ADVANCES AND CHALLENGES IN MICROPHYTOBENTHOS RESEARCH: FROM CELL BIOLOGY TO COASTAL ECOSYSTEM FUNCTION

EDITED BY: João Serôdio, David M. Paterson, Vona Meleder and Wim Vyverman
PUBLISHED IN: Frontiers in Marine Science

frontiers Research Topics

ISSN 1664-8714
ISBN 978-2-88966-296-8
DOI 10.3389/978-2-88966-296-8

About Frontiers

Frontiers is more than just an open-access publisher of scholarly articles: it is a pioneering approach to the world of academia, radically improving the way scholarly research is managed. The grand vision of Frontiers is a world where all people have an equal opportunity to seek, share and generate knowledge. Frontiers provides immediate and permanent online open access to all its publications, but this alone is not enough to realize our grand goals.

Frontiers Journal Series

The Frontiers Journal Series is a multi-tier and interdisciplinary set of open-access, online journals, promising a paradigm shift from the current review, selection and dissemination processes in academic publishing. All Frontiers journals are driven by researchers for researchers; therefore, they constitute a service to the scholarly community. At the same time, the Frontiers Journal Series operates on a revolutionary invention, the tiered publishing system, initially addressing specific communities of scholars, and gradually climbing up to broader public understanding, thus serving the interests of the lay society, too.

Dedication to Quality

Each Frontiers article is a landmark of the highest quality, thanks to genuinely collaborative interactions between authors and review editors, who include some of the world's best academicians. Research must be certified by peers before entering a stream of knowledge that may eventually reach the public - and shape society; therefore, Frontiers only applies the most rigorous and unbiased reviews.
Frontiers revolutionizes research publishing by freely delivering the most outstanding research, evaluated with no bias from both the academic and social point of view. By applying the most advanced information technologies, Frontiers is catapulting scholarly publishing into a new generation.

What are Frontiers Research Topics?

Frontiers Research Topics are very popular trademarks of the Frontiers Journals Series: they are collections of at least ten articles, all centered on a particular subject. With their unique mix of varied contributions from Original Research to Review Articles, Frontiers Research Topics unify the most influential researchers, the latest key findings and historical advances in a hot research area! Find out more on how to host your own Frontiers Research Topic or contribute to one as an author by contacting the Frontiers Editorial Office: researchtopics@frontiersin.org

ADVANCES AND CHALLENGES IN MICROPHYTOBENTHOS RESEARCH: FROM CELL BIOLOGY TO COASTAL ECOSYSTEM FUNCTION

Topic Editors:
João Serôdio, University of Aveiro, Portugal
David M. Paterson, University of St Andrews, United Kingdom
Vona Meleder, Université de Nantes, France
Wim Vyverman, Ghent University, Belgium

Image: João Serôdio.

Citation: Serôdio, J., Paterson, D. M., Meleder, V., Vyverman, W., eds. (2020). Advances and Challenges in Microphytobenthos Research: From Cell Biology to Coastal Ecosystem Function. Lausanne: Frontiers Media SA.
doi: 10.3389/978-2-88966-296-8

Table of Contents

frontiers in Marine Science

EDITORIAL
published: 12 November 2020
doi: 10.3389/fmars.2020.608729

Editorial: Advances and Challenges in Microphytobenthos Research: From Cell Biology to Coastal Ecosystem Function

João Serôdio[1]*, *David M. Paterson*[2], *Vona Méléder*[3] and *Wim Vyverman*[4]

[1] Department of Biology and CESAM—Centre for Environmental and Marine Studies, University of Aveiro, Aveiro, Portugal, [2] Sediment Ecology Research Group, Scottish Oceans Institute, School of Biology, University of St Andrews, Fife, United Kingdom, [3] Mer Molécules Santé (EA 21 60), Université de Nantes, Nantes, France, [4] Protistology & Aquatic Ecology, Ghent University, Ghent, Belgium

Keywords: microphytobenthos, diatoms, primary productivity, biodiversity, estuaries

Editorial on the Research Topic

Advances and Challenges in Microphytobenthos Research: From Cell Biology to Coastal Ecosystem Function

OPEN ACCESS

Edited and reviewed by:
Angel Borja,
Technological Center Expert in Marine and Food Innovation (AZTI), Spain

***Correspondence:**
João Serôdio
jserodio@ua.pt

Specialty section:
This article was submitted to Marine Ecosystem Ecology, a section of the journal Frontiers in Marine Science

Received: *21 September 2020*
Accepted: *30 September 2020*
Published: *12 November 2020*

Citation:
Serôdio J, Paterson DM, Méléder V and Vyverman W (2020) Editorial: Advances and Challenges in Microphytobenthos Research: From Cell Biology to Coastal Ecosystem Function. Front. Mar. Sci. 7:608729. doi: 10.3389/fmars.2020.608729

The microphytobenthos are fascinating communities of microalgae and cyanobacteria that inhabit benthic habitats in marine and freshwater ecosystems. These often apparently barren landscapes are in fact a "secret garden", harboring an immense microbial diversity and intense photosynthetic and biogeochemical activity (MacIntyre et al., 1996; Underwood and Kromkamp, 1999). On the intertidal flats of estuaries and beneath shallow coastal waters, the microphytobenthos are dominated by pennate diatoms, the most recently evolved and most diversified of this important group of protists (Kooistra et al., 2007; Benoiston et al., 2017).

Microphytobenthos have mostly been studied in temperate estuaries, but they have a widespread distribution from polar regions (Woelfel et al., 2014) to the tropics (Underwood, 2002). Over the last decades, microphytobenthos have attracted considerable interest mainly due to their role as a main contributor to the productivity of estuarine and shallow coastal areas (Hope et al., 2019). With a global annual gross primary production estimated to be in the order of 500 Mt of carbon, these ecosystems can be responsible for up to 20% of the ocean gross primary production although occupying only 0.03% of the ocean surface area (Pinckney, 2018). For estuarine ecosystems, microphytobenthos primary production can be comparable to that of the phytoplankton and can provide up to more than 50% of total ecosystem-level carbon fixation (Underwood and Kromkamp, 1999). Best known for their high photosynthetic activity and carbon fixation, their contribution to sediment stabilization and the strong links with invertebrate and vertebrate consumers, microphytobenthos communities have in recent years become the focus of multiple and apparently disparate disciplines such as photonics, photophysiology, community ecology, biogeochemistry, microbiology, evolutionary science, remote sensing and molecular biology.

This Research Topic aimed to bring together contributions on microphytobenthos research, to update current knowledge and uncover exciting future directions of strategic value, including

new methods and approaches, ultimately contributing to link cell biology and functional traits of diatoms and cyanobacteria to emerging properties observed at the community and ecosystem-level. This ebook comprises a collection of 20 articles, covering a wide range of topics, from cell motility and photophysiology to ecosystem-level productivity, reflecting the current interest in microphytobenthos diversity and functional traits, as well as in their role in the ecology of estuarine ecosystems. Most contributions to the Research Topic present results of original research, but the ebook also includes one mini-review and one perspective article. The majority of the articles refers to microphytobenthos communities from estuaries, covering over 14 ecosystems in Europe, North America, Australia and New Zealand.

The contributions to this Research Topic can be divided in five different groups, based on the topics addressed: (i) microphytobenthos primary productivity and biogeochemistry in tidal estuaries; (ii) motility and vertical migration of benthic diatoms and cyanobacteria; (iii) interactions between microphytobenthos and consumers; (iv) microphytobenthos diversity; and v) emerging topics.

A large number of articles (eight) addressed questions related to the role of microphytobenthos as primary producers in tidal estuaries, centered on the characterization of the spatio-temporal variability in biomass and productivity, often showing complex patterns due to spatial patchiness and the influence of tidal regimes. Most studies refer to locations in the European Atlantic coast (France, Portugal, Spain) and one to estuarine areas in Australia. Haro et al. investigated the seasonal variability in microphytobenthos biomass and productivity in a southern European coastal system (Cadiz Bay, Spain) and explored the influence of multiple environmental factors on the observed patterns. Daggers et al. used remote sensing data from high resolution satellite sensors to obtain a detailed characterization the spatio-temporal variability in microphytobenthos biomass across intertidal areas of the Westerschelde (The Netherlands). The studies by Méléder et al. and Savelli et al. combined modeling approaches with remote sensing data to estimate areal rates of carbon fixation for intertidal mudflats in the French Atlantic coast (Pertuis Charentais Sea, France). Frankenbach et al. used chlorophyll fluorescence techniques to directly compare the spatial and temporal variability of the photosynthetic activity of microphytobenthos and phytoplankton of the Ria de Aveiro (Portugal), showing that the areal and ecosystem-level productivity of the microphytobenthos may more than double the contribution by the phytoplankton. Redzuan and Underwood addressed the effects of sediment resuspension by tidal currents on the redistribution of microalgal biomass in the Colne Estuary (UK), while Tolhurst et al., using a manipulative approach, investigated the role of light and nutrients on microphytobenthos biomass and on the biogeochemistry of intertidal flats in the Sydney Harbor estuary (Australia). Pniewski and Piasecka-Jedrzejak investigated the operation of photoacclimatory and photoprotective mechanisms in a benthic diatom species, photophysiological processes key to enabling high rates of productivity under the variable light conditions, characteristic of shallow and intertidal habitats.

A second group of articles (five) addressed questions related to cell motility and vertical migration in microphytobenthos biofilms. Cellular motility is recognized as a key factor for the optimal exploitation of resources in the sedimentary microenvironment, directly related to the environmental rhythmicity of intertidal habitats. Barnett et al. and Prins et al. present results on the role of light intensity and color on the control of vertical migratory behavior of benthic diatoms, and its coupling with the operation of photophysiological photoprotective processes. Lichtenberg et al. investigated the role of light in the vertical migration of the relatively less studied cyanobacteria-dominated biofilms. While these studies refer to manipulative studies carried out under controlled laboratory conditions, Kromkamp et al. presents data collected *in situ* on the short-term and micro-scale (< 1 m) variation of microphytobenthos biomass and photosynthetic activity during diurnal low tide periods. The ebook also includes a mini-review by Marques da Silva et al., consisting of a theoretical study on the long-standing question of the relative energetic costs of vertical migration and physiological photoprotective mechanisms in motile diatoms.

A third group of articles (three) address topics related to the interactions between microphytobenthos and consumers inhabiting estuarine intertidal areas. Using bird exclusion experiments carried out on an intertidal flat, Booty et al. explored the effects of the presence of shorebirds on key sedimentary parameters such as the critical erosion threshold, and the influx and efflux of nitrate and phosphorous. The connections between microphytobenthos and shorebirds were also addressed by Schnurr et al. who linked the seasonal variation in fatty acid composition of benthic diatoms, and associated nutritional value, to the regular visits of shorebirds to the Fraser River estuary, Canada, during their annual migration. The fatty acid composition of benthic diatoms was also studied by Hope et al., in the context of anthropogenic nutrient enrichment and turbidity increase, considering the implications for the populations of deposit-feeding bivalves.

The important, but often understudied, topic of the diversity of microphytobenthos communities is also covered in this ebook with two articles. Virta et al. investigated the seasonal and inter-annual variation of the taxonomic and functional composition of the communities of benthic diatoms in a non-tidal system in the Baltic Finnish coast. Ribeiro et al. explored alternative methodological approaches, as excluding abundance data or rare species, taxonomic resolution, or use of size-based metrics, to characterize the diversity of benthic diatom communities inhabiting intertidal flats of the Tagus estuary (Portugal).

The Research Topic also includes two articles on emerging topics in microphytobenthos research. One article refers to the first use of untargeted metabolomic techniques to microphytobenthos biofilms, here with the purpose of characterizing the metabolite composition of extracellular polymeric substance excreted by benthic diatoms (Gaubert-Boussarie et al.). The other is a perspective article on

the predictable but largely unstudied effects of light pollution on benthic microalgal communities (Maggi and Serôdio).

DEDICATION

We dedicate this ebook to Jacco Kromkamp, an inspirational scientist whose meticulous work was an exemplar to others in the field. Jacco will be missed in the community and more so by those that knew him for his science and for his kind and gentle nature. He was always supportive and constructive with a lively sense of humor and it was a pleasure to share fieldwork and laboratory studies with him.

AUTHOR CONTRIBUTIONS

JS, DP, VM, and WV organized this Research Topic and wrote the editorial. All authors contributed to the article and approved the submitted version.

FUNDING

Thanks are due to FCT/MCTES for the financial support to CESAM (UIDP/50017/2020 + UIDB/50017/2020), through national funds, to JS, and to the NERC Blue-coast project to DMP (NE/N016009/1).

REFERENCES

Benoiston, A., Ibarbalz, F. M., Bittner, L., Guidi, L., Jahn, O., Dutkiewicz, S., et al. (2017). The evolution of diatoms and their biogeochemical functions. *Philos. Trans. R. Soc. B Biol. Sci.* 372:20160397. doi: 10.1098/rstb.2016.0397

Hope, J. A., Paterson, D. M., and Thrush, S. F. (2019). The role of microphytobenthos in soft-sediment ecological networks and their contribution to the delivery of multiple ecosystem services. *J. Ecol.* 108, 1365–2745.13322. doi: 10.1111/1365-2745.13322

Kooistra, H., Gersonde, R., Medlin, L., and Mann, D. (2007). "The origin and evolution of the diatoms: their adaptation to a planktonic existence," in *Evolution of Primary Producers in the Sea*, eds. P. G. Falkowski and A. Knoll (Amsterdam: Elsevier Academic Press), 207–249. doi: 10.1016/B978-012370518-1/50012-6

MacIntyre, H. L., Geider, R. J., and Miller, D. C. (1996). Microphytobenthos: the ecological role of the "secret garden" of unvegetated, shalow-water marine habitats. I. Distribution, abundance and primary production. *Estuaries* 19, 186–201. doi: 10.2307/1352224

Pinckney, J. L. (2018). A mini-review of the contribution of benthic microalgae to the ecology of the continental shelf in the south atlantic bight. *Estuar. Coasts* 41, 2070–2078. doi: 10.1007/s12237-018-0401-z

Underwood, G. J. C. (2002). Adaptations of tropical marine microphytobenthic assemblages along a gradient of light and nutrient availability in Suva Lagoon, Fiji. *Eur. J. Phycol.* 37, 449–462. doi: 10.1017/S0967026202003785

Underwood, G. J. C., and Kromkamp, J. (1999). "Primary production by phytoplankton and microphytobenthos in estuaries," in *Advances in Ecological Research* (San Diego, CA: Academic Press), 93–153. doi: 10.1016/S0065-2504(08)60192-0

Woelfel, J., Eggert, A., and Karsten, U. (2014). Marginal impacts of rising temperature on Arctic benthic microalgae production based on in situ measurements and modelled estimates. *Mar. Ecol. Prog. Ser.* 501, 25–40. doi: 10.3354/meps10688

Conflict of Interest: The authors declare that the research was conducted in the absence of any commercial or financial relationships that could be construed as a potential conflict of interest.

frontiers in Marine Science

ORIGINAL RESEARCH
published: 14 February 2020
doi: 10.3389/fmars.2020.00039

Microbenthic Net Metabolism Along Intertidal Gradients (Cadiz Bay, SW Spain): Spatio-Temporal Patterns and Environmental Factors

Sara Haro[1], Miguel Lara[1], Irene Laiz[2], Carlos José González[3], Julio Bohórquez[1], Emilio Garcia-Robledo[1], Alfonso Corzo[1] and Sokratis Papaspyrou[1]*

[1] Department of Biology, Faculty of Marine and Environmental Sciences, University of Cádiz, Cádiz, Spain, [2] Department of Applied Physics, University of Cádiz, Cádiz, Spain, [3] Division of Naval Support and Oceanography, Marine Hydrographic Institute, Spanish Navy, Cádiz, Spain

OPEN ACCESS

Edited by:
David M. Paterson, University of St Andrews, United Kingdom

Reviewed by:
Akkur Vasudevan Raman, Andhra University, India
Punyasloke Bhadury, Indian Institute of Science Education and Research Kolkata, India

****Correspondence:***
Sara Haro
sara.haro@uca.es

Specialty section:
This article was submitted to Marine Ecosystem Ecology, a section of the journal Frontiers in Marine Science

Received: *25 July 2019*
Accepted: *21 January 2020*
Published: *14 February 2020*

Citation:
Haro S, Lara M, Laiz I, González CJ, Bohórquez J, Garcia-Robledo E, Corzo A and Papaspyrou S (2020) Microbenthic Net Metabolism Along Intertidal Gradients (Cadiz Bay, SW Spain): Spatio-Temporal Patterns and Environmental Factors. Front. Mar. Sci. 7:39. doi: 10.3389/fmars.2020.00039

Microphytobenthos (MPB), the photosynthetic primary producing component of microbenthos, shows variable patterns in its biomass distribution along the intertidal gradient as a result of the interactions of factors such as light, tides, temperature, and grazing pressure. These patterns have been studied more extensively in northern European estuaries than southern European coastal systems. Even less information is available regarding temporal changes in MPB primary production rates in these systems. For this reason, we followed the seasonal changes in net production in light and dark respiration rates (determined by oxygen microelectrodes) and MPB biomass (estimated by sediment chlorophyll *a*) along the intertidal gradient of the inner Cadiz Bay during a year. Sediment cores were collected along two transects (five sampling stations per transect) with distinct sediment granulometry: one muddy [Puerto Real (PR)] and one muddy-sandy transect [San Fernando (SF)]. Our results show that MPB biomass and net production increased seawards reaching their maxima in winter. In contrast to what is observed in northern European systems, the higher solar irradiance and temperatures occurring in summer in southern Spain likely inhibit MPB production. In Cadiz Bay, spatial patterns of MPB biomass and net production depended on season and location due to the environmental heterogeneity observed. Environmental variables, analyzed by principal component analysis (PCA), were used to explain the variability of MPB metabolism by multiple regression. Selected principal component (PC) axes explained 60% of the net production in light and 41% of the dark respiration rates variability in PR, while they only accounted for 25% of the same rates in SF. The differences observed between transects and the variability in the environmental variables explaining them highlight the importance of considering the spatial heterogeneity of our system to estimate the contribution of MPB to the inner Cadiz Bay productivity. In our case, this contribution is significant accounting for up to 49% of the total benthic production of the inner Cadiz Bay intertidal sediments, confirming previous global estimates.

Keywords: microphytobenthos, primary production, metabolism, intertidal sediment, oxygen microelectrodes, chlorophyll

INTRODUCTION

Microphytobenthos (MPB), the photosynthetic community inhabiting the surface layer of euphotic sediments, plays a key role in the cycling of carbon and nitrogen in estuaries and other coastal shallow ecosystems, being able to contribute up to 50% of their total primary production (Underwood and Kromkamp, 1999). However, patterns of MPB biomass distribution and primary production vary strongly in estuarine ecosystems as a result of the high variability and interactions of environmental factors which characterizes these systems (Benyoucef et al., 2013). Among these factors, irradiance and temperature are the ones considered to most strongly affect MPB photosynthetic rates (Hancke and Glud, 2004; Migné et al., 2004; Davoult et al., 2009). In addition, a large number of other variables have been used to explain variations in MPB abundance and composition in time and space. Some of them include sediment type, tidal height, sediment desiccation and compaction, grazing pressure, salinity, topography, and nutrients availability both in the sediment porewater and the water column (Coelho et al., 2009; Jesus et al., 2009; Pratt et al., 2015; Garcia-Robledo et al., 2016).

The majority of studies focusing on the distribution of MPB biomass at the sediment surface have been performed using the pulse amplitude modulation (PAM) technique, spectral reflectance analysis, or remote sensing (Jesus et al., 2005; Murphy et al., 2008; Benyoucef et al., 2013). However, these methods do not measure directly microphytobenthic primary production (PP_{MPB}) or respiration. To quantify these processes, methods such as benthic chamber or whole core incubations, ^{14}C incorporation, or oxygen microsensor measurements are required. However, these methods are difficult to upscale in order to monitor intertidal areas at a large scale. As a result, little is known on the distribution of MPB primary production, respiration, and net metabolism rates at large spatial and temporal scales. Despite this shortcoming, oxygen microelectrodes have been used to determine the distribution of MPB production rates in time and space, showing good agreement with ^{14}C incubations data (Revsbech et al., 1981; Barranguet et al., 1998). Oxygen measurements are then usually upscaled to larger areas using several models of PP_{MPB} developed for the purpose (Pinckney and Zingmark, 1993; Serôdio and Catarino, 2000). Regardless of the method used, seasonal and spatial patterns of PP_{MPB}, similarly to MPB biomass, have been explained by a wide array of biotic and abiotic environmental variables depending on the environment studied (Hubas et al., 2006; Jesus et al., 2009; Orvain et al., 2012; Savelli et al., 2018).

Fluctuations in environmental variables result in MPB biomass changes on temporal scales ranging from days to seasons (Migné et al., 2004; Serôdio et al., 2005). MPB seasonal patterns seem to differ between northern and southern European estuaries. In northern Europe, the maximum of MPB biomass is observed in summer, whereas in southern Europe, in most cases, the maximum is found in winter and early spring (Van der Wal et al., 2010; Benyoucef et al., 2013; Brito et al., 2013; Garcia-Robledo et al., 2016; Savelli et al., 2018). Seasonal patterns with maximum values of MPB biomass in winter have also been reported at latitudes similar to those of southern Europe, in Korea and Japan (Goto et al., 2000; Koh et al., 2007; Kwon et al., 2016). In fact, intertidal MPB can adapt physiologically to a combined light-temperature stress gradient, such as that found along the Atlantic coast of southern Europe (Laviale et al., 2015). Therefore, latitudinal conditions of light and temperature seem to be important factors affecting seasonal and spatial patterns of MPB distribution.

The spatial distribution of MPB biomass ranges from centimeters to kilometers depending on the system (Guarini et al., 1998; Maggi et al., 2017). Along the intertidal gradient, the maximum MPB biomass is usually found at the high shore with biomass decreasing seawards. This pattern has been observed in both southern (Orvain et al., 2012; Brito et al., 2013; Maggi et al., 2017) and northern European estuaries (Van der Wal et al., 2010; Benyoucef et al., 2013), and is attributed to a higher irradiance dose in the upper shore (i.e., due to a shallower water column and a longer emersion period). However, in some southern European estuaries, the long emersion period in the upper shore produces greater sediment desiccation and exposure to extreme temperatures, inverting the trend described (Coelho et al., 2009; Laviale et al., 2015).

In the present study, we wanted to test two hypotheses: (1) annual maxima in biomass and primary production occur during the winter months at lower latitude temperate intertidal flats, in contrast to what has been generally observed at higher latitudes, and (2) higher biomass and net primary production occur at the upper shore, most likely due to a higher daily irradiance dose as a result of a lower light attenuation by the water column in comparison to the lower intertidal range. To test these hypotheses, we studied the seasonal distribution of MPB biomass and net metabolism (net production in light and dark respiration) along the intertidal gradient in the inner Cadiz Bay (Spain, southern Europe). In addition, we tried to identify environmental variables that could explain the variation in MPB net metabolism in the bay, both seasonally and in space, by multivariate and multiple regression analyses.

MATERIALS AND METHODS

Study Site and Sampling

The inner Cadiz Bay is a shallow water body, with an average depth of less than 3 m. The intertidal zone (maximum length 9.3 km; width 5.25 km) covers ∼60% of its surface. Sediment is predominantly mud (size grain $< 63\ \mu m$) (Sanchez De Lamadrid Rey and Muñoz Pérez, 1994; Carrasco et al., 2003). The bay is affected by semidiurnal tides that oscillate between a maximum tidal height of 1.75 m and a minimum of -1.5 m relative to the local mean sea level (MSL). Circulation is mainly controlled by tides, which is the main mechanism of water renovation. Strong easterly winds are frequent in the region and contribute to sediment resuspension (Gutiérrez et al., 2000; Ligero et al., 2005). Submerged vegetation changes along the intertidal gradient, mainly in locations with a high variability in sediment grain size along the intertidal zone (Morris et al., 2009; Lara et al., 2016) (**Figure 1**). In the inner Cadiz Bay, 70% of the intertidal area is covered by *Zostera noltei* meadows, 20% is bare sediment,

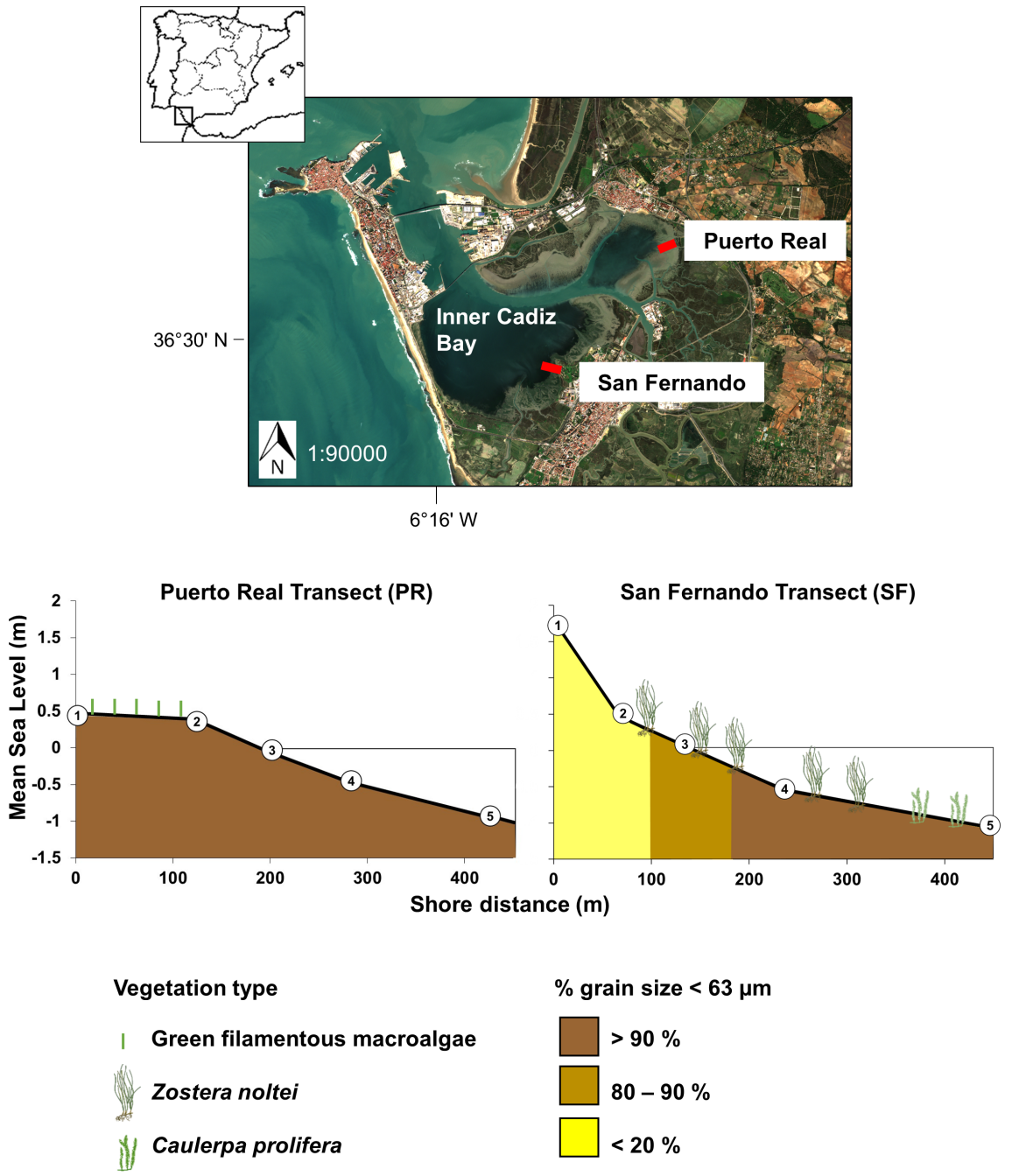

FIGURE 1 | Map of inner Cadiz Bay indicating the two studied transects: Puerto Real (PR) and San Fernando (SF). The lower panels indicate the slope profiles of each transect and the sampling stations as a function of shore distance (axis *x*) and mean sea level (axis *y*). The approximate distribution of grain size distribution (<63 µm) and vegetation species zonation are indicated.

occasionally covered in parts by green macroalgae, whereas the remaining 10% is shared between *Caulerpa prolifera* and *Cymodocea nodosa* meadows, which inhabit the lower fringe of the intertidal zone (Gómez Ordoñez, 2008; Brun et al., 2015). MPB community studies do not exist for the inner bay; however, published experimental data using sediment from the wider bay area indicate a dominance of diatoms which is disturbed in the presence of green macroalgal blooms in favor of cyanobacteria (Garcia-Robledo et al., 2008, 2012; Haro et al., 2019). Preliminary semi-quantitative data for the inner bay sediments based on molecular analyses indicate the presence of both diatoms and cyanobacteria throughout the intertidal area (J. Taylor pers. comm). Cyanobacteria show higher relative abundances (within prokaryotes) in the upper intertidal, especially in sandier

sediments. The most abundant genera include *Pleurocapsa* sp., *Phormidium* sp., and *Rivularia* sp. in sandy muddy sediments and *Lyngbya* sp. and *Coleofasciculus* sp. in muddy sediments. Diatoms also show higher relative abundance in the upper intertidal (within eukaryotic OTUs). Most common genera include *Amphora* sp., *Navicula* sp., *Nitzschia* sp., *Pleurosigma* sp., and *Placoneis* sp. in sandy muddy sediments and *Skeletonema* sp., *Gyrosigma* sp., and *Navicula* sp. in muddy sediments. A more detailed description of the sampling area can be found in Papaspyrou et al. (2013) and Jimenez-Arias et al. (2016).

Samplings were performed along two transects in the inner Cadiz Bay, each 500 m long, once per season (July and October 2016, and January and April 2017) (**Figure 1**). The two transects were selected to include the range of grain size distributions found in the area. In Puerto Real (PR), sediment is mainly mud, whereas in San Fernando (SF) a mixture of sand and mud. Five stations were distributed along each transect to cover from the upper intertidal (1.7 m above MSL in SF and 0.5 m in PR) to the lower intertidal (-1.5 m below MSL in both cases) (**Supplementary Table 1**). Samplings were performed during spring tides (average tidal coefficient of ∼80), at high tide to ensure access by rowboat along the entire transect. Samplings took place during the same week for both transects, 1 day per transect.

At each sampling station, six sediment cores (i.d. 5.2 cm; 27 cm length) were collected using a Kajak sediment sampler (model 13.030, KC, Denmark). Water column samples were also collected at each station. Cores and water samples were kept on ice until returning to the laboratory. Upon arrival to the laboratory, water column samples were immediately filtered through a GF/F filter and stored frozen (−20°C) until nutrient analyses. Sediment cores were placed in an aquarium connected to a tank filled with *in situ* seawater under constant temperature (18°C). The aquarium was illuminated with fluorescent lamps (Lumina 1080 Blau Aquaristic) at 200 μmol photon m^{-2} s^{-1} under a 12 h light: 12 h dark photoperiod. Three cores were sliced on the same day (upper 0.5 cm), the sediment centrifuged at 4700 × g for 20 min at 4°C, and the supernatant preserved at −20°C for porewater analysis.

Microsensor Measurements

Oxygen microprofiles were measured in each of three cores, in light and in darkness, using O_2 microelectrodes (50 μm tip size, Unisense A/S, Denmark). In order to obtain the maximum potential primary production rates, O_2 microprofiles in light were measured after 30 min under a saturating irradiance (1200 μmol photon m^{-2} s^{-1}). Dark respiration rates (R_D) and net production of the photosynthetic layer in light (P_N) were determined from the oxygen vertical profiles by applying Fick's first law (Revsbech and Jorgensen, 1983; Kühl et al., 1996). The oxygen diffusion coefficient was obtained from standard values for the prevailing conditions of salinity and temperature (Soetaert et al., 2010), and corrected for sediment tortuosity (Li and Gregory, 1974). Microprofiles were performed in areas within sediment cores where no macrophytes or macroalgae were present. In the few cases where macrophytes were abundant in sediment cores, they were carefully removed without disturbing the sediment surface, and microprofiles were measured only within clear bare sediment zones.

Sediment Variables

Once oxygen microprofiles were measured, the upper 0.5 cm sediment layer was obtained. A portion of fresh sediment (∼5 g) was used to determine sediment density as the weight of a known volume. Porosity was determined as the loss of water of a known volume of sediment sample after drying at 60°C for 72 h. The percentage of fines (< 63 μm) was determined by wet sieving after removing organic matter with hydrogen peroxide (H_2O_2) and dispersing the sediment with sodium hexametaphosphate $(NaPO_3)_6$ (Buchanan, 1984).

Pigments' content in the sediment was measured by extraction of ∼2 g of fresh sediment in 100% methanol buffered with $MgCO_3$, for 12 h at 4°C in darkness (Thompson et al., 1999). Samples were centrifuged at 4700 × *g* for 10 min (Sorvall Legend X1R; Thermo Scientific). Spectra of the extracts were obtained on a microplate reader (Multiskan GO; Thermo Scientific) before and after acidifying the methanol extract with 2 N hydrochloric acid in order to determine phaeopigments (pheo) content. Chl *a* and Chl *c*, and pheo were estimated according to Ritchie (2008) and Stal et al. (1984), respectively.

The remaining sediment was dried at 60°C for 72 h. One portion of the sediment (∼0.5 g) was used to determine the organic matter content by loss on ignition (Heiri et al., 2001). Total carbon and total nitrogen (TN) contents were determined in dried sediment samples. Organic carbon (OC) was determined as the difference between total carbon measured in dried sediment samples and inorganic carbon measured on a second replicate combusted previously at 550°C for 5 h. Both samples were analyzed on an elemental analyzer (LECO CHNS 932) at the Central Services of the University of A Coruña.

Sediment porewater and water column nutrient concentrations [NH_4^+, NO_2^-, NO_3^-, PO_4^{3-} and $Si(OH)_4$, hereafter referred to as dissolved silica, DSi] were measured following standard protocols (Grasshoff et al., 1999; Garcia-Robledo et al., 2014) on a microplate reader (Multiskan GO; Thermo Scientific).

Physical Variables

Mean sea level of every sampling point was computed with an independent mesh of data which combines the nautical charts 443A and 443B from the Marine Hydrographic Institute (IHM, Spain) with further topobathymetric measurements for certain localities (Tejedor et al., 1997). The value of MSL for a specific *XY* coordinate was approached by nearest neighbor criteria to the existing mesh. Euclidean distances to the reference nodes were calculated with the R package "geosphere" (Hijmans et al., 2017). This procedure allows to obtain the MSL of sampling points with a horizontal precision always higher than 28 m (i.e., assuming the worst scenario, with the point placed at the same distance from the four nodes), which is negligible due to the flat morphometry of Cadiz Bay. Longitudinal distances within the transects were calculated taking as a reference the station nearest to the shore (**Figure 1**).

Meteorological conditions (irradiance, temperature, rain, and wind speed) were obtained by the Junta de Andalucía meteorological station located in El Puerto de Santa María. Values were averaged for the week before each sampling (**Supplementary Figure 1**).

Annual Net Metabolism of the Microbenthic Intertidal Sediment

In order to estimate the contribution of MPB communities to the annual net metabolism of the intertidal zone of the inner Cádiz Bay, we used the P_N and R_D rates data obtained in the different sediment types (e.g., bare muddy sediment, bare sandy sediment, seagrass meadow sediment). Daily rates of P_N in light or R_D in darkness were obtained by multiplying with the hours of daylight or darkness, respectively. P_N rates were corrected for the variability in rates observed during daylight. To do this, given that measurements in the lab were always performed during the maximum daylight production phase, a diel correction factor was applied to account for the lower P_N rates at the beginning and end of the daylight phase (0.67 ± 0.3, $n = 4$, Haro et al., 2019). R_D rates were considered constant during the night (Haro et al., 2019). Daily P_N or R_D were assumed constant during each season and were corrected for temperature differences using a Q_{10} of 1.56 for P_N (Kwon et al., 2018) and 2.0 for R_D (Grant, 1986; Hancke and Glud, 2004). To compare the obtained data with the literature, rates in mmol O_2 m^{-2} $year^{-1}$ were converted to mmol C m^{-2} $year^{-1}$, assuming a photosynthetic quotient 1.2 mmol O_2: mmol C and a respiratory quotient 106 mmol O_2: 138 mmol C, and expressed in g C (Hedges et al., 2002). Finally, the annual net metabolism of the microbenthic intertidal sediment was calculated as the difference between the annual rates of P_N in light and R_D in darkness and multiplied by the surface cover of each habitat type in the intertidal area of the inner Cadiz Bay.

Statistical Analysis

In order to explore potential relationships, reduce the number of explanatory variables, and avoid collinearity effects in further analysis, a principal component analysis (PCA) was applied to the entire set of normalized environmental data (i.e., shore distance, MSL, % grain size < 63 μm, irradiance, air temperature, rainfall, wind speed, porosity, salinity, OC, TN, nutrients in the water column and porewater). Chl *a*, Chl *c*, and nutrients in porewater were log-transformed prior to analysis. Then, a multiple linear regression (MLR) model was applied using P_N or R_D as dependent variables and principal components (PCs) obtained from the PCA as explanatory ones (Cho et al., 2009; Lee et al., 2015). Given the biotic nature of chlorophyll and the direct link to MPB production, chlorophylls were maintained as independent variables and were not included in the initial PCA. Only PCs with eigenvalues higher than 1 were selected for MLR analysis (Jackson, 1993). Best Model variable selection procedures were employed to identify the best empirical equation of P_N, R_D, and MPB biomass (Zuur and Ieno, 2016). Analyses were carried out independently for each transect, due to their different nature in terms of granulometry and environmental features, as the contrasting results obtained by PCA corroborated. All statistical analysis was carried out using XLSTAT 2018 (Microsoft Office 2016).

RESULTS

Abiotic Environmental Variables

Sediment along the intertidal transects studied was mainly muddy-silt with the fine fraction (< 63 μm) accounting for $> 90\%$ (**Supplementary Table 2**), with the exception of the two upper intertidal stations in SF, where $< 20\%$ was fine sediment. A macrophytes species zonation was observed along the SF transect (**Figure 1**); *Z. noltei* was present in stations SF2–SF4, whereas dense *C. prolifera* canopies dominated in SF5. In PR, sediment was covered by a visible brown diatomaceous biofilm year round, although more intensely in winter. Green filamentous macroalgae were also observed in the upper shore in January.

Temperature showed the typical pattern for temperate systems with higher values in July (23.8 ± 1.7°C) and lower in January (10.1 ± 1.6°C) (**Supplementary Figure 1**). Rainfall was minimal during the days previous to the sampling with only 0.15 ± 0.3 mm registered the week before the autumn sampling. In spring, sampling occurred 1 week after a strong wind and slight rainfall event (**Supplementary Figure 1**).

Water Column and Porewater Nutrients

Water column nutrient concentrations were higher in general in PR than SF (**Figure 2A**). A clear decrease in DSi concentrations was observed seawards, less evident in PR. Water column PO_4^{3-} concentrations were mostly lower than 1 μM and showed a parallel trend to that of DSi. On the other hand, NO_3^- and NH_4^+ concentrations showed little variation in both transects, with relatively higher values observed in PR4 (7.9 ± 0.5 and 5.0 ± 0.4 μM, respectively). Overall, NO_3^- was slightly more abundant than NH_4^+ in PR (**Figure 2A**), while NO_2^- concentrations were below detection limits in both transects (data no shown).

In contrast to the water column, the highest concentrations of nutrients in the porewater were measured in SF (**Figure 2B**). Furthermore, a reverse trend to that of the water column was observed, with concentrations increasing toward lower intertidal stations. This trend was less evident in PR than in SF for almost all of the studied nutrients due to the higher concentrations found in the upper shore station. In contrast to water column, NH_4^+ was the most available form of inorganic nitrogen in the porewater.

Organic Carbon, Total Nitrogen, and Pigments

Organic carbon and TN contents were always higher at the sampling stations with sediment comprising of $> 90\%$ fine particles. Thus, in PR, OC content did not vary with MSL (∼3.5%), whereas in SF, it ranged from 4–5% in the muddy stations to less than 1% in the sandy stations (SF1 and SF2) (**Figure 3A**). TN content followed the same pattern as OC (**Figure 3B**). No temporal trends were observed for either OC or

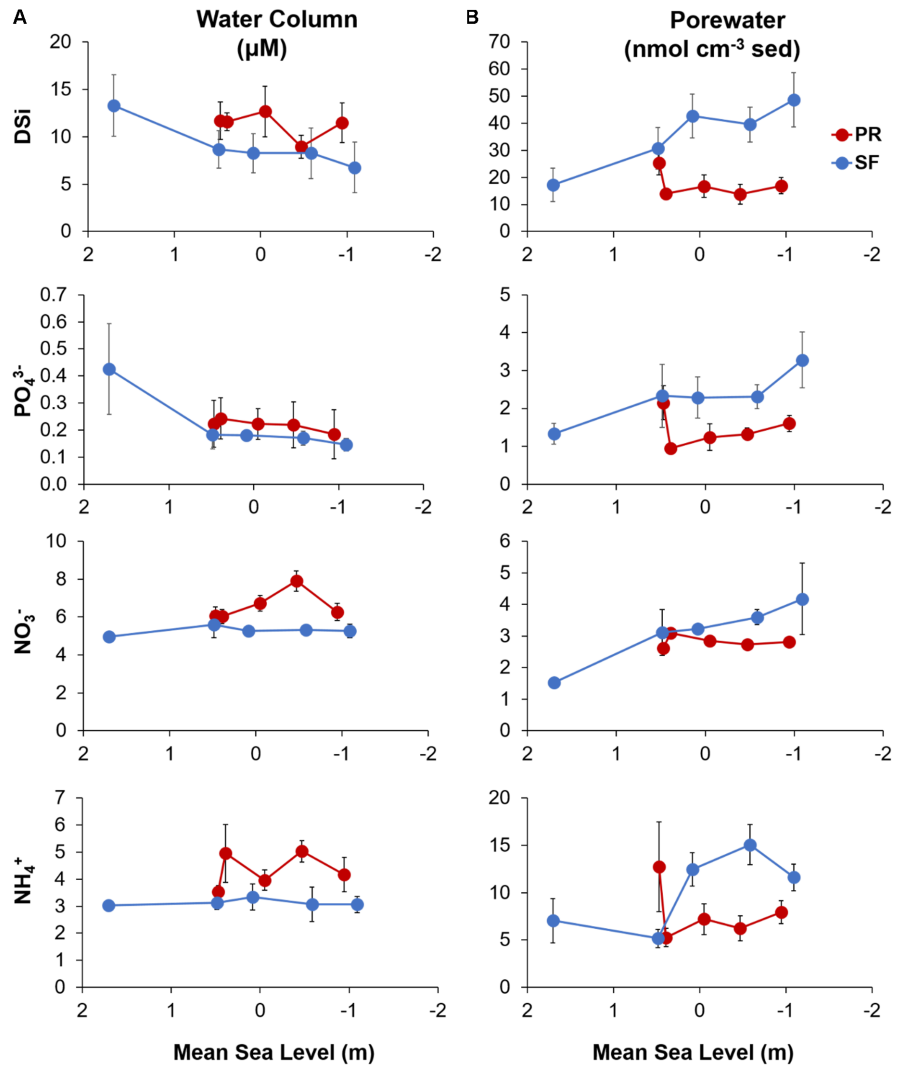

FIGURE 2 | Seasonal mean nutrients concentrations (DSi, NO_3^-, NH_4^+, and PO_4^{3-}) **(A)** in the water column and **(B)** the porewater plotted against mean sea level for the Puerto Real (PR; in red) and San Fernando (SF; in blue) transects. Water column and porewater values represent the mean ± SE (n = 4).

TN content. The OC to TN ratio (**Figure 3C**) was also constant along the transects in both PR (17.1 ± 0.4) and SF (13.5 ± 0.3), with the exception of station SF1, where a strong temporal variability was observed.

Microphytobenthos biomass was generally higher in SF than in PR (**Figure 4A**). The highest Chl *a* content was observed in both transects in January. In SF, Chl *a* content was threefold higher in January than in April. Distribution of MPB biomass between stations was more homogeneous in PR (average of 1.5 µg chl *a* cm^{-2}) than in SF where values ranged between 0.6 and 6.13 µg chl *a* cm^{-2}. In SF, the highest Chl *a* content was measured at stations SF3 and SF4. In PR, higher Chl *a* values were measured in the upper intertidal, whereas the opposite was true in January.

The Chl *c* to Chl *a* ratio showed high spatial variability in both transects (**Figure 4B**), with the lowest ratio observed at the lower intertidal level. In PR, the highest Chl *c* to Chl *a* ratio was found in January. In SF, differences between seasons were less evident. The pheo to Chl *a* ratio showed a larger spatial variability in SF (range between 1.38 and 0.07), whereas in PR, this ratio was relatively constant along the transect (average of 0.58) (**Figure 4C**). OC to Chl *a* ratio did not show clear trends along the transects, although in SF it increased slightly seawards, being up to three times higher in SF5 than in SF1 in April and October (**Figure 4D**).

Seasonal and Spatial Variability of MPB Net Metabolism

On average, P_N was higher in PR (4.0 ± 0.5 mmol O_2 m^{-2} h^{-1}) than in SF (1.7 ± 0.4 mmol O_2 m^{-2} h^{-1}) (**Figure 5A**). Rates of P_N in PR were much higher in January than during the rest of the seasons, increasing near the lower intertidal level. However, in April and October, although rates varied little along the intertidal, the highest P_N rates were measured at PR1. In contrast, spatial variability in SF was high, with a general

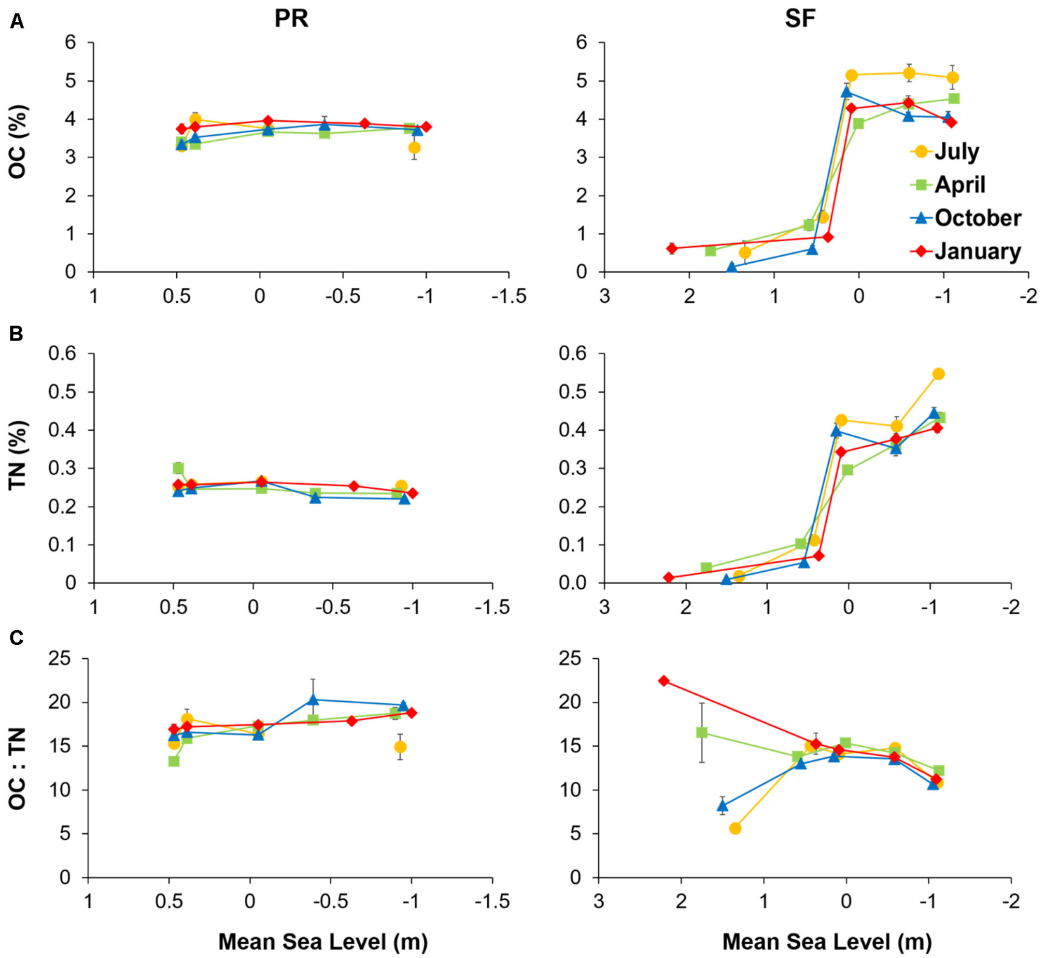

FIGURE 3 | (A) Sediment organic carbon (OC), **(B)** total nitrogen (TN), and **(C)** OC to TN ratio plotted against mean sea level for the Puerto Real (PR) and San Fernando (SF) transects in July (yellow), April (green), October (blue), and January (red). Values represent mean values ± SE (n = 3).

slight decrease in P_N seawards. No clear pattern was observed over time.

P_N rates normalized to Chl *a* content were five times higher in the PR transect (0.32 ± 0.1; n = 5) than the SF one (0.06 ± 0.1; n = 5) (**Figure 5B**). Differences between seasons were more evident in PR than in SF, with maximum values found in January (0.44 ± 0.04; n = 5). In PR, normalized P_N tended to increase seawards, whereas the opposite was true in winter. In SF, normalized P_N decreased slightly seaward, with P_N turning negative at station SF5.

Temporal patterns of R_D did not coincide between the two transects (**Figure 5C**). Although R_D was maximum in January and April in both PR and SF, R_D rates varied between seasons more in PR than in SF. Overall, a trend of decreasing rates was observed seawards in PR.

Interaction Between Environmental Variables

Principal components with eigenvalues higher than 1 explained 81.48 and 82.10% of the total variation of the PR and SF transects, respectively (**Table 1**). PC1 and PC2 explained approximately half of that variation (41.94 and 53.39% of the variance in PR and SF transects, respectively) (**Figure 6**). In PR, PC1 was mainly related with irradiance, temperature, salinity and water column nutrient concentrations, and PC2 with shore distance, MSL, and grain size. In SF, PC1 correlated with distance, MSL, grain size, and porewater nutrients, and PC2 with temperature, salinity, irradiance, and water column DSi concentration. OC presented high correlation with PC1 in both transects, slightly higher in SF. Around 12 and 13% of the variance in environmental variables (PC3) was attributed to rainfall in both transects. Overall, according to our PCA analysis, spatial variability dominated in SF in contrast to PR where temporal variability dominated (**Figure 6**).

Factors Controlling MPB Biomass

The PC axes selected by MRL analyses to explain the variations in time and space of the MPB biomass (estimated here by the Chl *a* content) in each transect accounted for 30% of the total variation. In PR, MPB biomass was best explained by PC2

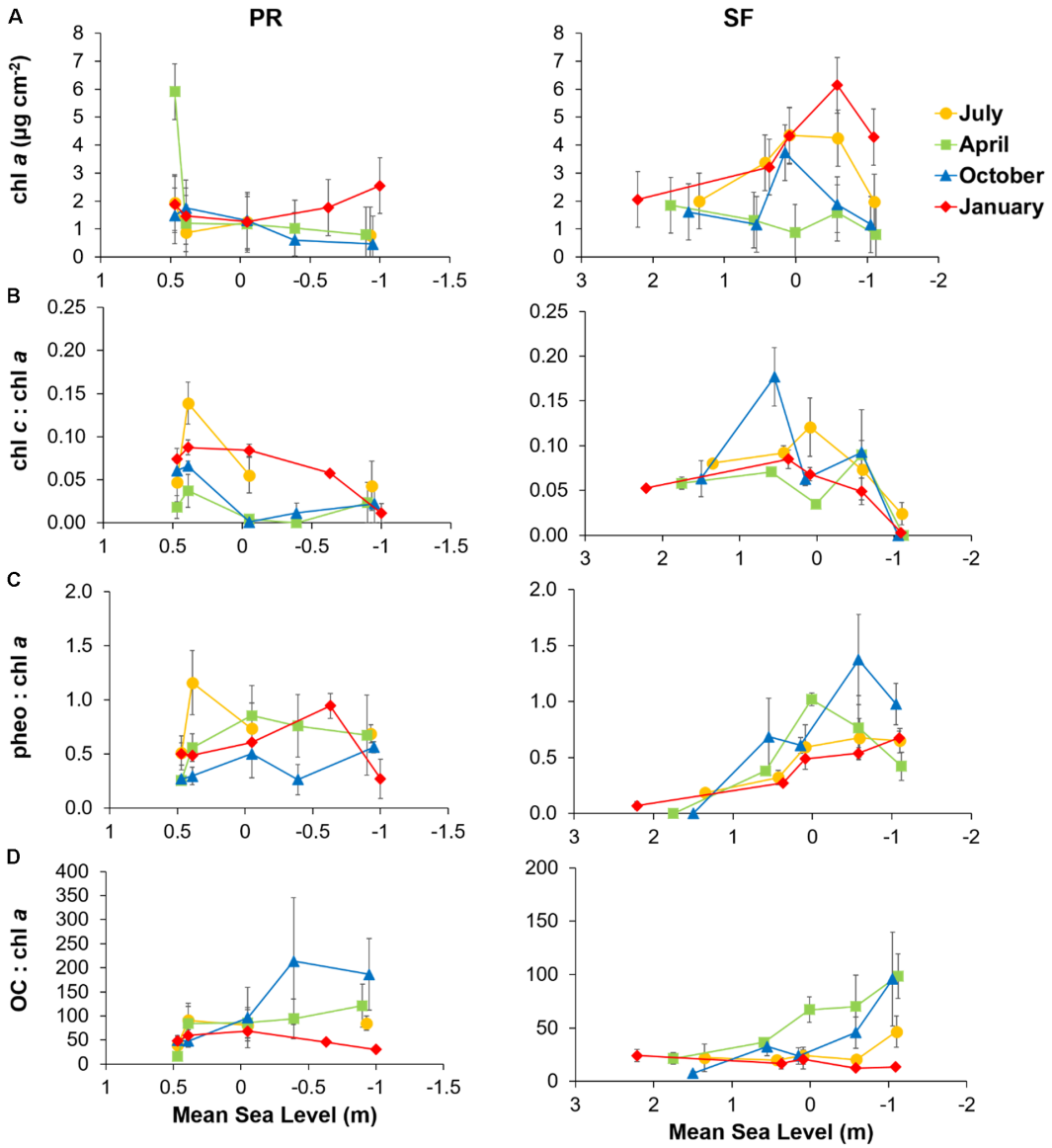

FIGURE 4 | (A) Sediment chlorophyll *a* (Chl *a*) content, **(B)** chlorophyll *c* to chlorophyll *a* ratio (Chl *c* to Chl *a*), **(C)** phaeopigments to chlorophyll *a* ratio (pheo to Chl *a*), and **(D)** organic carbon to chlorophyll *a* ratio (OC to Chl *a*) plotted against mean sea level (MSL) for the Puerto Real (PR) and San Fernando (SF) transects in July (yellow), April (green), October (blue), and January (red). Values represent means ± SE (n = 3).

(**Table 2**) composed primarily by shore distance, MSL, grain size, and TN (**Table 1**). On the other hand, MPB biomass in SF was explained mainly by PC5 (**Table 2**), related to NH_4^+ in the water column (**Table 1**), and to a lesser extent by PC2 which was related to temperature, salinity, irradiance, and DSi concentration in the water column.

Factors Controlling MPB Biomass and Sediment Metabolism

Principal component scores and MPB biomass (Chl *a* and Chl *c*) were used as independent variables in MLR to explain P_N in Cadiz Bay. In PR, 60% of the variance in P_N was explained by Chl *a* and PC1 (**Table 2**). Irradiance, temperature, salinity, and wind speed were positively correlated with PC1, while OC, PO_4^{3-}, and NH_4^+ in water column showed negative correlation with PC1 (**Table 1**). In SF, the variables tested could only explain 25% of the variation in P_N. The variables that significantly contributed to explaining this variability were Chl *c* and PC1 (**Table 2**). In SF, PC1 was negatively associated with MSL and positively with grain size, porosity, TN, OC, shore distance, and porewater nutrients (except PO_4^{3-}) (**Table 1**).

Environmental variables explained 41 and 25% of R_D in PR and SF, respectively (**Table 2**). In PR, PC3 and PC4 contributed significantly to explain variation in R_D. PC3 correlated with rainfall, DSi in the water column and NO_3^- and NH_4^+ in the

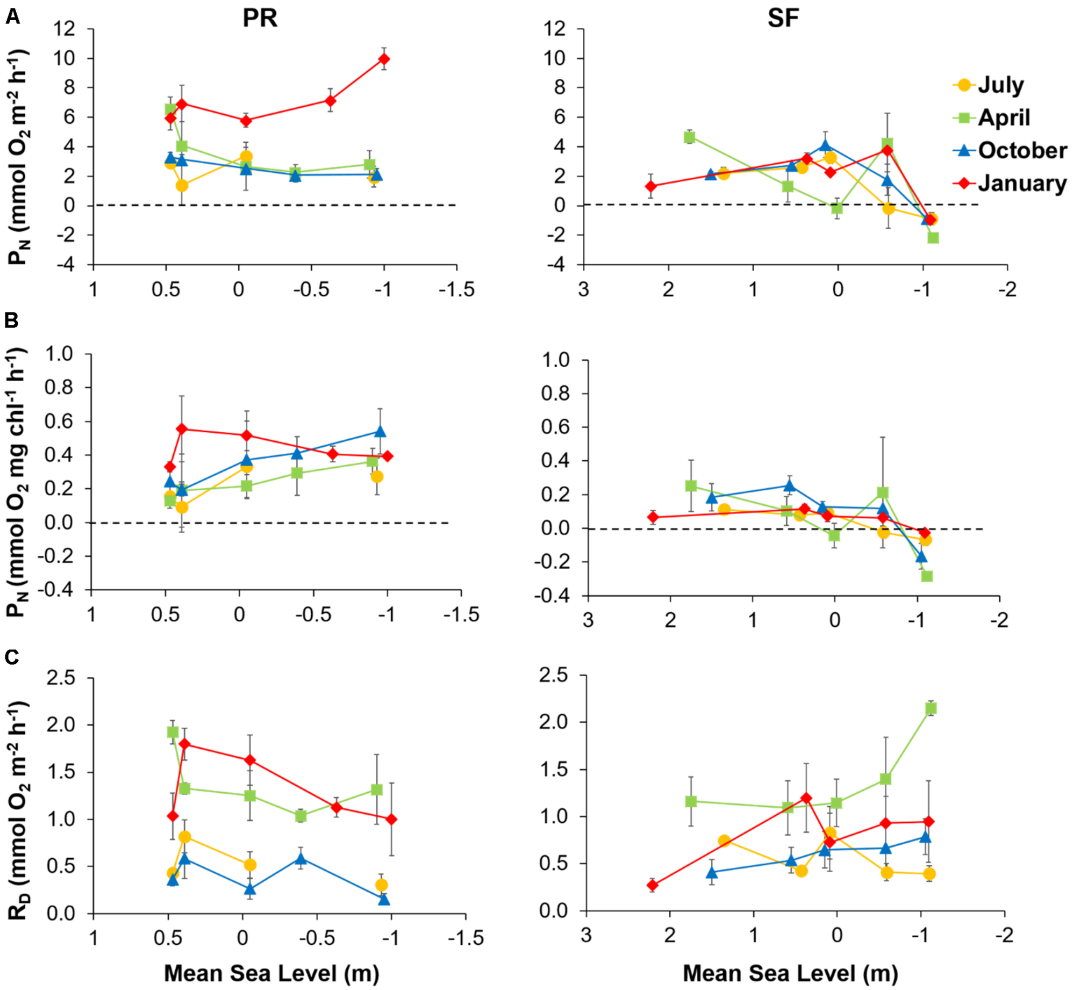

FIGURE 5 | (A) Net production in the photic layer (P_N), **(B)** respiration in darkness (R_D), and **(C)** P_N normalized by MPB biomass plotted against mean sea level (MSL) along the Puerto Real (PR) and San Fernando (SF) transects in July (yellow), April (green), October (blue), and January (red). Values represent means ± SE (n = 3).

porewater. PC4 was composed mostly by NO_3^- in the water column (**Table 1**). PC3 was the most influential variable of the two (**Table 2**). In SF, the variables selected were PC3 and PC1 (**Table 2**). In this case, PC3 was positively correlated with rainfall and negatively with wind speed (**Table 1**). PC1, as mentioned previously, was associated with MSL and grain size related variables (**Table 1**).

Annual Net Metabolism of the Microbenthic Intertidal Sediment

Daily microphytobenthic rates of P_N and R_D were integrated for every season for all seabed types. Microbenthic net metabolism was positive in all seasons except in April in *Z. noltei* sediments (**Figure 7**). The annual net metabolism of MPB (P_N - R_D) in bare muddy sediment (PR transect), in bare sandy sediment (SF1-2), and seagrass meadow sediment (SF3-4) was 73.3, 29.6, and 19.5 g C m^{-2}, respectively. Given that there was no indication of MPB being present in *C. prolifera* sediment, this habitat was not considered (SF5).

DISCUSSION

Biogeochemical Properties of Intertidal Sediments in Cadiz Bay

The inner Cadiz bay is a complex system, comprising of salt marshes, intertidal flats, seagrass meadows, and shallow subtidal areas. The two transects studied here showed clear differences in their elevation profiles, sediment granulometry, and vegetation cover, as a result of the hydrodynamic conditions and sediment morphodynamics in the bay (Kagan et al., 2003). The PR transect was more homogenous, dominated by fine sediment, without permanent vegetation, and a gentler slope across the gradient (**Figure 1**). Fine grain sediment, as that found in the PR transect, is the predominant sediment type within the bay (Sanchez De Lamadrid Rey and Muñoz Pérez, 1994; Carrasco et al., 2003). In contrast, the SF transect was more variable in terms of grain size distribution, showing also a steeper slope. In addition, the sediment in the SF transect was colonized by *Z. noltei* and *C. prolifera*, typical species of the vegetational zonation of

TABLE 1 | Correlation coefficients between environmental variables and significant components obtained by principal components analysis (wherein the selected components account for over 80% of environmental variability) for each of the two transects studied in Puerto Real (PR) and San Fernando (SF) seasonally during on year.

	PR							SF				
	PC1	**PC2**	**PC3**	**PC4**	**PC5**	**PC6**	**PC7**	**PC1**	**PC2**	**PC3**	**PC4**	**PC5**
Dist.	−0.341	**0.801**	0.089	−0.177	−0.224	0.152	0.320	**0.812**	−0.094	0.103	−0.089	−0.137
MSL	0.306	**−0.758**	−0.070	0.149	0.321	−0.254	−0.298	**−0.921**	0.025	−0.130	0.048	0.096
Grain size < 63 μm	0.021	**−0.740**	0.233	−0.228	−0.102	0.419	−0.211	**0.940**	−0.006	0.150	−0.074	0.026
Φ	−0.227	**0.584**	0.374	−0.322	0.204	0.021	0.025	**0.919**	0.032	0.153	−0.103	−0.038
Rain	−0.125	0.006	**0.786**	0.089	−0.163	−0.271	−0.258	−0.178	0.166	**0.756**	0.182	−0.433
Rad.	**0.813**	0.383	−0.177	−0.156	0.309	−0.041	−0.049	0.228	**0.749**	−0.594	−0.070	0.116
Temp.	**0.788**	0.376	0.150	−0.208	0.291	−0.097	−0.156	0.178	**0.903**	−0.163	−0.170	0.091
Wind	**0.485**	0.353	−0.477	0.448	−0.034	−0.298	0.074	0.157	0.563	**−0.697**	0.257	−0.199
Sal.	**0.723**	−0.044	0.269	−0.042	−0.157	0.004	−0.025	−0.184	**0.655**	0.497	−0.172	−0.102
WC.DSi	0.520	0.072	**0.588**	−0.004	0.384	−0.100	0.261	−0.202	**0.876**	0.164	−0.105	0.237
WC.PO4	**−0.627**	−0.358	0.386	0.202	0.201	−0.070	0.252	−0.394	0.424	0.412	**0.499**	0.051
WC.NO3	−0.205	0.459	−0.064	**0.543**	0.169	0.038	−0.431	0.055	−0.009	−0.167	**0.791**	−0.004
WC.NH4	**−0.659**	0.001	0.168	0.530	0.166	−0.116	0.107	0.133	−0.374	0.036	0.214	**0.836**
PW.DSi	0.499	−0.220	0.091	0.376	−0.223	−0.110	**0.522**	**0.585**	0.061	−0.076	0.556	−0.215
PW.PO4	0.401	0.151	−0.244	0.415	−0.085	**0.628**	−0.063	0.318	**0.473**	0.440	0.236	0.323
PW.NO3	−0.368	−0.020	**−0.504**	−0.180	0.488	−0.065	0.154	**0.675**	−0.065	−0.441	0.153	−0.142
PW.NH4	0.322	0.183	**0.567**	0.340	0.302	0.406	0.042	**0.633**	−0.036	0.243	0.397	0.082
OC	**−0.638**	0.109	−0.105	−0.030	0.457	0.207	−0.020	**0.923**	0.044	0.111	−0.205	0.079
TN	0.350	**−0.595**	−0.160	−0.054	0.266	0.184	0.354	**0.941**	0.042	0.172	−0.186	0.056

Nutrients in the porewater were log(x + 1) transformed. Values in bold correspond to the axis for which the squared cosine of the specific variable is the largest. Dist., shore distance; MSL, mean sea level; Rad., irradiance; Temp., temperature; Rain, rainfall; wind speed, Φ porosity; Sal., salinity, in water column (WC) and porewater (PW) nutrients (DSi, $NO_2^- + NO_3^-$, PO_4^{3-} and NH_4^+), OC organic carbon, and TN total nitrogen.

the inner Cadiz Bay benthic environment (**Figure 1**) (Gómez Ordoñez, 2008). These macrophytes can significantly contribute to the accumulation of finer grained sediment (Peralta et al., 2008; Greiner et al., 2016), which might explain the differences along the SF transect with increased fines content in the middle and lower intertidal.

Water column nutrients showed little differences between transects probably due to the relatively small distance between sampling points within the transect and the increased mixing in the water column due to tides and wind action (Kagan et al., 2003). Nonetheless, water column DSi and PO_4^{3-} tended to decrease seaward along the transects, indicating that the upper intertidal near the saltmarsh might act as a potential source of DSi and PO_4^{3-}, whereas concentrations of NO_3^- and NH_4^+ were rather constant. Interestingly, nutrient concentrations in the porewater followed an inverse trend to that observed in the water column, i.e., they tended to increase seaward. Nutrient concentrations in both the water column and the porewater were similar to those measured previously in the bay (Garcia-Robledo et al., 2016), with the exception of DSi. Concentrations of DSi in the porewater, particularly in SF, were up to 50 nmol cm^{-3}, double the maximum measured previously (Garcia-Robledo et al., 2016). Overall, higher nutrients concentrations in the porewater were measured in SF with a trend of increasing values seaward, in the presence of the seagrass *Z. noltei* at SF3 and SF4. This is not surprising since seagrass sediments are able to temporarily retain a high amount of nitrogen due to the trapping of particles from the water column, the biological immobilization of decomposing plant tissues via burial, and the stimulation of nitrogen fixation (Risgaard-Petersen et al., 1998; Barrón et al., 2006).

Stoichiometric ratios of inorganic nutrients (i.e., DSi:N and N:P) in the water column seem to indicate that MPB in Cadiz Bay could be strongly limited by P since the N:P ratio was generally higher than 22 (Hillebrand and Sommer, 1999). On the other hand, the DSi to N ratio was lower than 0.8 suggesting limitation by DSi, mainly in winter in both transects (Justiæ et al., 1995). In our study, we did not find any positive correlation between P_N or biomass and water column DSi, like the ones observed previously for MPB (Welker et al., 2002; Garcia-Robledo et al., 2016). In addition, a recent experimental study using sediment from the inner Bay of Cadiz has demonstrated that water column DSi concentration affects MPB primary production but not its biomass (Bohórquez et al., 2019). Although these data might suggest a DSi and P limitation which might affect the growth of diatoms (Cibic et al., 2007), previous published observations for sediments of the wider area (Garcia-Robledo et al., 2008, 2012; Haro et al., 2019) and preliminary data based on molecular analyses for intertidal sediments of the inner bay (J. Taylor pers comm) suggest that diatoms are ubiquitous and are the dominant microalgal group. Nevertheless, further analyses are required to quantify the contribution of the various algal groups to the MPB community composition along the intertidal area of Cádiz Bay and study the drivers behind possible community shifts in space and time.

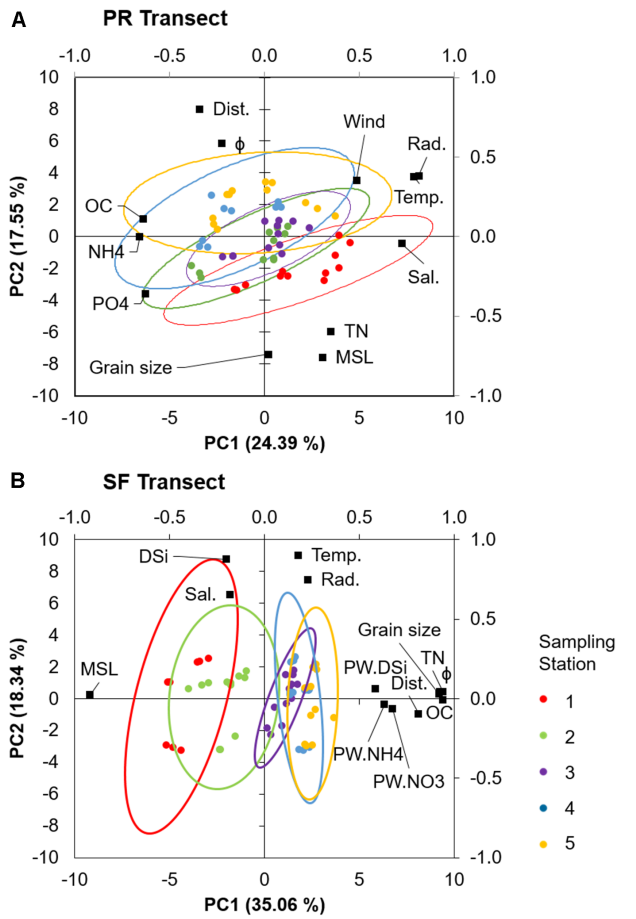

FIGURE 6 | Principal components analysis of environmental variables for the **(A)** Puerto Real (PR) and **(B)** San Fernando (SF) transects. Only variables for which the squared cosine is the largest in each axis are shown. Colored symbols represent the five stations sampled at each transect during the four sampling campaigns. The ellipses represent 95% confidence intervals for each station.

Sediment OC content variations were mainly related to sediment grain size, with limited variations over time. Thus, in PR, where the sediment was homogeneous and lacked areas with permanent macrophytes, no variations in OC were observed (**Figure 3A**) and values were similar to those measured previously in the inner bay (Papaspyrou et al., 2013; Jimenez-Arias et al., 2016). In SF, however, organic matter content changed drastically with grain size. OC values were ∼4 times higher in stations SF3–SF5, indicating a high input of OC to sediment, presumably from macrophyte detritus and exudates, as well as fine particles trapped within the meadows (Peralta et al., 2008; Greiner et al., 2016). This highlights the importance of macrophytes for the accumulation and burial of organic matter in vegetated areas, especially in the shallow inner Cadiz Bay (Jimenez-Arias et al., 2016).

Sediment OC to TN ratio, albeit slightly higher in PR, was similar in both transects, except in SF1 (**Figure 3C**). C:N ratios greater than 7.5 indicate sources of organic matter, other than microphytobenthic production (Hillebrand and Sommer, 1999) or high N mineralization rates (Sundbäck et al., 2004). The OC to TN ratios observed here were slightly higher than those found previously in muddy sediments close to the PR transect (∼10, Jimenez-Arias et al., 2016) and other intertidal flats (De Jonge, 1980; Oakes et al., 2010; Lee et al., 2018). On the other hand, a slight decrease in the OC to TN ratio at SF5 could be due to increased nitrogen fixation observed in *C. prolifera* beds (Chisholm and Moulin, 2003). At SF5, an increase in the OC to Chl *a* ratio (**Figure 4D**) was also observed suggesting an increase in fresh non-photosynthetic labile OC associated with particulate matter accumulated due to hydrodynamic effects within the canopy (Hendriks et al., 2010; Lara et al., 2016) or organic matter exudates by *C. prolifera* (Ruiz-Halpern et al., 2014).

Temporal and Spatial Patterns in the MPB Biomass

Microphytobenthos biomass patterns depend on the tight interaction between abiotic factors, such as light, nutrient availability, and resuspension, and biotic ones, such as grazing. Most studies on MPB have been conducted in intertidal areas of northern European estuaries and coastal settings with a humid continental climate (latitudes > 45°) (**Table 3**). In these regions, an annual maximum of biomass is found usually in summer, when higher temperatures and increased irradiance occur (Migné et al., 2004; Davoult et al., 2009; Van der Wal et al., 2010; Orvain et al., 2012), although in some cases different patterns have been found (Colijn and De Jonge, 1984; Underwood and Paterson, 1993; Thornton et al., 2002). In contrast, in southern European estuaries, with Mediterranean climate, the opposite temporal pattern is usually observed. In the Tagus estuary, for example, the MPB biomass was studied seasonally by remote sensing and was found to be maximum in winter (Brito et al., 2013), same as in Cadiz Bay (current study, Garcia-Robledo et al., 2016). Interestingly, studies worldwide in intertidal flats located at a similar latitude (i.e., around 35–38°) have found similar patterns with maxima in winter, e.g., the Ariake Sea in Japan (Koh et al., 2007), or the Saemangeum tidal flat in west Korea (Kwon et al., 2016) (**Table 3**).

Some discrepancies with respect to this general pattern have been reported for French estuaries. The calm conditions and the exposure to sunlight during low tide allow the development of higher MPB biomass in the intertidal zone in the Bay of Somme, the Mont Saint-Michael Bay or the Roscoff Aber Bay, at latitudes between 48 and 50° (Orvain et al., 2012), in the summer. In contrast, in the Brouage mudflat, at a lower latitude (45°), the highest biomass was reported between winter and early spring due to the grazing and thermo-inhibition in summer (Savelli et al., 2018) (**Table 3**). In our study, maximum Chl *a* values were found in winter. In addition to a possible thermo-inhibition, the lower MPB biomass in the summer could be a consequence of the combined effects of resuspension, turbidity, and grazing pressure. In Cadiz Bay, extreme wind events are especially frequent during summer and are known to increase sediment resuspension and turbidity, as well as produce sediment surface desiccation (**Supplementary Figure 1**) (Gutiérrez et al., 2000;

TABLE 2 | Multiple linear regression analysis of chlorophyll *a*, P_N in light, and R_D in darkness against the component variables obtained from the PCA analyses of the environmental variables for the Puerto Real (PR) and San Fernando (SF) transects.

	PR					SF				
Variables	**Value**	**Standard error**	***t***	**Pr > | *t*|**	**Adjusted R^2**	**Value**	**Standard error**	***t***	**Pr > | *t*|**	**Adjusted R^2**
Biomass										
Intercept	0.850	0.043	19.729	**<0.0001**	0.330	1.163	0.053	22.135	**<0.0001**	0.363
PC2	−0.121	0.024	−5.119	**<0.0001**		−0.079	0.028	−2.810	**0.007**	
PC5						0.241	0.047	5.103	**<0.0001**	
PC6	0.075	0.041	1.832	0.073						
P_N in light										
Intercept	0.044	0.535	0.081	0.935	0.608	0.568	0.492	1.154	0.254	0.251
Chl *a*	4.729	0.573	8.256	**<0.0001**						
Chl *c*						9.167	2.736	3.350	**0.001**	
PC1	−0.635	0.105	−6.059	**<0.0001**		−0.329	0.121	−2.716	**0.009**	
R_D in darkness										
Intercept	0.919	0.060	15.339	**<0.0001**	0.414	0.848	0.066	12.948	**<0.0001**	0.247
PC1						0.065	0.025	2.553	**0.014**	
PC3	−0.210	0.039	−5.417	**<0.0001**		−0.155	0.042	−3.724	**0.000**	
PC4	0.168	0.048	3.505	**0.001**						

In the case of P_N and R_D regressions, chl a and chl c were added as additional explanatory variables. Best model variable selection procedures were employed to identify the most parsimonious model that best explains the variations in the dependent variables. P values in bold indicate variables or principal components which significantly contributed to explain the patterns in MPB biomass, PN or RD according to the multiple linear regression analysis.

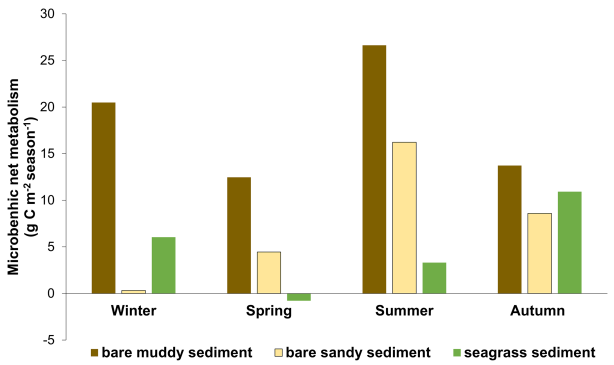

FIGURE 7 | Microbenthic net metabolism integrated for each season (90 days) (g C m^{-2}) in bare muddy sediment (brown), in bare sandy sediment (yellow), and seagrass meadow sediment (green). Daily P_N in light was corrected by a diel correction factor of 0.67 (Haro et al., 2019). Daily rates were corrected for temperature differences during the year using Q_{10}. Microbenthic net metabolism was calculated as the differences between daily rates of P_N and R_D. The annual net metabolism of MPB community in bare muddy sediment, bare sandy sediment, and seagrass meadow sediment were 73.3, 29.6, and 19.5 g C m^{-2} $year^{-1}$, respectively.

Kagan et al., 2003; Lara et al., 2018). In terms of grazing, higher rates have been reported for summer elsewhere, particularly during emersion (Cariou-Le Gall and Blanchard, 1995; Coelho et al., 2011). Available studies on the abundance of potential grazers in the inner Cadiz Bay (i.e., meiofauna) show variable results; higher meiofaunal abundance in the months of January and July in one case (Papaspyrou et al. unpubl. data) or in May in another (Bohórquez et al., 2013), therefore, the effect of grazing on the patterns observed in our transects cannot be evaluated at present.

Spatial patterns of MPB biomass studied here differed seasonally and between locations. At the muddy transect (PR), an increase seaward was observed during winter (i.e., the most productive period) whereas during the warmest months of the year values were more homogeneous or showed a slightly inverse trend. The seaward increase in winter seems to contrast with the spatial variations reported in other estuaries and tidal flats (Jesus et al., 2009; Van der Wal et al., 2010; Orvain et al., 2012; Brito et al., 2013; Kwon et al., 2016). These studies attributed the higher MPB biomass upper shore to the longer light exposure there and the decreased biomass lower shore to the light attenuation by the water column limiting MPB growth. However, although irradiance dosage is higher in the upper shore, the additional amount of light cannot be fully absorbed by the sediment due to a higher reflectance in emersion. This has been experimentally demonstrated for irradiances of up to 800 μmol photon m^{-2} s^{-1} in sandy (Kühl and Jorgensen, 1994; Haro et al., 2019), as well as muddy sediments (Balsam et al., 1998). Regardless, in Cadiz Bay and other intertidal systems located at lower latitudes, light limitation is generally lower in the lower shore because the incident solar irradiance is higher. Moreover, the lower intertidal experiences a shorter desiccation period which together with the higher solar irradiance could explain the higher biomass values found here. Nevertheless, long term studies integrating larger areas will be needed to determine whether the pattern observed here persists in time.

In the mixed sediment type transect (SF), maximum MPB biomass was found at the intermediate stations SF3 and SF4. The higher MPB biomass at these stations could be due to a positive interaction between MPB and seagrasses present at

TABLE 3 | Temporal and spatial variability of the MPB biomass (Chl-*a*), net production in light (PN), gross production (PG), and respiration in darkness (RD) in the intertidal areas of estuaries worldwide at latitudes from 53 to 33°N.

Variable	Estuary characteristics				Seasonal variability		Spatial variability		Temporal resolution		Spatial resolution	Analysis method	References
	Estuary	Country	Latitude	Substrate	Maximum	Minimum	Maximum	Minimum			Grid or Transect length (m) (Numbers of sampling stations)		
Biomass													
NDVI	Wadden Sea	Netherlands	53°20′N	Sandy	June	December	Upper	Lower	Monthly	2002–2008	250 × 250	RS	Van der Wal et al., 2010
NDVI	Ems-Dollard	Netherlands	53°25′N	Muddy-sandy	June	December	Upper	Lower	Monthly	2002–2008	250250	RS	Van der Wal et al., 2010
NDVI	Westerschelde	Netherlands	51°20′N	Sandy	May	December	Patch	Patch	Monthly	2002–2008	250 × 250	RS	Van der Wal et al., 2010
NDVI	Oosterschelde	Netherlands	51°35′N	Sandy	October	December	Patch	Patch	Monthly	2002–2008	250 × 250	RS	Van der Wal et al., 2010
NDVI	Thames	United Kingdom	51°35′N	Muddy-sandy	March–July	December	Upper	Lower	Monthly	2002–2008	250 × 250	RS	Van der Wal et al., 2010
NDVI	Wash	United Kingdom	52°55′N	Muddy-sandy	August	December	Upper	Lower	Monthly	2002–2008	250 × 250	RS	Van der Wal et al., 2010
NDVI	Humber	United Kingdom	53°35′N	Muddy-sandy	September	December	Upper	Lower	Monthly	2002–2008	250 × 250	RS	Van der Wal et al., 2010
NDVI	Brillantes_Loire	France	47°17′N	Muddy-sandy	–	–		–	Interannual	1991–2009	20 × 20	RS	Benyoucef et al., 2013
NDVI	Lavau_Loire	France	47°17′N	Mud	–	–		–	Interannual	1991–2009	20 × 20	RS	Benyoucef et al., 2013
NDVI	Brouage mudflat	France	45°54′N	Mud	March	May–August	–	–	February & July; April, July & November; February & April	2008; 2012; 2013	250 × 250	RS	Savelli et al., 2018
NDVI	Tagus, A Transect	Portugal	38°44′N	Muddy-sandy		–	Upper	Middle-lower	Bimonthly	2002–2004	270 (3)	NDVI	Jesus et al., 2009
NDVI	Tagus. V Transect	Portugal	38°44′N	Muddy-sandy	–	–	Middle-lower	Upper	Bimonthly	2002–2004	270 (3)	NDVI	Jesus et al., 2009
NDVI	Tagus	Portugal	38°44′N	Mud	December	May	Upper	Lower	December–April	2002–2003	20 × 20	RS	Brito et al., 2013
Chl-*a*	Colne	United Kingdom	51°50′N	Mud	Fall	Spring	Upper-middle	Lower	Monthly	1996–1998	10000 (4)	SC; Spec	Thornton et al., 2002
Chl-*a*	Bay of Somme, English Channel	France	50°13′N	Sandy	June	January	–	–	Quarterly	2000–2001	– (1)	SC; Spec	Migné et al., 2004

(Continued)

TABLE 3 | Continued

Variable	Estuary characteristics				Seasonal variability		Spatial variability		Temporal resolution		Spatial resolution	Analysis method	References
	Estuary	Country	Latitude	Substrate	Maximum	Minimum	Maximum	Minimum			Grid or Transect length (m) (Numbers of sampling stations)		
Chl-*a*	Baie des Veys, English Channel	France	49°22′N	Muddy-sandy	–	–	Upper	Lower	14-19 april; March	2003; 2004	500 × 500 (138)	SC; Spec	Orvain et al., 2012
Chl-*a*	Mont Saint-Michel Bay. Ca Transect	France	48°35′N	Mud	Depends on MSL	August	Middle	–	Quarterly	2003–2004	2000 (3)	SC; Spec	Davoult et al., 2009
Chl-*a*	Mont Saint-Michel Bay. Ch Transect	France	48°35′N	Sand	Depends on MSL	August	Upper	–	Quarterly	2003–2004	2500 (3)	SC; Spec	Davoult et al., 2009
Chl-*a*	Brouage mudflat	France	45°54′N	Mud	March	September	–	–	February & July; April, July & November; February & April	2008; 2012; 2013	250 × 250	SC; Spec	Savelli et al., 2018
Chl-*a*	Brouage mudflat in Marennes-Oleron Bay	France	45°50′N	Mud	May	December	–	–	November; May	2000; 2001	2600 (3)	SC; Spec	Orvain et al., 2007
Chl-*a*	Marennes-Oleron Bay	France	45°50′N	Mud	June	January	–	–	June–January	1995–1996	250 × 250	SC; Spec	Guarini et al., 1998
Chl-a	Livorno	Italy	43°47′N	Sandstone	September	March	–	–	March; September	2012; 2014	–	SC; Spec	Maggi et al., 2017
Chl-*a*	Tagus, A Transect	Portugal	38°44′N	Muddy-sandy	January–May	November	Upper	Middle-lower	Bimonthly	2002–2004	270 (3)	SC; Spec	Jesus et al., 2009
Chl-*a*	Tagus. V Transect	Portugal	38°44′N	Muddy-sandy	January–May	November & July	Middle-lower	Upper	Bimonthly	2002–2004	270 (3)	SC; Spec	Jesus et al., 2009
Chl-*a*	Tagus	Portugal	38°44′N	Mud	January	–	Upper	Lower	December–April	2002–2003	20 × 20	SC; Spec	Brito et al., 2013
Chl-*a*	Daebu mudflat	South Korea	37°12′N	Mud	March	January	–	–	Monthly	2008–2010	– (1)	SC; Spec	Kwon et al., 2018
Chl-*a*	Inner Cadiz Bay. PR Transect	Spain	36°30′N	Mud	January	July; October	Upper (except in January)	Lower (except in January)	Quarterly	2016–2017	420 (5)	SC; Spec	This study

(Continued)

TABLE 3 | Continued

Variable	Estuary characteristics				Seasonal variability		Spatial variability		Temporal resolution		Spatial resolution	Analysis method	References
	Estuary	Country	Latitude	Substrate	Maximum	Minimum	Maximum	Minimum			Grid or Transect length (m) (Numbers of sampling stations)		
Chl-*a*	Inner Cadiz Bay. SF Transect	Spain	36°28′N	Muddy-sandy	January	April; October	Middle	Upper	Quarterly	2016–2017	450 (5)	SC; Spec	This study
Chl-*a*	Inner Cadiz Bay	Spain	36°31′N	Mud	January	April	–	–	Monthly	2008	– (1)	SC; Spec	Garcia-Robledo et al., 2016
Chl-*a*	Gwanghwal_ Saemangeum	South Korea	35°30′N	Muddy-sand	Winter-Spring	Summer-Fall	Upper	Lower	Monthly	2004	30 × 30 (33)	RS; SC; Spec	Kwon et al., 2016
Chl-*a*	Gyehwa_ Saemangeum flat	South Korea	35°30′N	Muddy-sand	Winter-Spring	Fall	Upper-middle	Lower	Monthly	2004	30 × 30 (64)	RS; SC; Spec	Kwon et al., 2016
Chl-*a*	Isshiki flat, Mikawa Bay	Japan	34°46′N	Mud	Apri	October	–	–	Monthly	1997–1998	500 (5) and 290 (3)	SC; Spec	Goto et al., 2000
Chl-*a*	Nanaura mudflat, Ariake Sea	Japan	33°00′N	Mud	February	July	–	–	Every 2–3 weeks	2002–2003	– (1)	SC; Spec	Koh et al., 2007
Primary production													
P_G	Bay of Somme, English Channel	France	50°13′N	Sandy	June	February	–	–	Quarterly	2001–2002	–	BC	Migné et al., 2004
P_G	Roscoff Aber Bay	France	48°42′N	Muddy-coarse	August	February	Upper-middle	Lower	Monthly	2003–2004	2000 (3)	BC	Hubas et al., 2006
P_G	Mont Saint-Michal Bay. Ca Transect	France	48°35′N	Mud	August	February	Middle	Lower	Quarterly	2003–2004	2000 (3)	BC	Davoult et al., 2009
P_G	Mont Saint-Michel Bay. Ch Transect	France	48°35′N	Sand	April-August	February	Middle	Lower	Quarterly	2003–2004	2500 (3)	BC	Davoult et al., 2009
P_N	Brouage mudflat	France	45°54′N	Mud	Spring	Fall	–	–	February & July; April, July & November; February & April	2008; 2012; 2013	250 x 250	RS; model	Savelli et al., 2018

(Continued)

TABLE 3 | Continued

Variable	Estuarycharacteristics				Seasonal variability		Spatial variability		Temporal resolution		Spatial resolution	Analysis method	References
	Estuary	Country	Latitude	Substrate	Maximum	Minimum	Maximum	Minimum			Grid or Transect length (m) (Numbers of sampling stations)		
P_N	Daebu mudflat	South Korea	37°12′N	Mud	April	January	–	–	Monthly	2008–2010	– (1)	SC; OxM	Kwon et al., 2018
P_N	Inner Cadiz Bay	Spain	36°31′N	Mud	July	January	–	–	Monthly	2008	– (1)	SC; OxM	Garcia-Robledo et al., 2016
P_N	Inner Cadiz Bay. PR Transect	Spain	36°30′N	Mud	January	July; October	Upper (except in January)	Lower (except to January)	Quarterly	2016–2017	420 (5)	SC; OxM	This study
P_N	Inner Cadiz Bay. SF Transect	Spain	36°28′N	Muddy-sandy	January	April	Middle	Lower (Caulerpa prolifera)	Quarterly	2016–2017	450 (5)	SC; OxM	This study
P_G	Isshiki flat, Mikawa Bay	Japan	34°46′N	Mud	February–March	August	–	–	Monthly	1997–1998	500 (5) and 290 (3)	^{14} C	Goto et al., 2000
Respiration													
R_D	Roscoff Aber Bay	France	48°42′N	Muddy-coarse	July	February	Upper	Lower	Monthly	2003–2004	2000 (3)	BC	Hubas et al., 2006
R_D	Mont Saint-Michal Bay. Ca Transect	France	48°35′N	Mud	April	August	Lower	Upper	Quarterly	2003–2004	2000 (3)	BC	Davoult et al., 2009
R_D	Mont Saint-Michel Bay. Ch Transect	France	48°35′N	Sand	April	August	–	–	Quarterly	2003–2004	2500 (3)	BC	Davoult et al., 2009
R_D	Inner Cadiz Bay	Spain	36°31′N	Mud	April	January	–	–	Monthly	2008	– (1)	SC; OxM	Garcia-Robledo et al., 2016
R_D	Inner Cadiz Bay. PR Transect	Spain	36° 30′ N	Mud	April	October	Middle	Lower	Quarterly	2016–2017	420 (5)	SC; OxM	This study
R_D	Inner Cadiz Bay. SF Transect	Spain	36° 28′ N	Muddy-sandy	April	October; January	Lower	Upper	Quarterly	2016–2017	450 (5)	SC; OxM	This study

MSL, mean sea level; RS, remote sensing; Spec, Chl-a spectrophotometric analysis; SC, sediment cores; BC, benthic chamber; OxM, oxygen microelectrodes.

these stations due to the protection macrophytes provide to associated microalgal communities against resuspension (Lemley et al., 2017). In addition, the upper shore sediment at this transect was sandier and had a higher MSL (1.7 m), meaning longer emersion periods and faster draining (Dye, 1980). As a result, desiccation and temperature effects would be stronger in the upper shore. Various authors have reported higher MPB biomass in the middle-upper shore along the intertidal (**Table 3**) (Davoult et al., 2009; Benyoucef et al., 2013). Underwood (2001) suggested that the MPB distribution along the intertidal could show a peak somewhere between mid-tide and mean high water neap tide level (stations SF3 and SF4 in our transect), and not necessarily at the upper shore. This range of the intertidal offers optimum conditions for MPB growth; lower hydrodynamic conditions (i.e., lower resuspension compared with the lower shore) and reduced desiccation and irradiance effects, compared to the high shore. The mixed sediment type transect (SF) showed such a distribution, with MPB biomass even higher than PR in the intermediate stations. Overall, our data indicate that the spatial distribution of MPB along the intertidal is highly variable and site specific and that other methods such as remote sensing should be used to estimate spatial patterns in the bay due to the high spatial heterogeneity.

Sediment Primary Production and Respiration Along the Intertidal Gradient

Spatial and temporal patterns of P_N are not frequently studied. Instead, MPB biomass is used as a proxy for P_N given that the former can be estimated by a more direct and relatively fast technique (i.e., remote sensing). However, the conversion of MPB biomass to primary production values is not straightforward (Daggers et al., 2018; Méléder et al., 2018; Savelli et al., 2018), so direct measurements with oxygen microelectrodes or ^{14}C are essential (Brotas et al., 2003; Garcia-Robledo et al., 2016; Walpersdorf et al., 2017). In Cadiz Bay, P_N rates determined using microelectrodes were always positive in the PR transect and in the majority of the cases at the first four stations of the SF transect indicating an autotrophic community. However, at SF5, where *C. prolifera* meadows are present, sediment metabolism was net heterotrophic all year round. In the PR transect, P_N rates were surprisingly rather homogeneous during most of the year, with the exception of January, when they were three times higher and slightly increased downshore. In the SF transect, P_N rates exhibited a similar pattern for the above zero MSL stations of a slight increase toward the mid intertidal (with the exception of April when surprisingly the opposite was observed) coinciding with muddier sediments in the middle of the intertidal.

At the SF transect, the variables selected during the statistical analysis could explain only 25% of the variability in P_N. This is probably due to the larger variability and non-linear patterns in terms of gradient slope, vegetation type, and grain size distribution—and correlated variables, such as OC and porewater nutrient content—in SF compared to PR. The variables that explained better the pattern of P_N in SF were Chl *c* and PC1. The latter was composed principally by geo-morphological variables (MSL, shore distance, grain size, and porosity), OC, and porewater nutrients (**Tables 1**, **2**), highlighting the importance of the spatial variability along the SF transect (**Figure 6**). At this location, grain size distribution was negatively correlated to MSL (r = -0.838) and therefore it is difficult to discern between the two predictors. However, Orvain et al. (2012) reported that, in the macro-intertidal des Veys Bay (France), MPB biomass variability was mainly explained by grain size, whereas MSL only explained 2–3%. Likewise, Daggers et al. (2018) considered grain size distribution as one of the most important variables to predict P_N in the tidal environments of Oosterschelde and Westerschelde (Netherlands). In contrast, Hubas et al. (2006) determined that neither porewater nutrients, which in SF contributed to explain P_N, nor grain size controlled MPB net metabolism along a granulometric gradient in an intertidal area in the Roscoff Aber Bay (France). Instead, Hubas et al. (2006) determined that net metabolism of MPB was mainly controlled by temperature. However, in our case, when P_N were corrected for Q_{10} (**Supplementary Figure 2**), no differences were found in the spatio-temporal patterns. Lastly, the inclusion of Chl *c*, a characteristic pigment of benthic diatoms, among the variables best explaining MPB P_N corroborates that measured P_N rates with the microelectrodes were not affected by macrophytes but were a direct result of the MPB community production (mainly diatoms).

In PR, in contrast to SF, the selected model could explain a high percentage of P_N variability (60%). Sediment-related variables (e.g., grain size, porewater nutrients, organic matter) were more homogenous both in time and space and thus were not expected to contribute significantly in explaining the differences observed in metabolic rates. Indeed, the PC that explain the patterns in P_N was composed of meteorological variables (irradiance and temperature), OC, and water column nutrients (**Tables 1**, **2**). This highlights the strong effect seasonal acclimation of the MPB community has in these muddy sediments, and this despite the fact that the experimental conditions we used were the same year-round (saturating irradiance and constant temperature). Of course, other biotic, i.e., grazing, or physical factors, i.e., current speed, that were not studied in this work have also been proposed to explain P_N variability (Hubas et al., 2006; Van der Wal et al., 2008; Savelli et al., 2018). Their importance remains to be tested for the Cadiz Bay and could contribute to better explaining the spatial variability of P_N with respect to MSL.

Diel and seasonal variability also exists for R_D (Davoult et al., 2009) although this tends to be less pronounced than the one for P_N. R_D rates usually remain constant throughout the dark period for several days in laboratory experiments (Haro et al., 2019). In addition, preliminary experiments in microcosms with Cadiz Bay sediment found no substantial differences between R_D in emersion and immersion. However, *in situ* daily variations due to changes in tidal conditions have been reported elsewhere (Migné et al., 2009). Seasonality of R_D rates is mainly controlled by (1) temperature (Migné et al., 2004) and (2) variations in the activity of heterotrophic bacteria (which might explain up to 88% of sediment respiration, Hubas et al., 2006), with highest rates being expected in summer. Surprisingly, in Cadiz Bay, the highest rates were found in January in PR and April in SF (**Figure 5C**).

However, when correcting R_D rates for the temperature *in situ* (**Supplementary Figure 2**) (Hancke and Glud, 2004; Migné et al., 2004; Kwon et al., 2018), in both transects highest R_D rates were still found in spring, not in summer. On the one hand, this is probably due to a higher availability of labile OC in spring after the MPB and macroalgal blooms and on the other, to the high sediment temperatures in summer which can reach well above 30°C (Guarini et al., 1997), affecting negatively the resident microbial community which tends to show an optimum between 25–30°C (Thamdrup et al., 1998).

Regression analysis indicated that the variables that best explained R_D rates in the PR transect (41%) included the PC axes composed of principally of nutrients in the water column and the sediment. In contrast, in SF, the variables selected were the PC axes that were composed mainly of MSL, grain size gradient, OC, and porewater nutrient content, as well as some meteorological aspects (wind and rain), all of which explained 25% of the variation in R_D rates. The cause–effect relationship between R_D rates and the selected variables is not always clear and should be treated with caution. For example, OC carbon content was highly related to both grain size and MSL in SF; clearly, it is the higher OC availability in the sediment that can stimulate higher R_D rates. On the other hand, R_D rates did not reflect the significant differences observed in the OC content between the stations along the transect which was four to five times lower in the sandy compared to the muddy stations (**Figure 3A**). In the case of the nutrient concentrations, either in the water column or the porewater, the relationship can be bidirectional; higher R_D rates would result in increased mineralization rates and higher nutrient release to the sediment and porewater, while at the same time, higher nutrient concentrations can stimulate the growth of microorganisms, especially ones using anaerobic mineralization pathways, and thus the overall sediment metabolism (Canfield et al., 2005).

Contribution of PP_{MPB} to Total Benthic Production in Cadiz Bay Intertidal Sediments

The intertidal sediment in the inner Cadiz Bay is principally muddy with only 10% sandy areas (Sanchez De Lamadrid Rey and Muñoz Pérez, 1994). The annual rate of P_N in light for bare intertidal muddy sediment in the inner Cadiz bay was 105.8 g C m^{-2} $year^{-1}$, which is similar to that calculated for other estuaries with muddy sediment in southern Europe, e.g., 156 g C m^{-2} $year^{-1}$ for the Tagus Estuary in Portugal (Serôdio and Catarino, 2000) and 127 g C m^{-2} $year^{-1}$ for the Brouage mudflat in France (Savelli et al., 2018). The annual net metabolism for bare intertidal muddy sediment in inner Cadiz Bay was net autotrophic (73.3 g C m^{-2} $year^{-1}$). This was higher than that measured in other temperate estuaries; 25 g C m^{-2} $year^{-1}$ in the Seine Estuary (Migné et al., 2004), or even negative, −41 g C m^{-2} $year^{-1}$ in the Bay of Somme and −78 g C m^{-2} $year^{-1}$ in Mont Saint-Michel Bay, both on the English Channel in France (Spilmont et al., 2006; Migné et al., 2009). These mudflats exhibited annual R_D rates higher than the 32.5 g C m^{-2} $year^{-1}$ measured in our study. In bare sandy sediments in the inner Cadiz Bay, the annual net metabolism was lower, 29.6 g C m^{-2} $year^{-1}$. In the Roscoff Aber Bay, in France, an autotrophic annual metabolism of up to 16 g C m^{-2} $year^{-1}$ at the sandy sediments was reported by Hubas and Davoult (2006).

The intertidal area of the inner Cadiz Bay covers ∼60% of its surface (13 km^2, Sanchez De Lamadrid Rey and Muñoz Pérez, 1994). Of that, approximately 70% is covered by the seagrass *Z. noltei* and the remaining is bare sediment covered by MPB and occasionally green macroalgae (Gómez Ordoñez, 2008). According to the extracted values from grain size distribution maps (Sanchez De Lamadrid Rey and Muñoz Pérez, 1994), approximately 90% of the bare sediment in the inner Cadiz Bay is muddy. When the differences in vegetation and sediment type cover are taken into account, the annual net metabolism of MPB for bare sediment is 285.9 t C $year^{-1}$ (257.3 and 10.4 t C $year^{-1}$ for muddy and sandy sediments, respectively), whereas for the sandy-muddy sediment covered by *Z. noltei,* the contribution of MPB, based on the data from sampling stations SF3 and SF4 in SF, is 177.2 t C $year^{-1}$. Thus, the total annual metabolism attributed to intertidal MPB is 444.9 t C $year^{-1}$.

In order to calculate the MPB contribution to the total benthic production in intertidal sediments in the inner Cadiz Bay, we estimated the production of *Z. noltei*. Previous studies in the area have estimated the total annual production of *Z. noltei* in the Los Toruños area of Cadiz Bay to be 51 g C m^{-2} $year^{-1}$ (Brun et al., 2003), corresponding to an annual production for the entire bay of 464.1 t C $year^{-1}$. Therefore, 48.9% of the total intertidal benthic primary production would correspond to MPB. Similarly, Asmus and Asmus (2000) estimated that MPB production contributes up to 54% of the total primary production on an intertidal *Zostera* bed in the Wadden Sea, 347 g C m^{-2} $year^{-1}$ MPB production vs. 258 g C m^{-2} $year^{-1}$ for *Zostera*. Therefore, our data confirm the important contribution of MPB to the total primary production in coastal shallow systems (Underwood and Kromkamp, 1999) even in the presence of important primary producers such as seagrass meadows.

CONCLUSION

Our results suggest that the seasonal and spatial variability of MPB biomass and MPB P_N in different locations within the same system can be affected by different sets of environmental factors. This variability makes producing good PP predictive models with general applicability to different environments very difficult. Nonetheless, from system intercomparison, it seems that seasonal and spatial patterns of MPB P_N along the intertidal seem to depend on latitudinal conditions of daylight irradiance and temperature and on substrate type, the latter being strongly related with the hydrodynamic conditions in the zone in question. Clearly, more work, combining laboratory experiments and field studies, is needed to disentangle the relationships between MPB biomass and net metabolism and the rather high number of environmental variables that have been used to explain the standing stock of MPB and its biological activity in the intertidal zone. Most of these variables change at different spatio-temporal scales, complicating further the investigation on their role on MPB patterns. New techniques, such as the aquatic eddy correlation technique or *in situ* continuous oxygen profiling,

will allow exploring long-term changes of PP_{MPB} *in situ* with non-destructive techniques. This, in addition to the progress in remote sensing with the increasing availability of satellite images of increased quality and resolution, will aid in estimating with higher precision PP_{MPB} and its contribution to estuarine primary production.

DATA AVAILABILITY STATEMENT

The datasets are available on request. The raw data supporting the conclusions of this article will be made available by the authors, without undue reservation, to any qualified researcher.

AUTHOR CONTRIBUTIONS

All authors were involved in the study design. ML, IL, and CG selected the sampling stations. SH, ML, and AC carried out the samplings. SH and ML conducted the measurements. SH, ML, and SP participated in the statistical analysis of the data. All authors contributed to data interpretation. SH, ML, AC, and SP wrote the manuscript. All authors contributed to the manuscript revision and approved the final submitted version.

FUNDING

This study was supported by the Spanish Ministry of Economy and Business (MINECO) through the projects MICROBAHIA and MICROBAHIA2 (CTM2013-43857-R and CTM2017-82274-R) awarded to AC. SH was funded by a Ph.D. fellowship from the University of Cádiz, Spain.

SUPPLEMENTARY MATERIAL

The Supplementary Material for this article can be found online at: https://www.frontiersin.org/articles/10.3389/fmars.2020.00039/full#supplementary-material

REFERENCES

Asmus, H., and Asmus, R. (2000). Material exchange and food web of seagrass beds in the Sylt-Rømø Bight: how significant are community changes at the ecosystem level? *Helgol. Mar. Res.* 54, 137–150. doi: 10.1007/s101520050012

Balsam, W. L., Deaton, B. C., and Damuth, J. E. (1998). The effects of water content on diffuse reflectance spectrophotometry studies of deep-sea sediment cores. *Mar. Geol.* 149, 177–189. doi: 10.1016/s0025-3227(98)00033-4

Barranguet, C., Kromkamp, J., and Peene, J. (1998). Factors controlling primary production and photosynthetic characteristics of intertidal microphytobenthos. *Mar. Ecol. Prog. Ser.* 173, 117–126. doi: 10.3354/meps173117

Barrón, C., Middelburg, J. J., and Duarte, C. M. (2006). Phytoplankton trapped within seagrass (*Posidonia oceanica*) sediments are a nitrogen source: an in situ isotope labeling experiment. *Limnol. Oceanogr.* 51, 1648–1653. doi: 10.4319/lo.2006.51.4.1648

Benyoucef, I., Blandin, E., Lerouxel, A., Jesus, B., Rosa, P., Méléder, V., et al. (2013). Microphytobenthos interannual variations in a North-European estuary (Loire estuary, France) detected by visible-infrared multispectral remote sensing. *Estuar. Coast. Shelf Sci.* 136, 43–52. doi: 10.1016/j.ecss.2013.11.007

Bohórquez, J., Calenti, D., Garcia-Robledo, E., Papaspyrou, S., Jimenez-Arias, J. L., Gómez-Ramírez, E. H., et al. (2019). Water column dissolved silica concentration limits microphytobenthic primary production in intertidal sediments. *J. Phycol.* 55, 625–636. doi: 10.1111/jpy.12838

Bohórquez, J., Papaspyrou, S., Yúfera, M., Van Bergeijk, S. A., Garcia-Robledo, E., Jimenez-Arias, J. L., et al. (2013). Effects of green macroalgal blooms on the meiofauna community structure in the Bay of Cadiz. *Mar. Pollut. Bull.* 70, 10–17. doi: 10.1016/j.marpolbul.2013.02.002

Brito, A., Benyoucef, I., Jesus, B., Brotas, V., Gernez, P., Mendes, C. R., et al. (2013). Seasonality of microphytobenthos revealed by remote-sensing in a South European estuary. *Cont. Shelf Res.* 66, 83–91. doi: 10.1016/j.csr.2013.07.004

Brotas, V., Serôdio, J., Risgaard-Petersen, N., Dalsgaard, T., Serôdio, J., Ottosen, L., et al. (2003). In situ measurements of photosynthetic activity and respiration of intertidal benthic microalgal communities undergoing vertical migration. *Ophelia* 57, 13–26. doi: 10.1080/00785236.2003.10409502

Brun, F. G., Pérez-Lloréns, J. L., Hernández, I., and Vergara, J. J. (2003). Patch Distribution and Within-Patch Dynamics of the Seagrass Zostera noltii Hornem. in Los Toruños Salt-Marsh. Cadiz Bay, Natural Park, *Spain. Bot. Mar.* 46, 513–524. doi: 10.1515/BOT.2003.053

Brun, F. G., Vergara, J. J., and Morris, E. P. (2015). Diversidad de angiospermas marinas en la bahía de Cádiz: redescubriendo a Zostera marina. *Chron. Naturae* 5, 45–56.

Buchanan, J. B. (1984). "Sediment analysis," in *Methods for the Study of Marine Benthos*, eds N. A. Holme, and A. D. McIntyre, (London: Blackwell Scientific Publications), 41–64.

Canfield, D. E., Thamdrup, B., and Kristensen, E. (2005). "Aquatic Geomicrobiology," in *Advances in Marine Biology*. Cambridge, MA: Elsevier Academic Press.

Cariou-Le Gall, V., and Blanchard, G. F. (1995). Concentration from an intertidal muddy sediment. *Mar. Ecol. Prog. Ser.* 121, 171–179. doi: 10.3354/meps121171

Carrasco, M., López-Ramírez, J. A., Benavente, J., López-Aguayo, F., and Sales, D. (2003). Assessment of urban and industrial contamination levels in the bay of Cadiz. *SW Spain. Mar. Pollut. Bull.* 46, 335–345. doi: 10.1016/S0025-326X(02)00420-4

Chisholm, J. R. M., and Moulin, P. (2003). Stimulation of nitrogen fixation in refractory organic sediments by *Caulerpa taxifolia* (Chlorophyta). *Limnol. Oceanogr.* 48, 787–794. doi: 10.4319/lo.2003.48.2.0787

Cho, K. H., Kang, J.-H., Ki, S. J., Park, Y., Cha, S. M., and Kim, J. H. (2009). Determination of the optimal parameters in regression models for the prediction of chlorophyll-a: A case study of the Yeongsan Reservoir. *Korea. Sci. Total Environ.* 407, 2536–2545. doi: 10.1016/j.scitotenv.2009.01.017

Cibic, T., Blasutto, O., Falconi, C., and Fonda Umani, S. (2007). Microphytobenthic biomass, species composition and nutrient availability in sublittoral sediments of the Gulf of Trieste (northern Adriatic Sea). *Estuar. Coast. Shelf Sci.* 75, 50–62. doi: 10.1016/j.ecss.2007.01.020

Coelho, H., Cartaxana, P., Brotas, V., Queiroga, H., and Serôdio, J. (2011). Pheophorbide *a* in Hydrobia ulvae faecal pellets as a measure of microphytobenthos ingestion: variation over season and period of day. *Aquat. Biol.* 13, 119–126. doi: 10.3354/ab00356

Coelho, H., Vieira, S., and Serôdio, J. (2009). Effects of desiccation on the photosynthetic activity of intertidal microphytobenthos biofilms as studied by optical methods. *J. Exp. Mar. Bio. Ecol.* 381, 98–104. doi: 10.1016/j.jembe.2009.09.013

Colijn, F., and De Jonge, V. N. (1984). Primary production of microphytobenthos in the Ems-Dollard Estuary. *Mar. Ecol. Prog. Ser.* 14, 185–196. doi: 10.3354/meps014185

Daggers, T. D., Kromkamp, J., Herman, P. M. J., and van der Wal, D. (2018). A model to assess microphytobenthic primary production in tidal systems using satellite remote sensing. *Remote Sens. Environ.* 211, 129–145. doi: 10.1016/j.rse.2018.03.037

Davoult, D., Migné, A., Créach, A., Gévaert, F., Hubas, C., Spilmont, N., et al. (2009). Spatio-temporal variability of intertidal benthic primary production and respiration in the western part of the Mont Saint-Michel Bay (Western English

Channel. *France). Hydrobiologia* 620, 163–172. doi: 10.1007/s10750-008-9626-3

De Jonge, V. N. (1980). Fluctuations in the organic carbon to chlorophyll a ratios for estuarine benthic diatom populations. *Mar. Ecol. Prog. Ser.* 2, 345–353. doi: 10.3354/meps002345

Dye, A. H. (1980). Tidal fluctuations in biological oxygen demand in exposed sandy beaches. *Estuar. Coast. Mar. Sci.* 11, 1–8. doi: 10.1016/S0302-3524(80)80024-7

Garcia-Robledo, E., Bohórquez, J., Corzo, A., Jimenez-Arias, J. L., and Papaspyrou, S. (2016). Dynamics of inorganic nutrients in intertidal sediments: porewater, exchangeable, and intracellular pools. *Front. Microbiol.* 7:761. doi: 10.3389/fmicb.2016.00761

Garcia-Robledo, E., Corzo, A., García De Lomas, J., and van Bergeijk, S. A. (2008). Biogeochemical effects of macroalgal decomposition on intertidal microbenthos: a microcosm experiment. *Mar. Ecol. Prog. Ser.* 356, 139–151. doi: 10.3354/meps07287

Garcia-Robledo, E., Corzo, A., and Papaspyrou, S. (2014). A fast and direct spectrophotometric method for the sequential determination of nitrate and nitrite at low concentrations in small volumes. *Mar. Chem.* 162, 30–36. doi: 10.1016/j.marchem.2014.03.002

Garcia-Robledo, E., Corzo, A., Papaspyrou, S., and Morris, E. P. (2012). Photosynthetic activity and community shifts of microphytobenthos covered by green macroalgae. *Environ. Microbiol. Rep.* 4, 316–325. doi: 10.1111/j.1758-2229.2012.00335.x

Gómez Ordoñez, E. (2008). *Propiedades Ópticas y Teledetección de Macrófitos Marinos en la bahía de Cádiz, España*. Cadiz: UniversidaddeCádiz, 23.

Goto, N., Mitamura, O., and Terai, H. (2000). Seasonal variation in primary production of microphytobenthos at the Isshiki intertidal flat in Mikawa Bay. *Limnology* 1, 133–138. doi: 10.1007/s102010070019

Grant, J. (1986). Sensitivity of benthic community respiration and primary production to changes in temperature and light. *Mar. Biol.* 90, 299–306. doi: 10.1007/bf00569142

Grasshoff, K., Koroleff, K., and Ehrhardt, M. (1999). *Methods of Seawater Analysis*. Hoboken, NJ: Wiley Online Library.

Greiner, J. T., Wilkinson, G. M., McGlathery, K. J., and Emery, K. A. (2016). Sources of sediment carbon sequestered in restored seagrass meadows. *Mar. Ecol. Prog. Ser.* 551, 95–105. doi: 10.3354/meps11722

Guarini, J.-M., Blanchard, G. F., Bacher, C., Gros, P., Riera, P., Richard, P., et al. (1998). Dynamics of spatial patterns of microphytobenthic biomass: inferences from a geostatistical analysis of two comprehensive surveys in Marennes-Oléron Bay (France). *Mar. Ecol. Prog. Ser.* 166, 131–141. doi: 10.3354/meps166131

Guarini, J.-M., Blanchard, G. F., Gros, P., and Harrison, S. J. (1997). Modelling the mud surface temperature on intertidal flats to investigate the spatio-temporal dynamics of the benthic microalgal photosynthetic capacity. *Mar. Ecol. Prog. Ser.* 153, 25–36. doi: 10.3354/meps153025

Gutiérrez, J. M., Luna del Barco, A., Parrado, J. M., Sánchez, E., Fernández-Palacios, A., and Ojeda, J. (2000). Variaciones de turbidez de las aguas de la bahía de Cádiz determinadas a partir del análisis de imágenes Landsat TM. *Geogaceta* 27, 79–82.

Hancke, K., and Glud, R. N. (2004). Temperature effects on respiration and photosynthesis in three diatom-dominated benthic communities. *Aquat. Microb. Ecol.* 37, 265–281. doi: 10.3354/ame037265

Haro, S., Bohórquez, J., Lara, M., Garcia-Robledo, E., González, C. J., Crespo, J. M., et al. (2019). Diel patterns of microphytobenthic primary production in intertidal sediments: the role of photoperiod on the vertical migration circadian rhythm. *Sci. Rep.* 9, 13376. doi: 10.1038/s41598-019-49971-8

Hedges, J. I., Baldock, J. A., Gélinas, Y., Lee, C., Peterson, M. L., and Wakeham, S. G. (2002). The biochemical and elemental compositions of marine plankton: a NMR perspective. *Mar. Chem.* 78, 47–63. doi: 10.1016/S0304-4203(02)00009-9

Heiri, O., Lotter, A. F., and Lemcke, G. (2001). Loss on ignition as a method for estimating organic and carbonate content in sediments: reproducibility and comparability of results. *J. Paleolimnol.* 25, 101–110.

Hendriks, I. E., Bouma, T. J., Morris, E. P., and Duarte, C. M. (2010). Effects of seagrasses and algae of the Caulerpa family on hydrodynamics and particle-trapping rates. *Mar. Biol.* 157, 473–481. doi: 10.1007/s00227-009-1333-8

Hijmans, R. J., Williams, E., and Vennes, C. (2017). *Package "Geosphere" Spherical Trigonometry for Geographic Applications. Version 1.5-10* Available at: https://cran.r-project.org/web/packages/geosphere/geosphere.pdf (accessed May 26, 2019).

Hillebrand, H., and Sommer, U. (1999). The nutrient stoichiometry of benthic microalgal growth: Redfield proportions are optimal. *Limnol. Oceanogr.* 44, 440–446. doi: 10.4319/lo.1999.44.2.0440

Hubas, C., and Davoult, D. (2006). Does seasonal proliferation of Enteromorpha sp. affect the annual benthic metabolism of a small macrotidal estuary? (Roscoff Aber Bay, France). *Estuar. Coast. Shelf Sci* 70, 287–296. doi: 10.1016/j.ecss.2006.06.019

Hubas, C., Davoult, D., Cariou, T., and Artigas, L. (2006). Factors controlling benthic metabolism during low tide along a granulometric gradient in an intertidal bay (Roscoff Aber Bay, France). *Mar. Ecol. Prog. Ser.* 316, 53–68. doi: 10.3354/meps316053

Jackson, D. A. (1993). Stopping rules in principal components analysis: a comparison of heuristical and statistical approaches. *Ecology* 74, 2204–2214. doi: 10.2307/1939574

Jesus, B., Brotas, V., Marani, M., and Paterson, D. M. (2005). Spatial dynamics of microphytobenthos determined by PAM fluorescence. *Estuar. Coast. Shelf Sci.* 65, 30–42. doi: 10.1016/j.ecss.2005.05.005

Jesus, B., Brotas, V., Ribeiro, L., Mendes, C. R., Cartaxana, P., and Paterson, D. M. (2009). Adaptations of microphytobenthos assemblages to sediment type and tidal position. *Cont. Shelf Res.* 29, 1624–1634. doi: 10.1016/j.csr.2009.05.006

Jimenez-Arias, J. L., Mata, M. P., Corzo, A., Poulton, S. W., März, C., Sánchez-Bellón, A., et al. (2016). A multiproxy study distinguishes environmental change from diagenetic alteration in the recent sedimentary record of the inner Cadiz Bay (SW Spain). *Holocene* 26, 1355–1370. doi: 10.1177/0959683616640046

Justić, D., Rabalais, N. N., Turner, R. E., and Dortch, Q. (1995). Changes in nutrient structure of river-dominated coastal waters: stoichiometric nutrient balance and its consequences. *Estuar. Coast. Shelf Sci.* 40, 339–356. doi: 10.1016/S0272-7714(05)80014-9

Kagan, B. A., Álvarez, O., Izquierdo, A., Mañanes, R., Tejedor, B., and Tejedor, L. (2003). Weak wind-wave/tide interaction over a moveable bottom: results of numerical experiments in Cadiz Bay. *Cont. Shelf Res.* 23, 435–456. doi: 10.1016/S0278-4343(02)00223-6

Koh, C. H., Khim, J. S., Araki, H., Yamanishi, H., and Kenichi, K. (2007). Within-day and seasonal patterns of microphytobenthos biomass determined by co-measurement of sediment and water column chlorophylls in the intertidal mudflat of Nanaura. *Estuar. Coast. Shelf Sci.* 72, 42–52. doi: 10.1016/j.ecss.2006.10.005

Kühl, M., Glud, R. N., Ploug, H., and Ramsing, N. B. (1996). Microenvironmental control of photosynthesis and photosynthesis-coupled respiration in an epilithic cyanobacterial biofilm. *J. Phycol.* 32, 799–812. doi: 10.1111/j.0022-3646.1996.00799.x

Kühl, M., and Jorgensen, B. B. (1994). The light field of microbenthic communities: radiance distribution and microscale optics of sandy coastal sediments. *Limnol. Oceanogr.* 39, 1368–1398. doi: 10.4319/lo.1994.39.6.1368

Kwon, B.-O., Kim, H. C., Koh, C. H., Ryu, J., Son, S. H., Kim, Y. H., et al. (2018). Development of temperature-based algorithms for the estimation of microphytobenthic primary production in a tidal flat: a case study in Daebu mudflat. *Korea. Environ. Pollut.* 241, 115–123. doi: 10.1016/j.envpol.2018.05.032

Kwon, B.-O., Lee, Y., Park, J., Ryu, J., Hong, S., Son, S. H., et al. (2016). Temporal dynamics and spatial heterogeneity of microalgal biomass in recently reclaimed intertidal flats of the Saemangeum area. *Korea. J. Sea Res.* 116, 1–11. doi: 10.1016/j.seares.2016.08.002

Lara, M., Bohórquez, J., Jimenez-Arias, J. L., Crespo, J. M., Haro, S., Papaspyrou, S., et al. (2018). Microscale drivers of oxygen dynamics during emersion: Microphytobenthic production, sediment compaction and shifts on diffusivity. *Eur. Geosci. Union Gen. Assem. Geophys. Res. Abstr. Vol.* 20, EGU2018–EGU19488.

Lara, M., Bouma, T. J., Peralta, G., Van Soelen, J., and Pérez-Lloréns, J. L. (2016). Hydrodynamic effects of macrophyte microtopography: Spatial consequences of interspecific benthic transitions. *Mar. Ecol. Prog. Ser.* 561, 123–136. doi: 10.3354/meps11913

Laviale, M., Barnett, A., Ezequiel, J., Lepetit, B., Frankenbach, S., Méléder, V., et al. (2015). Response of intertidal benthic microalgal biofilms to a coupled light-temperature stress: evidence for latitudinal adaptation along the Atlantic coast

of Southern Europe. *Environ. Microbiol.* 17, 3662–3677. doi: 10.1111/1462-2920.12728

Lee, J.-H., Jeong, K.-S., Lee, D.-H., Park, K. S., and Woo, H. J. (2018). Elemental (C/N Ratios) isotope compositions (δ 13 C TOC and δ 15 N TN) of Surface Sediments from the Barrier Islands in the Nakdong River Estuary. *South Korea. J. Coast. Res.* 85, 36–40. doi: 10.2112/si85-008.1

Lee, Y., Ha, S.-Y., Park, H.-K., Han, M.-S., and Shin, K.-H. (2015). Identification of key factors influencing primary productivity in two river-type reservoirs by using principal component regression analysis. *Environ. Monit. Assess.* 187, 213. doi: 10.1007/s10661-015-4438-1

Lemley, D. A., Adams, J. B., and Strydom, N. A. (2017). Testing the efficacy of an estuarine eutrophic condition index: does it account for shifts in flow conditions? *Ecol. Indic.* 74, 357–370. doi: 10.1016/j.ecolind.2016.11.034

Li, Y.-H., and Gregory, S. (1974). Diffusion of ions in sea water and in deep-sea sediments. *Geochim. Cosmochim. Acta* 38, 703–714. doi: 10.1016/0016-7037(74)90145-8

Ligero, R. A., Barrera, M., and Casas-Ruiz, M. (2005). Levels of137Cs in muddy sediments of the seabed of the Bay of Cadiz, Spain. Part I. Vertical and spatial distribution of activities. *J. Environ. Radioact.* 80, 75–86. doi: 10.1016/j.jenvrad.2004.05.019

Maggi, E., Rindi, L., Dal Bello, M., Fontanini, D., Capocchi, A., Bongiorni, L., et al. (2017). Spatio-temporal variability in Mediterranean rocky shore microphytobenthos. *Mar. Ecol. Prog. Ser.* 575, 17–29. doi: 10.3354/meps12216

Méléder, V., Jesus, B., Barnett, A., Barillé, L., and Lavaud, J. (2018). Microphytobenthos primary production estimated by hyperspectral reflectance. *PLoS One* 13:e0197093. doi: 10.1371/journal.pone.0197093

Migné, A., Spilmont, N., Boucher, G., Denis, L., Hubas, C., Janquin, M.-A., et al. (2009). Annual budget of benthic production in Mont Saint-Michel Bay considering cloudiness, microphytobenthos migration, and variability of respiration rates with tidal conditions. *Cont. Shelf Res.* 29, 2280–2285. doi: 10.1016/j.csr.2009.09.004

Migné, A., Spilmont, N., and Davoult, D. (2004). In situ measurements of benthic primary production during emersion: seasonal variations and annual production in the Bay of Somme (eastern English Channel, France). *Cont. Shelf Res.* 24, 1437–1449. doi: 10.1016/j.csr.2004.06.002

Morris, E. P., Peralta, G., Benavente, J., Freitas, R., Rodrigues, A. M., Quintino, V., et al. (2009). Caulerpa prolifera stable isotope ratios reveal anthropogenic nutrients within a tidal lagoon. *Mar. Ecol. Prog. Ser.* 390, 117–128. doi: 10.3354/meps08184

Murphy, R. J., Tolhurst, T. J., Chapman, M. G., and Underwood, G. J. C. (2008). Spatial variation of chlorophyll on estuarine mudflats determined by field-based remote sensing. *Mar. Ecol. Prog. Ser.* 365, 45–55. doi: 10.3354/meps07456

Oakes, J. M., Eyre, B. D., Middelburg, J. J., and Boschker, H. T. S. (2010). Composition, production, and loss of carbohydrates in subtropical shallow subtidal sandy sediments: Rapid processing and long-term retention revealed by13C-labeling. *Limnol. Oceanogr.* 55, 2126–2138. doi: 10.4319/lo.2010.55.5.2126

Orvain, F., Lefebvre, S., Montepini, J., Sébire, M., Gangnery, A., and Sylvand, B. (2012). Spatial and temporal interaction between sediment and microphytobenthos in a temperate estuarine macro-intertidal bay. *Mar. Ecol. Prog. Ser.* 458, 53–68. doi: 10.3354/meps09698

Orvain, F., Sauriau, P.-G., Hir, P., Le Guillou, G., Cann, P., and Paillard, M. (2007). Spatio-temporal variations in intertidal mudflat erodability: Marennes-Oléron Bay, western France. *Cont. Shelf Res.* 27, 1153–1173. doi: 10.1016/j.csr.2006.05.013

Papaspyrou, S., Diz, P., Garcia-Robledo, E., Corzo, A., and Jimenez-Arias, J. L. (2013). Benthic foraminiferal community changes and their relationship to environmental dynamics in intertidal muddy sediments (Bay of Cadiz, SW Spain). *Mar. Ecol. Prog. Ser.* 490, 121–135. doi: 10.3354/meps10447

Peralta, G., van Duren, L., Morris, E., and Bouma, T. (2008). Consequences of shoot density and stiffness for ecosystem engineering by benthic macrophytes in flow dominated areas: a hydrodynamic flume study. *Mar. Ecol. Prog. Ser.* 368, 103–115. doi: 10.3354/meps07574

Pinckney, J. L., and Zingmark, R. G. (1993). Modeling the annual production of intertidal benthic microalgae in estuarine ecosystems. *J. Phycol.* 29, 396–407. doi: 10.1111/j.1529-8817.1993.tb00140.x

Pratt, D. R., Pilditch, C. A., Lohrer, A. M., Thrush, S. F., and Kraan, C. (2015). Spatial distributions of grazing activity and microphytobenthos reveal scale-dependent relationships across a sedimentary gradient. *Estuaries and Coasts* 38, 722–734. doi: 10.1007/s12237-014-9857-7

Revsbech, N. P., Jorgensen, B., and Brix, O. (1981). Primary production of microalgae in sediments measured by oxygen microprofile, H14CO3- fixation, and oxygen exchange methods. *Limnol. Oceanogr* 26, 717–730. doi: 10.4319/lo.1981.26.4.0717

Revsbech, N. P., and Jorgensen, B. B. (1983). Photosynthesis of benthic microflora measured with high spatial resolution by the oxygen microprofile method: capabilities and limitations of the method. *Limnol. Oceanogr.* 28, 749–756. doi: 10.4319/lo.1983.28.4.0749

Risgaard-Petersen, N., Dalsgaard, T., Rysgaard, S., Christensen, P. B., Borum, J., McGlathery, K. J., et al. (1998). Nitrogen balance of a temperate eelgrass Zostera marina bed. *Mar. Ecol. Prog. Ser.* 174, 281–291. doi: 10.3354/meps174281

Ritchie, R. J. (2008). Universal chlorophyll equations for estimating chlorophylls a, b, c, and d and total chlorophylls in natural assemblages of photosynthetic organisms using acetone, methanol, or ethanol solvents. *Photosynthetica* 46, 115–126. doi: 10.1007/s11099-008-0019-7

Ruiz-Halpern, S., Vaquer-Sunyer, R., and Duarte, C. M. (2014). Annual benthic metabolism and organic carbon fluxes in a semi-enclosed Mediterranean bay dominated by the macroalgae Caulerpa prolifera. *Front. Mar. Sci.* 1:67. doi: 10.3389/fmars.2014.00067

Sanchez De Lamadrid Rey, A., and Muñoz Pérez, J. L. (1994). *El Medio físico y Biológico en la Bahía de Cádiz: saco Interior. Dirección General de Investigación, Tecnología y Formación Agroalimentaria y Pesquera*. Seville: JuntadeAndalucía.

Savelli, R., Dupuy, C., Barillé, L., Lerouxel, A., Guizien, K., Philippe, A., et al. (2018). On biotic and abiotic drivers of the microphytobenthos seasonal cycle in a temperate intertidal mudflat: a modelling study. *Biogeosciences* 15, 7243–7271. doi: 10.5194/bg-15-7243-2018

Serôdio, J., and Catarino, F. (2000). Modelling the primary productivity of intertidal microphytobenthos: time scales of variability and effects of migratory rhythms. *Mar. Ecol. Prog. Ser.* 192, 13–30. doi: 10.3354/meps192013

Serôdio, J., Vieira, S., Cruz, S., and Barroso, F. (2005). Short-term variability in the photosynthetic activity of microphytobenthos as detected by measuring rapid light curves using variable fluorescence. *Mar. Biol.* 146, 903–914. doi: 10.1007/s00227-004-1504-6

Soetaert, K., Petzoldt, T., and Meysman, F. (2010). *Marelac: Tools for Aquatic Sciences. R package version 2.1*. Available at: https://cran.r-project.org/web/packages/marelac/vignettes/marelac.pdf (accessed June 03, 2018).

Spilmont, N., Davoult, D., and Migné, A. (2006). Benthic primary production during emersion: in situ measurements and potential primary production in the Seine Estuary (English Channel. *France). Mar. Pollut. Bull.* 53, 49–55. doi: 10.1016/j.marpolbul.2005.09.016

Stal, L. J., Van Gemerden, H., and Krumbein, W. E. (1984). The simultaneous assay of chlorophyll and bacteriochlorophyll in natural microbial communities. *J. Microbiol. Methods* 2, 295–306. doi: 10.1016/0167-7012(84)90048-4

Sundbäck, K., Linares, F., Larson, F., Wulff, A., and Engelsen, A. (2004). Benthic nitrogen fluxes along a depth gradient in a microtidal fjord: the role of denitrification and microphytobenthos. *Limnol. Oceanogr.* 49, 1095–1107. doi: 10.4319/lo.2004.49.4.1095

Tejedor, L., López, A., and Álvarez, O. (1997). *Determinación del Nivel Medio del Mar en la Bahía de Cádiz. En: IV Jornadas Españolas de Ingeniería de Costas y Puertos*. Spain: Serv. Publicaciones la Univ.

Thamdrup, B., Hansen, J. W., and Jørgensen, B. B. (1998). Temperature dependence of aerobic respiration in a coastal sediment. *FEMS Microbiol. Ecol.* 25, 189–200. doi: 10.1016/S0168-6496(97)00095-0

Thompson, R. C., Tobin, M. L., Hawkins, S. J., and Norton, T. A. (1999). Problems in extraction and spectrophotometric determination of chlorophyll from epilithic microbial biofilms: towards a standard method. *J. Mar. Biol. Assoc. UK* 79, 551–558. doi: 10.1017/S0025315498000678

Thornton, D. C. O., Dong, L. F., Underwood, G. J. C., and Nedwell, D. B. (2002). Factors affecting microphytobenthic biomass, species composition and production in the Colne Estuary (UK). *Aquat. Microb. Ecol.* 27, 285–300. doi: 10.3354/ame027285

Underwood, G. J. C. (2001). Microphytobenthos. *Encycl. Ocean Sci.* 3, 807–814. doi: 10.1016/b978-012374473-9.00213-7

Underwood, G. J. C., and Kromkamp, J. (1999). Primary production by phytoplankton and microphytobenthos in estuaries. *Adv. Ecol. Res.* 29, 93–153. doi: 10.1016/S0065-2504(08)60192-0

Underwood, G. J. C., and Paterson, D. M. (1993). Seasonal changes in diatom biomass, sediment stability and biogenic stabilization in the severn estuary. *J. Mar. Biol. Assoc. United Kingdom* 73, 871–887. doi: 10.1017/S0025315400034780

Van der Wal, D., Herman, P. M. J., Forster, R. M., Ysebaert, T., Rossi, F., Knaeps, E., et al. (2008). Distribution and dynamics of intertidal macrobenthos predicted from remote sensing: Response to microphytobenthos and environment. *Mar. Ecol. Prog. Ser.* 367, 57–72. doi: 10.3354/meps07535

Van der Wal, D., Wielemaker-van den Dool, A., and Herman, P. M. J. (2010). Spatial synchrony in intertidal benthic algal biomass in temperate coastal and estuarine ecosystems. *Ecosystems* 13, 338–351. doi: 10.1007/s10021-010-9322-9

Walpersdorf, E., Kühl, M., Elberling, B., Andersen, T. J., Hansen, B., Pejrup, M., et al. (2017). In situ oxygen dynamics and carbon turnover in an intertidal sediment (Skallingen. *Denmark). Mar. Ecol. Prog. Ser.* 566, 49–65. doi: 10.3354/meps12016

Welker, C., Sdrigotti, E., Covelli, S., and Faganeli, J. (2002). Microphytobenthos in the gulf of trieste (Northern Adriatic Sea): Relationship with labile sedimentary organic matter and nutrients. *Estuar. Coast. Shelf Sci.* 55, 259–273. doi: 10.1006/ecss.2001.0901

Zuur, A. F., and Ieno, E. N. (2016). A protocol for conducting and presenting results of regression-type analyses. *Methods Ecol. Evol.* 7, 636–645. doi: 10.1111/2041-210X.12577

Conflict of Interest: The authors declare that the research was conducted in the absence of any commercial or financial relationships that could be construed as a potential conflict of interest.

frontiers in Marine Science

ORIGINAL RESEARCH
published: 03 June 2020
doi: 10.3389/fmars.2020.00392

Seasonal and Spatial Variability in Patchiness of Microphytobenthos on Intertidal Flats From Sentinel-2 Satellite Imagery

*Tisja D. Daggers[1], Peter M. J. Herman[2,3] and Daphne van der Wal[1,4]**

[1] NIOZ Royal Netherlands Institute for Sea Research, Department of Estuarine and Delta Systems, Utrecht University, Yerseke, Netherlands, [2] Department of Marine and Coastal Systems, Deltares, Delft, Netherlands, [3] Department of Coastal Engineering, Delft University of Technology, Delft, Netherlands, [4] Faculty of Geo-Information Science and Earth Observation (ITC), University of Twente, Enschede, Netherlands

Understanding the spatial structure of microphytobenthos (MPB) on intertidal flats is necessary to gain insight in the benthic community structure and ecosystem processes. The increasing availability of high resolution satellite sensors provides the opportunity to better understand spatial patterns of MPB on various (meter to km) scales. We tested how MPB patch size (indicated by the range derived from a semi-variogram) and degree of patchiness (indicated by the sill) vary as function of seasons, salinity, tidal flat type (muddy fringing versus sandy mid-channel tidal flats) or ecotopes (defined by hydrodynamics, silt content and elevation), in the Westerschelde estuary, the Netherlands. We used Sentinel-2 imagery (2016–2019) with 10 m spatial resolution to derive (omnidirectional) semi-variogram parameters from the NDVI (used as indicator for MPB biomass) and evaluated (seasonality in) patchiness of MPB in the different categories. We demonstrated that MPB patch size (the range) remains constant from winter to summer, while the sill increased from winter to summer. The location of patches on tidal flats was variable throughout the year and shows a remarkable similarity with seasonality in the spatial heterogeneity of the silt content on tidal flats. The patch size and degree of patchiness is higher on relatively sandy mid-channel tidal flats than on relatively silt rich fringing tidal flats. This implies that spatial patterning of MPB biomass on the meso-scale is likely closely linked to abiotic conditions and that spreading processes or grazing activity play a minor role. We observed visually that some areas with a relatively high MPB biomass ('patches') remain visible throughout the year, while other patches were only present during a particular season.

Keywords: microphytobenthos, patchiness, intertidal flats, silt, remote sensing

OPEN ACCESS

Edited by:
Vona Meleder, Université de Nantes, France

Reviewed by:
Rodney Forster, University of Hull, United Kingdom
Jan Marcin Weslawski, Institute of Oceanology (PAN), Poland

****Correspondence:***
Daphne van der Wal
daphne.van.der.wal@nioz.nl

Specialty section:
This article was submitted to Marine Ecosystem Ecology, a section of the journal Frontiers in Marine Science

Received: *30 November 2019*
Accepted: *07 May 2020*
Published: *03 June 2020*

Citation:
Daggers TD, Herman PMJ and van der Wal D (2020) Seasonal and Spatial Variability in Patchiness of Microphytobenthos on Intertidal Flats From Sentinel-2 Satellite Imagery. Front. Mar. Sci. 7:392. doi: 10.3389/fmars.2020.00392

INTRODUCTION

Microphytobenthos (MPB) living on intertidal flats in estuaries, consisting of cyanobacteria and unicellular eukaryotic algae, can form a considerable part of the total primary production in estuaries (Underwood and Kromkamp, 1999). MPB on intertidal flats mainly consist of benthic diatoms (Meleder et al., 2007). Several studies have emphasized the key role of MPB in sustaining

intertidal food webs (Herman et al., 2000; Thrush et al., 2012; Christianen et al., 2017) and stabilizing the sediment (Orvain et al., 2004; Ubertini et al., 2015). Strong environmental gradients are present in estuarine ecosystems associated with distance to the mouth (salinity, temperature, and tidal amplitude) and elevation (current velocity and sediment composition) (Moreira et al., 1993). These environmental gradients, in turn, structure the spatial variability of biota, including the macrobenthic community and MPB.

Intertidal areas that are relatively homogeneous in terms of the environmental factors can be classified into ecotopes (Bouma et al., 2006; Baptist et al., 2019), and these may also structure the biota.

Meso-scale (i.e., meters to kilometers) and macro-scale (kilometers up to scale of an entire estuary) spatial variability in MPB biomass on intertidal sediments has often been associated with sediment characteristics, bathymetry and wave action (bottom–up control) (Guarini et al., 1998; Van der Wal et al., 2010b; Orvain et al., 2012; Brito et al., 2013; Benyoucef et al., 2014), while micro scale (up to ca 1 m) spatial variability has been associated with grazing by benthic fauna (top–down control) (Weerman et al., 2011). Orvain et al. (2012) identified median grain size of the sediment as the most important parameter explaining spatial variability of MPB, using a macro-scale *in situ* sampling campaign. Van der Wal et al. (2010b) identified positive correlations between MPB biomass and emersion duration, mud content and their interaction, using MODIS satellite imagery of various temperate tidal basins and estuaries. The species composition of benthic diatoms has been associated with sediment characteristics, with epipsammic (sand-fixed) species, mainly occurring in relatively sandy sediments and epipelic (migrating) species, dominating relatively silty sediments (Paterson et al., 1998). Seasonal variability in MPB biomass has been associated with abiotic factors such as irradiance, temperature, nutrient concentrations and wind velocity (Van der Wal et al., 2010b; Ubertini et al., 2012 and references therein).

The macrofaunal community is known to vary as function of current velocity, sediment composition and salinity (Van der Wal et al., 2008; Cozzoli et al., 2013). Macrobenthos may promote or inhibit MPB abundance through various mechanisms, including grazing and physical disturbances (bioturbation) (Solan et al., 2003). Bioturbation from motile infauna (e.g., bivalves, crustaceans, gastropods, and polychaetes) may contribute to the decline of MPB biomass through resuspension and burial below the photic zone (de Deckere et al., 2001; Andersen et al., 2002; Orvain et al., 2004). Small scale effects of macrofaunal grazing on spatial patterns of MPB have been observed, whereby fauna lowered MPB biomass and patchiness (Weerman et al., 2011). However, few studies have focused on meso-scale effects of macrofauna on spatial patterns of MPB biomass. In the Westerschelde, The Netherlands, species richness, biomass and abundance of macrofauna decreases with increasing grain size of the sediment, likely due to increasing hydrodynamic stress in sandy habitats (Cozzoli et al., 2013). The total biomass and number of species of macrofauna in the intertidal areas of the Westerschelde has been demonstrated to strongly decrease with decreasing salinity (Ysebaert et al., 2003). In the polyhaline zone, suspension feeders dominate in terms of biomass and decrease with decreasing salinity. Likewise, surface deposit feeders and sub-surface deposit feeders have a higher biomass in the polyhaline zone than in the mesohaline zone (Ysebaert et al., 2003).

Understanding of the spatial structure of microphytobenthos (MPB) on intertidal flats is necessary to understand community structure and ecosystem functioning (Murphy et al., 2008; Brito et al., 2013). The increasing availability of high resolution satellite sensors provides the opportunity to better understand spatial patterns of MPB on the scale at which ecosystem functioning can be analyzed (meso- and macro-scale). Furthermore, the increasing temporal resolution of satellite imagery may add to insight in changes in spatial patterns of MPB over time. As MPB usually forms small patches at a scale smaller than the resolution of most available satellite sensors, unmanned aerial vehicles (UAVs) may provide detailed information on spatial patterns of MPB on finer spatial scales (<1 m) (Ryu et al., 2014).

Few studies have addressed specific sizes of MPB patches on the meso- or macro-scale. Guarini et al. (1998) performed a geostatistical semi-variogram analysis on MPB biomass data collected in winter and summer (1 km grid resolution). The analysis revealed that patches of high MPB biomass were located at the same spots in summer and winter. A decrease in patch size was observed from summer to winter indicated by the semi-variogram range, which decreased from 6 to 2 km. The process leading to the observed pattern could not be identified. Morris (2005) performed *in situ* sampling campaigns on several tidal flats located in multiple estuaries and emphasized that, because of the dependency of chl-a distributions on topography and sediment properties, spatial patterns of chl-a can have a highly site specific nature.

In the Westerschelde, fringing tidal flats generally have a relatively high silt content, low hydrodynamic energy and high macrofaunal biomass compared to the relatively sandy tidal flats located in the mid-channel. We hypothesize that the degree of patchiness (represented by the sill of a semi-variogram) is lower and the patch size (represented by the range of a semi-variogram) of MPB is higher on mid-channel tidal flats than on fringing tidal flats. We expect that the higher hydrodynamic activity on mid-channel tidal flats compared to fringing tidal flats homogenizes spatial variation in MPB biomass, due to the high resuspension rates of MPB associated with higher current velocities (Lucas et al., 2000). The degree of patchiness is expected to decrease with decreasing salinity due to lower grazing and bioturbation by macrofauna, while the patch size (range) may increase with decreasing salinity.

We hypothesize that patch size and degree of patchiness of MPB increases during the expected spring bloom (early spring) and decreases again in summer and winter. Hereby, it is assumed that MPB biomass follows a constant-density model (Guarini et al., 1998), whereby an increase in MPB biomass expands the patch sizes when an 'optimum' MPB biomass at the center of the patch is reached. We expect that in spring, patch size

and degree of patchiness are mainly coupled to abiotic factors, while in summer macrofauna may influence these parameters by increased grazing activity and bioturbation.

We analyze the seasonality in spatial patterns in MPB along a longitudinal gradient in the Westerschelde estuary, Netherlands, using semi-variograms. Spatial patterns of MPB are studied on the meso-scale at study sites located in varying abiotic and biotic environments along the estuarine gradient. Differences in MPB patch sizes (range of the semi-variogram), degree of patchiness (sill of the semi-variogram), micro-scale variability (nugget of the semi-variogram) and total MPB biomass are compared among seasons, salinity, tidal flat type (fringing, relatively silty or mid-channel, relatively sandy) and ecotopes whereby available Sentinel-2 imagery (10 m resolution) from 2016 to 2019 is used.

MATERIALS AND METHODS

Study Sites

The study is performed in the Westerschelde, The Netherlands. The salinity decreases in upstream direction and varies from polyhaline to α-mesohaline. The selected study sites are located in a strongly polyhaline region (29.23 ± 1.36), weakly polyhaline region (23.96 ± 1.52) and α-mesohaline region (16.52 ± 2.04), respectively (**Figure 1**; Ysebaert et al., 2003). In each salinity zone, a tidal flat located in the mid-channel and a fringing tidal flat was selected. The sediment composition in the intertidal is similar along the estuarine gradient (Cozzoli et al., 2013).

MPB is the main benthic primary producer in the Westerschelde (Daggers et al., 2019). MPB biomass in the surface layer of intertidal sediments of the Westerschelde (i.e., the upper 2 mm) varies from approximately 5 to 300 mg chl *a* m^{-2} (Sahan et al., 2007; Daggers et al., 2019). In a study on the Molenplaat in the Westerschelde, MPB assemblages were dominated by benthic diatoms in spring and autumn, while in summer cyanobacteria and euglenoids became more abundant (Barranguet et al., 1997). In another study performed at the Molenplaat, benthic diatoms were found to be dominant in June (Kromkamp et al., 2006). Benthic diatoms consist of epipelic and epipsammic species. In a study on a brackish site in the Westerschelde, the epipsammic fraction was most abundant and dominated by *Achnantes delicatula*, *Opephora* cf. *perminuta,* and *Catenula adhaerens* (Sabbe, 1993), but many other (episammic) species can be found in the Westerschelde, such as *Rhaphoneis amphiceros* and *R. munitissima* (Sabbe and Vyverman, 1991). The epipelic diatom community composition is related locally to the tidal regime and sediment composition (Sabbe and Vyverman, 1991) and on the estuary scale to the salinity gradient, whereby brackish sites, e.g., contain *Navicula flanatica*, *N. gregaria*, *N. phyllepta*, *Gyrosigma* sp., *Stauphora salina* and *Tryblionella hungarica* and marine sites, e.g., contain the salt tolerant *Amphora* spp., *N. arenaria* var. *rostellata*, *N. microdsigitoradiata*, *N.* cf. *mollis* and *N. perminuta* (Sahan et al., 2007). The community composition of epipelic diatoms varies seasonally, notably at marine sites, containing a higher diversity and larger sized diatoms in late spring and summer than in early spring (Sahan et al., 2007).

Macroalgae densities are generally low and macroalgae are mainly located at the base of the dikes (Lucas and Holligan, 1999; Riera et al., 2000). Nevertheless, field surveys have revealed some patches with macroalgae (*Ulva* sp., *Vaucheria* sp.) in summer, particularly *Ulva* sp. at the southeastern side of the Molenplaat, and at the edge of a chenier on the southern side of Lage Springer.

The most common macrofauna species in the Westerschelde (observed in number of samples) are the capitellid worm *Heteromastus filiformis*, the saltwater clam *Macoma balthica*, the polychete worm *Pygospio elegans*, the sand digger shrimp *Bathyporeia* spp., the ragworm *Hediste diversicolor* and the mudsnail *Peringia ulvae* (Ysebaert et al., 2003).

Sentinel-2 Satellite Data and Pre-processing

Sentinel-2 MSI data for the tiles 31UES and 31UET from April 2016 to July 2019 were downloaded as level 1C data (before 2018) or level 2A (from 1 April 2017) from the Scientific hub at https://scihub.copernicus.eu. The level 1C data were atmospherically corrected using Sen2Cor v2.2; for level 2A the correction was already applied. For the atmospheric correction of the level 1C images, we assumed an aerosol type "maritime," and used the default cirrus correction. Further default settings ensured that the temperature profile and ozone content were determined from the metadata of the image with a LUT to determine the best fit for the measured ozone concentration, and visibility was automatically calculated and averaged from the scene using a dark pixel approach (all images had a visibility of >20 km, clear sky). The season was also taken from the image metadata. On all images, an empirical line calibration was applied to band 4 (surface reflectance in the red) and 8 (surface reflectance in the near-infrared) of each image, using a set of reference points with semi-invariant surfaces (e.g., roofs, deep clear water) and regressed to surface reflectances in band 4 and 8 of an atmospherically corrected image with clear sky (March 12th 2016). This normalization was applied to best compare the images in time. In all cases, regressions had fits of $R^2 > 0.74$ and in most cases $R^2 \geq 0.90$. The equations for both bands in each image are provided in **Supplementary Table S1**.

A Normalized Differential Vegetation Index (NDVI) was based on the resulting surface reflectance in band 4 (10 m resolution reflectance in the red RR) and band 8 (10 m resolution reflectance in the near-infrared RNIR), following (RNIR-RR)/(RR + RNIR) (Kromkamp et al., 2006; Van der Wal et al., 2010b; Daggers et al., 2018). Satellite images acquired during clear sky and low tide conditions were selected, considering groups of 3 images per season (**Table 1**). Pixels with clouds and cloud shadows were masked using manually defined polygons based on visual inspection of the image; such masks were applied for small areas in the sites of Rilland and Valkenisse on the image of July 5th 2019. The NDVI is used as proxy for MPB biomass on the emerged tidal flats, as elaborated below in section "Data analyses." This proxy is widely used (e.g., Kromkamp et al., 2006; Van der Wal et al., 2010b; Kazemipour et al., 2012) and validated for this purpose with chlorophyll-a data collected at

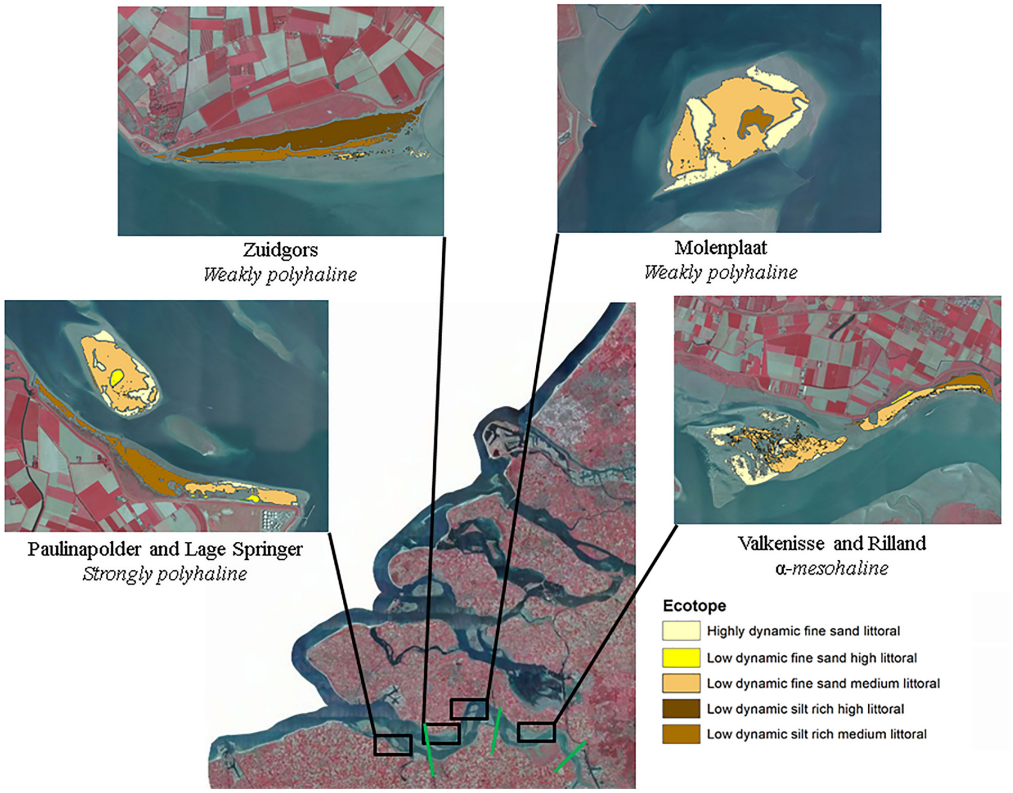

FIGURE 1 | Study sites. The boundaries between different salinity zones (strongly polyhaline, weakly polyhaline, and α-mesohaline) are indicated in green. The boundaries of the study areas are the outer boundaries of the displayed ecotopes and contain the part of the tidal flat that was emersed at all images (see 'Data analyses' for a detailed description of the followed procedure). Ecotope information was obtained from Rijkswaterstaat (2017). Source image: Esri, Aerial photograph of the Netherlands CIR - 25 cm resolution, 2017.

several sites along the estuarine gradient in the Dutch part of the Westerschelde (Daggers et al., 2018, 2019).

Ecotope and Bathymetry Maps

An ecotope map of the Westerschelde was obtained from Rijkswaterstaat (2017), and used to identify intertidal areas that are ecologically distinct (Bouma et al., 2006). The ecotope map of the Westerschelde considers the following abiotic factors for the ecotope classification of intertidal areas: hydrodynamics (high energy: maximum linear current velocity > 0.8 m/s, low energy: maximum linear current velocity < 0.8 m/s), depth (low littoral: 75% flood duration, medium high littoral: 75–25%, 25%) and sediment composition (silt rich: ≥25% silt, <63 μm; fine sand: >25% silt and median < 250 μm).

TABLE 1 | Overview of Copernicus Sentinel-2 MSI imagery used for data analyses.

Season	Satellite and sensor	Acquisition date (dd-mm-yyyy)	Acquisition time (UTC)	Water level (m NAP)	Tidal stage
Winter (December to February)	Sentinel-2B MSI	05-02-2018	10:53	−2.40	Outgoing
	Sentinel-2B MSI	12-12-2018	10:54	−2.24	Outgoing
	Sentinel-2B MSI	21-01-2019	10:55	−0.38	Incoming
Early spring(March to April)	Sentinel-2A MSI	11-04-2016	10:50	−2.52	Outgoing
	Sentinel-2A MSI	27-03-2017	10:50	−0.53	Incoming
	Sentinel-2B MSI	06-04-2018	10:50	−1.89	Outgoing
Late spring (May to June)	Sentinel-2A MSI	26-05-2017	10:50	−0.95	Incoming
	Sentinel-2B MSI	06-05-2018	10:50	−1.52	Outgoing
	Sentinel-2A MSI	30-06-2018	10:50	−1.31	Incoming
Summer(July)	Sentinel-2A MSI	20-07-2016	10:55	−0.73	Incoming
	Sentinel-2B MSI	15-07-2018	10:50	−1.56	Incoming
	Sentinel-2A MSI	05-07-2019	10:50	−1.55	Incoming

Water level and tidal stage at overpass were obtained from Rijkswaterstaat data at station Hansweert (data source: https://waterinfo.rws.nl).

Airborne LiDAR data of the intertidal areas of the Westerschelde (2014–2018) were also obtained from Rijkswaterstaat (cm spatial resolution); these data were used to characterize the tidal flats of interest in terms of their mean elevation and standard deviation.

Data Analyses

The pixels used for the semi-variogram analysis were selected using a mask. Pixels with NDVI < -0.05 were considered to be water, and were removed. The boundary NDVI value of -0.05 was determined empirically, as areas with NDVI values > -0.05 were visibly emersed. Pixels with an NDVI < 0 may contain some standing water. Pixels with NDVI > 0.3 were excluded to exclude areas containing macroalgae. A buffer of 10m along saltmarshes was applied, to exclude pioneer vegetation. Only pixels that were emersed and did not contain macroalgae or saltmarsh vegetation at all available imagery were used for further analyses, i.e., the same mask was applied to all images. Using the ecotope map, saltmarshes present at low to high densities, peat and hard substratum were excluded from the study area. A buffer of 20 m was applied between ecotopes, to prevent edge effects in the semi-variogram analyses per ecotope. Semi-variograms of NDVI (as a proxy for microphytobenthos biomass MPB on emerged sediments), were used to quantify the degree (sill) and scale (range) of MPB patchiness (Rossi et al., 1992; Legendre and Legendre, 2012) for each tidal flat per image using the gstat package version 2.0-2 (Pebesma, 2004) in R version 3.6.0. Variograms were fit using the following default initial parameters: the maximum lag was taken as one third of the maximum sample variogram distance, the nugget parameter was taken as the mean of the first three sample variogram values and the partial sill was given the mean of the last five sample variogram values. To obtain the lag interval, the maximum lag was divided into 15 equal lags. A fit was considered as 'converged' when the change in the weighted sum of squares of differences between the semi-variogrm model and sample variogram became less than 10^6 times the last value of this sum of squares. The nugget represents random variation on the sub-pixel scale (<10 m). Omnidirectional semi-variograms were calculated for each tidal flat separately at each date (**Table 1**), where a tidal flat is defined as a consecutive intertidal area with a minimum width of 100 m. Furthermore, semi-variograms were calculated per ecotope on each tidal flat (see **Figure 1** for an overview of ecotopes present). A spherical model gave the best semi-variogram fit (smallest sum of squared errors of the fitted model) at the majority of datasets as opposed to a Matern or exponential model and was therefore applied to all data. NDVI data per ecotope for which a semi-variogram could not be fitted, as autocorrelation was present in the entire study area, was excluded from further analyses (15% of ecotope data). The NDVI values were normally distributed (Shapiro–Wilk, $p > 0.05$). The NDVI data was (1) detrended using a 1st degree polynomial function to achieve stationary conditions, and (2) normalized by dividing by the standard deviation per tidal flat or ecotope.

Three images per season from winter to summer were considered (**Table 1**), whereby a distinction was made between early and late spring. The effect of season, salinity and tidal flat type (fringing or mid-channel) on MPB biomass, patch size (range), degree of patchiness (sill) and micro-scale variability (nugget) per tidal flat was quantified using an ANOVA test and HSD Tukey *post hoc* test. The residuals did not meet the normality assumption (Shapiro–Wilk, $p < 0.01$) and showed a somewhat right-tailed distribution as commonly observed in biological datasets. Variation in semi-variogram parameters calculated per ecotope per site was tested using an ANOVA and HSD Tukey *post hoc* test for the factors season, salinity and ecotope. We tested whether a linear correlation was present between the MPB biomass and sill using the Pearson product-moment correlation coefficient.

The locations on the tidal flats of interest where the NDVI was high or low, respectively, in particular seasons was similar over the years (2016–2019, inspected visually) and the NDVI was therefore averaged per season to produce maps with mean (non de-trended, non-normalized) NDVI per season. In addition, maps of the coefficient of variation in NDVI (calculated as σ/μ per pixel for the study period 2016-2019) were produced for each of the tidal flats and analyzed visually.

RESULTS

Site Characteristics

The selected tidal flats, i.e., the surface area selected for semi-variogram analysis ($-0.05 <$ NDVI < 0.30), had a similar surface area with the exception of Valkenisse ($\pm$ a factor 2 larger) and similar average MPB biomass, i.e., NDVI (**Table 2**). The percentage of area covered with silt rich sediment derived from the ecotope map was profoundly larger on fringing tidal flats than on mid-channel tidal flats. The average elevation of the sites was similar, although Zuidgors was located somewhat higher in the intertidal (1.45 m NAP).

Seasonality in MPB Biomass

The MPB biomass was higher in summer than in early spring (**Table 3**; ANOVA, $P = 0.004$, $F_{3,55} = 4.80$, $n = 72$; HSD Tukey, $p < 0.05$). The MPB biomass did not differ significantly between fringing and mid-channel tidal flats (ANOVA, $P = 0.9$, $F_{1,65} = 0.02$, $n = 72$) or among salinity zones (ANOVA, $P = 0.45$, $F_{2,65} = 0.81$, $n = 72$). Particularly at Zuidgors, Molenplaat and Valkenisse an increasing trend in MPB biomass was observed from early spring to summer, while a large amount of variation in the biomass was present in winter among the years 2016–2019 at most sites (**Figure 2**).

Semi-Variogram Parameters per Site

The range derived from the semi-variograms of the normalized NDVI showed a high degree of similarity among different dates at each site (**Figure 3** and **Supplementary Table S2**). The range of the semi-variogram (patch size) did not vary among seasons (ANOVA, $P = 0.17$, $F_{3,65} = 1.72$, $n = 72$) and appeared relatively constant throughout the year (**Figure 4**). Although the location of patches was in many cases constant throughout the year, the location of the patches may change over time (**Figure 6** and **Supplementary Figure S1**). The range was higher in the

TABLE 2 | General characteristics of the areas of interest of the selected tidal flats, i.e., $-0.05 < \text{NDVI} < 0.3$.

Site	Surface area (km^2)	NDVI (MPB) ($\mu \pm \sigma$)	% Silt rich area	Salinity	Tidal flat type	Height 2014-2018 $\mu \pm \sigma$ (m NAP*)
Paulinapolder	0.94	0.075 ± 0.037	63	Strongly polyhaline	Fringing	0.61 ± 0.05
Zuidgors	0.88	0.047 ± 0.031	96	Weakly polyhaline	Fringing	1.45 ± 0.18
Rilland	1.08	0.062 ± 0.029	26	α-mesohaline	Fringing	0.87 ± 0.08
Lage Springer	1.14	0.057 ± 0.034	1	Strongly polyhaline	Mid-channel	0.71 ± 0.06
Molenplaat	1.12	0.074 ± 0.029	5	Weakly polyhaline	Mid-channel	0.36 ± 0.10
Valkenisse	2.02	0.039 ± 0.038	0	α-mesohaline	Mid-channel	0.58 ± 0.54

**The elevation values are with regard to the Dutch ordnance system NAP (Normaal Amsterdams Peil), which is approximately similar to mean sea level.*

TABLE 3 | Statistics of MPB biomass and semi-variogram parameters calculated per site.

	MPB biomass			Nugget			Sill			Range		
	F	*P*	df	*F*	*P*	df	*F*	*P*	df	F	P	df
Season	4.80	0.004**	3,65	33.95	$2.54*10^{-13}$	3,65	20.60	$1.7*10^{-9}$***	3,65	1.72	0.17	3,65
Salinity	0.81	0.45	2,65	0.46	0.63	2,65	2.96	0.06	2,65	15.68	$2.77*10^{-6}$***	2,65
Type	0.02	0.90	1,65	6.85	0.01*	1,65	9.18	0.004**	1,65	12.28	0.0008***	1,65

*Significance level (P) is indicated by *** = 0, ** = 0.001, and * = 0.05.*

TABLE 4 | Statistics of MPB biomass and semi-variogram parameters calculated per ecotope.

	MPB biomass			Nugget			Sill			Range		
	F	*P*	df	*F*	*P*	df	*F*	*P*	df	*F*	*P*	df
Season	7.05	0.0002***	3,192	32.84	$<2*10^{-16}$	3,192	8.83	$1.6*10^{-5}$***	3,111	0.60	0.62	3,192
Salinity	0.39	0.67	2,192	2.67	0.07	2,192	3.81	0.02*	2,111	0.83	0.44	2,192
Ecotope	1.98	0.08	3,192	3.93	0.002**	5,192	3.02	0.01*	3,111	4.02	0.002**	5,192

*Significance level (P) is indicated by *** = 0, ** = 0.001, and * = 0.05.*

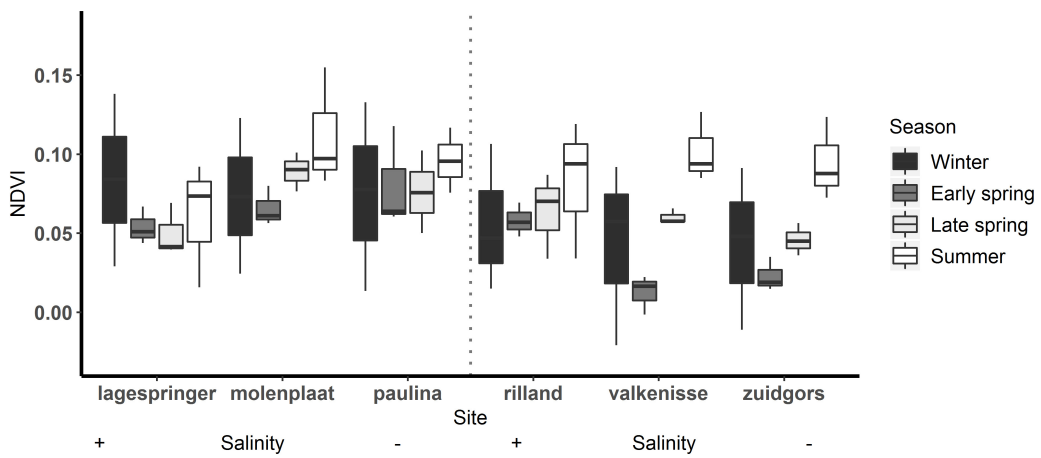

FIGURE 2 | MPB biomass, expressed as the NDVI, on each tidal flat per season. Winter: December to February, early spring: March to April, late spring: May to June, summer: July.

mesohaline zone (603 m) than in the weakly polyhaline (338 m) and strongly polyhaline zone (366 m) (ANOVA, $P = 2.77*10^{-6}$, $F_{2,65} = 15.68$, $n = 72$; HSD Tukey, $p < 0.0001$). Furthermore, the range was higher at tidal flats located in the mid-channel (510 m) than at fringing tidal flats (362 m) (ANOVA, $P < 0.001$, $F_{1,65} = 12.28$, $n = 72$; HSD Tukey, $p < 0.001$). The angle of the major range was estimated visually from anisotropy maps and was highly consistent throughout the year (Lage springer: ±135, Molenplaat: ±60, Paulinapolder: ±115, Rilland: ±70, Valkenisse: ±100, Zuidgors: ±80).

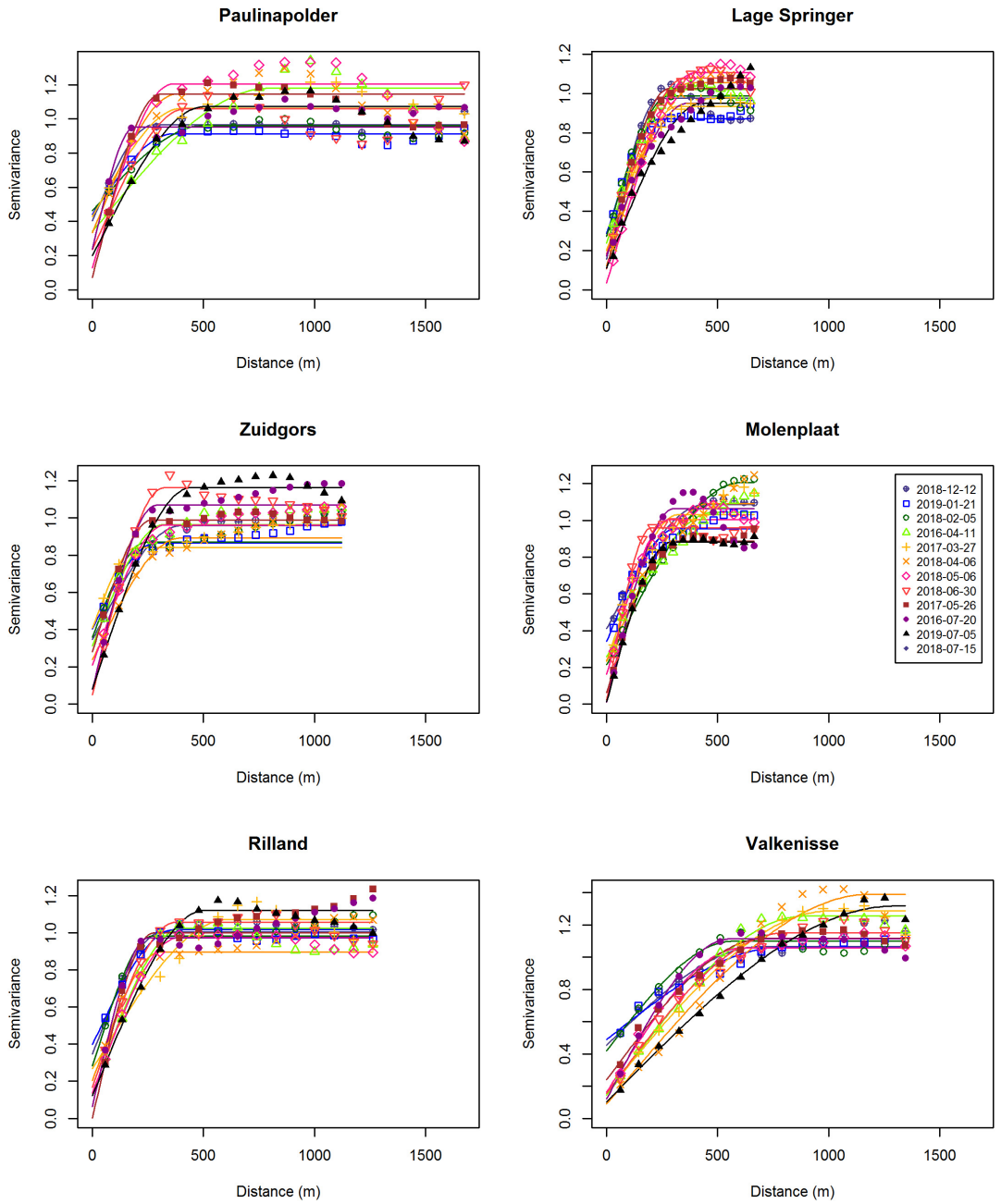

FIGURE 3 | Semi-variograms per site.

The sill showed an increasing trend throughout the year (**Figure 4**). The sill was higher in early spring, late spring, and summer than in winter and the sill was higher in summer than in early spring (ANOVA, $P = 1.7^{*}10^{-9}$, $F_{3,65} = 20.6$, $n = 72$; HSD Tukey, $p < 0.05$). The sill was higher on mid-channel tidal flats than on fringing tidal flats (ANOVA, $P = 0.004$, $F_{3,65} = 9.18$, $n = 72$; HSD Tukey, $p < 0.01$). The sill was not significantly correlated with MPB biomass (Pearson's $r = 0.17$, $p = 0.16$).

The nugget showed a decreasing trend throughout the year (**Figure 4**). The nugget did not vary significantly as function of salinity, but was lower in early spring, late spring and summer than in winter. Furthermore, the nugget was lower in late spring and summer than in early spring (ANOVA, $P = 2.54^{*}10^{-13}$, $F_{3,65} = 33.95$, $n = 72$; HSD Tukey, $p < 0.05$). The nugget was higher on fringing tidal flats than on mid-channel tidal flats (ANOVA, $P = 0.01$, $F_{3,65} = 6.85$, $n = 72$; HSD Tukey, $p < 0.05$).

Semi-Variogram Parameters per Ecotope

The range calculated per ecotope did not differ significantly among seasons or salinity zones (**Figure 5** and **Table 4**). The

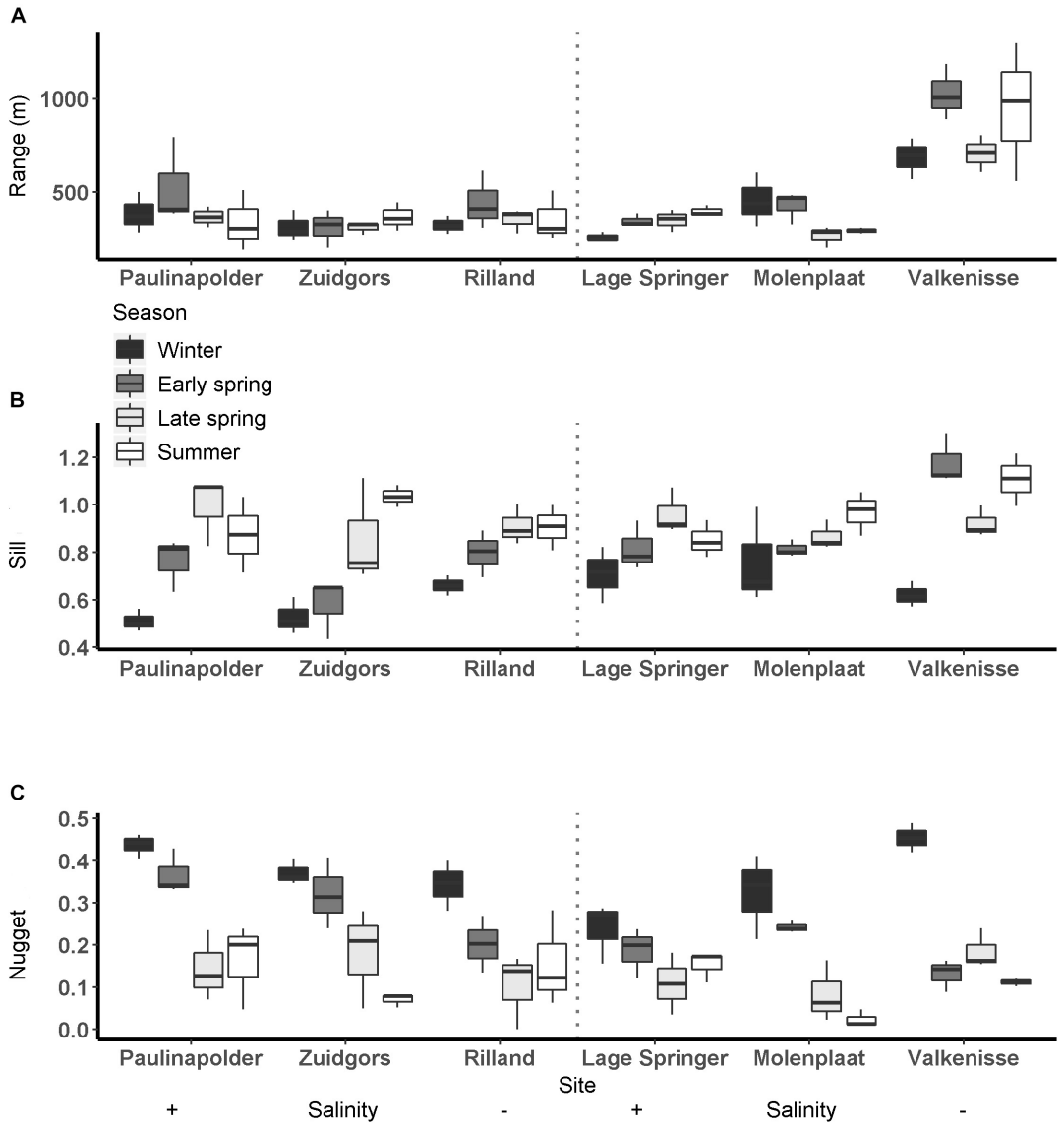

FIGURE 4 | Semi-variogram parameters per season per site at fringing (left) and mid-channel (right) tidal flats (**A**: range (m), **B**: sill, **C**: nugget).

range was higher in the 'low dynamic silt rich medium high littoral' ecotope than the 'low dynamic fine sand high littoral' ecotope (ANOVA, $P = 0.002$, $F_{3,111} = 4.02$, $n = 120$; HSD Tukey, $p = 0.02$). Furthermore, the range was lower in the 'low dynamic fine sand high littoral' ecotope than in the 'highly dynamic fine sand littoral' ecotope (HSD Tukey, $p = 0.001$). Lastly, the range was higher in the 'low dynamic fine sand medium high littoral' ecotope than in the 'low dynamic fine sand high littoral' ecotope (HSD Tukey, $p = 0.01$).

The sill calculated per ecotope was higher in late spring and summer than in winter (ANOVA, $P = 1.6^{*}10^{-5}$, $F_{3,111} = 8.83$, $n = 120$; HSD Tukey, $p < 0.001$). The sill did not differ significantly among ecotopes. The sill was higher in the weakly polyhaline zone than in the strongly polyhaline zone (ANOVA, $P = 0.02$, $F_{3,111} = 3.81$, $n = 120$; HSD Tukey, $p < 0.05$). The ANOVA test revealed significant differences in the variance between ecotopes (ANOVA, $P = 0.01$, $F_{3,111} = 3.01$, $n = 120$). However, an HSD Tukey test revealed no significant differences between individual ecotopes.

The nugget was higher in early spring, late spring and summer than in winter and higher in early spring than in summer (ANOVA, $P < 2^{*}10^{-16}$, $F_{3,111} = 32.84$, $n = 120$; HSD Tukey, $p < 0.05$). The nugget did not differ significantly among salinity zones. The nugget was higher in the 'low dynamic fine sand high littoral' ecotope than in the 'highly dynamic fine sand littoral' ecotope (ANOVA, $P < 0.002$, $F_{3,111} = 3.93$, $n = 120$; HSD Tukey, $p = 0.01$). The nugget was higher in the 'highly dynamic fine sand high littoral' ecotope than in the 'low dynamic fine sand medium high littoral' ecotope (HSD Tukey, $p = 0.02$).

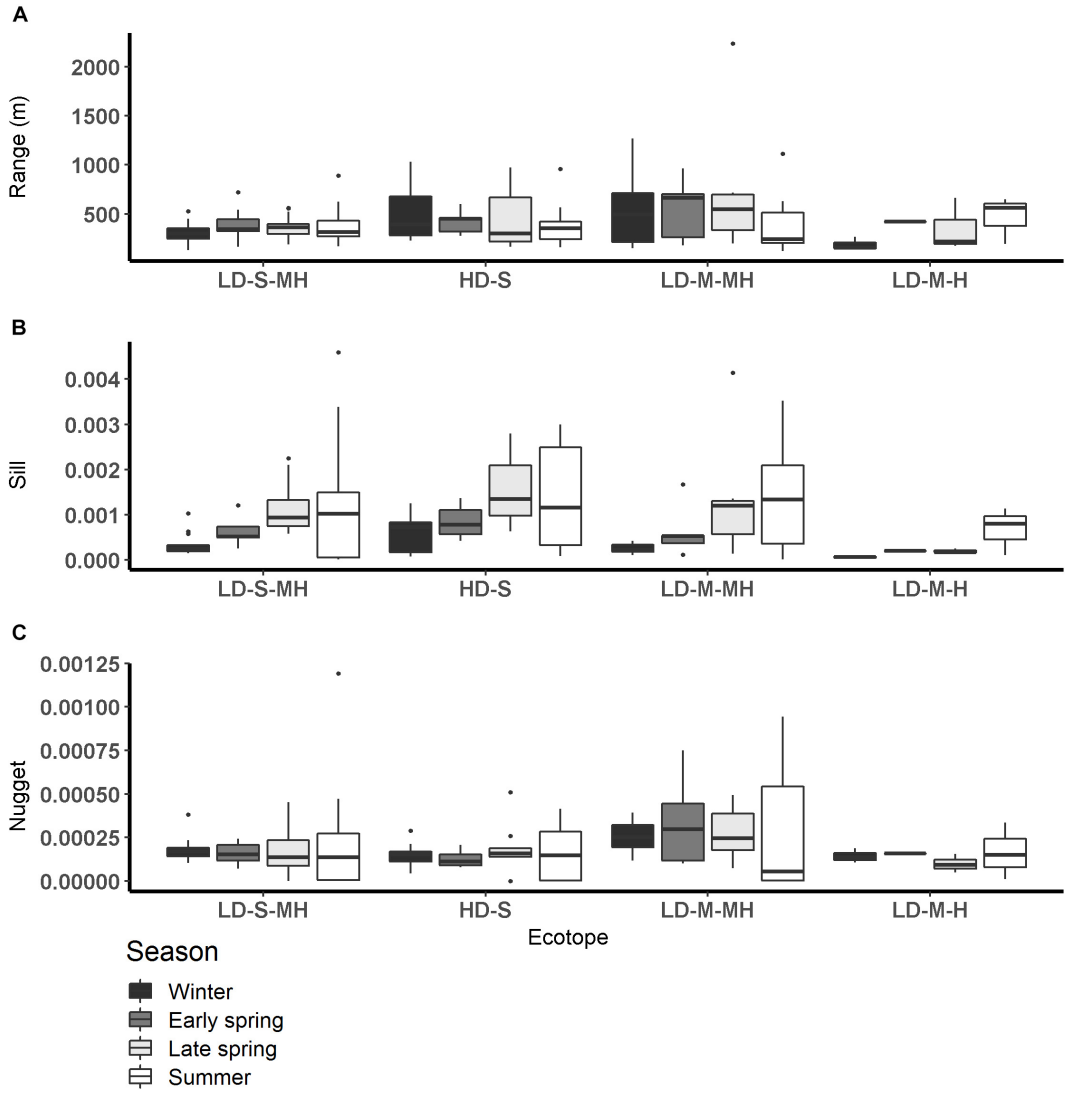

FIGURE 5 | Semi-variogram parameters per season per ecotope (**A**: range (m), **B**: sill, **C**: nugget). HD-S, Highly dynamic fine sand littoral; LD-S-MH, low dynamic fine sand medium high littoral; LD-M-H, low dynamic silt rich high littoral, and LD-M-MH, low dynamic silt rich medium high littoral.

Seasonality in the Location of Patches

Regular observation of the sites showed that that some areas with a relatively high MPB biomass ('patches') remain visible throughout the year, while other patches were only present during a particular season. For example, the patch located on the southeast side of the mid-channel tidal flat Lage Springer (**Figure 6**, a) can be clearly distinguished during all studied seasons. However, the patch located on the north side of Lage Springer was clearly visible in winter, but could hardly be detected in other seasons (**Figure 6**, b). At the fringing tidal flat Paulinapolder, an area of high MPB biomass was observed at the center of the tidal flat, which could not be distinguished clearly in winter or spring (**Figure 6**, c). At the mid-channel tidal flat Valkenisse, the MPB biomass was consistently higher on the southeast side of the tidal flat throughout the year and the region with a relatively high biomass appeared to increase in surface area from spring to summer (**Supplementary Figure S1**, a and **Figure 2**). The coefficient of variation confirmed that changes in MPB biomass were relatively low in this area (**Figure 7**, a). At the mid-channel tidal flat Molenplaat, the seasonal average of the MPB biomass was relatively high on the east side throughout the year (**Supplementary Figure S1**, b). The MPB biomass was most variable over time on the west side (**Figure 7**, b), where a patch appeared in late spring (**Supplementary Figure S1**, c). At the fringing tidal flats Zuidgors and Rilland, a cross-shore gradient from high to low in MPB biomass was present during all seasons. The MPB biomass was most variable throughout the year at low elevation at Zuidgors, Rilland and Valkenisse (**Figure 7**). In late spring, a band of high MPB biomass appeared at low elevation at Zuidgors (**Supplementary Figure S1**, d).

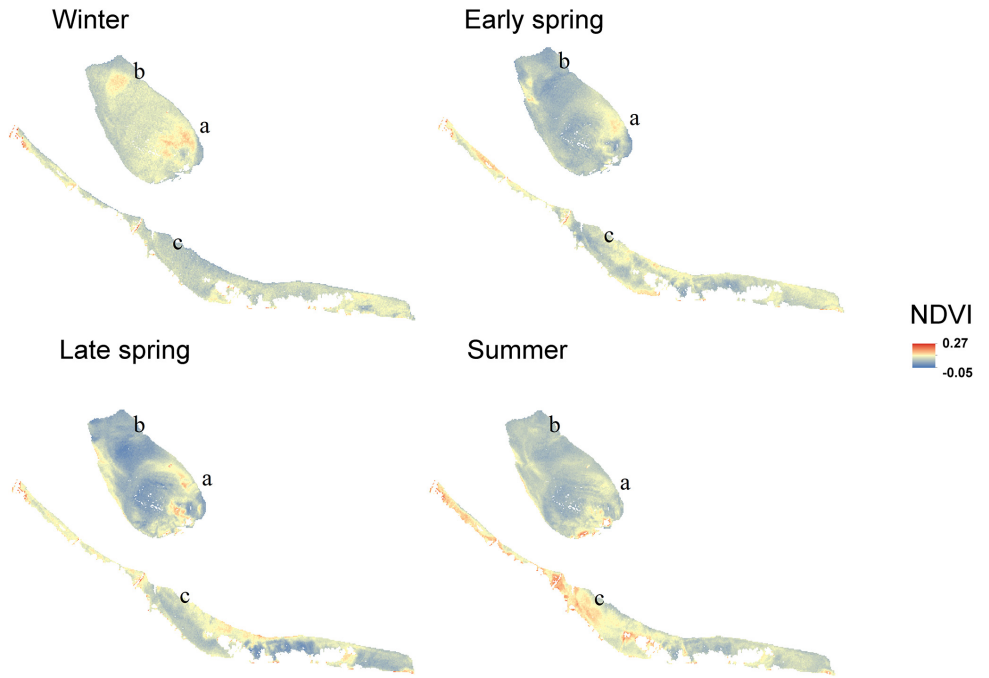

FIGURE 6 | NDVI maps averaged per season for 'Lage Springer' (mid-channel tidal flat) and 'Paulinapolder' (fringing tidal flat).

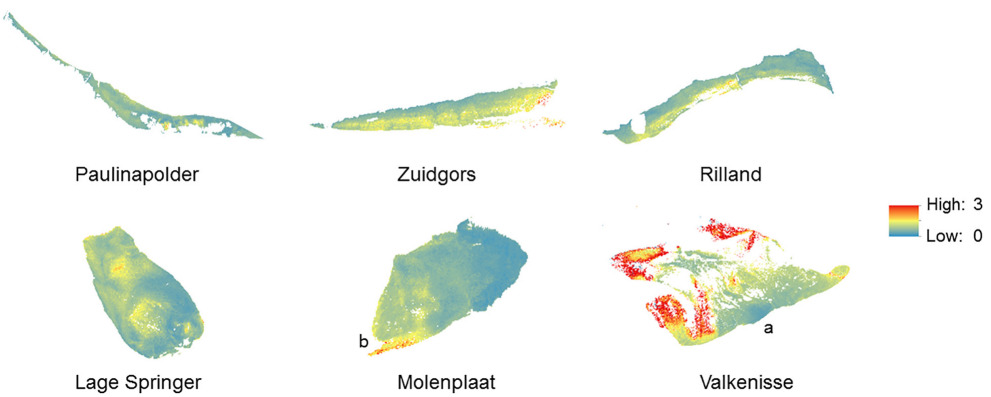

FIGURE 7 | Coefficient of variation of the NDVI (2016–2019). The coefficient of variation ranged from –5176 to 13565.

DISCUSSION

Spatial structure is a crucial component of ecological communities. Our results demonstrate that MPB show a remarkable seasonality in the degree of patchiness (sill) which increases from winter to summer, while the patch size (range) remains relatively constant. The location of the patches may change over time, which suggests that in these cases the increase in degree of patchiness is not associated with a general increase in MPB biomass but with locally changing abiotic conditions or grazing activity. Furthermore, the patch size and degree of patchiness is higher on relatively sandy mid-channel tidal flats than on relatively silt rich fringing tidal flats. This suggests that sediment composition plays an important role in pattern formation of MPB, as found in earlier studies (Morris, 2005; Meleder et al., 2007).

Seasonal Dynamics of MPB Biomass and Patterning

Our results demonstrate that the MPB biomass averaged per tidal flat increased from early spring to summer, while in winter MPB biomass was highly variable among the years 2016–2019. We did not observe a clear spring bloom. Following a constant-density model, as hypothesized, the patch size (range) would be expected to increase from early spring to summer accordingly. However, the range of MPB did not change significantly over time and visual observation showed that the location of areas with

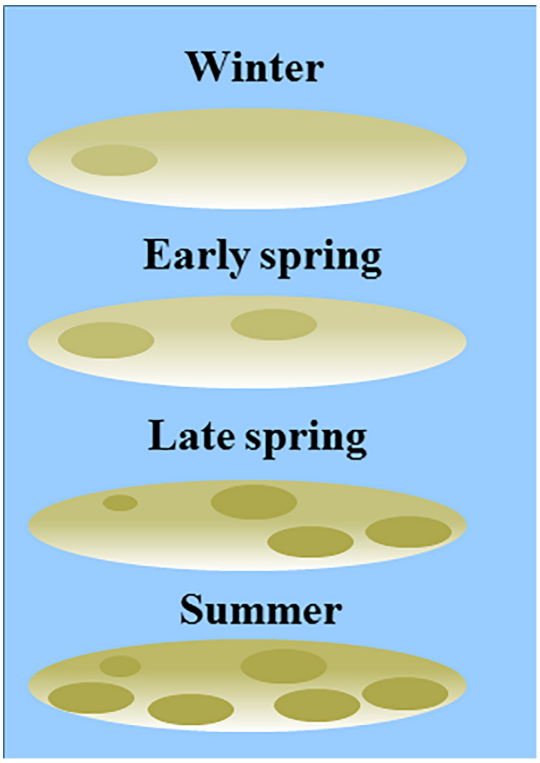

FIGURE 8 | Conceptual model of seasonality in patch size (based on the range derived from a semi-variogram) and degree of patchiness (sill derived from a semi-variogram) in MPB biomass, complemented by visual observations of the sites. No boundary values for areas of 'MPB patches' versus 'bare sediment' were used in the current study.

a relatively high MPB biomass changed throughout the seasons (**Supplementary Figure S1**). It should be noted that no boundary value for the NDVI was used to distinguish between 'MPB patches' versus 'bare sediment' in the current study. Variation in MPB biomass on tidal flats are gradual and the range derived from the semi-variogram quantifies the size of areas with a similar MPB biomass (referred to as 'patch'). A power law analysis using a definition of patches with a fixed NDVI threshold may provide further insight in changes in the number and size of patches throughout seasons (Weerman et al., 2012). Visual observation showed that, at most sites, areas with a relatively low MPB biomass increased in biomass from early spring to summer, while the biomass was highly variable in winter in 2016–2019. In some areas, MPB biomass remained low throughout the seasons (**Figure 8**). Furthermore, it was visually observed that the number of areas with a relatively high MPB biomass increases from early spring to summer. At a few tidal flats, the spatial configuration of patches remained relatively constant from winter to summer (Valkenisse, Molenplaat, and Rilland; **Supplementary Figure S1**). Visual observation showed that at Valkenisse and the eastern side of Molenplaat, areas with a relatively high MPB biomass expand over time (**Figure 8**). Valkenisse and Rilland are located in the mesohaline zone, where macrofaunal biomass is relatively low (Ysebaert et al., 2003) and, therefore, a minor influence of grazing activity or bioturbation on spatial patterns of MPB is expected. The consistent patch size throughout the year is not in line with the finding of Guarini et al. (1998), who studied spatial variability on a larger scale (1 km grid resolution) and found an increase in patch size from winter to summer along with an increasing MPB biomass. However, we did visually observe this phenomenon at Valkenisse and Molenplaat, where MPB biomass increased from early spring to summer and patches appeared to spread over the tidal flat (**Supplementary Figure S1**). This suggests that, depending on local environmental conditions, pattern formation may indeed follow a constant-density model.

The sill was significantly higher in late spring and summer than in winter at mid-channel and fringing tidal flats. This is in line with our hypothesis and may be associated with increased grazing activity and bioturbation by macrofauna or with changed abiotic conditions. The higher sill in late spring and summer than in winter was observed in all ecotopes ('low dynamic fine sand medium high littoral,' 'low dynamic silt rich medium high littoral,' and 'highly dynamic fine sand littoral') except the ecotope 'low dynamic silt rich high littoral.' This ecotope was only present at Zuidgors, where the MPB biomass visually appeared relatively homogeneous in winter, early spring and late spring. In summer, a patch emerged on the east side of the tidal flat (**Supplementary Figure S1**).

Spatial Patterning on Fringing Versus Mid-Channel Tidal Flats

As hypothesized, the patch size (range) was higher on mid-channel tidal flats than on fringing tidal flats. This suggests that the relatively high hydrodynamic activity on mid-channel tidal flats as opposed to fringing tidal flats homogenizes spatial variability in MPB biomass, possibly due to high resuspension rates associated with higher current velocities (Lucas et al., 2000). However, the observed difference was mainly due to the range being approximately a factor two higher at the site Valkenisse than all other study sites. Likewise, the range was significantly higher in the mesohaline zone than in the strongly and weakly polyhaline zone, mainly due to the range being higher at Valkenisse than at all other sites. At Valkenisse, there appears to be one prevalent patch on the southeastern side of the tidal flat which is present throughout the year. In summer, more heterogeneity in MPB biomass appears within the patch which may be associated with increased grazing activity by macrofauna or changed abiotic conditions. The higher range at this site compared to other tidal flats is expected to be associated with the higher hydrodynamic activity and lower macrofaunal biomass at this location compared to other sites, as this site is located in the α-mesohaline zone and is characterized by mega-ripples (cf. Van der Wal et al., 2017). However, the larger surface area of Valkenisse may also play a role (**Table 2**), as no correction for the size of the study areas was applied in the semi-variogram analysis. Expansion of the current study to other estuaries and coastal embayments may increase insight on the possible effect of tidal flat size on the range of MPB patches.

The sill was higher on mid-channel tidal flats than on fringing tidal flats. This is not in line with our hypothesis, which stated that

higher hydrodynamic energy and low macrofaunal biomass on mid-channel tidal flats is expected to homogenize MPB biomass. Instead, based on our findings, we suggest that the presence of an embankment at the top of the shore reduces the directionality in which heterogeneity in MPB biomass may emerge. At the fringing tidal flats, MPB patches mostly appeared in bands orientated alongshore (**Supplementary Figure S1**), as was observed by Guarini et al. (1998), while at mid-channel tidal flats patches have an omnidirectional character.

Structuring Processes

The proposition by Guarini et al. (1998) that seasonal dynamics of MPB biomass follow a constant density model is not supported by the current study, as the patch size remained constant throughout the year, but instead suggest a proportional-density model. Hereby, no relationship exists between the biomass of MPB and the occupied area, which is illustrated by the increase in MPB biomass over time while the patch size remained constant. From an ecological perspective, this implies that spatial patterning of MPB biomass is not governed by spreading processes.

Spatial variability of MPB biomass is caused by both physical and biological structuring processes. Morris (2005) found that the most important scales of variability in MPB biomass were around 200–300 m, $\leq$100 m and $\leq$2.5 m and that mean grain size and sediment sorting explain about 27% of the spatial variability in chl-a concentrations. A positive feedback exists between net silt accumulation and diatom growth, likely due to relatively high concentrations of nutrients in silt rich sediment compared to sandy sediments. Furthermore, diatoms secrete extracellular polymeric substances which lead to increased sediment cohesion, reducing the erodibility of sediment (Van De Koppel et al., 2001). This results in generally higher concentrations of MPB in silt rich sediment than in sandy sediments (Van der Wal et al., 2010b). The silt content of intertidal sediments in the Westerschelde retrieved from surface roughness estimates from ERS-2 SAR revealed changes in spatial heterogeneity in the silt content throughout the year (Van der Wal et al., 2010a). The seasonality in the spatial heterogeneity of the silt content observed in 2006 shows remarkable similarities with the seasonality in the spatial heterogeneity of MPB biomass surveyed in the current study. For example, the emerging MPB patch on the west side of the Molenplaat in late spring and summer (**Supplementary Figure S1**) coincides with a strong increase in silt content in summer (Van der Wal et al., 2010a). Furthermore, the high concentration of MPB biomass on the southeast side of Valkenisse corresponds with a high silt content at this location, which increases in surface area in summer like the surface area of MPB increases at this site. This provides a strong indication that seasonality in spatial patterns of MPB and silt content are linked on the meso-scale and that, on the meso-scale, grazing activity likely plays a minor role.

Spatial Patterning in Ecotopes

The patch size (range) was higher in the 'low dynamic silt rich medium high littoral' ecotope than the 'low dynamic fine sand high littoral,' confirming our previous conclusion that sediment composition is likely closely linked to pattern formation of MPB. In addition, the range was significantly higher in the 'low dynamic fine sand medium high littoral' ecotope than in the 'low dynamic fine sand high littoral' ecotope. Therefore, the factor 'elevation' is additionally expected to influence the patch size, which may be associated with the presence of a gradient in hydrodynamic conditions or grazing activity. However, the relatively small surface area of the latter ecotope in the Westerschelde is likely to influence the observed difference in the range here.

Future Requirements and Perspectives

Regular *in situ* monitoring campaigns of MPB in intertidal areas are rare and provide limited information on ecosystem dynamics on the meso-scale. The use of satellite remote sensing seems a promising method to monitor spatial patterning of MPB at this scale. We demonstrated that Sentinel-2 MSI imagery provides a useful information source for mapping and analyses of spatial heterogeneity and seasonality in MPB biomass. Our results demonstrate that the location of MPB patches and, therefore, available food for higher trophic levels (including benthic macrofauna) varies from winter to summer. This information can be accounted for in spatially explicit food web models or sediment transport modeling.

The proposed method could be used in tidal systems worldwide to investigate to what extent patch characteristics and their seasonal dynamics vary among systems. This may provide further insight into the contribution of e.g., climate, tidal regime and the specific morphology of tidal flats to seasonal dynamics of patch characteristics. Several studies where MPB biomass was quantified using the NDVI were performed in benthic diatom dominated estuaries (e.g., Kromkamp et al., 2006; Benyoucef et al., 2014; Daggers et al., 2018). However, further research is needed on possible effects of the microphytobenthic community composition (e.g., benthic diatoms versus euglenoids) on the relationship between the NDVI and MPB biomass. The relationship between the NDVI and MPB biomass should be calibrated for each site, as the relationship may vary per site and season.

CONCLUSION

Overall, we provided evidence that the degree of patchiness (sill derived from a semi-variogram) of MPB on the meso-scale varies from winter to spring, while the patch size (range derived from a semi-variogram) remains constant. The degree of patchiness and the patch size was higher on relatively sandy mid-channel tidal flats than on relatively silt rich fringing tidal flats. The location of patches may remain constant or vary throughout the year. The observed seasonality in MPB patchiness on the meso-scale appears to be closely linked to changes in the silt content.

DATA AVAILABILITY STATEMENT

The datasets generated for this study are available on request to the corresponding author.

AUTHOR CONTRIBUTIONS

DW and TD designed the study. TD compiled the data, performed the analysis, and wrote the manuscript. PH and DW contributed to the study design, analyses, interpretation of the data, and editing of the manuscript.

FUNDING

This research was supported by the "User Support Program Space Research" of the Netherlands Organization for Scientific Research (NWO grant no. ALW-GO 13/14 to DW).

ACKNOWLEDGMENTS

We gratefully acknowledge Annette Wielemaker for her assistance in data collection, pre-processing of the imagery, and valuable discussions on the used methodology.

SUPPLEMENTARY MATERIAL

The Supplementary Material for this article can be found online at: https://www.frontiersin.org/articles/10.3389/fmars.2020.00392/full#supplementary-material

REFERENCES

Andersen, T. J., Jensen, K. T., Lund-Hansen, L., Mouritsen, K. N., and Pejrup, M. (2002). Enhanced erodibility of fine-grained marine sediments by *Hydrobia ulvae*. *J. Sea Res.* 48, 51–58.

Baptist, M. J., Van der Wal, J. T., Folmer, E. O., Grawe, U., and Elschot, K. (2019). An ecotope map of the trilateral Wadden Sea. *J. Sea Res.* 152:101761. doi: 10.1016/j.seares.2019.05.003

Barranguet, C., Herman, P. M. J., and Sinke, J. J. (1997). Microphytobenthos biomass and community composition studied by pigment biomarkers: importance and fate in the carbon cycle of a tidal flat. *J. Sea Res.* 38, 59–70.

Benyoucef, I., Blandin, E., Lerouxel, A., Jesus, B., Rosa, P., Meleder, V., et al. (2014). Microphytobenthos interannual variations in a north-European estuary (Loire estuary, France) detected by visible-infrared multispectral remote sensing. *Estuar. Coast. Shelf Sci.* 136, 43–52. doi: 10.1016/j.ecss.2013.11.007

Bouma, H., de Jong, D. J., Twisk, F., and Wolfstein, K. (2006). *A Dutch Ecotope System for Coastal Waters (ZES.1). To Map The Potential Occurrence Of Ecological Communities In Dutch Coastal And Transitional Waters*. Middelburg: Rijkswaterstaat.

Brito, A. C., Benyoucef, I., Jesus, B., Brotas, V., Gernez, P., Mendes, C. R., et al. (2013). Seasonality of microphytobenthos revealed by remote-sensing in a South European estuary. *Cont. Shelf Res.* 66, 83–91. doi: 10.1016/j.csr.2013.07.004

Christianen, M. J. A., Middelburg, J. J., Holthuijsen, S. J., Jouta, J., Compton, T. J., van der Heide, T., et al. (2017). Benthic primary producers are key to sustain the Wadden Sea food web: stable carbon isotope analysis at landscape scale. *Ecology* 98, 1498–1512. doi: 10.1002/ecy.1837

Cozzoli, F., Bouma, T. J., Ysebaert, T., and Herman, P. M. J. (2013). Application of non-linear quantile regression to macrozoobenthic species distribution modelling: comparing two contrasting basins. *Mar. Ecol. Prog. Ser.* 475, 119–133. doi: 10.3354/Meps10112

Daggers, T. D., Kromkamp, J. C., Herman, P. M. J., and Van der Wal, D. (2018). A model to assess microphytobenthic primary production in tidal systems using satellite remote sensing. *Remote Sens. Environ.* 211, 129–145. doi: 10.1016/j.rse.2018.03.037

Daggers, T. D., Kromkamp, J. C., Herman, P. M. J., and Van der Wal, D. (2019). Corrigendum to " A model to assess microphytobenthic primary production in tidal systems using satellite remote sensing". *Remote Sens. Environ.* 211, 129–145.

de Deckere, E. M. G. T., Tolhurst, T. J., and de Brouwer, J. F. C. (2001). Destabilization of cohesive intertidal sediments by infauna. *Estuar. Coast. Shelf Sci.* 53, 665–669. doi: 10.1006/ecss.2001.0811

Guarini, J. M., Blanchard, G. F., Bacher, C., Gros, P., Riera, P., Richard, P., et al. (1998). Dynamics of spatial patterns of microphytobenthic biomass: inferences from a geostatistical analysis of two comprehensive surveys in Marennes-Oleron bay (France). *Mar. Ecol. Prog. Ser.* 166, 131–141.

Herman, P. M. J., Middelburg, J. J., Widdows, J., Lucas, C. H., and Heip, C. H. R. (2000). Stable isotopes as trophic tracers: combining field sampling and manipulative labelling of food resources for macrobenthos. *Mar. Ecol. Prog. Ser.* 204, 79–92. doi: 10.3354/Meps204079

Kazemipour, F., Launeau, P., and Meleder, V. (2012). Microphytobenthos biomass mapping using the optical model of diatom biofilms: application to hyperspectral images of Bourgneuf Bay. *Remote Sens. Environ.* 127, 1–13. doi: 10.1016/j.rse.2012.08.016

Kromkamp, J. C., Morris, E. P., Forster, R. M., Honeywill, C., Hagerthey, S., and Paterson, D. M. (2006). Relationship of intertidal surface sediment chlorophyll concentration to hyperspectral reflectance and chlorophyll fluorescence. *Estuar. Coasts* 29, 183–196. doi: 10.1007/Bf02781988

Legendre, P., and Legendre, L. (2012). "Spatial analysis," in *Numerical Ecology*, (Oxford: Elsevier), 785–858.

Lucas, C. H., and Holligan, P. M. (1999). Nature and ecological implications of algal pigment diversity on the molenplaat tidal flat (Westerschelde estuary, SW Netherlands). *Mar. Ecol. Prog. Ser.* 180, 51–64.

Lucas, C. H., Widdows, J., Brinsley, M. D., Salkeld, P. N., and Herman, P. M. J. (2000). Benthic-pelagic exchange of microalgae at a tidal flat. 1. Pigment analysis. *Mar. Ecol. Prog. Ser.* 196, 59–73.

Meleder, V., Rince, Y., Barille, L., Gaudin, P., and Rosa, P. (2007). Spatiotemporal changes in microphytobenthos assemblages in a macrotidal flat (Bourgneuf bay, France). *J. Phycol.* 43, 1177–1190. doi: 10.1111/j.1529-8817.2007.00423.x

Moreira, M. H., Queiroga, H., Machado, M. M., and Cunha, M. R. (1993). Environmental gradients in a southern Europe estuarine system: Ria de Aveiro, Portugal. Implications for soft bottom macrofauna colonization. *Neth. J. Aquat. Ecol.* 27, 465–482.

Morris, E. P. (2005). *Quantifying Primary Production Of Microphytobenthos: Application Of Optical Methods*. Ph. D thesis, University of Groningen, Groningen.

Murphy, R. J., Tolhurst, T. J., Chapman, M. G., and Underwood, A. J. (2008). Spatial variation of chlorophyll on estuarine mudflats determined by field-based remote sensing. *Mar. Ecol. Prog. Ser.* 365, 45–55. doi: 10.3354/Meps07456

Orvain, F., Lefebvre, S., Montepini, J., Sebire, M., Gangnery, A., and Sylvand, B. (2012). Spatial and temporal interaction between sediment and microphytobenthos in a temperate estuarine macro-intertidal bay. *Mar. Ecol. Prog. Ser.* 458, 53–68.

Orvain, F., Sauriau, P. G., Sygut, A., Joassard, L., and Le Hir, P. (2004). Interacting effects of Hydrobia ulvae bioturbation and microphytobenthos on the erodibility of mudflat sediments. *Mar. Ecol. Prog. Ser.* 278, 205–223. doi: 10.3354/Meps278205

Paterson, D. M., Wiltshire, K. H., Miles, A., Blackburn, J., Davidson, I., Yates, M. G., et al. (1998). Microbiological mediation of spectral reflectance from intertidal cohesive sediments. *Limnol. Oceanogr.* 43, 1207–1221.

Pebesma, E. J. (2004). Multivariable geostatistics in S: the gstat package. *Comput. Geosci.* 30, 683–691.

Riera, P., Stal, L. J., and Nieuwenhuize, J. (2000). Heavy delta N-15 in intertidal benthic algae and invertebrates in the Scheldt Estuary (The Netherlands): effect of river nitrogen inputs. *Estuar. Coast. Shelf Sci.* 51, 365–372. doi: 10.1006/ecss.2000.0684

Rijkswaterstaat (2017). *Toelichting op de zoute ecotopenkaart Westerschelde 2016: biologische monitoring zoute rijkswateren*. Delft: Rijkswaterstaat - Centrale Informatievoorziening.

Rossi, R. E., Mulla, D. J., Journel, A. G., and Franz, E. H. (1992). Geostatistical tools for modeling and interpreting ecological spatial dependence. *Ecol. Monogr.* 62, 277–314. doi: 10.2307/2937096

Ryu, J. H., Choi, J. K., and Lee, Y. K. (2014). Potential of remote sensing in management of tidal flats: a case study of thematic mapping in the Korean tidal flats. *Ocean Coast. Manag.* 102, 458–470. doi: 10.1016/j.ocecoaman.2014.03.003

Sabbe, K. (1993). Short-term fluctuations in benthic diatom numbers on an intertidal sandflat in the Westerschelde estuary (Zeeland, The Netherlands). *Hydrobiologia* 26, 275–284.

Sabbe, K., and Vyverman, W. (1991). Distribution of benthic diatom assemblages in the Westerschelde (Zeeland, The Netherlands). *Belg. Journ. Bot.* 124, 91–101.

Sahan, E., Sabbe, K., Creach, V., Hernandez-Raquet, G., Vyverman, W., Stal, L. J., et al. (2007). Community structure and seasonal dynamics of diatom biofilms and associated grazers in intertidal mudflats. *Aquat. Microb. Ecol.* 47, 253–266.

Solan, M., Germano, J. D., Rhoads, D. C., Smith, C., Michaud, E., Parry, D., et al. (2003). Towards a greater understanding of pattern, scale and process in marine benthic systems: a picture is worth a thousand worms. *J. Exp. Mar. Biol. Ecol.* 285, 313–338.

Thrush, S. F., Hewitt, J. E., and Lohrer, A. M. (2012). Interaction networks in coastal soft-sediments highlight the potential for change in ecological resilience. *Ecol Appl* 22, 1213–1223. doi: 10.1890/11-1403.1

Ubertini, M., Lefebvre, S., Gangnery, A., Grangere, K., Le Gendre, R., and Orvain, F. (2012). Spatial variability of benthic-pelagic coupling in an estuary ecosystem: consequences for microphytobenthos resuspension phenomenon. *PLoS One* 7:e44155. doi: 10.1371/journal.pone.0044155

Ubertini, M., Lefebvre, S., Rakotomalala, C., and Orvain, F. (2015). Impact of sediment grain-size and biofilm age on epipelic microphytobenthos resuspension. *J. Exp. Mar. Biol. Ecol.* 467, 52–64.

Underwood, G. J. C., and Kromkamp, J. (1999). Primary production by phytoplankton and microphytobenthos in estuaries. *Adv. Ecol. Res.* 29, 93–153. doi: 10.1016/j.scitotenv.2017.12.184

Van De Koppel, J., Herman, P. M. J., Thoolen, P., and Heip, C. H. R. (2001). Do alternate stable states occur in natural ecosystems? Evidence from a tidal flat. *Ecology* 82, 3449–3461.

Van der Wal, D., Herman, P. M. J., Forster, R. M., Ysebaert, T., Rossi, F., Knaeps, E., et al. (2008). Distribution and dynamics of intertidal macrobenthos predicted from remote sensing: response to microphytobenthos and environment. *Mar. Ecol. Prog. Ser.* 367, 57–72. doi: 10.3354/Meps07535

Van der Wal, D., van Kessel, T., Eleveld, M. A., and Vanlede, J. (2010a). Spatial heterogeneity in estuarine mud dynamics. *Ocean Dyn.* 60, 519–533. doi: 10.1007/s10236-010-0271-9

Van der Wal, D., Wielemaker-van den Dool, A., and Herman, P. M. J. (2010b). Spatial synchrony in intertidal benthic algal biomass in temperate coastal and estuarine ecosystems. *Ecosystems* 13, 338–351. doi: 10.1007/s10021-010-9322-9329

Van der Wal, D., Ysebaert, T., and Herman, P. M. J. (2017). Response of intertidal benthic macrofauna to migrating megaripples and hydrodynamics. *Mar. Ecol. Prog. Ser.* 585, 17–30. doi: 10.3354/meps12374

Weerman, E. J., Herman, P. M. J., and Van de Koppel, J. (2011). Top-down control inhibits spatial self-organization of a patterned landscape. *Ecology* 92, 487–495. doi: 10.1890/10-0270.1

Weerman, E. J., Van Belzen, J., Rietkerk, M., Temmerman, S., Kéfi, S., Herman, P. M. J., et al. (2012). Changes in diatom patch-size distribution and degradation in a spatially self-organized intertidal mudflat ecosystem. *Ecology* 93, 608–618. doi: 10.1890/11-0625.1

Ysebaert, T., Herman, P. M. J., Meire, P., Craeymeersch, J., Verbeek, H., and Heip, C. H. R. (2003). Large-scale spatial patterns in estuaries: estuarine macrobenthic communities in the Schelde estuary, NW Europe. *Estuar. Coast. Shelf Sci.* 57, 335–355. doi: 10.1016/S0272-7714(02)00359-351

Conflict of Interest: The authors declare that the research was conducted in the absence of any commercial or financial relationships that could be construed as a potential conflict of interest.

frontiers in Marine Science

ORIGINAL RESEARCH
published: 23 July 2020
doi: 10.3389/fmars.2020.00520

Mapping the Intertidal Microphytobenthos Gross Primary Production Part I: Coupling Multispectral Remote Sensing and Physical Modeling

Vona Méléder[1], Raphael Savelli[2], Alexandre Barnett[1,2], Pierre Polsenaere[3], Pierre Gernez[1], Philippe Cugier[4], Astrid Lerouxel[1], Anthony Le Bris[1,5], Christine Dupuy[2], Vincent Le Fouest[2] and Johann Lavaud[2,6]*

[1] *Mer Molécules Santé (EA 21 60), Université de Nantes, Nantes, France,* [2] *LIENSs 'Littoral ENvironnement et Sociétés' UMR 7266, Institut du Littoral et de l'Environnement, CNRS/Université de La Rochelle, La Rochelle, France,* [3] *Laboratoire Environnement Ressources des Pertuis Charentais (LER-PC), Ifremer, L'Houmeau, France,* [4] *Département Dynamiques de l'Environnement Côtier, Laboratoire d'Ecologie Benthique, Ifremer, Plouzané, France,* [5] *Centre d'Etude et de Valorisation des Algues (CEVA), Pleubian, France,* [6] *Takuvik Joint International Laboratory UMI3376, CNRS (France) & ULaval (Canada), Département de Biologie, Université Laval, Québec, QC, Canada*

OPEN ACCESS

Edited by:
Angel Borja, Technological Center Expert in Marine and Food Innovation (AZTI), Spain

Reviewed by:
Peter M. J. Herman, Delft University of Technology, Netherlands
Alfonso Corzo, University of Cádiz, Spain

***Correspondence:**
Vona Méléder
vona.meleder@univ-nantes.fr

Specialty section:
This article was submitted to Marine Ecosystem Ecology, a section of the journal Frontiers in Marine Science

Received: *20 December 2019*
Accepted: *08 June 2020*
Published: *23 July 2020*

Citation:
Méléder V, Savelli R, Barnett A, Polsenaere P, Gernez P, Cugier P, Lerouxel A, Le Bris A, Dupuy C, Le Fouest V and Lavaud J (2020) Mapping the Intertidal Microphytobenthos Gross Primary Production Part I: Coupling Multispectral Remote Sensing and Physical Modeling. Front. Mar. Sci. 7:520. doi: 10.3389/fmars.2020.00520

The gross primary production (GPP) of intertidal mudflat microphytobenthos supports important ecosystem services such as shoreline stabilization and food production, and it contributes to blue carbon. However, monitoring microphytobenthos GPP over a long-term and large spatial scale is rendered difficult by its high temporal and spatial variability. To overcome this issue, we developed an algorithm to map microphytobenthos GPP in which the following are coupled: (i) NDVI maps derived from high spatial resolution satellite images (SPOT6 or Pléiades), estimating the horizontal distribution of the microphytobenthos biomass; (ii) emersion time, photosynthetically active radiation (PAR), and mud surface temperature simulated from the physical model MARS-3D; (iii) photophysiological parameters retrieved from Production–irradiance (P–E) curves, obtained under controlled conditions of PAR and temperature, using benthic chambers, and expressing the production rate into mg C h^{-1} m^{-2} $ndvi^{-1}$. The productivity was directly calibrated to NDVI to be consistent with remote-sensing measurements of microphytobenthos biomass and was spatially upscaled using satellite-derived NDVI maps acquired at different seasons. The remotely sensed microphytobenthos GPP reasonably compared with *in situ* GPP measurements. It was highest in March with a daily production reaching 50.2 mg C m^{-2} d^{-1}, and lowest in July with a daily production of 22.3 mg C m^{-2} d^{-1}. Our remote sensing algorithm is a new step in the perspective of mapping microphytobenthos GPP over large mudflats to estimate its actual contribution to ecosystem functions, including blue carbon, from local and global scales.

Keywords: microphytobenthos, intertidal mudflat, gross primary production, remote sensing, NDVI, modeling

INTRODUCTION

Tidal mudflats are soft sediment coastal marine ecosystems that undergo regular tidal inundation. Their bare surface is colonized by biofilms constituted of photosynthetic microorganisms (microalgae and cyanobacteria), collectively known as microphytobenthos (MPB) (e.g., MacIntyre et al., 1996; Paterson and Hagerthey, 2001). Under temperate latitudes, MPB assemblages are mainly dominated by diatoms that form a brown dense biofilm at the sediment surface during daytime low tides (MacIntyre et al., 1996; Underwood and Kromkamp, 1999). Intertidal flats provide important ecosystem services such as biodiversity depositories, storm protection, and shoreline stabilization (Murray et al., 2018; Legge et al., 2020). They also provide essential food resource for higher trophic levels, from benthic fauna to birds (Herman et al., 2000; Kang et al., 2006; Jardine et al., 2015), and for pelagic organisms when MPB is resuspended in the water column (Perissinotto et al., 2003; Krumme et al., 2008). As such, they contribute to the so-called blue carbon (Otani and Endo, 2019; Legge et al., 2020). With sand and rocky flats, tidal mudflats are one of the most extensive coastal ecosystems, with a recent global area estimation of at least 127,921 km^2 (Murray et al., 2018). With a global annual gross primary production (GPP) estimated to be in the order of 0.5 Gt C y^{-1} (Cahoon, 1999), MPB are of key importance for local and global coastal ecosystem functions, including carbon budget. However, their actual contribution remains unknown, due to the lack of estimation at ecosystem scale (i.e., the entire mudflat). A more comprehensive mapping of these intertidal mudflats is therefore needed to improve the accuracy of coastal carbon budgets (Legge et al., 2020).

The spatial heterogeneity of intertidal mudflats, as well as the high degree of temporal variability in process rates, adds to the challenges of accurately quantifying carbon stocks and flows in coastal areas (Legge et al., 2020). MPB spatiotemporal distribution is highly variable, as it is driven by highly variable physical [photosynthetically active radiation (PAR), mud surface temperature (MST), tides, and waves] and biological (grazing, biostabilization, and bioturbation) factors (e.g., Pinckney and Zingmark, 1991; Kingston, 2002; Cohn et al., 2003; Consalvey et al., 2004; Spilmont et al., 2007; Coelho et al., 2009, 2011; Serôdio et al., 2012; Savelli et al., 2018). Such a variability impedes on an accurate and robust assessment of MPB contribution to the coastal and global marine carbon cycle. To assess MPB biomass and/or GPP, tidal mudflat measurements are usually limited to single-point sampling (e.g., Vieira et al., 2013; Orvain et al., 2014; Cartaxana et al., 2015; Pniewski et al., 2015). Station-based sampling makes it possible to locally assess MPB temporal dynamics, but it fails to describe MPB spatial and temporal variations at the scale of the entire mudflat (Forster and Kromkamp, 2006). Whereas only few studies have resolved MPB variability using sampling campaigns requiring time and important logistical resources (i.e., Guarini et al., 1998; Ubertini et al., 2012), satellite remote sensing appears to be the most efficient upscaling tool. Since the end of the last century, starting with Jobson et al. (1980) initiative, airborne and spaceborne remote sensing methods have been developing increasingly and are now more widely used for MPB studies (Méléder et al., 2003b; van der Wal et al., 2010; Brito et al., 2013; Benyoucef et al., 2014; Echappé et al., 2018). Remote sensing data can cover large spatial scales (from one meter to several kilometers), and vegetation indices such as the normalized difference vegetation index (NDVI) were successfully applied to multispectral broadband satellite sensors to map MPB biomass at the scale of a whole mudflat (e.g., Méléder et al., 2003b; van der Wal et al., 2010; Brito et al., 2013; Benyoucef et al., 2014; Echappé et al., 2018). However, although it is common use to estimate terrestrial vegetation GPP (e.g., Goetz et al., 1999; Huemmrich et al., 2010) and oceanic GPP (e.g., Babin et al., 2015) from space, remote sensing has never been used to map MPB GPP over an entire mudflat before the study by Daggers et al. (2018). While this recent study represents a major contribution to the field, their GPP model does not take into account the seasonal variability of photophysiology (Kromkamp and Forster, 2006) and also strongly depends on the relationship between NDVI and sediment MPB chlorophyll-*a* (Chl *a*) concentration, which is known to be highly sensitive to Chl *a* sampling depth, MPB vertical distribution, and MPB small-scale horizontal variability (Jesus et al., 2006). In order to resolve the NDVI versus Chl *a* issue, we propose here an original method where GPP is directly calibrated to NDVI. First, a GPP algorithm was obtained using laboratory measurements of NDVI and carbon fluxes (mg C h^{-1} m^{-2}) fitted on Production–Irradiance (P–E) curves. Second, the seasonal variability of the photophysiological parameters was taken into account in a series of laboratory experiments performed during winter, spring, and summer. Third, the NDVI-calibrated GPP algorithm was applied to high-resolution satellite images acquired during the three seasons and coupled to emersion time, mud surface temperature (MST), and light intensity (PAR) obtained from the physical model for Applications at Regional Scale (MARS-3D). Finally, we compared the remotely sensed GPP with field observations, and we discussed the ability of our algorithm to map MPB GPP at mudflat scale and to provide new insights on the role of MPB in the coastal carbon cycle.

MATERIALS AND METHODS

Study Site: Brouage Mudflat

The study site was located in the Pertuis Charentais Sea, a shallow semi-enclosed sea located on the French Atlantic coast (**Figure 1**). The tidal regime is semi-diurnal and macrotidal. The tidal range reaches up to ∼6 m during spring tides. This study focused on the Brouage mudflat which extends over 42 km^2 in the southeastern part of the area (**Figure 1**). The mudflat sediment is composed of very fine and cohesive grains (median grain size is 17 μm and 85% of grains have a diameter <63 μm; Bocher et al., 2007) distributed on a gentle slope (∼1/1000; Le Hir et al., 2000).

Periods of Investigation

The investigated periods for MPB primary production estimation by multispectral remote sensing and modeling were selected in accordance to the seasonal cycle of MPB biomass (**Figure 2**).

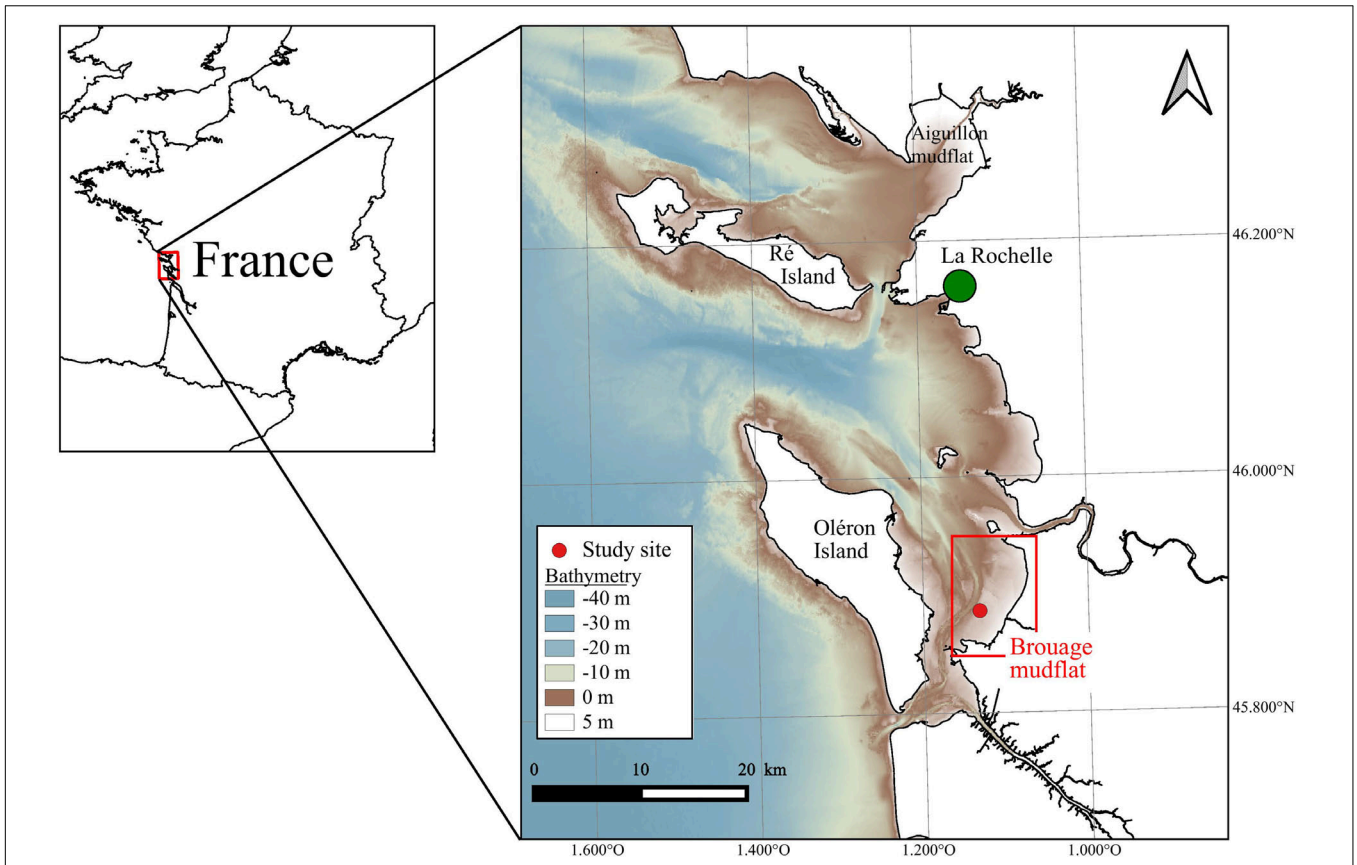

FIGURE 1 | The Pertuis Charentais, and the Brouage mudflat, France. The red point indicates the study site. Bathymetry is used in MARS-3D model (source: SHOM).

This cycle was extracted from a time series from 2000 to 2015, obtained by the processing of 582 low-tide images from the Moderate Resolution Imaging Spectroradiometer (MODIS) onboard the Terra satellite. MODIS Terra data [namely the Surface Reflectance Daily L2G Global 250 m SIN Grid product (MOD09GQ)] were used because the morning pass [10 to 11 h Universal Time (UT)] was better suited than the MODIS Aqua satellite afternoon pass to observe the emerged mudflat during spring low tides at our study site. The MOD09GQ product provides surface reflectance data in a red band (R_{red}, from 620 to 670 nm) and a near-infrared (NIR) band (R_{NIR}, from 841 to 876 nm) at a spatial resolution of 250 m and with a revisit time of 1 to 2 days. This medium spatial resolution has been previously demonstrated to be valid for the study of MPB seasonal dynamics in large intertidal areas (van der Wal et al., 2010). For the present study, 582 MODIS low-tide images were initially downloaded, from which 343 cloud-free scenes were eventually selected. An NDVI (Eq. 1) was computed as a proxy of MPB biomass. The NDVI quantifies the changes in the reflectance's spectral shape due to Chl *a* absorption in the red band and to the absence of absorption by pigments in the NIR plateau (Méléder et al., 2003b; Brito et al., 2013; Benyoucef et al., 2014; Echappé et al., 2018). The NDVI is a widely used vegetation index, relatively robust to the variability in sediment backgrounds (Barillé et al., 2011) and mainly driven by changes in algal biomass (i.e., the higher vegetation biomass, the higher the NDVI). Several methods have been developed to discriminate the MPB from other Chl-bearing intertidal vegetation (e.g., seagrass and macroalgae), from simple reflectance thresholds (Méléder et al., 2003b) to more complex clustering methods (Hossain et al., 2015). As previous field studies did not report significant areas colonized by macrophytes in the MPB-dominated Brouage mudflat (Lebreton, personal communication), the NDVI-derived biomass was non-ambiguously assigned here to MPB biofilms.

$$\mathrm{NDVI} = \frac{R_{NIR} - R_{red}}{R_{NIR} + R_{red}} \quad (1)$$

From this NDVI time series, three periods were selected for field campaigns and for laboratory P–E curve calibration (**Figure 2**): March, when MPB biomass reaches its highest level; July, corresponding to the lowest level; and May, corresponding to an intermediary level. For the three periods, the weather was also expected to be contrasted: low temperature and light intensity in March, higher temperature and light intensity in July, and intermediate temperature and light in May. Field campaigns occurred the 5th and 6th of May, 2015; the 2nd and 3rd of July, 2015; and the 5th of March, 2018. They included *in situ* measurements and sediment sampling for further laboratory experiments.

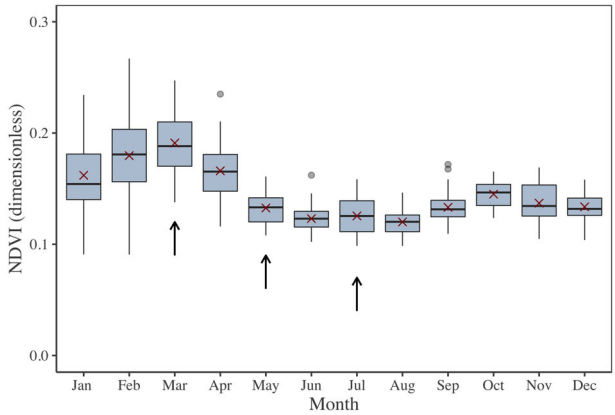

FIGURE 2 | NDVI 2000–2015 time series illustrating the MPB biomass seasonal cycle for the Brouage mudflat. NDVI was retrieved from Terra MODIS reflectance. Box plots were calculated for each month. The red crosses are the monthly average. Arrows show the three period of investigation (March, May, and July).

Gross Primary Production (GPP) Measurements

Field Campaigns

The sampling station was located at the "Merignac" site, in the Brouage mudflat (**Figure 1**, red dot 45°53′11.20″N; 1°7′538″W). CO_2 fluxes were measured at the air/sediment interface (enclosed sediment area of 165 cm^2 down to 5-cm depth) using the closed-chamber method described in Migné et al. (2002). Air CO_2 concentration (ppm) changes were monitored in the benthic chamber (0.8 L) continuously over an incubation period of 20 to 30 min, using an infrared gas analyzer (IRGA Li-840A, LI-COR, Lincoln, NE, United States) connected to a datalogger (Li-1400, LI-COR) with a 30-s frequency. CO_2 flux was calculated as the slope of the linear regression of CO_2 concentration (μmol mol^{-1}) against time (min) and expressed in mg C m^{-2} h^{-1}.

Transparent chambers were used to estimate the net benthic community production [NCP; balance between the community GPP and the community respiration (CR)]. Dark chambers were used to estimate the CR. Light and dark incubations were performed successively. Due to the tidal cycle duration, a maximum of four incubations were done per day (two transparents and two darks). The GPP expressed in mg C m^{-2} h^{-1} was computed following Migné et al. (2002) (Eq. 2):

$$GPP = NCP + CR \quad (2)$$

The biomass-specific productivity (P^b) was then computed from GPP. Here, the NDVI was used as a proxy of MPB biomass, and P^b was directly expressed in C m^{-2} h^{-1} $ndvi^{-1}$ (Eq. 3):

$$P^b = GPP/NDVI \quad (3)$$

The NDVI was computed from MPB reflectance spectra acquired using a JAZ (Ocean Optics, Largo, FL, United States) spectroradiometer (200–1100 nm; sampling: 0.3 nm; spectral resolution: 0.3–10 nm FWHM) pointed at an area of the MPB biofilm close to the benthic chambers. Because the spectral resolution of this detector was higher than a satellite multispectral detector, NDVI calculation was adapted (Eq. 1): the red reflectance, R_{red}, was considered as the averaged value of data at 675 nm ± 3 nm and the NIR reflectance, R_{NIR}, as the average at 750 nm ± 3 nm (Méléder et al., 2003a, 2010). NDVI was measured during the same period of each light incubations (equal to NCP estimation), and a time-averaged NDVI was used to standardize GPP in Eq. 3.

Synchronously, the incident photosynthetically active radiation (PAR, from 400 to 700 nm, in μmol photons m^{-2} s^{-1}) and mud surface temperature (MST, in °C) were continuously (every 30 s) measured (LS-C sensor plugged to a ULM-500 data-logger, Walz, Effeltrich, Germany) at the sediment surface, near to the chambers and to the area of reflectance acquisition and measurement of MPB Chl *a* biomass content. The latter was measured in the first 250 μm of sediment continuously sampled (every 5–10 min) by the "crème brulée" technique (Laviale et al., 2015). This technique, derived from the contact-core technique (Ford and Honeywill, 2002), consists of freezing by contact the top surface of sediment (here 250 μm) with a metal surface (1.5 cm^2) previously immersed in liquid nitrogen. The obtained sediment disks were stored in liquid nitrogen during field campaign and were kept at −80°C in the laboratory until pigment analysis. After freeze-drying of the sediment disks, pigments were extracted in a cold mixture (4°C) of 90% methanol/0.2 M ammonium acetate (90/10 vol/vol) and 10% ethyl acetate. Injection, HPLC device (Hitachi Lachrom Elite, Tokyo, Japan), pigment identification, and quantification were detailed before (Roy et al., 2011; Barnett et al., 2015). The Chl *a* amount in sediment was standardized to the sampled surface (1.5 cm^2) in order to be expressed in mg Chl *a* m^{-2}.

In an aim to assess MPB photophysiological status at tide time scale and check if changes occurred during incubation time, several photophysiological parameters (F_v'/F_m', rETR, α, and E_k) were measured continuously (every 5 to 10 min) using a Water-PAM fluorimeter (Fiber version, Walz, Effeltrich, Germany). For details, see **Supplementary Appendix A**. All *in situ* data (GPP, PAR, MST, biomass, and photophysiological parameters) were used as ground-truthing for laboratory P–E curve calibration and the remotely sensed GPP validation.

Laboratory Experiment for Production–Irradiance Curve Calibration

During the three field campaigns, the upper layer (approx. the top first centimeter) of sediment was collected and brought back to the laboratory. The mud was cleaned of fauna by sieving through a 500-μm mesh. The sediment was homogenized by thoroughly mixing and was spread as plane layer in plastic trays of 4-cm depth (Serôdio et al., 2012). A water layer was added for the night and sediment was left undisturbed overnight. The next morning, the water layer was manually removed by a syringe 3 h before the lowest water level timing expected *in situ* (i.e., at sampling site) and trays were kept in darkness at 22 ± 1°C. Experimentation started 1 h later, when the MPB biofilm started to darken in color at the sediment surface. It consisted of lighting up the trays one by one with an LED panel (LED Light SL 3500-E, Photo System

Instrument, Tøeboò, Czechia) at a given PAR (=E), varied from 5 to 2,200 μmol photons m^{-2} s^{-1} for 30 min at 22 ± 1°C, exactly in the optimal temperature range for MPB production (according to Blanchard et al., 1997). During the lightening, NCP was estimated through transparent benthic chamber incubations, following the same method as the field measurements (Migné et al., 2002). At the beginning and end of each light incubation, NDVI, sediment Chl *a* content, and photophysiological parameters using PAM-fluorimetry were measured the same way as *in situ* (see above). After illumination, CR was measured during the 20- to 30-min dark benthic chamber incubations. The same process was repeated as long as MPB was present at the surface of sediment (i.e., with similar measured NDVI) and for 8 to 11 Es. For each E, GPP was calculated as the sum between NCP and CR as done *in situ* (Eq. 2, Migné et al., 2002). GPP was then standardized by NDVI in order to directly express P^b in mg C m^{-2} h^{-1} $ndvi^{-1}$ (Eq. 3), so that the GPP algorithm could be consistently applied to satellite-derived NDVI maps (see section "Coupling Remote Sensing Data and Modeling: the GPP-Algorithm").

For the three campaigns (March, May, and July), a season-dependent P^b was obtained. For each season, several P–E models widely used in the literature [namely Platt et al. (1980), Eilers and Peeters (1988), Steele (1962), Platt and Jassby (1976), and the modified version of Platt and Jassby (1976)] were fitted to the P–E curves to select the best model to be integrated into the GPP-algorithm. The selection of the most appropriate model was done using the determination coefficient (r^2) and residual standard deviation (RSD) calculated using the in R-software. For details, see **Supplementary Appendix B**.

Data Analysis for Field Campaign and Laboratory Experiments

All data are available for download: 10.5281/zenodo0.3862068. Changes in MPB biomass (NDVI and Chl *a* content), photophysiological parameters measured by PAM-fluorimetry (F_v'/F_m', α, rETRm and E_k) and GPP and P^b were detected at a tidal time scale (i.e., during incubation) and at a monthly scale (March, May, and July). Knowing the potential high variability of environmental conditions (i.e., PAR, MST, and light dose calculated from PAR and emersion time), the objective was to check if biomass and photophysiological status changed drastically or not during the light incubation estimating GPP as well *in situ* and at the laboratory. In this aim, Spearman or Pearson correlations, and ANOVA or Kruskal–Wallis (KW) test were performed on all data using R software, after a Shapiro test, to test data normality. For details, see the **Supplementary Appendix A**.

Coupling Remote Sensing Data and Modeling: the GPP-Algorithm

The successive steps in the remotely sensed GPP procedure are described below and synthesized in **Figure 3**.

Remote Sensing Data

High-resolution satellite remote sensing was used to upscale the GPP algorithm to the whole mudflat, using the season-dependent, NDVI-specific P^b parameter. Multispectral images were selected from the SPOT, Landsat, and Pléiades archives following three acquisition criteria: (1) acquisition day as close as possible to the field campaign day, (2) acquisition time as close as possible to low tide timing (i.e., the lowest water height, when mudflat was the most exposed), and (3) cloud-free observation (cloud cover < 10%) with an almost zenithal sun. These criteria allowed us to select three images from the SPOT6 and Pléiades archive (one per field campaign, **Table 1**). The top-of-atmosphere data were converted into surface reflectance using the fast line of sight atmospheric analysis of spectral hypercubes (FLAASH, Matthew et al., 2000) atmospheric correction using the ENVI software. For a consistent analysis of the SPOT and Pléiades images, the same FLAASH parameters were applied to each image: United States atmospheric model with a visibility of 40 km, and a maritime aerosol model. The spectral images were registered in the WGS 84 UTM 30N coordinate system. Finally, the NDVI was calculated from the surface reflectance following Eq. (1) to map MPB biomass (Méléder et al., 2003b). As the SPOT6 and Pléiades data have similar spectral characteristics, the NDVI was not recalibrated between the two sensors (Echappé et al., 2018). The satellite-derived NDVI maps were used as inputs for the GPP-algorithm, in complement to other data (**Figure 3**).

Tidal Height and PAR Modeling

The tidal height and PAR were simulated over the Brouage mudflat by the 3D hydrodynamical MARS-3D (**Figure 3**). The bathymetry was extracted from the model numerical grid. The Navier–Stokes primitive equations were solved under assumptions of Boussinesq approximation, hydrostatic equilibrium, and incompressibility (Blumberg and Mellor, 1987; Lazure and Dumas, 2008). The numerical domain of the Pertuis Charentais Sea consisted of 100- × 100-m grid cells discretized over 20 sigma-levels. For details, see Lazure and Dumas (2008). The meteorological forces (i.e., 10 m wind speed, 2 m air temperature and relative humidity, atmospheric pressure at sea level, nebulosity, and solar fluxes) used to constrain MARS-3D were extracted from the Meteo France AROME model[1]. The tidal model CST FRANCE, developed by the SHOM (Simon and Gonella, 2007), forced MARS-3D at the domain boundaries. The tidal model solved the amplitude and phase of 115 harmonic constituents. Initial and boundary conditions of seawater temperature, salinity, current velocity, and sea surface height were extracted from the MANGAE 2500 Ifremer model of 2.5-km lateral resolution (Lazure et al., 2009). Simulated tidal height associated to bathymetry allowed to estimate the beginning, the end and thus the duration of emersion period of each grid cells. During emersion period, PAR intensity varied every 10 min at 100- × 100-m spatial resolution, but values were interpolated on the horizontal grid of satellite data (2 or 6 m, see **Table 1**) and used as inputs in the GPP-algorithm (**Figure 3**).

Mud Surface Temperature Modeling

The simulated mud surface temperature (MST) was obtained from the coupling of the MST model of Savelli et al. (2018)

[1]https://donneespubliques.meteofrance.fr

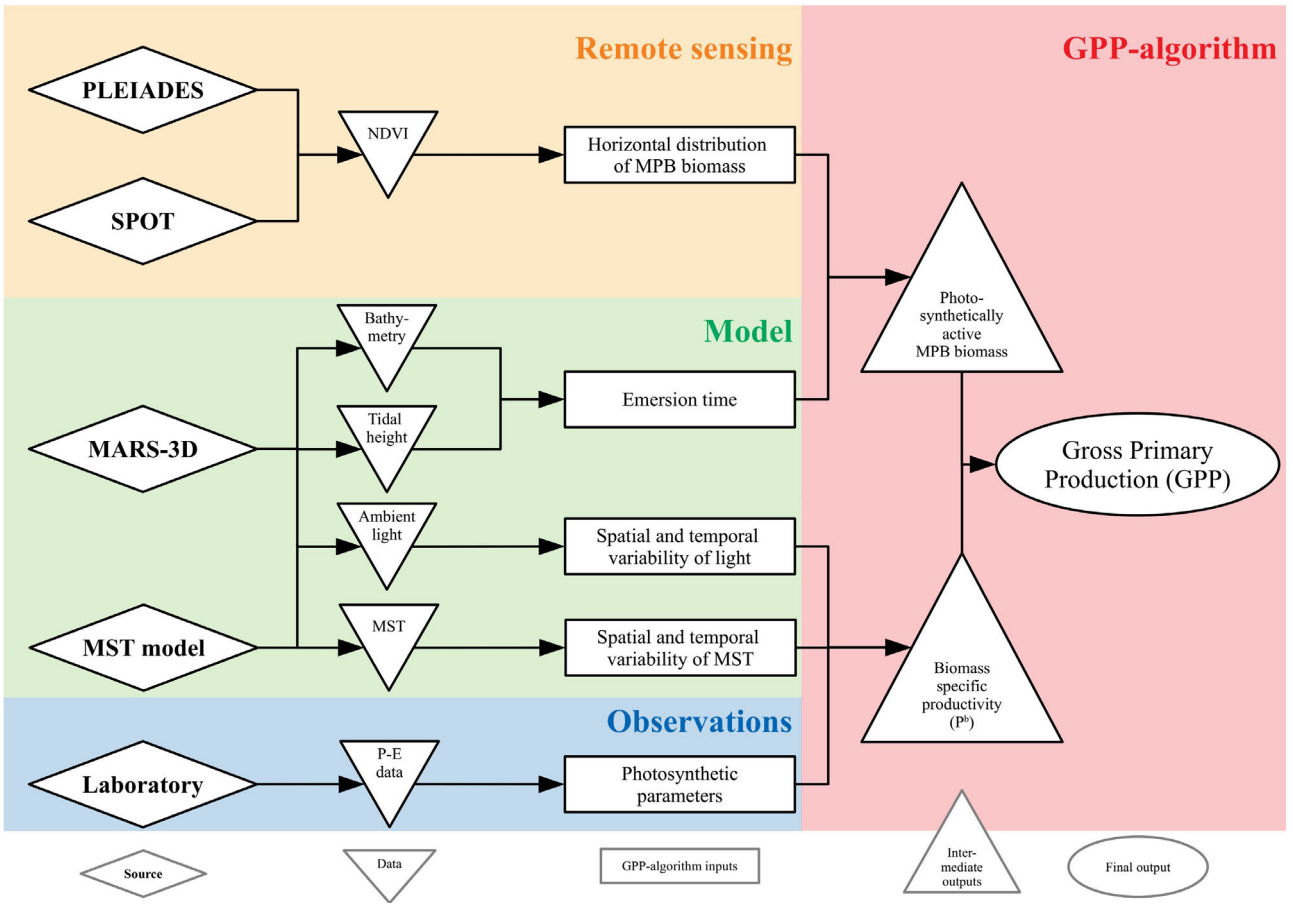

FIGURE 3 | Conceptual scheme of the MPB GPP-algorithm.

TABLE 1 | Satellite image characteristics used to map the horizontal distribution of the MPB biomass, expressed in NDVI.

Satellite	Spatial resolution (m)	Blue band (nm)	Green band (nm)	Red band (nm)	NIR band (nm)	Acquisition day (d/m/y)	Acquisition time (UT)	Low tide time (UT)	Water height (m)
SPOT 6	6	455–525	530–590	625–695	760–890	18/05/15	10:54	09:36	0.80
Pléiades	2	430–550	490–610	600–720	750–950	17/07/15	11:11	10:30	1.30
						03/03/18	11:25	10:46	0.44

with MARS-3D. The simulated heat fluxes in a 1-cm-deep sediment layer were solved by thermodynamic equations detailed in Savelli et al. (2018). The horizontal fluxes of heat were neglected. During exposure periods, the simulated MST resulted from heat exchanges between the sun, the atmosphere, and the sediment surface; from the conduction between mud and air; and from evaporation. The simulated MST of immersed mud was set to the temperature of the overlying seawater simulated by MARS-3D since MST was not used in this study. The MST differential equation was solved by the MARS-3D numerical scheme. For more details, see Savelli et al. (2018). During emersion period, MST varied at the same time resolution than PAR intensity (10 min and 100 × 100 m). But, as PAR, the MST values were interpolated on the horizontal grid of satellite data (2 or 6 m, see **Table 1**) and was used as input in the GPP algorithm (**Figure 3**).

GPP Algorithm

Finally, the GPP algorithm (**Figure 3**) coupled NDVI maps from SPOT and Pléiades scenes with forces by hydrodynamical MARS-3D. Whereas the NDVI estimates the horizontal distribution of MPB biomass, the MARS-3D model simulates the emersion time over the whole mudflat using the bathymetry and the tidal height. Coupled with the MPB biomass, the emersion time determined the photosynthetically active biomass at the mud surface. The MPB biomass detected by satellite was assumed to correspond to the fully established biofilm during the daytime low tide (total photosynthetically active

biomass). The migration behavior of MPB was introduced in the model through a progressive establishment of the total photosynthetically active biomass at the sediment surface, known to take place during 20 min at Brouage mudflat (Herlory et al., 2004). The MPB started to migrate at the sediment surface just after water removal to reach 50% of the total amount of the photosynthetically active biomass (=NDVI/2) after 10 min of emersion of respective grid cells. After 20 min, the MPB biofilm at the sediment surface was fully formed. 20 min before the immersion, downward migration started and only the half of the total photosynthetically active biomass was still at the surface 10 min before immersion. No biomass was at the surface when water overlaid the sediment. PAR and MST simulated by MARS-3D were used to constrain the algorithm: the selected P–E model and its respective parameters values fitted on the laboratory measurements were used to compute the P^b according to the simulated light conditions. The effect of MST was simulated using the Blanchard et al. (1996) model to compute the P^b variations according to the simulated temperature. Finally, combined with the horizontal distribution of the MPB biomass of the NDVI maps, the P^b (mg C m^{-2} h^{-1} $ndvi^{-1}$) was further used to map the remotely sensed GPP (mg C m^{-2} h^{-1}). The time resolution was 10 min (following PAR and MST variations), whereas the spatial resolution was the one of the SPOT or Pléiades image (2 or 6 m, see **Table 1**).

The current configuration of the GPP-algorithm was consistent only for intertidal mudflats composed by very fine cohesive grains over the Brouage mudflat (Poirier et al., 2010). Consequently, no-muddy areas were excluded of the GPP-algorithm and MST model used was developed and validated for the mud only (Savelli et al., 2018). Therefore, laboratory and *in situ* measurements were conducted only on muddy sediment. The GPP maps thus corresponded to MPB assemblages known to be dominated by epipelic diatoms at the study site (Haubois et al., 2005; Du et al., 2017).

GPP Maps Validation

The validation of the GPP model was performed in three steps for each seasonal experiment, using the field data acquired at the study site (see section "Gross Primary Production (GPP) measurements"). First, the simulated MST and PAR were compared to *in situ* measurements using a Mann Whitney (MW) test to assess the accuracy of the physical model. Second, the satellite derived NDVI was validated against field measurements. The GPP was then computed from satellite-derived NDVI maps coupled with the modeled PAR and MST data. The remotely sensed GPP maps were averaged hourly (mg C m^{-2} h^{-1}) over the emersion period, as well as daily-integrated period (mg C m^{-2} d^{-1}). Finally, the hourly remotely sensed GPP data was compared to *in situ* GPP measurement using a MW test.

To ensure that the delay between measurements for P–E calibration and image acquisition (2, 13, and 14 days in March, May, and July, respectively) was not an issue, simulated PAR were averaged during daytime emersion periods 2 weeks before each sampling/measurement session and image acquisition to be compared (MW tests). The main limitation was a change in physiology and metabolic acclimation status of MPB cells due to a change in light and temperature conditions during this delay, preventing the use of P–E photophysiological parameters retrieved from laboratory experiments to calibrate images acquired several days later.

RESULTS

Microphytobenthos GPP Variation Between Months

Field Campaigns

During field campaigns, PAR intensity and MST were significantly different between months (**Figures 4a,b**; KW test, $p \leq 0.001$). Minimum values were mainly measured in March for PAR and MST with 624 ± 10 µmol photons m^{-2} s^{-1} (mean ± SE) and 15.7 ± 0.1°C, respectively, whereas maximum values were reached in May for PAR ($1{,}509 \pm 27$ µmol photons m^{-2} s^{-1}) and July for MST (30.7 ± 0.2°C) (**Figures 4a,b**). According to its seasonal cycle (**Figure 2**), MPB biomass was higher in March than in May and July (KW test, $p \leq 0.001$) with averaged NDVI values and Chl *a* sediment content of 0.61 ± 0.01 and 95.2 ± 3.1 mg m^{-2}, respectively (**Figures 4c,d**). The GPP did not vary significantly among campaigns, although the minimum value was measured in March, and the highest was measured in July (**Figure 4e**). When GPP was standardized by NDVI to be expressed into biomass-specific productivity (P^b), this difference was more visible (**Figure 4f**) even if it was not significant (KW test, $p = 0.1$). Regarding photophysiological parameters measured by PAM-fluorimetry (F_v'/F_m', α, rETRm, and E_k), see **Supplementary Appendix A**. At the tidal scale, biomass (NDVI and Chl *a* content), but also PAM photophysiological parameters (F_v'/F_m', α, rETRm, and E_k) changed with PAR, light dose, and MST, illustrating the rapid responses of MPB (behavioral migration and/or physiology) to environmental conditions.

Laboratory Measurements for P–E Curve Calibration

During laboratory experiments, whereas temperature and PAR were controlled, the MPB biomass, expressed in NDVI or Chl *a* sediment content, changed with the sampling campaign date; as for *in situ*, it was the highest in March, with an averaged value of 0.57 ± 0.01 for NDVI and 97.7 ± 5.5 mg Chl *a* m^{-2} (three-way ANOVA, $p \leq 0.001$; **Figure 5** and **Supplementary Table A3**). The biomass at the sediment surface of the plastic trays globally did not change between PAR tested and during incubation time for a given month (see **Supplementary Table A3** for details). Consequently, GPP measured from benthic chamber incubations for each sediment tray were considered to correspond to a same MPB biomass. Biomass specific productivity, P^b was then obtained by dividing GPP by the averaged NDVI value over the sediment trays for each month: 0.57 ± 0.01 in March, 0.08 ± 0.01 in May, and 0.20 ± 0.01 in July (**Supplementary Figure A3a**). The shape of the relationship between P^b and the irradiance provided by artificial lighting (i.e., P–E curves) varied with seasons (**Figure 5**), as well the fitted photophysiological parameters from the five P–E models tested (**Supplementary Table B1**). The high r^2 and low RSD values demonstrated that

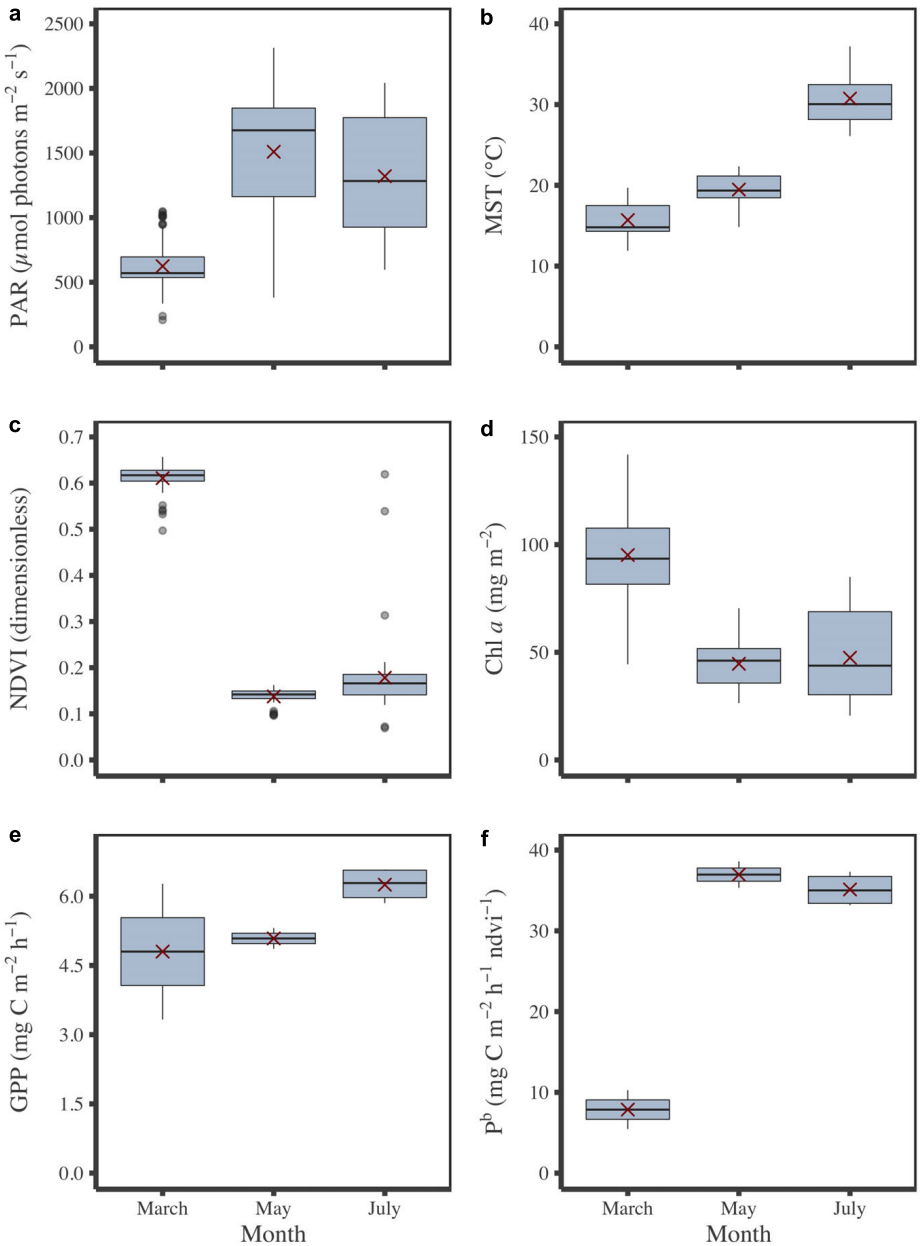

FIGURE 4 | Monthly variations of environmental and MPB parameters measured *in situ*. PAR **(a)**, MST **(b)**, biomass in NDVI **(c)** and Chl *a* content **(d)**, GPP **(e)** and P^b **(f)**. Red crosses correspond the mean values for the corresponding period.

all P-E models fitted well with the laboratory measurements (**Supplementary Table B2**). Because it exhibited the best fit to P–E laboratory measurements, the Eilers and Peeters (1988) model was selected to estimate and map remotely-sensed GPP using the GPP-algorithm.

Mapping Microphytobenthos GPP From NDVI Maps

Overall, SPOT and Pléiades provided consistent spatial distribution of MPB biomass, with a higher NDVI in the middle and lower areas of the mudflat than in the upper shore, especially in March and May (**Figure 6**). The Pléiades-derived NDVI varied from 0 to 0.4, with an averaged value of 0.2 ± 0.09 in March and of 0.14 ± 0.05 in July (**Figures 6a,c**), whereas the SPOT6-derived NDVI varied from 0 to 0.3, with an averaged value of 0.14 ± 0.05 in May (**Figure 6b**). Besides the seasonal variability, the difference in the sensors' spatial resolution could also partly explain the differences between SPOT6 and Pléiades. Compared to Pléiades (2 m), the lower spatial resolution of SPOT6 (6 m) smoothed out the fine-scale distribution of MPB biofilms, thus resulting in lower NDVI averages.

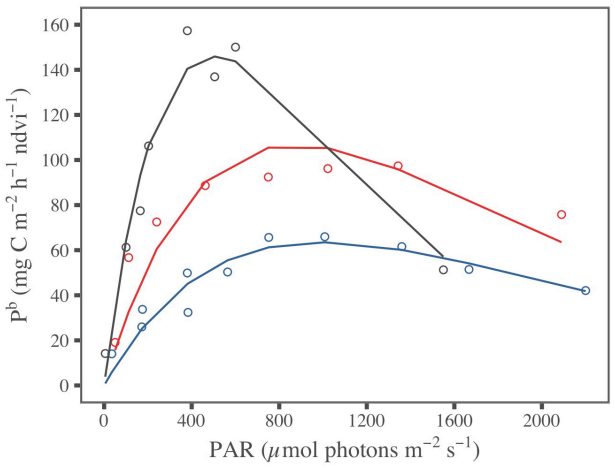

FIGURE 5 | Measured (dot) and predicted (line) biomass specific productivity (P^b) standardized by NDVI, fitted with the Eilers and Peeters (1988) P–E model for the three periods of investigation: March (blue), May (gray), and July (red).

Spatially resolved GPP rates were then modeled from the satellite-derived NDVI maps for each season (**Figure 7**). The short-scale temporal variability of the production factors was taken into account using the hourly PAR and MST MARS-3D simulations and the laboratory P–E curves (**Figure 5** and **Supplementary Table B1**). For each date of satellite acquisition, remotely sensed GPP was averaged over the daytime emersion period (**Figures 7a–c**) and eventually integrated to yield daily GPP maps (**Figures 7d–f**). GPP was at its maximum in March and its minimum in July (**Figures 7a,c**). The most productive areas of the mudflat were the middle and lower shores, with values up to 14.4 mg C m^{-2} h^{-1} in March and 10.8 mg C m^{-2} h^{-1} in May (**Figures 7a,b**). The upper shore was less productive with an hourly GPP of ∼7.5 mg C m^{-2} h^{-1} in March and ∼6.0 mg C m^{-2} h^{-1} in May (**Figures 7a,b**). The hourly GPP exhibited no spatial pattern in July, and GPP was low over the entire mudflat (∼1.8 mg C m^{-2} h^{-1}, **Figure 7c**). The mean daily-integrated GPP, reaching 50.2 ± 30.1 mg C m^{-2} d^{-1} in March, 40.9 ± 26.8 mg C m^{-2} d^{-1} in May, and 22.3 ± 20.5 mg C m^{-2} d^{-1} in July, allowed to integrate GPP over the mudflat, reaching, respectively, 2.06 (for an emerged surface of 41 km^2), 1.42 (for 34.5 km^2), and 0.80 tC d^{-1} (for 36 km^2) in March, May, and July (**Figures 7d–f**).

Validations

A Priori Physical Environment Validation

The MST and PAR conditions simulated by the MARS-3D model satisfactorily compared to the *in situ* conditions, even if there were some significant differences (**Figures 8a,b**). The delay between field campaigns and image acquisition was not an issue (**Figures 8c,d**): for the three periods, the averaged PAR and the MST 2 weeks before measurements and before images acquisition were not significantly different (**Figures 8c,d**). These observations mean that MPB cells were expected to be in a similar acclimation status during laboratory experiments and image acquisition. After these first validations, simulated MST and PAR, satellite images and calibrate P–E model were used in the GPP algorithm to predict and map GPP.

Measured *Versus* Estimated NDVI and GPP

The NDVI measured *in situ* was always higher than the remotely sensed NDVI at the study site (**Figure 9a**). In March, the NDVI measured *in situ* (0.61 ± 0.03) was almost 5-fold higher than the remotely sensed NDVI at the pixel corresponding to the study site (0.14). The NDVI measured *in situ* in May (0.14 ± 0.02) was 1.5-fold higher than the remotely sensed NDVI at the pixel of the study site (0.09). In July, the NDVI measured *in situ* (0.18 ± 0.09) was almost 1.8-fold higher than the remotely sensed NDVI at the pixel of the study site (0.1). Regarding the GPP, the measured value *in situ* varied from 4.8 ± 2.1 mg C m^{-2} h^{-1} in March to 6.3 ± 0.3 mg C m^{-2} h^{-1} in July (**Figures 4e**, **9b**), whereas the GPP remotely-sensed at the respective grid cell averaged during daytime emersion varied from 2.2 ± 1.4 mg C m^{-2} h^{-1} in July to 7.8 ± 3.1 mg C m^{-2} h^{-1} in March (**Figure 9b**). However, there was not significant difference between *in situ* and remotely sensed GPP (MW tests, **Figure 9b**).

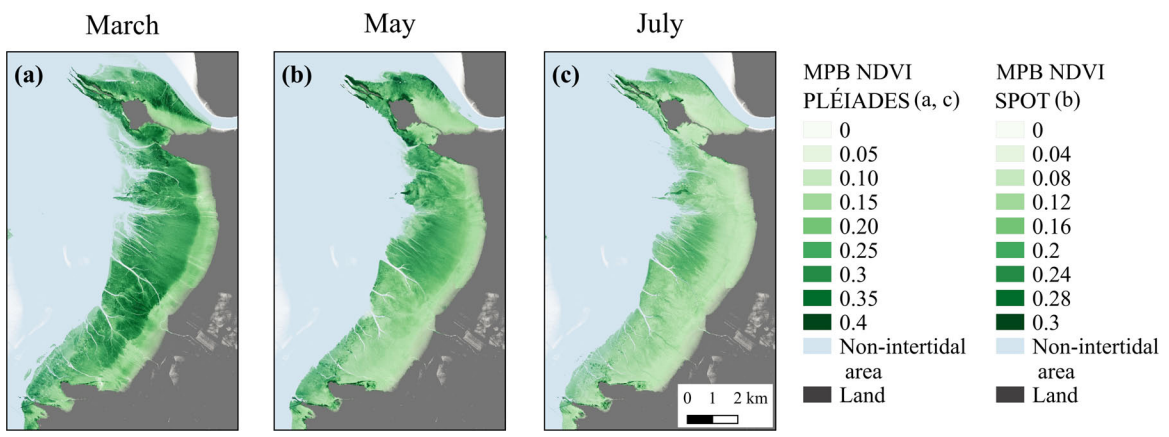

FIGURE 6 | MPB-specific NDVI from Pléiades satellite, March 3, 2018 **(a)**, and July 17, 2015 **(c)**, and from SPOT6 satellite, May 6, 2015 **(b)**.

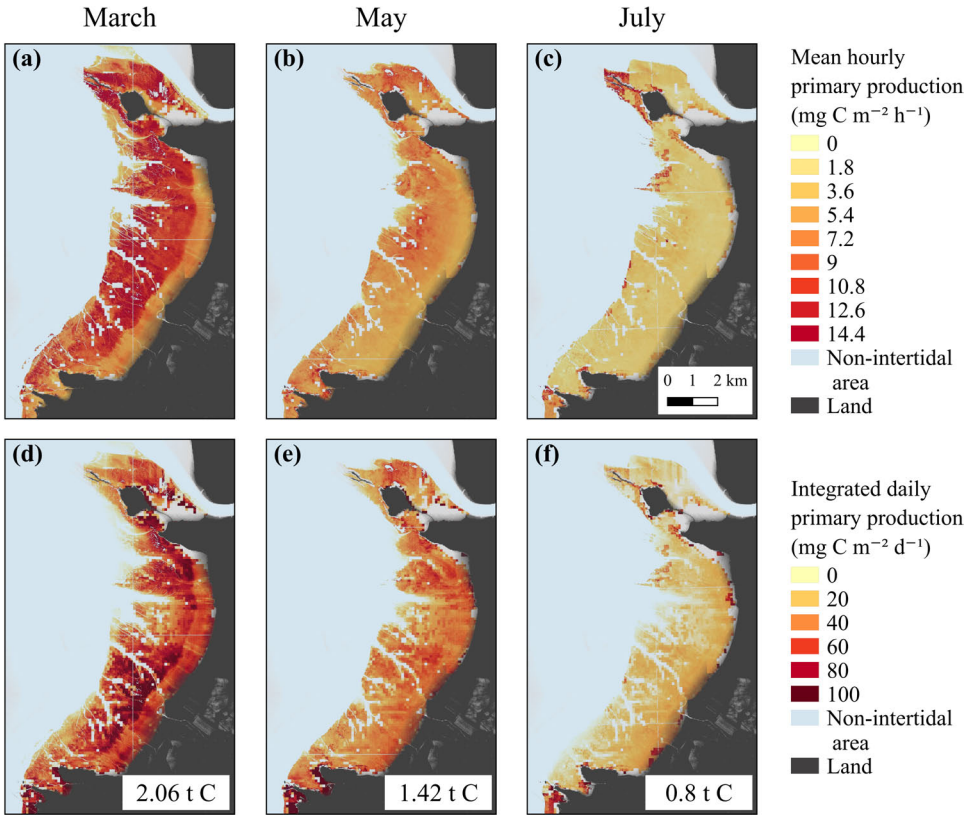

FIGURE 7 | Hourly (mg C m^{-2} h^{-1}) and daily (mg C m^{-2} d^{-1}) averaged remotely-sensed GPP from the GPP-algorithm based on Eilers and Peeters (1988) P–E model in March **(a,d)**, May **(b,e)**, and July **(c,f)**.

DISCUSSION

NDVI *Versus* Chl *a* GPP Standardization

In order to be able to upscale MPB biomass over an entire mudflat, NDVI has been used as a proxy of MPB abundance (e.g., Méléder et al., 2003b; van der Wal et al., 2010; Brito et al., 2013; Benyoucef et al., 2014; Echappé et al., 2018). Here, the NDVI 2000–2015 time series demonstrated a seasonal cycle characterized by a maximum of MPB biomass in winter–spring and a minimum in summer. This MPB seasonality observed in the Brouage mudflat is consistent with the seasonal pattern reported before for the same mudflat (Cariou-Le Gall and Blanchard, 1995; Savelli et al., 2018) and for other Northern European mudflats (van der Wal et al., 2010; Echappé et al., 2018).

Usually, on a local scale, GPP is standardized to the Chl *a* sediment content (e.g., Cahoon, 2006). Ideally, in order to convert our NDVI maps into GPP, a conversion of NDVI in Chl *a* sediment content should be performed. However, a direct relationship between NDVI and Chl *a* is a real issue for three main reasons. First, the relationship is known to be non-linear and to saturate for high values of Chl *a* (Méléder et al., 2003a; Serôdio et al., 2009; Barillé et al., 2011; Daggers et al., 2018). Second, there is an ongoing debate on the sediment depth to be sampled for Chl *a* content estimation in order to be in accordance with the sediment depth detected by sensors for NDVI calculation. Jesus et al. (2006) suggested the sampling of the first 150 μm, however, all depths tested along the first 2 mm were highly correlated, leading to similar NDVI for different Chl *a* contents (i.e., different depths). Moreover, the optical depth varies with the MPB biomass at the sediment surface, the sediment texture, the organic and water content, and the incident light wavelengths (Kühl et al., 1994; Jesus et al., 2006; Barillé et al., 2011; Kazemipour et al., 2011; Fisher et al., 2018). In the current study, the length of the path of the reflected light (i.e., the NDVI) is assumed to correspond to the photic zone, where the biomass is photosynthetically active, which rarely exceeds 500 μm for muddy sediments (Cartaxana et al., 2011). Third, the dilution of the reflectance signal from the sediment surface to the satellite sensor is variable. MPB-specific NDVI data obtained in this study from MODIS-Terra, SPOT6, and Pléiades satellites and measured *in situ* with a handheld field spectroradiometer reach, respectively, maximal values of 0.25, 0.30, and 0.40 for satellite and 0.60 *in situ*, meaning that maximum NDVI value decreases with spatial resolution. Even if such values are in the range of the MPB-specific NDVI derived from satellite data over temperate mudflats (Méléder et al., 2003b; van der Wal et al., 2010; Brito et al., 2013; Benyoucef et al., 2014; Echappé et al., 2018), their variability illustrates the different sensitivity between devices, but also the dilution

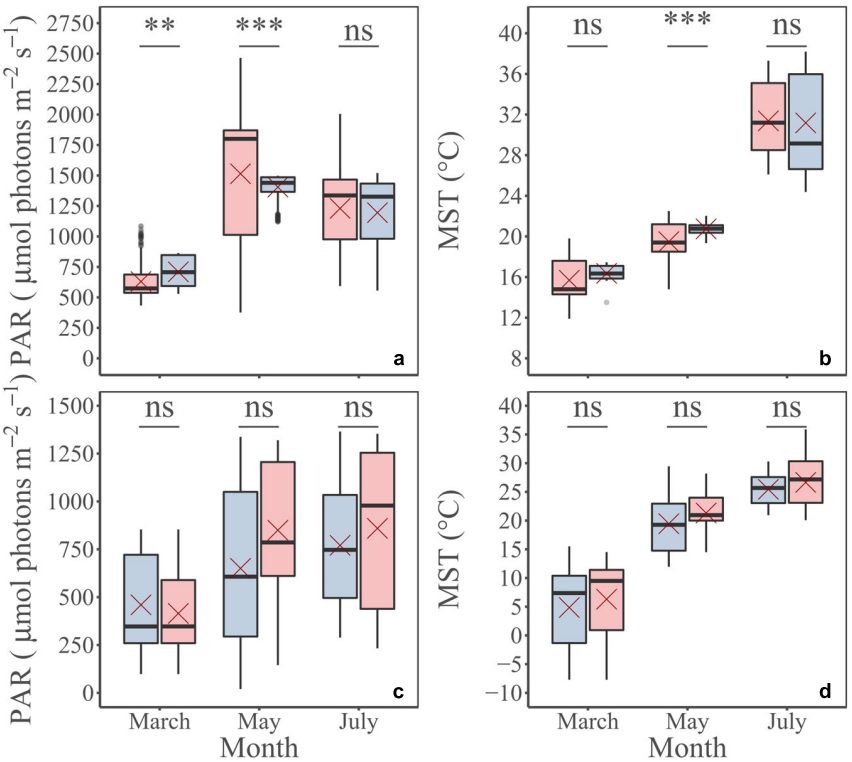

FIGURE 8 | *A priori* physical environment validation. PAR **(a)** and MST **(b)** measured *in situ* (blue) and simulated by MARS-3D (pink) for the same period: March, May, and July; PAR **(c)** and MST **(d)** simulated by MARS-3D, averaged during daytime emersion periods 2 weeks before *in situ* measurements (blue) and satellite scenes acquisitions (pink). Red crosses correspond the mean value of PAR and MST for the corresponding period. Mann Whitney test; *p*-value: ns, $p > 0.01$; $^{*}p \leq 0.01$; $^{**}p \leq 0.001$; $^{***}p \leq 0.0001$.

of the reflectance signal for larger surfaces, mainly due to the patchiness distribution of the MPB biofilm (Saburova et al., 1995; Jesus et al., 2006; Spilmont et al., 2011). Méléder et al. (2010) and Launeau et al. (2018) demonstrated previously that MPB patchiness is responsible for a reflectance signal, due to the non-linear mixing of individual MPB patches and apparent mud. This generates one Chl *a* content corresponding to diverse NDVI values and conversely, one NDVI value could correspond to diverse Chl *a* content. This non-linear mixing increases the difficulty to use the Chl *a* sediment content measured at local scale (a few millimeters squared) to map NDVI over several meters squared or kilometers squared. In the present study, the direct calibration of the GPP-algorithm in NDVI allowed to decrease bias due to uncertainties of the NDVI *versus* Chl *a* relationship. Nevertheless, and in spite of this major improvement, some issues remain, such as the NDVI saturation for high MPB biomass leading to a potential non-linear GPP-NDVI relation, which will need further investigation.

GPP Algorithm Physical Setting

The MST and PAR conditions simulated by the MARS-3D model compared well to the conditions measured in the field. The model-*versus*-*in situ* data comparison suggested that the 3D model can resolve with confidence the physical environment experienced by MPB at the sediment surface. In regards to the frequency of the atmospheric AROME model (1 h), the simulated PAR conditions varied less than the *in situ* observations. The 3D model could not reproduce the observed synoptic variations of irradiance at the sub-hourly scale that can induce a substantial variability in the remotely sensed GPP over an emersion period. In addition, the horizontal resolution of the 3D model (100 × 100 m) may also translate into model–data discrepancies. In the GPP-algorithm, the bathymetric level and simulated water height originating from 100- × 100-m grid cells delay the emersion timing by ∼30 min. However, considering this delay, the comparison of *in situ* and simulated physical conditions and GPP were made on the corresponding low tides. Most importantly, the preservation of the horizontal resolution of satellite data in order to capture the MPB patchiness suggests that the GPP algorithm can resolve with confidence the overall dynamics of MPB GPP at the tidal scale.

Ability of the GPP Algorithm to Map the Current Productive State of the Mudflat

Our study is not the first to assess MPB primary production coupling remotely sensing and physical–biological modeling. Daggers et al. (2018) proposed a first approach using (i) remotely sensed information on MPB biomass and on sediment mud content, (ii) surface irradiance and ambient temperature,

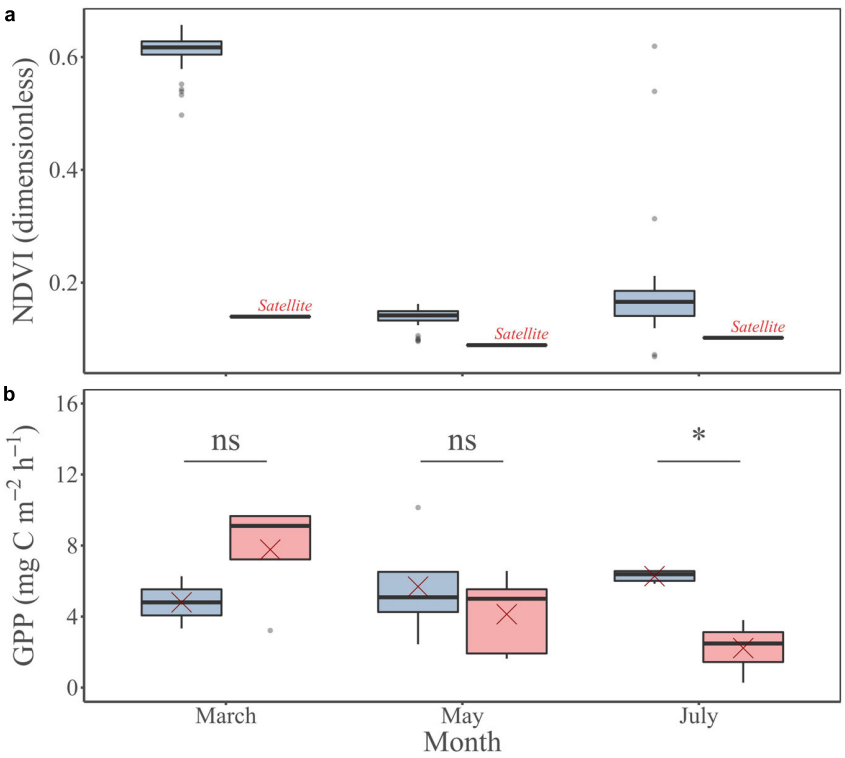

FIGURE 9 | MPB-specific NDVI **(a)** and GPP **(b)** measured *in situ* (blue) and remotely sensed (pink) at the study site for the three investigated periods: March, May, and July. Red crosses correspond the mean values for the corresponding period. Mann Whitney test, *p*-value: ns, $p > 0.01$; *$p \leq 0.01$; **$p \leq 0.001$; ***$p \leq 0.0001$.

(iii) directly measured photophysiological parameters by PAM fluorimetry, and (iv) a tidal model. The current GPP algorithm improves the (Daggers et al., 2018) approach by (i) the use of NDVI rather than the conversion of NDVI into Chl *a*, which introduces uncertainties (see section "Discussion" above); (ii) the use of MST rather than ambient temperature, which was identified as a weakness of their model; and (iii) photophysiological parameters derived directly from benthic chamber CO_2 exchange measurements on natural MPB communities in sediment under controlled conditions, rather than an averaged electron requirement (EE) rate derived from PAM fluorimetry. The EE used by Daggers et al. (2018) corresponds to the ETR efficiency for C fixation to translate ETR (μmol electrons m^{-2} s^{-1}) into C (mg C m^{-2} h^{-1}). However, it is known to vary with season, species, and site (Barranguet and Kromkamp, 2000), and the relationship between ETR and C-fixation can be non-linear, especially at irradiances exceeding E_k. The difficulty to use photophysiological parameters derived from PAM fluorimetry to predict C fixation was confirmed by the current study. PAM photophysiological parameters could vary rapidly even during the time of benthic chamber incubation (30-min duration) rendering the use of an averaged EE rate weakly representative of a given season, a given day and even a given emersion. To overcome this issue, we suggest to directly calibrate the P–E model with C-fixation standardized to NDVI values.

Additionally, the environmental conditions 2 weeks before measurements for the GPP algorithm calibration and 2 weeks before the acquisition of satellite images used to apply GPP algorithm were checked in the aim to support the representativeness of the photophysiological parameters. The conditions were similar, assuming the same photosynthetic capabilities of MPB during experiments for the calibration and during image acquisition. Otherwise, it would have been hazardous to apply the GPP algorithm on MPB that would have been differently acclimated between lab experiments and satellite image acquisitions.

The GPP algorithm uses a vertical migration scheme of MPB biomass within the upper layer of sediment, which is represented through the modulation of the total photosynthetically active biomass detected from the remotely sensed NDVI. Such a migration scheme in the GPP algorithm was set according to the observation of the progressive superficial sediment covering by MPB during emersion at our study site (Herlory et al., 2004). However, the migration speed can be faster [a few minutes; see Méléder et al. (2003b)] or slower [one hour; see Paterson et al. (1998)], and it is mainly controlled by the tidal cycle and the light climate and spectral quality (Pinckney and Zingmark, 1991; Spilmont et al., 2007; Coelho et al., 2011; Barnett et al., 2020; Prins et al., 2020), but also by temperature (Cohn et al., 2003), nutrient availability in the sub-surface of sediment (Kingston, 2002), and desiccation (Coelho et al., 2009). Currently, the GPP-algorithm does not include the short-term variations of MPB photosynthetically active biomass at the sediment surface (i.e., "micro-migrations"), as it has been also observed some

days/timings during our field campaigns. As suggested previously by Daggers et al. (2018), further research on the mechanisms and triggers that determine the vertical phototaxis of diatom cells in sediment is required to better predict and model intertidal MPB migration patterns and therefore changes in MPB photosynthetically active biomass at the sediment surface.

When constrained by the PAR and MST conditions simulated by the MARS-3D model, the remotely sensed GPP predicted by the GPP-algorithm reached rates up to 14 mg C m^{-2} h^{-1} or 100 mg C m^{-2} d^{-1}, similar to rates reported for other European mudflats (Barranguet et al., 1998; Underwood and Kromkamp, 1999; Cahoon, 2006; Hubas et al., 2006; Daggers et al., 2018; Frankenbach et al., 2020). These values further supports the key role of MPB in supporting the high productivity of temperate intertidal bare mudflats (e.g., Cahoon, 1999; Underwood and Kromkamp, 1999; Barranguet and Kromkamp, 2000) and its paramount support to local socio-economics (Lebreton et al., 2019). This growing recognition also supports the necessity for the worldwide consideration of mudflats as key ecosystems in the marine global carbon budget (Ciais et al., 2014; Legge et al., 2020).

The predicted and measured GPP reasonably compared. Both GPP show low seasonal variability, whereas the MPB biomass displays a pronounced seasonal cycle. This leads to lower P^b values during the period with the highest MPB biomass (i.e., March). It has been shown before that high MPB biomass does not always generate high production (Barranguet et al., 1998). During winter, the MPB biomass standing stock increases due to lower grazing activity (Thompson et al., 2000). As a consequence, MPB photosynthetically active biomass is mainly concentrated in an extremely thin layer at the sediment surface. However, such high concentration induces strong competition for light and nutrients, limiting the biomass specific productivity (P^b) (Barranguet et al., 1998; Stal, 2010; Vieira et al., 2016). This competition, compensated by high biomass, suggests a bottom-up regulation of the GPP in winter (by light, temperature, and nutrients), whereas a top-down control (by grazing activity) occurs in spring and summer.

CONCLUSION AND PERSPECTIVES: THE USE OF HYPERSPECTRAL REMOTE SENSING

The GPP algorithm developed in this study combines satellite remote sensing, laboratory measurements, and a 3D physical model. The algorithm is constrained by realistic simulated 2D fields of tidal heights, MST, and PAR. It is standardized by photophysiological parameters estimated from laboratory measurements on natural MPB communities in sediment and expressed in C fixation rates. In addition, the direct calibration of the algorithm in NDVI is a step forward to limiting outstanding bias due to NDVI to Chl *a* conversion. Moreover, the calibration of the GPP algorithm to NDVI allowed us to consistently apply the algorithm to satellite images. This study shows that:

- The NDVI data retrieved from the SPOT6 and Pléiades sensors were consistent with the seasonality of the MPB biomass previously reported for the study site, and their range was comparable to NDVI data from other European mudflats;
- The GPP-algorithm yields MPB GPP rates in the range of *in situ* GPP measurements, including the seasonal variability of GPP;
- The GPP algorithm was well-adapted to intertidal mudflats mostly composed by fine cohesive sediments dominated by motile epipelic diatoms, and it could be applied for similar habitats.

However, this study highlights several challenging issues that need to be tackled to better estimate MPB production on regional and global scales from *in situ* information:

- Photosynthetic ability changes over a range of time scales, from the emersion to the season via the tidal fortnight cycle. To overcome this issue, photophysiological parameters, and not only MPB biomass, have to be measured at the ecosystem level (i.e., entire mudflat scale). Currently, only hyperspectral remote sensing is able to capture such a detailed information based on fine pigment absorption features, as recently proposed for terrestrial vegetation (DuBois et al., 2018; Lees et al., 2018). This is an approach we have started to develop successfully on MPB (Méléder et al., 2018).
- Up-scaling remains the main issue. It could be overcome also using hyperspectral remote sensing as demonstrated recently by Launeau et al. (2018). The use of the optical properties retrieved from hyperspectral images to predict MPB biomass allows to remove the patchiness effect (=non-linear mixing) which build a linear relationship between MPB biomass and optical properties independent of the size of the analyzed surface. This approach could be applied for GPP mapping to improve the up-scaling bias.

DATA AVAILABILITY STATEMENT

All the data, inlcuding maps from GPP-algotithm, are avaible on a data repository (Zenodo): doi: 10.5281/zenodo.3862068.

AUTHOR CONTRIBUTIONS

VM, RS, VL, and JL developed the theoretical formalism. VM, RS, AB, PP, AL, and JL carried out the experiments. PG, AL, and ALB processed the remote sensing data. VM, RS, and VF designed the model and the computational framework. VM, RS, AB, and JL analyzed the data. VM and RS wrote the manuscript with inputs from all authors. All authors contributed to the final version of the manuscript.

FUNDING

This work was supported by (i) the DYCOFEL project, funded through the 2015 Fondation de France call "Quels littoraux

pour demain?"; (ii) the MIMOSA project, funded through the 2018 CNRS EC2CO-LEFE call; (iii) the HYPEDDY project, funded through the 2018–2020 Tosca-CNES call; (iv) the BIO-Tide project, funded through the 2015–2016 BiodivERsA COFUND call for research proposals, with the national funders BelSPO, FWO, ANR, and SNSF; (v) the public funds received in the framework of GEOSUD, a project (ANR-10-EQPX-20) of the program "Investissements d'Avenir," managed by the French National Research Agency; and (vi) the projects Littoral 1 and ECONAT funded by the Contrat de Plan Etat-Région (CPER) and the CNRS and the European Regional Development Fund. Pléiades and SPOT images were acquired by CNES's ISIS program, facilitating scientific access to imagery. Pléiades CNES 2015, 2018, Distribution Airbus DS, all rights reserved. Commercial uses forbidden. This research was part of fulfillment of the requirements for a Ph.D. degree (RS) at the Université de La Rochelle, France. RS was supported by a Ph.D. fellowship from the French Ministry of Higher Education, Research and Innovation.

ACKNOWLEDGMENTS

We thank the CNRS, Ifremer, the Université de Nantes, and the Université de La Rochelle for their support and V. Ouisse and N. Spilmont for their help with setting up the benthic chambers and with analyzing the CO_2 data.

SUPPLEMENTARY MATERIAL

The Supplementary Material for this article can be found online at: https://www.frontiersin.org/articles/10.3389/fmars.2020.00520/full#supplementary-material

REFERENCES

Babin, M., Bélanger, S., Ellingsen, I., Forest, A., Le Fouest, V., Lacour, T., et al. (2015). Estimation of primary production in the Arctic Ocean using ocean colour remote sensing and coupled physical–biological models: strengths, limitations and how they compare. *Overarching Perspect. Contemp. Future Ecosyst. Arct. Ocean* 139, 197–220. doi: 10.1016/j.pocean.2015.08.008

Barillé, L., Mouget, J. L., Méléder, V., Rosa, P., and Jesus, B. (2011). Spectral response of benthic diatoms with different sediment backgrounds. *Remote Sens. Environ.* 115, 1034–1042. doi: 10.1016/j.rse.2010.12.008

Barnett, A., Méléder, V., Blommaert, L., Lepetit, B., Gaudin, P., Vyverman, W., et al. (2015). Growth form defines physiological photoprotective capacity in intertidal benthic diatoms. *ISME J.* 9, 32–45. doi: 10.1038/ismej.2014.105

Barnett, A., Méléder, V., Dupuy, C., and Lavaud, J. (2020). The vertical migratory rhythm of intertidal microphytobenthos in sediment depends on the light photoperiod, intensity, and spectrum: evidence for a positive effect of blue wavelengths. *Front. Mar. Sci.* 7:212. doi: 10.3389/fmars.2020.00212

Barranguet, C., and Kromkamp, J. (2000). Estimating primary production rates from photosynthetic electron transport in estuarine microphytobenthos. *Mar. Ecol. Prog. Ser.* 204, 39–52. doi: 10.3354/meps204039

Barranguet, C., Kromkamp, J., and Peene, J. (1998). Factors controlling primary production and photosynthetic characteristics of intertidal microphytobenthos. *Mar. Ecol. Prog. Ser.* 173, 117–126. doi: 10.3354/meps173117

Benyoucef, I., Blandin, E., Lerouxel, A., Jesus, B., Rosa, P., Méléder, V., et al. (2014). Microphytobenthos interannual variations in a north-European estuary (Loire estuary, France) detected by visible-infrared multispectral remote sensing. *Estuar. Coast. Shelf Sci.* 136, 43–52. doi: 10.1016/j.ecss.2013.11.007

Blanchard, G., Guarini, J.-M., Gros, P., and Richard, P. (1997). Seasonal effect on the relationship between the photosynthetic capacity of intertidal microphytobenthos and temperature. *J. Phycol.* 3, 723–728. doi: 10.1111/j.0022-3646.1997.00723.x

Blanchard, G. F., Guarini, J.-M., Richard, P., Gros, P., and Mornet, F. (1996). Quantifying the short-term temperature effect on light-saturated photosynthesis of intertidal microphytobenthos. *Mar. Ecol. Prog. Ser.* 134, 309–313. doi: 10.3354/meps134309

Blumberg, A. F., and Mellor, G. L. (1987). A description of a three-dimensional coastal ocean circulation model. *Three Dimens. Coast. Ocean Models* 4, 1–16. doi: 10.1029/co004p0001

Bocher, P., Piersma, T., Dekinga, A., Kraan, C., Yates, M. G., Guyot, T., et al. (2007). Site-and species-specific distribution patterns of molluscs at five intertidal soft-sediment areas in northwest Europe during a single winter. *Mar. Biol.* 151, 577–594. doi: 10.1007/s00227-006-0500-4

Brito, A. C., Benyoucef, I., Jesus, B., Brotas, V., Gernez, P., Mendes, C. R., et al. (2013). Seasonality of microphytobenthos revealed by remote-sensing in a South European estuary. *Cont. Shelf Res.* 66, 83–91. doi: 10.1016/j.csr.2013.07.004

Cahoon, L. (2006). "Upscaling primary production estimates: Regional and global scale estimates of microphytobenthos production," in *Functionning of Microphytobenthos in Estuarines*, eds J. Kromkamp, J. Brouwer, G. Blanchard, R. Forster, and V. Créach (Amsterdam: Royal Netherlands Academy of Arts and Science), 99–108.

Cahoon, L. B. (1999). The role of benthic microalgae in neritic ecosystems. *Oceanogr. Mar. Biol.* 37, 47–86.

Cariou-Le Gall, V., and Blanchard, G. (1995). Monthly measurements of pigment concentration from an intertidal muddy sediment of Marennes-Oleron, France. *Mar. Ecol. Prog. Ser.* 121, 171–179. doi: 10.3354/meps121171

Cartaxana, P., Ruivo, M., Hubas, C., Davidson, I., Serôdio, J., and Jesus, B. (2011). Physiological versus behavioral photoprotection in intertidal epipelic and epipsammic benthic diatom communities. *J. Exp. Mar. Biol. Ecol.* 405, 120–127. doi: 10.1016/j.jembe.2011.05.027

Cartaxana, P., Vieira, S., Ribeiro, L., Rocha, R. J., Cruz, S., Calado, R., et al. (2015). Effects of elevated temperature and CO_2 on intertidal microphytobenthos. *BMC Ecol.* 15:10. doi: 10.1186/s12898-015-0043-y

Ciais, P., Sabine, C., Bala, G., Bopp, L., Brovkin, V., Canadell, J., et al. (2014). "Carbon and other biogeochemical cycles," in *Climate Change 2013: The Physical Science Basis. Contribution of Working Group I to the Fifth Assessment Report of the Intergovernmental Panel on Climate Change*, eds T. F. Stocker, D. Qin, G.-K. Plattner, M. Tignor, S. K. Allen, J. Boschung (Cambridge: Cambridge University Press), 465–570.

Coelho, H., Vieira, S., and Serôdio, J. (2009). Effects of desiccation on the photosynthetic activity of intertidal microphytobenthos biofilms as studied by optical methods. *J. Exp. Mar. Biol. Ecol.* 381, 98–104. doi: 10.1016/j.jembe.2009.09.013

Coelho, H., Vieira, S., and Serôdio, J. (2011). Endogenous versus environmental control of vertical migration by intertidal benthic microalgae. *Eur. J. Phycol.* 46, 271–281. doi: 10.1080/09670262.2011.598242

Cohn, S. A., Farrell, J. F., Munro, J. D., Ragland, R. L., Weitzell, R. E. Jr., and Wibisono, B. L. (2003). The effect of temperature and mixed species composition on diatom motility and adhesion. *Diatom Res.* 18, 225–243. doi: 10.1080/0269249x.2003.9705589

Consalvey, M., Jesus, B., Perkins, R. G., Brotas, V., Underwood, G. J. C., and Paterson, D. M. (2004). Monitoring migration and measuring biomass in benthic biofilms: the effects of dark/far-red adaptation and vertical migration on fluorescence measurements. *Photosynth. Res.* 81, 91–101. doi: 10.1023/b:pres.0000028397.86495.b5

Daggers, T. D., Kromkamp, J. C., Herman, P. M. J., and van der Wal, D. (2018). A model to assess microphytobenthic primary production in tidal systems using satellite remote sensing. *Remote Sens. Environ.* 211, 129–145. doi: 10.1016/j.rse.2018.03.037

Du, G., Yan, H., and Dupuy, C. (2017). Microphytobenthos as an indicator of environmental quality status in intertidal flats: case study of coastal ecosystem in Pertuis Charentais, France. *Estuar. Coast. Shelf Sci.* 196, 217–226. doi: 10.1016/j.ecss.2017.06.031

DuBois, S., Desai, A. R., Singh, A., Serbin, S. P., Goulden, M. L., Baldocchi, D. D., et al. (2018). Using imaging spectroscopy to detect variation in terrestrial ecosystem productivity across a water-stressed landscape. *Ecol. Appl.* 28, 1313–1324. doi: 10.1002/eap.1733

Echappé, C., Gernez, P., Méléder, V., Bruno, J., Cognie, B., Decottignies, P., et al. (2018). Satellite remote sensing reveals a positive impact of living oyster reefs on microalgal biofilm development. *Biogeosciences* 15, 905–918. doi: 10.5194/bg-15-905-2018

Eilers, P. H. C., and Peeters, J. C. H. (1988). A model for the relationship between light intensity and the rate of photosynthesis in phytoplankton. *Ecol. Model.* 42, 199–215. doi: 10.1016/0304-3800(88)90057-9

Fisher, A., Wangpraseurt, D., Larkum, A. W., Johnson, M., Kühl, M., Chen, M., et al. (2018). Correlation of bio-optical properties with photosynthetic pigment and microorganism distribution in microbial mats from Hamelin Pool, Australia. *FEMS Microbiol. Ecol.* 95:fiy219.

Ford, R. B., and Honeywill, C. (2002). Grazing on intertidal microphytobenthos by macrofauna: is pheophorbide a a useful marker? *Mar. Ecol. Prog. Ser.* 229, 33–42. doi: 10.3354/meps229033

Forster, R. M., and Kromkamp, J. C. (2006). "Estimating benthic primary production: scaling up from point measurements to the whole estuary," in *Functioning of Microphytobenthos in Estuaries*, eds J. C. Kromkamp, J. F. C. de brouwer, G. F. Blanchard, R. M. Forster, and V. Creach (Amsterdam: Edita -the Publishing House of the Royal), 109–120.

Frankenbach, S., Ezequiel, J., Plecha, S., Goessling, J. W., Vaz, L., Kühl, M., et al. (2020). Synoptic spatio-temporal variability of the photosynthetic productivity of microphytobenthos and phytoplankton in a tidal estuary. *Front. Mar. Sci.* 7:170. doi: 10.3389/fmars.2020.00170

Goetz, S. J., Prince, S. D., Goward, S. N., Thawley, M. M., and Small, J. (1999). Satellite remote sensing of primary production: an improved production efficiency modeling approach. *Ecol. Model.* 122, 239–255. doi: 10.1016/s0304-3800(99)00140-4

Guarini, J.-M., Blanchard, G., Bacher, C., Gros, P., Riera, P., Richard, P., et al. (1998). Dynamics of spatial patterns of microphytobenthic biomass: inferences from a geostatistical analysis of two comprehensive surveys in Marennes-Oléron Bay (France). *Mar. Ecol. Prog. Ser.* 166, 131–141. doi: 10.3354/meps166131

Haubois, A.-G., Sylvestre, F., Guarini, J.-M., Richard, P., and Blanchard, G. F. (2005). Spatio-temporal structure of the epipelic diatom assemblage from an intertidal mudflat in Marennes-Oléron Bay, France. *Estuar. Coast. Shelf Sci.* 64, 385–394. doi: 10.1016/j.ecss.2005.03.004

Herlory, O., Guarini, J.-M., Richard, P., and Blanchard, G. F. (2004). Microstructure of microphytobenthic biofilm and its spatio-temporal dynamics in an intertidal mudflat (Aiguillon Bay, France). *Mar. Ecol. Prg. Ser.* 282, 33–44. doi: 10.3354/meps282033

Herman, P. M. J., Middelburg, J. J., Widdows, J., Lucas, C. H., and Heip, C. H. R. (2000). Stable isotopes as trophic tracers: combining field sampling and manipulative labelling of food resources for macrobenthos. *Mar. Ecol. Prog. Ser.* 204, 79–92. doi: 10.3354/meps204079

Hossain, M. S., Bujang, J. S., Zakaria, M. H., and Hashim, M. (2015). The application of remote sensing to seagrass ecosystems: an overview and future research prospects. *Int. J. Remote Sens.* 36, 61–114. doi: 10.1080/01431161.2014.990649

Hubas, C., Davoult, D., Cariou, T., and Artigas, L. F. (2006). Factors controlling benthic metabolism during low tide along a granulometric gradient in an intertidal bay (Roscoff Aber Bay, France). *Mar. Ecol. Prog. Ser.* 316, 53–68. doi: 10.3354/meps316053

Huemmrich, K. F., Gamon, J. A., Tweedie, C. E., Oberbauer, S. F., Kinoshita, G., Houston, S., et al. (2010). Remote sensing of tundra gross ecosystem productivity and light use efficiency under varying temperature and moisture conditions. *Remote Sens. Environ.* 114, 481–489. doi: 10.1016/j.rse.2009.10.003

Jardine, C. B., Bond, A. L., Davidson, P. J., Butler, R. W., and Kuwae, T. (2015). Biofilm consumption and variable diet composition of Western Sandpipers (*Calidris mauri*) during migratory stopover. *PLoS One* 10:e0124164. doi: 10.1371/journal.pone.0124164

Jesus, B., Mendes, C. R., Brotas, V., and Paterson, D. M. (2006). Effect of sediment type on microphytobenthos vertical distribution: modelling the productive biomass and improving ground truth measurements. *J. Exp. Mar. Biol. Ecol.* 332, 60–74. doi: 10.1016/j.jembe.2005.11.005

Jobson, D. J., Zingmark, R. G., and Katzberg, S. J. (1980). Remote sensing of benthic microalgal biomass with a tower-mounted multispectral scanner. *Remote Sens. Environ.* 9, 351–362. doi: 10.1016/0034-4257(80)90039-5

Kang, C., Lee, Y., Eun, J. C., Shin, J., Seo, I., and Hong, J. (2006). Microphytobenthos seasonality determines growth and reproduction in intertidal bivalves. *Mar. Ecol. Prog. Ser.* 315, 113–127. doi: 10.3354/meps315113

Kazemipour, F., Méléder, V., and Launeau, P. (2011). Optical properties of microphytobenthic biofilms (MPBOM): Biomass retrieval implication. *J. Quant. Spectrosc. Radiat. Transf.* 112, 131–142. doi: 10.1016/j.jqsrt.2010.08.029

Kingston, M. B. (2002). Effect of subsurface nutrient supplies on the vertical migration of Euglena proxima (Euglenophyta). *J. Phycol.* 38, 872–880. doi: 10.1046/j.1529-8817.2002.t01-1-01197.x

Kromkamp, J., and Forster, R. M. (2006). "Development in microphytobenthos primary productivity studies," in *Functioning of Microphytobenthos in Estuaries*, eds J. Kromkamp, J. F. C. de Brouwer, G. F. Blanchard, R. M. Forster, and V. Creach (Amsterdam: Edita -the Publishing House of the Royal), 9–30.

Krumme, U., Keuthen, H., Barletta, M., Saint-Paul, U., and Villwock, W. (2008). Resuspended intertidal microphytobenthos as major diet component of planktivorous Atlantic anchoveta *Cetengraulis edentulus* (Engraulidae) from equatorial mangrove creeks. *Ecotropica* 14, 121–128.

Kühl, M., Lassen, C., and Jørgensen, B. B. (1994). Light penetration and light intensity in sandy marine sediments measured with irradiance and scalar irradiance fiber-optic microprobes. *Mar. Ecol. Prog. Ser.* 139–148. doi: 10.3354/meps105139

Launeau, P., Méléder, V., Verpoorter, C., Barillé, L., Kazemipour-Ricci, F., Giraud, M., et al. (2018). Microphytobenthos biomass and diversity mapping at different spatial scales with a hyperspectral optical model. *Remote Sens.* 10:716. doi: 10.3390/rs10050716

Laviale, M., Ezequiel, J., Pais, C., Cartaxana, P., and Serôdio, J. (2015). The "crème brûlée" sampler: a new high-resolution method for the fast vertical sampling of intertidal fine sediments. *J. Exp. Mar. Biol. Ecol.* 468, 37–44. doi: 10.1016/j.jembe.2015.03.013

Lazure, P., and Dumas, F. (2008). An external–internal mode coupling for a 3D hydrodynamical model for applications at regional scale (MARS). *Adv. Water Resour.* 31, 233–250. doi: 10.1016/j.advwatres.2007.06.010

Lazure, P., Garnier, V., Dumas, F., Herry, C., and Chifflet, M. (2009). Development of a hydrodynamic model of the Bay of Biscay. Validation of hydrology. *Cont. Shelf Res.* 29, 985–997. doi: 10.1016/j.csr.2008.12.017

Le Hir, P., Roberts, W., Cazaillet, O., Christie, M., Bassoullet, P., and Bacher, C. (2000). Characterization of intertidal flat hydrodynamics. *Cont. Shelf Res.* 20, 1433–1459. doi: 10.1016/s0278-4343(00)00031-5

Lebreton, B., Rivaud, A., Picot, L., Prévost, B., Barillé, L., Sauzeau, T., et al. (2019). From ecological relevance of the ecosystem services concept to its socio-political use. The case study of intertidal bare mudflats in the Marennes-Oléron Bay, France. *Ocean Coast. Manag.* 172, 41–54. doi: 10.1016/j.ocecoaman.2019.01.024

Lees, K. J., Quaife, T., Artz, R. R. E., Khomik, M., and Clark, J. M. (2018). Potential for using remote sensing to estimate carbon fluxes across northern peatlands–A review. *Sci. Total Environ.* 615, 857–874. doi: 10.1016/j.scitotenv.2017.09.103

Legge, O., Johnson, M., Hicks, N., Jickells, T., Diesing, M., Aldridge, J., et al. (2020). Carbon on the Northwest European Shelf: contemporary budget and future influences. *Front. Mar. Sci.* 7:143. doi: 10.3389/fmars.2020.00143

MacIntyre, H., Geider, R., and Miller, D. (1996). Microphytobenthos: the ecological role of the "secret garden" of unvegetated, shallow water marine habitats. I. Distribution, abundance and primary production. *Estuaries* 19, 186–201.

Matthew, M. W., Adler-Golden, S. M., Berk, A., Richtsmeier, S. C., Levine, R. Y., Bernstein, L. S., et al. (2000). "Status of atmospheric correction using a MODTRAN4-based algorithm," in *SPIE Proceedings of the Algorithms for Multispectral, Hyperspectral, and Ultraspectral Imagery VI*, Orlando, FL, 199–208.

Méléder, V., Barillé, L., Launeau, P., Carrere, V., and Rince, Y. (2003a). Spectrometric constraint in analysis of benthic diatom biomass using monospecific cultures. *Remote Sens. Environ.* 88, 386–400. doi: 10.1016/j.rse.2003.08.009

Méléder, V., Jesus, B., Barnett, A., Barillé, L., and Lavaud, J. (2018). Microphytobenthos primary production estimated by hyperspectral reflectance. *PLoS One* 13:e0197093. doi: 10.1371/journal.pone.0197093

Méléder, V., Launeau, P., Barillé, L., Combe, J. P., Carrere, V., Jesus, B., et al. (2010). "Hyperspectral imaging for mapping microphytobenthos in coastal areas," in *Geomatic Solutions for Coastal Environments*, eds M. Maanan and M. Robin (Hauppauge, NY: Nova Science Publishers, Inc), 71–139.

Méléder, V., Launeau, P., Barillé, L., and Rincé, Y. (2003b). Microphytobenthos assemblage mapping by spatial visible-infrared remote sensing in a shellfish ecosystem. *C. R. Biol.* 326, 377–389.

Migné, A., Davoult, D., Spilmont, N., Menu, D., Boucher, G., Gattuso, J. P., et al. (2002). A closed-chamber CO_2-flux method for estimating intertidal primary production and respiration under emersed conditions. *Mar. Biol.* 140, 865–869. doi: 10.1007/s00227-001-0741-1

Murray, N. J., Phinn, S. R., DeWitt, M., Ferrari, R., Johnston, R., Lyons, M. B., et al. (2018). The global distribution and trajectory of tidal flats. *Nature* 565, 222–225. doi: 10.1038/s41586-018-0805-8

Orvain, F., De Crignis, M., Guizien, K., Lefebvre, S., Mallet, C., Takahashi, E., et al. (2014). Tidal and seasonal effects on the short-term temporal patterns of bacteria, microphytobenthos and exopolymers in natural intertidal biofilms (Brouage, France). *J. Sea Res.* 92, 6–18. doi: 10.1016/j.seares.2014.02.018

Otani, S., and Endo, T. (2019). "CO_2 flux in tidal flats and salt marshes," in *Blue Carbon in Shallow Coastal Ecosystems*, eds T. Kuwae and M. Hori (Berlin: Springer), 223–250. doi: 10.1007/978-981-13-1295-3_8

Paterson, D. M., and Hagerthey, S. E. (2001). "Microphytobenhthos in contrasting coastal ecosytems: biology and Dynamics," in *Ecological Comparisons of Sedimentary Shores*, ed. K. Reise (Berlin: Spring-Verlag), 105–125.

Paterson, D. M., Wiltshire, K. H., Miles, A., Blackburn, J., Davidson, I., Yates, M. G., et al. (1998). Microbiological mediation of spectral reflectance from intertidal cohesive sediments. *Limnol. Oceanogr.* 43, 1207–1221. doi: 10.4319/lo.1998.43.6.1207

Perissinotto, R., Nozais, C., Kibirige, I., and Anandraj, A. (2003). Planktonic food webs and benthic-pelagic coupling in three South African temporarily-open estuaries. *Acta Oecol.* 24, S307–S316.

Pinckney, J., and Zingmark, R. G. (1991). Effects of tidal stage and sun angles on intertidal benthic microalgal productivity. *Mar. Ecol. Prog. Ser.* 76, 81–89. doi: 10.3354/meps076081

Platt, T., Gallegos, C., and Harrison, W. (1980). Photoinhibition of photosynthesis in natural assemblages of marine phytoplankton. *J. Mar. Res.* 38, 687–701.

Platt, T., and Jassby, A. D. (1976). The relationship between photosynthesis and light for natural assemblages of coastal marine phytoplankton. *J. Phycol.* 12, 421–430. doi: 10.1111/j.1529-8817.1976.tb02866.x

Pniewski, F. F., Biskup, P., Bubak, I., Richard, P., Latala, A., and Blanchard, G. (2015). Photo-regulation in microphytobenthos from intertidal mudflats and non-tidal coastal shallows. *Estuar. Coast. Shelf Sci.* 152, 153–161. doi: 10.1016/j.ecss.2014.11.022

Poirier, C., Sauriau, P.-G., Chaumillon, E., and Bertin, X. (2010). Influence of hydro-sedimentary factors on mollusc death assemblages in a temperate mixed tide-and-wave dominated coastal environment: implications for the fossil record. *Cont. Shelf Res.* 30, 1876–1890. doi: 10.1016/j.csr.2010.08.015

Prins, A., Deleris, P., Hubas, C., and Jesus, B. (2020). Effect of light intensity and light quality on diatom behavioral and physiological photoprotection. *Front. Mar. Sci.* 7:203. doi: 10.3389/fmars.2020.00203

Roy, S., Llewellyn, C., Egeland, E. S., and Johnsen, G. (2011). *Phytoplankton Pigments - Characterization, Chemotaxonomy and Applications in Oceanography*. Cambridge: Cambridge University Press.

Saburova, M. A., Polikarpov, I. G., and Burkovsky, I. V. (1995). Spatial structure of an intertidal sandflat microphytobenthic community as related to different spatial scales. *Mar. Ecol. Prog. Ser.* 129, 229–239. doi: 10.3354/meps129229

Savelli, R., Dupuy, C., Barillé, L., Lerouxel, A., Guizien, K., Philippe, A., et al. (2018). On biotic and abiotic drivers of the microphytobenthos seasonal cycle in a temperate intertidal mudflat: a modelling study. *Biogeosciences* 15, 7243–7271. doi: 10.5194/bg-15-7243-2018

Serôdio, J., Cartaxana, P., Coelho, H., and Vieira, S. (2009). Effects of chlorophyll fluorescence on the estimation of microphytobenthos biomass using spectral reflectance indices. *Remote Sens. Environ.* 113, 1760–1768. doi: 10.1016/j.rse.2009.04.003

Serôdio, J., Ezequiel, J., Barnett, A., Mouget, J.-L., Méléder, V., Laviale, M., et al. (2012). Efficiency of photoprotection in microphytobenthos: role of vertical migration and the xanthophyll cycle against photoinhibition. *Aquat. Microb. Ecol.* 67, 161–175. doi: 10.3354/ame01591

Simon, B., and Gonella, J. (2007). *La Marée Océanique Côtière*. Paris: Institut océanographique.

Spilmont, N., Migné, A., Seuront, L., and Davoult, D. (2007). Short-term variability of intertidal benthic community production during emersion and the implication in annual budget calculation. *Mar. Ecol. Prog. Ser.* 333, 95–101. doi: 10.3354/meps333095

Spilmont, N., Seuront, L., Meziane, T., and Welsh, D. T. (2011). There's more to the picture than meets the eye: sampling microphytobenthos in a heterogeneous environment. *Estuar. Coast. Shelf Sci.* 95, 470–476. doi: 10.1016/j.ecss.2011.10.021

Stal, L. J. (2010). Microphytobenthos as a biogeomorphological force in intertidal sediment stabilization. *Ecol. Eng.* 36, 236–245. doi: 10.1016/j.ecoleng.2008.12.032

Steele, J. H. (1962). Environmental control of photosynthesis in the sea. *Limnol. Oceanogr.* 7, 137–150. doi: 10.4319/lo.1962.7.2.0137

Thompson, R. C., Roberts, M. F., Norton, T. A., and Hawkins, S. J. (2000). "Feast or famine for intertidal grazing molluscs: a mis-match between seasonal variations in grazing intensity and the abundance of microbial resources," in *Island, Ocean and Deep-Sea Biology. Developments in Hydrobiology,* Vol. 152, eds M. B. Jones, J. M. N. Azevedo, A. I. Neto, A. C. Costa, A. M. F. Martins (Dordrecht: Springer), 357–367. doi: 10.1007/978-94-017-1982-7_33

Ubertini, M., Lefebvre, S., Gangnery, A., Grangeré, K., Le Gendre, R., and Orvain, F. (2012). Spatial variability of benthic-pelagic coupling in an estuary ecosystem: consequences for microphytobenthos resuspension phenomenon. *PLoS One* 7:e44155. doi: 10.1371/journal.pone.0044155

Underwood, G. J. C., and Kromkamp, J. (1999). Primary production by phytoplankton and microphytobenthos in estuaries. *Adv. Ecol. Res.* 29, 93–153. doi: 10.1016/s0065-2504(08)60192-0

van der Wal, D., Wielemaker-van den Dool, A., and Herman, P. M. (2010). Spatial synchrony in intertidal benthic algal biomass in temperate coastal and estuarine ecosystems. *Ecosystems* 13, 338–351. doi: 10.1007/s10021-010-9322-9

Vieira, S., Cartaxana, P., Máguas, C., and Marques da Silva, J. (2016). Photosynthesis in estuarine intertidal microphytobenthos is limited by inorganic carbon availability. *Photosynth. Res.* 128, 85–92. doi: 10.1007/s11120-015-0203-0

Vieira, S., Ribeiro, L., da Silva, J. M., and Cartaxana, P. (2013). Effects of short-term changes in sediment temperature on the photosynthesis of two intertidal microphytobenthos communities. *Estuar. Coast. Shelf Sci.* 119, 112–118. doi: 10.1016/j.ecss.2013.01.001

Conflict of Interest: The authors declare that the research was conducted in the absence of any commercial or financial relationships that could be construed as a potential conflict of interest.

frontiers in Marine Science

ORIGINAL RESEARCH
published: 09 October 2020
doi: 10.3389/fmars.2020.00521

Mapping the Intertidal Microphytobenthos Gross Primary Production, Part II: Merging Remote Sensing and Physical-Biological Coupled Modeling

Raphaël Savelli[1]*, *Vona Méléder*[2], *Philippe Cugier*[3], *Pierre Polsenaere*[4], *Christine Dupuy*[1], *Johann Lavaud*[1,5], *Alexandre Barnett*[1,2] and *Vincent Le Fouest*[1]

[1] LIttoral, ENvironnement et Sociétés (LIENSs), Université de La Rochelle, UMR 7266, CNRS-ULR, La Rochelle, France, [2] Mer Molécules Santé (MMS) - EA 21 60, Université de Nantes, Mer Molécules Santé, Nantes, France, [3] Département Dynamiques de l'Environnement Côtier, Laboratoire d'Ecologie Benthique, IFREMER, Plouzané, France, [4] IFREMER, Laboratoire Environnement et Ressources des Pertuis Charentais (LER-PC), BP133, La Tremblade, France, [5] Takuvik Joint International Laboratory UMI 3376, CNRS (France) & ULaval (Canada), Département de Biologie, Pavillon Alexandre-Vachon, Université Laval, Québec City, QC, Canada

OPEN ACCESS

Edited by:
Christian Grenz,
UMR7294 Institut Méditerranéen d'océanographie (MIO), France

Reviewed by:
Vanda Brotas,
University of Lisbon, Portugal
Rodrigo Riera,
Catholic University of the Most Holy Conception, Chile

***Correspondence:**
Raphaël Savelli
raphael.savelli1@univ-lr.fr

Specialty section:
This article was submitted to Marine Ecosystem Ecology, a section of the journal Frontiers in Marine Science

Received: 20 December 2019
Accepted: 08 June 2020
Published: 09 October 2020

Citation:
Savelli R, Méléder V, Cugier P, Polsenaere P, Dupuy C, Lavaud J, Barnett A and Le Fouest V (2020) Mapping the Intertidal Microphytobenthos Gross Primary Production, Part II: Merging Remote Sensing and Physical-Biological Coupled Modeling. Front. Mar. Sci. 7:521. doi: 10.3389/fmars.2020.00521

Microphytobenthos (MPB) at the sediment surface of intertidal mudflats are known to show a high spatial and temporal variability in response to the biotic and abiotic conditions prevailing at the mud surface. It makes long-term and large-scale monitoring of MPB Gross Primary Production (GPP) difficult to set up. In this study, we developed the first 3D physical-biological coupled model (MARS-3D) that explicitly simulates GPP of intertidal MPB at the mudflat scale, and we compared the outputs with *in situ* and space remote sensing MPB GPP data. We discuss the sources of discrepancies between the modeling and the remote sensing approach in the light of future developments to be done. For instance, the remote sensing algorithm provides a very synoptic view of the mudflat GPP. It is well-suited to achieve diagnostic estimates of MPB GPP at the synoptic spatial and temporal scale. By contrast, the MARS-3D model provides a more dynamic representation of the MPB activity and prognostic estimates of MPB GPP over the mudflat. It is very relevant to resolve the seasonal and inter-annual dynamics of MPB. Getting comparable GPP estimates derived from the remote sensing algorithm and 3D physical-biological coupled model will further require a better convergence in terms of equations structure, biological constants parameterization, and source data used (i.e., vegetation index vs. chlorophyll *a*). Setting a common parameterization in both the numerical model and remote sensing algorithm might be challenging in a perspective of mapping MPB PP over large mudflats from a synoptic to inter-annual time scale, but it could open the door to a new way of quantifying MPB GPP over large intertidal mudflats.

Keywords: microphytobenthos, intertidal mudflat, gross primary production, remote sensing, physical-biological modeling

1. INTRODUCTION

Benthic microalgae or microphytobenthos (MPB) inhabiting the sediment surface sustain a high biological production in intertidal mudflats (MacIntyre et al., 1996; Underwood and Kromkamp, 1999). As the main primary producers on intertidal mudflats, MPB are of key importance for higher trophic levels from benthic fauna to birds (Herman et al., 2000; Kang et al., 2006; Jardine et al., 2015) and for pelagic organisms that benefit MPB locally resuspended by tides and waves (Perissinotto et al., 2003; Krumme et al., 2008) but also exported to adjacent ecosystems (Saint-Béat et al., 2013). With a global annual Primary Production (PP) estimated to ∼500 million tons of Carbon (C; Cahoon, 1999), MPB also participate in the Blue Carbon (Otani and Endo, 2019). Guarini et al. (2008) suggested that MPB PP could represent a significant amount of carbon not considered in the global carbon cycle. However, their contribution to the global carbon budget remains unknown.

The spatial and temporal distribution of MPB over mudflats is highly variable, as it is driven by highly variable physical [light, mud surface temperature (MST), tides, waves, and current] and biological (grazing, biostabilization, and bioturbation) conditions (e.g., Admiraal, 1984; Blanchard et al., 1996; MacIntyre et al., 1996; Underwood, 2001; Morris and Kromkamp, 2003; Sahan et al., 2007; Salleh and McMinn, 2011; Kwon et al., 2014; Orvain et al., 2014a,b; Savelli et al., 2019). Such a variability impedes any accurate and robust assessment of the role played by MPB at the scale of the whole mudflat ecosystem and of its contribution to the carbon cycle. MPB PP and biomass measurements are usually limited to single-point sampling (e.g., Vieira et al., 2013; Orvain et al., 2014a; Cartaxana et al., 2015; Pniewski et al., 2015). This approach succeeds in capturing the MPB temporal dynamics but is rapidly limited when dealing with spatial and temporal variations of MPB PP and biomass at the scale of an entire mudflat. Only a few studies resolved the MPB spatial variability at the mudflat scale, as time and important logistical resources are required to meet this goal (e.g., Guarini et al., 1998; Ubertini et al., 2012). Remote sensing and physical-biological coupled modeling are then relevant and non-invasive approaches to infer on MPB dynamics (e.g., Guarini et al., 2000; Combe et al., 2005; van der Wal et al., 2010; Brito et al., 2013).

Jobson et al. (1980) initiated the use of remote sensing to assess the MPB biomass from a tower-mounted sensor designed to scan a mudflat of South Carolina (USA). Since then, airborne and space remote sensing methods were increasingly developed and more widely used in MPB studies (e.g., Méléder et al., 2003a; Brito et al., 2013; Benyoucef et al., 2014; Daggers et al., 2018). Remote sensing data can cover large spatial scales (∼ from one meter to several kilometers), and multispectral broadband sensors promise high quality data to map MPB biomass and PP over entire mudflats. Daggers et al. (2018) first coupled *in situ* measurements, satellite remote sensing data, and observed tidal heights to map synoptic MPB PP in spring at the scale of the Oosterschelde and Westerschelde estuaries (The Netherlands). Méléder et al. (2020) coupled *in situ* measurements, satellite remote sensing data, and data simulated (light, MST, and tidal height) by a 3D physical-biological coupled model to map synoptic MPB PP at three seasons over the large intertidal Brouage mudflat on the French Atlantic Coast.

Recently, remotely sensed estimates of vegetation index and of in water MPB chlorophyll *a* (Chl *a*) concentration were compared to model outputs in order to assess the model ability to simulate realistic MPB biomass levels over the Brouage mudflat (Savelli et al., 2018, 2019). Such a comparison does not exist for MPB PP. The recent development for the Brouage mudflat of a regional MPB Gross Primary Production (GPP) algorithm (Méléder et al., 2020) and of a 1D MPB GPP physical-biological coupled model (Savelli et al., 2018) allows for the comparison of MPB GPP estimates derived from space remote sensing and a prognostic modeling approach. The objective of this study is to infer the capacity of remote sensing and prognostic modeling to converge toward realistic MPB GPP estimates over the large Brouage mudflat. In this paper, we describe first the physical-biological coupled model developed in 3D in order to simulate the spatial and temporal dynamics of intertidal MPB. Second, we compare the model outputs with remotely sensed MPB GPP estimates coincident in space and time. Finally, we discuss the sources of discrepancies between the two approaches in the light of future developments to be done.

2. MATERIALS AND METHODS

2.1. Study Site

The Pertuis Charentais Sea is a shallow semi-enclosed sea where develops one of the biggest shellfish farming activity in Europe (Goulletquer, 1998). It receives riverine inputs originating from the agricultural watersheds of the Sèvre, Charente, and Seudre rivers (**Figure 1**). Located in the southern part of the Pertuis Charentais, the Brouage intertidal mudflat is a 42-km^2 intertidal mudflat composed of fine cohesive sediments (Bocher et al., 2007) distributed over a gentle slope (∼ 1/1,000; Le Hir et al., 2000). As in many other mudflats along the northern European Atlantic coast, a dense MPB biofilm develops at the sediment surface at low tide with Chl *a* concentrations reaching up to 25 mg Chl *a* m^{-2} (Guarini, 1998). The Brouage mudflat is responsible for a large part of the high PP reported in the Marennes-Oléron Bay (Struski and Bacher, 2006).

2.2. Observations

Field campaigns were conducted during spring and daytime low tides on 5–6 May and 2–3 July 2015. A total of 9 GPP estimates were derived from carbon fluxes at the air-sediment interface measured with benthic chambers. The CO_2 concentration was measured in the chambers continuously over a period of 20 to 30 min using an infrared gas analyzer (IRGA). At the same time, incident photosynthetically active radiation (400 to 700 nm; PAR, μmol photons m^{-2} s^{-1}) and temperature (°C) were measured (LS-C planar sensor plugged to a ULM-500 data-logger, Walz, Effeltrich, Germany) at the sediment surface near the chambers at a 30-s frequency. The MPB biomass was estimated continuously (every 5–10 min) by sediment sampling of the upper 250 μm layer by the "crème brulée" method (Laviale et al., 2015). 43 biomass samples were taken from the sediment surface. The Chl

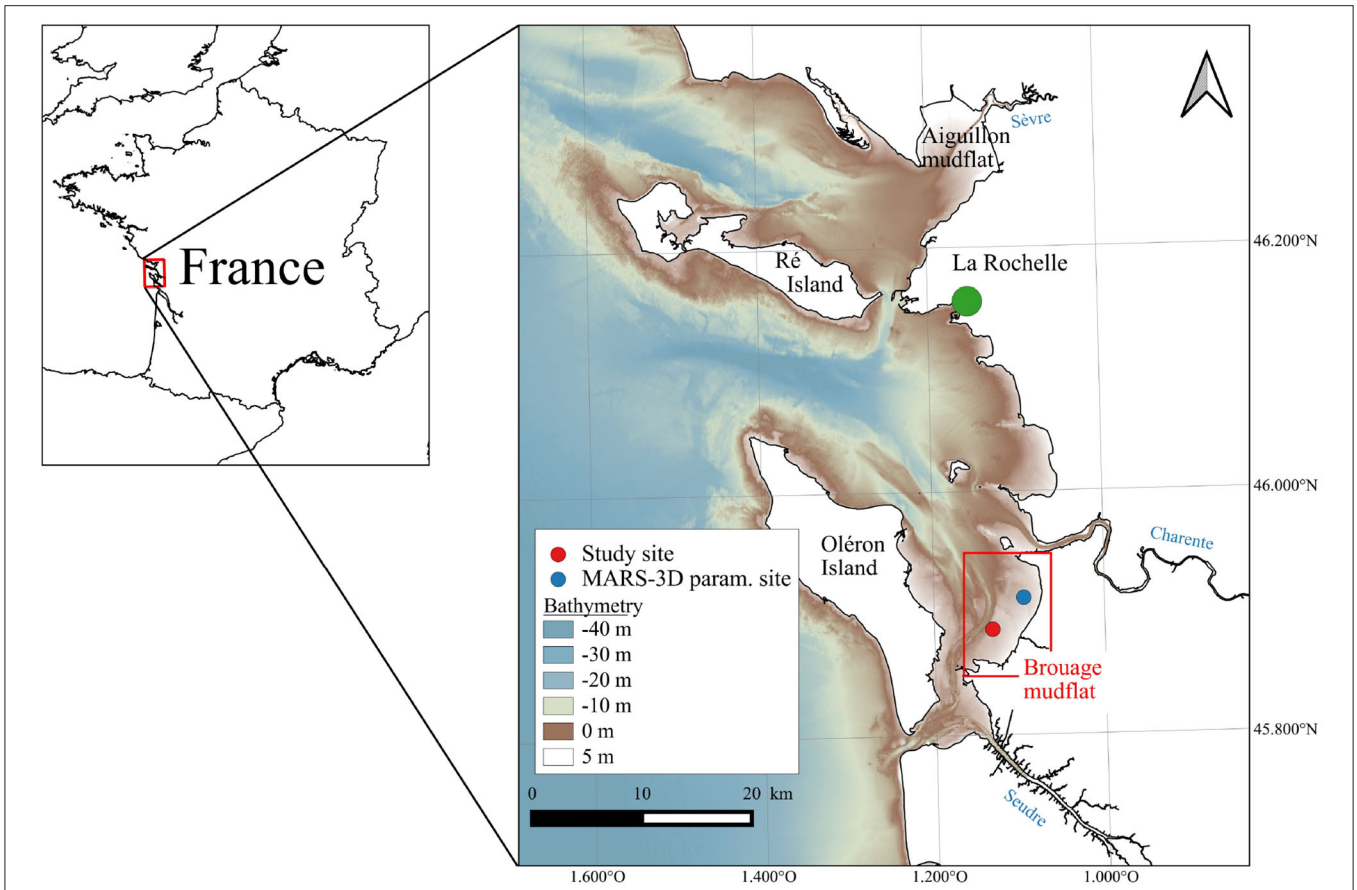

FIGURE 1 | Bathymetry of the model domain covering the Pertuis Charentais Sea (source: SHOM).

a content of sediment was determined by reversed phase HPLC (Hitachi High Technologies Co., Japan) calibrated for Chl *a*. The Chl *a* concentration was normalized to the sampled surface (1.5 cm^2) to be expressed in mg Chl *a* m^{-2}. The sampling protocol is fully detailed in Méléder et al. (2020).

2.3. The Coupled Physical-Biological 3D Model

2.3.1. The MARS-3D Model

The MARS-3D model (3D hydrodynamical Model for Applications at Regional Scale) is a regional ocean model that simulates the ocean physics (Lazure and Dumas, 2008). In this study, we used the regional configuration set up for the Pertuis Charentais area, including the Brouage mudflat. The model was discretized into 100 m by 100 m horizontal grid cells and 20 sigma-levels over depth. The model was run for the same domain as in Polsenaere et al. (2017) (**Figure 1**). The MARS-3D model is fully detailed in Lazure and Dumas (2008). Atmospheric forcings (10 m winds, air temperature, atmospheric pressure at sea level, nebulosity fraction, relative humidity, and downwelling solar fluxes) were provided by the Meteo France AROME model (https://donneespubliques.meteofrance.fr). At the open boundaries of the numerical grid, the MARS-3D model was forced by tidal amplitudes and phases of 115 harmonic constituents from the cstFRANCE tidal model developed by the French marine service for hydrography and oceanography (SHOM; Simon and Gonella, 2007). Initial and boundary conditions of seawater temperature, salinity, current velocity, and sea surface height were derived from the MANGAE 2500 Ifremer model (Lazure et al., 2009).

2.3.2. The Mud Surface Temperature Model

The mud surface temperature model used in Savelli et al. (2018) was coupled to MARS-3D. Thermodynamic equations detailed in Savelli et al. (2018) simulated heat fluxes within a 1 cm deep sediment layer. No horizontal fluxes were considered. In their study, Savelli et al. (2018) successfully compared the simulated MST with 1 min MST data measured *in situ* on the Brouage mudflat. The differential equation of heat energy balance was solved by the MARS-3D numerical scheme. The MST model is fully detailed in Savelli et al. (2018).

2.3.3. The MPB Model

The MPB model used in Savelli et al. (2018) was also coupled to MARS-3D. The MPB model simulated the MPB biomass in both the surface biofilm (*S*, mg Chl *a* m^{-2}) and sediment first centimeter (*F*, mg Chl *a* m^{-2}), and the grazer biomass (*Peringia*

ulvae, *Z*, and mg C m^{-2}) at the sediment surface. The MPB model accounted for vertical MPB migrations driven by diurnal and tidal cycles through exchanges of MPB biomass between *S* and *F* (Guarini et al., 2000). The *P. ulvae* growth was sustained by grazing on the MPB biofilm. It was controlled by the MST and MPB biomass in the biofilm. The biomass-specific photosynthetic rate P^b [mg C (mg Chl *a*)$^{-1}$ h^{-1}] was regulated by MST and PAR according to the models of Blanchard et al. (1996) and Platt and Jassby (1976), respectively. In the present study, the MPB biomass in the biofilm referred to the variable $S*$ introduced by Savelli et al. (2018) that represented the *S* compartment that incorporated the *S* instantaneous production of biomass [mg Chl *a* m^{-2}], which is directly transferred to *F*. The MPB model and differential equations are fully detailed in Savelli et al. (2018).

The physical-biological coupled model was initialized with a spin-up starting from 12 September 2014 00:00:00 UTC to 1 January 2015 00:00:00 UTC. The variables *F*, *S*, and *Z* were initially set to 100 mg Chl *a* m^{-2}, 0 mg Chl *a* m^{-2} and 1,000 mg C m^{-2}, respectively. The physical-biological coupled model was then run from 1 January 2015 00:00:00 UTC to 1 January 2016 00:00:00 UTC.

2.4. Remotely Sensed MPB GPP

The MPB GPP algorithm developed by Méléder et al. (2020; GPP-algo) coupled Normalized Difference Vegetation Index data (NDVI; Tucker, 1979) derived from the SPOT and Pléiades satellite sensors with MARS-3D derived forcings. In the GPP-algo, the remotely sensed GPP was obtained by constraining with tidal heights, light levels and mud surface temperature simulated by MARS-3D the horizontal distribution of MPB biomass estimated from the NDVI data and modulated by MPB vertical migration. The photosynthetic rate of MPB in the GPP-algo [P^b, mg C (NDVI)$^{-1}$ m^{-2} h^{-1}] was estimated by the temperature and light-related production models of Blanchard et al. (1996) and Eilers and Peeters (1988) parameterized with photophysiological parameters fitted on the laboratory measured light curves (α the initial slope of the curve, E_{opt} the optimum irradiance for photosynthesis, and P^b_{max} the photosynthetic capacity). The GPP-algo is fully detailed in Méléder et al. (2020).

2.5. Comparison of Remotely Sensed and Simulated MPB GPP

We compared the MPB GPP remotely sensed and simulated by MARS-3D on satellite acquisition matching days in May and July 2015. We ran two model setups. In the first run, the maximum photosynthetic capacity [P^b_{MAX}, mg C (mg Chl *a*)$^{-1}$ h^{-1}] was seasonally estimated by Blanchard et al. (1997; MARS-3D$_{season}$ run). In a second run, P^b_{MAX} was set from *in situ* GPP measurements in May and July 2015 (MARS-3D$_{synoptic}$ run). P^b_{MAX} was estimated from the measured biomass-specific production rate P^b [mg C (mg Chl *a*)$^{-1}$ h^{-1}], light, and MST from which we retrieved values of P^b_{MAX} with the models of Blanchard et al. (1996) and Platt and Jassby (1976) parameterized with photophysiological parameters (β the shape parameter of the production-temperature relationship, T_{opt} the temperature optimum for MPB photosynthesis, T_{max} the maximum temperature for MPB photosynthesis and E_k the light saturation parameter) from Savelli et al. (2018). We iterated values of P^b_{MAX} by a dichotomous analysis based on the intermediate value theorem (Bolzano, 1817). In MARS-3D$_{synoptic}$, the MPB GPP was simulated in days matching the *in situ* measurements with MARS-3D parameterized with the mean value of P^b_{MAX} iterated during *in situ* measurements in May and July 2015.

First, we took advantage of the MARS-3D$_{season}$ model to investigate the seasonal dynamics of MPB biomass and GPP (**Figure 2**). Second, we explored the spatial distribution of MPB biomass and GPP simulated by MARS-3D$_{season}$ (**Figure 2**). Then, we compared, in a single-point approach, P^b_{MAX} and GPP extracted from the MARS-3D$_{season}$ and MARS-3D$_{synoptic}$ grid cell corresponding to the sampling site with *in situ* measurements and GPP-algo (**Figure 2**). Finally, we compared fields of MPB GPP obtained with MARS-3D$_{synoptic}$ and GPP-algo (**Figure 2**).

3. RESULTS

3.1. Simulated Physical Environment by MARS-3D

PAR and MST data simulated by MARS-3D were validated with *in situ* MST and PAR data at the study site (**Figures 3A,B**). In May, the simulated PAR (1404.9 ± 101.3 μmol photons m^{-2} s^{-1}) was significantly different than the measured PAR (1514.7 ± 532.4 μmol photons m^{-2} s^{-1}; Mann–Whitney test, $p < 0.01$; **Figure 3A**). In July, the simulated PAR (1195.1 ± 305 μmol photons m^{-2} s^{-1}) was not significantly different from the measured PAR (1230 ± 306 μmol photons m^{-2} s^{-1}; Mann–Whitney test, $p = 0.04$). With respect to MST, with 20.7 ± 0.6°C in May, the simulated MST was significantly different than the MST measurements (19.5 ± 1.8°C; Mann–Whitney test, $p < 0.01$). In July, the simulated MST (31.2 ± 5°C) was not significantly different from the measured one (31.4 ± 3.4°C; Mann–Whitney test, $p = 0.1$; **Figure 3B**).

3.2. Seasonal MPB Dynamics Simulated at the Sampling Site

In the MARS-3D$_{season}$ run, the MPB biomass simulated in the sediment 1st cm reached one seasonal maximum on 25 February and 30 December with ∼190 mg Chl *a* m^{-2} in 2015 (**Figure 4A**). The seasonal minimum of MPB biomass simulated in the sediment occurred on 22 August with 34.2 mg Chl *a* m^{-2} (**Figure 4A**). The MPB biomass in the biofilm simulated in the MARS-3D$_{season}$ run was 20.6 ± 11.25 mg Chl *a* m^{-2} at the study site and varied from 0 to 44.3 mg Chl *a* m^{-2} (**Figure 4B**). The mean hourly GPP during daytime emersion simulated in the MARS-3D$_{season}$ run was 71.3 ± 65.4 mg C m^{-2} h^{-1} (**Figure 4C** and **Table 1**). Similarly to MPB biomass simulated in the biofilm, it was highly variable ranging from 0 to 278.8 mg C m^{-2} h^{-1} and often reached GPP levels similar to those measured in May and July 2015 (**Figure 4C**). The mean daily GPP simulated in the MARS-3D$_{season}$ run at the study site was 359.9 ± 229.5 mg C m^{-2} d^{-1} (**Table 1**). Such simulated GPP rates resulted in an annual GPP at the study site of 131 g C m^{-2} yr^{-1} (**Table 1**).

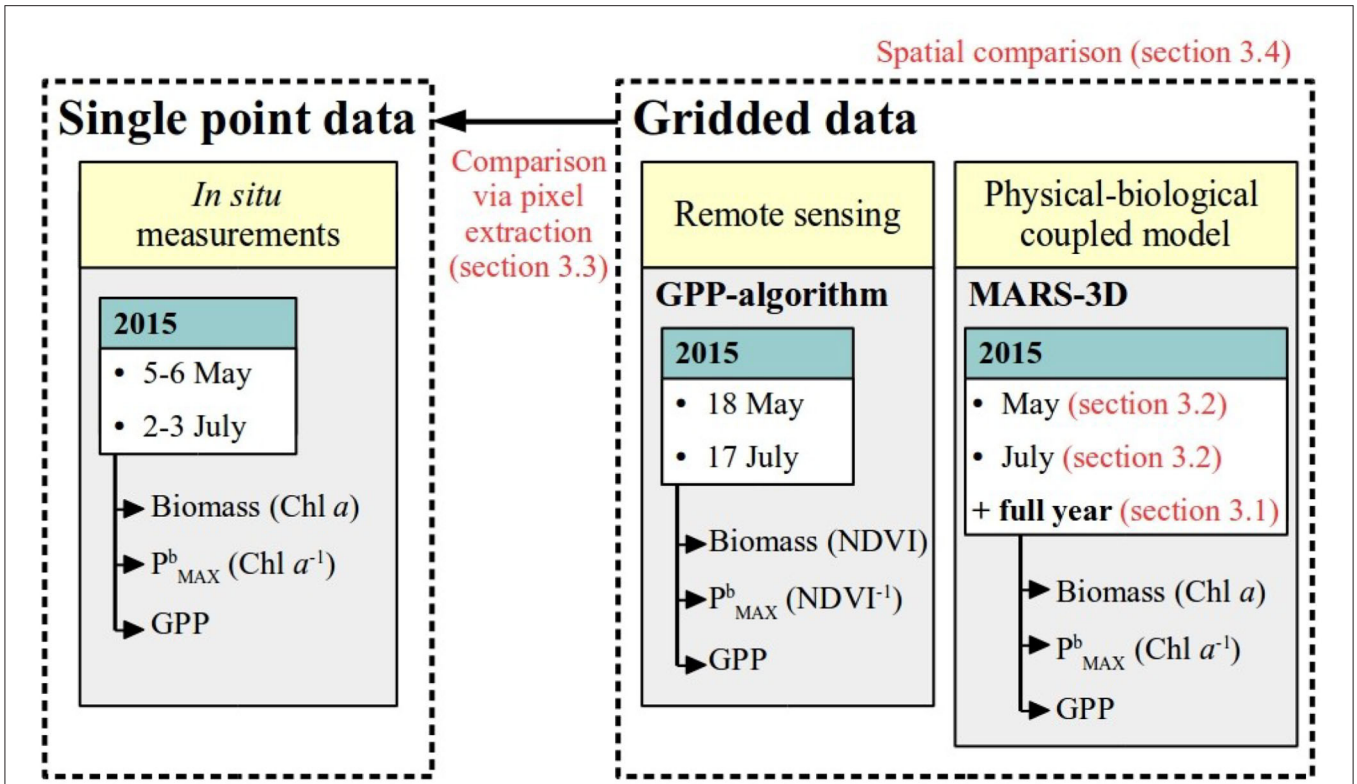

FIGURE 2 | Methods for MPB GPP estimation used in this study.

3.3. MPB GPP Simulated Over the Whole Mudflat

The MPB biomass in the biofilm simulated in MARS-3D$_{season}$ on satellite acquisition matching days in May 2015 was ∼40 and 35 mg Chl *a* m^{-2} on the upper and lower shore, respectively (**Figure 5A**). The MPB biomass simulated in the biofilm on satellite acquisition matching days in July 2015 was relatively homogeneous over the mudflat and was lower than in May 2015 with ∼25 and 20 mg Chl *a* m^{-2} (**Figure 5B**). In May 2015, the hourly GPP simulated in the MARS-3D$_{season}$ run on satellite acquisition matching days was relatively homogeneous over the mudflat with values of 130 mg C m^{-2} h^{-1} (**Figure 6A**). In July 2015, the hourly GPP simulated in the MARS-3D$_{season}$ run on satellite acquisition matching days was higher on the southern part of the mudflat (∼ 40 mg C m^{-2} h^{-1}) than on the northern part (∼ 20 mg C m^{-2} h^{-1}; **Figure 6B**). In May 2015, the daily integrated GPP simulated in MARS-3D$_{season}$ was higher on the upper shore (∼900 mg C m^{-2} d^{-1}) than on the lower shore (∼700 mg C m^{-2} d^{-1}; **Figure 6C**). Integrated over the mudflat, GPP simulated in MARS-3D$_{season}$ during satellite acquisition matching day in May 2015 was 19.5 t C (**Figure 6C**). In July 2015, similarly to the hourly GPP, the daily GPP simulated in the MARS-3D$_{season}$ run on satellite acquisition matching days was higher on the southern part of the mudflat (∼ 250 mg C m^{-2} d^{-1}) than on the northern part (∼ 100 mg C m^{-2} d^{-1}; (**Figure 6C**). It represented 3.8 t C, once integrated over the mudflat (**Figure 6D**).

3.4. MPB GPP Single-Point Comparison: Simulated vs. Remotely Sensed and *in situ* Data

P^b_{MAX} retrieved from iterations on *in situ* measurements was in average 0.26 ± 0.11 and 0.67 ± 0.30 mg C (mg Chl *a*)$^{-1}$ h^{-1} in May and July 2015, respectively (**Figure 7A** and **Table 2**). In the MARS-3D$_{season}$ run, P^b_{MAX} was ∼9.4 and 6.4 mg C (mg Chl *a*)$^{-1}$ h^{-1} in days matching the *in situ* measurements in May and July 2015, respectively (**Figure 7A** and **Table 2**). It was hence 36- and 9-fold higher than P^b_{MAX} retrieved from *in situ* measurements in May and July 2015, respectively (**Figure 7A** and **Table 2**). In the MARS-3D$_{season}$ run, the MPB biomass simulated in the biofilm during the field campaign was on average 21.7 ± 12.5 and 21.1 ± 9.5 mg Chl *a* m^{-2} in May and July 2015, respectively (**Figure 7B**). It was not significantly different than the measured MPB biomass in the biofilm in May and July 2015 (Mann–Whitney test: $p = 0.31$ and 0.95, respectively; **Figure 7B**). The simulated GPP in the MARS-3D$_{season}$ run in days matching the *in situ* measurements (164.8 ± 66.7 mg C m^{-2} h^{-1}) was on average 29- to 40-fold higher than the measured (5.69 ± 3.22 mg C m^{-2} h^{-1}) and remotely sensed (4.13 ± 2.22 mg C m^{-2} h^{-1}) GPP in May 2015, respectively (Mann–Whitney test: $p < 0.01$; **Figure 7C** and **Table 2**). In July 2015, GPP simulated in the MARS-3D$_{season}$ run (41.3 ± 43.6 mg C m^{-2} h^{-1}) was significantly different than *in situ* (6.3 ± 0.3 mg C m^{-2} h^{-1}) and remotely sensed GPP (2.2 ± 1.4

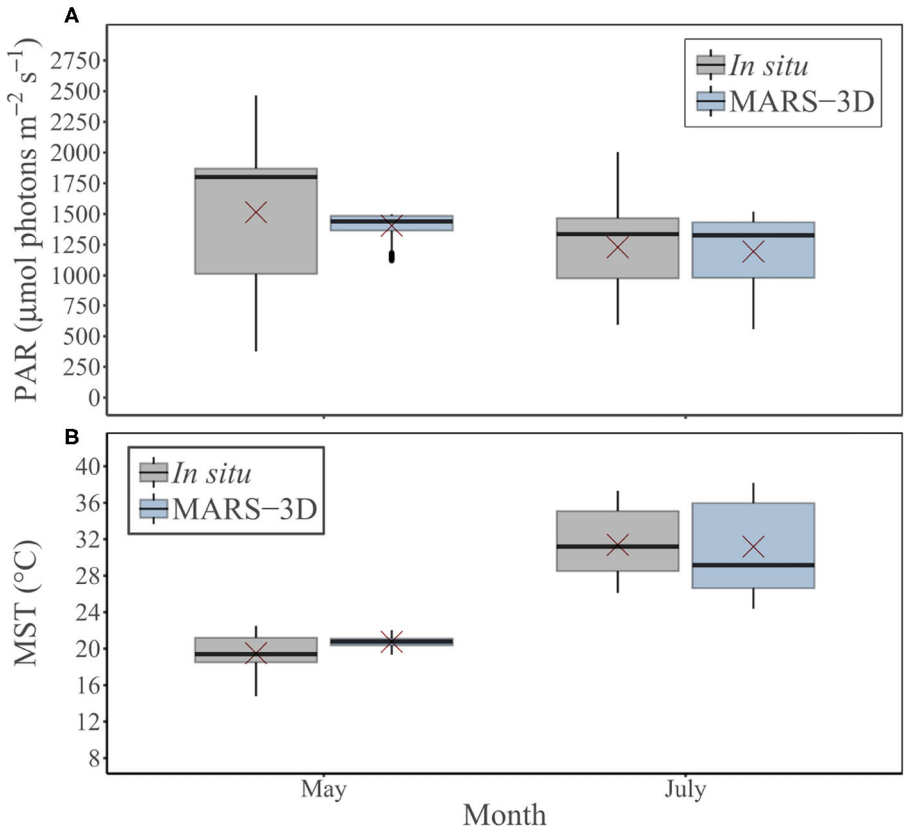

FIGURE 3 | Measured and simulated **(A)** PAR (μmol photons m^{-2} s^{-1}) and **(B)** MST (°C) by MARS-3D during *in situ* sampling days in May and July 2015. Red crosses correspond the mean value of PAR and MST for the corresponding period.

mg C m^{-2} h^{-1}; Mann–Whitney test: $p < 0.01$; **Figure 7C** and **Table 2**).

In the MARS-3D$_{synoptic}$ run, i.e., with a mean P^b_{MAX} based on *in situ* measurements in May and July 2015 (0.26 ± 0.11 and 0.67 ± 0.30 mg C (mg Chl *a*)$^{-1}$ h^{-1}, respectively; **Figure 8A**), the MPB biomass simulated in the biofilm was consistent with the estimates measured *in situ* (Mann–Whitney test: $p = 0.6$ and 0.62, respectively; **Figure 8B**). The mean MPB biomass simulated in the MARS-3D$_{synoptic}$ run on *in situ* sampling days in May 2015 was 17.8 ± 9.9 mg Chl *a* m^{-2} (**Figure 8B**). In July 2015, it was 17.3 ± 9.9 mg Chl *a* m^{-2} (**Figure 8B**). In the MARS-3D$_{synoptic}$ run, the simulated GPP compared to GPP measured *in situ* and derived from GPP-algo on *in situ* sampling days. With values of 5.1 ± 2.13 mg C m^{-2} h^{-1} in May 2015, GPP simulated in the MARS-3D$_{synoptic}$ run was not significantly different than GPP measured *in situ* and derived from GPP-algo (Mann–Whitney test: $p = 0.9$ and 0.5; **Figure 8C** and **Table 2**). In July 2015, GPP simulated in the MARS-3D$_{synoptic}$ run (5.25 ± 4.78 mg C m^{-2} h^{-1}) was not significantly different than GPP measured *in situ* and derived from GPP-algo (Mann–Whitney test: $p = 0.6$ and 0.08, respectively in July 2015; **Figure 8C** and **Table 2**).

3.5. Sensitivity of the Model to P^b_{MAX} Variability

The parametrization of P^b_{MAX} in the MARS-3D$_{synoptic}$ run resulted in much lower simulated GPP values over the whole mudflat on satellite acquisition matching days in May and July 2015 than in the MARS-3D$_{season}$ run (**Figure 9**). In May 2015, the daily integrated GPP simulated in MARS-3D$_{synoptic}$ was homogeneous over the mudflat reaching value of ∼22 mg C m^{-2} d^{-1} (**Figure 9A**). Integrated over the whole mudflat, GPP was 0.54 t C in the MARS-3D$_{synoptic}$ run. In July 2015, the daily integrated GPP simulated in the MARS-3D$_{synoptic}$ run was higher on the upper shore (∼24 mg C m^{-2} d^{-1}) than on the lower shore (∼15 mg C m^{-2} d^{-1}; **Figure 9B**). It resulted in a simulated spatially integrated GPP of 0.40 t C in the MARS-3D$_{synoptic}$ run (**Figure 9A**).

Compared to the remotely sensed GPP data, the use of P^b_{MAX} based on synoptic field data in the MARS-3D$_{synoptic}$ run resulted into slightly lower daily integrated GPP simulated over the mudflat in May 2015 (−21.2 ± 58.2 mg C m^{-2} d^{-1}; **Figure 9E**). Integrated over the mudflat, the simulated GPP decreased by 0.88 t C compared to the remotely sensed GPP estimate (**Figure 9E**). Aside from the extreme upper shore of the southern part of

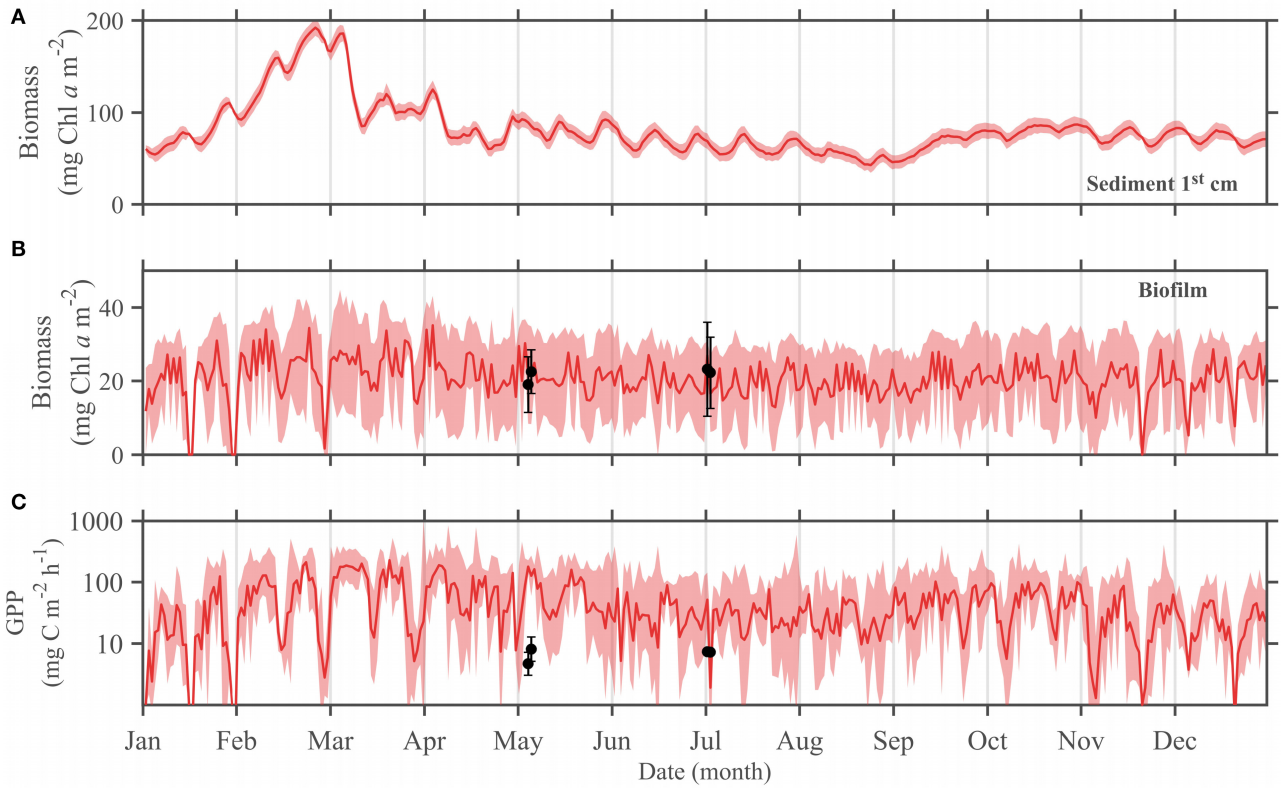

FIGURE 4 | Simulated mean seasonal cycle (MARS-3D$_{season}$ run) of the 2015 **(A)** daily mean MPB biomass in the sediment 1st cm, **(B)** daily mean MPB biomass in the biofilm (mg Chl *a* m^{-2}) and **(C)** hourly GPP (mg C m^{-2} h^{-1}; log scale) averaged during daytime low tides at the sampling site. The bold line is the temporal mean over the respective periods and shaded areas correspond to the temporal standard deviation. Black dots and error bars correspond to the mean and standard deviation of the Chl *a* (mg Chl a m^{-2}) and GPP measured *in situ*.

TABLE 1 | Simulated GPP estimates (MARS-3D$_{season}$ run) at the sampling site in 2015.

Variables	Units	Values
Hourly GPP	mg C m^{-2} h^{-1}	71.3 ± 65.4
Daily GPP	mg C m^{-2} d^{-1}	359.9 ± 229.5
Annual GPP	g C m^{-2} yr^{-1}	131

the mudflat where MARS-3D did not simulate MPB, the GPP differences were particularly high on patches in the central and northern part of the mudflat with differences up to 40 mg C m^{-2} d^{-1} in May 2015 (**Figure 9E**). The GPP differences between the MARS-3D$_{synoptic}$ run and the GPP-algo were lower in July 2015 than in May 2015. The mean GPP difference was −3.82 ± 15.7 mg C m^{-2} d^{-1} in July 2015 (**Figure 9F**). The MARS-3D$_{synoptic}$/GPP-algo difference of mudflat-integrated GPP in July 2015 was −0.40 t C (**Figure 9F**). The high temporal variability of P^b_{MAX} impeded therefore a convergence of its estimation between the modeling and space remote sensing approach. Consequently, it was a very sensitive parameter in the model as it mediated strong differences in GPP estimates between the MARS-3D$_{synoptic}$ and MARS-3D$_{season}$ runs.

4. DISCUSSION

4.1. Simulated and Remotely Sensed MPB GPP Estimates

The GPP simulated in the MARS-3D$_{season}$ run model is much higher than GPP measured *in situ*. Over the mudflat, the GPP simulated in the MARS-3D$_{season}$ run is also higher than the GPP derived from the GPP-algo developed by Méléder et al. (2020) for the whole mudflat. However, both the model (MARS-3D$_{season}$) and the remote sensing algorithm provide hourly and daily GPP rates in the range of GPP values reported in the literature (Cahoon, 1999; Underwood and Kromkamp, 1999; Daggers et al., 2018).

Given that the MARS-3D model is constrained by simulated water height and meteorological parameters, it is sensitive to likely inaccuracies in the forcings that might impede the model to resolve the high temporal variability of the physical environment. Nevertheless, simulated PAR and MST data lie within the range of *in situ* measurements and the impact of such inaccuracies on GPP estimates may be limited. As the MPB biomass simulated in the biofilm in the MARS-3D$_{season}$ run is also consistent with *in situ* measurements, the MARS-3D$_{season}$ run-observations GPP discrepancies can be attributed to differences in the MPB maximum photosynthetic capacity (P^b_{MAX}) used in the

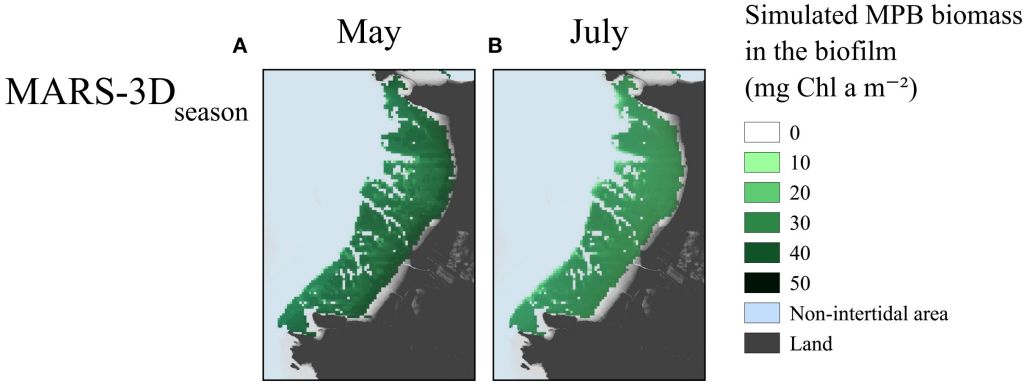

FIGURE 5 | Maximum MPB biomass simulated in the biofilm (mg Chl *a* m^{-2}) on satellite acquisition matching days in **(A)** May and **(B)** July 2015.

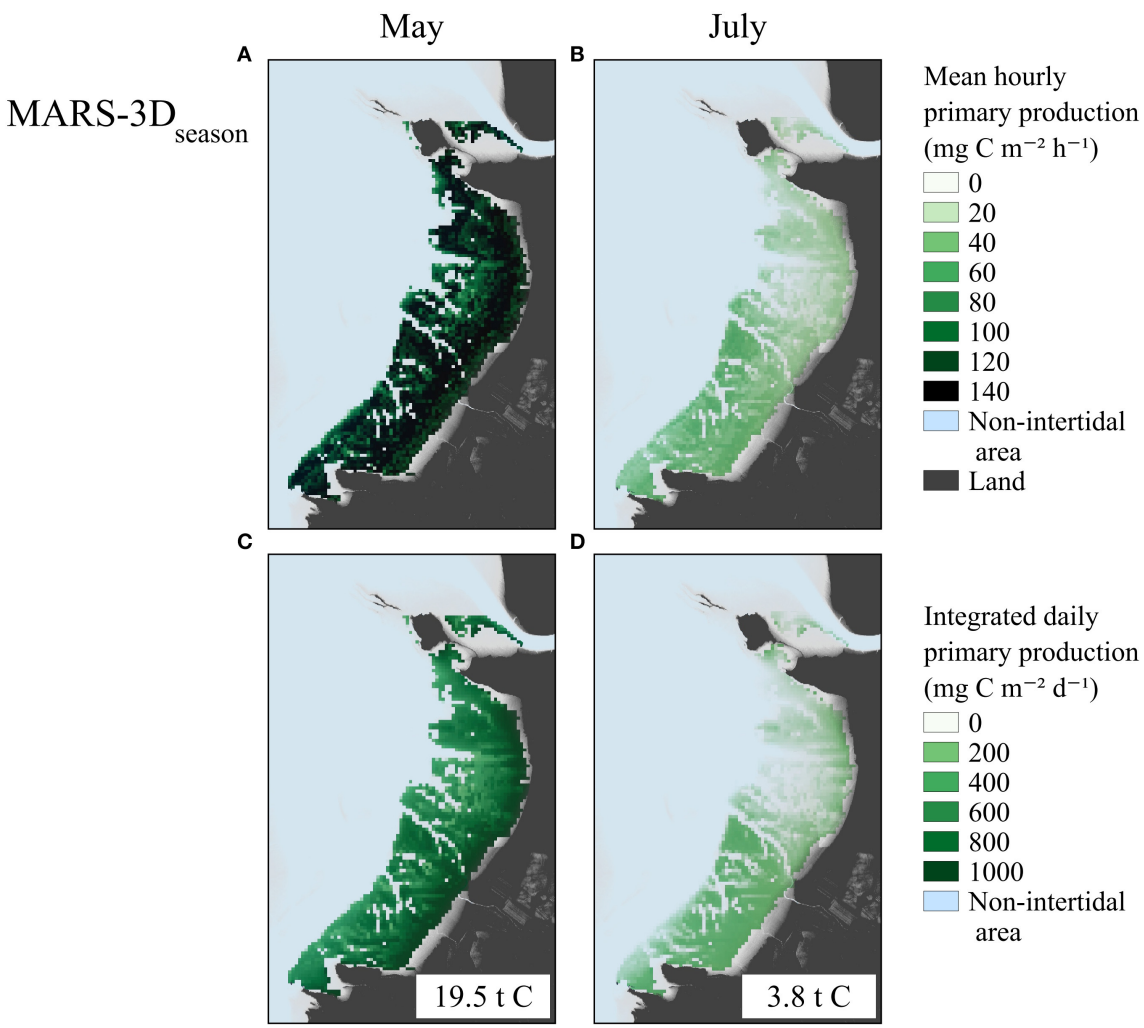

FIGURE 6 | Mean hourly (mg C m^{-2} h^{-1}) and daily integrated (mg C m^{-2} d^{-1}) GPP simulated in the MARS-$3D_{season}$ run on satellite acquisition matching days in May **(A,C)** and July 2015 **(B,D)**. Values indicated in white frames in **(C,D)** correspond to the GPP spatially integrated over the mudflat in t C.

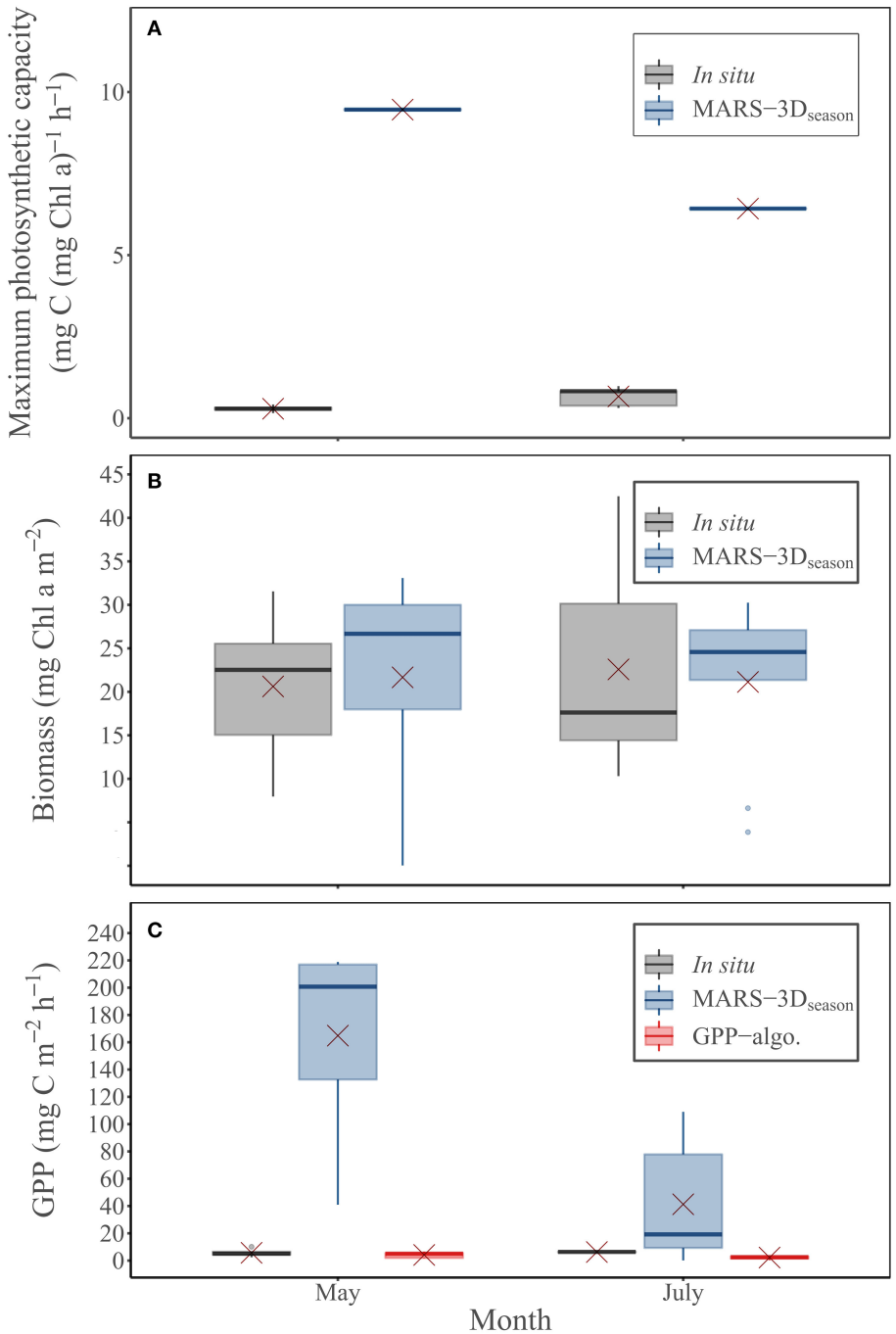

FIGURE 7 | Measured and simulated (MARS-3D$_{season}$ run) **(A)** maximum photosynthetic capacity (P^b_{MAX}, mg C (mg Chl *a*)$^{-1}$ h^{-1}) and **(B)** MPB biomass in the biofilm (mg Chl *a* m^{-2}) during *in situ* sampling days in May and July 2015. **(C)** MPB GPP (mg C m^{-2} h^{-1}) measured and predicted by the MARS-3D$_{season}$ run and the GPP-algo during *in situ* sampling days in May and July 2015. Red crosses correspond the mean value of PAR and MST for the corresponding period.

MARS-3D$_{season}$ run and estimated in the field in May and July 2015 at the study site. When set up with P^b_{MAX} comparable to the measured values, the GPP simulated in the MARS-3D$_{synoptic}$ run better compared to *in situ* GPP measurements. This suggests that, at the mudflat scale, MPB GPP estimates derived from remote sensing and the model are sensitive to the MPB photophysiological parameters (P^b_{MAX} but also the other temperature and light-related photosynthesis parameters such as the temperature optimum and maximum for MPB photosynthesis, the shape parameter of the production-temperature relationship and the light saturation parameter) and their spatio-temporal variability.

TABLE 2 | Measured and simulated maximum photosynthetic capacity (P^b_{MAX}) and hourly GPP in May and July 2015.

Months	Variables	*In situ*	GPP-algo	MARS-3D$_{season}$	MARS-3D$_{synoptic}$
May	P^b_{MAX} [mg C (mg Chl *a*)$^{-1}$ h^{-1}]	0.26 ± 0.11	per NDVI	9.4	Set to *in situ*
	Hourly GPP [mg C m^{-2} h^{-1}]	5.69 ± 3.22	4.13 ± 2.22	164.8 ± 66.7	5.1 ± 2.13
July	P^b_{MAX} [mg C (mg Chl *a*)$^{-1}$ h^{-1}]	0.67 ± 0.3	per NDVI	6.4	Set to *in situ*
	Hourly GPP (mg C m^{-2} h^{-1})	6.3 ± 0.3	2.2 ± 1.4	41.3 ± 43.6	5.25 ± 4.78

4.2. From Synoptic to Seasonal GPP Estimates

The GPP-algo developed by Méléder et al. (2020) is parameterized with synoptic measurements of the photosynthetic activity and the related photophysiological parameters (P^b_{MAX} and also the optimal irradiance for photosynthesis and the initial slope of the production-irradiance relationship) of MPB cells collected during the field campaigns. It is therefore well-suited to depict the high temporal variability of the MPB photosynthetic response to the physical environment. However, GPP estimates from space remote sensing are restricted to the satellite data availability, which depends on the satellite revisit time, the cloud cover and the time window of acquisition during the day (Daggers et al., 2018; Méléder et al., 2020). Despite this limitation, remote sensing GPP algorithms are relevant to estimate MPB GPP at the synoptic time scale (Daggers et al., 2018; Méléder et al., 2020).

When parameterized with synoptic *in situ* estimate of P^b_{MAX}, the MARS-3D model simulates GPP values that also compare to the *in situ* estimates. However, such a parametrization does only apply to a specific location at a specific time. Despite GPP simulated in MARS-3D$_{season}$ on *in situ* sampling days depart from measured GPP, daily and annual GPP simulated at the study site in 2015 (359.9 ± 229.5 mg C m^{-2} d^{-1} and 131 g C m^{-2} yr^{-1}, respectively) are consistent with the literature (Cahoon, 1999; Underwood and Kromkamp, 1999; Savelli et al., 2018, 2019). Annual MPB GPP estimates can be obtained from extrapolation of daily GPP (3.65 to 93.99 g C m^{-2} yr^{-1}; Méléder et al., 2020) derived from GPP-algo. However, the high MPB GPP variability at the hourly scale makes such extrapolations to be considered with caution. In contrast, the relatively consistent GPP values simulated at high frequency (12 s time step) in MARS-3D$_{season}$ over a year are likely to be used with more confidence for estimating GPP at the seasonal scale. The MPB model used in this study is adapted from the 1D model developed and validated in Savelli et al. (2018), which reasonably simulates the MPB dynamics in the Brouage mudflat for the year 2008. Similarly to Savelli et al. (2018), the seasonal cycle of MPB biomass simulated at the study site in 2015 is characterized by a spring bloom, a summer depression and a fall bloom. The fair agreement between the MPB biomass in the biofilm simulated in MARS-3D with the time-coincident observations suggests that overall the model simulates with some confidence the MPB dynamics at the seasonal scale in 2015.

4.3. From Single-Point to Mudflat GPP Estimates

MPB GPP estimates derived from remote sensing algorithms and physical-biological coupled models depend on the photophysiological parameters values and as such, on their sampling location on the mudflat. On a sandflat of the Bay of Paranaguá (Brazil), Fonseca et al. (2008) measured with benthic chambers higher PP rates in the upper and middle shores (1.9–2.1 g C m^{-2} d^{-1} and 1.3–2.2 g C m^{-2} d^{-1}, respectively) than in the lower shore (0.24–0.27 g C m^{-2} d^{-1}). Cook et al. (2004) measured CO_2 fluxes at the air-sediment interface at two tidal levels of a mudflat located in Tasmania. The uptake of inorganic carbon (total CO_2) at the benthic interface was higher on the upper shore (up to 15,000 μmol m^{-2} h^{-1}) than on the lower shore (up to 6,000 μmol m^{-2} h^{-1}), suggesting a higher benthic GPP on the upper shore than on the lower shore. On the Brouage mudflat, the relatively low GPP over the whole area depicted by the GPP-algo (Méléder et al., 2020) may be the result of a parametrization of the algorithm based on photophysiological parameters estimated on potentially low-productive MPB cells collected on the lower shore. Conversely, the photophysiological parameters used in the MARS-3D parameterization were derived from MPB cells collected on the middle shore of the Brouage mudflat (**Figure 1**; Blanchard et al., 1997). Consequently, when applied to the entire mudflat, such a parametrization may result in a GPP overestimation, especially on the lower shore as suggested by the MARS-3D$_{season}$-*in situ* measurements mismatch reported in the lower shore. Such a model-data mismatch is reduced in the MARS-3D$_{synoptic}$ run when the MARS-3D model is parameterized using MPB photophysiological parameters estimated on mud samples gathered on the lower Brouage shore.

Remote sensing algorithms and physical-biological coupled model GPP estimates rely on the photosynthetically active MPB biomass at the mud surface. While the remote sensing algorithm uses NDVI data, the MARS-3D model uses Chl *a* concentration simulated in the biofilm to infer on the horizontal distribution of MPB biomass at the mud surface. NDVI data provide a synoptic view of the MPB activity for a given time. Combining these NDVI snapshots over time (i.e., a diurnal cycle) requires us to account for the MPB vertical migration scheme during daytime low tides. Daggers et al. (2018) introduced the MPB vertical migrations in their remote sensing algorithm by modulating the PP rate during the first hour of the daytime emersion period. In their algorithm (GPP-algo), Méléder et al.

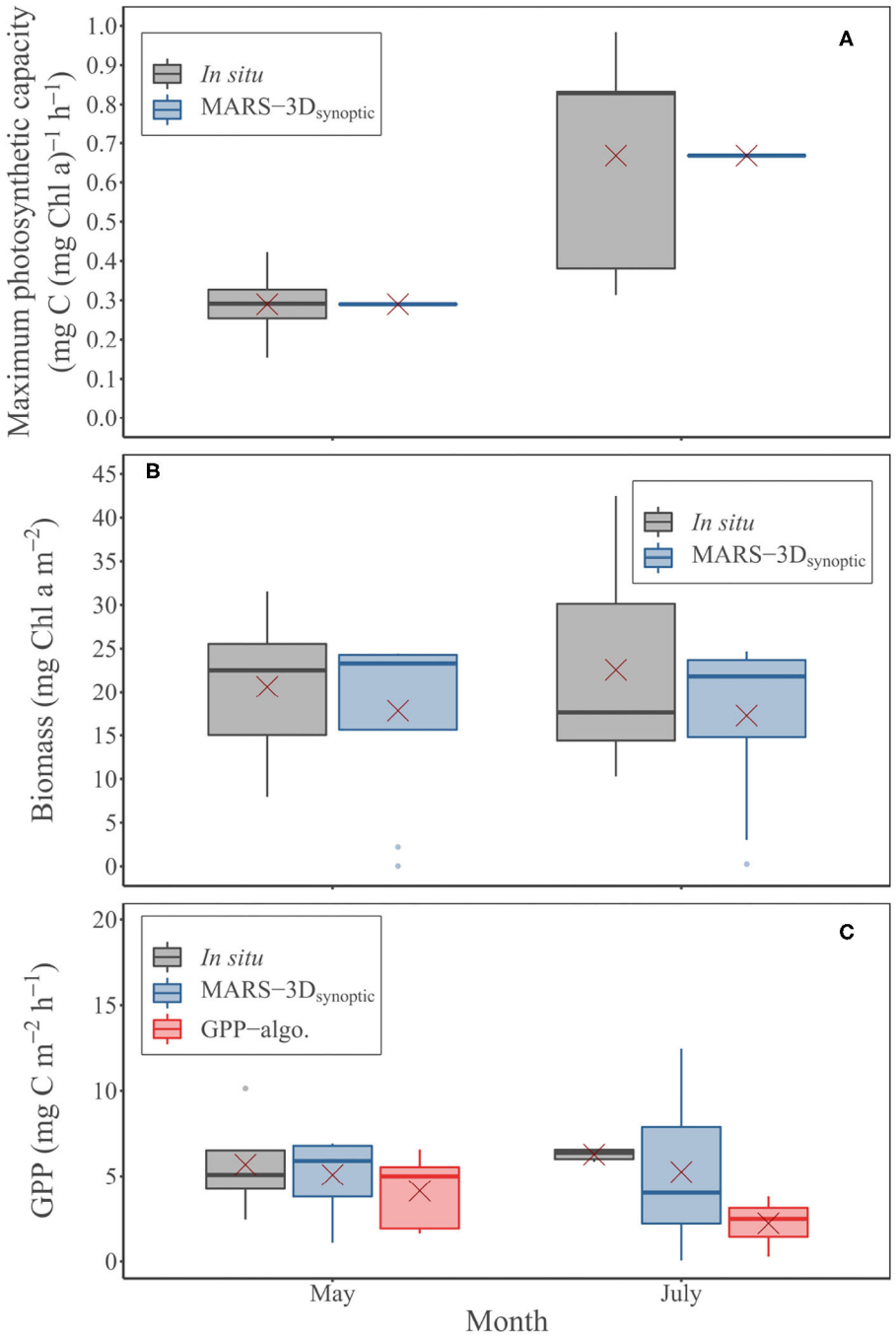

FIGURE 8 | Measured and simulated (MARS-3D$_{synoptic}$ run) **(A)** maximum photosynthetic capacity (P^b_{MAX}, mg C (mg Chl *a*)$^{-1}$ h^{-1}) and **(B)** MPB biomass in the biofilm (mg Chl *a* m^{-2}) during *in situ* sampling days in May and July 2015. **(C)** MPB GPP (mg C m^{-2} h^{-1}) measured and predicted by the MARS-3D$_{synoptic}$ run and GPP-algo during *in situ* sampling days in May and July 2015. Red crosses correspond the mean value of PAR and MST for the corresponding period.

(2020) assumed that the MPB biomass detected by satellite corresponds to the fully-established biofilm during the daytime low tide (total photosynthetically active biomass). Méléder et al. (2020) considered therefore a progressive establishment of the total photosynthetically active biomass at the sediment surface. In the MARS-3D model, the MPB biomass simulated in the biofilm follows the MPB vertical scheme described by Guarini et al. (2000). MPB cells migrate upward from the lower 1st cm sediment to the sediment surface during daytime low tides. At nightfall or at the time the flood begins, MPB cells migrate back downward. As the MPB biomass simulated in the biofilm in the MARS-3D model compares to the time-coincident field

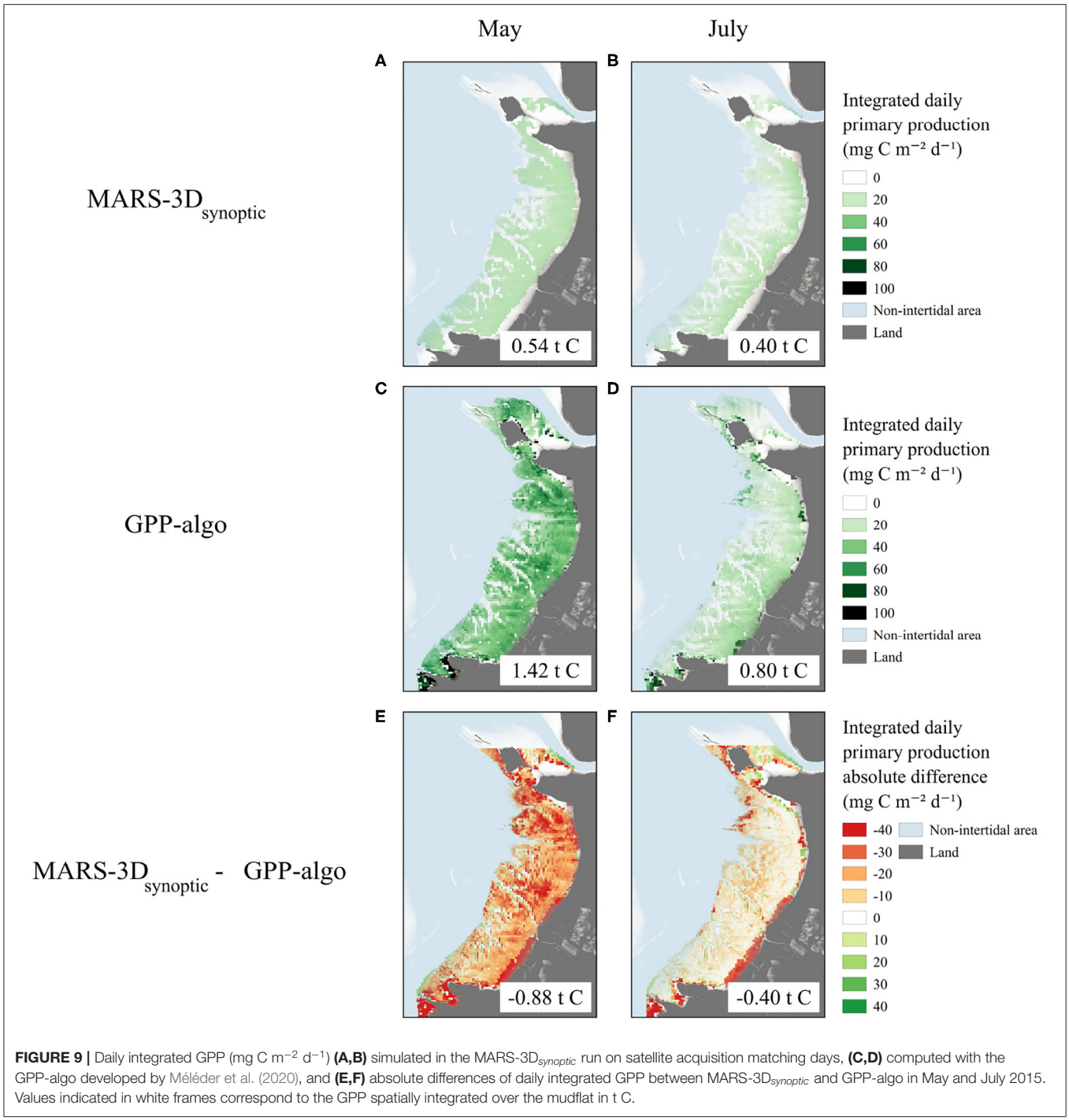

FIGURE 9 | Daily integrated GPP (mg C m^{-2} d^{-1}) **(A,B)** simulated in the MARS-3D$_{synoptic}$ run on satellite acquisition matching days, **(C,D)** computed with the GPP-algo developed by Méléder et al. (2020), and **(E,F)** absolute differences of daily integrated GPP between MARS-3D$_{synoptic}$ and GPP-algo in May and July 2015. Values indicated in white frames correspond to the GPP spatially integrated over the mudflat in t C.

measurements, the model can resolve with some confidence the temporal variability of the MPB biomass in the biofilm. However, no gridded data of benthic Chl *a* are available to assess the ability of the MARS-3D model to resolve the spatial variability of the MPB biomass in the biofilm. In the MARS-3D model (MARS-3D$_{season}$), the MPB biomass simulated in the biofilm is slightly higher on the upper shore than on the lower shore on satellite acquisition matching days. However, the time-coincident NDVI data suggest a higher MPB biomass on the lower and middle shores than on the upper shore (Méléder et al., 2020). Comparing the MARS-3D model (Chl *a*) and GPP-algo (NDVI) is difficult as the NDVI-Chl *a* relationship is not linear, especially at high values of Chl *a* (Méléder et al., 2003a,b; Serôdio et al., 2009). The remote sensing of the MPB biomass in Chl *a* units from hyperspectral imaging might overcome the MPB biomass units mismatch (Kazemipour et al., 2012; Launeau et al., 2018).

The horizontal resolution of satellite data and 3D regional models is also a critical issue when estimating GPP of patchy-distributed MPB. Méléder et al. (2020) report high differences in the NDVI signal between *in situ* and satellite observations and between different satellite sensors due to the dilution of the NDVI signal with the increasing pixel size and the patchiness distribution of the biofilm (Saburova et al., 1995; Spilmont et al., 2011). As the horizontal resolution of the MARS-3D model (100 m) and the remote sensing algorithm developed by Méléder et al. (2020) (from 2 to 6 m) differs, confronting quantitatively remotely sensed and simulated GPP per unit of surface must be considered with caution. The high horizontal resolution of remote sensing data is appropriate to monitor the MPB patchiness, which is not the case of the MARS-3D model. For this reason, remotely sensed GPP estimates are more suitable for comparison with synoptic *in situ* measurements.

5. CONCLUSIONS

This study is a first attempt to simulate the 3D MPB dynamics at the scale of an entire intertidal mudflat. Combined with a novel space remote sensing approach to assess MPB GPP, it allows for a first comparison of MPB GPP estimates derived from a remote sensing algorithm (GPP-algo) and a regional 3D physical-biological coupled model. The remote sensing algorithm provides a very synoptic view of the mudflat GPP. It is well-suited to achieve diagnostic estimates of MPB GPP at the synoptic spatial and temporal scale. By contrast, the 3D physical-biological model provides a more dynamic representation of the MPB activity as well as prognostic estimates of MPB GPP over the mudflat. It is very relevant to resolve the seasonal and inter-annual dynamics of MPB. Furthermore, the coupling of the intertidal and pelagic domains in the regional 3D model could be envisaged in the future to assess the fate in the coastal ocean of fresh organic carbon resulting from MPB GPP. However, a refinement of its horizontal numerical mesh is required to resolve the MPB patchiness and to allow a better comparison with high resolution remote sensing data in the future. With respect to remote sensing, GPP algorithms are still limited by the too low spectral resolution of the multispectral (3–10 bands) satellite sensors and by the data availability. Hyperspectral remote sensing is able to capture photosynthetic capabilities and GPP, as recently proposed for terrestrial vegetation (DuBois et al., 2018; Lees et al., 2018). This approach starts to be develop successfully on MPB by Méléder et al. (2018). Furthermore, airborne hyperspectral data (hundreds of bands) could complement space satellite remote sensing data in an era of remote sensing drone aircraft democratization (Launeau et al., 2018). The start-up of the Deutsches Zentrum für Luft- und Raumfahrt Earth Sensing Imaging Spectrometer (DESIS) on-board of the International Space Station could also enable the development of Earth Observation algorithms based on hyperspectral images from space. Confronting GPP derived from remote sensing algorithms and 3D physical-biological models will require a better convergence in terms of equations structure, biological constants parameterization, and source data used (i.e., NDVI vs. Chl *a*). Such a convergence would provide very complementary tools for diagnostic and prognostic analyses of the MPB GPP evolution at mudflat scales. While space remote sensing algorithms may provide a more realistic view of the MPB dynamics at the mudflat scale, 3D coupled physical-biological models can fill the gap left by space remote sensing strongly impacted at these latitudes by cloud cover, hence allowing for an annual budget of MPB GPP. Consequently, remote sensing algorithms and 3D coupled physical-biological models can be combined to monitor in an operational way MPB GPP from the synoptic to the annual scale and to achieve annual MPB GPP budget for large intertidal mudflats. Such a convergence was acclaimed in Babin et al. (2015) for phytoplankton in remote environments, whereas, for mudflats, remote sensing is pivotal for PP monitoring. Such an achievement will however require spatial and temporal surveys of the MPB photophysiological parameters across tidal heights in order to better assess the MPB photosynthetic response in time and space and better parameterize the remote sensing algorithms and models. Assessing the photosynthetic response of MPB to its highly variable environment is a challenge for the coming years in a perspective of quantifying MPB PP over large productive mudflats from a synoptic to inter-annual time scale.

DATA AVAILABILITY STATEMENT

Several chapters of RS.'s PhD thesis will use the model presented in this study. As a consequence, the model data presented in this study were archived in a ZENODO repository (https://zenodo.org/record/4022383), which will be available after an embargo period corresponding to the completion of this PhD thesis (December 2020).

AUTHOR CONTRIBUTIONS

RS, VM, VL, PC, PP, CD, and JL set the conceptual framework of this study. RS, PC, VL, and PP coupled the MPB model to MARS-3D. VM, RS, AB, PP, and JL carried out the experiments. RS, AB, and JL analyzed the data. RS wrote the manuscript. RS, VM, VL, PC, PP, CD, JL, and AB reviewed the manuscript. All authors contributed to the final version of the manuscript.

FUNDING

This work was supported by (i) the DYCOFEL project, funded through the 2015 Fondation de France call Quels littoraux pour demain?; (ii) the MIMOSA project, funded through the 2018 CNRS EC2CO-LEFE call; (iii) the HYPEDDY project, funded through the 2018–2020 Tosca-CNES call; (iv) the BIO-Tide project, funded through the 2015–2016 BiodivERsA COFUND call for research proposals, with the national funders BelSPO, FWO, ANR, and SNSF; (v) the public funds received in the framework of GEOSUD, a project (ANR-10-EQPX-20) of the program Investissements d'Avenir, managed by the French

National Research Agency; and (vi) the projects Littoral 1 and ECONAT funded by the Contrat de Plan Etat-Région (CPER) and the CNRS and the European Regional Development Fund. Pléiades and SPOT images were acquired by CNES's ISIS program, facilitating scientific access to imagery. Pléiades CNES 2015, 2018, Distribution Airbus DS, all rights reserved. Commercial uses forbidden. This research was part of fulfillment of the requirements for a Ph.D. degree (RS) at the Université de La Rochelle, France. RS was supported by a Ph.D. fellowship from the French Ministry of Higher Education, Research and Innovation.

ACKNOWLEDGMENTS

The authors acknowledge Meteo France for providing meteorological data and the Institut National de l'Information Géographique et Forestière (IGN) and the Service Hydrographique et Océanographique de la Marine (SHOM) for providing the digital elevation model of Charente Maritime LITTO3D®. The authors acknowledge the Pôle de Calcul et de Données Marines (PCDM) for providing DATARMOR storage, data access and computational resources.

REFERENCES

Admiraal, W. (1984). The ecology of estuarine sediment inhabiting diatoms. *Prog. Phycol. Res.* 3, 269–314.

Babin, M., Bélanger, S., Ellingsen, I., Forest, A., Le Fouest, V., Lacour, T., et al. (2015). Estimation of primary production in the Arctic Ocean using ocean colour remote sensing and coupled physical-biological models: strengths, limitations and how they compare. *Prog. Oceanog.* 139, 197–220. doi: 10.1016/j.pocean.2015.08.008

Benyoucef, I., Blandin, E., Lerouxel, A., Jesus, B., Rosa, P., Méléder, V., et al. (2014). Microphytobenthos interannual variations in a north-European estuary (Loire estuary, France) detected by visible-infrared multispectral remote sensing. *Estuar. Coast. Shelf Sci.* 136, 43–52. doi: 10.1016/j.ecss.2013.11.007

Blanchard, G. F., Guarini, J.-M., Gros, P., and Richard, P. (1997). Seasonal effect on the relationship between the photosynthetic capacity of intertidal microphytobenthos and temperature. *J. Phycol.* 33, 723–728. doi: 10.1111/j.0022-3646.1997.00723.x

Blanchard, G. F., Guarini, J.-M., Richard, P., Gros, P., and Mornet, F. (1996). Quantifying the short-term temperature effect on light- saturated photosynthesis of intertidal microphytobenthos. *Mar. Ecol. Prog. Ser.* 134, 309–313. doi: 10.3354/meps134309

Bocher, P., Piersma, T., Dekinga, A., Kraan, C., Yates, M. G., Guyot, T., et al. (2007). Site-and species-specific distribution patterns of molluscs at five intertidal soft-sediment areas in northwest Europe during a single winter. *Mar. Biol.* 151, 577–594. doi: 10.1007/s00227-006-0500-4

Bolzano, B. (1817). *Analytischer Beweis des Lehrsatzes, daß zwischen je zwey Werthen, die ein entgegensetztes Resultat gew ähren, wenigstens eine reelle Wurzel der Gleichung liege*. Gedruckt bei Gottlieb Haase.

Brito, A. C., Benyoucef, I., Jesus, B., Brotas, V., Gernez, P., Mendes, C. R., et al. (2013). Seasonality of microphytobenthos revealed by remote-sensing in a South European estuary. *Continent. Shelf Res.* 66, 83–91. doi: 10.1016/j.csr.2013.07.004

Cahoon, L. (1999). The role of benthic microalgae in neritic ecosystems. *Oceanogr. Mar. Biol.* 37, 47–86.

Cartaxana, P., Vieira, S., Ribeiro, L., Rocha, R. J., Cruz, S., Calado, R., et al. (2015). Effects of elevated temperature and CO 2 on intertidal microphytobenthos. *BMC Ecol.* 15:10. doi: 10.1186/s12898-015-0043-y

Combe, J.-P., Launeau, P., Carrère, V., Despan, D., Méléder, V., Barillé, L., et al. (2005). Mapping microphytobenthos biomass by non-linear inversion of visible-infrared hyperspectral images. *Remote Sens. Environ.* 98, 371–387. doi: 10.1016/j.rse.2005.07.010

Cook, P. L., Butler, E. C., and Eyre, B. D. (2004). Carbon and nitrogen cycling on intertidal mudflats of a temperate Australian estuary. I. Benthic metabolism. *Mar. Ecol. Prog. Ser.* 280, 25–38. doi: 10.3354/meps280025

Daggers, T. D., Kromkamp, J. C., Herman, P. M., and Van Der Wal, D. (2018). A model to assess microphytobenthic primary production in tidal systems using satellite remote sensing. *Remote Sens. Environ.* 211, 129–145. doi: 10.1016/j.rse.2018.03.037

DuBois, S., Desai, A. R., Singh, A., Serbin, S. P., Goulden, M. L., Baldocchi, D. D., et al. (2018). Using imaging spectroscopy to detect variation in terrestrial ecosystem productivity across a water-stressed landscape. *Ecol. Appl.* 28, 1313–1324. doi: 10.1002/eap.1733

Eilers, P., and Peeters, J. (1988). A model for the relationship between light intensity and the rate of photosynthesis in phytoplankton. *Ecol. Modell.* 42, 199–215. doi: 10.1016/0304-3800(88)90057-9

Fonseca, A., Brandini, N., da Costa Machado, E., and Brandini, F. P. (2008). Variação espacial e sazonal da produção primária microfitobêntica em uma planície entremarés subtropical, baía de paranaguá, paraná-Brasil. *INSULA Rev. Bot.* 37:19. doi: 10.5007/2178-4574.2008v37p19

Goulletquer, P. (1998). "Shellfish culture in France: present status and new approaches to optimise production," in *Proceedings of the Twenty-Ninth annual Shellfish Conference*, 69–80. Available online at: https://archimer.ifremer.fr/doc/00000/3094/

Guarini, J.-M. (1998). *Modélisation de la dynamique du microphytobenthos des vasieres intertidales du bassin de Marennes-Oléron. Effets des synchroniseurs physiques sur la régulation de la production* (Ph.D. thesis). Université Pierre & Marie Curie, Paris.

Guarini, J.-M., Blanchard, G. F., Bacher, C., Gros, P., Riera, P., Richard, P., et al. (1998). Dynamics of spatial patterns of microphytobenthic biomass: inferences from a geostatistical analysis of two comprehensive surveys in Marennes-Oléron Bay (France). *Mar. Ecol. Prog. Ser.* 166, 131–141. doi: 10.3354/meps166131

Guarini, J.-M., Blanchard, G. F., Gros, P., Gouleau, D., and Bacher, C. (2000). Dynamic model of the short-term variability of microphytobenthic biomass on temperate intertidal mudflats. *Mar. Ecol. Prog. Ser.* 195, 291–303. doi: 10.3354/meps195291

Guarini, J.-M., Chauvaud, L., and Coston-Guarini, J. (2008). Can the intertidal benthic microalgal primary production account for the "Missing Carbon Sink"? *J. Oceanogr. Res. Data* 1, 12–19.

Herman, P. M. J., Middelburg, J. J., Widdows, J., Lucas, C. H., and Heip, C. H. R. (2000). Stable isotopes as trophic tracers: combining field sampling and manipulative labelling of food resources for macrobenthos. *Mar. Ecol. Prog. Ser.* 204, 79–92. doi: 10.3354/meps204079

Jardine, C. B., Bond, A. L., Davidson, P. J., Butler, R. W., and Kuwae, T. (2015). Biofilm consumption and variable diet composition of Western Sandpipers (*Calidris mauri*) during migratory stopover. *PLoS ONE* 10:e0124164. doi: 10.1371/journal.pone.0124164

Jobson, D. J., Zingmark, R. G., and Katzberg, S. J. (1980). Remote sensing of benthic microalgal biomass with a tower-mounted multispectral scanner. *Remote Sens. Environ.* 9, 351–362. doi: 10.1016/0034-4257(80)90039-5

Kang, C., Lee, Y., Eun, J. C., Shin, J., Seo, I., and Hong, J. (2006). Microphytobenthos seasonality determines growth and reproduction in intertidal bivalves. *Mar. Ecol. Prog. Ser.* 315, 113–127. doi: 10.3354/meps315113

Kazemipour, F., Launeau, P., and Méléder, V. (2012). Microphytobenthos biomass mapping using the optical model of diatom biofilms: application to hyperspectral images of bourgneuf bay. *Remote Sens. Environ.* 127, 1–13. doi: 10.1016/j.rse.2012.08.016

Krumme, U., Keuthen, H., Barletta, M., Saint-Paul, U., and Villwock, W. (2008). Resuspended intertidal microphytobenthos as major diet component of planktivorous Atlantic anchoveta Cetengraulis edentulus (Engraulidae) from equatorial mangrove creeks. *Ecotropica* 14, 121–128.

Kwon, B.-O., Koh, C.-H., Khim, J. S., Park, J., Kang, S.-G., and Hwang, J. H. (2014). The relationship between primary production of microphytobenthos

and tidal cycle on the Hwaseong mudflat, west coast of Korea. *J. Coast. Res.* 30, 1188–1196. doi: 10.2112/JCOASTRES-D-11-00233.1

Launeau, P., Méléder, V., Verpoorter, C., Barillé, L., Kazemipour-Ricci, F., Giraud, M., et al. (2018). Microphytobenthos biomass and diversity mapping at different spatial scales with a hyperspectral optical model. *Remote Sens.* 10:716. doi: 10.3390/rs10050716

Laviale, M., Barnett, A., Ezequiel, J., Lepetit, B., Frankenbach, S., Méléder, V., et al. (2015). Response of intertidal benthic microalgal biofilms to a coupled light-temperature stress: evidence for latitudinal adaptation along the Atlantic coast of Southern Europe. *Environ. Microbiol.* 17, 3662–3677. doi: 10.1111/1462-2920.12728

Lazure, P., and Dumas, F. (2008). An external-internal mode coupling for a 3d hydrodynamical model for applications at regional scale (MARS). *Adv. Water Resour.* 31, 233–250. doi: 10.1016/j.advwatres.2007.06.010

Lazure, P., Garnier, V., Dumas, F., Herry, C., and Chifflet, M. (2009). Development of a hydrodynamic model of the bay of biscay. Validation of hydrology. *Continent. Shelf Res.* 29, 985–997. doi: 10.1016/j.csr.2008.12.017

Le Hir, P., Roberts, W., Cazaillet, O., Christie, M., Bassoullet, P., and Bacher, C. (2000). Characterization of intertidal flat hydrodynamics. *Continent. Shelf Res.* 20, 1433–1459. doi: 10.1016/S0278-4343(00)00031-5

Lees, K., Quaife, T., Artz, R., Khomik, M., and Clark, J. (2018). Potential for using remote sensing to estimate carbon fluxes across northern peatlands-a review. *Sci. Tot. Environ.* 615, 857–874. doi: 10.1016/j.scitotenv.2017.09.103

MacIntyre, H. L., Geider, R. J., and Miller, D. C. (1996). Microphytobenthos: the ecological role of the "secret garden" of unvegetated, shallow-water marine habitats. I. Distribution, abundance and primary production. *Estuaries* 19, 186–201. doi: 10.2307/1352224

Méléder, V., Barillé, L., Launeau, P., Carrere, V., and Rincé, Y. (2003b). Spectrometric constraint in analysis of benthic diatom biomass using monospecific cultures. *Remote Sens. Environ.* 88, 386–400. doi: 10.1016/j.rse.2003.08.009

Méléder, V., Jesus, B., Barnett, A., Barillé, L., and Lavaud, J. (2018). Microphytobenthos primary production estimated by hyperspectral reflectance. *PLoS ONE* 5:e0197093. doi: 10.1371/journal.pone.0197093

Méléder, V., Launeau, P., Barillé, L., and Rincé, Y. (2003a). Cartographie des peuplements du microphytobenthos par télédétection spatiale visible-infrarouge dans un écosystème conchylicole. *Comptes Rendus Biologies* 326, 377–389. doi: 10.1016/S1631-0691(03)00125-2

Méléder, V., Savelli, R., Barnett, A., Polsenaere, P., Gernez, P., Cugier, P., et al. (2020). Mapping the intertidal microphytobenthos gross primary production part I: coupling multispectral remote sensing and physical modeling. *Front. Mar. Sci.* 7:520. doi: 10.3389/fmars.2020.00520

Morris, E. P., and Kromkamp, J. C. (2003). Influence of temperature on the relationship between oxygen-and fluorescence-based estimates of photosynthetic parameters in a marine benthic diatom (Cylindrotheca closterium). *Eur. J. Phycol.* 38, 133–142. doi: 10.1080/0967026031000085832

Orvain, F., De Crignis, M., Guizien, K., Lefebvre, S., Mallet, C., Takahashi, E., et al. (2014a). Tidal and seasonal effects on the short-term temporal patterns of bacteria, microphytobenthos and exopolymers in natural intertidal biofilms (Brouage, France). *J. Sea Res.* 92, 6–18. doi: 10.1016/j.seares.2014.02.018

Orvain, F., Guizien, K., Lefebvre, S., Bréret, M., and Dupuy, C. (2014b). Relevance of macrozoobenthic grazers to understand the dynamic behaviour of sediment erodibility and microphytobenthos resuspension in sunny summer conditions. *J. Sea Res.* 92, 46–55. doi: 10.1016/j.seares.2014.03.004

Otani, S., and Endo, T. (2019). "Co2 flux in tidal flats and salt marshes," in *Blue Carbon in Shallow Coastal Ecosystems*, eds T. Kuwae and M. Hori (Singapore: Springer), 223–250. doi: 10.1007/978-981-13-1295-3_8

Perissinotto, R., Nozais, C., Kibirige, I., and Anandraj, A. (2003). Planktonic food webs and benthic-pelagic coupling in three South African temporarily-open estuaries. *Acta Oecol.* 24(Suppl 1), S307–S316. doi: 10.1016/S1146-609X(03)00028-6

Platt, T., and Jassby, A. D. (1976). The relationship between photosynthesis and light for natural assemblages of coastal marine phytoplankton. *J. Phycol.* 12, 421–430. doi: 10.1111/j.1529-8817.1976.tb02866.x

Pniewski, F. F., Biskup, P., Bubak, I., Richard, P., Latała, A., and Blanchard, G. F. (2015). Photo-regulation in microphytobenthos from intertidal mudflats and non-tidal coastal shallows. *Estuar. Coast. Shelf Sci.* 152, 153–161. doi: 10.1016/j.ecss.2014.11.022

Polsenaere, P., Soletchnik, P., Le Moine, O., Gohin, F., Robert, S., Pépin, J.-F., et al. (2017). Potential environmental drivers of a regional blue mussel mass mortality event (winter of 2014, Breton sound, France). *J. Sea Res.* 123, 39–50. doi: 10.1016/j.seares.2017.03.005

Saburova, M. A., Polikarpov, I. G., and Burkovsky, I. V. (1995). Spatial structure of an intertidal sandflat microphytobenthic community as related to different spatial scales. *Mar. Ecol. Prog. Ser.* 129, 229–239. doi: 10.3354/meps129229

Sahan, E., Sabbe, K., Creach, V., Hernandez-Raquet, G., Vyverman, W., Stal, L. J., et al. (2007). Community structure and seasonal dynamics of diatom biofilms and associated grazers in intertidal mudflats. *Aquat. Microb. Ecol.* 47, 253–266. doi: 10.3354/ame047253

Saint-Béat, B., Dupuy, C., Bocher, P., Chalumeau, J., De Crignis, M., Fontaine, C., et al. (2013). Key features of intertidal food webs that support migratory shorebirds. *PLoS ONE* 8:e76739. doi: 10.1371/journal.pone.0076739

Salleh, S., and McMinn, A. (2011). The effects of temperature on the photosynthetic parameters and recovery of two temperate benthic microalgae, Amphora cf. Coffaeformis and Cocconeis cf. sublittoralis (bacillariophycae)[1]. *J. Phycol.* 47, 1413–1424. doi: 10.1111/j.1529-8817.2011.01079.x

Savelli, R., Bertin, X., Orvain, F., Gernez, P., Dale, A., Coulombier, T. et al. (2019). Impact of chronic and massive resuspension mechanisms on the microphytobenthos dynamics in a temperate intertidal mudflat. *J. Geophys. Res.* 124, 3752–3777. doi: 10.1029/2019JG005369

Savelli, R., Dupuy, C., Barillé, L., Lerouxel, A., Guizien, K., Philippe, A., et al. (2018). On biotic and abiotic drivers of the microphytobenthos seasonal cycle in a temperate intertidal mudflat: a modelling study. *Biogeosciences* 15, 7243–7271. doi: 10.5194/bg-15-7243-2018

Serôdio, J., Cartaxana, P., Coelho, H., and Vieira, S. (2009). Effects of chlorophyll fluorescence on the estimation of microphytobenthos biomass using spectral reflectance indices. *Remote Sens. Environ.* 113, 1760–1768. doi: 10.1016/j.rse.2009.04.003

Simon, B., and Gonella, J. (2007). *La marée océanique côtière*. Institut Océanographique.

Spilmont, N., Seuront, L., Meziane, T., and Welsh, D. T. (2011). There's more to the picture than meets the eye: sampling microphytobenthos in a heterogeneous environment. *Estuar. Coast. Shelf Sci.* 95, 470–476. doi: 10.1016/j.ecss.2011.10.021

Struski, C., and Bacher, C. (2006). Preliminary estimate of primary production by phytoplankton in Marennes-Oléron Bay, France. *Estuar. Coast. Shelf Sci.* 323–334. doi: 10.1016/j.ecss.2005.09.007

Tucker, C. J. (1979). Red and photographic infrared linear combinations for monitoring vegetation. *Remote Sens. Environ.* 8, 127–150. doi: 10.1016/0034-4257(79)90013-0

Ubertini, M., Lefebvre, S., Gangnery, A., Grangeré, K., Le Gendre, R., and Orvain, F. (2012). Spatial variability of benthic-pelagic coupling in an estuary ecosystem: consequences for microphytobenthos resuspension phenomenon. *PLoS ONE* 7:e44155. doi: 10.1371/journal.pone.0044155

Underwood, G. J. C. (2001). "Microphytobenthos," in *Encyclopedia of Ocean Sciences*, ed J. H. Steele (Oxford: Academic Press), 1770–1777. doi: 10.1006/rwos.2001.0213

Underwood, G. J. C., and Kromkamp, J. C. (1999). "Primary production by phytoplankton and microphytobenthos in estuaries," in *Estuaries, Volume 29 of Advances in Ecological Research*, eds D. Nedwell and D. Raffaelli (Academic Press), 93–153. doi: 10.1016/S0065-2504(08)60192-0

van der Wal, D., Wielemaker-van den Dool, A., and Herman, P. M. J. (2010). Spatial synchrony in intertidal benthic algal biomass in temperate coastal and estuarine ecosystems. *Ecosystems* 13, 338–351. doi: 10.1007/s10021-010-9322-9

Vieira, S., Ribeiro, L., da Silva, J. M., and Cartaxana, P. (2013). Effects of short-term changes in sediment temperature on the photosynthesis of two intertidal microphytobenthos communities. *Estuar. Coast. Shelf Sci.* 119, 112–118. doi: 10.1016/j.ecss.2013.01.001

Conflict of Interest: The authors declare that the research was conducted in the absence of any commercial or financial relationships that could be construed as a potential conflict of interest.

frontiers in Marine Science

ORIGINAL RESEARCH
published: 24 March 2020
doi: 10.3389/fmars.2020.00170

Synoptic Spatio-Temporal Variability of the Photosynthetic Productivity of Microphytobenthos and Phytoplankton in a Tidal Estuary

Silja Frankenbach[1†], João Ezequiel[1†‡], Sandra Plecha[2,3‡], Johannes W. Goessling[4,5], Leandro Vaz[2], Michael Kühl[4], João Miguel Dias[2], Nuno Vaz[2] and João Serôdio[1]*

[1] Department of Biology – Centre for Environmental and Marine Studies, University of Aveiro, Aveiro, Portugal, [2] Department of Physics – Centre for Environmental and Marine Studies, University of Aveiro, Aveiro, Portugal, [3] Instituto Dom Luiz (IDL), Faculdade de Ciências da Universidade de Lisboa (FCUL), Lisbon, Portugal, [4] Marine Biological Section, Department of Biology, University of Copenhagen, Helsingør, Denmark, [5] International Iberian Nanotechnology Laboratory, Braga, Portugal

OPEN ACCESS

Edited by:
Dongyan Liu,
East China Normal University, China

Reviewed by:
Yujue Wang,
Yantai Institute of Coastal Zone Research (CAS), China
Gang Li,
South China Sea Institute of Oceanology, China
Li Zou,
Ocean University of China, China

***Correspondence:**
Silja Frankenbach
s.frankenback@ua.pt

[†] These authors share first authorship

[‡] Present address:
João Ezequiel,
RAIZ – Instituto de Investigação da Floresta e Papel, Aveiro, Portugal
Sandra Plecha,
Instituto Dom Luiz, Faculty of Sciences, University of Lisbon, Lisbon, Portugal

Specialty section:
This article was submitted to Marine Ecosystem Ecology, a section of the journal Frontiers in Marine Science

Received: *04 December 2019*
Accepted: *04 March 2020*
Published: *24 March 2020*

Citation:
Frankenbach S, Ezequiel J, Plecha S, Goessling JW, Vaz L, Kühl M, Dias JM, Vaz N and Serôdio J (2020) Synoptic Spatio-Temporal Variability of the Photosynthetic Productivity of Microphytobenthos and Phytoplankton in a Tidal Estuary. Front. Mar. Sci. 7:170. doi: 10.3389/fmars.2020.00170

Tidal estuaries are regarded as highly important ecosystems, mostly due to their high primary productivity and associated role as carbon sinks. In these ecosystems, primary productivity is mainly due to the photosynthetic carbon fixation by phytoplankton and microphytobenthos. The productivity of the two communities has been mostly studied separately, and directly comparable estimates of their carbon fixation rates in the same estuary are relatively scarce. The present study aimed to characterize the spatio-temporal variability of the productivity of phytoplankton and microphytobenthos in a tidal estuary, the Ria de Aveiro (Portugal). The productivity of the two communities was determined using a common methodological approach, based on measurements of *in vivo* chlorophyll fluorescence, allowing the estimation of the annual ecosystem-level budget for carbon fixation by the two groups. Productivity rates were determined based on synoptic *in situ* measurements of absolute rates of electron transport rate of photosystem II, using Pulse Amplitude Modulation fluorometry. Chlorophyll fluorescence indices were accompanied by measurements of salinity, temperature, water turbidity, solar irradiance, and planktonic and benthic microalgal biomass. Measurements were carried out hourly, along four spring-neap tidal cycles distributed along 1 year, on three sites of the estuary. The most pronounced trends in the spatio-temporal variability of the photophysiology and productivity of the two communities were the following: (i) maximum biomass and productivity were reached later for microphytobenthos (summer-autumn) than for phytoplankton (spring-summer); (ii) the absorption cross-section of PSII was generally higher for phytoplankton; (iii) the two groups showed a similar photoacclimation state, but microphytobenthos appeared as high light-acclimated when compared to phytoplankton. Biomass-specific productivity was on average higher for phytoplankton than for microphytobenthos, averaging 68.0 and 19.1 mg C mg Chl a^{-1} d^{-1}, respectively. However, areal depth-integrated production rates were generally higher for the microphytobenthos than for the phytoplankton, averaging 264.5 and

140.0 mg C m^{-2} d^{-1}, respectively. On an annual basis, phytoplankton productivity averaged 49.9 g C m^{-2} yr^{-1} while the productivity of microphytobenthos averaged 105.2 g C m^{-2} yr^{-1}. When upscaling to the whole estuary, annual primary production rates of phytoplankton and microphytobenthos reached 4894.3 and 7534.0 t C yr^{-1}, respectively, representing 39.4 and 60.6% of the combined total of 12428.3 t C yr^{-1} determined for the two communities in the Ria de Aveiro.

Keywords: chlorophyll *a* fluorescence, estuaries, diatoms, microphytobenthos, photoacclimation, photosynthesis, phytoplankton, productivity

INTRODUCTION

Estuaries and coastal zones support a variety of important ecosystem services, including nutrient cycling, flood control, and provision of nursery ground for a large diversity of marine animal species (Hope et al., 2019). At the same time, these areas are currently under direct threat from heavy human use, such as industrial and agricultural activities, littering and global climate changes (Barbier et al., 2011). The importance attributed to these habitats is largely justified by their high rates of primary productivity, ranking among the highest in both aquatic and terrestrial ecosystems, supporting important food webs and affecting atmospheric carbon sequestration (McLusky and Elliott, 2007). In tidal estuaries and shallow coastal zones, primary productivity is mostly due to the photosynthetic carbon fixation by phytoplankton and microphytobenthos (Underwood and Kromkamp, 1999). Although estuarine primary productivity is often considered to be mainly due to phytoplankton photosynthetic activity, the contribution of microphytobenthos can be significant in tidal systems, having been estimated to reach up to 50% of ecosystem-level carbon fixation (Cadée and Hegeman, 1974; Joint, 1978). This is due to the light-limitation of phytoplankton productivity, associated to the high turbidity of the water column caused by sediment resuspension by strong tidal currents (Ubertini et al., 2012; Pratt et al., 2014), and, on the other hand, to the large intertidal areas formed during low tide, which harbor dense and highly productive microphytobenthos communities (Van Colen et al., 2014).

The assessment of the primary productivity of estuarine areas is crucial to evaluate their role as carbon sinks, a question particularly relevant in the current context of increasing of atmospheric carbon levels due to anthropogenic action (Bauer et al., 2013). However, the primary productivity of phytoplankton and microphytobenthos communities have been generally studied separately and only a relatively small number of studies have attempted to provide directly comparable estimates of carbon fixation rates of the two groups in the same estuary (Cadée and Hegeman, 1974; Joint, 1978; Fielding et al., 1988; Caffrey et al., 2014). This is likely due to differences in the methodologies used to quantify photosynthetic activity and carbon fixation in the water column and in the sediment. The difficulties in obtaining comparable estimates for phytoplankton and microphytobenthos have been long recognized (Underwood and Kromkamp, 1999) and are essentially due to the drastic differences in the vertical scale of the photic zone in the water column (meters) and the sediment (micrometers). This has hampered not only the estimation of integrated pelagic-benthic production budgets but also the evaluation of the relative importance of both communities.

This work aimed to assess the integrated pelagic-benthic productivity in a tidal estuarine system, the Ria de Aveiro (Portugal), by estimating photosynthetic rates of both phytoplankton and microphytobenthos communities using a common methodological approach. The primary productivity of phytoplankton and microphytobenthos was estimated based on measurements of *in vivo* chlorophyll fluorescence indices combining the functional absorption cross section and the effective quantum yield of photosystem II (PSII), enabling the calculation of absolute rates of electron transport at PSII, which is expected to be closely related with rates of photosynthetic carbon fixation (Kromkamp et al., 1998; Migné et al., 2007; Schreiber et al., 2012; Morelle et al., 2018). Measurements were carried out on water and sediment samples, collected on different sites of the estuary, selected to cover a wide range of conditions, including distance to the mouth of the estuary or sediment grain size, and covering the main scales of temporal variability in the estuarine environment (hourly, fortnightly and seasonal). This approach allowed for the detailed characterization of the spatio-temporal variability of benthic and pelagic photosynthetic activity, ultimately yielding the estimation of an ecosystem-level budget of photosynthetic carbon fixation by phytoplankton and microphytobenthos for the whole estuary.

MATERIALS AND METHODS

Study Area, Sampling and Sample Processing

The study was carried out in the Ria de Aveiro a coastal lagoon located in the northwest coast of Portugal (40′38′N - 08′45′W). The Ria de Aveiro comprises four main channels (S. Jacinto, Mira, Ílhavo and Espinheiro), receiving fresh water from five rivers (Vouga, Antuã, Cáster, Boco and Valas de Mira) (Araújo et al., 2008). It connects to the Atlantic Ocean by a single artificial inlet, allowing water circulation patterns typical of a tidal estuary (Vaz and Dias, 2008). The Ria de Aveiro is a mesotidal system, with mean tidal amplitude of 2 m, and amplitudes of 0.6 m in neap tides and 3.2 m in spring tides (Vaz and Dias, 2008).

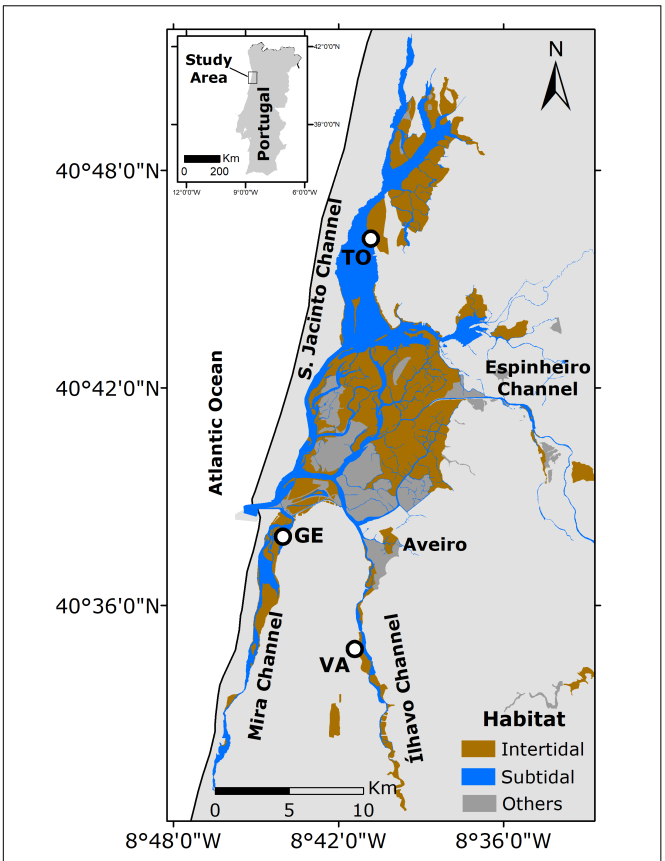

FIGURE 1 | Ria de Aveiro, Portugal. The different habitats are highlighted in green, for intertidal areas, blue for subtidal areas, and gray for other areas (e.g., salt pans). Sampling sites are marked with a black dot: Vista Alegre (VA), Gafanha da Encarnação (GE), and Torreira (TO).

It is a shallow, well-mixed system, with an average depth of ca. 1 m (Dias et al., 1999). Further characterization of physical, geomorphological, and ecological features of the Ria de Aveiro can be found elsewhere (Dias et al., 1999, 2003; Tomás et al., 2014; Bueno-Pardo et al., 2018).

Three sampling sites were selected, based on their contrasting characteristics, namely location (channels, distance to the ocean), hydrodynamics, salinity and sediment granulometry (**Figure 1**): Gafanha da Encarnação, located in the Mira channel and closest to the mouth of the estuary, characterized by sandy sediments (GE; 40°35′18″ N, 08°41′06″ W); Vista Alegre, located in the Canal de Ílhavo, characterized by fine muddy sediments (VA; 40°37′12″ N, 08°44′54″ W); Torreira, in the S. Jacinto channel, characterized by coarser muddy sand (TO; 40.758403 N, 8.676949 W). The three sampling sites are described in more detail in Frankenbach et al. (2019).

Sampling was carried along four spring-neap tidal cycles, distributed over the period between July 2013 and June 2014, to assess seasonal variability (summer: 16–18 and 23–25 July 2013; autumn: 29–31 October and 4–6 November 2013; winter: 12–13 and 18–20 February 2014; spring: 27–29 May and 3–5 June 2014). For each neap or spring tidal period, sampling was carried out on the three sites on consecutive days, one for each site. During each sampling day, samples were collected hourly, from sunrise to sunset, and all measurements were carried out *in situ* (see below) immediately following collection. Water samples were collected from surface water (ca. 0.5 m deep), at the shoreline (GE) or from an overlying bridge (VA, TO), using a bucket and transferred into 1.5 L bottles. Sediment samples were collected only during daytime low tide exposure, using Plexiglas corers (3.6 cm internal diameter), and were subsampled for quantification of chlorophyll *a*, as an indicator of surface biomass (see below) by cryo-sampling using mini contact cores ("crème brûlée" technique; Laviale et al., 2015). Different sample depths were collected for each sampling site, to match the expected depth of the photic zone on each type of sediment (0.25, 0.5, and 2.0 mm for VA, GE, and TO respectively). Samples were flash frozen immediately after collection and kept in liquid nitrogen until further analysis in the laboratory. Microphytobenthos cell suspensions were collected from the sediment surface using the lens tissue technique (Eaton and Moss, 1966). Two layers of lens tissue (Lens cleaning tissue 105, Whatman) were placed on the sediment surface for 1 h and the upper piece was collected and resuspended in falcon tubes with 10 ml of filtered seawater. Chlorophyll *a* fluorescence was measured immediately after preparation of the suspensions (1.25 ml).

Physical Parameters

Photosynthetic active radiation (E, 400–700 nm; see **Table 1** for notation) was measured hourly, at the time of sample collection, using a quantum meter (Model MQ-200, Apogee Instruments, Logan, UT, United States). Sediment temperature was measured with an infrared thermometer (ScanTemp 410, Tematec GmbH, Hennef, Germany). Water temperature, salinity and turbidity (NTU) were measured using a multi-parameter Sonde YSi 6600 (YSI incorporated, Yellow Springs, OH, United States) at the same locations used for collecting water. This allowed to measure salinity in a range from 0 to 70 ppt (±0.1 ppt), temperature from −5 to 50°C (±0.15 °C) and turbidity from 0 to 1000 NTU (±0.3 NTU).

Biomass

Biomass of phytoplankton and microphytobenthos was estimated by quantifying chlorophyll *a* content. Water samples (1 L, one replicate per sampling point) were filtered in cellulose nitrate filters (0.8 μm pore size, 47 mm diameter) and immediately frozen at −80°C until pigment extraction. Sediment samples (three replicates per sampling point), collected with mini contact cores, were kept frozen prior to the pigment extraction. Chlorophyll *a* content was quantified spectrophotometrically following Lorenzen (1967). Pigments from all samples were extracted in 90% aqueous acetone. Samples were homogenized in a vortex, to ensure a good mixing between the sample (filters, sediments or pellets, depending on the sample type) and the extraction solvent. Extraction was done in the dark, at 4°C, for 24 h. Samples were centrifuged (3000 g, 10 min, 4°C) and the absorptance of the supernatant was read in a spectrophotometer (Thermo Fisher Scientific, Waltham, United States) at 664 and 750 nm, with acetone 90% used as a blank. Acidification was

TABLE 1 | Notation.

Parameter	Description
α	Initial slope of a rETR vs. E curve [μmol quanta^{-1} m^2 s]
σ_{II}	Absorption cross-section of PSII [nm^2]
Chl *a*	Chlorophyll *a* concentration [mg Chl *a* m^{-3} or mg Chl *a* m^{-2}]
Css	Concentration of cohesive sediments [mg L^{-1}]
d	Day
E	PAR irradiance [μmol quanta m^{-2} s^{-1}]
E_k	Light-saturation parameter of a rETR vs. E curve [μmol quanta m^{-2} s^{-1}]
E(z)	PAR irradiance [μmol quanta m^{-2} s^{-1}] at depth z
ETR	Absolute electron transport rate of PSII [e$^-$ PSII^{-1} s^{-1}]
$_r$ETR	Relative electron transport rate of PSII [dimensionless]
$_r$ETR$_m$	Maximum rETR in a rETR vs. E curve [dimensionless]
F_o, F_m	Minimum and maximum fluorescence of a dark-adapted sample [arbitrary units]
F_s, F_m'	Steady-state and maximum fluorescence of a light-adapted sample [arbitrary units]
F_v/F_m	Maximum quantum yield of PSII [dimensionless]
$\Delta F/F_m$'	Effective quantum yield of PSII [dimensionless]
FRRF	Fast repetition rate fluorometry
GE	Gafanha da Encarnação
k_s	Light extinction coefficient in the sediment [mm^{-1}]
k_w	Light extinction coefficient in the water column [m^{-1}]
M(C), M(Chl)	Molar mass of carbon and chlorophyll *a* [g mol^{-1}]
MPB	Microphytobenthos
ne(O_2)	Number of electrons required for evolution of 1 molecule of O_2 [e$^-$ $O_2{}^{-1}$]
NT	Neap tides
P	Depth-integrated photosynthetic rate [mg C m^{-2} h^{-1}]
P^B	Biomass-specific photosynthetic rate [mg C mg Chl *a*$^{-1}$ d^{-1}]
PAR	Photosynthetic active radiation
PP	Phytoplankton
PQ	Photosynthetic quotient [mol C mol $O_2{}^{-1}$)]
PSII	Photosystem II
PSU	Number of chlorophyll *a* molecules per photosynthetic unit [Chl *a* PSII^{-1}]
RLC	Rapid light-response curve
rO_2	Rate of O_2 evolution [mmol O_2 mg Chl *a*$^{-1}$ s^{-1}]
ST	Spring tides
TO	Torreira
Turb	Turbidity [mg L^{-1}]
VA	Vista Alegre
yr	Year
z	Depth

done by adding 12 μl of HCl 1 M. Chlorophyll *a* content was expressed per volume as mg m^{-3} (phytoplankton) or per area mg m^{-2} (microphytobenthos).

Chlorophyll *a* Fluorescence

Chlorophyll *a* fluorescence was measured using a Multi-Color PAM fluorometer, controlled by the PamWin V3.12w software (Heinz Walz GmbH, Effeltrich, Germany). Blue light (peaking at 440 nm) was used for the measuring and actinic light, and for the saturating light pulses. In the MCP-D detector unit, a RG 665 long pass filter (>650 nm, 3 mm RG665, Schott) was used. Fluorescence of cell suspensions was measured in a 10 × 10 mm quartz cuvette using the ED-101US/MD optical unit, coupled to a magnetic stirrer (PHYTO-MS Miniature Magnetic Stirrer, Walz). Fluorescence of microphytobenthos suspensions was measured using the MCP-BK Optical Unit for Leaf Measurements (Walz). The fluorometer was zeroed using filtered seawater as a blank (cells suspensions) or by pointing the MCP-BK Optical Unit to empty space (sediment samples). Measurements were carried out by running a user-defined Script-file, comprising the following steps: 30 s of darkness; measurement of the absorption cross section of PSII (σ_{II}; see below); 30 s of darkness; rapid light curves (RLC; see below); 60 s of actinic light, of intensity matching the solar irradiance at the moment of sample collection; measurement of the effective quantum yield ($\Delta F/F_m$', see below). During the periods of darkness, far-red illumination (725 nm) was applied to induce the fully re-oxidation of the plastoquinone pool. The first measurement of each RLC was taken as a proxy for the maximum quantum yield of PSII, F_v/F_m. Samples were magnetically stirred between measurements. At each occasion, measurements were carried out on three replicates.

Absorption Cross Section of PS II

The absorption cross section of PS II, σ_{II}, was measured from the O–I1 rise kinetics, following Schreiber et al. (2012). The O–I1 rise kinetics was measured under strong light (440 nm), using the pre-programmed Sigma 1000_MT.FTM fast trigger file. σ_{II} was then calculated by running the special fitting routine O-I1 Fit (PamWin V3.12w software, Walz), based on the reversible radical pair model of PS II (Schreiber et al., 2012).

Effective Quantum Yield and Relative Electron Transport Rate of PSII

The effective quantum yield ($\Delta F/F_m$') and the relative electron transport rate of PSII (rETR) were calculated from the fluorescence parameters F_s and F_m' (steady-state and maximum fluorescence of a light adapted sample, respectively) and the incident photosynthetically active radiation (E; measured *in situ* or applied as actinic light by the fluorometer), by Genty et al. (1989):

$$\frac{\Delta F}{F_m'} = \frac{F_m' - F_s}{F_m'} \quad (1)$$

and

$$rETR = E\frac{F_m' - F_s}{F_m'} \quad (2)$$

Light-Response Curves of rETR

Rapid light-response curves (RLCs) of rETR were generated by sequentially applying 12 incremental lights steps (between 0 and 2180 μmol quanta m^{-2} s^{-1}) of 10 s. RLCs were described by estimating the initial slope (α), the maximum rETR ($rETR_m$) and the photoacclimation parameter E_k, by fitting the model of Eilers and Peeters (1988) as described in Frankenbach et al. (2018).

Absolute ETR and Carbon Fixation Rates

Absolute rates of electron transport at PSII were estimated following the rationale described by Schreiber et al. (2012), based on the determination of the rate of quantum absorption per PSII (e^- $PSII^{-1}$ s^{-1}):

$$ETR = \sigma_{II}\ L\ E\ \frac{\Delta F/F_m^{'}}{F_v/F_m} \quad (3)$$

with L being the Avogadro's constant (0.6022 mol^{-1}). Carbon fixation rates (biomass-specific photosynthetic hourly rates; mg C mg Chl a^{-1} h^{-1}) were estimated from (i) hourly rates of O_2 evolution (mmol O_2 mg Chl a^{-1} s^{-1}), estimated by:

$$rO_2 = \frac{ETR}{PSU\ ne\,(O_2)\ M\,(Chl)} \quad (4)$$

where PSU is the number of chlorophyll *a* molecules per photosynthetic unit, ne(O_2) is the number of electrons required for evolution of 1 molecule of O_2 and M(Chl) is the molar mass of chlorophyll *a* (893.49 g mol^{-1}); and (ii) the ratio of oxygen produced per fixed carbon (photosynthetic quotient, PQ; mol C mol $O_2{}^{-1}$):

$$P^B = \frac{rO_2}{PQ} M\,(C)\ 3600 \quad (5)$$

where M(C) is the molar mass or carbon (12.01 g mol^{-1}) and 3600 is the conversion factor for hourly rates. PSU and ne(O_2) were assumed to be equal to 600 Chl *a* $PSII^{-1}$ and 5 e^- $O_2{}^{-1}$, respectively, based on the experimental data compiled by Suggett et al. (2010). PQ was assumed to be 1.1 mol C mol $O_2{}^{-1}$ (Kromkamp et al., 2008). All these parameters were assumed to remain constant across sampling sites and dates of sampling. Daily carbon fixation rates were calculated by integrating the hourly rates for each daytime period.

Areal Rates of Carbon Fixation

Areal rates of carbon fixation were estimated by integrating over depth the biomass-specific photosynthetic rates calculated by Eq. (5), using the method described by MacIntyre et al. (1996). For each depth *z* below the surface of the water (phytoplankton) or the sediment (microphytobenthos): (i) incident irradiance E(z) was calculated from light the attenuation coefficient k_w or k_s (for the water column and sediments, respectively; see below) assuming an exponential decrease with depth; (ii) the biomass-specific photosynthetic rate P^B(z) was calculated from the light-response curve (P^B vs. E) measured for the corresponding sampling time and site, using E(z) as an input; light-response curves of P^B were calculated by applying Eqs. 3–5 to the rETR vs. E curves (RLCs). P^B(z) was calculated for depth intervals Δz of 10^{-6} mm (sediment) or 10^{-6} m (water column) and depth-integrated rate P (mg C m^{-2} h^{-1}) was calculated summing over all depth intervals and multiplying by the chlorophyll *a* concentration, Chl *a*, assumed to be distributed evenly within the water column or the sediment (mg Chl *a* m^{-3}):

$$P = \sum_z P^B\,(z)\ \ \Delta z\ Chl\mathrm{a} \quad (6)$$

For the microphytobenthos, $P^B(z)$ was calculated based on the light curves measured on cells collected in lens tissues, integrated numerically over depth using the attenuation coefficient measured for each type of sediment. Chlorophyll *a* concentration (mg Chl *a* m^{-3}) was calculated considering the volume sampled by the contact core used for each sampling site. For the phytoplankton, $P^B(z)$ was depth integrated from the surface until the maximum depth of the water column at each sampling moment.

Light Attenuation Coefficients

Spectral scalar irradiance profiles of PAR in sediments of the sampling sites were measured with a custom-made scalar field radiance probe connected to a spectrophotometer (USB 2000+, Ocean Optics, Duiven, Netherlands), and recorded using the spectral acquisition software Spectra Suite (Ocean Optics). The custom-made sensor consisted of a light diffusing sphere with a diameter of 90 μm, attached to the coated tip of a tapered optical fiber (Rickelt et al., 2016). The sensor was mounted on a motorized micromanipulator and positioned on the sediment surface in a 45° angle to minimize self-shading. To account for the insertion angle, the sensor was moved downwards in 141.4 μm steps to record spectral irradiance profiles in vertical depths of 100 μm increments. Spectral data were normalized to the incident downwelling irradiance recorded on a black non-reflective surface at the same position relative to light source and sediment surface. The light attenuation coefficients (k_s, mm^{-1}) were determined by the slope of the linear decay of the natural logarithm transformed percentage of incident light intensity as a function of depth, down to a maximum depth of 0.8 mm (Kühl, 2005). Measurements were replicated on three different samples per sampling site.

For the water column, the light extinction coefficient, k_w (m^{-1}), was estimated from measurements of turbidity (Turb, NTU), assuming to be proportional to the concentration of cohesive sediments (Css, mg L^{-1}), using the following relationships (Portela, 1996; Vaz et al., 2019):

$$Css\ =\ 3.42\ Turb\ +\ 3.0 \quad (7)$$

and

$$k_w\ =\ 0.036\ Css\ +\ 1.24 \quad (8)$$

Estimation of Ecosystem-Level Annual Primary Productivity

A tentative estimate of the annual primary productivity of the phytoplankton and microphytobenthos of the entire estuary was calculated by multiplying the daily rates P, measured at each season and tidal cycle (spring vs. neap), by the number of days of each season (91 days, 1/4 of the year) corresponding to spring tides or to neap tides (45.5 days). Daily rates were calculated by summing the hourly rates determined for each day of sampling. Upscale to the whole estuary was done by considering the total flooded area of the estuary (phytoplankton) and the area corresponding to intertidal flats (microphytobenthos). The former was estimated from the

mean value between the area covered by water during mean high tide and during mean low tide (89.2 and 64.9 km^2, respectively; Lopes et al., 2013). The areas corresponding to each type of sediment type were the ones determined in Frankenbach et al. (2019): 34, 16 and 5 km^2 for TO, GE and VA, respectively. The area corresponding to the phytoplankton was estimated to reach 100 km^2, by adding the subtidal and the total intertidal areas calculated by Frankenbach et al. (2019). The modeling approach used to estimate the area rates of carbon fixation by phytoplankton and microphytobenthos is summarized in **Figure 2**.

Statistical Analysis

Measurements made on different sampling sites and occasions were compared by applying two-way ANOVAs, and by *post hoc* Tukey HSD test. Assumptions of normality and homoscedasticity were verified prior to analysis using the Shapiro–Wilk test and Levene's test, respectively. In case of violation of assumptions, data were log transformed. All statistical analyses were carried out using Statistica 10 (StatSoft, Tulsa, OK, United States).

RESULTS

Hourly Variability in Physical Conditions, Photophysiology, and Biomass-Specific Productivity

Figures 3–5 illustrate the typical hourly variability in abiotic and photophysiological parameters in the three sampling sites for 2 days, on neap and spring tides, during July 2013. A marked hourly variability in abiotic factors was observed in both the water column and intertidal sediments. Water column turbidity varied markedly during the tidal cycle, typically reaching higher values during low tide (**Figures 3–5A,B**) and showing short periods of very high values close to the tidal ebb (**Figures 3A,B**) or flood (**Figure 4B**).

Water temperature was relatively constant during high tide (deeper water column), typically increasing along the ebb, especially when occurring at mid-day (neap tides; **Figures 3D**, **4C,D**, **5D**). On some days, on the site closest to the mouth of the estuary (GE), a sharp inversion of water temperature could be observed at the mid of the low tide period, associated with an equally marked change of salinity, revealing a sudden replacement of water masses at the sampling site, from freshwater-dominated (higher temperature, low salinity) to oceanic (lower temperature, high salinity) (**Figure 4D**). The tides had a measurable impact on the water temperature, as the incoming oceanic seawater during flood was often substantially cooler than the estuarine water. Sediment temperature exhibited the same general pattern as the water column, with higher values being recorded during low tide, when sediment was exposed (**Figures 3–5C,D**), but especially during spring tides, when low tide occurred at mid-day (**Figures 3–5D**). The sediment was typically warmer than water column, often reaching values above 25°C (**Figure 3D**), as measurements were taken during diurnal low tide, when the sediment surface was exposed to direct sunlight.

Water column salinity was often lower during low tides, when the influence of freshwater was the greatest, and higher in high tide, reaching values typical of seawater (around 35). This pattern of variation was more marked in site GE, the one closest the estuary mouth (e.g., **Figures 4C,D**). On site TO, water salinity remained virtually constant due to reduced influx of fresh water in that canal (**Figures 3C,D**).

Phytoplankton biomass, as measured by chlorophyll *a* concentration in the water column, showed a large hourly variability, particularly in sites TO and GE during spring tides (**Figures 3E,F**, **4F**). Maximum values tended to occur during the low tide periods (**Figures 3–5F**). Variations from about 1.5 to 7.5 mg Chl *a* m^{-3} in a period of 4 h were observed in site TO (**Figure 3F**). At site VA, the farthest from the estuary mouth, hourly variations were much smaller (**Figures 5E,F**). In contrast with the water column, the chlorophyll *a* content of the sediment did not show a consistent pattern of variation, although in some instances the two parameters displayed a similar pattern of variation, with maximum values during the low tide periods (**Figure 4F**).

The effective quantum yield of PSII, $\Delta F/F_m'$, also varied markedly along the day, both for phytoplankton and microphytobenthos. The same overall pattern was observed for the two groups, with values varying from 0.5 to 0.6 during early morning or late afternoon, and around 0.1, when solar irradiances were the highest. For the phytoplankton, this pattern was observed in all days, with $\Delta F/F_m'$ mainly responding (inversely) to solar irradiance, irrespectively of tidal stage. During neap tides, an almost symmetrical pattern was found, with the decrease of $\Delta F/F_m'$ observed during the morning recovering completely during the afternoon (**Figures 3–5G**). On days during spring tides, the recovery of $\Delta F/F_m'$ appeared incomplete (**Figures 3–5H**), likely associated to the shallower water column during the middle of the day, allowing the exposure of the cells to higher light levels, higher temperature and lower salinity, conditions prone to cause a higher slowly reversible photodamage. For the microphytobenthos, $\Delta F/F_m'$ values were generally similar to those of phytoplankton, following the same overall trend of varying inversely with incident solar irradiance (**Figures 3–5G,H**).

The absorption cross section of PS II, σ_{II}, was characterized by a large variability between replicates, especially for phytoplankton (e.g., **Figures 3–5G**). Both for phytoplankton and microphytobenthos, σ_{II} varied similarly to $\Delta F/F_m'$, largely responding inversely to solar irradiance (e.g., **Figure 3G**, microphytobenthos). However, σ_{II} seemed to be more affected by tidal stage, as in some days it did not decrease under high solar irradiance if under high tide (**Figures 4G,H**; phytoplankton and microphytobenthos). σ_{II} was consistently lower for microphytobenthos than for phytoplankton. Clear trends of hourly variation were not very evident, although a tendency to vary inversely with irradiance could be identified (e.g., **Figures 3–5H**).

Short-term photoacclimation status, as measured by RLC parameters α and $rETR_m$, varied hourly both for phytoplankton

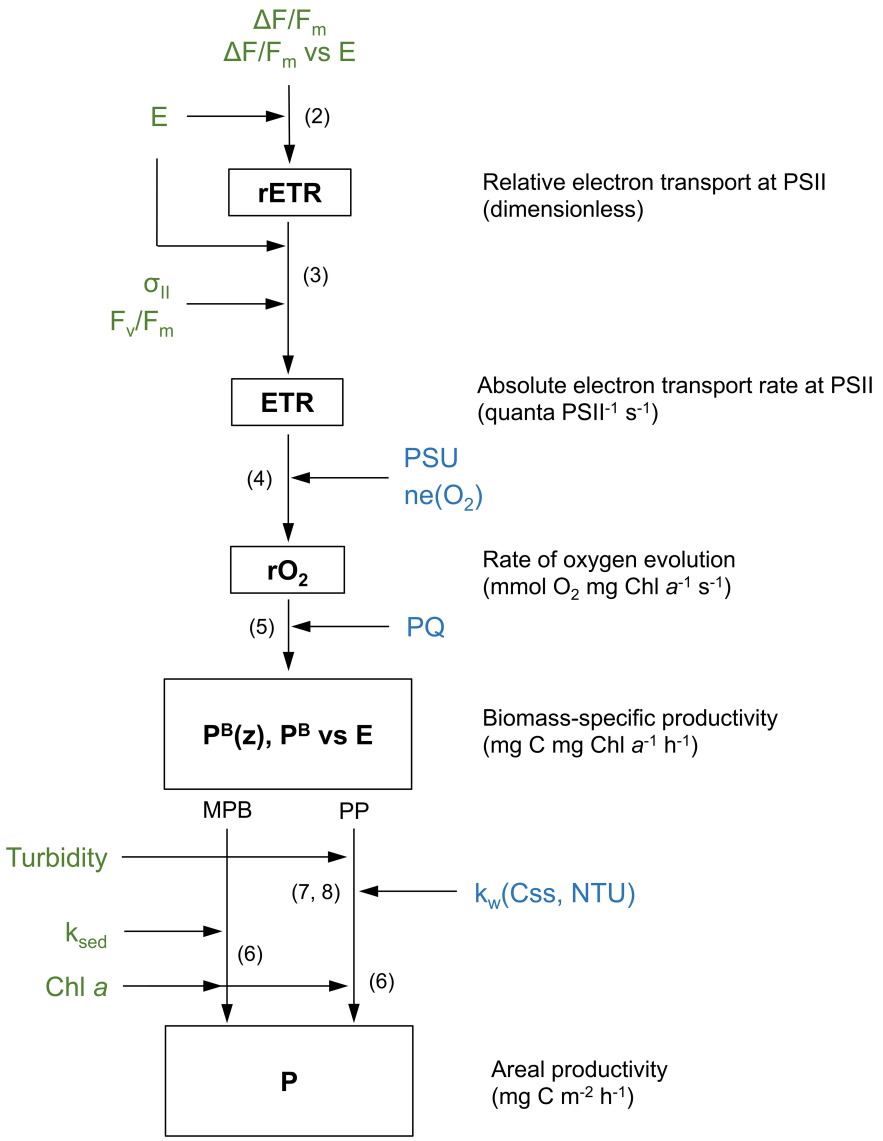

FIGURE 2 | Schematic describing the modeling workflow followed in this study. Biomass-specific productivity rates (P^B, mg C mg Chl a^{-1} h^{-1}) were calculated from irradiance (E) and fluorescence-based parameters (F_v/F_m, $\Delta F/F_m'$, σ_{II}). Productivity per unit area was calculated by depth-integrating P^B using light-response curves of P^B, chlorophyll *a* content, and light attenuation. Depth-integration was carried out differently for phytoplankton (PP) and microphytobenthos (MPB), using light attenuation coefficient for the water column (k_w) and the sediment (k_s), respectively. Parameters in green were measured in this study. Parameters in blue were taken from published sources. Numbers represent the equations describing each step.

and microphytobenthos. However, changes in photoacclimation status were driven mostly by changes in $rETR_m$ than in α. On most days, $rETR_m$ varied markedly, showing a well-defined pattern of variation, increasing toward the middle of the day, and reaching minimum values at beginning and end of the day (**Figures 4**, **5I,J**). In the case of phytoplankton, light-limited photosynthesis (denoted by α) remained relatively constant along the day, on most days (e.g., **Figures 4I**, **5J**), but occasionally showed erratic, short-term variations (**Figure 3J**). In the case of microphytobenthos, α and $rETR_m$ values were similar to those measured in the water column, although rETR varied following less defined trends, and more variable in absolute terms: similar (**Figure 3I**), significantly lower (**Figure 4I**) or significantly higher (**Figure 4J**).

Spatio-Temporal Variability: Fortnight and Seasonal Time Scales

Mean daily solar irradiance (average of hourly values measured during the whole photoperiod) varied markedly with season, with maximum values being measured in July and in May/June (**Figures 6A–C**). However, the variation in incident solar irradiance between spring and neap tides was partially due to changes in cloud cover during the sampling days (**Figures 6A–C**). Considering the high turbidity of the water column, the total

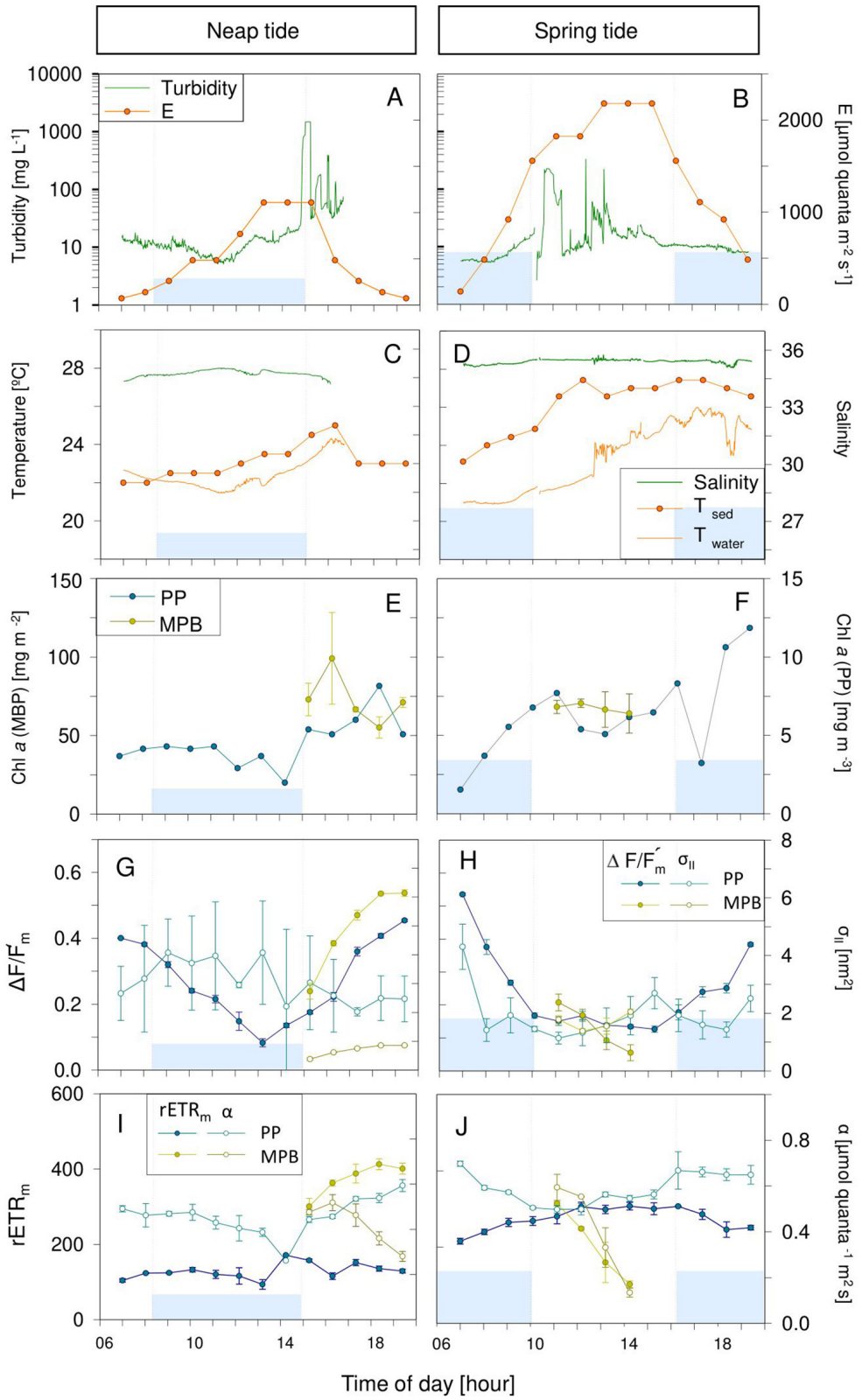

FIGURE 3 | Hourly variation of abiotic **(A–D)** and photophysiological **(E–J)** parameters along one day in Torreira (TO) during neap **(A,C,E,G,I)** and spring tide **(B,D,F,H,J)** in July 2013. Blue areas represent high tide; vertical bars demonstrate the beginning and end of the high tide. Mean values of three replicates. Error bars represent one standard error. PP, phytoplankton; MPB, microphytobenthos.

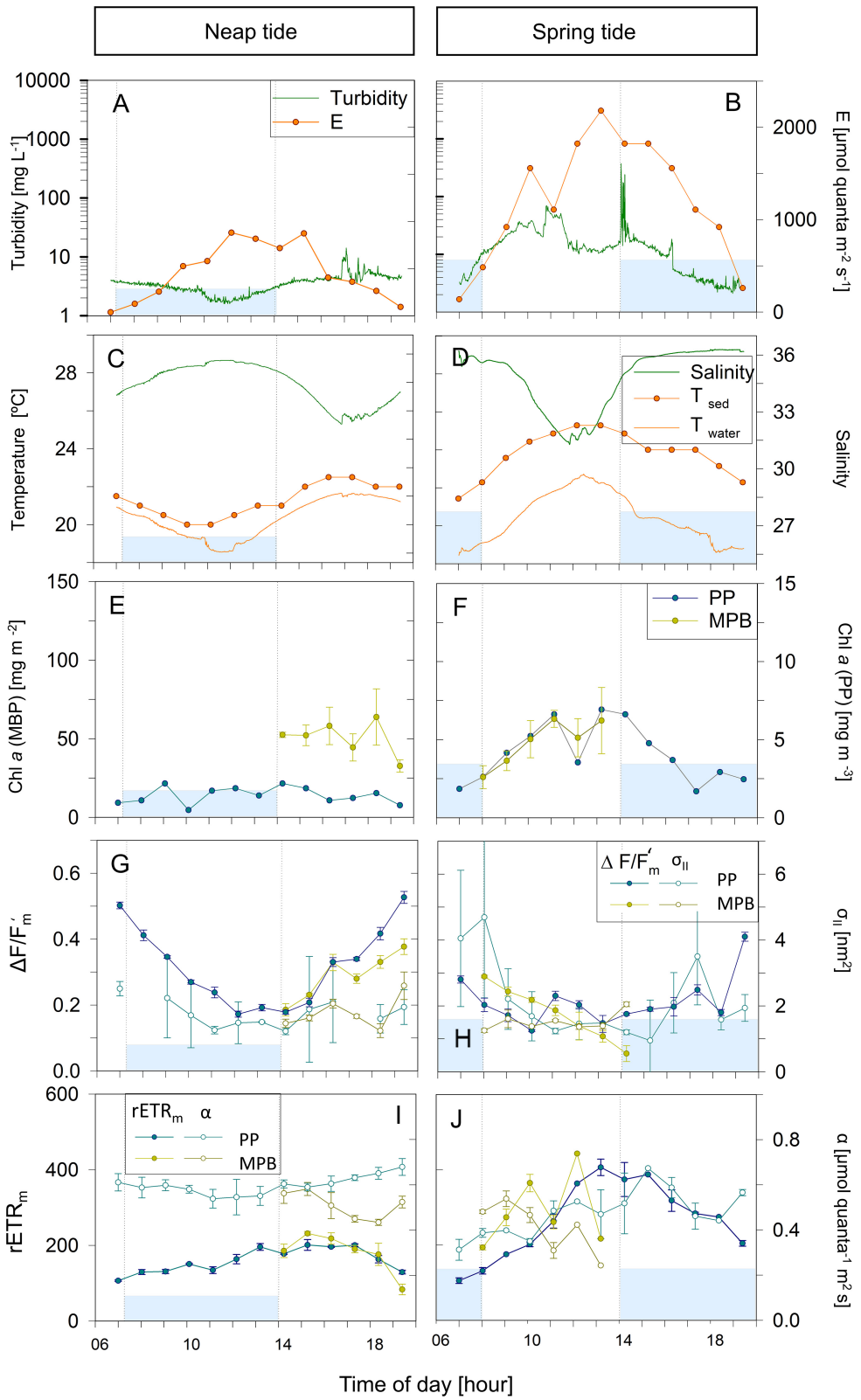

FIGURE 4 | Hourly variation of abiotic **(A–D)** and photophysiological **(E–J)** parameters along one day in Gafanha de Encarnação (GE) during neap **(A,C,E,G,I)** and spring tide **(B,D,F,H,J)** in July 2013. Blue areas represent high tide; vertical bars demonstrate the beginning and end of the high tide. Mean values of three replicates. Error bars represent one standard error. PP, phytoplankton; MPB, microphytobenthos.

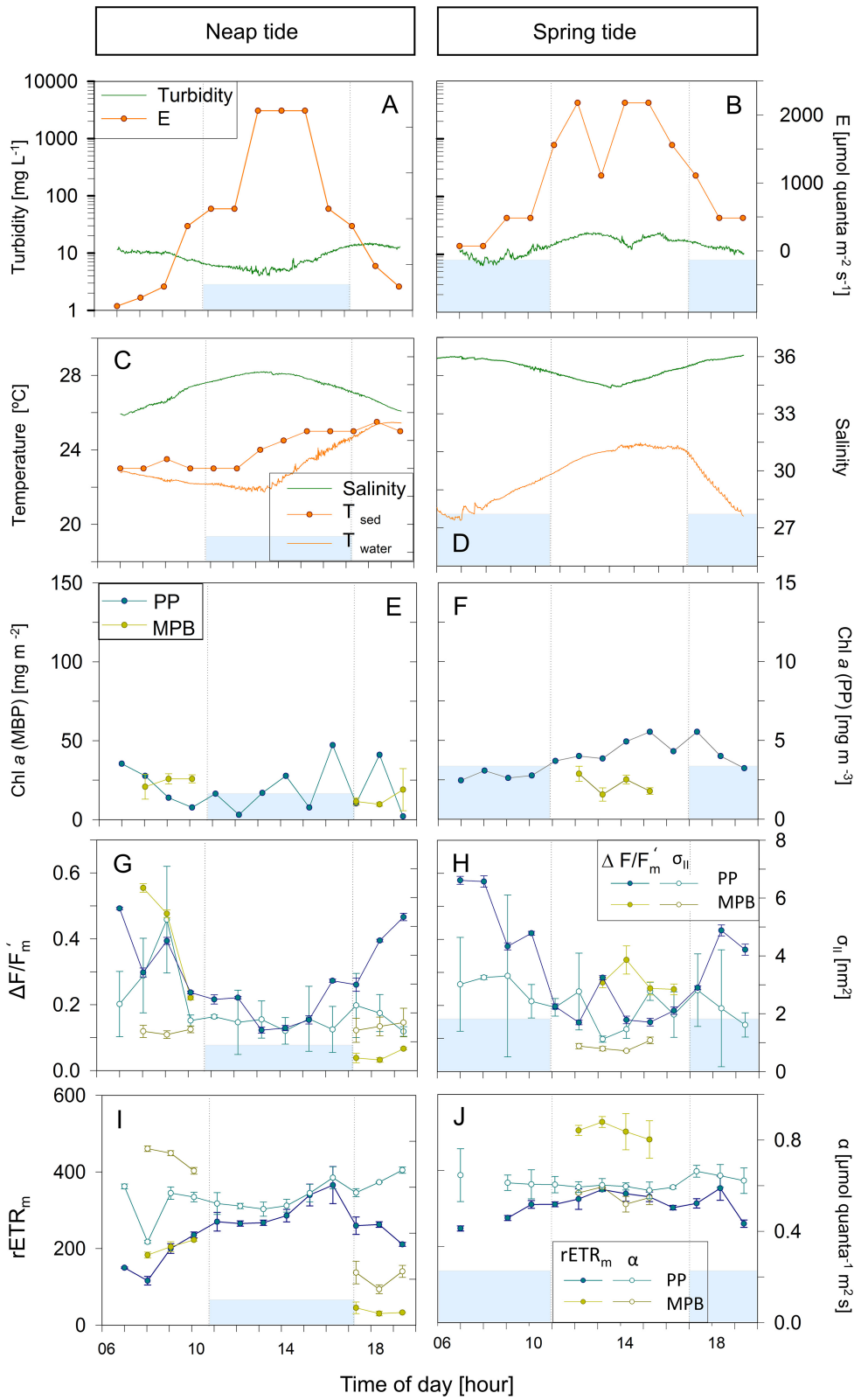

FIGURE 5 | Hourly variation of abiotic **(A–D)** and photophysiological **(E–J)** parameters along one day in Vista Alegre (VA) during neap **(A,C,E,G,I)** and spring tide **(B,D,F,H,J)** in July 2013. Blue areas represent high tide; vertical bars demonstrate the beginning and end of the high tide. Mean values of three replicates. Error bars represent one standard error. No temperature data available for the spring tide sampling day (D). PP, phytoplankton; MPB, microphytobenthos.

daily light doses received at the intertidal sites varied substantially on the timing of the low tide period (**Figures 6A–C**). Also, because of the delay in tidal propagation inside the estuary, causing the timing of low tide to vary between the sampling sites, a systematic variation in daily solar light dose received in the three sites was observed. Water turbidity was relative constant across sampling sites and seasons, being affected mainly by tide, but a tendency for higher values during autumn and winter was observed. Occasional peaks in turbidity were measured, causing a large data dispersion (e.g., TO, July; **Figure 6A**).

Water and sediment temperature showed a clear seasonal variation in all sampling sites, with maximum average values occurring in July (23.3 ± 1.83°C for water in TO, and 28.3 ± 0.96°C in sediments at VA) and minimum values (10.3 ± 0.63°C, for water at TO and 12.3 ± 0.58°C for sediments in GE) being observed in February. A virtually identical seasonal pattern was found for all sampling sites (**Figures 6D–F**). The seasonal variation in water temperature was closely followed by equally large changes in water salinity, at all sampling sites. Highest average salinities were observed in July (35.0 ± 0.52), and the minimum values in February (2.0 ± 2.47), directly resulting from the seasonal variation in freshwater input (**Figures 6D–F**). Minimum salinity values, close to zero, were recorded in winter at site VA, the sampling site locate farthest from the mouth of the estuary (**Figure 6F**).

Both the biomass of phytoplankton and microphytobenthos (as expressed per unit area) varied significantly with seasons (ANOVA, $F_{3,817} = 319.54$; $P < 0.001$; and $F_{3,317} = 13.54$; $P < 0.001$, respectively; **Figures 5G–I**). However, the two communities differed regarding the timing when the maximum biomass was reached, its variation with spring-neap tidal cycle, and its spatial distribution. In the case of the phytoplankton, maximum average values were observed in spring and summer, and the lowest in winter (**Figures 6G–I**). In contrast, microphytobenthos biomass reached maximum values later in the year, in summer and autumn. On average, the biomass of phytoplankton was significantly higher in spring than in neap tides (ANOVA, $F_{1,817} = 25.14$; $P < 0.001$), although an exception to this general pattern was observed in May/June (**Figure 6I**). For the microphytobenthos, the differences between spring and neap tides were overall not significant (ANOVA, $F_{1,317} = 1.47$; $P = 0.226$), despite some marked differences at particular moments (February and October/November, **Figures 6H,I**). Both phytoplankton and microphytobenthos biomass varied significantly between sampling sites (ANOVA, $F_{2,817} = 25.14$; $P < 0.001$, and $F_{2,317} = 45.07$; $P < 0.001$, respectively), and in both cases the highest values were measured at site TO. In the case of phytoplankton, the remaining two sites did not differ significantly (Tukey HSD, $P > 0.05$). Regarding the microphytobenthos, all sampling sites differed from each other (Tukey HSD, $P < 0.001$ for all pairwise comparisons), the lowest biomass values being found for site VA (**Figures 6G–I**).

Phytoplankton and microphytobenthos also differed regarding the spatio-temporal variability of photophysiological parameters $\Delta F/F_m$' and σ_{II}. In the case of the phytoplankton, both $\Delta F/F_m$' and σ_{II} varied significantly with seasons (ANOVA, $F_{3,820} = 230.74$; $P < 0.001$ and $F_{3,705} = 43.63$; $P < 0.001$, respectively; **Figures 6J–O**), the maximum values being measured in summer and the minimum in winter (**Figures 6K,L**). In the case of microphytobenthos $\Delta F/F_m$' and σ_{II} also varied significantly with seasons ($F_{3,335} = 48.02$; $P < 0.001$ and $F_{3,335} = 27.44$; $P < 0.001$, respectively). However, maximum values were observed during autumn ($\Delta F/F_m$') or summer (σ_{II}), while minimum values were measured in spring, for both parameters (**Figures 6M–O**).In the case of the phytoplankton, $\Delta F/F_m$' varied significantly between spring and neap tides (higher values during spring tides) (ANOVA, $F_{1,820} = 67.01$; $P < 0.001$), while σ_{II} did not show significant differences (ANOVA, $F_{1,705} = 1.78$; $P > 0.1$). The opposite pattern was observed for microphytobenthos, with σ_{II} varying between spring and neap tides (ANOVA, $F_{1,335} = 10.65$; $P < 0.01$), and $\Delta F/F_m$' increasing significantly from neap to spring tides (ANOVA, $F_{1,335} = 15.414$; $P < 0.001$). In terms of spatial variation, phytoplankton showed a significant variation in $\Delta F/F_m$' between sampling sites (ANOVA, $F_{2,820} = 28.04$; $P < 0.001$), with maximum values occurring at TO and minimum ones at VA, while no differences among sites were found regarding σ_{II} (ANOVA, $F_{2,705} = 2.29$; $P > 0.1$). In the case of the microphytobenthos, $\Delta F/F_m$' also varied significantly between sampling sites (ANOVA, $F_{2,335} = 6.61$; $P < 0.01$), with maximum values being observed for site VA and minimum for site GE. σ_{II} varied significantly between sites (ANOVA, $F_{2,335} = 22.46$; $P < 0.001$), but showed the opposite pattern, with maximum values occurring at site GE and minimum ones at VA (**Figures 6M–O**). Still regarding the parameters $\Delta F/F_m$' and σ_{II}, phytoplankton and microphytobenthos differed not only concerning their spatio-temporal variability, but also in terms of their absolute values. While $\Delta F/F_m$' showed comparable values for the two groups (0.43 ± 0.16 and 0.47 ± 0.09, respectively; ANOVA, $F_{1,44} = 1.13$; $P > 0.1$), σ_{II} was significantly higher in the case of the phytoplankton (1.80 ± 1.19 and 1.19 ± 0.03 for phytoplankton and microphytobenthos, respectively; ANOVA, $F_{1,44} = 25.25$, $P < 0.001$).

Regarding the photoacclimation state, phytoplankton samples showed a significant seasonal variability in both light-limited (α) and light-saturated ($rETR_m$) photosynthetic activity (ANOVA, $F_{3,751} = 456.82$; $P < 0.001$ and $F_{3,749} = 307.2$; $P < 0.001$, respectively), with maximum and minimum values occurring in spring and in winter, respectively (**Figures 6P–R**). The two parameters were also significantly higher during spring than during neap tides (ANOVA, $F_{1,751} = 71.44$; $P < 0.001$ and $F_{1,749} = 74.80$; $P < 0.001$, respectively). Spatially, differences were found only regarding α (ANOVA, $F_{2,751} = 41.37$; $P < 0.001$), with maximum values being reached at site TO and minimum ones at site VA (**Figures 6P,R**). Regarding the microphytobenthos, also both α and $rETR_m$ varied significantly among seasons (ANOVA, $F_{3,335} = 7.661$; $P < 0.001$ and $F_{3,334} = 46.44$; $P < 0.001$, respectively), but maximum values were reached in autumn and minimum ones in winter (**Figures 6S–U**). As observed for the phytoplankton, both parameters showed significantly higher values during spring tides than during neap tides (ANOVA, $F_{1,335} = 5.44$; $P < 0.05$ and $F_{1,334} = 81.94$; $P < 0.001$, for α and $rETR_m$ respectively). Both α and $rETR_m$ varied significantly between sampling sites (ANOVA, $F_{2,335} = 8.654$; $P < 0.001$

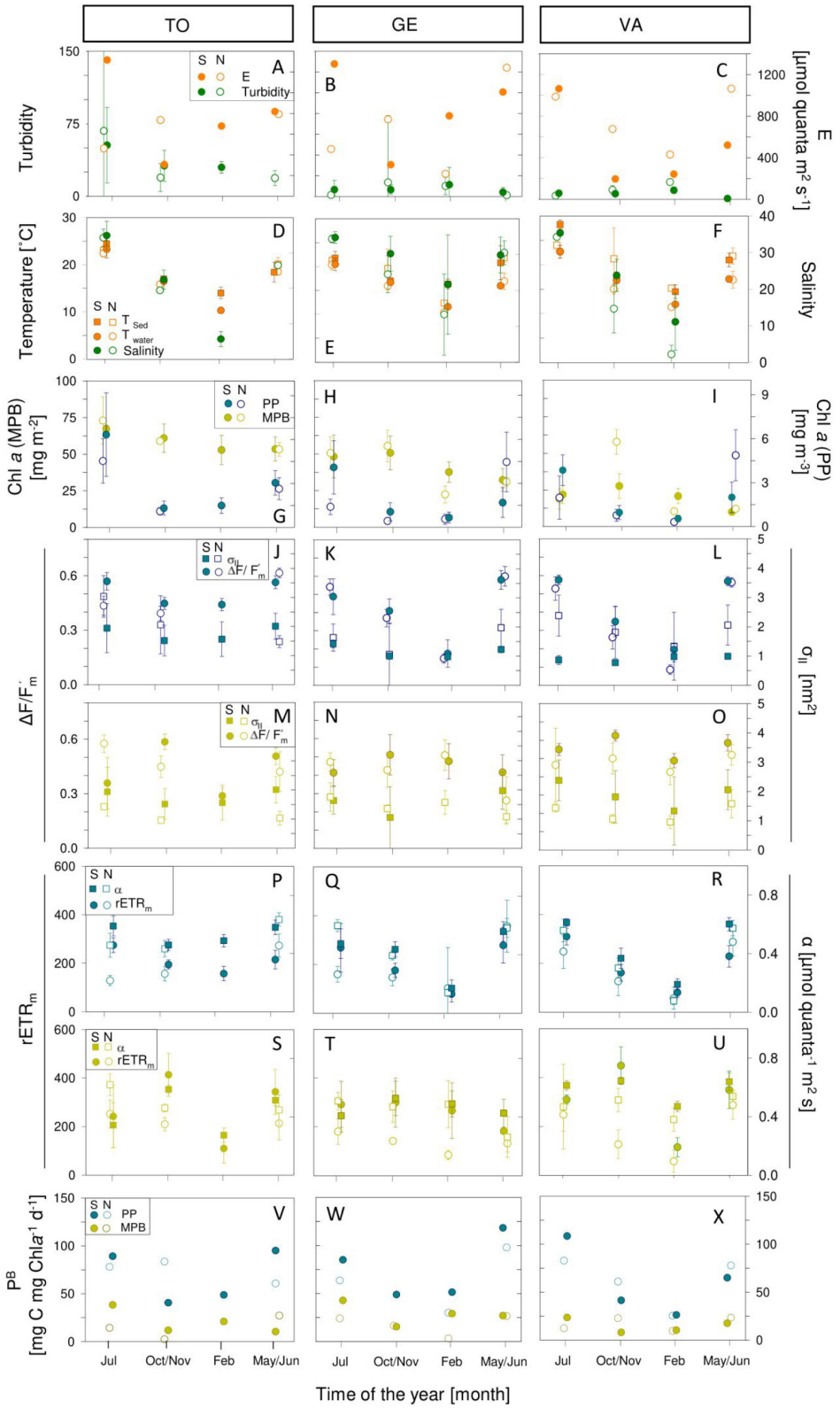

FIGURE 6 | Seasonal variation of abiotic **(A–F)** and photophysiological **(G–X)** parameters in sampling sites Torreira (TO; **A,D,G,J,M,P,S,V)**, Gafanha da Encarnação (GE; **B,E,H,K,N,Q,T,W**) and Vista Alegre (VA; **C,F,I,L,O,R,U,X**) during spring (full circles) and neap tide (empty circles), for phytoplankton (blue) and microphytobenthos (yellow). Mean values of three replicates. Error bars represent one standard error. PP, phytoplankton; MPB, microphytobenthos.

and $F_{2,334}$ = 3.45; $P < 0.05$, respectively), in both cases reaching higher values at site VA and minimum values at site GE (**Figures 6T,U**).

This large spatio-temporal variability in α and $rETR_m$ was reflected in substantial variations in the photoacclimation parameter E_k (data not shown). For both communities, E_k varied significantly over seasons (ANOVA, $F_{3,754}$ = 4.3; $P < 0.01$ and $F_{3,334}$ = 39.91; $P < 0.001$, respectively), reaching maximum values in spring and autumn (phytoplankton) or in spring (microphytobenthos). For both types of samples, E_k was significantly higher during spring than during neap tides (ANOVA, $F_{1,754}$ = 4.6; $P < 0.05$ and $F_{1,334}$ = 79.10; $P < 0.001$, for phytoplankton and microphytobenthos, respectively). For the phytoplankton, E_k varied significantly between sampling sites (ANOVA, $F_{2,754}$ = 11.6; $P < 0.001$), the highest values occurring at site VA and the minimum at site TO. In contrast, no significant differences were found between sampling sites for microphytobenthos ($F_{1,334}$ = 0.77; P = 0.466). Overall, the photoacclimation state of phytoplankton and microphytobenthos appeared to be very similar, with E_k values averaging 490.8 ± 211.7 and 491.5 ± 175.7 μmol quanta m^{-2} s^{-1}, respectively. However, with the exception of the winter sampling period, E_k was higher for microphytobenthos (ranging from 490.7 ± 197.5 in summer to 561.9 ± 124.9 μmol quanta m^{-2} s^{-1} in spring), than for phytoplankton (ranging from 408.5 ± 28.5 in summer to 473.6 ± 107.7 μmol quanta m^{-2} s^{-1} in spring).

Biomass-Specific Productivity

Despite the differences observed in the physical conditions between the water column and intertidal sediments, and between the photophysiological and photoacclimation state of phytoplankton and microphytobenthos, the spatio-temporal patterns of variability of daily biomass-specific rates, P^B, of the two communities was relatively similar (**Figures 6V–X**). For both communities, the daily rates of carbon fixation varied significantly with season (ANOVA, $F_{3,719}$ = 58.56; $P < 0.001$ and $F_{3,315}$ = 17.40; $P < 0.001$, respectively) and phase of the spring-neap tidal cycle (ANOVA, $F_{1,719}$ = 4.83; $P < 0.05$ and $F_{1,315}$ = 5.19; $P < 0.05$, respectively). Maximum values were obtained for summer and spring, during spring tides, and minimum values for winter and neap tides. No significant differences were found between sampling sites. However, the absolute values of P^B were on average higher for the phytoplankton than for the microphytobenthos, averaging 68.0 ± 26.1 and 19.1 ± 10.3 mg C mg Chla^{-1} d^{-1}, respectively.

Light Attenuation Coefficients

The vertical light profiles measured in sediment samples from the three sampling sites revealed an exponential attenuation of downwelling irradiance, enabling a very good fit of an exponential model (**Figure 7**). The attenuation coefficient k_s ranged from 3.9 ± 0.8 mm^{-1} (TO) to 9.0 ± 0.8 mm^{-1} (VA), GE reaching the intermediate value of 6.1 ± 0.6 mm^{-1}.

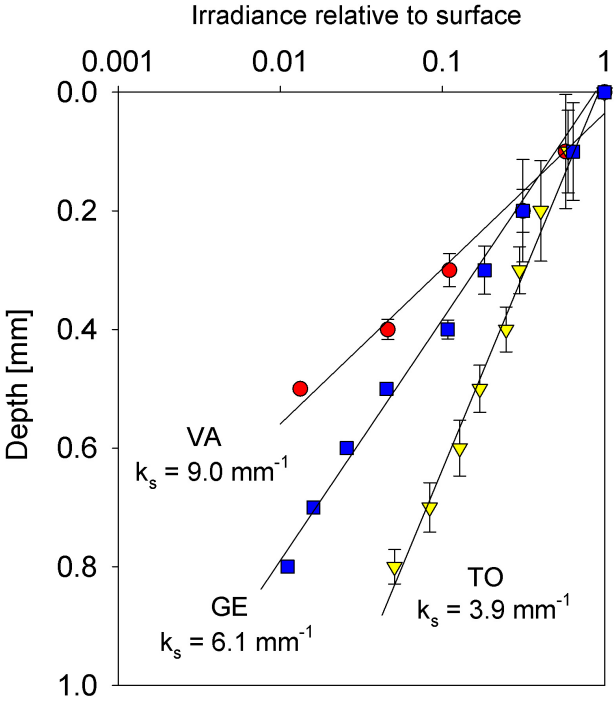

FIGURE 7 | Vertical profile of spectrally averaged irradiance (percentage of incident irradiance) in intertidal sediments of the three sampling sites Vista Alegre (VA), Gafanha da Encarnação (GE) and Torreira (TO). Numbers are the downwelling light attenuation coefficients (k_s) for each type of sediment. Mean values of three replicates. Error bars represent one standard error.

Areal Production Rates

Despite the fact that the rates of biomass-specific production were higher for phytoplankton (**Figure 6**), the depth-integrated areal rates of microphytobenthos were often much higher, due to the higher biomass involved in photosynthetic activity (**Figures 8A–D**). The difference between the two groups was particularly large when the periods of low tide occurred at the middle of the day (e.g., **Figures 8B–D**). The higher productivity of microphytobenthos was also found when comparing daily rates, despite the shorter periods of light exposure considered for their calculation (264.5 ± 228.8 and 140.4 ± 154.8 mg C m^{-2} d^{-1}, respectively; **Figures 9A–C**). Maximum daily rates of carbon fixation ranged from 8.1 (winter, neap tides, GE) to 505.0 (summer, spring tides, TO) mg C m^{-2} d^{-1} for the phytoplankton, and from 25.6 (winter, spring tides, GE) to 909.0 (summer, spring tides, TO) mg C m^{-2} d^{-1}, for the microphytobenthos.

The marked seasonal and fortnight variability of the biomass and the photosynthetic performance was reflected on a significant variation in daily rates of areal production between seasons and spring-neap tide conditions (**Figures 8**, **9**), of both phytoplankton ($F_{3,309}$ = 75.26; $P < 0.001$ and $F_{1,309}$ = 11.19; $P < 0.001$, comparing between seasons and spring-neap tides, respectively) and microphytobenthos ($F_{3,309}$ = 75.26; $P < 0.001$ and $F_{1,309}$ = 11.19; $P < 0.001$; comparing between seasons and spring-neap tides, respectively). In both cases, maximum

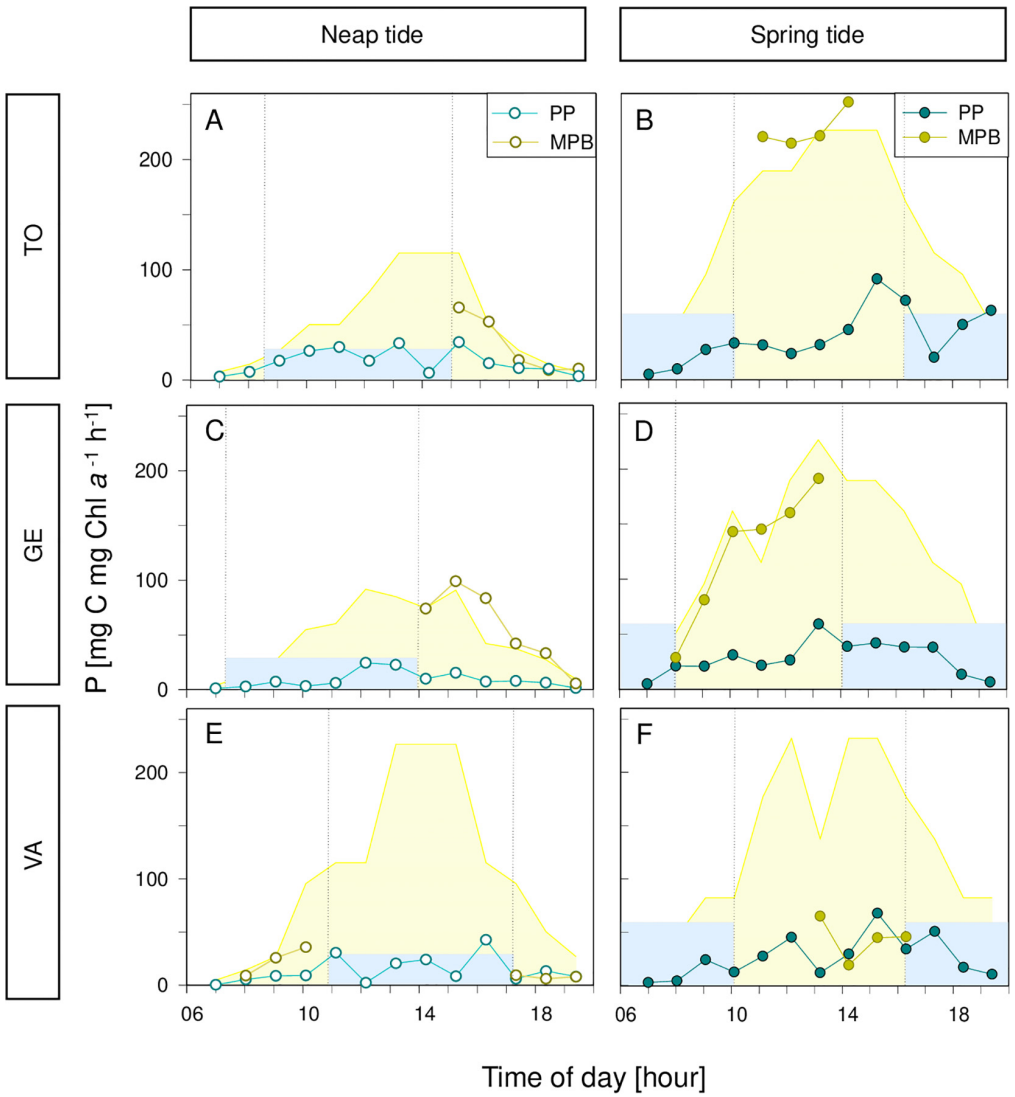

FIGURE 8 | Hourly rates of biomass-specific primary production of phytoplankton (PP) and microphytobenthos (MPB) along two days in July 2013, on tides **(A,C,E)** and spring tides **(B,D,F)**, at the three sampling sites, Torreira (TO; **A,B**), Gafanha da Encarnação (GE; **C,D**) and Vista Alegre (VA; **E,F**). Areas in the background represent corresponding solar irradiance. Blue areas represent high tide; vertical bars demonstrate the beginning and end of the high tide.

values were attained in spring and summer, and during spring tides, and minimum values occurred on winter, during neap tides. Significant differences were also present regarding the spatial distribution. For the phytoplankton, large variations were found ($F_{2,309}$ = 7.66; $P < 0.001$), showing maximum daily production for site TO and lower but comparable rates for sites GE an VA. For the microphytobenthos, significant variations between sampling sites were also observed ($F_{2,309}$ = 12.31; $P < 0.001$), but maximum values were observed for site TO and minimum for site VA.

Upscaling to Ecosystem-Level Productivity

The data used to upscale the areal primary production rates to ecosystem-level values are summarized in **Table 2**. Per unit area, microphytobenthos productivity was the highest, with exception of the site VA, for which the values of the two groups were similar. Phytoplankton rates averaged 49.9 g C m^{-2} yr^{-1}, ranging from 44.7 to 51.8 g C m^{-2} yr^{-1}, for sites VA and GE, respectively. Microphytobenthos productivity rates averaged 105.2 g C m^{-2} yr^{-1}, ranging between 43.4 to 164.4 g C m^{-2} yr^{-1}, for sites VA and TO, respectively. This tendency was reinforced when upscaling to the whole estuary, despite the larger area accounted for the phytoplankton, and the primary production carried out by the microphytobenthos and by the phytoplankton were found to attain, respectively, 7534.0 and 4894.3 and t C yr^{-1}, representing 60.6 and 39.4% of the global primary production of the two communities in the Ria de Aveiro, that reached 12428.3 t C yr^{-1}.

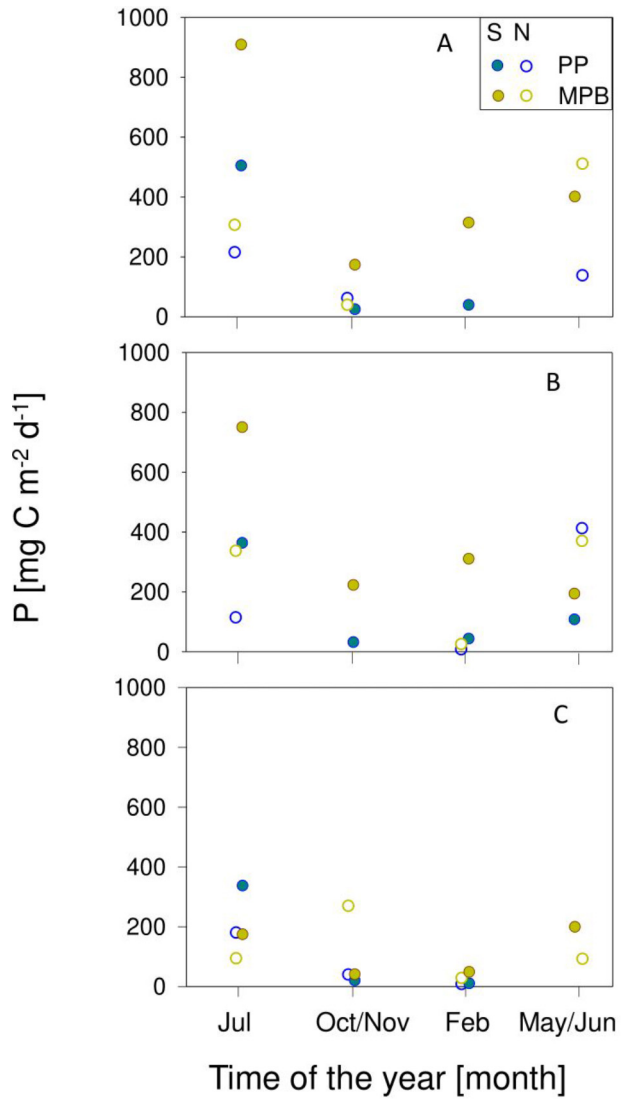

FIGURE 9 | Seasonal variation of daily rates of primary production of phytoplankton (PP) and microphytobenthos (MPB) during spring (S) and neap (N) tides in sampling sites Torreira **(A)**, Gafanha da Encarnação **(B)**, and Vista Alegre **(C)**.

TABLE 2 | Summary of the data used for the upscaling of local areal primary production rates (g C m^{-2} yr^{-1}) to ecosystem-level carbon fixation budget (t C yr^{-1}).

	Site	Area km^2	Areal production g C m^{-2} yr^{-1}	Total production t C yr^{-1}
Phytoplankton	TO	33.3	50.31	1676.9
	GE	33.3	51.76	1725.3
	VA	33.3	44.76	1492.1
	Total	100.0		4894.3
				(39.4%)
Microphytobenthos	TO	34.0	164.40	5589.6
	GE	16.0	107.97	1727.6
	VA	5.0	43.36	216.78
	Total	55.0		7534.0
				(60.6%)
			Total	12428.3

Percentages refer to the proportion of primary production of phytoplankton or microphytobenthos relatively to the total.

DISCUSSION

Abiotic Factors

The sampling program carried out in this study allowed to cover a large variability in hourly, fortnight and seasonal time scales in all physical parameters measured for the three studied sampling sites. Seasonal variability was pronounced for both the water column and the intertidal sediments, namely regarding temperature, salinity and turbidity. In both habitats, a strong fortnight variability was superimposed on the seasonal cycle. In the intertidal habitat, stronger and faster changes were observed during tidal ebb and flood, associated to sudden changes between immersion and exposure to sunlight and wind. In the case of the intertidal communities, it is known that the experienced environmental variability is likely characterized by a wider range of conditions than those registered only during the low tide periods, mainly due to the contrast between the conditions during submersion under high tide (not monitored in this study) and air and light exposure during low tide (de Jonge and Van Beusekom, 1995; Koh et al., 2007; Pratt et al., 2014). These patterns of temporal variability were essentially the same in all sampling sites, despite the different time delay of the tidal propagation within the estuary. The observed patterns of spatial and temporal environmental variability are typical of tidal estuaries, strongly dominated by the tidal rhythm (Serôdio and Catarino, 1999; Brito et al., 2009; Kwon et al., 2012). In the sampling sites of the Ria de Aveiro, low tide tends to occur at mid-day during spring tides, and early in the morning and in late afternoon during neap tides. This causes a strong fortnight pattern of variability in physical conditions, particularly in the intertidal areas (Serôdio et al., 2008). The solar irradiance received varied between maximum values during spring tides to minimum values during neap tides, when direct exposure to light was restricted to two short periods, one during early morning and one during late afternoon. The strong periodicity of physical parameters propagated into a large variability in phytoplankton and microphytobenthos biomass and photosynthetic activity, ultimately determining their spatial-temporal patterns of productivity.

Biomass

The synoptic sampling of the water column and intertidal sediments with a high temporal resolution allowed a detailed comparison of the spatio-temporal variability of phytoplankton and microphytobenthos regarding biomass, photophysiology, photosynthetic performance, and productivity. In what regards biomass, the direct comparison of absolute values for microphytobenthos and phytoplankton is usually compromised by well-known difficulties, related to the determination of biomass values using directly comparable units. Ecologically relevant estimates, expressed as unit area (e.g., mg Chl *a* m^{-2}) are

very dependent on the criteria used for the vertical integration of volumetric measurements (Flemming, 2000; Serôdio et al., 2001; Laviale et al., 2015). While these difficulties were not completely resolver in this study, the concurrent sampling of planktonic and benthic biomass allowed comparing the overall patterns of spatial and temporal variability.

The spatio-temporal variation of phytoplankton and microphytobenthos biomass coincided in several aspects, namely a large variation over seasons, spring-neap tidal cycles, and a large variation over sampling sites, with TO showing the highest values. This overall tendency for the two communities to co-vary spatio-temporally, especially regarding the seasonal time scale, is likely tied to their common control by major abiotic factors, like irradiance and temperature, which varied markedly over seasons (de Jonge et al., 2012; Liu et al., 2018; Haro et al., 2019). Both phytoplankton and microphytobenthos biomass varied seasonally, but maximum values were observed later for the microphytobenthos (summer–autumn) than for the phytoplankton (spring, summer). The earlier peaking of phytoplankton biomass may be due to the more pronounced seasonal variation in favorable conditions for growth in the water column than in the sediment. The high nutrient availability in the water column commonly observed at the end of winter in estuaries and coastal areas (Vidal et al., 2017; Vajravelu et al., 2018), together with the start of favorable light and temperature conditions in spring, may have caused the phytoplankton to respond more promptly in terms of growth and accumulation of biomass. The sharp decrease observed in autumn, also typically observed for estuaries (Pennock and Sharp, 1986; Tian et al., 2009; Vidal et al., 2017), is likely associated to nutrient depletion caused by intense uptake during spring and summer. On the other hand, seasonal changes in growth conditions for the microphytobenthos might not be as relevant as for the water column, especially regarding nutrient availability, commonly considered not limiting in this habitat all year round (Davis and McIntire, 1983; Brotas et al., 1995). This, together with the continuation of favorable light and temperature conditions until autumn months, may explain the prolonging of high biomass levels into later in the year. The seasonal variation of microphytobenthos biomass, namely the lower values observed in Spring may thus be related to other factors, namely the increase in feeding activity by grazers (Vieira et al., 2012).

The occurrence of a significant fortnight variability in phytoplankton biomass, with maxima during spring tides, may be associated to the fact that during these periods the shallower water column of low tide coincides with the maximum solar irradiance, allowing a more efficient illumination of the phytoplankton populations (Pennock and Sharp, 1986; Mallin and Pearl, 1992; Madariaga, 2002). Also, the higher water currents during spring tides are associated to increased resuspension rates of sediment and benthic cells, which may have contributed to the higher chlorophyll *a* content and nutrients in the water column (Delgado et al., 1991; de Jonge and Van Beusekom, 1995; Ubertini et al., 2012; Pratt et al., 2014). For microphytobenthos, a tendency for higher biomass values during spring tides was also observed, that can be associated to the fact that the periods of low tide and light exposure occurring during the middle of the day favor daily photosynthetic rates and growth. However, the observed variation in the accumulation of biomass was not statistically significant, either because the fortnight variability in growth conditions was not sufficiently marked, or because of the confounding effects of varying favorable weather conditions during the periods before each sampling days.

Spatially, the coincidence of higher amounts of both planktonic and benthic biomass at the GE sampling site may be related to higher rates of resuspension-deposition associated to stronger tidal currents, that would cause a larger transfer of microalgal biomass from the benthos to the water column (Delgado et al., 1991; de Jonge and Van Beusekom, 1995; Brito et al., 2009). The reasons for the higher abundance of benthic biomass at this site are uncertain, but maybe related to higher nutrient availability, caused by the combination of finer sediment granulometry, favoring organic matter remineralization, and of possible agricultural run-off, originated in the farm fields bordering the canal of the estuary where the sampling site is located (Sousa et al., 2017; Bueno-Pardo et al., 2018; Vaz et al., 2019).

Photophysiology and Photoacclimation State

The photophysiological parameters $\Delta F/F_m$' and σ_{II} were, on short times scales, mostly controlled by changes in incident irradiance, showing large and rapid (minutes to hours) variations during daytime periods, as observed in other studies (Serôdio et al., 2008; Houliez et al., 2013; Schreiber and Klughammer, 2013). However, both $\Delta F/F_m$' and σ_{II}, of phytoplankton and microphytobenthos, showed also consistent patterns of variation on longer time scales, denoting changes in the photophysiological and photoacclimation state. $\Delta F/F_m$' largely followed the trends observed for the biomass of in the two groups, regarding seasonality (peaking in summer and in autumn, respectively), and the variation along the spring-neap tidal cycle (higher during spring tides in the case of the phytoplankton; not varying significantly in the case of the microphytobenthos) and spatial distribution (higher values at site TO, both communities). The similarity between the spatio-temporal variation of $\Delta F/F_m$' and biomass suggests that the accumulation of biomass may be directly related with conditions enabling a better photosynthetic performance. The higher $\Delta F/F_m$' values for the phytoplankton observed during spring tides may be associated to the increased availability of nutrients caused by the higher resuspension rates typical of the faster tidal currents occurring during spring tides, but also more favorable conditions in terms of temperature or photoperiod. The lack of significant variations in $\Delta F/F_m$' in microphytobenthos samples may result from the fact that, in the sedimentary environment, photosynthesis is more limited by light conditions than nutrient availability, which may support a good photophysiological condition along the spring-neap tidal cycle.

Regarding σ_{II}, there was a general tendency to follow the patterns of spatial and temporal variation of $\Delta F/F_m$' and biomass, namely concerning seasonal and fortnight time scales for phytoplankton. In other cases, $\Delta F/F_m$' and σ_{II} diverged from

each other, indicating the independent short-term regulation of the processes controlling the two parameters. A marked difference between the photophysiology of the phytoplankton and the microphytobenthos was revealed by the consistently higher values of σ_{II} measured for the phytoplankton. Higher values of σ_{II} are indicative of larger PSII antenna sizes, capable of higher light absorption efficiency, beneficial in low light environments and typical of low-light acclimated organisms (Ragni et al., 2008; Schreiber et al., 2012; Ware et al., 2015). Such high σ_{II} values may be advantageous for the planktonic microalgae inhibiting the highly turbid waters of the Ria de Aveiro estuary, where the experienced light regime calls for the optimization of light absorption. The lower σ_{II} values measured in the microphytobenthos samples are, on the other hand, symptomatic of a smaller PSII antenna, consistent with a high light environment, as the one at the sediment surface when directly exposed to sunlight during low tide. Smaller antennae sizes are also consistent with high light-acclimation, as allow a reduction in potential photodamage of PSII and photoinhibition of photosynthesis (Gordillo et al., 2001).

The results on photoacclimation state obtained from RLCs repeat, in general terms, the overall patterns of spatio-temporal variability in biomass, $\Delta F/F_m$' and, to a lesser extent, σ_{II}: α and $rETR_m$ reaching maximum values during summer (phytoplankton) and autumn (microphytobenthos), during spring tides (both communities), and at sampling site TO (phytoplankton). The marked seasonal photoacclimation in photophysiological parameters $\Delta F/F_m$' and σ_{II} described above was confirmed by comparable large changes in the photoacclimation parameter E_k, for both phytoplankton and microphytobenthos. The highest E_k values observed during summer and the lowest values observed during winter denote a variation from a high light-acclimation state to a low light-acclimation following the change in light conditions between the two contrasting seasons. Although not as clear as for σ_{II}, the differences observed between E_k measured in phytoplankton and in microphytobenthos samples, showing a tendency for higher values in the later, supports that the benthic communities appear as high-light acclimated, when compared to their planktonic counterparts.

The photoacclimation state of microphytobenthos appeared to vary fortnightly, as higher values of $\Delta F/F_m$' α and $rETR_m$ were measured during spring tides when compared to neap tides. This is most likely a consequence of the higher light dose received during spring tides rather than an effect of tidal height (Haro et al., 2019). The high light acclimation state of estuarine intertidal microphytobenthos has been referred before, supported by relatively high values of E_k (Serôdio et al., 2005; Frankenbach et al., 2018). It has been explained by the exposure to high solar irradiance levels during low tide periods, and, especially in the case of assemblages dominated by motile diatoms (epipelic), by the use of vertical migration as a form of control of light exposure within the photic zone of the sediment (Serôdio et al., 2001; Consalvey et al., 2004; Ezequiel et al., 2015; Haro et al., 2019). Curiously, microphytobenthos samples did not show a significant variation in the photoacclimation state between sites, as opposed to what was previously reported for the sites VA and GE (Frankenbach et al., 2018). This discrepancy may be explained by the fact that the mention study analyzed samples collected during a short period of three consecutive days (thus not covering different stages along the spring-neap tidal cycle), and that the photophysiological measurements were carried out in the laboratory, remove from the high variability *in situ* environment.

Biomass-Specific, Areal and Ecosystem-Level Productivity

In this study, the daily biomass-specific rates of productivity, P^B, were derived from the photophysiological parameters related to light usage efficiency ($\Delta F/F_m$' and σ_{II}) integrated over daylight hours. As such, the patterns of spatio-temporal variation of P^B largely followed the ones observed for those parameters. Probably due to the larger values of σ_{II} measured in the water column, the production rates of the phytoplankton resulted substantially higher than those of the microphytobenthos, for all sampling occasions and sites. The incorporation of photosynthetic biomass and the vertical light attenuation in the water and the sediment in the calculation of daily areal productivity rates did not alter the overall patterns of spatio-temporal distribution. However, it resulted in the inversion of the relative importance of phytoplankton and microphytobenthos. As expressed by units of area, benthic carbon fixation rates were on average 1.9 times higher than those in the water column. Despite the fact that the productivity rates determined in this study were based on chlorophyll fluorescence measurements, they fitted well within the range published values, based on the direct quantification of carbon fixation or oxygen evolution, for both estuarine phytoplankton and microphytobenthos (**Table 3**).

Regarding phytoplankton, the average annual rate of 49.8 g C m^{-2} y^{-1} appears as relatively low considering the median value of 252 g C m^{-2} y^{-1} reported by the exhaustive meta-analysis study of Cloern et al. (2014). According to the classification of Nixon (1995), the studied sites of the Ria de Aveiro could be classified as oligotrophic, as they fall below the limit of 100 g C m^{-2} y^{-1}. On the other hand, the average annual rate of 105.3 g C m^{-2} y^{-1} determined for the microphytobenthos, is remarkably close to the value of 100 g C m^{-2} y^{-1}, taken as the typical value for primary production rate on estuarine intertidal flats (Underwood and Kromkamp, 1999; Daggers et al., 2018).

The relative contribution of the phytoplankton and the microphytobenthos to the ecosystem-level productivity has been discussed for decades (Underwood and Kromkamp, 1999). Studies that directly compared the two communities have reported that the productivity of microphytobenthos could surpass the one of phytoplankton, reaching between 48.9% (Fielding et al., 1988) to 63.5% (Joint, 1978) of their combined contributions, and, in some cases, reaching over 50% of total estuarine carbon fixation (Cadée and Hegeman, 1974; Joint, 1978). The results of the present study showed that, despite the larger area accounted for the phytoplankton, the primary production carried out by the microphytobenthos may reach around 60% of the 12 kt C yr^{-1} annual rate estimated for the whole Ria de Aveiro. This estimate is amongst the highest

TABLE 3 | Daily and annual primary productivity rates of phytoplankton and microphytobenthos in published studies and as measured in this study (average and range of variation).

	Areal production		References
Phytoplankton	Daily (mg C m^{-2} d^{-1})	134.1 (8.1–505.0)	This study
		0.23–1.18	Morelle et al., 2018[a]
		0.69	Cloern et al., 2014
		2–778	Gameiro et al., 2011
		1.2–4.8	Kromkamp et al., 2008
	Annual (g C m^{-2} yr^{-1})	49.9 (44.7–51.8)	This study
		252	Cloern et al., 2014
		140–700	Underwood and Kromkamp, 1999
		77–92	Gameiro et al., 2011
		64.8	Morelle et al., 2018
Microphytobenthos	Daily (mg C m^{-2} d^{-1})	259.8 (25.6–909.0)	This study
		1–2888[b]	MacIntyre et al., 1996
		50–200	Daggers et al., 2018
		5–1900	Underwood and Kromkamp, 1999
		427	Serôdio and Catarino, 2000
	Annual (g C m^{-2} yr^{-1})	105.2 (43.4–164.4)	This study
		142	Savelli et al., 2018
		47–178	Brotas et al., 1995
		156	Serôdio and Catarino, 2000
		60–300	Underwood and Kromkamp, 1999

Average values unless stated otherwise. [a]*Maximum daily values.* [b]*Range of compiled values.*

reported in the literature, and close to the value of 63.5% obtained by Joint (1978).

Assumptions and Limitations of Chlorophyll Fluorescence-Based Productivity Estimates

With the aim of obtaining an integrated characterization of the spatio-temporal variability of the photosynthetic activity and productivity of benthic and planktonic microalgal communities, this study employed a synoptic sampling plan to measure the activity of phytoplankton and microphytobenthos under *in situ* conditions, on the same sites and on the same days, and with the same high temporal resolution. Key for the parallel close comparison of the two communities was the use of the same chlorophyll fluorescence-based technique for planktonic and benthic samples.

A novelty of this study was the estimation, to our knowledge for the first time, of production rates of microphytobenthos based on measurements of absolute rates of PSII electron transport (ETR). Previous studies have used chlorophyll fluorescence to estimate productivity rates of microphytobenthos, but they were based on determinations of relative ETR, integrated on empirically derived indices (Barranguet and Kromkamp, 2000; Serôdio et al., 2007). For the phytoplankton, the use of absolute ETR-based indices for the estimation of productivity rates has been addressed extensively for a long time, mostly based on 'pump-and-probe' (e.g., Kolber and Falkowski, 1993; Sakshaug et al., 1997) or 'fast repetition rate fluorometry' (FRRF) (Kromkamp et al., 2008; Lawrenz et al., 2013; Boatman et al., 2019) protocols. The protocol used in the present study, developed only recently, and specifically for the MC-PAM, and has been used only a few times, and only for phytoplankton (Morelle and Claquin, 2018; Morelle et al., 2018). While being also based on single-turnover pulses, this protocol is somewhat different from the pump-and-probe or FRRF approaches (Schreiber et al., 2012). Although no direct comparison between the two types of instruments and protocols has been carried out, the results of the present study regarding σ_{II}, a parameter crucial for the determination of absolute ETR values, are comparable and well within the range of values obtained with FRRF-based instruments.

This study is also novel because absolute ETR-based productivity estimates were applied to both phytoplankton and microphytobenthos. This approach presents several well-known significant operational advantages as compared to traditional methods based on the direct determination based on carbon fixation or oxygen evolution. In the context of the present study, it allowed for direct comparison of the two groups regarding the characterization of photoacclimation state, quantification of photosynthetic activity, and estimation of primary productivity.

The approach followed in this study is however based on several important assumptions. These apply to both phytoplankton and microphytobenthos, and can be categorized as follows:

(a) Conversion of fluorescence indices to biomass-specific carbon fixation rates. The method associated to the MC-PAM requires the *a priori* assumption of the value of PSU, ne(O_2) and PQ (Eqs. 4,5) (Schreiber et al., 2012). A compilation of experimental data compiled by Suggett et al. (2010) shows that ne(O_2), the number of electrons required for evolution of 1 molecule of O_2, varies from below 1 to above 11 e^- $O_2{}^{-1}$. However, the values measured for diatoms, dinoflagellates and haptophytes, the dominant groups in the phytoplankton and microphytobenthos of the Ria de Aveiro (Vidal et al., 2017; Frankenbach et al., 2018) vary between 3 and 6 e^- $O_2{}^{-1}$. In this study, ne(O_2) was assumed to reach 5 e^- $O_2{}^{-1}$, a value similar to those used by other authors (Kromkamp et al., 2008; Schreiber et al., 2012; Morelle and Claquin, 2018; Morelle et al., 2018). The photosynthetic quotient, PQ, was assumed be 1.1 mol C mol $O_2{}^{-1}$, a value commonly accepted, including in studies on estuarine phytoplankton (Kromkamp et al., 2008). PSU, the number of chlorophyll *a* molecules per photosynthetic unit is the most variable parameters required to calculate P^B from fluorescence measurements, having a larger direct impact on the final carbon fixation rates. For eukaryotes, the values assumed for PSU have varied from 500 (Schreiber et al., 2011; Lawrenz et al., 2013) and 1000 Chl *a* $PSII^{-1}$ (Schreiber et al., 2012;

Morelle and Claquin, 2018; Morelle et al., 2018). For diatoms, dinoflagellates and haptophytes, PSU varies between ca. 300 and 700, averaging around 620 Chl *a* $PSII^{-1}$ (Suggett et al., 2010). In the present study, PSU was assumed to be 600 Chl *a* $PSII^{-1}$, a value considered representative of the main groups that dominate the phytoplankton and the microphytobenthos in the Ria de Aveiro. In the absence of more detailed data, the same value was assumed for both groups although it is conceivable that it may differ between phytoplankton and the microphytobenthos, not only due to different taxonomic composition as to differences in photoacclimation state. All things considered, it seems unlikely that a depart from these assumptions would significantly affect the main conclusions of this study. Even considering the widest range of variation of ne(O_2), PQ and PSU, the large difference between the areal and ecosystem-based productivity of phytoplankton and microphytobenthos would likely still hold.

(b) Depth-integration of biomass-specific carbon fixation rates to areal productivity. An implicit assumption of the approach used in this study was to consider, for both the phytoplankton and the microphytobenthos, that the biomass and photosynthetic activity was constant over depth. That is, that the responses measured for samples collected at a single depth (water column) or at the surface (sediment) represent the ones in the remaining regions of the photic zones. For the phytoplankton this assumption seems realistic, due to the homogeneity of the shallow and turbulent water column, caused by the strong tidal currents of the Ria de Aveiro. In the case of the microphytobenthos, this approach may be more problematic, especially due to the fact that the measurements were carried out on cells in suspension, under conditions possibly not representative of the vertically heterogenous physico-chemical environment of the sediment (MacIntyre et al., 1996; Serôdio, 2003).

(c) Upscaling of areal to ecosystem-level productivity. Critical for a realistic evaluation of the planktonic and benthic productivity at the estuary-level, both in absolute as in relative terms, is the correct accounting of the area of intertidal and subtidal habitats, associated to phytoplankton and microphytobenthos productivity. Also important is to consider the time of day, and its variation along the spring-neap tidal cycle, when low or high tides occur, which determine the light incident on exposed tidal flats and light penetration in the water column. In this study, due to the lack of detailed information, estuarine-level production was calculated from spatially and temporal-averaged productivity rates. Another potentially important source of error affecting the absolute estimates of annual productivity of the two groups (but not their relative importance) is the fact that the annual estimates were directly conditioned by the particular conditions (mainly solar irradiance) of the days of measurements. As such, the annual budgets here reported should be seen as tentative estimates. The error associated to this approach is hard to quantify and can only be assessed with a much more extensive sampling program. An additional assumption was to consider that no benthic productivity occurred during immersion in high tide. However, this common assumption seems justified by the high turbidity of the water column and vertical migratory behavior of benthic diatoms (Serôdio and Catarino, 2000; Daggers et al., 2018).

DATA AVAILABILITY STATEMENT

The datasets generated for this study are available on request to the corresponding author.

AUTHOR CONTRIBUTIONS

JE, NV, JD, and JS planned and designed the research plan and fieldwork. JE, SP, NV, and JS carried out the fieldwork. JG and MK measured the vertical profiles of light in the sediment. SF, JE, and JS analyzed the data and wrote the draft of the manuscript. All authors edited and revised the manuscript.

FUNDING

The research was funded by the Portuguese Foundation for Science and Technology (FCT), through Project BioChangeR (PTDC/AAC-AMB/121191/2010), project Evo-Sym (POCI-01-0145-FEDER-028751), funded by FEDER, through COMPETE2020 - Programa Operacional Competitividade e Internacionalização (POCI), and by national funds (OE), through FCT/MCTES, and the fellowships BI/UI88/6484/2013 (JE), SFRH/BD/86788/2012 (SF), and SFRH/BD/103973/2014 (LV). NV was funded by national funds (OE), through FCT, in the scope of the framework contract foreseen in the numbers 4, 5, and 6 of the article 23, of the Decree-Law 57/2016, of August 29, changed by Law 57/2017, of July 19. This study was also supported by a Sapere-Aude Advanced grant from the Danish Council for Independent Research/Natural Sciences (MK) and an instrument grant from the Carlsberg Foundation (MK). Thanks are also due to CESAM (UID/AMB/50017 - POCI-01- 0145-FEDER-007638) and (UIDP/50017/2020+UIDB/50017/2020), to FCT/MEC through national funds (PIDDAC), and the co-funding by the FEDER, within the PT2020 Partnership Agreement and Compete 2020.

REFERENCES

Araújo, I., Dias, J., Pugh, D., Araujo, I., Dias, J., and Pugh, D. (2008). Model simulations of tidal changes in a coastal lagoon, the Ria de Aveiro (Portugal). *Cont. Shelf Res.* 28, 1010–1025. doi: 10.1016/j.csr.2008.02.001

Barbier, E. B., Hacker, S. D., Kennedy, C., Koch, E. W., Stier, A. C., and Silliman, B. R. (2011). The value of estuarine and coastal ecosystem services. *Ecol. Monogr.* 81, 169–193. doi: 10.1890/10-1510.1

Barranguet, C., and Kromkamp, J. (2000). Estimating primary production rates from photosynthetic electron transport in estuarine microphytobenthos. *Mar. Ecol. Prog. Ser.* 204, 39–52. doi: 10.3354/meps204039

Bauer, J. E., Cai, W.-J., Raymond, P. a, Bianchi, T. S., Hopkinson, C. S., and Regnier, P. a. G (2013). The changing carbon cycle of the coastal ocean. *Nature* 504, 61–70. doi: 10.1038/nature12857

Boatman, T. G., Geider, R. J., and Oxborough, K. (2019). Improving the accuracy of single turnover active fluorometry (STAF) for the estimation of phytoplankton primary productivity (PhytoPP). *Front. Mar. Sci.* 6:319. doi: 10.3389/fmars.2019.00319

Brito, A., Newton, A., Tett, P., and Fernandes, T. F. (2009). Temporal and spatial variability of microphytobenthos in a shallow lagoon: Ria Formosa (Portugal). *Estuar. Coast. Shelf Sci.* 83, 67–76. doi: 10.1016/j.ecss.2009.03.023

Brotas, V., Cabrita, T., Portugal, A., Serôdio, J., and Catarino, F. (1995). Spatio-temporal distribution of the microphytobenthic biomass in intertidal flats of Tagus Estuary (Portugal). *Hydrobiologia* 30, 93–104. doi: 10.1007/BF00024451

Bueno-Pardo, J., García-Seoane, E., Sousa, A. I., Coelho, J. P., Morgado, M., Frankenbach, S., et al. (2018). Trophic web structure and ecosystem attributes of a temperate coastal lagoon (Ria de Aveiro. Portugal). *Ecol. Modell.* 378, 13–25. doi: 10.1016/j.ecolmodel.2018.03.009

Cadée, G. C., and Hegeman, J. (1974). Primary production of the benthic microflora living on tidal flats in the Dutch Wadden Sea. *Neth. J. Sea Res.* 8, 260–291. doi: 10.1016/0077-7579(74)90020-9

Caffrey, J. M., Murrell, M. C., Amacker, K. S., Harper, J. W., Phipps, S., and Woodrey, M. S. (2014). Seasonal and inter-annual patterns in primary production, respiration, and net ecosystem metabolism in three estuaries in the northeast Gulf of Mexico. *Estuaries Coasts* 37, 222–241. doi: 10.1007/s12237-013-9701-5

Cloern, J. E., Foster, S. Q., and Kleckner, A. E. (2014). Phytoplankton primary production in the world's estuarine-coastal ecosystems. *Biogeosciences* 11, 2477–2501. doi: 10.5194/bg-11-2477-2014

Consalvey, M., Paterson, D. M., and Underwood, G. J. C. (2004). The ups and downs of life in a benthic biofilm: migration of benthic diatoms. *Diatom Res.* 19, 181–202. doi: 10.1080/0269249X.2004.9705870

Daggers, T. D., Kromkamp, J. C., Herman, P. M. J., and van der Wal, D. (2018). A model to assess microphytobenthic primary production in tidal systems using satellite remote sensing. *Remote Sens. Environ.* 211, 129–145. doi: 10.1016/j.rse.2018.03.037

Davis, M. W., and McIntire, C. D. (1983). Effects of physical gradients on the production dynamics of sediment-associated algae. *Mar. Ecol. Prog. Ser.* 13, 103–114. doi: 10.3354/meps013103

de Jonge, V. N., and Van Beusekom, J. E. E. (1995). Wind and tide induced resuspension of sediment and microphytobenthos in the Ems estuary. *Limnol. Oceanogr.* 40, 766–778.

de Jonge, V. N. V., de Boer, W. F. W., De Jong, D. D. J., and Brauer, V. V. S. (2012). Long-term mean annual microphytobenthos chlorophyll a variation correlates with air temperature. *Mar. Ecol. Prog. Ser.* 468, 43–56. doi: 10.3354/meps09954

Delgado, M., de Jonge, V. N., Peletier, H., Jonge, V. N., and Peletier, H. (1991). Experiments on resuspension of natural microphytobenthos populations. *Mar. Biol.* 108, 321–328. doi: 10.1007/BF01344347

Dias, J. M., Lopes, J. F., and Dekeyser, I. (1999). Hydrological characterisation of Ria de Aveiro, Portugal, in early summer. *Oceanol. Acta* 22, 473–485. doi: 10.1016/s0399-1784(00)87681-1

Dias, J. M., Lopes, J. F., and Dekeyser, I. (2003). A numerical system to study the transport properties in the Ria de Aveiro lagoon. *Ocean Dyn.* 53, 220–231. doi: 10.1007/s10236-003-0048-5

Eaton, J. W., and Moss, B. (1966). The estimation of numbers and pigment content in epipelic algal populations. *Limnol. Oceanogr.* 11, 584–595. doi: 10.4319/lo.1966.11.4.0584

Eilers, P. H. C. H. C., and Peeters, J. C. H. C. H. (1988). A model for the relationship between light intensity and the rate of photosynthesis in phytoplankton. *Ecol. Modell.* 42, 199–215. doi: 10.1111/jpy.12060

Ezequiel, J., Laviale, M., Frankenbach, S., Cartaxana, P., and Serôdio, J. (2015). Photoacclimation state determines the photobehaviour of motile microalgae: the case of a benthic diatom. *J. Exp. Mar. Bio. Ecol.* 468, 11–20. doi: 10.1016/j.jembe.2015.03.004

Fielding, P. J., Damstra, K. S. J., and Branch, G. M. (1988). Benthic diatom biomass, production and sediment chlorophyll in langebaan lagoon, South Africa. *Estuar. Coast. Shelf Sci.* 27, 413–426. doi: 10.1016/0272-7714(88)90097-2

Flemming, B. (2000). Mass physical properties of muddy intertidal sediments: some applications, misapplications and non-applications. *Cont. Shelf Res.* 20, 1179–1197. doi: 10.1016/s0278-4343(00)00018-2

Frankenbach, S., Azevedo, A. A., Reis, V., Dias, D., Vaz, L., Dias, J. M., et al. (2019). Functional resilience of PSII, vertical distribution and ecosystem-level estimates of subsurface microphytobenthos in estuarine tidal flats. *Cont. Shelf Res.* 182, 46–56. doi: 10.1016/j.csr.2019.05.018

Frankenbach, S., Schmidt, W., Frommlet, J., and Serôdio, J. (2018). Photoinactivation, repair and the motility-physiology trade-off in microphytobenthos. *Mar. Ecol. Prog. Ser.* 601, 41–57. doi: 10.3354/meps12670

Gameiro, C., Zwolinski, J., and Brotas, V. (2011). Light control on phytoplankton production in a shallow and turbid estuarine system. *Hydrobiologia* 669, 249–263. doi: 10.1007/s10750-011-0695-3

Genty, B., Briantais, J.-M. M., and Baker, N. R. (1989). The relationship between the quantum yield of photosynthetic electron transport and quenching of chlorophyll fluorescence. *Biochim. Biophys. Acta Gen. Subj.* 990, 87–92. doi: 10.1016/s0304-4165(89)80016-9

Gordillo, F. J. L. L., Jimenez, C., Chavarria, J., Niell, F. X., Jiménez, C., Chavarría, J., et al. (2001). Photosynthetic acclimation to photon irradiance and its relation to chlorophyll fluorescence and carbon assimilation in the halotolerant green alga Dunaliella viridis. *Photosynth. Res.* 68, 225–235. doi: 10.1023/A:1012969324756

Haro, S., Bohórquez, J., Lara, M., González, C. J., Crespo, J. M., Papaspyrou, S., et al. (2019). Diel patterns of microphytobenthic primary production in intertidal sediments : the role of photoperiod on the vertical migration circadian rhythm. *Sci. Rep.* 9:13376. doi: 10.1038/s41598-019-49971-8

Hope, J. A., Paterson, D. M., and Thrush, S. F. (2019). The role of microphytobenthos in soft-sediment ecological networks and their contribution to the delivery of multiple ecosystem services. *J. Ecol.* 1–16. doi: 10.1111/1365-2745.13322

Houliez, E., Lizon, F., Lefebvre, S., Artigas, L. F., and Schmitt, F. G. (2013). Short-term variability and control of phytoplankton photosynthetic activity in a macrotidal ecosystem (the Strait of Dover, eastern English Channel). *Mar. Biol.* 160, 1661–1679. doi: 10.1007/s00227-013-2218-4

Joint, I. R. (1978). Microbial production of an estuarine mudflat. *Estuar. Coast. Mar. Sci.* 7, 185–195. doi: 10.1016/0302-3524(78)90074-9

Koh, C.-H., Khim, J. S., Araki, H., Yamanishi, H., and Koga, K. (2007). Within-day and seasonal patterns of microphytobenthos biomass determined by co-measurement of sediment and water column chlorophylls in the intertidal mudflat of Nanaura, Saga, Ariake Sea, Japan. *Estuar. Coast. Shelf Sci.* 72, 42–52. doi: 10.1016/j.ecss.2006.10.005

Kolber, Z., and Falkowski, P. G. (1993). Use of active fluorescence to estimate phytoplankton photosynthesis in situ. *Limnol. Oceanogr.* 38, 1646–1665. doi: 10.4319/lo.1993.38.8.1646

Kromkamp, J., Barranguet, C., and Peene, J. (1998). Determination of microphytobenthos PSII quantum yield efficiency and photosynthetic activity by means of variable chlorophyll fluorescence. *Mar. Ecol. Prog. Ser.* 162, 45–55. doi: 10.3354/meps162045

Kromkamp, J. C., Dijkman, N. A., Peene, J., Simis, S. G. H., and Gons, H. J. (2008). Estimating phytoplankton primary production in Lake IJsselmeer (The Netherlands) using variable fluorescence (PAM-FRRF) and C-uptake techniques. *Eur. J. Phycol.* 43, 327–344. doi: 10.1080/09670260802080895

Kühl, M. (2005). Optical microsensors for analysis of microbial communities. *Methods Enzymol.* 397, 166–199. doi: 10.1016/s0076-6879(05)97010-9

Kwon, B.-O. O., Khim, J. S., Park, J., Ryu, J., Kang, S.-G. G., and Koh, C.-H. H. (2012). Short-term variability of microphytobenthic primary production associated with in situ diel and tidal conditions. *Estuar. Coast. Shelf Sci.* 112, 236–242. doi: 10.1016/j.ecss.2012.07.029

Laviale, M., Ezequiel, J., Pais, C., Cartaxana, P., and Serôdio, J. (2015). The "crème brûlée" sampler: a new high-resolution method for the fast vertical sampling of intertidal fine sediments. *J. Exp. Mar. Bio. Ecol.* 468, 37–44. doi: 10.1016/j.jembe.2015.03.013

Lawrenz, E., Silsbe, G., Capuzzo, E., Ylöstalo, P., Forster, R. M., Simis, S. G. H. H., et al. (2013). Predicting the electron requirement for carbon fixation in seas and oceans. *PLoS One* 8:e58137. doi: 10.1371/journal.pone.0058137

Liu, B., de Swart, H. E., and de Jonge, V. N. (2018). Phytoplankton bloom dynamics in turbid, well-mixed estuaries: a model study. *Estuar. Coast. Shelf Sci.* 211, 137–151. doi: 10.1016/j.ecss.2018.01.010

Lopes, C. L., Azevedo, A., and Dias, J. M. (2013). Flooding assessment under sea level rise scenarios: Ria de Aveiro case study. *J. Coast. Res.* 65, 766–771. doi: 10.2112/si65-130.1

Lorenzen, C. J. (1967). Determination of chlorophyll and pheo-pigments: spectrophotometric equations. *Limnol. Oceanogr.* 12, 343–346. doi: 10.4319/lo.1967.12.2.0343

MacIntyre, H. L., Geider, R. J., and Miller, D. C. (1996). Microphytobenthos: the ecological role of the "secret garden" of unvegetated, shalow-water marine habitats. I. Distribution, abundance and primary production. *Estuaries* 19, 186–201. doi: 10.2307/1352224

Madariaga, I. (2002). Short-term variations in the physiological state of phytoplankton in a shallow temperate estuary. *Hydrobiologia* 475–476, 345–358. doi: 10.1023/A:1020391425989

Mallin, M. A., and Pearl, H. W. (1992). Effects of variable irradiance on phytoplankton productivity in shallow estuaries. *Limnol. Oceanogr.* 37, 54–62. doi: 10.4319/lo.1992.37.1.0054

McLusky, D. S., and Elliott, M. (2007). Transitional waters: a new approach, semantics or just muddying the waters? *Estuar. Coast. Shelf Sci.* 71, 359–363. doi: 10.1016/j.ecss.2006.08.025

Migné, A., Gévaert, F., Créach, A., Spilmont, N., Chevalier, E., Davoult, D., et al. (2007). Photosynthetic activity of intertidal microphytobenthic communities during emersion: in situ measurements of chlorophyll fluorescence (PAM) and CO2 flux (IRGA). *J. Phycol.* 43, 864–873. doi: 10.1111/j.1529-8817.2007.00379.x

Morelle, J., and Claquin, P. (2018). Electron requirements for carbon incorporation along a diel light cycle in three marine diatom species. *Photosynth. Res.* 137, 201–214. doi: 10.1007/s11120-018-0491-2

Morelle, J., Schapira, M., Orvain, F., Riou, P., Lopez, P. J., Pierre-Duplessix, O., et al. (2018). Annual phytoplankton primary production estimation in a temperate estuary by coupling PAM and carbon incorporation methods. *Estuaries Coasts* 41, 1337–1355. doi: 10.1007/s12237-018-0369-8

Nixon, S. W. (1995). Coastal marine eutrophication: a definition, social causes, and future concerns. *Ophelia* 41, 199–219. doi: 10.1080/00785236.1995.10422044

Pennock, J. R., and Sharp, J. H. (1986). Phytoplankton production in the Delaware Estuary: temporal and spatial variability. *Mar. Ecol. Prog. Ser.* 34, 143–155. doi: 10.3354/meps034143

Portela, L. (1996). *Modelação Matemática da Hidrodinâmica e dos Processos de Qualidade da Água no Estuário do Tejo*. Lisboa: Instituto Superior Técnico.

Pratt, D. R., Pilditch, C. A., Lohrer, A. M., and Thrush, S. F. (2014). The effects of short-term increases in turbidity on sandflat microphytobenthic productivity and nutrient fluxes. *J. Sea Res.* 92, 170–177. doi: 10.1016/j.seares.2013.07.009

Ragni, M., Airs, R. L., Leonardos, N., and Geider, R. J. (2008). Photoinhibition of PSII in *Emiliania huxleyi* (Haptophyta) under high light stress: the roles of photoacclimation, photoprotection, and photorepair. *J. Phycol.* 44, 670–683. doi: 10.1111/j.1529-8817.2008.00524.x

Rickelt, L. F., Lichtenberg, M., Trampe, E. C. L., and Kühl, M. (2016). Fiber-optic probes for small-scale measurements of scalar irradiance. *Photochem. Photobiol.* 92, 331–342. doi: 10.1111/php.12560

Sakshaug, E., Bricaud, A., Dandonneau, Y., Falkowski, P. G., Kiefer, D. A., Legendre, L., et al. (1997). Parameters of photosynthesis: definitions, theory and interpretation of results. *J. Plankton Res.* 19, 1637–1670. doi: 10.1093/plankt/19.11.1637

Savelli, R., Dupuy, C., Barillé, L., Lerouxel, A., Guizien, K., Philippe, A., et al. (2018). On biotic and abiotic drivers of the microphytobenthos seasonal cycle in a temperate intertidal mudflat: a modelling study. *Biogeosciences* 15, 7243–7271. doi: 10.5194/bg-15-7243-2018

Schreiber, U., and Klughammer, C. (2013). Wavelength-dependent photodamage to *Chlorella* investigated with a new type of multi-color PAM chlorophyll fluorometer. *Photosynth. Res.* 114, 165–177. doi: 10.1007/s11120-013-9801-x

Schreiber, U., Klughammer, C., and Kolbowski, J. (2011). High-end chlorophyll fluorescence analysis with the MULTI-COLOR-PAM. I. Various light qualities and their applications. *PAM Appl. Notes* 1, 1–21.

Schreiber, U., Klughammer, C., and Kolbowski, J. (2012). Assessment of wavelength-dependent parameters of photosynthetic electron transport with a new type of multi-color PAM chlorophyll fluorometer. *Photosynth. Res.* 113, 127–144. doi: 10.1007/s11120-012-9758-1

Serôdio, J. (2003). A chlorophyll fluorescence index to estimate short-term rates of photosynthesis by intertidal microphytobenthos. *J. Phycol.* 39, 33–46. doi: 10.1046/j.1529-8817.2003.02043.x

Serôdio, J., and Catarino, F. (1999). Fortnightly light and temperature variability in estuarine intertidal sediments and implications for microphytobenthos primary productivity. *Aquat. Ecol.* 33, 235–241. doi: 10.1023/A:1009989229098

Serôdio, J., and Catarino, F. (2000). Modelling the primary productivity of intertidal microphytobenthos: time scales of variability and effects of migratory rhythms. *Mar. Ecol. Prog. Ser.* 192, 13–30. doi: 10.3354/meps192013

Serôdio, J., Da Silva, J. M., and Catarino, F. (2001). Use of in vivo chlorophyll a fluorescence to quantify short-term variations in the productive biomass of intertidal microphytobenthos. *Mar. Ecol. Prog. Ser.* 218, 45–61. doi: 10.3354/meps218045

Serôdio, J., Vieira, S., and Barroso, F. (2007). Relationship of variable chlorophyll fluorescence indices to photosynthetic rates in microphytobenthos. *Aquat. Microb. Ecol.* 49, 71–85. doi: 10.3354/ame01129

Serôdio, J., Vieira, S., and Cruz, S. (2008). Photosynthetic activity, photoprotection and photoinhibition in intertidal microphytobenthos as studied in situ using variable chlorophyll fluorescence. *Cont. Shelf Res.* 28, 1363–1375. doi: 10.1016/j.csr.2008.03.019

Serôdio, J., Vieira, S., Cruz, S., and Barroso, F. (2005). Short-term variability in the photosynthetic activity of microphytobenthos as detected by measuring rapid light curves using variable fluorescence. *Mar. Biol.* 146, 903–914. doi: 10.1007/s00227-004-1504-6

Sousa, A. I., Calado, R., Cleary, D. F. R., Nunes, C., Coimbra, M. A., Serôdio, J., et al. (2017). Effect of spatio-temporal shifts in salinity combined with other environmental variables on the ecological processes provided by *Zostera noltei* meadows. *Sci. Rep.* 7:1336. doi: 10.1038/s41598-017-01359-2

Suggett, D. J., Moore, C. M., and Geider, R. J. (2010). "Estimating aquatic productivity from active fluorescence measurements," in *Chlorophyll a Fluorescence in Aquatic Sciences: Methods and Applications, Developments in Applied Phycology 4*, eds D. J. Suggett, O. Prasil, and M. A. Borowitzka, (Dordrecht: Springer), 103–127. doi: 10.1007/978-90-481-9268-7_6

Tian, T., Merico, A., Su, J., Staneva, J., Wiltshire, K., and Wirtz, K. (2009). Importance of resuspended sediment dynamics for the phytoplankton spring bloom in a coastal marine ecosystem. *J. Sea Res.* 62, 214–228. doi: 10.1016/j.seares.2009.04.001

Tomás, L. M., Rodrigues, M., Fortunato, A. B., Azevedo, A., Leitão, P. C., Oliveira, A., et al. (2014). Salinity modelling accuracy of a coastal lagoon: a comparative river flow analysis of basin model vs. traditional approaches. *J. Coast. Res.* 70, 586–591. doi: 10.2112/SI70-099.1

Ubertini, M., Lefebvre, S., Gangnery, A., Grangeré, K., Le Gendre, R., and Orvain, F. (2012). Spatial variability of benthic-pelagic coupling in an estuary ecosystem: consequences for microphytobenthos resuspension phenomenon. *PLoS One* 7:e44155. doi: 10.1371/journal.pone.0044155

Underwood, G. J. C., and Kromkamp, J. (1999). Primary production by phytoplankton and microphytobenthos in estuaries. *Adv. Ecol. Res.* 29, 93–153. doi: 10.1016/s0065-2504(08)60192-0

Vajravelu, M., Martin, Y., Ayyappan, S., and Mayakrishnan, M. (2018). Seasonal influence of physico-chemical parameters on phytoplankton diversity, community structure and abundance at Parangipettai coastal waters, Bay of Bengal, South East Coast of India. *Oceanologia* 60, 114–127. doi: 10.1016/j.oceano.2017.08.003

Van Colen, C., Underwood, G. J. C., Serôdio, J., and Paterson, D. M. (2014). Ecology of intertidal microbial biofilms: mechanisms, patterns and future research needs. *J. Sea Res.* 92, 2–5. doi: 10.1016/j.seares.2014.07.003

Vaz, N., and Dias, J. M. (2008). Hydrographic characterization of an estuarine tidal channel. *J. Mar. Syst.* 70, 168–181. doi: 10.1016/j.jmarsys.2007.05.002

Vaz, N., Vaz, L., Serôdio, J., and Dias, J. M. (2019). A modeling study of light extinction due to cohesive sediments in a shallow coastal lagoon under well mixed conditions. *Sci. Total Environ.* 694:133707. doi: 10.1016/j.scitotenv.2019.133707

Vidal, T., Calado, A. J., Moita, M. T., and Cunha, M. R. (2017). Phytoplankton dynamics in relation to seasonal variability and upwelling and relaxation

patterns at the mouth of Ria de Aveiro (West Iberian Margin) over a four-year period. *PLoS One* 12:e0177237. doi: 10.1371/journal.pone.0177237

Vieira, S., Coelho, H., Nolasco, R., Serôdio, J., Barnes, R. S. K. K., and Queiroga, H. (2012). Repeated cycles of immersion and emersion amplify the crawling rhythm of the intertidal gastropod *Hydrobia ulvae*. *J. Mar. Biol. Assoc. U. K.* 92, 565–570. doi: 10.1017/S0025315411000853

Ware, M. A., Belgio, E., and Ruban, A. V. (2015). Photoprotective capacity of non-photochemical quenching in plants acclimated to different light intensities. *Photosynth. Res.* 126, 261–274. doi: 10.1007/s11120-015-0102-4

Conflict of Interest: The authors declare that the research was conducted in the absence of any commercial or financial relationships that could be construed as a potential conflict of interest.

frontiers in Marine Science

ORIGINAL RESEARCH
published: 07 July 2020
doi: 10.3389/fmars.2020.00496

Movement of Microphytobenthos and Sediment Between Mudflats and Salt Marsh During Spring Tides

Nurul S. Redzuan[1,2]* *and Graham J. C. Underwood*[1]

[1] School of Life Sciences, University of Essex, Colchester, United Kingdom, [2] Faculty of Science and Marine Environment, Universiti Malaysia Terengganu, Kuala Terengganu, Malaysia

The movement of sediment and associated microphytobenthos (MPB) between the upper mudflat and salt marsh in a macrotidal estuary was investigated by comparing the variability of benthic chlorophyll *a* (Chl. *a*) and suspended Chl. *a* during flood and ebb spring tides during the 2015 supermoon event. Sampling was carried out for 4 days in August and September. Flood-tide water carried significantly higher amounts of Chl. *a* from the mudflat transition zone onto the salt marsh compared to the amount of leaving the salt marsh during ebb tides. Suspended solid loads, suspended Chl. *a* concentrations, and diatom species composition provided evidence that resuspended mudflat sediments containing biofilm material were transferred onto the salt marsh by flood tide. Significant negative correlations between sediment Chl. *a* concentrations on the upper mudflat transition zone and Chl. *a* concentrations in flood-tide water indicated biostabilization of sediments by biofilms reducing sediment resuspension. Mean wind speed had a significant positive effect on resuspending Chl. *a* from the salt marsh sediment surface into the ebb tide ($p < 0.001$). The amount of Chl. *a* being resuspended in flood and ebb tidal waters was significantly correlated with MPB biomass on the sediment surface on the mudflat and salt marsh, respectively. Resuspended diatoms over the mudflat during high tide shared a total of 54.3% similar species with diatoms recorded in flood tidal water over the salt marsh. Diatom taxa characteristic of salt marsh assemblages, and some deposited diatom taxa were resuspended and carried off the salt marsh during ebb tide. Resuspension of Chl. *a* in both flood and ebb waters was significantly controlled by the tidal range (both significant at $p < 0.001$). During spring tides, there was a net movement of characteristic MPB mudflat diatom taxa and sediment from the adjacent mudflat to the salt marsh, contributing to the accumulation of material within vegetated marshes during summer months.

Keywords: microphytobenthos, diatom species, suspended sediment, suspended Chl. *a*, flood tide, ebb tide

OPEN ACCESS

Edited by:
David M. Paterson, University of St Andrews, United Kingdom

Reviewed by:
Clarisse Mallet, UMR 6023 Laboratoire Microorganismes Génome et Environnement (LMGE), France
Lourenço Soares Ribeiro, Center for Marine and Environmental Sciences (MARE), Portugal

***Correspondence:**
Nurul S. Redzuan
nurulshahida@umt.edu.my

Specialty section:
This article was submitted to Marine Ecosystem Ecology, a section of the journal Frontiers in Marine Science

Received: *30 November 2019*
Accepted: *03 June 2020*
Published: *07 July 2020*

Citation:
Redzuan NS and Underwood GJC (2020) Movement of Microphytobenthos and Sediment Between Mudflats and Salt Marsh During Spring Tides. Front. Mar. Sci. 7:496. doi: 10.3389/fmars.2020.00496

INTRODUCTION

Tidal flats are important coastal and estuarine habitats (Peterson and Peterson, 1979) that play a vital role in ecosystem services. The tidal flats occurring along coastlines are barriers to wave and wind energy (Scholz and Liebezeit, 2012; Leonardi et al., 2015). Tidal flats can be categorized by tide level into supratidal, intertidal, and subtidal zones. The sediment surface of intertidal flats

(mudflats) and supratidal flats (salt marsh) are exposed to diurnal or semidiurnal cycles of tides. While mudflats are generally covered by all tides within the neap tide periods in North West Europe, vegetated salt marsh grows above the mean high water neap tide level (Beeftink and Rozema, 1988; de Leeuw et al., 1994) and so is only covered with seawater during spring tides. Upper salt marsh, located in the supratidal area and vegetated with herbs, grasses, and low shrubs (Xin et al., 2013), are only subjected to tidal immersion during the highest spring tides. This results in a greater range of environmental conditions within salt marsh sediments, with higher levels of desiccation, rainfall, temperature, and nutrient delivery through tidal water (Chesman et al., 2006). Salinity ranges of salt marshes are greater than on adjacent mudflats (McKew et al., 2011). Underwood (1997) reported a salinity range between 16 and 210 in salt marsh of the Blackwater Estuary, Essex, while adjacent mudflat salinity ranged between 22 and 39. Periods of tidal cover replenish salt marsh sediments with nutrients and reestablish seawater conditions.

Salt marshes provide a range of ecosystem functions, such as denitrification and nutrient biogeochemistry (Seitzinger, 1973; Ogilvie et al., 1997; Underwood, 1997; Cibic et al., 2007), primary production and carbon storage (Macreadie et al., 2013; Mueller et al., 2019), wave attenuation and coastal protection (Shepard et al., 2011; Yang et al., 2012), food provisioning (Grothues and Able, 2003; Banerjee et al., 2017), and cultural benefits that are important ecosystem services for human society. There has been significant research into how to protect, enhance, and restore salt marshes to preserve these functions in the face of changing environmental pressures on coasts (Reed et al., 2018). Salt marshes can trap and accrete sediment brought in on high tides and grow vertically in the tidal frame, enabling them to keep pace with historic rates of relative sea level rise (Horton and Sawai, 2010). Many salt marshes have a short cliff face between the salt marsh platform and the adjacent mudflat (Reed et al., 2018). Sediment block collapse (slumping) in this transition zone and the dynamics of wave action and the height differences between mudflat, transition zone, and salt marsh can cause lateral erosion of marshes, while providing a source of sediment for vertical growth (Green and Coco, 2014; Ladd et al., 2019). Wave energy, tidal range, flood–ebb tides, and spring-neap tidal cycles are potentially factors that affect the resuspension and deposition of sediment in the tidal flats (French and Spencer, 1993; French et al., 2009; Green, 2011; Reed et al., 2018). The patterns of lateral salt marsh growth or loss and vertical height accretion are therefore dependent on wave climate, local fetch, the supply of sediment to the adjacent mudflats, relative seal level changes, and a range of biological interactions that can stabilize or destabilize sediments (Green and Coco, 2014; Reed et al., 2018).

Microphytobenthic (MPB) biofilms (mixed assemblages of eukaryotic and prokaryotic microorganisms and associated extracellular mucilage) are important agents for biostablization on mudflat and salt marsh sediments, increasing the erosional shear stress needed for sediment to erode (Paterson, 1989; Spears et al., 2008). Microphytobenthos have been attributed as primary colonizers in succession (Coles, 1979) and are important primary producers and biogeochemical agents in coastal sediments. Resuspension of microphytobenthos occurs when erosive forces exceed the shear stress of the sediment bed, and MPB can be carried in the suspended sediment load and can resettle elsewhere in the estuarine system (Koh et al., 2006; Ubertini et al., 2012). MPB are more abundant on unvegetated mudflats than under the vegetation canopy of European salt marshes, but the deposition onto marshes provides a source of new cells, organic material, and sediments. Redzuan (2017) observed coupling between the MPB on the transition zone and the salt marsh in the Colne Estuary, United Kingdom, with higher species similarity between transition and salt marsh MPB assemblages during spring tides than in the neap tides. Some common mudflat MPB species such as *Diploneis didyma*, *Pleurosigma angulatum*, *Surirella ovata*, *Gyrosigma scalproides*, *Gyrosigma wansbeckii*, and *Nitzschia sigma* showed increased relative abundance on salt marsh sediments during spring tide.

The aim of this study was to investigate the transfer of sediment and MPB between the transition zone of mudflats and the adjacent salt marsh surface and the relationships between sediment movement and four abiotic factors: wind speed, tidal range, rainfall, and sun hours. We hypothesized that wind speed and tidal range would increase sediment movement, with lower rainfall and higher sun hours promoting biostabilization and reducing resuspension. In addition to measuring suspended solids and microphytobenthic biomass (Chl. *a*), we used diatom species composition as a biomarker indicating the source of resuspended sediment. We hypothesized that diatom taxa characteristic of mudflat MPB would be associated with the suspended sediment during flood tide and deposited on the salt marsh. If no resuspension of salt marsh sediment occurred at high tide, then the diatom composition in the ebb-tide water would reflect that of the flood-tide water. However, if salt marsh sediment resuspension did occur, the ebb-tide water would carry a diatom assemblage more typical of a salt marsh sediment diatom flora.

MATERIALS AND METHODS

Sampling Strategy and Sample Processing

Two sampling surveys, involving four consecutive sampling days during the spring tide across the transition zone on the mudflat and the salt marsh, were carried out in August 2015 (survey 1, 30.08.15 to 02.09.15) and September 2015 (survey 2, 26.09.15 to 29.09.15) (**Figure 1**). The relatively shallow-water depth over the salt marsh surface even during spring tides can prevent successful deployment of sediment traps to collect any suspended sediment samples. Our study coincided with the "supermoon" event (the closest approaches the moon makes to the earth in its elliptical orbit), peaking on the 28th September 2015, which resulted in increased spring tide ranges (5.3–6.1 m) and greater flooding of the salt marshes in the Colne Estuary, enabling the collection of suspended sediment samples on the salt marsh.

Two sampling plots (0.5 m × 4.5 m, built of five 0.5 m × 0.5 m quadrats distanced at 0.5 m between each other and perpendicularly to the water channel, **Figure 1A**) were laid out, one on the upper transition zone of the mudflat and one of

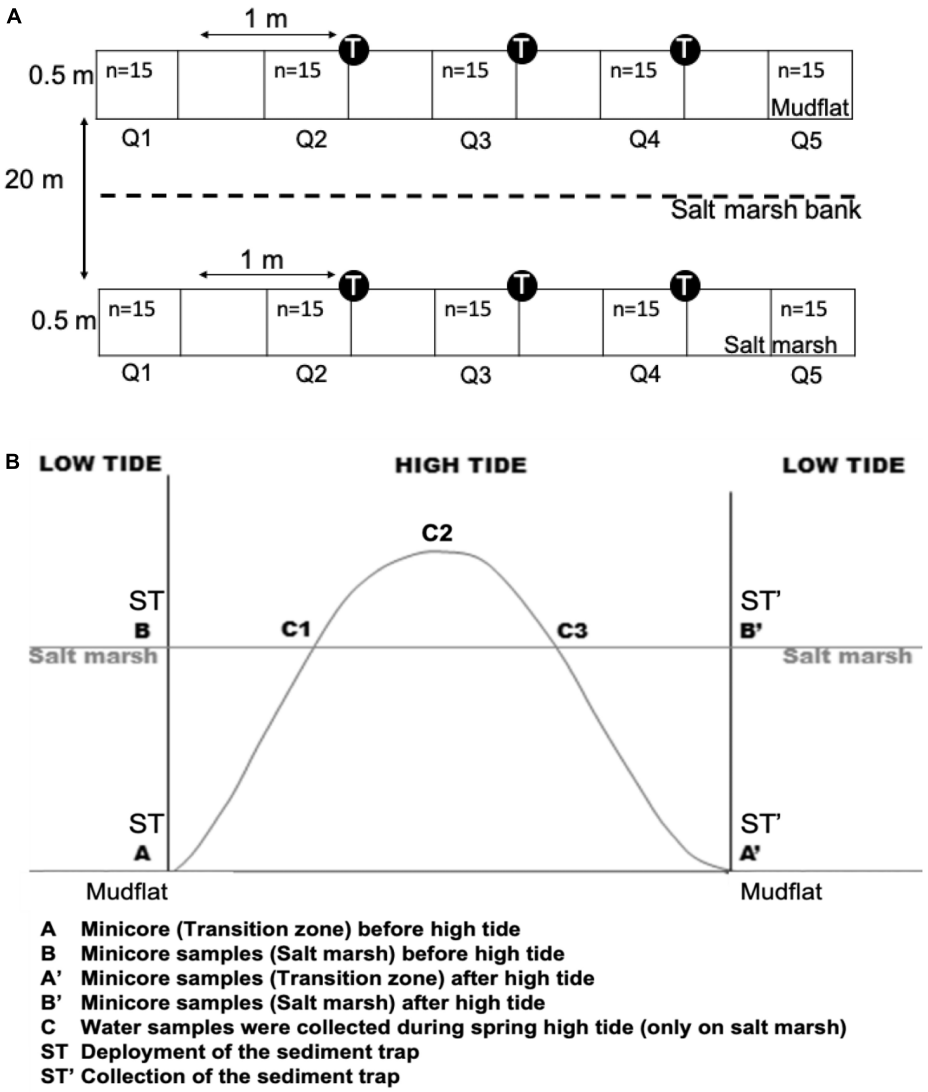

FIGURE 1 | (A) Technical diagram of the plots (0.5 m × 4.5 m) built from five quadrats distanced at 0.5 m each, in which $n = 15$ samples were collected on mudflat and salt marsh. The $n = 15$ were pooled in the laboratory to make up triplicate samples for each quadrat, which then made up a sample size of $n = 5$ for each zone. *T* and *Q*, respectively, indicate sediment trap and quadrat; **(B)** sampling strategy carried out on the transition zone of mud flat (MF) and salt marsh (SM) at Fingringhoe Wick, Colne Estuary, Essex, United Kingdom, in August and September 2015. The sediment trap (ST) ($n = 3$) was deployed before the high tide and was collected after one period of tidal cover on each sampling day. C1 indicates water sample collection on flood and (C3) ebb tides. The unit of replication, $n = 3$.

the salt marsh. The size of the plot was decided after taking into account time to deploy and to collect sediment traps and to obtain sediment samples during each tidal cycle (**Figure 1B**). Three different sets of data were obtained from the plot on each day of sampling (**Supplementary Material A**): (1) surface sediment Chl. *a* concentration (MPB biomass) before and after tidal cover; (2) suspended sediment and associated Chl. *a* concentrations in sediment traps after high tide; and (3) suspended sediment and Chl. *a* during flood and ebb tides over the salt marsh surface (see **Supplementary Material A**). Fifteen sediment surface samples (top 2 mm) were randomly obtained from each quadrat ($n = 5$) on the mudflat and salt marsh (twice, collected once before and once after one daytime high tide event) (**Figure 1B**) using minicores (20-ml syringe cut at the end with 2.836 cm^2 diameter). Fifteen field replicates (n) were taken within each quadrat, as $n = 12$ proved to have the least sampling error at this spatial scale (Redzuan, 2017). The samples were immediately transferred into cold–dark containers and were preserved for Chl. *a* and colloidal carbohydrate (CC) analyses and MPB cell counts. Three sediment traps (inverted 850-mL plastic bottles with the bases removed, attached vertically to canes) were systematically placed along each plot (**Figure 1A** at a 1-m interval in each zone (**Figure 1A**). The suspended sediment samples in the traps were collected, labeled, and transferred into 1-liter bottles immediately after the high tide. Triplicate tidal water samples during flood tide (C1) and ebb tide (C3) were collected (only on salt marsh) into 500-ml

bottles by hand to investigate the effect of tidal resuspension on water column Chl. *a* and CC concentrations and cell counts (**Figure 1B**). All samples were kept in cold and dark containers and returned to the laboratory for processing.

Sample Processing

In the laboratory, sediment samples from the fifteen collected minicores for each quadrat were pooled and mixed thoroughly, after which triplicate subsamples (n = 3) (technical replicates) were freeze dried for Chl. *a* (Lorenzen, 1967) and CC (Hanlon et al., 2006) analyses. Additionally, another triplicate set of sediment samples was collected and preserved in 0.5% w/v glutaraldehyde. These preserved samples were acid washed (Underwood, 1994) for permanent slide preparation for diatom cell counts.

Sediment trap water (250 ml) and tidal water samples (250 ml) were filtered using 12.5 and 4.5-cm GF/F Whatman filter paper, respectively. Tidal water samples were filtered through the smaller-size filter paper due to low sediment concentration (based on observation). The filtered sediments were freeze dried for Chl. *a* (Lorenzen, 1967) and CC (Hanlon et al., 2006) analyses. For permanent slide preparation and diatom cell count, a volume of 50 ml water sample from both the suspended and tidal water samples were taken after agitation of the main sample and transferred into plastic 15-ml centrifuge tubes. Samples were preserved with 0.5% w/v glutaraldehyde before going through an acid-washing procedure to make permanent diatom slides following Underwood (1994).

A total of 300 and 250 diatom valves were counted for each of the triplicate sediment surface samples for the mudflat and the salt marsh, respectively. Only 150 and 100 valves were counted for the triplicate suspended and tidal water samples, respectively, due to their low cell density. Each taxon was expressed in relative abundance (%).

Weather-Related Abiotic Factors

Four weather-related abiotic factors, the percentage of cloud cover (%), the tidal range (m), the mean wind speed (m s^{-1}, averaged wind speed data for the 2 days preceding and on sampling day), and the sum of rainfall (mm, sum of rainfall of 2 days pre sampling and on the sampling day), were measured. Data for the cloud cover, sum of rainfall, and wind speed were obtained online on www.worldweatheronline.com/Colchester-weather-histor/Essex/GB.aspx. Tidal range data were obtained from Brightlingsea tide tables[1]. Cloud cover was chosen to indicate the potential light attenuation and also the weather (cloudy or sunny) at the study site.

Statistical Analyses

T-tests were performed using SPSS 25 to evaluate the variability in both Chl. *a* (log transformed) and CC (log transformed) concentrations in the top 2-mm sediment surface between before (LT 1) and after (LT 2) tidal immersion on the transition zone and the salt marsh. One-way ANOVA tests were used to investigate the variability of the Chl. *a* (log transformed) and CC (log transformed) in both the sediment surface and suspended in the water column among sampling days across the sampling surveys. Weather-related abiotic factors were analyzed using one-way ANOVA using day and survey as factors to determine their variability at both factor levels. Daily variability in Chl. *a* concentrations in both the flood and ebb tides (survey 1, 2) was investigated by using two-way ANOVA. The day and the sampling survey were treated as the factors for the ANOVA analyses; significant variability is reported at significance levels $p < 0.05$, $p < 0.01$, and $p < 0.001$.

Pearson correlation coefficients were used to determine the relationship between the measured variables (Chl. *a*, CC, suspended sediment Chl. *a*, and Chl. *a* in tidal water samples) with the weather-related abiotic factors.

Modified Morisita's similarity index was used to calculate the percentage similarity between the MPB-diatom species composition on the transition zone and salt marsh sediment surfaces, in sediment traps (on transition zone) and in the flood and ebb-tide samples, using the Multi Variate Statistical Package (MVSP) 3.1 software (Kovach, 1999). Before the analyses, the overall data for each taxon were averaged and $\log_{10}$ $n + 1$ transformed. NMDS, ANOSIM, and SIMPER analyses were conducted on the diatom species-abundance Bray Curtis dissimilarity matrix, using R version 4.0 with the package vegan (Oksanen et al., 2019; R Core Team, 2020).

RESULTS

Temporal Variability in Microphytobenthic and Suspended Biomass Related to Tides and Weather Factors

Chl. *a* concentrations in the top 2-mm sediment surface on the transition zone of the mudflat and salt marsh before (LT 1) and after (LT 2) the immersion period showed no significant differences across a flood–ebb cycle (**Figures 2A,B**). There were significant differences in the sediment CC concentration on the transition zone between the low tides ($F_{1,60}$ = 235.2, $p < 0.001$) but no consistent pattern of being higher or lower before and after tidal cover (**Figure 2C**). The presence of fine particulate organic matter in the salt marsh sediments interfered with the carbohydrate assay, which meant it was not possible to determine accurate CC concentrations in the salt marsh sediments.

Chl. *a* concentrations in the top 2-mm cm^{-2} sediment displayed strong temporal variation at daily time scales on both zones in both surveys (**Figure 3**; survey 1, $F_{3,40} = 80.73$, $p < 0.001$; survey 2, $F_{3,40}$ = 29.34, $p < 0.001$) on the transition zone of the mudflat (**Figure 3A**). There was significantly higher mudflat sediment Chl. *a* during Survey 2 (overall average 14.8 ± 1.28 μg Chl. *a* cm^{-2}) than during survey 1 (8.0 ± 0.6 μg Chl. *a* cm^{-2}) ($F_{1,80}$ = 26.693, $p < 0.001$). Chl. *a* concentrations on the salt marsh in both surveys showed a pattern of decrease followed by an increase after 3 days (**Figure 2B**; survey 1,

[1]http://www.visitmyharbour.com/tides/90/uk-tables/brightlingsea-tide-tables

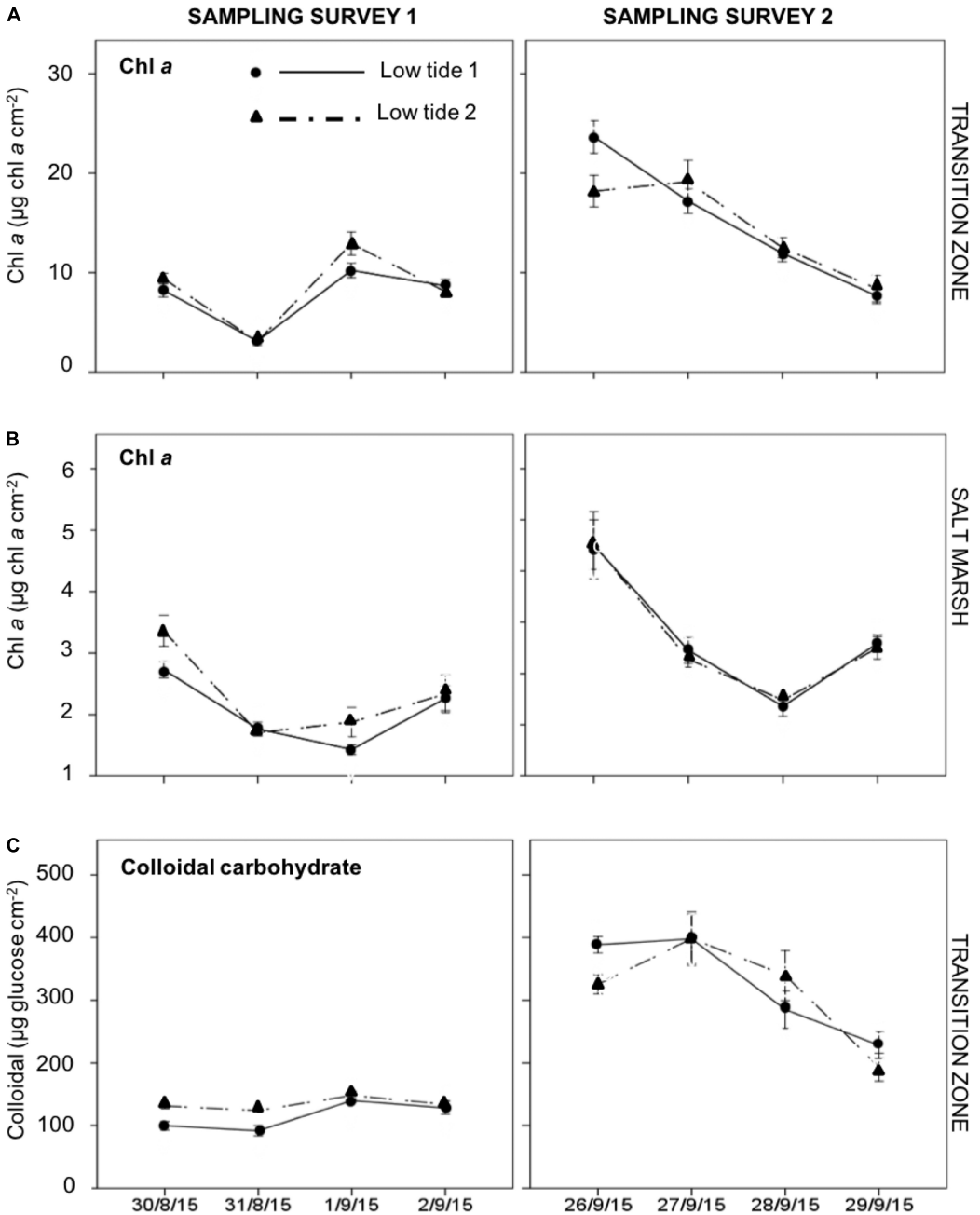

FIGURE 2 | Daily changes in Chl *a* concentration (µg cm^{-2}) in the top 2-mm sediment surface on the; **(A)** transition zone of the mudflat; **(B)** salt marsh; and **(C)** colloidal carbohydrate on the transition zone, sampled during low tide 1 (LT1) and low tide 2 (LT2) in sampling survey 1 and survey 2 at Fingringhoe Wick, Colne Estuary, Essex, United Kingdom, in August and September 2015. Values are mean ± SE, $n = 5$.

$F_{3,40} = 15.965$, $p < 0.01$; survey 2 $F_{3,40} = 38.173$, $p < 0.001$). On the mudflat transition zone, there was a strong positive correlation ($r = 0.812$, $p < 0.001$) between the concentrations of Chl. *a* and CC across sampling days in both surveys (**Figure 2** and **Supplementary Material B**).

There were significant differences in the weather-related abiotic factors between days and between survey periods (**Table 1**). The mean sediment Chl. *a* concentration on the transition zone was significantly negatively correlated with all four abiotic factors, with cloud showing the strongest negative correlation (**Table 2**) (r value > -0.5). The mean Chl. *a* concentration on the salt marsh was negatively correlated ($r > -0.5$) with increasing tidal range (**Table 2**). Salt marsh Chl. *a* concentrations were also significantly negatively correlated with averaged wind speed for 3 days ($r = -0.172$, $p < 0.05$) and tidal range ($r = -0.551$, $p < 0.001$) (**Table 2**).

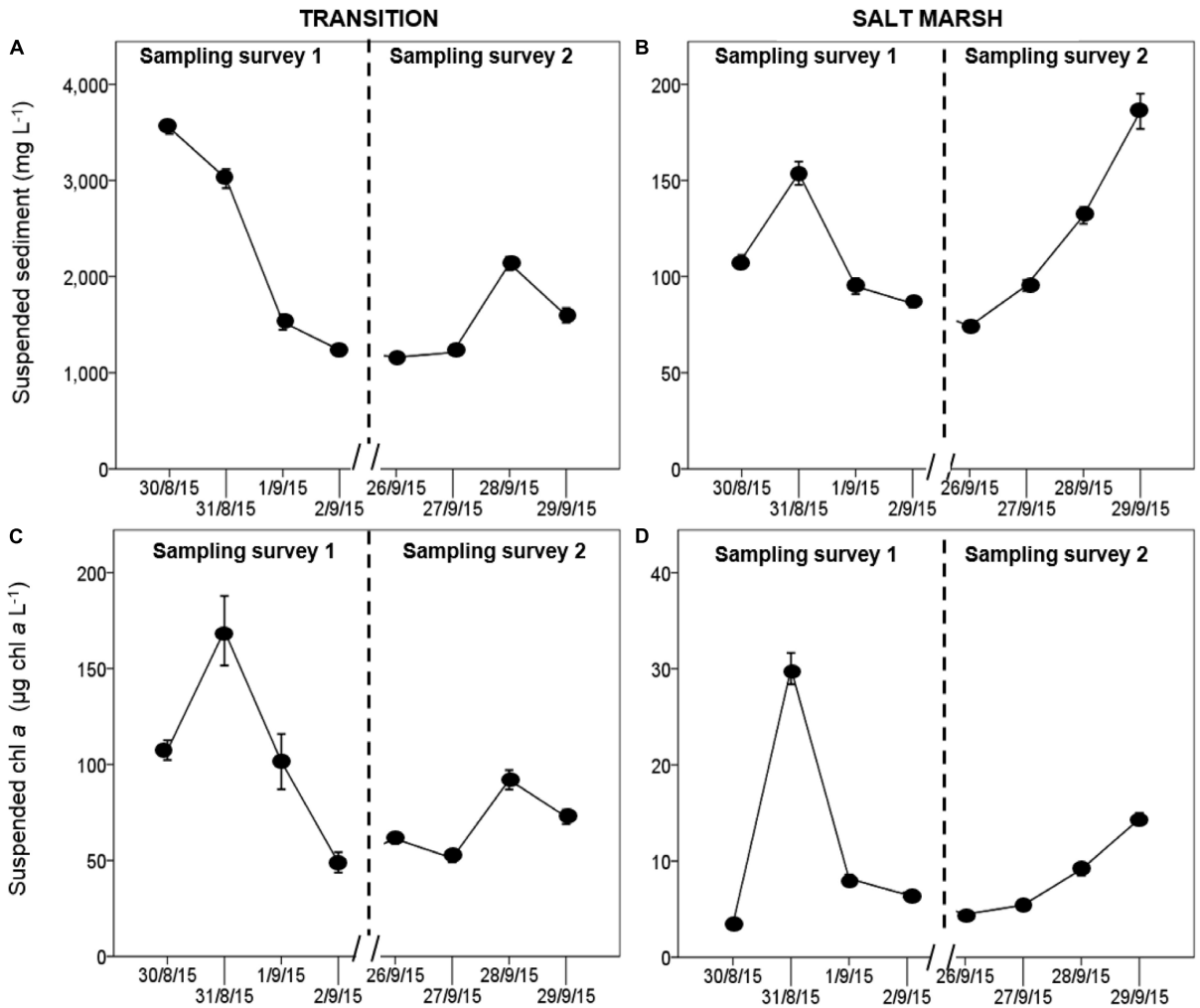

FIGURE 3 | Daily changes in suspended sediment **(A,B)** and suspended sediment associated Chl. *a* **(C,D)** per L of water (obtained by sediment trap) over the transition zone of the mud flat and the salt marsh during two periods of sampling in August and September 2015 at Fingringhoe Wick, Colne Estuary, Essex, United Kingdom Values are mean ± SE, $n = 3$.

TABLE 1 | Daily changes in the weather-related abiotic factors and tidal range during sampling surveys 1 and 2, at Fingringhoe Wick, Colne Estuary, Essex, United Kingdom, in 2015.

Sampling survey	Date	Weather-related abiotic factors			
		Sum of rainfall (m)	Mean wind speed (ms^{-1})	Cloud cover (%)	Tidal range (m)
1	30th August	2.8	2.9	89.0	5.7
	31st August	7.0	3.3	100.0	6.0
	1st September	6.5	3.8	57.0	6.0
	2nd September	6.8	3.8	31.0	5.9
2	26th September	2.9	3.1	7.0	5.3
	27th September	0.1	2.7	16.0	5.7
	28th September	0.1	3.0	47.0	6.1
	29th September	0.1	3.7	30.0	6.1

There were significant negative correlations between sediment Chl. *a* concentrations and both suspended sediment load and suspended Chl. *a* in the water column during immersion (**Table 2**), with the strongest negative correlations on the transition zone and the lowest correlation coefficients for the marsh surface (**Table 2**). Suspended solid loads were high,

TABLE 2 | Correlations between Chl. *a* concentration with weather-related abiotic factors and suspended water properties during August and September 2015 on two different intertidal zones at Fingringhoe Wick, Colne Estuary, Essex, United Kingdom.

	Pearson correlation coefficients (r)					
	Weather-related abiotic factors				Suspended	
Zones	**Sum of rainfall**	**Mean wind speed**	**Cloud cover**	**Tidal range**	**Suspended sediment**	**Suspended Chl. *a***
Transition zone of the mudflat	−0.207**	−0.299***	−0.652***	−0.462***	−0.605***	−0.472***
Salt marsh	ns	−0.172*	−0.267***	−0.551***	−0.398***	−0.260***

The Pearson's correlation coefficients were performed on pooled Chl. a data of surveys 1 and 2.

exceeding 1,000 mg L^{-1} over the transition zone of the mudflat and between 100 and 200 mg L^{-1} on the salt marsh (**Figure 3**). Suspended Chl. *a* concentrations showed similar patterns with suspended sediment load (sediment trap data). There was significantly higher suspended sediment on the 30th and the 31st August (*post hoc* Tukey HSD, $p < 0.001$) (**Figure 3A**) and suspended Chl. *a* (*post hoc* Tukey HSD, $p < 0.001$) (**Figure 3B**) in the water column than other days. Suspended Chl. *a* concentrations in the water column over the salt marsh were significantly positively correlated with mean wind speed and with tidal range (**Supplementary Material C**), even if the high values from 31 Aug 2015 were discounted, (i.e., $r = 0.40$, $p < 0.05$ (mean wind speed); $r = 0.7$, $p < 0.001$ (tidal range).

MPB Coupling Between the Transition Zone (Mudflat) and the Salt Marsh

Chl. *a* concentrations over the salt marsh were significantly higher in the flood tidal water (23.90 ± 1.43 μg Chl. *a* L^{-1}) than in the ebb [19.46 ± 0.89 μg Chl. *a* L^{-1}, $F_{1,48} = 7.105$, $p < 0.05$ (overall data), **Figure 4**]. Only the Chl. *a* in the flood tide on the 1st and 2nd Sept 2015 showed lower values than the ebb, which was potentially closely linked to the weather condition (windy and rainy) on these two sampling days. The difference between the flood and ebb-tide concentrations of suspended Chl. *a* indicates retention of sediment within the salt marsh.

The water column Chl. *a* concentration in flood-tide water samples on the salt marsh was significantly negatively correlated with the Chl. *a* concentration on the transition zone of the mud flat sediment surface [$r = -0.774$, $p < 0.001$ (**Figure 5A**)]. The correlation was stronger than the correlation between flood tide Chl. *a* and Chl. *a* on the salt marsh ($r = -0.410$, $p < 0.001$) (**Figure 5B**). During ebb tides, there was evidence for the wash away of MPB from the salt marsh. The significantly higher salt marsh sediment Chl. *a* in survey 2 (2.71 ± 0.15 μg Chl. *a* cm^{-2}) than in survey 1 (2.18 ± 0.10 μg Chl. *a* cm^{-2}) was associated with relatively lower Chl. *a* in the ebb-tide water samples in the survey 2 (17.79 ± 1.07 μg Chl. *a* L^{-1}) than in survey 1 (21.13 ± 1.29 μg Chl. *a* L^{-1}). These data revealed the significant negative correlation between ebb-tide Chl. *a* concentrations and Chl. *a* in the top 2-mm sediment surface of the salt marsh (**Figure 5B**). The correlation coefficient was higher than for the correlation during flood tides (**Figure 5A**). During our period of study, rainfall had no significant effect on water column Chl. *a* concentrations in either flood- or ebb-tide water over the marsh. Increasing wind speed caused shallow-water mixing on the salt marsh surface (**Figure 6A**), resulting in increased suspended Chl. *a* load in ebb tides (**Figure 6B**). Cloud cover and tidal range were both positively correlated with flood-tide Chl. *a* concentration, with tidal range also influencing ebb-tide water concentrations (**Figures 6C,D**).

There were significant differences in the taxonomic composition of the diatom assemblages present on the mudflat and salt marsh and in the sediment traps and flood and ebb-tide waters (**Figure 7A**, ANOSIM, $r = 0.989$, $p < 0.001$). The mudflat flora (64 taxa) was characterized by a number of abundant large *Gyrosigma* and *Pleurosigma* species, *Diploneis didyma*, *Synedra*, and *Nitzschia* (SIMPER, $p < 0.01$ or less, **Table 3**). Eighteen of the 64 taxa identified on the mudflats were also found in the salt marsh assemblages (**Table 3**). Characteristic salt marsh taxa (34 taxa) included two *Opephora* species, *Neidium* sp., *Nitzschia vitrea*, and *Surirella fastuosa* (SIMPER, $p < 0.01$ or less).

There was 65.4% similarity in diatom community composition between the assemblages on the transition zone mudflats and those in sediment trap tide (**Figure 7B**) and a 54.3% assemblage similarity between the transition zone diatom assemblages (sediment and water) with the diatoms present in flood-tide samples over the salt marsh (**Figure 7B**). A number of abundant mudflat taxa, notably *Gyrosigma balticum*, *G. limosum*, *Psammodictyon panduriforme*, and the *Synedra* species were not found in the sediment traps or flood-tide samples or present in the salt marsh (**Table 3**). All the mudflat taxa present in the flood-tide water samples were also found on the salt marsh. In addition, there were a number of planktonic diatom genera found in the flood-tide samples (*Coscinodiscus*, *Stephanodiscus*, *Actinoptychus*, and *Rhizosolenia*, data not shown). The ebb-tide water column diatom assemblage (14 taxa) had 72.6% similarity with the species composition on the salt marsh sediment surfaces (**Figures 7A,B**) and was most dissimilar to the nudflat flora (**Figure 7A**). Eight taxa were found only in both the salt marsh and the ebb-tide water samples (**Table 3**). Overall, the species composition of Group B (characterized by MPB originating from the mudflat) shared a total of 31.8% similarity with MPB associated with salt marsh sediments and ebbing tides (Group C) (**Figure 7B**, **Supplementary Material D**). Five taxa that were abundant in the ebb-tide samples, *Surirella ovata*, *Diploneis didyma*, *D. litoralis*, *Nitzschia sigma*, and *Actinoptychus undulatus*, were also found in varying relative abundances in all the other four sample types (**Table 3**).

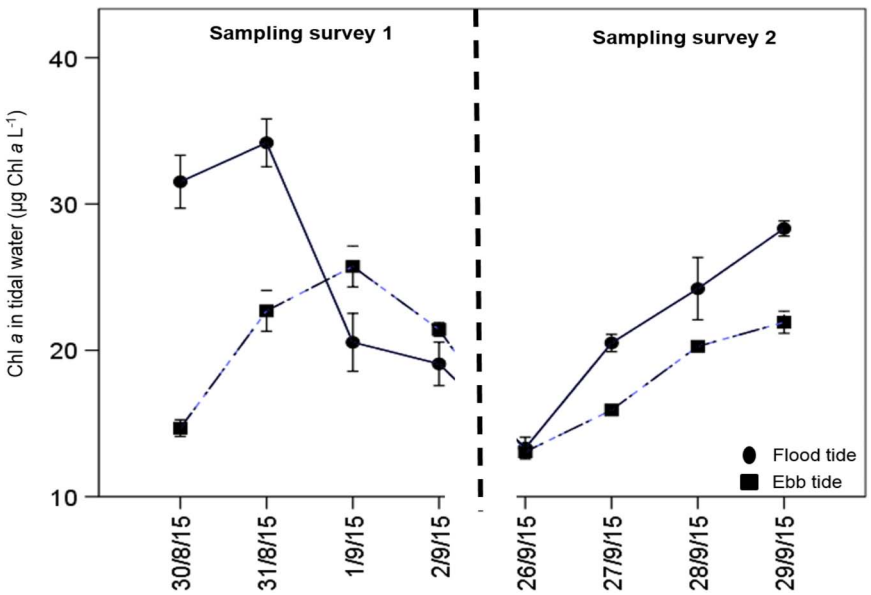

FIGURE 4 | Daily variability in water column Chl. *a* in flood and ebb tidal water on the same tide over the salt marsh in both surveys 1 and 2 at Fingringhoe Wick, Colne Estuary, Essex, United Kingdom, in August and September 2015. Values are mean ± SE, n of tidal water = 3. The difference between the flood and ebb lines material retained on the marsh over the tidal cycle.

DISCUSSION

This study did not find any significant reduction in MPB Chl. *a* concentration in the top 2-mm sediment surface before and after high-tide emersion periods during spring tides on both the transition and the salt marsh. Other studies in the Colne estuary have found significant "wash away" from mudflats during tidal cover (Bellinger et al., 2009; Taylor et al., 2013), and modeling shows this can be a significant process in MPB biomass dynamics on mudflats (Savelli et al., 2019). High levels of microspatial variability in MPB biomass (Spilmont et al., 2011; Taylor et al., 2013) may mask individual localized losses on any particular patch of sediment. Our sampling design integrated microspatial patchiness to look at the larger scale of meters. It is clear that some resuspension related to abiotic weather factors (particularly tidal range, wind, and cloud) did occur (**Table 2**) but that the mass lost was not sufficient to reduce the Chl *a* stocks remaining in the sediments. Koh et al. (2007) found a significant positive correlation between the daily mean of Chl. *a* concentration and both the Chl. *a* concentrations sampled at two different emersion periods of similar sampling day. There is a significant pool of microphytobenthic biomass within sediments, which undergoes micro-migration cycles (Underwood et al., 2005), so loss of some surface biomass may not be detectable against this larger Chl *a* signal. A strong contributor to reducing wash away is the presence of vertical migratory rhythms of MPB responding to tidal and diel conditions (Smith and Underwood, 1998; Underwood et al., 2005). Downward vertical migration has been reported to reduce the effect of MPB biofilm "wash away" by the tidal current (Fidalgo et al., 2002) and its associated wind (de Jonge and van Beusekom, 1995) and wave (Easley et al., 2005) energies during spring tide immersion (Riggs, 2002). During our period of study, wind speeds were relatively low and not sufficient to produce mass failure of the sediment bed. However, the diatom biomarkers suggest that there was differential removal of taxa under the conditions of our study. A number of large diatom taxa dominant on the mudflats were not found in the suspended sediments. Taxa such as *G. balticum* live in short mucilage tubes in sediments and are very active and rapid vertical migrators (Jönnson et al., 1994). *Gyrosigma balticum* also do not remain on the sediment surface throughout periods of tidal exposure (Underwood et al., 2005) but move down before tidal immersion, and other taxa show a similar behavior. Other taxa, such as *Synedra* and *Psammodictyon* are large cells and perhaps less likely to be resuspended, especially if they are bound into a mucilage matrix. So though some species avoided resuspension, a wide range of other mudflat taxa were present in the flood water and caught in sediment traps, for example *Pleurosigma angulatum*, which remains at the mudflat surface throughout periods of tidal exposure (Underwood et al., 2005). The high similarity in assemblage composition indicates that a transfer of biofilm material into the water column with incoming tides did occur.

The ability of MPB biofilms to reduce erosion by increasing the sediment critical erosion threshold has been reported in numerous studies (Paterson, 1989, 1994; Underwood and Paterson, 1993). This biostabilization is due in part to the production of mucilage (colloidal carbohydrates) that forms layers that protect the underlying sediment (Ubertini et al., 2012, 2015), and this is closely related to diatom biomass (**Supplementary Material B**). We found overall a negative relationship between sediment Chl *a* and water column Chl *a*

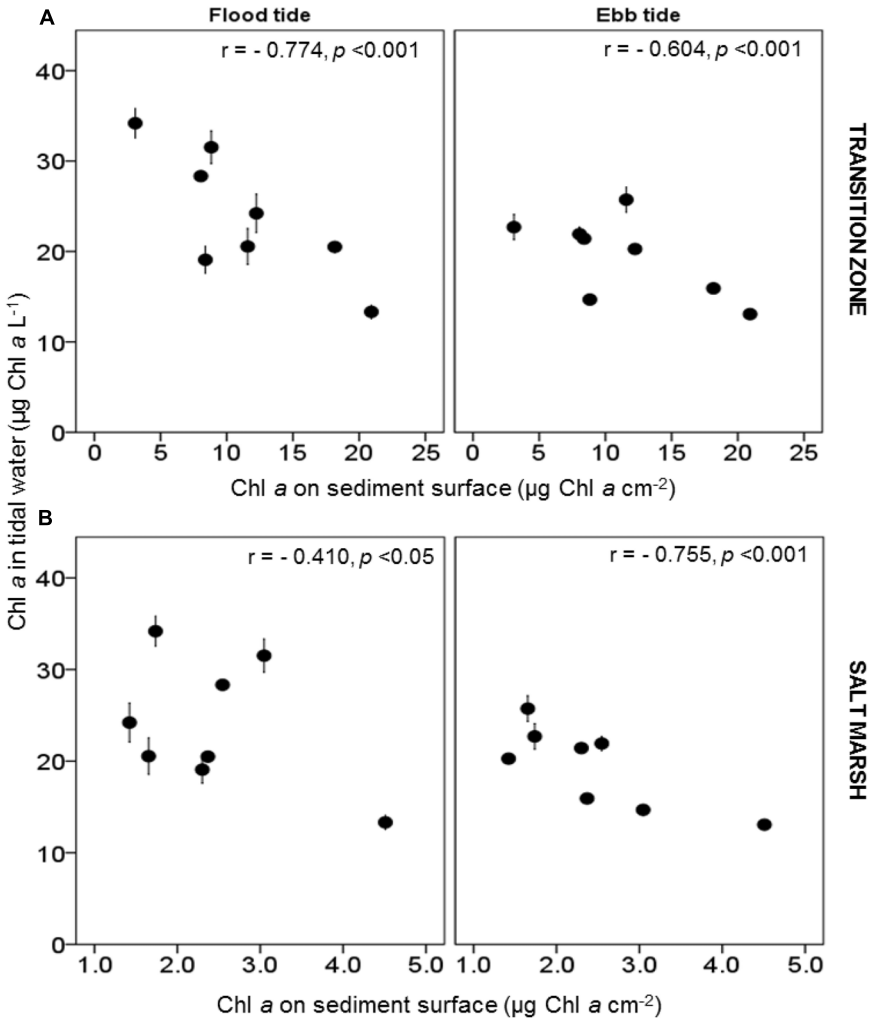

FIGURE 5 | Relationship between Chl. *a* concentration (µg L^{-1}) in flood and ebb-tide water (mean values ± SE, $n = 3$) with the Chl. *a* concentration in the top 2 mm per cm^2 sediment surface of the **(A)** transition zone of the mudflat and; **(B)** salt marsh at Fingringhoe Wick, Colne Estuary, Essex, United Kingdom, in August and September 2015. Pearson's correlation coefficients (r) on daily mean of flood and ebb data.

(**Table 2**), indicating that denser biofilms reduce resuspension. It is also known that under higher light conditions, benthic diatoms will produce excess colloidal carbohydrate, increasing the potential for biostabilization (Perkins et al., 2001). The percentage of cloud cover was also positively correlated with increased suspended Chl. *a* concentrations in flood-tide samples on the salt marsh (**Figures 6Ci,ii**) and lower sediment Chl *a* concentrations. A higher percentage of cloud cover represents lower light conditions that may be partly responsible for lower reduce Chl. *a* concentrations (Serôdio et al., 2006) and reduced biostabilization (Gerbersdorf et al., 2009; Du et al., 2010) by MPB on the transition zone, facilitating resuspension. Other factors cannot be discounted, such as biofilm age, which can affect biostabilization potential, or varying sediment sizes (Ubertini et al., 2015). In our study, the sediments across the whole site are uniformly fine cohesive sediments, so there were no grain size changes. Other unmeasured biotic and abiotic factors may have influenced our results, demonstrating the many potential interactions influencing biofilm sediment processes in the field.

Lower Chl. *a* concentrations on the salt marsh sediment surface were associated with higher suspended sediment and suspended Chl. *a* concentration during immersion in spring tide (**Table 2**). Salt marsh biofilms are also more mixed in their species composition (Zong and Horton, 1998) and in this study were characterized by non-motile diatom taxa such as *Opephora* and *Actinoptychus*. Underwood (1997) reported that only when MPB assemblages consisted of more than 50% epipelic diatom on salt marsh was there a relationship between biomass and colloidal carbohydrate concentrations in the sediment surface. Therefore, the potential for biostabilization by MPB on salt marshes could be related to MPB biomass and species composition. Taxa like *Opephora* are widely distributed in estuaries across a range of sediment types (Sabbe and Vyverman, 1995), as part of the tychoplankton, and they can be resuspended and carried

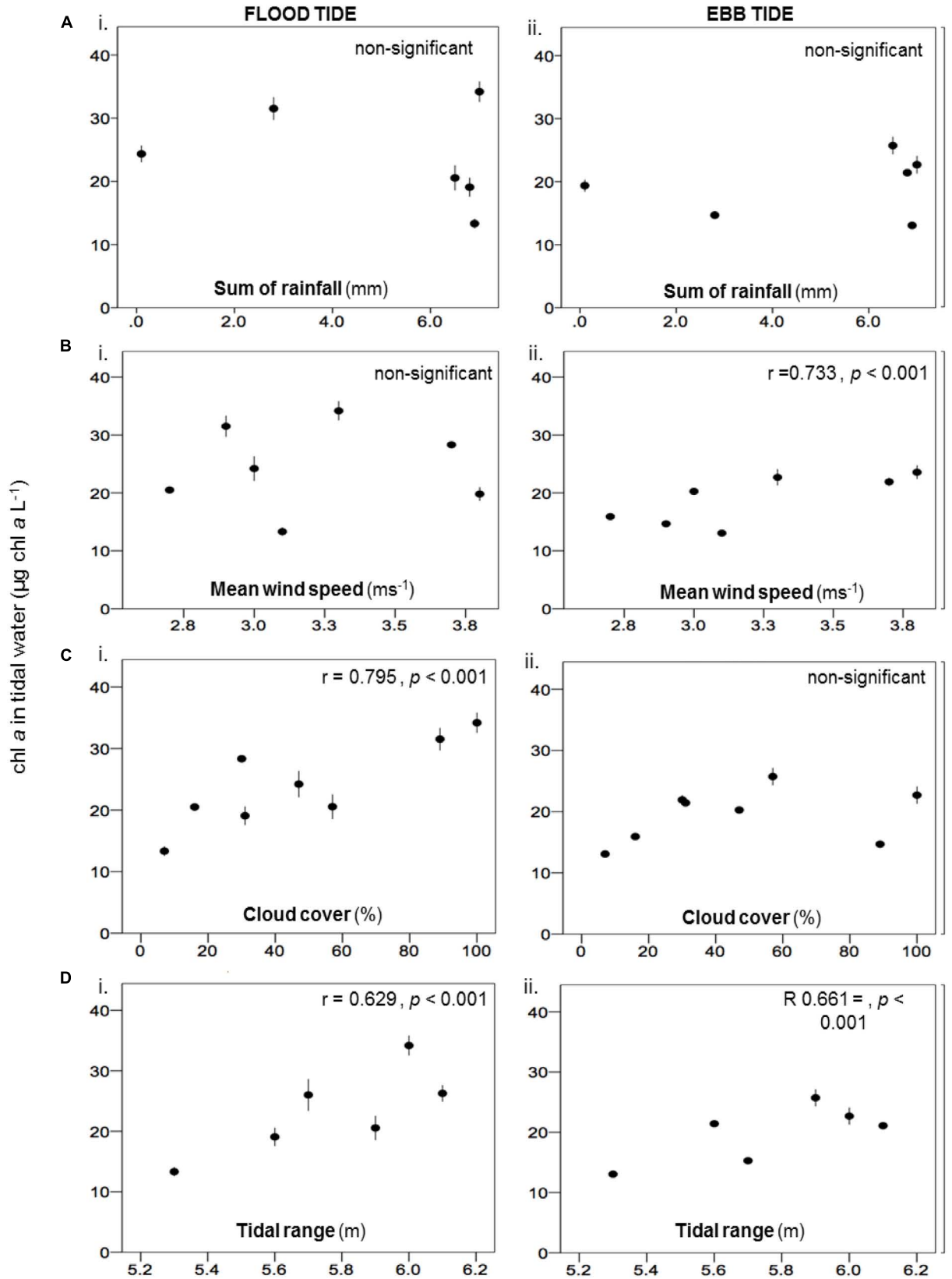

FIGURE 6 | Relationship between water column Chl. *a* concentration (mean ± SE, *n* = 3) in (i) flood and (ii) ebb-tide water over the salt marsh with **(A)** sum of rainfall for 3 days; **(B)** averaged wind speed for 3 days; **(C)** percentage of cloud cover; and **(D)** the tidal range, during spring tides at Fingringhoe Wick, Colne Estuary, Essex, United Kingdom, in August and September 2015.

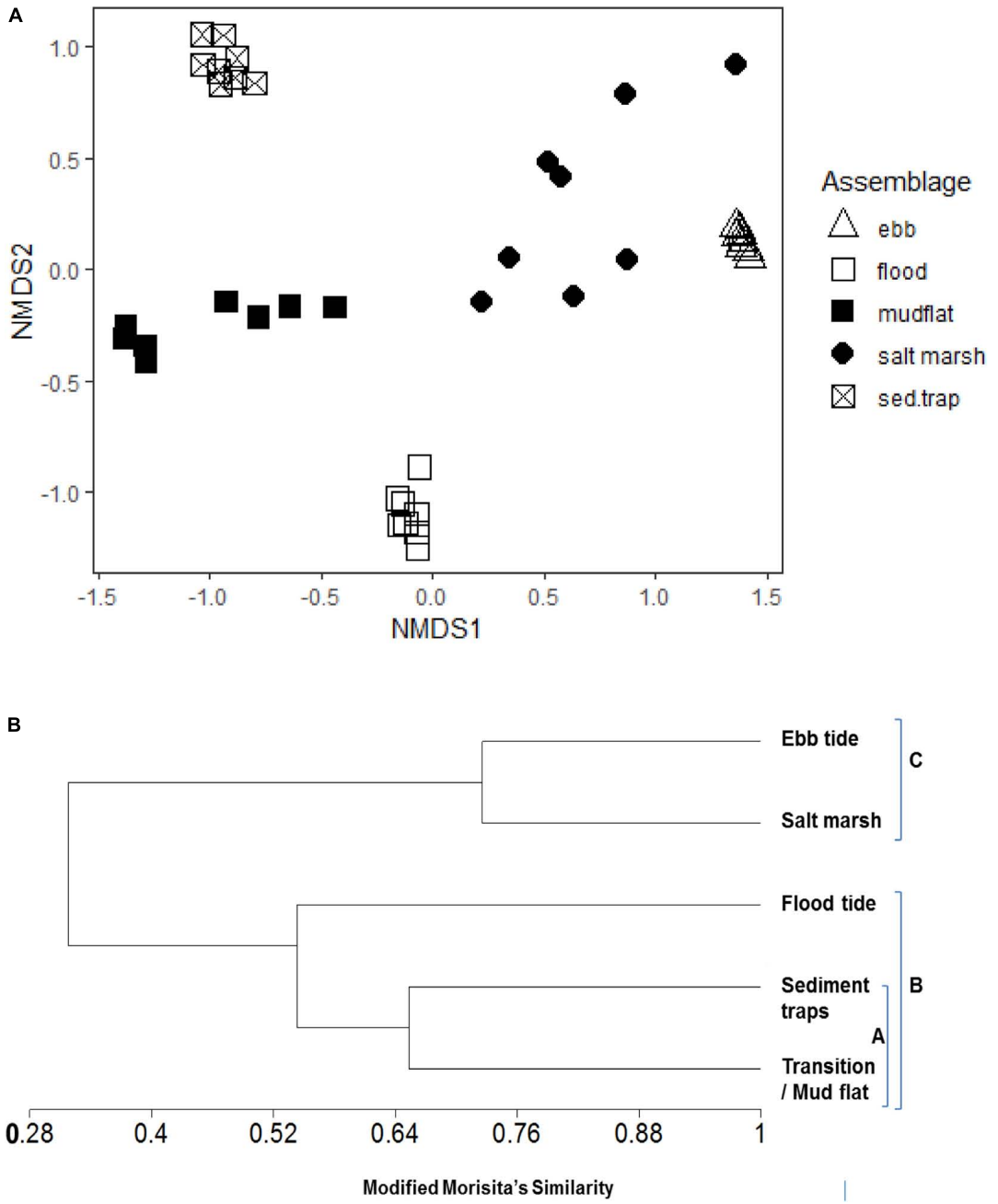

FIGURE 7 | (A) NMDS plot of species composition of diatom assemblages (relative abundance) sampled from ebb-tide water, salt marsh sediment surface, flood-tide water, sediment traps (deployed on transition zone of the mudflat), and transition zone of the mudflat sediment surface samples. **(B)** Dendrogram showing% similarity (Modified Morista's) in MPB diatom species composition for the five assemblage types.

around with sediment (Underwood, 1994). Salt marsh plants slow water flow and enhance sediment deposition, trapping sediments around their roots and also on their leave surfaces (Mason et al., 2003; Reed et al., 2018; Ladd et al., 2019). This "trapping" of sediment may facilitate the deposition of those mudflat taxa also found in the salt marsh assemblage (**Table 3**).

Wind speed and tidal range during spring tides were the two abiotic factors that were important in MPB resuspension on the salt marsh. Loss of Chl. *a* from salt marsh biofilms is promoted by increasing tidal range (Horton et al., 2006). The negative effect of increased tidal range on Chl. *a* concentrations on the sediment surface is potentially associated with water depth and the wind speed (de Jonge and van Beusekom, 1995; van der Wal et al., 2010; Savelli et al., 2019). Wind speed is positively correlated with wave height at the study site (Redzuan, 2017), so that increases in suspended Chl. *a* and sediment concentrations

TABLE 3 | Relative abundance ± SE (%) (n = 8) of MPB diatom species present in mudflat and salt marsh sediments and sampled in sediment traps and in flood and ebb-tide water at Fingringhoe Wick, Colne Estuary, Essex, United Kingdom.

MPB species	On sediment surface		In sediment trap on transition zone	Collected in flood tide on salt marsh	Collected in ebb tide on salt marsh
	Mud flat	Salt marsh			
Gyrosigma balticum #	21.88 ± 1.78	–	–	–	–
Gyrosigma limosum #	4.45 ± 1.08	–	–	–	–
Psammodictyon panduriforme #	5.47 ± 0.48	–	–	–	–
Synedra sp. #	4.17 ± 0.62	–	–	–	–
Synedra sp. 1#	4.35 ± 0.65	–	–	–	–
Tryblionella sp. 2#	4.03 ± 0.35	–	–	–	–
Pleurosigma angulatum	3.32 ± 0.47	1.89 ± 0.49	2.95 ± 0.34	3.66 ± 1.29	–
*Surirella ovata**	0.60 ± 0.24	1.68 ± 0.33	1.44 ± 0.25	2.06 ± 0.19	6.04 ± 0.92
*Diploneis didyma**, #	5.47 ± 1.06	3.34 ± 0.68	5.74 ± 0.68	1.98 ± 0.70	6.12 ± 0.88
Nitzschia dubia	1.05 ± 0.26	0.70 ± 0.33	0.78 ± 0.17	1.92 ± 0.68	–
*Nitzschia sigma**, #	4.02 ± 0.79	2.18 ± 0.45	3.85 ± 0.48	1.83 ± 0.65	7.68 ± 1.19
Navicula gregaria	1.95 ± 0.24	3.52 ± 0.81	1.83 ± 0.33	1.77 ± 0.63	–
*Actinoptychus undulatus**	0.58 ± 0.18	0.32 ± 0.19	0.13 ± 0.04	1.60 ± 0.57	8.21 ± 1.60
Gyrosigma wansbeckii #	4.12 ± 0.69	0.83 ± 0.30	3.99 ± 0.59	1.55 ± 0.55	–
Navicula sp. 1	2.83 ± 0.37	0.88 ± 0.36	0.85 ± 0.01	1.49 ± 0.53	–
Navicula gracilis	0.93 ± 0.23	1.23 ± 0.26	0.96 ± 0.24	1.41 ± 0.50	–
Pleurosigma sp. 1	3.95 ± 0.81	0.50 ± 0.29	1.81 ± 0.31	1.41 ± 0.50	–
Berkeleya scopulorum	2.40 ± 0.65	1.02 ± 0.41	4.76 ± 0.73	1.36 ± 0.48	–
Stauroneis producta	0.80 ± 0.24	0.15 ± 0.09	2.01 ± 0.19	1.36 ± 0.48	–
*Diploneis litoralis**	0.78 ± 0.31	2.20 ± 0.52	2.21 ± 0.36	1.30 ± 0.46	6.64 ± 1.28
Nitzschia scalproides	2.40 ± 0.63	0.45 ± 0.19	2.46 ± 0.30	1.25 ± 0.44	–
Gyrosigma scalproides #	5.28 ± 1.03	3.18 ± 0.61	4.66 ± 0.47	1.20 ± 0.42	–
Achnanthes longipes	1.08 ± 0.31	0.57 ± 0.33	2.06 ± 0.19	0.92 ± 0.32	–
Raphoneis amphiceros	1.45 ± 0.41	1.68 ± 0.45	0.75 ± 0.19	0.64 ± 0.23	–
Amphora sp. 1*	–	1.43 ± 0.58	–	–	8.39 ± 1.00
Nitzschia sp. 1*	–	7.30 ± 0.95	–	–	7.80 ± 0.98
Opephora sp. 2*	–	13.95 ± 1.85	–	–	7.68 ± 1.19
*Surirella fastuosa**	–	3.5 ± 0.82	–	–	7.45 ± 0.72
Neidium sp.*	–	10.68 ± 1.55	–	–	7.42 ± 1.23
*Nitzschia vitrea**	–	5.37 ± 0.59	–	–	7.33 ± 1.09
*Diploneis stroemii**	–	1.99 ± 0.78	–	–	6.96 ± 1.41
Opephora sp. 1*	–	14.3 ± 1.42	–	–	6.71 ± 1.11
*Nitzschia bilobata**	–	6.27 ± 0.89	–	–	5.56 ± 1.15
Overall species recorded	64	34	30	27	14

Hashtag (#) indicates taxa, which represent the top 10 most common species on the mudflat. Asterisk (*) indicates diatom species potentially involved in resuspension on the salt marsh during ebb tide. The relative abundance was calculated based on the pooled overall (surveys 1, 2) data in August and September 2015. Taxa ordered in the table by major habitat groupings and then abundance in flood or ebb-tide water.

on the salt marsh will be a product of water depth and wave energy (Leonardi et al., 2015). The wind speed values during this study were less that those found by de Jonge and van Beusekom (1995) to cause major resuspension, but even lower speeds can resuspend surface cells and sediments loosely associated in a "fluff" layer (Savelli et al., 2019). Such resuspension of biofilm material also weakens the potential for further biostabilization, leading to further resuspension (Ubertini et al., 2015). This chronic resuspension may play an important role in the gradual transfer of material from mudflats to salt marshes (as is clearly indicated by the diatom assemblage composition data), rather than major erosional and resuspension events, which also cause sediments to be lost from salt marshes (Ladd et al., 2019).

As hypothesized, greater tidal range positively increased suspended Chl. *a* concentrations and had a significant negative correlation with Chl. *a* concentrations on sediment surfaces of the salt marsh (**Table 2**). These two correlations further supported the occurrence of opposing influences on the salt marsh at our study site, which potentially caused the lower relative abundance of dominant salt marsh MPB species during spring tides (Redzuan, 2017). Tidal cover is reported to replenish resources such as nutrients on the salt marshes sediment (Blanchard et al., 2001), which may support MPB growth, but is also reported as one of major disturbance to MPB biofilms of the zone (Horton et al., 2006; Le Rouzic, 2012). It is clear that a number of characteristic salt marsh diatom taxa were resuspended and

carried off the marsh in the ebb tides, indicating that some resuspension of salt marsh sediments did occur, even under the relatively benign summer weather conditions during this study.

Earlier work conducted in 2013 (Redzuan, 2017) highlighted that the diatom species composition in MPB assemblages on salt marsh, which mostly comprised small, "edaphic," and epiphytic species during neap tides (Zong and Horton, 1998), was found to shift its assemblage composition toward diatom species common on the transition zone and the mudflat during spring tides. Characteristic mudflat taxa groups such as *Pleurosigma*, *Gyrosigma*, large *Nitzschia* spp., *Diploneis*, *Navicula gregaria*, and dominant on European mudflats (Underwood et al., 1998; Ribeiro et al., 2013) were found both in overlying water on the salt marsh and in marsh sediments. Suspended diatom assemblages in the flood-tide samples (sampled on salt marsh) were most similar to the transition zone MPB diatom assemblages (**Figure 7**), indicating that MPB coupling between the transition zone and the salt marsh occurs during flood tides. Flood-tide tidal currents have been reported by Koh et al. (2006) to cause simultaneous MPB resuspension on the mudflat, appearing to carry MPB biomass from the transition zone onto the salt marsh during the spring tide.

Chl. *a* concentrations on salt marsh sediment surfaces were negatively correlated with the suspended Chl. *a* in ebb and flood tides (**Figure 6B**). Species composition data showed that five out of the six dominant MPB species on the salt marsh sediment surface in neap tide were recorded in the ebb-tide tidal water samples (**Table 3**). The observation further supported the hypothesis that there was resuspension and possibly wash away of some epipelic, edaphic, and epiphytic salt marsh MPB species during ebb tides. Such taxa (e.g., *Opephora*) do not form EPS-rich biofilms that provide protection from resuspension or were more oligohaline to freshwater taxa, e.g., *Neidium* (Licursi et al., 2010). Disturbance during submersion in Spring tides has been shown to decrease in microphytobenthic biomass on the salt marshes (Le Rouzic, 2012).

CONCLUSION

This study confirmed that transfer of MPB biomass and sediments within a single mudflat and salt marsh tidal flat system can occur over individual tides in the absence of acute erosion events. Resuspension of MPB in both flood and ebb tidal waters strongly connected to spring tide tidal range. Biostabilization was implicated in controlling the amount of MPB resuspension on the mudflat transition zone and was closely linked to the availability of sunlight (based on the cloud cover percentage). Both flood and ebb tides resulted in exchanges of MPB between the zones. Weather-related abiotic factors, cloud cover and wind, were responsible for controlling the MPB exchange. Transfer of mudflat material was confirmed by the presence of particular diatom taxa and high levels of assemblage similarity, both on the flood tide (from the mudflat) and on the ebb tide (from the salt marsh). This present study was only carried out for 8 days in two different sampling surveys and covered non-storm event periods. During this time, a net movement of sediment from the mudflat onto the salt marsh was evident, which would support accretion of the marsh surface. Diatom assemblage analysis can act as a biomarker for that process. Further studies are needed to understand the exchange process of MPB over annual cycles that are influential in maintaining MPB biomass coupling in the estuarine ecosystem.

DATA AVAILABILITY STATEMENT

The datasets generated for this study are available on request to the corresponding author.

AUTHOR CONTRIBUTIONS

NR and GU designed the study and wrote the manuscript. NR conducted the fieldwork, laboratory, and data analyses. All authors contributed to the article and approved the submitted version.

FUNDING

NR was funded by the Malaysia Ministry of Higher Education and Universiti Malaysia Terengganu. This work was partly supported by the United Kingdom Natural Environment Research Council, Coastal Biodiversity and Ecosystem Services program (Ref NE/J01561X/1), to GU.

ACKNOWLEDGMENTS

We acknowledge excellent fieldwork and technical support provided by Mr. J. Green, Mr. R. Smart, and Mrs. T. Cresswell-Maynard.

SUPPLEMENTARY MATERIAL

The Supplementary Material for this article can be found online at: https://www.frontiersin.org/articles/10.3389/fmars.2020.00496/full#supplementary-material

REFERENCES

Banerjee, K., Sappal, S., Ramachandran, P., and Ramachandran, R. (2017). Salt marsh: ecologically important, yet least studied blue carbon ecosystems in India. *J. Clim. Chang.* 3, 59–72. doi: 10.3233/JCC-170014

Beeftink, W. G., and Rozema, J. (1988). "The nature and functioning of salt marshes," in *Pollution of the North Sea: An Assessment*, eds W. Salomons, B. L. Bayne, E. K. Duursma, and U. Förstner (Berlin: Springer), 59–87. doi: 10.1007/978-3-642-73709-1_4

Bellinger, B. J., Underwood, G. J. C., Ziegler, S. E., and Gretz, M. R. (2009). Significance of diatom-derived polymers in carbon flow dynamics within

estuarine biofilms determined through isotopic enrichment. *Aquat. Microb. Ecol.* 55, 169–187. doi: 10.3354/ame01287

Blanchard, F., Guarini, J., Orvain, F., and Sauriau, P. (2001). Dynamic behaviour of benthic microalgal biomass in intertidal mudflats. *Mar. Biol. Assoc. U. K.* 82, 85–100. doi: 10.1016/s0022-0981(01)00312-4

Chesman, B. S., Burt, G. R., and Langston, W. J. (2006). Characterisation of european marine sites: essex estuaries, European marine site. *J. Mar. Biol. Assoc. Spec. Publ.* 17, 1–28.

Cibic, T., Blasutto, O., Falconi, C., and Umani, S. F. (2007). Microphytobenthic biomass, species composition and nutrient availability in sublittoral sediments of the gulf of trieste (Northern Adriatic Sea). *Estuar. Coast. Shelf Sci.* 75, 50–62. doi: 10.1016/j.ecss.2007.01.020

Coles, S. M. (1979). "Benthic microalgal populations on intertidal sediments and their role as precursors to salt marsh development," in *Ecological Processes In Coastal Environments: The First European Symposium Of The British Ecological Society*, eds R. L. Jefferies and A. J. Davy (Oxford: Blackwell Scientific), 25–42.

de Jonge, V. N., and van Beusekom, J. E. E. (1995). Wind- and tide-induced resuspension of sediment and microphytobenthos from tidal flats in the Ems estuary. *Limnol. Oceanogr.* 40, 776–778. doi: 10.4319/lo.1995.40.4.0776

de Leeuw, J., Apon, L. P., Herman, P. M. J., de Munck, W., and Beeftink, W. G. (1994). The response of salt marsh vegetation to tidal reduction caused by the oosterschelde storm-surge barrier. *Hydrobiologia* 282, 335–353. doi: 10.1007/BF00024640

Du, G. Y., Oak, J.-H., Li, H., and Chung, I.-K. (2010). Effect of light and sediment grain size on the vertical migration of benthic diatoms. *Algae* 25, 133–140. doi: 10.4490/algae.2010.25.3.133

Easley, J. T., Hymel, S. N., and Plante, C. J. (2005). Temporal patterns of benthic microalgal migration on a semi-protected beach. *Estuar. Coast. Shelf Sci.* 64, 486–496. doi: 10.1016/j.ecss.2005.03.013

Fidalgo, E., Costa, P., Brotas, V., Cancela, and Da Fonseca, L. (2002). Physical characterisation and microphytobenthos biomass of estuarine and lagoon environments of the Southwest coast of Portugal. *Limnetica* 21, 69–80.

French, A. J. R., Spencer, T., Murray, A. L., Arnold, N. S., Small, T., and Wetlands, T. (2009). Coastal geostatistical analysis of sediment deposition in two small tidal Wetlands, Norfolk, UK. *J. Coast. Res.* 11, 308–321.

French, R., and Spencer, T. (1993). Dynamics of sedimentation in a tide-dominated backbarrier salt marsh, Norfolk, UK. *Mar. Geol.* 110, 315–331. doi: 10.1016/0025-3227(93)90091-9

Gerbersdorf, S. U., Westrich, B., and Paterson, D. M. (2009). Microbial extracellular polymeric substances (EPS) in fresh water sediments. *Microb. Ecol.* 58, 334–349. doi: 10.1007/s00248-009-9498-8

Green, M., and Coco, G. (2014). Review of wave-driven sediment resuspension and transport in estuaries. *Rev. Geophys.* 52:437. doi: 10.1002/2013RG000437

Green, M. O. (2011). Very small waves and associated sediment resuspension on an estuarine intertidal flat. *Estuar. Coast. Shelf Sci.* 93, 449–459. doi: 10.1016/j.ecss.2011.05.021

Grothues, T. M., and Able, K. W. (2003). Response of juvenile fish assemblages in tidal salt marsh creeks treated for phragmites removal. *Estuaries* 26, 563–573. doi: 10.1007/BF02823731

Hanlon, A. R. M., Bellinger, B., Haynes, K., Xiao, G., Hofmann, T. A., Gretz, M. R., et al. (2006). Dynamics of extracellular polymeric substance (EPS) production and loss in an estuarine, diatom-dominated, microalgal biofilm over a tidal emersion-immersion period. *Limnol. Oceanogr.* 51, 79–93. doi: 10.4319/lo.2006.51.1.0079

Horton, B. P., Corbett, R., Culver, S. J., Edwards, R. J., and Hillier, C. (2006). Modern saltmarsh diatom distributions of the Outer Banks, North Carolina, and the development of a transfer function for high resolution reconstructions of sea level. *Estuar. Coast. Shelf Sci.* 69, 381–394. doi: 10.1016/j.ecss.2006.05.007

Horton, B. P., and Sawai, Y. (2010). Diatoms as indicators of former sea levels, earthquakes, tsunamis, and hurricanes. *Appl. Environ. Earth Sci.* 8, 357–372. doi: 10.1017/CBO9780511763175.020

Jönnson, B., Sundbäck, K., and Nilsson, C. (1994). An upright life-form of an epipelic motile diatoms: on the behaviour of *Gyrosigma balticum*. *Eur. J. Phycol.* 29, 11–15. doi: 10.1080/09670269400650421

Koh, C. H., Jong, S. K., Araki, H., Yamanishi, H., Mogi, H., and Koga, K. (2006). Tidal resuspension of microphytobenthic chlorophyll a in a nanaura mudflat, Saga, Ariake Sea, Japan: flood-ebb and spring-neap variations. *Mar. Ecol. Prog. Ser.* 312, 85–100. doi: 10.3354/meps312085

Koh, C. H., Khim, J. S., Araki, H., Yamanishi, H., and Koga, K. (2007). Within-day and seasonal patterns of microphytobenthos biomass determined by co-measurement of sediment and water column Chlorophylls in the intertidal mudflat of Nanaura, Saga, Ariake Sea, Japan. *Estuar. Coast. Shelf Sci.* 72, 42–52. doi: 10.1016/j.ecss.2006.10.005

Kovach, W. L. (1999). *A Multivariate Statistical Package*. Wales: Kovach Computing Service.

Ladd, C. J. T., Duggan-Edwards, M. F., Bouma, T. J., and Pagès, J. F. (2019). Sediment supply explains long-term and large-scale patterns in salt marsh lateral expansion and erosion. *Geophys. Res. Lett.* 46:315. doi: 10.1029/2019GL083315

Le Rouzic, B. (2012). Changes in photosynthetic yield (Fv/Fm) responses of salt-marsh microalgal communities along an osmotic gradient (Mont-Saint-Michel Bay, France). *Estuar. Coast. Shelf Sci.* 115, 326–333. doi: 10.1016/j.ecss.2012.09.012

Leonardi, N., Ganju, N. K., and Fagherazzi, S. (2015). A linear relationship between wave power and erosion determines salt-marsh resilience to violent storms and hurricanes. *Proc. Natl. Acad. Sci. U.S.A.* 113, 64–68. doi: 10.1073/pnas.1510095112

Licursi, M., Gómez, N., and Donadelli, J. (2010). Ecological optima and tolerances of coastal benthic diatoms in the freshwater-mixohaline zone of the Río de la Plata estuary. *Mar. Ecol. Prog. Ser.* 418, 105–117. doi: 10.3354/meps08865

Lorenzen, C. J. (1967). Determination of chlorophyll and pheo-pigments: Spectrophotometric equations. *Limnol. Oceanogr.* 12, 343–346. doi: 10.4319/lo.1967.12.2.0343

Macreadie, P. I., Hughes, A. R., and Kimbro, D. L. (2013). Loss of "Blue Carbon" from coastal salt marshes following habitat disturbance. *PLoS One* 8:e069244. doi: 10.1371/journal.pone.0069244

Mason, C. F., Underwood, G. J. C., Baker, N. R., Davey, P. A., Davidson, I., Hanlon, A., et al. (2003). The role of herbicides in the erosion of salt marshes in eastern England. *Environ. Pollut.* 122, 41–49. doi: 10.1016/S0269-7491(02)00284-1

McKew, B. A., Taylor, J. D., McGenity, T. J., and Underwood, G. J. C. (2011). Resistance and resilience of benthic biofilm communities from a temperate saltmarsh to desiccation and rewetting. *ISME J.* 5, 30–41. doi: 10.1038/ismej.2010.91

Mueller, P., Do, H. T., Jensen, K., and Nolte, S. (2019). Origin of organic carbon in the topsoil of Wadden Sea salt marshes. *Mar. Ecol. Prog. Ser.* 624, 39–50. doi: 10.3354/meps13009

Ogilvie, B., Nedwell, D. B., Harrison, R. M., Robinson, A., and Sage, A. (1997). High nitrate, muddy estuaries as nitrogen sinks: the nitrogen budget of the River Colne estuary (United Kingdom). *Mar. Ecol. Prog. Ser.* 150, 217–228. doi: 10.3354/meps150217

Oksanen, J., Blanchet, G., Friendly, M., Kindt, R., Legendre, P., McGlinn, D., et al. (2019). *Vegan: Community Ecology Package. R Package Version 2.5-6*.

Paterson, D. M. (1994). "Microbiological mediation of sediment structure and behaviour," in *Microbial Mats NATO ASI Series (Series G: Ecological Sciences)*, Vol. 35, eds L. J. Stal and P. Caumette (Berlin: Springer), 97–109.

Paterson, D. M. (1989). Short-term changes in the erodibility of intertidal cohesive sediments related to the migratory behavior of epipelic diatoms. *Limnol. Oceanogr.* 34, 223–234. doi: 10.4319/lo.1989.34.1.0223

Perkins, R. G., Underwood, G. J. C., Brotas, V., Snow, G. C., Jesus, B., and Ribeiro, L. (2001). Responses of microphytobenthos to light: primary production and carbohydrate allocation over an emersion period. *Mar. Ecol. Prog. Ser.* 223, 101–112. doi: 10.3354/meps223101

Peterson, H., and Peterson, N. M. (1979). *The Ecology of Intertidal Flats of North Carolina: A Community Profile*. Slidell, LA: United States Fish and Wildlife Service, Office of Biological Services, 73.

R Core Team (2020). *R: A Language And Environment For Statistical Computing*. Vienna: R Foundation for Statistical Computing.

Redzuan, N. S. (2017). *Microphytobenthos (MPB) Biomass Variability And Sediment-Water Column Exchanges On An Intertidal Flat: Influence Of Weather-Related Abiotic Factors Across Neap-Spring-Neap Tidal Cycle*. Ph. D. thesis, University of Essex, Colchester.

Reed, D., van Wesenbeeck, B., Herman, P. M. J., and Meselhe, E. (2018). Tidal flat-wetland systems as flood defenses: understanding biogeomorphic controls. *Estuar. Coast. Shelf Sci.* 213, 269–282. doi: 10.1016/j.ecss.2018.08.017

Ribeiro, L., Brotas, V., Rincé, Y., and Jesus, B. (2013). Structure and diversity of intertidal benthic diatom assemblages in contrasting shores: a case

study from the Tagus estuary. *J. Phycol.* 49, 258–270. doi: 10.1111/jpy.12031

Riggs, S. R. (2002). "Life at the edge of North Carolina's coastal system: the geologic controls," in *Life at the Edge of the Sea: Essays on North Carolina's Coast and Coastal Culture*, eds C. Beal and C. Prioli (Wilmington, NC: Coastal Carolina Press), 63–95.

Sabbe, K., and Vyverman, W. (1995). Taxonomy, morphology and ecology of some widespread representatives of the diatom genus opephora. *Eur. J. Phycol.* 30, 235–249. doi: 10.1080/09670269500651011

Savelli, R., Bertin, X., Orvain, F., Gernez, P., Dale, A., Coulombier, T., et al. (2019). Impact of chronic and massive resuspension mechanisms on the microphytobenthos dynamics in a temperate intertidal mudflat. *JGR Biogeosci*. 124, 3752–3777. doi: 10.1029/2019JG005369

Scholz, B., and Liebezeit, G. (2012). Microphytobenthic dynamics in a Wadden Sea intertidal flat – Part II: seasonal and spatial variability of non-diatom community components in relation to abiotic parameters. *Eur. J. Phycol.* 47, 120–137. doi: 10.1080/09670262.2012.665251

Seitzinger, S. P. (1973). Denitrification in freshwater and coastal marine ecosystems: ecological and geochemical significance. *Limnol. Oceanogr.* 33, 702–724. doi: 10.4319/lo.1988.33.4part2.0702

Serôdio, J., Coelho, H., Vieira, S., and Cruz, S. (2006). Microphytobenthos vertical migratory photoresponse as characterised by light-response curves of surface biomass. *Estuar. Coast. Shelf Sci.* 68, 547–556. doi: 10.1016/j.ecss.2006.03.005

Shepard, C. C., Crain, C. M., and Beck, M. W. (2011). The protective role of coastal marshes: a systematic review and meta-analysis. *PLoS One* 6:e027374. doi: 10.1371/journal.pone.0027374

Smith, D. J., and Underwood, G. J. C. (1998). Exopolymer production by intertidal epipelic diatoms. *Limnol. Oceanogr.* 43, 1578–1591. doi: 10.4319/lo.1998.43.7.1578

Spears, B. M., Saunders, J. E., Davidson, I., and Paterson, D. M. (2008). Microalgal sediment biostabilisation along a salinity gradient in the Eden Estuary, Scotland: unravelling a paradox. *Mar. Freshw. Res.* 59, 313–321. doi: 10.1071/MF07164

Spilmont, N., Seuront, L., Meziane, T., and Welsh, D. T. (2011). There's more to the picture than meets the eye: sampling microphytobenthos in a heterogeneous environment. *Estuar. Coast. Shelf Sci.* 95, 470–476. doi: 10.1016/j.ecss.2011.10.021

Taylor, J. D., McKew, B. A., Kuhl, A., McGenity, T. J., and Underwood, G. J. C. (2013). Microphytobenthic extracellular polymeric substances (EPS) in intertidal sediments fuel both generalist and specialist EPS-degrading bacteria. *Limnol. Oceanogr.* 58, 1463–1480. doi: 10.4319/lo.2013.58.4.1463

Ubertini, M., Lefebvre, S., Gangnery, A., Grangeré, K., Le Gendre, R., and Orvain, F. (2012). Spatial variability of benthic-pelagic coupling in an estuary ecosystem: consequences for microphytobenthos resuspension phenomenon. *PLoS One* 7:e044155. doi: 10.1371/journal.pone.0044155

Ubertini, M., Lefebvre, S., Rakotomalala, C., and Orvain, F. (2015). Impact of sediment grain-size and biofilm age on microphytobenthos resuspension. *J. Exp. Mar. Biol. Ecol.* 467, 52–64. doi: 10.1016/j.jembe.2015.02.007

Underwood, G. J. C. (1994). Seasonal and spatial variation n epipelic diatom assemblages in the Severn estuary. *Diatom Res.* 9, 451–472. doi: 10.1080/0269249x.1994.9705319

Underwood, G. J. C. (1997). Microalgal colonization in a saltmarsh restoration scheme. *Estuar. Coast. Shelf Sci.* 44, 471–481. doi: 10.1006/ecss.1996.0138

Underwood, G. J. C., Hanlon, A. R. M., Oxborough, K., and Baker, N. R. (2005). Patterns in microphytobenthic primary productivity: species-specific variation in migratory rhythms and photosynthetic efficiency in mixed-species biofilms. *Am. Soc. Limnol. Oceanogr.* 50, 755–767. doi: 10.4319/lo.2005.50.3.0755

Underwood, G. J. C., and Paterson, D. M. (1993). Recovery of intertidal benthic diatoms after biocide treatment and associated sediment dynamics. *J. Marine Biol. Assoc. UK.* 73, 25–45. doi: 10.1017/S002531540003263X

Underwood, G. J. C., Phillips, J., and Saunders, K. (1998). Distribution of estuarine benthic diatom species along salinity and nutrient gradients. *Eur. J. Phycol.* 33, 173–183. doi: 10.1080/09670269810001736673

van der Wal, D., Wielemaker-van den Dool, A., and Herman, P. M. J. (2010). Spatial synchrony in intertidal benthic algal biomass in temperate coastal and estuarine ecosystems. *Ecosystems* 13, 338–351. doi: 10.1007/s10021-010-9322-9

Xin, P., Li, L., and Barry, D. A. (2013). Tidal influence on soil conditions in an intertidal creek-marsh system. *Water Resour. Res.* 49, 137–150. doi: 10.1029/2012WR012290

Yang, S. L., Shi, B. W., Bouma, T. J., Ysebaert, T., and Luo, X. X. (2012). Wave attenuation at a salt marsh margin: a case study of an exposed coast on the yangtze estuary. *Estuar. Coast.* 35, 169–182. doi: 10.1007/s12237-011-9424-4

Zong, Y., and Horton, B. P. (1998). Diatom zones across intertidal flats and coastal saltmarshes in Britain. *Diatom Res.* 13, 375–394. doi: 10.1080/0269249X.1998.9705456

Conflict of Interest: The authors declare that the research was conducted in the absence of any commercial or financial relationships that could be construed as a potential conflict of interest.

frontiers in Marine Science

ORIGINAL RESEARCH
published: 26 June 2020
doi: 10.3389/fmars.2020.00419

The Effect of Shading and Nutrient Addition on the Microphytobenthos, Macrofauna, and Biogeochemical Properties of Intertidal Flat Sediments

Trevor J. Tolhurst[1,2]*, *M. G. Chapman*[1] *and R. J. Murphy*[1]

[1] *Centre for Research on Ecological Impacts of Coastal Cities, Marine Ecology Laboratories A11, School of Life and Environmental Sciences, The University of Sydney, Sydney, NSW, Australia,* [2] *Centre for Ocean and Atmospheric Sciences, School of Environmental Sciences, University of East Anglia, Norwich, United Kingdom*

OPEN ACCESS

Edited by:
David M. Paterson, University of St. Andrews, United Kingdom

Reviewed by:
Conrad Pilditch, The University of Waikato, New Zealand
Paulo Cartaxana, University of Aveiro, Portugal
Rachel Joy Harris, Loxahatchee River District, Jupiter, FL, United States

***Correspondence:**
Trevor J. Tolhurst
t.tolhurst@uea.ac.uk

Specialty section:
This article was submitted to Marine Ecosystem Ecology, a section of the journal Frontiers in Marine Science

Received: *17 October 2019*
Accepted: *13 May 2020*
Published: *26 June 2020*

Citation:
Tolhurst TJ, Chapman MG and Murphy RJ (2020) The Effect of Shading and Nutrient Addition on the Microphytobenthos, Macrofauna, and Biogeochemical Properties of Intertidal Flat Sediments. Front. Mar. Sci. 7:419. doi: 10.3389/fmars.2020.00419

Proliferation of urban structures and mangrove forests in estuaries are altering the shading of intertidal sediments. Urbanization also tends to increase nutrient loads in estuaries, which can have numerous direct and indirect effects on estuarine flora and fauna. Mangrove canopy shades the sediment and provides nutrients to the ecosystem via leaf litter. Microphytobenthos, macrofauna, sediment erodibility, and various biogeochemical properties of sediments have been shown to differ significantly between unshaded intertidal sediment and nearby sediment under a mangrove canopy. This study tested the effects of experimental manipulation of shading and addition of nutrients on the microphytobenthos, macrofauna, sediment erodibility, and selected biogeochemical properties of exposed intertidal flat next to the seaward edge of a mangrove forest. In the first of two experiments, plots were shaded with roofs to give lightly shaded plots and heavily shaded plots, for comparison with unshaded control plots; nutrients were added in an orthogonal design. Sediment and benthos were sampled after 2 weeks. Nutrients were omitted in the second experiment, with plots sampled after 2 weeks or approximately 3 months. The only effect of nutrients was a small negative effect on chlorophyll *a* and colloidal carbohydrate. Light shading (clear roofs) generally increased measures of microphytobenthos biomass (e.g., F_o and chlorophyll *a*) and biogeochemical properties associated with microphytobenthos such as colloidal carbohydrate. Heavy shading (black roofs) generally decreased measures of microphytobenthos biomass and microphytobenthos-associated biogeochemical properties. Effects on the fauna were much smaller and inconsistent with previous studies, after 3 months, assemblages were different under heavy shading compared to light shading and unshaded control plots, with differences primarily driven by changes in the oligochaetes. Natural or anthropogenic changes in shading at larger spatial scales are likely therefore to directly and indirectly change microphytobenthos,

sediment properties, macrofauna and hence ecosystem functions; but any flow-on effects to the fauna are difficult to predict without further experiments to understand the indirect and direct responses of fauna to changing microphytobenthos and properties of intertidal sediment.

Keywords: microphytobenthos, shade, macrofauna, biogeochemical, mangrove forest, intertidal flat, urbanization, ecosystem function

INTRODUCTION

Many important changes occur in estuaries subjected to increased urban development, including eutrophication, pollution, disturbances associated with boating, increased sedimentation and many others (Chapman et al., 2008; Whitfield and Elliot, 2011). There has been a proliferation of artificial structures into intertidal and shallow subtidal areas (Glasby and Connell, 1999; Chapman and Underwood, 2011; Firth et al., 2016; Bishop et al., 2017), which replace natural habitats; often providing habitat of very different structure and altering physical conditions, such as by shading of nearby sediment. Most research has focused on the organisms inhabiting the structures themselves (e.g., Chapman, 2003), or on fish in adjacent waters (Able et al., 1998; Clynick et al., 2008; Munsch et al., 2014), rather than the surrounding sediment.

As well as directly altering the environment, anthropogenic impacts can cause significant shifts in ecological structure; for example, there has been widespread net loss of mangrove forest area worldwide (Morrisey et al., 2010), but there are locations with large terrigenous sediment supply and accreting intertidal flats, where mangrove forests are spreading into adjacent habitat (Saintilan and Williams, 1999; Morrisey et al., 2010). This has been attributed to anthropogenic impacts such as: climate change, increased inputs of nutrients to estuaries and catchment deforestation causing increased erosion of terrestrial sediment and hence increased estuarine sedimentation (Morrisey et al., 2010).

Urban development can directly and/or indirectly alter water turbidity, which alters the amount of light reaching the underlying sediment bed (i.e., it causes shading) and alters nutrient load, which in turn can alter plankton, phytobenthos such as seagrass (Hauxwell et al., 2003) and microphytobenthos (Stutes et al., 2006). Algal blooms, either on the sediment-surface or in the overlying water column, have been associated with eutrophication, which can cause major changes to benthic assemblages (Raffaelli, 1999). The relative importance of direct changes to sediment due to shading caused by these blooms, or indirect changes due to anoxia or other processes associated with the algae is not always clear. Shading of habitat can be very important in determining distributions and abundances of organisms, which may be affected either directly by changes in environmental stress, or indirectly via changes to biotic relationships (e.g., Wiens, 1976; Defew et al., 2004; Kon et al., 2011). On rocky shores and seawalls, shading can increase or decrease amounts of algae and change sessile assemblages (Williams, 1994; Blockley, 2007) or cause mobile animals to aggregate (Takada, 1999). Van Colen et al. (2015) demonstrated that in non-shaded controls and bare sediment treatments, microphytobenthos biomass (chlorophyll *a*) was positively related to the density of *Macomona liliana*, while no significant linear relationship was found between both variables in shaded sediments; shading-induced changes in bioturbation interference also determined meiofauna densities. Thrush et al. (2014) demonstrated that shade on sandflats altered the interaction network between sediment biogeochemical fluxes, productivity, and macrofauna. However, Pratt et al. (2015) showed there were no significant differences in a multivariate metric of ecosystem function nor the constituent ecosystem function variables between shaded and non-shaded plots on a sandflat. Lundkvist et al. (2007) demonstrated that light is an important forcing factor in the biostabilization of cohesive sediments. Sanger et al. (2004) showed reduced density of saltmarsh vegetation under docks in South Carolina, although it is not known whether this was a direct effect of shade on the plants themselves, or an indirect effect via changes to sediment. Saunders and Connell (2001) showed increased numbers of spirorbid polychaetes on mangrove pneumatophores that were shaded by surrounding seagrass. Subsequent experiments, using artificial substrata, indicated that this was a direct effect of shading on recruitment.

Relatively few experiments have looked at effects of shade on microphytobenthos in unvegetated soft sediments, and they have yielded inconsistent results. A series of experiments in Manukau Harbour investigated the effects of experimental manipulation of shade and grazing pressure on unvegetated sandflat sediments (e.g., Thrush et al., 2014; Harris et al., 2015; Van Colen et al., 2015). They demonstrated that reductions in incident sunlight changed the interaction network between sediment biogeochemical fluxes, productivity, and macrofauna, but did not find an increase in erosion threshold with increasing microphytobenthos biomass. Defew et al. (2002) showed a change in the size of mudflat diatoms in low light conditions in the laboratory in response to shading, but there were no changes in species richness and little effect on biomass, carbohydrate production and photophysiology. When both temperature and shading were manipulated, mudflat microphytobenthic assemblages illustrated a variety of responses to the different conditions, including changes in biomass, pigment ratios, species richness and diversity (Defew et al., 2004). Stutes et al. (2006) showed an effect of shading on micro-algae in the field, but only when there was a large amount of natural light. Given microphytobenthos are important drivers of ecosystem functioning, including food web dynamics (Byers and Grabowski, 2014), sediment erodibility (Black et al., 2002; Tolhurst et al., 2009; Grabowski et al., 2011) and biogeochemical properties of sediments

(e.g., Tolhurst et al., 2008; Murphy and Tolhurst, 2009), changes in microphytobenthic communities caused by changes in shading and/or nutrients could cause numerous knock-on effects on the sediments they inhabit and other organisms.

The canopy of mangrove trees can cast deep shade over the substratum. Previous work has shown that intertidal benthic assemblages differ between muddy substratum that is continuously shaded, periodically shaded and nearby unshaded substratum (Chapman and Tolhurst, 2004, 2007; Tolhurst and Chapman, 2007; Kon et al., 2010, 2011; Tolhurst et al., 2010). Leaf litter is the largest constituent of mangrove organic matter contributing to food chains (Lee, 2008), the decomposition of which releases nutrients to the ecosystem (Kamruzzaman et al., 2019), although this release is slower in temperate climates compared to tropical ones (Gladstone-Gallagher et al., 2014a). The shaded habitat under the canopy of the mangroves typically has greater amounts of leaf litter, which may affect macrofauna. For example, Lee (1999) demonstrated increased colonization of defaunated intertidal sand in buckets by the addition of mangrove detritus, whilst Gladstone-Gallagher et al. (2014b) found small changes in the relative abundances of a few dominant taxa in response to the addition of mangrove detritus to intertidal flats.

Thus, the expansion of mangrove forests and proliferation of man-made structures into more open habitats (e.g., saltmarsh, mudflat, and sandflat), can result in significant changes to environmental conditions, such as the amount of shading and nutrients, with knock-on effects for ecosystem structure and function. Yet, it remains unclear how much the previously found differences in benthos and properties of the sediment in differently shaded microhabitats are caused by variation in shading, and how much by variation in other components such as leaf litter and nutrients.

Although quantified patterns of differences are essential to underpin causal models, observation alone is not sufficient to distinguish among the many potential models that can explain any pattern (Underwood et al., 2000). Manipulative field experiments allow direct tests of different competing models that can explain a set of observations. The effects of shade may be complex in muddy sediments because shade may directly affect benthos and not sediment, affect sediment and not benthos, or affect both, resulting in highly complex interactions.

This study examined the effects of artificially shading unvegetated intertidal soft sediment adjacent to mangrove forests in Sydney Harbour estuary to mimic the effects of shading by mangrove canopy or man-made structures. The previous differences documented between biota and sedimentary features between the substratum under mangrove canopy and adjacent unshaded intertidal flats (Chapman and Tolhurst, 2004; Tolhurst and Chapman, 2007) could be due to the effect of the shade from the canopy, increased nutrients under mangrove trees from the mangrove detritus, a combination of these two factors, or some other unknown factor(s). If differences are due to shade alone, it was predicted that the addition of shading to sun-exposed substratum would alter the sediment and the benthos to resemble that generally found under canopy. Specifically, it was predicted that amphipods and insect larvae would increase in number and oligochaetes and polychaetes would decrease in shaded habitats. It was similarly predicted that microphytobenthos would increase under the shaded roofs, which would lead to increased amounts of photosynthetic pigments and colloidal carbohydrate with concomitant increases in the erosion threshold, proportion of fine-grained sediment, and a decrease in erosion rate. Alternatively, if the original differences identified were due to increased nutrients in the sediments under the trees from the greater amounts of filamentous algae and leaf litter, it was predicted that shading would have no effect, but the addition of nutrients to the sediment would lead to the differences in biota and abiotic variables described above. If both shading and increased nutrient levels under canopy caused the original patterns, an interaction between increased shading and added nutrients would be necessary to lead to the original patterns identified.

MATERIALS AND METHODS

Study Sites

Two sites in Sydney Harbour estuary, Tambourine Bay and Gore Creek were chosen, the former being one of the locations where the original observations were made (Chapman and Tolhurst, 2007; Tolhurst and Chapman, 2007). They are in very sheltered embayments of Sydney Harbour estuary, with little wave-action except during storms, nor much boat activity. The only public use of the study sites is occasional harvesting for bait (pers. obs.), but the sites were generally undisturbed. They have shallow intertidal flats that are emersed during low tide and during high tide the water is <2 m deep, with a narrow strip of mangroves and urban development, including seawalls, at their landward edge. Grain size in the embayments is spatially and temporally variable resulting in mixed intertidal flats, for example at Tambourine Bay mean mud (<63 μm) content is 36.6% (S.E. 6.35, n = 15), with a range of 15.5–99.5% (data converted from mud mass density in Tolhurst and Chapman, 2007). Further physico-chemical data from Sydney Harbour estuary, including from Tambourine Bay can be found in Markich and Jeffree (2019). Data and modeling of nutrients and suspended sediment in the estuary can be found in Birch et al. (2010). The phytobenthos at the study sites include green filamentous algae, diatoms and cyanobacteria. The diatoms and cyanobacteria rarely form visible biofilms like they do in other estuaries around the world, whilst the green filamentous algae often form visible mats on the sediment surface and provide many of the same functions as microphytobenthos (Fagherazzi et al., 2013).

Field Methods

Two field experiments were completed, with the second modified according to the results obtained from the first. The first was on an intertidal flat at Tambourine Bay, Sydney Harbour (see Tolhurst and Chapman, 2007 for details). On the 22nd February 2005, thirty six 0.25 m^2 plots, with 4 m between adjacent plots, were allocated randomly to nine treatments. Twelve were left undisturbed as an unshaded control and twelve shaded with 0.25 m^2 roofs of black Perspex (heavy shading), held

approximately 10–15 cm off the surface of the sediment by plastic pipe legs in each corner of the plot. To test for effects of the physical structure of the roofs (other than shading), 12 plots were similarly covered with clear Perspex roofs as a procedural control; however, unquantified observations indicated that a thin layer of sediment settled on the roofs and although it was regularly removed, the sediment under the clear roofs was lightly shaded compared to the unshaded control plots, although not as deeply shaded as the plots with the black roofs. Thus, the three shading treatments were unshaded control, lightly shaded and heavily shaded.

Four replicate plots of each treatment were not further manipulated and four of each were supplied with nutrients. A flexible plastic tube, 1.5 cm in diameter and with small holes 15 cm apart along its length, was formed into a ring and filled with Osmocote (Scotts Osmocote Plus, Roses Superfeeder, 15% N, 5.2% P, 10% K). Laboratory tests showed that this supplied nutrients continually throughout a 4-week period and, although amounts of nutrients decreased with time, their concentrations were always more than twice the background level. These rings were carefully buried in the sediment surrounding each plot to a depth of 2 cm. Thus, plots were surrounded by a supply of nutrients, with no disturbance to the plot itself. A procedural control, a similar ring without Osmocote, was applied to the remaining 12 plots (4 of each of the shading treatments).

Two weeks later, data from this experiment were collected over 2 days because it was not possible to collect all the samples on the same day. Days were nested within sites to avoid confounding spatial and temporal patterns (Tolhurst and Chapman, 2005), although previous work has shown no significant differences in benthos nor sediment over 2 days (Tolhurst and Chapman, 2007). Accurate quantification and analysis of all pigments present requires destructive sampling and HPLC analysis, which is laborious and expensive (Jeffrey et al., 1999). Remote sensing techniques have advantages over destructive sampling (Murphy et al., 2008), spectroradiometry can reliably estimate the relative amount of absorption by a range of pigments, or groups of pigments (Murphy et al., 2005a). In each plot, the reflectance spectra (350–1,050 nm, in 1 nm intervals) were taken in 2 replicate randomly chosen areas under ambient light using an Analytical Spectral Devices (ASD) FieldSpec Pro spectroradiometer (ASD, Boulder, CO, United States details in Murphy et al., 2005a,b). Spectra were taken using an 8° fore-optic, from a height of 35 cm, thus measuring reflectance from an area of mud the same size as the subsequent contact core sediment samples (5 cm diameter). Each spectral measurement was an average of 30 individual spectra. Immediately prior to the collection of each spectrum, a calibration spectrum was taken from a ∼99% reflective panel of spectralon. Two and four replicate spectra were taken from each plot for experiments 1 and 2, respectively. The same replicate 5 cm diameter areas were then dark-adapted for 15 min with foil chambers and the microphytobenthic biomass (F_o) and 'health' (F_v/F_m) measured using a Heinz Walz Diving Pulse Amplitude Modulation (PAM) fluorometer (Honeywill et al., 2002).

Next a 5 cm diameter, ∼2 mm deep, cryogenic contact core sample was taken from the same spot as the PAM and spectroradiometer measurements. These cores were immediately wrapped in aluminum foil, stored in liquid nitrogen and returned to the laboratory. The thickness of each core was measured to calculate core volume so the biogeochemical data could be expressed as concentrations (mass density), because of potential confounding of data expressed as content (mass fraction; Perkins et al., 2003; Tolhurst et al., 2005). Then, all samples were weighed, lyophilized in the dark (to prevent degradation of pigments) and stored at −70°C in the dark before analysis of biogeochemical sediment properties.

The erosion thresholds and relative erosion rate (suspension index, S_i) of the sediment were measured adjacent to the sampled areas using a Cohesive Strength Meter (CSM), for more details see Tolhurst et al. (1999) and Vardy et al. (2007). Finally, two benthic sediment cores, 8.5 cm diameter and 5.0 cm deep, were collected from each plot to sample the surface macrofauna. Just the surface was sampled because the mangrove roots prevented sampling of deeper sediments in the previous work on which this study is based Chapman and Tolhurst (2004). Two syringe cores of sediment, 2 cm diameter and 2 cm deep, were collected to measure grain size and organic matter.

The second experiment was set up in two bays, Tambourine Bay and Gore Creek on 21st April, 2005. Twenty-four plots were established in each site and allocated randomly to unshaded control, lightly (clear roofs) and heavily shaded (black roofs) treatments. Fertilizer manipulation was not included because of the lack of a response in the first experiment. Approximately 2 weeks later, on the 5th May, 2005, 12 of the plots (n = 4 for each treatment) at Gore Creek were sampled as before to test whether the patterns found previously at Tambourine Bay were also found at Gore Creek. The roofs were then re-used to set up two additional plots of each treatment at each site, giving a total of six plots for each treatment. These were sampled approximately 3 months later, over 2 days on the 4th and 5th July, 2005, but because a large storm destroyed most of the plots at Gore Creek, only data from Tambourine Bay were available for analysis. On the 4th July, 2005, light intensity readings were taken in three plots of each treatment and under the adjacent mangrove canopy.

Laboratory Methods

The type and relative abundance of pigments were obtained from the 2nd-derivative reflectance spectra (Murphy and Tolhurst, 2009). Reflectance spectra were calculated by dividing the mud spectrum by the calibration spectrum. To derive absolute reflectance this quotient was then multiplied by the panel calibration factors provided by the manufacturer of the panel. The relative amount of absorption by pigments was estimated using derivative analysis of the reflectance spectra. First, spectra within each plot were averaged. Second-order derivatives were then calculated from the average spectra using the combined differentiation and smoothing method of Savitzky and Golay (1964), with a 20 nm smoothing window. Fourth-order derivative spectra may be better at separating individual pigments (Bidigare et al., 1989), but were not used here because they were too "noisy" due to the small reflectance of the mud. Second-order derivative spectra are centered on zero with peaks in

the spectrum representing absorption maxima of pigments. The relative amounts of pigments in each plot-average spectrum were calculated by automatically identifying the maximum value in the 2nd derivative above zero and its wavelength position, for each major absorption in the spectrum. The identity of pigments was inferred by comparing the wavelength locations of maximal absorption with the published wavelengths of *in vivo* absorption maxima (Bidigare et al., 1989; Smith and Alberte, 1994; Aguirre-Gomez et al., 2001). Absorptions were identified at 419 nm (chlorophyll *a*), 434 nm (probably a mixture of chlorophylls *a* and *c*), 471 nm (chlorophyll *b*), 493 nm and 587 nm (carotenoids and xanthophylls), 618 nm (chlorophyll *a*), 630 nm (chlorophyll *c*), and 675 nm (chlorophyll *a*).

The benthic cores were sieved over 500 μm mesh and the retained fauna preserved in a 10% solution of formol-seawater before being sorted under a microscope. Taxonomic resolution was mixed from broad groups (e.g., oligochaetes and nematodes), through families (polychaetes) to species/morphospecies (amphipods, gastropods) because: (i) the taxonomy of many of these groups is not well-known or identification keys are not easily available and (ii) identification of these fauna at mixed resolution is suitable to identify spatial and temporal patterns of variation of these fauna within and among habitats (e.g., Chapman, 1998; Chapman and Tolhurst, 2004).

Contact core samples were used to measure a suite of biogeochemical properties: chlorophyll *a* and *b*, colloidal and total carbohydrate, water concentration, mud, sand and organic matter using standard methods (see Murphy and Tolhurst, 2009; Chapman et al., 2010 for more details). The concentration of water was calculated from the contact core as $(Wt_{wet} - Wt_{dry})$/core volume in cm^3, where: Wt_{wet} = wet weight of the sediment; Wt_{dry} = dry weight of the sediment. The colloidal carbohydrates (the water-soluble fraction of carbohydrates) and total carbohydrates were measured from a sub-sample of each contact core using the sulphuric acid-phenol Dubois assay (Dubois et al., 1956). Data were calculated as glucose equivalents using a standard curve and expressed as mass density (μg cm^{-3} for colloidal carbohydrate and mg cm^{-3} for total carbohydrate). Approximately 0.2 g of the freeze-dried sample was used for the assay of colloidal carbohydrate and 0.0025–0.005 g for the assay of total carbohydrate. Chlorophylls *a* and *b* were measured spectrophotometrically from a sub-sample of the contact core using a dimethyl formamide (DMF) extraction, following the equations of Porra et al. (1989) and expressed as mass density (μg cm^{-3}):

$$\text{Chlorophyll } a = 12\,(A_{664} - A_{750}) - 3.11\,(A_{647} - A_{750})$$

$$\text{Chlorophyll } b = 20.78(A_{647} - A_{750}) - 4.88(A_{664} - A_{750})$$

Where *A* are the absorptions at the specified wavelengths.

Organic matter was determined from each contact core and each syringe core by ashing the remaining sediment in a furnace at 450°C, with the sediment weighed pre- and post-ashing and data expressed as mass density (g cm^{-3}). The grain size was then measured by washing the ashed sediment through a mini 63 μm sieve, of known weight. The sieve containing the remaining sand sized sediment was then freeze-dried and re-weighed to determine the mass density of sand (>63 μm g cm^{-3}) and mud (<63 μm g cm^{-3}).

Statistical Methods

Biotic assemblages and the suite of sedimentary variables were analyzed using multivariate analyses of variance (Permanova; Anderson, 2001). The biotic data used matrices of Bray–Curtis dissimilarities and untransformed data and the abiotic data used matrices of normalized Euclidean distances. Levels of probability were estimated from 999 permutations of the data using the reduced model (Anderson, 2001). When factors were significant (at $P < 0.05$), the means were illustrated in nMDS plots (Clarke, 1993) and means compared using *t*-tests within the Permanova statistical package. The biota and abiotic variables that contributed most to the significant differences among relevant means were identified using SIMPER, which provides the contributions of each individual taxon/abiotic variable to the mean dissimilarity between any two variables.

Univariate data (e.g., abundances of individual taxa, the number of taxa, individual sedimentary variables and individual pigment bands) were analyzed using analysis of variance (ANOVA). First, heterogeneity of variances was tested using Cochran's test and, if significant, significant F-ratios were interpreted with caution. Differences among means for factors with significant F-ratios were identified using Student–Newman–Keuls (SNK) tests (Underwood, 1997a). For all analyses, nutrients (plus/minus/procedural control) and shading (black roofs/clear roofs/no roofs) were treated as fixed factors, with plots nested within the nutrient x shading interaction. Each site and time were analyzed separately. The differences among treatments, when significant, were over and above plot differences.

RESULTS

Amounts of Shading

The light readings showed that average light intensities (photosynthetic photon flux density) on the day of measurement were 1,048 μmol m^{-2} s^{-1} (*SE* = 31) in the unshaded control plots, 4.6 μmol m^{-2} s^{-1} (*SE* = 0.93) under black roofs, 648 μmol m^{-2} s^{-1} (*SE* = 53.4) under clear roofs and 64 μmol m^{-2} s^{-1} (*SE* = 1.1) under the mangrove canopy. The black roof produced sediment more heavily shaded than that under the mangrove canopy, whilst the clear roof produced sediment more lightly shaded than that under the mangrove canopy. The clear roofs decreased average light intensities by approximately 38%, mangrove canopy by approximately 94% and the black roofs by over 99.5%. Therefore, the term lightly shaded refers to clear roofs, the term heavily shaded refers to black roofs and unshaded control refers to plots with no shading.

Changes After 2 Weeks, Tambourine Bay and Gore Creek: Fauna

In the first experiment at Tambourine Bay, 45 taxa were identified, including ten families of polychaetes, seven species

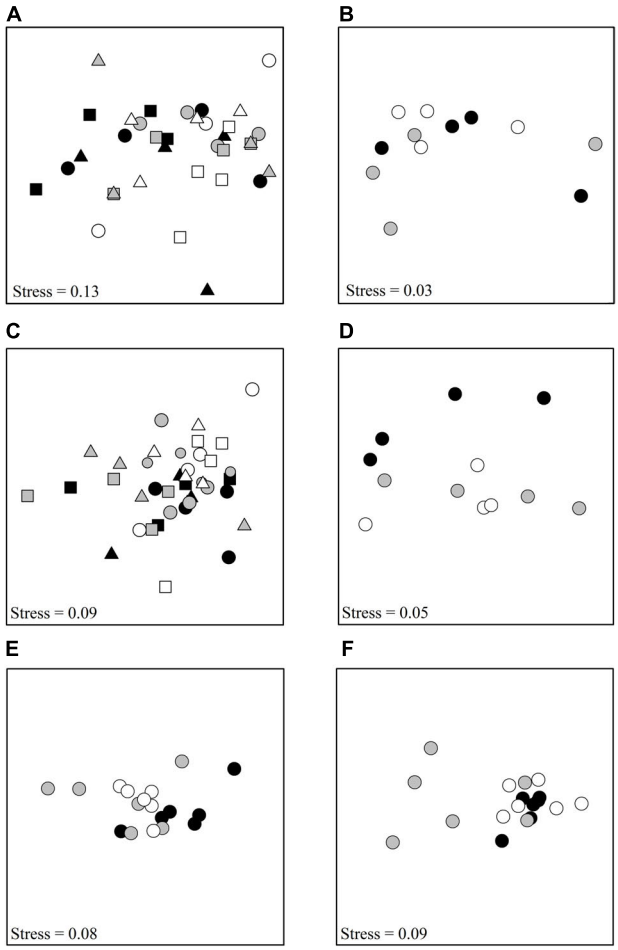

FIGURE 1 | nMDS plots showing differences among treatments, **(A)** Tambourine Bay macrofauna after 2 weeks, **(B)** Gore Creek macrofauna after 2 weeks, **(C)** Tambourine Bay properties of sediment after 2 weeks, **(D)** Gore Creek properties of sediment after 2 weeks, **(E)** Tambourine Bay macrofauna after 3 months, **(F)** Tambourine Bay properties of sediment after 3 months. For panels **(A,C)**, each point represents 1 plot; black – heavily shaded plots with black roofs, gray – lightly shaded plots with clear roofs, white – unshaded control plots; circles – with nutrients, square – procedural control (buried plastic ring), triangle – no additional nutrients. For the rest of the panels, each point represents 1 plot; black – heavily shaded plots with black roofs, gray – lightly shaded plots with clear roofs, white – unshaded control plots.

of amphipods, eight species of bivalves and groups such as nematodes, insect larvae and oligochaetes. Of the >4,000 individuals, approximately 70% were polychaetes (39% were spionids). Analysis using PERMANOVA (Anderson, 2001) on untransformed data showed no significant effect of either factor (Shading or Nutrients), nor significant interaction ($P > 0.05$ for all terms in the analysis; **Figure 1A**) and, thus, no effect of either factor on the faunal assemblage as a whole.

The number of taxa, families of polychaetes and abundances of oligochaetes, capitellids, spionids, amphipods, bivalves and nematodes (which together made up 85% of individuals) were each analyzed using analyses of variance (**Table 1A**). There were no significant differences among treatments, nor general consistent trends for most data. In some cases, this was due to very small differences among treatments (e.g., the number of taxa in **Figure 2**). In other cases (e.g., abundances of bivalves, amphipods, and oligochaetes), taxa were extremely variable among some or all treatments (**Figure 2**). Heavy shading did, however, reduce abundance of spionids and capitellids as was predicted, although this was only significant for capitellids (**Table 1A** and **Figure 2**). Adding fertilizer had no significant effect on any of the fauna (**Table 1A**).

In the second experiment at Gore Creek, there were 27 taxa after 2 weeks, including eight families of polychaetes, one species of amphipods, six species of bivalves and groups, such as nematodes, insect larvae and oligochaetes. Again, there was no significant effect of shading (PERMANOVA; $P > 0.80$) (**Figure 1B**). Nor were there any effects of shading on the number of taxa, families of polychaetes, nor abundances of oligochaetes, capitellids, sabellids, spionids, or bivalves (**Figure 3**, all F-ratios for Treatment had $P > 0.05$).

Changes After 2 Weeks, Tambourine Bay and Gore Creek: Sediment Properties

The properties of the sediment (F_o, F_v/F_m, chlorophyll *a* and *b*, colloidal and total carbohydrate, erosion threshold, erosion rate, mud in contact core and syringe core, sand in contact core and syringe core, organic matter in contact core and syringe core and amount of water) from experiment 1 at Tambourine Bay after 2 weeks were analyzed as normalized Euclidean distances using PERMANOVA. In contrast to the fauna, there was a statistically significant effect of shading in experiment 1 ($P < 0.01$), with all treatments significantly different from each other (at $P < 0.05$). Nevertheless, the nMDS (**Figure 1C**) shows considerable overlap among the different treatments.

The percentage contribution of each variable to Euclidean distance measures among the different levels of shading was calculated for each variable. Sediment in plots without roofs was primarily distinguished from that with light shading by amounts of water (10% of the average distance measure), colloidal carbohydrate (8%) and F_o (8%). The two types of roof were mainly distinguished by F_o and F_v/F_m (10 and 9%, respectively) and chlorophyll *a* extracted from the contact cores (8%).

Analyses of the sedimentary variables for experiment 1 at Tambourine Bay after 2 weeks gave no significant effects of either treatment (shade and fertilizer) on most variables (**Tables 1B,C** and **Figure 4**). Light shading caused a significant increase in: F_o, concentration of chlorophyll *a* and water (**Table 1B** and **Figure 4**). There was a strong effect of shading on concentrations of colloidal carbohydrate (**Table 1B**), with decreased values under both amounts of shading, particularly the heavily shaded ones, which was opposite to what was predicted, but as predicted, there was no significant effect on total carbohydrate. There was a significant decrease in the concentration of sand in the absence of nutrient addition under light shading (**Table 1C** and **Figure 4**).

In contrast to the fauna, there was a small, but significant effect of fertilizer on chlorophyll *a* and colloidal carbohydrate (**Table 1B**), although Student–Newman–Keuls (SNK) tests could

TABLE 1 | ANOVA for macrofauna and properties of sediments in plots subjected to Shading (Sh), addition of Nutrients (N) and appropriate control treatments, experiment 1 at Tambourine Bay after 2 weeks; details in text. 20 mm is data from syringe core, 2 mm is data from contact core, 2 samples from each of $n = 4$ replicate plots.

(A)

Source	df	No. taxa	Fams. Poly.	Oligochaetes	Capitellids	Spionids	Amphipods	Bivalves	Nematodes
Sh	2	-	–	–	*	–	–	–	–
N	2	–	–	–	–	–	–	–	–
ShxN	4	–	–	–	–	–	–	–	–
P(ShxN)	27	**	–	–	–	–	***	–	–

(B)

Source	df	F_o	F_v/F_m	Chl. *a*	Chl. *b*	Coll. Carb.	Total Carb.	Eros. thres.	Eros. rate
Sh	2	**	–	*	–	**	–	–	–
N	2	–	–	*	–	*	–	–	–
ShxN	4	–	–	–	–	–	–	–	–
P(ShxN)	27	*	–	*	**	***	***	–	–

(C)

Source	df	Mud (20 mm)	Mud (2 mm)	Sand (20 mm)	Sand (2 mm)	Organics (20 mm)	Organics (2 mm)	Water (2 mm)
Sh	2	–	–	*	*	–	–	**
N	2	–	–	–	–	–	–	–
ShxN	4	–	–	–	–	–	–	–
P(ShxN)	27	–	**	*	*	**	**	*

*Asterisks indicate significance, *$p < 0.05$, **$p < 0.01$, ***$p < 0.001$. For treatments to be significant, the difference among them must be greater than the plot to plot variation.*

not distinguish among means. In each case, there were smaller concentrations of chlorophyll *a* and colloidal carbohydrate in the plots with added fertilizer (**Figure 4**), which was opposite to what was predicted.

In experiment 1 at Tambourine Bay, after 2 weeks, there was no significant effect of fertilizer on any of the pigment bands (data not shown), but there were significant differences in the amounts of pigments between shading treatments (**Figure 5A**). The amount of chlorophyll *a*, as measured by the absorption at 675 nm was significantly different between each of the three shade treatments. Absorptions by pigments at 587, 618, and 630 nm were significantly greater under light shading, but there was no significant difference in absorption between the unshaded control plots and heavy shading. There was a significant difference between shade treatments at 493 nm, but the SNK test could not differentiate between treatments. At 419 nm absorption was significantly smaller under light shading than heavy shading and unshaded control plots.

In experiment 2, at Gore Creek after 2 weeks, roofs had no significant effect on the sediment (PERMANOVA; $p > 0.20$), even though the nMDS plots clearly separated the plots with heavy shading from the other treatments (**Figure 1D**). Separate analysis of the individual properties using ANOVA revealed significant reductions in F_o, F_v/F_m and colloidal carbohydrate ($F_{2,21} = 6.72$, 6.35, and 6.47, respectively, all $P < 0.01$) under the heavy shading (**Figure 6**), although the decrease in F_v/F_m was small. No other variables showed any significant effect of shading treatments (**Figure 6**).

In experiment 2, at Gore Creek after 2 weeks, absorptions by pigments at 618 nm were significantly different among shading treatments (**Figure 5B**), but the SNK test could not differentiate means. Absorption by pigments at 675 nm were significantly smaller under heavy shading than both light shading and unshaded control plots, which were not significantly different from each other.

Changes After ∼3 Months, Tambourine Bay

Data were only available from Tambourine Bay because the experiment at Gore Creek was lost to a storm. For both the fauna and sediment, nMDS plots and ANOSIM (Clarke, 1993) showed no significant difference between the plots which had been in place for 2 weeks less than the others. Thus, all plots were analyzed together.

Tambourine Bay: Fauna

After ∼3 months, there were 47 taxa, including nine families of polychaetes, 11 species of amphipods, six species of bivalves, three species of gastropods, five species of isopods and various broad groups, such as nematodes, insect larvae, oligochaetes, copepods, etc. Pairwise comparisons showed that heavily shaded plots had significantly different benthic fauna to the lightly shaded and unshaded control plots, which were similar (PERMANOVA; $p < 0.05$; **Figure 1E**).

Differences were primarily due to abundances of oligochaetes (which contributed 24% to the total dissimilarity between heavily

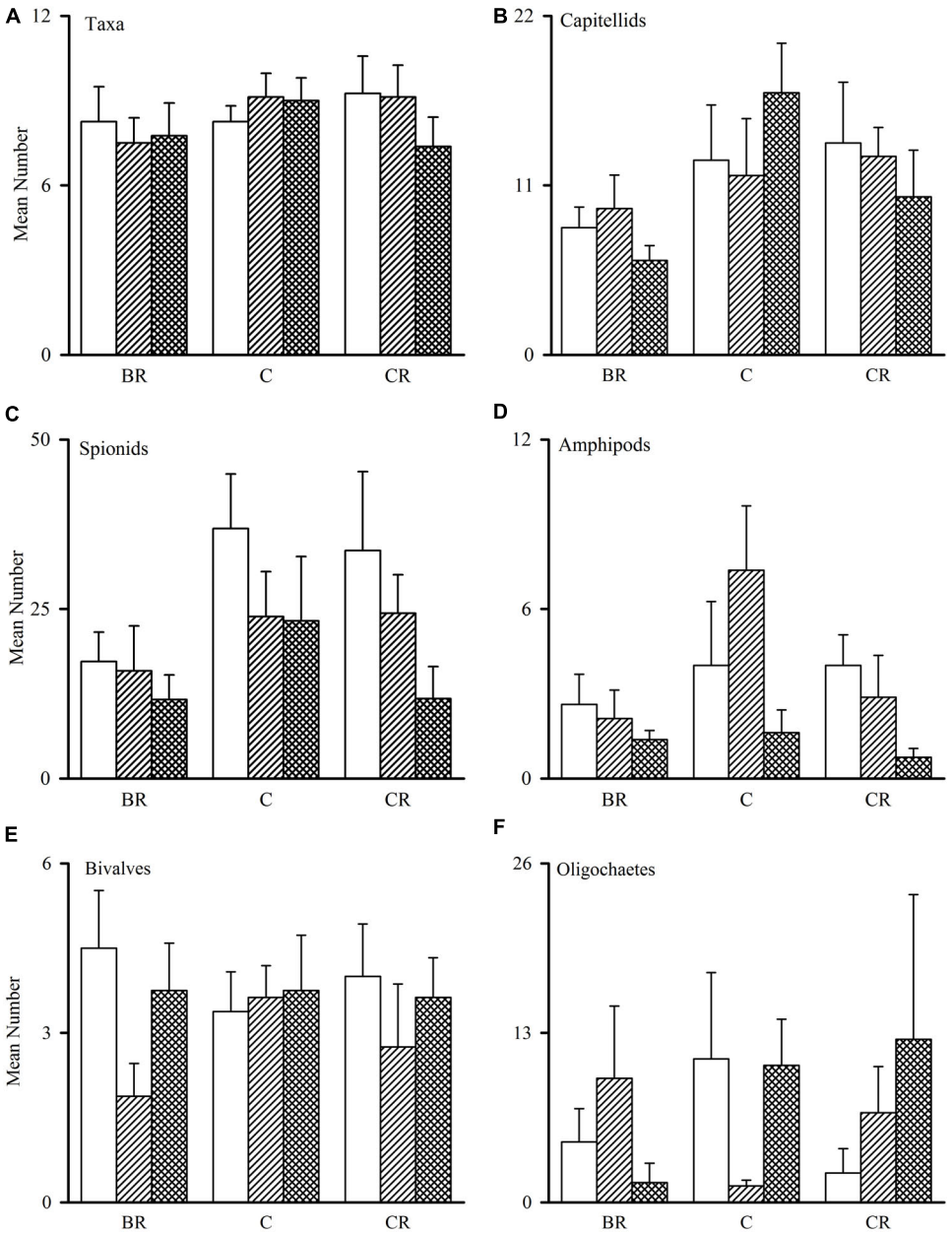

FIGURE 2 | Tambourine Bay macrofauna after 2 weeks, mean (*SE.*; $n = 4$ plots). Panel **(A)** numbers of all taxa and abundances of **(B)** capitellids, **(C)** spionids, **(D)** amphipods, **(E)** bivalves, and **(F)** oligochaetes in heavily shaded plots with black roofs (BR), lightly shaded plots with clear roofs (CR) or unshaded control plots (C), when provided with added nutrients (white bars), no nutrients (linear hatched bars) or the associated procedural control (crosshatched bars).

shaded and lightly shaded plots, 23% to the dissimilarity between heavy shading plots and unshaded control plots), sabellids (17 and 12%, respectively), spionids (17 and 19%, respectively) and one species of gammarid amphipod (11% for the latter comparison only).

The number of taxa, families of polychaetes and abundances of oligochaetes, capitellids, nereidids, sabellids, spionids, amphipods, and nematodes were analyzed using analysis of variance, the other taxa being too sparse for analysis, i.e., data dominated by zeroes and singletons (**Table 2**). Several of these taxa showed significant variability among replicate plots, but only the number of taxa and abundances of amphipods showed significant differences among treatments. SNK tests could not identify the differences among treatments for the number of taxa, although there were fewer under heavy shading and more under the light shading (**Figure 7**). Abundances of amphipods were significantly reduced under both sets of roofs, which indicates an experimental artifact. Despite the strong contribution of oligochaetes to the multivariate patterns and large decreases in oligochaete, sabellid, and nereidid polychaete abundance under

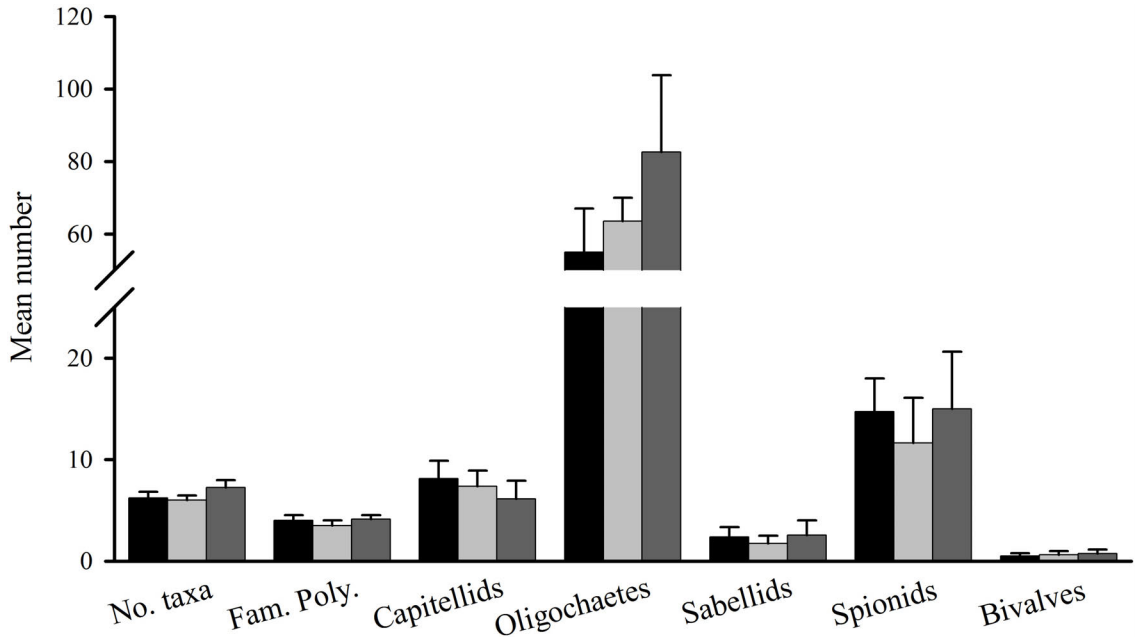

FIGURE 3 | Gore Creek macrofauna after 2 weeks, mean (*SE*; $n = 4$ plots) number of taxa, families of polychaetes and abundances of capitellids, oligochaetes, sabellids, spionids, and bivalves in plots with black roofs (black bars), clear roofs (dark gray bars), or control plots (light gray bars).

heavy shading (**Figure 7**), there was no significant effect of heavy shading (**Table 2**).

Tambourine Bay: Properties of Sediment

After ∼3 months, roofs had no significant effect on the sediment (PERMANOVA, $P > 0.25$), mostly due to very large and significant differences among plots. It is clear from **Figure 1F**, that four of the six plots with light shading were very different from the other two plots with light shading, which plotted together with those with heavy shading and the unshaded control plots. These two plots with light shading were not the plots that had been in the field 2 weeks less than the other plots with light shading.

Although differences were not significant, because four of the six plots with light shading were clearly separated from the other plots on the nMDS plot (**Figure 1F**), SIMPER determined which variables most contributed to differences in sediment between the plots with light shading and the unshaded control plots, or those with heavy shading. The entire range of variables measured contributed similar amounts to the differences, with no single property contributing large amounts to the overall differences in sediments.

In contrast to the fauna, there were significant differences among treatments for many of these properties of sediments; these were F_o, F_v/F_m, chlorophyll *a*, water, total and colloidal carbohydrate and sand in both types of core (**Tables 2B,C** and **Figure 8**). In general, there were more significant differences in the biochemical properties than in the physical properties of the sediment. There were no significant differences in threshold or rate of erosion, despite the significant changes in the amount of microphytobenthos, water and sand in the surface sediment.

Most significant differences in the properties of the sediment were between the plots with light shading and the other treatments (SNK tests). There was significantly more chlorophyll *a*, F_o, total and colloidal carbohydrate and water under the light shading than in the other two treatments (**Figure 8**). In all analyses, heavily shaded and unshaded control plots did not differ significantly, despite reduced measures of F_o, chlorophyll *a* and colloidal carbohydrate under heavy shading (**Figure 8**). F_v/F_m showed the opposite pattern to F_o, being significantly smaller under the light shading.

Although there were significant effects of treatments on amounts of sand, SNK tests could not distinguish among the means. There appeared to be an artifact associated with roofs influencing the amounts of sand and mud, with increased mud and decreased amounts of sand under both sets of roofs compared to the unshaded control plots. The rate of erosion was greatest under heavy shading and least under light shading (**Figure 8**). The threshold of erosion did not differ significantly among treatments, but was slightly reduced under heavy shading.

After 3 months at Tambourine Bay, absorption by pigments at 419 nm was significantly less under light shading than under heavy shading and unshaded control plots, which were not significantly different to each other (**Figure 5C**). There was no significant difference in absorption among shading treatments at 471 nm. At 675 nm heavily shaded plots had significantly smaller amounts of absorption than both lightly shaded and unshaded control plots, which were not significantly different to each other. For all other wavelengths, light shading showed significantly greater amounts of absorption than both heavily shaded and unshaded control plots, which were not significantly different to each other (**Figure 5C**).

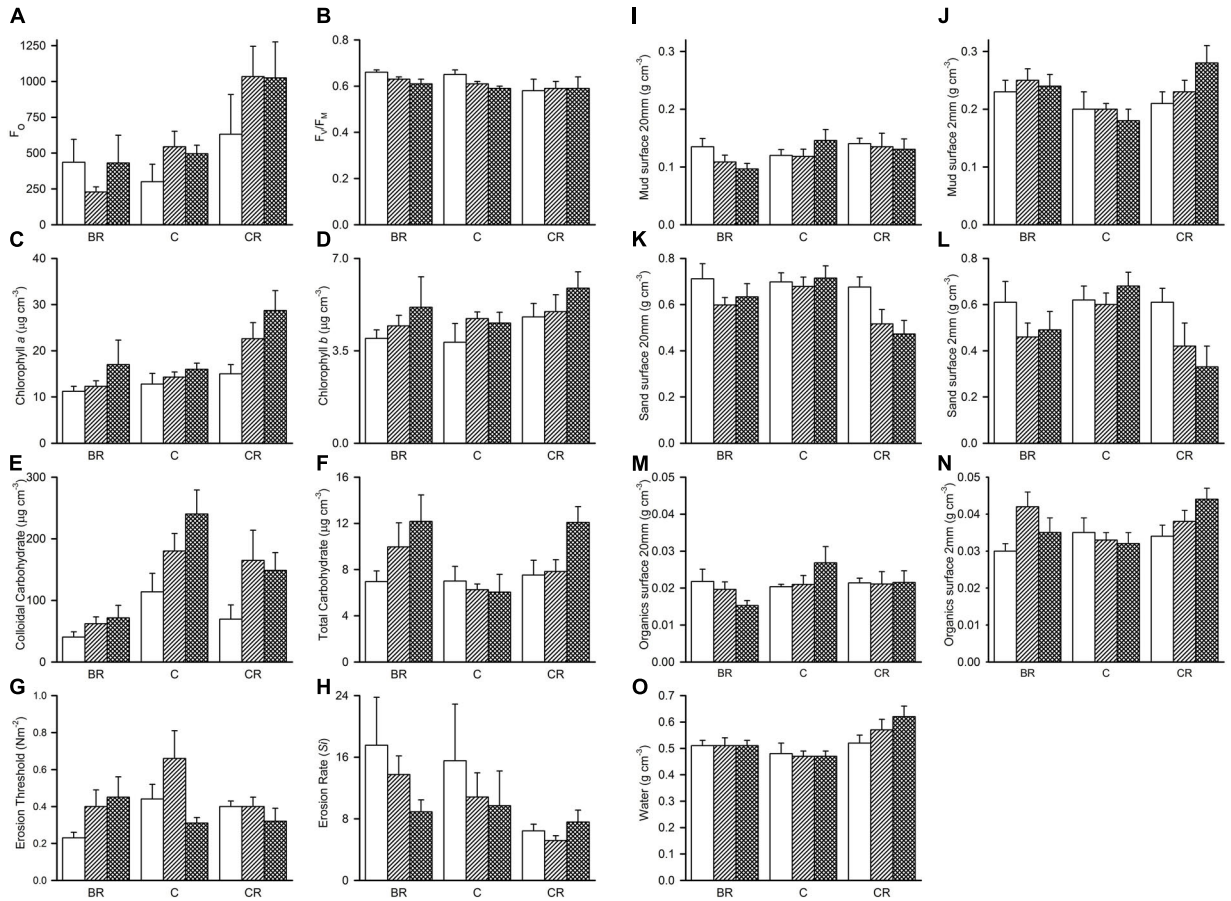

FIGURE 4 | Tambourine Bay properties of sediment after 2 weeks, mean (*SE*; $n = 4$ plots) in plots with black roofs (BR), clear roofs (CR), or unshaded control plots (C), when provided with added nutrients (white bars), no nutrients (linear hatched bars), or the associated procedural control (crosshatched bars). Panel **(A)** F_o, **(B)** F_v/F_m, **(C)** chlorophyll *a*, **(D)** chlorophyll *b*, **(E)** colloidal carbohydrates, **(F)** total carbohydrates, **(G)** erosion threshold, **(H)** erosion rate, **(I)** mud from 20 mm deep core, **(J)** mud from 2 mm deep core, **(K)** sand from 20 mm deep core, **(L)** sand from 2 mm deep core, **(M)** organics from 20 mm deep core, **(N)** organics from 2 mm core, and **(O)** water from 2 mm deep core. F_o and F_v/F_m measured with a PAM (unitless); erodibility measured with a CSM, erosion threshold (N m^{-2}), erosion rate (dimensionless); all other measures are mass density (wt per cm^{-3}).

DISCUSSION

These experiments show that both light shading (produced by the clear roofs) and heavy shading (produced by the black roofs) can, within a few weeks, cause significant changes in microphytobenthos, properties of sediments and some macrofauna. In contrast, there was little to no effect of addition of nutrients. Shading by saltmarsh plants has been found to cause similar changes, altering physical properties, shifting microphytobenthos communities to diatom dominance and altering macrofaunal community composition (Whitcraft and Levin, 2007). This suggests that shading is a fundamental driver of intertidal sediment ecosystem structure and function in these Australian habitats.

Effects of Roofs

Mangroves in Sydney Harbour are patchy and do not form a dense forest, hence their shading of sediment is patchy at the edges and shaded patches are often comparatively small. We did our experiment on the edges of the mangrove forests, where the sizes of the naturally shaded patches and our experimental plots more closely match. However, the size we chose for our plots was a trade-off between area shaded and having a manageable roof size. In addition, our shading manipulation was a persistent change in shading, similar to that caused by structures such as bridges; whereas shading due to immersion and emersion is periodic and hence so are the impacts (Drylie et al., 2018). Thus, the extrapolation of our findings to larger scale and different types of shading should be treated with appropriate caution.

Originally, the clear roofs were incorporated into the experiment as a procedural control to unconfound contrasts between the unshaded control plots and the heavily shaded plots, which potentially differed not only with respect to shading, but in other factors that may be altered by the presence of the roofs, e.g., changes to water-movement, reduced predation, mobile fauna sheltering under roofs during high and/or low tide, etc. (Miller and Gaylord, 2007). For amphipod abundance there appeared to be an experimental artifact of roofs, with a significant decrease

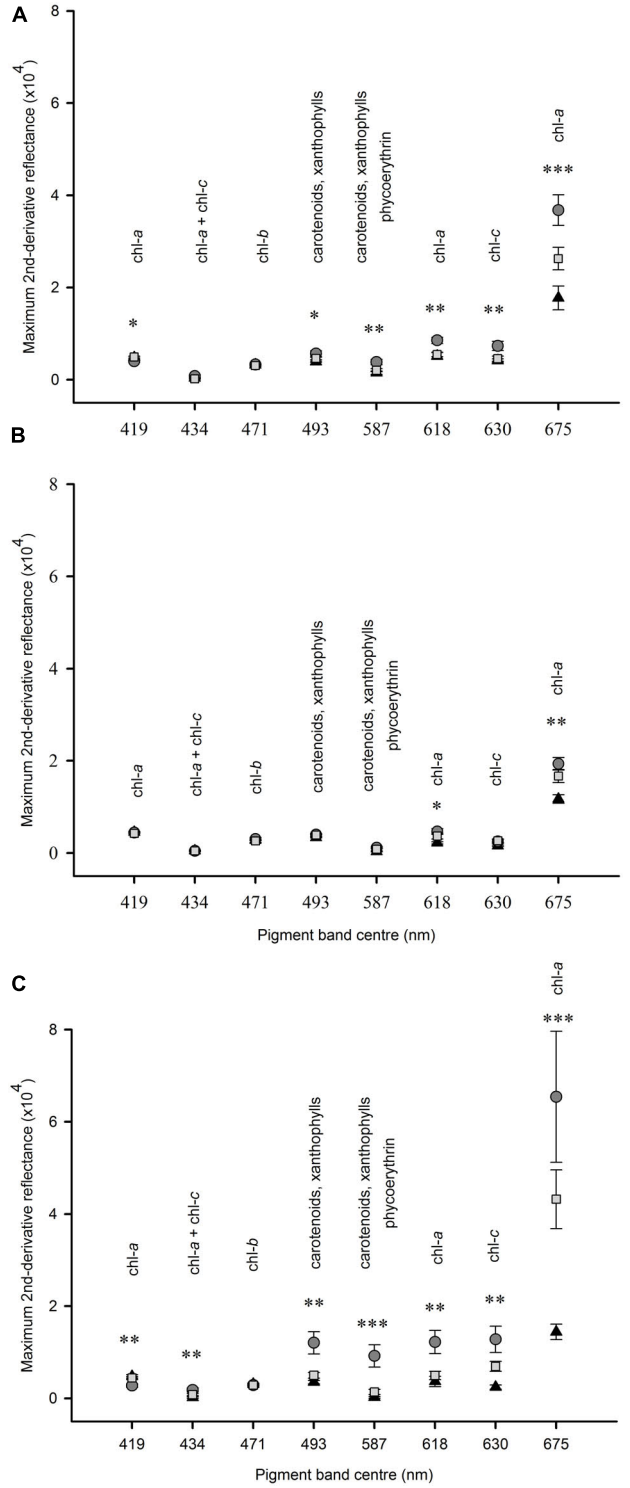

FIGURE 5 | Mean (SE) amount of absorption by pigments at different wavelengths between 400 and 800 nm under heavy shading (▲); light shading (●); unshaded control plots (■). Panel **(A)** after 2 weeks at Tambourine Bay, $n = 2$; **(B)** after 2 weeks at Gore Creek, $n = 4$; **(C)** after 3 months at Tambourine Bay, $n = 4$. Data were analyzed using ANOVA on untransformed data, asterisks indicate significance, $*p < 0.05$, $**p < 0.01$, $***p < 0.001$.

in abundances of amphipods after 3 months under both sets of roofs compared to the unshaded control plots. For most of the significant responses shown by the taxa and the sedimentary properties to shading, measures under the clear and black roofs showed opposite directional responses, so are very unlikely to be due to an artifact associated with the structure itself.

Effects of Addition of Nutrients

The only significant effect was a small decrease in biochemically measured chlorophyll *a* and colloidal carbohydrate in the plots with added nutrients. This was opposite to what would be predicted if algal growth was nutrient limited. Despite biotic processing of mangrove leaves increasing nutrients in sediment (Camilleri, 1992) and nutrient addition altering faunal assemblages (Morris and Keough, 2003); adding a source of nutrients to sediments does not always result in either measurable increases in nutrients (Douglas et al., 2016), nor changes to fauna (Rossi, 2006), nor an overall increase in primary productivity or biomass of microphytobenthos (Stutes et al., 2006; Cebrián et al., 2012), but can alter assemblage structure (Gladstone-Gallagher et al., 2014b), for example by inducing cyanobacterial blooms (Armitage and Fong, 2004).

The effect of nutrient addition can also be mediated by other organisms, for example the crab *Pachygrapsus crassipes*, via processes such as bioturbation, reduced the relative importance of nutrients to soft-sediment benthic assemblages (Armitage and Fong, 2006). It is possible that the crab species found in our sites, such as the burrowing *Heloecius cordiformis*, have a similar effect on nutrients. Nutrient additions to intertidal flats have been shown to increase chlorophyll *a* concentration in the sediment by 90%, but only where resource uptake efficiency and the accumulation of algae in plots were facilitated by the addition of high densities of a burrowing bivalve (Eriksson et al., 2017).

These results suggest that microphytobenthos in this part of Sydney Harbour are not nutrient limited, although it has been shown that fertilizer application rate and sediment properties influence enrichment level (Douglas et al., 2016) and it is possible that we did not get sufficient nutrient release to detect an effect. The results also suggest that the differences in patterns of microphytobenthos, carbohydrates and fauna found between unshaded sediment without large amounts of surface litter and the shaded sediment with surface litter (Chapman and Tolhurst, 2004, 2007; Tolhurst and Chapman, 2007), represents a much more complex interaction of many different factors (see below sections and Kon et al., 2010) than a simple increase in nutrients derived from leaf litter. A unified approach to field-based sediment nutrient enrichment experiments is required to enhance comparisons and future meta-analyses (Douglas et al., 2016).

Effects of Shading on the MPB and Properties of the Sediment

Changes in the properties of sediments due to shading were primarily in the measures of microphytobenthos and properties known to be altered by them. This is most likely due to the

altered light availability, although changes to temperature and moisture may have also contributed. Visual observations and the changes in sediment properties indicate that there was generally an increase in microphytobenthos biomass in the lightly shaded plots and a decrease in the more heavily shaded plots. Fewer variables were significantly altered at Gore Creek, demonstrating spatial variability in the response to shading. Originally, chlorophyll *a* and colloidal carbohydrate were predicted to increase under black roofs (heavy shading), because of the patterns previously documented between unshaded mud and mud shaded by the mangrove canopy (Chapman and Tolhurst, 2004; Tolhurst and Chapman, 2007), which the black roofs were expected to mimic. However, the black roofs caused more shading than the mangrove canopy and there was either no significant response in chlorophyll *a* and colloidal carbohydrate or the opposite response occurred. Altered light intensity directly causes shifts in the microphytobenthos, e.g., in: pigment ratios, amount of chlorophyll proteins, species composition, growth, survival, migration of motile species, number and/or size of light harvesting subunits (Gallagher et al., 1984; Hust et al., 1999; Defew et al., 2004; Jesus et al., 2006; Stutes et al., 2006; van Leeuwe et al., 2008; Perkins et al., 2010; Cartaxana et al., 2016); although the contribution of an indirect effect of shading via macrofauna cannot be ruled out. In the unshaded control plots, high light levels are most probably driving motile microphytobenthos cell migration downward in the sediment profile or inducing photoinhibition, at least during parts of the day. Under heavy shading, light availability is probably limiting microphytobenthic photosynthesis.

On rocky shores and seawalls, shading ameliorates stressful conditions (Blockley, 2007), for example by decreasing physical stresses associated with emersion during low tide, particularly temperature and desiccation (Thompson et al., 2004). Mangrove canopy directly alters physical conditions such as temperature and moisture, with concomitant changes to sediment properties and organisms (Kon et al., 2011). Latitude and its effects on temperature, insolation and day-length play an important role in regulating microphytobenthos biomass and their response to shading. Murphy et al. (2009) suggested that increased insolation and temperatures were responsible for a decrease in microphytobenthos biomass during warmer months in these intertidal flats. The results from Tambourine Bay after 3 months are in line with that suggestion, with the light shading at least partially emulating conditions found in cooler months (i.e., increased sediment moisture and decreased light intensity). The increased concentration of water in the sediment under light shading is probably due to shading decreasing temperatures and evaporation during emersion (Kon et al., 2010), and/or the increase in microphytobenthos biomass, and decrease in sand increasing water retention (the method for measuring water does not differentiate between pore water and water found within organisms). The increase in colloidal carbohydrate at Tambourine Bay after 3 months is probably primarily due to the increase in microphytobenthos, which are known to correlate with amounts of carbohydrate (Underwood, 1997b; Tolhurst et al., 2008). Over the whole study, however, the differences in pigments and photosynthetic measures are mixed, suggesting that either the microphytobenthic community is mixed, exhibiting unique responses, or that something else in addition to the microphytobenthos is impacting the carbohydrates.

After 3 months, heavily shaded plots showed directional responses in sediment properties in line with a reduction in microphytobenthos (except for grain size), including reductions in F_o, chlorophyll *a*, colloidal carbohydrate, erosion threshold and total carbohydrate; and increased erosion rate and water; although the differences were not always significant (**Figure 8**). The lightly shaded plots showed directional responses in line with an increase in microphytobenthos biomass; including increases in F_o, chlorophyll *a*, chlorophyll *b*, colloidal carbohydrate, total carbohydrate, erosion threshold, mud (both types of core), and water; and decreased erosion rate and amounts of sand (both types of core), although the differences were not always significant (**Figure 8**).

The amounts and types of pigments in microphytobenthos can yield important information on the composition of the microphytobenthic assemblage (reviewed by Millie et al., 1993). Amounts of pigments can also change in response to variations in the intensity and wavelength distribution of incident light. Carotenoids, for example, play an important role in protecting algae from intense sunlight (Young and Britton, 1990) and changes in amounts of their oxidized derivatives, xanthophylls, are known to occur over relative short time-intervals in some micro-algae (e.g., Demers et al., 1991).

After 2 weeks in Tambourine bay (experiment 1), shading had a significant effect on the amounts of pigments (as measured by the strength of their absorption spectra), with carotenoids, xanthophylls, chlorophyll *a* (419, 618, and 675 nm) and chlorophyll *c* (630 nm) greater in lightly shaded plots than where plots were either heavily shaded or unshaded. The absorption due to chlorophyll *a* at 675 nm was greatest in lightly shaded plots and smallest in heavily shaded plots, indicating that microphytobenthos biomass was increased in lightly shaded plots and decreased under more heavy shading. This agrees with the F_o and biochemically measured chlorophyll *a* data. These data do not indicate that pigments were responding differently between treatments at this time.

After 2 weeks in Gore Creek (experiment 2), there was little effect of shading on absorptions, with a small significant decrease in chlorophyll *a* (618 and 675 nm) under heavy shading, indicating a small decrease in microphytobenthos biomass. Again, there was no indication that pigments were responding differently between treatments.

After 3 months at Tambourine Bay (experiment 2) absorption by chlorophylls *a*, *b* and *c* (419, 424, and 471 nm) was so strong that the spectrum became flat and individual bands could not be easily resolved. This may explain why differences in absorption among treatments were smaller in this spectral region compared with other absorptions at longer wavelengths caused by the same pigments (compare chlorophyll *a* derivative reflectance at 419 nm with that at 675 nm in **Figure 5C**). The different amount and direction of responses in absorption at different wavelengths under different shading treatments suggests that as well as changes in microphytobenthos biomass, there may be some

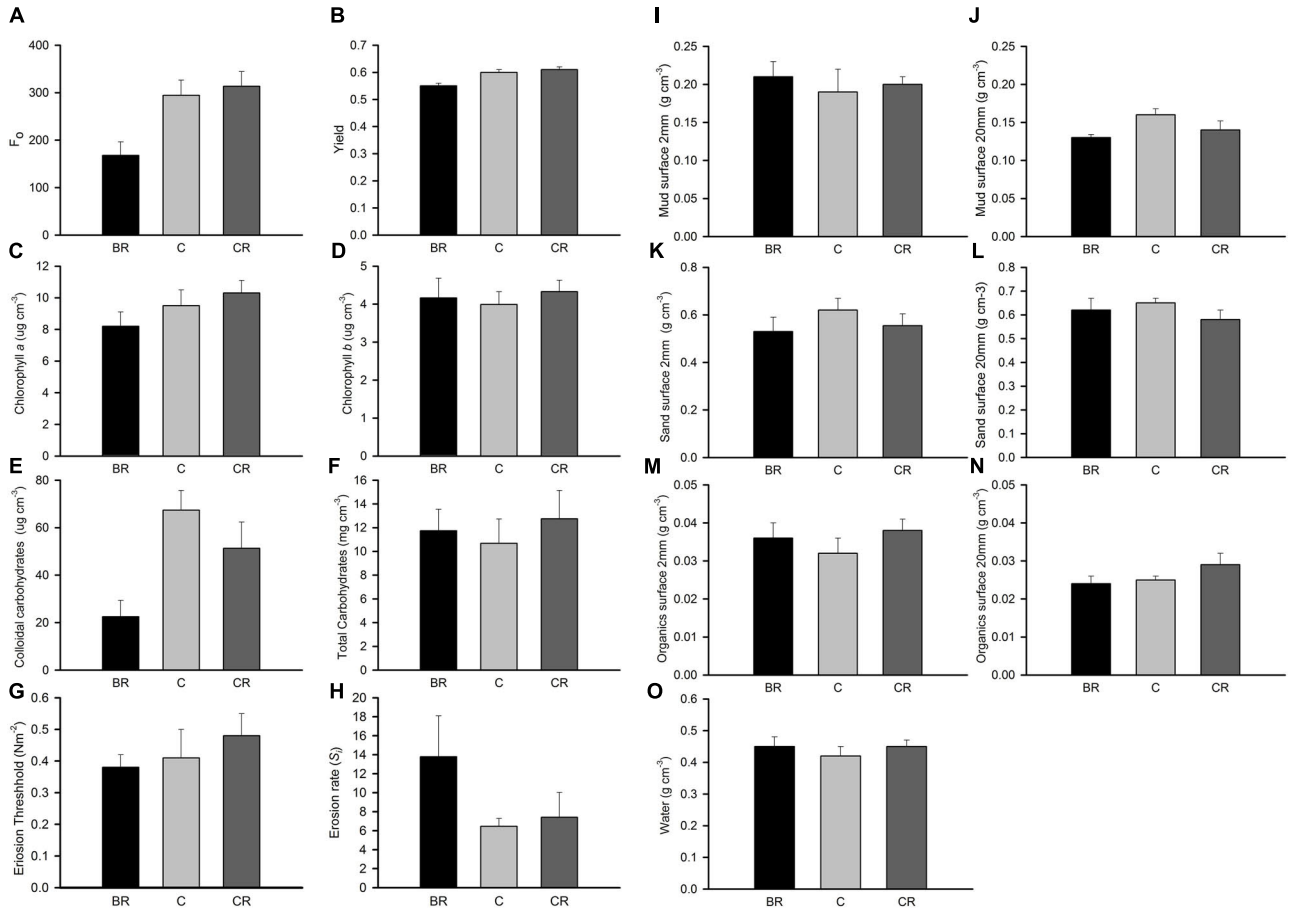

FIGURE 6 | Gore Creek properties of sediment after 2 weeks, mean (SE) for panel **(A)** F_o, **(B)** yield, **(C)** chlorophyll *a*, **(D)** chlorophyll *b*, **(E)** colloidal carbohydrates, **(F)** total carbohydrates, **(G)** erosion threshold, **(H)** erosion rate, **(I)** mud from 2 mm deep core, **(J)** mud from 20 mm deep core, **(K)** sand from 2 mm deep core, **(L)** sand from 20 mm deep core, **(M)** organics from 2 mm deep core, **(N)** organics from 20 mm deep core, and **(O)** water from 2 mm deep core. F_o and F_v/F_m measured with a PAM (unitless); erodibility measured with a CSM, erosion threshold (N m^{-2}), erosion rate (dimensionless); all other measures are mass density (wt per cm^{-3}).

TABLE 2 | Analyses of major components of fauna and selected properties of sediments in plots (P) subjected to Shading (Sh), with appropriate control treatment; experiment 2 at Tambourine Bay after 3 months; details in text.

(A)

Source	df	No. taxa	Fams. Poly.	Oligochaetes	Capitellids	Spionids	Sabellids	Nereidids	Amphipods	Nematodes	Bivalves
Sh	2	*	–	–	–	–	–	–	*	–	–
P(Sh)	15	–	*	–	*	–	–	**	*	–	**

(B)

Source	df	F_o	F_v/F_m	Chl. *a*	Chl. *b*	Coll. Carb	Total Carb.	Eros. thres.	Eros. rate
Sh	2	**	*	**	–	**	**	–	–
P(Sh)	15	***	*	***	***	**	–	–	–

(C)

Source	df	Mud (20 mm)	Mud (2 mm)	Sand (20 mm)	Sand (2 mm)	Organics (20 mm)	Organics (2 mm)	Water (2 mm)
Sh	2	–	–	**	*	–	–	*
P(Sh)	15	*	***	–	*	–	–	*

*2 samples from each of n = 6 replicate plots. Asterisks indicate significance, *p < 0.05, **p < 0.01, ***p < 0.001.*

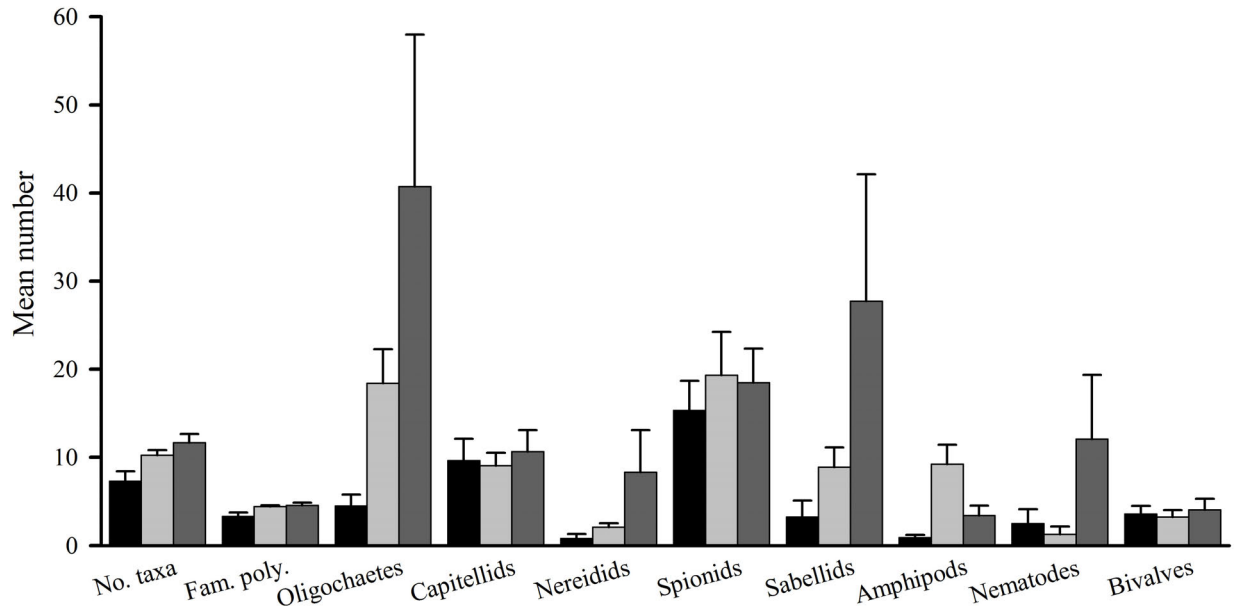

FIGURE 7 | Tambourine Bay macrofauna after 3 months. Mean (*SE*; $n = 6$ plots) number of taxa, families of polychaetes and abundance of oligochaetes, capitellids, nereidids, spionids, sabellids, amphipods, nematodes, and bivalves in heavily shaded plots with black roofs (black bars), lightly shaded plots with clear roofs (dark gray bars), and unshaded control plots (light gray bars).

physiological shifts in pigment composition and/or behavioral responses such as migration by diatoms and/or a change in the species composition of the microphytobenthos assemblage due to different amounts of shading. Directional changes in absorption due to chlorophyll *c* (630 nm) suggest that there might have been greater numbers of diatoms under lightly shaded conditions and fewer under heavily shaded conditions. This would support the interpretation that the increase in colloidal carbohydrates under light shading was due to microphytobenthos, because diatoms are known to secrete copious amounts of carbohydrates (Underwood and Smith, 1998; Paterson et al., 2000; Tolhurst et al., 2008) and removal of microphytobenthos with algaecide in these habitats causes significant reduction in colloidal carbohydrate (Murphy and Tolhurst, 2009).

When light levels are large, excess photosynthetic production, particularly in diatoms, is used to produce extracellular carbohydrates that can be utilized later, for example at night (Lancelot and Mathot, 1985; de Brouwer and Stal, 2002). The patterns in colloidal carbohydrate (heavy shading < unshaded controls < light shading) suggest that in heavily shaded plots there is a reduction in carbohydrate production and the utilization of available carbohydrates; when there is no shading there is less carbohydrate production compared to lightly shaded plots (possibly due to photoinhibition and/or high temperatures); whilst under light shading there is excess carbohydrate production. Measurements of the seasonal changes in microphytobenthos on these intertidal flats using spectroradiometry and PAM fluorescence demonstrated that microphytobenthos biomass increased in cooler months and decreased in warmer months (Murphy et al., 2009), suggesting that the effects of shading on microphytobenthos may be partially due to changes in temperature and moisture as well as altered light intensity.

It is possible that the fauna also affects the carbohydrates, most likely through total carbohydrates. For example, there were increased numbers of worms in unshaded sediment, which are known to secrete carbohydrates during construction of burrows (Meadows et al., 1990). However, whilst carbohydrates may be increased locally on burrow surfaces, the net effects of worms and other fauna tends to be a reduction in colloidal carbohydrates (Hu et al., 1995; de Deckere et al., 2001). Further work is required to elucidate causative relationships between the fauna and properties of the sediments, such as carbohydrates and how these relate to carbohydrate production from other sources, such as bacteria.

Both types of roof (levels of shading) tended to decrease the concentration of sand in the surface ∼2 mm of sediment, with a particularly large decrease after 3 months in lightly shaded sediment, accompanied by a concomitant increase in water (**Figure 8**). The concentration of mud, however, showed relatively small changes. The reduction in sand concentration and increase in water concentration means there was a shift to finer grained, less consolidated surface sediment under both types of roof after 3 months. This may represent a direct artifact of the roofs, e.g., by altering local hydrodynamics (there was evidence of this at Gore Creek after the storm) or an indirect effect, via changes in the microphytobenthos and fauna. Diatom biofilms are better at stabilizing finer sediment than coarser sediment (Fagherazzi et al., 2013), suggesting microphytobenthos preferentially trap fine sediment. The decreased amount of sand is thus consistent with both an artifact of the roofs on hydrodynamics, and an increased biomass of microphytobenthos.

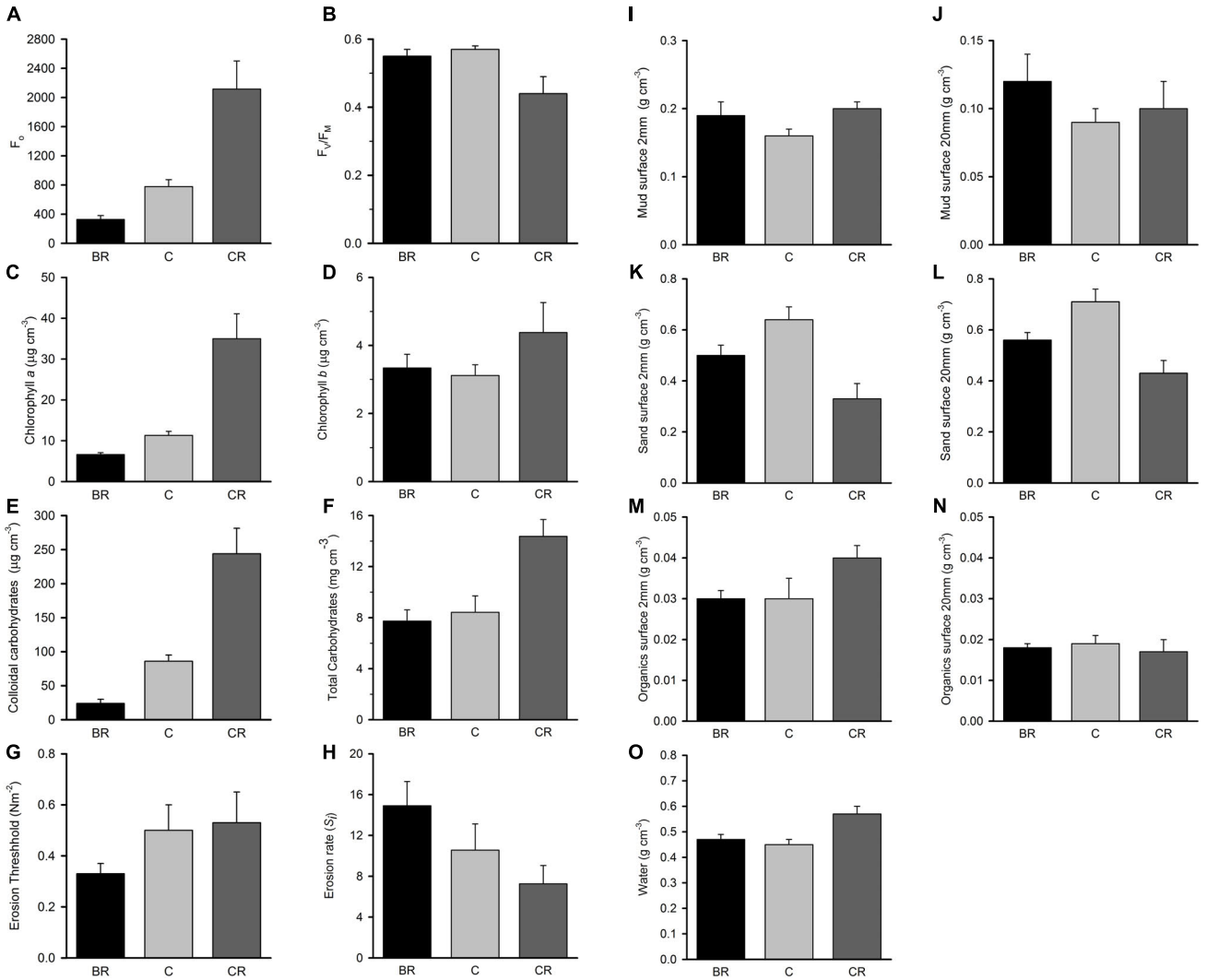

FIGURE 8 | Tambourine Bay properties of sediment after 3 months, mean (SE) for panel **(A)** F_o, **(B)** F_v/F_m, **(C)** chlorophyll *a*, **(D)** chlorophyll *b*, **(E)** colloidal carbohydrates, **(F)** total carbohydrates, **(G)** erosion threshold, **(H)** erosion rate, **(I)** mud from 2 mm deep core, **(J)** mud from 20 mm deep core, **(K)** sand from 2 mm deep core, **(L)** sand from 20 mm deep core, **(M)** organics from 2 mm deep core, **(N)** organics from 20 mm deep core, and **(O)** water from 2 mm deep core. F_o and F_v/F_m measured with a PAM (unitless); erodibility measured with a CSM, erosion threshold (N m^{-2}), erosion rate (dimensionless); all other measures are mass density (wt per cm^{-3}).

Despite considerable increases in microphytobenthos under light shading and decreases under heavy shading, there were only relatively minor changes in erosion threshold and relative erosion rate (S_i). This was surprising because microphytobenthos are known to stabilize sediments (Tolhurst et al., 2006a,b; Tolhurst et al., 2008). Similar limited effects on erodibility in response to shading have been found in work on the sandflats in Manukau Harbour (Harris et al., 2015). Directional responses were, however, generally consistent with the changes in microphytobenthos biomass and biostabilization, particularly for the relative erosion rate (S_i heavy shading > unshaded controls > light shading). The limited effect of shading on erodibility can be explained by consideration of the other sediment properties, changes in macrofauna and the nature of biostabilization. The large changes in amounts of sand, water and to a lesser extent mud suggest that there was a shift to finer grained, unconsolidated sediment under each type of roof, which would be less stable than the unshaded control sediment. These changes in the physical composition of the sediment would act in an antagonistic fashion to the stabilizing effect of the microphytobenthos. Oligochaetes were more abundant in lightly shaded sediment and less abundant in heavily shaded sediment and have been shown to significantly reduce algal biomass at the sediment surface (van Regteren et al., 2017), probably with cascading effects causing a reduction in sediment stability and increase in erodibility. Thus, an increase in oligochaetes would also act in an antagonistic fashion to the stabilizing effect of the microphytobenthos and could explain why the

effect of shading on microphytobenthos and related sediment properties were not as large as otherwise might be expected. Thus, the net effect of changes in physical properties, macrofauna and microphytobenthos are to increase sediment erodibility in heavily shaded conditions and generally decrease erodibility in lightly shaded conditions, although effects were generally small. Antagonistic effects and variability in the relative magnitude of the physical and biological contributions to erodibility would explain why the lightly shaded sediment is not always more stable than the unshaded sediment, despite the general increase in microphytobenthos in lightly shaded conditions. Finally, microphytobenthos do not always stabilize sediment (e.g., Sutherland et al., 1998; Tolhurst et al., 2008).

Effects of Shading on the Fauna

Despite clear effects of shading on the sediment, it had less effect on the fauna. Shading was predicted to increase abundances of amphipods and insect larvae and decrease abundances of oligochaetes and polychaetes in accordance with patterns of abundance found between unshaded mud and shaded mud under the canopy of the trees (Chapman and Tolhurst, 2004; Tolhurst and Chapman, 2007). In a mangrove forest in Thailand, manipulative experiments by Kon et al. (2010) showed species richness and abundance of epifauna increased in shaded treatments due to lower temperature and higher moisture.

After 2 weeks, there was no effect of shading on the entire assemblage in either location. There were, however, changes to individual taxa, some of which were as predicted. Heavy shading in experiment 1 at Tambourine Bay did not decrease abundance of all polychaetes, only reducing abundance of spionids and capitellids (**Figure 2**), which made up the majority of the worms. Oligochaetes were decreased in both shading treatments when nutrients were added and increased in both shading treatments when nutrients were not added, but increased in lightly shaded plots and unshaded plots in the procedural control for nutrient addition. This is difficult to explain. After 2 weeks in experiment 2 at Gore Creek, abundance of oligochaetes also decreased slightly in deeply shaded plots, as predicted, but increased under light shading (**Figure 3**). Spionids and capitellids are opportunistic taxa, with abundances that change rapidly in response to changes in resources (Levin, 1984). Because many small polychaetes are capable of dispersal through the water-column, the decrease in abundance may have been due to emigration or mortality. Spionids primarily live in temporary tubes, feeding across the surface of the mud around the tubes, whereas capitellids are shallow deposit-feeders. The decreases in capitellids and spionids under shade are likely to be a direct response to reduction of food; either the amount of microphytobenthos, or perhaps bacteria, or meiofauna.

After 3 months, there were significant changes in the faunal assemblage in deeply shaded plots compared to the other treatments. This was primarily due to large decreases in oligochaetes and sabellid polychaetes, but there was little change in the numbers of capitellids or spionids. In lightly shaded plots, abundance of oligochaetes, nereids, sabellids, and nematodes increased, which is opposite to what was predicted (Chapman and Tolhurst, 2004; Tolhurst and Chapman, 2007), although differences were not statistically significant due to the large variability in the data (**Figure 7**). Insect larvae and amphipods, predicted to increase in the shade, showed no significant change, suggesting that shading alone does not determine their natural patterns of abundance in mangroves. They are probably more influenced by other factors such as physical structure of mangrove plants or the distribution/amounts of leaf litter detritus (Chen and Ye, 2011), which can offer shelter and food.

Future Research

There is a wide variety of different types of natural and anthropogenic shading on intertidal flats, including persistent (e.g., docks, jetties, and mangrove canopy) and transient (moored boats, turbidity, and planktonic algal blooms), which vary spatially and temporally. This study shows that both light and heavy shading can significantly alter properties and processes at the sediment-water interface over a relatively short time period. Future studies should investigate how the different types, frequencies and duration of shade stress alter properties and processes on intertidal flats to identify specific thresholds or optimum conditions, with the ultimate goal of minimizing negative anthropogenic impacts to these environments.

CONCLUSION

Shading had major effects on microphytobenthos and related sediment properties, but patterns were not always as predicted and there was less of an effect on the macrofauna. Changes in the amount and intensity of shading of intertidal sediments, e.g., from anthropogenic (wharves, jetties etc.) or natural sources (mangrove forests) will alter various components of intertidal flat sediments, particularly microphytobenthos and associated properties. Changes in the microphytobenthos only caused small changes in sediment erodibility. Further research on the effects of shading on microphytobenthos, including detailed taxonomic analysis are required to determine the contributions of changes in biomass, species composition, photoinhibition, physiology, pigment composition and migration to the patterns found here. As shown in the current study, changes to the macrofauna are complex and variable, so before any environmental effects of increased shading on fauna can be understood, it is necessary to separate direct effects of shading on fauna from indirect effects, such as the changes to microphytobenthos or other resources. This requires appropriate experimental designs that can separate and measure the relative strengths of direct and indirect interactions between the biota and the sediment and the influence of external environmental conditions on these interactions. This is a major challenge for intertidal flat research.

DATA AVAILABILITY STATEMENT

The raw data supporting the conclusions of this article will be made available by the authors, without undue reservation, to any qualified researcher.

AUTHOR CONTRIBUTIONS

MC, TT, and RM conceptualized the study and designed the experiments. TT and RM participated in the field setup and sampling. MC analyzed the macrofauna data. TT analyzed the CSM, PAM, and biogeochemical data. RM analyzed the spectroradiometry data. TT, MC, and RM wrote the manuscript.

FUNDING

This study was funded by the Australian Research Council through their Special Research Centre programme, an ARC Discovery Grant (DP0559073), the Centre for Research on Ecological Impacts of Coastal Cities, and The University of Sydney. TT received additional support during writing from the University of East Anglia.

ACKNOWLEDGMENTS

Many research support staff in the Centre assisted in the field and laboratory, in particular C. Myers. The project has benefited from numerous discussions with A. J. Underwood and comments on the manuscript from A. Jackson.

REFERENCES

Able, K. W., Manderson, J. P., and Studholme, A. L. (1998). The distribution of shallow water juvenile fishes in an urban estuary: the effects of manmade structures in the lower Hudson river. *Estuaries* 21, 731–744.

Aguirre-Gomez, R., Weeks, A. R., and Boxall, S. R. (2001). The identification cation of phytoplankton pigments from absorption spectra. *Int. J. Remote Sens.* 22, 315–338. doi: 10.1080/014311601449952

Anderson, M. J. (2001). A new method for non-parametric multivariate analysis of variance. *Aust. Ecol.* 26, 32–46. doi: 10.1111/j.1442-9993.2001.01070.pp.x

Armitage, A. R., and Fong, P. (2004). Upward cascading effects of nutrients: shifts in a benthic microalgal community and a negative herbivore response. *Oecologia* 139, 560–567. doi: 10.1007/s00442-004-1530-6

Armitage, A. R., and Fong, P. (2006). Predation and physical disturbance by crabs reduce the relative impacts of nutrients in a tidal mudflat. *Mar. Ecol. Prog. Ser.* 313, 205–213. doi: 10.3354/meps313205

Bidigare, R. R., Morrow, J. H., and Kiefer, D. A. (1989). Derivative analysis of spectral absorption by photosynthetic pigments in the Western Sargasso Sea. *J. Mar. Res.* 47, 323–341. doi: 10.1357/002224089785076325

Birch, G. F., Cruickshank, B., and Davis, B. (2010). Modelling nutrient loads to Sydney estuary (Australia). *Environ. Monit. Assess.* 167, 333–348. doi: 10.1007/s10661-009-1053-z

Bishop, M. J., Mayer-Pinto, M., Airoldi, L., Firth, L. B., Morris, R. L., Loke, L. H. L., et al. (2017). Effects of ocean sprawl on ecological connectivity: impacts and solutions. *J. Exp. Mar. Biol. Ecol.* 492, 7–30. doi: 10.1016/j.jembe.2017.01.021

Black, K. S., Tolhurst, T. J., Paterson, D. M., and Hagerthey, S. E. (2002). Working with natural cohesive sediments. *J. Hydraul. Eng.* 128, 2–8. doi: 10.1061/(asce)0733-9429(2002)128:1(2)

Blockley, D. J. (2007). Effect of wharves on intertidal assemblages on seawalls in Sydney Harbour, Australia. *Mar. Environ. Res.* 63, 409–427. doi: 10.1016/j.marenvres.2006.10.007

Byers, J. E., and Grabowski, J. H. (2014). "Soft-sediment communities," in *Marine Community Ecology*, eds M. D. Bertness, J. F. Bruno, B. R. Silliman, and J. J. Stachowicz, (Sunderland, MA: Sinauer), 227–249.

Camilleri, J. C. (1992). Leaf-litter processing by invertebrates in a mangrove forest in Queensland. *Mar. Biol.* 114, 139–145.

Cartaxana, P., Cruz, S., Gameiro, C., and Kühl, M. (2016). Regulation of intertidal microphytobenthos photosynthesis over a diel emersion period is strongly affected by diatom migration patterns. *Front. Microbiol.* 7:872. doi: 10.3389/fmicb.2016.00872

Cebrián, J., Stutes, A. L., Phipps, S., Stutes, J. P., Christiaen, B., and Pennock, J. R. (2012). Effects of short-term sediment nutrient enrichment and grazer (*Neritina reclivata*) removal on sediment microalgae in a shallow eutrophic estuary (Alabama, USA). *Rev. Biol. Trop.* 60, 1687–1706.

Chapman, M. G. (1998). Relationships between spatial patterns of benthic assemblages in a mangrove forest using different levels of taxonomic resolution. *Mar. Ecol. Prog. Ser.* 162, 71–78. doi: 10.3354/meps162071

Chapman, M. G. (2003). Paucity of mobile species on constructed seawalls: effects of urbanization on biodiversity. *Mar. Ecol. Prog. Ser.* 264, 21–29. doi: 10.3354/meps264021

Chapman, M. G., Blockley, D., People, J., and Clynick, B. (2008). "Effect of urban structures on diversity of marine species," in *Ecology of Cities And Towns: A Comparative Approach*, eds M. McDonnell, J. Breuste, and A. K. Hahs, (Cambridge: Cambridge University Press), 156–176. doi: 10.1017/cbo9780511609763.010

Chapman, M. G., and Tolhurst, T. J. (2004). The relationship between invertebrate assemblages and bio-dependent properties of sediment in urbanized temperate mangrove forests. *J. Exp. Mar. Biol. Ecol.* 304, 51–73.

Chapman, M. G., and Tolhurst, T. J. (2007). Relationships between benthic macrofauna and biogeochemical properties of sediments at different spatial scales and among different habitats in mangrove forests. *J. Exp. Mar. Biol. Ecol.* 343, 96–109.

Chapman, M. G., Tolhurst, T. J., Murphy, R. J., and Underwood, A. J. (2010). Complex and inconsistent patterns of variation in benthos, micro-algae and sediment over multiple spatial scales. *Mar. Ecol. Prog. Ser.* 398, 33–47. doi: 10.3354/meps08328

Chapman, M. G., and Underwood, A. J. (2011). Evaluation of ecological engineering of "armoured" shorelines to improve their value as habitat. *J. Exp. Mar. Biol. Ecol.* 400, 302–311.

Chen, G. C., and Ye, Y. (2011). Restoration of *Aegiceras corniculatum* mangroves in Jiulongjiang Estuary changed macro-benthic faunal community. *Ecol. Eng.* 37, 224–228. doi: 10.1016/j.ecoleng.2010.10.003

Clarke, K. R. (1993). Non-parametric multivariate analyses of changes in community structure. *Aust. J. Ecol.* 18, 117–143. doi: 10.1111/j.1442-9993.1993.tb00438.x

Clynick, B. G., Chapman, M. G., and Underwood, A. J. (2008). Fish assemblages associated with urban structures and natural reefs in Sydney. *Australia. Aust. Ecol.* 33, 140–150. doi: 10.1111/j.1442-9993.2007.01802.x

de Brouwer, J. F. C., and Stal, L. J. (2002). Daily fluctuations of exopolymers in cultures of the benthic diatoms *Cylindrotheca closterium* and *Nitzschia* sp (Bacillariophyceae). *J. Phycol.* 38, 464–472. doi: 10.1046/j.1529-8817.2002.01164.x

de Deckere, E., Tolhurst, T. J., and de Brouwer, J. F. C. (2001). Destabilization of cohesive intertidal sediments by infauna. *Estuar. Coast. Shelf Sci.* 53, 665–669. doi: 10.1006/ecss.2001.0811

Defew, E. C., Paterson, D. M., and Hagerthey, S. E. (2002). The use of natural microphytobenthic assemblages as laboratory model systems. *Mar. Ecol. Prog. Ser.* 237, 15–25. doi: 10.3354/meps237015

Defew, E., Perkins, R., and Paterson, D. (2004). The influence of light and temperature interactions on a natural estuarine microphytobenthic assemblage. *Biofilms* 1, 21–30. doi: 10.1017/s1479050503001054

Demers, S., Roy, S., Gagnon, R., and Vignault, C. (1991). Rapid light-induced-changes in cell fluorescence and in Xanthophyll-cycle pigments of *Alexandrium excavatum* (Dinophyceae) and *Thalassiosira pseudonana* (Bacillariophyceae) - a photo-protection mechanism. *Mar. Ecol. Prog. Ser.* 76, 185–193. doi: 10.3354/meps076185

Douglas, E. J., Pilditch, C. A., Hines, L. V., Kraan, C., and Thrush, S. F. (2016). In situ soft sediment nutrient enrichment: a unified approach to eutrophication field experiments. *Mar. Poll. Bull.* 111, 287–294. doi: 10.1016/j.marpolbul.2016.06.096

Drylie, T. P., Lohrer, A. M., Needham, H. R., Bulmer, R. H., and Pilditch, C. A. (2018). Benthic primary production in emerged intertidal habitats provides resilience to high water column turbidity. *J. Sea Res.* 142, 101–112. doi: 10.1016/j.seares.2018.09.015

Dubois, M., Gilles, K. A., Hamilton, J. K., Rebers, P. A., and Smith, F. (1956). Colorimetric method for determination of sugars and related substances. *Anal. Chem.* 28, 350–356. doi: 10.1021/ac60111a017

Eriksson, B. K., Westra, J., van Gerwen, I., Weerman, E., van der Zee, E., van der Heide, T., et al. (2017). Facilitation by ecosystem engineers enhances nutrient effects in an intertidal system. *Ecosphere* 8:e02051. doi: 10.1002/ecs2.205

Fagherazzi, S., Fitzgerald, D. M., Fulweiler, R. W., Hughes, Z. J., Wiberg, P. L., McGlathery, K. J., et al. (2013). "12.13 ecogeomorphology of tidal flats," in *Treatise on Geomorphology*, ed. J. Shroder, (San Diego: Academic Press), 201–220. doi: 10.1016/b978-0-12-374739-6.00403-6

Firth, L. B., Knights, A. M., Bridger, D., Evans, A. J., Mieszkowska, N., Moore, P. J., et al. (2016). Ocean sprawl: challenges and opportunities for biodiversity management in a changing world. *Oceanogr. Mar. Biol.* 54, 193–269.

Gallagher, J. C., Wood, A. M., and Alberte, R. S. (1984). Ecotypic differentiation in the marine diatom *Skeletonema costatum* - Influence of light-intensity on the photosynthetic apparatus. *Mar. Biol.* 82, 121–134. doi: 10.1007/bf00394096

Gladstone-Gallagher, R. V., Lundquist, C. J., and Pilditch, C. A. (2014a). Mangrove (*Avicennia marina* subsp. australasica) litter production and decomposition in a temperate estuary. *New Zeal. J. Mar. Fresh. Res.* 48, 24–37. doi: 10.1080/00288330.2013.827124

Gladstone-Gallagher, R. V., Lundquist, C. J., and Pilditch, C. A. (2014b). Response of temperate intertidal benthic assemblages to mangrove detrital inputs. *J. Exp. Mar. Biol. Ecol.* 460, 80–88. doi: 10.1016/j.jembe.2014.06.006

Glasby, T. M., and Connell, S. D. (1999). Urban structures as marine habitats. *Ambio* 28, 595–598.

Grabowski, R. C., Droppo, I. G., and Wharton, G. (2011). Erodibility of cohesive sediment: the importance of sediment properties. *Earth Sci. Rev.* 105, 101–120. doi: 10.1016/j.earscirev.2011.01.008

Harris, R. J., Pilditch, C. A., Hewitt, J. E., Lohrer, A. M., Van Colen, C., Towsend, M., et al. (2015). Biotic interactions influence sediment erodibility on wave-exposed sandflats. *Mar. Ecol. Prog. Ser.* 523, 15–30. doi: 10.3354/meps11164

Hauxwell, J., Cebrian, J., and Valiela, I. (2003). Eelgrass *Zostera marina* loss in temperate estuaries: relationship to land-derived nitrogen loads and effect of light limitation imposed by algae. *Mar. Ecol. Prog. Ser.* 247, 59–73. doi: 10.3354/meps247059

Honeywill, C., Paterson, D. M., and Hagerthy, S. E. (2002). Determination of microphytobenthic biomass using pulse-amplitude modulated minimum fluorescence. *Eur. J. Phycol.* 37, 485–492. doi: 10.1017/s0967026202003888

Hu, S., Coleman, D. C., Hendrix, P. F., and Beare, M. H. (1995). Biotic manipulation effects on soil carbohydrates and microbial biomass in a cultivated soil. *Soil Biol. Biochem.* 27, 1127–1135. doi: 10.1016/0038-0717(95)00041-c

Hust, M., Krumbein, W. E., and Rhiel, E. (1999). An immunochemical in situ approach to detect adaptation processes in the photosynthetic apparatus of diatoms of the Wadden Sea sediment surface layers. *J. Microbiol. Methods* 38, 69–80. doi: 10.1016/s0167-7012(99)00077-9

Jeffrey, S. W., Wright, S. W., and Zapata, M. (1999). Recent advances in HPLC pigment analysis of phytoplankton. *Mar. Freshwat. Res.* 50, 879–896.

Jesus, B., Perkins, R. G., Mendes, C. R., Brotas, V., and Paterson, D. M. (2006). Chlorophyll fluorescence as a proxy for microphytobenthic biomass: alternatives to the current methodology. *Mar. Biol.* 150, 17–28. doi: 10.1007/s00227-006-0324-2

Kamruzzaman, M. D., Basak, K., Paul, S. K., Ahmed, S., and Osawa, A. (2019). Litterfall production, decomposition and nutrient accumulation in Sundarbans mangrove forests, Bangladesh. *Forest Sci. Technol.* 15, 24–32. doi: 10.1080/21580103.2018.1557566

Kon, K., Kurokura, H., and Tongnunui, P. (2010). Effects of the physical structure of mangrove vegetation on a benthic faunal community. *J. Exp. Mar. Biol. Ecol.* 383, 171–180. doi: 10.1016/j.jembe.2009.11.015

Kon, K., Kurokura, H., and Tongnunui, P. (2011). Influence of a microhabitat on the structuring of the benthic macrofaunal community in a mangrove forest. *Hydrobiologia* 671, 205–216. doi: 10.1007/s10750-011-0718-0

Lancelot, C., and Mathot, S. (1985). Biochemical fractionation of primary production by phytoplankton in Belgian coastal waters during short-term and long-term incubations with C-14C Bicarbonate. 1. Mixed diatom populations. *Mar. Biol.* 86, 219–226. doi: 10.1007/bf00397507

Lee, S. Y. (1999). Tropical mangrove ecology: physical and biotic factors influencing ecosystem structure and function. *Aust. J. Ecol.* 24, 355–366. doi: 10.1046/j.1442-9993.1999.00984.x

Lee, S. Y. (2008). Mangrove macrobenthos: assemblages, services, and linkages. *J. Sea Res.* 59, 16–29. doi: 10.1016/j.seares.2007.05.002

Levin, L. A. (1984). Life-history and dispersal patterns in a dense infaunal polychaete assemblage - Community structure and response to disturbance. *Ecology* 65, 1185–1200. doi: 10.2307/1938326

Lundkvist, M., Grue, M., Friend, P. L., and Flindt, M. R. (2007). The relative contributions of physical and microbiological factors to cohesive sediment stability. *Cont. Shelf Res.* 27, 1143–1152. doi: 10.1016/j.csr.2006.01.021

Markich, S. J., and Jeffree, R. A. (2019). Physico-chemical and key metal data for surface waters and sediments of the Sydney and Hawkesbury estuaries, Australia. *Data Brief* 252, 813–824. doi: 10.1016/j.dib.2019.104255

Meadows, P. S., Tait, J., and Hussain, S. A. (1990). Effects of estuarine infauna on sediment stability and particle sedimentation. *Hydrobiologia* 190, 263–266. doi: 10.1007/bf00008194

Miller, L. P., and Gaylord, B. (2007). Barriers to flow: the effects of experimental cage structures on water velocities in high-energy subtidal and intertidal environments. *J. Exp. Mar. Biol. Ecol.* 344, 215–228. doi: 10.1016/j.jembe.2007.01.005

Millie, D. F., Paerl, H. W., and Hurley, J. P. (1993). Microalgal pigment assessments using high-performance liquid chromatography - a synopsis of organismal and ecological applications. *Can. J. Fish. Aquat. Sci.* 50, 2513–2527. doi: 10.1139/f93-275

Morris, L., and Keough, M. J. (2003). Variation in the response of intertidal infaunal invertebrates to nutrient additions: field manipulations at two sites within Port Phillip Bay, Australia. *Mar. Ecol. Prog. Ser.* 250, 35–49. doi: 10.3354/meps250035

Morrisey, D. J., Swales, A., Dittmann, S., Morrison, M. A., Lovelock, C. E., and Beard, C. M. (2010). The ecology and management of temperate mangroves. *Oceanogr. Mar. Biol.* 48, 43–60.

Munsch, S. H., Cordell, J. R., Toft, J. D., and Morgan, E. E. (2014). Effects of seawalls and piers on fish assemblages and juvenile salmon feeding behavior. *N. Am. J. Fish. Manag.* 34, 814–827. doi: 10.1080/02755947.2014.910579

Murphy, R. J., and Tolhurst, T. J. (2009). Effects of experimental manipulation of algae and fauna on the properties of intertidal soft sediments. *J. Exp. Mar. Biol. Ecol.* 379, 77–84. doi: 10.1016/j.jembe.2009.08.005

Murphy, R. J., Tolhurst, T. J., Chapman, M. G., and Underwood, A. J. (2005a). Estimation of surface chlorophyll-a on an emersed mudflat using field spectrometry: accuracy of ratios and derivative-based approaches. *Int. J. Remote Sens.* 26, 1835–1859. doi: 10.1080/01431160512331326530

Murphy, R. J., Tolhurst, T. J., Chapman, M. G., and Underwood, A. J. (2005b). Remote-sensing of benthic chlorophyll: should ground-truth data be expressed in units of area or mass? *J. Exp. Mar. Biol. Ecol.* 316, 69–77. doi: 10.1016/j.jembe.2004.10.006

Murphy, R. J., Tolhurst, T. J., Chapman, M. G., and Underwood, A. J. (2009). Seasonal distribution of chlorophyll on mudflats in New South Wales, Australia measured by field spectrometry and PAM fluorometry. *Estuar. Coast. Shelf Sci.* 84, 108–118. doi: 10.1016/j.ecss.2009.06.003

Murphy, R. J., Underwood, A. J., Tolhurst, T. J., and Chapman, M. G. (2008). Field-based remote-sensing for experimental intertidal ecology: case studies using hyperspatial and hyperspectral data for New South Wales (Australia). *Remote Sens. Environ.* 112, 3353–3365. doi: 10.1016/j.rse.2007.09.016

Paterson, D. M., Tolhurst, T. J., Kelly, J. A., Honeywill, C., de Deckere, E. M. G. T., Huet, V., et al. (2000). Variations in sediment properties, Skeffling mudflat, Humber Estuary, UK. *Cont. Shelf Res.* 20, 1373–1396. doi: 10.1016/s0278-4343(00)00028-5

Perkins, R. G., Honeywill, C., Consalvey, M., Austin, H. A., Tolhurst, T. J., and Paterson, D. M. (2003). Changes in microphytobenthic chlorophyll *a* and EPS resulting from sediment compaction due to dewatering: opposing patterns in concentration and content. *Cont. Shelf Res.* 23, 575–586. doi: 10.1016/s0278-4343(03)00006-2

Perkins, R. G., Lavaud, J., Serôdio, J., Mouget, J.-L., Cartaxana, P., Rosa, P., et al. (2010). Vertical cell movement is a primary response of intertidal benthic

biofilms to increasing light dose. *Mar. Ecol. Prog. Ser.* 416, 93–103. doi: 10.3354/meps08787

Porra, R. J., Thompson, W. A., and Kriedemann, P. E. (1989). Determination of accurate extinction coefficients and simultaneous-equations for assaying Chlorophyll *a* and Chlorophyll *b* extracted with 4 different solvents - Verification of the concentration of Chlorophyll standards by atomic-absorption spectroscopy. *Biochim. Biophys. Acta* 975, 384–394. doi: 10.1016/s0005-2728(89)80347-0

Pratt, D. R., Lohrer, A. M., Thrush, S. F., Hewitt, J. E., Townsend, M., Cartner, K., et al. (2015). Detecting subtle shifts in ecosystem functioning in a dynamic estuarine environment. *PLoS One* 10:e0133914. doi: 10.1371/journal.pone.0133914

Raffaelli, D. (1999). Nutrient enrichment and trophic organisation in an estuarine food web. *Acta Oecol.* 20, 339–461.

Rossi, F. (2006). Small-scale burial of macroalgal detritus in marine sediments: effects of *Ulva* spp. on the spatial distribution of macrofauna assemblages. *J. Exp. Mar. Biol. Ecol.* 332, 84–95. doi: 10.1016/j.jembe.2005.11.003

Saintilan, N., and Williams, R. J. (1999). Mangrove transgression into saltmarsh environments in south-east Australia. *Glob. Ecol. Biogeog.* 8, 117–124. doi: 10.1046/j.1365-2699.1999.00133.x

Sanger, D. M., Holland, A. F., and Gainey, C. (2004). Cumulative impacts of dock shading on *Spartina alterniflora* in South Carolina estuaries. *Environ. Manage.* 33, 741–748.

Saunders, R. J., and Connell, S. D. (2001). Interactive effects of shade and surface orientation on the recruitment of spirorbid polychaetes. *Aust. Ecol.* 26, 109–115. doi: 10.1111/j.1442-9993.2001.01090.pp.x

Savitzky, A., and Golay, M. J. E. (1964). Smoothing and differentiation of data by simplified least squares procedures. *Analyt. Chem.* 36, 1627–1639. doi: 10.1021/ac60214a047

Smith, C. M., and Alberte, R. S. (1994). Characterization of in-vivo absorption features of Chlorophyte, Phaeophyte and Rhodophyte algal species. *Mar. Biol.* 118, 511–521. doi: 10.1007/bf00350308

Stutes, A. L., Cebrian, J., and Corcoran, A. A. (2006). Effects of nutrient enrichment and shading on sediment primary production and metabolism in eutrophic estuaries. *Mar. Ecol. Prog. Ser.* 312, 29–43. doi: 10.3354/meps312029

Sutherland, T. F., Grant, J., and Amos, C. L. (1998). The effect of carbohydrate production by the diatom *Nitzschia curvilineata* on the erodibility of sediment. *Limnol. Oceanogr.* 43, 65–72.

Takada, Y. (1999). Influence of shade and number of boulder layers on mobile organisms on a warm temperate boulder shore. *Mar. Ecol. Prog. Ser.* 189, 171–179.

Thompson, R. C., Norton, T. A., and Hawkins, S. J. (2004). Physical stress and biological control regulate the producer-consumer balance in intertidal biofilms. *Ecology* 85, 1372–1382.

Thrush, S. F., Hewitt, J. E., Parkes, S., Lohrer, A. M., Pilditch, C., Woodin, S. A., et al. (2014). Experimenting with ecosystem interaction networks in search of threshold potentials in real-world marine ecosystems. *Ecology* 95, 1451–1457.

Tolhurst, T. J., Black, K. S., and Paterson, D. M. (2009). Muddy sediment erosion: insights from field studies. *J. Hydraul. Eng.* 135, 73–87.

Tolhurst, T. J., Black, K. S., Shayler, S. A., Mather, S., Black, I., Baker, K., et al. (1999). Measuring the in situ erosion shear stress of intertidal sediments with the cohesive strength meter (CSM). *Est. Coast. Shelf Sci.* 49, 281–294.

Tolhurst, T. J., and Chapman, M. G. (2005). Spatial and temporal variation in the sediment properties of an intertidal mangrove forest: implications for sampling. *J. Exp. Mar. Biol. Ecol.* 317, 213–222.

Tolhurst, T. J., and Chapman, M. G. (2007). Patterns in biogeochemical properties of sediments and benthic animals among different habitats in mangrove forests. *Aust. Ecol.* 32, 775–788.

Tolhurst, T. J., Consalvey, M., and Paterson, D. M. (2008). Changes in cohesive sediment properties associated with the growth of a diatom biofilm. *Hydrobiologia* 596, 225–239.

Tolhurst, T. J., Defew, E. C., de Brouwer, J. F. C., Wolfstein, K., Stal, L. J., and Paterson, D. M. (2006a). Small-scale temporal and spatial variability in the erosion threshold and properties of cohesive intertidal sediments. *Cont. Shelf Res.* 26, 351–362.

Tolhurst, T. J., Defew, E. C., and Dye, A. (2010). Lack of correlation between surface macrofauna, meiofauna, erosion threshold and biogeochemical properties of sediments within an intertidal mudflat and mangrove forest. *Hydrobiologia* 652, 1–13.

Tolhurst, T. J., Defew, E. C., Perkins, R. G., Sharples, A., and Paterson, D. M. (2006b). The effects of tidally-driven temporal variation on measuring intertidal cohesive sediment erosion threshold. *Aquat. Ecol.* 40, 521–531.

Tolhurst, T. J., Underwood, A. J., Perkins, R. G., and Chapman, M. G. (2005). Content versus concentration: effects of units of measuring the biogeochemical properties of soft sediments. *Est. Coast. Shelf Sci.* 63, 665–673.

Underwood, A. J. (1997a). *Experiments in Ecology: Their Logical Design and Interpretation Using Analysis of Variance*. Cambridge: Cambridge University Press.

Underwood, A. J., Chapman, M. G., and Connell, S. D. (2000). Observations in ecology: you can't make progress on processes without understanding the patterns. *J. Exp. Mar. Biol. Ecol.* 250, 97–115.

Underwood, G. J. C. (1997b). Microalgal colonization in a saltmarsh restoration scheme. *Estuar. Coast. Shelf Sci.* 44, 471–481.

Underwood, G. J. C., and Smith, D. J. (1998). Predicting epipelic diatom exopolymer concentrations in intertidal sediments from sediment chlorophyll. *Microb. Ecol.* 35, 116–125.

Van Colen, C., Thrush, S. F., Parkes, S., Harris, R., Woodin, S. A., Wethey, D. S., et al. (2015). Bottom–up and top–down mechanisms indirectly mediate interactions between benthic biotic ecosystem components. *J. Sea Res.* 98, 42–48.

van Leeuwe, M. A., Brotas, V., Consalvey, M., Forster, R. M., Gillespie, D., Jesus, B., et al. (2008). Photoacclimation in microphytobenthos and the role of xanthophyll pigments. *Eur. J. Phycol.* 43, 123–132.

van Regteren, M., Ten Boer, R., Meesters, E. H., and De Groot, A. V. (2017). Biogeomorphic impact of oligochaetes (Annelida) on sediment properties and *Salicornia* spp. seedling establishment. *Ecosphere* 8:e01872. doi: 10.1002/ecs2.1872

Vardy, S., Saunders, J. E., Tolhurst, T. J., Davies, P. A., and Paterson, D. M. (2007). Calibration of the high-pressure cohesive strength meter (CSM). *Cont. Shelf Res.* 27, 1190–1199.

Whitcraft, C. R., and Levin, L. A. (2007). Regulation of benthic algal and animal communities by salt marsh plants: impact of shading. *Ecology* 88, 904–917.

Whitfield, A., and Elliot, M. (2011). "Ecosystem and biotic classifications of estuaries and coasts," in *Treatise on Estuarine and Coastal Science*, Vol. 1, eds E. Wolanski, and D. McLusky, (Amsterdam: Elsevier), 99–124.

Wiens, J. A. (1976). Population responses to patchy environments. *Ann. Rev. Ecol. Syst.* 7, 81–120.

Williams, G. A. (1994). The relationship between shade and molluscan grazing in structuring communities on a moderately-exposed tropical rocky shore. *J. Exp. Mar. Biol. Ecol.* 178, 79–95.

Young, A., and Britton, G. (1990). "Carotenoids and stress," in *Stress Responses in Plants: Adaptation and Acclimation Mechanisms*, eds R. G. Alscher, and J. R. Cumming, (New York, NY: Wiley-Liss), 87–112.

Conflict of Interest: The authors declare that the research was conducted in the absence of any commercial or financial relationships that could be construed as a potential conflict of interest.

frontiers in Marine Science

ORIGINAL RESEARCH
published: 29 May 2020
doi: 10.3389/fmars.2020.00381

Photoacclimation to Constant and Changing Light Conditions in a Benthic Diatom

Filip Pniewski and Iwona Piasecka-Jędrzejak*

Institute of Oceanography, University of Gdańsk, Gdynia, Poland

Photoacclimation to constant and changing light conditions was studied in the benthic diatom *Nitzschia* cf. *aurariae* isolated from the littoral zone of the Baltic Sea. The diatom was grown under a wide range of irradiances, i.e., 15–350 μmol photons m^{-2} s^{-1} with the photoperiod of 16 h of light and 8 h of darkness. In the first experiment, three levels of a constant light were applied, i.e., 30, 115, and 350 μmol photons m^{-2} s^{-1}. In the second experiment, the diatom was exposed to two ranges of changing light conditions, i.e., the lower-range of variable light, i.e., 15–30–150 μmol photons m^{-2} s^{-1}, and the higher-range of variable light, i.e., 30–60–350 μmol photons m^{-2} s^{-1}. The cellular content of photosynthetic (chlorophyll *a* and fucoxanthin), as well as photoprotective pigments (diadinoxanthin and diatoxanthin), was determined by the total daily light doses. The de-epoxidation state of the xanthophyll cycle reached higher values in cultures maintained under variable light regimes. The analysis of photosynthesis-irradiance curves suggested that *N.* cf. *aurariae* acclimated primarily through the changes in the number of photosynthetic units (PSU). Higher photosynthetic rates observed under variable irradiance indicated the maximization of photosynthesis at lower light intensities. In constant high light, the diatom accumulated more photoprotective pigments, however, the activity of the xanthophyll cycle was limited. Under variable light regimes wide changes in the de-epoxidation state allowed for efficient photoprotection, depending on the light intensities applied. Photoprotection appeared to represent an interplay between long-term photoacclimation and rapid adjustment to ambient light conditions within the constraints set by the former. Prolonged exposure to high light caused a decrease in photosynthetic rates. However, the stable growth of the diatom across the applied light intensities showed that it can survive periods of potentially stressful light conditions. Acclimation mechanisms observed in the studied diatom were consistent with those observed in microalgae present in habitats characterized by high irradiance and rapid changes in light conditions.

Keywords: photoacclimation, photosynthetic units, photosynthesis-irradiance curves, photosynthetic pigments, diatoms, Baltic

OPEN ACCESS

Edited by:
João Serôdio,
University of Aveiro, Portugal

Reviewed by:
Johann Lavaud,
Centre National de la Recherche Scientifique (CNRS), France
Torsten Jakob,
Leipzig University, Germany

****Correspondence:***
Filip Pniewski
filip.pniewski@ug.edu.pl

Specialty section:
This article was submitted to Marine Ecosystem Ecology, a section of the journal Frontiers in Marine Science

Received: *15 October 2019*
Accepted: *04 May 2020*
Published: *29 May 2020*

Citation:
Pniewski F and Piasecka-Jędrzejak I (2020) Photoacclimation to Constant and Changing Light Conditions in a Benthic Diatom. Front. Mar. Sci. 7:381. doi: 10.3389/fmars.2020.00381

INTRODUCTION

Microphytobenthos is a collection of photosynthetic organisms inhabiting various substrata in shallow aquatic environments, with diatoms being the most prominent algal group (Round, 1981). It is a key player in marine ecosystems as it may be responsible for a considerable proportion of the primary production (Blanchard and Cariou-Le Gall, 1994). Microphytobenthos facilitates the biogeochemical cycling of major nutrients and mediates their fluxes at the water-sediment surface (Sundbäck et al., 2006). It also stabilizes sediments, and due to resuspension is an important food source not only to benthic but also pelagic organisms (Sutherland et al., 1998; Lucas et al., 2001; Saint-Béat et al., 2014).

Microphytobenthos is subjected to a wide and often, rapid variations in ecological variables with light being a crucial factor. Light drives and dictates its photosynthetic processes and thus governs its species composition, biomass distribution, and productivity (e.g., MacIntyre et al., 1996; Underwood, 2005). The underwater light field strongly differs from that of terrestrial habitats, as the light intensity can be a few orders of magnitude lower, and its spectral composition can be altered by the water quality (Depauw et al., 2012). In marine environments, light depends on incident solar radiation, seasons, the time of day and atmospheric conditions, such as cloud cover, mist, and pollution, etc. Light passing through water is attenuated due to the absorptive and scattering water properties caused by water itself, the presence of dissolved organic matter and suspended particles (Dring, 1998). The movement of water due to tides and wind-induced waves, also influences light conditions. Tides reduce light intensity through sediment resuspension, while waves cause rapid focusing and defocusing of light (caustic light), resulting in flashes of extremely high light. Sediment granulometry also influences light conditions; in muddy sediments, light is fully attenuated at a depth of a fraction of a millimeter, and in sandy sediments it can penetrate deeper, up to several millimeters (Kühl et al., 1994; Cartaxana et al., 2011).

Being exposed to such extreme irradiance changes, microphytobenthos require complex adaptive mechanisms maximizing the rate of photosynthesis and CO_2 fixation under limiting light conditions, whilest minimizing the damage induced by high light intensities. The balance between these processes is achieved through numerous photoacclimatory and photoprotective mechanisms, spanning various time scales (e.g., Depauw et al., 2012). Short-term regulation of photosynthesis is a reversible process, which enables immediate tracking of changes in the light intensity (Raven and Geider, 2003). For example, the activity of Rubisco accounts for the variations in maximum photosynthetic rates (MacIntyre et al., 2000). Whereas the xanthophyll cycle, which is based on covalent changes in the chromatophores, alters the capacity to quench the excitation energy by down-regulating PSII activity, and thus limits possible photo-damage (Goss et al., 2006). Long-term acclimation, on the other hand, requires altering the gene expression, manifested in the changes of the photosynthetic apparatus (Eberhard et al., 2008). Falkowski and Owens (1980) divided long-term acclimation responses into two categories, namely: a photoacclimation strategy, involving a change in the number of photosynthetic units (PSU) and a strategy, in which light acclimation is accomplished by altering the size of PSU.

The shallow and essentially non-tidal coastal areas of the Baltic Sea provide favorable conditions for the development of microphytobenthos (usually below <1 m depth). Sandy sediments promote the growth of epipsammic species, which tend to be small, with no or strongly limited ability to move (unlike epipelic species, which conversely, are large and motile). As a result epipsammon photo-regulates relying on its physiology (e.g., Cartaxana et al., 2011). In the Baltic Sea, diatoms may constitute up to 60% of the epipsammon biomass, therefore, to understand their ecological dominance, this study investigated the photosynthetic activity of the benthic diatom *Nitzschia* cf. *aurariae* Cholnoky 1966, a typical representative of the Baltic epipsammic communities (Pniewski et al., 2015). The main goal was to assess the effect of variable light conditions on the *N.* cf. *aurariae* long-term photoacclimation and photoprotection. In order to do so the diatom was grown under different light regimes, i.e., in constant and in changing light, the photo-regulation mechanisms and the activity of the xanthophyll cycle were examined through the analyses of changes in (1) pigment composition, (2) the shape of photosynthesis vs. light (P-E) curves and (3) variable fluorescence (the maximum quantum yield of photosystem II and the non-photochemical quenching).

MATERIALS AND METHODS

Diatom Culture and Experimental Conditions

The study was carried out on the benthic diatom *N.* cf. *aurariae* isolated from the sediment samples collected in Puck Bay located in the southern part of the Baltic Sea, in the proximity of Władysławowo (54°43′N, 18°34′E). The strain (BA 156) is maintained as a unialgal culture in the Culture Collection of the Baltic Algae (CCBA) at the Gdańsk University, and it is grown in the f/2 medium (Guillard, 1975) prepared from Baltic seawater (with salinity of ca. 6.7), at 50 μmol photons m^{-2} s^{-1} and 17°C (**Figure 1**). *N.* cf. *aurariae* belongs to rather small-size diatoms [10.8-(11.6)-12.6 μm long, and 2.9-(3.4)-4 μm broad, n = 30, in brackets the average value is provided]. It is a widespread cosmopolitan species, commonly occurring in the Baltic Sea (Witkowski et al., 2000).

Experiments were conducted with cultures grown in 100 ml Erlenmeyer flask filled with 50 ml of the f/2 medium (Guillard, 1975) prepared from artificial seawater with salinity of 7, which were kept in a growth chamber at the constant temperature of 17°C. The cultures were grown for 7 days until they reached the exponential growth phase under three different light regimes, i.e., constant light (CL) and two variable light regimes (VL). Under constant light conditions, three different levels of light were applied, i.e., 30 (low light, LL), 115 (medium light, ML), and 350 (high light, HL) μmol photons m^{-2} s^{-1}. Under variable light, the irradiance was increased automatically from the lowest to the highest level of light at fixed time intervals; after a period of darkness, the samples were illuminated with the lowest level

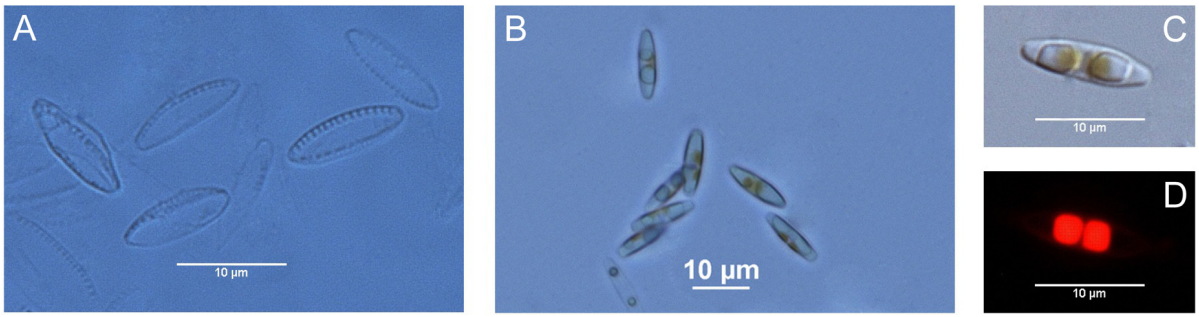

FIGURE 1 | Morphological characteristics of *N.* cf. *aurariae*, frustuls mounted in Naphrax **(A)**, living cells observed under 40x **(B)** and 100x oil immersion objective **(C)**, epifluorescence microscopy of chloroplasts **(D)**.

of light for 3 h, after which the light was increased to reach the medium light intensity for another 3 h, and then the highest light was applied for 4 h. Subsequently, the light intensity was decreased in the reversed order at the same time intervals. In the first variant of variable light regimes, i.e., the lower range (LRVL – lower-range variable light), the following set of light intensities was applied, 15 (low light), 30 (medium light), and 150 (high light) µmol photons m^{-2} s^{-1}, whereas in the second one, the higher range (HRVL – higher-range variable light), these were 30 (low light), 60 (medium light), and 350 (high light) µmol photons m^{-2} s^{-1} (**Supplementary Figure S1**). For each light regime, a photoperiod of 16 h of light and 8 h of darkness was used. Illumination was provided with a set of fluorescent lamps Philips TLD 36 W emitting cool white light. At each applied light level, measurements were performed after an hour of illumination. The oxygen evolution measurements were repeated at 1-h intervals. All measurements were performed on independent biological samples.

Growth Rates

The growth of the diatoms was monitored by cell count using a hemocytometer with the Bürker grid. Specific growth rates (µ, d^{-1}) were calculated according to the equation provided by Fogg and Thake (1987).

Photosynthetic Pigments Analysis

Five millimeter aliquots of cell suspension were taken and filtered through GF/C Whatman glass filters (25 mm diameter) under low vacuum and then frozen and stored at −20°C until further analysis. Pigments were extracted using 4 ml of cold 90% acetone (HPLC grade) at −20°C for 4 h (Strickland and Parsons, 1972). Subsequently, extracts were centrifuged (7000 rpm, 10 min) and filtered through PTFE filters. Pigments were separated with the Waters liquid chromatograph comprising a double pump (Waters 515) system and equipped with the Diode Array Detector 440 (set at 440 nm). Pigment separation was performed using reverse phase chromatography (RP-HPLC) (250 × 4.6 mm LiChrospher 100, octadecylsilica bonded phase with the particle size of 5 µm) following optimized analytical gradient protocol provided by Pniewski (2020). The HPLC system was calibrated using high purity pigment standards purchased from The International Agency for 14C Determination DHI Institute for Water and Environment in Denmark. Pigments were identified from their absorbance spectra and retention times and quantified according to the procedure described by Mantoura and Repeta (1997).

Photosynthesis vs. Irradiance (P-E) Curves

After a 7-day cultivation period, the final concentration of chlorophyll *a* (Chl*a*) reached 2.00 ± 0.3, 0.91 ± 0.07, 1.0 ± 0.17, 2.21 ± 0.15, 2.12 ± 0.04 mg l^{-1} at LL, ML, HL, LRVL, and HRVL, respectively. Net oxygen evolution was performed using the Chlorolab 2 system equipped with the DW2/2 liquid-phase chamber unit with an integral oxygen electrode (Hansatech, Norfolk, United Kingdom) (Hansatech, Norfolk, United Kingdom). The system was kept at a constant temperature of 17°C by connecting it to a circulating water bath (Julabo Labortechnik, Seelbach, Germany). Light was provided by LH11/2R high-intensity red LED probe with the maximum light value of 1700 µmol photons m^{-2} s^{-1}, which was measured with a Quantitherm Light meter (Hansatech, Norfolk, United Kingdom) placed inside the DW2/2 chamber. Polarographic measurements were performed using 2 ml cell suspension aliquots. P-E curves were constructed by measuring oxygen production rates at 10 stepwise increments of light each of which was applied for 5 min (11, 40, 85, 145, 225, 450, 650, 990, 1385, and 1700 µmol photons m^{-2} s^{-1}). Dark respiration was measured for 10 min prior to the constructing of the light curve. Oxygen evolution rates were expressed per cell and Chl*a* unit. Subsequently, the model provided by Platt et al. (1980) was mathematically fitted to the obtained data in order to estimate photosynthetic parameters, i.e., the maximum photosynthetic capacity (GP_{max}), the maximum photosynthetic efficiency (α) and the light saturation index ($E_k = GP_{max}/\alpha$).

Fluorescence Measurements

Chl*a* variable fluorescence was measured using a computer-operated FMS1 system (Hansatech, Norfolk, United Kingdom) equipped with an amber light (594 nm) emitting diode to excite fluorescence and a PIN-photodiode with $l > 700$ nm filter to detect it. An internal halogen lamp (8 V/20 W) was the source

of actinic and saturating light. All measurements were performed with a 5.5-mm-diameter Fiberoptic kept perpendicular to the sample placed in the temperature-controlled DW2/2 chamber at a constant distance of 4 mm.

The cell suspension subsamples were harvested at an exponential growth phase and filtered onto Whatman GF/C filters under low vacuum (Jesus et al., 2006). Next, small subsamples were cut out from the filter, placed onto a small plastic base, and put into a DW2/2 chamber (Hansatech, Norfolk, United Kingdom) and filled with the medium in which the cells were grown. Prior to each measurement, samples were dark-adapted for 15 min. Next, a pulse of saturating light (SP > 3500 μmol photons m^{-2} s^{-1} for 400 ms) was applied to measure minimum (F_o) and maximum fluorescence (F_m) in the dark-adapted state, then the maximum quantum yield of photosystem II (PSII) [$F_v/F_m = (F_m - F_o)/F_m$] was calculated (Schreiber, 2004). Subsequently, actinic light (AL) of an intensity matching growth irradiance was applied. Once the steady-state was achieved, usually within 8 min of illumination, a saturating pulse was applied to measure a steady-state fluorescence level (F) and maximum fluorescence (F_m') in the light-adapted state. These allowed calculating the non-photochemical quenching [NPQ = (F_m-F_m')/F_m'] (Genty et al., 1989; Serôdio et al., 2005).

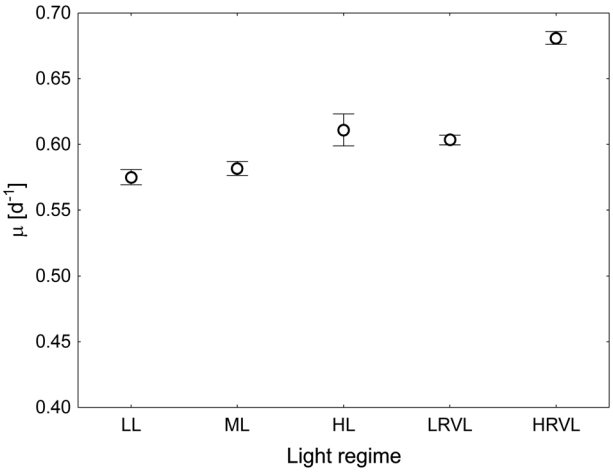

FIGURE 2 | Specific growth rates of *N.* cf. *aurariae* grown under various light regimes, i.e., constant light: low light (LL) – 30, medium light (ML) – 115, high light (HL) – 350 μmol photons m^{-2} s^{-1}, lower range variable light (LRVL), i.e., irradiance varying within the range of 15–150 μmol photons m^{-2} s^{-1}, and higher range variable light (HRVL), i.e., irradiance varying within the range 30–350 μmol photons m^{-2} s^{-1}. Each data point is the mean of 3 independent cultures, error bars represent standard error.

Statistics

The mean values of all analyzed parameters were compared separately for each applied light regime using the one-way analysis of variance (ANOVA). *Post hoc* comparisons were performed with Tukey HSD test. To describe linear relationships between analyzed variables, if present, the Pearson correlation coefficient was applied. All statistical analyses were performed using Statistica 10 (StatSoft Inc., United States). The results of statistical tests are provided in **Supplementary Information**.

RESULTS

Growth Rates

The cell count showed that the diatom *N.* cf. *aurariae* grew under all applied light regimes. Considering the fact that there were no statistically significant differences between applied light intensities within each variable light regime, i.e., the lower- (LRVL) and higher-range (HRVL) variable light, all of the obtained growth rate (m) values were pooled together. Comparing constant light levels, a significant difference between low (LL) and high (HL) light (30 and 350 μmol photons m^{-2} s^{-1}, respectively; **Supplementary Table S1**) (Tukey HSD test, $p < 0.05$) was observed. The m value obtained for the lower-range variable light (LRVL) did not vary from the value obtained for the cells from the constant high light (Tukey HSD test, $p > 0.05$). The highest m was found in cells grown at the higher-range variable light (HRVL) (**Figure 2**).

Pigments

Cellular pigment content changed significantly under applied light conditions (**Supplementary Table S2**). Under constant light, photosynthetic pigments, including chlorophyll *a* (Chl*a*) (**Figure 3A**) and fucoxanthin (Fuco) decreased, while the content of the xanthophyll cycle pigments, namely: diadinoxanthin and diatoxanthin (Dd + Dt), increased (Tukey HSD test, $p < 0.05$). No significant changes were observed with respect to chlorophyll *c* (Chl*c*) and β-carotene (β-car). Under the lower-range variable light, the content of all pigments did not vary significantly. Conversely, under the higher-range variable light, only Chl*c* and β-car remained unchanged. Under constant light conditions, the xanthophylls pool [(Dd + Dt)/Chl*a*] increased ca. Ten-fold, reaching the highest value at the highest applied irradiance (350 μmol photons m^{-2} s^{-1}, corresponding to the TDLD of 20.2 μmol photons m^{-2}; **Figure 3B**) (Tukey HSD test, $p < 0.05$). Whereas cells grown at both variable light regimes showed no change in (Dd + Dt)/Chl*a* (ANOVA, $p > 0.05$) comparing the applied light levels. When the content of Chl*a* was analyzed as a function of total daily light dose (TDLD). It was shown that the values calculated for cells grown under variable light conditions matched the decreasing pattern set by values obtained for cells from the constant light (**Figure 3A**). Fuco followed the same variation pattern (data not shown). The xanthophylls pool [(Dd + Dt)/Chl*a*] values from LRVL and HRVL, likewise, fitted the constant light pattern (**Figure 3B**). Furthermore, direct comparison of values obtained for cultures from ML and HRVL, as they received almost the same TDLDs, showed no statistically significant differences considering Chl*a* and (Dd + Dt)/Chl*a* as well (Tukey HSD test, $p < 0.05$). Under each light regime, the de-epoxidation state [Dt/(Dd + Dt)] differed considerably between the applied light levels (ANOVA, $p < 0.05$; **Figure 4**). In constant light, Dt/(Dd + Dt) was two-fold higher at the highest applied irradiance (350 μmol photons m^{-2} s^{-1}) comparing it to the lowest one (30 μmol photons m^{-2} s^{-1}) (Tukey HSD

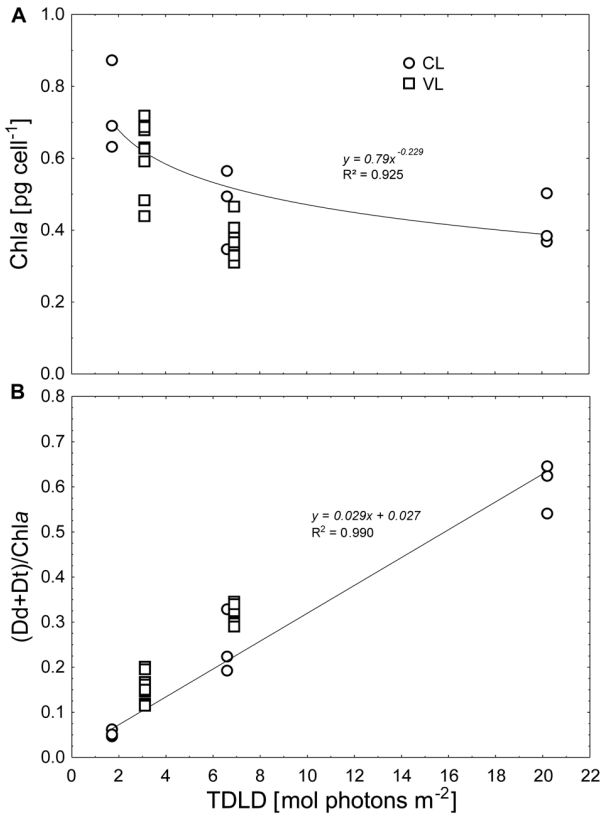

FIGURE 3 | Chlorophyll *a* content **(A)** and xanthophylls pool (Dd + Dt)/Chl*a* **(B)** as a function of total daily light doses (TDLD) in *N.* cf. *aurariae* grown under different light regimes: constant light (CL) (○), and variable light (□).

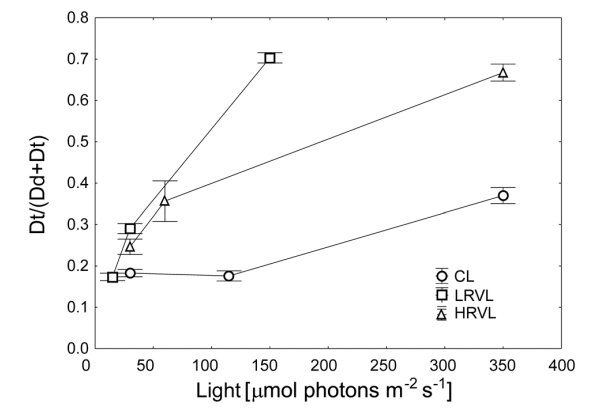

FIGURE 4 | De-epoxidation state [Dt/(Dt + Dd)] in *N.* cf. *aurariae* grown under different light regimes: constant light (CL) (○), i.e., 30, 115, and 350 μmol photons m^{-2} s^{-1}, lower range variable light (LRVL) (□), i.e., 15, 30, and150 μmol photons m^{-2} s^{-1}, and higher range variable light (HRVL) (△), i.e., 30, 60, and 350 μmol photons m^{-2} s^{-1}. Each data point is the mean of 3 independent cultures, error bars represent standard error.

test, $p < 0.05$), whereas in variable light, the Dt/(Dd + Dt) values increased ca. three and four times in LRVL and HRVL, respectively (Tukey HSD test, $p < 0.001$).

P-E Curves and Photosynthetic Parameters

The fitting of the mathematical model (Platt et al., 1980) to the data was always good, with R^2 exceeding the value of 0.9. The photosynthetic response of the diatom varied significantly between applied light conditions (ANOVA, $p < 0.05$, **Figure 5** and **Supplementary Figure S2**). In constant light, GP_{max} expressed per cell basis (GP_{max}/cell) decreased at higher light intensities, ca. two and four times at ML and HL, respectively (Tukey HSD test, $p < 0.05$; **Figure 5A** and **Supplementary Table S3**). When expressed per Chl*a* basis, no change was observed between LL and ML, whereas at HL GP_{max}/Chl*a* was two-fold lower (Tukey HSD test, $p < 0.05$; **Figure 5B**). The a values for cells grown at LL and ML did not differ (Tukey HSD test, $p > 0.05$; **Supplementary Table S3**), while at HL α/cell significantly decreased (Tukey HSD test, $p > 0.05$; **Figure 5C**). When expressed per Chl*a* unit, statistical tests showed no difference in α/Chl*a* (Tukey HSD test, $p > 0.05$; **Figure 5D**). Although some variations in the shape of the P-E curves were observed in cultures maintained under variable light (LRVL and HRVL as well), differences between the values of these parameters were not statistically significant when comparing the applied light levels (ANOVA, $p > 0.05$). The means of both parameters calculated for cells from the variable light regimes were systematically higher with respect to those of the constant light regimes (**Figure 5**). Particular pairs of means were compared, i.e., LL and LRVL, ML and HRVL, as they had similar Chl*a* content. GP_{max}/cell obtained for cells from LRVL differed significantly from LL (Tukey HSD test, $p < 0.05$). On the other hand, no significant differences were found between ML and HRVL (Tukey HSD test, $p > 0.05$; **Figure 6**). When comparing the same pairs of α/cell means, it was found that they showed significant differences (Tukey HSD test, $p < 0.05$). Generally, similar patterns were also observed in GP_{max}/Chl*a* and α/Chl*a* (data not shown). Despite some variations in the light saturation index (E_k), its values estimated for cultures acclimated to LL and ML did not differ significantly (ANOVA, $p < 0.5$; **Supplementary Table S3**), while at the highest light, E_k markedly decreased (Tukey HSD test, $p < 0.05$). The same variation pattern was also exhibited by cells maintained in variable light (**Supplementary Table S3**).

PAM Fluorescence and Dt Molecules Concentration

Under each light regime, the fluorescence parameters varied significantly (ANOVA, $p < 0.5$, **Supplementary Table S4**). Under constant light, F_v/F_m decreased significantly at high light (ANOVA, $p > 0.5$). In variable light, the trend was more pronounced; the wider the range of the applied light intensities, the larger the decrease in F_v/F_m was observed. The dynamics of F_v/F_m showed a negative correlation with the de-epoxidation state (**Figure 7A**). NPQ rose with the increase in the light intensity. At the constant light regimes, the sharp NPQ increase was recorded at ML compared to LL, followed by its significant build-up at HL. This pattern was further reflected in the relationship between NPQ and Dt, which was broken down

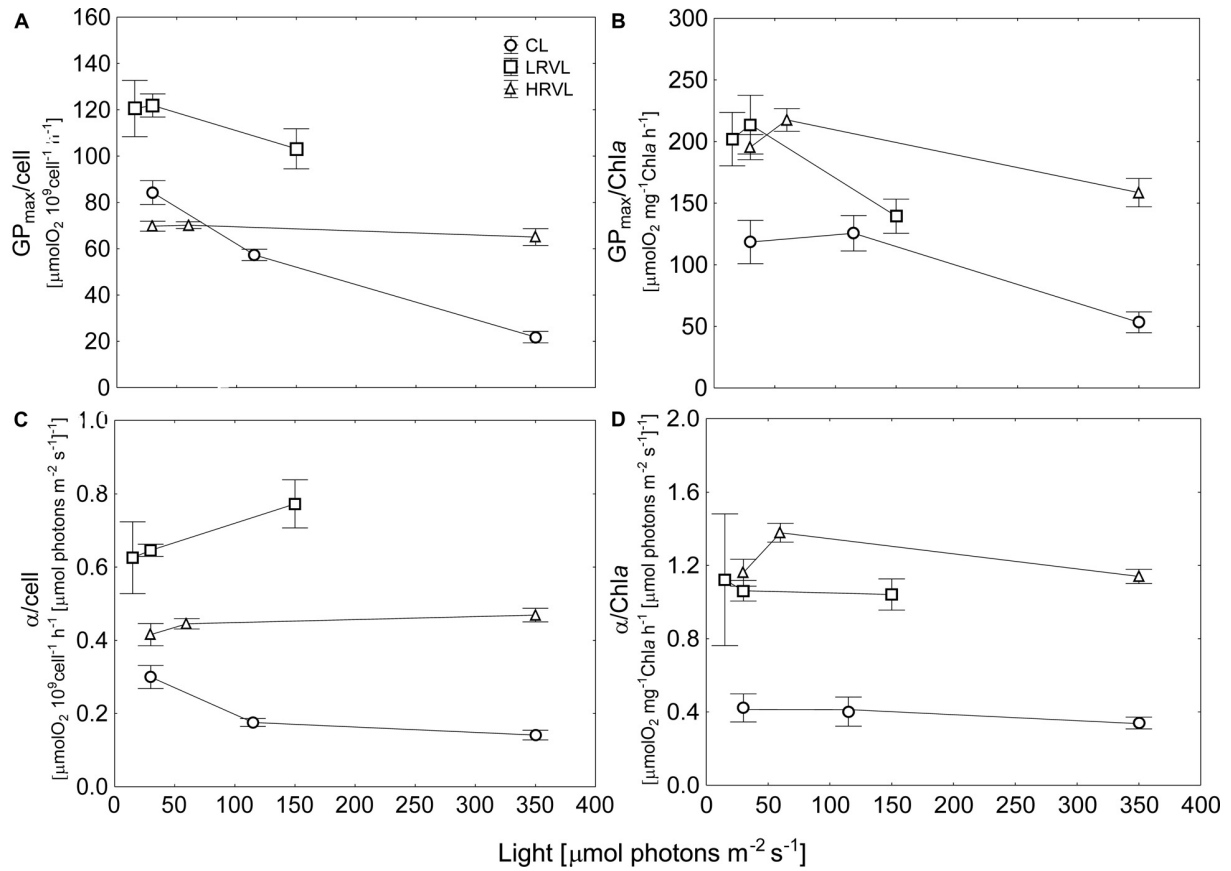

FIGURE 5 | Photosynthetic parameters, the gross maximum photosynthetic capacity expressed per cell (GP_{max}/cell) **(A)**, the gross maximum photosynthetic capacity expressed per Chla unit (GP_{max}/Chl*a*) **(B)**, the maximum photosynthetic efficiency expressed per cell (α/cell) **(C)**, the maximum photosynthetic efficiency expressed per Chl*a* unit (α/Chl*a*) **(D)**, in N. cf. aurariae grown under different light regimes: constant light (CL) (○), i.e., 30, 115, 350 μmol photons m^{-2} s^{-1}, lower range variable light (LRVL) (□), i.e., 15, 30, 150 μmol photons m^{-2} s^{-1}, and higher range variable light (HRVL) (△), i.e., 30, 60, 350 μmol photons m^{-2} s^{-1}. Each data point is the mean of 3 independent cultures, error bars represent standard error.

into two linear correlations formed by values obtained for cells from LL and ML; ML and HL. The slope of the former was 0.332, whereas for the latter it decreased to 0.068 (**Figure 7B**). Under both variable light regimes, at the lowest light levels NPQ was rarely measured (due to the fact that F_m values were lower than F_m') despite Dt molecules being present (3.6 ± 0.47 at 15 μmol photons m^{-2} s^{-1} and 12.5 ± 1.22 at 30 μmol photons m^{-2} s^{-1} under LRVL and HRVL, respectively, data not shown). The NPQ increased linearly with the increase in Dt content, reaching values similar to those exhibited by cultures from ML and HL (**Figure 7B**).

DISCUSSION

Photoacclimation allows an adjustment of a photosynthetic apparatus for varying light conditions. It also serves to minimize growth variations under changing environmental conditions (as it may also be affected by other variables such as temperature and the availability of nutrients) (e.g., Dubinsky and Stambler, 2009; Lacour et al., 2018; Liefer et al., 2018). This process is reflected in photosynthetic pigment content and, by extension, in the variations of P-E curves, which enable identification of main photoacclimation strategies (Richardson et al., 1983).

The applied variations of light intensities changed pigment composition. The primary acclimation mechanism involved a decrease of the photosynthetic pigments, which is a typical response in microalgae to increasing irradiance (e.g., Ruivo et al., 2011). Pigment composition was determined by the applied TDLD. Similar results were observed in the green alga *Dunaliella tertiolecta* when the sinusoidal light regime was applied (Havelková-Doušová et al., 2004). Previous studies showed that microalgae do not acclimate to the average, but somewhat lower irradiance when grown under highly fluctuating light conditions thus substantiating the importance of the light regime (e.g., van de Poll et al., 2007). In this study, *N.* cf. *aurariae* was incubated for several days under changing light conditions emulating, in a simplified manner, a diurnal irradiance variation (which partially explains differences between results obtained here and in other studies; e.g., Flameling and Kromkamp, 1997) and therefore it can be

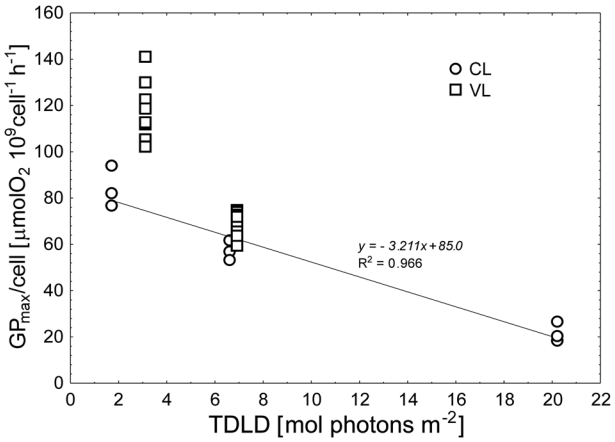

FIGURE 6 | Maximum photosynthetic capacity expressed per cell (GP_{max}/cell) as a function of total daily light doses (TDLD) in *N.* cf. *aurariae* grown under different light regimes: constant light (CL) (○), and variable light (□).

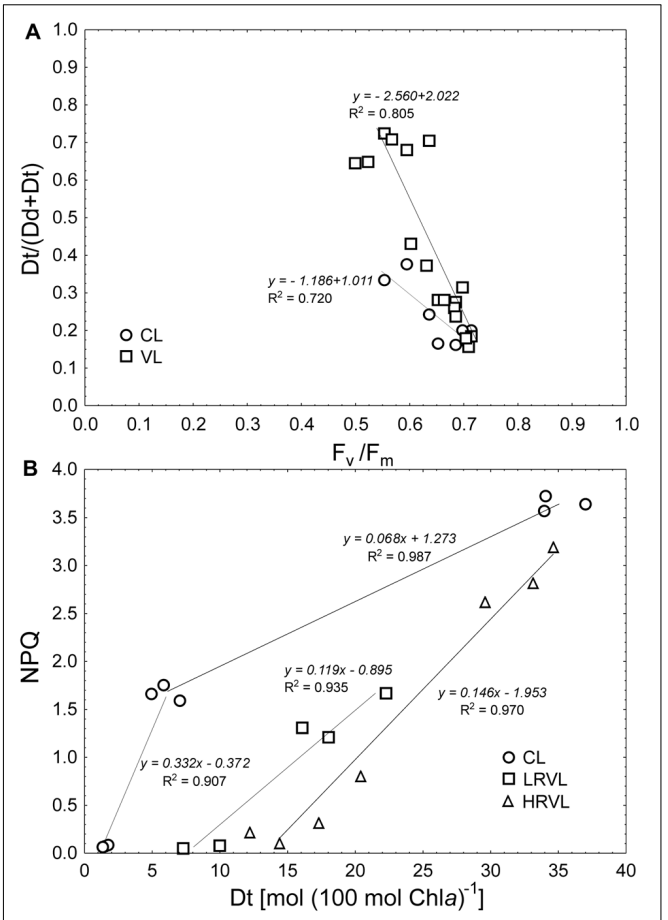

FIGURE 7 | Relationship between de-epoxidation state [Dt/(Dd + Dt)] and the maximum quantum yield of photosystem II (F_v/F_m) **(A)** in *N.* cf. *aurariae* grown under different light regimes: (1) constant light (CL) (○), and variable light (□), and non-photochemical quenching (NPQ) and diatoxanthin (Dt) concentration **(B)** in *N.* cf. *aurariae* grown under different light regimes: constant light (CL) (○), lower range variable light (LRVL) (□), and higher range variable light (HRVL) (△).

assumed that the changes in pigment content reflected long-term photoacclimation.

Changes in the content of Chl*a* can be associated with the change in the size and/or number of photosynthetic units (defined as the functional photosynthetic structure comprising the reaction centers together with their accessory pigments and electron carriers (Falkowski and Owens, 1980). Newly synthesized Chl*a* molecules can be added to the already existing PSU or by building up a new one, determining a response of microalgae to changing light conditions (Dring, 1998). These changes can be identified by analyzing variations in the shape of P-E curves produced for microalgae acclimated to diverse light conditions (i.e., low and high light), and several predictive models were provided (Richardson et al., 1983; Sakshaug et al., 1997). Their interpretation, however, strongly depends on the unit to which photosynthetic rates are expressed as they may give different images of photoacclimation (MacIntyre et al., 2002).

In the diatoms grown under constant light conditions, the initial slope (α) as well as the maximum photosynthetic capacity (GP_{max}), expressed on a per cell basis decreased when grown at higher light intensities. The observed phenotypic responses of P-E curves correspond with models depicting changes in the PSU number (Prézelin, 1981; Richardson et al., 1983). To the best of our knowledge, such variations in the shape of P-E curves have not been previously reported for diatoms. However, it is interesting to note that the same variation pattern was also found in another Baltic diatom, i.e., *Opephora* sp., isolated from the same location (unpublished data). Previous studies showed that the light-shade photoacclimation, and by extension, the underlying photoacclimation mechanism might be related to the ecological niches occupied by phototrophs (e.g., Falkowski and Owens, 1980). The mechanism involving changes in the number of PSU was reported in green algae and dinoflagellates (e.g., Prézelin and Sweeney, 1978; Falkowski and Owens, 1980). It was also observed in *Skeletonema costatum*, although it was accompanied by the changes in the size of PSU (Kromkamp and Limbeek, 1993). A photoacclimation strategy based on the change in the PSU number has been considered to be more favorable in habitats with highly fluctuating light (Falkowski and Owens, 1980; Behrenfeld et al., 1998). In the coastal shallows of the Baltic Sea, microalgae experience highly variable light conditions not only due to the seasonal and daily changes in light intensity. They can easily be transported deeper into the sediment due to bioturbation and sediment movement (Josefson et al., 2012), where they can undergo prolonged periods of darkness. They can also be moved to the water column, experiencing light conditions typical of phytoplankton (Pliński, 1993), where, due to the turbidity, the average irradiance decreases while light fluctuations increase. Thus, photoacclimation in *N.* cf. *aurariae* through the hypothesized changes in the PSU number coincides with the light climate characteristics typical of its habitat.

Comparing cultures from the constant and variable light regimes, i.e., LL vs. LRVL and ML vs. HRVL, it was shown that despite comparable Chl*a* contents, and in the latter similar TDLDs, LRVL and HRVL cultures had different photosynthetic traits. This confirmed the substantial influence of the light regime and demonstrated that the diatom optimized photosynthesis accordingly. The LRVL and HRVL cultures were also characterized by lower E_k values (ca. two-fold on average), showing that photosynthesis was saturated at lower irradiances. Changes in photosynthetic parameters observed in cultures grown under variable light regimes might have resulted from further alternations in the number of PSUs (as it was indicated to be the primary acclimatory mechanism). With regard to the fact that no significant differences in the Chl*a* content values were observed, it can be presumed that changes in the size of PSUs also occurred. This can be supported by the fact that changes in the PSU size primarily affect the photosynthetic efficiency (a) (Dubinsky and Stambler, 2009); in both compared cultures pairs (i.e., LL vs. LRVL and ML vs. HRVL) a expressed on a per cell and Chl*a*, decreased 2.5 times on average. A change in the number, as well as the size of PSUs induced by variable light regimes, was previously reported in diatoms (Kromkamp and Limbeek, 1993). The authors showed that in fluctuating light, *S. costatum* acclimated by increasing the number and decreasing the size of PSUs. Moreover, it was also shown that in cultures receiving higher TDLD, α/Chl*a* and GP_{max}/Chl*a* increased in cells from fluctuating light as compared to those maintained under the sinusoidal light regime. Similar variations in the aforementioned parameters were also observed when the cultures receiving an approximate TDLDs, i.e., ML and HRVL, were compared. Thus, it could be cautiously speculated that under variable light regimes, *N.* cf. *aurariae* also increased the number of PSUs and decreased their size. A higher number of PSUs with relatively small size seems to be particularly beneficial to algae inhabiting environments of variable light conditions. They facilitate effective light harvesting at low light and enhance the capacity for compensatory changes in PSII at higher irradiance, decreasing the risk of overexcitation of PSII (Behrenfeld et al., 1998).

In HL cells, maximum photosynthetic rates were strongly reduced. Previous studies argued that such photosynthesis impairment could be caused by high light-induced damage of PSII (e.g., Samuelsson and Richardson, 1982). Photodamage lowers the number of PSU and thus decreases both a and GP_{max}; a usually decreases first until a critical percentage of PSII centers is deactivated. After that, any additional photodamage causes a decrease in GP_{max} (Vassiliev et al., 1994; Behrenfeld et al., 1998). Regarding the fact that photoinhibition is not only a light- but also a time-dependent process (Henley, 1993; Blanchard et al., 2004; Serôdio et al., 2012), long-term exposure to elevated irradiance (350 μmol photons m^{-2} s^{-1}) indicated that *N.* cf. *aurariae* experienced high light stress. Under variable light conditions, on the other hand, the photoinhibitory effect of high light was diminished, possibly due to the shorter exposure time (4 vs. 16 h) as well as a putative decrease in the PSU size. Also a high light period was followed by low light, which stimulates D1 turnover and PSII repair (Behrenfeld et al., 1998; Tyystjärvi, 2013). Generally, the capacity for repair of PSII in epipelic and epispammic species was shown to be greater than suffered photodamage. Although epipsammon species seem to rely more on the reduction of photoinactivation due to physiological photoprotection rather than costly repair mechanisms (Frankenbach et al., 2018). Thus, the limited (mostly statistically insignificant) decrease in photosynthetic rates obtained when the diatom was exposed to the highest light levels under the variable light regimes could possibly be an effect of the up-regulation of photoprotection (Henley, 1993; Zhu and Green, 2010). Moreover, photoinhibition may also be considered as a photoprotective mechanism. Damaged PSII itself can act as non-photochemical quenchers (Matsubara and Chow, 2004; Zavafer et al., 2019), preventing over-reduction of the photosynthetic electron transport chain (Rumeau et al., 2007). As a result, *N.* cf. *aurariae* was able to achieve a certain balance between photoinhibition and photoprotection, resulting in sufficient photosynthesis supporting its growth. And consequently, enabling the diatom to survive prolonged periods of high light.

The cultures grown under constant light conditions exhibited a similar growth rate independent of light intensity. There was no considerably lower growth rate at LL, as it was reported for other diatoms (e.g., Mouget et al., 1999). Alternatively, it could be stated that the growth of *N.* cf. *aurariae* at HL, although still higher than at LL and ML, was somewhat restricted due to the inability of the diatom to acclimate to high irradiance. In variable light, when the diatom was mainly exposed to low light intensities (15–30 and 30–60 μmol photons m^{-2} s^{-1} at LR and HRVL, respectively, for 12 out of 16 h of illumination period), growth rates were even higher. Such results partially explain environmental observations showing that *N.* cf. *aurariae* was present in epispammic communities throughout the year, and it was most frequently found in autumn (Pniewski, 2010), when lower irradiance predominates (monthly means of light intensity at the sea surface are below ca. 345 μmol photons m^{-2} s^{-1}; Kaczmarek and Dera, 1998). Nonetheless, increased photosynthetic rates under variable light conditions suggested that the diatom, due to its specific photoacclimation (i.e., an increased number and decreased size of PSU), could also benefit from the shorter high light illumination periods.

In constant light, the xanthophylls pool [(Dd + Dt)/Chl*a*] was determined by the applied TDLD. As with the Chl*a* content, (Dd + Dt)/Chl*a* for LR and HLVL fitted the pattern set by the values obtained from the constant light cultures. Both xanthophylls, i.e., Dd and Dt, form the one-step reaction xanthophyll cycle, allowing diatoms to instantaneously balance excitation energy and/or ensure photoprotection (e.g., Lhor and Wilhelm, 1999; Goss and Jakob, 2010; Lavaud and Lepetit, 2013). The main difference between cells grown under constant and variable light conditions was the activity of the xanthophyll cycle; Dt/(Dd + Dt) was almost twice as high in variable light as at constant high light. A high amount of Dt molecules is crucial for efficient photoprotection, enabling NPQ build-up responsible for the thermal dissipation of

excess energy (Lavaud et al., 2004; Zhu and Green, 2010). Recent studies showed that NPQ, as well as the xanthophyll cycle, are species/strain-specific traits regulating a functional response of microalgae to varying light conditions (e.g., Lavaud et al., 2007; Lavaud and Lepetit, 2013). In benthic diatoms, it was proven that photoprotective mechanisms are also strongly dependent on their growth form. The data obtained here coincided with features characteristic for non-motile epispammic diatoms (Barnett et al., 2015; Blommaert et al., 2017). *N.* cf. *aurariae* was able to reach very high NPQ (which agrees with NPQ values previously observed in Baltic microphytobenthos; Pniewski et al., 2017), regardless of the light regime. In ML cultures of *N.* cf. *aurariae*, the xanthophylls pool increased (as compared to LL), while no change in the de-epoxidation state was observed. This indicated that the NPQ was developed due to higher Dt accumulation, originating from a larger xanthophylls pool and not from an increased de-epoxidiaiton state (Blommaert et al., 2018). However, in HL cells, together with the increased (Dd + Dt)/Chl*a* values, Dt/(Dd + Dt) also increased. The prominence of the de-epoxidation state was even greater in variable light, and it was dependent on the light intensities applied. Such observations are also consistent with previous reports showing a stronger de-epoxidation state in diatom-dominated epipsammic communities (e.g., Jesus et al., 2009; Cartaxana et al., 2011; Pniewski et al., 2015). A high NPQ capacity in epipsammic diatoms was shown to be their main photoprotection mechanism as they have no or strongly limited behavioral control over their light environment (Barnett et al., 2015; Frankenbach et al., 2018).

In constant light, NPQ increased with the content of Dt molecules. However, this relationship was not linear. At HL, despite a sharp increase in Dt, the expected build-up of NPQ was not observed. Furthermore, despite the fact that in cells from the variable light regimes, at low light intensities (i.e., 15 and 30 μmol photons m^{-2} s^{-1}) a substantial amount of Dt molecules was already present, NPQ could not be measured, or it was very low. This suggests that not all Dt molecules participated to the NPQ development. The possible explanation could be the presence of Dt molecules in the lipid matrix of thylakoids and protein-bound Dt in PSI, which may help to avoid lipid peroxidation, and to scavenge ROS reducing the possibility of oxidative damage (Lepetit et al., 2010; Lavaud and Lepetit, 2013). These additional Dt pools (i.e., not involved in NPQ development) could play an essential role in photoprotection, especially under constant high light conditions, preventing further PSII inactivation and preserving its functionality as turnover of D1 is inhibited at saturating light intensities (Behrenfeld et al., 1998). Growing the diatom under various light conditions suggested that its photoprotection was based on a certain balance between (Dd + Dt) content and the de-epoxidation state (Lacour et al., 2018). Long-term photoacclimation regulated the xanthophylls pool according to the received TDLD, and it seemed that it also determined the distribution of the xanthophyll cycle pigments in the cell (at least with respect to their involvement, or lack of it, in the NPQ build-up), while the de-epoxidation state acted as a fine-tuning process allowing precise regulation of the dissipation of excess energy, as required by specific light intensities. This further shows that epipsammic diatoms use various mechanisms to cope with changing light (Blommaert et al., 2017).

The F_v/F_m values decreased at higher light intensities; before measurements, samples were dark-adapted for 15 min, retaining some fraction of NPQ ("dark" NPQ) and thus lowering F_v/F_m. Such observations were reported in various diatom species as well as microphytobenthos communities (e.g., Serôdio et al., 2005; Lacour et al., 2018). "Dark" NPQ is often observed after prolonged exposure to high light resulting from the restricted epoxidation of Dt to Dd as Dt epoxidase functions more effectively in low light than in darkness (Goss et al., 2006; Lavaud and Lepetit, 2013). It can also be developed in the dark due to the chlororespiratory proton gradient (Jakob et al., 2001; Serôdio et al., 2005). The presence of "dark" NPQ is considered as an advantageous feature allowing diatoms to maintain their antenna system in a dissipative state promptly providing photoprotection upon rapid light exposure (Lavaud and Goss, 2014). Such an adaptation seems to be particularly relevant in species occupying habitats with highly fluctuating light, including sediments of coastal shallows (Perkins et al., 2011).

CONCLUSION

Previous studies carried out on the Baltic epipsammic assemblages dominated by diatoms showed that they are characterized by high primary production, similar to epipelic communities and that they are resistant to high light. They also quickly respond to changing light conditions (Pniewski et al., 2015, 2017, 2018). The photophysiological properties of microalgal communities seem to be the resultant characteristics typical of their members. The data obtained provided evidence for the considerable photoacclimatory potential of *N.* cf. *aurariae* that can help to ensure the resilience of microphytobenthos communities, especially under lower light conditions. The cultures grown in constant light showed general long-term photoacclimation patterns of the species. Whereas, variable light regimes depicted specific modifications in their photosynthetic characteristics. The photosynthesis of *N.* cf. *auraraie* was more efficient at lower light intensities, which may be explained by the fact that in its natural environment, the diatom can experience subsaturating irradiance (or even darkness) for an extended time. In contrast, photoprotection represented an interplay between long-term photoacclimation and rapid adjustment to ambient light conditions within the constraints set by the former. Diminished photosynthetic rates under constant high light indicated that the diatom can suffer from prolonged exposure to excess irradiance, most likely resulting from lower light acclimation. Overall, the adaptive plasticity of the studied diatom seems to be developed as a response to variable light conditions characteristic of its natural habitat, i.e., coastal shallows, and shaped by the lifestyle and growth

form of the diatom. It can also be tentatively assumed that the physiological versatility of *N.* cf. *aurariae* facilitated its ecological success as one of the most common diatoms in the Baltic epipsammon.

DATA AVAILABILITY STATEMENT

The datasets generated for this study are available on request to the corresponding author.

AUTHOR CONTRIBUTIONS

FP developed the idea and performed HPLC pigment analyses. IP-J prepared and carried out the experiments as well as performed growth, photosynthesis, and fluorescence measurements. FP and IP-J performed statistical analyses and wrote the manuscript.

FUNDING

This study was funded within the statutory funds of the Department of Marine Ecosystems Functioning at the Institute of Oceanography University of Gdańsk.

ACKNOWLEDGMENTS

We thank John Breslin and Daniel Naude for language consultations, and two reviewers for critical comments on the manuscript.

SUPPLEMENTARY MATERIAL

The Supplementary Material for this article can be found online at: https://www.frontiersin.org/articles/10.3389/fmars.2020.00381/full#supplementary-material

REFERENCES

Barnett, A., Méléder, V., Blommaert, L., Lepetit, B., Gaudin, P., Vyverman, W., et al. (2015). Growth form defines physiological photoprotective capacity in intertidal benthic diatoms. *ISME J.* 9, 32–42. doi: 10.1038/ismej.2014.105

Behrenfeld, M. J., Prasil, O., Kolber, Z. S., Babin, M., and Falkowski, P. G. (1998). Compensatory changes in Photosystem II electron turnover rates protect photosynthesis from photoinhibition. *Photosynth. Res.* 58, 259–268. doi: 10.1023/A:1019894720789

Blanchard, G. F., and Cariou-Le Gall, V. (1994). Photosynthetic characteristic of microphytobenthos in Marennes-Oléron Bay, France: preliminary results. *J. Exp. Mar. Biol. Ecol.* 182, 1–14.

Blanchard, G. F., Guarini, J.-M., Dang, C., and Richard, P. (2004). Characterizing and quantifying photoinhibition in intertidal microphytobenthos. *J. Phycol.* 40, 692–696.

Blommaert, L., Huysman, M. J. J., Vyverman, W., Lavaud, J., and Sabbe, K. (2017). Contrasting NPQ dynamics and xanthophyll cycling in a motile and a non-motile intertidal benthic diatom. *Limnol. Oceanogr.* 62, 1466–1479.

Blommaert, L., Lavaud, J., Vyverman, W., and Sabbe, K. (2018). Behavioural versus physiological photoprotection in epipelic and epipsammic benthic diatoms. *Eur. J. Phycol.* 53, 146–155.

Cartaxana, P., Ruivo, M., Hubas, C., Davidson, I., Serôdio, J., and Jesus, B. (2011). Physiological versus behavioral photoprotection in intertidal epipelic and epipsammic benthic diatom communities. *J. Exp. Mar. Biol. Ecol.* 405, 120–127.

Depauw, F. A., Rogato, A., d'Alcalá, M. R., and Falciatore, A. (2012). Exploring the molecular basis of responses to light in marine diatoms. *J. Exp. Bot.* 63, 1575–1591. doi: 10.1093/jxb/ers005

Dring, M. J. (1998). *The Biology of Marine Plants*. Cambridge: Cambridge University Press, 43–66.

Dubinsky, Z., and Stambler, N. (2009). Photoacclimation processes in phytoplankton: mechanisms, consequences, and applications. *Aquat. Microb. Ecol.* 56, 163–176.

Eberhard, S., Finazzi, G., and Wollman, F.-A. (2008). The dynamics of photosynthesis. *Annu. Rev. Genet.* 42, 462–515.

Falkowski, P. G., and Owens, T. G. (1980). Light-shade adaptation. *Plant Physiol.* 66, 592–595.

Flameling, I. A., and Kromkamp, J. (1997). Photoacclimation of *Scenedesmus protuberans* (Chlorophyceae) to fluctuating irradiances simulating vertical mixing. *J. Plankton Res.* 19, 1011–1024.

Fogg, G. E., and Thake, B. (1987). *Algal Culture and Phytoplankton Ecology*. Madison, WI: The University of. Wisconsin press.

Frankenbach, S., Schmidt, W., Frommlet, J. C., and Serôdio, J. (2018). Photoinactivation, repair and the motility-physiology trade-off in microphytobenthos. *Mar. Ecol. Prog. Ser.* 601, 41–57.

Genty, B., Briantais, J.-M., and Baker, N. R. (1989). The relationship between the quantum yield of photosynthetic electron transport and quenching of chlorophyll fluorescence. *Biochim. Biophys. Acta* 990, 87–92.

Goss, R., and Jakob, T. (2010). Regulation and function of xanthophyll cycle-dependent photoprotection in algae. *Photosynth. Res.* 106, 103–122. doi: 10.1007/s11120-010-9536-x

Goss, R., Pinto, E. A., Wilhelm, C., and Richter, M. (2006). The importance of a highly active and ΔpH-regulated diatoxanthin epoxidase for the regulation of the PS II antenna function in diadinoxanthin cycle containing algae. *J. Plant Physiol.* 163, 1008–1021. doi: 10.1016/j.jplph.2005.09.008

Guillard, R. L. (1975). "Culture of phytoplankton for feeding marine invertebrates," in *Culture of Marine Invertebrate Animals*, eds W. L. Smith and M. N. Chanle (New York, NY: Plenum Press), 29–60.

Havelková-Doušová, H., Prášil, O., and Behrenfeld, M. J. (2004). Photoacclimation of *Dunaliella tertiolecta* (Chlorophyceae) under fluctuating irradiance. *Photosynthetica* 42, 273–281.

Henley, W. J. (1993). Measurement and interpretation of photosynthetic light-response curves in algae in the context of photoinhibition and diel changes. *J. Phycol.* 29, 729–739.

Jakob, T., Goss, R., and Wilhelm, C. (2001). Unusual pH-dependence of diadinoxanthin de-epoxidase activation causes chlororespiration induced accumulation of diatoxanthin in the diatom Phaeodactylum tricornutum. *J. Plant Physiol.* 158, 383–390.

Jesus, B., Brotas, V., Ribeiro, L., Mendes, C. R., Cartaxana, P., and Paterson, D. M. (2009). Adaptations of microphytobenthos assemblages to sediment type and tidal position. *Cont. Shelf Res.* 29, 1624–1634.

Jesus, B., Perkins, R. G., Mendes, C. R., Brotas, V., and Paterson, D. M. (2006). Chlorophyll fluorescence as a proxy for microphytobenthic biomass: alternatives to the current methodology. *Mar. Biol.* 150, 17–28.

Josefson, A. B., Norkko, J., and Norkko, A. (2012). Burial and ecomposition of plant pigments in surface sediments of the Baltic Sea: role of oxygen and benthic fauna. *Mar. Ecol. Prog. Ser.* 455, 33–49.

Kaczmarek, S., and Dera, J. (1998). Radiation flux balance of the sea-atmosphere system over the southern Baltic Sea. *Oceanologia* 40, 277–306.

Kromkamp, J., and Limbeek, M. (1993). Effect of short-term variaition in irradiance on light harvesting and photosynthesis of the marine diatom *Skeletonema costatum*: a laboratory study simulating vertical mixing. *J. Gen. Microbiol.* 1993, 2277–2284.

Kühl, M., Lassen, C., and Jørgensen, B. B. (1994). Light penetration and light intensity in sand marine sediments measured with irradiance and scalar irradiance fiber-optic microprobes. *Mar. Ecol. Prog. Ser.* 105, 139–148.

Lacour, T., Larivière, J., Ferland, J., Bruyant, F., Lavaud, J., and Babin, M. (2018). The role of sustained photoprotective non-photochemical quenching in low temperature and high light acclimation in the bloom-forming arctic diatom *Thalassiosira gravida*. *Front. Mar. Sci.* 5:354. doi: 10.3389/fmars.2018.00354

Lavaud, J., and Goss, R. (2014). "The peculiar features of non-photochemical fluorescence quenching in diatoms and brown algae," in *Non-Photochemical Quenching and Energy Dissipation in Plants, Algae and Cyanobacteria*, eds B. Demmig-Adams, G. Garab, W. Adams, and Govindjee (Dordrecht: Springer Netherlands), 421–443.

Lavaud, J., and Lepetit, B. (2013). An explanation for the inter-species variability of the photoprotective non-photochemical chlorophyll fluorescence quenching in diatoms. *Biochim. Biophys. Acta* 1827, 294–302. doi: 10.1016/j.bbabio.2012.11.012

Lavaud, J., Rousseau, B., and Etienne, A.-L. (2004). General features of photoprotection by energy dissipation in planktonic diatoms (Bacillariophyceae). *J. Phycol.* 40, 130–137.

Lavaud, J., Strzepek, R. F., and Kroth, P. G. (2007). Photoprotection capacity differs among diatoms: possible consequences on the spatial distribution of diatoms related to fluctuations in the underwater light climate. *Limnol. Oceanogr.* 52, 1188–1194.

Lepetit, B., Volke, D., Gilbert, M., Wilhelm, C., and Goss, R. (2010). Evidence for the existence of one antenna-associated, lipid-dissolved and two protein-bound pools of diadinoxanthin cycle pigments in diatoms. *Plant Physiol.* 154, 1905–1920. doi: 10.1104/pp.110.166454

Lhor, M., and Wilhelm, C. (1999). Algae displaying the diadinoxanthin cycle also possess the violaxanthin cycle. *Proc. Natl. Acad. Sci. U.S.A.* 96, 8784–8789. doi: 10.1073/pnas.96.15.8784

Liefer, J. D., Garg, A., Campbell, D. A., Irwin, A. J., and Finkel, Z. V. (2018). Nitrogen starvation induces distinct photosynthetic responses and recovery dynamics in diatoms and prasinophytes. *PLoS One* 13:e0195705. doi: 10.1371/journal.pone.0195705

Lucas, C. H., Banham, C., and Holligan, P. M. (2001). Benthic-pelagic exchange of microalgae at a tidal flat. 2. Taxonomic analysis. *Mar. Ecol. Prog. Ser.* 212, 39–52.

MacIntyre, H. L., Geider, R. J., and Miller, D. C. (1996). Microphytobenthos: the ecological role of the "secret garden" of unvegetated, shallow-water marine habitats. I. Distribution, abundance and primary production. *Estuaries* 19, 186–201.

MacIntyre, H. L., Kana, T. M., Anning, T., and Geider, R. J. (2002). Photoacclimation of photosynthesis irradiance response curves and photosynthetic pigments in microalgae and cyanobacteria. *J. Phycol.* 38, 17–38.

MacIntyre, H. L., Kana, T. M., and Geider, R. J. (2000). The effect of water motion on short-term rates of photosynthesis by marine phytoplankton. *Trends Plant Sci.* 5, 12–17. doi: 10.1016/s1360-1385(99)01504-6

Mantoura, R. F. C., and Repeta, D. J. (1997). "Calibration methods for HPLC," in *Phytoplankton Pigments in Oceanography: Guidelines to Modern Methods*, eds S. W. Jeffrey, R. F. C. Mantoura, and S. W. Wright (Paris: UNESCO Publishing), 407–428.

Matsubara, S., and Chow, W. S. (2004). Populations of photoinactivated photosystem II reaction centers characterized by chlorophyll a fluorescence lifetime in vivo. *Proc. Natl. Acad. Sci. U.S.A.* 101, 18234–18239. doi: 10.1073/pnas.0403857102

Mouget, J.-L., Tremblin, G., Morant-Manceau, A., Morançais, M., and Robert, J.-M. (1999). Long-term photoacclimation of *Haslea ostrearia* (Bacillariophyta): effect of irradiance on growth rates, pigment content and photosynthesis. *Eur. J. Phycol.* 34, 109–115.

Perkins, R. G., Kromkamp, J. C., Serôdio, J., Lavaud, J., Jesus, B., Mouget, J. L., et al. (2011). "The application of variable chlorophyll fluorescence to microphytobenthic biofilms," in *Chlorophyll a Fluorescence in Aquatic Sciences: Methods and Applications*, eds J. D. Suggett, O. Prášil, and A. M. Borowitzka (Dordrecht: Springer Netherlands), 237–275.

Platt, T., Gallegos, C. L., and Harrison, W. G. (1980).). Photoinhibition of photosynthesis in natural assemblages of marine phytoplankton. *J. Mar. Res.* 38, 687–701.

Pliński, M. (1993). "Fitoplankton," in *Zatoka Pucka*, ed. K. Korzeniewski (Gdańsk: Fundacja Rozwoju Uniwersytetu Gdańskiego), 378–387.

Pniewski, F. (2010). *Photosynthetic Performance of Microphytobenthos from Intertidal Mudflats in Aiguillon Bay (Atlantic coast, France) and Non-tidal Coastal Shallows of Puck Bay (Baltic Sea, Poland)*. Ph.D. thesis, University of Gdańsk, Gdynia.

Pniewski, F. (2020). HPLC separation of cyanobacterial and algal photosynthetic pigments. *Biologia* 75, 223–233. doi: 10.2478/s11756-019-00407-8

Pniewski, F. F., Biskup, P., Bubak, I., Richard, P., Latała, A., and Blanchard, G. (2015). Photoregulation in microphytobenthos from intertidal mudflats and non-tidal coastal shallows. *Estuar. Coast. Shelf Sci.* 152, 153–161.

Pniewski, F. F., Richard, P., Latała, A., and Blanchard, G. (2017). Non–photochemical quenching in epipsammic and epipelic microalgal assemblages from two marine ecosystems. *Cont. Shelf Res.* 136, 74–82.

Pniewski, F. F., Richard, P., Latała, A., and Blanchard, G. (2018). Long- and short-term photoacclimation in epipsammon from non-tidal coastal shallows compared to epipelon from intertidal mudflat. *J. Sea Res.* 136, 1–9.

Prézelin, B. B. (1981). "Light reactions in photosynthesis," in *Physiological Bases of Phytoplankton Ecology*, ed. T. Platt (Ottawa, ON: Fisheries Research Board of Canada), 1–46.

Prézelin, B. B., and Sweeney, B. M. (1978). Photoadaptation of photosynthesis in *Gonyaulax polyedra*. *Mer. Biol.* 48, 27–35.

Raven, J. A., and Geider, R. J. (2003). "Adaptation, acclimation and regulation in algal photosynthesis," in *Photosynthesis in Algae*, eds A. W. D. Larkum, S. E. Douglas, and J. A. Raven (Dordrecht: Academic Publisher), 385–412. doi: 10.1038/nature08587

Richardson, K., Beardall, L., and Raven, J. A. (1983). Adaptation of unicellular algae to irradiance: an analysis of strategies. *New Phytol.* 93, 157–191.

Round, F. E. (1981). *The Ecology of Algae*. Cambridge: Cambridge University Press, 653.

Ruivo, M., Amorin, A., and Cartaxana, P. (2011). Effects of growth phase and irradiance on phytoplankton pigment ratios: implications for chemotaxonomy in coastal waters. *J. Plankton Res.* 33, 1012–1022.

Rumeau, D., Peltier, G., and Cournac, L. (2007). Chlororespiration and cyclic electron flow around PSI during photosynthesis and plant stress response. *Plant Cell Environ.* 30, 1041–1051. doi: 10.1111/j.1365-3040.2007.01675.x

Saint-Béat, B., Dupuy, C., Agogué, H., Carpentier, A., Chalumeau, J., Como, S., et al. (2014). How does the resuspension of the biofilm alter the functioning of the benthos–pelagos coupled food web of a bare mudflat in Marennes-Oléron Bay (NE Atlantic)? *J. Sea Res.* 92, 144–157.

Sakshaug, E., Bricaud, A., Dandonneau, Y., Falkowski, P. G., Kiefer, D. A., Legendre, L. L., et al. (1997). Parameters of photosynthesis: definitions, theory and interpretation of results. *J. Plankton Res.* 19, 1637–1670.

Samuelsson, G., and Richardson, K. (1982). Photoinhibition at low quantum flux densities in marine dinoflagellate (*Amphidinium carterae*). *Mar. Biol.* 70, 21–26.

Schreiber, U. (2004). "Pulse-amplitude-modulation (PAM) fluorometry and saturation pulse method: an overview," in *Chlorophyll a Fluorescence. A Signature of Photosynthesis*, eds G. C. Papageorgiou and Govindjee (Dordrecht: Springer), 279–319.

Serôdio, J., Cruz, S., Vieira, S., and Brotas, V. (2005). Non-photochemical quenching of chlorophyll fluorescence and operation of the xanthophyll cycle in estuarine microphytobenthos. *J. Exp. Mar. Biol. Ecol.* 326, 157–169.

Serôdio, J., Ezequiel, J., Barnett, A., Mouget, J.-L., Méléder, V., Laviale, M., et al. (2012). Efficiency of photoprotection in microphytobenthos: role of vertical migration and the xanthophyll cycle against photoinhibition. *Aquat. Microb. Ecol.* 67, 161–175.

Strickland, I. D. H., and Parsons, T. R. (1972). *A Practical Handbook of Seawater Analysis*. Ottawa, ON: Fisheries Research Board of Canada, 310.

Sundbäck, K., Miles, A., and Linares, F. (2006). Nitrogen in nontidal littoral sediments: role of microphytobenthos and denitrification. *Estuaries Coasts* 29, 1196–1211.

Sutherland, T. F., Grant, J., and Amos, C. L. (1998). The effect of carbohydrate production by the diatom *Nitzschia curvilineata* on the erodibility of sediment. *Limnol. Oceanogr.* 43, 65–72.

Tyystjärvi, E. (2013). Photoinhibition of photosystem II. *Int. Rev. Cell. Mol. Biol.* 300, 243–303.

Underwood, G. J. C. (2005). Microalgal (microphytobenthic) biofilms in shallow coastal waters: how important are species? *Proc. Calif. Acad. Sci.* 56, 162–169.

van de Poll, W. H., Visser, R. J. W., and Buma, A. G. J. (2007). Acclimation to a dynamic irradiance regime changes excessive irradiance sensitivity of *Emiliania huxleyi* and *Thalassiosira weissflogii*. *Limnol. Oceanogr.* 52, 1430–1438.

Vassiliev, I. R., Prasil, O., Wyman, K. D., and Kolber, Z. (1994). Inhibition of PSII photochemistry by PAR and UV radiation in natural phytoplankton communities. *Photosynth. Res.* 42, 51–64. doi: 10.1007/BF00019058

Witkowski, A., Lange-Bertalot, H., and Metzeltin, A. (2000). *Diatom Flora of Marine Coast I*. Koönigstein: A.R.G. Ganter, 369–370.

Zavafer, A., Iermak, I., Cheah, M. H., and Chow, W. S. (2019). Two quenchers formed during photodamage of phostosystem II and the role of one quencher in preemptive photoprotection. *Sci. Rep.* 9:17275. doi: 10.1038/s41598-019-53030-7

Zhu, S.-H., and Green, B. R. (2010). Photoprotection in the diatom *Thalassiosira pseudonana*: role of LI818-like proteins in response to high light stress. *Biochim. Biophys. Acta.* 1797, 1449–1457. doi: 10.1016/j.bbabio.2010.04.003

Conflict of Interest: The authors declare that the research was conducted in the absence of any commercial or financial relationships that could be construed as a potential conflict of interest.

frontiers in Marine Science

ORIGINAL RESEARCH
published: 21 April 2020
doi: 10.3389/fmars.2020.00212

The Vertical Migratory Rhythm of Intertidal Microphytobenthos in Sediment Depends on the Light Photoperiod, Intensity, and Spectrum: Evidence for a Positive Effect of Blue Wavelengths

Alexandre Barnett[1,2], Vona Méléder[1,2], Christine Dupuy[1] and Johann Lavaud[1,3]*

[1] UMR7266 LIENSs 'Littoral, Environnement et Sociétés', Institut du Littoral et de l'Environnement, CNRS/Université de La Rochelle, La Rochelle, France, [2] UPRES EA 2160 MMS 'Mer, Molécules, Santé', Faculté des Sciences et Techniques, Université de Nantes, Nantes, France, [3] UMI3376 Takuvik, CNRS/ULaval, Département de Biologie, Université Laval, Quebec City, QC, Canada

OPEN ACCESS

Edited by:
Dongyan Liu,
East China Normal University, China

Reviewed by:
Guang Gao,
Xiamen University, China
Deyong Sun,
Nanjing University of Information Science and Technology, China

****Correspondence:***
Alexandre Barnett
alexandre.barnett@univ-nantes.fr

Specialty section:
This article was submitted to Marine Ecosystem Ecology, a section of the journal Frontiers in Marine Science

Received: *25 January 2020*
Accepted: *18 March 2020*
Published: *21 April 2020*

Citation:
Barnett A, Méléder V, Dupuy C and Lavaud J (2020) The Vertical Migratory Rhythm of Intertidal Microphytobenthos in Sediment Depends on the Light Photoperiod, Intensity, and Spectrum: Evidence for a Positive Effect of Blue Wavelengths. Front. Mar. Sci. 7:212. doi: 10.3389/fmars.2020.00212

Estuarine intertidal flats strong biological productivity is mainly based on the activity of benthic microalgae communities or microphytobenthos (MPB), mostly dominated by diatoms. Epipelon is a major MPB growth form comprising motile species, which perform repeated "vertical migration" patterns in the upper sediment layers according to tidal and diurnal cycles with upward migration at the beginning of the daylight emersion and downward migration before immersion starts. Although this fascinating behavior has been extensively studied for more than a century, many of its features remain uncharacterized. Epipelon migratory rhythms are believed to be driven by an endogenous internal clock of unknown nature in combination with diverse environmental stimuli. Among the environmental stimuli impacting on MPB vertical migration, light is probably the most important. Rhythmic changes in surface abundance of natural MPB assemblages were therefore continuously assessed at high frequency by Imaging-PAM fluorimetry in fresh sediment sampled at different seasons, comprising 85 migration profiles from 40 sediment samplings over 2 years, and exposed to different light conditions without any other environmental stimuli (i.e., no tidal-like water flow and stable optimal temperature). In particular, we manipulated (i) the 24-h natural photoperiod MPB that was acclimated to in order to disentangle the tight link between the diurnal and tidal rhythmicity of epipelon migration, and (ii) the light spectrum in order to potentially influence MPB accumulation at the surface of sediment. We found that the migration rhythmicity mapped onto the tidal cycle but that it was modulated, and even overridden, by the diurnal cycle and by the irradiance level during daytime periods with a positive phototactic upward migration up to a certain threshold (in our conditions, 120 μmol photons m^{-2} s^{-1} of white light). Also, we found blue wavelengths (465 nm) triggered

MPB surface accumulation, as compared to other wavelengths (white, green, and red) in patterns that were intensity-dependent and species-dependent. In particular, we found two species, *Navicula spartinetensis* and *Gyrosigma fasciola*, which strongly migrate up under blue light and could potentially be used as model species for further studying the light-responses of intertidal MPB.

Keywords: blue light, diatoms, intertidal flats, pigments, migration, photoperiod

INTRODUCTION

Estuarine intertidal flats are among the most productive ecosystems on Earth (Underwood and Kromkamp, 1999). They play a paramount role in the functioning of coastal food-webs and they support essential local socio-economic activities (Lebreton et al., 2019). Tidal flats high biological productivity is mainly based on the activity of benthic microalgal communities or microphytobenthos (MPB) (Admiraal, 1984; Lebreton et al., 2019). In temperate marine areas, MPB is mostly dominated by diatoms (Ribeiro et al., 2013), which display a high degree of taxonomic and functional diversity (Kooistra et al., 2007; Barnett et al., 2015; Nakov et al., 2018). A major growth form of MPB diatoms is epipelon, which mostly inhabits fine cohesive sediments and comprises raphid diatom species moving freely in between sediment particles. The motility of epipelic diatoms is ensured by a slit (raphe) in their cell wall (frustule), which allows for directional and reversible locomotion (Cohn, 2001; Cohn et al., 2016) driven by highly sophisticated suites of micromovements (Apoya-Horton et al., 2006; Bertrand, 2008). Motility is a key adaptation to the intertidal sedimentary habitat providing epipelic diatoms with many ecological benefits including the colonization of microhabitats with specific light, nutrient, and temperature conditions, coping with environmental extreme variations, optimization of photosynthetic productivity, pheromonal-based sexual attraction, and tidal resuspension avoidance (see Consalvey et al., 2004; Marques Da Silva et al., 2017; Nakov et al., 2018, and references therein). The most known and fascinating display of this motile behavior is the "vertical migration" occurring in the upper sediment layers (Consalvey et al., 2004). Typically, at the beginning of daylight emersion (but not during nighttime), epipelic diatoms move upward and form dense and transient photosynthetic biofilms at the surface of sediment. Then, generally before and/or when immersion and/or night start, they move back downward in the deeper sediment layers. This rhythmic pattern repeats according to tides and photoperiod and is continuously reset to match the daily and fortnightly tide timings and the progressive seasonal changes in day length. Vertical migration was proposed to confer MPB with the ability to optimally exploit the physicochemical gradients of the intertidal sediments for performing photosynthesis and carbon fixation in well-lit upper sediment layers, spatially disconnected from cell division in nutrient-rich, stable, and darkened deeper layers (Saburova and Polikarpov, 2003; Consalvey et al., 2004). In that framework, the acquisition of motility obviously appears as the central motor of pennate diatom adaptation to life, and dominance, in intertidal sediments (Kooistra et al., 2007; Nakov et al., 2018).

Rhythmic MPB vertical migration has been recognized as a key regulating factor of MPB photosynthetic activity and mudflat primary productivity (Serôdio et al., 2005; Spilmont et al., 2007; Haro et al., 2019). The conceptualization of MPB migration dynamics (Guarini et al., 2008) opened a path to improvements in coupled biological-physical modeling attempts of mudflat primary production (Guarini et al., 2006). In this framework, the quantification of the MPB photosynthetically active biomass (PAB) at the surface of sediment (Herlory et al., 2005) and the precise measurement of its spatial and temporal dynamics (Consalvey et al., 2004), as well as its photosynthetic productivity (Kwon et al., 2012; Cartaxana et al., 2016a; Haro et al., 2019), have received major interest. It is generally accepted that rhythmic MPB migration is first governed by the tidal and diurnal cycles, which, together, control the light availability at the surface of sediment. Therefore, among the numerous environmental stimuli that impact on epipelon motility (i.e., temperature, salinity, nutrient availability, depth of the oxic sediment layer, etc.), light is probably the most important (Consalvey et al., 2004). Intertidal MPB indeed experience an extremely complex and continuously changing light environment (Paterson and Hagerthey, 2001), depending on a multifaceted combination of turbidity of the shallow water column at high tide (HT), and open-field–like light fluctuations at low tide (LT). The sediment-dependent light penetration generates (Kuhl and Jorgensen, 1994; Cartaxana et al., 2016b): (i) a photic zone condensed to the first hundreds of μm, (ii) a deeper light penetration in coarser sediment versus more cohesive fine mud, and (iii) a stronger depth attenuation of the blue band (450–500 nm) of the visible light spectrum and thus a steeper gradient of blue light compared to other spectral bands.

Previous attempts have successfully manipulated the light environment of MPB in controlled laboratory conditions, especially in order to disentangle the impact of the tidal and diurnal cycles on the rhythm of MPB vertical migration (Kwon et al., 2012; Haro et al., 2019). Nevertheless, these studies were performed on permanently submersed intertidal sediment, thereby artificially exacerbating the diurnal versus the tidal response as reported for *in situ* subtidal sediment (Ni Longphuirt et al., 2006). Additionally, only one previous work (Wenderoth and Rhiel, 2004) has explored the effect of monochromatic wavelengths on daytime MPB vertical migration. Therefore, the present study is a further complementary step: we used imaging Chl *a* fluorimetry on freshly sampled intertidal sediment to continuously measure at high frequency the changes in surface epipelic PAB without any other abiotic stimuli than light (i.e., in

particular, no sediment submersion or tidal-like water flow, and stable optimal temperature). We thereby explored the integrative effects of light photoperiod, intensity, and spectrum at different time scales from the emersion timing to seasonal on the rhythmic changes in MPB abundance at the surface of sediment. We have found that intertidal MPB vertical migration rhythm (i) primary tracks the tidal and diurnal cycles but to different extents, (ii) is strongly modulated by light intensity and spectrum, (iii) positively influenced by blue wavelengths at the species level by increasing the presence and abundance of cells at the surface of sediment.

MATERIALS AND METHODS

Study Site and Sediment Harvesting

Sediment samples were regularly collected at LT from March 2011 to March 2013 (**Supplementary Table S1**) in the upper zone (500 m from the shore, ca. 4 m above the marine chart datum) in the bay of l'Aiguillon ("Esnandes" site, 46°15.36′ N, 1°8.55′ W), an intertidal mudflat site on the Atlantic French coast (**Figure 1**). There, sediment is mostly composed of fine muddy particles (particle size <63 μm) (Herlory et al., 2004) and is hereafter referred to as "muddy sediment." Occasionally, sediment was also sampled in the bay of Bourgneuf ("Lyarne" site, 47°2′35″ N, 1°59′59″ W) where sediment is composed of muddy sand (63–200 μm particles) (Méléder et al., 2007) and hereafter referred to as "sandy-muddy sediment." For both sites, the MPB community is largely dominated by diatoms throughout the year (Herlory et al., 2004; Méléder et al., 2007). The upper layer (approximately the top first centimeter) of sediment was collected at LT and immediately brought back to the laboratory. After sieving through a 500-μm mesh to remove macrofauna, especially the mud snail *Peringia* species, the sediment was homogenized by thorough mixing and was spread as a plane layer in 4-cm-depth plastic trays (Serôdio et al., 2012). In order to keep the sediment hydrated throughout the measurements, it was homogenized each 24 h at the time of the *in situ* HT (i.e.,

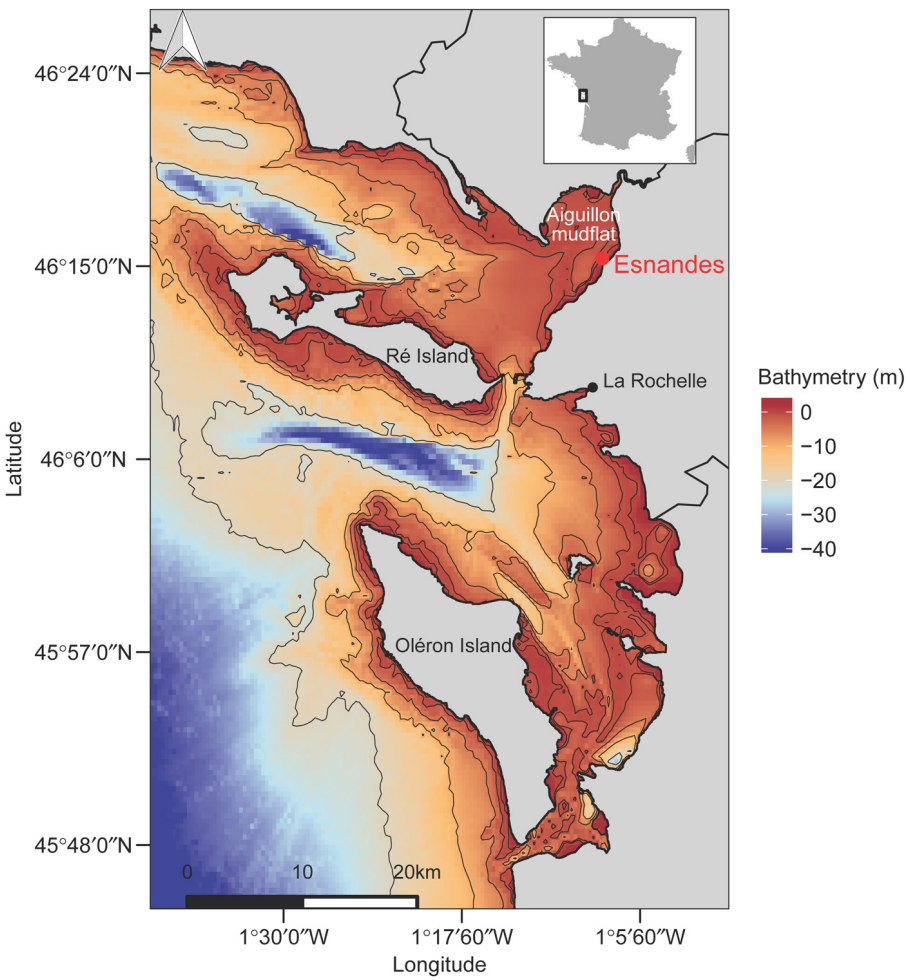

FIGURE 1 | A map of the Pertuis Charentais, France, showing the Bay of l'Aiguillon and the location of our sampling site, Esnandes (red dot). Bathymetry was retrieved from the General Bathymetric Chart of the Oceans (GEBCO International) database and plotted using R software with the use of the marmap package (Pante and Simon-Bouhet, 2013).

corresponding to the highest water level at the site of sampling) with filtered (GF/F, 0.7 μm) fresh seawater. In these conditions, MPB conserved its natural migratory rhythm for several days (5 ± 1 days; **Supplementary Figure S1**).

Monitoring of the Motile MPB Abundance Under Different Light Conditions

The "instantaneous" Chl *a* fluorescence F_t was used as a proxy for the MPB biomass present at the surface of sediment (see section "Monitoring of the Changes in the MPB PAB at the Surface of Sediment by Imaging-PAM Fluorimetry"). F_t measurements were converted into Chl *a* concentration per surface of sediment (Chl *a* m^{-2}) as detailed in **Supplementary Figure S2**. F_t was continuously monitored for 24 h on sediment trays placed under an Imaging-PAM fluorometer (Maxi-PAM M-series; Walz, Effeltrich, Germany) and by using its blue (470 nm) detecting beam (settings: intensity 0, frequency 1, measuring frequency 900 s). A map of the irradiance provided by the detecting beam at the surface of sediment tray is shown in **Supplementary Figure S3**. Five "areas of interest" of 6.4 cm^2, corresponding to 1,500 pixels (Serôdio et al., 2012), and for which the F_t values of all pixels are averaged, were randomly selected. This way, and even if the sediment was well homogenized before each measurement, random "areas of interest' were used as pseudoreplicates for each sediment tray so that each measurement took into account possible remaining heterogeneity of the Chl *a* fluorescence signal across the tray. All experiments were carried out at 20°C, which is optimal for MPB activity throughout the year (Blanchard et al., 1997; Savelli et al., 2018). The reason for maintaining the temperature optimal for all experiments, whatever the season sampling, was to focus only on the effect of light, and therefore to discard effect of temperature on MPB migration that could have potentially confound the output of our experiments.

For each experiment, two phases were recorded: (1) Phase 1: "MPB migration control", the first 24-h tidal cycle (based on the *in situ* water level at the site of sampling) was recorded under "ambient filtered true light" conditions (i.e., light passing by the window of the laboratory, 24-h natural photoperiod, no direct sunlight) as a control for the changes of the MPB biomass at the surface of the sediment; this option was chosen over an artificial light control in order to take into account the photoperiod and irradiance seasonal changes while keeping the ambient light conditions favorable to MPB migration in the laboratory (i.e., to, for instance, avoid photoinhibitory conditions in summer); (2) Phase 2: after homogenization of the sediment with seawater (see above), the second 24-h tidal cycle was monitored under different conditions of light intensities and spectra using 4 LED panels (FloraLEDs; Plant Climatics, Wertingen, Germany): darkness (Imaging-PAM and sediment tray placed under a black box), "white" light (20, 120, and 350 μmol photons m^{-2} s^{-1}, respectively, the minimum, intermediate, and maximum intensities reached by the mix of different LED sources with 459- and 553-nm maximum wavelengths), blue light (BL; 10, 40, and 120 μmol photons m^{-2} s^{-1}, respectively, the minimum, intermediate, and maximum intensities reached at 465 nm), red light (180 μmol photons m^{-2} s^{-1}, which was the maximum intensity reached at 677 nm, with and without far red 748 nm), and green light (10 and 40 μmol photons m^{-2} s^{-1}, the minimum and maximum intensities reached by "white" light with a 530-nm filter; 124 Dark Green Lee filter; Lee, Andover, England) (full spectra in **Supplementary Figure S4**). For each light condition, a new sediment tray was used, and a new "MPB migration control" was recorded.

We additionally performed "desynchronization experiments" where the photoperiod was artificially inverted. For doing so, during the "control" Phase 1, the day/night photoperiod was artificially provided following the 24-h natural photoperiod timings by applying a "white light" of 120 μmol photons m^{-2} s^{-1} with the LED panels. During Phase 2, the photoperiod was artificially inverted by applying the same white light during the natural night period and darkness during the natural day period.

The profiles of MPB abundance at the surface of the sediment were analyzed by computing two parameters: (1) the maximum MPB abundance reached during the daytime period of the measurement, (2) the area under the curve that integrates total MPB abundance changes during the 24-h monitoring over the first 24 h of "MPB migration control." In previous works (Guarini et al., 2006; Coelho et al., 2011), the maximum and integrated MPB abundances were, respectively, used as proxies for the maximum and for the total PAB of MPB present at the surface of the sediment. The graphic analysis of PAB was performed using Excel 2010; total PAB was computed with the Integral (gamma.xla) macro provided by http://fordom.free.fr.

For all experiments and under all light conditions described above (**Supplementary Table S2**), we regularly probed the "instantaneous" effective quantum yield of photosystem II (PS II) photochemistry (ΦPSII*inst*, see section "Chlorophyll *a* Fluorescence Yield and Light Curves") under current light conditions and when the daytime maximum MPB abundance was reached:

$$\Phi\text{PS II}inst = \frac{F'_{\mathrm{m}} - F_{\mathrm{t}}}{F'_{\mathrm{m}}} \quad (1)$$

where F_t is the "instantaneous" Chl *a* fluorescence yield, and F_m' the maximum Chl *a* fluorescence yield measured by firing a saturating pulse (see section "Chlorophyll *a* Fluorescence Yield and Light Curves").

Sediment Sampling

Sediment cores (diameter 3.2 cm, height 3 cm) were collected in the sediment tray for pigments (see section "Pigments Analysis") and species diversity (see section "Diatom Species Identification and Diversity Analysis") analyses. Sampling was performed during the "control" and BL conditions for different seasons: 10 μmol photons m^{-2} s^{-1} BL summer, and 40 and 120 μmol photons m^{-2} s^{-1} BL winter and summer, and at three timings of the corresponding *in situ* tidal cycle: (1) at the timing of the *in situ* LT (i.e., corresponding to the lowest water level at the site of sampling), (2) 3 h before LT (BLT), and (3) 3 h after LT (ALT). The sediment cores were immediately frozen in liquid nitrogen and stored at −80°C.

Pigments Analysis

The pigment content of sediment was determined by reversed phase HPLC (Hitachi High Technologies Co., Tokyo, Japan) calibrated for Chl *a* (expressed in μg Chl *a* cm^{-2}; **Supplementary Figure S2**). In order to decipher the vertical pigment content, the surface of three sediment cores (see section "Sediment Sampling") was cut in three sublayers (0–200, 200–400, and 400–600 μm) with a cryomicrotome (Leica CM1850; Leica Microsystems Nusslch GmbH, Nussloch, Germany). The sediment samples were lyophilized during 24 h, and the pigments were extracted with 0.5 mL of a mixture of 90% methanol/0.2 M ammonium acetate (90/10 vol/vol) and 10% ethyl acetate (Lepetit et al., 2013). Pigment quantification was as described before (Jakob et al., 1999), and Chl *a* content was normalized to the sediment dry weight (g^{-1}). The xanthophyll de-epoxidation state (DES in%) was calculated as:

$$\mathrm{DES} = \frac{\mathrm{DT}}{\mathrm{DD} + \mathrm{DT}} \times 100 \quad (2)$$

where DD is the diadinoxanthin, the epoxidized form; and DT is the diatoxanthin, the de-epoxidized form.

Chlorophyll *a* Fluorescence Yield and Light Curves

In order not to disturb the monitoring of MPB biomass changes with the Imaging-PAM and to discard potential limitations in the measurement of photosynthetic performance by Imaging fluorimetry (Vieira et al., 2013), the Chl *a* fluorescence yield was monitored on the MPB containing sediment surface with a Water-PAM fluorometer (Fiber version; Walz) at the same timings as the sediment sampling, that is, BLT, LT, and ALT (see section "Sediment Sampling"). Chlorophyll *a* fluorescence was excited by a non-actinic modulated 460-nm light, and a saturating pulse of BL (3,000 μmol photons m^{-2} s^{-1}) was fired in order to, respectively, measure the minimum (F_0) and the maximum (F_m) PS II fluorescence yield on sediment previously dark-adapted for 10 min. The maximum quantum yield of PS II photochemistry was calculated as the ratio F_v/F_m, where

$$F_\mathrm{v} = F_\mathrm{m} - F_0 \quad (3)$$

Rapid light curves (RLCs) were recorded in triplicates at three different randomly selected locations on the sediment tray. The sediment surface was exposed to eight successive light steps of increasing intensity (E) provided by the LED source of the Water-PAM. The duration of each light step was 30 s as recommended before (Lefebvre et al., 2011). Rapid light curves allowed construction of PSII relative electron transport rate (rETR) versus E curves and non-photochemical quenching (NPQ) versus E curves. Relative electron transport rate was calculated as

$$\mathrm{rETR} = \Phi\mathrm{PS\ II} \times \mathrm{E} \quad (4)$$

Where

$$\Phi\mathrm{PS\ II} = \frac{F_{\mathrm{m}'} - F'}{F_{\mathrm{m}'}} \quad (5)$$

F' being the fluorescence steady-state yield measured after 30-s illumination at a given E, and F_m', the maximum fluorescence yield measured at the end of each E by firing a saturating pulse. Non-photochemical quenching was calculated as

$$\mathrm{NPQ} = \frac{F_\mathrm{m} - F_{\mathrm{m}'}}{F_{\mathrm{m}'}} \quad (6)$$

NPQ_m was the maximum NPQ induced during the RLC protocol. The rETR-E curves were fitted with the mathematical model of Eilers and Peeters (1988). It allowed extraction of $rETR_m$, the maximum rETR (rETRm, the asymptote of the curve); α, the use light efficiency (the slope at the beginning of the curve); and E_k, the light saturation parameter:

$$E_\mathrm{k} = \frac{\mathrm{rETR_m}}{\alpha} \quad (7)$$

Diatom Species Identification and Diversity Analysis

Frozen cores were carefully melted, and "Crème brulée" samplers (Laviale et al., 2015) were used to collect the first 250 μm of sediment (Ø 1.4 cm, 1.5 cm^2). To facilitate cell observation and determination, definitive slides were made after their separation from sediment using Ludox HS-40 colloidal silica (SPCI S.A., St. Denis de la Plaine, France) as described before (Méléder et al., 2007). A 48-h decantation allowed separation between cells (at the bottom of the tube) and mineral particles (in Ludox). Settled material was rinsed by centrifugation in distilled water (at least five times) and observed with a photonic microscope. Definitive slides were made after cremation (2 h, 450°C) to observe clean diatom cell frustules mounted in a high-resolution diatom mountant (Naphrax; Brunel Microscopes Ltd., Chippenham, Wiltshire, United Kingdom). Species were identified based on morphology (Witkowski, 2000; Ribeiro, 2010). When photonic microscopy was inconclusive, scanning electron microscopy was used. For species composition analysis, a total of ∼300 diatom frustules were counted to determine specific abundances.

Statistical Analysis

Total and maximum PAB: they were analyzed using one-way analysis of variance (ANOVA) to estimate which PAB proxy was the most impacted by which of the light conditions used. *RLC photosynthetic parameters:* the effects of (i) light conditions (BL 10 and 120 μmol photons m^{-2} s^{-1} and their respective control) and of (ii) the tide sampling timing (BLT, LT, and ALT) were tested using a two-way ANOVA. *Pigment content of sediment:* the effect of the season (Winter and Summer), the light conditions (control winter and summer, and BL 10, 40, and 120 μmol photons m^{-2} s^{-1}), and of the tide sampling timing (BLT, LT, and ALT) were tested using a three-way ANOVA. When significant, ANOVA tests were followed by a *post hoc* Tukey test to highlight differences. *Diatom species abundance:* Hclustering was performed with the Ward.D method in order to group the diatom species and to highlight the groups of interest. All statistical analyses were performed using R software (R Foundation for Statistical Computing, Vienna, Austria).

RESULTS

Vertical Migration Pattern of MPB as a Function of Sediment Type, LT Timing, and Seasons

We monitored MPB abundance at the surface of sediment over 24 h under our light control conditions of 24-h natural photoperiod) at the surface of muddy [dominated by motile epipelon (Serôdio et al., 2012) and sandy-muddy sediments (dominated by epipsammon (Méléder et al., 2007)] (**Figure 2**). For muddy sediment, very low surface MPB abundance occurred at night but rapidly increased with the sun rising, going on through the daytime period until reaching a maximum at approximately solar noon before it decreased (**Figure 2A**). This bell-like pattern also closely followed the daytime period *in situ* water level at the site of sediment sampling (spring tide), although the sediment was continuously exposed to air in our laboratory conditions. Coincidentally, MPB abundance increased from the day HT to the LT timing, reaching a maximum at a timing close to the one of the lowest *in situ* water level (11:15–12:00 vs. 12:00 h Universal Time), and it then decreased from LT timing toward HT (**Figure 2A**). These rhythmic changes in MBP abundance were maintained for 5 ± 1 days in our laboratory conditions with, importantly, a sustained daily shift and therefore time correspondence between the timings of LT and of surface MPB maximal abundance (**Supplementary Figure S1**). Simultaneously, we probed ΦPSII*inst*, the "instantaneous" effective quantum yield of PS II photochemistry, when the maximum MPB abundance was reached to check if our laboratory conditions negatively influenced photosynthetic potential of MPB and therefore its light response, which was confirmed as not being the case with ΦPSII*inst* remaining at near optimal levels of 0.689 ± 0.004. Such verification of ΦPSII*inst* was subsequently performed for all experiments under all light conditions tested (**Supplementary Table S2**). For sandy-muddy sediment, we observed a similar (i) coincidence between the maximum MPB surface abundance with solar noon and (ii) inverse relationship between MPB abundance changes and *in situ* water level with a maximum MPB abundance occurring exactly at LT timing (**Figure 2B**). Nevertheless, major differences appeared compared to muddy sediment: (1) integrated MPB abundance was higher at night, (2) MPB maximum abundance was approximately five times lower during daytime emersion, (3) the speed to reach the MPB maximum abundance was much slower, and (4) after reaching its maximum, MPB abundance remained mostly stable, thus breaking the inverse relationship with the *in situ* water level. ΦPSII*inst* again remained high (0.666 ± 0.004, **Supplementary Table S2**).

Because it provided the strongest and clearest signal, we went on studying migration phenomenon with muddy sediments only. When the *in situ* LT timing did not coincide with solar noon (as in **Figure 2A**), the pattern of MPB abundance changes was different. Two main patterns complementary to **Figure 2A** are shown in **Supplementary Figure S5** (**Supplementary Figure S5A**: neap tide, **Supplementary Figure S5B**: spring tide). When *in situ* LT timing (18:07 h UT) was close to sunset (19:15 h UT), MPB abundance started to increase just after the timing of *in situ* HT, again reaching a maximum significantly before (16:55 h UT) LT timing and sunset, so that MPB abundance reached an

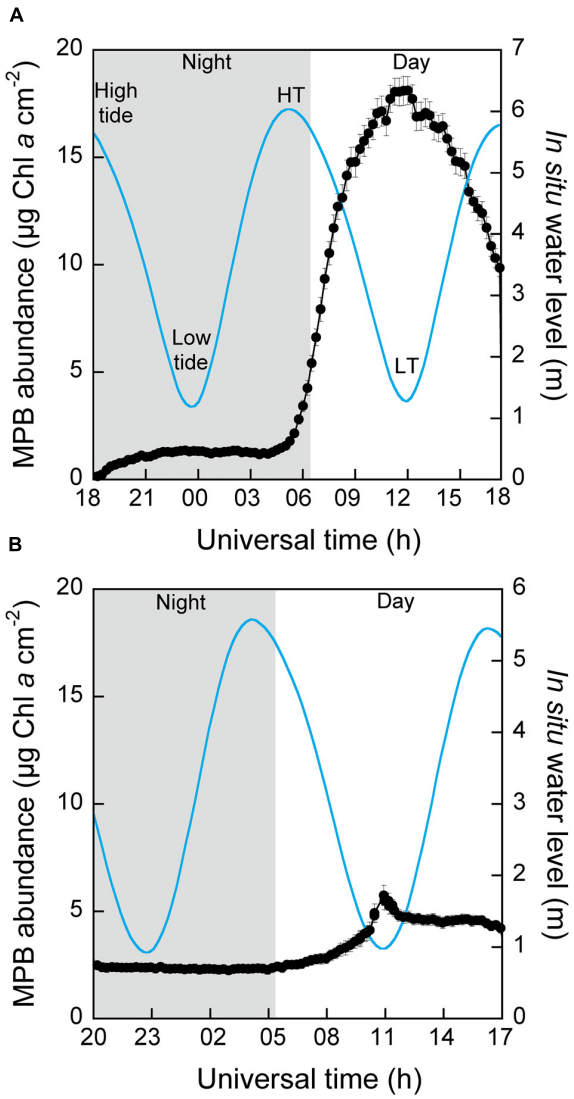

FIGURE 2 | Microphytobenthos (MPB) abundance (µg Chl *a* cm^{-2}) at the surface of sediment and *in situ* water level (m) at the site of sampling as a function of universal time (h UT) measured continuously for 24 h under control light conditions (i.e., 24-h natural photoperiod) for **(A)** muddy sediment mostly inhabited by epipelic diatoms and **(B)** sandy-muddy sediment mostly inhabited by epipsammic diatoms. Black line: MPB abundance (µg Chl *a* cm^{-2}); blue line: water level (m) at the site of sampling; gray and white backgrounds: the natural night and day periods, respectively. Microphytobenthos abundance was derived from Chl *a* fluorescence (F_t level) as measured with an Imaging-PAM and HPLC analysis of Chl *a* sediment content (**Supplementary Figure S2**); values are the mean ± SD of 5 Imaging-PAM "areas of interest" on the sediment tray. Water-level data were retrieved from the Service Hydrographique et Océanographique de la Marine (SHOM, France) database. See Section "Materials and Methods" for further details, and **Supplementary Figure S5** for MPB abundance patterns when the low tide timing was close to sunset and/or sunrise (i.e., spring and neap tides).

approximately 0 value only 3 h after sunset (**Supplementary Figure S5A**). When *in situ* LT timing was close to sunrise (∼1 h 15 after sunrise), the maximum MBP abundance followed two patterns as a function of the preceding *in situ* LT timing event (i.e., neap tide or spring tide, respectively): (1) when the later was just before sunset (∼1 h 15), MPB abundance started to increase the same way as during the preceding daytime period, that is, following the *in situ* water level decrease independent of the day–night alternation (here ∼2 h before sunrise) and reaching its maximum just after the *in situ* LT timing with no coincidence with solar noon (**Supplementary Figure S5A**); (2) when the preceding *in situ* LT was at night, MPB abundance started increasing with sunrise, reaching its maximum after the *in situ* LT timing and at a time closer to solar noon (**Supplementary Figure S5B**).

Taking into account these patterns and their variations, we compiled 85 profiles from 40 sediment samplings over 2 years (**Supplementary Table S1**) in order to compute (i) the total PAB (Guarini et al., 2006; Coelho et al., 2011) of MPB present at the surface of sediment (the integrated area under the curve), and (ii) the maximum surface PAB reached during daytime LT period. Note that total PAB was computed over 24 h, including nighttime, in order to analyze both MPB abundance changes occurring during daytime (**Figure 2A**) and closer to sunrise and/or sunset (**Supplementary Figure S5**). When PAB was plotted versus the *in situ* level of low waters, there was no clear trend (**Figure 3A** and **Supplementary Figure S6A**). When plotted versus the *in situ* LT timing, a clearer pattern was observed (**Figure 3B** and **Supplementary Figure S6B**): (i) the maximum and total PAB were recorded at daytime LT timings independent of the season; (ii) there was a tendency for the highest values of maximum PAB to be reached when the LT timing coincided with solar noon (ca. 12:00 ± 2:00 h UT) as in **Figure 2A**. When plotted versus sampling date (**Figure 3C** and **Supplementary Figure S6C**), the highest PAB values occurred by the end of winter–beginning of spring, they decreased to reach a minimum in summer and autumn and increased again through the next winter. For all experiments, ΦPSII*inst* was high (0.681 ± 0.026, **Supplementary Table S2**).

Vertical Migration Pattern of MPB as a Function of Light Regimes

In a following step, we manipulated the 24-h natural photoperiod to study its impacts on MPB abundance changes at the surface of sediment. First, we artificially replaced the daytime period by night resulting in 24-h continuous darkness and the other way around (**Figures 4A,B**, respectively). Before such manipulation, MPB migration was recorded for 24 h the same way as described in **Figure 2A**, reaching a similar maximum PAB: 15.8 ± 0.7 μg Chl *a* cm^{-2} (**Figure 4A**) and 16.0 ± 0.7 μg Chl *a* cm^{-2} (**Figure 4B**). When exposed to 24-h darkness, changes in MPB abundance followed a similar pattern as during the preceding 24 h of 24-h natural photoperiod, except the maximum PAB reached during subjective daytime period was lower: 11.3 ± 0.9 μg Chl *a* cm^{-2} (**Figure 4A**); ΦPSII*inst* remained high (**Supplementary Table S2**). When exposed to

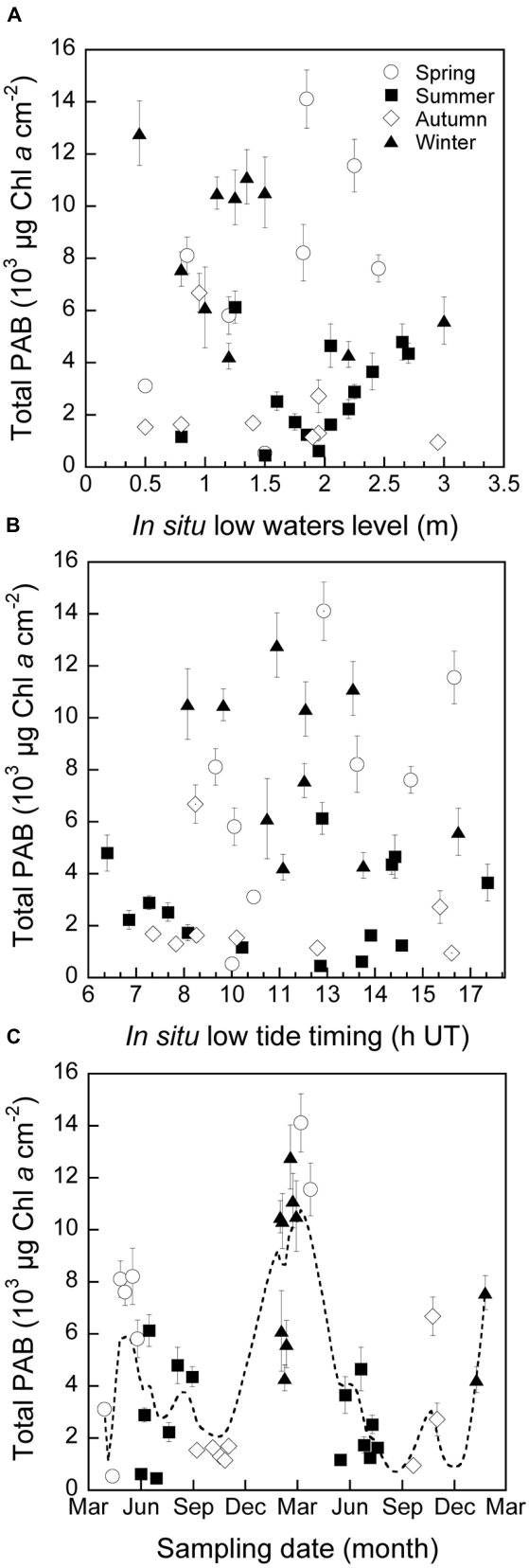

FIGURE 3 | Continued

FIGURE 3 | Microphytobenthos total photosynthetically active biomass (PAB) at the surface of muddy sediment as function of **(A)** low water level at the site of sampling (i.e., the lowest water level, which depends on the tidal amplitude), **(B)** the low tide timing (h UT) at the site of sampling (i.e., corresponding to the lowest water level), and **(C)** the date of sampling (month abbreviations are Mar, March; Jun, June; Sep, September; Dec, December). In order to facilitate visualization, months were pooled under season labels: spring (circles), summer (squares), autumn (diamonds), and winter (triangles). Values are the mean ± SD of 5 Imaging-PAM "areas of interest" on the sediment tray. Water level and low tide timing data were retrieved from the Service Hydrographique et Océanographique de la Marine (SHOM, France) database.

24-h light (**Figure 4B**), MBP abundance immediately increased upon onset of the artificial light even if during subjective nighttime period, reaching a maximum (5.9 ± 0.6 μg Chl *a* cm^{-2}) at a time coinciding with the *in situ* LT timing and maintaining at this maximum. During the following daytime period, (i) the increase in MPB abundance was slower than during the first 24-h daytime period so that the occurrence of the maximal PAB was delayed by approximately 2 h (i.e., it occurred 90 min after the *in situ* LT timing instead of 30 min before), and (ii) the value of maximum PAB was much higher: 24.7 ± 0.6 μg Chl *a* cm^{-2}. Although ΦPSII*inst* decreased, it remained relatively high (0.588 ± 0.037, **Supplementary Table S2**).

In a second manipulation, we aimed at desynchronizing MPB migration from the 24-h natural photoperiod and eventually from the *in situ* tidal cycle. We continuously monitored MPB migration over several days, and after a first 24-h exposure to an artificial light regime exactly matching the 24-h natural photoperiod, we inverted it by exposing the sediment to darkness during subjective daytime (starting Day 2) and by applying the same artificial light as in **Figure 4B** during subjective nighttime periods (**Figure 4C**). After 1 day under the new light regime (Days 2–3 in **Figure 4C**), MPB abundance changes showed a similar pattern as for the short-time experiments described in **Figures 4A,B**. This pattern was kept along the 4 following days with a maximum PAB always reached by the end of the light period would it be during artificial daytime (Day 1, similar as **Figure 4B**, and coinciding with the timing of the *in situ* LT) or subjective nighttime (the following days). Of paramount interest was the fact that in the meantime the timings of the *in situ* LT shifted by 60 ± 15 min per day. It generated a complete loss of synchronization between the timing of maximum PAB with the timing of the *in situ* LT (compare with **Supplementary Figure S1**), so that by the end of the experiment the maximum PAB was reached at a time nearly coinciding with the timing of the *in situ* HT (03:00 vs. 04:20, Day 6, **Figure 4C**). ΦPSII*inst* was 0.648 ± 0.008 for Day 1 and 0.671 ± 0.009 for the following days (**Supplementary Table S2**).

Vertical Migration Pattern of MPB as a Function of Light Intensity and Light Spectrum

We furthermore tested the effect of light intensities and wavelengths on the PAB at surface of sediment at all seasons, through experiments with the same light conditions performed at different seasons, thus taking into account seasonal changes in MPB abundance (**Figure 3C**). Results are compiled in **Figure 5**, **Supplementary Figure S7**, and **Supplementary Table S3**. In order to compare all light conditions, data were normalized on the control light conditions, which were systematically performed before each light treatment (i.e., the first 24-h MPB migration under 24-h natural photoperiod as in **Figure 2A**). Note that (i) we worked at equivalent PAR ("photosynthetically active radiation"); for technical reasons, we could not work at equivalent PUR ("photosynthetically usable radiation"); (ii) due to technical limitation of our LED panels, we could not use the same PAR for all wavelengths; in particular, monochromatic wavelengths did not reach the highest "white" light PAR (350 μmol photons m^{-2} s^{-1}); (iii) the statistical analysis was significant only when considering total PAB (one-way ANOVAs, $p \leq 0.05$, **Supplementary Table S3**) rather than maximum PAB (one-way ANOVAs, $p > 0.05$, **Supplementary Table S3**). Based on Tukey *post hoc* test, we could draw the following observations. Among all light treatments: (i) a significantly lower total PAB was observed in sustained darkness [39% ± 2% of the control ($p \leq 0.05$) compared to 120 μmol photon m^{-2} s^{-1} white light and BL and to 40 μmol photons m^{-2} s^{-1} green light; see **Figure 4A** and **Supplementary Table S3**]; (ii) the significantly ($p \leq 0.05$) highest total PAB values were reached for lights of 120 μmol photons m^{-2} s^{-1} ("white" and blue, 144% ± 3% and 176% ± 38% of the control, respectively). Yet, lower or higher irradiances generated no significant changes or a significant decrease in total PAB independent of the wavelength (**Supplementary Table S3**). ΦPSII*inst* was high under all light conditions: 0.642 ± 0.047 (**Supplementary Table S2**).

More precisely (**Figure 5** and **Supplementary Table S3**), under "white" light, total PAB significantly increased with irradiance (from 20 to 120 μmol photons m^{-2} s^{-1}) and decreased thereafter (from 120 to 350 μmol photons m^{-2} s^{-1}), so that total PABs under 20 and 350 μmol photons m^{-2} s^{-1} were not significantly different. Under BL (465 nm), total PAB significantly increased with intensity (from 10 to 120 μmol photons m^{-2} s^{-1}); noteworthy is the effect of an irradiance as low as 10 μmol photons m^{-2} s^{-1} of BL, which generated a total PAB as high as 75% ± 2.77% of the control. Green light (530 nm) did not trigger a response significantly different from the control light conditions (40 μmol photons m^{-2} s^{-1}) and darkness (10 μmol photons m^{-2} s^{-1}). Unfortunately, with our setup, we could not test higher green light intensities. The maximum intensity of red light (677 nm, with and without far red 748 nm, 180 μmol photons m^{-2} s^{-1}) did not trigger a total PAB significantly different from the control light.

Effect of BL on the MPB Pigment Content, Photosynthetic Performance, and Diatom Species Composition During Vertical Migration

Because we observed a specific BL positive effect, we analyzed potential changes in (i) the pigment content, (ii) the photosynthetic performance, and (iii) the species composition

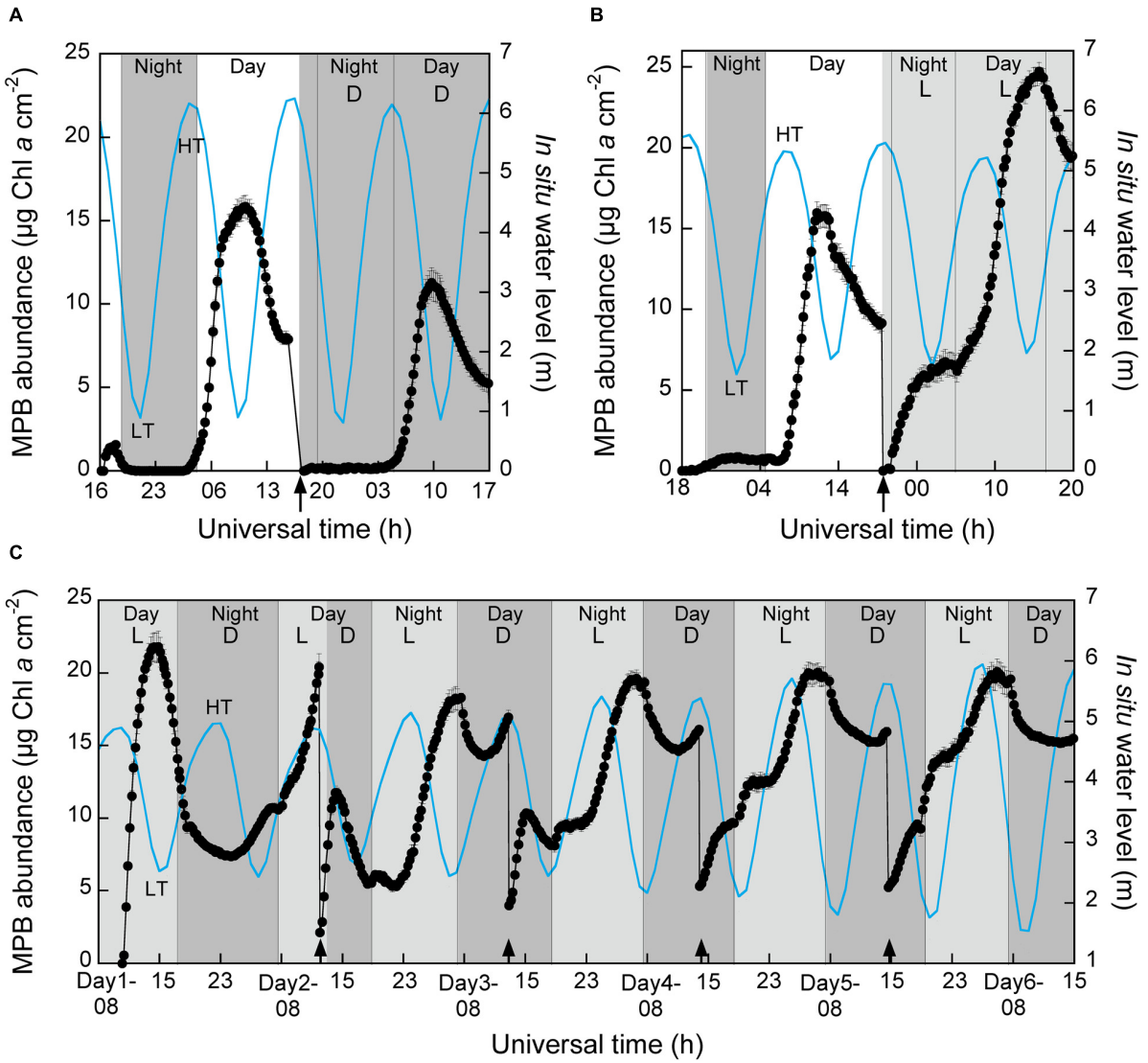

FIGURE 4 | Microphytobenthos abundance (µg Chl *a* cm^{-2}) at the surface of muddy sediment, and *in situ* water level (m) at the site of sampling as function of universal time (h UT), and monitored under different light regimes: **(A)** control light conditions for the first natural night/day period ("Night" and "Day" backgrounds) followed by artificial darkness (D) for the second night/day period; **(B)** control light conditions for the first natural night/day period followed by continuous artificial "white" light (L, 120 µmol photons m^{-2} s^{-1}) for the second night/day period, **(C)** artificial "white" light (L) followed by artificial darkness (D) for the first night/day period (Day 1), followed by artificially inverted night/day period (starting Day 2) for the four following days (Days 3–6). Low tide and HT, low tide and HT *in situ* timings, respectively, as in **Figure 2**. Black line: MPB abundance (µg Chl *a* cm^{-2}); blue line: water level (m) at the site of sampling; dark gray and light gray backgrounds: the night and day periods, respectively; arrows indicate the timings for which the sediment was stirred with fresh seawater. Microphytobenthos abundance was derived from Chl *a* fluorescence (F_t level) as measured with an Imaging-PAM and HPLC analysis of Chl *a* sediment content (**Supplementary Figure S2**); values are the mean ± SD of 5 Imaging-PAM "areas of interest" on the sediment tray. Water-level data were retrieved from the Service Hydrographique et Océanographique de la Marine (SHOM, France) database. See the Section "Materials and Methods" for further details.

of MPB during its migration [at the *in situ* LT timing, 3 h before (BLT) and after (ALT)] under BL exposure of different intensities (10, 40, and 120 µmol photons m^{-2} s^{-1}) and for winter and summer sediments, when total PAB was the highest and the lowest, respectively (**Figure 3C**).

Pigment Content and Photosynthetic Performance

Pigments were analyzed at three depths (0–200, 200–400, and 400–600 µm; **Supplementary Table S4**) and expressed relative to Chl *a* in order to normalize for pigment changes due to changes in MPB abundance with seasons and/or tidal cycle (**Figure 3**); 600 ± 100 µm is usually the depth of the photic zone in fine sediments, and 200–250 µm is where photoprotection is the highest (Cartaxana et al., 2011). We found significant differences in winter versus summer sediments exposed to light control conditions and for most sampling times (LT, BLT, and ALT), as well as some significant differences under BL versus control light conditions (detailed description, **Supplementary Table S4**).

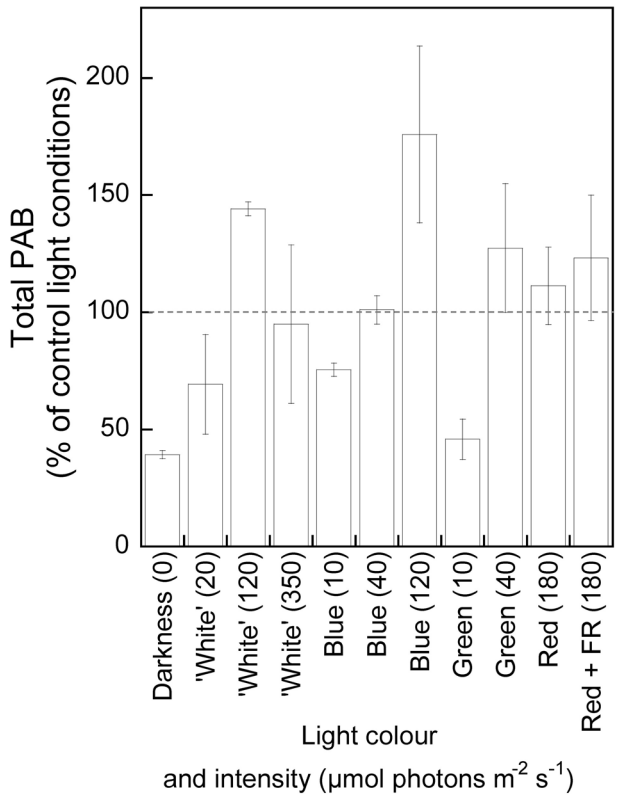

FIGURE 5 | Microphytobenthos total photosynthetically active biomass (PAB in% of the control light conditions) at the surface of muddy sediment and under different light exposures of 24 h. Values are the mean ± SD of n measurements for each light condition. The light conditions were as follows: darkness (0 µmol photons m^{-2} s^{-1}, $n = 2$), "white" light (emission maxima at 459 and 553 nm, 20 µmol photons m^{-2} s^{-1}, $n = 2$; 120 µmol photons m^{-2} s^{-1}, $n = 2$; 350 µmol photons m^{-2} s^{-1}, $n = 2$), blue light (465 nm, 10 µmol photons m^{-2} s^{-1}, $n = 2$; 40 µmol photons m^{-2} s^{-1}, $n = 5$; 120 µmol photons m^{-2} s^{-1}, $n = 5$), green light (530 nm, 10 µmol photons m^{-2} s^{-1}, $n = 2$; 40 µmol photons m^{-2} s^{-1}, $n = 4$), red light (180 µmol photons m^{-2} s^{-1}, 677 nm; without far-red-FR, 748 nm, $n = 3$ and with FR, $n = 2$). Control light condition (24-h natural photoperiod) values were set to 100% (performed before each light treatment). See **Supplementary Figure S4** for the full emission spectrum of each LED color and **Supplementary Figure S7** for MPB maximum PAB data.

However, we observed no changes in MPB pigment content, and especially in BL absorbing carotenoids, to relate with the BL positive effect on vertical MPB migration described above (see section "Vertical Migration Pattern of MPB as a Function of Light Intensity and Light Spectrum").

Because most of the significant differences in pigment content were observed for sediment sampled in summer (**Supplementary Table S4**), we analyzed MPB photosynthetic performances in summer only and for the BL lowest and highest intensities (10 and 120 µmol photons m^{-2} s^{-1}) (**Table 1**). F_v/F_m (which is equivalent to ΦPSII*inst* after dark acclimation of MPB) was high and stable for all BL treatments and their respective controls (two-way ANOVA, $p > 0.05$ for all factors, **Table 1**). Because they could not be monitored during a restricted timeframe (i.e., two consecutive weeks), the two controls significantly differed in $rETR_m$ and E_k, both parameters of the control for BL-10 (sampling end of May) being lower than the control for BL-120 (sampling end of July) (two-way ANOVA, $p \leq 0.001$ for the light effect, different groups with the Tukey test, **Table 1**). While exposure to BL-10 µmol did not yield any significant changes in photosynthetic performance (similar group with Tukey test; **Table 1**), BL-120 generated a significant decrease in $rETR_m$ and E_k for all *in situ* tide timings (different group with Tukey test; **Table 1**) but no significant changes in α (two-way ANOVA, $p > 0.05$ for all factors). There was also a tendency for higher NPQ_m values under BL-120 LT versus control conditions (two-way ANOVA, $p \leq 0.05$ for the light effect).

Diatom Species Composition

The MPB species composition was analyzed in the 0- to 250-µm sediment layer. Forty-nine species were identified including a large majority of pennate diatoms and of epipelic representatives (**Supplementary Table S5**). Because only two species, *Navicula phyllepta* and *Navicula spartinetensis*, were present in all samples, we first proceeded with an Hcluster analysis showing that most of the species (left cluster, **Supplementary Figure S8A**) have a very low abundance. In a second step (**Supplementary Figure S8B**), we proceeded with the 19 species that were present at least once >5% of the total MPB relative abundance. This way, two species, *N. spartinetensis* and *G. fasciola*, were highlighted. The species relative abundance of all experiments (**Figure 6**) showed that (i) only the exposure to BL-40 generated major changes (**Figures 6B,D**), and (ii) these changes concerned *N. spartinetensis* in summer (**Figure 6B**, pale blue) and *G. fasciola* in winter (**Figure 6D**, yellow). In order to discard a potential effect of changes in the relative abundance of other motile species on *N. spartinetensis* and *G. fasciola* (i.e., for instance their relative abundance would be artificially increased by a decrease in the relative abundance of other motile species), we normalized the relative abundance of the 12 motile species (among the selected 19) encountered in the light conditions of interest (summer and winter, BL-40) to the relative abundance of non-motile species as a common and stable basis: if the abundance of a given species would increase relative to non-motile species, we would assume an upward migration and *vice versa*. This analysis (**Supplementary Figure S9**) confirmed that *N. spartinetensis* and *G. fasciola* were indeed the two species whose abundances increased relative to the pool of non-motile species under BL and that the response of *N. spartinetensis* was particularly strong.

More precisely, for both species, BL induced an increase in abundance at the surface of sediment, all along the LT period (**Supplementary Figure S10**). *Gyrosigma fasciola* was massively present at the surface of sediment (50% of the total abundance of 19 most present species) already by the beginning of LT (BLT) while appearing only by the end of the LT (ALT) under control light conditions (**Supplementary Figure S10B**). Noteworthy were the observations highlighting a respective specific effect of a certain BL dose in the two species: (i) while *N. spartinetensis* abundance continuously increased to reach a maximum of approximately 85% relative abundance at ALT timing, *G. fasciola* abundance decreased by approximately

TABLE 1 | Photosynthetic parameters of microphytobenthos (MPB) exposed to blue (465 nm) light conditions (the blue 10 and 120 μmol photon m^{-2} s^{-1} intensities between brackets) and their respective control light conditions: because the two blue light exposures could not be performed simultaneously, it was necessary to perform measurements under control light conditions independently for each of them.

		Control	Blue (10)	Control	Blue (120)
BLT	F_v/F_m	0.74 ± 0.02	0.72 ± 0.05	0.74 ± 0.03	0.72 ± 0.03
	α	0.63 ± 0.06	0.63 ± 0.05	0.63 ± 0.05	0.62 ± 0.06
	$rETR_m$	38.78 ± 6.96^{bc}	40.35 ± 7.58^{bc}	92.3 ± 19.71^{a}	54.25 ± 11.14^{b}
	E_k	66.58 ± 10.43^{bcd}	65.53 ± 16.36^{bcd}	146.21 ± 26.08^{a}	88.29 ± 18.45^{b}
	NPQ_m	1.11 ± 0.12^{ab}	1.05 ± 0.20^{ab}	1.01 ± 0.19^{ab}	1.11 ± 0.48^{ab}
LT	F_v/F_m	0.75 ± 0.02	0.74 ± 0.02	0.72 ± 0.02	0.74 ± 0.03
	α	0.63 ± 0.05	0.64 ± 0.05	0.63 ± 0.05	0.63 ± 0.07
	$rETR_m$	36.32 ± 6.48^{bc}	36.44 ± 7.93^{bc}	91.7 ± 15.18^{a}	45.63 ± 11.78^{bc}
	E_k	60.77 ± 9.47^{bcd}	58.54 ± 16.9^{cd}	147.4 ± 20.05^{a}	67.65 ± 11.47^{bcd}
	NPQ_m	1.05 ± 0.18^{ab}	1.06 ± 0.26^{ab}	1.08 ± 0.26^{ab}	1.45 ± 0.46^{a}
ALT	F_v/F_m	0.73 ± 0.03	0.74 ± 0.02	0.71 ± 0.02	0.72 ± 0.07
	α	0.61 ± 0.06	0.64 ± 0.06	0.68 ± 0.07	0.58 ± 0.07
	$rETR_m$	29.93 ± 8.60^{c}	35.72 ± 8.58^{bc}	81.82 ± 20.56^{a}	47.53 ± 3.41^{bc}
	E_k	49.55 ± 10.11^{d}	58.23 ± 15.19^{cd}	129.02 ± 25.22^{a}	87.35 ± 18.53^{bc}
	NPQ_m	0.93 ± 0.17^{b}	0.99 ± 0.24^{b}	1.10 ± 0.22^{ab}	1.29 ± 0.35^{ab}

Two-way analysis of variance were performed to test the effect of light conditions and of the tide sampling timing. Post hoc Tukey test was further performed to group values. For each photosynthetic parameter, values with the same letter are not significantly different. F_v/F_m, maximum quantum yield of PSII photochemistry (no units); α, maximum light efficiency use (relative units); $rETR_m$, maximum relative photosynthetic electron transport rate (μmol electrons m^{-2} s^{-1}); E_k, light saturation coefficient (μmol photons m^{-2} s^{-1}); NPQ_m, maximum NPQ (no units); BLT, 3 h before low tide; LT, low tide timing at the site of sampling (i.e., corresponding to the lowest water level); ALT, 3 h after low tide. Values are the mean ± SD of 3 measurements.

20%; (ii) for *N. spartinetensis*, a BL-10 and BL-120 did not induce changes in abundance relative to control light conditions (**Figures 6A,C**); the same was true for *G. fasciola* response to BL-120 (BL-10 was not tested). Finally, and to a much lower extent, other *Navicula* species (especially *Navicula phyllepta* and *Navicula gregaria*) might show a positive response to BL (**Figure 6** and **Supplementary Figure S9**).

DISCUSSION

Monitoring of the Changes in the MPB PAB at the Surface of Sediment by Imaging-PAM Fluorimetry

The use of coupled Chl *a* fluorescence with imaging techniques has proven to be of paramount interest to monitor the temporal changes in MPB biomass, in particular with an Imaging-PAM fluorometer (Du et al., 2010; Vieira et al., 2013; Blommaert et al., 2018). Imaging of Chl *a* fluorescence allows assessment of the dynamics of the "photosynthetically active (or productive) biomass" (PAB) at the surface of sediment (Herlory et al., 2005; Guarini et al., 2008). In the present study, we have used Imaging-PAM fluorimetry to assess changes in PAB in a continuous mode with measurements every 900 s over several days with less than 15-min stop for watering and mixing the sediment tray every 24 h. The main advantage of imaging-fluorimetry compared to other fluorimeters (for instance, the Water-PAM fiber version or the Diving-PAM) is its non-invasive feature; there is no contact with the sediment surface (Vieira et al., 2013). This way, (i) MPB biofilm structure is not disturbed, (ii) its light microenvironment is less biased, and (iii) changes in MPB abundance can be followed simultaneously with regular measurement of photosynthetic performances (for instance, here, ΦPSII*inst*) taking into account potential limitations (Vieira et al., 2013). More precisely here, we have monitored F_t, the "instantaneous" Chl *a* fluorescence yield as measured with the detecting beam of the Imaging-PAM. The interest in using F_t instead of the well-known MPB biomass proxy F_0 (Consalvey et al., 2005) was to avoid darkening of the MPB, which is known to induce counteracting downward migration, and would have therefore disrupted rhythmic dynamics in MPB migration. Stock et al. (2019) also noticed that F_0 could be successfully replaced by F_t under some experimental conditions [see also Ni Longphuirt et al. (2006)]. We verified that F_t was well correlated to the Chl *a* content of sediment surface (R^2 = 0.84), a correlation as strong as the ones previously reported between F_t (Ni Longphuirt et al., 2006) or F_0 (Honeywill et al., 2002; Serôdio et al., 2006) and Chl *a*. Although the detecting beam was used with minimal irradiance settings, to be as close as possible to non-actinic conditions, still 0.81 ± 0.08 μmol photons m^{-2} s^{-1} were generated at the surface of sediment trays. It appeared, *a posteriori*, that this intensity of blue wavelength (470 nm) was sufficiently effective in triggering positive, albeit limited, upward migration of MPB (see section "Influence of the Light Spectrum on the Amount of PAB Present at the Surface of Sediment: Specific Effect of BL Wavelengths"). This effect was most obvious with the 5.1% ± 4.0% total PAB at night (as compared to control light conditions), which is not expected to occur (see section "What Influences the Most the Amount of PAB Present at the Surface of Sediment: Tides or Light?"). This is nevertheless consistent with earlier findings reporting an effect of irradiances as low as 0.5 to 1 μmol photons m^{-2} s^{-1} in triggering the directional motility of epipelic diatoms (Paterson, 1986; Cohn and Weitzell, 1996; Wenderoth and Rhiel, 2004). There would be

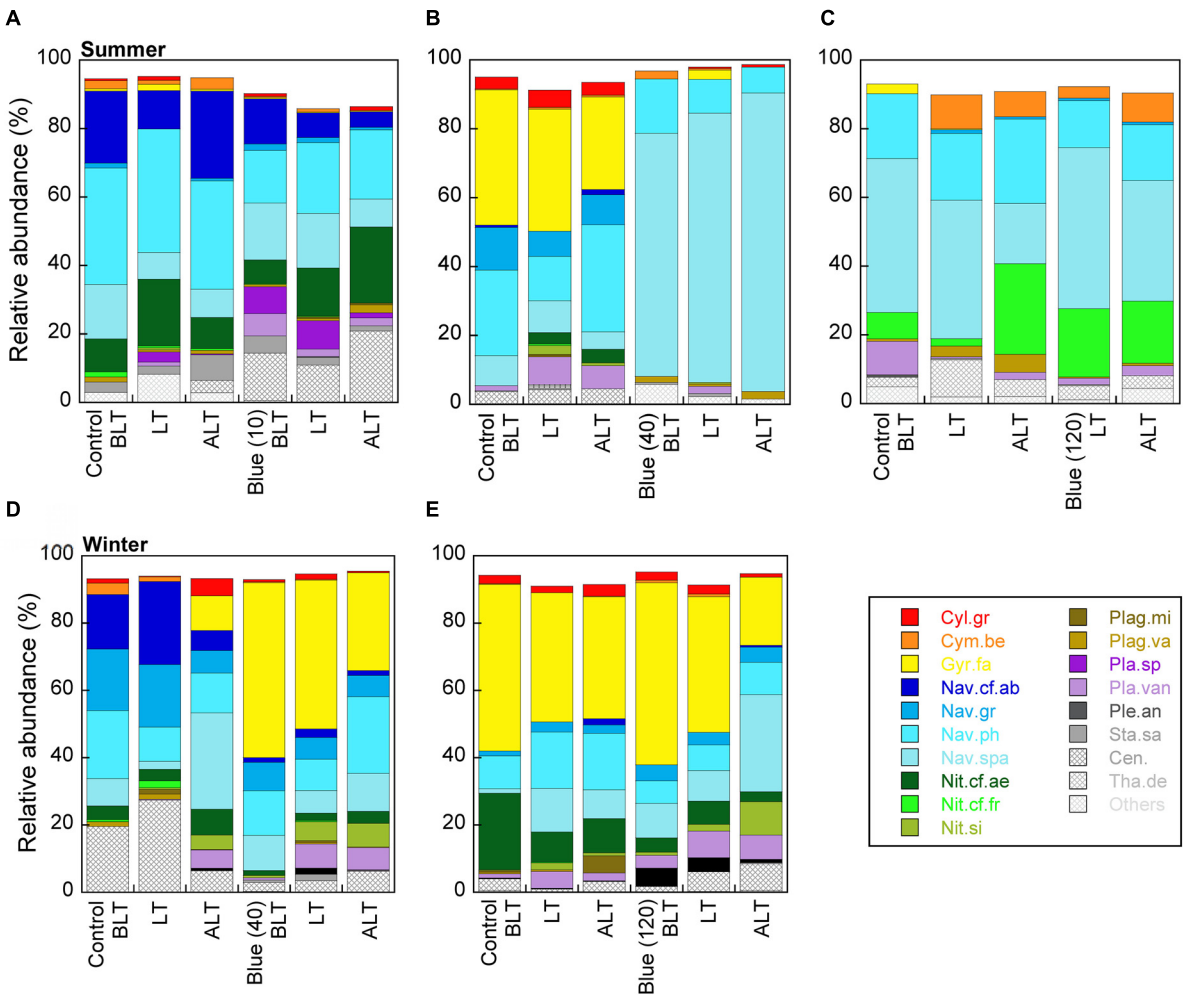

FIGURE 6 | Cumulative relative abundance of the 19 diatom species found at least once >5% of the total relative MPB abundance in the upper layer (0–250 μm) of muddy sediment for the three timings of the *in situ* low tide at the sampling site (BLT-3 h before low tide, LT-low tide timing, ALT-3 h after low tide) and for two seasons and different light conditions: **(A–C)** summer blue (465 nm) light treatment with three increasing light intensities: **(A)** 10, **(B)** 40, and **(C)** 120 μmol photons m^{-2} s^{-1} with their respective control (24-h natural photoperiod) light conditions; **(D,E)** winter blue light treatment with two light intensities: **(D)** 40 and **(E)** 120 μmol photons m^{-2} s^{-1} with their respective control light conditions. The full list of species with their full names is found in Supplementary Table S5. A zoom of winter and summer 40 μmol photons m^{-2} s^{-1} blue light treatments with focus on *Navicula spartinetensis* and *Gyrosigma fasciola* is shown in **Supplementary Figure S10**.

two ways of avoiding this drawback: (1) instead of measuring F_t, to use the red and near-infrared LEDs of the Imaging-PAM LED panel to measure an NDVI index shown to be well correlated with Chl *a* sediment content (Blommaert et al., 2018); (2) to replace the blue Imaging-PAM measuring head by the red (650–660 nm) one for measuring F_t, which most likely (see section "Influence of the Light Spectrum on the Amount of PAB Present at the Surface of Sediment: Specific Effect of BL Wavelengths") will not trigger MPB migration at night.

These minor technical limitations being considered, our experimental setup allowed us to reliably monitor MPB migration dynamics *ex situ*. The patterns we observed in muddy sediment dominated by epipelic diatoms at different times of the day and as a function of LT timings (i.e., at solar noon or close to sunset and/or sunrise, see section "Vertical Migration Pattern of MPB as a Function of Sediment Type, LT Timing, and Seasons") were well in accordance with those accurately described decades ago both *in situ* and in the laboratory (Consalvey et al., 2004). Of primary importance here was the checking of several prerequisites for further experimental manipulation. As others before (Consalvey et al., 2004), (i) we could observe a migratory rhythm of natural MPB assemblages in laboratory-controlled conditions and without any artificially recreated tidal rhythm (i.e., alternation of emersion/immersion); (ii) this migratory rhythm was precisely related to the *in situ* LT timings (i.e., corresponding to the lowest water level at the sampling site) and to the day length (photoperiod); (iii) migratory rhythm was maintained for 5 ± 1 consecutive days with only sea-watering and sediment mixing every 24 h at the exact timing of *in situ* HT; (iv) migratory rhythm was maintained whatever the season at which the sediment was sampled (albeit the amplitude was different, see below); (v) the photosynthetic potential of MBP

(ΦPSII*inst*) was preserved. In fact, our conditioning of sediment was good enough, and our experimental setup sensitive enough so that we could record the MPB activity even in sandy sediment dominated by epipsammic diatoms. Epipsammic species are generally immotile except for representatives that are capable of micromovements within the sphere of the sediment particle to which they are attached, or from a particle to another (Harper, 1969; Round, 1979). Here, when compared to muddy sediment, we could observe (i) a stronger night basal Chl *a* fluorescence signal probably due to the deeper penetration of the Imaging-PAM detecting beam in the coarser sediment, and (ii) a slower, weaker but sustained increase in MPB abundance at the surface of sediment around daytime solar noon *in situ* LT timing that we interpret as the motile epipsammic and/or the small proportion of epipelic diatoms moving toward the light source (Harper, 1969; Cartaxana et al., 2011), and thus increasing the fluorescence signal. By compiling all of our MPB migration profiles, we could draw a general scheme of surface PAB changes as a function of tidal amplitude, LT timing, and seasons, at our study site. Because the later was upper-shore (i.e., 500 m from the shore, approximately 4 m above the marine chart datum), MPB was often emerged, even for low tidal amplitude. This situation likely explains why we did not observe any clear correlation in PAB changes with the *in situ* tidal amplitude and LT timing (see also Brotas et al., 1995; Jesus et al., 2009; Coelho et al., 2011). However, surface PAB was strongly related to the sampling season with the highest values observed by the end of winter–beginning of spring. This general seasonal pattern strikingly matches the one recorded through the analysis of a 15-year satellite remote sensing time-series over the Brouage mudflat located just south of our sampling site (Méléder et al., unpublished). This result is of crucial importance for future up-scaling approaches for the estimation of intertidal mudflat primary production (Daggers et al., 2018), the present experimental setup providing a reliable intermediary step between *in situ* measurements and satellite images.

What Influences the Most the Amount of PAB Present at the Surface of Sediment: Tides or Light?

It is generally accepted that the rhythmic MPB vertical migration in intertidal sediment and the surface PAB accumulation are governed by the tidal and diurnal cycles together (Consalvey et al., 2004; Coelho et al., 2011). There are nevertheless situations where tides have a more limited influence and/or light a stronger influence; in such conditions, MPB migration strongly matches with diurnal photoperiodic and irradiance (see below) changes (see, for instance, Mitbavkar and Anil, 2004; Ni Longphuirt et al., 2006). It highlights the possibility to disentangle the tight link between the tidal and diurnal rhythmicity of MPB migration. We thus manipulated the 24-h natural photoperiod of MPB in order to try desynchronizing MPB migration pattern from the tidal and/or diurnal cycles. Differently from previous works (Kwon et al., 2012; Haro et al., 2019), we did not submerse the sediment in order to avoid potentially exacerbated photoperiodic response as in subtidal sediments (Ni Longphuirt et al., 2006). Our experiments have shown that (i) MPB migration can persist for 5 ± 1 days *ex situ* following *in situ* tidal cycle and photoperiod even when permanently maintained emerged (although homogenized with seawater every 24 h); (ii) in neap tide situation (i.e., LT timings close to sunset and sunrise), MPB migration occurs irrespective of the photoperiod and is primarily modeled onto the tidal cycle; (iii) under 24-h darkness or light exposure, MPB migration goes on matching the LT timing of the subjective day or night; (iii) within few days, it is possible to completely desynchronize MPB migration from the tidal cycle to force it matching photoperiod such as in *in situ* subtidal sediments (Ni Longphuirt et al., 2006) or intertidal sediments immerged *ex situ* (Paterson, 1986; Haro et al., 2019). These observations confirm and complete previous ones [see the synthesis by Consalvey et al. (2004), as well as more recent works where MPB migration was experimentally manipulated *ex situ* (Coelho et al., 2011; Kwon et al., 2012; Haro et al., 2019)]. Also important are the many *in situ* observations that (see Happey-Wood and Jones, 1988; Consalvey et al., 2004; Coelho et al., 2011) (i) MPB at the surface of sediment appears to "anticipate" the incoming tide by migrating downward, although this behavior is not systematic; (ii) MPB migrates downward even during emersion at dusk or when darkened.

Taken all together, these features support the endogenous nature of intertidal MPB migration rhythmicity, which is first modeled onto the tidal cycle [so-called "lunidian clock" phased on the lunar day length and cycle (Palmer, 2000)], which can be modulated (i.e., entrained and/or reset; Haro et al., 2019), potentiated, and even overridden, by the diurnal cycle, also potentially controlled by an endogenous circadian clock, in some situations. Quantification of the "potentiating" effect of non-stressful light can be attempted using PAB values under prolonged darkness and continuous light exposures: respectively, 39% ± 2% and 144% ± 3% of control light conditions, strikingly similar to previous reports (approximately 40% in darkness and approximately 130–155% at optimal irradiance) (Sauer et al., 2002; Coelho et al., 2011). These values would mean that light can potentiate the tidal effect on surface PAB accumulation by a factor of 1.6 under 24-h natural photoperiod conditions to more than 2.5 in optimal laboratory conditions (see also Coelho et al., 2011). It was proposed before that endogenous clock(s) would control cell gravitaxy to match the tidal cycle and cell phototaxy to match the diurnal cycle (see Mitbavkar and Anil, 2004; Coelho et al., 2011; Frankenbach et al., 2014). Saburova and Polikarpov (2003) additionally proposed that the central biological driver of rhythmic MPB migration is the cell division cycle and its spatial disconnection from photosynthesis; that is, the cell cycle occurs in the stable and nutrient-rich deep sediment layers during immersion/at night, and it needs the photochemical energy and organic carbon that is generated and stored at the surface of sediment during daytime emersion (Underwood et al., 2005; Marques Da Silva et al., 2017). This temporal (light vs. dark periods) metabolic decoupling in diatoms has been further demonstrated (Skogen Chauton et al., 2013). The

endogenously controlled rhythmic MPB migration, modeled onto intertidal flat environmental conditions, would allow MPB to perform surface and depth biological processes in the most optimal conditions. Although endogenous circadian clocks, their components and regulation, have been well detailed in several algal lineages, they remain uncharacterized in diatoms (Noordally and Millar, 2015), with the exception of the recent discovery of a time-keeping molecular component, which controls the diel rhythmic expression of many genes (Annunziataa et al., 2019).

Both lunar and solar day major drivers can be in turn modulated by other environmental stimuli (temperature, nutrients, salinity, pH, etc.; see Consalvey et al., 2004), and by other light features: light spectrum (see section "Influence of the Light Spectrum on the Amount of PAB Present at the Surface of Sediment: Specific Effect of BL Wavelengths") and irradiance. Indeed, during emersion, the light availability at the surface and in sediment is also defined by the course of the sun during the daytime period, by open-field–like incident irradiance fluctuations and by the sediment-dependent light penetration, which varies with several features [particle size, content in pore water, etc. (Kuhl and Jorgensen, 1994)]. Many studies have reported how the level of irradiance controls epipelic diatom phototaxis in a biphasic way. While up to a certain irradiance threshold light promotes upward migration and the formation of the MPB biofilm, beyond this threshold it conversely induces downward migration and decreases surface PAB (see, for instance, Serôdio et al., 2006; Laviale et al., 2016). It is believed that motility along the sediment light gradient allows MPB both to optimize photosynthesis and to avoid stressful light conditions (i.e., above the photosynthetic capacity of cells). In the present study, the phototactic behavior of epipelic MPB was well illustrated by the PAB present at the surface of sediment as a function of "white" light irradiance with a maximum reached for 120 μmol photons m^{-2} s^{-1}. Similar values (i.e., range 100–250 μmol photons m^{-2} s^{-1}) were also reported in previous studies on both MPB natural communities (Perkins et al., 2002; Serôdio et al., 2006; Laviale et al., 2016; Du et al., 2018) and isolated epipelic diatom species (McLachlan et al., 2009; Du et al., 2010; Ezequiel et al., 2015). This feature was essential for two reasons: (i) it allowed us to validate the relevance of our experimental setup, and especially its ability to well preserve MPB light response in the sediment, and (ii) it allowed us to draw reference light conditions for maximizing the surface PAB, two necessary conditions for further testing together the effect of light intensity and spectrum on MPB migration.

Influence of the Light Spectrum on the Amount of PAB Present at the Surface of Sediment: Specific Effect of BL Wavelengths

In the present study, surface PAB accumulation was positively influenced by blue (465 nm) and possibly by green (530 nm) wavelengths, but not by red ones (677 nm, with or without far red). Although green light generated a similar PAB accumulation than BL for the same intensity (40 μmol photons m^{-2} s^{-1}), our experimental setup did not allow to test higher green light intensities to unambiguously conclude the responses to green light. It was previously demonstrated that green light (>510–520 nm) generally has a lower effect than BL (450 ± 20 nm) on phototactic directional cell movements (Nultsch, 1971; Cohn et al., 2004, 2015, 2016). Differently, red light of low or moderate intensity usually has no/little effect or negative effect on directional motility of diatoms and their accumulation, although this response is species-specific (Cohn and Weitzell, 1996; McLachlan et al., 2009; Cohn et al., 2015). These reports partially explain the action spectrum of MPB abundance at the surface of sediment at low irradiance (5 μmol photons m^{-2} s^{-1}) showing a strong positive effect of blue wavelengths (440 ± 10 nm), limited effect of greens (500–550 nm), and a moderate effect of red (680 nm) (Wenderoth and Rhiel, 2004).

Here, as regards to the specific effect of blue wavelengths, we have found that (i) BL induced a ×1.8 ± 0.4 total PAB increase compared to the "white" light control at the same intensity of 120 μmol photons m^{-2} s^{-1}; (ii) PAB accumulation was irradiance-dependent with a positive effect from 10 to 120 μmol BL photons m^{-2} s^{-1}; (iii) PAB accumulation was species-specific with two taxa, namely, *N. spartinetensis* and *G. fasciola* (and probably other *Navicula* species to a lesser extent), which strongly reacted (i.e., from 0 to 10% relative presence at the surface of sediment to up to more than 80%) at 40 μmol BL photons m^{-2} s^{-1}; (iv) their surface accumulation was independent of the season: the BL effect was observed with both winter and summer sediments for a particular species. These features fit well with previous reports. In general, blue wavelengths have a positive effect (up to a certain irradiance threshold, see Cohn et al., 2004; McLachlan et al., 2009) on surface PAB (×1.4 to ×1.8, Wenderoth and Rhiel, 2004) by modulating the speed to which epipelic diatoms move directionally (Nultsch, 1971; Cohn and Weitzell, 1996; McLachlan et al., 2009; Cohn et al., 2015). This BL photosensitivity is species-specific (McLachlan et al., 2009; Cohn et al., 2015), and it is detected at least at the tips of pennate cells (Cohn et al., 1999). The way blue wavelengths act at the cellular level and how the "BL signal" might be transduced is still unclear in diatoms, although significant recent advances have been made (Jaubert et al., 2017). It was early proposed (Nultsch, 1971) that pigments, chlorophylls and carotenoids, should act as primary harvesters and transducers to trigger the previously described action spectrum of MPB motility, and especially photokinesis (i.e., change of motility speed; Wenderoth and Rhiel, 2004). The latter would directly depend on the energy provided by photosynthesis, which itself is driven by actinic wavelengths, and obviously BL. In that respect, the optical properties of the photonic crystal-like structures of the diatom frustule are highly relevant; they have been shown to shape the availability of light and of specific wavelengths inside the cell, thereby potentiating pigment light-harvesting and photosynthetic efficiency (Goessling et al., 2018a,b). Interestingly, the frustule of one of our most BL-reactive species, *G. fasciola*,

was shown to be transparent when the frustule of other epipelic species significantly (up to 20%) attenuated the transmission of blue wavelengths (Goessling et al., 2018a). While BL attenuation can be advantageous to decrease potentially harmful incident irradiance, its nearly 100% transmission under low/moderate irradiance could support specific BL signaling inside the cell. These interspecies differences in frustule optical properties were claimed to additionally modulate the light availability inside the biofilm itself (Goessling et al., 2018a). Taken together with the fact that a species response to BL can be modulated by the presence of other species in its close surrounding (Cohn et al., 2016), it points out to the importance of the species consortium composition, which varies year around (this study, Haubois et al., 2005). Therefore, wavelengths, together with irradiance, would fine tune the differential rhythmic MPB migratory behavior and surface PAB accumulation versus the sediment light climate at the cell, species, and consortium (i.e., biofilm) levels.

However, in the present study, upon 24-h exposure, we did not observe any specific BL effect on (i) MPB pigment content, and especially carotenoids, independent of the irradiance, of the season, and of the sediment depth (down to 600 μm); (ii) MPB photosynthetic performances, independent of the irradiance. Therefore, the positive BL effect we observed was based on molecular cell components that were already present at the beginning of the light treatment (such as pigments), and it was not due to a surge in photosynthetic performance, that is, higher surface PAB accumulating because of more diatom cells photosynthesizing better under BL. Although we do not question the importance of the frustule optical properties and of photopigments in triggering the BL-enhanced PAB with the irradiance-dependent PAB increase being a proof of such role, we aim at seeking for alternative complementary answers. Photoreceptors have been proposed before to play a central role in the positive upward phototaxis of epipelic MPB to blue wavelengths (Wenderoth and Rhiel, 2004; McLachlan et al., 2009). In the recent years, three types of BL photoreceptors have been identified in planktonic diatom models including cryptochromes and a family unique to stramenopiles, aureochromes (Jaubert et al., 2017). Aureochromes control the onset of diatom cell division (mitosis) (Huysman et al., 2013), and BL stimulates growth rate and biofilm formation of the epipelic representative *Navicula* species (Cao et al., 2013). Therefore, the BL increase in surface PAB we observed could also be due to the proliferation of diatom cells. Because blue wavelengths are rapidly attenuated with sediment depth (Kuhl and Jorgensen, 1994), it is possible that BL, in conjunction with the necessary level of photochemical energy and organic carbon stored during emersion (Underwood et al., 2005; Marques Da Silva et al., 2017), could act as a trigger for mitosis when migrating downward, which, according to Saburova and Polikarpov (2003), are coupled. Furthermore, recent highlights on the role of photoreceptors in the rhythmic light response of diatoms (see Jaubert et al., 2017 for a synthesis) point out to a highly complex regulatory molecular network of light-dependent (such as the photoperiod) and independent (such as the tidal cycle) biological rhythms. It is very likely that sophisticated cross-talks between light perception (by frustule, pigments, and photoreceptors), photosynthetic metabolism, and endogenous regulators (circadian clock components) occur to finely tune the light response of diatoms beyond photoperiod (see section "What Influences the Most the Amount of PAB Present at the Surface of Sediment: Tides or Light?"). Obviously, such a network would be a strong asset for epipelic diatoms in coping with the multifaceted intertidal sediment light climate.

CONCLUSION

The present study strengthens the view that the vertical migratory rhythm of motile MPB diatoms in intertidal sediment is of endogenous nature and is first mapped onto the tidal cycle with the migration rhythm driven by a "lunidian clock" phased on the lunar day length and cycle. Migration rhythmicity is further modulated, and even overridden in some conditions, by light, including the diurnal cycle and the irradiance level during daytime periods. Optimal light conditions can significantly "potentiate" the tidal effect on the accumulation of PAB at the surface of sediment during emersion. Additionally, we found a strong positive effect of blue wavelengths (465 nm) on surface PAB accumulation as compared to others (white, green, and red lights). This effect is intensity- and species-dependent (i.e., some species strongly react to BL, whereas others do not). We propose that, in addition to photopigments and frustule optical properties, BL photoreceptors (cryptochromes and aureochromes) might play a crucial role in regulating the presence and abundance of PAB at the surface of intertidal sediment. We found two new potential model species, *N. spartinetensis* and *G. fasciola*, which strongly react to blue wavelengths. The fact that *N. spartinetensis* shows a much smaller size than *G. fasciola*, and probably a different migratory behavior (see Wenderoth et al., 2004; Underwood et al., 2005) is an additional asset. The complementary use of the epipelic model *Seminavis robusta* (Blommaert et al., 2017, 2018), which genome has been sequenced, will allow to search for molecular players, such as timekeepers (Annunziataa et al., 2019), photoreceptors (Jaubert et al., 2017), and diurnal-responsive genes (see Meyer et al., 2003; Blommaert et al., 2020), of the rhythmic migratory light-tuned response of intertidal epipelic MPB.

DATA AVAILABILITY STATEMENT

All datasets generated for this study are included in the article/**Supplementary Material**.

AUTHOR CONTRIBUTIONS

AB and JL contributed to the conception and design of the study. AB performed the experiments. AB, VM, and

JL performed samples and data analyses. AB wrote the first draft of the manuscript. All authors contributed to manuscript revision, read and approved the submitted version.

FUNDING

This work was supported by the Centre National de la Recherche Scientifique-CNRS, the University of La Rochelle-ULR, the Contrat Plant Etat Région-CPER "Littoral" 2007–2013, the Region Poitou-Charentes-CG17, and by the Natural Sciences and Engineering Research Council-NSERC (Discovery grant to JL).

ACKNOWLEDGMENTS

The authors thank I. Benyoucef for his help with the preparation of definitive slides, the identification and the counting of diatom cells, J.-L. Mouget for the access to the Water-PAM, X. Cousin for the access to the cryomicrotome, and D. Campbell for the critical reading of the manuscript.

SUPPLEMENTARY MATERIAL

The Supplementary Material for this article can be found online at: https://www.frontiersin.org/articles/10.3389/fmars.2020.00212/full#supplementary-material

REFERENCES

Admiraal, W. (1984). "The ecology of estuarine sediment inhabiting diatoms," in *Progress Phycology Research*, eds F. E. Round and D. J. Chapman (Bristol: Biopess Limited), 269–314.

Annunziataa, R., Rittera, A., Fortunato, A. E., Manzotti, A., Cheminant-Navarro, S., Agier, N., et al. (2019). bHLH-PAS protein RITMO1 regulates diel biological rhythms in the marine diatom *Phaeodactylum tricornutum*. *Proc. Natl Acad. Sci. U.S.A.* 116, 13137–13142. doi: 10.1073/pnas.1819660116

Apoya-Horton, M. D., Yin, L., Underwood, G. J. C., and Gretz, M. R. (2006). Movement modalities and responses to environmental changes of the mudflat diatom *Cylindrotheca Closterium* (Bacillariophyceae)1. *J. Phycol.* 42, 379–390. doi: 10.1111/j.1529-8817.2006.00194.x

Barnett, A., Méléder, V., Blommaert, L., Lepetit, B., Gaudin, P., Vyverman, W., et al. (2015). Growth form defines physiological photoprotective capacity in intertidal benthic diatoms. *ISME J.* 9, 32–45. doi: 10.1038/ismej.2014.105

Bertrand, J. (2008). Mouvements des diatomées VIII: synthèse et hypothèse. *Diatom Res.* 23, 19–29. doi: 10.1080/0269249x.2008.9705734

Blanchard, G., Guarini, J.-M., Gros, P., and Richard, P. (1997). Seasonal effect on the relationship between photosynthetic capacity of intertidal microphytobenthos and temperature. *J. Phycol.* 33, 723–728. doi: 10.1111/j.0022-3646.1997.00723.x

Blommaert, L., Huysman, M. J., Vyverman, W., Lavaud, J., and Sabbe, K. (2017). Contrasting NPQ dynamics and xanthophyll cycling in a motile and a non-motile intertidal benthic diatom. *Limnol. Oceanogr.* 62, 1466–1479. doi: 10.1002/lno.10511

Blommaert, L., Lavaud, J., Vyverman, W., and Sabbe, K. (2018). Behavioural versus physiological photoprotection in epipelic and epipsammic benthic diatoms. *Eur. J. Phycol.* 53, 146–155. doi: 10.1080/09670262.2017.1397197

Blommaert, L., Vancaester, E., Huysman, M. J. J., Osuna-Cruz, C. M., D'hondt, S., Lavaud, J., et al. (2020). Light regulation of LHCX genes in the benthic diatom *Seminavis robusta*. *Front. Mar. Sci.* 7:192. doi: 10.3389/fmars.2020.00192

Brotas, V., Cabrita, T., Portugal, A., Serôdio, J., and Catarino, F. (1995). Spatio-temporal distribution of the microphytobenthic biomass in intertidal flats of Tagus Estuary (Portugal). *Hydrobiologia* 300, 93–104. doi: 10.1007/bf00024451

Cao, S., Wang, J., and Chen, D. (2013). Settlement and cell division of diatom *Navicula* can be influenced by light of various qualities and intensities. *J. Basic Microbiol.* 53, 884–894. doi: 10.1002/jobm.201200315

Cartaxana, P., Cruz, S., Gameiro, C., and Kühl, M. (2016a). Regulation of intertidal microphytobenthos photosynthesis over a diel emersion period is strongly affected by diatom migration patterns. *Front. Microbiol.* 7:872. doi: 10.3389/fmicb.2016.00872

Cartaxana, P., Ribeiro, L., Goessling, J. W., Cruz, S., and Kühl, M. (2016b). Light and O2 microenvironments in two contrasting diatom-dominated coastal sediments. *Mar. Ecol. Progr. Ser.* 545, 35–47. doi: 10.3354/meps11630

Cartaxana, P., Ruivo, M., Hubas, C., Davidson, I., Serôdio, J., and Jesus, B. (2011). Physiological versus behavioral photoprotection in intertidal epipelic and epipsammic benthic diatom communities. *J. Exp. Mar. Biol. Ecol.* 405, 120–127. doi: 10.1016/j.jembe.2011.05.027

Coelho, H., Vieira, S., and Serôdio, J. (2011). Endogenous versus environmental control of vertical migration by intertidal benthic microalgae. *Eur. J. Phycol.* 46, 271–281. doi: 10.1080/09670262.2011.598242

Cohn, S. A. (2001). ""Photo-stimulated effects on diatom motility,"," in *Photomovement*, eds D.-P. Häder and M. Lebert (Amsterdam: Elsevier), 375–401. doi: 10.1016/s1568-461x(01)80017-x

Cohn, S. A., Bahena, M., Davis, J. T., Ragland, R. L., Rauschenberg, C. D., and Smith, B. J. (2004). Characterisation of the diatom photophobic response to high irradiance. *Diatom Res.* 19, 167–179. doi: 10.1080/0269249x.2004.9705869

Cohn, S. A., Dunbar, S., Ragland, R. L., Schulze, J., Suchar, A., Weiss, J., et al. (2016). Analysis of light quality and assemblage composition on diatom motility and accumulation rate. *Diatom Res.* 31, 173–184. doi: 10.1080/0269249x.2016.1193058

Cohn, S. A., Halpin, D., Hawley, N., Ismail, A., Kaplan, Z., Kordes, T., et al. (2015). Comparative analysis of light-stimulated motility responses in three diatom species. *Diatom Res.* 30, 213–225. doi: 10.1080/0269249x.2015.1058295

Cohn, S. A., Spurck, T. P., and Pickett-Heaps, J. D. (1999). High energy irradiation at the leading tip of moving diatoms causes a rapid change of cell direction. *Diatom Res.* 14, 193–206. doi: 10.1080/0269249x.1999.9705466

Cohn, S. A., and Weitzell, R. E. (1996). Ecological considerations of diatom cell motility I. Characterization of motility and adhesion in four diatom species. *J. Phycol.* 32, 928–939. doi: 10.1111/j.0022-3646.1996.00928.x

Consalvey, M., Paterson, D. M., and Underwood, G. J. C. (2004). The ups and downs of life in a benthic biofilm: migration of benthic diatoms. *Diatom Res.* 19, 181–202. doi: 10.1080/0269249x.2004.9705870

Consalvey, M., Perkins, G. R., Paterson, D. M., and Underwood, G. J. C. (2005). PAM fluorescence: a beginners guide for benthic diatomists. *Diatom Res.* 20, 1–22. doi: 10.1080/0269249x.2005.9705619

Daggers, T. D., Kromkamp, J. C., Herm, P. M. J., and Van Der Wal, D. (2018). A model to assess microphytobenthic primary production in tidal systems using satellite remote sensing. *Remote Sens. Environ.* 211, 129–145. doi: 10.1016/j.rse.2018.03.037

Du, G. Y., Oak, J. H., Li, H., and Chung, I. K. (2010). Effect of light and sediment grain size on the vertical migration of benthic diatoms. *Algae* 25, 133–140. doi: 10.4490/algae.2010.25.3.133

Du, G. Y., Yan, H., Liu, C., and Moa, Y. (2018). Behavioral and physiological photoresponses to light intensity by intertidal microphytobenthos. *Chinese J. Oceanol. Limnol.* 36, 293–304. doi: 10.1007/s00343-017-6099-0

Eilers, P. H. C., and Peeters, J. C. H. (1988). A model for the relationship between light intensity and the rate of photosynthesis in phytoplankton. *Ecol. Model.* 42, 199–215. doi: 10.1016/0304-3800(88)90057-9

Ezequiel, J., Laviale, M., Frankenbach, S., Cartaxana, P., and Serôdio, J. (2015). Photoacclimation state determines the photobehaviour of motile microalgae: the case of a benthic diatom. *J. Exp. Mar. Biol. Ecol.* 468, 11–20. doi: 10.1016/j.jembe.2015.03.004

Frankenbach, S., Pais, C., Martinez, M., Laviale, M., Ezequiel, J., and Serôdio, J. (2014). Evidence for gravitactic behaviour in benthic diatoms. *Eur. J. Phycol.* 49, 429–435. doi: 10.1080/09670262.2014.974218

Goessling, J. W., Frankenbach, S., Ribeiro, L., Serôdio, J., and Kühl, M. (2018a). Modulation of the light field related to valve optical properties of raphid diatoms: implications for niche differentiation in the microphytobenthos. *Mar. Ecol. Progr. Ser.* 588, 29–42. doi: 10.3354/meps12456

Goessling, J. W., Yanyan, Y., Cartaxana, P., Maibohm, C., Rickelt, L. F., Trampe, E. C. L., et al. (2018b). Structure-based optics of centric diatom frustules: modulation of the *in vivo* light field for efficient diatom photosynthesis. *New Phytol.* 219, 122–134. doi: 10.1111/nph.15149

Guarini, J.-M., Blanchard, G., and Richard, P. (2006). "Modelling the dynamics of the microphytobenthic biomass and primary production in European intertidal mudflats," in *Functioning of Microphytobenthos in Estuaries*, eds J. Kromkamp, J. F. C. De Brouwer, G. Blanchard, R. M. Forster, and V. Créach (Amsterdam: Royal Netherlands Academy of Arts and Sciences), 187–226.

Guarini, J.-M., Saric, N., and Moritz, C. (2008). Modelling the dynamics of the microalgal biomass in semi-enclosed shallow-water ecosystems. *Ecol. Model.* 211, 267–278. doi: 10.1016/j.ecolmodel.2007.09.011

Happey-Wood, C. M., and Jones, P. (1988). Rhythms of vertical migration and motility in intertidal benthic diatoms with particular reference to *Pleurosigma angulatum*. *Diatom Res.* 3, 83–93. doi: 10.1080/0269249x.1988.9705018

Haro, S., Bohórquez, J., Lara, M., Garcia-Robledo, E., González, C. J., Crespo, J. M., et al. (2019). Diel patterns of microphytobenthic primary production in intertidal sediments: the role of photoperiod on the vertical migration circadian rhythm. *Sci. Rep.* 9:13376.

Harper, M. A. (1969). Movement and migration of diatoms on sand grains. *Br. Phycol. J.* 4, 97–103. doi: 10.1080/00071616900650081

Haubois, A.-G., Sylvestre, F., Guarini, J.-M., Richard, P., and Blanchard, G. F. (2005). Spatio-temporal structure of the epipelic diatom assemblage from an intertidal mudflat in Marennes-Oléron Bay, France. *Estuar. Coast Shelf Sci.* 64, 385–394. doi: 10.1016/j.ecss.2005.03.004

Herlory, O., Blanchard, G. F., Planche, S., Huet, V., and Richard, P. (2005). Does the size of the microphytobenthic biofilm on intertidal mudflats depend on the available photosynthetic biomass? *Mar. Ecol. Progr. Ser.* 298, 95–100. doi: 10.3354/meps298095

Herlory, O., Guarini, J.-M., Richard, P., and Blanchard, G. F. (2004). Microstructure of microphytobenthic biofilm and its spatio-temporal dynamics in an intertidal mudflat (Aiguillon Bay, France). *Mar. Ecol. Progr. Ser.* 282, 33–44. doi: 10.3354/meps282033

Honeywill, C., Paterson, D. M., and Hagerthey, S. E. (2002). Determination of microphytobenthic biomass using pulse-amplitude modulated minimum fluorescence. *Eur. J. Phycol.* 37, 485–492. doi: 10.1017/s0967026202003888

Huysman, M. J., Fortunato, A. E., Matthijs, M., Costa, B. S., Vanderhaeghen, R., Van Den Daele, H., et al. (2013). AUREOCHROME1a-mediated induction of the diatom-specific cyclin dsCYC2 controls the onset of cell division in diatoms (*Phaeodactylum tricornutum*). *Plant Cell* 25, 215–228. doi: 10.1105/tpc.112.106377

Jakob, T., Goss, R., and Wilhelm, C. (1999). Activation of diadinoxanthin de-epoxidase due to a chlororespiratory proton gradient in the dark in the diatom *Phaeodactylum tricornutum*. *Plant Biol.* 1, 76–82. doi: 10.1111/j.1438-8677.1999.tb00711.x

Jaubert, M., Bouly, J.-P., D'alcala, M. R., and Falciatore, A. (2017). Light sensing and responses in marine microalgae. *Trends Plant Biol.* 37, 70–77. doi: 10.1016/j.pbi.2017.03.005

Jesus, B., Brotas, V., Ribeiro, L., Mendes, C. R., Cartaxana, P., and Paterson, D. M. (2009). Adaptations of microphytobenthos assemblages to sediment type and tidal position. *Cont. Shelf Res.* 29, 1624–1634. doi: 10.1016/j.csr.2009.05.006

Kooistra, W. H. C. F., Gersonde, R. K., Medlin, L. G., and Mann, D. (2007). "The origin and evolution of the diatoms: their adaptation to a planktonic existence," in *Evolution of Primary Producers in the Sea*, eds P. G. Falkowski and A. H. Knoll (Burlington: Academic Press), 207–249. doi: 10.1016/b978-012370518-1/50012-6

Kuhl, M., and Jorgensen, B. B. (1994). The light field of microbenthic communities: radiance distribution and microscale optics of sandy coastal sediments. *Limnol. Oceanogr.* 39, 1368–1398. doi: 10.4319/lo.1994.39.6.1368

Kwon, B.-O., Khim, J. S., Park, J., Ryu, J., Kang, S.-G., and Koh, C.-H. (2012). Short-term variability of microphytobenthic primary production associated with in situ diel and tidal conditions. *Estuar. Coast Shelf Sci.* 112, 236–242. doi: 10.1016/j.ecss.2012.07.029

Laviale, M., Ezequiel, J., Pais, C., Cartaxana, P., and Serôdio, J. (2015). The "crème brûlée" sampler: a new high-resolution method for the fast vertical sampling of intertidal fine sediments. *J. Exp. Mar. Biol. Ecol.* 468, 37–44. doi: 10.1016/j.jembe.2015.03.013

Laviale, M., Frankenbach, S., and Serôdio, J. (2016). The importance of being fast: comparative kinetics of vertical migration and non-photochemical quenching of benthic diatoms under light stress. *Mar. Biol.* 160:10.

Lebreton, B., Rivaud, A., Picot, L., Prévost, B., Barillé, L., Sauzeau, T., et al. (2019). From ecological relevance of the ecosystem services concept to its sociopolitical use. The case study of intertidal bare mudflats in the Marennes-Oléron Bay, France. *Ocean Coast. Manage* 172, 41–54. doi: 10.1016/j.ocecoaman.2019.01.024

Lefebvre, S., Mouget, J.-L., and Lavaud, J. (2011). Duration of rapid light curves for determining the photosynthetic activity of microphytobenthos biofilm *in situ*. *Aquat. Bot.* 95, 1–8. doi: 10.1016/j.aquabot.2011.02.010

Lepetit, B., Sturm, S., Rogato, A., Gruber, A., Sachse, M., Falciatore, A., et al. (2013). High light acclimation in the secondary plastids containing diatom *Phaeodactylum tricornutum* is triggered by the redox state of the plastoquinone pool. *Plant Physiol.* 161, 853–865. doi: 10.1104/pp.112.207811

Marques Da Silva, J., Cruz, S., and Cartaxana, P. (2017). Inorganic carbon availability in benthic diatom communities: photosynthesis and migration. *Phil. Trans. R. Soc. B* 372:20160398. doi: 10.1098/rstb.2016.0398

McLachlan, D. H., Brownlee, C., Taylor, A. R., Geider, R. J., and Underwood, G. J. C. (2009). Light-induced motile responses of the estuarine benthic diatoms *Navicula Perminuta* and *Cylindrotheca Closterium* (Bacillariophyceae). *J. Phycol.* 45, 592–599. doi: 10.1111/j.1529-8817.2009.00681.x

Méléder, V., Rincé, Y., Barillé, L., Gaudin, P., and Rosa, P. (2007). Spatiotemporal changes in microphytobenthos assemblages in a macrotidal flat (Bourgneuf Bay,France). *J. Phycol.* 43, 1177–1190. doi: 10.1111/j.1529-8817.2007.00423.x

Meyer, T., Hust, M., Marquardt, J., Krumbein, W. E., and Rhiel, E. (2003). A methodological approach to investigate steady state fucoxanthin chlorophyll a /c binding protein mRNA levels in Wadden Sea sediments. *Internatl. Microbiol.* 6, 33–39. doi: 10.1007/s10123-003-0098-z

Mitbavkar, S., and Anil, A. C. (2004). Vertical migratory rhythms of benthic diatoms in a tropical intertidal sand flat: influence of irradiance and tides. *Mar. Biol.* 145, 9–20.

Nakov, T., Beaulieu, J. M., and Alverson, A. J. (2018). Accelerated diversification is related to life history and locomotion in a hyperdiverse lineage of microbial eukaryotes (Diatoms, Bacillariophyta). *New Phytol.* 219, 462–473. doi: 10.1111/nph.15137

Ni Longphuirt, S., Leynaert, A., Guarini, J.-M., Chauvaud, L., Claquin, P., Herlory, O., et al. (2006). Discovery of microphytobenthos migration in the subtidal zone. *Mar. Ecol. Progr. Ser.* 328, 143–154. doi: 10.3354/meps328143

Noordally, Z. B., and Millar, A. J. (2015). Clocks in algae. *Biochemistry* 54, 171–183. doi: 10.1021/bi501089x

Nultsch, W. (1971). Phototactic and photokinetic action spectra of the diatom *Nitzschia communis*. *Photochem. Photobiol.* 14, 705–712. doi: 10.1111/j.1751-1097.1971.tb06209.x

Palmer, J. D. (2000). The clocks controlling the tide-associated rhythms of intertidal animals. *BioEssays* 22, 32–37. doi: 10.1002/(sici)1521-1878(200001)22:1<32::aid-bies7>3.0.co;2-u

Pante, E., and Simon-Bouhet, B. (2013). Marmap: a package for importing, plotting and analyzing bathymetric and topographic data in R. *PLoS One* 8:e73051. doi: 10.1371/journal.pone.0073051

Paterson, D. M. (1986). The migratory behaviour of diatom assemblages in a laboratory tidal micro-ecosystem examined by low temperature scanning electron microscopy. *Diatom Res.* 1, 227–239. doi: 10.1080/0269249x.1986.9704971

Paterson, D. M., and Hagerthey, S. E. (2001). ""Microphytobenthos in contrasting coastal ecosystems: biology and dynamics,"," in *Ecological Comparisons of Sedimentary Shores*, ed. K. Reise (Berlin: Springer-Verlag), 106–125.

Perkins, R. G., Oxborough, K., Hanlon, A. R. M., Underwood, G. J. C., and Baker, N. R. (2002). Can chlorophyll fluorescence be used to estimate the rate of photosynthetic electron transport within microphytobenthic biofilms? *Mar. Ecol. Progr. Ser.* 228, 47–56. doi: 10.3354/meps228047

Ribeiro, L. (2010). *Intertidal Benthic Diatoms of the Tagus Estuary: Taxonomic Composition and Spatial-Temporal Variation*. Ph.D. thesis, Universidade de Lisboa, Lisboa.

Ribeiro, L., Brotas, V., Rince, Y., and Jesus, B. (2013). Structure and diversity of intertidal benthic diatom assemblages in contrasting shores: a case study from the Tagus estuary. *J. Phycol.* 49, 258–270. doi: 10.1111/jpy.12031

Round, F. E. (1979). A diatom assemblage living below the surface of intertidal sand flats. *Mar. Biol.* 54, 219–223. doi: 10.1007/bf00395784

Saburova, M. A., and Polikarpov, I. G. (2003). Diatom activity within soft sediments: behavioural and physiological processes. *Mar. Ecol. Progr. Ser.* 251, 115–126. doi: 10.3354/meps251115

Sauer, J., Wenderoth, K., Maier, U. G., and Rhiel, E. (2002). Effects of salinity, light and time on the vertical migration of diatom assemblages. *Diatom Res.* 17, 189–203. doi: 10.1080/0269249x.2002.9705538

Savelli, R., Dupuy, C., Barillé, L., Lerouxel, A., Guizien, K., Philippe, A., et al. (2018). On biotic and abiotic drivers of the microphytobenthos seasonal cycle in a temperate intertidal mudflat: a modelling study. *Biogeosciences* 15, 7243–7271. doi: 10.5194/bg-15-7243-2018

Serôdio, J., Coelho, H., Vieira, S., and Cruz, S. (2006). Microphytobenthos vertical migratory photoresponse as characterised by light-response curves of surface biomass. *Estuar. Coast Shelf Sci.* 68, 547–556. doi: 10.1016/j.ecss.2006.03.005

Serôdio, J., Ezequiel, J., Barnett, A., Mouget, J.-L., Méléder, V., Laviale, M., et al. (2012). Efficiency of photoprotection in microphytobenthos: role of vertical migration and the xanthophyll cycle against photoinhibition. *Aquat. Microb. Ecol.* 67, 161–175. doi: 10.3354/ame01591

Serôdio, J., Vieira, S., Cruz, S., and Barroso, F. (2005). Short-term variability in the photosynthetic activity of microphytobenthos as detected by measuring rapid light curves using variable fluorescence. *Mar. Biol.* 146, 903–914. doi: 10.1007/s00227-004-1504-6

Skogen Chauton, M., Winge, P., Brembu, T., Vadstein, O., and Bones, A. M. (2013). Gene regulation of carbon fixation, storage, and utilization in the diatom *Phaeodactylum tricornutum* acclimated to light/dark cycles. *Plant Physiol.* 161, 1034–1048. doi: 10.1104/pp.112.206177

Spilmont, N., Migné, A., Seuront, L., and Davoult, D. (2007). Short-term variability of intertidal benthic community production during emersion and the implication in annual budget calculation. *Mar. Ecol. Progr. Ser.* 333, 95–101. doi: 10.3354/meps333095

Stock, W., Blommaert, L., Daveloose, I., Vyverman, W., and Sabbe, K. (2019). Assessing the suitability of Imaging-PAM fluorometry for monitoring growth of benthic diatoms. *J. Exp. Mar. Biol. Ecol.* 513, 35–41. doi: 10.1016/j.jembe.2019.02.003

Underwood, G. J. C., and Kromkamp, J. C. (1999). "Primary production by phytoplankton and microphytobenthos in estuaries," in *Advance Ecology Research*, eds D. B. Nedwell and D. G. Raffaelli (Cambridge, MA: Academic Press), 93–153. doi: 10.1016/s0065-2504(08)60192-0

Underwood, G. J. C., Perkins, R. G., Consalvey, M. C., Hanlon, A. R. M., Oxborough, K., Baker, N. R., et al. (2005). Patterns in microphytobenthic primary productivity: species-specific variation in migratory rythms and photosynthetic efficiency in mixed-species biofilms. *Limnol. Oceanogr.* 50, 755–767. doi: 10.4319/lo.2005.50.3.0755

Vieira, S., Ribeiro, L., Jesus, B., Cartaxana, P., and Da Silva, J. M. (2013). Photosynthesis assessment in microphytobenthos using conventional and imaging pulse amplitude modulation fluorometry. *Photochem. Photobiol.* 89, 97–102. doi: 10.1111/j.1751-1097.2012.01224.x

Wenderoth, K., Marquardt, J., and Rhiel, E. (2004). The big trail: many migrate at the expense of few. *Diatom Res.* 19, 115–122. doi: 10.1080/0269249x.2004.9705611

Wenderoth, K., and Rhiel, E. (2004). Influence of light quality and gassing on the vertical migration of diatoms inhabiting the Wadden Sea. *Helgoland Mar. Res.* 58, 211–215. doi: 10.1007/s10152-004-0187-1

Witkowski, A. (2000). Diatom flora of marine coasts I. *Iconogr. Diatomol.* 7, 1–925.

Conflict of Interest: The authors declare that the research was conducted in the absence of any commercial or financial relationships that could be construed as a potential conflict of interest.

frontiers in Marine Science

ORIGINAL RESEARCH
published: 21 April 2020
doi: 10.3389/fmars.2020.00203

Effect of Light Intensity and Light Quality on Diatom Behavioral and Physiological Photoprotection

Antoine Prins[1,2†], Paul Deleris[1], Cédric Hubas[2] and Bruno Jesus[1,3†]*

[1] Mer Molécules Santé EA 2160, Faculté des Sciences et des Techniques, Université de Nantes, Nantes, France, [2] Muséum National d'Histoire Naturelle, FRE BOREA 2030, MNHN-IRD-CNRS-SU-UCN-UA, Station Marine de Concarneau, Concarneau, France, [3] Biosystems & Integrative Sciences Institute, Faculty of Sciences, University of Lisbon, Lisbon, Portugal

In this study, we investigated the different photoregulation responses of diatom dominated natural biofilms to different light intensities and wavelengths, over a tidal cycle in the laboratory. We compared the overall effect of light spectral quality from its light absorption (*Qphar*) dependent effect. Two different conditions were compared to study photoprotective strategies: sediment (migrational) and without sediment (non-migrational). Three different colors (blue, green, and red) and two light intensities (low light, LL at 210 μmol.photons.m^{-2}.s^{-1} and high light, HL at 800 μmol.photons.m^{-2}.s^{-1}) showed strong interactions in inducing behavioral and physiological photoprotection. Non-migrational biofilm non-photochemical quenching (*NPQ*) was much more reactive to blue HL than red HL while it did not differ in LL. We observed a biphasic *NPQ* response with a light threshold between 200 and 250 μmol.photons.m^{-2}.s^{-1} of *Qphar* that elicited the onset of physiological photoprotection. Similar HL differences were not observed in migrational biofilms due to active vertical migration movements that compensated light saturating effects. Our results showed that within migrational biofilms there was an interaction between light quality and light intensity on cell accumulation pattern at the sediment surface. This interaction led to inverse diatom accumulation patterns between blue and red light at the same intensity: LL (blue + 200.67%, red + 123.96%), HL (blue + 109.15%, red + 150.34%). These differences were largely related to the differential amount of light absorbed at different wavelengths and highlighted the importance of using wavelength standardized intensities. Different vertical migration patterns significantly affected the total pigment content measured at the surface, suggesting that cell could migrate downward more than 2 mm as a photoregulatory response. Colloidal carbohydrates patterns paralleled the vertical migration movements, highlighting their possible role in diatom motility. Our data strongly suggests a wavelength and Qphar dependent light stress threshold that triggers upward and downward movements to position microphytobenthic diatoms at their optimal depth.

Keywords: diatoms, fluorescence, PAM, migration, photoprotection

OPEN ACCESS

Edited by:
Wim Vyverman,
Ghent University, Belgium

Reviewed by:
Graham J. C. Underwood,
University of Essex, United Kingdom
Reimund Goss,
Leipzig University, Germany

****Correspondence:***
Antoine Prins
antoine.prins@univ-nantes.fr;
taone@hotmail.fr

† These authors have contributed equally to this work

Specialty section:
This article was submitted to Marine Ecosystem Ecology, a section of the journal Frontiers in Marine Science

Received: *30 November 2019*
Accepted: *16 March 2020*
Published: *21 April 2020*

Citation:
Prins A, Deleris P, Hubas C and Jesus B (2020) Effect of Light Intensity and Light Quality on Diatom Behavioral and Physiological Photoprotection. Front. Mar. Sci. 7:203. doi: 10.3389/fmars.2020.00203

INTRODUCTION

Mycrophytobenthos dominated mudflats are highly productive coastal ecosystems (MacIntyre et al., 1996; Underwood and Kromkamp, 1999) and diatom biofilms forming at the sediment surface during each diurnal tidal cycle are often at the source of this high productivity (e.g., Paterson et al., 2003). These biofilms are also responsible for a range of important biogeochemical processes including sediment stabilization (Paterson, 1989; Yallop et al., 1994), modulation of oxygen availability (Walpersdorf et al., 2017), as well as influencing carbon turnover and availability through the production of polymeric exudates (Perkins et al., 2001; Taylor et al., 2013) which in turns affects microbial diversity (Haynes et al., 2007). Epipelic diatoms, i.e., motile diatoms that move around sediment particles (Round, 1965), exhibit marked vertical movements inside the sediment matrix (Round and Happey, 1965; Consalvey et al., 2004b) that can be divided in two types: an endogenous circadian cycle synchronized with daily emersion periods whereby cells migrate to the sediment surface forming biofilms; and smaller fine tuning vertical adjustments positioning cells at optimal light levels, functioning as a photo-regulation mechanism (Perkins et al., 2001; Jesus et al., 2006; Cartaxana et al., 2011; Serôdio et al., 2012). The circadian rhythms are endogenously controlled and are kept for several days in laboratory conditions without artificial tides and exposed to continuous light (Round and Happey, 1965; Paterson, 1986; Serôdio et al., 1997; Mitbavkar and Anil, 2004; Coelho et al., 2011). The smaller photo-regulation movements are one of the main photo-regulation mechanisms of epipelic diatoms (Jesus et al., 2009; Perkins et al., 2010; Cartaxana et al., 2011; Laviale et al., 2016), while epipsammic diatoms (strongly associated to sediment grains) depend mainly on the thermal dissipation of excessive light energy through the xanthophyll cycle (XC) to photo-regulate (Cartaxana et al., 2011; Barnett et al., 2015; Blommaert et al., 2018). The XC relies on the presence of a transthylakoidal proton gradient to de-epoxidise diadinoxanthin (Diad) into its energy-dissipation form diatoxanthin (Diat). It presumably induces a conformational shift in the light harvesting antennas that leads to excess energy being dissipated by heat through a non-photochemical quenching (NPQ) process (e.g., Olaizola and Yamamoto, 1994; Lavaud et al., 2004; Lavaud and Goss, 2014). Several studies have tried to quantify the relative importance of the two photo-regulation mechanisms (e.g., Perkins et al., 2010; Serôdio et al., 2012), notably by using migration inhibitors (Cartaxana and Serôdio, 2008) to separate the photo-regulatory effect of the XC from the vertical movements. Overall, published data shows that microphytobenthos depend on both photo-regulation mechanisms but that the two strategies are strongly dependent on their life forms (i.e., epipelic vs. epipsamic) (Cartaxana et al., 2011; Barnett et al., 2015). A few studies have investigated the trade-off between vertical migration (VM) and NPQ (Perkins et al., 2010; Serôdio et al., 2012; Barnett et al., 2015; Laviale et al., 2016; Blommaert et al., 2018). Diatoms movements have been differentiated in phototaxis and photokinesis (Nultsch, 1971; Häder, 1986). The former describing an oriented movement toward or away from a light source and the latter describing the speed of the movement as a response to light fluence rate (McLachlan et al., 2009). Both positive and negative phototaxis, toward and away from light, have been reported for different diatoms and different light intensities (Nultsch, 1971; Cohn et al., 1999; Du et al., 2010; Ezequiel et al., 2015). Benthic diatoms, in the absence of light cues, may also exhibit negative gravitaxis inducing upward movements to the sediment surface (Frankenbach et al., 2014). Most studies on diatom movement, growth and photosynthetic properties have investigated the effect of light intensity regardless of light spectra (Perkins et al., 2001; Paterson et al., 2003; Underwood et al., 2005; Jesus et al., 2006; Chevalier et al., 2010; Jauffrais et al., 2015). Light intensity is a wavelength weighted energy measurement that refers to the total number of photons received per unit area in a given time. Its use has been widely spread in photosynthetic studies because photosynthetic photochemical reactions are driven by total amount of photon received rather than the amount of energy received by each photon (Kume, 2018). In the aforementioned studies (Perkins et al., 2001; Paterson et al., 2003; Underwood et al., 2005; Jesus et al., 2006; Chevalier et al., 2010; Jauffrais et al., 2015) light has been integrated over the photosynthetic active radiation (PAR) spectrum, not accounting for the spectral variations within the light spectrum. However, these changes in light composition can affect diatom photo-protective capacity and photo-acclimation to high light intensities (Phaeodactylum tricornutum) (Schellenberger Costa et al., 2013a; Brunet et al., 2014). Light composition can also affect locomotion speed thereby affecting diatom vertical migration (Wenderoth and Rhiel, 2004; McLachlan et al., 2009). Spectral differences affect the relative proportion of photons available at each wavelength per unit area in a given time. In turn this modify on one hand the total amount of energy and on the other hand specific interactions, i.e., absorptions, with different structures such as diatoms' pigments and chromophores. It is unknown whether light quality changes only modulate the amount of light being absorbed by diatoms or if there are other effect, possibly due to differential energy levels and other confounding factors. To differentiate between chromatic differential absorption and other effects we compared intensity with Qphar (Gilbert et al., 2000) which is the photosynthetically absorbed radiation weighing in specific absorption coefficients of the major pigments. Currently, no studies exist on the effect of light quality regarding the two main diatom photo-regulation mechanisms. The objective of the current study was to investigate the effect of light spectral composition and light intensity on diatom physiological and behavioral photo-regulation mechanisms throughout a tidal cycle, using MPB assemblages in natural sediment and assemblages immobilized on petri dishes. Light quality effects will firstly be studied from an intensity perspective before considering their effect from an absorbance point of view.

MATERIALS AND METHODS

Site and Sampling

The sampling site was located in La Couplasse mudflats (Bourgneuf Bay, 47.015753, −2.024148) and sampling was

carried out on February 2018 during low tide. It is a non-protected area that did not require a permit for this kind of biological material sampling. Superficial sediment (upper 5 mm) was scrapped and transported back to the laboratory where it was spread out evenly in trays and submerged with water from the site in a room with natural lighting, allowing for the reconstitution of the biofilm the next day. The sediment at this site is dominated by benthic epipelic diatoms (e.g., Hernández Fariñas et al., 2017).

Experimental Setup

Water was drained from the trays on the day after the sampling and 3 h prior to the expected low tide we added two layers of lens tissue on top of the sediment. The sediment was then exposed to natural light from a window to facilitate biofilm vertical migration. Lens tissues were recovered at the middle of the virtual emersion time (low-tide peak), thereby harvesting the microalgae that had migrated to the sediment surface during the first 3 h (Eaton and Moss, 1966). Cells were extracted from the lens tissues by gently scrapping them into site-filtered sea water and kept in darkness before further use. On the second day, 5 h before expected low tide and 2 h before the beginning of the experiment 48 black microplates wells (22 mm diameter and 18 mm depth) were filled with either the same mud used for extraction or clean lens tissue inoculated with algal suspension. Mud samples contained both migratory and non-migratory diatoms from the field. Half were filled with one lens tissue layer and inoculated with 2 mL of algal suspension; the other half was filled with mud (15 mm) and 0.5 mL of algal suspension. To facilitate handling the 12 wells microplates were cut in rows of 4 wells containing each 3 replicates and a dark control (**Figure 1**). Mud and lens tissue samples will henceforth respectively be referred as migrational and non-migrational biofilms.

Light Treatments

LEDs light sources (SL 3500 – PSI) were calibrated with a light sensor (MSC15 – Gigahertz-Optik) to deliver 800 μmol.photons.m^{-2}.s^{-1} from a 30 cm distance onto the microplates. Three monochromatic lights were used to set up three light conditions: Red (635 nm, FWHM 20 nm), Green (528 nm, FWHM 34 nm) and Blue (444 nm, FWHM 20 nm). To produce low intensities condition neutral filters were applied on each color to reduce light intensity to 210 μmol.photons.m^{-2}.s^{-1}. Dark condition was obtained by covering microplate wells with dark tape. All treatments were replicated three times.

PAM Chlorophyll Fluorescence

Fluorescence was measured with an imaging-PAM (WALZ – Germany) using blue Luxeon LEDs (450 nm) for both actinic illumination and saturating pulses. Absorptivity was measured with the same instrument using a different set of incorporated LEDs, red (660 nm) and infrared (780 nm) performing a pixel by pixel comparison of images recorded under the two lights using the equation: Absorptivity = 1 – (Red/Infrared). The microplates were placed at 20 cm from the camera (CCD IMAG-K4) to optimize lens focus and illumination. Fluorescence measurements consisted of rapid light curves (RLC) from which all photosynthetic parameters were calculated. RLCs were carried in sequences, starting with migrational 800 μmol.photons.m^{-2}.s^{-1} RGB followed by non-migrational 800 μmol.photons.m^{-2}.s^{-1} RGB then migrational 210 μmol.photons.m^{-2}.s^{-1} RGB and finally non-migrational 210 μmol.photons.m^{-2}.s^{-1} RGB. The time elapsed between the first and last measurement was 25 min. The first RLC measurement (T0) was done 3 h before expected low tide and in darkness, it was followed by three time measurements: T1, done 1.5 h before low tide and after 1.5 h of illumination; T2, synchronized with low tide and after 3 h of illumination; and T3, 1.5 h after low tide with 4.5 h of illumination. RLCs consisted of 12 lights levels (0, 4, 18, 41, 74, 142, 279, 518, 745, 986, 1302, 2342 μmol.photons.m^{-2}.s^{-1}) with 30 s steps. RLC parameters α-slope and *rETRm* were estimated by fitting Silsbe and Kromkamp (2012) modified equation of Eilers and Peeters (1988).

$$\phi II_i = \frac{Fm' - F'}{Fm'} \quad (1)$$

$$\phi II\,(E) = rETRm + \alpha - \text{slope} + \frac{\alpha - \text{slope}}{E * Eopt * (Eopt * E - 2)} \quad (2)$$

Where F' and Fm' are respectively the fluorescence yield under actinic light and the maximum fluorescence yield after a light saturating pulse at each RLC step; E is the light intensity in μmol.photons.m^{-2}.s^{-1}; ϕII_i is the photosystem II effective quantum efficiency at each i steps of the RLC. ϕII_1 correspond to the optimal photosystem II quantum efficiency measured during the first step of the RLC. $\phi II(E)$ refers to light-dependent changes of ϕII. From fitting $\phi II(E)$ the following photosynthetic parameters were estimated: the initial slope of the RLC (α-slope) under limiting irradiance, the maximum relative electron transport rate of the RLCs (*rETRm*) and the optimal light parameter (*Eopt*) of ϕII versus E curves. *Eopt* corresponds to the irradiance (μmol.photons.m^{-2}.s^{-1}) at which ETR saturates and where further increment of light induces photoprotection. Continuous light exposure prevented measurements of the fully oxidized photosystem II at the different time of the tide. In these conditions direct NPQ measurements proved to be impractical due to the cofounding effect of NPQ relaxation and migration. Instead α-slope was used as a proxy for NPQ induction and relaxation. It has been shown to be inversely proportional to NPQ allowing to trace short-term changes in NPQ levels without dark incubation (Cruz and Serôdio, 2008).

Pigments

At the end of the experiment (T3) the migrational samples were sampled by freezing with liquid nitrogen and contact cores (1 cm diameter and 2 mm deep). They were then stored in a −80°C freezer and freeze dried before further processing. Pigment extraction was performed in a dark chamber using acetone (90%), sonicated for 90 s, followed by overnight extraction at 4°C. HPLC analysis was performed according to Van Heukelem method (Heukelem and Thomas, 2001) using a 1 ml/min flow for 36 min with methanol (solvent B) and

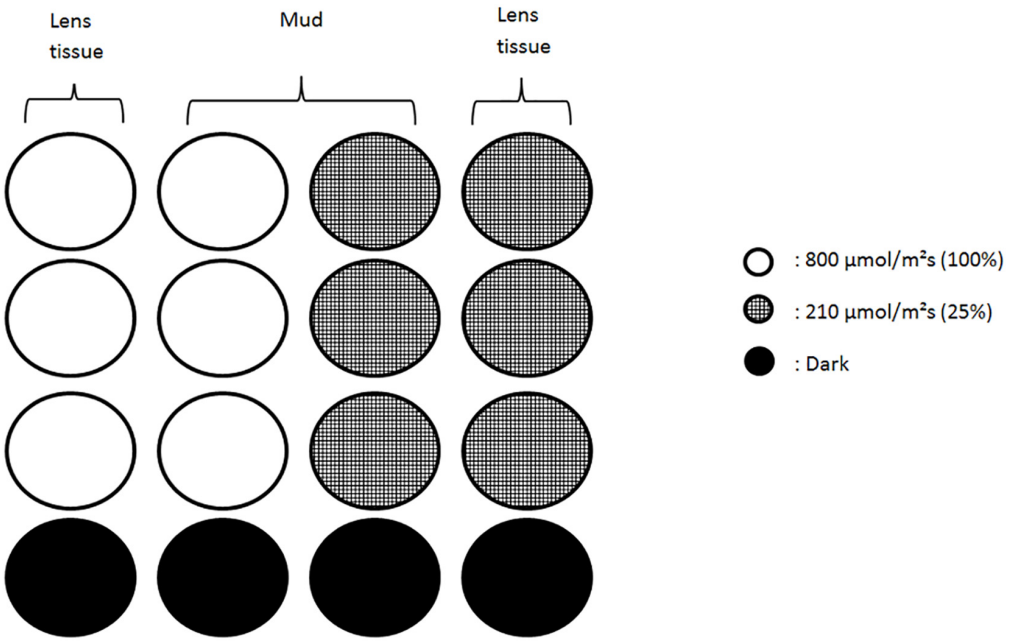

FIGURE 1 | Schematic of the wells set up under each color. Each column of four wells was independently bound and contained three replicates and a dark control. Lens tissue wells were filled with a suspension of migrating diatoms collected from the mud. Wells with mud contained natural assemblages of algae/diatom dominated by epipelic species. Low light conditions (210 µmol.photons.m^{-2}.s^{-1}) were obtained using neutral filters.

methanol/TBAA-28 mM (70/30 – solvent A) going from 5 to 95% of solvent B and vice versa for solvent A. Injection volume was 100 µL with 28.5 µL sample and 71.5 µL TBAA 28 mM. An Agilent Eclipse XDB-C8 column was used at 60°C. Detection was done at 450 and 665 nm using a diode array detector. Approximately 0.17 g of sediment and 1.5 ml of solvent were used for each sample. Identification and pigment concentrations were calibrated using the response factors (RF) of pigments standards (DHI-Danemark). Data analysis was conducted on relative percentage of pigments. The de-epoxidative state (DES) was calculated as Diat/(Diat + Diad). Pigment determination was not performed on non-migrating biofilms due to lack of biological material for the different analysis.

Absorption Spectra

To compare whether differences in light color responses were due to total light absorbed or other chromatic effect a pigment weighted light absorption (*Qphar*) was calculated. *Qphar(λ)* correspond to the amount and proportion of light absorbed by the cells at different wavelengths. It is calculated according to a modified Eq. (4) of Gilbert et al. (2000). The specific *in vitro* absorption coefficients of microphytobenthos samples a_{mpb} were reconstructed according to Eq. (3).

$$a_{mpb}(\lambda) = \sum_{i}^{n} a_i(\lambda)^* C_i \quad (3)$$

$$Qphar(\lambda) = Q(\lambda) - (Q(\lambda)^* e^{-a_{ph}(\lambda)}) \quad (4)$$

$a(\lambda)$ is the concentration specific absorption coefficient in m^2g^{-1}, its values were obtained from the literature (Clementson and Wojtasiewicz, 2019). *C* is the pigment specific average concentration within all contact cores in $mg.g^{-1}$. *Q(λ)* is the photosynthetically available radiation at the top of the sediment or in lens tissue in µmol.photons.m^{-2}.s^{-1}. Pigments used for reconstruction of the light absorption spectrum were chlorophyll *a*, chlorophyll *c2*, fucoxanthin, β-carotene, diadinoxanthin and diatoxanthin.

Carbohydrates and Proteins

At T3, migrational and non-migrational samples were frozen and stored at −80°C for carbohydrate and protein quantification. Colloidal (soluble) fractions were extracted from thawed samples. They were first mixed in 2 mL of artificial sea water for 1.5 h (Orbital shaker, YELLOWline), then the supernatant was removed and the remaining sediment was mixed again with 2 mL of artificial sea water and 300 mg of Dowex Marathon Cex change resin to extract the bound (attached to sediment particles) fraction. Carbohydrate and protein quantification were done by spectroradiometry (Genesys 10S Uv/Vis) using the colorimetric reactions methods of DuBois et al. (1956) for carbohydrates and a modified Lowry method for proteins (Frølund et al., 1996).

Species Identification

Algal suspensions were preserved with glutaraldehyde (4%) and sediment cores were frozen with liquid nitrogen, respectively stored at 4 and −80°C. Three vials were filled with 1.5 mL of algal suspension while sediment cores were first placed in ludox (®HS-40 coloidal silica) to separate cells from the

sediment and were then resuspended in a known volume of water and cleaned up following the protocol by Consalvey (2002). Succinctly, it consisted of a 24 h oxidation in saturated potassium permanganate solution, followed by the addition of hydrochloric acid for 2 h at 70°C. Lastly, cells were rinsed seven times with ultrapure water in a final volume of 1.5 mL. A 50 µl subsample was permanently mounted on microscope slides using NaphraxTM. Cell counting, observation and identification of diatom valves were made with an optical microscope (Olympus). At 1000 magnification, 10 zones were chosen using randomly generated numbers and counted in five different slides until more than 400 individuals were counted. Identification was performed using the literature (Paulmier, 1997; Ribeiro, 2010; Mertens et al., 2014). Biovolumes were retrieved from the literature (Olenina et al., 2006; Ribeiro, 2010) and calculated according to morphologically based equations (Hillebrand et al., 1999; Olenina et al., 2006).

Statistical Analysis

All statistical analyses were performed using R (R Core Team, 2017). Two-ways analysis of covariance (ANCOVA) were performed to compare datasets possessing a time variable with a linear regression. This comprised analysis of absorptivity, ϕII_1 and α-slope over time for the different treatments of either same color or same light intensity. Pigment compositions were tested using a permutational multivariate analysis of variance using distance matrices based on Bray–Curtis dissimilarity index. Multivariate homogeneity of group dispersions was tested with a permutation-based test. Pigment and EPS differences between treatments were tested using two-way analysis of variance (ANOVA), after normality and homogeneity of variance had been verified using Shapiro–Wilk and Barlett tests, respectively. Individual differences were tested using *Post hoc* Tukey HSD tests. A principal components analysis (PCA) was used to visualize the pigment variance between treatments.

RESULTS

Species Composition

The dominant species in the non-migrational biofilms were: *Navicula meulemansii* (71.8%), *Navicula spartinetensis* (17.3%), *Gyrosigma limosum* (5.3%), *Gyrosigma wansbecki* (3.8%), and *Pleurosigma angulatum* (1.3%) (**Figure 2**). The migrational biofilm was dominated by *Navicula meulemansii* (30.42%), *Thalassiosira* cf. *proschkinae* (11.47%), *Navicula spartinetensis* (10.7%), *Gyrosigma limosum* (7.0%), *Gyrosigma wansbeckii* (5.7%), *Thalassiosira* cf. *pseudonana* (4.5%), *Odontella aurita* (3.74%), *Raphoneis amphiceros* (2.49%), *Tryblionella* sp. (2.0%), *Coconeis speciosa* (2.0%), *Nitzschia* cf. *lorenziana* (2.0%), *Thalassiosira* cf. *angulata* (1.7%), *Pleurosigma angulatum* (1.7%) (**Figure 2**).

Photosynthetic Activity as a Function of Color-Dependent Light Intensity (Qphar)

Photosynthetic active radiation intensity is a widely used measure of standardized light dosage that can be compared across a variety of experiments. However, when light spectral composition is taken into account this measurement becomes flawed due to the fact that photosynthetic organisms absorb light differently, depending on their pigment composition. Thus direct comparisons of similar light intensities at different wavelengths are hindered by potentially different photoprotective reactions. Recalculating the total intensity absorbed at each wavelength (*Qphar*) produced six different intensities. These Qphar intensities were respectively 63.8 (R210), 76.2 (G210), 198.3 (B210), 255.02 (B800), 305.01 (G800) and 793.29 (B800) $\mu mol.photons.m^{-2}.s^{-1}$ (**Figure 3**). Migrational and non-migrationnal biofilms (**Figure 3**) displayed a Qphar threshold where alpha values switched from a NPQ relaxation state to a light induced NPQ production. Alpha is inversely proportional to NPQ intensity and a characteristic shift from values over 100% to values below 100% indicated a threshold where light started inducing physiological photoprotection throught NPQ increase. This threshold was observed between 200 and 250 $\mu mol.photons.m^{-2}.s^{-1}$ of Qphar (**Figure 3**) effectively separating our treatments in low light (LL) when it is below 200 $\mu mol.photons.m^{-2}.s^{-1}$ and high light (HL) when above 250 $\mu mol.photons.m^{-2}.s^{-1}$ of Qphar.

Vertical Migration Absorptivity Changes at the Surface

Absorptivity increased over time in all treatments subjected to light and decreased in the dark control (**Figure 4**). Light intensity had a significant effect on the absorptivity changes in red, blue and green wavelengths (ANCOVA, $p < 0.05$). Time also had a significant effect on absorptivity changes in red, green, blue, and dark treatments (ANCOVA, $p < 0.05$), with no significant interaction between time and light intensity. Within each set of light intensities there was also a significant effect of light color (ANCOVA, $p < 0.001$), and light color over time (ANCOVA, $p < 0.05$) which differed in the two conditions (HL and LL). Red and blue treatments showed different effects at the two light intensities, with blue absorptivity increasing 101% in LL and only 9% in HL; while red absorptivity increased 50% in HL and only 24% in LL (**Figure 4**). The dark control showed a decrease in absorptivity over time.

Optimal PSII Quantum Efficiency (ϕII_1)

On average, optimal PSII quantum efficiency (ϕII_1) in a dark adapted state at T0 were significantly higher ($p < 0.001$ *t*-test) for migrational biofilms (mean = 0.607) than non-migrational biofilms (mean = 0.401). Non-migrational treatments were characterized by a ϕII_1 increase in LL and ϕII_1 decrease in HL, with significant effects of time (ANCOVA, $p < 0.01$), light intensity (ANCOVA, $p < 0.001$) and intensity over time (ANCOVA, $p < 0.001$). Non-migrational biofilms ϕII_1 was affected differently by the light color in LL and HL treatments (**Figure 5**). With the exception of dark and red, ϕII_1 in HL showed significant differences between colors ($p < 0.001$), time ($p < 0.001$) and color over time ($p < 0.001$). Contrastingly, ϕII_1 in LL samples increased significantly over time ($p < 0.001$) and remained constant in dark controls. There were no significant

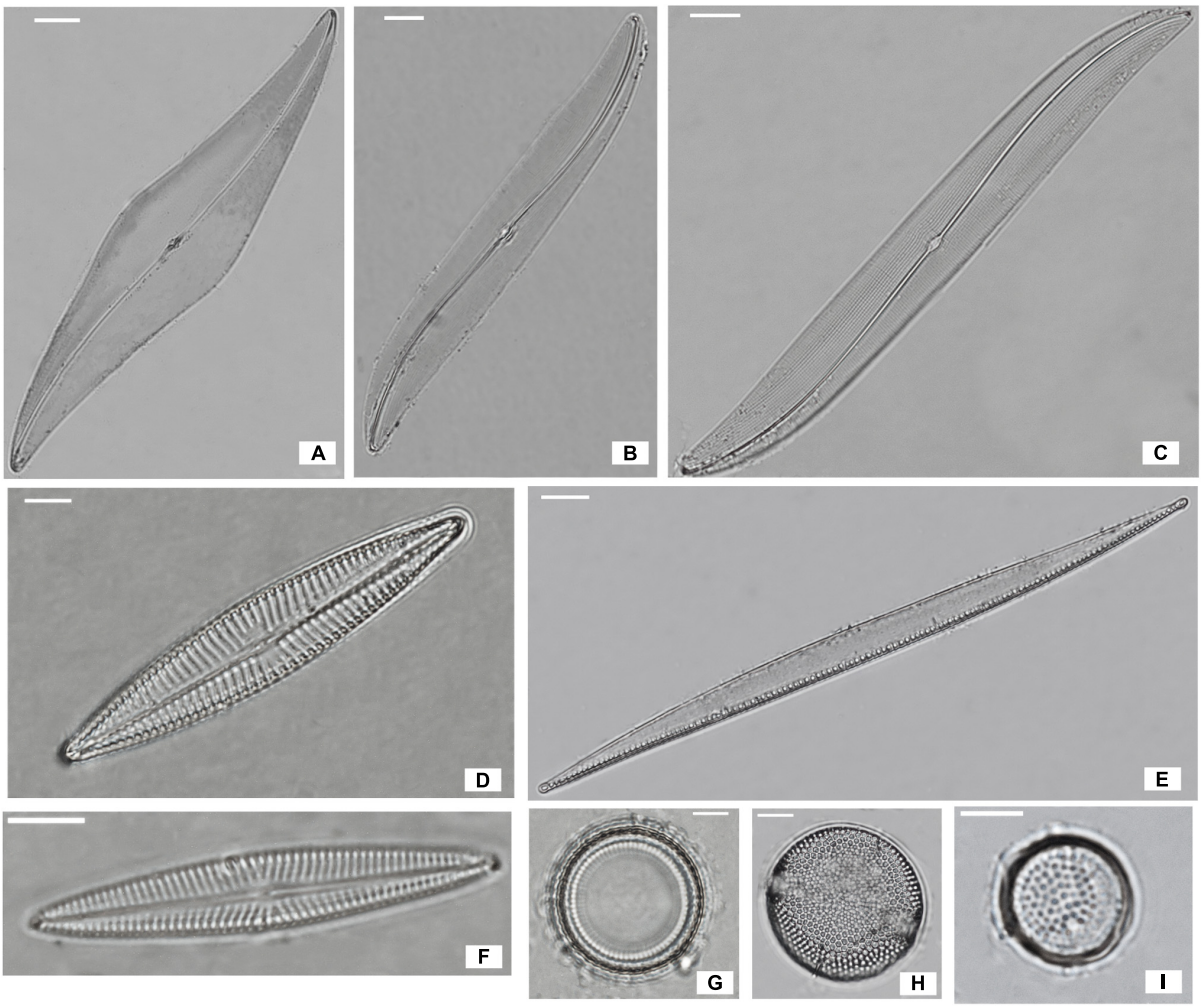

FIGURE 2 | Most abundant diatoms species of Bay de Bourgneuf site; **(A)** *Pleurosigma angulatum* (scale bar = 20 μm); **(B)** *Gyrosigma limosum* (5 μm); **(C)** *Gyrosigma wansbecki* (10 μm); **(D)** *Navicula spartinetensis* (5 μm); **(E)** *Nitzschia* cf. *lorenziana* (10 μm); **(F)** *Navicula meulemansii* (5 μm); **(G)** *Thalassiosira* cf. *pseudonana* (5 μm); **(H)** *Thalassiosira* cf. *angulata* (5 μm); **(I)** *Thalassiosira* cf. *proschkinae* (5 μm).

differences in LL ϕII_1 between colors and colors over time (**Figure 5**). ϕII_1 of all migrational biofilms increased in LL and decreased in HL, with significant effects of time ($p < 0.001$), intensity ($p < 0.001$), and intensity over time ($p < 0.001$) (**Figure 5**). All migrational HL biofilms (apart from control) showed a significant ϕII_1 decrease over time ($p < 0.001$) and no significant differences between colors and colors over time. With the exception of green and blue samples, the LL migrational ϕII_1 differed significantly between color treatments with significant effect of color ($p < 0.001$), time ($p < 0.05$), and color over time ($p < 0.01$).

RLC Parameters

Changes in α-slope were strongly correlated with ϕII_1 (Pearson correlation of 0.99, $p < 0.001$) with α-slope increasing in all LL treatments and decreasing in all HL treatments over time (**Tables 1**, **2**). There was a significant effect of light intensity and light color in all α-slope values that were always significantly different from the dark controls over time (ANCOVA, $p < 0.001$) (**Figure 6**). α-slope significantly decreased with time in HL migrational biofilms and significantly increased with time in migrational LL biofilms (ANCOVA, $p < 0.001$), with no significant differences between color and light color over time (**Figure 6**). In migrational LL biofilms only red samples showed significantly higher α-slope values than the other two colors (ANCOVA, $p < 0.05$). The biggest significant difference in α-slope values was observed in non-migrational HL samples were α-slope significantly decreased between colors ($p < 0.001$), over time ($p < 0.001$) and between colors over time ($p < 0.001$) (**Figure 6**).

Changes in *rETRm* over the course of the experiment were strongly influenced by light color and light intensity (**Tables 1**, **2**). In all samples and all conditions *rETRm* systematically increased from T0 to T1 and then depending on the conditions either continuously decreased or increased. LL non-migrational biofilm was the only condition where *rETRm* kept increasing throughout

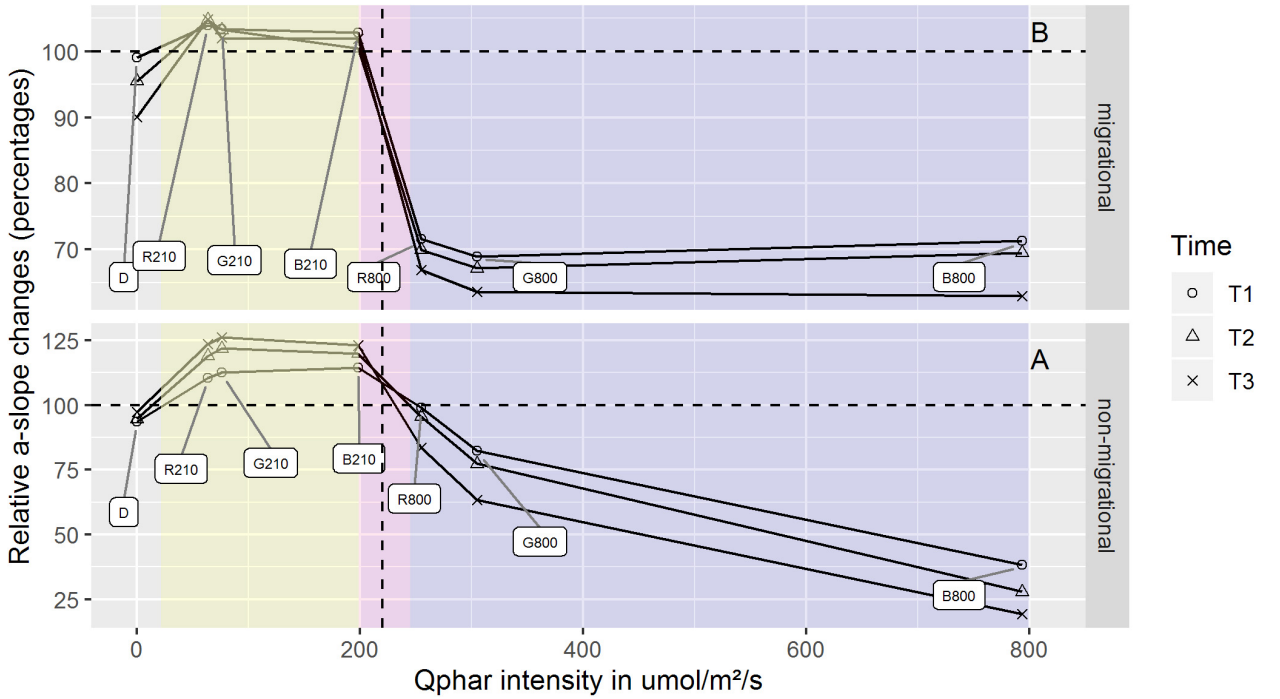

FIGURE 3 | α-slope changes for differing Qphar intensities. α-slope are displayed as percentages of the initial value prior to illumination. Qphar recalculated intensities are 63.8 (R210), 76.2 (G210), 198.3 (B210), 255.02 (R800), 305.01 (G800), and 793.29 (B800) μmol.photons.m^{-2}.s^{-1}. The area below 200 μmol.photons.m^{-2}.s^{-1} (yellow) correspond to non-stressful light conditions where NPQ is relaxing while the area above 250 μmol.photons.m^{-2}.s^{-1} (purple) correspond to stressful light inducing NPQ. The boundary and threshold between LL Qphar and HL Qphar is represented in pink. n = 3 for each point.

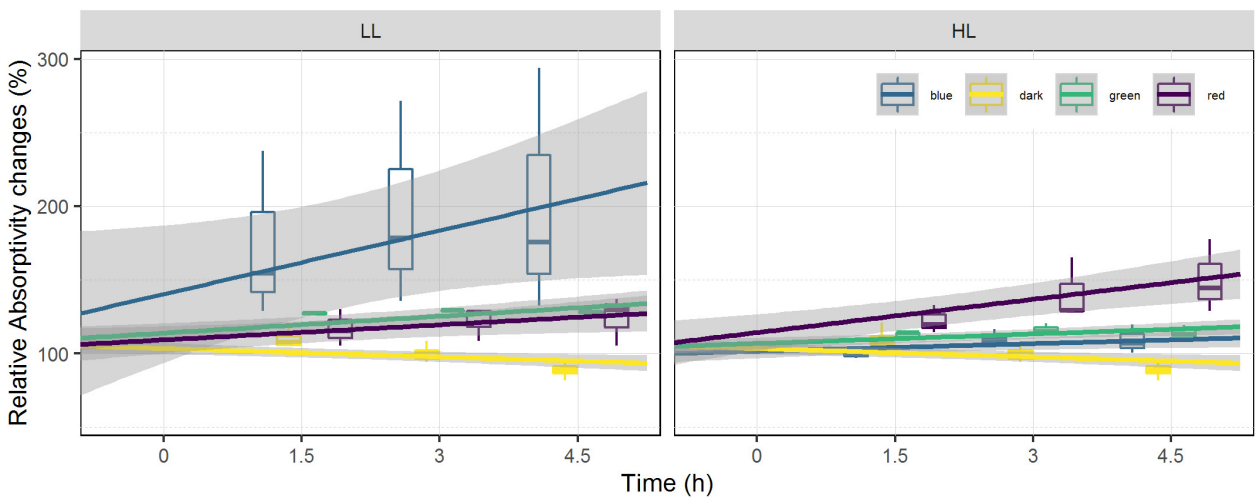

FIGURE 4 | Relative absorptivity changes at the surface of the sediment. Absorptivity is displayed as percentage of the initial value prior to illumination (at T0). It is used as a biomass proxy at the surface of the sediment. Each color has been fitted with a linear model where confidence interval (0.95) are represented in gray (n = 3).

the whole experiment (with the exception of blue T3). *rETRm* color treatments were significantly higher than dark controls ($p < 0.01$) while not significantly differing between each color. On the contrary in HL all treatments significantly differed ($p < 0.01$) with the exception of red and dark. At the end of the light exposure in non-migrational biofilms there was a significant effect of intensity ($p < 0.001$) on *rETRm* values exemplified by a 44% decrease in blue HL and a 224% increase in LL compared to initial values. In all migrational biofilms *rETRm* increased to their maximum value at T1 and then slowly decreased over

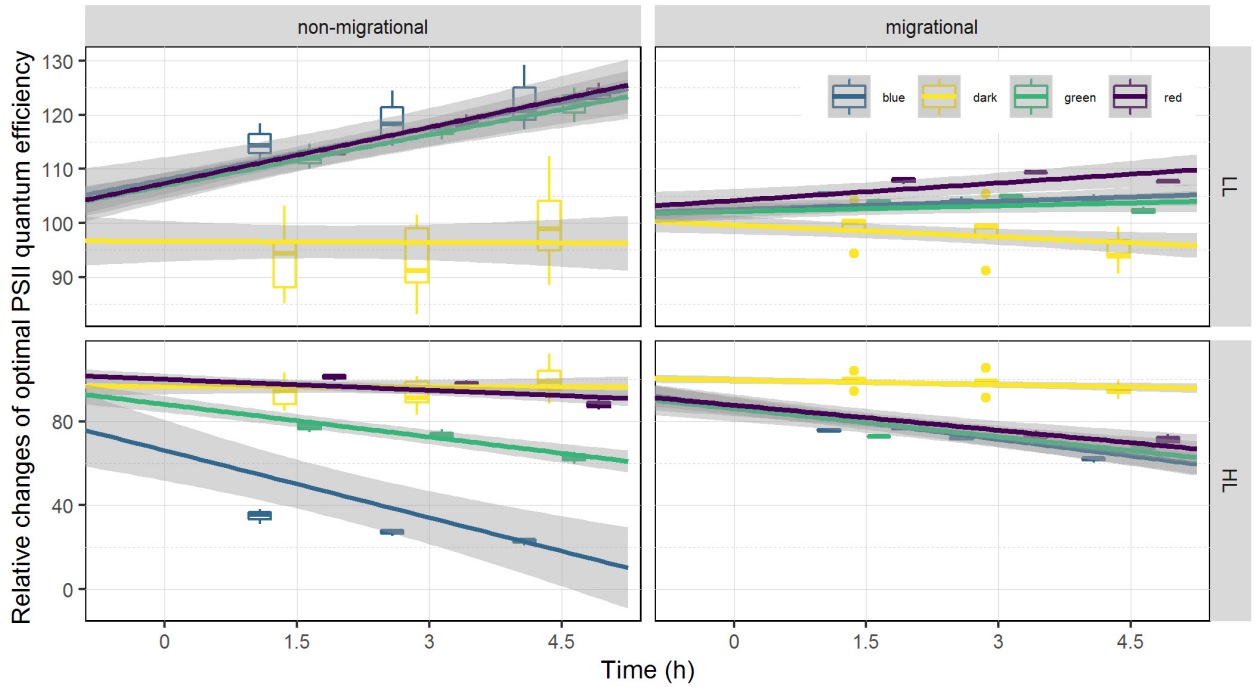

FIGURE 5 | Relative changes of optimal photosystem two light efficiency ϕII_1. ϕII_1 is displayed as percentage of the initial value prior to illumination (at T0). Each color has been fitted with a linear model where confidence interval (0.95) are represented in gray (n = 3).

TABLE 1 | Photosynthetic parameters and ϕII_1 values obtained from rapid light curve fitting of ϕII(E) within the non-migrational biofilm.

		Blue		Dark	Green		Red	
µmol.photons.m^{-2}.s^{-1}		**800**	**210**	**NA**	**800**	**210**	**800**	**210**
α-slope	T0	0.38 ± 0.002	0.39 ± 0.01	0.37 ± 0.017	0.37 ± 0.01	0.37 ± 0.01	0.37 ± 0.004	0.37 ± 0.011
	T1	0.15 ± 0.012	0.44 ± 0.003	0.34 ± 0.007	0.31 ± 0.003	0.42 ± 0.011	0.37 ± 0.004	0.41 ± 0.01
	T2	0.11 ± 0.007	0.46 ± 0.008	0.34 ± 0.01	0.29 ± 0.004	0.45 ± 0.007	0.35 ± 0.004	0.44 ± 0.01
	T3	0.07 ± 0.007	0.48 ± 0.008	0.36 ± 0.014	0.24 ± 0.007	0.47 ± 0.004	0.31 ± 0.007	0.46 ± 0.008
ϕII	T0	0.41 ± 0.002	0.42 ± 0.012	0.4 ± 0.019	0.4 ± 0.013	0.4 ± 0.012	0.39 ± 0.004	0.4 ± 0.012
	T1	0.14 ± 0.015	0.48 ± 0.004	0.37 ± 0.024	0.31 ± 0.004	0.45 ± 0.011	0.4 ± 0.007	0.45 ± 0.014
	T2	0.11 ± 0.006	0.5 ± 0.008	0.37 ± 0.015	0.29 ± 0.002	0.47 ± 0.008	0.38 ± 0.002	0.47 ± 0.013
	T3	0.09 ± 0.006	0.51 ± 0.011	0.39 ± 0.018	0.25 ± 0.008	0.49 ± 0.002	0.35 ± 0.007	0.49 ± 0.008
rETRm	T0	40.8 ± 3	45.7 ± 3	39.2 ± 7.5	38.8 ± 2	41.4 ± 3	33.6 ± 2	38.7 ± 3
	T1	52.7 ± 7	98.4 ± 1	65.35 ± 10.5	79.3 ± 3	86.5 ± 7	73.2 ± 2	75.5 ± 6
	T2	30.8 ± 5	110 ± 5	74.45 ± 8.5	67.8 ± 3	102.9 ± 7	70.2 ± 1	88.7 ± 7
	T3	17.8 ± 1	104.1 ± 5	77.45 ± 11.5	45.3 ± 2	103.7 ± 4	49.3 ± 2	92.9 ± 5

Equation derived from Silsbe and Kromkamp (2012) modified equation of Eilers and Peeters (1988). The entire well was used as a region of interest. n = 3. ± : standard deviations.

time. Only red light displayed a significant *rETRm* difference between intensities ($p < 0.05$). Overall blue light treatments had a significant higher *rETRm* than samples of the same intensity with the exception of red LL.

Pigments and EPS

Mean total pigment content is a proxy of the biomass within the 2 upper mm (**Figure 7**). At T3 the mean total pigment content (**Figure 7**) resembled the patterns observed in absorptivity measured at T3 (**Figure 4**) that were marked by an interaction of light quality and light intensity ($p < 0.05$), producing opposite effects at LL and HL. In the LL treatment, the highest mean total pigment content was found under blue light while the lowest content was found in red. The opposite trend was observed in HL with the highest mean total pigment content observed under red light and lowest in blue light.

The average pigment composition of migrational biofilms at the end of the experiment was: chlorophyll *a* (Chl *a*, 40.8%), fucoxanthin (Fuco, 37.8%), diadinoxanthin (Diad, 8.8%), chlorophyll *c1* (Chl *c1*, 3.8%), diatoxanthin (Diat, 2.54%),

TABLE 2 | Photosynthetic parameters and ϕII_1 values obtained from rapid light curve fitting of ϕII(E) within the migrationnal biofilm.

		Blue		Dark	Green		Red	
μmol.photons.m^{-2}.s^{-1}		**800**	**210**	**NA**	**800**	**210**	**800**	**210**
α-slope	T0	0.59 ± 0.006	0.59 ± 0.003	0.57 ± 0.009	0.59 ± 0.003	0.59 ± 0.002	0.57 ± 0.003	0.58 ± 0.002
	T1	0.42 ± 0.005	0.6 ± 0.004	0.57 ± 0.0145	0.41 ± 0.004	0.61 ± 0.008	0.41 ± 0.003	0.6 ± 0.005
	T2	0.41 ± 0.006	0.59 ± 0.004	0.55 ± 0.018	0.4 ± 0.006	0.61 ± 0.001	0.4 ± 0.01	0.61 ± 0.003
	T3	0.37 ± 0.007	0.6 ± 0.006	0.52 ± 0.014	0.38 ± 0.006	0.6 ± 0.005	0.38 ± 0.012	0.61 ± 0.004
ϕII	T0	0.61 ± 0.007	0.61 ± 0.002	0.6 ± 0.01	0.61 ± 0.005	0.62 ± 0.002	0.59 ± 0.001	0.61 ± 0.001
	T1	0.46 ± 0.009	0.65 ± 0.004	0.6 ± 0.025	0.45 ± 0.002	0.64 ± 0.005	0.45 ± 0.004	0.65 ± 0.005
	T2	0.44 ± 0.011	0.64 ± 0.003	0.59 ± 0.033	0.43 ± 0.004	0.65 ± 0.001	0.43 ± 0.012	0.66 ± 0.001
	T3	0.38 ± 0.01	0.64 ± 0.007	0.57 ± 0.022	0.41 ± 0.005	0.63 ± 0.004	0.42 ± 0.015	0.65 ± 0.003
rETRm	T0	126.3 ± 7	135.9 ± 6	132.55 ± 6.5	131.5 ± 5	138 ± 5	122.5 ± 6	135.5 ± 3
	T1	207.6 ± 18	221 ± 16	172.95 ± 16.5	168.9 ± 1	200.6 ± 10	155.1 ± 5	200.6 ± 6
	T2	189.9 ± 21	188.5 ± 21	169.4 ± 15.5	153.4 ± 5	169.3 ± 12	133.5 ± 9	182.8 ± 7
	T3	184.6 ± 23	171.1 ± 22	159.35 ± 9.5	144.1 ± 5	147.9 ± 12	121.4 ± 10	166.4 ± 7

Equation derived from Silsbe and Kromkamp (2012) modified equation of Eilers and Peeters (1988). The entire well was used as a region of interest. n = 3. ± : standard deviations.

chlorophyll *c2* (Chl *c2*, 2%), alpha and beta-carotene (αβ car, 1.9%), chlorophyll *b* (chl *b*, 1%) and antheraxanthin (anth, 0.8%). Color, light intensity and their interaction had a significant effect ($p < 0.001$) on the relative percentage of pigments (**Figure 8**). The PCA results (**Figure 8**) show that the two main axes explained 57.5% of the variance between pigments, with color treatments aligned along the two axes. Light intensity accounted for 23.1% of the total variance (Between Class Analysis) with significant percentage differences in Diat ($p < 0.001$), Diad ($p < 0.01$), Fuco ($p < 0.01$), and Chl c1 ($p < 0.01$). A *post hoc* test showed a higher percentage of Diat ($p < 0.001$) in all HL treatments (**Figure 8**).This was further exemplified by the significant higher ($p < 0.001$) DES (**Table 3**) in HL compared to LL. Color treatments accounted for 27.4% of the total variance with significant pigment percentage differences of Chl a ($p < 0.001$), Fuco ($p < 0.001$), Anth ($p < 0.001$), Diad ($p < 0.01$), and Diat ($p < 0.01$). *Post hoc* tests showed significant higher Chl a pigment percentage in blue treatments compared to red ones ($p < 0.001$) and higher Fuco percentage in red light ($p < 0.05$) compared to the other two colors. The interaction effect of color and intensity accounted for 67.3% of the total variance with significant pigment percentage differences of Fuco ($p < 0.01$), Diad ($p < 0.01$), Anth ($p < 0.05$), Diat ($p < 0.01$), Chl *a* ($p < 0.05$). Amongst these interaction effects there was a significantly lower Diat ($p < 0.01$) in blue HL compared to the other two colors.

Non-migrational biofilms showed significant differences in colloidal carbohydrates (CC) with higher CC content observed in HL ($p < 0.05$) (**Figure 9**). In HL, there was no significant difference between colors for any carbohydrate fraction nevertheless the variance was very high in blue and red CC. Overall, the carbohydrate contents measured in non-migrational biofilms were very small, which led to values below the detection threshold in bound carbohydrates (BC) and to high variability in CC. There were no significant differences between treatments and controls for all protein measurements *(data not shown)*. The average protein concentration was 0.0114 (± 0.0025) μg.mm^{-2} for non-migrational biofilms and 0.0608 (± 0.010) μg.mm^{-2} for migrational biofilms.

Migrational biofilm CC contents were significantly different between color ($p < 0.001$), light intensity ($p < 0.05$) and their interaction ($p < 0.05$) (**Figure 9**). All color treatments with the exception of red LL had significantly higher CC contents than the dark controls ($p < 0.05$). The interaction effect led to contrasting results at the different light intensities with no significant CC differences between colors in HL while at LL lower CC concentrations were observed in red in comparison to blue ($p < 0.01$). The BC concentrations of the migrational biofilms were also significantly affected by color ($p < 0.001$), with blue treatment having higher BC contents than dark control ($p < 0.05$) in both LL and HL while red treatment only had a higher BC contents than dark control under HL intensities ($p < 0.05$).

DISCUSSION

Both light intensity and light quality had a significant effect on diatom photo-regulation mechanisms (migration and NPQ), with clear differences being observed between migrational and non-migrational biofilms, confirming that vertical migration movements within the sediment matrix plays a major role in diatom photo-regulation.

Species Composition

The diatoms that were present in both migrational and non-migrational biofilms were typical epipelic diatoms from the Bourgneuf bay site, similar to the assemblages observed by Méléder et al. (2007). *Navicula spartinetensis* is found exclusively in intertidal muddy sediments and is one of the most commonly found epipelic species in European Atlantic coasts (Ribeiro, 2010). The only species that had not yet been described for this site was *Navicula meeulmansii*. However, *N. meeulmansii* has only recently been described as a cosmopolitan species tolerating wide range of salinities (Mertens et al., 2014), which

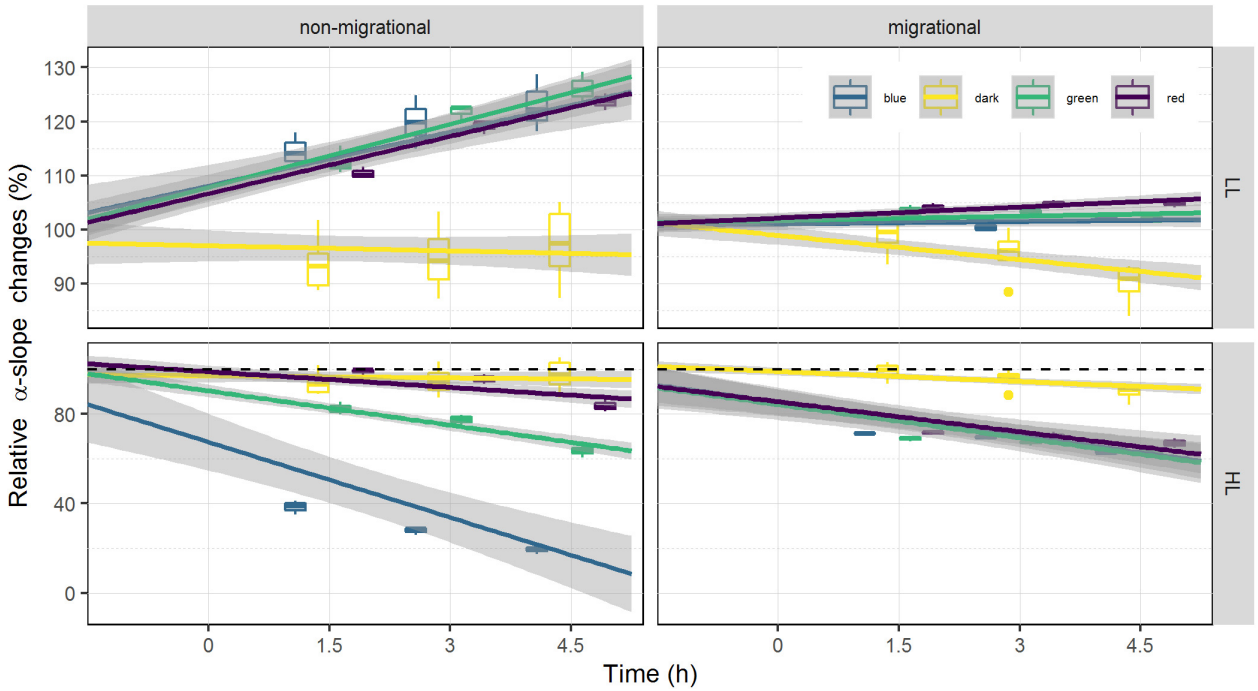

FIGURE 6 | Relative changes of α-slope. α-slope is displayed as percentage of the initial value prior to illumination (at T0). α-slope variations is used as a proxy of NPQ as it is inversely proportional. Each color has been fitted with a linear model where confidence interval (0.95) are represented in gray (n = 3).

may have been previously described as *Navicula phyllepta* or *Navicula microdigitoradiata* in the other studies from this ecosystem (Méléder et al., 2007; Hernández Fariñas et al., 2017). These epipelic diatoms are known to photo-regulate using both physiological and behavioral photoprotection (Cartaxana et al., 2011; Laviale et al., 2015). The species differences observed between the two treatments were mainly related to the non-migrational nature of *Thalassiosira* cf. *proschkinae*, *Thalassiosira* cf. *pseudonana*, *Thalassiosira* cf. *angulata*, *Odontella aurita*, *Raphoneis amphiceros*, *Coconeis speciosa*, and *Nitzschia lorenziana* which will not be captured by our sampling method (Eaton and Moss, 1966). Nevertheless, the two biofilms were strongly dominated by migratory species: *Navicula meulemansii*, *Navicula spartinetensis*, *Gyrosigma limosum*, *Gyrosigma wansbecki* and *Pleurosigma angulatum* and their biovolumes were strongly dominated by *Gyrosigma limosum*, *Gyrosigma wansbecki* and *Pleurosigma angulatum* that, albeit present only in relatively small numbers, correspond to 18.5, 48.1, 22.6 and 17.3, 51.7, 22.2% of the total biovolume (non-migrational and migrational, respectively).

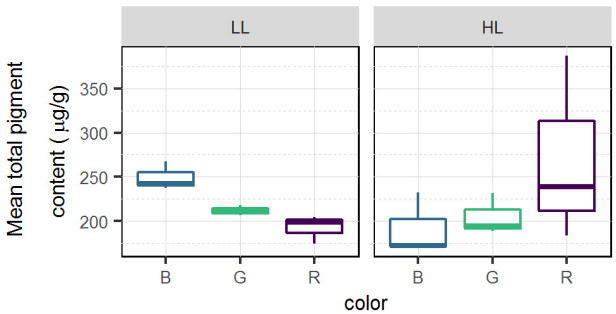

FIGURE 7 | Average total pigment content ($\mu g.g^{-1}$) for each light color and intensity in migrational biofilm (n = 3). Pigments were sampled on the top 2 mm of the sediment using contact cores.

Physiological Photoprotection

In the non-migrational biofilms cells were artificially constrained to immobility and thus had to rely solely on physiological photoprotection to cope with changing light environment. This immobility was characterized by an increase in ϕII_1 and *α-slope* in the LL condition (**Figures 5**, **6**). A ϕII_1 increase indicates that a higher proportion of absorbed light was being used for photosystem II (PSII) photochemistry implying a concomitant decrease in NPQ from the start of the experiment. This is coherent with the α-slope increase observed in the LL non-migrational biofilms (**Figure 6**) as RLC α-slope increases have been shown to be proportional to NPQ reversal (Cruz and Serôdio, 2008). An α-slope increase over time indicates that a significant amount of NPQ had accumulated overnight in all conditions and was being dissipated over the course of the experiment in the LL conditions. Diatom dark NPQ induction has been previously observed and attributed to a transthylakoidal pH-gradient dependent activation of the XC cycle, due to chlororespiration or to the reverse operation of ATP synthase (Ting and Owens, 1993; Jakob et al., 1999; Dijkman and Kroon,

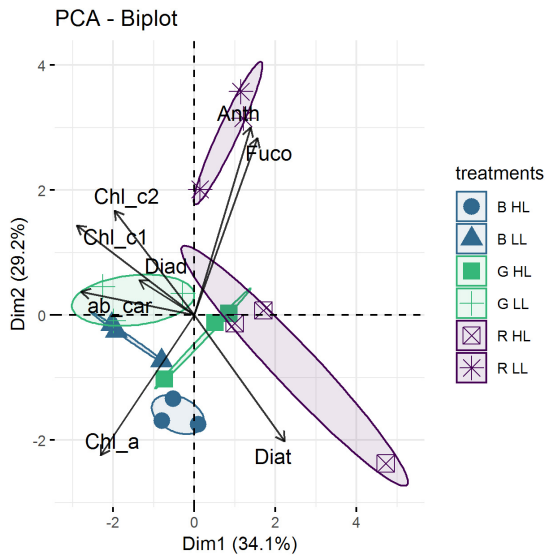

FIGURE 8 | Representation of Principal component analysis (PCA) calculated with pigment percentages from $\mu g.g^{-1}$. The first two PCA dimensions accounted for 29.3 and 26.2%, respectively, of the total variance. Replicates of the same treatment ($n = 3$) are grouped by confidence interval ellipses (0.95).

2002; Mouget et al., 2004). The decrease of NPQ and the consequent increase of both α-slope and ϕII_1 under LL could be explained by the gradual dissipation of the transthylakoidal proton gradient under low fluence rates (Consalvey et al., 2004a; Serôdio et al., 2005). This NPQ dissipation attests that the LL intensity condition was indeed perceived, for each color, as a non-stressful factor and did not require the development of photoprotective mechanisms hence a gradually increasing *rETRm* (**Table 1**).Within the LL treatments there was no significant differences between NPQ dissipation despite varying Qphar values (**Figure 3**, non-migrational) indicating that below 200 $\mu mol.photons.m^{-2}.s^{-1}$ of Qphar, NPQ build up was not modulated by the amount of light absorbed. This was further exemplified by the absence of noteworthy differences in EPS that were characterized by the same amount of carbohydrates (**Figure 9**) and proteins. Under HL exposure in non-migrational biofilms photosynthetic parameters ϕII_1 and α-slope showed less NPQ induction under red light (**Figure 6**) with no significant differences between red and dark treatments. Comparatively, green and especially blue light induced much more NPQ build-up in non-migrational HL samples (**Figure 6**). CC concentrations were also significantly higher in HL than LL. These changes in CC production/secretion could reflect a need to readjust the carbohydrate:protein ratio within the cell as an "overflow metabolism" that helps coping with the stressful environmental conditions imposed by exposure to high light intensities (Staats et al., 2000; Orvain et al., 2003; Underwood et al., 2004; Takahashi et al., 2009). At HL there was a strong inverse correlation of $r = -0.92$ ($p < 0.001$) between α-slope and Qphar (**Figure 3**). The same correlation was not observed between CC and Qphar as CC content were not significantly different in HL (**Figure 9**). The physiological role of CC in photoprotection therefore seemed limited to whether or not NPQ was induced but not proportional to the amount of NPQ induction. There was a threshold between 200 and 250 $\mu mol.photons.m^{-2}.s^{-1}$ of Qphar where light started inducing physiological photoprotection. Despite not having pigment data for the non-migrational biofilms, α-slope and ϕII_1 values observed in HL non-migrational biofilms suggested that blue light, notably due to its higher Qphar value would have had a higher effect in inducing the xantophyll cycle as observed by the strong decrease in α-slope (**Figure 6**) and rETRm (**Table 1**), in comparison to the other two light colors. Previous observations, using similar Qphar intensities (Schellenberger Costa et al., 2013a) or using wavelength dependent absorption cross-section of PSII (PSII effective $quanta.s^{-1}$) (Schreiber et al., 2012), have shown that despite these standardization growing diatoms in blue light induced significant higher NPQ and *ETRm* values compared to red light (Schreiber et al., 2012; Schellenberger Costa et al., 2013a,b; Jungandreas et al., 2014). Diatoms possess a number of photoreceptors, including blue light sensing aureochrome and red/far-red light sensing phytochrome, hypothesized to mediate photoprotective

TABLE 3 | Main pigment concentration in $ug.g^{-1}$ for migrational biofilm.

	Blue		Green		Red	
$\mu mol.photons.m^{-2}.s^{-1}$	800	210	800	210	800	210
Chl *a*	78.58 ± 14.8	102.85 ± 6.72	81.27 ± 8.79	85.99 ± 3.4	106.81 ± 42.6	74.98 ± 6.34
Fuco	69.38 ± 13.03	93.74 ± 6.13	75.98 ± 9.7	77.47 ± 1.96	101.11 ± 39.71	74.28 ± 6.76
Chl *c1*	6.96 ± 1.53	9.87 ± 0.84	7.9 ± 0.76	8.35 ± 0.5	9.41 ± 3	7.35 ± 0.79
Chl *c2*	3.76 ± 0.7	4.72 ± 0.51	3.97 ± 0.49	4.2 ± 0.34	4.84 ± 1.43	3.79 ± 0.37
Chl *b*	2.62 ± 0.82	2.51 ± 0.08	1.7 ± 0.05	1.77 ± 0.14	2.35 ± 1.15	1.69 ± 0.23
ab car	3.62 ± 0.78	4.97 ± 0.33	3.93 ± 0.38	3.84 ± 0.22	4.43 ± 1.11	3.52 ± 0.26
Anth	1.33 ± 0.15	1.53 ± 0.14	1.56 ± 0.08	1.74 ± 0.03	2.2 ± 0.69	2.37 ± 0.24
Diad	15.83 ± 2.79	21.3 ± 1.32	17.28 ± 2.47	20.32 ± 0.6	22.86 ± 8.46	16.36 ± 1.19
Diat	5.91 ± 1.26	3.81 ± 0.08	7.22 ± 0.53	3.53 ± 0.22	10.4 ± 5.02	3.08 ± 0.18
DES	0.27 ± 0.31	0.15 ± 0.06	0.29 ± 0.18	0.15 ± 0.27	0.31 ± 0.37	0.16 ± 0.13

Pigments were sampled on the top 2 mm of the sediment using contact cores. n = 3. ± : standard deviations.

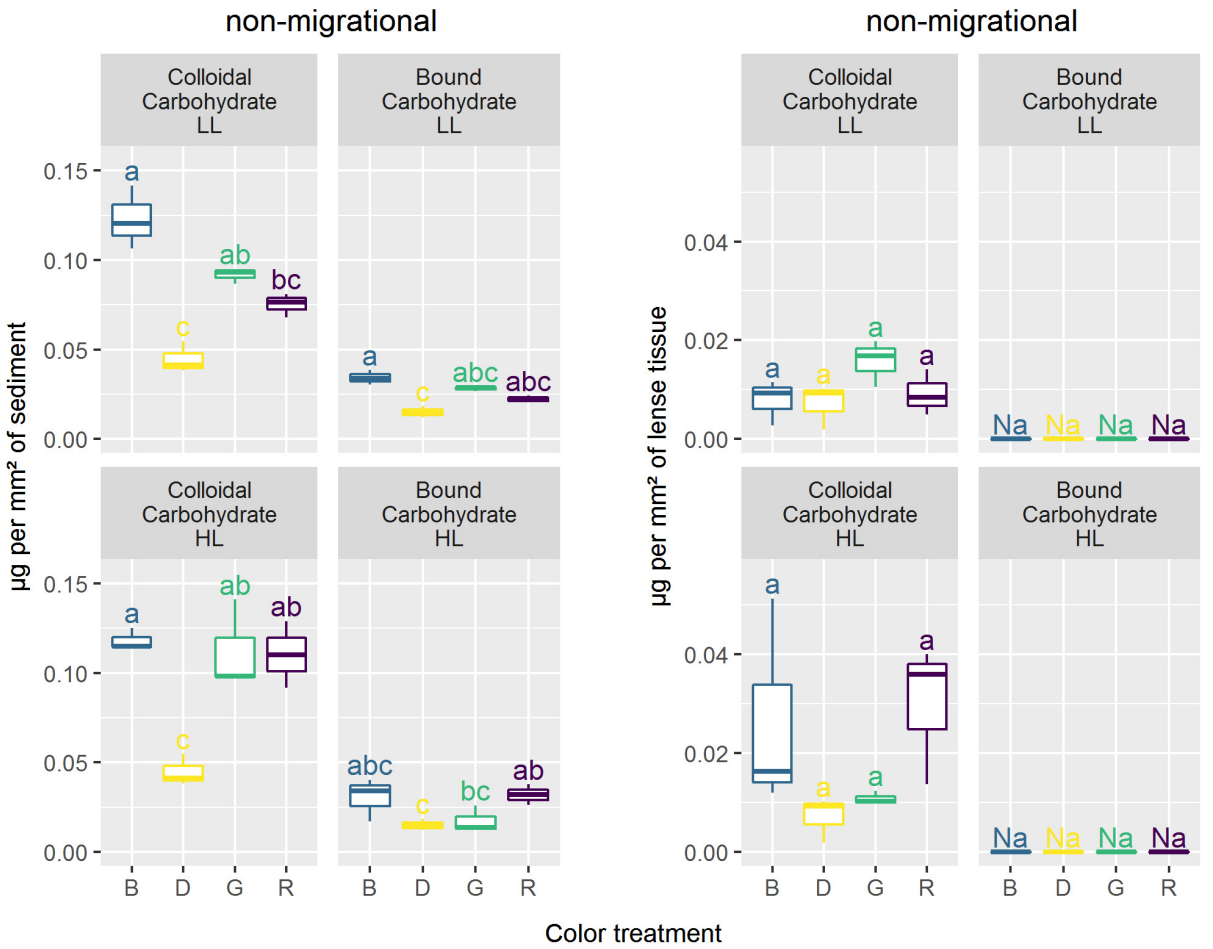

FIGURE 9 | Carbohydrates concentration ($\mu g.mm^{-2}$) in coloidal and bound fraction for the different lights. Similar letters correspond to treatments not significantly different from Tukey multiple comparisons between colors and intensity within each carbohydrate fraction with an alpha of 0.05.

responses (Depauw et al., 2012 and reference therein). The blue photoreceptor Aureochrome 1a was found to repress HL acclimation of *Phaeodactylum tricornutum* in both blue and red light implying a mediated pathway between these lights and aureochrome (Schellenberger Costa et al., 2013b). Similarly, but without correcting for wavelength specific absorption, Brunet et al. (2014) found that *Pseudo-nitzschia multistriata* could not induce HL acclimation with monochromatic wavelengths and required both blue and red light sensing to regulate DES and NPQ production. All aforementioned studies used monospecific culture grown under very different light regime favoring long term acclimation. To our knowledge the effect of light quality on physiological photoprotection has not been investigated on scales of minutes to hours making comparison between studies extremely challenging. Besides, specific absorption and Qphar measurements are highly variable, species specific and susceptible to changes due to DES variation (Fujiki and Taguchi, 2001), cell volume (Fujiki and Taguchi, 2001), "pigment package" effect (Bidigare et al., 1990) and *in vivo* bathochromic shifts (Bidigare et al., 1990). Ideally Qphar should be monitored continuously but is not the only chromatic effect of light and may sometime prove to be unadapted to quantitatively measure light. For instance, frustule nanostructure may change upon exposure to different monochromatic wavelengths (Su et al., 2015) consequently modifying photonic properties either in increasing blue light absorption by the frustule (Yamanaka et al., 2008) or in increasing blue light scalar irradiance thus enhancing the effective intensity of blue light (Goessling et al., 2018). Such effect would not be integrated in Qphar calculation. Consequently, it is uncertain whether different physiological responses at different color wavelengths were only a reflection of different Qphar values or if other chromatics differences would exist.

Biofilm Movement

Light quality effects on migration were strongly dependent on light intensity, with certain wavelengths inducing variable migration responses. Namely, blue and red colors induced intense upward migration movements in LL and HL, respectively. A stronger migration response and diatom accumulation in blue light has been supported by Nultsch (1971) early work on *Nitzschia communis* as well as McLachlan et al. (2009) on *Navicula perminuta* where wavelengths up to 540 µm induced

positive phototropism while red wavelengths did not. Similarly, Wenderoth and Rhiel (2004) observed cell accumulations 1.8 times higher in blue compared to white light (low fluence rate 5 μmol.photons.m^{-2}.s^{-1}). The cited studies were done at low light levels and are consistent with the absorptivity increases we observed in blue LL in comparison to green, red and dark (**Figure 4**), supporting the hypothesis that at low fluence rates blue wavelengths are more efficient at stimulating diatom movements. In diatoms, several light sensors have been evidenced and hypothesized to be involved in the light quality responsive changes in motility (McLachlan et al., 2009; Cohn et al., 2015). Changes in light intensities have been shown to be most sensitive in modulating the whole cell movement near the distal ends of the raphes (Cohn et al., 1999, 2015) and a putative photo-detection system could involve an aureochrome. However, biochemical and functional characterization of these photoreceptors and their chromophores is still very limited (Depauw et al., 2012; Wilhelm et al., 2014). The existence of different species specific motile responses to light quality (Cohn et al., 2015) as well as the lack of current identified receptors at the tips of the cells hinder further conclusions on the role of these photoreceptors. The high correlation, observed in LL, between absorptivity and Qphar (r = 0.74, $p < 0.001$) suggests that the different migrational responses were a response to the amount of Qphar rather than selective effect of different wavelength and their specific interaction with photoreceptors. Changes observed in absorptivity (**Figure 4**) were paralleled by mean total pigment content (**Figure 7**) for different intensity and treatments. Although this correlation (r = 0.75) was not statistically significant (p = 0.09) it could indicate that the absorptivity parameter, which was measured at the sediment surface, was linked to the biomass (pigments) measured in the 2 mm deep contact core. This strong correlation could imply that cells would have migrated deeper than 2 mm in the lower absorptivity samples. Diatom speeds have not been often measured in natural sediments but the few available datasets supports the possibility that diatoms could have migrated more than 2 mm during the course of the experiment (4.5 h). Namely, using values presented by Hay et al. (1993) the biofilm would have been able to move at least 2.7 mm in the 4.5 h. The downward migration in blue HL could be related to a light-stress response due to higher Qphar values resulting in less accumulation of cells at the sediment surface. This light stress would be accompanied by an increase in NPQ build-up, which would induce a photoprotective downward response or a reduced upward migration in blue light from the start of the experiment. This would be consistent with previous observations that have described light thresholds between 500 and 1000 μmol.photons.m^{-2}.s^{-1} for inducing an avoidance response for both blue (450 nm) and green (550 nm) lights (Cohn, 2001). Furthermore, there is a general consensus that diatom photoaccumulation and photodispersal are intensity dependent whereby low to moderate white light stimulate upward migration and high light promotes downward migration (Serôdio et al., 2008; Du et al., 2010, 2018; Perkins et al., 2010; Coelho et al., 2011; Laviale et al., 2016). The absorptivity changes followed a typical biphasic dose response to Qphar shifting from a positive phototaxis at a theoric maximum between 200 and 250 μmol.photons.m^{-2}.s^{-1} to a negative or downregulated positive phototaxis. Our hypothesis is that above 250 μmol.photons.m^{-2}.s^{-1} of Qphar the onset and amount of NPQ – proportional to Qphar – (**Figure 3**) downregulated behavioral positive phototaxis. However, the light intensity thresholds and the spectral limits described in previous works are very variable and it is possible that the recorded differences are partially the result of the complexity of measuring light environments inside the sediment. Many factors will affect the light received by a diatom incorporated in microphytobenthic biofilms, e.g., organic matter, type of sediment particles, biofilm density, species composition, water content, etc. All these factors will produce different absorption and scattering effects that will affect the intensity and light spectral quality (e.g., Kühl et al., 1994). Nonetheless, regardless of light color, absorptivity increased significantly with time in both LL and HL treatments in comparison to dark controls, which suggests that light intensities were never high enough to completely inhibit upward migration in our conditions. Benthic diatoms are capable of positioning themselves in a light gradient at sediment depths where light exposure is optimal. This optimal depth may vary with photoacclimation status and light intensity tolerance tresholds that induce photoinhibition (Ezequiel et al., 2015) and our data supports the hypothesis that diatom optimal depth will vary as an interaction between light intensity and light quality to adjust to the optimal Qphar light.

Behavioral and Physiological Interplay

The LL migrational biofilms showed a similar trend of increasing ϕII_1 as the LL non-migrational biofilms albeit with less intensity (**Figure 5**). The smaller ϕII_1 increase in migrational biofilms is likely due to an already higher absolute ϕII_1 value at the onset of the experiment. $\phi II_1$and α-slope in LL migrational biofilms increased significantly more under red light, perhaps as a positive tradeoff for having produced little CC (**Figure 9**) and migrated less than other colors (**Figure 4**). In LL intensities there was significant carbohydrate production in blue and green light which was not seen in the non-migrational biofilm. Colloidal carbohydrate concentration (**Figure 9**), mean total pigment (**Figure 7**) and absorptivity (**Figure 4**) followed the same pattern, being highest in blue and lowest in red. These similar patterns could be the result of polysaccharide secretion produced by diatoms during their vertical movements (Pniewski et al., 2015). At these non-stressful LL intensities photo-regulation was mainly dominated by behavioral positive phototaxi to increase light exposure as a response to increasing Qphar values. Exposing migrational biofilms to HL induced a decrease in α-slope and ϕII, which implied physiological photoprotection due to stress exerted by the light intensities. Analysis of the relative pigment percentage showed significant differences (**Figure 8**). HL samples were characterized by a significant higher Diat relative concentration and a lower relative concentration of Diad which is consistent with the xanthophyll cycle operation (Olaizola and Yamamoto, 1994; Lavaud et al., 2004). Colorwise there were no significant DES differences between color treatments (**Table 3**) despite very different Qphar amount. Similarly, at

HL in migrational biofilms, despite a differential migration between colors there were no significant differences in either α-slope (**Figure 3**) or EPS secretion for different colors. This implies that, even if blue light has the potential to induce an higher NPQ and DES (see physiological photoprotection discussion), diatoms can migrate to different sediment depths. Diatoms seemed to position themselves at an optimal depth as a response to the interaction between light intensity and spectral composition. At these depths they might maximize their CC production for both behavioral and physiological photoprotection, thus showing no obvious differences in CC concentration between the different colors (**Figure 9**). These result contrasts with previous observations (Perkins et al., 2001) that did not find significant colloidal carbohydrates accumulation differences at the end of the migration between shaded and unshaded biofilms. It is noteworthy to stress that samples from natural sediments will contain EPS from a range of sources (bacteria, detritus, and dissolved organic matter) (Smith and Underwood, 1998) and while our extraction technique has been proposed as a standardized method for microphytobenthos (Takahashi et al., 2009) other extraction techniques may have had different EPS fractions making comparison with previous studies difficult (Underwood et al., 1995, 2004; Smith and Underwood, 2000; De Brouwer and Stal, 2002). It is possible that blue and red photoreceptors are involved in tailoring the specific behavioral photoprotective responses. In natural conditions blue/red ratio is a very informative cue for diatoms, changing during tides, twilight and with depth (Ragni and D'Alcalà, 2004; Spitschan et al., 2016). However the exact pathway and signal cascading remain to be elucidated. We hypothesize that the trigger for the vertical migration movements and behavioral photoprotection is linked to an NPQ mechanism or some other light-stress induced mechanism, e.g., ROS production. This would be in agreement with other observations of diatoms using motility to select their optimal light exposure based on their photophysiological status (Ezequiel et al., 2015; Cartaxana et al., 2016) emphasizing the behavioral role of migration in regulating photosynthesis. Nevertheless, while migration compensated the different NPQ and DES levels observed in non-migrational biofilm between the different color treatments we still observed higher *rETRm* values in blue light migrational biofilms (**Table 2**). These differences show that despite an active behavioral photoprotection mechanism, light specific wavelengths affected photosynthesis differently. Further investigation on the role of photoreceptors, wavelength specific chloroplast aggregation (Furukawa et al., 1998; Noyes et al., 2008) or frustule waveguiding properties (Shihira-Ishikawa et al., 2007) could shed some light on the underlying mechanisms between these two types of photoprotection.

CONCLUSION

Overall there was a strong interaction between light intensity and spectral quality in inducing diatoms migration and behavioral photoprotection. The difficult task of disentangling the respective role of light inherent properties showcased how relevant considering both light quality and intensity helped understanding the underlying mechanisms of biofilm photoprotection. While not accounting for all chromatic effects of light, the use of Qphar proved to finely integrate and correctly correlate to the light quality and intensity interactions. The higher impact of blue light in stimulating ETR and NPQ development in comparison to red remains to be elucidated but was largely dependent on how much light was being absorbed. These differences are largely reduced in the sediment biofilms due to finely tuned vertical migration movements, supporting the hypothesis of epipelic diatom photoprotection being governed by behavioral mechanisms. Furthermore, it strongly suggests a wavelength and Qphar dependent light stress threshold that triggers NPQ development and consequently override or downregulate upward movements. Our data supports the hypothesis that diatoms accumulation and migration can extend deeper than 2 mm. The absence of light cues at these depths and the fast migration in a matter of few hours could have implication for future experimental design of microphytobenthos migrational studies.

DATA AVAILABILITY STATEMENT

All datasets generated for this study are included in the article/supplementary material.

AUTHOR CONTRIBUTIONS

AP, BJ, PD, and CH: conceptualization. AP, CH, and BJ: formal analysis, visualization, and writing – review and editing. AP and BJ: investigation and writing – original draft. BJ and CH: methodology and validation.

FUNDING

This research was supported under the BIO-Tide project, funded through the 2015–2016 BiodivERsA COFUND call for research proposals, with the national funders BelSPO, FWO, ANR, and SNSF.

REFERENCES

Barnett, A., Méléder, V., Blommaert, L., Lepetit, B., Gaudin, P., Vyverman, W., et al. (2015). Growth form defines physiological photoprotective capacity in intertidal benthic diatoms. *ISME J.* 9, 32–45. doi: 10.1038/ismej.2014.105

Bidigare, R. R., Ondrusek, M., Fisheries, S., and Kiefer, D. A. (1990). "In-vivo absorption properties of algal pigments," in *Proceedings of the 1990 Technical Symposium on Optics, Electro-Optics, and Sensors*, Orlando, FL, 290–301. doi: 10.1117/12.21451

Blommaert, L., Lavaud, J., Vyverman, W., and Sabbe, K. (2018). Behavioural versus physiological photoprotection in epipelic and epipsammic benthic diatoms. *Eur. J. Phycol.* 53, 146–155. doi: 10.1080/09670262.2017.1397197

Brunet, C., Chandrasekaran, R., Barra, L., Giovagnetti, V., Corato, F., and Ruban, A. V. (2014). Spectral radiation dependent photoprotective mechanism in the

diatom Pseudo-nitzschia multistriata. *PLoS One* 9:e87015. doi: 10.1371/journal.pone.0087015

Cartaxana, P., Cruz, S., Gameiro, C., and Kühl, M. (2016). Regulation of intertidal microphytobenthos photosynthesis over a diel emersion period is strongly affected by diatom migration patterns. *Front. Microbiol.* 7:872. doi: 10.3389/fmicb.2016.00872

Cartaxana, P., Ruivo, M., Hubas, C., Davidson, I., Serôdio, J., and Jesus, B. (2011). Physiological versus behavioral photoprotection in intertidal epipelic and epipsammic benthic diatom communities. *J. Exp. Mar. Biol. Ecol.* 405, 120–127. doi: 10.1016/j.jembe.2011.05.027

Cartaxana, P., and Serôdio, J. (2008). Inhibiting diatom motility: A new tool for the study of the photophysiology of intertidal microphytobenthic biofilms. *Limnol. Oceanogr. Methods* 6, 466–476. doi: 10.4319/lom.2008.6.466

Chevalier, E., Gévaert, F., and Créach, A. (2010). In situ photosynthetic activity and xanthophylls cycle development of undisturbed microphytobenthos in an intertidal mudflat. *J. Exp. Mar. Biol. Ecol.* 385, 44–49. doi: 10.1016/j.jembe.2010.02.002

Clementson, L. A., and Wojtasiewicz, B. (2019). Dataset on the absorption characteristics of extracted phytoplankton pigments. *Data Brief* 24:103875. doi: 10.1016/j.dib.2019.103875

Coelho, H., Vieira, S., and Serôdio, J. (2011). Endogenous versus environmental control of vertical migration by intertidal benthic microalgae. *Eur. J. Phycol.* 46, 271–281. doi: 10.1080/09670262.2011.598242

Cohn, S. A. (2001). Chapter 13 Photo-stimulated effects on diatom motility. *Compr. Ser. Photosci.* 1, 375–401. doi: 10.1016/S1568-461X(01)80017-X

Cohn, S. A., Halpin, D., Hawley, N., Ismail, A., Kaplan, Z., Kordes, T., et al. (2015). Comparative analysis of light-stimulated motility responses in three diatom species. *Diatom Res.* 30, 213–225. doi: 10.1080/0269249X.2015.1058295

Cohn, S. A., Spurck, T. P., and Pickett-Heaps, J. D. (1999). High energy irradiation at the leading tip of moving diatoms causes a rapid change of cell direction. *Diatom Res.* 14, 193–206. doi: 10.1080/0269249X.1999.9705466

Consalvey, M. (2002). *The Structure and Function of Microphytobenthic Biofilms*. Available online at: https://hdl.handle.net/10023/2682 (accessed February 03, 2020).

Consalvey, M., Jesus, B., Perkins, R. G., Brotas, V., Underwood, G. J., and Paterson, D. M. (2004a). Monitoring migration and measuring biomass in benthic biofilms: the effects of dark/far-red adaptation and vertical migration on fluorescence measurements. *Photosyn. Res.* 81, 91–101. doi: 10.1023/B:PRES.0000028397.86495.b5

Consalvey, M., Paterson, D. M., and Underwood, G. J. C. (2004b). The ups and downs of life in a benthic biofilm: migration of benthic diatoms. *Diatom Res.* 19, 181–202. doi: 10.1080/0269249X.2004.9705870

Cruz, S., and Serôdio, J. (2008). Relationship of rapid light curves of variable fluorescence to photoacclimation and non-photochemical quenching in a benthic diatom. *Aquat. Bot.* 88, 256–264. doi: 10.1016/j.aquabot.2007.11.001

De Brouwer, J. F., and Stal, L. J. (2002). Daily fluctuations of exopolymers in cultures of the benthic diatoms *Cylindrotheca closterium* and *Nitzschia* sp. (Bacillariophyceae). *J. Phycol.* 38, 464–472. doi: 10.1046/j.1529-8817.2002.01164.x

Depauw, F. A., Rogato, A., D'Alcalá, M. R., and Falciatore, A. (2012). Exploring the molecular basis of responses to light in marine diatoms. *J. Exp. Bot.* 63, 1575–1591. doi: 10.1093/jxb/ers005

Dijkman, N. A., and Kroon, B. M. A. (2002). Indications for chlororespiration in relation to light regime in the marine diatom *Thalassiosira weissflogii*. *J. Photochem. Photobiol. B Biol.* 66, 179–187.

Du, G., Yan, H., Liu, C., and Mao, Y. (2018). Behavioral and physiological photoresponses to light intensity by intertidal microphytobenthos. *J. Oceanol. Limnol.* 36, 293–304.

Du, G. Y., Oak, J.-H. H., Li, H., and Chung, I.-K. K. (2010). Effect of light and sediment grain size on the vertical migration of benthic diatoms. *Algae* 25, 133–140. doi: 10.4490/algae.2010.25.3.133

DuBois, M., Gilles, K. A., Hamilton, J. K., Rebers, P. A., and Smith, F. (1956). Colorimetric method for determination of sugars and related substances. *Anal. Chem.* 28, 350–356. doi: 10.1021/ac60111a017

Eaton, J. W., and Moss, B. (1966). The estimation of numbers and pigment content in epipelic algal populations. *Limnol. Oceanogr.* 11, 584–595. doi: 10.4319/lo.1966.11.4.0584

Eilers, P. H. C., and Peeters, J. C. H. (1988). A model for the relationship between light intensity and the rate of photosynthesis in phytoplankton. *Ecol. Model.* 42, 199–215. doi: 10.1111/jpy.12060

Ezequiel, J., Laviale, M., Frankenbach, S., Cartaxana, P., and Serôdio, J. (2015). Photoacclimation state determines the photobehaviour of motile microalgae: the case of a benthic diatom. *J. Exp. Mar. Biol. Ecol.* 468, 11–20. doi: 10.1016/j.jembe.2015.03.004

Frankenbach, S., Pais, C., Martinez, M., Laviale, M., Ezequiel, J., and Serôdio, J. (2014). Evidence for gravitactic behaviour in benthic diatoms. *Eur. J. Phycol.* 49, 429–435. doi: 10.1080/09670262.2014.974218

Frølund, B., Palmgren, R., Keiding, K., and Nielsen, P. H. (1996). Extraction of extracellular polymers from activated sludge using a cation exchange resin. *Water Res.* 30, 1749–1758.

Fujiki, T., and Taguchi, S. (2001). Relationship between light absorption and the xanthophyll-cycle pigments in marine diatoms. *Plankton Biol. Ecol.* 48, 96–103.

Furukawa, T., Watanabe, M., and Shihira-Ishikawa, I. (1998). Green- and blue-light-mediated chloroplast migration in the centric diatom *Pleurosira laevis*. *Protoplasma* 203, 214–220. doi: 10.1007/BF01279479

Gilbert, M., Domin, A., Becker, A., and Wilhelm, C. (2000). Estimation of primary productivity by chlorophyll a *in vivo* fluorescence in freshwater phytoplankton. *Photosynthetica* 38, 111–126. doi: 10.1023/A:1026708327185

Goessling, J. W., Frankenbach, S., Ribeiro, L., Serôdio, J., and Kühl, M. (2018). Modulation of the light field related to valve optical properties of raphid diatoms: implications for niche differentiation in the microphytobenthos. *Mar. Ecol. Prog. Ser.* 588, 29–42. doi: 10.3354/meps12456

Häder, D.-P. (1986). Signal perception and amplification in photomovement of prokaryotes. *Biochim. Biophys. Acta* 864, 107–122.

Hay, S. I., Maitland, T. C., and Paterson, D. M. (1993). The speed of diatom migration through natural and artificial substrata. *Diatom Res.* 8, 371–384. doi: 10.1080/0269249x.1993.9705268

Haynes, K., Hofmann, T. A., Smith, C. J., Ball, A. S., Underwood, G. J. C., and Osborn, A. M. (2007). Diatom-derived carbohydrates as factors affecting bacterial community composition in estuarine sediments. *Appl. Environ. Microbiol.* 73, 6112–6124.

Hernández Fariñas, T., Ribeiro, L., Soudant, D., Belin, C., Bacher, C., Lampert, L., et al. (2017). Contribution of benthic microalgae to the temporal variation in phytoplankton assemblages in a macrotidal system. *J. Phycol.* 53, 1020–1034. doi: 10.1111/jpy.12564

Heukelem, L. V., and Thomas, C. S. (2001). Computer-assisted high-performance liquid chromatography method development with applications to the isolation and analysis of phytoplankton pigments. *J. Chromatogr. A* 910, 31–49.

Hillebrand, H., Dürselen, C.-D., Kirschtel, D., Pollingher, U., and Zohary, T. (1999). Biovolume calculation for pelagic and benthic microalgae. *J. Phycol.* 35, 403–424. doi: 10.1046/j.1529-8817.1999.3520403.x

Jakob, T., Goss, R., and Wilhelm, C. (1999). Activation of diadinoxanthin de-epoxidase due to a chlororespiratory proton gradient in the dark in the diatom *Phaeodactylum tricornutum*. *Plant Biol.* 1, 76–82. doi: 10.1111/j.1438-8677.1999.tb00711.x

Jauffrais, T., Drouet, S., Turpin, V., Méléder, V., Jesus, B., Cognie, B., et al. (2015). Growth and biochemical composition of a microphytobenthic diatom (*Entomoneis paludosa*) exposed to shorebird (*Calidris alpina*) droppings. *J. Exp. Mar. Biol. Ecol.* 469, 83–92. doi: 10.1016/j.jembe.2015.04.014

Jesus, B., Brotas, V., Ribeiro, L., Mendes, C. R., Cartaxana, P., and Paterson, D. M. (2009). Adaptations of microphytobenthos assemblages to sediment type and tidal position. *Cont. Shelf Res.* 29, 1624–1634. doi: 10.1016/j.csr.2009.05.006

Jesus, B., Perkins, R. G., Consalvey, M., Brotas, V., and Paterson, D. M. (2006). Effects of vertical migrations by benthic microalgae on fluorescence measurements of photophysiology. *Mar. Ecol. Prog. Ser.* 315, 55–66. doi: 10.3354/meps315055

Jungandreas, A., Costa, B. S., Jakob, T., Von Bergen, M., Baumann, S., and Wilhelm, C. (2014). The acclimation of *Phaeodactylum tricornutum* to blue and red light does not influence the photosynthetic light reaction but strongly disturbs the carbon allocation pattern. *PLoS One* 9:e99727. doi: 10.1371/journal.pone.0099727

Kühl, M., Lassen, C., and Jorgensen, B. B. (1994). Light penetration and light intensity in sandy marine sediments measured with irradiance and scalar irradiance fiber-optic microprobes. *Mar. Ecol. Prog. Ser.* 105, 139–148. doi: 10.3354/meps105139

Kume, A. (2018). Importance of the green color, absorption gradient, and spectral absorption of chloroplasts for the radiative energy balance of leaves. *J. Plant Res.* 130, 501–514. doi: 10.1007/s10265-017-0910-z

Lavaud, J., and Goss, R. (2014). "The peculiar features of non-photochemical fluorescence quenching in diatoms and brown algae," in *Non-Photochemical Quenching and Energy Dissipation in Plants, Algae and Cyanobacteria*, eds B. Demmig-Adams, G. Garab, W. Adams III, and Govindjee (Dordrecht: Springer), 421–443. doi: 10.1007/978-94-017-9032-1_20

Lavaud, J., Rousseau, B., and Etienne, A. L. (2004). General features of photoprotection by energy dissipation in planktonic diatoms (Bacillariophyceae). *J. Phycol.* 40, 130–137. doi: 10.1046/j.1529-8817.2004.03026.x

Laviale, M., Barnett, A., Ezequiel, J., Lepetit, B., Frankenbach, S., Méléder, V., et al. (2015). Response of intertidal benthic microalgal biofilms to a coupled light-temperature stress: evidence for latitudinal adaptation along the Atlantic coast of Southern Europe. *Environ. Microbiol.* 17, 3662–3677. doi: 10.1111/1462-2920.12728

Laviale, M., Frankenbach, S., and Serôdio, J. (2016). The importance of being fast: comparative kinetics of vertical migration and non-photochemical quenching of benthic diatoms under light stress. *Mar. Biol.* 163:10.

MacIntyre, H. L., Geider, R. J., and Miller, D. C. (1996). Microphytobenthos: the ecological role of the "Secret Garden" of unvegetated, shallow-water marine habitats. I. Distribution, abundance and primary production. *Estuaries* 19, 186–201. doi: 10.2307/1352224

McLachlan, D. H., Brownlee, C., Taylor, A. R., Geider, R. J., and Underwood, G. J. C. (2009). Light-induced motile responses of the estuarine benthic diatoms Navicula perminuta and *Cylindrotheca closterium* (bacillariophyceae). *J. Phycol.* 45, 592–599. doi: 10.1111/j.1529-8817.2009.00681.x

Méléder, V., Rincé, Y., Barillé, L., Gaudin, P., and Rosa, P. (2007). Spatiotemporal changes in microphytobenthos assemblages in a macrotidal flat (Bourgneuf Bay, France). *J. Phycol.* 43, 1177–1190. doi: 10.1111/j.1529-8817.2007.00423.x

Mertens, A., Witkowski, A., Lange-Bertalot, H., Ribeiro, L., and Rhiel, E. (2014). *Navicula meulemansii* sp. nov., (Bacillariophyaceae) from brackish waters in Europe and the U.S.A. Nova Hedwigia 98, 201–212. doi: 10.1127/0029-5035/2013/0152

Mitbavkar, S., and Anil, A. C. (2004). Vertical migratory rhythms of benthic diatoms in a tropical intertidal sand flat: Influence of irradiance and tides. *Mar. Biol.* 145, 9–20.

Mouget, J. L., Rosa, P., and Tremblin, G. (2004). Acclimation of Haslea ostrearia to light of different spectral qualities - Confirmation of 'chromatic adaptation' in diatoms. *J. Photochem. Photobiol. B Biol.* 75, 1–11. doi: 10.1016/j.jphotobiol.2004.04.002

Noyes, J., Sumper, M., and Vukusic, P. (2008). Light manipulation in a marine diatom. *J. Mater. Res.* 23, 3229–3235. doi: 10.1557/jmr.2008.0381

Nultsch, W. (1971). Phototactic and photokinetic action spectra of the diatom Nitschia communis. *Photochem. Photobiol.* 14, 705–712. doi: 10.1111/j.1751-1097.1971.tb06209.x

Olaizola, M., and Yamamoto, H. Y. (1994). Short-term response of the diadinoxanthin cycle and fluorescence yield to high irradiance in Chaetoceros muelleri (Bacillariophyceae). *J. Phycol.* 30, 606–612. doi: 10.1111/j.0022-3646.1994.00606.x

Olenina, I., Hajdu, S., Edler, L., Andersson, A., Wasmund, N., Busch, S., et al. (2006). *Biovolumes and size-classes of phytoplankton in the Baltic Sea HELCOM Balt.Sea Environ. Proc. No. 106*. Available online at: http://helcom.fi/Lists/Publications/BSEP106.pdf (accessed February 03, 2020).

Orvain, F., Galois, R., Barnard, C., Sylvestre, A., Blanchard, G., and Sauriau, P. G. (2003). Carbohydrate production in relation to microphytobenthic biofilm development: an integrated approach in a tidal mesocosm. *Microb. Ecol.* 45, 237–251.

Paterson, D. (1989). Short-term changes in the erodibility of intertidal cohesive sediments related to the migratory behaviour of epipelic diatoms. *Limnol. Oceanogr.* 34, 223–234. doi: 10.4319/lo.1989.34.1.0223

Paterson, D. M. (1986). The migratory behaviour of diatom assemblages in a laboratory tidal scanning electron microscopy micro-ecosystem examined by low temperature. *Diatom Res.* 1, 227–239. doi: 10.1080/0269249X.1986.9704971

Paterson, D. M., Perkins, R., Consalvey, M., and Underwood, G. J. C. (2003). "Ecosystem function, cell micro-cycling and the structure of transient biofilms," in *Fossil and Recent Biofilms*, eds W. E. Krumbein, D. M. Paterson, and G. A. Zavarzin (Dordrecht: Springer), 47–63. doi: 10.1007/978-94-017-0193-8_3

Paulmier, G. (1997). *Atlas des Diatomophycées des Côtes Françaises et des Aires Marines Adjacentes*. Available online at: https://archimer.ifremer.fr/doc/00000/2452/ (accessed February 03, 2020).

Perkins, R., Underwood, G., Brotas, V., Snow, G., Jesus, B., and Ribeiro, L. (2001). Responses of microphytobenthos to light: primary production and carbohydrate allocation over an emersion period. *Mar. Ecol. Prog. Ser.* 223, 101–112. doi: 10.3354/meps223101

Perkins, R. G., Lavaud, J., Serôdio, J., Mouget, J. L., Cartaxana, P., Rosa, P., et al. (2010). Vertical cell movement is a primary response of intertidal benthic biofilms to increasing light dose. *Mar. Ecol. Prog. Ser.* 416, 93–103. doi: 10.3354/meps08787

Pniewski, F. F., Biskup, P., Bubak, I., Richard, P., Latała, A., and Blanchard, G. (2015). Photo-regulation in microphytobenthos from intertidal mudflats and non-tidal coastal shallows. *Estuar. Coast. Shelf Sci.* 152, 153–161. doi: 10.1016/j.ecss.2014.11.022

R Core Team (2017). *R: A Language and Environment for Statistical Computing*. Vienna: R Foundation for Statistical Computing.

Ragni, M., and D'Alcalà, M. R. (2004). Light as an information carrier underwater. *J. Plankton Res.* 26, 433–443. doi: 10.1093/plankt/fbh044

Ribeiro, L. L. (2010). *Intertidal Benthic Diatoms of the Tagus Estuary: Taxonomic Composition and Spatial-Temporal Variation*. Ph.D. dissertation, University of Lisbon, Lisbon.

Round, F. E. (1965). The epipsammon; a relatively unknown freshwater algal association. *Br. Phycol. Bull.* 2, 456–462. doi: 10.1080/00071616500650071

Round, F. E., and Happey, C. M. (1965). Persistent, vertical-migration rhythms in benthic microflora: Part IV a diurnal rhythm of the epipelic diatom association in non-tidal flowing water. *Br. Phycol. Bull.* 2, 463–471. doi: 10.1080/00071616500650081

Schellenberger Costa, B., Jungandreas, A., Jakob, T., Weisheit, W., Mittag, M., and Wilhelm, C. (2013a). Blue light is essential for high light acclimation and photoprotection in the diatom *Phaeodactylum tricornutum*. *J. Exp. Bot.* 64, 483–493. doi: 10.1093/jxb/ers340

Schellenberger Costa, B., Sachse, M., Jungandreas, A., Bartulos, C. R., Gruber, A., Jakob, T., et al. (2013b). Aureochrome 1a is involved in the photoacclimation of the diatom *Phaeodactylum tricornutum*. *PLoS One* 8:e74451 doi: 10.1371/journal.pone.0074451

Schreiber, U., Klughammer, C., and Kolbowski, J. (2012). Assessment of wavelength-dependent parameters of photosynthetic electron transport with a new type of multi-color PAM chlorophyll fluorometer. *Photosyn. Res.* 113, 127–144.

Serôdio, J., Cruz, S., Vieira, S., and Brotas, V. (2005). Non-photochemical quenching of chlorophyll fluorescence and operation of the xanthophyll cycle in estuarine microphytobenthos. *J. Exp. Mar. Biol. Ecol.* 326, 157–169. doi: 10.1016/j.jembe.2005.05.011

Serôdio, J., Da Silva, J. M., and Catarino, F. (1997). Nondestructive tracing of migratory rhythms of intertidal benthic microalgae using in vivo chlorophyll a fluorescence. *J. Phycol.* 33, 542–553. doi: 10.1111/j.0022-3646.1997.00542.x

Serôdio, J., Ezequiel, J., Barnett, A., Mouget, J. L., Meåéder, V., Laviale, M., et al. (2012). Efficiency of photoprotection in microphytobenthos: role of vertical migration and the xanthophyll cycle against photoinhibition. *Aquat. Microb. Ecol.* 67, 161–175. doi: 10.3354/ame01591

Serôdio, J., Vieira, S., and Cruz, S. (2008). Photosynthetic activity, photoprotection and photoinhibition in intertidal microphytobenthos as studied in situ using variable chlorophyll fluorescence. *Cont. Shelf Res.* 28, 1363–1375. doi: 10.1016/j.csr.2008.03.019

Shihira-Ishikawa, I., Nakamura, T., Higashi, S. I., and Watanabe, M. (2007). Distinct responses of chloroplasts to blue and green laser microbeam irradiations in the centric diatom *Pleurosira laevis*. *Photochem. Photobiol.* 83, 1101–1109. doi: 10.1111/j.1751-1097.2007.00167.x

Silsbe, G. M., and Kromkamp, J. C. (2012). Modeling the irradiance dependency of the quantum efficiency of photosynthesis. *Limnol. Oceanogr. Methods* 10, 645–652. doi: 10.4319/lom.2012.10.645

Smith, D. J., and Underwood, G. J. (2000). The production of extracellular carbohydrates by estuarine benthic diatoms: the effects of growth phase and

light and dark treatment. *J. Phycol.* 36, 321–333. doi: 10.1046/j.1529-8817.2000.99148.x

Smith, D. J., and Underwood, G. J. C. (1998). Exopolymer production by intertidal epipelic diatoms. *Limnol. Oceanogr.* 43, 1578–1591. doi: 10.4319/lo.1998.43.7.1578

Spitschan, M., Aguirre, G. K., Brainard, D. H., and Sweeney, A. M. (2016). Variation of outdoor illumination as a function of solar elevation and light pollution. *Sci. Rep.* 6:26756. doi: 10.1038/srep26756

Staats, N., Stal, L. J., and Mur, L. R. (2000). Exopolysaccharide production by the epipelic diatom *Cylindrotheca closterium*: effects of nutrient conditions. *J. Exp. Mar. Biol. Ecol.* 249, 13–27.

Su, Y., Lundholm, N., Friis, S. M., and Ellegaard, M. (2015). Implications for photonic applications of diatom growth and frustule nanostructure changes in response to different light wavelengths. *Nano Res.* 8, 2363–2372.

Takahashi, E., Ledauphin, J., Goux, D., and Orvain, F. (2009). Optimising extraction of extracellular polymeric substances (EPS) from benthic diatoms: comparison of the efficiency of six EPS extraction methods. *Mar. Freshw. Res.* 60, 1201–1210. doi: 10.1071/MF08258

Taylor, J. D., McKew, B. A., Kuhl, A., McGenity, T. J., and Underwood, G. J. C. (2013). Microphytobenthic extracellular polymeric substances (EPS) in intertidal sediments fuel both generalist specialist EPS-degrading bacteria. *Limnol. Oceanogr.* 58, 1463–1480. doi: 10.4319/lo.2013.58.4.1463

Ting, C. S., and Owens, T. G. (1993). Photochemical and nonphotochemical fluorescence quenching processes in the diatom *Phaeodactylum tricornutum*. *Plant Physiol.* 101, 1323–1330.

Underwood, G. J., Boulcott, M., Raines, C. A., and Waldron, K. (2004). Environmental effects on exopolymer production by marine benthic diatoms: dynamics, changes in composition, and pathways of production. *J. Phycol.* 40, 293–304. doi: 10.1111/j.1529-8817.2004.03076.x

Underwood, G. J., and Kromkamp, J. (1999). Primary production by phytoplankton and microphytobenthos in estuaries. *Adv. Ecol. Res.* 29, 93–153.

Underwood, G. J. C., Paterson, D. M., and Parkes, R. J. (1995). The measurement of microbial carbohydrate exopolymers from intertidal sediments. *Limnol. Oceanogr.* 40, 1243–1253. doi: 10.4319/lo.1995.40.7.1243

Underwood, G. J. C., Perkins, R. G., Consalvey, M. C., Hanlon, A. R. M., Oxborough, K., Baker, N. R., et al. (2005). Patterns in microphytobenthic primary productivity : species-specific variation in migratory rhythms and photosynthetic efficiency in mixed-species biofilms. *Limnol. Oceanogr.* 50, 755–767. doi: 10.4319/lo.2005.50.3.0755

Walpersdorf, E., Kühl, M., Elberling, B., Andersen, T., Hansen, B., Pejrup, M., et al. (2017). In situ oxygen dynamics and carbon turnover in an intertidal sediment (Skallingen, Denmark). *Mar. Ecol. Prog. Ser.* 566, 49–65. doi: 10.3354/meps12016

Wenderoth, K., and Rhiel, E. (2004). Influence of light quality and gassing on the vertical migration of diatoms inhabiting the Wadden Sea. *Helgoland Mar. Res.* 58, 211–215.

Wilhelm, C., Jungandreas, A., Jakob, T., and Goss, R. (2014). Light acclimation in diatoms: from phenomenology to mechanisms. *Mar. Genomics* 16, 5–15. doi: 10.1016/j.margen.2013.12.003

Yallop, M. L., Winder, B. de, Paterson, D. M., and Stal, L. J. (1994). Comparative structure, primary production and biogenic stabilization of cohesive and non-cohesive marine sediments inhabited by microphytobenthos. *Estuar. Coast. Shelf Sci.* 39, 565–582.

Yamanaka, S., Yano, R., Usami, H., Hayashida, N., Ohguchi, M., Takeda, H., et al. (2008). Optical properties of diatom silica frustule with special reference to blue light. *J. Appl. Phys.* 103:074701. doi: 10.1063/1.2903342

Conflict of Interest: The authors declare that the research was conducted in the absence of any commercial or financial relationships that could be construed as a potential conflict of interest.

frontiers in Marine Science

ORIGINAL RESEARCH
published: 25 May 2020
doi: 10.3389/fmars.2020.00359

Vertical Migration Optimizes Photosynthetic Efficiency of Motile Cyanobacteria in a Coastal Microbial Mat

*Mads Lichtenberg†, Paulo Cartaxana† and Michael Kühl**

Marine Biological Section, Department of Biology, University of Copenhagen, Copenhagen, Denmark

Microbial mats are diverse and stratified microbial biofilm communities characterized by steep gradients in light, temperature and chemical parameters. Their high optical density creates a competition for light among phototrophic microalgae and bacteria residing in the uppermost mat layers. Strategies to counter such resource limitation include metabolic investment in protective and light-harvesting pigments enabling exploitation of separate niches in terms of irradiance and spectral composition, or investment in motility to enable migration to an optimal light microenvironment. We used microsensor measurements of light, temperature and gross photosynthesis in coastal microbial mats dominated by motile cyanobacteria and colorless sulfur bacteria to study how migration affected their radiative energy-budgets and relative photosynthetic efficiency. The optical density of the microbial mat was extremely high, and >99% of incident irradiance of visible light (400–700 nm) was attenuated <0.4 mm below the surface. While energy conservation efficiency did not change dramatically with previous light acclimation, vertical profiles of photosynthetic efficiency showed a shift in the position of maximum efficiency of ∼0.2 mm, depending on light treatment. Besides avoidance of unfavorable chemical conditions such as high sulfide levels, vertical migration over short distances thus enable cyanobacteria to track zones with optimal light exposure thereby efficiently counteracting detrimental effects of excessive light at the surface and insufficient light deeper in the mat.

Keywords: biofilm, light, microenvironment, microsensors, photosynthesis, cyanobacteria

OPEN ACCESS

Edited by:
Vona Meleder, Université de Nantes, France

Reviewed by:
Bo Barker Jørgensen, Aarhus University, Denmark
Dirk de Beer, Max-Planck-Gesellschaft (MPG), Germany

****Correspondence:***
Michael Kühl
mkuhl@bio.ku.dk

†Present address:
Mads Lichtenberg, Costerton Biofilm Center, University of Copenhagen, Copenhagen, Denmark
Paulo Cartaxana, Departamento de Biologia & CESAM & ECOMARE, Universidade de Aveiro, Aveiro, Portugal

Specialty section:
This article was submitted to Marine Ecosystem Ecology, a section of the journal Frontiers in Marine Science

Received: *24 September 2019*
Accepted: *27 April 2020*
Published: *25 May 2020*

Citation:
Lichtenberg M, Cartaxana P and Kühl M (2020) Vertical Migration Optimizes Photosynthetic Efficiency of Motile Cyanobacteria in a Coastal Microbial Mat. Front. Mar. Sci. 7:359. doi: 10.3389/fmars.2020.00359

INTRODUCTION

Light-exposed coastal sediments in shallow waters and intertidal areas are often colonized by benthic microalgae and cyanobacteria, which under the absence of animal grazing (typically under environmental extremes such as desiccation, high salinity or sulfide levels) can form complex stratified microbial biofilm communities, i.e., microbial mats (Stal, 1995), that stabilize the sediment by excretion of exopolymers. Microbial mats are densely populated and highly compacted, vertically stratified microbial communities characterized by steep gradients of physical (light and temperature) and chemical parameters (Kühl et al., 1996; Dillon et al., 2009; Al-Najjar et al., 2012; De Beer and Stoodley, 2013). The uppermost layers of coastal microbial mat layers are typically dominated by diatoms on top of a dense green cyanobacterial layer that is often dominated

by *Microcoleus chtonoplastes* and various other motile, filamentous cyanobacteria (Wieland et al., 2003; Fourcans et al., 2004; Dillon et al., 2009). Often, purple sulfur bacteria and green filamentous anoxygenic phototrophs are found below the cyanobacteria followed by a reduced black layer of precipitated iron sulfide (Jørgensen, 1982). Besides light-driven sulfide oxidation by anoxygenic phototrophs, sulfide can also be oxidized efficiently by colorless sulfur bacteria such as filamentous *Beggiatoa* spp. (Nelson and Castenholz, 1981) that are motile and produce white patches in the microbial mat at the oxygen-sulfide interface (Jørgensen and Revsbech, 1983).

Light is the primary energy source for photosynthetic microbial mats. Due to the high density of photopigments, organic matter, and sediment particles, light is subject to intense scattering and absorption within microbial mats (Kühl and Jørgensen, 1994; Kühl et al., 1994). This can lead to an extremely narrow photic zone (Kühl et al., 1997) and a rapid change in spectral composition with depth (Lassen et al., 1992; Cartaxana et al., 2016b). Ploug et al. (1993) related changes in light quality in a coastal microbial mat to the vertical zonation of a population of diatoms over a dense filamentous cyanobacteria layer that largely sustained their oxygenic photosynthesis via phycobiliproteins with absorption characteristics complementary to chlorophylls. Similarly, complementary use of visible and near-infrared radiation by chlorophylls/phycobilins vs. bacteriochlorophylls enables coexistence of dense populations of oxygenic phototrophs on top of anoxygenic phototrophs (Kühl and Fenchel, 2000). Apart from light, other parameters such as nutrient availability or the presence of sulfide may vertically limit photosynthesis in microbial mats (Stal, 1995; Kühl et al., 1996; Wieland et al., 2003).

The ecological success of benthic microbes in optically dense and vertically stratified communities has recurrently been linked to cell motility allowing individual microbes to search for optimal environmental conditions regarding crucial parameters such as light, temperature, O_2 or nutrient availability (Whale and Walsby, 1984; Bebout and Garcia-Pichel, 1995; Bhaya, 2004; Serôdio et al., 2006). Complex migratory rhythms determined by day/night cycles, tidal regimes, UV exposure and changes in irradiance levels have been described for both diatom- and cyanobacteria-dominated phototrophic mat communities (Bebout and Garcia-Pichel, 1995; Serôdio et al., 2006; Coelho et al., 2011). Similar strategies to optimize photon capture are known in terrestrial plants, where the position of chloroplast in palisade and mesophyll layers in leaves can change depending on light levels and light field directionality, i.e., diffuse versus collimated light (Vogelmann, 1993; Gorton et al., 1999; Wada et al., 2003). Raphidic diatoms, filamentous cyanobacteria and *Beggiatoa* spp. are able to glide within an extracellular polymeric matrix at speeds of 0–10 $\mu m\ s^{-1}$ (Glagoleva et al., 1980; Richardson and Castenholz, 1987; Hoiczyk, 2000; Gupta and Agrawal, 2007; Kamp et al., 2008; Tamulonis et al., 2011). Because of the steep light gradient, migration and the resultant vertical redistribution of the productive biomass have important consequences for both the photobiology of the phototrophs and the net primary productivity of the microbial mat ecosystem (Bebout and Garcia-Pichel, 1995; Cartaxana et al., 2016b).

Recent studies have focused on the efficiency with which light is utilized and converted to chemical energy via photosynthesis in cyanobacterial mats and mixed cyanobacteria-diatom biofilms (Al-Najjar et al., 2010, 2012). In these studies, relatively low photosynthetic efficiencies were estimated for microbial mats compared with ecosystems with a more open canopy-like organization such as coarse sediments (Lichtenberg et al., 2017), macroalgal stands (Sand-Jensen et al., 2007), corals (Brodersen et al., 2014), or terrestrial forest communities (Terashima et al., 2016), where light propagation is not hindered to the same extent by self-shading and photosynthetic inactive components. How the photosynthetic efficiency of biofilms and microbial mats is modulated by the migration of motile phototrophic populations remains to be studied in detail. In this study, we used fiber-optic scalar irradiance and field radiance microprobes in combination with O_2 and temperature microsensors to investigate the radiative energy budget for the euphotic zone in a coastal microbial mat dominated by motile cyanobacteria and colorless sulfur bacteria. We investigated how photosynthetic efficiency of oxygenic phototrophs in the microbial mat was affected by changes in vertical biomass distribution imposed by acclimating the microbial mat to different light conditions.

MATERIALS AND METHODS

Sample Collection and Preparation

Microbial mats were collected from a periodically desiccated sand flat in Aggersund, Limfjorden, Denmark. The water level at the sample site is mainly determined by wind and local current patterns, and the mats can experience desiccation for extended periods. The sampled mats were dark green/black in appearance and were dominated by filamentous cyanobacteria (*Microcoleus* spp. and other motile morphotypes). Beneath the cyanobacterial band, a population of the sulfur bacteria *Beggiatoa* spp. was found. See Nielsen et al. (2015) for more details of the microbial mat and sampling site.

Mat samples were collected using small plastic trays ($7 \times 2 \times 5$ cm) and were brought back to a field laboratory (Rønbjerg Marine Research Station, Aarhus University, Denmark), where they were incubated submerged in seawater (20°C; Salinity = 27) under a low photon irradiance (∼75 μmol photons $m^{-2}\ s^{-1}$) of photosynthetically active radiation (PAR, 400–700 nm) provided by a halogen lamp. Within few hours of incubation, the mat turned dark green as motile cyanobacteria aggregated and extensive bubble formation from oxygenic photosynthesis appeared on the surface of the mat.

During measurements, the mat samples were transferred to a flow chamber ($25 \times 8 \times 8$ cm) that provided a stable laminar flow (∼2 cm s^{-1}) of aerated seawater (room temperature = 21–23°C; Salinity = 27) (see also Brodersen et al., 2014; Lichtenberg et al., 2017) that minimized bubble formation due to enhanced mass transfer between the microbial mat and water. The flow chamber was connected to a 25 L aquarium where water was recirculated through. Light was provided vertically from above by a white LED lamp (KL-2500 LED, Schott, Germany; color temperature of 5600K) equipped with a collimating lens. The incident irradiance

(400–700 nm) from the lamp was regulated electronically without spectral distortion. The downwelling photon irradiance was measured with a calibrated photon irradiance meter (ULM-500, Walz GmbH, Germany) equipped with a factory-calibrated photon irradiance detector (LI-192S, LiCor, United States). Incident spectral irradiance was also measured in radiometric units (W m^{-2} nm^{-1}) with a calibrated spectroradiometer (Jaz ULM, Ocean Optics, United States). All sensors were mounted in a 45° angle (relative to the vertically incident light) on a motorized micromanipulator (MU-1, PyroScience, Germany), which could be controlled by the manufacturer's software (Profix, PyroScience, Germany). All measurements were performed under an incident photon irradiance (400–700 nm) of 1000 μmol photons m^{-2} s^{-1} as provided by the white LED lamp. This light level was chosen as a saturating irradiance based on a previously measured photosynthesis – irradiance curve (PI). For each profile a new horizontal position in a mat was randomly chosen. Prior to measurements, the vertical distribution of biomass was modulated by incubating the biofilm samples for at least 3 h in either darkness, low light (∼75 μmol photons m^{-2} s^{-1}) or high light (1000 μmol photons m^{-2} s^{-1}), respectively. Upon increasing the irradiance to 1000 μmol photons m^{-2} s^{-1}, scalar irradiance and gross photosynthesis were measured immediately, reflecting the systems immediate response to the new irradiance. Profiles of O_2 and temperature were illuminated for 10 min at 1000 μmol photons m^{-2} s^{-1} before measurements, and we note that the mats were therefore not measured under steady state (see also discussion).

Light Measurements

Spectral scalar irradiance was measured with a fiber-optic scalar irradiance microprobe (spherical tip diameter ∼70 μm) (Rickelt et al., 2016) connected to a fiber-optic spectrometer (USB2000+, Ocean Optics, United States). Spectral downwelling irradiance, $E_d(\lambda)$, was measured with the microprobe tip positioned in a black, non-reflective, light-well at the same distance from the light source as the mat surface (see **Table 1** for definition of abbreviations). In the mat samples, spectral scalar irradiance, $E_0(\lambda)$ was measured in vertical increments of 0.1 mm. These measurements were then corrected for exposure time of the spectrophotometer and normalized to similarly corrected downwelling irradiance spectra yielding scalar irradiance transmittance spectra in different mat layers in % of $E_d(\lambda)$, i.e., $100 \cdot E_0(\lambda)/E_d(\lambda)$.

Spectral attenuation coefficients of scalar irradiance, $K_0(\lambda)$ were calculated for specific depth intervals in the microbial mats as (Kühl, 2005):

$$K_0(\lambda) = -ln\frac{(E_0(\lambda)_1/E_0(\lambda)_2)}{z_2 - z_1}$$

where $E_0(\lambda)_1$ and $E_0(\lambda)_2$ are the spectral scalar irradiances measured at depth z_1 and z_2, respectively.

Similarly, depth profiles and attenuation coefficients of PAR, K_0, were calculated from integrated values over the spectral region of interest. Light measurements <420 nm exhibited noisy signals and increasing amounts of stray light from within the detector and integrations were therefore carried out from 420–700 nm (henceforth mentioned as PAR). In deeper layers of the mat, integration of the measurements encompassed regions in the blue part of the spectrum exhibiting very noisy signals and an increasing contribution from stray light in the spectrometer, and these noisy signals were therefore excluded.

Reflectance of the microbial mat surface was measured with a fiber-optic field radiance miniprobe (flat cut tip diameter = 1 mm) connected to the same fiber-optic spectrometer used for scalar irradiance measurements. The PAR reflectance (R_{PAR}) was calculated from the upwelling irradiance [$E_u(\lambda)$], here measured as the backscattered spectral radiance assuming Lambertian (diffuse) backscatter from the mat surface (Kühl and Jørgensen, 1994), and the downwelling irradiance [$E_d(\lambda)$] measured as the backscattered spectral radiance measured over a white Lambertian reflectance standard (99%; Spectralon, Labsphere, United States) as (Kühl, 2005):

$$R_{PAR} = \int_{420}^{700} \frac{E_u(\lambda)}{E_d(\lambda)} d\lambda$$

The acceptance angle of light collection through the fiber depends on the numerical aperture (NA) of the fiber and the refractive index of the medium. Since $E_d(\lambda)$ was estimated in air, and $E_u(\lambda)$ was measured in water we corrected for the acceptance angle differences by the relation $\Theta_a = sin^{-1}\left(\frac{NA}{RI_w}\right)$, where Θ_a is the acceptance angle, NA is the numerical aperture of the fiber (0.22) and RI_w is the refractive index of water (1.33).

Microsensor Measurements of O_2 Concentration and Gross Photosynthesis

Vertical depth profiles of O_2 concentration were measured using Clark-type O_2 microelectrodes (tip diameter = 25 μm, OX-25, Unisense A/S, Aarhus, Denmark) with fast response time (<0.5 s) and low stirring sensitivity (<1–2%) (Revsbech, 1989), connected to a pA-meter (Unisense A/S, Aarhus, Denmark) and interfaced through an A/D converter (DCR-16, PyroScience, Germany) to data acquisition software (Profix, PyroScience, Germany). The O_2 signals were also recorded on a strip-chart recorder (BD 12E; Kipp & Zonen BV, Netherlands) connected to the pA-meter. Sensor signals were linearly calibrated at experimental temperature and salinity from measurements in the aerated free flowing water in the flow-chamber and in anoxic zones in the sediment. Depth profiles of O_2 concentration were measured in 0.1 mm increments relative to the mat surface position determined by placing the sensor tip at the mat surface (z = 0 mm), as observed through a USB microscope (AM7013MZT Dino-Lite, AnMo Electronics Corporation, Taiwan). The sensor tip was then moved to 1.5 mm above the mat surface ($z = -1.5$ mm) and from here profiles were measured in steps of 100 μm until reaching anoxic mat layers (z∼1.5 mm).

The volume-specific rate of gross photosynthesis [PS(z) in nmol O_2 cm^{-3} s^{-1}] was measured using the light/dark shift method (Revsbech and Jørgensen, 1983) in vertical steps of 0.1 mm starting from just above the microbial mat surface until the depth where no immediate O_2 signal changes were observed upon darkening. Areal rates of gross photosynthesis [PS(a) in

nmol O_2 cm^{-2} s^{-1}] were calculated by integrating the volumetric rates over depth.

Temperature Microsensor Measurements

Temperature profiles were measured using thermocouple microsensors (tip diameter = 50 μm, TP-50, Unisense A/S, Aarhus, Denmark) connected to a thermocouple meter (Unisense A/S, Aarhus, Denmark) and interfaced through an A/D converter (DCR-16, PyroScience, Germany) to data acquisition software (Profix, PyroScience, Germany). Signals were linearly calibrated against a high precision digital thermometer (± 0.2°C; Testo 110, Testo AG, Germany) in seawater of different temperatures. The areal heat dissipation from the microbial mat was calculated using Fourier's law of conduction using the linear temperature gradient in the thermal boundary layer (TBL) and the thermal conductivity of seawater (k = 0.6 W m^{-1} K^{-1}):

$$J_H = k\frac{\partial T}{\partial z}$$

The downward heat dissipation could not be directly calculated from the measured temperature profiles, and were estimated from the principle of energy conservation as the difference between the absorbed light energy and the sum of photosynthesis and upward heat flux (both in energy units).

Energy Calculations

To obtain absolute scalar irradiance spectra, we multiplied the measured transmittance spectra for each depth with the measured incident radiometric spectra (in W m^{-2}). By using Planck's equation:

$$E_\lambda = h\,\frac{c}{\lambda},$$

where E_λ is the energy of a photon with a wavelength λ, h is Planck's constant ($6.626 \cdot 10^{-34}$ W s^2) and c is the speed of light in vacuum (in m s^{-1}), we then converted absolute scalar irradiance spectra to absolute spectra of photon scalar irradiance [$E_0(z)$ in μmol photons m^{-2} s^{-1} nm^{-1}].

The total absorbed light energy in the mat (J_{ABS} in J m^{-2} s^{-1}), i.e., the vector irradiance, was calculated from the downwelling spectral irradiance $E_d(\lambda)$ and the irradiance reflectance as:

$$J_{ABS} = \int_{420}^{700} E_d(\lambda)(1 - R(\lambda))d\lambda$$

The amount of energy dissipated via photosynthesis was calculated by multiplying the areal photosynthesis rates [PS(a)] with the Gibbs free energy from the light reactions, where O_2 is produced by the photolysis of water. Including the formation of ATP this yields 482.9 kJ (mol O_2) $^{-1}$ (Thauer et al., 1977).

Energy budgets for the entire photic zone were calculated under the assumption that the total energy stored in photosynthesis (J_{PS}), and dissipated via heat (J_H) and reflection (R) balanced the incoming radiative energy (J_{IN}):

$$J_{IN} = J_H + J_{PS} + R \text{ and } J_{IN} - R = J_{ABS} = J_H + J_{PS}$$

To investigate how photosynthetic quantum efficiency varied with depth in the microbial mat, we calculated relative photosynthetic efficiencies (in mol O_2 (mol photons) $^{-1}$ mm^{-1}) by dividing the photosynthetic rates in a specific depth layer with the photon scalar irradiance just above that layer (Lassen et al., 1992). We note that the calculated efficiency parameter does not reflect the true quantum efficiency, where depth specific photosynthesis is related to the number of absorbed photons in that particular depth (see section Discussion).

HPLC Pigment Analysis

Sediment samples of the 0-0.5 mm surface layer were collected using the "crème brûlée" sampler described by Laviale et al. (2015) and stored at −80°C. Approximately 100 mg of sampled mat material were ground with a micro pestle and extracted in a mixture of acetone and methanol (7:2). Samples were sonicated (S-4000, Branson Ultrasonic Corporation, United States) for 20 s to improve pigment extraction and were then centrifuged for 60 s at 13,400 rpm. Supernatants were filtered through 0.45 μm PTFE-membranes and immediately injected in a HPLC (1260 Infinity, Agilent Technologies, United States). Fifteen microliter of 1 M ammonium acetate was added to each HPLC vial prior to injection as a resolution-improving agent. The solvent gradient was set up according to Frigaard et al. (1997) with a 69 min elution program, a flow rate of 1.0 mL min^{-1} and an injection volume of 100 μL. Chromatographic separation was carried out using a C18 Ascentis column for reverse phase chromatography (5 μm particle size; L × I.D: 25 cm × 4.6 mm). Pigments were identified from their characteristic retention times and absorbance spectra.

RESULTS

Light, Temperature, and Photosynthesis

Microprofiles of photon scalar irradiance in the dense microbial mat were measured after incubation in dark, low light (75 μmol photons m^{-2} s^{-1}), and high light (1000 μmol photons m^{-2} s^{-1}), respectively, which yielded a different spatial organization of motile microbes in the mat (**Figure 1**). In the low light-acclimated state, a cyanobacterial layer formed near the surface, while in the high light-acclimated state the cyanobacteria were found in deeper layers. In the dark-acclimated mat, a dense whitish layer of colorless *Beggiatoa* spp. formed at the surface with the cyanobacteria located just below the colorless sulfur bacteria (**Figure 1**).

The vertical attenuation of photosynthetically active radiation (PAR, 400–700 nm) with depth in the microbial mat did not follow a mono-exponential decay, but exhibited variable attenuation in different layers depending on light acclimation and the distribution of biomass in the mat (**Figures 2A–C**). In the low light acclimated state, the strongest attenuation of PAR was found in the top 0.2 mm (K_0 = 13.9 mm^{-1}), whereas the underlying part of the microbial mat (0.3–0.5 mm) showed a slightly lower attenuation of PAR scalar irradiance (K_0 = 10.3 mm^{-1}). In the high light-acclimated state this trend was reversed, where the attenuation of PAR in the top layer (K_0 = 10.6 mm^{-1}) was lower

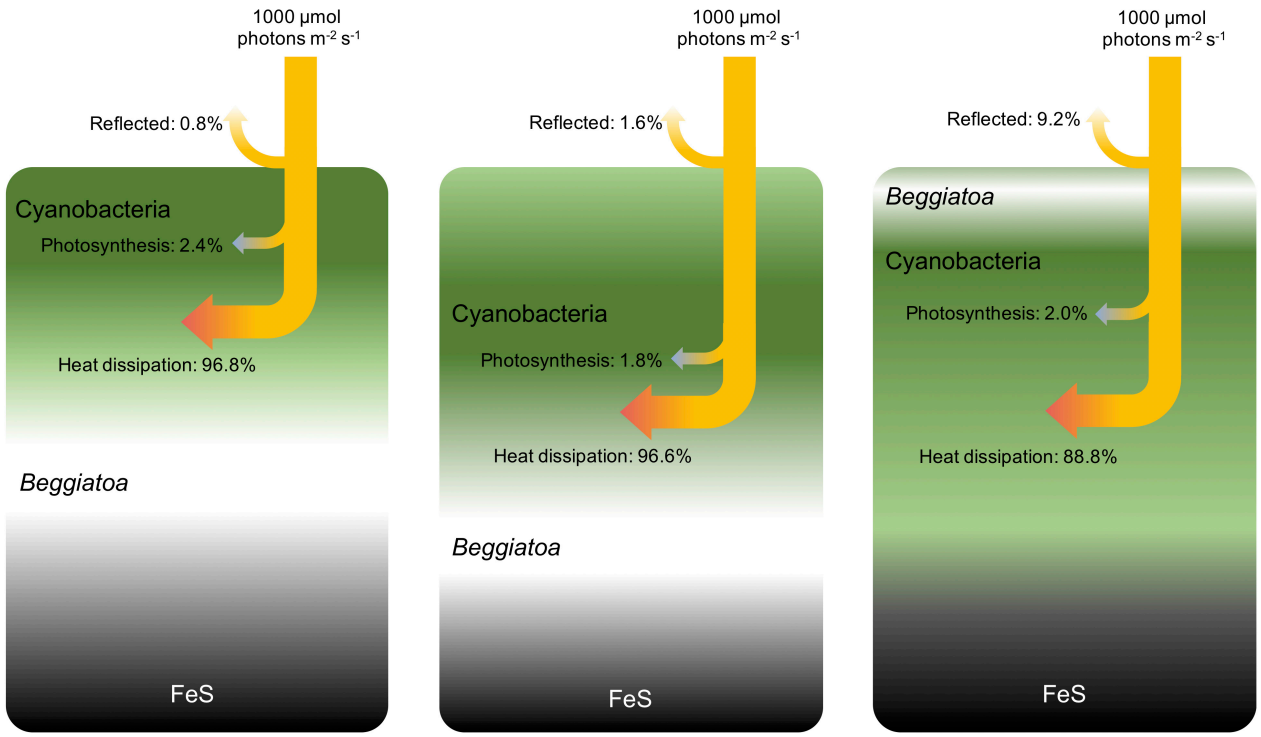

FIGURE 1 | Conceptual drawing of the biomass distribution during different light acclimation scenarios and the corresponding radiative energy budgets of the entire photic zone measured under an incident photon irradiance of 1000 µmol photons m^{-2} s^{-1}. The surface layers of the microbial mat were dominated by dense populations of motile cyanobacteria (*Microcoleus* sp. and other filamentous species) and filamentous sulfide oxidizing bacteria (*Beggiatoa* spp.). Beneath the narrow photic zone, a dark FeS-containing sediment layer was present. In low light, the upper layers became oxidized driving the O_2-H_2S interface and thus *Beggiatoa* deeper into the mat, while the motile cyanobacteria moved toward the mat surface under non-inhibitory light levels. In high light, a larger part of the biofilm is oxidized, *Beggiatoa* moved further down, while motile cyanobacteria in the top layers started to move downwards to avoid high photoinhibitory light levels at the microbial mat surface. In darkness, the entire mat became anoxic and the *Beggiatoa* moved to the mat surface forming a white layer on top of the cyanobacteria, to avoid the high levels of H_2S and remain at the O_2-H_2S interface (Preisler et al., 2007), whereas the cyanobacteria remained in a dense layer underneath.

than in deeper layers of the microbial mat (K_0 = 16.5 mm^{-1}). In the dark-acclimated state, a lower attenuation of PAR was found in the top 0.2 mm (K_0 = 5.8 mm^{-1}) of the microbial mat followed by a very steep attenuation from 0.2 to 0.4 mm depth (K_0 = 22.2 mm^{-1}).

Spectral attenuation of scalar irradiance in the PAR region was enhanced around absorption maxima of most abundant photopigments commonly found in cyanobacterial mats, e.g., Chl *a* (440 nm; 675 nm), phycocyanin (620 nm) and phycoerythrin (565 nm) (**Figures 2D–F**). HPLC analysis revealed the presence of other cyanobacterial pigments such as myxoxanthophyll, zeaxanthin, oscillaxanthin and β,ε-carotene in the upper 0.5 mm of the mat, along with BChl *a* indicative of anoxygenic phototrophs (**Figure 3**). Due to the strong light attenuation in the mat, <1% of PAR surface scalar irradiance remained just 0.4 mm below the biofilm surface (**Figure 2**). The very high light-attenuation of PAR (400–700 nm) and dense pigmentation of the microbial mat resulted in low surface reflection (**Figure 1**). In the low-light acclimated state, only 0.75% of the incident light was reflected, whereas the reflection from the mat surface in the high light-acclimated state was twice as high (1.6%). In the dark-acclimated state, where the surface of the microbial mat was covered by a whitish layer of motile, filamentous colorless sulfur bacteria (*Beggiatoa* spp.), the reflection increased ∼10-fold to 9.2% of the incident irradiance.

Most of the incident irradiance in the PAR region was thus readily absorbed in the mat, and the majority of the absorbed light was dissipated as heat as quantified from the heat flux over a ∼1.2 mm thick thermal boundary layer (TBL) (**Figure 4**). Under similar flow and thus TBL thickness, the mat surface heating differed slightly depending on light acclimation, where the surface temperature of the high light-acclimated mat increased by 0.3°C as compared to the low light-acclimated mat showing a mat surface temperature increase of 0.24°C. Lowest surface heating was measured when illuminating the dark-acclimated mat reaching a surface temperature increase of 0.2°C.

Due to the high light-attenuation, the euphotic zone of the microbial mat was restricted to the uppermost 0.6 to 0.8 mm (**Figure 5**). The depth distribution of gross photosynthesis rates varied with light acclimation, and very high rates were observed

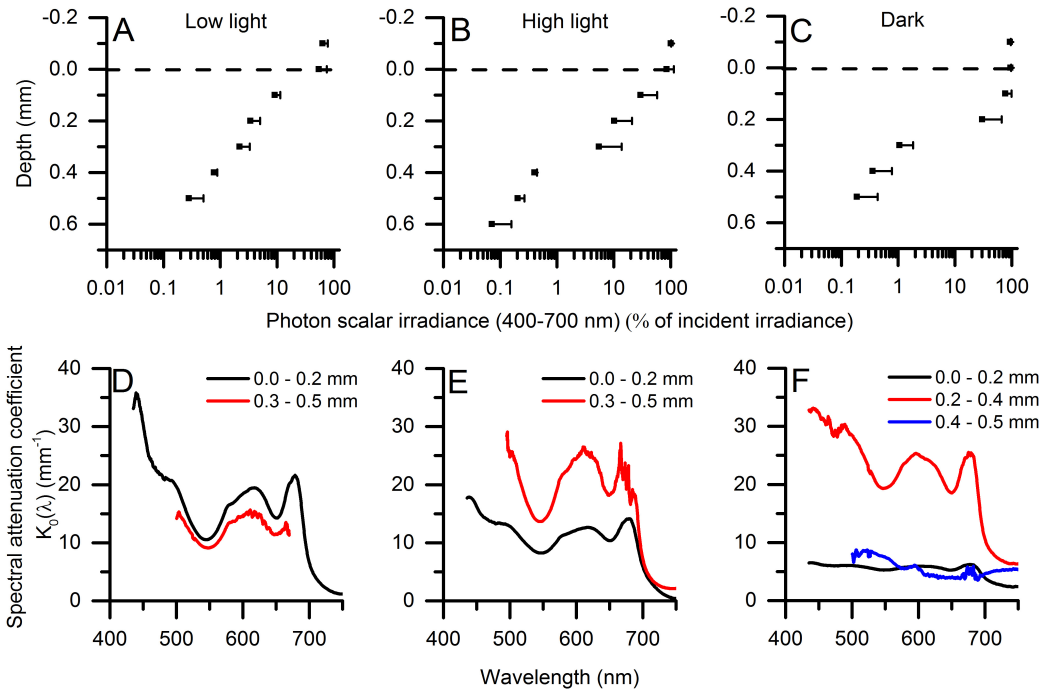

FIGURE 2 | (A–C) Vertical microprofiles of photon scalar irradiance (PAR; 420–700 nm) (in μmol photons m^{-2} s^{-1}). The dashed line indicates the biofilm surface. [means ± 1 SD (only + SD shown for clarity); n = 3]. PAR attenuation coefficients, K_0, were estimated in the upper- and lower part of the biofilm (0.0–0.2 mm; 0.3–0.5 mm) from the slope of linear regressions on natural logarithm transformed data (R^2 > 0.95 for all plots). **(D–F)** Shows spectral attenuation coefficients, $K_0(\lambda)$ (in mm^{-1}) in different zones of the biofilm (n = 3). The measurements were done in low light-acclimated (left panels), high light-acclimated (middle panels), and dark-acclimated biofilms (right panels). At depth in the mats, very low light levels led to decreasing signal to noise ratios and increasing contributions by straylight in the spectrometer at shorter wavelengths and spectra were therefore truncated.

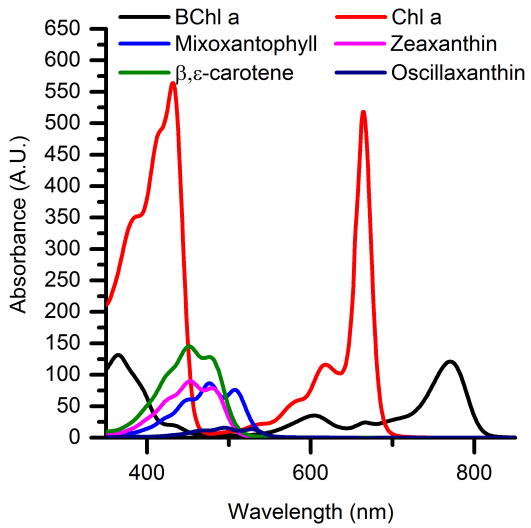

FIGURE 3 | Relative absorbance spectra of predominant photopigments found in the upper 0.5 mm of the microbial mat as investigated with HPLC analysis.

in all treatments (up to 30 nmol O_2 cm^{-3} s^{-1}). In the low light-acclimated state, peaks of gross photosynthesis were found at the mat surface and 0.3 mm beneath the surface. In the high light-acclimated state, the photosynthetic rates near the surface were diminished, while a stronger sub-surface peak in gross photosynthesis was found around 0.2 mm below the mat surface. The dark-acclimated mat showed a small photosynthesis peak near the mat surface and a sub-surface peak at 0.3–0.4 mm depth (**Figure 5**). However, the O_2 concentration profiles between light acclimations were quite similar and did not show any clear differences in e.g., O_2 penetration depth (**Figure 5**).

Energy Budgets

The vector irradiance, i.e., the net downwelling radiative energy flux (400–700 nm), was very similar between light acclimations and amounted to 218.0 ± 5.6 W m^{-2}. However, the heat dissipation from the mat to the water differed between light incubations, where the dark-acclimated mat exhibited the lowest upward heat dissipation of 140 W m^{-2}, the heat dissipation in the low light-acclimated mat was 144 W m^{-2}, and the highest heat dissipation was measured in the high light-acclimated mat reaching 179 W m^{-2}.

Depth integrated gross (oxygenic) photosynthesis only accounted for a small part of the absorbed light energy. The highest amount of radiative energy stored via photosynthesis was measured in the low light-acclimated microbial mat and amounted to 5.4 ± 0.7 W m^{-2}, while the high light- and the dark-acclimated mat conserved 4.06 ± 1.6 W m^{-2} and 4.8 ± 1.1 W m^{-2}, respectively.

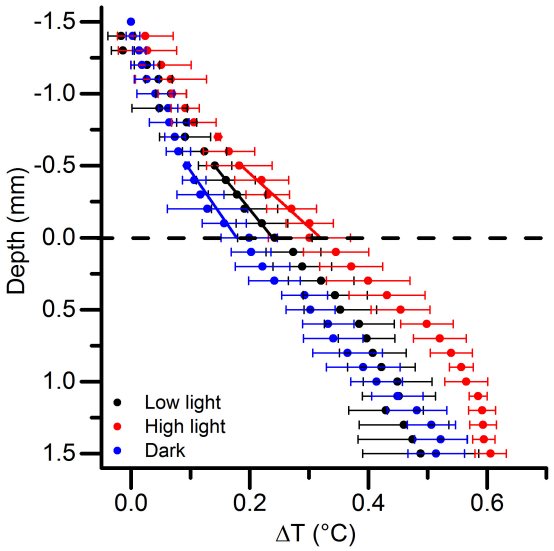

FIGURE 4 | Vertical microprofiles of temperature increase (ΔT in°C) relative to the free-flowing water temperature under an incident photon irradiance of 1000 μmol photons m^{-2} s^{-1}. The dashed line indicates the microbial mat surface. Black, red, and blue symbols represent measurements in a low light-, high light-, and dark-adapted mats, respectively. The straight black, red and blue lines indicate the linear regressions used to estimate the areal heat dissipation from the microbial mat. Data points with error bars represent means ± 1 SD (n = 3).

Relative to the incident energy, the photosynthetic energy conservation efficiency for the entire photic zone thus only accounted for ∼2% (2.1, 2.4, and 1.8% for the dark-, low light-, and high light-acclimated biofilm, respectively), while the majority of incident light energy was dissipated as heat (**Figure 1**).

Relative Photosynthetic Efficiencies

Depth profiles of relative photosynthetic efficiencies in the microbial mat were calculated by normalizing the measured volumetric gross photosynthesis rates at each depth to the scalar irradiance incident to that depth. Such profiles showed sub-surface peaks in relative photosynthetic efficiency in all light acclimation states of the microbial mat (**Figure 6**). In the low light-acclimated mat, a peak in relative efficiency was located closest to the surface at 0.3 mm depth. The dark-acclimated mat exhibited highest relative photosynthetic efficiencies 0.4 mm beneath the surface, while the highest relative photosynthetic efficiencies in the high light acclimated mat were found near the lower boundary of the photic zone at 0.5 mm below the mat surface.

DISCUSSION

Radiative energy budgets in microbenthic systems have previously been studied in cyanobacterial mats and biofilms (Al-Najjar et al., 2010, 2012), sediments (Lichtenberg et al., 2017), and corals (Brodersen et al., 2014), albeit under the assumption of a homogenous depth distribution of biomass. In the studied microbial mat, dense populations of phototrophic microalgae and cyanobacteria reside in steep gradients of resource stratification shaped by communities of photo-, chemo-, and heterotrophic microorganisms creating a steep redox gradient (van Gemerden, 1993). Consequently, the physical and chemical landscape in such microbial mats can change, within less than one mm, from intense sun exposure (>1000 μmol photons m^{-2} s^{-1}) and O_2 supersaturation (up to 2 mM) to complete darkness and a reduced anoxic sediment high in H_2S (Jørgensen, 1982).

The studied microbial mat exhibited an extremely high optical density and attenuation of PAR, where >99% of the surface irradiance was effectively absorbed <0.4 mm below the microbial mat surface. Light was thus the primary limiting resource for microbial phototrophs in the mat. One strategy to remain competitive under light limitation is to complement light absorption by Chl *a*, the main light harvesting pigment in oxygenic photosynthesis, by metabolic investment in producing a range of accessory pigments absorbing a broader part of the available light spectrum and channeling it to the photosynthetic reaction centers (Stomp et al., 2007; Trampe and Kühl, 2016; Kühl et al., 2020). HPLC pigment analysis of the upper 0.5 mm of the microbial mat revealed that very efficient light absorption was achieved by a mixture of light harvesting pigments from cyanobacteria (Chl *a*, mixoxanthophyll, zeaxanthin, oscillaxanthin and β,ε-carotene) and anoxygenic phototrophs (BChl *a*), able to absorb light from the UV-B well into the NIR region (**Figure 3**). We did not find any signs of typical diatom light harvesting pigments (fucoxanthin, diadinoxanthin or Chl *c*) or the far-red absorbing chlorophylls *d* or *f* in either measurements of scalar irradiance or by HPLC analysis.

The attenuation of light was stratified with depth and varied between the different acclimation states. In all acclimations, we found strong spectral attenuation from typical cyanobacterial pigments confirmed by the HPLC pigment analysis. In low light acclimated mats the strongest spectral attenuation was in the top 0.2 mm while the strongest spectral attenuation was found deeper (0.3–0.5 mm) in the high light acclimated mats.

Consequently, low surface reflection was observed in the low and high light-acclimated microbial mats. In the low light-acclimated mat, the cyanobacterial population was located near the surface and only 0.75% of the incident irradiance was backscattered, while in the high light-acclimated state, the motile cyanobacteria migrated downward changing the surface biomass composition leading to higher reflectance. During dark-acclimation, the surface of the biofilm became anoxic and a layer of the motile, filamentous colorless sulfur bacteria *Beggiatoa* formed on the mat surface. *Beggiatoa* spp. are sulfide oxidizing bacteria known to store granules of elemental sulfur (Nelson and Castenholz, 1981), which make the filaments appear white due to strong light scattering, which in our measurements increased the surface reflectance to 9.2% of the incident irradiance. Multiple scattering in sediments and coral tissues have previously been shown to increase the scalar irradiance in top layers (Kühl and Jørgensen, 1994; Wangpraseurt et al., 2012) which could explain the very low attenuation of light in the top layers of the dark-acclimated mat (**Figure 2**). Light-dependent migration

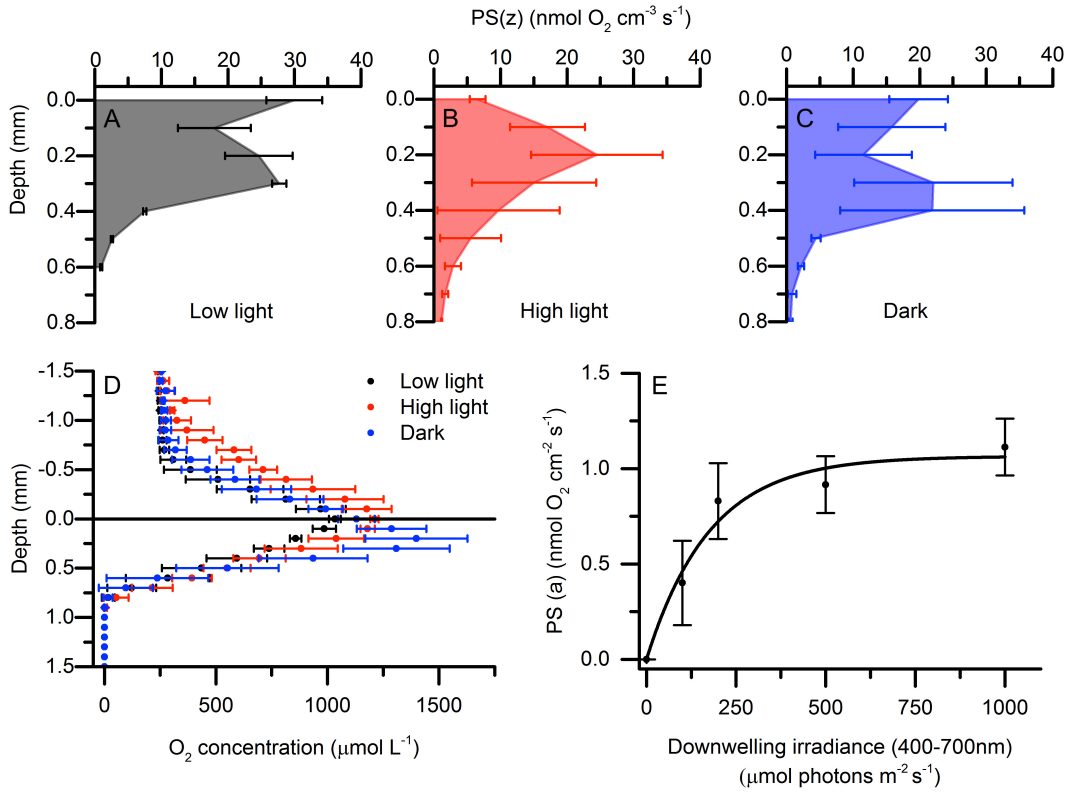

FIGURE 5 | Depth distribution of volumetric gross photosynthesis rates [PS(z)] under an incident photon irradiance of 1000 µmol photons m^{-2} s^{-1}. Measurements were done in a low light-acclimated **(A)**, high light-acclimated **(B)**, and dark-acclimated **(C)** microbial mat. Data points with error bars represent means ± 1 SD (n = 3). **(D)** Depth profiles of O_2 concentration in low light, high light, and dark acclimated microbial mats measured under a downwelling photon irradiance (400–700 nm) of 1000 µmol photons m^{-2} s^{-1}(means ± 1SD; n = 3). **(E)** Areal photosynthetic rates [PS(a)] vs. irradiance curve using 30 min acclimation to each irradiance (means ± 1 SD; n = 3). Data was fitted with an exponential saturation model (Webb et al., 1974).

patterns of cyanobacteria and *Beggiatoa* thus clearly modulated the radiative energy input to the microbial mat.

The strong light absorption in the uppermost mat layers, resulted in very high local photosynthetic rates reaching >30 nmol O_2 cm^{-3} s^{-1}. This is about 2–5 fold higher than rates measured in most other cyanobacteria-dominated microbial mats (Al-Najjar et al., 2012), but e.g., comparable to rates measured in a highly stratified intertidal mudflat community dominated by motile diatoms (Cartaxana et al., 2016b) and in a cultivated diatom biofilm (Jensen and Revsbech, 1989). We investigated photosynthesis under high light exposure of microbial mats exhibiting different distributions of motile microbes in response to different light history. Investigations of photosynthesis under increasing irradiances in motile microbial systems are complex as migrating cells under changing light can change the spatial characteristics of the biofilm/mat and thereby potentially affect light exposure and distribution in different mat layers (Kühl et al., 1997). In the present study, the main aim was thus to investigate how the migration of motile cyanobacteria affected photosynthetic efficiency under different spatial organization of phototrophs in the microbial mat.

This is experimentally challenging, and we note that these measurements were not performed under steady-state conditions. The change to higher light than the acclimation irradiance will start to move the mat toward a new steady-state and rates and profiles will thus be measured under transient "quasi steady-state" conditions. The measurements of scalar irradiance and gross photosynthesis reflect the community's response to high light in the current distribution of biomass. The distribution of O_2 and temperature is, however, more complex to interpret, as the distribution of O_2 is determined by the interplay between diffusion, production and consumption, while the temperature profiles are determined by the local heat dissipation and heat transfer properties. These are slower processes and will move toward a steady state on the same time scale as motility driven biomass redistribution in such compact systems as the studied mats.

Areal rates of oxygenic photosynthesis, integrated across the entire euphotic zone, did not differ markedly between different light acclimations (0.99, 1.11, and 0.84 nmol O_2 cm^{-2} s^{-1} for dark-, low light- and high light-acclimated samples, respectively) under the high saturating photon irradiance used for the energy budget measurements. It is however noted that the lowest areal photosynthetic rates were observed in the high light-acclimated state. One could speculate that the longer acclimation period to high light could have given the phototrophs, in this treatment,

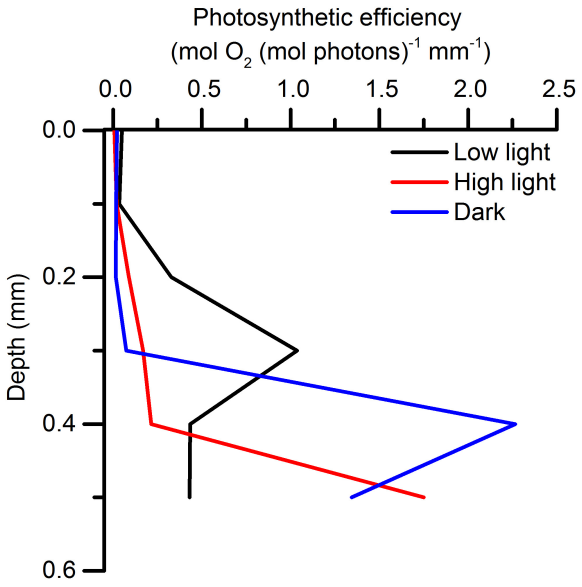

FIGURE 6 | Photosynthetic efficiencies [in mol O_2 (mol photons) $^{-1}$ mm^{-1}] calculated from volume-specific gross photosynthesis rates and the photon scalar irradiance incident to the corresponding depth in a low light-, high light-, and dark-acclimated biofilm (means; $n = 3$).

time to adjust their balance between photosynthesis and non-photochemical quenching (NPQ) processes. One of the most important short-term regulatory mechanisms to avoid photo damage is NPQ, where excess energy decays from singlet excited chlorophyll (^{1}Chl*) into heat dissipation (Müller et al., 2001). This mechanism significantly lowers the effective quantum yield of photosynthesis but avoids the formation of reactive singlet oxygen ($^1O_2$*) by the triplet state of chlorophyll (^{3}Chl*) (Müller et al., 2001), which can have long term detrimental effects on the photosystems by degradation of the D1 protein; an important component in photosystem II (Nymark et al., 2009). The higher rates displayed by the top population for the dark- and low-light acclimated mats could therefore be a product of the more open reaction centers before regulating the different NPQ components that operate on time scales from a few minutes to a few hours (Kress and Jahns, 2017).

Photophobic responses or phototaxis enabling movement along a light gradient (Jekely, 2009) are alternative strategies of photoprotection, enabling motile phototrophs to align their position at optimum irradiance in light gradients (Tamulonis et al., 2011) depending on the status of the electron transport chain and time of the day (Burns and Rosa, 1980). *Microcoleus chtonoplastes* displays light dependent migration preferring moderate to low light levels (Ramsing and Prufert-Bebout, 1994), and other studies have found that as little as a 4% difference in light intensity between "head" and "tail" of a cyanobacterial filament can trigger their movement (Häder, 1987). From our measured depth profiles of gross oxygenic photosynthesis, it appears that the distance of vertical migration was limited to only 0.2 to 0.3 mm. However, due to the steep light gradients in the investigated microbial mat, the changes in the light field over such short distances are dramatic, and cyanobacteria migrating 200 μm deeper into the mat experienced a >84-fold decrease in scalar irradiance (**Figure 2C**; 0.4–0.2 mm) from >350 μmol photons m^{-2} s^{-1} to < 10 μmol photons m^{-2} s^{-1}. Such strong changes in light exposure upon migration distances of a few 100 μm have previously been demonstrated in hypersaline cyanobacterial mats (Kühl et al., 1997). Consequently, the spatial distribution of gross photosynthesis varied with light acclimation, probably as a result of migrations of the cyanobacteria and *Beggiatoa*.

Other triggers for migration could also play a role in the observed redistribution of biomass. Sulfide is well known to cause migration due to its cytotoxicity (Whale and Walsby, 1984). Sulfide was most likely present in high concentrations in the studied mats due to i) the black FeS layer below the photic zone, ii) the presence of BChl *a*, indicative of anoxygenic phototrophs that oxidize hydrogen sulfide to sulfur, and the presence of a dense population of *Beggiatoa* known to thrive at the interface of strong O_2 and sulfide concentration gradients. Earlier microsensor measurements in microbial mats from the same sampling site also demonstrated significant sulfide production and light-driven dynamics of O_2, pH and sulfide in the uppermost mat layers (Nielsen et al., 2015). As stated above, *Microcoleus* prefer moderate to low light levels and their migratory behavior is thus probably due to a combination of photophobic movement and sulfide avoidance, although they can grow in H_2S concentrations up to 974 μM (de Wit and van Gemerden, 1987).

Compared to earlier studies of heat dissipation in corals and microbial mats (Jimenez et al., 2008; Al-Najjar et al., 2010; Brodersen et al., 2014), we found a relatively small heat dissipation from the biofilm surface into the water column and the surface temperature of the microbial mat increased by only ∼0.3°C. However, the heat dissipation in deeper mat layers was larger than expected. The zone of maximum temperature increase was expected to be found in the same zone as the largest energy deposition, i.e., in the upper few hundred micrometers of the microbial mat, where >90% of the incident light was attenuated. However, the heat dissipation below 0.5 mm depth was in the same order of magnitude as the upward heat dissipation and reached higher temperatures (**Figure 4**). We note that below the dense photic zone, a black layer of precipitated iron sulfide was found, and absorption of light energy in this sediment layer apparently contributed significantly to the heating of the microbial mat, but this remains speculative. While we did not measure temperature deep enough in the sediment to be able to calculate the downward transport of heat, we estimated from the principle of energy conservation that the downward heat flux contributed about 20–50% of the total heat dissipation.

The amount of photochemically conserved energy did not change markedly between different light acclimation states of the microbial mat when investigated at similar high irradiance, despite the higher reflection and lower heat dissipation observed in the dark-acclimated biofilms. Consequently, the photosynthetic energy conservation was 2.1, 2.4, and 1.8% of the incident energy, for dark-, low light-, and high light-acclimated

TABLE 1 | Definition of abbreviations.

Abbreviation	Definition	Unit
TBL	Thermal boundary layer	
PAR	Photosynthetic active radiation (420–700 nm)	
PS(z)	Volume-specific rate of gross photosynthesis	nmol O_2 cm^{-3} s^{-1}
PS(a)	Areal rate of gross photosynthesis	nmol O_2 cm^{-2} s^{-1}
J_{PS}	Areal rate of gross photosynthesis in energy terms	J m^{-2} s^{-1}
$J_{H\uparrow}$	Upward heat flux	J m^{-2} s^{-1}
$J_{H\downarrow}$	Downward heat flux	J m^{-2} s^{-1}
J_H	$J_{H\uparrow} - J_{H\downarrow}$	J m^{-2} s^{-1}
$E_d(\lambda)$	Downwelling photon irradiance	Counts nm^{-1}
$E_0(\lambda)$	Spectral scalar irradiance	% of $E_d(\lambda)$
$E_0(z)$	Local scalar irradiance availability	µmol photons m^{-2} s^{-1}
J_{IN}	Incident light energy	J m^{-2} s^{-1}
J_{ABS}	Absorbed light energy	J m^{-2} s^{-1}
R	Irradiance reflectance	
K_0	Diffuse attenuation coefficient of PAR	mm^{-1}
$K_0(\lambda)$	Spectral attenuation coefficient	mm^{-1}

biofilms, respectively. This indicates that by migration, the phototrophic community can apparently sustain similar energy conservation efficiencies, while avoiding the detrimental effects of excessive light when situated near the surface.

The vertical stratification of relative photosynthetic efficiencies (**Figure 6**) can either be ascribed to (i) a higher density of biomass contributing to photosynthesis, or (ii) an overall higher efficiency caused by higher cell specific pigment content and/or higher absorption cross section, in that area (Iglesias-Prieto and Trench, 1994, 1997; Falkowski and Raven, 2007; Al-Najjar et al., 2010). However, in our measurements we found differences in the vertical positions of the peaks of relative photosynthetic efficiency depending on light acclimation. At the cellular level, regulation of the pigment density and the absorption cross section of antennae pigments occurs on a longer time scale than the acclimation time used in these experiments, although the formation of zeaxanthin from β-carotene is a short term photoprotective mechanism (Falkowski and Raven, 2007). Given the time scale, the difference in vertical position of the peaks in relative photosynthetic efficiencies, can thus primarily be ascribed to migration.

In a fluctuating light environment, phototrophs can modulate light exposure/harvesting either by regulating pigment densities or by moving to a different light environment. For this mechanism to be energetically successful, the cost of motility must present an advantage compared to employment of regulation of light harvesting or photoprotective pigments. The cost of motility was estimated for *Oscillatoria* to be 0.2–5% of the energy generated by oxidative phosphorylation (Halfen and Castenholz, 1971). This is a relatively low cost considering that in a dense microbial system, where oxygenic phototrophs not only have to cope with alternating light environments but also steep and dynamic chemical gradients of e.g., pH and sulfide. Motility may thus be an important trait for phototrophs in microbial mats enabling rapid optimization of their light exposure and chemical microenvironment. Migration of cyanobacterial populations can also mitigate effects of continuous sedimentation and overgrowth by other microbes (Whale and Walsby, 1984).

Previously, photosynthetic quantum efficiencies in microbial mats have been calculated by applying a model that estimates the local quantity of absorbed light, which is then correlated to the local rates of gross photosynthesis (Al-Najjar et al., 2010). However, this model assumes a homogenous distribution of light absorption (i.e., biomass), which makes the application of such a model problematic in a motile community exhibiting photomovement. Calculations using the model of Al-Najjar et al. (2010) on our data showed apparent photosynthetic quantum efficiencies, about 2-fold higher than the theoretical maximum of 0.125 (i.e., 8 photons needed to produce 1 O_2 molecule). We speculate that the presence of a black ferrous sulfide layer in close proximity to the phototrophs also interfered with such estimations of the local density of absorbed light. However, the distribution of sand particles, organic matter and photosynthetic biomass was not further quantified, and a correction for this possible artifact was not attempted. Therefore, we estimated relative quantum efficiencies of photosynthesis by relating the depth specific gross photosynthesis rates to the scalar irradiance incident to that point following the approach of Lassen et al. (1992), who also found that the position of maximum quantum efficiencies changed with light exposure. The relative quantum efficiencies estimated in our mat samples were, however, up to three times higher than values reported by Lassen et al. (1992) for a less compacted microbial mat.

The photosynthetic efficiency depends on photo-pigmentation and other biotic/abiotic substances contributing to light absorption (Al-Najjar et al., 2012) but also on complex interplay between cyanobacteria and sulfur oxidizers (Klatt et al., 2016). Thus, the microscale 3D structure of the microbial mat will have an influence on the light availability and the energy balance of the system, where more open systems will display larger photic zones and different responses to changes in light environment as compared to more compacted systems

(Lichtenberg et al., 2017). How such microscale canopy-like effects in microbial mats are affected by the presence of much higher densities of abiotic matter in comparison to e.g., plant canopies remain to be studied in more detail.

CONCLUSION

We conclude that cyanobacteria can sustain high relative photosynthetic efficiencies by vertical migration in response to shifting light conditions, thereby optimizing the overall capacity of light absorption and photosynthetic activity against a backdrop of dynamic chemical gradients of O_2, pH and sulfide. This was evident from the overall photosynthetic energy conservation efficiency that did not change with light acclimation but showed vertical differences in the distribution of maximum relative photosynthetic efficiency. Further studies could investigate how distribution and efficiency of gross photosynthesis respond to changing light environment in microbial mats with vertically fixed populations of phototrophs in different depth horizons, e.g., by applying a motility inhibitor (Cartaxana et al., 2016a). In very compact systems such as the mats studied here it is, however, difficult to resolve local differences due to the spatial resolution of the microsensors and methodology to non-invasively monitor biomass distributions. In less compacted systems (e.g., mats like studied by Wieland and Kühl, 2000; Saenger et al., 2006; Lichtenberg et al., 2017) with more open structures and thereby less steep gradients of the physico-chemical parameters, local differences in energy deposition would be easier to describe in more detail.

Our study adds novel insight to the regulation of photosynthesis in compacted microbial mats and biofilms. In terms of energy conservation and photosynthetic efficiency, such systems are often regarded less efficient due to their more or less flat topography (e.g., Al-Najjar et al., 2012). However, there is increasing evidence that microstructural changes can modulate light harvesting and photosynthesis in dense photosynthetic biofilms and tissues, and that such systems can exhibit canopy-like properties at a microscale, where a more open microstructure and/or modulation of the scattering and lateral distribution of incident light seems to govern higher photosynthetic efficiency (e.g., Wangpraseurt et al., 2014; Lichtenberg et al., 2016, 2017; Lyndby et al., 2016). In the present study, we show that reorganization of the phototrophs via migration is yet another functional trait that helps optimize overall light harvesting and photosynthesis in biofilms and microbial mats.

DATA AVAILABILITY STATEMENT

The datasets generated for this study are available on request to the corresponding author.

AUTHOR CONTRIBUTIONS

ML, PC, and MK designed the experiments and analyzed the data. ML and PC performed the experiments. ML wrote the manuscript with editorial input from PC and MK.

FUNDING

This study was supported by grants from the Independent Research Fund Denmark (DFF-1323-00065B and DFF- 8021-00308B) (MK). PC acknowledges support from FCT/MCTES through CESAM (UIDB/50017/2020+UIDP/50017/2020).

ACKNOWLEDGMENTS

We thank Lars Rickelt for construction of scalar irradiance microprobes, and Sofie Jakobsen for excellent technical assistance. The members of the Microenvironmental Research Group provided useful feedback, help and suggestions during the experimental and analysis part of this study. Parts of this manuscript were included in the Ph.D. thesis of ML (Lichtenberg, 2017).

REFERENCES

Al-Najjar, M. A., de Beer, D., Kühl, M., and Polerecky, L. (2012). Light utilization efficiency in photosynthetic microbial mats. *Environ. Microbiol.* 14, 982–992. doi: 10.1111/j.1462-2920.2011.02676.x

Al-Najjar, M. A. A., de Beer, D., Jørgensen, B. B., Kühl, M., and Polerecky, L. (2010). Conversion and conservation of light energy in a photosynthetic microbial mat ecosystem. *ISME J.* 4, 440–449. doi: 10.1038/ismej.2009.121

Bebout, B. M., and Garcia-Pichel, F. (1995). UV B-induced vertical migrations of cyanobacteria in a microbial mat. *Appl. Environ. Microb.* 61, 4215–4222.

Bhaya, D. (2004). Light matters: phototaxis and signal transduction in unicellular cyanobacteria. *Mol. Microbiol.* 53, 745–754. doi: 10.1111/j.1365-2958.2004.04160.x

Brodersen, K. E., Lichtenberg, M., Ralph, P. J., Kühl, M., and Wangpraseurt, D. (2014). Radiative energy budget reveals high photosynthetic efficiency in symbiont-bearing corals. *J. R. Soc. Interf.* 11:20130997. doi: 10.1098/rsif.2013.0997

Burns, N. M., and Rosa, F. (1980). *In situ* measurement of the settling velocity of organic carbon particles and 10 species of phytoplankton. *Limnol. Oceanogr.* 25, 855–864.

Cartaxana, P., Cruz, S., Gameiro, C., and Kühl, M. (2016a). Regulation of intertidal microphytobenthos photosynthesis over a diel emersion period is strongly affected by diatom migration patterns. *Front. Microbiol.* 7:872. doi: 10.3389/fmicb.2016.00872

Cartaxana, P., Ribeiro, L., Goessling, J. W. L., Cruz, S., and Kühl, M. (2016b). Light and O2 microenvironments in two contrasting diatom-dominated coastal sediments. *Mar. Ecol. Prog. Ser.* 545, 35–47.

Coelho, H., Vieira, S., and Serôdio, J. (2011). Endogenous versus environmental control of vertical migration by intertidal benthic microalgae. *Eur. J. Phycol.* 46, 271–281.

De Beer, D., and Stoodley, P. (2013). "Microbial biofilms," in *The Prokaryotes - Applied Bacteriology and Biotechnology*, eds E. Rosenberg, E. DeLong, E. Stackebrandt, S. Lory, and F. Thompson (Berlin: Springer-Verlag), 343–372.

de Wit, R., and van Gemerden, H. (1987). Oxidation of sulfide to thiosulfate by *Microcoleus chtonoplastes*. *FEMS Microbiol. Ecol.* 45, 7–13.

Dillon, J. G., Miller, S., Bebout, B., Hullar, M., Pinel, N., and Stahl, D. A. (2009). Spatial and temporal variability in a stratified hypersaline microbial mat community. *FEMS Microbiol. Ecol.* 68, 46–58. doi: 10.1111/j.1574-6941.2009.00647.x

Falkowski, P., and Raven, J. A. (2007). *Aquatic Photosynthesis*, 2nd Edn, Princeton: Princeton University Press.

Fourcans, A., de Oteyza, T. G., Wieland, A., Solé, A., Diestra, E., van Bleijswijk, J., et al. (2004). Characterization of functional bacterial groups in a hypersaline microbial mat community (Salins-de-Giraud, Camargue, France). *FEMS Microbiol. Ecol.* 51, 55–70. doi: 10.1016/j.femsec.2004.07.012

Frigaard, N. U., Takaichi, S., Hirota, M., Shimada, K., and Matsuura, K. (1997). Quinones in chlorosomes of green sulfur bacteria and their role in the redox-dependent fluorescence studied in chlorosome-like bacteriochlorophyll c aggregates. *Arch. Microbiol.* 167, 343–349.

Glagoleva, T. N., Glagolev, A. N., Gusev, M. V., and Nikitina, K. A. (1980). Protonmotive force supports gliding in cyanobacteria. *FEBS Lett.* 117, 49–53.

Gorton, H. L., Williams, W. E., and Vogelmann, T. C. (1999). Chloroplast movement in *Alocasia macrorrhiza*. *Physiol. Plant.* 106, 421–428.

Gupta, S., and Agrawal, S. C. (2007). Survival and motility of diatoms *Navicula grimmei* and *Nitzschia palea* affected by some physical and chemical factors. *Folia Microbiol.* 52, 127–134. doi: 10.1007/BF02932151

Häder, D. P. (1987). "Photomovement," in *The Cyanobacteria*, ed. P. Fay (Amsterdam: Elsevier Science Publishers), 325–345.

Halfen, L. N., and Castenholz, R. W. (1971). Energy expenditure for gliding motility in a blue-green alga. *J. Phycol.* 7, 258–260.

Hoiczyk, E. (2000). Gliding motility in cyanobacteria: observations and possible explanations. *Arch. Microbiol.* 174, 11–17. doi: 10.1007/s002030000187

Iglesias-Prieto, R., and Trench, R. K. (1994). Acclimation and adaptation to irradiance in symbiotic dinoflagellates. Responses of the photosynthetic unit to changes in photon flux density. *Mar. Ecol. Prog. Ser.* 113, 163–175.

Iglesias-Prieto, R., and Trench, R. K. (1997). Acclimation and adaptation to irradiance in symbiotic dinoflagellates. II. Response of chlorophyll-protein complexes to different photon-flux densities. *Mar. Biol.* 130, 23–33.

Jekely, G. (2009). Evolution of phototaxis. *Philos. T. R. Soc. B* 364, 2795–2808.

Jensen, J., and Revsbech, N. P. (1989). Photosynthesis and respiration of a diatom biofilm cultured in a new gradient growth chamber. *FEMS Microbiol. Ecol.* 5, 29–38.

Jimenez, I. M., Kühl, M., Larkum, A. W. D., and Ralph, P. J. (2008). Heat budget and thermal microenvironment of shallow-water corals: do massive corals get warmer than branching corals? *Limnol. Oceanogr.* 53, 1548–1561.

Jørgensen, B. B. (1982). Ecology of the bacteria of the sulfur cycle with special reference to anoxic oxic interface environments. *Philos. T. R. Soc. B* 298, 543–561. doi: 10.1098/rstb.1982.0096

Jørgensen, B. B., and Revsbech, N. P. (1983). Colorless sulfur bacteria, *Beggiatoa spp. and Thiovulum spp. in O*2 and H2S microgradients. *Appl. Environ. Microb.* 45, 1261–1270.

Kamp, A., Roy, H., and Schulz-Vogt, H. N. (2008). Video-supported analysis of *Beggiatoa* filament growth, breakage, and movement. *Microb. Ecol.* 56, 484–491. doi: 10.1007/s00248-008-9367-x

Klatt, J. M., Meyer, S., Häusler, S., Macalady, J. L., de Beer, D., and Polerecky, L. (2016). Structure and function of natural sulphide-oxidizing microbial mats under dynamic input of light and chemical energy. *ISME J.* 10, 921–933. doi: 10.1038/ismej.2015.167

Kress, E., and Jahns, P. (2017). The dynamics of energy dissipation and xanthophyll conversion in *Arabidopsis* indicate an indirect photoprotective role of zeaxanthin in slowly inducible and relaxing components of non-photochemical quenching of excitation energy. *Front. Plant Sci.* 8:2094. doi: 10.3389/fmicb.2016.002094

Kühl, M. (2005). Optical microsensors for analysis of microbial communities. *Environ. Microbiol.* 397, 166–199. doi: 10.1016/S0076-6879(05)97010-9

Kühl, M., and Fenchel, T. (2000). Bio-optical characteristics and the vertical distribution of photosynthetic pigments and photosynthesis in an artificial cyanobacterial mat. *Microb. Ecol.* 40, 94–103. doi: 10.1007/s002480000061

Kühl, M., Glud, R. N., Ploug, H., and Ramsing, N. B. (1996). Microenvironmental control of photosynthesis and photosynthesis-coupled respiration in an epilithic cyanobacterial biofilm. *J. Phycol.* 32, 799–812.

Kühl, M., and Jørgensen, B. B. (1994). The light-field of microbenthic communities - radiance distribution and microscale optics of sandy coastal sediments. *Limnol. Oceanogr.* 39, 1368–1398.

Kühl, M., Lassen, C., and Jørgensen, B. B. (1994). "Optical properties of microbial mats: Light measurements with fiber-optic microprobes," in *Microbial Mats*, eds L. Stal and P. Caumette (Berlin: Springer), 149–166.

Kühl, M., Lassen, C., and Revsbech, N. P. (1997). A simple light meter for measurements of PAR (400 to 700 nm) with fiber-optic microprobes: application for P vs E0(PAR) measurements in a microbial mat. *Aquat. Microb. Ecol.* 13, 197–207.

Kühl, M., Trampe, E., Mosshammer, M., Johnson, M., Larkum, A. W. D., Frigaard, N.-U., et al. (2020). Substantial near-infrared radiation-driven photosynthesis of chlorophyll *f*-containing cyanobacteria in a natural habitat. *eLife* 9:e50871. doi: 10.7554/eLife.50871

Lassen, C., Ploug, H., and Jørgensen, B. B. (1992). Microalgal photosynthesis and spectral scalar irradiance in coastal marine sediments of Limfjorden Denmark. *Limnol. Oceanogr.* 37, 760–772.

Laviale, M., Ezequiel, J., Pais, C., Cartaxana, P., and Serôdio, J. (2015). The "creme brulee" sampler: a new high-resolution method for the fast vertical sampling of intertidal fine sediments. *J. Exp. Mar. Biol. Ecol.* 468, 37–44.

Lichtenberg, M. (2017). *Microscale Canopy Interactions in Aquatic Phototrophs*. Ph.D. dissertation, University of Copenhagen.

Lichtenberg, M., Brodersen, K. E., and Kühl, M. (2017). Radiative energy budgets of phototrophic surface-associated microbial communities and their photosynthetic efficiency under diffuse and collimated light. *Front. Microbiol.* 8:452. doi: 10.3389/fmicb.2016.00452

Lichtenberg, M., Larkum, A. W. D., and Kühl, M. (2016). Photosynthetic acclimation of *Symbiodinium in hospite* depends on vertical position in the tissue of the scleractinian coral *Montastrea curta*. *Front. Microbiol.* 7:230. doi: 10.3389/fmicb.2016.00230

Lyndby, N. H., Kühl, M., and Wangpraseurt, D. (2016). Heat generation and light scattering of green fluorescent protein-like pigments in coral tissue. *Sci. Rep.* 6:26599. doi: 10.1038/srep26599

Müller, P., Li, X. P., and Niyogi, K. K. (2001). Non-photochemical quenching. A response to excess light energy. *Plant Physiol.* 125, 1558–1566. doi: 10.1104/pp.125.4.1558

Nelson, D. C., and Castenholz, R. W. (1981). Organic nutrition of *Beggiatoa sp*. *J. Bacteriol.* 147, 236–247.

Nielsen, M., Revsbech, N. P., and Kühl, M. (2015). Microsensor measurements of hydrogen gas dynamics in cyanobacterial microbial mats. *Front. Microbiol.* 6:726. doi: 10.3389/fmicb.2016.00726

Nymark, M., Valle, K. C., Brembu, T., Hancke, K., Winge, P., Andresen, K., et al. (2009). An integrated analysis of molecular acclimation to high light in the marine diatom *Phaeodactylum tricornutum*. *PLoS One* 4:e7743. doi: 10.1371/journal.pone.0007743

Ploug, H., Lassen, C., and Jørgensen, B. B. (1993). Action spectra of microalgal photosynthesis and depth distribution of spectral scalar irradiance in a coastal marine sediment of Limfjorden, Denmark. *FEMS Microbiol. Ecol.* 12, 69–78.

Preisler, A., de Beer, D., Lichtschlag, A., Lavik, G., Boetius, A., and Jorgensen, B. B. (2007). Biological and chemical sulfide oxidation in a *Beggiatoa* inhabited marine sediment. *ISME J.* 1, 341–353. doi: 10.1038/ismej.2007.50

Ramsing, N. B., and Prufert-Bebout, L. (1994). "Motility of *Microcoleus chthonoplastes* subjected to different light intensities quantified by digital image analysis," in *Microbial Mats*, eds L. J. Stal and P. Caumette (Berlin: Springer), 183–191.

Revsbech, N. P. (1989). An oxygen microsensor with a guard cathode. *Limnol. Oceanogr.* 34, 474–478.

Revsbech, N. P., and Jørgensen, B. B. (1983). Photosynthesis of benthic microflora measured with high spatial-resolution by the oxygen microprofile method - capabilities and limitations of the method. *Limnol. Oceanogr.* 28, 749–756.

Richardson, L. L., and Castenholz, R. W. (1987). Diel vertical movements of the cyanobacterium *Oscillatoria terebriformis* in a sulfide-rich hot spring microbial mat. *Appl. Environ. Microb.* 53, 2142–2150.

Rickelt, L., Lichtenberg, M., Trampe, E., and Kühl, M. (2016). Fiber-optic probes for small scale measurements of scalar irradiance. *Photochem. Photobiol.* 92, 331–342. doi: 10.1111/php.12560

Saenger, C., Miller, M., Smittenberg, R. H., and Sachs, J. P. (2006). A physico-chemical survey of inland lakes and saline ponds: Christmas Island (Kiritimati) and Washington (Teraina) Islands, Republic of Kiribati. *Saline Syst.* 2:8. doi: 10.1186/1746-1448-2-8

Sand-Jensen, K., Binzer, T., and Middelboe, A. L. (2007). Scaling of photosynthetic production of aquatic macrophytes - a review. *Oikos* 116, 280–294.

Serôdio, J., Coelho, H., Vieira, S., and Cruz, S. (2006). Microphytobenthos vertical migratory photoresponse as characterised by light-response curves of surface biomass. *Estuar. Coast. Shelf S* 68, 547–556.

Stal, L. J. (1995). Physiological ecology of cyanobacteria in microbial mats and other communities. *New Phytol.* 131, 1–32.

Stomp, M., Huisman, J., Stal, L. J., and Matthijs, H. C. (2007). Colorful niches of phototrophic microorganisms shaped by vibrations of the water molecule. *ISME J.* 1, 271–282. doi: 10.1038/ismej.2007.59

Tamulonis, C., Postma, M., and Kaandorp, J. (2011). Modeling filamentous cyanobacteria reveals the advantages of long and fast trichomes for optimizing light exposure. *PLoS One* 6:e22084. doi: 10.1371/journal.pone.00022084

Terashima, I., Ooeda, H., Fujita, T., and Oguchi, R. (2016). Light environment within a leaf. II. Progress in the past one-third century. *J. Plant Res.* 129, 353–363. doi: 10.1007/s10265-016-0808-1

Thauer, R. K., Jungermann, K., and Decker, K. (1977). Energy conservation in chemotrophic anaerobic bacteria. *Bacteriol. Rev.* 41, 100–180.

Trampe, E., and Kühl, M. (2016). Chlorophyll *f* distribution and dynamics in cyanobacterial beachrock biofilms. *J. Phycol.* 52, 990–996. doi: 10.1111/jpy.12450

van Gemerden, H. (1993). Microbial mats - a joint venture. *Mar. Geol.* 113, 3–25.

Vogelmann, T. C. (1993). Plant-tissue optics. *Annu. Rev. Plant. Phys.* 44, 231–251.

Wada, M., Kagawa, T., and Sato, Y. (2003). Chloroplast movement. *Annu. Rev. Plant. Biol.* 54, 455–468.

Wangpraseurt, D., Larkum, A. W. D., Franklin, J., Szabo, M., Ralph, P. J., and Kühl, M. (2014). Lateral light transfer ensures efficient resource distribution in symbiont-bearing corals. *J. Exp. Biol.* 217, 489–498. doi: 10.1242/jeb.091116

Wangpraseurt, D., Larkum, A. W. D., Ralph, P. J., and Kühl, M. (2012). Light gradients and optical microniches in coral tissues. *Front. Microbiol.* 3:316. doi: 10.3389/fmicb.2016.00316

Webb, W. L., Newton, M., and Starr, D. (1974). Carbon dioxide exchange of *Alnus rubra* - a mathematical model. *Oecologia* 17, 281–291. doi: 10.1007/BF00345747

Whale, G. F., and Walsby, A. E. (1984). Motility of the cyanobacterium *Microcoleus chthonoplastes* in mud. *Br. Phycol. J.* 19, 117–123.

Wieland, A., and Kühl, M. (2000). Irradiance and temperature regulation of oxygenic photosynthesis and O2 consumption in a hypersaline cyanobacterial mat (Solar Lake. Egypt). *Mar. Biol.* 137, 71–85.

Wieland, A., Kühl, M., McGowan, L., Fourcans, A., Duran, R., Caumette, P., et al. (2003). Microbial mats on the Orkney Islands revisited: microenvironment and microbial community composition. *Microb. Ecol.* 46, 371–390. doi: 10.1007/s00248-002-0108-2

Conflict of Interest: The authors declare that the research was conducted in the absence of any commercial or financial relationships that could be construed as a potential conflict of interest.

frontiers in Marine Science

ORIGINAL RESEARCH
published: 22 July 2020
doi: 10.3389/fmars.2020.00562

Microscale Variability in Biomass and Photosynthetic Activity of Microphytobenthos During a Spring-Neap Tidal Cycle

Jacco C. Kromkamp[1], Ed Morris[2] and Rodney M. Forster[3]**

[1] Royal Netherlands Institute for Sea Research, Department of Estuarine and Delta Systems, Utrecht University, Utrecht, Netherlands, [2] Vizzuality, Madrid, Spain, [3] Hull Marine Laboratory, Department of Biological and Marine Sciences, University of Hull, Hull, United Kingdom

Carbon fixation by microphytobenthic algae of intertidal flats often dominates the total primary production of turbid, temperate estuaries. Whilst remote sensing can accurately measure the spatial distribution of photosynthetic biofilms at the mesoscale (1–300 m), variability at smaller scales requires *in-situ* investigation. Here, changes in biomass and photosynthetic activity of microphytobenthos (MPB) at the micro-scale (<1 m) were investigated. Biomass of MPB was estimated from repeated high resolution spectral measurements carried out at intervals along a short transect. Whilst the mean concentration of MPB remained constant over time, considerable variability in the spatial and temporal dimensions was measured. The biofilm grew and diminished along the transect over time, and net growth and loss rates could be established under natural conditions. Daily vertical migration was observed for the first time in an undisturbed sediment, and was modeled as a function of solar elevation and tidal angle. Top down factors such as grazing, or physical disturbance, played an important role in the changes in biomass. Photosynthetic activity was measured with portable fluorometers: one device used an artificial light source, the other measured the effective photosystem-II quantum efficiency ($\Delta F/F_m'$) *in-situ* with solar irradiance. No evidence was found for photoinhibition, with F_v/F_m values consistently high, indicating an ability of the diatom biofilm to remain productive under periods of high irradiance. The maximum rate of photosynthesis reached with artificial light was rarely achieved *in-situ*, even with full solar exposure. There was, however, a very good agreement between the predicted rate at ambient irradiance, and that actually measured. Composite photosynthesis-irradiance curves over the whole experimental period were similar, and showed the same initial slopes, but the maximum rate of relative photosynthetic electron transport ($rETR_m$) based on the *in-situ* measurement was lower. When total depth-averaged primary production during low tide was calculated, the differences between methods varied between 5 and 13%, and were smallest when surface irradiance values were highest. These results show that the protocol used to measure the photosynthetic activity of the MPB had only minor importance on the overall productivity estimate compared to accurate knowledge of photosynthetically active biomass and irradiance.

Keywords: microphytobenthos, microscale variability, surface biofilm, photosynthetic activity, chlorophyll fluorescence, vertical migration, photosynthetic electron transport, estuary

OPEN ACCESS

Edited by:
Vona Meleder, Université de Nantes, France

Reviewed by:
Elena Maggi, University of Pisa, Italy
James L. Pinckney, University of South Carolina, United States

****Correspondence:***
Jacco C. Kromkamp
jacco.kromkamp@nioz.nl
Rodney M. Forster
r.forster@hull.ac.uk

Specialty section:
This article was submitted to Marine Ecosystem Ecology, a section of the journal Frontiers in Marine Science

Received: *06 December 2019*
Accepted: *18 June 2020*
Published: *22 July 2020*

Citation:
Kromkamp JC, Morris E and Forster RM (2020) Microscale Variability in Biomass and Photosynthetic Activity of Microphytobenthos During a Spring-Neap Tidal Cycle. Front. Mar. Sci. 7:562. doi: 10.3389/fmars.2020.00562

INTRODUCTION

Benthic microalgal communities are important ecological players on intertidal estuarine sediments. They can be responsible for a significant fraction of the total estuarine primary production (MacIntyre et al., 1996; Underwood and Kromkamp, 1999; Christianen et al., 2017), providing a range of ecosystem services (Hope et al., 2019), such as provision of a highly nutritious food source that can be used directly or indirectly by higher trophic levels including important wading bird populations (Kuwae et al., 2008). Microphytobenthos (MPB) can also be considered important ecosystem engineers as the presence of surface biofilms gives enhanced resistance against erosion (Paterson, 1989; Paterson and Black, 1999; Decho, 2000; Underwood and Paterson, 2003). This effect is most prominent on muddy, cohesive diatom-dominated sediments, where the excretion of extracellular polymeric substances improves the stabilization of mudflats (Smith and Underwood, 2000; Tolhurst et al., 2003). Of particular note here are microbial communities dominated by epipelic, pennate diatoms – biofilms of this type can accumulate multiple layers of cells with areal chlorophyll concentrations of over 200 mg m^{-2} (Forster et al., 2006; Sahan et al., 2007; Jesus et al., 2009).

Whilst the seasonal appearance of intertidal MPB blooms can display a remarkable synchronicity at the sea-basin scale (van der Wal et al., 2010), geostatistical analysis of *in-situ* data and remote sensing images has shown that MPB show spatial patchiness at a range of smaller distances (Ibrahim et al., 2014). Semivariograms constructed on MPB samples typically show a *range* (distance at which samples are not spatially autocorrelated) of 50–500 m (Morris, 2005; Orvain et al., 2012; Ibrahim et al., 2014). There are few estimates of microscale variability in MPB biomass i.e., at distances less than the typical spread of replicate samples at a point station (1–3 m).

In addition to spatial variability in the horizontal dimension, MPB of mud-dominated tidal flats exhibit a pronounced vertical variability due to migrations of diatom cells toward and away from the surface. The vertical migration may be driven by an endogenous clock as cells only come to the surface during low tide, and only when the low tide is during the day: at night cells remain below the sediment surface (Pinckney and Zingmark, 1991; Serôdio et al., 1997; Jesus et al., 2006). Due to the changes in photosynthetic biomass exposed to the light, vertical migration is a strong driver of daily primary production (Kwon et al., 2012; Haro et al., 2019). In addition to the tidally driven migration, epipelic diatoms may also change depth in relation to the light intensity and avoid too high light conditions (Cartaxana et al., 2008). The fact that, even after prolonged exposure to high light, effective photosynthetic quantum efficiencies can still be high prompted Kromkamp et al. (1998) to propose the concept of vertical "micro-migration" where cells at the surface migrate to slightly deeper layers in the sediment in order to prevent over-exposure to damaging irradiances or CO_2-limitation, whereas others cells migrate to the surface. Thus, the biofilm at the sediment surface is a dynamic, productive system where cells at the very surface are continuous being replaced by others (Marques da Silva et al., 2017). In contrast to vegetated coastal environments such as seagrass beds and salt marshes, very few estimates of the contribution of MPB to coastal primary production, or long-term carbon storage ("blue carbon") are available (Cahoon, 1999 for global MPB; Howard et al., 2017 for coastal vegetation).

Several techniques to measure the photosynthetic activity and primary production of MPB are available (see Kromkamp and Forster (2006) for a review on methodologies), which together with consideration of the above-mentioned spatio-temporal variability, may lead to better global estimates of MPB carbon fixation (Forster and Kromkamp, 2006). Measurements of variable fluorescence, using pulse-amplitude modulated (PAM) type fluorimeters have been used widely to assess the photosynthetic activity of intact MPB biofilms (Barranguet and Kromkamp, 2000; Cruz and Serôdio, 2008; Perkins et al., 2010). The advantage of this technique is that the photosynthetic activity can be assessed rapidly, making many measurements possible during a single low tide emersion period. Several different means of measuring the cardinal parameters of the photosynthesis-irradiance relationship using the variable fluorescence technique have been developed. Theoretically, "rapid light curves" measured on undisturbed biofilms, without a prior dark acclimation, and with short light steps, should measure photosynthetic rates close to that *in-situ*. Previous work has shown that the physiological information derived from photosynthesis-irradiance curves depends on the methodology used (Perkins et al., 2006; Serôdio et al., 2013). Following measurement of electron transport rates, conversion of relative rates of photosynthesis to depth integrated carbon-fixation rate is complicated because the variable fluorescence technique requires calibration. In experiments on the electron requirement for carbon fixation, Barranguet and Kromkamp (2000) obtained a conversion factor of 0.043 when the depth-integrated rates of relative electron transport was regressed against depth-integrated rates of carbon-fixation obtained from short-term ^{14}C-incubations on MPB suspended in water. However, it can be expected that this value will depend on the environmental conditions (Lawrenz et al., 2013). Quantifying the light absorbed by the surface biofilm is difficult but taking the baseline fluorescence level (F_o) as a proxy for the light absorbed has shown to be a useful approach (Serôdio, 2003). Méléder and co-workers have developed an optical primary production model based on hyperspectral reflectance (Méléder et al., 2018; Launeau et al., 2018), but the model needs further validation with *in-situ* data.

Here, a 2-week period of intensive, non-destructive optical measurements of an intertidal mudflat is used to address unknowns in three key areas of MPB ecology: spatial and temporal variability of surface photosynthetic biofilms, patterns of vertical migration allowing biofilm formation on the sediment surface, and environmental controls of photosynthesis in undisturbed MPB biofilms in the field in relation to the use of variable fluorescence. The development of small-scale patchiness and photosynthetic activity was measured quasi-continuously during a spring-neap cycle in a temperate estuarine setting. High resolution optical measurements were used to track changes in surface photosynthetic biomass, and photosynthesis was measured using a rapid light curve

(RLC) with sequential increases in irradiance, together with measurement of photosystem-II quantum efficiency under naturally fluctuating solar irradiance. As the latter gives an instantaneous measurement of the photosynthetic activity it should be possible to assess if the standard sequential RLCs give the same information, or that the method introduces artifacts. Together, the data set allows the investigation of the effect of patchiness and changing environmental conditions during the spring-neap cycle on the photosynthetic activity.

MATERIALS AND METHODS

Study Site

The experiment took place during May 2003 at a site in the Kapelle Bank, in the Westerschelde estuary (**Figure 1**). The site was located close to the foot of a dyke (Netherlands National Grid, RD 056368, 386506 or WGS84: N 51°27.539′E 003°58.078′), at a shore height with equal immersion and emersion times of approximately 6 h. At the beginning of the experiment on 15 May the whole of this intertidal bay had a dense cover of epipelic diatoms. The measurements were taken approximately 5 m from the foot of the dike. A sampling bridge was constructed from wooden pallets and bricks in order to reach the site without causing disturbance (**Figure 2**).

A frame was placed at the front of the sampling bridge, creating a 1.05 m long transect along which detailed hyperspectral reflectance measurements were made at eight evenly spaced positions along the transect in order to follow the dynamics in MPB biomass. The bridge was removed after every sampling in order to prevent changes in current velocity during the high water period. Two anchor points ensured that the frame was always in the exact same location. Sampling was done at 2-day intervals for a period of 2 weeks during daytime low tides, with 15 min-to-hourly measurement intervals. The final sampling was on 28 May. Fluorescence measurements for photosynthetic activity were measured just outside the frame in order not to disturb the biomass dynamics along the 1 m transect.

Measurements

Two optical techniques were used to quantify MPB biomass: chlorophyll fluorescence (Honeywill et al., 2002; Jesus et al., 2005; Kromkamp et al., 2006), and hyperspectral reflectance (Forster and Jesus, 2006; Kromkamp et al., 2006). The advantage of the latter technique is that the signal is not influenced by fluorescence quenching in bright light, which can lead to an underestimation of the real chlorophyll concentration at the sediment surface. Indices based on hyperspectral reflectance measurements (such as the normalized difference vegetation index (NDVI; Kromkamp et al., 2006) have been shown to correlate very well with measured chlorophyll concentrations of the sediment surface, thus opening the applicability of remote sensing techniques to study spatial distribution patterns of MPB over large scales using drones or satellite remote sensing (van der Wal et al., 2010; Daggers et al., 2018; Launeau et al., 2018).

Reflectance Measurements

Hyperspectral reflectance was measured with a Ramses ARC-VIS spectrometer (TriOS optical sensors, Germany) with a 7° field of view as Lu_s/Lu_r where Lu is the reflected upwelling radiance

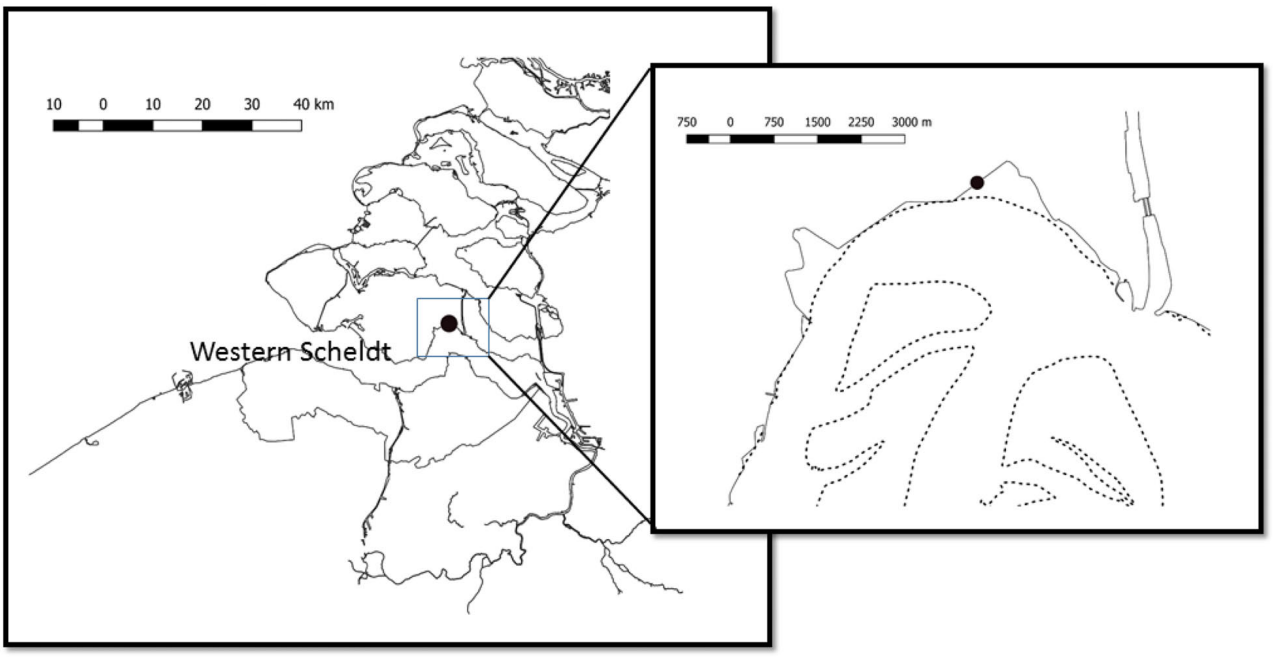

FIGURE 1 | Location of the study site at the Kapelle Bank within the Westerschelde (Western Scheldt) estuary in the south-west of Netherlands. The dotted lines show the mean low tide line delimiting intertidal flats.

FIGURE 2 | Setup of the sampling platform showing the removable "bridge" to the 1-m transect marked by the vertical frame to the left of the image.

from the sediment and the reflectance standard, respectively. A white polystyrene plate served as standard. The reflectance of this plate was calibrated against a white Spectralon reflectance standard with 99% reflectance (Labsphere Inc., North Sutton, NH, United States). The spectral characteristics of polystyrene plate differed less than 5% as compared to the Spectralon standard (Kromkamp et al., 2006). Dynamic changes in MPB biomass during low tide were followed using the normalized difference vegetation index (NDVI) which was calculated as NDVI = (R750 – R675)/(R750 + R675) where R750 and R675 are the measured reflectances at 750 and 675 nm, respectively. A linear relationship between NDVI and chlorophyll-*a* (chl *a*) concentrations (as mg chla m^{-2}) was found by Kromkamp et al. (2006). Although NDVI values could be converted to chl *a* using the relationship published in that paper specific for the Westerschelde mud habitat (Grid YA, chl *a* = 437 × NDVI + 21), we choose to present the raw NDVI values as a proxy for MPB biomass to facilitate comparison with other MPB remote sensing studies. Reflectance measurements were performed at 15 cm intervals along the 1.05 m transect with duplicate measurements at hourly intervals. In total, 826 reflectance spectra were collected over 2 weeks.

Relative growth rate was estimated as the change in NDVI for a sampling position between successive measurement events at time 1 and time 2:

$$RGR = (\ln(NDVI_2) - \ln(NDVI_1))/(t_2 - t_1)$$

Vertical migration of the biomass was predicted using the model of Pinckney and Zingmark (1991). A standardized tide angle was obtained by multiplying the time interval between the time of measurement and the previous time of high tide with a conversion factor, which was obtained from the time interval between successive high tides divided by 360°. The sun angle at a particular time was calculated by dividing the time interval between local sunrise and sunset by 180° and multiplying this difference with the same conversion factor. Three NDVI proxies were calculated: (1) The measured normalized average NDVI along the transect where the initial value upon arrival at the site immediately after tidal emersion was set to 1. (2) The raw predicted NDVI: this property was calculated as [(A × tide + sun angle) + B] + (C × sun angle) + D, where A (=2.020073), B (0.452419), C (0.375736), and D (0.452149) are fit constants. (3) The normalized predicted NDVI. The Solver function of Microsoft Excel was used to optimize the model fit over the 2-week period by optimizing the values of A, B, C, and D.

Variable Fluorescence Measurements

Photosynthetic activity was measured in two ways:

(1) A Diving-PAM (Walz GmbH, Germany) measured at 5 min intervals the *in-situ* activity of the undisturbed MPB biofilm. This was done by placing the optical fiber of the Diving-PAM in a customized holder with a 45° angle very close to a randomly selected area of the sediment surface. The angle of the fiber ensured that the fiber did not cast a shadow on the sediment. At the same time the ambient solar irradiance was measured using the light sensor of the Diving-PAM which was cross calibrated against a LiCor LI-190R photosynthetically active radiation (PAR) quantum sensor.
(2) Rapid light curves were made using a Mini-PAM (Walz GmbH, Germany) with 15 min dark acclimation and 30 s light steps. The optical fiber of the MiniPAM was placed in a custom-made dark chamber in such a way that the tip of the fiber was held vertically 4 mm above the sediment surface. At this distance the irradiance values generated by the RLC protocol of the mini-PAM using an internal halogen light source were calibrated using the same LiCor LI-190R as used for calibrating the Diving-PAM PAR values.

The measurement of minimal and maximum fluorescence was done before (F_o) and during a saturating flash (F_m) using previously optimized instrument settings for both variants of the method.

Quality control: fluorescence values below the detection limit of the fluorimeters were removed. The quantum yield (F_v/F_m in the dark-acclimated state, or $\Delta F/F_m'$ in the light, Kromkamp and Forster, 2006) was calculated from $F_v = F_m - F_o$ after subtraction of a blank value determined on chlorophyll-free sediment. After QC, a total of 709 dark-adapted F_v/F_m measurements, 793 $\Delta F/F_m$' measurements in natural sunlight, and 109 RLCs with artificial light were measured over 2 weeks. Data were stored in a relational database to enable linkages to be built between environmental data and optical data. The data in this paper can be obtained from the following http://www.vliz.be/en/imis?module=datasetanddasid=1213. Results were summarized into 1-h time blocks for further analysis.

The relative rate of photosystem-II electron transport (rETR) was calculated as rETR = PAR × Y_{II}, where Y_{II} is the effective quantum efficiency measured by the variable fluorescence technique (Kromkamp and Forster, 2006). The RLCs were fitted using the model of Webb et al. (1974). The parameters describing the fit are $rETR_m$ (the maximum rate of rETR) and α_{rETR} (the initial slope), E_k (the irradiance at which rETR saturated was calculated as $rETR_m/\alpha_{rETR}$. In addition, α_{rETR} was also calculated using linear regression through the initial points of the RLC, as the fitting of the data especially at high light influenced the value of the initial slope.

Statistical analyses were carried out in R (R Core Team, 2018) using R-studio (RStudio Team, 2020).

Ancillary Measurements

Air temperatures were measured with a thermometer whereas sediment temperatures were measured with a DivingPAM temperature probe placed in the surface layer. Solar irradiance values were recorded with a LiCor-LI190R-PAR quantum sensor in the field, and a LI-1000 datalogger on the roof of the institute located 10 km from the field site. Rain data from the nearest station at Vlissingen was obtained from the Dutch Meteorological Office (KNMI, available at https://climexp.knmi.nl/data/rxrx310.dat).

RESULTS

Meteorological Conditions During the Study

The measurement series started on spring tides centered on 15 to 20 May, during which time the prevailing weather conditions were overcast skies with light rainfall and cool daily mean air temperatures of between 11.1 and 14.2°C (**Figure 3**). Overcast conditions continued as tidal range decreased toward neap tides centered on 22 to 26 May, before a period of clearer skies, light winds, no precipitation, and increasing air temperature became established for the remainder of the experiment (**Figure 3**). Mud surface temperature (MST) tracked air temperature on cloudy days, but absorption of solar energy caused an additional warming on days with high PAR, resulting in warming of the surface to over 25°C. An empirical linear relationship was established relating MST to PAR over the duration of the study, with 43 paired temperature data points:

MST = b+(a*PAR); where b is the initial temperature of the mud surface upon emersion (10°C), and a is a scaling factor of 0.012. r^2 of the relationship was 0.73.

Changes in MPB Biomass

An average NDVI of 0.269 (with a standard deviation 0.134, lowest value 0.051, highest value 0.690) was estimated for the whole study period, across all times and grid positions.

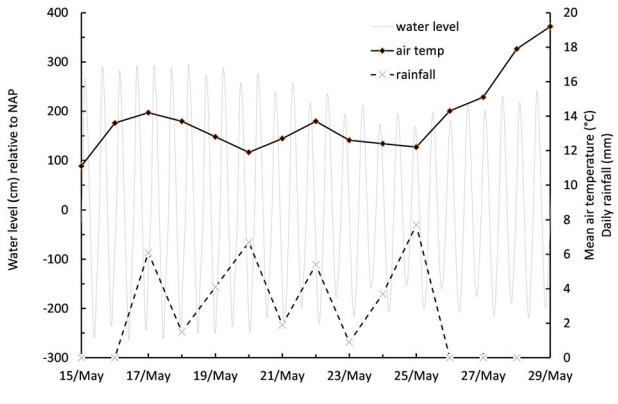

FIGURE 3 | Meteorological and tidal conditions during the measurement period from May 15 to May 28.

Conversion to chl *a* resulted in a mean value of 138 mg m^{-2}, which was within the expected range for the spring growth period of MPB at this and other temperate intertidal sites. However, within the overall mean NDVI value over 14 days was hidden a great deal of variability both spatially (at microscale) and temporally (hourly, daily).

Microscale spatial variability was estimated from the coefficient of variability (CV; standard deviation/mean) values along the transect line for each measurement day. Initially, CV was low with values of between 26 and 29% for the period 15 May to 19 May, then variability increased sharply to 63% on the following measurement day (21 May). This was due to a rise in NDVI at position 7, with falls in NDVI at all other positions (**Figures 4**, **5**). Spatial variability then decreased to 60% on 23 May and decreased further to 40% by the final measuring day. The mean spatial CV across the experimental period was 42%.

Other than positions 3 and 8, which decreased in NDVI over the spring-neap cycle, all other positions showed an increase in biomass (**Figure 4**), however, biomass was generally lowest around day 6 to 8, after which some increase was noticeable again. Analysis of the position-specific relative growth rate between successive sampling events showed that the number of events with a decreased NDVI (27 events with RGR from −0.51 to 0 d^{-1}) was approximately equal to the number of events with a positive growth rate (30 events with RGR from 0 to 0.57 d^{-1}). The spatial patterns become more obvious when the NDVI data are plotted as a contour plot (**Figure 5**). Growth rate was positive with a mean value of 0.38 d^{-1} for all positions over the first 2 days, followed by a 6-day period of declining NDVI from 19 to 23 May (**Figures 4**, **5**), then a phase of weak positive growth through to 28 May. Integrating NDVI values over the whole 2-week period gave an overall growth rate of 0.02 d^{-1}, resulting in an increase in NDVI of 40% in 2 weeks. The mean temporal CV across the experimental period was 47%.

It was apparent from **Figure 4**, where within-day values are shown, that a pronounced daily variability in NDVI at the different positions along the 1 m transect was also present. Further examination showed a clear and predictable pattern, with an increase in values in the first 2 h following exposure of the tidal flat, followed by a later decrease before the tide returned. The extent and shape of the profile varied per location and day. For detailed analysis, the daily pattern of NDVI at position 2 was plotted for 4 days throughout the series with different incident irradiance levels (**Figure 6**), thus showing the extent of dynamic behavior due to vertical migration and giving a clear demonstration of how quickly the surface photosynthetic biomass can change.

The examples in **Figure 6** clearly suggested that the timing of the migration was coupled to both the timing of the low tide and time of day, as the maximum recorded NDVI values were intermediate between the times of low tide (marked with red line), and time of peak irradiance. Temporary decreases in NDVI, for example at 09:00 on day 5 (19 May) were occasionally observed in association with a decrease in solar irradiance due to clouds, but this was not consistent. A large decrease in irradiance around 11:00 on Day 3 (17 May) was not followed by a

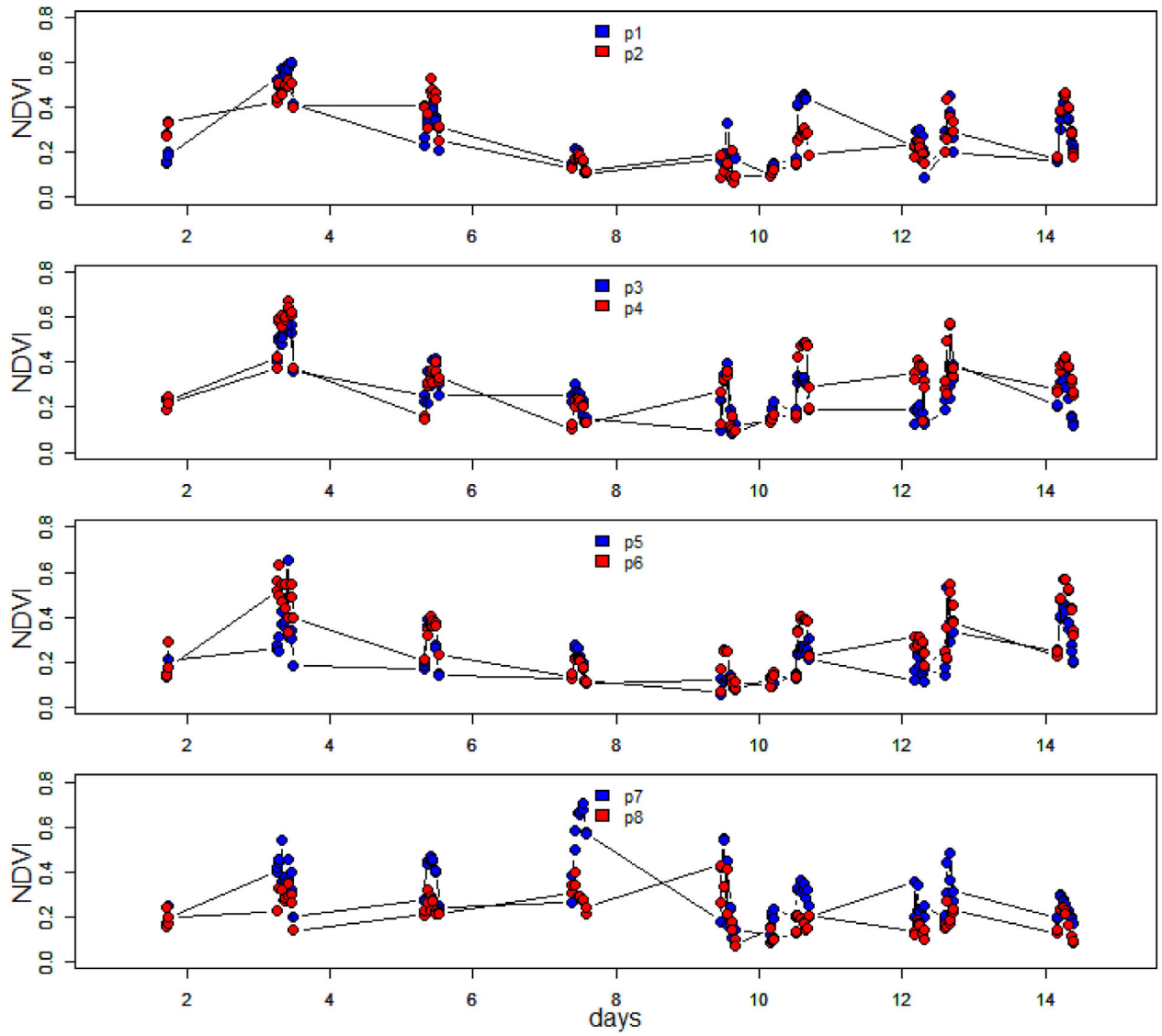

FIGURE 4 | Time series of hourly averaged NDVI over the spring-neap-spring measuring period at the eight different positions along the 1-m transect. The site was sampled every 2 days.

decrease in NDVI. On day 14 the mudflat was visited early in the morning at sunrise and it was noticed that the algae had already migrated to the sediment surface during the end of night, with a NDVI value of 0.25.

To further investigate the dependency on tidal state and time of day, the change in NDVI was calculated for each tidal period in relation to the initial NDVI value upon first exposure. A predicted NDVI for each time point was then calculated using tidal and solar elevation coefficients according to Pinckney and Zingmark (1991) (see section "Materials and Methods" for details). Graphs of measured versus predicted NDVI clearly showed that the timing of the migration was more coupled strongly to the timing of the tide (**Figure 7**), with a weaker association with solar elevation. Instances of NDVI rising as solar elevation was decreasing were recorded on the afternoon and evening tides of day 12 and 14. Deviations from the predicted values occurred on days 3, 9, and 10 (**Figure 7**). The predicted level of surface biomass failed to appear on day 3 and day 9, whereas biomass on day 10 was higher than predicted from the initial values. Plotted as a function of the measured normalized NDVI values, the predicted values from tidal and sun angle modeling show a correlation (**Figure 8**; $r^2 = 0.59$ $n = 103$). The role of the tidal cycle alone as the leading factor in determining the pattern of surface biomass was demonstrated by a high r^2 of 0.56 when solar angle was excluded. Excluding the anomalous days 3, 9, and 10 improved the r^2 value to 0.87.

Photosynthetic Activity

Maximum quantum efficiencies (dark-acclimated F_v/F_m) during the low tide periods are plotted in **Figure 9**. Sampling started

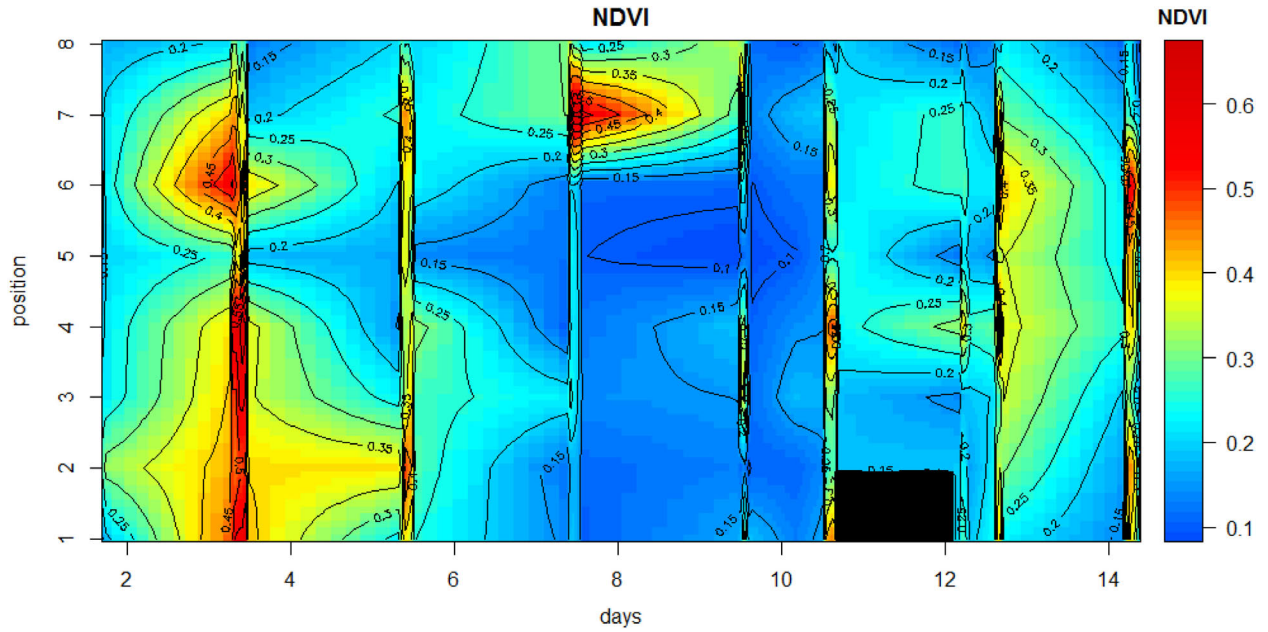

FIGURE 5 | Contour plot of the changes in NDVI along the 1-m transect during the measuring period. The days on which no measurements were carried out were omitted from the data plot in order to avoid gaps in the plot.

on the evening tide of Day 1 (15 May) with high F_v/F_m values (above 0.75). On day 3, F_v/F_m values were high during the initial phase of the morning low tide as the irradiance was still low (see **Supplementary Figure S1**). When the irradiance rapidly rose to >1500 μmol photons m^{-2} s^{-1} around 9:00, F_v/F_m decreased over time to 0.68. F_v/F_m values remained consistently high (up to 0.77) during the early morning and late evenings of the entire experiment, although small differences were noticeable between days. F_v/F_m on day 5 was higher than on day 7 which correspond to the fact that irradiance values reached higher values on day 7 than on day 5 (**Supplementary Figure S1**), but differences were small and values never were smaller than 0.66. Days 9 and 10 had similar irradiance values and the F_v/F_m values were also very similar. Days 12 and 14 showed a small decline in F_v/F_m, during the morning low tide period, which was more pronounced in day 14 as the low tide extended more into the morning when F_v/F_m decreased steadily from 0.75 at 4:30 to 0.66 at 9:30. Both days had clear skies and irradiance rose steady to 1500 μmol photons m^{-2} s^{-1} during the end of the morning low tide at day 14.

Rapid light curves (RLC) were measured between 5 and 18 times per day during the low tide phase. The initial slope of the RLC showed more variability than dark-acclimated F_v/F_m, with values lower during periods of high PAR (**Supplementary Figure S2**). In contrast, the maximum rates of light-saturated relative photosynthetic electron transport ($rETR_m$) had a mean value of 592 units, but showed considerable variability, as shown as a function of time during low tide (**Figure 10**). For example, during the morning of day 3 it can be seen that the hourly mean $rETR_m$ almost doubled over 5 h from 350 to ∼ 700 (relative units). During this period light intensities were rather low (<500 μmol photons m^{-2} s^{-1}, see **Supplementary Figure S1**). Between 9:00 and 11:00 $rETR_m$ transiently dropped to 460–512 units, and this coincided with a period of higher irradiance (>1200 μmol photons m^{-2} s^{-1}, see **Supplementary Figure S1**). Values recovered later in the afternoon when the surface irradiance decreased again. On day 5, which was overcast with PAR values <500 μmol photons m^{-2} s^{-1}, $rETR_m$ remained relatively stable at a value of 540 to 620 except for two higher values at 9:00 and 12:00. On day 7, $rETR_m$ remained relatively stable from 10:00 to 13:00 then rose to the highest value recorded in the 2 week period of 933 units at 14:00 (datapoint off upper limit of **Figure 10** *y*-axis). On days 9 and 10, $rETR_m$ varied around 600, except for a low value of 330 units at 15:00. The first low tide of day 12 showed a threefold increase in $rETR_m$ (but with fluctuations), which coincided with the morning increase in irradiance on a cloudless day. Interestingly, this increase occurred despite a very small decrease in F_v/F_m, showing that F_v/F_m is a poor predictor for the photosynthetic potential. The same pattern was seen on the morning low tide of day 14 with values increasing from 540 to 850 units. The afternoon period of decreasing irradiance during the second low tide on day 12 showed decreasing $rETR_m$. Although the daily values in $rETR_m$ were rather similar, the differences between the days were significant (Wilcoxon text, W = 9801, p-value < $2.2e^{-16}$). In a multiple regression, mud temperature at the time of measurement was weakly positively related to ETR_{max} but instantaneous irradiance did not have a significant effect. $rETR_m$ and α_{rETR} were not related (**Supplementary Figure S3**), indicating E_k-independent photoacclimation (Behrenfeld et al., 2004).

The light saturation parameter E_k is shown in **Supplementary Figure S4**. As the variability in the α_{rETR} was rather limited and

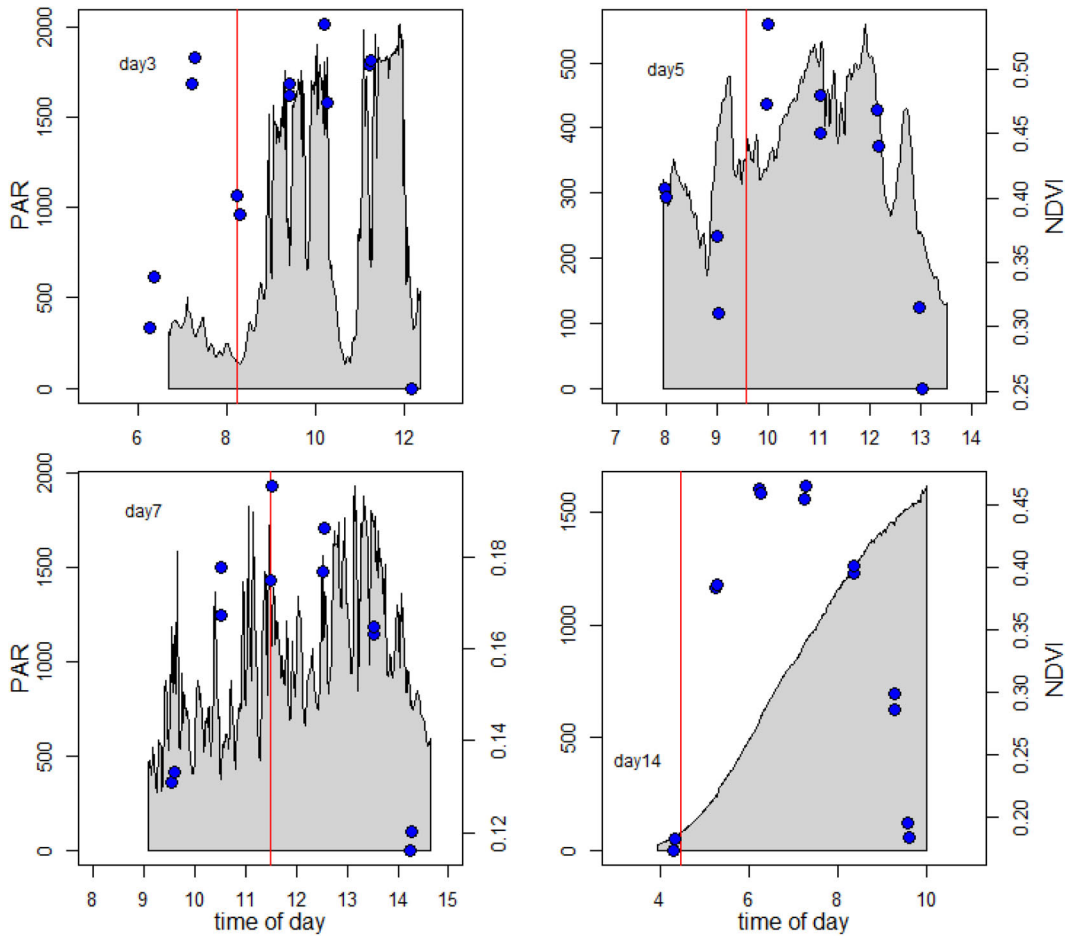

FIGURE 6 | Vertical migration patterns. The blue symbols show the measured NDVI data. The gray area shows the surface solar irradiance during the measuring period. The vertical red line gives the time of low tide.

not related to changes in $rETR_m$, changes in E_k followed those in $rETR_m$ closely.

Apart from measuring the light-dependent photosynthetic activity with RLCs using the inbuilt light source of a portable fluorimeter, the *in-situ* quantum efficiency of the surface biofilm with natural solar irradiance was measured using a second PAM instrument. Simultaneous recording of the solar irradiance allowed the calculation of the *in-situ* rETR from light-acclimated PSII yields. From the artificial light RLCs taken within the same hourly time interval the rETR at the same light intensity as that recorded for solar-exposed biofilms was calculated, and the two rates compared to each other (**Figure 10**). On day 1, the solar *in-situ* measurements were missing. On day 3 the rETR measured at 7:00 and 10:00 were identical, but for the other time points the rETR rates calculated from the RLCs were slightly higher than the ones based on the *in-situ* measurements (**Figure 10**). Nevertheless, the daily pattern in photosynthetic activity was rather similar. On days 5, 9, and 10 the results of both measurements were virtually identical. On day 7 the estimates of rETR at 10:00, 11:00 and 13:00 GMT were similar but at 12:00 and 14:00 rETR derived from the RLCs were lower than those based on the *in-situ* measurements (thus the opposite results as compared to day 3). On day 12, rETR based on the RLCs of the last time point of the morning low tide and the first point of the afternoon low tide gave higher values than the ones based on the *in-situ* measurements, and on day 14 the RLCs gave in general slightly higher rETR values than the ones determined with the solar *in-situ* measurements. But in all cases, both approaches gave the same daily patterns and the results were often very similar. It is apparent from **Figure 10** that the theoretical maximum rate of electron transport, $rETR_m$, was rarely reached, even with solar irradiances over 1000 μmol photons m^{-2} s^{-1}. Complete light saturation was only reached on days 3 and 7 (**Figure 10**), and all other days showed that the operationally achieved rate of electron transport was well below the theoretical maximum.

The two independent measurements of rETR were plotted as a single "composite" RLC (**Figure 11**). Both curves were similar, but the *in-situ* composite RLC with solar irradiance had a higher α_{rETR} and a lower $rETR_m$ when compared to the same data obtained from the RLC made with the artificial light source and step-wise increases in irradiance. The values of both type of measurements were fitted according to the

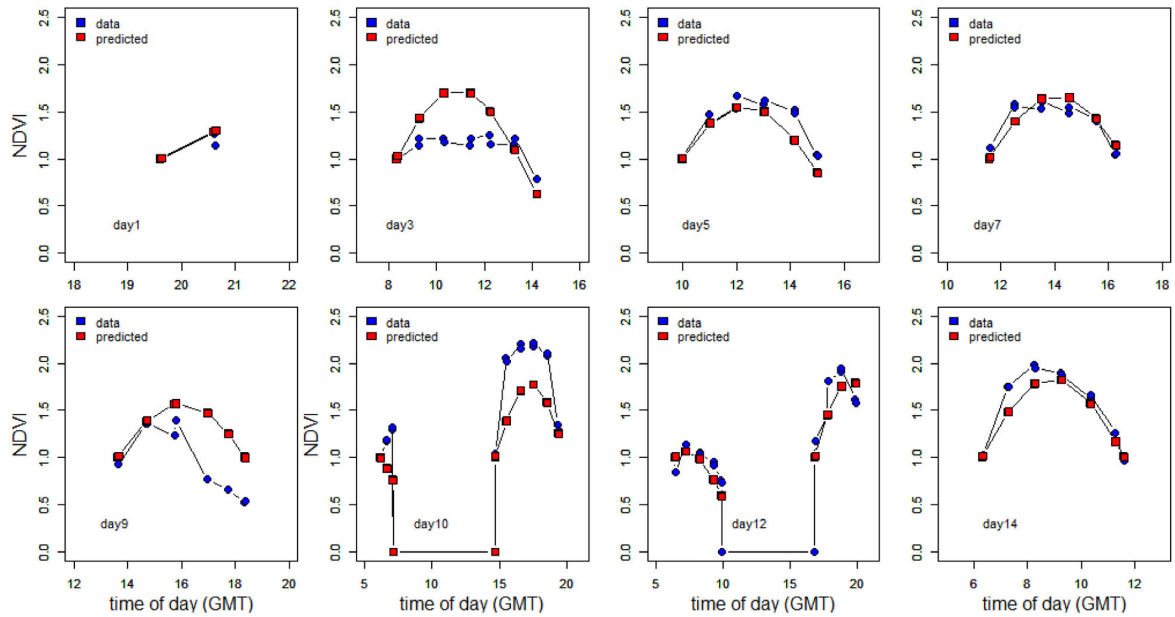

FIGURE 7 | Measured vs. predicted NDVI values. The NDVI values were normalized to the initial values measured immediately after emersion of the tidal flat.

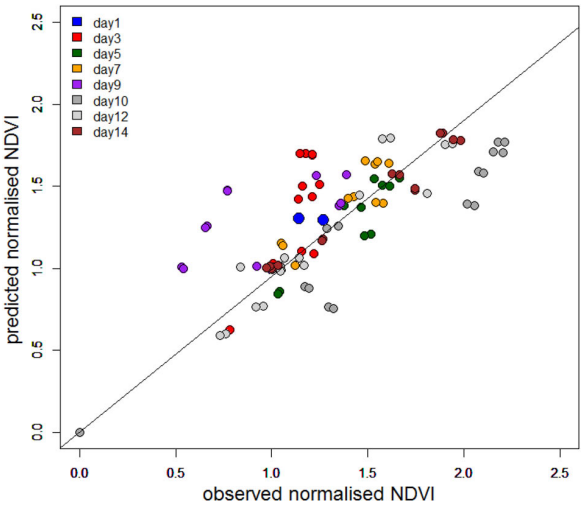

FIGURE 8 | Predicted normalized NDVI using the model of Pinckney and Zingmark (1991) against normalized NDVI from field measurements.

photosynthesis model of Webb et al. (1974) in order to get the RLC parameters describing the relationships between the surface incident PAR and the relative rate of photosynthetic electron transport (**Table 1**). To test if these differences were significant, a non-linear method in R which included the method as factor was applied. The results showed that the initial slopes of the synthetic light curves (α_{rETR}) between the two methods were not significantly different. The differences in the maximum rate of rETR were significant (p = 0.034) (see **Supplementary Table S1** for details).

To investigate the effect of different method choice on daily sediment integrated primary production we modeled 3 days (day 3, 5, and 7) using the hourly averaged irradiance and assumed a light attenuation coefficient within the sediment of 2.5 mm^{-1} or 3 mm^{-1} (Forster and Kromkamp, 2006). This was done using the fit parameters describing the RLCs shown in **Table 1**. The results of this exercise show that if the data from the RLCs are used (RLCfit), the total depth-integrated production rate during the low tide period is lower than the results obtained from the *in-situ* derived fit-constants. At first glance this might seem surprising, as the $rETR_m$ based on the RLC data is higher than the one obtained from the *in-situ* measurements, but the crossover points of both curves is approximate 600 μmol photons m^{-2} s^{-1}, so as long as the surface irradiance <600 μmol photons m^{-2} s^{-1} the higher α_{rETR} of the *in-situ* fitted data will return higher productivity values, and this was observed (although they were not significantly different as the α_{rETR} values were not significantly different). The difference depended on the surface irradiance: on day 5 irradiance values were lowest, and the productivity obtained from the RLC-fitted data was 87% from those based on the *in-situ* data. With higher irradiance, the difference was smaller: on day 3 several hours exceeded 1500 μmol photons m^{-2} s^{-1} and in this case the difference was within ∼ 5%. The differences in the estimates were independent of the K_d-value (**Table 2**).

DISCUSSION

The aim of this work had three components: (1) to investigate the nature of microscale patchiness of diatom-dominated biofilms over a typical growth period (spring-neap tidal cycle), (2) to investigate the nature of vertical migration under natural

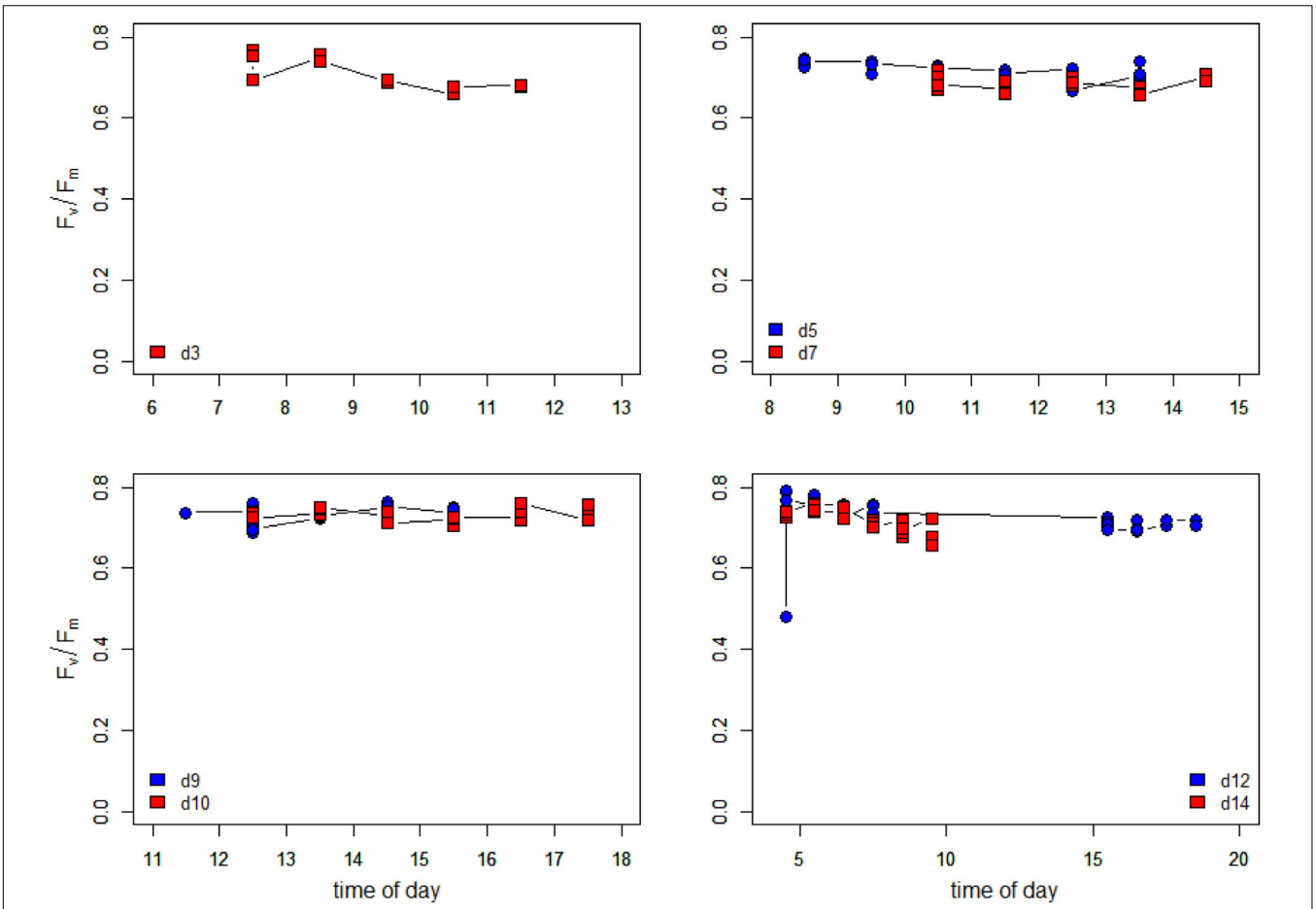

FIGURE 9 | Changes in the maximum PSII efficiency (dark-acclimated F_v/F_m) during the days of the measurements. Data are the average of hourly time blocks.

conditions and (3) to quantify the rate of photosynthesis over an extended period, and to compare different measuring approaches (artificial light given as sequential light curves versus steady-state photosynthesis in natural solar irradiance). The work took place during the spring growth period when diatom-dominated biofilms are a major ecological feature of temperate soft-sediment intertidal zones (van der Wal et al., 2010). A conspicuous surface biofilm was well-established over the entire tidal flat at the start of the measurement period, and observations of the wider area around the experiment suggested that biomass was maintained at a constant level throughout the spring-neap-spring cycle. A revisit of the site in June showed that the surface biofilm had greatly decreased, leaving no visible patches of MPB. For the one-meter transect itself, although there was no net increase or decrease in mean photosynthetic biomass during the sampling period, continuous changes in the surface concentration were evident in space and time.

Using NDVI as proxy, the extent of microscale variability was revealed to be of similar magnitude in space and in time. The picture made visible by the contour plot clearly shows that local high patches of biomass can disappear quickly and establish themselves at a nearby but different location. The overall patterns showed some dependency on the tide: at the start and end of the experiment the low tides were in general in the middle of the day whereas on days 10–14 the low tides were in the early morning and evening. Nevertheless, high biomass could develop under both tidal conditions as shown when days 3 and 5 (low tide during the middle of the day) and day 12 and 14 (high tide at the middle of the day) were compared. Tidal phase is not the only factor explaining the biomass development. The correlation between maximum NDVI and total light exposure was very weak and not significant (r^2 = 0.11, p = 0.47). It is likely that the spatial dynamics in MPB biomass were mainly the result of varying local grazing pressure. Periods of increasing microphytobenthic biomass, due to growth and division of diatom cells, were matched by periods of loss due to grazing, bioturbation (leading to deep burial of cells), or resuspension events. Net growth rate estimated from successive reflectance measurements at 2-day intervals showed maximum values of 0.38 d^{-1}, equivalent to a doubling time of 1.8 days. In comparison, an MPB growth rate of 0.46 d^{-1} was recorded during early growth of a diatom biofilm in a tidal mesocosm tank from which all grazers had been removed (Morris et al., 2008). Loss rates were of the same order as growth rates, and the dominance of growth

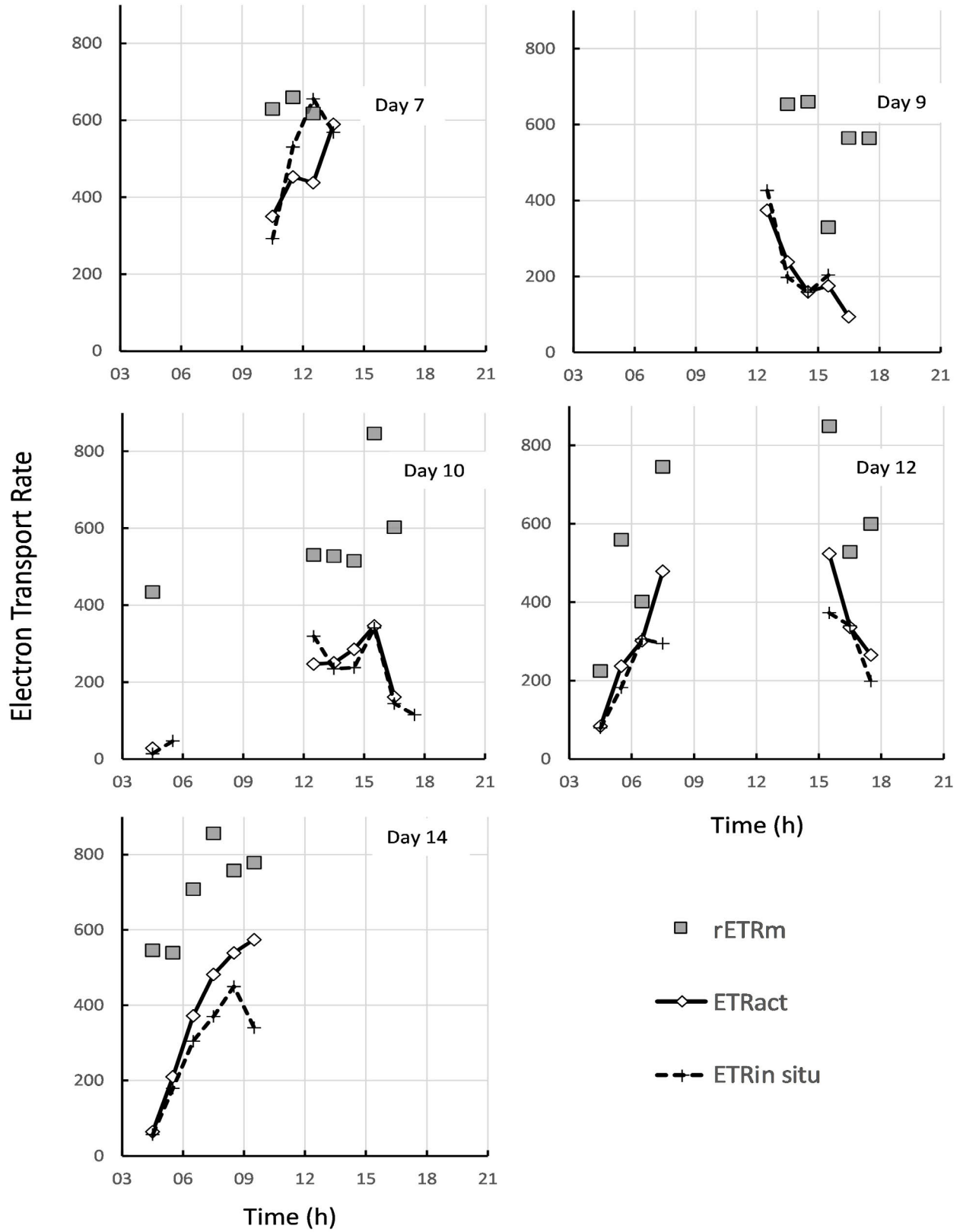

FIGURE 10 | Comparison of the theoretical maximum rate of electron transport $rETR_m$ estimated from rapid light curves (gray squares), with the estimated *in-situ* ETR in ambient light (gray diamonds), and the actual *in-situ* rate measured directly in ambient solar irradiance (dashed line with crosses).

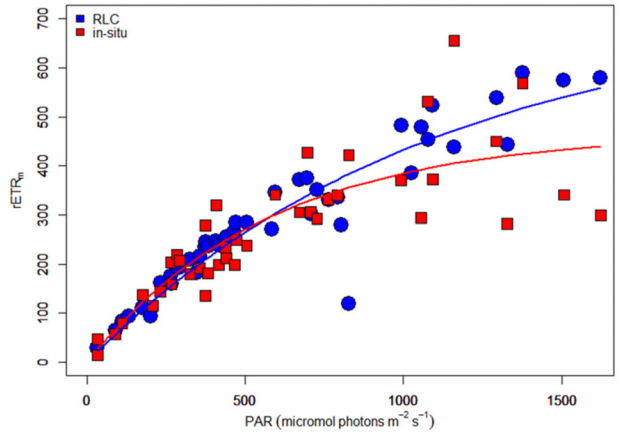

FIGURE 11 | "Composite" rapid light curves (electron transport rate versus irradiance) based on data obtained with sequential steps of increasing artificial light (blue dots) or naturally varying ambient solar irradiance data (red squares). The lines give the predicted rETR rates obtained from a fit of the data to the equation of Webb et al. (1974).

TABLE 1 | Fit parameters [obtained using the model of Webb et al. (1974) for the composite RLC shown in **Figure 11**].

	RLC parameters obtained from fitted data				
	rETRm	**std-err**	**alpha**	**std-err**	***p***
RLC	726.4	91.4	0.658	0.050	<0.001
In-situ	468.3	48.6	0.808	0.101	<0.001

TABLE 2 | Total depth integrated relative photosynthetic electron transport rates (relative units) for the low tide period shown in days 3, 5, and 7 (**Figure 5**).

	K_d = 2.5 mm^{-1}			K_d = 3 mm^{-1}		
	Day 3	**Day 5**	**Day 7**	**Day 3**	**Day 5**	**Day 7**
RLC_{fit}	11214	4272	6750	9344	3558	5622
RLC-*in-situ*	11817	4938	7577	9849	4114	6313
Ratio	0.95	0.87	0.89	0.95	0.87	0.89

Only the fit parameters and the hourly averaged irradiance data of these days were used.

or loss could change within a distance of 10 cm. For example, position 6 had a decrease in NDVI of −0.32 d^{-1} between 21 and 23 May, whereas its neighboring position 7 increased by 0.23 d^{-1}.

At present, there are no suitable remote imaging systems with sufficient spatial, temporal and spectral resolution to enable the dynamics revealed here using *in-situ* instruments to be investigated over wider scales. Medium resolution satellite images of 10 to 30 m pixel size can be obtained from Landsat-8 and Sentinel-2, but cloud-free images are usually available only once or twice per month. Further investigation of microscale MPB population dynamics may be possible using repeated imaging over successive tidal cycles with high-resolution cameras or scanners mounted on unmanned aerial vehicles, or fixed cameras at a suitable height with narrow-band wavelength filters to capture red/infrared spectral differences. Accurate geo-correction would be essential in order to locate pixels in exactly the same position for calculation of growth and loss rates over time. If such methods were to be used, a complete semi-variogram covering all spatial scales from cm to km could be constructed, allowing not only patch size to be further defined, but carbon fixation estimates at the tidal flat scale to be improved.

The MPB community in these plots clearly showed a vertical migration pattern, with the regular appearance and disappearance of the surface biofilm being easily visible to the naked eye, and quantifiable by means of repeated spectral measurements. The amount of chlorophyll present in the surface biofilm increased by a factor of 1.5 to 2 during low tide, before decreasing just before immersion. It is still unknown whether this cycle is determined by a daily oscillator or by a tidal cycle or both. Haro et al. (2019) presented evidence, based on a Fourier analysis of the daily patterns, that the vertical migration in the absence of tides was controlled by an endogenous circadian rhythm that was entrained by the photoperiod and that the vertical migration behavior could immediately be reset by the photoperiod. However, the authors state that the influence of an *in-situ* tidal signal cannot be discarded. Pinckney and Zingmark (1991), however, were able to model the migratory behavior of MPB as a function of both tidal and sun angles, suggesting both factors play a role. This is corroborated by our results that also clearly show that the timing of the migration shifts with the tide. Whether these differences were related to decreases in irradiance during cloud cover events, causing negative phototaxis, is not clear, as low irradiance per se did not always cause a decrease in NDVI. A cellular tidal clock is most likely involved although it cannot be excluded that the diurnal clock determining the circadian rhythm is reset daily by the shifting tides and thus compensates for the shift in the tide. Clearly more experimental work is needed to resolve this question, and to explain occasions when anomalous migration patterns were observed. On days 9 and 10 a bell-shaped migration curve was observed, but it was the magnitude of migration which differed from the prediction, whereas NDVI values on day 3 changed little throughout the tidal cycle until the final hour of emersion. The spectral reflectance technique would be most suitable for use in migration investigations, giving an unambiguous high-frequency estimate of chlorophyll concentration in the surface biofilm. A good relationship was established between measured and modeled NDVI values using the Pinckney and Zingmark (1991) approach. If tidal and solar data are available for a site, further refinement of relationships such as this could be used to extrapolate the daily dynamics of MPB biofilms from single-point measurements i.e., a midday satellite overpass.

It was observed that the cells reached the surface within 1–2 h and stayed at the surface for about 3–4 h. As NDVI values at the beginning of low tide or at the end of the low tide were low, most of the MPB population appeared to consist of species able to perform vertical migration. In contrast to several other authors (Serôdio et al., 2006; Perkins et al., 2010) we did not observe downward migration as a result of high light intensities. This does not mean that the cells were not affected by the high

irradiances: clear signs of downregulation of α_{rETR} were observed on sunny days (e.g., days 3, 12, and 14), but this downregulation did not occur when the irradiance conditions fluctuated rapidly (e.g., day 7 on **Supplementary Figure S2**). The question whether this decrease in α_{rETR} signifies photoinhibition (i.e., caused by damage to the photosystem-II) or dynamic downregulation cannot be answered with certainty as we did not study recovery kinetics of α_{rETR} in low light or measured intact and damaged D1-proteins, but the fact that F_v/F_m had very high values, and was essentially constant over the period, makes it likely that dynamic downregulation is the cause of this decrease in α_{rETR}. The diatom biofilm was able to remain productive under prolonged periods of high irradiance.

The maximum rates of relative photosynthetic electron transport showed greater variability during the day than light-limited photosynthesis (α_{rETR}). In general, $rETR_m$ had lowest values immediately after tidal exposure, and increased following the upward migration of cells to the surface. Activation of the RuBisCO enzyme following a prolonged period of dark acclimation is the most likely cause of this increase (MacIntyre and Geider, 1996). During the low tide period, increases and decreases of up to threefold were measured within short time intervals. These changes in $rETR_m$ were not related to decreases in F_v/F_m, which stayed rather constant, or to changes in α_{rETR}. The use of an artificial light source to generate RLCs has the advantage that the light steps given are known and repeatable, but the light received at the sediment surface does depend on a highly accurate positioning of the fiber-optic cable with respect to the surface biofilm (in these experiments – 4 mm distance). Small errors in positioning, for example if the supporting plastic chamber sinks into the soft sediment, can potentially reduce the distance to the sediment and increase the irradiance received. This would cause an underestimation of ETR.

A potential problem with using fluorescence measurements on the surface biofilm is that variable fluorescence originating below the surface ("deep layer fluorescence") will cause an overestimation of the true effective quantum efficiency which can cause serious overestimation of the true rate of electron transport at higher irradiance (Forster and Kromkamp, 2004; Serôdio, 2004). A similar observation has been made for corals (Wangpraseurt et al., 2019). This degree of overestimation is also dependent on the vertical distribution of MPB in the sediment as it changes the amount of cells in the photic layer in the sediment, and Morelle et al. (2018) suggested a method to correct for this artifact. In addition, the vertical migration itself has been shown to influence photosynthetic activity and productivity as the biomass of the MPB in the photic zone will change as a result of the migratory behavior (Cartaxana et al., 2008). Optical artifacts would lead to a positive relationship between F_o and $rETR_m$ but in the field measurements here, a negative relationship with F_o was found ($rETR_m = -0.606 \times F_o + 843$, $r^2 = 0.32$, $p < 0.0001$).

Of the other factors likely to play a role in the dynamic behavior of $rETR_m$, temperature was the most important one as a correlation between sediment temperature and $rETR_m$ was observed. A measurement of the true mud surface temperature within the dark chamber used for light curve measurements was not made, instead an estimate of the adjacent temperature of solar-exposed mud was made. It is likely that the temperature within the chamber cooled during the short period of measurement, and hence a recommendation for future measurements of this type would be to add a miniature seawater-proof thermistor to the instrument.

Rapid light curves have the advantage that they can be used to measure the photosynthetic properties quickly, but the information retrieved from RLCs depend very much on the protocol used as explained in the introduction (see Perkins et al. (2010) for an extensive review on this topic). Two techniques were used to measure the photosynthetic activity of the diatom biofilms: (1) Normal (sequential) rapid light curves, with a 30 s light step and a 1 min dark acclimation period. (2) *in-situ* measurements of the effective PSII quantum efficiency ($\Delta F/F_m'$) which was converted to relative rates of photosynthetic electron transport by multiplying it with the solar irradiance. These latter measurements thus measured the "real" photosynthetic activity as the biofilm was not shaded or touched in any way, and the incident irradiance was known with high accuracy (i.e., no artifact due to distance from the light course). The sequential RLCs used a maximum irradiance of 2000 μmol photons m^{-2} s^{-1} to generate light-saturated photosynthetic electron transport. $rETR_m$ measured in this way was almost always higher than the instantaneous ETR measured under ambient irradiance, indicating that on the majority of tidal exposures photosynthesis was not fully light-saturated. When ETR from RLCs was calculated for the same irradiance as the *in-situ* solar, results show clearly that both methods gave nearly identical results as can be seen in **Figure 10**: both types of measurements follow the same daily patterns. The shape of the ETR-irradiance curves were very similar, but the RLC-based data showed a significantly higher $rETR_m$ and a slightly lower α_{rETR}. Spectral differences between the halogen light source of the PAM instrument, and natural sunlight, may account for some of the differences, as well as the temperature difference between inside and outside of the RLC chamber mentioned above. Calculation of the total primary production over depth during a low tide period for the irradiances measured during the period showed that the *in-situ* measurements gave between 5 and 13% higher production estimates (due to the higher light affinity, α_{rETR}), and that the differences became smaller with higher surface irradiance (a result of the "crossing over" of the LC, see **Figure 11**). The results also showed that spatial differences in biomass did not affect the shape of the LC and that basically the photosynthetic parameters did not change during the 14-day spring-neap-spring cycle, despite the fact that occasional differences in $rETR_m$ during the day were observed. From a modeling perspective, the fact that the cardinal parameters of photosynthesis changed little during this period would simplify the scaling-up of production estimates. We can thus conclude that the RLC-protocol that was used can be obtained to generate a synoptic map of RLC-parameters at different sites and different environment conditions. *In-situ* reflectance and fluorescence techniques can be used alongside remote sensing in order to better quantify the productivity of intertidal soft sediment systems.

DATA AVAILABILITY STATEMENT

The data in this article can be obtained from the following: http://www.vliz.be/en/imis?module=datasetanddasid=1213.

AUTHOR CONTRIBUTIONS

JK and RF wrote the manuscript with contributions from EM. RF designed the database in which the data was stored. All authors contributed to the article and approved the submitted version.

FUNDING

This work was carried for the HIMOM project, funded by a grant from the 5th European Framework Programme (Contract No. EVK-CT-2001-00052).

SUPPLEMENTARY MATERIAL

The Supplementary Material for this article can be found online at: https://www.frontiersin.org/articles/10.3389/fmars.2020.00562/full#supplementary-material

REFERENCES

Barranguet, C., and Kromkamp, J. (2000). Estimating primary production rates from photosynthetic electron transport in estuarine microphytobenthos. *Mar. Ecol. Prog. Ser.* 204, 39–52. doi: 10.3354/meps204039

Behrenfeld, M. J., Prasil, O., Babin, M., and Bruyant, F. (2004). In search of a physiological basis for covariations in light-limited and light-saturated Photosynthesis1. *J. Phycol.* 40, 4–25. doi: 10.1046/j.1529-8817.2004.03083.x

Cahoon, L. B. (1999). The role of benthic microalgae in neritic ecosystems. *Oceanogr. Mar. Biol. Annu. Rev.* 37, 47–86.

Cartaxana, P., Brotas, V., and Serôdio, J. (2008). Effects of two motility inhibitors on the photosynthetic activity of the diatoms *Cylindrotheca closterium* and *Pleurosigma angulatum*. *Diatom Res.* 23, 65–74. doi: 10.1080/0269249x.2008.9705737

Christianen, M. J. A., Middelburg, J. J., Holthuijsen, S. J., Jouta, J., Compton, T. J., van der Heide, T., et al. (2017). Benthic primary producers are key to sustain the Wadden Sea food web: stable carbon isotope analysis at landscape scale. *Ecology* 98, 1498–1512. doi: 10.1002/ecy.1837

Cruz, S., and Serôdio, J. (2008). Relationship of rapid light curves of variable fluorescence to photoacclimation and non-photochemical quenching in a benthic diatom. *Aquat. Bot.* 88, 256–264. doi: 10.1016/j.aquabot.2007.11.001

Daggers, T. D., Kromkamp, J. C., Herman, P. M. J., and van der Wal, D. (2018). A model to assess microphytobenthic primary production in tidal systems using satellite remote sensing. *Rem. Sens. Environ.* 211, 129–145. doi: 10.1016/j.rse.2018.03.037

Decho, A. W. (2000). Microbial biofilms in intertidal systems: an overview. *Cont. Shelf Res.* 20, 1257–1273. doi: 10.1016/s0278-4343(00)00022-4

Forster, R. M., Créach, V., Sabbe, K., Vyverman, W., and Stal, L. J. (2006). Biodiversity-ecosystem function relationship in microphytobenthic diatoms of the Westerschelde estuary. *Mar. Ecol. Prog. Ser.* 311, 191–201. doi: 10.3354/meps311191

Forster, R. M., and Jesus, B. (2006). Field spectroscopy of estuarine intertidal habitats. *Int. J. Rem. Sens.* 27, 3657–3669. doi: 10.1080/01431160500500367

Forster, R. M., and Kromkamp, J. C. (2004). Modelling the effects of chlorophyll fluorescence from subsurface layers on photosynthetic efficiency measurements in microphytobenthic algae. *Mar. Ecol. Prog. Ser.* 284, 9–22. doi: 10.3354/meps284009

Forster, R. M., and Kromkamp, J. C. (2006). Upscalling primary production-Estimating benthic primary production: scaling up from point measurements to the whole estuary. *Verh. K. Ned. Akad. Wet.* 2, 109–122.

Haro, S., Bohórquez, J., Lara, M., Garcia-Robledo, E., González, C. J., Crespo, J. M., et al. (2019). Diel patterns of microphytobenthic primary production in intertidal sediments: the role of photoperiod on the vertical migration circadian rhythm. *Sci. Rep.* 9, 1–10.

Honeywill, C., Paterson, D. M., and Hagerthey, S. E. (2002). Determination of microphytobenthic biomass using pulse- amplitude modulated minimum fluorescence. *Eur. J. Phycol.* 37, 485–492. doi: 10.1017/s0967026202003888

Hope, J. A., Paterson, D. M., and Thrush, S. F. (2019). The role of microphytobenthos in soft-sediment ecological networks and their contribution to the delivery of multiple ecosystem services. *J. Ecol.* 108, 815–830. doi: 10.1111/1365-2745.13322

Howard, J., Sutton-Grier, A., Herr, D., Kleypas, J., Landis, E., Mcleod, E., et al. (2017). Clarifying the role of coastal and marine systems in climate mitigation. *Front. Ecol. Environ.* 15:1451. doi: 10.1002/fee.1451

Ibrahim, E., Adam, S., De Wever, A., Govaerts, A., Vervoort, A., and Monbaliu, J. (2014). Investigating spatial resolutions of imagery for intertidal sediment characterization using geostatistics. *Cont. Shelf Res.* 85, 117–125. doi: 10.1016/j.csr.2014.05.012

Jesus, B., Brotas, V., Marani, M., and Paterson, D. M. (2005). Spatial dynamics of microphytobenthos determined by PAM fluorescence. *Estuar. Coast. Shelf Sci.* 65, 30–42. doi: 10.1016/j.ecss.2005.05.005

Jesus, B., Brotas, V., Ribeiro, L., Mendes, C. R., Cartaxana, P., and Paterson, D. M. (2009). Adaptations of microphytobenthos assemblages to sediment type and tidal position. *Cont. Shelf Res.* 29, 1624–1634. doi: 10.1016/j.csr.2009.05.006

Jesus, B., Perkins, R., Consalvey, M., Brotas, V., and Paterson, D. (2006). Effects of vertical migrations by benthic microalgae on fluorescence measurements of photophysiology. *Mar. Ecol. Prog. Ser.* 315, 55–66. doi: 10.3354/meps315055

Kromkamp, J., Barranguet, C., and Peene, J. (1998). Determination of microphytobenthos PSII quantum efficiency and photosynthetic activity by means of variable chlorophyll fluorescence. *Mar. Ecol. Prog. Ser.* 162, 45–55. doi: 10.3354/meps162045

Kromkamp, J. C., and Forster, R. M. (2006). Photosynthesis in marine diatom assemblages-Developments in microphytobenthos primary productivity studies. *Verh. K. Ned. Akad. Wet.* 2, 9–30.

Kromkamp, J. C., Morris, E. P., Forster, R. M., Honeywill, C., Hagerthey, S., and Paterson, D. M. (2006). Relationship of intertidal surface sediment chlorophyll concentration to hyperspectral reflectance and chlorophyll fluorescence. *Estuar. Coasts* 29, 183–196. doi: 10.1007/bf02781988

Kuwae, T., Beninger, P. G., Decottignies, P., Mathot, K. J., Lund, D. R., and Elner, R. W. (2008). Biofilm grazing in a higher vertebrate: the western sandpiper *Calidris mauri*. *Ecology* 89, 599–606. doi: 10.1890/07-1442.1

Kwon, B. O., Khim, J. S., Park, J., Ryu, J., Kang, S. G., and Koh, C. H. (2012). Short-term variability of microphytobenthic primary production associated with *in situ* diel and tidal conditions. *Estuar. Coast. Shelf Sci.* 112, 236–242. doi: 10.1016/j.ecss.2012.07.029

Launeau, P., Méléder, V., Verpoorter, C., Barillé, L., Kazemipour-Ricci, F., Giraud, M., et al. (2018). Microphytobenthos biomass and diversity mapping at different spatial scales with a hyperspectral optical model. *Rem. Sens.* 10:716. doi: 10.3390/rs10050716

Lawrenz, E., Silsbe, G., Capuzzo, E., Ylöstalo, P., Forster, R. M., Simis, S. G. H., et al. (2013). Predicting the electron requirement for carbon fixation in seas and oceans. *PLoS One* 8:e58137. doi: 10.1371/journal.pone.0058137

MacIntyre, H. L., and Geider, R. J. (1996). Regulation of rubisco activity and its potential effect on photosynthesis during mixing in a turbid estuary. *Mar. Ecol. Prog. Ser.* 144, 247–264. doi: 10.3354/meps144247

MacIntyre, H. L., Geider, R. J., and Miller, D. C. (1996). Microphytobenthos - the ecological role of the secret garden of unvegetated, shallow-water marine habitats. 1. distribution, abundance and primary production. *Estuaries* 19, 186–201.

Marques da Silva, J., Cruz, S., and Cartaxana, P. (2017). Inorganic carbon availability in benthic diatom communities: photosynthesis and migration. *Philos. Trans. R. Soc. B Biol. Sci.* 372:20160398. doi: 10.1098/rstb.2016.0398

Méléder, V., Jesus, B., Barnett, A., Barillé, L., and Lavaud, J. (2018). Microphytobenthos primary production estimated by hyperspectral reflectance. *PLoS One* 13:e0197093. doi: 10.1371/journal.pone.0197093

Morelle, J., Orvain, F., and Claquin, P. (2018). A simple, user friendly tool to readjust raw PAM data from field measurements to avoid over- or underestimating of microphytobenthos photosynthetic parameters. *J. Exp. Mar. Bio. Ecol.* 503, 136–146. doi: 10.1016/j.jembe.2018.02.007

Morris, E. (2005). *Quantifying Primary Production of Microphytobenthos: Application of Optical Methods*. Ph. D. Thesis, University of Groningen. Groningen.

Morris, E. P., Forster, R., Peene, J., and Kromkamp, J. C. (2008). Coupling between Photosystem II electron transport and carbon fixation in microphytobenthos. *Aquat. Microb. Ecol.* 50, 301–311. doi: 10.3354/ame01175

Orvain, F., Lefebvre, S., Montepini, J., Sébire, M., Gangnery, A., and Sylvand, B. (2012). Spatial and temporal interaction between sediment and microphytobenthos in a temperate estuarine macro-intertidal bay. *Mar. Ecol. Prog. Ser.* 458, 53–68. doi: 10.3354/meps09698

Paterson, D. M. (1989). Short-term changes in the erodibility of intertidal cohesive sediments related to the migratory behaviour of epipelic diatoms. *Limnol. Oceanogr.* 34, 223–234. doi: 10.4319/lo.1989.34.1.0223

Paterson, D. M., and Black, K. S. (1999). "Water flow, sediment dynamics and benthic biology," in *Advances in Ecological Research*, eds D. M. Paterson and K. Black (Cambridge, MA: Academic Press Inc), 155–193. doi: 10.1016/s0065-2504(08)60193-2

Perkins, R. G., Kromkamp, J. C., Serôdio, J., Lavaud, J., Jesus, B., Mouget, J. L., et al. (2010). "The application of variable chlorophyll fluorescence to microphytobenthic biofilms," in *Chlorophyll a Fluorescence in Aquatic Sciences: Methods and Applications*, eds D. A. Duggett, O. Prasil, and M. A. Borowitzka (Dordecht: Springer), 277–292.

Perkins, R. G., Mouget, J. L., Lefebvre, S., and Lavaud, J. (2006). Light response curve methodology and possible implications in the application of chlorophyll fluorescence to benthic diatoms. *Mar. Biol.* 149, 703–712. doi: 10.1007/s00227-005-0222-z

Pinckney, J., and Zingmark, R. (1991). Effects of tidal stage and sun angles on intertidal benthic microalgal productivity. *Mar. Ecol. Prog. Ser.* 76, 81–89. doi: 10.3354/meps076081

R Core Team (2018). *R: A Language and Environment for Statistical Computing*. Vienna: R Foundation for Statistical Computing.

RStudio Team (2020). *RStudio: Integrated Development for R*. Boston, MA: RStudio, PBC. Available online at: http://www.rstudio.com/

Sahan, E., Sabbe, K., Creach, V., Hernandez-Raquet, G., Vyverman, W., Stal, L., et al. (2007). Community structure and seasonal dynamics of diatom biofilms and associated grazers in intertidal mudflats. *Aquat. Microb. Ecol.* 47, 253–266. doi: 10.3354/ame047253

Serôdio, J. (2003). A chlorophyll fluorescence index to estimate short-term rates of photosynthesis by intertidal microphytobenthos. *J. Phycol.* 39, 33–46. doi: 10.1046/j.1529-8817.2003.02043.x

Serôdio, J. (2004). Analysis of variable chlorophyll fluorescence in microphytobenthos assemblages: implications of the use of depth-integrated measurements. *Aquat. Microb. Ecol.* 36, 137–152. doi: 10.3354/ame036137

Serôdio, J., Coelho, H., Vieira, S., and Cruz, S. (2006). Microphytobenthos vertical migratory photoresponse as characterised by light-response curves of surface biomass. *Estuar. Coast Shelf Sci.* 68, 547–556. doi: 10.1016/j.ecss.2006.03.005

Serôdio, J., Da Silva, J. M., and Catarino, F. (1997). Nondestructive tracing of migratory rhythms of intertidal benthic microalgae using in vivo chlorophyll a fluorescence. *J. Phycol.* 33, 542–553. doi: 10.1111/j.0022-3646.1997.00542.x

Serôdio, J., Ezequiel, J., Frommlet, J., Laviale, M., and Lavaud, J. (2013). A method for the rapid generation of nonsequential light-response curves of chlorophyll fluorescence. *Plant Physiol.* 163, 1089–1102. doi: 10.1104/pp.113.225243

Smith, D. J., and Underwood, G. J. C. (2000). The production of extracellular carbohydrates by estuarine benthic diatoms: the effects of growth phase and light and dark treatment. *Eur. J. Phycol.* 35, 173–182.

Tolhurst, T. J., Jesus, B., Brotas, V., and Paterson, D. M. (2003). "Diatom migration and sediment armouring — an example from the Tagus Estuary, Portugal," in *Migrations and Dispersal of Marine Organisms*, eds M. B. Jones, A. Ingólfsson, G. V. Helgason, E. Ólafsson, K. Gunnarsson, and J. Svavarsson (Berlin: Springer), 183–193. doi: 10.1023/b:hydr.0000008474.33782.8d

Underwood, G. J. C., and Kromkamp, J. (1999). Primary production by phytoplankton and microphytobenthos in estuaries. *Adv. Ecol. Res.* 29, 93–153. doi: 10.1016/s0065-2504(08)60192-0

Underwood, G. J. C., and Paterson, D. M. (2003). The importance of extracellular carbohydrate production by marine epipelic diatoms. *Adv. Bot. Res.* 40, 183–240. doi: 10.1016/s0065-2296(05)40005-1

van der Wal, D., van den Dool, A. W., and Herman, P. M. J. (2010). Spatial synchrony in intertidal benthic algal biomass in temperate coastal and estuarine ecosystems. *Water* 13, 338–351. doi: 10.1007/s10021-010-9322-9

Wangpraseurt, D., Lichtenberg, M., Jacques, S. L., Larkum, A. W. D., and Kühl, M. (2019). Optical properties of corals distort variable chlorophyll fluorescence measurements. *Plant Physiol.* 179, 1608–1619. doi: 10.1104/pp.18.01275

Webb, W. L., Newton, M., and Starr, D. (1974). Carbon dioxide exchange of *Alnus rubra*: a mathematical model. *Oecologia* 17, 281–291. doi: 10.1007/bf00345747

Conflict of Interest: The authors declare that the research was conducted in the absence of any commercial or financial relationships that could be construed as a potential conflict of interest.

frontiers in Marine Science

MINI REVIEW
published: 18 June 2020
doi: 10.3389/fmars.2020.00433

Travelling Expenses: The Energy Cost of Diel Vertical Migrations of Epipelic Microphytobenthos

Jorge Marques da Silva[1]*, *Bernardo Duarte*[2] and *Andrei Borissovitch Utkin*[3,4]

[1] Faculty of Sciences, BioISI - Biosystems and Integrative Sciences Institute, Universidade de Lisboa, Lisbon, Portugal, [2] MARE – Marine and Environmental Sciences Centre, Faculty of Sciences, Universidade de Lisboa, Lisbon, Portugal, [3] INOV INESC Inovação, Lisbon, Portugal, [4] CeFEMA, Universidade de Lisboa, Lisbon, Portugal

The physiology of the diel movements of epipelic microphytobenthic diatoms is not fully understood. As well, the evolutionary pressures that led to migratory behavior and the ecological role of vertical migrations remain unknown. The behavioral photoprotection hypothesis, according to which the diatoms move along the vertical light gradient to find their optimal light environment, is the most generally accepted. However, the motion is associated with an energy cost that has not been fully acknowledged before. To throw light on this issue, we looked at the mechanisms of diatom locomotion and reviewed their patterns of movement. Making use of published data, we estimated an energy cost of 0.12 pJ for a typical diatom cell to move upward (or downward) in a 400 μm photic zone. This amounts to 3.93×10^{-18} mol of ATP, which are released by the oxidation of 1.31×10^{-19} mol of glucose. This represents only 0.0001% of the daily net photosynthetic production of a typical microphytobenthic diatom cell, showing that diel vertical migrations have a negligible impact on cell and ecosystem energy budget. Even though the migration energy cost of individual cells may depart almost two orders of magnitude from the central value presented for a typical diatom (depending on cell size, velocity of displacement, and viscosity of the medium), the maximum value calculated is still negligible from the metabolic and ecologic point of view. Results show that behavioral photoprotection might be an energetically cheap mechanism, offering competitive advantages when compared with structural/physiological photoprotection.

Keywords: microphytobenthos, diatoms, sediments, migration, energy

OPEN ACCESS

Edited by:
Wim Vyverman,
Ghent University, Belgium

Reviewed by:
Olivier Pringault,
Institut de Recherche Pour le Développement (IRD), France
Ulisses Miranda Azeiteiro,
University of Aveiro, Portugal

***Correspondence:**
Jorge Marques da Silva
jmlsilva@fc.ul.pt

Specialty section:
This article was submitted to Marine Ecosystem Ecology, a section of the journal Frontiers in Marine Science

Received: *06 December 2019*
Accepted: *18 May 2020*
Published: *18 June 2020*

Citation:
Marques da Silva J, Duarte B and Utkin AB (2020) Travelling Expenses: The Energy Cost of Diel Vertical Migrations of Epipelic Microphytobenthos. Front. Mar. Sci. 7:433. doi: 10.3389/fmars.2020.00433

LOCOMOTION OF DIATOMS

Locomotion is present among unicellular organisms (prokaryotes and eukaryotes) and eukaryotic cells of multicellular organisms. The locomotion of unicellular eukaryotes (e.g., free-living protozoa) is mainly used for feeding, whereas it plays a central role in the development of multicellular organisms. Also, in the latter type of organisms, specialized cells can move inside the body for specific reasons, such as leukocytes, which move to grant immune response, being able to travel long distances in the organs in just a few hours (Vargas et al., 2017). Eukaryotic cells and unicellular organisms evolved several mechanisms of locomotion (Chowdhury, 2013). The specific locomotion mechanism of a given organism is dependent on the characteristics of its natural habitat. If the organism lives in a liquid medium, it will swim or, in certain cases, adjust its position on the water column by changing its floatability (Villareal, 1992). If the organism lives in a thin film

at the interface between a solid surface and liquid medium, or in the interior of a three-dimensional matrix, gliding will be its preferred way of locomotion (Sibley et al., 1998; Spormann, 1999). Some microorganisms may exhibit several mechanisms of locomotion. The term "amoeboid migration," named after the protozoon *Amoeba proteus*, subsume several of those cellular mechanisms, ranging from blebbing motility to entirely actin-polymerization-based gliding. These apparently different mechanisms, however, might be variants of an archetypal one, showing different contributions of actin protrusion, actomyosin contraction, and substrate adhesion, where blebbing and gliding represent the extreme versions of a common "ameboid" locomotion (Lammermann and Sixt, 2009). Generally speaking, three different locomotion mechanisms have been postulated: (i) force generated by polymerization of cytoskeletal protein filaments (actin and microtubules), (ii) force generated by cytoskeletal motors by their interactions with filamentous tracks, and (iii) forces of hydrostatic (osmotic) origin (Chowdhury, 2013). In the present review we will address only the force generated by polymerization of cytoskeletal protein filaments, since it seems the only one to be involved in diatom locomotion. The motility of the colonial diatom *Bacillaria paxillifera* was the subject of the first research on diatoms ever published, by the Danish naturalist Otto Friedrich Müller in 1783 (Ussing et al., 2005). The synchronized movement of the individual diatom cells in the colony captured the inspiration of generations of scientists, intrigued by the mechanism of locomotion, since no mobile parts were visible. In fact, the pennate diatom *Bacillaria paxillifer* forms a colony where the adjacent cells smoothly and almost continuously slide, without any visible motility structure, such as cilia or flagella. Although the ecological and physiological significance of this movement is still unknown, some progress has been made on the elucidation of its mechanism. In fact, imaginative models on diatom motility have a long-standing history (Edgar, 1982). The theory of jet propulsion goes back to XIX century. In the first half of the XX century several models appeared: West (1916) and Fritsch (1935) reviewed several authors and described models as diverse as the ones based on cilia, pseudopodia, mucilaginous filaments, osmotic currents, undulating membranes, contractile protoplasm, streaming protoplasm, gas expulsion, and water jets (Hopkins and Drum, 1966). However, these models were not resounding, and another hypothesis of diatom locomotion—an actin-based motility model—was suggested by Edgar and Pickett-Heaps (1983) and Edgar and Zavortink (1983). Initially, the raphe mucilage strands (EPS, extracellular polymeric substances) adhere to the substratum during the gliding process. Additionally, transmembrane components are linked to actin bundles that lie underneath the plasmalemma at the raphe. Afterwards, a force applied to the transmembrane protein (e.g., putative myosin)/actin connectors, parallel to the actin bundle, produces movement of the transmembrane proteins through the cell, and consequent movement of the cell in the direction opposite to the force (Aumeier and Menzel, 2012). A similar mechanism has been proposed to explain the locomotion of other protists that exhibit substrate-adherence mediated gliding (Preston and King, 1996; Dobrowolski et al., 1997; Pinder et al., 1998). A variant of the Edgar model has been proposed to explain the locomotion of *Navicula* sp., postulating that it is done via two or more pseudopods or stalks projected out of the frustules. The adhesion can be secure due to the pull-off of one pseudopod or stalk from the substratum through EPS, and the positive pressure is produced to balance the adhesion because of the push-down of another pseudopod or stalk against the substratum. Because of the positive pressure, traction is produced, acting as a driving force of movement, and the other pseudopod or stalk can detach from the substratum, ensuing the locomotion (Wang et al., 2013). Therefore, locomotion requires two steps: temporary adhesion to the substrate, and subsequent detachment to allow displacement. Though Edgar and co-workers explained that the mucilage is detached on reaching the apical raphe ending called helictoglossa (Edgar and Pickett-Heaps, 1983), there is no empirical evidence supporting this assumption, since the expected aggregation of EPS at the helictoglossa has never been observed (Wang et al., 2013).

Cytoskeleton-disrupting drugs were used to examine the importance of actin, myosin, and microtubules in diatom gliding, providing additional evidence of their putative role. Contradictory results were found, with some drugs showing the ability to inhibit diatom gliding, where others failed to do it (Poulsen et al., 1999). Since gliding was hampered by the known actin inhibitors cytochalasin A and latrunculin A and by the myosin inhibitor 2,3-butanedione monoxime, it is thought to be driven by the actomyosin system of these diatoms (Edgar and Pickett-Heaps, 1982; Edgar and Zavortink, 1983; Poulsen et al., 1999). Latrunculin A and B inhibit actin assemblage, since they form an incompetent complex with monomeric actin, leading to F-actin depolymerization (Coué et al., 1987; Ayscough et al., 1997). In fact, in *B. paxillifer*, the actin bundles along the raphe disappeared after a short treatment (1 min) with latrunculin B and reappeared shortly after the removal of this drug (Yamaoka et al., 2016). However, it is not possible to exclude additional indirect effects of latrunculin in diatom motility, e.g., impairing the transport of secretion vesicles to the raphe (Poulsen et al., 1999), as postulated in the model of Edgar.

In any case, cumulative evidence points to a key role of the raphe in the mechanism of locomotion. In fact, only pennate diatoms exhibit true motility. These diatoms have bilateral symmetry and possess a long slit on the frustule (the raphe), which is required to substrate adherence and gliding (Poulsen et al., 1999). EPS, common to all motile diatoms, are excreted through or near the raphe by exocytosis, aiding to the adherence to the substrate (Edgar and Pickett-Heaps, 1982, 1983; Edgar, 1983; McConville et al., 1999). Arguably, the mucilage is cut when arrives at the end of the raphe. The cut is done by the polar fissure, a specific structure of the frustule, and the mucilage remains on the substratum leaving a trace of the gliding motion. Thus, involvement of the mucilage in gliding is also postulated (Poulsen et al., 1999). However, the previous models based exclusively in their excretion have been abandoned. This was partly due to the high energetic cost attributed to EPS synthesis, hindering locomotion. Nonetheless, the formation of certain polysaccharides, as polyuronic acids, requires little energy consumption, providing there is enough supply of glucose.

Therefore, secretion of this type of polysaccharide need not to have a high energetic cost for a photosynthetic cell, when compared with more complex molecules such as acetylated glucosamines (Edgar, 1982). Since motility depends on the secreted mucilage to substrate adhesion, granting traction, it is difficult to separate adhesion from motility processes (Poulsen et al., 1999). However, recent results from Cartaxana et al. (2016) showed that the interdependence of motility and adhesion is not so tight as previously thought. In an experiment where the responses of adhesion and gliding speed to temperature were simultaneously measured, the authors found that *Pinnularia viridis* significantly lost substrate adhesion at temperatures above 20°C, in contrast with *Nitzschia linearis,* but both species increased gliding speed. The interspecific differences observed between the effects of temperature on motility and adhesion are not surprising, since myosins are strongly conserved among plant groups, whereas mucilage composition is quite diverse, even among diatoms, resulting in differential adhesion to substrates. Another remaining problem is how to explain bidirectionality. It was suggested that the presence of two actin bundles should play a key role. One hypothesis is that two actin bundles have different polarity, myosin motors changing their moving track from one to the other actin bundle during reversion of direction. Another hypothesis admit that the two actin bundles have the same polarity and that several classes of myosins are involved (Wells et al., 1999). The determination of the polarity of the actin bundles will help unravel this uncertainty.

Vertical Movements on Microphytobenthos

Benthic epipelic diatoms usually colonize substrates (intertidal mudflats) with more than 80% of silt (very fine inorganic particles, which are habitually held in suspension by minor water movements at the sediment surface) and clay (mostly colloids of hydrated aluminum silicate, together with iron and other impurities) (see e.g., Elliott et al., 1998). The photic zone of a typical sediment is 0–0.5 mm. Scalar irradiance at the surface (0–0.1 mm) may be higher (∼114%) than the incident downward irradiation but it decreases exponentially to non-detectable values at 0.8 mm. This is more than the thickness of some artificial diatom biofilms (*Pinularia* sp.) formed in Petri dishes (150–380 μm Harbich, 2019). The dimensions of the pennate diatoms are also very variable. Wang et al. (2013) reported for *Navicula* sp. 10–15 μm length (longitudinal axis) and 4–5 μm wide (transversal axis). Benthic pennate diatoms inhabiting soft intertidal sediments often exhibit active motility within the substrates they inhabit (Cohn and Disparti, 1994; Serôdio et al., 1997, 2001, 2006; Du et al., 2010), in a way strongly dependent from light and other environmental conditions (Cohn and Weitzell, 1996; Cohn et al., 1999, 2015; Falciatore et al., 2000; Serôdio et al., 2006; McLashlan et al., 2012) and synchronized with daily and tidal cycles (Pinckney and Zingmark, 1993). Albeit diatoms' vertical movements were previously known, the disentanglement of its details progressed significantly with the utilization of non-invasive optical techniques such as pulse amplitude modulated fluorometry (Serôdio et al., 1997), imaging pulse amplitude modulated fluorometry (Vieira et al., 2013) and laser induced fluorescence (Utkin et al., 2013; Marques da Silva and Utkin, 2018). These diatoms accumulate at the surface of the sediment during daytime low tide and migrate downward before tidal flooding and/or sunset. Upward migration during daytime low tide allows the cells to reach the sediment photic zone, causing substantial changes on the community algal biomass engaged in photosynthesis (Vieira et al., 2011) and making these communities significant contributors to the primary production of estuarine and coastal areas (Svensson et al., 2014). It has been suggested that downward migration reduces the cells' risk of predation and facilitates the absorption of nutrients (Saburova and Polikarpov, 2003). In addition to this diel, partly endogenous, migration cycles, epipelic diatoms may also migrate downward when exposed to high irradiation (Kromkamp et al., 1998; Perkins et al., 2001; Cartaxana et al., 2011). The observation of this photophobic migration led to the formulation of the theory of "micromigration," according to which cells continuously change their position within the light gradient, avoiding photoinhibition and increasing photosynthetic performance (Kromkamp et al., 1998; Underwood et al., 2005; Marques da Silva et al., 2017). Light quality also plays a role on diatom movement (Cohn et al., 2004; Perkins et al., 2010). Photophobic responses of pennate diatoms (Cohn et al., 1999, 2015) is based on light perception by one or more photosensitive molecules that seems to act as light sensors in diatoms (Ishikawa et al., 2009; Depaw et al., 2012; Costa et al., 2013), changing the way how mucilage filaments interact with the underlying system of actin/myosin (Edgar and Pickett-Heaps, 1983; Edgar and Zavortink, 1983; Poulsen et al., 1999). Different diatom species have specific sensibility to irradiation wavelength and intensity (Underwood et al., 2005; Serôdio et al., 2006; Cohn et al., 2015). Besides the importance of these movements to diatoms' ecological success, the species-specific EPS secretion associated with motility is involved in complex biochemical interactions and contribute to the stabilization of the algal and microbial environment (Paterson, 1989; Sutherland et al., 1998; Poulsen et al., 2014; Amin et al., 2015). Interestingly, EPS play similar stabilizing roles in very different ecosystems, such as the cyanobacteria-dominated biological soil crusts (Adessi et al., 2018), and they play a key role on the complex microorganization of paradigmatic bacterial biofilms (Marques da Silva and Casetta, 2019). The layer of EPS displays viscoelasticity, so it is neither purely viscous nor purely elastic. The viscous property of the gel adds the movement of diatoms within a biofilm (Harbich, 2019).

Significant fortnight and seasonal differences on the vertical migration patterns of benthic diatoms have been observed and related to the timing of the low tide, previous light history, and composition of the diatom populations (Serôdio et al., 2008). Vertical community migration movements upward and downward are typically completed in 20 min (Hopkins and Drum, 1966 and references therein) but recently Cartaxana et al. (2016) reported the beginning of downward migration almost 2 h before tidal flooding. Maximum gliding speed reported for diatoms was ∼20 μm s^{-1} (Yamaoka et al., 2016) (**Table 1**), but this was attained in the very specific situation of gliding in the colonial species *Bacillaria paxillifera*. Murase et al. (2011) refer maximum gliding speed an order of magnitude lower (1–2 μm s^{-1}) and Wang et al. (2013) cast doubts in the capacity of the

TABLE 1 | Maximum gliding speed of diatoms.

References	Species	Maximum speed ($\mu m\ s^{-1}$)	Notes
Yamaoka et al. (2016)	*Bacillaria paxillifera*	20	Colonial diatom; adjacent cells glide over each other
Kooistra et al. (2003)	*Toxarium undulatum*	3.5	Maximum speed of 6 $\mu m\ s^{-1}$ was observed, but only for 10 s; speeds of 0.5–2 $\mu m\ s^{-1}$ were more common. Observation of horizontal trajectories in liquid culture medium
Murase et al. (2011)	*Navicula* sp.	1.7	Average velocity of 39 cells over a 600 s period was 1.1 $\mu m\ s^{-1}$; velocity of individual cells ranged from 0.5 to 1.7 $\mu m\ s^{-1}$. Observation of horizontal trajectories in sea water
Edgar (1979)	*Navicula cuspidata*	19.2	Diatoms moving underside a microscope glass coverslip
	Navicula viridula	30.5	
	Amphora ovalis	12.4	
	Nitzschia sublinearis	22.2	
	Nitzschia sigmoidea	28.7	
	Nitzschia acicularis	21.0	
	Cymatopleura solea	5.9	
Harper (1967) in Harper (1977)	*Amphora ovalis*	4.5	Not-determined
	Nitzschia linearis	24	
	Nitzshia sigmoidea	17	
	Cymatopleura solea	14	
	Navicula oblonga	20	
	Gyrosigma acuminatum	15	
	Suriella biseriata	10	
Gupta and Agrawal (2007)	*Nitzschia grimmei*	5.5	Mixed population of the two species gliding in soil liquid supernatant (no differences between the species)
	Nitzschia palea	5.5	
Hay et al. (1993)	*Gyrosigma spencerii*	4.7	Horizontal movement over an artificial sediment (kaolin)
		0.17	Vertical movement in an artificial sediment (kaolin)
		0.19	Vertical movement in a natural sediment

current models of diatom locomotion to support even these lower speeds. Nonetheless, gliding speeds from 4 to 12 $\mu m\ s^{-1}$ were reported (Edgar, 1979; Kooistra et al., 2003; Gupta and Agrawal, 2007). It must be noted, however, that these results were obtained in artificial systems where diatoms moved over a plan surface. They may not entirely reflect diatoms' movement in the complex three-dimensional matrix of epipelic MPB. Furthermore, one order of magnitude lower velocities was reported for vertical movements, when compared with horizontal movements (Hay et al., 1993; Consalvey et al., 2004), see **Table 1**.

Both increased nutrient availability (Passy, 2007; Lange et al., 2011) and higher temperatures have been suggested to cause increased diatom motility. On one hand, it was suggested that a motile life form would be more competitive in a resource-rich environment. On the other hand, changes in the mechanism of locomotion in motile diatoms may be induced by higher temperature: the viscosity of the cytoplasm in the raphe has been shown to decrease with increased temperature, thus making the motile diatoms capable to move faster at higher temperature. Consequently, global warming may increase the competitive advantage of motile over non-motile diatoms (Svensson et al., 2014). However, when temperature exceeds a certain threshold (30–35°C) a sudden and significant (but reversible) decrease of motility is observed (Cartaxana et al., 2016). This type of temperature response (exhibiting a steady increase of speed followed to a drastic drop to near zero) strongly resembles the response of enzymatic activity to temperature, where an increase of activity is observed to the point where the enzyme undergoes denaturation (Palmer, 1991). In addition to temperature and light, diatom locomotion (and adhesion) may also be influenced by the presence of other diatoms species, since different species will compete differently for limited resources (Cartaxana et al., 2016). Different locomotion and adhesion characteristics may determine the localizations and stratification within the biofilm community. Sediment porosity (quantity of pore space) and permeability (potential water flow) may also play a role in epipelic diatoms' movements. Particle size, its mixture and compaction impact the permeability or percolation rate, with low porosity and permeability in fine grained sediment and vice versa for sands (Elliott et al., 1998). Physical characteristics impact the energy costs of diatom movements within the sediment.

ENERGY COSTS OF VERTICAL MIGRATIONS

Mechanical Work That Must Be Performed to Rise to the Sediment Surface

Simplified Energetic Description of the Diatom Locomotion

The minimum energy requirement for a motile diatom to elevate to the sediment surface can be estimated on the basis of the

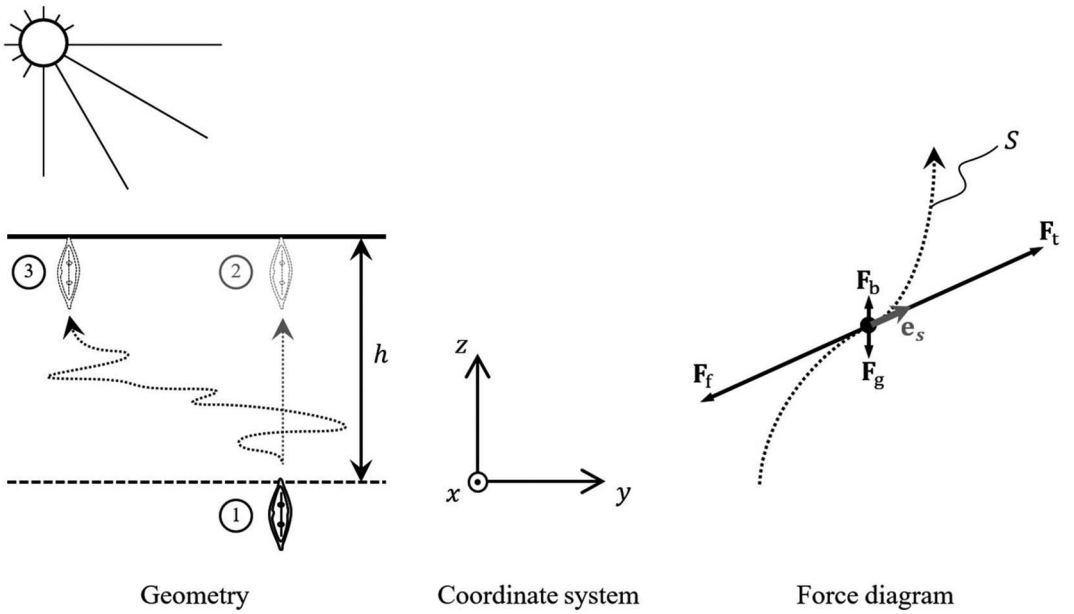

FIGURE 1 | Vertical migratory movements of a motile diatom rising to the surface through a photic sediment layer of depth h.

mechanical work it must do to overcome the forces affecting its body in the sediment. A diatom rising to the surface from the photic sediment depth h (**Figure 1**) must do the mechanical work A_m

$$A_m = -\int_{\mathbb{S}} \mathbf{F}_\Sigma(s)\cdot \mathbf{ds}$$

against the total force $\mathbf{F}_\Sigma$ acting along diatom's (in general, curved) path $\mathbb{S}$ in the sediment parametrized in the Cartesian coordinates of **Figure 1** (x, y, z) via the arc length s (see e.g., Taalman and Kohn, 2014)

$$x = x(s),\ \ y = y(s),\ \ z = z(s),\quad ds^2 = dx^2 + dy^2 + dz^2.$$

The dot represents the scalar product of $\mathbf{F}_\Sigma$ and local displacement **ds**. The total force $\mathbf{F}_\Sigma$ comprises the gravitational force $\mathbf{F}_g = m_d\mathbf{g} = -\rho_d V_d g\mathbf{e}_z$, the buoyancy force $\mathbf{F}_b = \rho_l V_d g\mathbf{e}_z$ and the friction force of the sediment $\mathbf{F}_f = \mathbf{F}_f(s)$. Here m_d and V_d stand for the mass and volume of the diatom, ρ_d and ρ_l are the densities of the diatom and the liquid composing the sediment (water of certain degree of salinity), $\mathbf{g} = -g\mathbf{e}_z$ is the gravitational acceleration ($g \approx 9.8\,\mathrm{m\ s^{-2}}$) and $\mathbf{e}_z$ is a unit vector associated with the vertical axis z.

Taking a conventional model diatom of the size of $10 \times 10 \times 100\ \mu\mathrm{m}^3$ (Edgar, 1982) and supposing that both ρ_d and ρ_l are of the same magnitude as the water density, $\rho_w \approx 1{,}000\,\mathrm{kg\ m^{-3}}$, one can readily assess the order of magnitude of the gravitational and buoyancy forces at the level of $\rho_w V_d g \simeq 10^{-11}$ N. Even without taking into account the fact that the two forces tend to compensate each other—producing the net effect of magnitude $\delta\rho V_d g$, where $\delta\rho = |\rho_d - \rho_l| \ll \rho_w$—one can exclude them from further discussion due to their smallness with respect to the friction force $\mathbf{F}_f$, whose estimation will be presented below.

Within the framework of the inertialess movement approximation—conventionally used for small objects traveling the most part of its trajectory at nearly constant longitudinal velocity under the action of balanced traction and friction forces (see e.g., Dukhin et al., 1995)—we suppose

$$\left|\mathbf{F}_t + \mathbf{F}_f\right| = \left|m_d \frac{d\mathbf{v}_d}{dt}\right| \ll \left|\mathbf{F}_f\right| = F_f$$

(here $\mathbf{v}_d$ is the velocity of the diatom motion) and get at once $\mathbf{F}_t = -\mathbf{F}_f$. As far as the friction force is always directed against the local infinitesimal displacement (speed direction) we have

$$\mathbf{F}_f = -F_f \frac{\mathbf{ds}}{ds} = -F_f \mathbf{e}_s \ \Rightarrow\ \mathbf{F}_t = F_t \mathbf{e}_s$$

where $\mathbf{e}_s$ is the unit vector tangential to the diatom trajectory, as shown in the force diagram of **Figure 1**.

Now the mechanical work estimation takes the form of an integral of the tractive force $\mathbf{F}_t$ over the diatom path $\mathbb{S}_h$ to the surface ($z = h$)

$$\begin{aligned} A_m &= -\int_{\mathbb{S}_h} \mathbf{F}_\Sigma(s)\cdot \mathbf{ds} \approx -\int_{\mathbb{S}_h} \mathbf{F}_f(s)\cdot \mathbf{ds} \approx \int_{\mathbb{S}_h} \mathbf{F}_t(s)\cdot \mathbf{ds} \\ &= \int_{\mathbb{S}_h} F_t(s)\,\mathbf{e}_s\cdot \mathbf{ds} = \int_0^{S_h} F_t(s)ds \end{aligned}$$

where $s = 0$ corresponds to the starting point of the diatom locomotion, S_h is the diatom path length and $F_t(s)$ represents the module of the tractive force at the point $x(s)$, $y(s)$, $z(s)$.

Introducing an average tractive force $\overline{F}$ acting upon the diatom during its motion from $s = 0$ to $s = S_h$, we can reduce the mechanical work estimation to

$$A_m = \int_0^{S_h} F_t(s)ds \approx \int_0^{S_h} \overline{F}ds \approx \overline{F}\int_0^{S_h} ds = \overline{F}S_h.$$

The simplest estimate of this quantity from below relates to the shortest rectilinear vertical path to the surface, ①→② in **Figure 1**. In this case $S_h = h$ and

$$A_m = A_m^{\updownarrow} \approx \overline{F}h.$$

The value of h corresponds to the thickness of the photic sediment layer, attenuating the sunlight by a factor of 10 and for estuarine sediments can be estimated at about 400 μm (see e.g., Kühl et al., 1997; Consalvey et al., 2004). The experimental data that allow to estimate $\overline{F}$ are related to measurements by Harper and Harper (1967), yielding 8×10^{-10} and 1.1×10^{-8} N for *Nitzschia sigmoidea* and *Nitzschia linearis*, respectively. For the typical locomotion speed of 10 μm s^{-1} (Edgar, 1982; Consalvey et al., 2004) and a model $10 \times 10 \times 100$ μm^3 diatom, such a resistance force was estimated by Edgar (1982) as ca. 10^{-10} N. Taking this last value as a rough estimation of the average traction force required for the locomotion, we get $A_m^{\updownarrow} \approx 0.04$ pJ.

Assessment of the Depth-to-Surface Path Length

The actual path $\mathbb{S}$ of the diatom traveling to the surface may be quite distinct from the straight line, representing a complicated curve like one linking positions ① and ③ in **Figure 1**. In the absence of complete nanoscale description of the sediment structure and the possibility of prediction of the diatom behavior, the process of its migration to the sediment surface can only be described within the framework of the stochastic approach, in which the shape of $\mathbb{S}$ is represented by the arc-length-dependent stochastic variables $x(s)$, $y(s)$, $z(s)$. For all practical purposes of the current research, the stochastic process description can be reduced to a single dimensionless chaoticity parameter

$$\sigma \stackrel{\text{def}}{=} \frac{\mathbb{E}\left\{S_h\left(x(s),\ y(s), z(s)\right)\right\}}{h},$$

where $\mathbb{E}\left\{S_h\left(x(s),\ y(s), z(s)\right)\right\}$ is the mathematical expectation of the path length S_h defined by the random process of the diatom walk along the trajectory $x(s)$, $y(s), z(s)$ toward the surface, starting from state ① ($s = 0$, $z(s) = 0$) and ending in state ③ ($s = S_h : z(S_h) = h$), when the substrate surface $z = h$ is reached. Having σ defined, one can assess the long-run average value of the required energy expense for the mechanical work as

$$\overline{A_m} = \overline{F}\,\mathbb{E}\left\{S_h\left(x(s),\ y(s), z(s)\right)\right\} = \overline{F}\sigma h = \sigma A_m^{\updownarrow}, \quad \sigma > 1,$$

where $\sigma \sim 1$ in the case of highly directional vertical motion and $\sigma \gg 1$ for the case of highly chaotic or bidirectional-gliding motion (Yamaoka et al., 2016).

Concrete estimations of $\mathbb{E}\left\{S_h\left(x(s),\ y(s), z(s)\right)\right\}$, as well as σ and $\overline{A_m}$, may be obtained on the basis of various stochastic models describing, to one degree or another, the real movement of different types of diatoms in accordance to their "decision making" and the sediment granularity or by analysis of recorded diatom tracks. For a very rough estimation of the path chaoticity, one can take the geometric mean of the two extreme values of 1 (rectilinear path) and 10 (highly chaotic motion), yielding an indicative value of $\sigma = 3$. For this figure, we readily have an estimation of the characteristic required energy expense of about 0.12 pJ.

Using the algorithm of the friction force estimation by Edgar (1982), we can readily provide a rough assessment of the migration energy cost for a wide range of the diatom species and locomotion conditions. Being based on the work against the viscous force in the thin film separating the raphe (active) face of the cell from the solid particles of substratum—following Edgar, the film thickness is taken to be 0.1 μm—this fully mechanistic approach does not depend on the locomotion type.

Let us introduce the specific energy expenditure per 1 μm of the displacement in the desired direction

$$\overline{a_m} = \overline{A_m}/h = \overline{F}\sigma,$$

to be measured in femtojoule per micrometer [fJ μm^{-1}]. Acting this way, we get rid of the *explicit* dependence of the assessment from the thickness of the photic sediment layer h. Notably, for some, especially small path lengths, $\overline{a_m}$ may depend on h through the chaoticity parameter, which makes it desirable to provide the estimation for the entire characteristic range $1 \leq \sigma \leq 10$, eventually corresponding to different sediment layer thicknesses that can be observed in real conditions. Another parameter, playing one of the key roles in Edgar's calculation of the force, is the medium viscosity, which as well is subjected to significant variation due to changes in temperature, salinity, traces of the surface-active substances, etc. Given such variety of conditions, the energy expenditure can conventionally be presented in the form of plots of $\overline{a_m}$ vs. σ, the vertical bar showing the uncertainty $\delta(\overline{a_m})$ due to possible variation of the medium viscosity, assessed in accordance with the classical data related to water (Engineeringtoolbox.com, 2020) in the temperature range from 0 to 40°C. Such plots are depicted in **Figure 2** for the most illustrative results related to the species of **Table 1**.

Plot (A) represents $\overline{a_m}(\sigma)$ for the group of relatively fast and large diatoms: *Navicula viridula*, migrating with the locomotion speed $v_l = 30.5$ μm s^{-1} (Edgar, 1979) and having the mean surface area of valve face of its cells $\overline{\Omega} = 519$ μm^2 (Diatoms org, 2020a); *Bacillaria paxillifera* of $v_l = 20$ μm s^{-1} (Yamaoka et al., 2016) and $\overline{\Omega} = 485$ μm^2 (Diatoms org, 2020b); and the model diatom of $v_l = 10$ μm s^{-1} and $\overline{\Omega} = 1{,}000$ μm^2 (Edgar, 1982). For this group the specific energy expenditure $\overline{a_m}$ varies from ca. 0.04 (model diatom, rectilinear path in low-viscosity liquid component of the substrate) to 2.5 fJ μm^{-1} (*Navicula viridula*, highly chaotic motion in high-viscosity liquid).

The same plot represents another characteristic group of slower diatoms in two extreme dimensions: *Nitzschia grimmei* and *Nitzschia palea* collected while growing almost equally in a mixed population, of $v_l = 5.5$ μm s^{-1} and small $\overline{\Omega} = 90$ μm^2 (Gupta and Agrawal, 2007) as well as *Gyrosigma*

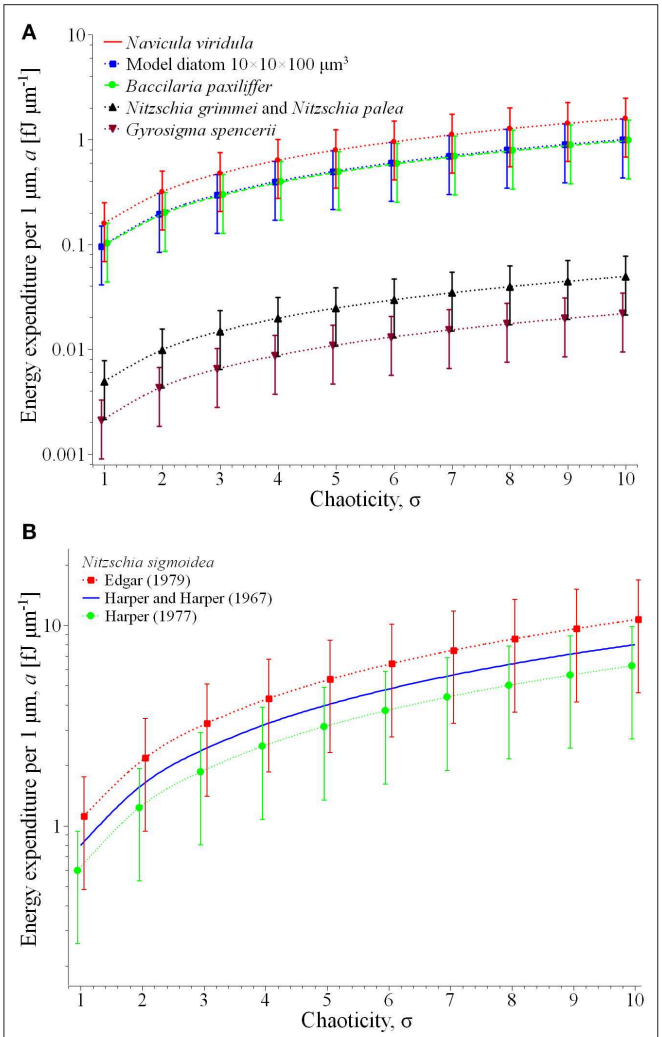

FIGURE 2 | Energy expenditure per 1 μm of the displacement in the desired direction for the most representative species of **Table 1 (A)** and comparison of the specific results for *Nitzschia sigmoidea* **(B)**.

spencerii of $v_l = 0.19\,\mu m\ s^{-1}$ (Hay et al., 1993) and large $\overline{\Omega} = 1{,}151\ \mu m^2$ (Phytolab, 2020). Here the energy expenditure assessment yields far lesser figures, from about 0.0009 (*Gyrosigma spencerii*, rectilinear path and low viscosity) to 0.075 fJ μm^{-1} (*Nitzschia grimmei* and *Nitzschia palea*, highly chaotic motion in high-viscosity liquid).

Plot (B) illustrates a comparison of the theoretical estimate of energy expenditure for *Nitzschia sigmoidea* based on Edgar's calculation of the force $\overline{F}$ for two different values of the locomotion speed, 17 and 28.7 $\mu m\ s^{-1}$ reported respectively by Harper (1977) and Edgar (1979). As can be seen from the extension of the vertical bars of the plot, the apparently contradictory reported results may be explained by different environmental conditions of observations—in particular, unequal viscosities of the liquid phase of the substrate—in which the same traction force may result to different friction-limited velocities of locomotion. Remarkably, the results are very well-coordinated with the alternative assessment based on the experimental value $\overline{F} = 8 \times 10^{-10}$ N reported by Harper and Harper (1967), represented in the plot by a solid line (no vertical bars as there is no force variation).

Metabolic Energy Requirement and Ecological Implications

The energy expended in the vertical migration of a typical diatom cell over a 400 μm photic zone—0.12 pJ—corresponds to 0.0287 pcal. Since the hydrolysis of one mol of ATP releases ∼7,300 cal, the energy expended in the vertical migration of a cell amounts to 3.93×10^{-18} mol ATP. Albeit the theoretical yield of the full oxidation of one mol of glucose is 38 mol ATP, because of losses due to membrane leakage and the cost of transporting pyruvate and ADP into the mitochondrial matrix, more realistic estimates point to 30 mol of ATP per mol of glucose (Rich, 2003). Therefore, the vertical migration of a cell requires the respiration of 1.31×10^{-19} mol of glucose.

Serôdio and Catarino (2000) measured hourly net oxygen production in microphytobenthos mats in the field ranging from 1 to 15 mmol $O_2\ m^{-2}\ h^{-1}$ which correspond to 20–300 fmol $O_2\ h^{-1}$ per cell. If these values are compared the data regarding *Phaeodactylum tricornutum* axenic cultures at 18°C (150 fmol $O_2\ h^{-1}$ per cell; Feijão et al., 2018), we see that the observed field values are very similar to the ones measured experimentally in the lab. Taking into account that diatoms only migrate during daylight and that intertidal banks only experience one tidal cycle during the day, it is possible to assume that diatoms are only exposed to sunlight for a maximum of 4 h per day (Serôdio and Catarino, 2000). Having this value in mind, the average daily net primary productivity of a diatom cell would correspond to 640 fmol $O_2\ d^{-1}$ per cell (considering minimum and maximum values of 80 and 1,200 fmol $O_2\ d^{-1}$ per cell, respectively). Assuming a 1:1 stoichiometry between O_2 evolution and CO_2 fixation, and that 6 carbon atoms are needed for each glucose molecule, the average amount of glucose produced would be 106.7 fmol d^{-1} per cell. This would mean an impact in terms of glucose expenses of 0.0001% of the daily glucose production. Even considering a two paths travel (upward and downward) these values—pertaining a typical diatom cell—remain extremely low. Even though the migration energy consumption may vary almost two orders of magnitude above and below this typical value, depending on the size of the diatom cell, the velocity, and chaocity of displacement and the viscosity of the medium (see section Assessment of the Depth-to-Surface Path Length and **Figure 2**), the maximum fraction of the daily energy allocated to migration would be 0.01%, still a low figure. This contrasts with the energy costs of movement determined for some prokaryotic microorganisms. It is, however, difficult to generalize this comparison, since bacteria have evolved a remarkable diversity of motility systems to adapt to different environments, including swimming in aqueous media, as well as twitching, swarming and gliding on solid and semi-solid surfaces. Albeit significant advances have been made in understanding swimming and swarming motilities powered by flagella, and twitching motility powered by Type IV pili, little is known about gliding motility (Luciano et al., 2011; Nan and

Zusman, 2016), the one most directly comparable with diatom motility, where quantitative estimations of energy consumption are virtually absent. As regards swimming, Mitchell (2002) reported a universal inverse relation between the amount of energy expenditure by unit of body mass and the body mass of the organism. Taking the examples this author provides for bacteria, we calculated that these would roughly spent between 0.0004 pcal (the smaller cells) and 2 pcal (the larger cells) to move along the 400 μm of the typical photic zone in microphytobenthos, which fits in the interval between 0.0003 and 3 pcal that we calculated for diatoms. In ecological terms, the low energy cost of epipelic diatoms' vertical migration points out to a highly efficient mechanism of behavioral photoprotection, having a small impact on the ecosystem metabolism. Using this migration mechanism, a square meter of a microphytobenthos mat (considering a cell density of 5×10^{11} cells per square meter; Jesus et al., 2006) releases <0.0001% of the carbon absorbed to the environment, this vertical movement having an almost neglectable effect on the diatom carbon stock. This is important considering that these organisms play a key role as ecosystem engineers and are at the basis of the mudflat trophic chain, fueling not only the sediment secondary productivity (e.g., organic matter mineralization), but also providing food for grazers, inputting significant amounts of carbon-based energy into the estuarine food webs. Moreover, this also reinforces the role of the autotrophic mats as marine carbon sinks and key players in the biological carbon pump at highly efficient rates.

CONCLUSION

Diatom migration costs rely on several parameters and assumptions that can vary through sediments and microphytobenthic communities. Nevertheless, and considering several average assumptions, a very rough assessment of the energy required for the mechanical diatom motion through the sediment is provided using the conventional inertialess movement approximation. It becomes clear that diatom migration energy expenses depend largely on the chaocity of the *path length* S_h rather than on the *vertical displacement h*, making chaotic curved paths highly expensive in terms of energy costs. The lack of information about the statistical properties of the (random) diatom paths in the granular sediments, which impedes reliable assessment of the mathematical expectation of the path length, constitutes a significant research gap that can potentially be bridged using contemporary approaches to the motion modeling. In particular, the *asymmetric persistent random walk* model (see e.g., Rossetto, 2018) can yield the desired mathematical expectation on the basis of properly assessed transport mean free paths for the upward and downward motion. Alternatively, the path length can be assessed analyzing a representative set of the diatom paths recorded during experimental research. Remarkably, both approaches are hard to implement: For the statistical models, the mean free path (along which the diatom moves quasi rectilinearly) depends on numerous parameters related to the diatom "decision making" and the sediment granularity (average grain size, its dispersion, etc.) that are hard to estimate. An equally hard task is tracking a particular diatom during its migration within highly opaque bulk of the sediment. Nevertheless, and as abovementioned, it is possible to have some average assumptions as basis in order to attain some estimations of the energetic costs associated with the diatom migrations. This was estimated linking both mechanical and biochemical features, resulting in very low energetic costs for the typical diatom cell. This reinforces the key role of vertical migration as an economic mechanism to avoid potential photoinhibition caused by excessive solar radiation on the top of the sediments and maintain the carbon fixation rates of these microphytobenthic communities elevated, and thus greatly contributing to the sediment organic matter, fuelling not only the sediment secondary productivity but also providing energy to higher trophic levels.

AUTHOR CONTRIBUTIONS

JM conceived the idea. AU and BD did the calculations. All the authors discussed and wrote the manuscript.

FUNDING

The authors would like to thank Fundação para a Ciência e a Tecnologia (FCT) for funding the research via project grants PTDC/CTA-AMB/30056/2017 (OPTOX), UID/MAR/04292/2019, UID/MULTI/04046/2019 and UID/MULTI/00612/2019. B. Duarte was supported by an FCT investigation contract (CEECIND/00511/2017).

REFERENCES

Adessi, A., Cruz de Carvalho, R., De Philippis, R., Branquinho, C., and Marques da Silva, J. (2018). Microbial extracellular polymeric substances improve water retention in dryland biological soil crusts. *Soil Biol. Biochem*. 116, 67–69. doi: 10.1016/j.soilbio.2017.10.002

Amin, S. A., Hmelo, L. R., van Tol, H. M., Durham, B. P., Carlson, L. T., Heal, K. R., et al. (2015). Interaction and signalling between a cosmopolitan phytoplankton and associated bacteria. *Nature* 522, 98–101. doi: 10.1038/nature14488

Aumeier, C., and Menzel, D. (2012). "Secretion in the diatoms," in *Secretions and Exudates in Biological Systems,* eds *J. M. Vivanco*, *and F. Baluška (Berlin Heidelberg: Springer-Verlag)*, 221–250. doi: 10.1007/978-3-642-23047-9_10

Ayscough, K. R., Stryker, J., Pokala, N., Sanders, M., Crews, P., and Drubin, D. G. (1997). High rates of actin filament turnover in budding yeast and roles for actin in establishment and maintenance of cell polarity revealed using the actin inhibitor latrunculin-A. *J. Cell Biol.* 137, 399–416. doi: 10.1083/jcb.137.2.399

Cartaxana, P., Cruz, S., Gameiro, C., and Kühl, M. (2016). Regulation of intertidal microphytobenthos photosynthesis over a diel emersion period is strongly affected by diatom migration patterns. *Front. Microbiol.* 7:872.doi: 10.3389/fmicb.2016.00872

Cartaxana, P., Ruivo, M., Hubas, C., Davidson, I., Serôdio, J., and Jesus, B. (2011). Physiological versus behavioral photoprotection in intertidal epipelic and epipsammic benthic diatom communities. *J. Exp. Mar. Biol. Ecol.* 405, 120–127. doi: 10.1016/j.jembe.2011.05.027

Chowdhury, D. (2013). Stochastic mechano-chemical kinetics of molecular motors: A multidisciplinary enterprise from a physicist's perspective. *Phys. Rep*. 529, 1–197. doi: 10.1016/j.physrep.2013.03.005

Cohn, S. A., Bahena, M., Davis, J. T., Ragland, R. L., Rauschenberg, C. D., and Smith, B. L. (2004). Characterization of the diatom photophobic response to high irradiance. *Diatom Res*. 19, 167–179. doi: 10.1080/0269249X.2004.9705869

Cohn, S. A., and Disparti, N. C. (1994). Environmental factors influencing diatom cell motility. *J. Phycol*. 30, 818–828. doi: 10.1111/j.0022-3646.1994.00818.x

Cohn, S. A., Halpin, D., Hawley, N., Ismail, A., Kaplan, Z., Kordes, T., et al. (2015). Comparative analysis of light-stimulated motility responses in three diatom species. *Diatom Res*. 30, 213–225. doi: 10.1080/0269249X.2015.1058295

Cohn, S. A., Spurck, T. P., and Pickett-Heaps, J. D. (1999). High energy irradiation at the leading tip of moving diatoms causes a rapid change in cell direction. *Diatom Res*. 14, 193–206. doi: 10.1080/0269249X.1999.9705466

Cohn, S. A., and Weitzell, R. E. Jr. (1996). Ecological considerations of diatom motility. *I.* characterization of motility and adhesion in four diatom species. *J. Phycol*. 32, 928–939. doi: 10.1111/j.0022-3646.1996.00928.x

Consalvey, M., Paterson, D. M., and Underwood, G. J. C. (2004). The ups and downs of life in a benthic biofilm: migration of benthic diatoms. *Diatom Res*. 19, 181–202. doi: 10.1080/0269249X.2004.9705870

Costa, B. S., Sachse, M., Jungandreas, A., Bartulos, C. R., Gruber, A., Jakob, T., et al. (2013). Aureochrome 1a is involved in the photoacclimation of the diatom *Phaeodactylum tricornutum*. *PLoS ONE* 8:e74451. doi: 10.1371/journal.pone.0074451

Coué, M., Brenner, S. L., Spector, I., and Korn, E. D. (1987). Inhibition of actin polymerization by Latrunculin A. *FEBS Lett*. 213, 316–318. doi: 10.1016/0014-5793(87)81513-2

Depaw, F. A., Rogato, A., D'alcal,á, M. R., and Falciatore, A. (2012). Exploring the molecular basis of responses to light in marine diatoms. *J. Exp. Bot*. 63, 1575–1591. doi: 10.1093/jxb/ers005

Diatoms org (2020a). *Species: Navicula viridula.* Available online at: https://diatoms.org/species/navicula_viridula (accessed April 21, 2020).

Diatoms org (2020b). *Species: Bacillaria Paxillifera.* Available online at: https://diatoms.org/species/bacillaria_paxillifera (accessed April 21, 2020).

Dobrowolski, J. M., Carruthers, V. B., and Sibley, L. D. (1997). Participation of myosin in gliding motility and host cell invasion by *Toxoplasma gondii*. *Mol. Microbiol*. 26, 163–173. doi: 10.1046/j.1365-2958.1997.5671913.x

Du, G. Y., Oak, J. H., Li, H., and Chung, I. K. (2010). Effect of light and sediment grain size on the vertical migration of benthic diatoms. *Algae* 25, 133–140. doi: 10.4490/algae.2010.25.3.133

Dukhin, S. S., Kretzschmar, G., and Miller, R. (1995). *Dynamics of Adsorption at Liquid Interfaces: Theory, Experiment, Application*. Amsterdam; New York, NY: Elsevier.

Edgar, L. A. (1979). Diatom locomotion: computer assisted analysis of cine film. *Br. Phycol. J*. 14, 83–101. doi: 10.1080/00071617900650111

Edgar, L. A. (1982). Diatom locomotion: a consideration of movement in a highly viscous situation. *Br. Phycol. J*. 17, 243–251. doi: 10.1080/00071618200650261

Edgar, L. A. (1983). Mucilage secretions of moving diatoms. *Protoplasma* 118, 44–48. doi: 10.1007/BF01284745

Edgar, L. A., and Pickett-Heaps, J. D. (1982). Ultrastructural localization of polysaccharides in the motile diatom *Navicula cuspidata*. *Protoplasma* 113, 10–22. doi: 10.1007/BF01283035

Edgar, L. A., and Pickett-Heaps, J. D. (1983). The mechanism of diatom locomotion. *I.* an ultrastructural study of the motility apparatus. *Proc. R. Soc. Lond. B* 218, 331–343. doi: 10.1098/rspb.1983.0042

Edgar, L. A., and Zavortink, M. (1983). The mechanism of diatom locomotion. II. Identification of actin. *Proc. R. Soc. Lond. B* 218, 345–348. doi: 10.1098/rspb.1983.0043

Elliott, M., Nedwell, S., Jones, N. V., Read, S. J., Cutts, N. D., and Hemingway, K. L. (1998). *Intertidal Sand and Mudflats & Subtidal Mobile Sandbanks. An Overview of Dynamic and Sensitivity Characteristics for Conservation Management of Marine SACs*. Vol. 2. Oban: Scottish Association for Marine Science (UK Marine SACs Project).

Engineeringtoolbox.com (2020). *Water - Dynamic and Kinematic Viscosity* Available online at: https://www.engineeringtoolbox.com/water-dynamic-kinematic-viscosity-d_596.html (accessed *April* 18, 2020).

Falciatore, A., D'alcala, R., Croot, P., and Bowler, C. (2000). Perception of environmental signals by a marine diatom. *Science* 288, 2363–2366. doi: 10.1126/science.288.5475.2363

Feijão, E., Gameiro, C., Franzitta, M., Duarte, B., Caçador, I., Cabrita, M. T., et al. (2018). Heat wave impacts on the model diatom *Phaeodactylum tricornutum*: searching for photochemical and fatty acid biomarkers of thermal stress. *Ecol. Indicators* 95, 1026–1037. doi: 10.1016/j.ecolind.2017.07.058

Fritsch, F. E. (1935). *The Structure and Reproduction of the Algae*. Vol. 1. Cambridge, CA: Cambridge University Press.

Gupta, G., and Agrawal, S. C. (2007). Survival and motility of diatoms *Navicula grimmei* and *Nitzschia palea* affected by some physical and chemical factors. *Folia Microbiol*. 52, 127–134. doi: 10.1007/BF02932151

Harbich, T. (2019). *Movement in EPS matrix: Biofilms on substrate*. Available online at: https://www.diatoms.de/en/biofilms-on-substrate (accessed October 31, 2019).

Harper, M. A. (1967). *Locomotion of diatoms and 'clumping' of blue-green algae* (Ph.D. Thesis). University of Bristol.

Harper, M. A. (1977). "Movements," in *The Biology of Diatoms.* ed D. Werner (Oxford: Blackwell Scientific Publications), 224–249.

Harper, M. A., and Harper, J. F. (1967). Measurements of diatom adhesion and their relationship with movement. *Br. Phycol. Bull.* 3, 195–207. doi: 10.1080/00071616700650051

Hay, S. I., Maitland, T. C., and Paterson, D. M. (1993). The speed of diatom migration through natural and artificial substrata. *Diatom Res*. 8, 371–384. doi: 10.1080/0269249X.1993.9705268

Hopkins, J. T., and Drum, R. W. (1966). Diatom motility: an explanation and a problem. *Br. Phycol. Bull*. 3, 63–67. doi: 10.1080/00071616600650081

Ishikawa, M., Takahashi, F., Nozaki, H., Nagasato, C., Motomura, T., and Kataoka, H. (2009). Distribution and phylogeny of the blue light receptors aureochromes in eukaryotes. *Planta* 230, 543–552. doi: 10.1007/s00425-009-0967-6

Jesus, B., Mendes, C. R., Brotas, V., and Paterson, D. M. (2006). Effect of sediment type on microphytobenthos vertical distribution: modelling the productive biomass and improving ground truth measurements. *J. Exp. Mar. Biol. Ecol*. 332, 60–74. doi: 10.1016/j.jembe.2005.11.005

Kooistra, W. H. C. F., De Stefano, M., Mann, D. G., Salma, N., and Medlin, L. K. (2003). Phylogenetic position of Toxarium, a pennate-like lineage within the centric diatoms (Bacillariophyceae). *J. Phycol*. 39, 185–197. doi: 10.1046/j.1529-8817.2003.02083.x

Kromkamp, J., Barranguet, C., and Peene, J. (1998). Determination of microphytobenthos PSII quantum efficiency and photosynthetic activity by means of variable chlorophyll fluorescence. *Mar. Ecol. Prog. Ser*. 162, 45–55. doi: 10.3354/meps162045

Kühl, M., Lassen, C., and Revsbech, N. (1997). A simple light meter for measurements of PAR (400 to 700 nm) with fiber-optic microprobes: application for P vs E0(PAR) measurements in a microbial mat. *Aquat. Microb. Ecol*. 13, 197–207. doi: 10.3354/ame013197

Lammermann, T., and Sixt, M. (2009). Mechanical modes of 'amoeboid' cell migration. *Curr. Opin. Cell Biol*. 21, 636–644. doi: 10.1016/j.ceb.2009.05.003

Lange, K., Liess, A., Piggott, J. J., Townsend, C. R., and Matthaei, C. D. (2011). Light, nutrients and grazing interact to determine stream diatom community composition and functional group structure. *Freshw. Biol*. 56, 264–278. doi: 10.1111/j.1365-2427.2010.02492.x

Luciano, J., Agrebi, R., Le Gall, A. V., Wartel, M., Fiegna, F., Ducret, A., et al. (2011). Emergence and modular evolution of a novel motility machinery in Bacteria. *PLoS Gene.* 7:e1002268. doi: 10.1371/journal.pgen.1002268

Marques da Silva, J., and Casetta, E. (2019). "Why a species-based approach to biodiversity is not enough. lessons from multispecies biofilms," in *From Assessing to Conserving Biodiversity,* eds E. Casetta, J. Marques da Silva, and D. Vecchi (Berlin: Springer), 195–217. doi: 10.1007/978-3-030-10991-2_9

Marques da Silva, J., Cruz, S., and Cartaxana, P. (2017). Inorganic carbon availability in benthic diatom communities: photosynthesis and migration. *Philos. Trans. R. Soc. Lond. B* 372:20160398.doi: 10.1098/rstb.2016.0398

Marques da Silva, J., and Utkin, A. B. (2018). Application of laser induced fluorescence in functional studies of photosynthetic biofilms. *Processes* 6:227.doi: 10.3390/pr6110227

McConville, M. J., Wetherbee, R., and Bacic, A. (1999). Subcellular location and composition of the wall and secreted extracellular sulphated polysaccharides/proteoglycans of the diatom *Stauroneis amphioxys* Gregoty. *Protoplasma* 206, 188–200. doi: 10.1007/BF01279266

McLashlan, D. H., Underwood, G. J. C., Taylor, A. R., and Brownlee, C. (2012). Calcium release from intracellular stores is necessary for the photophobic

response in the benthic diatom *Navicula perminuta* (Bacillariophyceae). *J. Phycol*. 48, 675–681. doi: 10.1111/j.1529-8817.2012.01158.x

Mitchell, J. G. (2002). The energetics and scaling of search strategies in Bacteria. *Am. Nat*. 160, 727–740. doi: 10.1086/343874

Murase, A., Kubota, Y., Hirayama, S., Kumashiro, Y., Okano, T., Mayama, S., et al. (2011). Two-dimensional trajectory analysis of the diatom Navicula sp. *using a micro chamber. J. Microbiol. Methods* 87, 316–319. doi: 10.1016/j.mimet.2011.09.006

Nan, B., and Zusman, D. R. (2016). Novel mechanisms power bacterial gliding motility. *Mol. Microbiol.* 101, 186–193. doi: 10.1111/mmi.13389

Palmer, T. (1991). *Understanding Enzymes, 3rd Edn*. Chichester: Ellis Horwood Limited.

Passy, S. I. (2007). Diatom ecological guilds display distinct and predictable behavior along nutrient and disturbance gradients in running waters. *Aquat. Bot*. 86, 171–178. doi: 10.1016/j.aquabot.2006.09.018

Paterson, D. M. (1989). Short-term changes in the erodibility of intertidal cohesive sediments related to the migratory behavior of epipelic diatoms. *Limnol. Oceanogr*. 34, 223–234. doi: 10.4319/lo.1989.34.1.0223

Perkins, R. G., Lavaud, J., Serôdio, J., Mouget, J. L., Cartaxana, P., Rosa, P., et al. (2010). Vertical cell movement is a primary response of intertidal benthic biofilms to increasing light dose. *Mar. Ecol. Prog. Ser*. 416, 93–103. doi: 10.3354/meps08787

Perkins, R. G., Underwood, G. J. C., Brotas, V., Snow, G. C., Jesus, B., and Ribeiro, L. (2001). Responses of microphytobenthos to light: primary production and carbohydrate allocation over an emersion period. *Mar. Ecol. Prog. Ser*. 223, 101–112. doi: 10.3354/meps223101

Phytolab (2020). *Gyrosigma spencerii. Ann Arbor: University of Michigan. reatLakesDiatomHomePage/Gyrosigma/Gyrosigma*Available online at: http://umich.edu/~phytolab/Gspencerii/Gyrosigmaspenceriicard.html#authority (accessed April 22, 2020).

Pinckney, J., and Zingmark, R. G. (1993). Photophysiological responses of intertidal benthic microalgal communities to *in situ* light environments: methodological considerations Limnol. *Oceanogr* 38, 1373–1383. doi: 10.4319/lo.1993.38.7.1373

Pinder, J. C., Fowler, R. E., Dluzewski, A. R., Bannister, L. H., Lavin, F. M., Mitchell, G. H., et al. (1998). Actomyosin motor in the merozoite of the malaria parasite, *Plasmodium falciparum*: implication for red cell invasion. *J. Cell Sci*. 111, 1831–1839.

Poulsen, N., Kroger, N., Harrington, M. J., Brunner, E., Paasch, S., and Buhmann, M. T. (2014). Isolation and biochemical characterization of underwater adhesives from diatoms. *Biofouling* 30, 513–523. doi: 10.1080/08927014.2014.895895

Poulsen, N. C., Spector, I., Spurck, T. P., Schultz, T. F., and Wetherbee, R. (1999). Diatom gliding is the result of an actin-myosin motility system. *Cell Motil. Cytoskel*. 44, 23–33. doi: 10.1002/(SICI)1097-0169(199909)44:1<23::AID-CM2>3.0.CO;2-D

Preston, T. M., and King, C. A. (1996). Strategies for cell-substratum dependent motility among protozoa. *Acta Protozool*. 35, 3–12.

Rich, P. R. (2003). The molecular machinery of Keilin's respiratory chain. *Biochem. Soc. Trans*. 31, 1095–1105. doi: 10.1042/bst0311095

Rossetto, V. (2018). The one-dimensional asymmetric persistent random walk. *J. Stat. Mech*. 2018:043204. doi: 10.1088/1742-5468/aab507

Saburova, M. A., and Polikarpov, I. G. (2003). Diatom activity within soft sediments: behavioural and physiological processes. *Mar. Ecol. Prog. Ser*. 251, 115–126. doi: 10.3354/meps251115

Serôdio, J., and Catarino, F. (2000). Modelling the primary productivity of intertidal microphytobenthos: time scales of variability and effects of migratory rhythms. *Mar. Ecol. Prog. Ser*. 192, 13–30. doi: 10.3354/meps192013

Serôdio, J., Coelho, H., Vieira, S., and Cruz, S. (2006). Microphytobenthos vertical migratory photoresponse as characterised by light-response curves of surface biomass. *Estuar. Coast. Shelf Sci*. 68, 547–556. doi: 10.1016/j.ecss.2006.03.005

Serôdio, J., Marques da Silva, J., and Catarino, F. (1997). Nondestructive tracing of migratory rhythms of intertidal benthic microalgae using *in vivo* chlorophyll a fluorescence. *J. Phycol*. 33, 542–553. doi: 10.1111/j.0022-3646.1997.00542.x

Serôdio, J., Marques da Silva, J., and Catarino, F. (2001). Use of *in vivo* chlorophyll a fluorescence to quantify short-term variations in the productive biomass of intertidal microphytobenthos. *Mar. Ecol. Prog. Ser*. 218, 45–61. doi: 10.3354/meps218045

Serôdio, J., Vieira, S., and Cruz, S. (2008). Photosynthetic activity, photoprotection and photoinhibition in intertidal microphytobenthos as studied *in situ* using variable chlorophyll fluorescence. *Cont. Shelf Res*. 28, 1363–1375. doi: 10.1016/j.csr.2008.03.019

Sibley, L. D., Håkansson, S., and Carruthers, V. B. (1998). Gliding motility: an efficient mechanism for cell penetration. *Curr. Biol*. 8, R12–R14. doi: 10.1016/S0960-9822(98)70008-9

Spormann, A. M. (1999). Gliding motility in bacteria: insights from studies of *Myxococcus xanthus*. *Microbiol. Mol. Biol. Rev*. 63, 621–641. doi: 10.1128/MMBR.63.3.621-641.1999

Sutherland, T. F., Grant, J., and Amos, C. L. (1998). The effect of carbohydrate production by the diatom *Nitzschia curvilieata* on the erodibility of sediment. *Limnol. Oceanogr* 43, 65–72. doi: 10.4319/lo.1998.43.1.0065

Svensson, F., Norberg, J., and Snoeijs, P. (2014). Diatom cell size, coloniality and motility: Trade-offs between temperature, salinity and nutrient supply with climate change. *PLoS ONE* 9:e109993. doi: 10.1371/journal.pone.0109993

Taalman, L., and Kohn, P. (2014). *Calculus*. New York, NY: W.H. Freeman and Company.

Underwood, G. J. C., Perkins, R. G., Consalvey, M. C., Halon, A. R. M., Oxborough, K., Baker, N. R., et al. (2005). Patterns in microphytobenthic primary productivity: species-specific variation in migratory rhythms and photosynthetic efficiency in mixed-species biofilms. *Limnol. Oceanogr* 50, 755–767. doi: 10.4319/lo.2005.50.3.0755

Ussing, A. P., Gordon, R., Ector, L., Buczko, K., Desnitskiy, A. G., and Vanlandingham, S. A. (2005). *The colonial diatom "Bacillaria paradoxa": chaotic gliding motility, Lindenmeyer model of colonial morphogenesis, and bibliography, with translation of O.F. Müller (1783), about a peculiar being in the beach-water"*. Ruggell: Gantner Verlag.

Utkin, A. B., Vieira, S., Marques da Silva, J., Lavrov, A., Leite, E., and Cartaxana, P. (2013). Compact low-cost detector for *in vivo* assessment of microphytobenthos using laser induced fluorescence. *Opt Spectrosc.* 114, 471–474. doi: 10.1134/S0030400X13030259

Vargas, P., Barbier, L., Saéz, P. J., and Piel, M. (2017). Mechanisms for fast cell migration in complex environments. *Curr. Opin. Cell Biol*. 48, 72–78. doi: 10.1016/j.ceb.2017.04.007

Vieira, S., Lavrov, A., Utkin, A., Santos, A., Vilar, R., Marques da Silva, J., et al. (2011). Effects of migration on intertidal microphytobenthos biomass measured by laser-induced fluorescence (LIF). *Mar. Ecol. Prog. Ser*. 432, 45–52. doi: 10.3354/meps09157

Vieira, S., Ribeiro, L., Jesus, B., Cartaxana, P., and Marques da Silva, J. (2013). Photosynthesis assessment in microphytobenthos with conventional and imaging pulse amplitude modulation fluorometry. *Photochem. Photobiol.* 89, 97-102. doi: 10.1111/j.1751-1097.2012.01224.x

Villareal, T. A. (1992). Buoyancy properties of the giant diatom *Ethmodiscus*. *J. Plankton Res*. 14, 459–463. doi: 10.1093/plankt/14.3.459

Wang, J., Cao, S., Du, C., and Chen, D. (2013). Underwater locomotion strategy by a benthic pennate diatom *Navicula* sp. *Protoplasma* 250, 1203–1212. doi: 10.1007/s00709-013-0502-2

Wells, A. L., Lin, A. W., Chen, L. Q., Safer, D., Cain, S. M., Hasson, T., et al. (1999). Myosin VI is an actin-based motor that moves backwards. *Nature* 401, 505–508. doi: 10.1038/46835

West, G. S. (1916). *Algae*. Vol. 1. Cambridge, CA: Cambridge University Press.

Yamaoka, N., Suetomo, Y., Yoshihisa, T., and Sonobe, S. (2016). Motion analysis and ultrastructural study of a colonial diatom, *Bacillaria paxillifer*. *Microscopy* 65, 211–221. doi: 10.1093/jmicro/dfv375

Conflict of Interest: The authors declare that the research was conducted in the absence of any commercial or financial relationships that could be construed as a potential conflict of interest.

frontiers in Marine Science

ORIGINAL RESEARCH
published: 25 August 2020
doi: 10.3389/fmars.2020.00685

Shorebirds Affect Ecosystem Functioning on an Intertidal Mudflat

James M. Booty[1], Graham J. C. Underwood[2], Amie Parris[2], Richard G. Davies[3] and Trevor J. Tolhurst[1]*

[1] School of Environmental Sciences, University of East Anglia, Norwich, United Kingdom, [2] School of Life Sciences, University of Essex, Colchester, United Kingdom, [3] School of Biological Sciences, University of East Anglia, Norwich, United Kingdom

Ecosystem functioning and services have provided a rationale for conservation over the past decades. Intertidal muddy sediments, and the microphytobenthic biofilms that inhabit them, perform crucial ecosystem functions including erosion protection, nutrient cycling and carbon sequestration. It has been suggested that predation on sediment macrofauna by shorebirds may impact biofilms, and shorebirds are known to consume biofilm, potentially causing significant top-down effects on mudflat ecosystem functioning. We carried out an exclusion experiment on the Colne Estuary, Essex, to examine whether shorebird presence significantly affects sediment erodibility measured with a Cohesive Strength Meter (CSM) and microphytobenthos biomass measured using PAM fluorescence (F_O) and chlorophyll *a* content. We also tested for treatment effects on sediment-water nutrient fluxes [nitrate, nitrite, ammonia, phosphate and dissolved organic carbon (DOC)] during periods of both dark and light incubation. Excluding shorebirds caused statistically significant changes in regulating and provisioning ecosystem functions, including mudflat erodibility and nutrient fluxes. The presence of shorebirds lowered the sediment critical erosion threshold τ_{cr}, reduced nitrate fluxes into the sediment under illumination, lowered nitrate efflux, and reduced phosphate uptake, compared to sediments where birds were excluded. There were no significant differences in macrofauna community composition within the sediment between treatments after 45 days of bird exclusion, suggesting a direct link between shorebird presence or absence and the significant differences in biofilm-related variables. This study introduces previously unknown effects of shorebird presence on ecosystem functions within this system and highlights an area of shorebird science that could aid joint conservation and human provisioning action.

Keywords: shorebirds, ecosystem function, microphytobenthos biofilm, sediment erosion, nutrient flux

OPEN ACCESS

Edited by:
David M. Paterson, University of St Andrews, United Kingdom

Reviewed by:
Diana Hamilton, Mount Allison University, Canada
João Serôdio, University of Aveiro, Portugal

****Correspondence:***
James M. Booty
j.booty@uea.ac.uk;
james_booty@hotmail.co.uk

Specialty section:
This article was submitted to Marine Ecosystem Ecology, a section of the journal Frontiers in Marine Science

Received: *15 October 2019*
Accepted: *28 July 2020*
Published: *25 August 2020*

Citation:
Booty JM, Underwood GJC, Parris A, Davies RG and Tolhurst TJ (2020) Shorebirds Affect Ecosystem Functioning on an Intertidal Mudflat. Front. Mar. Sci. 7:685. doi: 10.3389/fmars.2020.00685

INTRODUCTION

Ecosystem functioning and ecosystem services have provided a rationale for conservation over the past decades (Cabello et al., 2012). Intertidal mudflat ecosystem functions include nutrient cycling, erosion protection and carbon sequestration, which mediate associated services (Foster et al., 2013). Intertidal flats provide natural 'soft' coastal erosion defense by reducing wave energy, lowering water velocities and thereby shear stress on the estuary bed (Spalding et al., 2014). Benthic microalgae [microphytobenthos (MPB)] form complex matrices of cells, sediments and extra

polymeric substances (EPS) (Underwood and Paterson, 2003). These biofilms have a stabilizing effect on surface sediments, reducing erodibilty and aiding in the accumulation of particles and microbes (Gerbersdorf and Wieprecht, 2015). Estuarine sediments and biofilms are central components in estuarine nutrient cycles, ultimately affecting fluxes of these nutrients between land and sea (Thornton et al., 2007; Nedwell et al., 2016). Organic compounds are recycled and remineralized within sediments, particularly in coastal marine areas where nitrogen and phosphorous loads can be very high (Correll et al., 1992; Hochard et al., 2010). Nitrogen loading into marine systems can lead to eutrophication and decline in water quality, making its source and removal pathways of high interest (Burgin and Hamilton, 2007) and changes in nutrient loads can impact benthic communities (Culhane et al., 2019). MPB mediate fluxes of NO_3^-, NO_2^-, PO_4^{3-} and NH_4^+ between the water column and sediment layers (Sundback et al., 1991; Correll et al., 1992; Feuillet-Gerard et al., 1997), contributing to this process either by direct uptake/release or by altering oxygen concentration (Sundback and Graneli, 1988). Dissolved organic carbon (DOC) may also provide an important part of both global and coastal carbon sinks (Maher and Eyre, 2010; Legge et al., 2020), making effects on DOC fluxes in this environment relevant to anthropogenic climate change effects and mitigation (McKinley et al., 2016).

Mud and sand flats are essential habitats for the survival of resident and migratory overwintering shorebirds (Burton et al., 2006), which feed primarily upon infaunal and epifaunal invertebrates (Bowgen et al., 2015). Some small sandpiper species *Calidris* spp. also directly consume biofilm during, or in preparation for, migration (Kuwae et al., 2008; Jardine et al., 2015). Grazing of MPB and bioturbation by macrofauna can lead to alterations in sediment erodibility and other ecosystem functions (de Deckere et al., 2001; Hale et al., 2019). This poses questions regarding the effect of biofilm removal and bioturbation by shorebirds (Mathot et al., 2018), which may have significant knock-on effects altering ecosystem functions.

Research suggests that shorebirds could have significant direct and/or indirect effects on ecosystem function, e.g., via the impacts of foraging on macrofauna and/or biofilm or disturbance and reworking of sediment (Orvain et al., 2014b; Mathot et al., 2018). In the Bay Of Fundy (BOF), semipalmated sandpipers *Calidris pusilla* appeared to cause an ecological cascade effect by reducing densities of their mud shrimp prey *Corophium volutator*, which caused biofilm proliferation, leading to an increase in sediment stability (Daborn et al., 1993). However, subsequent research in the BOF has not indicated a trophic cascade effect, possibly due to compensatory interactions by macrofauna (Hamilton et al., 2006; Cheverie et al., 2014). Trophic webs and ecosystem functioning were compared in the Marenne-Oleron Bay, France, indicating that estuarine trophic webs including shorebirds have enhanced primary productivity through increased nutrient cycling (Saint-Beat et al., 2013). Despite evidence that estuarine shorebirds may significantly alter ecosystem functioning, the majority of shorebird research has an ornithological focus and potential top down effects on ecosystem functions such as erosion defense and nutrient cycling have not yet been experimentally tested (Mathot et al., 2018). The ecology of intertidal sediments is complex, compensatory interactions can mask effects (Hamilton et al., 2006), including trophic cascades (Fahimipour et al., 2017). Manipulative experiments are a valuable tool, to be utilized alongside 'natural' or 'observational' experiments to assess possible ecological mechanisms behind processes observed at wider spatial or temporal scales (Rogers et al., 2012).

The Colne Estuary, Essex, United Kingdom is a complex of habitats featuring many sand and mudflats, protected internationally under The Conservation of Habitats and Species (Amendment) (EU Exit) Regulations 2019, for supporting over 30,000 shorebirds. Our study site within the Colne Estuary, the Fingringhoe Wick Site of Special Scientific Interest (SSSI), was a location for the six year Coastal Biodiversity and Ecosystem Service Sustainability research program (CBESS), which provides key background information on the biotic and abiotic characteristics of the site.

Changes in community composition and mudflat characteristics can be rapid, occurring over months (Sahan et al., 2007; Rosa et al., 2008; Murphy and Tolhurst, 2009) weeks (Daborn et al., 1993; Hamilton et al., 2006), days (de Deckere et al., 2001; Tolhurst et al., 2008) and even hours (Tolhurst et al., 2006a,b). We designed and carried out a two month field exclusion experiment, supplemented by laboratory measurements, to investigate shorebird effects on two ecosystem functions, namely erosion protection (using a measure of sediment erodibility as a proxy) and nutrient cycling (including nitrate, nitrite, ammonia, phosphate and DOC). We tested three hypotheses: (1) surface biofilm biomass would be significantly altered in the presence of shorebirds, (2) sediment erodibility would be significantly altered in the presence of shorebirds and (3) nutrient fluxes between the sediment and water column would be significantly different between treatments (shorebird presence and absence) with flux direction and magnitude for different nutrient species increasing with greater MPB biomass.

MATERIALS AND METHODS

Description of Study Site

Fieldwork was undertaken between 20 January and 03 April 2017 on the mudflat adjacent to Geedon Saltings at Fingringhoe Wick Essex Wildlife Trust Nature Reserve, Essex, United Kingdom (grid reference TM 05065 19030). This time period covered the peak overwintering and start of the migratory periods for shorebirds in the East of England. The study location comprised an area of mudflat approximately 400 m^2 situated on the upper shore. Observations during 2016 noted flocks of dunlin *Calidris alpina* and knot *Calidris canutus*, and scattered individual redshank *Tringa totanus* and gray plover *Pluvialis squatarola* foraging at the study site on receding and incoming tides. The study location was set within a larger area of estuarine mudflat, approximately 130,000 m^2 of which could be visually surveyed for shorebird activity from a fixed point (Geedon hide).

Previous CBESS studies showed that during winter, sediment at the site is mostly silts and clays, with a very low proportion of sand (maximum 'very fine sand' content in a sample was

6.5%; coarser sand contents were all lower than this), with sediment particle size at the site predominantly <63 μm (mean 95.9 % ± 0.3 SE). Mean D_{50} = 6.9 μm ± 0.2 SE; Mean D_{16} = 1.9 μm ± 0.04 SE; D_{95} = 66.9 μm ± 13.2 SE (D_x = particle diameter representing the x% cumulative percentile) (Wood et al., 2015). Mean percentage surface sediment water content at the site is 62.3 ± 0.4 SE (Maunder and Paterson, 2015). This site lies within the polyhaline section of the estuary, with salinity ranging from 18-30, depending on freshwater flow conditions, with lower salinity during winter (Nedwell et al., 2016).

CBESS research also included sampling of fauna within the Colne estuary, demonstrating that during winter fish were absent, with only Ctenophores recorded during Fyke netting (Wood et al., 2015). Macrofauna recorded during winter CBESS research included ragworm *Hediste diversicolor*, mud snail *Peringia ulvae*, Baltic clam *Macoma balthica* and nematodes across a total of 22 quadrat sites, in which three samples were taken at each (Wood et al., 2015). A year-long fish sampling study carried out at two different locations along the estuary where our experiment was undertaken, found that fish were absent at all sampled sites during January, and absent from three out of five sites during February (Green et al., 2009). Where fish were present at two sites during February, total abundance (fish 100 m^{-2}) was approximately 2, and less than 1 during March (Green et al., 2009).

Experiment Design

The manipulative experiment was set up on 20 January 2017 (day 0). The experimental layout was a randomized design of 20 spatial plots (**Figure 1**), each 1 m x 1 m, allocated to two treatment levels; control (shorebirds present in open un-manipulated plots) and exclosure (shorebirds absent), with n = 10 replicates of each treatment. Previous work in the estuary showed that spatial variability in biofilm abundance is greatest at the fine scale and small at the meter scale (Taylor et al., 2013; Nedwell et al., 2016), therefore a completely randomized design was employed to maximize statistical power of the experiment. Exclosures were bamboo frames, approximately 30 cm in height, covered on all sides (including the top) by opaque 'fruit-cage' bird exclusion netting (plastic mono-thread) with a 2 cm aperture. Exclosures prevented access to the sediment by birds, but allowed access to infauna and small fish (<2 cm width). All plots were at least three meters apart, to allow sampling from all sides and prevent plots unduly influencing each other. Exclosure and control plots were unpaired and separated by similar distances, with treatments arranged sequentially to reduce the potential for spatial bias. The exact locations of plots were selected to represent the heterogeneity within the wider mudflat. No scouring or bite marks indicating the presence of larger fish (Eggold and Motta, 1992) were found within any plots during the experiment. Plots were arranged parallel to the tide line (within a minute of immersion/emersion time of one another). Plots were situated on the upper shore, where shorebirds spend most time foraging due to the longer emersion time (Granadeiro et al., 2006). Camera footage (see below) and direct observation recorded no events of birds standing on exclosures (behavior which may otherwise have caused input of droppings into exclosure absence plots as well as control presence plots) (Schrama et al., 2013; Jauffrais et al., 2015).

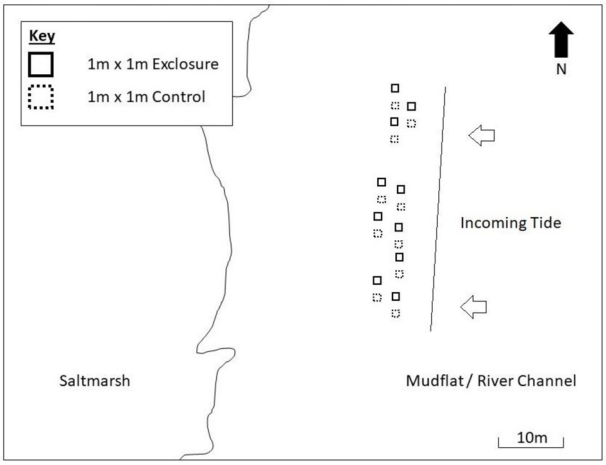

FIGURE 1 | Experimental layout adjacent to Geedon Saltings, Essex Wildlife Trust Fingringhoe Wick, Essex (grid reference TM 05065 19030).

Assessment of Possible Experimental Artifacts

To test the effect of the exclosures on the water flow within the study area, a 'plaster ball dissolution test' was carried out on days 17 and 18 (Cheverie et al., 2014). No significant difference was detected between plaster dissolution rates in control plots and exclosure plots (t = -1.057; df = 8; p = 0.322), demonstrating that our exclosures had no significant effects on tidal water flows in the vicinity of the mudflat surface.

Exclosure shading tests were carried out after the experiment to prevent additional mudflat disturbance, during a sunny day (cloud cover < 10%), hence resulting in an estimation of shading at the higher end of the actual range during the study period. Shading effects on Photosynthetically Active Radiation (PAR) reaching the sediment surface in exclosures were small (9.9%), and of a similar level to that in other manipulative studies in this type of environment (Cheverie et al., 2014). Further information reinforcing this conclusion is given in the discussion.

A Go-Pro HERO 4 camera fitted with a Cam-Do Blink time lapse controller mounted within a Cam-Do Solar-X enclosure (Cam-Do Solutions, 2017) was deployed to monitor bird activity within the study area for four weeks (21 February 2017 to 21 March 2017). This was mounted on a vertical pole 3.5 m above the saltmarsh at grid ref: TM 05031 19032. The camera captured a still of the plots every five minutes during daylight hours. Although species identification was not possible using captured images, numbers within the field of view were used to broadly determine whether numbers of birds using the study area were consistent with those recorded during visual surveys.

Weather data were collected during the experimental period [peak wind speed (km h^{-1}), daily precipitation (hours day^{-1}) and peak temperature (°C)], and plotted against biofilm biomass (F_o) and shorebird numbers to assess potential effects of

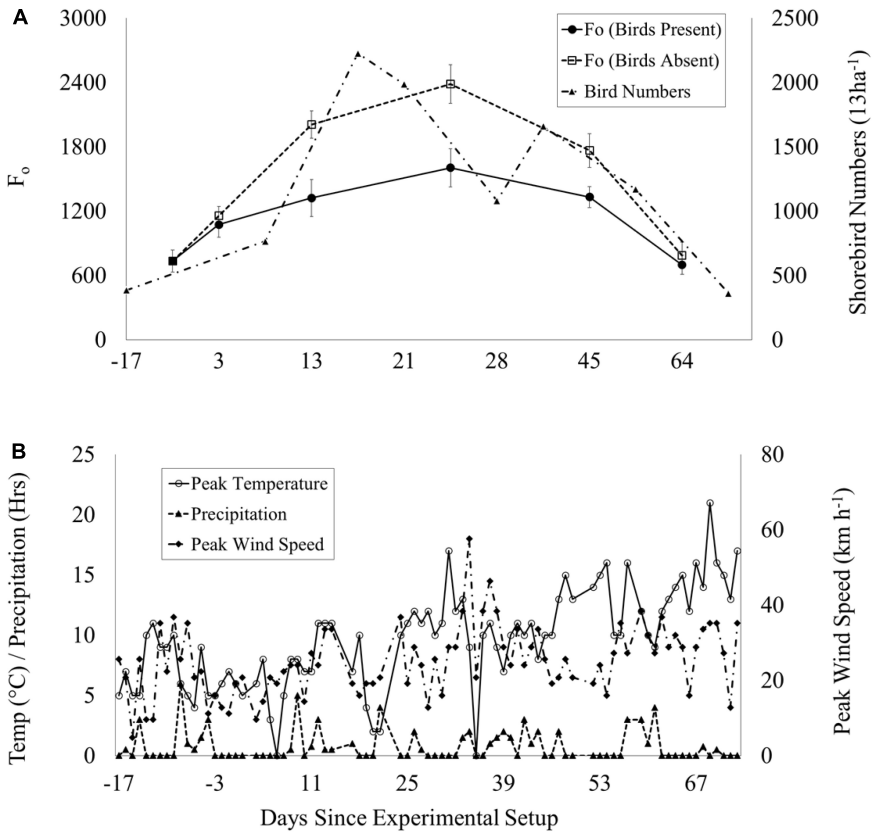

FIGURE 2 | Time series during the experimental period (03 Jan – 03 April 2017): **(A)** Mean F_o (±SE, n = 50) in shorebird presence (solid line, filled circles)/absence (dotted line, unfilled squares) plots and total peak shorebird count (multi-dash line, filled triangles). Dip in numbers on day 28 coincides with disturbance of flocks by marsh harrier. **(B)** Weather data per day: peak temperature (°C): solid line with unfilled circles, peak wind speed (km h^{-1}): multi-dash with filled diamonds and precipitation (hours): dash with filled triangles.

these variables on the experiment, such as extreme weather events, which can have significant effects on shorebird activity (Sutherland et al., 2012) and mudflat characteristics (Tolhurst et al., 2006b; Fagherazzi et al., 2017; Hale et al., 2019). No extreme weather events occurred during the experiment and no evidence was found of a relationship between F_o and daily precipitation (hours), peak temperature (°C) and peak wind speed (km h^{-1}) during the experiment (**Figures 2A,B**), although the potential for delayed responses has not been assessed. However, all plots were subject to the same weather and this is not considered to be a constraint to the experiment.

Response Variables

Between day variation in mudflat characteristics have been shown to be of greater significance than within day variation (Tolhurst and Chapman, 2005), therefore repeated measures of F_o were made to compensate for this effect. **Table 1** shows dates and days at which sampling events took place. On 20 January 2017, immediately following plot setup, 'day 0' minimum fluorescence (F_o) measurements were taken using a pulse amplitude modulated fluorometer (PAM, Walz, Effeltrich, Germany) to determine MPB biomass (Honeywill et al., 2002). MPB are key drivers of intertidal flat properties and processes (e.g., Murphy and Tolhurst, 2009), so to determine when the full sampling event would be most likely to detect any effects we monitored F_o (as a proxy for MPB biomass) on days 3, 13 and 26, as a convenient indication of treatment effects, to determine when erodibility and nutrient flux variables should be measured and to confirm that early in the experiment there were no significant differences between treatments. F_o was also measured on day 45 to evaluate the effect of shorebird presence/absence on MPB biomass and associated properties, and on day 64 to determine if trends continued. A subset of 6 exclosure and 6 control plots were measured on day 3 for a total of 60 F_o measurements (n = 5 in each of the 12 plots); subsequently all plots were measured, for a total of 100 F_o measurements (n = 5 in each of the 20 plots) on days 13, 26, 45, and 64 to investigate how surface MPB biomass responded to shorebird presence/absence over time.

Due to the large number of measurements required in each plot during a tidal cycle and considering the impact of dewatering during the tidal cycle (Maggi et al., 2013; Orvain et al., 2014a; Fagherazzi et al., 2017) a 5 min low light partial dark adaption treatment was used prior to each PAM measurement, which is a preferred method to conventional dark adaption for the measurement of minimum fluorescence as a proxy of MPB

TABLE 1 | Dates and numbers of days into the experiment that field sampling events occurred between 03 January and 03 April 2017 on the mudflat adjacent to Geedon Saltings at Fingringhoe Wick Essex Wildlife Trust Nature Reserve, Essex, United Kingdom (grid reference TM 05065 19030).

Date	Day	Event
03 Jan	−17	Shorebird monitoring
20 Jan	0	Experiment setup and F_o sampling
23 Jan	3	F_o sampling
27 Jan	7	Shorebird monitoring
02 Feb	13	F_o sampling
03 Feb	14	Shorebird monitoring
10 Feb	21	Shorebird monitoring
15 Feb	26	F_o sampling
17 Feb	28	Shorebird monitoring
24 Feb	35	Shorebird monitoring
06 March	45	F_o sampling, critical shear strength sampling, contact core and flux core collection.
10 March	49	Shorebird monitoring
25 March	64	F_o sampling
03 April	73	Shorebird monitoring

biomass (Jesus et al., 2006b). Sampling was carried out during periods of clear weather with little wind and no rain, at least one hour after the tide had exposed the sampling area to allow initial drying of plots. A consistent low light sampling environment was achieved using plastic 40 mm (diameter) × 60 mm (length), cylindrical opaque dark adaption chambers with a 6 mm aperture hole at the top. This also enabled *in-situ* sampling with the PAM fluorometer without removal of the chamber. This reduced the variation in light intensity during the measuring period. To further eliminate potential effects of varying light intensity and sediment water content during sampling events, exclosure and control plot sampling was alternated. To minimize the effect of varying light intensity and phase of vertical migration between sampling events, sampling periods were timed to cover low tides peaking as close to midday as possible.

Our experience of the site is that variability at the meter scale is low (Redzuan, 2017). Additionally, the repeated F_o sampling (described above) gives further confidence that plots were not significantly different at the beginning of the experiment. All *in situ* mudflat variables were measured on 06 March 2017, after 45 days of shorebird exclusion, to test the effect that a period of shorebird exclusion had on selected mudflat properties. Sampling included *in-situ* measurements of F_o (as described above), *in-situ* sediment critical erosion threshold (τ_{cr}) using a Cohesive Strength Meter (CSM) (three measurements within six plots of each treatment, total 36 measurements) (Tolhurst et al., 1999; Vardy et al., 2007) and contact coring for analysis of chlorophyll *a* content (three measurements within seven plots of each treatment; total 42 measurements) (Honeywill et al., 2002). Flux cores (Perspex tubes of 0.1 m diameter and approximately 0.2 m in depth) were also collected (one from each plot) for laboratory analysis of nutrients and macrofauna.

Contact cores (surface ∼2 mm) were freeze dried in the dark and chlorophyll *a* extracted using cold methanol over 24 h, and measured spectrophotometrically, correcting for phaeopigments (Stal et al., 1984).

Flux cores were carefully returned to the laboratory within an hour of leaving the site and immersed in seawater from the site, within oxygenated and temperature and light controlled indoor mesocosms (Thornton et al., 1999). Rubber bungs were used to ensure equal headspace volume across cores. Cores were left submerged and open to settle overnight prior to sampling on the following day. Throughout headspace water sampling, Perspex lids were tightly fitted to prevent leakage. Magnetic stirrers maintained water flow over the sediment surface. On 07 and 08 March 2017 these were sampled for sediment-water biogeochemical fluxes of nitrate, nitrite, ammonia, phosphate and dissolved organic carbon (DOC). Headspace seawater samples were taken at the beginning and end of 2 h dark and light incubation periods. Cores were left for at least one hour to adjust to light levels prior to each incubation. Sampling was completed according to general methods described by Thornton et al. (1999). Flux measurements were repeated in both light and dark conditions, using 500W halogen 'daylight' lamps to provide 'lit' conditions (500 μmol m^{-2} s^{-1} PAR) and covering mesocosms with opaque Perspex covers to provide 'dark' conditions. Water samples were analyzed for their nutrient concentrations using a Seal AA3 segmented flow Nutrient Analyzer (SEAL Analytical Inc.).

Individual cores used for nutrient flux measurements were subsequently sieved (500 μm mesh) to retain macrofauna. Macrofauna were preserved in 95% ethanol and identified to species level (where possible) using a microscope, quantified and densities (m^{-2}) calculated. Through data comparison with previous work at the site (Wood et al., 2015) we were confident that sufficient sampling had been undertaken to assess potential differences in community composition between shorebird presence and absence plots.

Bird surveys began on 03 January 2017 (−17 days) and were carried out at least every two weeks (see **Table 1**) to monitor the level and type of use of the study area by shorebirds. Monitoring began before the experimental setup to ensure current use of the study area by shorebirds and aid in deciding the best location for the experimental plots. Surveys were carried out using the 'look-see' methodology (Bibby et al., 2000), from a fixed location (Geedon Hide; TM 05081 19170). Surveys were undertaken for at least 2 h either side of low-tide, including as much of these timeframes as possible (four hours maximum) within daylight constraints. Particular care was taken to also include visual observation of the tideline crossing the plots wherever possible. Counts of species within the surrounding visible mudflat were taken every half hour. Continual observation of the study area was made, quantifying numbers and identifying species entering presence plots throughout the surveys. Equipment included a 20−60 × 82 telescope and 10 × 42 binoculars. No birds were recorded within or on the absence plots during any of the surveys. During F_o measurements, shorebird tracks were noted within all presence plots at some point during the study, indicating use of all presence plots by shorebirds. No tracks were recorded in any absence plots at any point during the experiment.

Statistical Analysis

To evaluate the effects of shorebird presence and time (days) on biofilm biomass throughout the experimental period, we used a linear mixed-effects model (plot nested in treatment) to analyze F_o data with plot as a random effect and time (day) and bird presence/absence as fixed effects. This model was run using NLME package in R version 4.0.

To evaluate the effect of shorebird presence/absence on MPB biomass and sediment erodibility, F_o (days 3, 13, 26, 45, and 64), chlorophyll *a* (from surface 2 mm) (day 45) and critical erosion threshold (day 45) data were analyzed using a mixed model, two-way nested ANOVA design with (plot nested in treatment) with plot as a random factor and shorebird presence/absence as a fixed factor, using the GMAV (1997) statistical package (University of Sydney, Australia). Although baseline data were not collected, ANOVA detects differences between treatments over and above variability among individual plots (Underwood, 1997). To counteract the issue of multiple comparisons we used Bonferroni correction testing each hypothesis at a confidence level of 0.01 (0.05/5).

To evaluate the effect of shorebird presence/absence on nutrient flux (day 45), nutrient data were analyzed using a two-way orthogonal ANOVA design with dark/light incubation and shorebird presence/absence as fixed factors, using the GMAV (1997) statistical package (University of Sydney, Australia). Where Cochran's test was significant (ammonium and phosphate), data were normalized by rank transformation and the analysis repeated. We also used reversals in flux (for example an efflux from the sediment in the absence of shorebirds becoming an influx into the sediment in the presence of shorebirds) as an indication of changes suggesting 'ecologically significant' implications for ecosystem functioning.

To assess whether shorebird presence/absence had significantly altered macroinvertebrate community structure, day 45 taxa density was analyzed using R version 3.6.1 with vegan package. Non-metric multidimensional scaling (NMDS, Bray-Curtis dissimilarity, 20 restarts) was used to visualize differences in community structure at day 45 in two dimensions (Clarke, 1993). The MDS had a stress 0.037, therefore considered an adequate representation (Clarke, 1993). Analysis of similarities (ANOSIM) was also performed to test quantitatively for differences in community structure between shorebird presence and absence.

To assess the potential for biases associated with the exclosures, plaster ball dissolution (days 17 and 18) and shading effect (post experiment) data were also analyzed using a one-way orthogonal ANOVA, using the GMAV (1997) statistical package (University of Sydney, Australia).

To evaluate shorebird pressure on the mudflat, species count data were first converted into 'bird-days,' by calculating the sum of the number of each shorebird species present on every count, multiplied by the number of days between that and the subsequent count (Gill et al., 2001; Lewis et al., 2014). This allowed comparison of shorebird pressure on the wider mudflat. Only species considered regular foragers on mudflats and recorded foraging on the surrounding mudflat were included in this analysis; for example lapwing *Vanellus vanellus* and golden plover *Pluvialis apricaria* were removed due to their high dependence, and almost exclusive foraging, on coastal grassland and arable fields (Mason and Macdonald, 1999). Furthermore, these species were recorded roosting on the mid to low shore only during low tides, further reducing the likelihood that they contributed to any effects within the upper shore study site. To compare mudflat variables with density of species recorded in presence plots, count numbers of such species were $\log_{10}$ transformed and plotted over time with mean F_o in shorebird presence and absence.

RESULTS

Microphytobenthic Biomass

Results of the linear mixed effects model show a highly significant difference in F_o (measure of MPB surface chlorophyll *a*) between shorebird presence and absence, with F_o higher in the bird exclosure treatments. There was no significant effects of time (days) or interaction between treatment with time (**Table 3**).

F_o initially increased in shorebird presence and absence plots, increasing more rapidly in absence plots, peaking on day 26 before decreasing (**Figure 2A**). On day 3, there was no significant difference in F_o between shorebird presence and absence plots, but on day 13 this difference had become significant. The largest difference was measured on day 26, when mean F_o in shorebird presence and absence plots was highly significantly different (**Table 3**).

The two subsequent sampling events (days 45 and 64) showed decreasing F_o with progressively smaller differences between presence and absence plots. Mean F_o in shorebird absence plots was still higher on day 45 but was not significantly different (Bonferroni corrected 0.01 significance level), and by day 64, F_o levels were very similar between treatments (**Figure 2A**). There was no significant difference in chlorophyll *a* content ($\mu g\ g^{-1}$) in the top ~2 mm of sediment between presence and absence plots on day 45 (**Figure 3B**).

Sediment Erodibility

To evaluate the effect of shorebirds on erosion protection, erosion threshold (τ_{cr}) was measured on day 45. Significantly greater erosion threshold was found in shorebird absence plots than in presence plots (**Figure 3C**, **Table 3**).

Sediment-Water Nutrient Fluxes

There was significantly greater net nitrate influx into the sediment when shorebirds were absent compared to when they were present (**Figure 4A**) and a significantly greater net nitrite efflux from the sediment into the water column when shorebirds were present (Figre 4B).

There was no significant difference in net phosphate flux between shorebird presence and absence plots. However, under lit conditions mean values changed from an influx into the sediment to a small efflux into the water column (**Figure 4D**), which is considered ecologically significant.

There was no significant difference in net dissolved organic carbon (DOC) flux between shorebird presence and absence

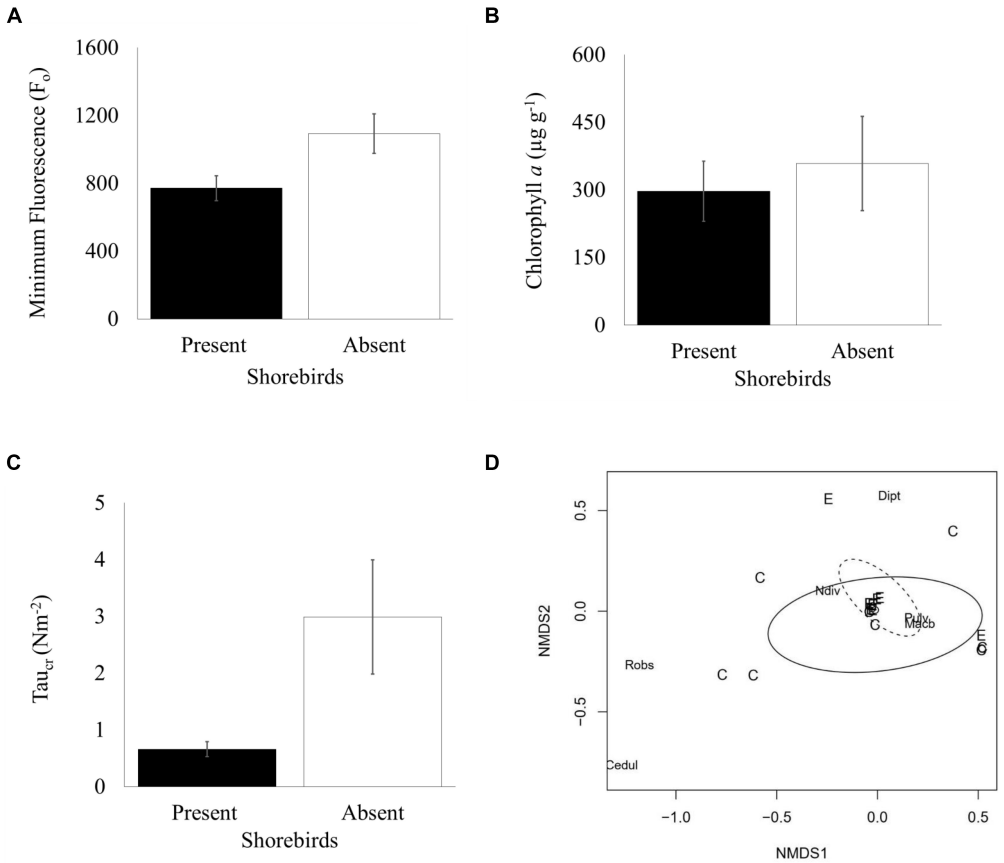

FIGURE 3 | Measured characteristics in shorebird presence/absence on day 45 (06 March 2017) **(A)** Mean F_O (±SE, n = 50) **(B)** Mean chlorophyll *a* content in top ~2 mm (µg g^{-1}) (±SE, n = 14) **(C)** Mean erosion threshold (τ_{cr}) (±SE, n = 36) **(D)** Non-metric multidimensional scaling (MDS) plot depicting Bray-Curtis dissimilarity in community composition (shorebird presence = solid oval; shorebird absence = dotted oval, C = shorebird presence, E = shorebird absence, Cedul = *C. edule*, Robs = *R. obtusa*, Dipt = Chironomidae, Pulv = *P. ulvae*, Ndiv = *N. diversicolor*).

plots (**Figure 4E**). However, in shorebird presence during light incubation, we found a large reversal in flux direction of DOC into the sediment rather than the water column (**Figure 4E**).

No significant difference in ammonium flux between the sediment and water column was found (**Figure 4C**).

Macrofauna Density

To evaluate the indirect effect of shorebirds on erosion protection, nutrient cycling and carbon sequestration via changes in macrofauna density, the numbers of macrofauna were counted (from the same cores used for the nutrient measurements). Macrofauna recorded on day 45 were mud snails *P. ulvae*, Baltic clams *Macoma balthica*, midge larvae (Chironomidae), ragworms *Hediste diversicolor*, Arctic barrel-bubble *Retusa obtusa* and common cockles *Cerastoderma edule*. Mean densities (m^{-2}) in each treatment are shown in **Table 4**. Raw macrofauna counts revealed presence of a single specimen of *C. edule* and *R. obtusa* in only two and three plots, respectively. *H. diversicolor* counts were also sparse (see **Table 4**). On day 26 *P. ulvae* was visually noted on the mudflat surface for the first time during F_o sampling. Mud snails can compensate for the loss of higher predators on intertidal mudflats (Hamilton et al., 2006; Cheverie et al., 2014). This species was subsequently present within the study area during all F_o sampling events, noted throughout the study site in presence and absence plots.

The non-metric Multi-Dimensional Scaling (nMDS) plot (**Figure 3D**) indicated that macrofauna communities between treatments were not significantly dissimilar; a large overlap between community composition is indicated, although the spread of data points is larger in shorebird presence demonstrating larger variability in community composition. ANOSIM confirmed there was no significant difference in community composition between shorebird presence and absence plots ($R = -0.038$, $P = 0.623$).

Bird Surveys

Over the study period, 10 shorebird species were recorded using the wider mudflat, with a total of 78,811 bird days (**Table 2**). Of these, three were recorded in the presence plots; *C. alpina* (84 bird-days), *T. totanus* (35 bird-days) and *P. squatarola* (28 bird-days). Camera data indicated that numbers of shorebirds using the study area were broadly consistent with those counted during surveys. Although the image quality (due to distance from the plots) made detection of individual birds difficult, flocks were

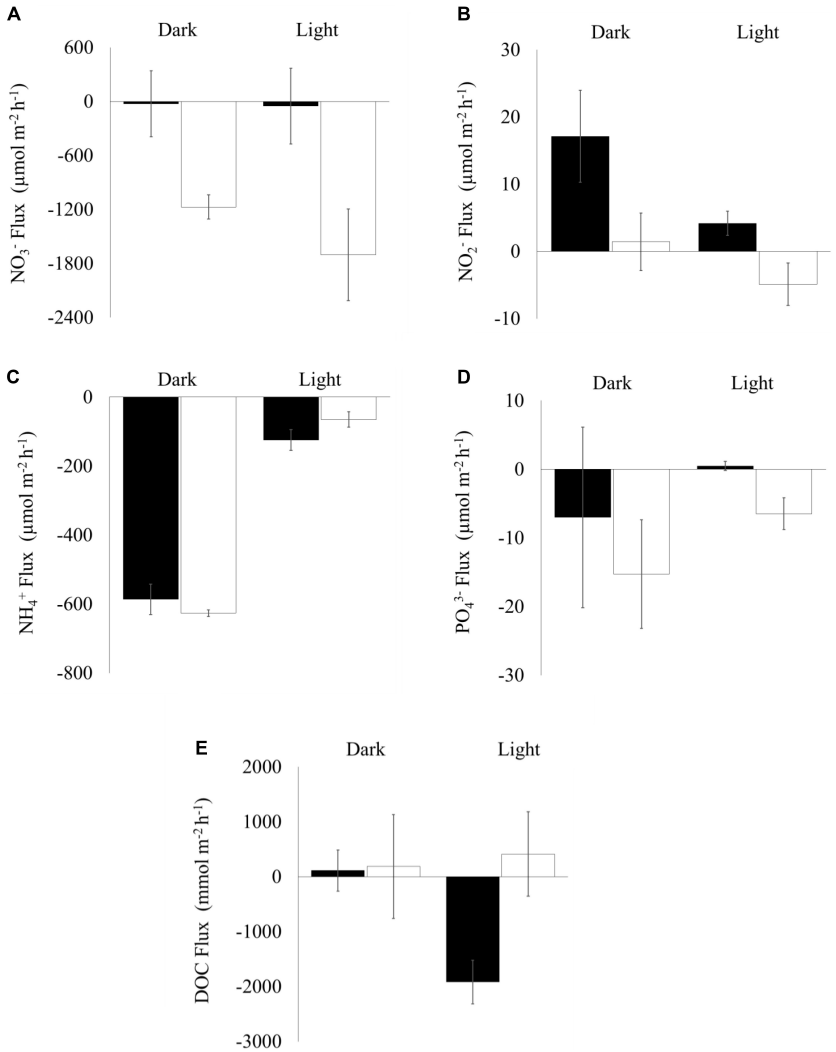

FIGURE 4 | Sediment-water nutrient fluxes (Mean ± SE, n = 10) during light and dark incubations in cores collected from shorebird presence (filled bars) and absence (unfilled bars) plots on day 45 (06 March 2017). X-axis marks zero flux, positive values show flux out of the sediment, negative values show flux into the sediment: **(A)** NO_3^-, **(B)** NO_2^-, **(C)** NH_4^+, **(D)** PO_4^{3-}, and **(E)** Dissolved Organic Carbon (DOC).

noted using the plots, often as the tideline crossed them. Flocks were noted on camera footage in and around the plots between 23 February and 5 March (day before main sampling event).

The experimental plots were laid out in an area of mudflat representing approximately 0.3% of the area visually surveyed. Peak *C. alpina*, *P. squatarola,* and *T. totanus* numbers within experimental plots comprised approximately 0.16%, 0.35%, and 0.8% (respectively) of peak numbers within the survey area, thus within the same order of magnitude as that expected based on the areas of plots and the overall mudflat area.

DISCUSSION

Excluding shorebirds caused significant changes in regulating and provisioning ecosystem functions, including mudflat erodibility, nutrient fluxes and carbon sequestration. Effects on MPB biofilm biomass and erodibility were, however, not as predicted in our hypotheses. We suggest that these effects were driven by shorebird bioturbation of surface sediments and MPB biofilms and possible direct grazing of MPB by *C. alpina*.

Effects on MPB and Erodibility

Hypothesis 1 was not rejected; our linear mixed-effects model showed a highly significant difference in F_o between shorebird presence and absence, with no significant interaction between other factors (see **Table 3**). Significantly greater MPB F_o values were found in shorebird absence plots on days 13 and 26. By day 45 the difference had become less significant, to the extent of being non-significant when Bonferroni correction was applied (0.01 level). Despite this, on day 45 the difference in F_o remained visually notable in the field, which is reflected in **Figure 2A**. These differences between treatments occurred during a period of increased shorebird activity in the study area. Despite the

TABLE 2 | Bird-days estimated for each species recorded foraging within the survey area between the 20th of January and the 3rd of April 2017 on the mudflat adjacent to Geedon Saltings at Fingringhoe Wick Essex Wildlife Trust Nature Reserve, Essex, United Kingdom (grid reference TM 05065 19030).

Species	*Calidris alpina*	*Calidris canutus*	*Pluvialis squarola*	*Arenaria interpres*	*Tringa totanus*	*Limosa limosa*	*Limosa lapponica*	*Recurvirostra avosetta*	*Numenius arquata*	*Haematopus ostralegus*
Bird Days	53,853	9,363	6,358	103	3,735	1,541	430	2,888	405	135

decline in surveyed shorebird numbers on day 28, the 83 ha^{-1} shorebirds present at this point was notably greater than at the beginning or end of the experiment (when numbers were 30 and 28 ha^{-1}, respectively) (**Figure 2A**). The survey visit on day 28 is also considered to be an underestimate due to the flushing of a large proportion of the foraging shorebirds on the incoming tide by a marsh harrier *Circus aeruginosus*. Differences in F_o between shorebird presence and absence on days 3 and 64 were non-significant and occurred when shorebird numbers were smaller, suggesting that the effects found may be dependent upon shorebird density.

There was no significant dissimilarity in macrofauna community structure between shorebird presence and absence plots (**Figure 3D**). The present study recorded a greater diversity of species at the study site than during previous large scale work at the site (Wood et al., 2015), albeit the majority of infaunal species were present sporadically and in very low numbers (see **Table 4**). This validates our macrofauna sampling effort, in that we had enough replicates to detect all species known to be present, despite likely patchiness in invertebrate distributions (Van Colen, 2018). These findings differ to suggestions that a top-down ecological cascade effect driven by shorebirds can increase biofilm biomass (Daborn et al., 1993), supporting instead more recent work (Hamilton et al., 2006; Cheverie et al., 2014). Our results provide strong indication that, through bioturbation and/or grazing (and/or a yet unknown pathway), shorebirds can have a significant reductive effect on the biomass of surface MPB biofilms. Thus, shorebirds can alter key ecosystem functions such as erosion protection and nutrient cycling via direct and/or indirect effects on MPB. The increase in MPB in the absence of shorebirds concurs with results reported by Hamilton et al. (2006), where the authors acknowledge that this finding is the opposite to that expected in the event of a trophic cascade. On day 45 bulk chlorophyll *a* content within the surface 2 mm of sediments showed the same directional response as surface biofilm biomass and was also not significantly different. Bioturbation and grazing by macrofauna can significantly affect surface MPB biomass and resuspension (Grant and Daborn, 1994; Hagerthey et al., 2002; Harris et al., 2015); but as macrofauna were not significantly different between our shorebird presence/absence plots, and motile macrofauna could access all plots, the changes in MPB biomass are highly unlikely to have been due to macrofauna. Physical effects of birds upon primary producers is evident within many freshwater and marine environments (Cadee, 1990; Mitchell and Perrow, 1998; Nacken and Reise, 2000) and physical mixing of intertidal mud has been shown to significantly reduce chlorophyll *a*, F_o, and colloidal carbohydrate (Tolhurst et al., 2012). It follows that physical disturbance (bioturbation) by shorebirds in our study location, through foraging (including biofilm grazing in some species) and tracking (walking), can have a significant effect upon MPB biomass and related sediment properties. These results suggest that bioturbation by shorebirds can be a more significant driver of effects on MPB than trophic cascades. Further work is required to confirm the mechanisms by which shorebirds in this part of the world reduce MPB biomass.

Hypothesis 2 was not rejected, sediment critical erosion threshold (τ_{cr}) was significantly smaller when shorebirds were present than when they were absent (see **Figure 3C**). This pattern is most likely to have been driven by both direct bioturbation during walking and feeding of shorebirds on the mudflat surface and, because MPB commonly significantly increase mudflat erosion threshold (Hale et al., 2019; Hope et al., 2020), indirectly by grazing decreasing the biomass of MPB. The exact mechanistic pathway(s) and their magnitude require further investigation. The erosion shear stresses exerted on intertidal mudflats by combined waves and tides are very variable, but commonly in the 0–1 Nm^{-2} range and typically below 4 Nm^{-2} (Christie and Dyer, 1998; Whitehouse and Mitchener, 1998). Thus, the τ_{cr} measurements suggest that erosion would occur frequently (i.e., during most tidal cycles) in the presence of shorebirds and much less frequently in the absence of shorebirds. Given the importance of sediment erodibility for many ecosystem functions (Hubas et al., 2018; Hope et al., 2020), including nutrient fluxes and erosion protection; the effect of shorebirds on erodibility demonstrates their importance as ecosystem engineers (Passarelli et al., 2014) and their significant role in ecosystem functioning.

Although F_o is widely used as a proxy for MPB biomass, it is important to acknowledge that this relationship varies depending upon the physiological state and taxonomic composition of MPB due to vertical migration of MPB (Serodio et al., 2001, 2006; Serodio, 2004; Du et al., 2018). By standardizing our time of sampling within the tidal exposure period, tidal migration rhythms influencing F_o were accounted for between treatments. Though changes in the relationship between F_o and Chl *a* over time may have occurred, we found significant differences in F_o between treatments at each time of sampling. Our results show the same directional response of F_o and Chl *a* to shorebird presence, suggesting an underlying relationship in this case. Actual Chl *a* concentration varies vertically within the sediment depending upon factors such as MPB migration, light intensity, water content and sediment compaction (Perkins et al., 2003; Tolhurst et al., 2003; Jesus et al., 2006a; Maggi et al., 2013) and also shows temporal changes. We did not design our sampling regime to specifically focus on the F_o to Chl *a* relationship, which requires a higher level of sampling granularity.

Effects on Nutrient Fluxes

Hypothesis 3 was not rejected; statistically significant differences in the fluxes of nitrate, nitrite and dissolved organic carbon (DOC), were found between presence and absence treatments.

TABLE 3 | Linear mixed-effects / ANOVA models and results for each variable and sampling time between the 20th of January and the 3rd of April 2017 on the mudflat adjacent to Geedon Saltings at Fingringhoe Wick Essex Wildlife Trust Nature Reserve, Essex, United Kingdom (grid reference TM 05065 19030).

Variable (day if not day 45) / Model	**Factor**	**Source**			
		numDF	**denDF**	***F***	***P***
Linear Mixed Model					
F_o = MEAN x P/A x TIME x Plot(TIME)	Sampling Days = TIME	1	3	0.91	0.58
	Presence/Absence = P/A	1	85	22.2	<0.0001
	P/A x TIME	1	85	1.64	0.204
ANOVA Models		**df**	**MS**	***F***	***P***
Chlorophyll *a* ug g^{-1} = MEAN + P/A + Plot(P/A) + RES	Presence/Absence = P/A	1	39516	0.3	0.596
	Plots (P/A)	12	133337	2.34	0.031
	Residual	24	56973		
Erosion threshold Nm^{-2} = MEAN + P/A + Plot(P/A) + RES	Presence/Absence = P/A	1	14.4	8.44	0.016
	Plots (P/A)	10	1.7	3.85	0.003
	Residual	24	0.44		
F_o (day 3) = MEAN + P/A + Plot(P/A) + RES	Presence/Absence = P/A	1	105588	0.28	0.61
	Plots (P/A)	10	376213	0.67	0.75
	Residual	48	564759		
F_o (day 13) = MEAN + P/A + Plot(P/A) + RES	Presence/Absence = P/A	1	11777938	9.23	0.007
	Plots (P/A)	18	1275748	1.94	0.024
	Residual	80	658534		
F_o (day 26) = MEAN + P/A + Plot(P/A) + RES	Presence/Absence = P/A	1	15245120	8.56	0.009
	Plots (P/A)	18	1781747	3.04	0.0003
	Residual	80	564759		
F_o (day 45) = MEAN + P/A + Plot(P/A) + RES	Presence/Absence = P/A	1	4723233	4.93	0.039
	Plots (P/A)	18	957343	1.42	0.145
	Residual	80	673677		
F_o (day 64) = MEAN + P/A + Plot(P/A) + RES	Presence/Absence = P/A	1	200435	0.32	0.581
	Plots (P/A)	18	633507	3.58	<0.00001
	Residual	80	177121		
Ammonium = MEAN + D/L + P/A + D/L x P/A + RES	Dark/Light = D/L	1	4000	124.03	<0.0001
	Presence/Absence = P/A	1	16.9	0.52	0.47
	D/L x P/A	1	152.1	4.72	0.114
	Residual	36	32.25		0.037
Phosphate = MEAN + D/L + P/A + D/L x P/A + RES	Dark/Light = D/L	1	448.9	3.57	0.067
	Presence/Absence = P/A	1	136.9	1.09	0.304
	D/L x P/A	1	211.6	1.68	0.203
	Residual	36	125.85		
Nitrate = MEAN + D/L + P/A + D/L x P/A + RES	Dark/Light = D/L	1	773375	0.47	0.496
	Presence/Absence = P/A	1	19546821	11.95	0.001
	D/L x P/A	1	637317	0.39	0.536
	Residual	36	1635096		
Nitrite = MEAN + D/L + P/A + D/L x P/A + RES	Dark/Light = D/L	1	929	4.27	0.046
	Presence/Absence = P/A	1	1534	7.05	0.01
	D/L x P/A	1	110	0.50	0.483
	Residual	36	218		
Dissolved organic carbon = MEAN + D/L + P/A + D/L x P/A + RES	Dark/Light = D/L	1	8137880	1.65	0.208
	Presence/Absence = P/A	1	14457171	2.92	0.096
	D/L x P/A	1	12738121	2.58	0.117
	Residual	36	4943100		

Orders of magnitude changes in the scale of some fluxes were observed (nitrate ∼100x, nitrite ∼10x and DOC ∼2000x). Despite not being formally significant, the reversal of phosphate flux into/out of the sediment is considered to be ecologically significant. These results suggest that shorebirds significantly alter ecosystem functioning associated with nutrient cycling

TABLE 4 | Count of each macrofauna species recorded within each core extracted from the study area on Day 45 (06 March 2017) on the mudflat adjacent to Geedon Saltings at Fingringhoe Wick Essex Wildlife Trust Nature Reserve, Essex, United Kingdom (grid reference TM 05065 19030).

Species/Family	Treatment (shorebirds present = P, shorebirds absent = A)	Mean Count (m^{-2})
Peringia ulvae	P	$31,669 \pm 5,014$
	A	$30,226 \pm 3,376$
Macoma balthica	P	$1,980 \pm 366$
	A	$1,796 \pm 213$
Nereis diversicolor	P	99 ± 33
	A	170 ± 35
Chironomidae	P	552 ± 347
	A	$2,574 \pm 2,086$
Retusa obtusa	P	42 ± 0
	A	0
Cerastoderma edule	P	29 ± 18
	A	0

(Saint-Beat et al., 2013; Mathot et al., 2018; Hope et al., 2020) and carbon storage (Maher and Eyre, 2010). Differences in the surface active MPB biomass (F_o) can explain the nutrient flux alterations by shorebirds. Photosynthesis and nutrient assimilation by MPB significantly affects nutrient flux rates, including nitrate (Dong et al., 2000) and phosphate (Sundback et al., 1991). Further, the EPS matrix within MPB biofilms provides additional organic matter to support heterotrophic bacteria, which reduce nitrite to nitrous oxide (Dong et al., 2002). We found evidence to suggest that the presence of shorebirds can significantly reduce nitrate uptake into intertidal sediments (**Figure 3A**). The reduction of active surface MPB biofilms by shorebirds is a likely mechanism that may reduce nitrate and phosphate uptake, nitrification, coupled nitrification-denitrification, and through the reduction of extracellular organic carbon, reduce bacterial degradation rates (Thornton et al., 2007).

Our findings suggest that shorebird effects on MPB can limit the drawdown of nitrate, nitrite and phosphate into sediments in an already nitrate rich estuary (Thornton et al., 2007). The observed alterations of nutrient fluxes suggest that shorebirds play a significant role in estuarine nutrient pathways, effectively controlling and engineering nutrient fluxes between the sediment and water column (Passarelli et al., 2014, 2018). Bioturbation by macrofauna is known to significantly affect nitrate and ammonia fluxes at the study site and elsewhere, through sediment reworking, ventilation and burrowing (Nizzoli et al., 2007). We suggest that bioturbation by shorebirds (Mathot et al., 2018) is likely to have contributed to the significant effects found here.

While the measured nutrients were typically characterized by a reduction in fluxes into the sediment from shorebird presence, DOC flux into sediment from shorebird presence increased significantly in lit conditions. It is possible that through the observed reduction of MPB biomass by shorebirds, competition for nutrients may have been reduced, allowing bacteria to proliferate and increase assimilation of DOC and ammonium (Amin et al., 2012). Migratory birds can also introduce bacteria to communities (Steiniger, 1969) via fecal droppings (Muller, 1965) and external tissues (Muza et al., 2000), potentially further increasing these process rates. These results indicate that changes in shorebird abundance could affect wider ecosystem functioning such as carbon sequestration and coastal biogeochemistry more broadly (Nedwell et al., 2016; Hope et al., 2020).

Secondary Effects

Use of the mid and upper shore at low tide by *C. alpina*, despite often being a 'tide follower' (Granadeiro et al., 2006), may have been driven by the visual cues of MPB communities on the mudflats, either as a cue for the presence of invertebrate prey or to feed upon MPB directly (Hamilton et al., 2003; Drouet et al., 2015; Jimenez et al., 2015). *C. alpina* is an opportunistic feeder with a broad diet (Dierschke et al., 1999) using visual and tactile foraging cues (Drouet et al., 2015), and possibly exploited areas with high diatom biomass to maximize the breadth of feeding opportunity.

Avian guano (in particular shorebird droppings) is a potentially important source of nutrients in coastal areas (Schrama et al., 2013). It has been suggested that *C. alpina* droppings increase growth rate and biomass of the diatom species *Entomoneis paludosa* through increases in nitrogen and phosphorous input to the sediment (Jauffrais et al., 2015). However, the Colne estuary has very high nutrient loads (McMellor and Underwood, 2014; Nedwell et al., 2016) and MPB biomass was smaller, rather than larger in shorebird presence, suggesting that nutrient enrichment of biofilms by guano is not a major mechanism in this case. These findings reflect the complexity of the real-world scenario compared to laboratory studies (Jauffrais et al., 2015); in the present study shorebirds reduced MPB biomass on the upper shore. This indicates that the effects of bioturbation and/or grazing by shorebirds, which lead to alterations in ecosystem functioning, significantly outweigh the effects of nutrient input via guano in our study site.

Shorebirds significantly affect ecosystem functions (nutrient flux and erodibility), at least within the upper shore, in a temperate climate during late winter. However, these effects are likely to vary temporally and spatially (Underwood and Paterson, 1993; Gerwing et al., 2015) depending as they do upon the abundances and functioning of other organisms present (Underwood, 1994; Norazlimi and Ramli, 2014). For example, we found that shorebird effects were temporary and seasonal, restricted to an approximately one month period when shorebird density peaked at the study site (**Figure 2A**). This suggests that the observed phenomenon is seasonally and density dependent, reliant on sufficient density of shorebirds (which are present in larger densities during winter) to cause effects on ecosystem functioning. Similarly, compensatory grazing by the mud snail Peringia ulvae may have limited the temporal effect of shorebirds on MPB during this study, effectively resetting the state of the system as bird density declined (Hamilton et al., 2006; Cheverie et al., 2014). The collapse of the shorebird effect on F_o was concomitant with the emergence of large numbers of *P. ulvae*. This MPB grazer was first noticed on the mudflat surface on day 26, was noted spread across the mudflat within all plots (**Table 4**), and can rapidly reduce the abundance and thickness of biofilms (Sahan et al., 2007). Subsequently the difference in F_o between treatments steadily decreased, eventually becoming non-significant. On day 45, no significant

difference between macrofaunal communities was evident. It is our interpretation that the snails had a homogenizing effect on biofilm distribution. Once the snails emerged and while birds remained, the effects of the birds became weaker. Once the birds left, continued grazing by the snails removed the residual bird effects (compensatory effect). Despite our restriction to observational evidence regarding the temporal change in numbers of *P. ulvae*, it is known that mudsnails can mask effects on MPB (Hamilton et al., 2006; Cheverie et al., 2014) and it is plausible that this occurred here, reducing the detectability of ecosystem function effect pathways. Here we highlight that shorebirds play a key community role in the regulation and control of ecosystem function, through inter and intraguild interactions with macrofauna and MPB with which they are intrinsically linked (Kuwae et al., 2012; Cheverie et al., 2014).

We found no evidence to suggest that macrofauna community structure differed between shorebird presence and absence, however, such effects have been detected in Canada in exclusion experiments on semipalmated sandpiper C. pusilla, where reductions in C. volutator densities were found (Hamilton et al., 2006; Cheverie et al., 2014). The differences between these studies may be due to geographic or shorebird species differences, or due to the fact that *C. volutator* is not present at our study site.

We also emphasize that differences in MPB surface biomass between treatments eventually became non-significant, despite shorebird exclosures remaining in-situ. We conclude therefore that shorebirds, rather than experimental artifacts, drove the measured MPB biomass changes and subsequent effects on ecosystem functions.

CONCLUSION

Here we have identified previously unknown effects of shorebirds on ecosystem functioning. Although limitations are acknowledged regarding the link between F_o measurements and actual Chl *a* content, the end effect of shorebird presence on erodibility and nutrient fluxes was found to be significant, and a large amount of existing literature indicates that MPB are highly likely to drive this effect. The removal of shorebirds significantly increased surface biofilm F_o and sediment erosion threshold. Shorebird absence was also found to affect nutrient cycling regimes and carbon sequestration on the mudflat; differences in biofilm biomass led to significant alterations in the flux of nutrients under lit conditions, including nitrate, nitrite and phosphate, all of which showed an increased flux into the sediment in the absence of shorebirds. The uptake of DOC in the light into the sediment was significantly greater in the presence of shorebirds.

The mechanism by which shorebirds reduced biofilm biomass was not experimentally tested, although the literature provides a number of possible drivers including physical disturbance (bioturbation) through tracking (walking) and foraging. Considering the presence of large numbers of *C. alpina*, which has been shown to consume MPB, it is plausible that direct consumption of biofilm may have contributed, but this is not confirmed. The lack of significant differences in macrofauna densities between treatments suggests that altered numbers of these invertebrates were not driving a change in bioturbation or grazing on the biofilms, and thus were not a significant driver of the measured effects.

The finite period of effects and community interactions between shorebirds, macrofauna and MPB reduce the clarity of the situation regarding consequences of declining shorebird species on coastal ecosystem functions. The work presented here indicates a potential shorebird density-dependent effect, resulting in stronger impacts on ecosystem function by birds during winter that may be 'reset' by other organisms or reduced bird densities in spring and summer. This reflects the complexity of intertidal mudflat ecosystem functions (Passarelli et al., 2018; Hale et al., 2019), but is a step forward in disentangling the many factors influencing them. This research indicates that shorebirds play a significant role in the ecosystem functions provided by intertidal mudflats, including erosion protection, nutrient cycling and carbon sequestration. However, further research is required, involving longer-term, larger-scale experiments, to better understand the mechanisms behind ecosystem function regulation by shorebirds.

DATA AVAILABILITY STATEMENT

The datasets generated for this study are available on request to the corresponding author.

AUTHOR CONTRIBUTIONS

JB conducted the initial experimental design and background research, performed primary data analysis and interpretation, was the primary manuscript author and led field and lab work. GU was a Ph.D. supervisor and provided quality control of the experimental design, flux core methodology, data analysis and interpretation. AP performed the laboratory data analysis of contact cores (Chl *a* concentrations) and some flux core samples (dissolved organic carbon) and contributed to the manuscript. RD was a Ph.D. supervisor and provided quality control of data interpretation regarding ecological community effects. TT was the Ph.D. project originator, primary supervisor and provided quality control of the experimental design, sediment properties measurements methodologies, data analysis and interpretation. GU, RD, and TT were manuscript reviewers and contributors. All authors contributed to the article and approved the submitted version.

FUNDING

This work was supported by the Natural Environment Research Council (grant number NE/L002582/1) and undertaken in partnership between the University of East Anglia and University of Essex within the EnvEast Doctoral Training Partnership.

ACKNOWLEDGMENTS

We thank John Green, Claire Passarelli, Tania Creswell-Maynard, Belinda Gillett-Booty, Alister Killingsworth, Christopher Bridge,

Matt Cole, David Booty, Barbara Booty, Ken Hudgell, and David Smith for their assistance in the field and the lab. We thank Essex Wildlife Trust for their permission and cooperation. We thank Charlie Williams at Natural England for his cooperation and permission regarding the SSSI. We thank DH for her invaluable review and input during the publication process. Additional support was also provided by the University of East Anglia and EnvEast during fieldwork and writing.

REFERENCES

Amin, S. A., Parker, M. S., and Armbrust, E. V. (2012). Interactions between diatoms and bacteria. *Microbiol. Mol. Biol. Rev.* 76, 667–684. doi: 10.1128/MMBR.00007-12

Bibby, C. J., Burgess, N. D., Hill, D. A., and Mustoe, S. (2000). *Bird Census Techniques*. London: Academic Press.

Bowgen, K. M., Stillman, R. A., and Herbert, R. J. H. (2015). Predicting the effect of invertebrate regime shifts on wading birds: insights from Poole Harbour, UK. *Biol. Conserv.* 186, 60–68. doi: 10.1016/j.biocon.2015.02.032

Burgin, A., and Hamilton, K. (2007). Have we overemphasized the role of denitrification in aquatic ecosystems? A review of nitrate removal pathways. *Front. Ecol. Environ.* 5, 89–96. doi: 10.1890/1540-929520075[89:HWOTRO]2.0.CO;2

Burton, N. H. K., Rehfisch, M. M., Clark, N. A., and Dodd, S. G. (2006). Impacts of sudden winter habitat loss on the body condition and survivial of redshank *Tringa totanus*. *J. Appl. Ecol.* 43, 464–473. doi: 10.1111/j.1365-2664.2006.01156.x

Cabello, J., Fernandez, N., Alcaraz-Segura, D., Oyonarte, C., Pineiro, G., Altesor, A., et al. (2012). The ecosystem functioning dimension in conservation: insights from remote sensing. *Biodivers. Conserv.* 21, 3287–3305. doi: 10.1007/s10531-012-0370-7

Cadee, G. C. (1990). Feeding traces and bioturbation by birds on a tidal flat, Dutch Wadden Sea. *Ichnos* 1, 23–30. doi: 10.1080/10420949009386328

Cheverie, A. V., Hamilton, D. J., Coffin, M. R. S., and Barbeau, M. A. (2014). Effects of shorebird predation and snail abundance on an intertidal mudflat community. *J. Sea Res.* 92, 102–114. doi: 10.1016/j.seares.2014.03.011

Christie, M. C., and Dyer, K. R. (1998). "Measurements of the turbid tidal edge over the Skeffling mudflats," in *Sedimentary Processes in the Intertidal Zone*, Vol. 138, eds K. S. Black, D. M. Paterson, and A. Cramp, (London: Geological Society).

Clarke, K. R. (1993). Non-parametric multivariate analyses of changes in community structure. *Aust. J. Ecol.* 18, 117–143. doi: 10.1111/j.1442-9993.1993.tb00438.x

Correll, D. L., Jordan, T. E., and Weller, D. E. (1992). Nutrient Flux in a Landscape: effects of coastal land use and terrestrial community mosaic on nutrient transport to coastal waters. *Estuaries* 15, 431–442. doi: 10.2307/1352388

Culhane, F. E., Briers, R. A., Tett, P., and Fernandes, T. F. (2019). Response of a marine benthic invertebrate community and biotic indices to organic enrichment from sewage disposal. *J. Mar. Biol. Assoc. U.K.* 99, 1721–1734. doi: 10.1017/S0025315419000857

Daborn, G. R., Amos, C. L., Brylinsky, M., Christian, H., Drapeau, G., Faas, R. W., et al. (1993). An ecological cascade effect: migratory birds affect stability of intertidal sediments. *Limnol. Oceanogr.* 38, 225–231. doi: 10.4319/lo.1993.38.1.0225

de Deckere, E. M. G. T., Tolhurst, T. J., and de Brouwer, J. F. C. (2001). Destabilization of cohesive intertidal sediments by infauna. *Estuar. Coast. Shelf Sci.* 53, 665–669. doi: 10.1006/ecss.2001.0811

Dierschke, V., Kube, J., Probst, S., and Brenning, U. (1999). Feeding ecology of dunlins *Calidris alpina* staging in the southern Baltic Sea, 1. Habitat use and food selection. *J. Sea Res.* 42, 49–64. doi: 10.1016/S1385-1101(99)00013-1

Dong, L. F., Nedwell, D. B., Underwood, G. J. C., Thornton, D. C. O., and Rusmana, I. (2002). Nitrous oxide formation in the Colne Estuary, England: the central role of nitrite. *Appl. Environ. Microbiol.* 68, 1240–1249. doi: 10.1128/AEM.68.3.1240-1249.2002

Dong, L. F., Thornton, D. C. O., Nedwell, D. B., and Underwood, G. J. C. (2000). Denitrification in sediments of the River Colne estuary, England. *Mar. Ecol. Prog. Ser.* 203, 109–122. doi: 10.3354/meps203109

Drouet, S., Turpin, V., Godet, L., Cognie, B., Cosson, R. P., and Decottignies, P. (2015). Utilisation of intertidal mudflats by the Dunlin *Calidris alpina* in relation to microphytobenthic biofilms. *J. Ornithol.* 156, 75–83. doi: 10.1007/s10336-014-1133-x

Du, G., Yan, H., Liu, C., and Mao, Y. (2018). Behavioural and physiological photoresponses to light intensity by intertidal microphytobenthos. *J. Oceanol. Limnol.* 36, 293–304. doi: 10.1007/s00343-017-6099-0

Eggold, B. T., and Motta, P. J. (1992). Ontogenetic dietary shifts and morphological correlates in striped mullet, *Mugil cephalus*. *Environ. Biol. Fishes* 34, 139–158. doi: 10.1007/BF00002390

Fagherazzi, S., Viggato, T., Vieillard, A. M., Mariotti, G., and Fulweiler, R. W. (2017). The effect of evaporation on the erodibility of of mudflats in a mesotidal estuary. *Estuar. Coast. Shelf Sci.* 194, 118–127. doi: 10.1016/j.ecss.2017.06.011

Fahimipour, A. K., Anderson, K. E., and Williams, R. J. (2017). Compensation masks tropic cascades in complex food webs. *Theor. Ecol.* 10, 245–253. doi: 10.1007/s12080-016-0326-8

Feuillet-Gerard, M., Gouleau, D., Blanchard, G., and Joassard, L. (1997). Nutrient fluxes on an intertidal mudflat in Marennes-Oleron Bay, and influence of the emersion period. *Aquat. Living Resour.* 10, 49–58. doi: 10.1051/alr:1997005

Foster, N. M., Hudson, M. D., Bray, S., and Nicholls, R. J. (2013). Intertidal mudflat and saltmarsh conservation and sustainable use in the UK: a review. *J. Environ. Manage.* 126, 96–104. doi: 10.1016/j.jenvman.2013.04.015

Gerbersdorf, S. U., and Wieprecht, S. (2015). Biostabilisation of cohesive sediments: revisiting the role of abiotic conditions, physiology and diversity of microbes, polymeric secretion and biofilm architecture. *Geobiology* 13, 68–97. doi: 10.1111/gbi.12115

Gerwing, T. G., Drolet, D., Barbeau, M. A., Hamilton, D., and Gerwing, A. M. A. (2015). Resilience of an intertidal infaunal community to winter stressors. *J. Sea Res.* 97, 40–49. doi: 10.1016/j.seares.2015.01.001

Gill, J. A., Sutherland, W. J., and Norris, K. (2001). Depletion models can predict shorebird distribution at different spatial scales. *Proc. R. Soc.* 268, 369–376. doi: 10.1098/rspb.2000.1386

Granadeiro, J. P., Dias, M. P., Martins, R. C., and Palmeirim, J. M. (2006). Variation in numbers and behaviour of waders during the tidal cycle: implications for the use of estuarine sediment flats. *Acta Oecol.* 29, 293–300. doi: 10.1016/j.actao.2005.11.008

Grant, J., and Daborn, G. (1994). The effects of bioturbation on sediment transport on an intertidal mudflat. *Neth. J. Sea Res.* 32, 63–72. doi: 10.1016/0077-7579(94)90028-0

Green, B. C., Smith, D. J., Earley, S. E., Hepburn, L. J., and Underwood, G. J. C. (2009). Seasonal changes in community composition and trophic structure of fish populations of five salt marshes along the Essex coastline, United Kingdom. *Estuar. Coast. Shelf Sci.* 85, 247–256. doi: 10.1016/j.ecss.2009.08.008

Hagerthey, S. E., Defew, E. C., and Paterson, D. M. (2002). Influence of *Corophium volutator* and *Hydrobia ulvae* on intertidal benthic diatom assemblages under different nutrient and temperature regimes. *Mar. Ecol. Prog. Ser.* 245, 47–59. doi: 10.3354/meps245047

Hale, R., Jacques, R. O., and Tolhurst, T. J. (2019). Determining how functionally diverse intertidal sediment species preserve mudflat ecosystem properties after abrupt biodiversity loss. *J. Coast. Res.* 35, 389–396. doi: 10.2112/JCOASTRES-D-17-00197.1

Hamilton, D. J., Barbeau, M. A., and Diamond, A. W. (2003). Shorebirds, mud snails, and *Corophium volutator* in the upper Bay of Fundy, Canada: predicting bird activity on intertidal mudflats. *Can. J. Zool.* 81, 1358–1366. doi: 10.1139/z03-130

Hamilton, D. J., Diamond, A. W., and Wells, P. G. (2006). Shorebirds, snails, and the amphipod (*Corophium volutator*) in the upper Bay of Fundy: top-down vs. bottom-up factors, and the influence of compensatory interactions on mudflat ecology. *Hydrobiologia* 567, 285–306. doi: 10.1007/s10750-006-0062-y

Harris, R. J., Pilditch, C. A., Greenfield, B. L., Moon, V., and Kroncke, I. (2015). The influence of benthic macrofauna on the erodibility of intertidal sediments with varying mud content in three New Zealand estuaries. *Estuaries Coasts* 39, 815–828. doi: 10.1007/s12237-015-0036-2

Hochard, S., Pinazo, C., Grenz, C., Burton Evans, J. L., and Pringault, O. (2010). Impact of microphytobenthos on the sediment biogeochemical cycles:

a modelling approach. *Ecol. Model.* 221, 1687–1701. doi: 10.1016/j.ecolmodel.2010.04.002

Honeywill, H., Paterson, D., and Hagerthey, S. (2002). Determination of microphytobenthic biomass using pulse-amplitude modulated minimum fluorescence. *Eur. J. Phycol.* 37, 485–492. doi: 10.1007/BF00391943

Hope, J. A., Paterson, D. M., and Thrush, S. F. (2020). The role of microphytobenthos in soft-sediment ecological networks and their contribution to the delivery of multiple ecosystem services. *J. Ecol.* 108, 815–830. doi: 10.1111/1365-2745.13322

Hubas, C., Passarelli, C., and Paterson, D. M. (2018). "Microphytobenthic biofilms: composition and interactions," in *Mudflat Ecology*, ed. P. G. Beninger, (Cham: Springer).

Jardine, C. B., Bond, A. L., Davidson, P. J. A., Butler, R. W., and Kuwae, T. (2015). Biolfilm consumption and variable diet composition of Western sandpipers (*Calidris mauri*) during migratory stopover. *PLoS One* 10:e0124164. doi: 10.1371/journal.pone.0124164

Jauffrais, T., Drouet, S., Turpin, V., Meleder, V., Jesus, B., Cognie, B., et al. (2015). Growth and biochemical composition of a microphytobenthic diatom (*Entomoneis paludosa*) exposed to shorebird (*Calidris alpina*) droppings. *J. Exp. Mar. Biol. Ecol.* 469, 83–92. doi: 10.1016/j.jembe.2015.04.014

Jesus, B., Perkins, R. G., Consalvey, M., Brotas, V., and Paterson, D. M. (2006a). Effects of vertical migrations by benthic micro-algae on fluorescence measurements of photophysiology. *Mar. Ecol. Prog. Ser.* 315, 55–66. doi: 10.3354/meps315055

Jesus, B., Perkins, R. G., Mendes, C. R., Brotas, V., and Paterson, D. M. (2006b). Chlorophyll fluorescence as a proxy for microphytobenthic biomass: alternatives to the current methodology. *Mar. Biol.* 150, 17–28. doi: 10.1007/s00227-006-0324-2

Jimenez, A., Elner, R. W., Favaro, C., Rickards, K., and Ydenberg, R. C. (2015). Intertidal biofilm distribution underpins differential tide-following behavior of two sandpiper species (*Calidris mauri* and *Calidris alpina*) during northward migration. *Estuar. Coast. Shelf Sci.* 155, 8–16. doi: 10.1016/j.ecss.2014.12.038

Kuwae, T., Beninger, P. G., Decottignes, P., Mathot, K. J., Lund, D. R., and Elner, R. W. (2008). Biofilm grazing in a higher vertebrate: the Western Sandpipier, *Calidris mauri*. *Ecology* 89, 599–606. doi: 10.1890/07-1442.1

Kuwae, T., Miyoshi, E., Hosokawa, S., Ichimi, K., Hosoya, J., Amano, T., et al. (2012). Variable and complex food web structures revealed by exploring missing trophic links between birds and biofilm. *Ecol. Lett.* 15, 347–356. doi: 10.1111/j.1461-0248.2012.01744.x

Legge, O., Johnson, M., Hicks, N., Jickells, T., Diesing, M., Aldridge, J., et al. (2020). Carbon on the Northwest European Shelf: contemporary Budget and Future Influences. *Front. Mar. Sci.* 7:143. doi: 10.3389/fmars.2020.00143

Lewis, L. J., Kelly, T. C., and Davenport, J. (2014). Black-tailed Godwits Limosa limosa islandica and Redshanks *Tringa totanus* respond differently to macroalgal mats in their foraging areas. *Wader Study Group Bull.* 121, 21–29.

Maggi, E., Jackson, A. C., Tolhurst, T. J., Underwood, A. J., and Chapman, M. G. (2013). Changes in microphytobenthos fluorescence over a tidal cycle: implications for sampling designs. *Hydrobiologia* 701, 301–312. doi: 10.1007/s10750-012-1291-x

Maher, D. T., and Eyre, B. D. (2010). Benthic fluxes of dissolved organic carbon in three temperate Australian estuaries: implications for global estimates of benthic DOC fluxes. *J. Geophys. Res.* 115:G04039. doi: 10.1029/2010JG001433

Mason, C. F., and Macdonald, S. M. (1999). Estuarine Feeding by Lapwings *Vanellus vanellus* and *Golden Plovers Pluvialis apricaria*. *Wildfowl* 50, 205–207.

Mathot, K. J., Piersma, T., and Elner, R. W. (2018). "Shorebirds as integrators and indicators of mudflat ecology," in *Mudflat Ecology*, ed. P. G. Beninger, (Cham: Springer).

Maunder, J., and Paterson, D. M. (2015). Coastal Biodiversity and Ecosystem Service Sustainability (CBESS) Surface Sediment Water Content in Saltmarsh and Mudflat Habitats. Avaialable online at: https://data.gov.uk/dataset/d98a5989-60e1-4eb6-838c-54ca9141a460/coastal-biodiversity-and-ecosystem-service-sustainability-cbess-surface-sediment-water-content-in-saltmarsh-and-mudflat-habitats (accessed September, 2019).

McKinley, G. A., Pilcher, D. J., Fay, A. R., Lindsay, K., Long, M. C., and Lovenduski, N. S. (2016). Timescales for detection of trends in the ocean carbon sink. *Nature* 530, 469–472. doi: 10.1038/nature16958

McMellor, S., and Underwood, G. J. C. (2014). Water policy effectiveness: 30 years of change in the hypernutrified Colne estuary, England. *Mar. Pollut. Bull.* 81, 200–209. doi: 10.1016/j.marpolbul.2014.01.018

Mitchell, S. F., and Perrow, M. R. (1998). "Interactions between grazing birds and macrophytes," in *The Structuring Role of Submerged Macrofytes in Lakes. Ecological Studies (Analysis and Synthesis)*, Vol. 131, eds E. Jeppesen, M. Sondergaard, and K. Christoffersen, (New York, NY: Springer),

Muller, G. (1965). *Salmonella* in bird faeces. *Nature* 207:1315. doi: 10.1038/2071315a0

Murphy, R. J., and Tolhurst, T. J. (2009). Effects of experimental manipulation of algae and fauna on the properties of intertidal soft sediments. *J. Exp. Mar. Biol. Ecol.* 379, 77–84. doi: 10.1016/j.jembe.2009.08.005

Muza, M. M., Burtt, E. H. Jr., and Ichida, J. M. (2000). Distribution of bacteria on feathers of some Eastern North American birds. *Wilson Bull.* 112, 432–435. doi: 10.1676/0043-5643(2000)112[0432:dobofo]2.0.co;2

Nacken, M., and Reise, K. (2000). Effects of herbivorous birds on intertidal seagrass beds in the northern Wadden Sea. *Helgol. Mar. Res.* 54, 87–94. doi: 10.1007/s101520050006

Nedwell, D. B., Underwood, G. J. C., McGenity, T. J., Whitby, C., and Dumbrell, A. J. (2016). The Colne Estuary: a long-term microbial ecology observatory. *Adv. Ecol. Res.* 55, 227–281. doi: 10.1016/bs.aecr.2016.08.004

Nizzoli, D., Bartoli, M., Cooper, M., Welsh, D. T., Underwood, G. J. C., and Pierluigi, V. (2007). Implications for oxygen, nutrient fluxes and denitrification rates during the early stage of sediment colonisation by the polychaete *Nereis* spp. in four estuaries. *Estuar. Coast. Shelf Sci.* 75, 125–134. doi: 10.1016/j.ecss.2007.03.035

Norazlimi, N., and Ramli, R. (2014). Temporal variation of shorebirds population in two different mudflats areas. *Int. J. Biol. Biomol. Agric. Food Biotechnol. Eng.* 8, 1314–1320.

Orvain, F., de Crignis, M., Guizien, K., Lefebvre, S., Mallet, C., Takahachi, E., et al. (2014a). Tidal and seasonal effects on the short-term temporal patterns of bacteria, microphytobenthos and exopolymers in natural intertidal biofilms (Brouage, France). *J. Sea Res.* 92, 6–18. doi: 10.1016/j.seares.2014.02.018

Orvain, F., Guizien, K., Lefebvre, S., Beret, M., and Dupuy, C. (2014b). Relevance of macrozoobenthic grazers to understand the dynamic behavior of sediment erodibility and microphytobenthos resuspension in sunny summer conditions. *J. Sea Res.* 92, 46–55. doi: 10.1016/j.seares.2014.03.004

Passarelli, C., Hubas, C., and Paterson, D. M. (2018). "Mudflat ecosystem engineers and services," in *Mudflat Ecology. Aquatic Ecology Series*, Vol. 7, ed. P. Beninger, (Cham: Springer).

Passarelli, C., Olivier, F., Paterson, D. M., Meziane, T. M., and Hubas, C. (2014). Organisms as cooperative ecosystem engineers in intertidal flats. *J. Sea Res.* 92, 92–101. doi: 10.1016/j.seares.2013.07.010

Perkins, R. G., Honeywill, C., Consalvey, M., Austin, H. A., TOlhurst, T. J., and Paterson, D. M. (2003). Changes in microphytobenthic chlorophyll a and EPS resulting from sediment compaction due to de-watering: opposing patterns in concentration and content. *Cont. Shelf Res.* 23, 575–586. doi: 10.1016/S0278-4343(03)00006-2

Redzuan, N. S. (2017). *Microphytobenthos (MPB) Biomass Variability and Sediment-Water Column Exchanges on an Intertidal Flat : Influence of Weather-Related Abiotic Factors Across Neap-Spring-Neap Tidal Cycles*. Ph.D. thesis, University of Essex, Colchester.

Rogers, H., Hille Ris Lambers, J., Miller, R., and Tewksbury, J. J. (2012). 'Natural experiment' demonstrates top-down control of spiders by birds on a landscape level. *PLoS One* 7:e43446. doi: 10.1371/journal.pone.0043446

Rosa, S., Granadeiro, J. P., Vinagre, C., Franca, S., Cabral, H. N., and Palmeirim, J. M. (2008). Impact of predation on the polychaete *Hediste diversicolor* in estuarine tidal flats. *Estuar. Coast. Shelf Sci.* 78, 655–664. doi: 10.1016/j.ecss.2008.02.001

Sahan, E., Sabbe, K., Creach, V., Hernandez-Raquet, G., Vyverman, W., Stal, L. J., et al. (2007). Community structure and seasonal dynamics of diatom biofilms and associated grazers in intertidal mudflats. *Aquat. Microb. Ecol.* 47, 253–266. doi: 10.3354/ame047253

Saint-Beat, B., Dupuy, C., Bocher, P., Chalumeau, J., De Crignis, M., Fontaine, C., et al. (2013). Key features of intertidal food webs that support migratory shorebirds. *PLoS One* 8:e76739. doi: 10.1371/journal.pone.0076739

Schrama, M., Jouta, J., Berg, M. P., and Olff, H. (2013). Food web assembly at the landscape scale: using stable isotopes to reveal changes in trophic structure during succession. *Ecosystems* 16, 627–638. doi: 10.1007/s10021-013-9636-5

Serodio, J. (2004). Analysis of variable chlorophyll fluorescence in microphytobenthos assemblages: implications of the use of depth integrated measurements. *Aquat. Microb. Ecol.* 36, 137–152. doi: 10.3354/ame036137

Serodio, J., Coelho, H., Vieira, S., and Cruz, S. (2006). Microphytobenthos vertical migratory photoresponse as characterised by light-response curves of surface biomass. *Estuar. Coast. Shelf Sci.* 68, 547–556. doi: 10.1016/j.ecss.2006.03.005

Serodio, J., Marques da Silva, J., and Catarino, F. (2001). Use of in vivo chlorophyll a fluorescence to quantify short-term variations in the productive biomass of intertidal microphytobenthos. *Mar. Ecol. Prog. Ser.* 218, 45–61. doi: 10.3354/meps218045

Spalding, M. D., McIvor, A. L., Beck, M. W., Koch, E. W., Moller, I., Reed, D. J., et al. (2014). Coastal ecosystems: a critical element of risk reduction. *Conserv. Lett.* 7, 293–301. doi: 10.1111/conl.12074

Stal, L. J., van Gemerden, H., and Krumbein, W. E. (1984). The simultaneous assay of chlorophyll and bacteriochlorophyll in natural microbial communities. *J. Microbiol. Methods* 2, 295–306. doi: 10.1016/0167-7012(84)90048-4

Steiniger, F. (1969). Transport of micro-organisms by migratory birds between Europe and South Africa, in relation to bird-ringing and disinfection. *J. Afr. Ornithol.* 40, 283–297. doi: 10.1080/00306525.1969.9639129

Sundback, K., Enoksson, V., Graneli, W., and Pettersson, K. (1991). Influence of sublittoral microphytobenthos on the oxygen and nutrient flux between sediment and water: a laboratory continuous-flow study. *Mar. Ecol. Prog. Ser.* 74, 263–279. doi: 10.3354/meps074263

Sundback, K., and Graneli, W. (1988). Influence of microphytobenthos on the nutrient flux between sediment and water: a laboratory study. *Mar. Ecol. Prog. Ser.* 43, 63–69. doi: 10.3354/meps043063

Sutherland, W. J., Alves, J. A., Amano, T., Chang, C. H., Davidson, N. C., Finlayson, C. M., et al. (2012). A horizon scanning assessment of current and potential future threats to migratory shorebirds. *IBIS* 154, 663–679. doi: 10.1111/j.1474-919x.2012.01261.x

Taylor, J. D., McKew, B. A., Kuhl, A., McGenity, T. J., and Underwood, G. J. C. (2013). Microphytobenthic extracellular polymeric substances (EPS) in intertidal sediments fuel both generalist and specialist EPS-degrading bacteria. *Limnol. Oceanogr.* 58, 1463–1480. doi: 10.4319/lo.2013.58.4.1463

Thornton, D. C. O., Dong, L. F., Underwood, G. J. C., and Nedwell, D. B. (2007). Sediment-water inorganic nutrient exchange and nitrogen budgets in the Colne Estuary, UK. *Mar. Ecol. Prog. Ser.* 337, 63–77. doi: 10.3354/meps337063

Thornton, D. C. O., Underwood, G. J. C., and Nedwell, D. B. (1999). Effect of illumination and emersion period on the exchange of ammonium across the estuarine sediment-water interface. *Mar. Ecol. Prog. Ser.* 184, 11–20. doi: 10.3354/meps184011

Tolhurst, T. J., Black, K. S., Shayler, S. A., Mather, S., Black, I., Baker, K., et al. (1999). Measuring the in situ erosion shear stress of intertidal sediments with the cohesive strength meter (CSM). *Estuar. Coast. Shelf Sci.* 49, 281–294. doi: 10.1006/ecss.1999.0512

Tolhurst, T. J., and Chapman, M. G. (2005). Spatial and temporal variation in the sediment properties of an intertidal mangrove forest: implications for sampling. *J. Exp. Mar. Biol. Ecol.* 317, 213–222. doi: 10.1016/j.jembe.2004.11.026

Tolhurst, T. J., Chapman, M. G., Underwood, A. J., and Cruz, J. J. (2012). Technical Note: the effects of five different defaunation methods on biogeochemical properties of intertidal sediment. *Biogeosciences* 9, 3647–3661. doi: 10.5194/bg-9-3647-2012

Tolhurst, T. J., Defew, E. C., de Brouwer, J. F. C., Wolfstein, K., Stal, L. J., and Paterson, D. M. (2006a). Small-scale temporal and spatial variability in the erosion threshold and properties of cohesive intertidal sediments. *Cont. Shelf Res.* 26, 351–362. doi: 10.1016/j.csr.2005.11.007

Tolhurst, T. J., Friend, P. L., Watts, C., Wakefield, R., Black, K. S., and Paterson, D. M. (2006b). The effects of rain on the erosion threshold of intertidal cohesive sediments. *Aquatic Ecol.* 40, 533–541. doi: 10.1007/s10452-004-8058-z

Tolhurst, T. J., Jesus, B., Brotas, V., and Paterson, D. M. (2003). Diatom migration and sediment armouring - an example from the Tagus Estuary, Portugal. *Hydrobiologia* 503, 183–193. doi: 10.1007/978-94-017-2276-6_20

Tolhurst, T. J., Watts, C. W., Vardy, S., Saunders, J. E., Consalvey, M. C., and Paterson, D. M. (2008). The effects of simulated rain on the erosion threshold and biogeochemical properties of intertidal sediments. *Cont. Shelf Res.* 28, 1217–1230. doi: 10.1016/j.csr.2008.01.005

Underwood, A. J. (1997). *Experiments in Ecology: Their Logical Design and Interpretation Using Analysis of Variance*. Cambridge: Cambridge University Press.

Underwood, G. J. C. (1994). Seasonal and spatial variation in epipelic diatom assemblages in the severn estuary. *Diatom Res.* 9, 451–472. doi: 10.1080/0269249X.1994.9705319

Underwood, G. J. C., and Paterson, D. M. (1993). Seasonal changes in diatom biomass, sediment stability and biogenic stabilization in the Severn Estuary. *J. Mar. Biol. Assoc. U.K.* 73, 871–887. doi: 10.1017/S0025315400034780

Underwood, G. J. C., and Paterson, D. M. (2003). The importance of extracellular carbohydrate production by marine epipelic diatoms. *Adv. Bot. Res.* 40, 184–240. doi: 10.1016/S0065-2296(05)40005-1

Van Colen, C. (2018). "The upper living levels: Invertebrate macrofauna," in *Mudflat Ecology*, ed. P. G. Beninger, (Cham: Springer), 7.

Vardy, S., Saunders, J. E., Tolhurst, T. J., Davies, P. A., and Paterson, D. M. (2007). Calibration of the high-pressure cohesive strength meter (CSM). *Cont. Shelf Res.* 27, 1190–1199. doi: 10.1016/j.csr.2006.01.022

Whitehouse, R. J. S., and Mitchener, H. J. (1998). Observations of the morphodynamic behaviour of an intertidal mudflat at different timescales. *Geol. Soc. Spec. Publ.* 139, 255–271. doi: 10.1144/gsl.sp.1998.139.01.21

Wood, C. L., Hawkins, S. J., Godbold, J. A., and Solan, M. (2015). *Coastal Biodiversity and Ecosystem Service Sustainability (CBESS) Sediment Particle Size in Mudflat and Saltmarsh Habitats*. Avaialble online at: https://catalogue.ceh.ac.uk/documents/4e6a2e58-6916-4212-8b2e-e30942b0a05a (accessed September, 2019).

Conflict of Interest: The authors declare that the research was conducted in the absence of any commercial or financial relationships that could be construed as a potential conflict of interest.

frontiers in Marine Science

CORRECTION
published: 01 December 2020
doi: 10.3389/fmars.2020.619563

Corrigendum: Shorebirds Affect Ecosystem Functioning on an Intertidal Mudflat

James M. Booty[1], Graham J. C. Underwood[2], Amie Parris[2], Richard G. Davies[3] and Trevor J. Tolhurst[1]*

[1] School of Environmental Sciences, University of East Anglia, Norwich, United Kingdom, [2] School of Life Sciences, University of Essex, Colchester, United Kingdom, [3] School of Biological Sciences, University of East Anglia, Norwich, United Kingdom

OPEN ACCESS

Edited and reviewed by:
David M. Paterson, University of St Andrews, United Kingdom

***Correspondence:**
James M. Booty
j.booty@uea.ac.uk;
james_booty@hotmail.co.uk

Specialty section:
This article was submitted to Marine Ecosystem Ecology, a section of the journal Frontiers in Marine Science

Received: *20 October 2020*
Accepted: *30 October 2020*
Published: *01 December 2020*

Citation:
Booty JM, Underwood GJC, Parris A, Davies RG and Tolhurst TJ (2020) Corrigendum: Shorebirds Affect Ecosystem Functioning on an Intertidal Mudflat. Front. Mar. Sci. 7:619563. doi: 10.3389/fmars.2020.619563

Keywords: shorebirds, ecosystem function, microphytobenthos biofilm, sediment erosion, nutrient flux

A Corrigendum on

Shorebirds Affect Ecosystem Functioning on an Intertidal Mudflat
by Booty, J. M., Underwood, G. J. C., Parris, A., Davies, R. G., and Tolhurst, T. J. (2020). Front. Mar. Sci. 7:685. doi: 10.3389/fmars.2020.00685

In the original article, there was a mistake in the legend for **Table 2** as published. Estimated bird days are presented as total for the survey area, not per hectare. The correct legend appears below.

Table 2. Bird-days estimated for each species recorded foraging within the survey area between the 20th of January and the 3rd of April 2017 on the mudflat adjacent to Geedon Saltings at Fingringhoe Wick Essex Wildlife Trust Nature Reserve, Essex, United Kingdom (grid reference TM 05065 19030).

The authors apologize for this error and state that this does not change the scientific conclusions of the article in any way. The original article has been updated.

frontiers in Marine Science

ORIGINAL RESEARCH
published: 18 February 2020
doi: 10.3389/fmars.2020.00063

Peak Abundance of Fatty Acids From Intertidal Biofilm in Relation to the Breeding Migration of Shorebirds

Peter J. Schnurr[1], Mark C. Drever[2], Robert W. Elner[2], John Harper[3] and Michael T. Arts[1]*

[1] Department of Chemistry and Biology, Ryerson University, Toronto, ON, Canada, [2] Environment & Climate Change Canada, Delta, BC, Canada, [3] Coastal & Ocean Resources, Victoria, BC, Canada

Intertidal biofilm is a thin layer of microbes and meiofauna enmeshed in an extracellular polymeric matrix within and on top of mudflat sediment. This medium provides a dynamic resource for a variety of consumers in estuarine habitats, and is rich in essential fatty acids that birds require for long-distance migration. We measured seasonal changes in biofilm fatty acid content from spring to summer on the Fraser River Estuary, one of the richest and most important ecosystems for migrant and wintering waterbirds in Canada. Fatty acid content in biofilm showed a strong seasonal pattern with a peak in the spring that is associated with the northward migration of Western Sandpipers (*Calidris mauri*) to their breeding grounds. This peak is linked to the abundance and physiological state, and hence nutritional condition, of epipelic diatoms, which, in turn, depend on a combination of mudflat topography, salinity, temperature, and nutrients that can fluctuate widely with the freshwater inputs from the Fraser River. Specifically, areas with higher elevation (i.e., ∼1 m) had longer periods of exposure to ambient conditions (i.e., light, warm temperatures, gas exchange into/out of biofilms) that facilitated more biofilm growth and higher fatty acid content. Moreover, springtime changes in water chemistry (i.e., salinity/osmotic stresses and nutrients) and temperature facilitated the production of higher overall total lipid/fatty acid contents in the mudflat biofilms compared to summer. Effective conservation of migrating shorebirds depends on the protection of underlying processes at important stopover sites that promote biofilm communities to escalate their production of lipids, including essential fatty acids, during key times of the year.

Keywords: biofilm, diatoms, estuary, fatty acids, mudflat, omega-3, shorebird migration, western sandpiper

OPEN ACCESS

Edited by:
Vona Meleder, Université de Nantes, France

Reviewed by:
Cédric Hubas, Muséum National d'Histoire Naturelle, France
Diana Hamilton, Mount Allison University, Canada

****Correspondence:***
Mark C. Drever
mark.drever@canada.ca

Specialty section:
This article was submitted to Marine Ecosystem Ecology, a section of the journal Frontiers in Marine Science

Received: *11 October 2019*
Accepted: *28 January 2020*
Published: *18 February 2020*

Citation:
Schnurr PJ, Drever MC, Elner RW, Harper J and Arts MT (2020) Peak Abundance of Fatty Acids From Intertidal Biofilm in Relation to the Breeding Migration of Shorebirds. Front. Mar. Sci. 7:63. doi: 10.3389/fmars.2020.00063

INTRODUCTION

North American avifauna have suffered a net loss approaching 3 billion birds, or ∼29% relative to 1970 abundance estimates, including steep declines in migratory shorebird species (Rosenberg et al., 2019). The authors attributed this collapse to the "loss of ecosystem integrity, function and services." For migratory shorebirds, a key aspect of ecosystem integrity is the functional quality

of the stopover locations that are so vital to the success of their annual migrations. Often these stopover sites are hotspots of biological diversity and productivity and, more often than not, occur in estuarine ecosystems (Butler et al., 2001). Given ongoing declines in bird numbers, it is of paramount importance, from a conservation perspective, to identify and delineate the most critical aspects underpinning the integrity of estuarine ecosystems for migrating shorebirds. Here, we seek to achieve this goal by linking the temporal and spatial dynamics of essential fatty acids, as available in the microphytobenthos, to the needs of migrating shorebirds.

Much of the primary productivity in estuarine environments comes from microphytobenthos (Underwood and Kromkamp, 1999), including biofilm, a thin layer of microbes and meiofauna embedded in an extracellular polymeric matrix that forms on intertidal mudflats. The individual microbial cells grow and reproduce within sediment pores (e.g., clay, silt, and sand) and on the top of the mudflat, and are exposed to ambient conditions during low-tide periods. Mudflat biofilms in the intertidal zone are grazed by marine invertebrates (Herman et al., 2000), fish (Carpentier et al., 2014), and, of key interest here, migratory shorebirds (Elner et al., 2005; Kuwae et al., 2008, 2012; Mathot et al., 2010; Jardine et al., 2015).

Algal taxa, particularly diatoms, are major sources of essential fatty acids for consumers in aquatic food webs (Kelly and Scheibling, 2012; Quinn et al., 2017). Although many consumers require, to various degrees, specific fatty acids, our focus is on the Western Sandpiper (*Calidris mauri*). Western Sandpipers extensively graze estuarine intertidal mudflat biofilm (Elner et al., 2005; Kuwae et al., 2008), which serves as a primary source of fatty acids to meet their energetic and physiological demands, particularly during their northward breeding migration each spring (Schnurr et al., 2019). Fats are a preferred migratory fuel because they represent a compact and energy-dense resource compared to carbohydrates and proteins (Guglielmo, 2010). During migration, 90% of the energy required by birds can be derived from lipids, primarily stored as saturated fatty acids (SFA) and monounsaturated fatty acids (MUFA; Guglielmo, 2010), directly or indirectly derived from algae. Further, algae are the main producers (globally) of critically important long-chain polyunsaturated fatty acids (LC-PUFA), including eicosapentaenoic acid (EPA; 20:5n–3) and docosahexaenoic acid (DHA; 22:6n–3) (Hixson et al., 2015). These PUFA are essential to many vertebrates, including birds (Viegas et al., 2017), which benefit from ingesting at least some PUFA (pre-formed) in their diets (Arts et al., 2001).

PUFA are also known to be physiologically important for long distance migration in birds. Consumption of PUFA can increase unsaturation levels of phospholipids in muscle cell membranes (Maillet and Weber, 2007; Weber, 2009), resulting in enhanced membrane fluidity (i.e., decreases in membrane lipid order), which increases permeability, including transmembrane lipid transport (Maillet and Weber, 2006; Weber, 2009). For example, high amounts of EPA and DHA in diets of Semipalmated Sandpipers (*Calidris pusilla*) enhance oxidative capacity in cellular mitochondria (Maillet and Weber, 2007), positively promoting energy availability required for long distance flights. When muscle cells of Sanderling (*Calidris alba*) were treated *in vitro* with n–3 PUFA supplementation, cells increased basal and maximal oxygen consumption (Young, 2019). In addition, PUFA are the precursors of hormones involved in inflammation and cell proliferation, which can facilitate muscle recovery over arduous migration periods (Price, 2010). Therefore, understanding the mechanisms by which estuarine habitats serve to furnish birds with these essential nutrients is essential to effective conservation of migration stopover sites.

Estuarine biofilm communities are dominated by diatoms (Underwood and Paterson, 1993), which can rapidly accumulate fatty acids under specific environmental conditions and growth phases (Schnurr et al., 2019). Under ideal growth conditions diatoms grow and reproduce maximally, causing them to rapidly produce membrane lipids (required for cell division), which consist mostly of phospholipids containing relatively higher proportions of PUFA. When environmental conditions change rapidly (i.e., as a result of an environmental stress), algal cells reduce their rate of cell division and instead store carbon fixed during photosynthesis as triacylglycerol (TAG) – which is comprised of a relatively higher proportion of SFA and MUFA – in lipid droplets located in the cytoplasm (Hu et al., 2008; Yi et al., 2014). For example, marine diatoms in coastal and estuarine ecosystems often experience osmotic stress (Kirst, 1989), and this stress (associated with sudden changes in salinity) induces a lipid/fatty acid accumulation response (Hu and Gao, 2006; Sharma et al., 2012; Mohan and Devi, 2014).

Here, we compared the organic content, and total lipid, chlorophyll-*a*, and fatty acid contents of intertidal biofilm during spring and summer; two time periods during which shorebirds are migrating northward and southward, respectively, through the Fraser River estuary, British Columbia, Canada. The way in which Western Sandpipers move through the Pacific Flyway differs between the two periods (O'Reilly and Wingfield, 1995; Franks et al., 2014). Northward migration is characterized by huge flocks that rapidly move through to the breeding grounds over narrow time windows (Warnock and Bishop, 1998; Drever et al., 2014). In contrast, southward migration occurs over a protracted period during which birds move through in smaller flocks at a slower pace (Butler et al., 1996). If migrating birds are broadly synchronizing the timing of their northward migration with the peak availability of fatty acids in estuarine biofilm, then seasonal changes in total lipid and fatty acid content should mirror the differences in shorebird use between spring and summer. Given that the realized fatty acid content of estuarine mudflat biofilms is likely a result of complex interactions among a variety of environmental conditions (Schnurr et al., 2019), our aim was to understand how spatial and temporal environmental conditions affect biofilm organic and fatty acid content during these two seasons. Specifically, we investigated how biofilm organic and fatty acid content in biofilms were affected by spatial variables such as mudflat elevation (and how that affects mudflat exposure time), proximity to shore, proximity to the outlet of the Fraser River, and by time-varying factors,

including salinity, temperature, nutrient concentrations, and light conditions.

MATERIALS AND METHODS

Sampling Dates

Sampling dates were selected to represent the spring (northward) and summer (southward) migration periods in 2017 for Western Sandpipers and Dunlin (*Calidris alpina*), another common shorebird. Sampling during spring migration was conducted during three campaigns: Campaign 1 occurred April 9–14, Campaign 2 occurred April 21–27, and Campaign 3 occurred May 10–18. Peak northward migration of Western Sandpipers in 2017 occurred around 28 April 2017 (MCD, unpublished data). As the southward migration period occurs over a longer timeframe (i.e., months) than the northward migration (Franks et al., 2014), the two final sampling campaigns were conducted a month apart (August 2–5 and September 5–9) during the summer. These sampling periods occurred during a mix of spring and neap tides (**Supplementary Material**).

Biofilm Sampling Locations

The Fraser River estuary is located south of the City of Vancouver (49.2827° N, 123.1207° W) in southwest British Columbia (**Figure 1**). It is one of the richest and most important ecosystems for migrant and wintering waterbirds in Canada (Butler and Campbell, 1987). Sampling locations (n = 24) (**Figure 1**) were determined according to the following criteria: (1) areas that Western Sandpipers are known to utilize for foraging during their stopover periods; and (2) areas across north-south and east-west transects to understand gradients of proximity to shore and proximity to freshwater river outlets within the estuary. A "spine" of sampling locations was set directly adjacent to provincial government monitoring sites so that we could share their salinity data. Temperature probes were deployed along a north-south transect of sampling locations. East-west transects were perpendicular to the main axis of the "spine" locations to determine whether there was an offshore-onshore spatial gradient in biofilm organic and fatty acid content (**Figure 1**).

Field Sampling Procedures

Biofilm Sampling

Biofilm samples (n = 354) were collected during the five campaigns using the same standard procedure. All samples were collected as the mudflat was exposed during ebbing tides, but some were exposed longer (i.e., range of 10–180 min) than others. Upon arrival at each sampling site, a 2.5 × 2.5 m sampling quadrat was set-up on the ground. This quadrat was divided into a sampling grid, whereby the x- and y-axis had 10 equally spaced 25 cm segments. A random number generator was used to determine sampling locations (n = 3) within the quadrat using the segments as guides. Triplicate biofilm samples were taken, whereby a spatula was used to scrape the top ∼2 mm layer of the biofilm at each location, resulting in a ∼1,000 cm^2 sampling area per biofilm sample. These biofilm samples were deposited into 50 ml Falcon^{TM} tubes and immediately stored in a cooler containing dry ice.

Water Sampling for Nutrient Analysis

Water samples were collected for dissolved nutrient analyses by attaching four 100 ml aluminum cans to each stake that marked a sampling location. The aluminum cans were attached ∼12, 25, 35, and 45 cm above the mud surface, so that, upon tidal flooding, each container would fill with water representative of that height and time. Once the tide receded the following day, the cans were removed and contents combined to create a composite sample representative of the flood period on each date at each location. Composite water samples (n = 118) were stored in a 4°C refrigerator until they were transported to the Pacific Environmental Science Centre, North Vancouver, British Columbia for analysis of macronutrients (soluble reactive phosphorus, nitrate, nitrite, and ammonia). A sub-volume of each sample (n = 118) was sent to the Canada Centre for Inland Waters (CCIW), Burlington, Ontario, for silica analyses.

Temperature and Salinity Data Collection

Temperature and salinity data were continuously collected along the spine (i.e., stations A1-G1; **Figure 1**). Alpha Mach iBWetLand 22L (model AM015) temperature sensors and data loggers recorded temperature at 15-min intervals, with a resolution of 0.1°C. Similarly, INW CT2X Conductivity Smart Sensor logged salinity data at 5-min intervals, with a resolution of 0.001 Practical Salinity Units (PSU). Dry zeros were excluded (i.e., when not inundated), and 5th, 50th, and 95th percentiles were calculated for each 24 h and 72-h period around each biofilm sample. Because all these values were strongly inter-correlated (**Supplementary Material**), we narrowed the list of possible variables by choosing measures related to specific biological hypotheses (**Table 1**).

Elevation and Distance Measures

Sample locations were referenced to relevant geographic features using the geospatial tools in Esri ArcMap. Distances of sample locations from the high-water line (HWL) were estimated as the shortest distance from the Canadian Hydrographic Service (CHS) digital HWL to sample location. Distances from the midline of the Fraser River outflow were estimated from the shortest distance between the CHS digital low-water line (that delineated Canoe Passage) to sample location (**Figure 1**). Elevation measures were obtained as available from LiDAR and Orthophotos taken on the estuary during flights conducted on 23 July 2013. Elevation was determined as an average of the points surrounding each sample location, and corresponds to geodetic elevations in meters, using mean sea level as the zero value.

Laboratory Procedures and Analyses

Organic Content

All frozen (−80°C) biofilm samples were lyophilized for 2–3 days until completely dry in a freeze-drier (Labconco FreeZone 2.5). Dry biofilm samples were then homogenized using a porcelain mortar and pestle. Ash free dry weight (AFDW) of each sample was determined by taking ∼3 g subsample from the homogenized

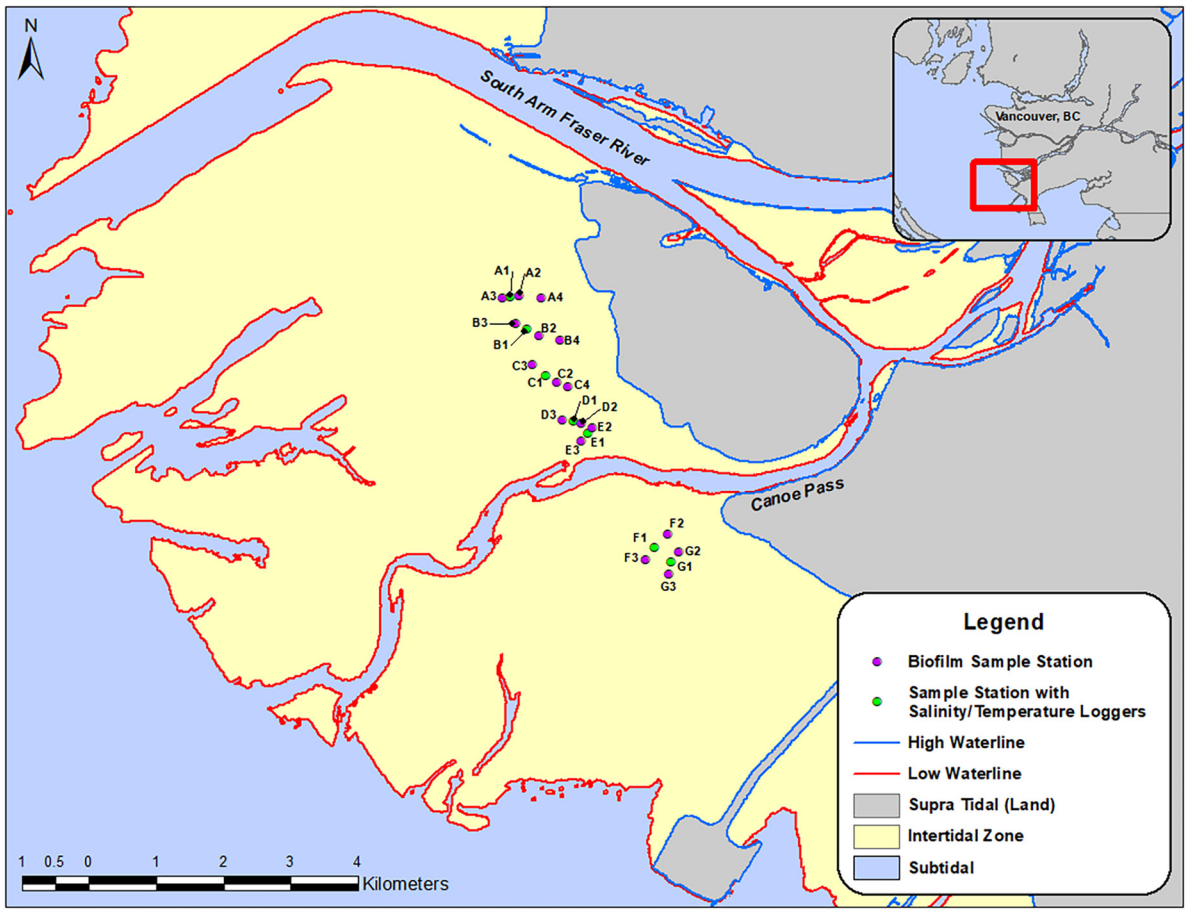

FIGURE 1 | Map of the Roberts Bank study site, with symbols indicating biofilm-sampling locations, April-September 2017. Inset shows the region south of the city of Vancouver, British Columbia, Canada, and the location of the study area within the outflow of the south arm of the Fraser River. Round symbols indicate sampling stations for biofilm measures, and stations in red included monitoring units for salinity and temperature.

sample, and ashing them in an oven at 550°C for 24 h to volatize all organic material, and then re-weighing the samples to determine the difference in mass (i.e., before and after ashing the samples). Organic content was expressed as the percent of the difference from the before-sample.

Chlorophyll-*a* Content

A subsample of each biofilm sample was used to determine chlorophyll content using a procedure adapted from Arar (1997), and conducted in low lighting conditions to prevent photo-oxidation of extracted chlorophyll compounds. Depending on the organic fraction of each sample, a specific mass was weighed out to achieve ∼20 mg of organic biomass within the subsample. The chlorophyll within the subsample was then extracted with 10 mL of 9:1 acetone: water in a grinding tube exposed to grinding for 2 min at 500 rpm. Solution and solid biomass contents were transferred from the grinding tube to a centrifugation tube, whereby the sample steeped in a dark refrigerator (4°C) for 20–23 h. After steeping, samples were centrifuged for 15 min at 675 g, and the supernatant was analyzed using spectrophotometry (Agilent Cary 60 UV-Vis Spectrophotometer) and 1 cm^3 quartz cuvette. A 9:1 acetone: water blank was used to zero the instrument before absorbance measurements were taken. Absorbance values were measured at 750, 664, 647, and 630 nm and applied to the equation [chlorophyll-*a* (mg/L) = 11.85 × abs664 nm – 1.54 × abs647 nm −0.08 × abs630 nm (Arar, 1997)]. Note, abs750 was subtracted from each of the absorbance measurements at the other three wavelengths for chlorophyll because abs750 is for suspended particles that may affect absorbance readings of chlorophyll pigments. Mass of chlorophyll within the extracted sample was determined by multiplying Chlorophyll-*a* concentration by volume of acetone: water used (10 mL), and that mass was normalized to both the mass of sample and the AFDW, as described above. These Chlorophyll-a values were not adjusted for phaeophytin levels.

Total Lipid and Fatty Acid Analysis

A subsample of each biofilm sample was used to determine total lipid and fatty acid content of mudflat biofilms. As with the chlorophyll sample sizes, each sample mass used equated to ∼20 mg of organic content when considering the AFDW (organic

TABLE 1 | Explanatory variables for modeling spatial and temporal variation in measures of biofilm organic and fatty acid content.

Covariate	Rationale
Total Inorganic Nitrogen	Nitrogen is an essential nutrient in cell growth, homeostasis, and other cellular activities, whose availability can limit growth of marine diatoms.
Soluble Reactive Phosphorus	Phosphates are essential nutrients in cell growth, PUFA accumulation, homeostasis, and other cellular activities, whose availability can limit growth of marine diatoms.
Silica	Silica forms the basis of the frustule exoskeleton of diatoms, and its availability can limit growth of diatoms.
Particle Size Distribution Median	Particle size distribution of the substrate can affect the vertical migration of diatoms and is a proxy for tidal/wave energy, which affects biofilm presence. The median represented the most common particle size.
Salinity (24 h) 50 percentile	Salinity is associated with community composition of the microbial communities found in biofilm.
Temperature (24 h) 50th percentile	Photosynthetic capacity of microphytobenthos can vary with temperature. The median value was chosen to represent the average conditions experienced during each sampling date.
Temperature (24 h) 95th percentile	Photosynthetic capacity and thus primary productivity may have upper thermal limits. Fatty acid synthesis rates may be reduced if temperatures are too high. The 95th percentile was chosen to represent the upper range of the conditions experienced in each sampling date
Distance to Canoe Passage	The influence of the Fraser River freshet may vary as a function of distance to the main outflow in the study area.
Distance to High Water Line (HWL)	Tidal/wave energy causes varying shear stresses, thereby affecting accumulation of biomass in mudflat sediments - areas closer to high water line should have lower tidal/wave energies. Nutrient inputs from terrestrial sources should also vary as a function from distance to shore, represented by the high water line.
Elevation	The elevation of the mudflat will determine the amount of time a sampling site is exposed to air, which will determine the amount of light and ambient conditions (i.e., temperature and CO_2 concentrations) the biofilms will be exposed to, thus affecting growth and fatty acid accumulation.

fraction) of the homogenized sample. The Folch extraction method (Folch et al., 1957) was used to extract the lipid from each of the samples. Tricosanoic acid (23:0; Nu-Chek Prep, Inc), which does not commonly occur naturally in this ecosystem, was used to quantify methylation efficiencies during the extraction and methylation procedures. The aqueous layer was discarded during the extraction because all fatty acids were dissolved in the chloroform layer. After extraction, the lipid-chloroform solution was evaporated under a nitrogen blanket before being re-suspended in 2.0 mL of hexane. Two-100 mL aliquots of the lipid-hexanes solution were taken to evaporate in a pre-weighed aluminum tin (∼0.25 mL). The mass difference after evaporation was used to gravimetrically determine the amount of total lipid in the biofilm samples.

The remaining lipid-hexanes solution was methylated with a 1% solution of H_2SO_4 in anhydrous methanol (2 mL), which was heat catalyzed for 90 min at 90°C (VWR Digital 2 block heater). After 90 min, a 1 mL aliquot of deionized water was added to samples to stop the reaction, and a 4 mL aliquot of hexanes was added to extract the fatty acids. The solution was then centrifuged at 2,500 rpm for 5 min to separate the hexanes and aqueous layers. The fatty acid-hexanes phase was separated from the aqueous phase with a Pasteur pipette, then dispensed into a clean centrifuge tube. Each sample was then re-extracted two more times with 4 mL hexane aliquots and combined into the sample in the centrifuge tube. Samples were once again evaporated until dry under a nitrogen blanket and re-suspended in 540 μL of hexanes. The final fatty acid-hexanes solution was pipetted into a Gas Chromatograph (GC) vial and stored at −80°C until analysis.

A Shimadzu GC2010 Plus GC, equipped with an AOC-20i autosampler and a Flame Ionization Detector (FID), was used to identify and quantify the fatty acids in biofilm samples. The GC was fitted with a Supelco SP-2560, 100 m × 0.25 mm column used for fatty acid methyl esters (FAME). Samples were injected in splitless mode. Initial column temperature was 60°C, which was then increased at 15°C per minute until 180°C, followed by 2°C per minute to 240°C. The column was held at 240°C for 5 min to elute all fatty acids potentially remaining in the column. Helium was the carrier gas with a flow rate of 1.2 mL/min. The injector and detector temperatures were both at 250°C through the duration of all sample runs. Fatty acids were identified by matching retention times from the FAME standard GLC-463 (Nu-Chek Prep, Inc) to the unknown peaks in the samples. Fatty acids were quantified by creating a series of dilutions of the FAME standard mix GLC-463 (Nu-Chek Prep, Inc), producing calibration curves for each of the fatty acids of interest after running them on the GC, then calculating the concentrations of the unknowns from the peak area of the fatty acid within the unknown. Methylation efficiencies were determined by comparing the theoretical amount of Tricosanoic Acid (23:0) added to each sample (10.2 μg) to the amount actually determined to be within each sample. All fatty acid mass fractions were then adjusted for methylation efficiencies, then normalized to both the mass of sample and the AFDW, as described above.

Particle Size Distribution Analysis

Particle size distribution analysis was conducted on samples collected in May, and assumed to have been constant throughout the study period. Analyses were conducted by the Department of Materials Science and Engineering, University of Toronto, based on several grams of lyophilized and homogenized samples. A Horiba Partica LA-950 Laser Diffraction Particle Size Analyzer was used, and summary statistics (median, mean, D10, D90) were derived for each location. D10 is the particle size diameter of the smallest grains (10th percentile of weight distribution), and D90 is the particle size diameter of the largest grains in the sample (90th percentile of weight distribution).

Water Sample Nutrient Analyses

Analysis for nutrients key to diatom growth were determined in the water column above each sampling site during tidal flood periods at the time of biofilm sampling. Before analyses, all samples were filtered with a 0.45 μm cellulose acetate membrane filter. Analyses for nitrite, nitrate and ammonia was

colorimetric using Standard Method 4500-NO2-I (nitrite as nitrogen), Standard Method 4500-NO3-I (nitrate as nitrogen), and Standard Method 4500-NH3 H (ammonia as nitrogen), respectively, flow injection analysis, and Lachat Flow Injection System (APHA et al., 2017). Analysis for soluble reactive phosphorus was colorimetric using the Standard Method 4500-P F (phosphorus), a continuous flow analyzer method, and a Technicon AutoAnalyzer II System – segmented flow. Each analyte of interest within a sample was reacted with specific chemicals and analyzed at a wavelength specific to each chemical complex. The protocols for analysis, including the reactant chemicals and wavelengths used for colorimetric analysis are included in each method, which are cited in the References section. Total inorganic nitrogen (TIN) was calculated from a summation of the nitrate, nitrite, and ammonia data collected. Analyses for silica was conducted by Inductively Coupled Plasma-Optical Emission Spectrometry (ICP-OES) (Thermo Scientific; Model ICAP 6300 Duo) using standard solutions produced in the Environment and Climate Change Canada lab at the Canadian Centre for Inland Waters.

Data Analyses

Data Selection and Biofilm Variables

We used a series of eight variables to represent the organic, total lipid, and fatty acid content of biofilm. Organic content was expressed as the mass of the organic fraction divided by the mass of the sample weight (g/g). Total lipid and fatty acid content varied both as a fraction of the organic matter within the sample, and by the total amount of organic matter enmeshed in the sediment. Therefore, our metric for total lipid and fatty acid content (that would be available to foraging birds) was normalized per gram of sample, such that:

$$\mu g \text{ fatty acid/g sample} = \mu g \text{ fatty acid/g organics} \times \text{g organics/g sample}$$

We summed the fatty acid mass fractions into major groups based on their saturation levels, including total values for SFA, MUFA, and PUFA, including n–3, and n–6 fatty acids. Results are presented on a per gram basis, and summary statistics on measures normalized to AFDW are included in the **Supplementary Material**.

We considered two different combinations of summed fatty acids to test two hypotheses about (1) physiological condition of diatoms, and (2) community composition of biofilm. First, we recognized that algal cells accumulate TAG when they stop or slow down dividing, e.g., during periods of stress (Sharma et al., 2012). Since cells are dividing at a reduced rate, they are not building/accumulating new membranes, which are primarily composed of PUFA-rich phospholipids. Thus, the ratio of (SFA + MUFA)/PUFA would be elevated during these stress periods, as diatoms would be expected to produce proportionately more TAG relative to phospholipids. A ratio with a value >2.0 would indicate a preferential accumulation of total SFA and MUFA in excess of that which would be predicted if all fatty acid groups were present in the same amounts. Second, we assessed proportions of specific fatty acids relative to total fatty acids as chemotaxonomic biomarkers for microbial community composition (Dalsgaard et al., 2003; Kelly and Scheibling, 2012). We used the following markers: the sum of 16:1n–7 + EPA for diatoms (Shin et al., 2008), the sum of 22:6n–3 (DHA) + 18:1n–9 for dinoflagellates (Kelly and Scheibling, 2012), 18:2n–6 for cyanobacteria, and the sum of odd-chain length fatty acids for bacteria (Kunihiro et al., 2014). We acknowledge the inherent uncertainty in using such biomarkers (i.e., some fatty acids may be found in several taxa within microphytobenthos), and treat any results with the understanding that they only provide broad indices of species turnover.

Selection of Covariates

We examined correlations among three datasets derived from three separate sources (biofilm measures, salinity and temperature values from station devices, and nutrient analysis measures) by calculating Pearson correlation matrices among all variables within each data source (**Supplementary Material**). From these correlations, we identified a series of response and explanatory variables to identify important spatial and seasonal covariates of biofilm organic and fatty acid content related to known or hypothesized relationships between biofilm, diatoms, and environmental conditions (**Table 1**).

To examine how the fatty acid content of the biofilm changed over time, we fitted a mixed effects model to each biofilm measure with sampling date as a categorical explanatory variable. Sampling station was included as a random effect to account for the repeated measures design, and controlled for consistent spatial differences. Biofilm measures were $\log_e$-transformed to normalize residuals. We tested for significance of the date term with a Type III Analysis of Variance (i.e., using Type III sums of squares) using the Satterthwaite's method [package *lmerTest* in R (Kuznetsova et al., 2017)], and a critical alpha level of $P = 0.00625$ to accommodate for multiple tests on correlated dependent variables. For each model, we checked the residuals for normality and heteroscedasticity. To differentiate whether biofilm measures varied among sampling dates, we conducted Tukey's all-pair comparisons using the glht function in package *multcomp* in R (Hothorn et al., 2008), and used a compact letter display to reveal groupings of data that were not statistically different.

Correlations With Covariates

We estimated the effect of each covariate individually using a mixed effects modeling approach. A mixed effects model was fitted with each biofilm measure as the response variable, including each covariate as a fixed effect in a model that also included date and sampling station as separate categorical random effects. All covariates were centered and scaled by subtracting the mean and dividing by the standard deviation (i.e., z-score), which allowed inferences about relative effect sizes by directly comparing parameter estimates. Because salinity and temperature data were only available for a subset of the stations their inclusion in a combined model would have resulted in loss of significant quantities of data related to other covariates, and therefore this approach using a series of tests allowed us to make best use of available data.

We tested for significance of each covariate with a *t*-test using the Satterthwaite's method [package lmerTest in R (Kuznetsova et al., 2017)]. For each model, we checked the residuals for normality and heteroscedasticity, and calculated pseudo-R^2 values (Nakagawa et al., 2017) using package piecewiseSEM (Lefcheck, 2016) in R. Two pseudo-R^2 values were derived for each model: the marginal R^2 considers only the variance explained by the fixed effects, and the conditional R^2 by both the fixed and random effects.

RESULTS

Temporal Trends in Biofilm Measures

The organic content of the sampled sediment ranged between 2 and 3% of the total sample mass, with a tendency toward higher values in August and September (**Figure 2**). Total lipid varied between a mean of 608 and 719 μg/g biofilm during April and May, respectively, and then declined to 450–237 μg/g biofilm in August and September, respectively. Median Chlorophyll-a values ranged from 32 to 47 μg/g biofilm with no clear seasonal pattern.

The five most abundant fatty acids found in biofilm during spring/summer sampling included 16:0 (palmitic acid), 16:1n–7 (palmitoleic acid) 20:5n–3 (EPA), 22:3n–3 (docosatrienoic acid), and 22:6n–3 (DHA) (**Table 2**). All summed measures of fatty acid content varied widely by date, with highest values observed on April 24 and May 11 (**Figure 2**; $F_{4,325} > 15.2$, $p < 0.0001$). For example, SFA had a mean value of 46 μg/g biofilm on 11 April, which doubled to 98 and 104 μg/g biofilm on 24 April and 11 May, respectively. Total SFA then declined to 64 and 44 μg/g biofilm during the August and September sample dates, similar to values observed in early spring (**Figure 2**). This same pattern of an approximate doubling in measures of fatty acid content from values observed in early spring to late April and May, followed by a decline to summer and early fall period (August/September), was apparent in all the summed measures of fatty acids, including SFA, MUFA, PUFA, n–3, and n–6 fatty acids (**Figure 2**).

The (SFA + MUFA)/PUFA ratio varied strongly by sampling date ($F_{4,325} = 25.8$, $p < 0.0001$) ranging from 2.3 to 2.9 in spring to 1.9–2.1 in summer. Confidence intervals for summer values of the ratio overlapped 2.0, indicating that summed SFA and MUFA were not being preferentially accumulated during August and September.

The biomarkers for microbial community composition also showed strongly seasonal variation (**Figure 3**; $F_{4,325} = 4.8$, $p < 0.001$). The marker for diatoms varied from 40 to 44% during the spring samples, and then dropped to ∼36% during summer samples. This change was accompanied by concurrent increases in the markers for dinoflagellates, cyanobacteria and bacteria, indicating a shift in the community composition of biofilm between spring and summer.

Correlations With Covariates

Covariates related to nutrients and water conditions varied among sampling dates (**Figure 4**). TIN was highest (0.25 mg/L) from 11 April to 11 May), after which values remained at ∼0.10 mg/L throughout summer. Similarly, phosphorus declined from 0.021 mg/L in the 11 April to 11 May period, to an average of 0.01 mg/L throughout summer. Both silica and salinity showed clear patterns related to the Fraser River freshet. Silica ranged between 3.2 and 5.1 mg/L and demonstrated little variance over time, except for a strong peak on 11 May, when silica increased to a mean value of 10.8 mg/L. Median salinity from the past 24 h, when averaged across locations, had a mean value of 13.7 PSU in April, which declined over the spring to its lowest mean value of 1.9 PSU during the freshet period in May, and then increased to range between 15−16 PSU during August and September. Median temperature from the past 24 h (i.e., before biofilm sampling) increased from 9.5°C on 11 April to ∼20°C in August and September. The 95th percentile of temperature ranged from a mean of 17°C in April to >22°C by September.

Biofilm measures were significantly correlated with a suite of spatial attributes and water conditions, of which elevation, salinity (24 h) 50th percentile, temperature (24 h) 50th percentile, and temperature (24 h) 95th percentile were the most influential, with details varying by each of the eight biofilm measures (**Table 3**). Elevation also had a strong and positive effect on all biofilm measures (**Table 3**), indicating the important role played by local topography in determining biofilm organic and fatty acid content. The other spatial covariate, distance to the HWL, was also negatively correlated with organic content, chlorophyll-a, and SFA, indicating higher values closer to shore (**Table 3**).

Soluble reactive phosphorus, TIN, and silica showed correlations with biofilm measures. Contrary to expectations, soluble reactive phosphorus and TIN had consistent and negative correlations with measures of fatty acid content (**Table 3**). Silica had a negative correlation with organic content and a positive correlation with measures of fatty acid content (**Table 3**).

The two measures of temperature had contrasting correlations with biofilm measures: the 95th percentile of temperature over the past 24 h had a negative association with organic content and chlorophyll-*a*, whereas median temperature was positively correlated with organic content (**Table 3**). Of the variables related to water conditions, median salinity over the past 24 h had negative correlations with SFA, n–3, and PUFA, and a positive correlation with total lipid (**Table 3**).

DISCUSSION

Shorebirds often travel many thousands of kilometers on their annual migrations between wintering and breeding areas. These arduous journeys are only possible if the birds are able to re-fuel with energy and nutrients thereby maintaining themselves in top physiological condition. To achieve this, birds depend on key stopover sites to provide safe staging places to recover and restock the energy and essential nutrients required for the next leg of their migration (Warnock, 2010). Disruptions to habitat quantity or quality at stopover sites can lead to steep declines in shorebird numbers (Weber et al., 1999; Studds et al., 2017). However, it is not just the location of stopover sites

TABLE 2 | Summary of fatty acid profiles.

			April 11		April 24		May 11		Aug 3		Sept 7	
Group	**Trivial nomenclature**	**Molecular formula**	**μ**	**SD**	**μ**	**SD**	**μ**	**SD**	**μ**	**SD**	**μ**	**SD**
SFA	Myristic acid	14:0	8.3	14.0	45.1	90.1	30.3	60.7	19.5	72.3	7.7	9.7
MUFA	Myristoleic acid	14:1n–5	0.0	0.0	0.0	0.0	0.0	0.0	0.0	0.0	0.0	0.0
SFA	Pentadecanoic acid	15:0	3.7	5.4	21.8	46.0	15.1	28.8	11.8	14.8	11.5	16.2
MUFA		15:1n–5	0.2	0.5	1.3	2.8	1.2	2.2	0.9	1.1	1.4	2.1
SFA	Palmitic acid	16:0	40.3	36.6	241.5	499.9	166.0	301.1	62.3	130.4	34.5	34.7
MUFA	Palmitoleic acid	16:1n–7c	54.9	53.6	320.9	713.8	212.6	387.8	47.8	45.9	35.8	36.7
MUFA		16:1n–7t	1.6	1.5	8.5	19.5	10.4	35.7	1.3	1.7	0.5	0.4
SFA	Margaric acid	17:0	0.7	0.8	4.6	9.5	2.9	5.1	2.5	2.6	2.3	2.8
MUFA		17:1n–7	0.6	1.1	3.8	8.5	3.4	5.8	2.3	3.7	2.3	4.2
SFA	Stearic acid	18:0	2.7	2.3	19.4	39.2	15.2	30.2	5.8	4.8	4.5	3.8
MUFA	Oleic acid	18:1n–9c	4.6	6.3	17.6	33.6	13.3	23.7	21.9	81.9	7.7	7.9
MUFA		18:1n–9t	0.2	0.3	1.3	2.7	0.8	1.8	0.5	0.7	0.2	0.2
MUFA	Petroselinic acid	18:1n–12c	0.2	0.2	1.2	2.5	1.4	4.1	0.3	1.1	0.2	0.5
MUFA	Vaccenic acid	18:1n–7c	6.1	6.6	39.3	84.5	27.0	48.5	14.0	34.5	7.3	7.0
MUFA		18:1n–7t	0.2	0.4	1.5	5.7	1.6	7.4	0.2	0.2	0.2	0.4
SFA	Nonadecylic acid	19:0	0.2	0.3	0.7	1.2	1.1	2.2	0.2	0.2	0.1	0.1
MUFA		19:1n–12	0.6	1.3	3.1	10.3	1.1	2.2	0.8	1.4	1.5	3.5
PUFA	Linoleic acid (LNA)	18:2n–6c	1.8	1.9	12.2	31.3	7.3	12.9	13.8	59.7	2.6	2.8
SFA	Arachidic acid	20:0	0.5	0.5	5.0	11.3	3.6	7.8	1.2	1.2	0.7	0.5
PUFA	α-Linoleic acid (GLA)	18:3n–6	1.0	1.0	6.1	12.6	5.3	9.1	1.6	2.1	1.3	1.6
MUFA		20:1n–15	0.0	0.0	0.0	0.0	0.0	0.0	0.0	0.0	0.0	0.0
MUFA		20:1n–12	0.4	0.7	2.9	6.3	2.4	4.9	1.1	1.5	0.8	1.5
MUFA	Gondoic acid	20:1n–9	0.3	0.3	2.4	5.4	1.6	3.7	0.6	1.7	0.3	0.3
PUFA	α-Linoleic acid (ALA)	18:3n–3	1.3	1.8	8.1	16.6	5.5	12.1	19.1	96.2	1.1	1.3
SFA		19:0	0.0	0.0	0.0	0.0	0.0	0.0	0.0	0.0	0.0	0.0
PUFA	Eicosadienoic acid	20:2n–6	2.8	4.8	14.9	29.7	10.9	23.0	2.2	2.7	1.9	1.9
PUFA	Docosatrienoic acid	22:3n–3	10.1	4.9	105.2	241.8	83.7	290.0	0.5	0.5	0.3	0.3
SFA	Behenic acid	22:0	1.0	0.9	4.8	9.2	5.2	11.0	2.4	1.9	1.3	1.0
PUFA	Dihomo-γ-linolenic acid	20:3n–6	0.4	0.4	2.4	5.1	2.1	3.8	1.0	1.0	0.7	0.8
MUFA	Cetoleic acid	22:1n–11	0.0	0.0	0.0	0.0	0.0	0.0	0.0	0.0	0.0	0.0
MUFA	Erucic acid	22:1n–9	0.6	1.7	2.2	4.3	1.7	5.0	0.3	0.6	0.3	0.4
PUFA	Eicosatrienoic acid	20:3n–3	0.3	0.4	1.6	3.2	1.0	2.0	0.9	2.9	0.4	0.3
PUFA	Arachidonic acid (ARA)	20:4n–6	2.9	1.6	19.1	42.0	17.8	35.0	9.2	9.7	6.1	5.2
PUFA	Docosadienoic acid	22:2n–6	0.8	1.4	3.2	6.3	2.4	4.7	0.9	2.0	0.6	0.5
SFA	Lignoceric acid	24:0	1.6	1.2	9.7	19.7	10.6	21.2	4.5	3.9	2.5	1.9
PUFA	Eicosapentaenoic acid (EPA)	20:5n–3	39.3	58.7	194.0	401.4	152.2	287.4	37.0	38.5	28.4	25.6
MUFA	Nervonic acid	24:1n–9	0.2	0.3	2.2	6.7	0.7	1.5	0.1	0.2	0.1	0.1
PUFA	Docosatetraenoic acid	22:4n–6	0.3	0.2	1.9	3.9	1.5	3.2	0.9	1.2	0.6	0.7
PUFA	Docosapentaenoic acid (DPA)	22:5n–6	0.0	0.0	0.0	0.0	0.0	0.0	0.0	0.0	0.0	0.0
PUFA	docosapentaenoic acid (DPA)	22:5n–3	1.1	1.2	7.2	15.4	6.1	11.2	3.6	11.2	1.4	1.6
PUFA	Docosahexaenoic acid (DHA)	22:6n–3	7.3	11.7	49.5	104.7	33.7	64.2	10.9	5.6	9.6	6.8

Means and standard deviations are expressed as Mass Fraction of Fatty Acid Methyl Esters (μg FAME/g of biofilm sample; obtained by multiplying by proportion of organic content in samples – see Methods) of biofilm on Roberts Bank, British Columbia, 2017. N for April 11 = 71; N for April 24 = 72; N for May 11 = 72; N for Aug 3 = 69; N for September 7 = 69. Group refers to the saturation level of each fatty acid: SFA, saturated fatty acids; MUFA, monounsaturated fatty acids, and PUFA, polyunsaturated fatty acids.

that determines their suitability, there is also a confluence of physical and chemical factors that, operating synergistically, make them ideal places for the generally well-timed production (mainly in the biofilm) of accessible energy and essential nutrients required by shorebirds during their annual migrations (Mathot et al., 2018).

We demonstrate that intertidal mudflat biofilm in the Fraser River estuary, especially in spring when these communities are dominated by diatoms, is a rich source of lipid and essential fatty acids. These riches of energy and nutrients occur around the same time that Western Sandpipers and other shorebirds make their annual northward migration through the area in

large congregations (Drever et al., 2014; Schnurr et al., 2019). These seasonal changes in fatty acid content may result from three (non-mutually exclusive) processes: (i) changes in the proportion of diatom biomass within the biofilm which results in more fatty acids; (ii) physiological changes within diatoms already present on the mudflats, resulting in an increase in per cell total lipid and individual fatty acid content, and (iii) seasonal species turnover within the biofilm community. Here, we describe the spatial and temporal confluence of triggers that stimulate lipid production in diatoms, and discuss how each of them may function to promote the observed temporal trajectory of essential fatty acids in these intertidal mudflat biofilm communities.

Spatial Variability

Spatially, we found measures of organic content, total lipid, chlorophyll-a, and fatty acids tended to be higher closer to the HWL and at sites with raised elevation (**Table 3**). Elevated areas have longer times (i.e., several hours per tidal period) when the mudflat is exposed to ambient air conditions. These conditions likely allow algal cells to photosynthesize at higher rates since they are exposed to higher photon flux densities, warmer springtime temperatures (Schnurr et al., 2019), and higher rates of gas exchange (i.e., CO_2 into the cells and O_2 out of the biofilms). The sites closer to shore would have longer exposure times (to ambient air conditions) and may experience less shear stress associated with tidal and wave energy (Underwood and Paterson, 1993). Generally, low shear stress facilitates formation and growth of thicker algal biofilms (de Brouwer et al., 2005; Besemer et al., 2007). The positive correlation with elevation might also reflect the presence of intertidal hummocks, which appear to be associated with higher densities of epipelic diatoms (Beninger et al., 2018).

Differences in Diatom Biomass

Spring is a time of rapid change in the Fraser River estuary. Temperature, day length and photon flux densities increase (Schnurr et al., 2019), and the tidal cycles switch such that lowest tides occur during daylight hours rather than overnight (Thomson, 1981). These higher photon flux densities (Jensen and Revsbech, 1989; Schnurr and Allen, 2015; Schnurr et al., 2016b) and temperatures (Blanchard et al., 1997; Kudo et al., 2000; Jiang and Gao, 2004; Scholz and Liebezeit, 2013) result in enhanced rates of photosynthesis and growth in microphytobenthos. Since diatoms are the main primary producers in intertidal biofilm at our study site (Beninger et al., 2011; Schnurr et al., 2019), increases in photosynthetic activity likely cause increases in overall diatom biomass in the biofilm. Thus, we found a positive correlation between organic content and temperature (24 h) 50th percentile (**Table 3**). Temperatures in the 15−20°C range foster ideal benthic diatom growth rates (Admiraal, 1976). The spring temperatures experienced on Roberts Bank in 2017 were often within these optimal temperatures (**Figure 4**), and outside temperature ranges that can result in growth inhibition and/or cell death (Thompson and Guo, 1992; Kudo et al., 2000; Jiang and Gao, 2004; Woelfel et al., 2014). Although not measured directly, the effect of photon flux density is encapsulated by the strong effect of date on the measures of fatty acid abundance. In addition, the diatom fatty acid biomarkers were higher in the spring compared to summer (**Figure 3**), consistent with the hypothesis that higher fatty acid content of biofilm results from an overall higher proportion of diatom biomass.

We found that fatty acid content was significantly reduced during summer, and this was likely a result of temperatures that were too high for diatoms to grow and reproduce. Indeed, we regularly observed maximal daytime temperatures on mudflat biofilms in the summertime to be greater than 33°C, which is above optimal temperatures for diatom growth (Thompson and Guo, 1992; Kudo et al., 2000; Jiang and Gao, 2004; Woelfel et al., 2014). Higher temperatures during summer would have also resulted in a stronger "de-watering" effect, wherein changes in the sediment bulk density can result in lower measures of Chl *a* content of microphytobenthos (Perkins et al., 2003).

Physiological Changes

Differences in fatty acid content of biofilm between spring and summer may also occur from physiological changes within the diatom communities themselves. The existence of a lipid accumulation response during spring was supported by the larger (SFA + MUFA)/PUFA ratios that ranged from 2.3 to 2.9, indicating a preferential production of triacylglycerol relative to summer samples. Laboratory studies have shown lipid accumulation in microalgae occurs in two stages (Rodolfi et al., 2009). First, when all requirements for growth are met, microalgae divide rapidly and synthesize (mostly) phospholipid-dominated membrane lipids, which are predominately composed of MUFA and PUFA (Solovchenko, 2012). Second, when any growth factor becomes limiting, cells enter a lipid-producing phase characterized by a slowdown or cessation of cell division accompanied by an accumulation of triacylglycerol, predominantly composed of SFA and MUFA (Sharma et al., 2012; Solovchenko, 2012). Fatty acid content during the spring sampling dates showed a wide variance, with some locations having very high values relative to the mean (**Figure 2**). Total fatty acid values had a double mode distribution, and these very high values could account for up to 85% of the total fatty acid content in the spring samples (**Supplementary Material**). Presently we have no way to differentiate the relative roles of increases in diatom biomass and lipid accumulation response in determining the total amount of fatty acids in intertidal biofilm, and we suggest that these local sites with very high values result from their combined action, i.e., very high local bursts of fatty acids become available when diatoms that are experiencing good growing conditions are suddenly triggered to accumulate lipid.

Sudden shifts in water chemistry such as salinity or pH can cause lipid accumulation responses in microalgae (Sharma et al., 2012). On Roberts Bank, the daily discharge of the Fraser River increases steadily during April and May on account of the spring freshet fueled by snow melt (**Supplementary Material**), and this influx of freshwater into the tidal estuary results in rapid changes in salinity and water chemistry. We consider rapid changes in salinity as the strongest driver in the lipid

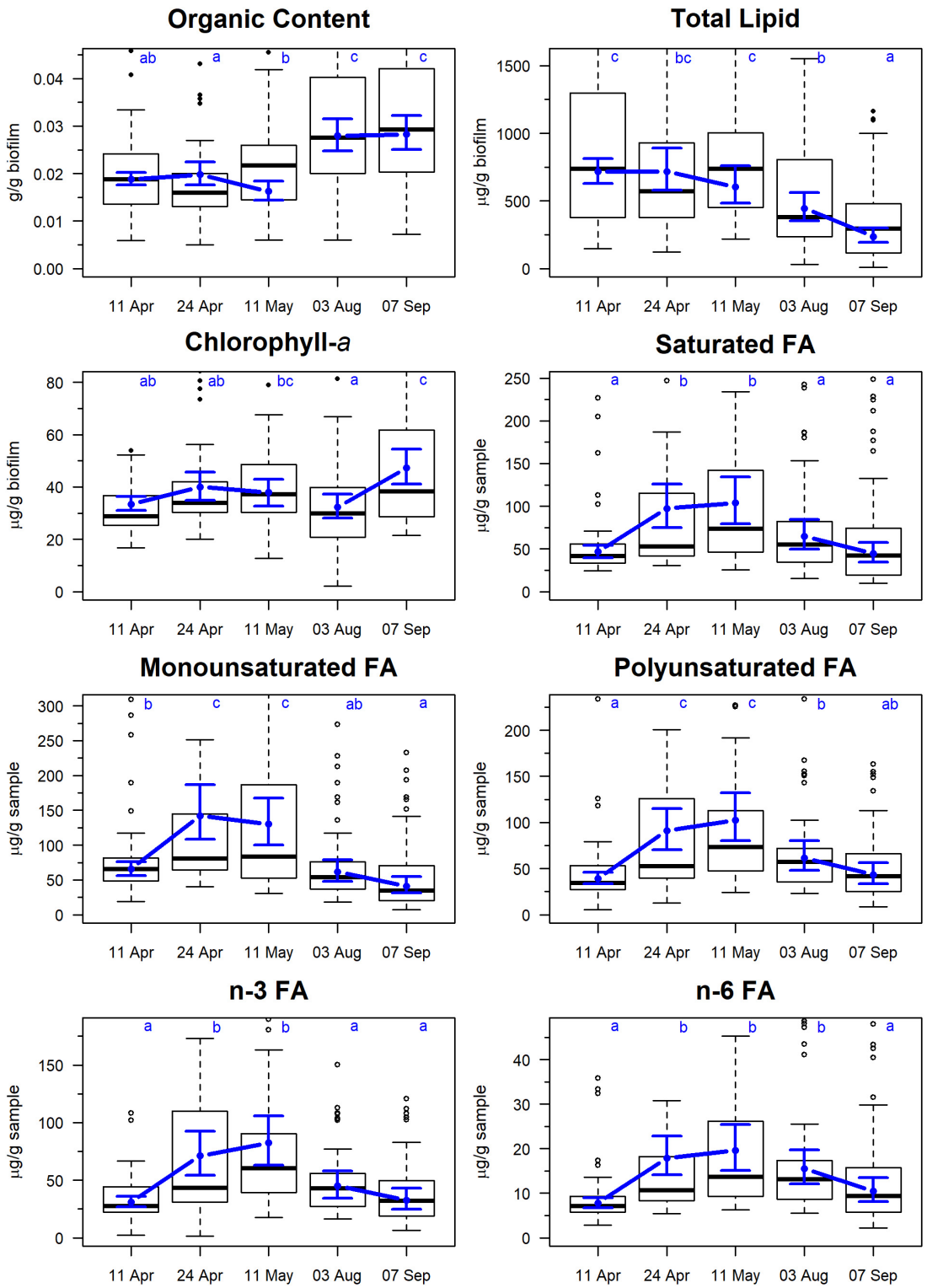

FIGURE 2 | Temporal changes in biofilm measures on Roberts Banks mudflats located on the Fraser River estuary, British Columbia, April-September 2017. Biofilm measures are expressed in units of per 1 g of sample, including inedible sediment. Note that *y*-axis extends from 0 to 0.90 percentile of each measure to avoid compression of scale from outliers. Box plots represent the distribution of observed values, where midline is the median, with the upper and lower limits of the box being 75th and 25th percentiles. Whiskers extend up to 1.5 × the interquartile range, and outliers are depicted as points. Blue circles indicate predicted means from linear mixed effects models, and bounds are 95% predictions intervals from fixed effects. Letters indicate groupings that are not statistically significantly different according to Tukey's pairwise comparisons.

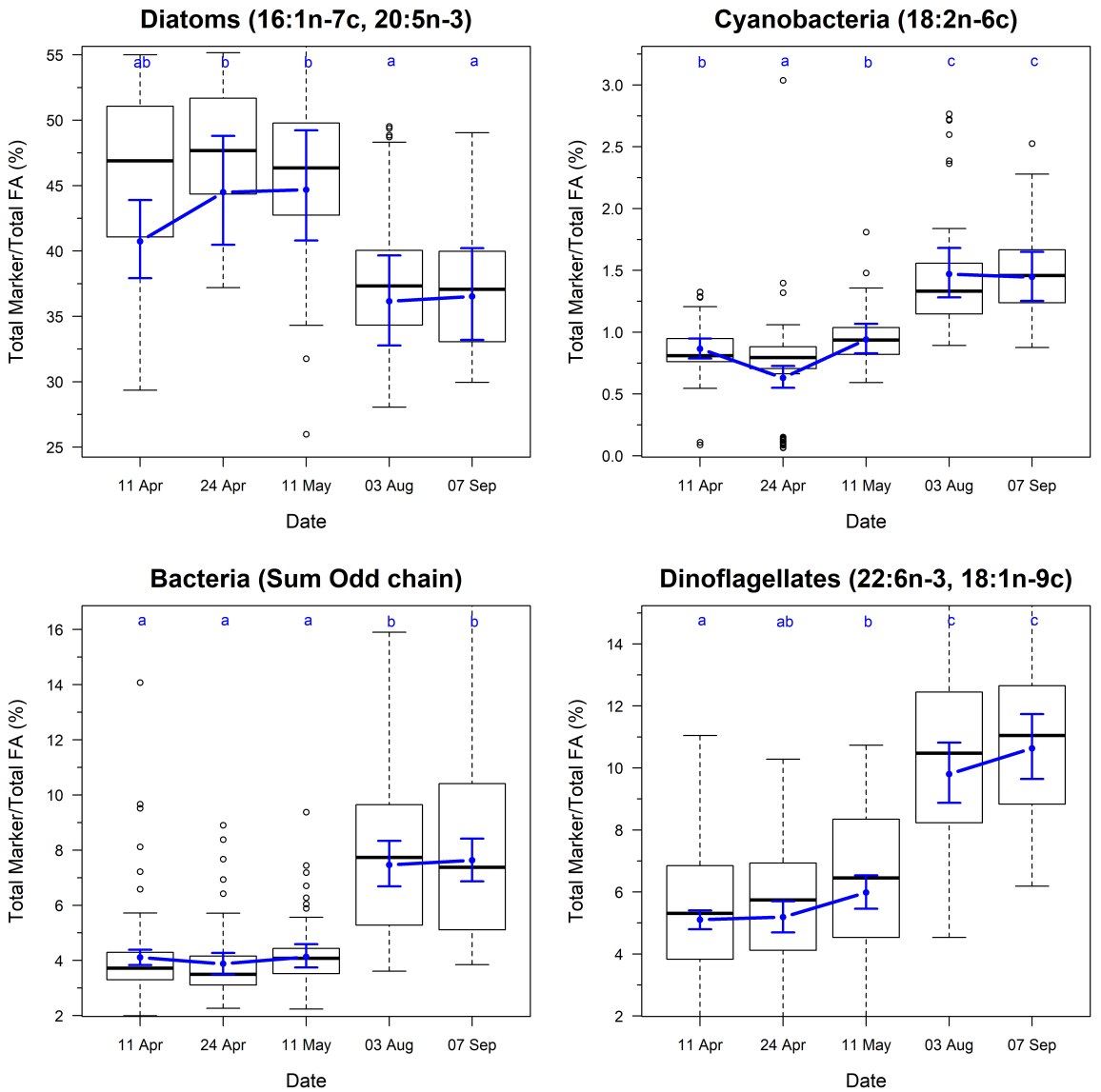

FIGURE 3 | Temporal changes in the ratio of fatty acid groups and chemotaxonomic markers on Roberts Banks mudflats located on the Fraser River estuary, British Columbia, April-September 2017. Note that *y*-axis for biomarker plots extend from 0.025 to 0.975 percentiles of each measure to avoid compression of scale from outliers. Box plots represent the distribution of observed values, where midline is the median, with the upper and lower limits of the box being 75th and 25th percentiles. Whiskers extend up to 1.5 × the interquartile range, and outliers are depicted as points. Blue circles indicate predicted means from linear mixed effects models, and bounds are 95% prediction intervals from fixed effects. Letters indicate groupings that are not statistically significantly different according to Tukey's pairwise comparisons.

accumulation response because the rapid drop in salinity in May coincided with the peak abundance of fatty acids (**Figure 4**), and the covariate modeling (**Table 3**) indicated salinity had a stronger role on fatty acid content than temperature. Further, seasonal changes are accompanied by wide daily fluctuations related to tidal cycles (i.e., salinity wedges), whereby dense saltwater flooding the mudflats causes a spike in salinity (Correll, 1978) until the tide peaks and then begins to recede, when diffusion and currents cause the salinity to decrease. This twice-daily event would contribute to a lipid accumulation response in response to the osmotic/salinity stress. In the spring, fatty acid content was highest during the May samples, which occurred during spring tides (**Supplementary Material**) that, in addition to resulting in longer exposure times, would have accentuated daily variance in salinity.

A lipid accumulation response can be also induced by factors such as changes in nutrients, light levels, and temperature (Sharma et al., 2012; Schnurr et al., 2016a). Diatoms can increase their total lipid (including fatty acids) contents (up to three-fold) when "starved" of nitrogen and/or silica for relatively short periods of time (i.e., 4–120 h) (Opute, 1974; Shifrin and Chisholm, 1981; Roessler, 1988; Sriharan et al., 1991;

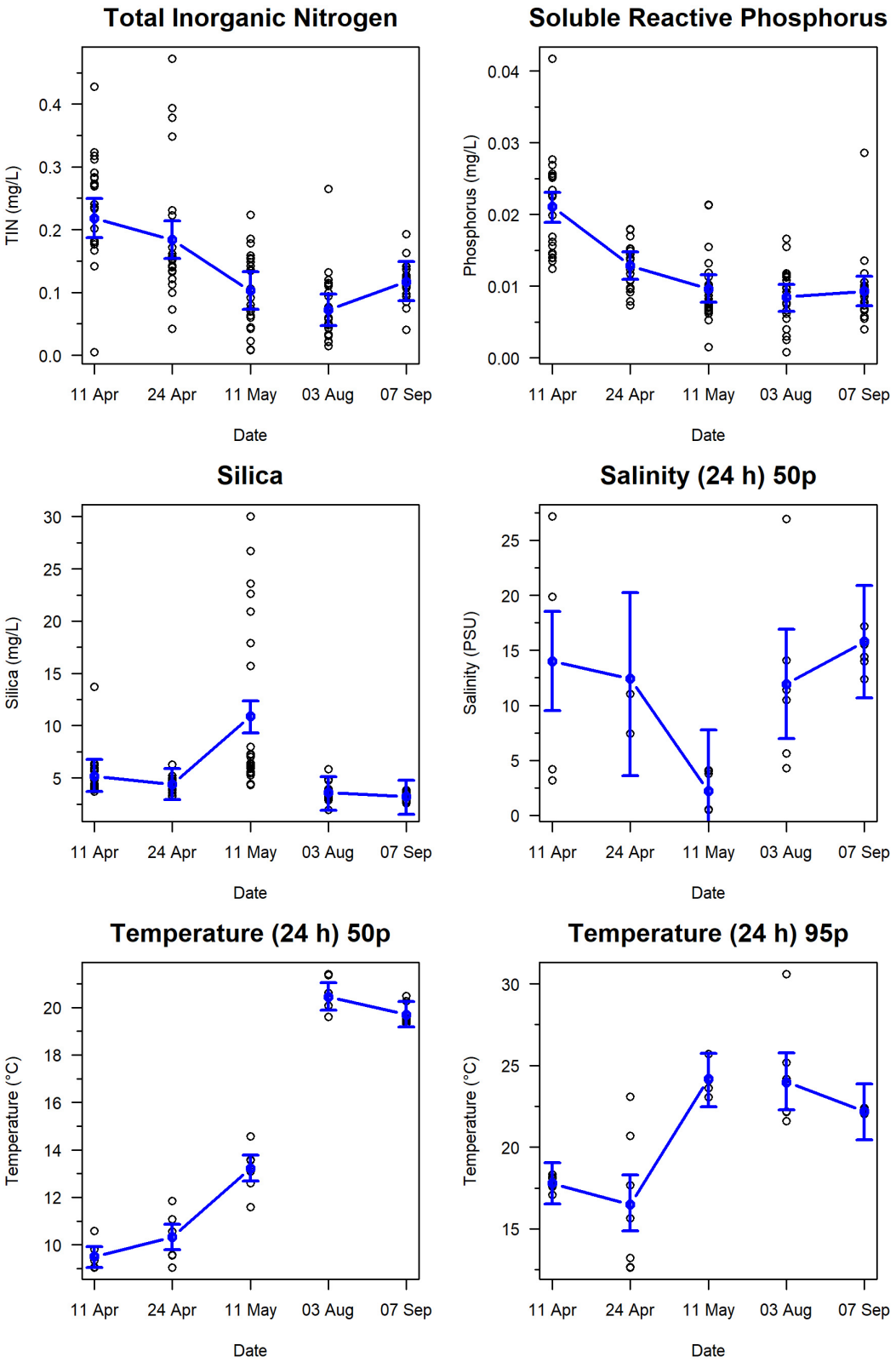

FIGURE 4 | Temporal changes in nutrients and water conditions on Roberts Bank, Fraser River Delta, British Columbia, 2017. Blue circles indicate predicted means, and bounds are 95% prediction intervals from linear mixed effects models. Variables plotted are Total Inorganic Nitrogen, Soluble Reactive Phosphorus, Silica, Salinity (24 h) 50 percentile, Temperature (24 h) 50th percentile, and Temperature (24 h) 95th percentile.

TABLE 3 | Effects of covariates on measures of biofilm organic and fatty acid (FA) content.

Biofilm measure	Covariate	β	SE(β)	P	Marginal R^2	Conditional R^2
Organic content	Temperature (24 h) 50th percentile	0.14	0.05	0.061	0.10	0.30
	Distance to High Water Line (HWL)	−0.13	0.06	0.029	0.06	0.48
	Elevation	0.12	0.06	0.044	0.05	0.48
	Temperature (24 h) 95th percentile	−0.11	0.06	0.082	0.05	0.46
	Silica	−0.07	0.03	0.012	0.02	0.49
Total lipid	Elevation	0.40	0.08	0.000	0.17	0.51
	Salinity (24 h) 50th percentile	0.22	0.12	0.085	0.04	0.73
	Soluble Reactive Phosphorus	0.16	0.05	0.004	0.03	0.53
Chlorophyll-a	Elevation	0.26	0.06	0.000	0.19	0.49
	Temperature (24 h) 95th percentile	−0.15	0.05	0.002	0.11	0.69
	Distance to High Water Line (HWL)	−0.14	0.08	0.094	0.05	0.50
SFA	Elevation	0.38	0.09	0.000	0.12	0.37
	Salinity (24 h) 50th percentile	−0.32	0.16	0.052	0.07	0.41
	Total Inorganic Nitrogen	−0.21	0.06	0.001	0.04	0.40
	Distance to High Water Line (HWL)	−0.20	0.11	0.092	0.03	0.38
	Silica	0.14	0.06	0.022	0.02	0.36
MUFA	Elevation	0.36	0.08	0.000	0.10	0.40
	Total Inorganic Nitrogen	−0.18	0.06	0.004	0.03	0.44
	Silica	0.15	0.06	0.018	0.02	0.38
PUFA	Salinity (24 h) 50th percentile	−0.30	0.15	0.058	0.07	0.38
	Elevation	0.26	0.09	0.011	0.06	0.37
	Total Inorganic Nitrogen	−0.18	0.06	0.004	0.03	0.38
	Silica	0.16	0.06	0.009	0.02	0.35
	Soluble Reactive Phosphorus	−0.14	0.07	0.037	0.02	0.34
n–3 fatty acids	Salinity (24 h) 50th percentile	−0.31	0.15	0.049	0.08	0.39
	Elevation	0.24	0.10	0.023	0.05	0.35
	Total Inorganic Nitrogen	−0.18	0.06	0.006	0.03	0.37
	Silica	0.16	0.06	0.011	0.02	0.33
	Soluble Reactive Phosphorus	−0.15	0.07	0.031	0.02	0.33
n–6 fatty acids	Elevation	0.30	0.08	0.002	0.08	0.34
	Total Inorganic Nitrogen	−0.18	0.06	0.003	0.03	0.35
	Silica	0.16	0.06	0.009	0.02	0.34
	Soluble Reactive Phosphorus	−0.12	0.06	0.058	0.01	0.31

Beta coefficients are derived from mixed effects models (see text for details), and sorted by absolute values from largest to smallest. P-values shown as 0.00 are <0.001. Marginal R^2 considers only the variance explained by the fixed effects, and the conditional R^2 by both the fixed and random effects (the total variance explained by the model). Only covariates that met a cut-off of $p < 0.1$ are included.

Hu et al., 2008). Although the negative correlations between fatty acid content with N and P (**Table 3**) are consistent with lipid accumulation response, these nutrients on Roberts Bank changed gradually over time (**Figure 4**), and therefore we interpret this correlation as a seasonal depletion, and that N and P are not limiting in a nutrient-rich marine environment. Silica had a negative correlation with organic content, and a positive correlation with measures of fatty acid content (**Table 3**). Silica (driven by the freshet) is likely fueling the diatom productivity selectively, wherein diatoms require this nutrient to form their exterior frustules, in contrast to other taxa in the microphytobenthos.

Community Composition

The composition of algal communities can have a pronounced effect on their fatty acid profiles (Galloway and Winder, 2015; Schnurr and Allen, 2015). Thus, differences in fatty acid content between spring and summer may have also resulted from changes in community composition of the intertidal biofilm. The Roberts Bank diatom community is dominated by *Navicula* spp. and *Nitzschia* spp. (Beninger et al., 2011; Schnurr et al., 2019). Based on fatty acid markers, we suggest that the overall diatom biomass within the biofilm declines from spring to summer (**Figure 3**), a change accompanied by an increase in bacteria, cyanobacteria, and dinoflagellates. The highest temperatures (>30°C) observed in the summertime would inhibit diatom growth and reproduction (Renaud et al., 1994; Kudo et al., 2000; Jiang and Gao, 2004; Scholz and Liebezeit, 2013; Woelfel et al., 2014), but favor the growth of cyanobacteria, chlorophytes and bacteria (Schnurr and Allen, 2015). These changes tie the fatty acid content of biofilm to the presence of epipelic diatoms, with the caveat that the effect of species turnover on fatty acid content of intertidal biofilm needs to be better explored with more detailed taxonomic data.

Implications for Shorebird Migration

Hitherto, there has been only a limited understanding of why shorebirds choose where, when and how long to stop and forage during long-distance migration. For example, why Western Sandpipers stop at only a few large estuarine mudflats during their northward breeding migration along the Pacific Flyway (Mathot et al., 2018), but are dissipated over multiple smaller sites on their return to non-breeding grounds, has been enigmatic (O'Reilly and Wingfield, 1995). Conventional ornithological hypotheses to explain this dichotomy in migration strategies are based on either access to energy (Farmer and Wiens, 1999) or predation threats (Lank et al., 2003). Our finding that the northward arrival of Western Sandpipers and other shorebirds on Roberts Bank mirrors seasonal increases in total lipid and in the abundance of essential fatty acids found in intertidal biofilm provides a new explanation. The discovery complements previous studies demonstrating that shorebirds alter their foraging behaviors to select areas with high microphytobenthic biomass (Drouet et al., 2015; Jiménez et al., 2015) and the activities of shorebirds can significantly affect benthic diatom growth (Jauffrais et al., 2015). The inference is that migration success for shorebirds hinges on their presence at a stopover site that generally coincides with maximal total lipid and fatty acid production at the site. In the case of Roberts Bank, the main trigger for benthic diatoms switching to their lipid/fatty acid accumulation phase appears to be stress associated with high amplitude oscillations in salinity. We speculate that equivalent mechanisms triggering lipid/fatty acid accumulation responses in diatom-dominated biofilm assemblages are likely also affecting the quality of migratory stopover locations on mudflats elsewhere on the Pacific and along other international flyways. Investigating the existence of and, if so, elucidating the nature of stress triggers at all these sites should be a research priority. Of particular importance is discerning whether these triggers are driven by similar salinity-associated circumstances to Roberts Bank or an alternative mechanism. Meanwhile, maintaining the salinity trigger is an imperative for the effective conservation of migratory shorebirds in the Fraser River estuary and, if a pattern emerges on other stopover sites, this new understanding would galvanize a paradigm shift in shorebird conservation worldwide.

Springtime accumulation of biofilm biomass and fatty acids represents a crucial "pulse" of fuel and essential nutrients into estuarine food webs. Invertebrate populations foraging on primary producers in the microphytobenthos can show rapid increases in abundance (Sahan et al., 2007), and thus accumulation of lipid and fatty acids up the food web (i.e., into fish, birds, etc.). Given the important role of essential fatty acids in the growth and reproduction of a wide variety of organisms within aquatic food webs (Kainz et al., 2004), understanding the physiological response of algae/diatoms to complex and interacting environmental factors in estuarine mudflats is fundamental to designing strategies to conserve and protect migrating birds and estuarine ecosystems in their entirety. We found that total lipid and fatty acid content in biofilm on mudflats varied between spring and summer and that these nutritionally important compounds were significantly affected by the outflow of freshwater from the Fraser River. To the north of our study site lies Sturgeon Bank, another large estuarine mudflat that has experienced extensive alterations to its coastal oceanography and sediment transport (Atkins et al., 2016). The Sturgeon Bank area now sees reduced use by shorebirds during the critical northward migration period relative to Roberts Bank (Jardine et al., 2015). Such differences underscores the need to protect these mudflat habitats in as pristine a state as possible so they may continue to furnish shorebirds with the energy and essential fatty acids required for long-distance migration.

DATA AVAILABILITY STATEMENT

The raw data supporting the conclusions of this article will be made available by the authors, without undue reservation, to any qualified researcher.

AUTHOR CONTRIBUTIONS

RE, MA, PS, and JH conceived and designed the study. PS collected the data. MD and JH contributed data. MD performed the statistical analyses. PS, MD, RE, JH, and MA wrote the manuscript.

FUNDING

Funding for this work was provided by the Vancouver Airport Fuel Facilities Corporation to MA and PS, Environment and Climate Change Canada to MD and RE, and Natural Sciences and Engineering Research Council of Canada to MA (NSERC Discovery Grant #04537-2014).

ACKNOWLEDGMENTS

Lipid and fatty acid analyses (Ryerson University) were assisted by Serena Egidio, Clara Romany, and Cristina Mudalige. Daniel Stewart and Megan Lievesley provided excellent assistance on the mudflats collecting data and samples. Brad Mason of the Community Mapping Network provided the elevation measures. Nutrient analyses were conducted by Environment and Climate Change Canada's National Laboratory for Environmental Testing, Burlington, Ontario, and the Pacific Environmental Science Centre, North Vancouver, British Columbia. Brent Gurd (Province of British Columbia) and Eric Balke (Ducks Unlimited Canada) contributed salinity data.

SUPPLEMENTARY MATERIAL

The Supplementary Material for this article can be found online at: https://www.frontiersin.org/articles/10.3389/fmars.2020.00063/full#supplementary-material

REFERENCES

Admiraal, W. (1976). Influence of light and temperature on the growth rate of estuarine benthic diatoms in culture. *Mar. Biol.* 39, 1–9. doi: 10.1007/bf00395586

APHA, AWWA, and WEF (2017). *Standard Methods for the Examination of Water and Wastewater, current online edition*. Washington, DC: American Public Health Association, 20001–23710.

Arar, E. J. (1997). *In Vitro Determination of Chlorophylls a, b, c1 + c2 and Pheopigments in Marine and Freshwater Algae by Visible Spectrometry (Method 446.0)*. Ohio: National Exposure Research Laboratory Office of Research and Development U.S. Environmental Protection Agency Cincinnati.

Arts, M. T., Ackman, R. G., and Holub, B. J. (2001). "Essential fatty acids" in aquatic ecosystems: a crucial link between diet and human health and evolution. *Can. J. Fish. Aquatic Sci.* 58, 122–137. doi: 10.1139/f00-224

Atkins, R. J., Tidd, M., and Ruffo, G. (2016). Sturgeon Bank, Fraser River delta, BC, Canada: 150 years of human influences on salt marsh sedimentation. *J. Coast. Res.* 75(Suppl.1), 790–795.

Beninger, P. G., Cuadrado, D., and van de Koppel, J. (2018). in *Sedimentary and Biological Patterns on Mudflats*, ed. P. G. Beninger, (Cham: Springer), 185–211.

Beninger, P. G., Elner, R. W., Morancais, M., and Decottignies, P. (2011). Downward trophic shift during breeding migration in the shorebird *Calidris mauri* (Western Sandpiper). *Mar. Ecol. Prog. Ser.* 428, 259–269. doi: 10.3354/meps09050

Besemer, K., Singer, G., Limberger, R., Chlup, A. K., Hochedlinger, G., Hödl, I., et al. (2007). Biophysical controls on community succession in stream biofilms. *Appl. Environ. Microbiol.* 73, 4966–4974. doi: 10.1128/aem.00588-07

Blanchard, G. F., Guarini, J. M., Gros, P., and Richard, P. (1997). Seasonal effect on the relationship between the photosynthetic capacity of intertidal microphytobenthos and temperature. *J. Phycol.* 33, 723–728. doi: 10.1111/j.0022-3646.1997.00723.x

Butler, R. W., and Campbell, R. W. (1987). *The Birds of the Fraser River Delta: Populations, Ecology and International Significance*. Occasional Paper. Ottawa: Canadian Wildlife Service, 73.

Butler, R. W., Davidson, N. C., and Morrison, R. G. (2001). Global-scale shorebird distribution in relation to productivity of near-shore ocean waters. *Waterbirds* 24, 224–232.

Butler, R. W., Delgado, F. S., de la Cueva, H., Pulido, V., and Sandercock, B. K. (1996). Migration routes of the Western Sandpiper. *Wilson Bull.* 180, 662–672.

Carpentier, A., Como, S., Dupuy, C., Lefrançois, C., and Feunteun, E. (2014). Feeding ecology of *Liza* spp. in a tidal flat: evidence of the importance of primary production (biofilm) and associated meiofauna. *J. Sea Res.* 92, 86–91. doi: 10.1016/j.seares.2013.10.007

Correll, D. L. (1978). Estuarine productivity. *Bioscience* 28, 646–650. doi: 10.2307/1307395

Dalsgaard, J., St John, M., Kattner, G., Müller-Navarra, D. C., and Hagen, W. (2003). Fatty acid trophic markers in the pelagic marine environment. *Adv. Mar. Biol.* 46, 225–340. doi: 10.1016/s0065-2881(03)46005-7

de Brouwer, J. D., Wolfstein, K., Ruddy, G. K., Jones, T. E. R., and Stal, L. J. (2005). Biogenic stabilization of intertidal sediments: the importance of extracellular polymeric substances produced by benthic diatoms. *Microb. Ecol.* 49, 501–512. doi: 10.1007/s00248-004-0020-z

Drever, M. C., Lemon, M. J., Butler, R. W., and Millikin, R. L. (2014). Monitoring populations of Western Sandpipers and Pacific Dunlins during northward migration on the Fraser River Delta, British Columbia, 1991–2013. *J. Field Ornithol.* 85, 10–22. doi: 10.1111/jofo.12045

Drouet, S., Turpin, V., Godet, L., Cognie, B., Cosson, R. P., and Decottignies, P. (2015). Utilisation of intertidal mudflats by the Dunlin Calidris alpina in relation to microphytobenthic biofilms. *J. Ornithol.* 156, 75–83. doi: 10.1007/s10336-014-1133-x

Elner, R. W., Beninger, P. G., Jackson, D. L., and Potter, T. M. (2005). Evidence of a new feeding mode in western sandpiper (Calidris mauri) and dunlin (Calidris alpina) based on bill and tongue morphology and ultrastructure. *Mar. Biol.* 146, 1223–1234. doi: 10.1007/s00227-004-1521-5

Farmer, A. H., and Wiens, J. A. (1999). Models and reality: time–energy trade-offs in pectoral sandpiper (*Calidris melanotos*) migration. *Ecology* 80, 2566–2580. doi: 10.1890/0012-9658(1999)080%5B2566:martet%5D2.0.co;2

Folch, J., Lees, M., and Sloane Stanley, G. H. (1957). A simple method for the isolation and purification of total lipids from animal tissues. *J. Biol. Chem.* 226, 497–509.

Franks, S., Lank, D. B., and Wilson, W. H. (2014). "Western sandpiper (*Calidris mauri*)," in *The birds of North America online*, ed. P. Rodewald, (Ithaca: Cornell Laboratory of Ornithology), doi: 10.2173/bna.90

Galloway, A. W. E., and Winder, M. (2015). Partitioning the relative importance of phylogeny and environmental conditions on phytoplankton fatty acids. *PLoS One* 10:e0130053. doi: 10.1371/journal.pone.0130053

Guglielmo, C. G. (2010). Move that fatty acid: fuel selection and transport in migratory birds and bats. *Integr. Comp. Biol.* 50, 336–345. doi: 10.1093/icb/icq097

Herman, P. M. J., Middelburg, J. J., Widdows, J., Lucas, C. H., and Heip, C. H. R. (2000). Stable isotopes as trophic tracers: combining field sampling and manipulative labelling of food resources for macrobenthos. *Mar. Ecol. Prog. Ser.* 204, 79–92. doi: 10.3354/meps204079

Hixson, S. M., Sharma, B., Kainz, M. J., Wacker, A., and Arts, M. T. (2015). Production, distribution, and abundance of long-chain omega-3 polyunsaturated fatty acids: a fundamental dichotomy between freshwater and terrestrial ecosystems. *Environ. Rev.* 23, 414–424. doi: 10.1139/er-2015-0029

Hothorn, T., Bretz, F., and Westfall, P. (2008). Simultaneous inference in general parametric models. *Biometr. J.* 50, 346–363. doi: 10.1002/bimj.200810425

Hu, H., and Gao, K. (2006). Response of growth and fatty acid compositions of *Nannochloropsis* sp. to environmental factors under elevated CO2 concentrations. *Biotechnol. Lett.* 28, 987–992. doi: 10.1007/s10529-006-9026-6

Hu, Q., Sommerfeld, M., Jarvis, E., Ghirardi, M., Posewitz, M., Seibert, M., et al. (2008). Microalgal triacylglycerols as feedstocks for biofuel production: perspectives and advances. *Plant J.* 54, 621–639. doi: 10.1111/j.1365-313X.2008.03492.x

Jardine, C. B., Bond, A. L., Davidson, P. J., Butler, R. W., and Kuwae, T. (2015). Biofilm consumption and variable diet composition of Western Sandpipers (*Calidris mauri*) during migratory stopover. *PLoS One* 10:e0124164. doi: 10.1371/journal.pone.0124164

Jauffrais, T., Drouet, S., Turpin, V., Méléder, V., Jesus, B., Cognie, B., et al. (2015). Growth and biochemical composition of a microphytobenthic diatom (*Entomoneis paludosa*) exposed to shorebird (*Calidris alpina*) droppings. *J. Exp. Mar. Biol. Ecol.* 469, 83–92. doi: 10.1016/j.jembe.2015.04.014

Jensen, J., and Revsbech, N. P. (1989). Photosynthesis and respiration of a diatom biofilm cultured in a new gradient growth chamber. *FEMS Microbiol. Ecol.* 62, 29–38. doi: 10.1111/j.1574-6968.1989.tb03655.x

Jiang, H., and Gao, K. (2004). Effects of lowering temperature during culture on the production of polyunsaturated fatty acids in the marine diatom *Phaeodactylum tricornutum* (*Bacillariophyceae*). *J. Phycol.* 40, 651–654. doi: 10.1111/j.1529-8817.2004.03112.x

Jiménez, A., Elner, R. W., Favaro, C., Rickards, K., and Ydenberg, R. C. (2015). Intertidal biofilm distribution underpins differential tide-following behavior of two sandpiper species (*Calidris mauri* and *Calidris alpina*) during northward migration. *Estuar. Coast. Shelf Sci* 155, 8–16. doi: 10.1016/j.ecss.2014.12.038

Kainz, M., Arts, M. T., and Mazumder, A. (2004). Essential fatty acids in the planktonic food web and their ecological role for higher trophic levels. *Limnol. Oceanogr.* 49, 1784–1793. doi: 10.4319/lo.2004.49.5.1784

Kelly, J. R., and Scheibling, R. E. (2012). Fatty acids as dietary tracers in benthic food webs. *Mar. Ecol. Prog. Ser.* 446, 1–22. doi: 10.3354/meps09559

Kirst, G. O. (1989). Salinity tolerance of eukaryotic marine algae. *Ann. Rev. Plant Physiol. Plant Mol. Biol.* 40, 21–53. doi: 10.1093/gbe/evw152

Kudo, I., Miyamoto, M., Noiri, Y., and Maita, Y. (2000). Combined effects of temperature and iron on the growth and physiology of the marine diatom *Phaeodactylum tricornutum* (*Bacillariophyceae*). *J. Phycol.* 36, 1096–1102. doi: 10.1046/j.1529-8817.2000.99042.x

Kunihiro, T., Veuger, B., Vasquez-Cardenas, D., Pozzato, L., Le Guitton, M., Moriya, K., et al. (2014). Phospholipid-derived fatty acids and quinones as markers for bacterial biomass and community structure in marine sediments. *PLoS One* 9:e96219. doi: 10.1371/journal.pone.0096219

Kuwae, T., Beninger, P. G., Decottignies, P., Mathot, K. J., Lund, D. R., and Elner, R. W. (2008). Biofilm grazing in a higher vertebrate: the western sandpiper *Calidris mauri*. *Ecology* 89, 599–606. doi: 10.1890/07-1442.1

Kuwae, T., Miyoshi, E., Hosokawa, S., Ichimi, K., Hosoya, J., Amano, T., et al. (2012). Variable and complex food web structures revealed by exploring missing trophic links between birds and biofilm. *Ecol. Lett.* 15, 347–356. doi: 10.1111/j.1461-0248.2012.01744.x

Kuznetsova, A., Brockhoff, P. B., and Christensen, R. H. B. (2017). lmerTest package: tests in linear mixed effects models. *J. Stat. Softw* 82, 1–26.

Lank, D. B., Butler, R. W., Ireland, J., and Ydenberg, R. C. (2003). Effects of predation danger on migration strategies of sandpipers. *Oikos* 103, 303–319. doi: 10.1034/j.1600-0706.2003.12314.x

Lefcheck, J. S. (2016). piecewiseSEM: piecewise structural equation modelling in R for ecology, evolution, and systematics. *Methods Ecol. Evol.* 7, 573–579. doi: 10.1111/2041-210x.12512

Maillet, D., and Weber, J. M. (2006). Performance-enhancing role of dietary fatty acids in a long-distance migrant shorebird: the Semipalmated Sandpiper. *J. Exp. Biol.* 209, 2686–2695. doi: 10.1242/jeb.02299

Maillet, D., and Weber, J. M. (2007). Relationship between n-3 PUFA content and energy metabolism in the flight muscles of a migrating shorebird: evidence for natural doping. *J. Exp. Biol.* 210, 413–420. doi: 10.1242/jeb.02660

Mathot, K. J., Lund, D. R., and Elner, R. W. (2010). Sediment in stomach contents of Western Sandpipers and Dunlin provide evidence of biofilm feeding. *Waterbirds* 33, 300–306. doi: 10.1675/063.033.0305

Mathot, K. J., Piersma, T., and Elner, R. W. (2018). "Shorebirds as integrators and indicators of mudflat ecology," in *Mudflat Ecology*, ed. P. G. Beninger, (Switzerland: Springer Nature), 309–338. doi: 10.1007/978-3-319-99194-8_12

Mohan, S. V., and Devi, M. P. (2014). Salinity stress induced synthesis to harness biodiesel during dual mode cultivation of mixotrophic microalgae. *Bioresour. Technol.* 165, 288–294. doi: 10.1016/j.biortech.2014.02.103

Nakagawa, S., Johnson, P. C., and Schielzeth, H. (2017). The coefficient of determination R2 and intra-class correlation coefficient from generalized linear mixed-effects models revisited and expanded. *J. R. Soc. Interf.* 14:20170213. doi: 10.1098/rsif.2017.0213

Opute, F. (1974). Lipid and fatty acid composition of diatoms. *J. Exp. Bot.* 25, 823–835. doi: 10.1093/jxb/25.4.823

O'Reilly, K. M., and Wingfield, J. C. (1995). Spring and autumn migration in Arctic shorebirds: same distance, different strategies. *Am. Zool.* 35, 222–233. doi: 10.1093/icb/35.3.222

Perkins, R. G., Honeywill, C., Consalvey, M., Austin, H. A., Tolhurst, T. J., and Paterson, D. M. (2003). Changes in microphytobenthic chlorophyll a and EPS resulting from sediment compaction due to de-watering: opposing patterns in concentration and content. *Continental Shelf Res.* 23, 575–586. doi: 10.1016/s0278-4343(03)00006-2

Price, E. R. (2010). Dietary lipid composition and avian migratory flight performance: development of a theoretical framework for avian fat storage. *Comp. Biochem. Physiol. Part A* 157, 297–309. doi: 10.1016/j.cbpa.2010.05.019

Quinn, J. T., Hamilton, D. J., and Hebert, C. E. (2017). Fatty acid composition and concentration of alternative food of Semipalmated Sandpipers (*Calidris pusilla*) in the upper Bay of Fundy Canada. *Can. J. Zool.* 95, 565–573. doi: 10.1139/cjz-2016-0246

Renaud, S. M., Parry, D. L., and Thinh, L. V. (1994). Microalgae for use in tropical aquaculture I: gross chemical and fatty acid composition of twelve species of microalgae from the Northern Territory Australia. *Journal of Applied Phycology.* 6, 337–345. doi: 10.1007/bf02181948

Rodolfi, L., Zittelli, G. C., Bassi, N., Padovani, G., Biondi, N., Bonini, G., et al. (2009). Microalgae for oil: strain selection, induction of lipid synthesis and outdoor mass cultivation in a low-cost photobioreactor. *Biotechnol. Bioeng.* 102, 100–112. doi: 10.1002/bit.22033

Roessler, P. G. (1988). Effects of silicon deficiency on lipid composition and metabolism in the diatom *Cyclotella cryptica*. *J. Phycol.* 24, 394–400. doi: 10.1111/j.1529-8817.1988.tb00189.x

Rosenberg, K. V., Dokter, A. M., Blancher, P. J., Sauer, J. R., Smith, A. C., Smith, P. A., et al. (2019). Decline of the North American avifauna. *Science* 366, 120–124. doi: 10.1126/science.aaw1313

Sahan, E., Sabbe, K., Creach, V., Hernandez-Raquet, G., Vyverman, W., Stal, L. J., et al. (2007). Community structure and seasonal dynamics of diatom biofilms and associated grazers in intertidal mudflats. *Aquatic Microb. Ecol.* 47, 253–266. doi: 10.3354/ame047253

Schnurr, P. J., and Allen, D. G. (2015). Factors affecting algae biofilm growth and lipid production: a review. *Renewable Sustain. Energ. Rev.* 52, 418–429. doi: 10.1016/j.rser.2015.07.090

Schnurr, P. J., Drever, M. C., Kling, H. J., Elner, R. W., and Arts, M. T. (2019). Seasonal changes in fatty acid composition of estuarine intertidal biofilm: implications for western sandpiper migration. *Estuar., Coast. Shelf Sci.* 224, 94–107. doi: 10.1016/j.ecss.2019.04.047

Schnurr, P. J., Espie, G. S., and Allen, D. G. (2016a). The effect of photon flux density on algal biofilm growth and internal fatty acid concentrations. *Algal Res.* 16, 349–356. doi: 10.1016/j.algal.2016.04.001

Schnurr, P. J., Molenda, O., Edwards, E., Espie, G. S., and Allen, D. G. (2016b). Improved biomass productivity in algal biofilms through synergistic interactions between photon flux density and carbon dioxide concentration. *Bioresour. Technol.* 219, 72–79. doi: 10.1016/j.biortech.2016.06.129

Scholz, B., and Liebezeit, G. (2013). Biochemical characterization and fatty acid profiles of 25 benthic marine diatoms isolated from the Solthörn tidal flat (southern North Sea). *J. Appl. Phycol.* 25, 453–465. doi: 10.1007/s10811-012-9879-0

Sharma, K. K., Schuhmann, H., and Schenk, P. M. (2012). High lipid induction in microalgae for biodiesel production. *Energies* 5, 1532–1553. doi: 10.3390/en5051532

Shifrin, N. S., and Chisholm, S. W. (1981). Phytoplankton lipids: interspecific differences and effects of nitrate, silicate and light-dark cycles. *J. Phycol.* 17, 374–384. doi: 10.1111/j.1529-8817.1981.tb00865.x

Shin, P. K., Yip, K. M., Xu, W. Z., Wong, W. H., and Cheung, S. G. (2008). Fatty acid as markers to demonstrating trophic relationships among diatoms, rotifers and green-lipped mussels. *J. Exp. Mar. Biol. Ecol.* 357, 75–84. doi: 10.1016/j.jembe.2008.01.002

Solovchenko, A. (2012). Physiological role of neutral lipid accumulation in eukaryotic microalgae under stresses. *Russian J. Plant Physiol.* 59, 192–202.

Sriharan, S., Bagga, D., and Nawaz, M. (1991). The effects of nutrient and temperature on biomass, growth, lipid production, and fatty acid composition of *Cyclotella cryptica* Reimann. Lewin and Guillard. *Appl. Biochem. Biotechnol.* 2, 317–326. doi: 10.1007/bf02922611

Studds, C. E., Kendall, B. E., Murray, N. J., Wilson, H. B., Rogers, D. I., Clemens, R. S., et al. (2017). Rapid population decline in migratory shorebirds relying on Yellow Sea tidal mudflats as stopover sites. *Nat. Commun.* 8:14895. doi: 10.1038/ncomms14895

Thompson, P. A., and Guo, M. (1992). Effects of variation in temperature. I. on the biochemical composition of eight species of marine phytoplankton. *J. Phycol.* 28, 481–488. doi: 10.1111/j.0022-3646.1992.00481.x

Thomson, R. E. (1981). "Oceanography of the British Columbia coast," in *Canadian Special Publication of Fisheries and Aquatic Sciences*, Vol. 56, ed. Canada. Dept. of Fisheries and Oceans, (Ottawa: Department of Fisheries and Oceans), 291.

Underwood, G. J., and Paterson, D. M. (1993). Seasonal changes in diatom biomass, sediment stability and biogenic stabilization in the Severn Estuary. *J. Mar. Biol. Assoc. U. K.* 73, 871–887. doi: 10.1017/s0025315400034780

Underwood, G. J. C., and Kromkamp, J. (1999). Primary production by phytoplankton and microphytobenthos in estuaries. *Adv. Ecol. Res.* 29, 93–153. doi: 10.1016/s0065-2504(08)60192-0

Viegas, I., Araújo, P. M., Rocha, A. D., Villegas, A., Jones, J. G., Ramos, J. A., et al. (2017). Metabolic plasticity for subcutaneous fat accumulation in a long-distance migratory bird traced by 2H2O. *J. Exp. Biol.* 220, 1072–1078. doi: 10.1242/jeb.150490

Warnock, N. (2010). Stopping vs. staging: the difference between a hop and a jump. *J. Avian Biol.* 41, 621–626. doi: 10.1111/j.1600-048x.2010.05155.x

Warnock, N., and Bishop, M. A. (1998). Spring stopover ecology of migrant Western Sandpipers. *Condor* 100, 456–467. doi: 10.2307/1369711

Weber, J. M. (2009). The physiology of long-distance migration: extending the limits of endurance metabolism. *J. Exp. Biol.* 212, 593–597. doi: 10.1242/jeb.015024

Weber, T. P., Houston, A. I., and Ens, B. J. (1999). Consequences of habitat loss at migratory stopover sites: a theoretical investigation. *J. Avian Biol.* 30, 416–426.

Woelfel, J., Schoknecht, A., Schaub, I., Enke, N., Schumann, R., and Karsten, U. (2014). Growth and photosynthesis characteristics of three benthic diatoms from the brackish southern Baltic Sea in relation to varying environmental conditions. *Phycologia* 53, 639–651. doi: 10.2216/14-019.1

Yi, H. Y., Lu, Y., Zheng, J. W., Yang, W. D., and Liu, J. S. (2014). Biochemical and genetic engineering of diatoms for polyunsaturated fatty acid biosynthesis. *Mar. Drugs* 12, 153–166. doi: 10.3390/md12010153

Young, K. G. (2019). *Growth Characteristics and Lipid Metabolism of Cultured Migratory Bird Skeletal Muscle Cells*. London, ON: Western University.

Conflict of Interest: The authors declare that this study received funding from Vancouver Airport Fuel Facilities Corporation. The funder was not involved in the study design, collection, analysis, interpretation of data, the writing of this article or the decision to submit it for publication.

JH was employed by company Coastal & Ocean Resources.

The remaining authors declare that the research was conducted in the absence of any commercial or financial relationships that could be construed as a potential conflict of interest.

frontiers in Marine Science

ORIGINAL RESEARCH
published: 20 August 2020
doi: 10.3389/fmars.2020.00695

Effect of Nutrient Enrichment and Turbidity on Interactions Between Microphytobenthos and a Key Bivalve: Implications for Higher Trophic Levels

Julie A. Hope[1], Judi Hewitt[2,3], Conrad A. Pilditch[4], Candida Savage[5,6] and Simon F. Thrush[1]*

[1] Institute of Marine Science, University of Auckland, Auckland, New Zealand, [2] National Institute of Water and Atmospheric Research, Hamilton, New Zealand, [3] Department of Statistics, University of Auckland, Auckland, New Zealand, [4] School of Science, University of Waikato, Hamilton, New Zealand, [5] Department of Marine Science, University of Otago, Dunedin, New Zealand, [6] Department of Biological Sciences, University of Cape Town, Rondebosch, South Africa

OPEN ACCESS

Edited by:
João Serôdio, University of Aveiro, Portugal

Reviewed by:
Francis Orvain, UMR7208 Biologie des Organismes et Écosystèmes Aquatiques (BOREA), France
David M. Paterson, University of St Andrews, United Kingdom

***Correspondence:**
Julie A. Hope
j.a.hope@hull.ac.uk;
julie.anne.hope@gmail.com

Specialty section:
This article was submitted to Marine Ecosystem Ecology, a section of the journal Frontiers in Marine Science

Received: *25 November 2019*
Accepted: *31 July 2020*
Published: *20 August 2020*

Citation:
Hope JA, Hewitt J, Pilditch CA, Savage C and Thrush SF (2020) Effect of Nutrient Enrichment and Turbidity on Interactions Between Microphytobenthos and a Key Bivalve: Implications for Higher Trophic Levels. Front. Mar. Sci. 7:695. doi: 10.3389/fmars.2020.00695

Benthic diatoms are a high-quality food resource providing essential fatty acids to benthic grazers. Different stressors may alter the proportion of diatoms and other microalgae and thus can affect the quality as well as quantity of food available to benthic consumers. Microphytobenthos (MPB) lipid biomarkers were assessed in a field experiment to elucidate changes to the biosynthesis of fatty acids (FA) under nitrogen (N) enrichment (three levels) at eight intertidal sites that spanned a turbidity gradient. Influences on the flow of carbon and energy were determined using FA biomarkers of a functionally important deposit-feeding tellinid bivalve (*Macomona liliana*). Site-specific effects of N enrichment were detected in MPB quantity and quality measurements. Enrichment generally increased MPB biomass (chl a) across all sites, while the proportion of diatom associated fatty acid biomarkers was more variable at some sites. Analysis of sediment FA biomarkers and environmental variables suggested that changes to the microbial community composition and quality were related to water clarity and mud content of the bed. The ability of the MPB to utilize the increased nitrogen, as indicated by the resource use efficiency index, was also important. Despite the increase in MPB biomass, lipid reserves in the tissue of *M. liliana*, a primary consumer of MPB, were reduced (by up to 6 orders of magnitude) in medium and high N addition plots compared to control plots. Further, the nutritional quality of the bivalves to higher trophic levels [indicated by a lower ratio of essential FAs (ω3:ω6)] was reduced in high treatment plots compared to control plots suggesting the bivalves were adversely affected by nutrient enrichment but not due to a reduction in food availability. This study suggests anthropogenic nutrient enrichment and turbidity may indirectly alter the structure and function of the benthic food web, in terms of carbon flow and ecosystem

productivity. This may indirectly change the interactions between MPB and key bivalves as suspended sediment concentrations and nutrient enrichment continue to increase globally. This has implications for various ecosystem functions that are mediated by these interactions, such as nutrient cycling as well as primary and secondary production.

Keywords: fatty acid biomarkers, benthic microalgae, MPB, nutrient enrichment, turbidity, soft sediment ecology, food quality, trophic interactions

INTRODUCTION

Global population increases and land-use change are causing degradation of coastal and estuarine environments (Thrush et al., 2004; Foley et al., 2005). Primarily this degradation is due to the inputs of contaminants, nutrients and sediment from the catchment area that have drastic effects on sediment-dwelling organisms that are essential for ecological function (Thrush et al., 2004). In New Zealand, nearly 200 million tons of terrestrial soil are transported annually from land to sea (Hicks et al., 2011), with sediment deposition smothering, and altering the behavior of functionally important infauna (Cummings et al., 2003; Woodin et al., 2012; Townsend et al., 2014). This in turn can modify biogeochemical gradients and productivity in the sediment (Lohrer et al., 2006; Norkko et al., 2010). Increases in sedimentation are often associated with greater nutrient availability within estuarine systems and reductions in water clarity as turbidity increases (De Jonge et al., 2002; Lovelock et al., 2007). The shift in resource limitation (from nutrients to light) can degrade ecological networks and significantly affect ecosystem function as species interactions are modified (O'Meara et al., 2017).

Primary productivity is the source of energy in most marine food webs. Microphytobenthos (MPB) on the sediment surface can be stimulated by increased nutrient availability associated with the input of fine sediments, but simultaneously become light limited during immersion due to higher turbidity (Drylie et al., 2018). The reduction in light can significantly reduce MPB biomass or photosynthetic capacity (Kromkamp et al., 1995; Cahoon and Safi, 2002; Du et al., 2017), but MPB can also behaviorally and physiologically adapt to low light levels (Cartaxana et al., 2016). Photo-acclimation and migration allow MPB to efficiently adapt to low light conditions but this often results in decreased overall production, with concomitant effects on marine food webs (Consalvey et al., 2004; Migné et al., 2007; Jesus et al., 2009; Serôdio et al., 2012). In addition to the individual cell responses to light, the MPB community composition may be modified as low light or higher nutrient inputs select for different taxa (Gattuso et al., 2006; Hopes and Mock, 2015). For example, the biomass of primary producers may increase with nutrient inputs, but diversity can decrease in response to other limiting resources (Burson et al., 2018) or grazer diversity (Balvanera et al., 2006). MPB quality, and the biosynthesis and transfer of essential fatty acids (FAs) to consumers is rarely considered when assessing the impacts of anthropogenic stressors on soft sediment ecosystem function (Bachok et al., 2006; Bueno-pardo et al., 2018). Yet primary producer quality, indicated by FAs, can often be more important for primary consumers than food quantity (Guo et al., 2016). Light intensity and nutrient availability are considered to be two of the most important factors that determine algae quality and quantity in lakes and streams (Sterner et al., 1997), but the importance of this has rarely been considered in estuarine environments.

Intertidal MPB underpin multiple ecosystem functions and services (Hope et al., 2019). These photosynthetic organisms are the sole source for omega-3 and omega-6 essential fatty acids (EFA) to higher trophic levels and the synthesis of these essential nutrients can be affected by light and nutrient conditions (Hill et al., 2011). MPB are not only important for the flow of energy to higher organisms, but critical for elemental cycling and habitat formation (Sundbäck et al., 2006; Fricke et al., 2017). While bacteria are the main players in the biogeochemical cycling of nitrogen (Cook et al., 2004b), the MPB oxygenate the sediment surface and provide a labile carbon source for N-cycling bacteria, facilitating processes such as denitrification (Tobias et al., 2003; Cnudde et al., 2015). These effects interact through their associations with infauna and bacteria in the sediment (Thrush et al., 2006; Sundbäck et al., 2010). It is therefore important to understand how light and nutrient conditions alter the quantity and quality of MPB not only in their role as a food resource for higher organisms but also for the potential effects on multiple other ecosystem functions.

Several biochemical traits such as stable isotopes and fatty acid biomarkers can be used to determine the nutritional quality of primary producers and consumers (Galloway et al., 2012; Cnudde et al., 2015; Marzetz et al., 2017). In particular, several studies have demonstrated that the synthesis of fatty acid biomarkers can be influenced by changing light, temperature and nutrient conditions (Hill et al., 2011; Jónasdóttir et al., 2019). The resulting changes to the 'quality' of primary producers in terms of FA synthesis can be more important than primary producer quantity for regulating carbon transfer (Müller-Navarra et al., 2000; Marzetz et al., 2017). While some FAs are ubiquitous to all organisms, several taxonomic or functional groups of MPB can be characterized by the presence, ratios or associations between different FAs (Parrish et al., 2000). For example, FAs such as 16:1ω7 (Palmitoleic acid), eicosapentaenoic acid (EPA, 20:5ω3) and docosahexaenoic acid (DHA, 22:6ω3) (Brett and Müller-Navarra, 1997) are mainly produced by MPB such as diatoms, dinoflagellates and cyanobacteria (Volkman et al., 1998). Diatoms are known to be a highly nutritious, high quality, food resource that are rich in these essential fatty acids (EFAs), with specific FAs such as γ-linolenic acid (GLA, 18:3ω6) indicative of cyanobacteria (Yang et al., 2016). Changes to the quality (in terms of EFA synthesis or taxonomical groups) of this food resource will

in turn affect the nutritional quality of higher organisms which cannot efficiently synthesize EFAs *de novo* (Parrish et al., 2000; Bell et al., 2003). Omega-3 FAs (in particular EPA and DHA) are not only vital for the growth and development of herbivores but are critical for reproductive success in many bivalve species (Fearman et al., 2009) and several other physiological processes in organisms including humans (Knauer and Southgate, 1999; Emata et al., 2004; Institute of Medicine [IOM], 2011; Galloway and Winder, 2015; Sprague et al., 2016).

It has been demonstrated that eutrophication in lake systems can reduce the proportion of EPA and DHA transferred to higher organisms from primary producers (Strandberg et al., 2015; Taipale et al., 2016). Furthermore, it is known that cyanobacteria and chlorophytes often dominate the phytoplankton in eutrophic waters (Scheffer and Van Nes, 2007; Berthold et al., 2018) which contain different FA biomarkers. However, there is a lack of similar investigations in marine systems where the focus has been on lipid classes rather than specific FAs (Pinturier-Geiss et al., 2002). Changes to key EFAs and other FAs associated with nutritious diatoms can therefore be used as primary producer and consumer quality indicators (Antonio and Richoux, 2014), and may help to reveal the effects of various anthropogenic stressors such as eutrophication in marine systems. Elevated nitrogen levels can lead to eutrophication with nitrogen toxicity and hypoxia directly and indirectly affecting the growth, survival and reproduction of organisms such as bivalves (Hickey and Martin, 1999; Camargo and Alonso, 2006; Thrush et al., 2017). However, changes to the quantity and quality of their primary food resource, the MPB may also indirectly affect consumer health, influencing activity levels and reproductive success.

Our main objective was to assess the combined effect of light and nutrients on MPB quantity and their nutritional quality as a basal food resource for a functionally important deposit-feeding bivalve (*M. liliana*) within the natural environment. We manipulated sediment porewater nitrogen concentrations across eight estuarine sites in the North Island of New Zealand that encompassed a natural gradient of turbidity. We hypothesized that porewater nitrogen enrichment would alter both the quantity and quality of MPB and the transfer of energy and nutrients from MPB to the deposit-feeder. A secondary hypothesis was that the effects of elevated porewater nitrogen would be site-dependent due to the differences in turbidity across the sites.

MATERIALS AND METHODS

Experimental Design

To assess the effects of elevated porewater nitrogen, we conducted a field experiment across eight sites in four estuaries of the North Island of New Zealand that represent a natural turbidity gradient (**Figure 1** and **Supplementary Table S1**). Photosynthetically active radiation (PAR) sensors (Odyssey, Dataflow Systems Pty Ltd., Christchurch, New Zealand) were deployed 10 cm above sediment surface at each intertidal site for approximately 7 months prior to sampling to measure average daily high and low tide PAR (sensors were exposed during low tide). Daytime, mean high-tide (immersed) PAR ranged from < 150 μmol m^{-2} s^{-1} to > 900 μmol m^{-2} s^{-1} across the selected sites (**Figure 2A**). As a proxy for turbidity, we derived a percentage clarity measure based on the proportion of light detected from exposed PAR sensors (during daytime low tide) and the submerged sensor (during daytime high tide), as a relative clarity index (**Figure 2B**). A clarity value near 100% indicates high water clarity/low turbidity (as clear water allows more of the incident light to the bed during immersion) and a value closer to 0% indicates low water clarity/high turbidity.

At each site, three replicate 9 m^2 plots were randomly allocated to one of three nitrogen treatments; high fertilizer addition (600 g N m^{-2}), medium fertilizer addition (150 g N m^{-2}), or a disturbance control (0 g N m^{-2}). Previous N enrichment experiments have successfully simulated eutrophic estuarine sediments using the above concentrations and application method (see below, Douglas et al., 2016). As nitrogen is typically the limiting nutrient in these systems (Rodil et al., 2011) a slow release nitrogen only fertilizer (Nutricote® N fertilizer [140 days, 40-0-0 N:P:K]) was added to 180 evenly distributed holes (20 holes m^{-2}) within each 9 m^2 plot to 15 cm depth using a 3 cm diameter hand-held corer. Douglas et al. (2016) have demonstrated that burial at this depth successfully elevates nitrogen in surface sediments (top 0–2 cm). Nutricote® quickly hydrolyzes to ammonium (NH_4^+) from urea (Lomstein et al., 1989). Ammonium (NH_4^+) is the most common form of nitrogen in New Zealand soft sediments (Tay et al., 2013) and the form of N most readily assimilated by microalgae (Underwood and Kromkamp, 1999; Risgaard-Petersen et al., 2004; Riekenberg et al., 2017). Control plots at each site ($n = 3$) were cored and the sediment then replaced without the addition of fertilizer to replicate the physical disturbance associated with the fertilizer additions in other treatments. All treatments were randomly distributed within the area.

Rationale for Species and Indicators Used in the Study

Macomona liliana is a facultative deposit-feeding tellinid that plays a key role in multiple ecosystem functions on New Zealand intertidal sandflats. Their activities can alter rates of organic matter degradation and nutrient cycling (Thrush et al., 2006; Volkenborn et al., 2012; Woodin et al., 2012). These roles are a result of their complex feedbacks with the MPB which they graze upon and stimulate through nutrient regeneration, and facilitation of biogeochemical cycling through their sediment reworking. *M. liliana* were used as a model benthic primary consumer while intertidal sediment surface (0–2 cm) samples were used to characterize MPB quality and quantity. While *M. liliana* are capable of suspension feeding, their primary feeding mode is deposit-feeding (Pridmore et al., 1991) and strong but complex relationships with the MPB have been demonstrated (Thrush et al., 2004). Furthermore, previous investigations have demonstrated that resuspended MPB are the primary food resource in NZ estuaries for both deposit and suspension feeders (Savage et al., 2012; Jones et al., 2017). As FAs are a primary component of lipids and play a

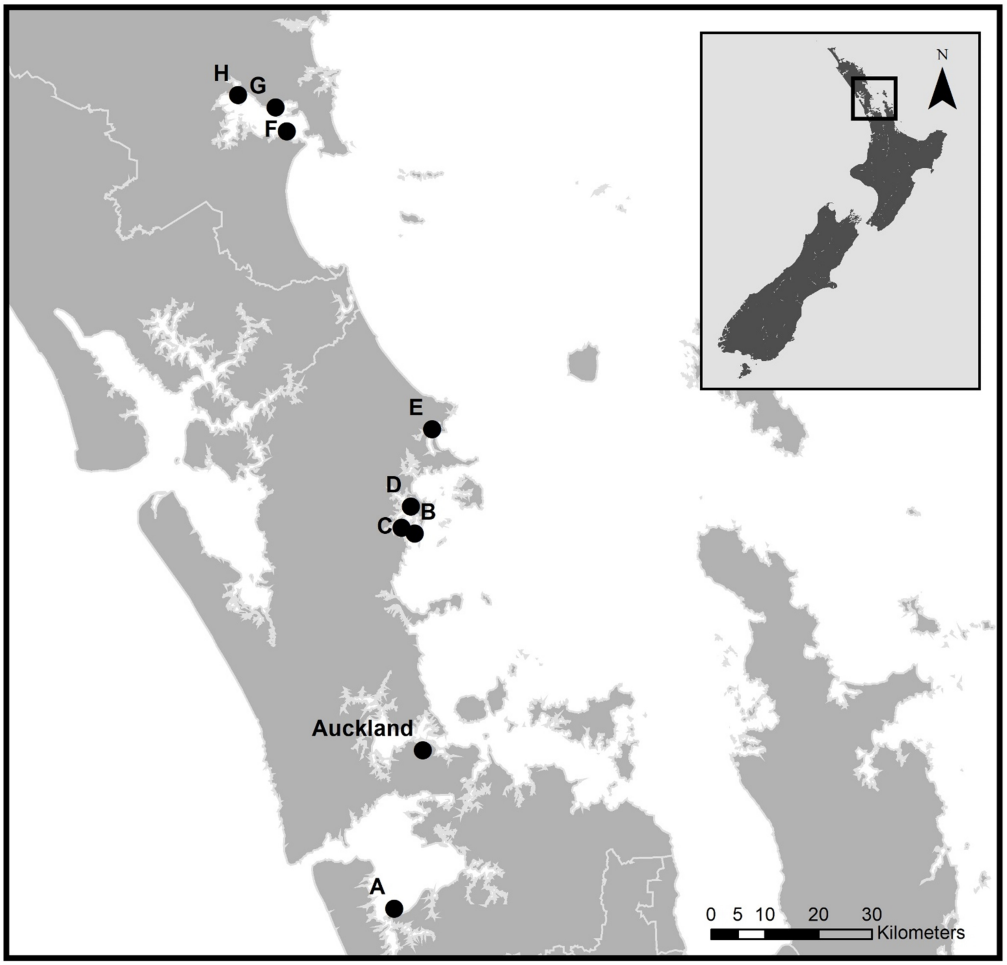

FIGURE 1 | Location of the eight field sites across the North Island of New Zealand (inset) and their proximity to Auckland City. **(A)** Manakau Harbor (MK); **(B)**, **(C)** and **(D)** Mahurangi Harbor sites 1-3 respectively (MH1, MH2, MH3); **(E)** Whangateau Harbor (WG); **(F)**, **(G)** and **(H)** Whangarei Harbor sites 1-3 respectively (WR1, WR2, WR3). GPS co-ordinates are provided in **Supplementary Table 1**.

fundamental role as an energy and nutrient source to higher organisms, FA biomarkers and other biochemical traits (lipid content, MPB biomass) were employed to determine MPB quantity and quality, MPB community responses and dietary intake in *M. liliana.*

As individual fatty acid biomarkers provide limited information, key ratios indicative of MPB community composition, were selected for examination (**Table 1**). These included: the diatom index of the MPB assemblage to determine the relative dominance of diatoms over dinoflagellates (Antonio and Richoux, 2014); and the proportion of bacterial FAs (BaFA) which can indicate the proportion of aerobic and anaerobic bacteria and degree of decomposition (Jaschinski et al., 2008; Ruano et al., 2012). These indices were also used to determine the relative ingestion or retention of essential FAs in bivalves or the ingestion of carbon that has first been processed through the microbial loop. Other FA biomarkers such as the ratio of ω3:ω6 PUFAs, and the proportion of EPA + DHA, were also examined as useful indicators of the nutritional quality of the primary producers, or 'health' of the bivalves (Vargas et al., 1998; Ruano et al., 2012).

Sample Collection and Processing

Sampling was conducted between October and November 2017, approx. 7 months after the initial nitrogen enrichment of the plots. During mid-morning low tides, four sediment cores (0–1 cm depth, 2.6 cm dia.) were randomly collected and pooled for biochemical analyses from each plot (giving 3 replicates per nutrient treatment, per site). An additional 5 cores were sampled and pooled from each replicate plot to determine particle size distribution and porosity (0–2 cm depth, 2.6 cm dia.) and 4 cores were pooled from each replicate plot for porewater nutrient analysis (0-2 cm depth, 2.6 dia.); again providing 3 replicates per nutrient treatment per site. The pooled sediment cores from within each replicate plot were used to ensure adequate sediment for subsequent analyses, and to account for the spatial variability across the 9 m^2 plots in biochemical properties, such as microphytobenthic (MPB) biomass.

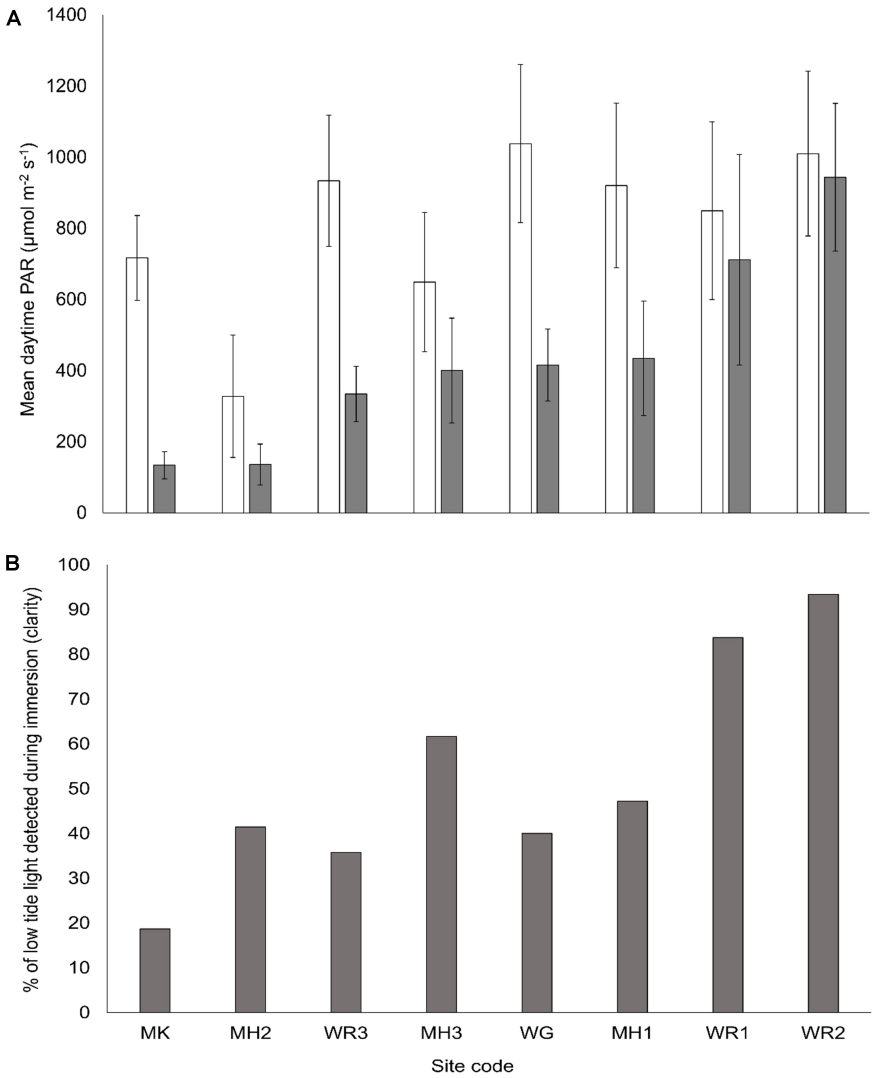

FIGURE 2 | (A) Mean daily photosynthetically active radiation (PAR, ± SE) measured 10 cm above the sediment surface for daytime low tide (white bars) and high tide (gray bars) for the 7 months period between the experiment setup and sampling. Daytime averaged from 2 h after sunrise to 2 h before sunset on days when low tides corresponded with daylight hours. **(B)** Relative clarity at each site over the 7 month period. Values close to 100% indicate the majority of incident light (emerged sensors) is detected by the submerged sensor (during immersion periods). Values close to zero mean very little incident light is reaching the submerged sensor.

Sediment samples for biochemical analysis (see below) were foil wrapped, immediately flash frozen in liquid nitrogen and transported to a −80°C freezer until processed to preserve FA biomarkers and chlorophyll content. Porewater samples were stored on ice in the dark until extracted in the laboratory. Duplicate 13 cm dia. cores were collected to a depth of 15 cm for the gathering of adult *M. liliana* specimens (> 20 mm shell length) from within each plot. Specimens were rinsed of sediment, foil wrapped and flash frozen in the field to be transferred to a −80°C freezer until further analysis. *M. liliana* were collected from all sites with the exception of MH2 and WR1, where specimens could not be detected in plots across all three nutrient treatments. These sites were excluded from further FA analysis of *M. liliana* tissue. Particle size distribution (PSD) was determined from freeze-dried sediments using a Malvern Mastersizer 2000 (range 0.05–2000 μm) (Singer et al., 1988) after the removal of organic matter with 10% hydrogen peroxide solution and disaggregation using 6% calgon.

Biochemical Properties

Total *M. liliana* biomass (incl. shell) was measured from the cores in each plot and biomass standardized to kg *M. liliana* m^{-2}. Whole organisms ($n > 3$) were freeze dried and homogenized to determine the animals' lipid reserves (conditional status) and fatty acid biomarkers. Sediment OM content was determined by loss on ignition of dried sediments at 450°C for 4 h, following Parker (1983). Porewater was extracted by adding 4 mL of deionized water to sediments, centrifuging at 3500 RPM for 10 min and filtering the extract through Whatman GF/C (1.1 μm) filters (Lohrer et al., 2010). Thawed extracts

TABLE 1 | Fatty acid (FA) biomarkers and indices used to indicate the presence of various Microphytobenthos (MPB) taxa in surface sediments and bivalve tissue.

FA contribution/ratio	Indicative of	References
Sediment analysis		
20:5ω3, 16:1ω7/16:0	Proportion of diatoms in the MPB	Dalsgaard et al., 2003
22:6ω3/20:5ω3 (DHA/EPA)	Relative dominance of dinoflagellates over diatoms	Parrish et al., 2000
C15:0 + C17:0	Proportion of aerobic and anaerobic bacteria in the sediment	Jaschinski et al., 2008; Ruano et al., 2012
(16:1ω7 + 20:5ω3)/ (18:1ω9 + 18:4ω3 + 22:6ω3)	Relative dominance of diatoms over dinoflagellates and other taxa	Antonio and Richoux, 2014
ω3:ω6 PUFA ratio	Indicator of MPB nutritional quality	Jaschinski et al., 2008; Ruano et al., 2012
Bivalve analysis		
22:6ω3/20:5ω3 (DHA/EPA)	Change in dietary intake of primary producers	Parrish et al., 2000
C15:0 + C17:0	Dietary intake of aerobic and anaerobic bacteria or carbon processed via the microbial loop	Jaschinski et al., 2008; Ruano et al., 2012
(16:1ω7 + 20:5ω3)/ (18:1ω9 + 18:4ω3 + 22:6ω3)	Diatom index – dominance of diatoms in the diet of consumers	Antonio and Richoux, 2014
ω3:ω6 PUFA ratio	Indicator of nutritional quality in bivalve consumers	Jaschinski et al., 2008; Ruano et al., 2012

Indicators of MPB and bivalve nutritional quality are centered around the importance of omega-3 fatty acids (ω3).

were analyzed for ammonium (NH_4^+), using standard methods for seawater analysis on a Lachat QuickChem 8500 + FIA (Zellweger Analytics Inc., Milwaukee, WI, United States) with concentrations corrected for sediment porosity and dilutions. Porewater concentrations were used to determine the effectiveness of nitrogen enrichment of the plots across the sites. Further, to assess the effects of N enrichment across the turbidity gradient the ratio between each sites high-tide light level (PAR) and the mean porewater NH_4^+ (light: NH_4^+) of treatment plots were calculated. This ratio has previously been used to assess the changes in microalgae fatty acid synthesis due to shifts in the ratio of available light and nutrients (Hill et al., 2011).

Chlorophyll a (chl a) and pheophytin (pheo) contents were determined from surficial sediments using a 90% acetone extraction to quantify MPB biomass and degradation products respectively (Lorenzen, 1967). Pigments were extracted in the dark for 24 h at 4°C using homogenized, freeze-dried sediment (∼1 g). Acetone was selected as it is best suited for spectrophotometric assay (Ritchie, 2006). Changes in resource use efficiency (RUE) was calculated as the ratio between sediment chlorophyll a concentrations and porewater concentration of the limiting nutrient; nitrogen in these systems. RUE is an ecological measure that defines the proportion of supplied resources that is then converted into new biomass (Hodapp et al., 2019). It is a useful metric to illustrate the change in resource use efficiency as higher concentrations of key nutrients become available to the MPB (Eriksson et al., 2017). An increase in RUE indicates that the MPB are efficiently assimilating the identified nutrient (nitrogen in this case) and converting it to biomass. Aliquots of tissue from freeze-dried bivalves and sediments were used to assess total lipids using a modified Bligh and Dyer (1959) and lipid content determined using the sulfo-phospho-vanillin (SPV) spectrophotometric method (Byreddy et al., 2016). Total fatty acid (TFA) composition was determined following a one-step direct transesterification method (Lepage and Roy, 1986; Zárate et al., 2016). The full details of the extraction and identification of FAs is provided in the **Supplementary Material**. All biochemical properties discussed in this section were standardized by either sediment/tissue weight or by the surface area of the sediment core as deemed appropriate (Tolhurst et al., 2005).

Identified FAs were first expressed as a percentage of the total FAs (TFAs) identified in each sample (% TFA) or as a ratio between two FAs if a dominance indicator was used. All FAs are designated as X:YωZ, where X is the number of carbon atoms, Y is the number of double bonds and Z is the position of the ultimate double bond from the terminal methyl. Full details are available in the **Supplementary Methods**. Specifically, eicosapentaenoic acid (EPA, 20:5ω3) and docosahexaenoic acid (DHA, 22:6ω3) which are vital for the growth and development of mollusks, fish and humans (Knauer and Southgate, 1999; Emata et al., 2004; Institute of Medicine [IOM], 2011; Sprague et al., 2016) were analyzed.

Data Analyses

Changes in MPB biomass and key FA biomarkers were tested across the different nutrient treatments (control, medium, high). To test the effects of nutrient enrichment and site on biochemical properties and FA biomarkers of the sediment and bivalves (**Table 2**), separate two-way PERMANOVAs based on Euclidean distance matrices (PRIMER, V7, Anderson et al., 2008) were run using a fixed factor nutrient (3 levels), a random factor of site (8 levels) and an interaction term. A total of 9999 permutations were applied to residuals under a reduced model. Monte Carlo *p*-values were also considered for the significance of differences among factors. Pairwise comparisons were performed using a *post hoc* test with the Bonferroni correction.

To summarize relationships between MPB quality indicators and sediment properties (**Table 2**) we used canonical analysis of principal components (CAP, Anderson et al., 2008), based on the Euclidean distance matrix of MPB quality indicators. Similarly, relationships between *M. liliana* biomarkers and biochemical traits (listed in **Table 2**), environmental and MPB/sediment indicators were summarized by CAP analysis based on the Euclidean distance matrix of *M. liliana* FA biomarkers. CAP was used rather than distance-based redundancy analysis (dbRDA) as the feedbacks between the different variables precludes the definition of any clear explanatory and response variables. All data used in the CAP analyses were normalized using a fourth-root transformation. The number of PCO axes (*m*) was chosen to exclude redundant axes, but include as much of the original variability in the dataset while minimizing the leave one out residual sum of squares (Anderson et al., 2008).

TABLE 2 | Biochemical properties and FA biomarkers used for univariate and multivariate analyses.

	Variables	Sediment analysis	Bivalve analysis
Quality indicator variables	% EPA (20:5ω3)	X	
	% DHA (22:6ω3)	X	
	Diatom index (Antonio and Richoux, 2014)	X	X
	Ratio of ω3:ω6 PUFA	X	X
	MPB biomass (Chl a)	X	
	BaFAs (C15:0 + C17:0)	X	X
	Bivalve Biomass		X
Environmental properties	Ratio of Light:NH_4^+	X	X
	PW NH_4^+ concentration	X	
	Mean grain size		X
	% Mud	X	
Sediment properties	RUE of MPB	X	
	Sediment diatom index		X
	Sediment BaFAs (C15:0 + C17:0)		X

Quality indicators marked with an X were used in multivariate analyses. Environmental properties were assessed against these matrices for both sediment and bivalve data. Additional indicators from the sediment were explored against the bivalve data to assess whether changes in the quality and quantity of MPB in the sediment were reflected in changes to the quality indicators of the bivalves. Diatom index under quality indicators is the diatom index of bivalves.

RESULTS

Sediment Nutrients and Grain Size

The relative clarity of overlying water varied from 19% in the Manukau Harbor (MK, low clarity and high turbidity) to 93% at Whangarei 2 (WR2, high clarity and low turbidity, **Figure 2B**). The addition of fertilizer to the sediment resulted in elevated surface porewater NH_4^+ concentrations (0–2 cm sediment depth) across all sites. Enrichment was proportional to the amount of fertilizer added, in that the final elevated porewater NH_4^+ concentrations varied between sites (**Figure 3A**), but higher N additions elevated the final concentrations of medium and high plots compared to controls (C < M < H plots, Pseudo-F = 9.0, $P < 0.001$). Mean grain size ranged from very fine to medium sand (63–500 μm; Wentworth, 1922), and all sites had a mean mud content < 10% (**Figure 3B**). Neither mean grain size nor mud content, varied significantly with the nutrient enrichment of the sediment, but site differences were detected for both factors (Pseudo-F = 25.7, $P < 0.001$, Pseudo-F = 20.7, $P < 0.001$ respectively, **Table 3**).

Changes to Microbial Communities

Nitrogen enrichment and site differences in turbidity influenced various microbial indicators in the sediment (**Table 3**). Nitrogen enrichment typically increased MPB biomass (chl a) but effects were site-specific (**Figure 4A**). At a number of sites, [MH1, MH2, WR1, WR2], high variability in the MPB biomass prohibited the detection of significant increases between control plots and medium or high N addition plots, while at two of the sites [MH1, WR1], MPB biomass was elevated in medium treatment but not in high treatment plots (**Figure 4A**). Several sites also exhibited a higher sediment diatom index [MK, WR3, MH3, MH1 and control-medium treatments at WR1], while the other sites displayed no differences between N treatments (**Figure 4B**). Interestingly, the proportion of diatoms in the MPB (diatom index) of control sediments across the sites exhibited no significant relationship with water clarity ($P < 0.05$). The EPA content of the sediment (characteristic FA biomarker for diatoms), increased with nitrogen treatment but there were no significant site differences detected (**Table 3**). The MPB were not effectively utilizing the higher N concentrations available in the porewater in enrichment plots as indicated by the reduced resource use efficiency (RUE, **Figure 5**). The proportion of aerobic and anaerobic bacteria-associated FAs (BaFAs) in the sediment varied primarily across the sites and not specifically with elevated nitrogen.

We further examined Pearson correlation coefficients between the turbidity proxy (% clarity) and measured variables for each nutrient treatment independently. With the exclusion of the Manukau (MK) site, MPB biomass of control plots was higher at sites with greater water clarity ($r^2 = 0.73$, **Figure 6**). The relationship between MPB biomass and clarity essentially disappeared with N enrichment ($r^2 = 0.08$ and 0.07 for medium and high N treatments respectively). Similarly, while BaFAs in control plots correlated significantly with water clarity (**Figure 7**, $r^2 = 0.67$), the relationships in medium ($r^2 = 0.05$) and high ($r^2 = 0.05$) nitrogen treated plots were diminished.

Changes to the Bivalve *M. liliana*

The biomass (**Figure 8**) and total lipid content (**Figure 9A**) of *M. liliana* was reduced with nitrogen enrichment at the majority of sites, with a significant interaction between site and N enrichment detected (**Table 3**). While most sites had significant reductions in both metrics, no effect of nitrogen enrichment was apparent for biomass at MK (**Figure 8**) or lipids at WG (**Figure 9A**). Coinciding with a decrease in the overall biomass of bivalves in N enriched plots and a depletion in lipid reserves of the bivalves that were collected in the plots, there was a significant decrease in the nutritional quality of the bivalves (ratio of ω3:ω6 fatty acids (**Figure 9B**) across the majority of sites with nitrogen additions (**Table 3**). The effects of elevated nitrogen on the diatom index and the EPA + DHA content of *M. liliana* tissue was also site dependent. At Manukau (MK) and Whangarei site 3 (WR3) the proportion of diatoms and intake of EPA + DHA in the diet of *M. liliana* were significantly reduced under elevated nitrogen levels (**Figures 9C,D**) whereas at Whangateau Harbor (WG), the intake of diatoms (diatom index), bivalve quality (ω3:ω6 ratio and the EPA + DHA content) all increased (**Figures 9B–D**).

Relationships Between *M. liliana*, MPB and Environmental Variables

Overall the CAP trace statistic (tr = 0.68, $P < 0.001$) together with the ordination plot suggests that the matrix of MPB quantity (biomass) and quality (FA biomarkers) in the sediment were strongly related to several measured sediment and environmental

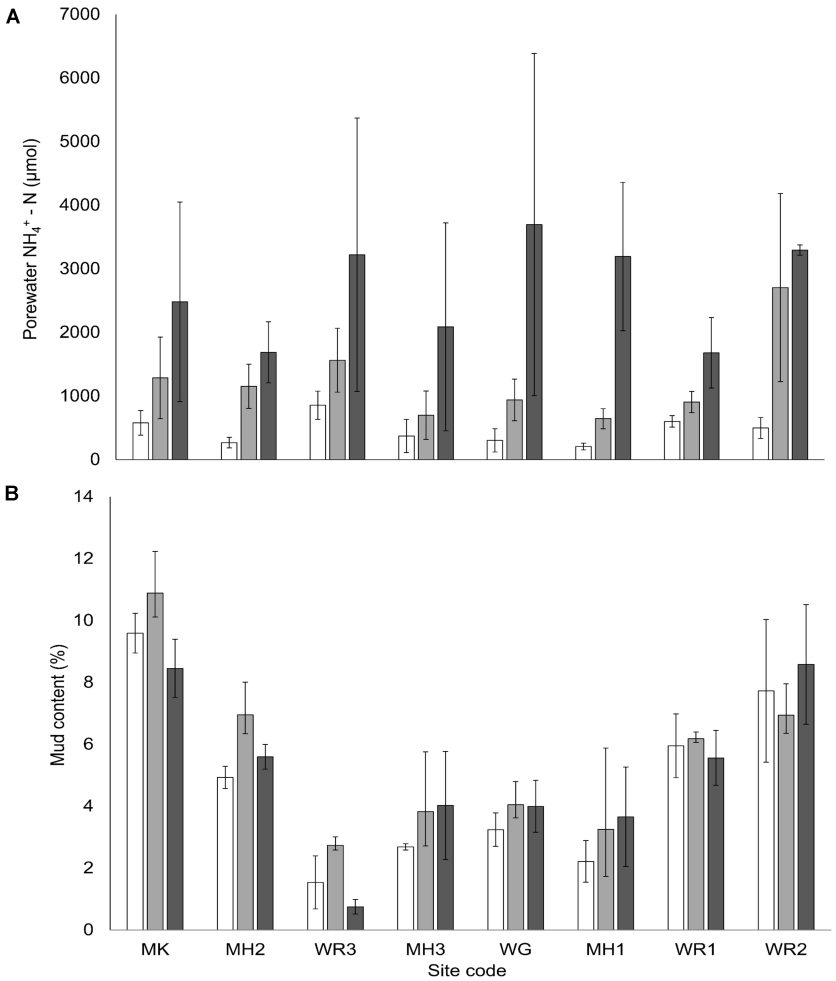

FIGURE 3 | (A) Mean porewater NH_4^+-N concentration (µM, ± SE, n = 3) of surface sediment (0–2 cm depth) for each treatment at each site. **(B)** Mean mud content (%, ± SE, n = 3) for each treatment at each site, and nutrient treatment. Nutrient addition treatments; white bars – control plots (0 g N m^{-2} addition), light gray – medium plots (150 g N m^{-2} addition and dark gray – high plots (600 g N m^{-2} addition).

properties (**Figure 10**). Diagnostics revealed the first three axes encapsulated around 96% of the variability in the resemblance matrix and minimized the residual sum of squares. The variables most strongly related to CAP1 were the sediment mud content (r^2 = 0.47), the resource use efficiency (RUE) of the MPB (r^2 = 0.25) and the percent clarity (r^2 = -0.17). The second axis (CAP2) was related to porewater NH_4^+ concentration (r^2 = 0.36) and the ratio between light and nutrient availability (Light: NH_4^+, r = 0.20). The third axis contributed even less (CAP3, δ^2 = 0.11) and was primarily related to the Light: NH_4^+ ratio and RUE of the MPB (r^2 = 0.15 for both).

Interestingly, the CAP ordination of *M. liliana* tissue data displayed contrasting results (**Figure 11**, tr = 0.76, $P < 0.01$). Instead of being dominated by one axis, the first two axes were of similar importance (δ^2 = 0.32 and 0.30, respectively), with the third axis contributing markedly less (δ^2 = 0.09). The environmental and MPB variables associated with the first axis (CAP1) were the mean grain size of the bed ($r^2 = -0.45$), however the 2nd axis (CAP2) was associated with the ratio between the light availability and porewater nitrogen (Light:NH_4^+ ratio, $r^2 = -0.35$) and the proportion of diatoms (r^2 = 0.38) and bacterial-associated FAs ($r^2 = -0.22$) as well as the clarity of the water column ($r^2 = -0.14$, **Figure 11**).

DISCUSSION

This study demonstrates that elevated porewater nitrogen affects the proportion of diatom- and bacteria-specific fatty acid biomarkers available in the sediment to primary deposit feeding consumers. Changes to FA biomarkers and MPB biomass were different across the sites, and a number of variables were related to the overlying water clarity. Our data suggest that the proportion of bacterial FA biomarkers was higher when water column turbidity was lower. Further, the positive correlation between MPB biomass and water clarity under ambient nitrogen conditions (controls) suggests reduced light availability in turbid estuaries may limit MPB growth. The exception to this was

TABLE 3 | Results of univariate Permanova tests for differences in sediment and biochemical properties using nitrogen enrichment (N) (fixed) and site (S) (random) as predictors.

Compartment	Parameter	Factor	Pseudo-F	p (perm)
Sediment	Mud content	S	25.7	< 0.001
	Mean grain size	S	20.7	< 0.001
	BaFAs (C15:0 + C17:0)	S	5.4	< 0.001
	MPB biomass (chl a)	N x S	2.5	< 0.01
	Diatom index (sed)	N x S	2.1	< 0.05
	%EPA	N	3.2	< 0.05
M.liliana tissue	Bivalve biomass	N x S	2.0	< 0.05
	Lipid content	N x S	2.5	< 0.05
	Ratio of ω3:ω6	N x S	3.0	< 0.01
	Diatom index (biv)	N x S	2.4	< 0.05

Significant ($P < 0.05$) main effects or interactions are displayed with Pseudo-F (number) and significance levels.

of course the high biomass MPB detected at the Manukau harbor (MK) despite high turbidity. Low light and high nutrient availability has been evident at the MK site for a number of years (Cahoon and Safi, 2002) and as such the MPB present may be photoacclimated to lower light (Veach and Griffiths, 2018). Previous studies have demonstrated that productivity during low tide can compensate for the lack of productivity during immersion in highly turbid sites similar to the Manukau (Drylie et al., 2018). It has previously been highlighted that there is a need for multiple stressor studies that incorporate a wide range of habitat conditions and species interactions (Crain et al., 2008). Our context-dependent results emphasize the complexity of these interactions and the fundamental need for large-scale field studies to encapsulate a wide range of ecological effects.

Our findings, suggest that effects of increased nitrogen loading on the functional role of MPB may depend on the environmental context (background nutrient levels and sediment type). Context dependency and legacy effects in ecological field studies are well documented, but can provide a wealth of information that cannot be provided by laboratory investigations (Thrush et al., 2000; Norkko et al., 2006). In these predominantly non-cohesive, low nutrient soft-sediments, the addition of nitrogen may have increased the quantity and quality of the MPB but their functional role in the system and trophic interactions were altered as the increase in essential FAs associated with diatoms were not reflected in the consumers The quality and quantity of MPB both increased with nitrogen enrichment but the magnitude of the effects were again site dependent. The correlations between MPB biomass and water clarity observed in control plots disappeared with N enrichment of the sediment suggesting the increase in nitrogen availability in the sediment facilitated the growth of the MPB by providing them with the nutrients required during low tide periods. Primary producers of course require both light and nutrients for growth and to reproduce (Kromkamp et al., 1995). Carbon is obtained through photosynthesis which relies on light availability, while key nutrients such as nitrogen and phosphorus are obtained from their environment (Longphuirt et al., 2009). The positive response of the MPB biomass to nitrogen additions suggests that the MPB growth across the sites before experimental enrichment was nitrogen limited (Underwood and Kromkamp, 1999). Non-cohesive sediments, associated with greater hydrodynamic energy, often have lower MPB biomass and nutrient capacity than muddy sediments (Cook et al., 2004a; Eyre et al., 2011). Remineralization and tight coupling of the nutrients within sandy sediments can however provide sufficient nutrients to sustain the MPB community and benthic metabolism (Cook et al., 2004a; Sundback and Mcglathery, 2005). Nonetheless, these differences in the sedimentary environment influence the rate and pathway of OM degradation (Ferguson et al., 2004). While an increase in RUE would suggest that the MPB are effectively using the additional nitrogen added to the system, a reduction (which we observed) suggests that N is now in excess following porewater enrichment and the MPB demand is no longer able to keep up with the supply of this nutrient from the porewater.

As inputs of nitrogen and sediment from catchments to coastal and estuarine environments continues to increase (Howarth, 2008; Hicks et al., 2011), these two stressors synergistically interact to affect the quality and quantity of primary food resources and their consumers. Elevated sediments enhance turbidity and limit light availability to the MPB and decrease their ability to assimilate nutrients at the sediment-water interface (Underwood and Kromkamp, 1999; Pratt et al., 2014), as we have seen in the RUE above. This causes an increase in the release of nutrients to the water column that further stimulate the phytoplankton enhancing turbidity effects. While we have examined the effects of N enrichment across a natural turbidity gradient that is attributed more to suspended sediment concentrations rather than phytoplankton blooms, our data suggest that as nutrient concentrations increase there may be a breakdown in the relationship between key consumers such as *M. liliana* and MPB across the light gradient. Understanding and predicting the effects of multiple stressors in the field is difficult, but critical to improving our understanding of anthropogenic effects in the real world (Crain et al., 2008; Thrush et al., 2012). Our study provides real-world information on the complexity associated with trophic interactions across a range of different sedimentary habitats. Furthermore, we provide further evidence of the potential impacts of eutrophication in understudied, low nutrient systems on carbon flow from primary producers to consumers. We stress that this is not only dependent on the adaptation of the MPB to particular stressors but will be influenced by feedbacks associated with differences in the response of higher trophic levels to the same perturbations (Thrush et al., 2006; Crain et al., 2008).

At two sites (MH2 and WR1), *M. liliana* were absent in nitrogen enriched plots. At sites where we did obtain *M. liliana* specimens, these bivalves from enriched plots had decreased lipid energy reserves. Plausible explanations for the reduced lipids energy reserves and lower nutritional quality of the bivalves include the accumulation of ammonium in the sediment becoming a chemical stressor to biota (Camargo and Alonso, 2006; Simpson et al., 2013). In other bivalves this type of stress response, the reductions in lipid content, has been related to oxidative stress and lipid peroxidation (Coutteau et al., 1996; De Almeida et al., 2007).

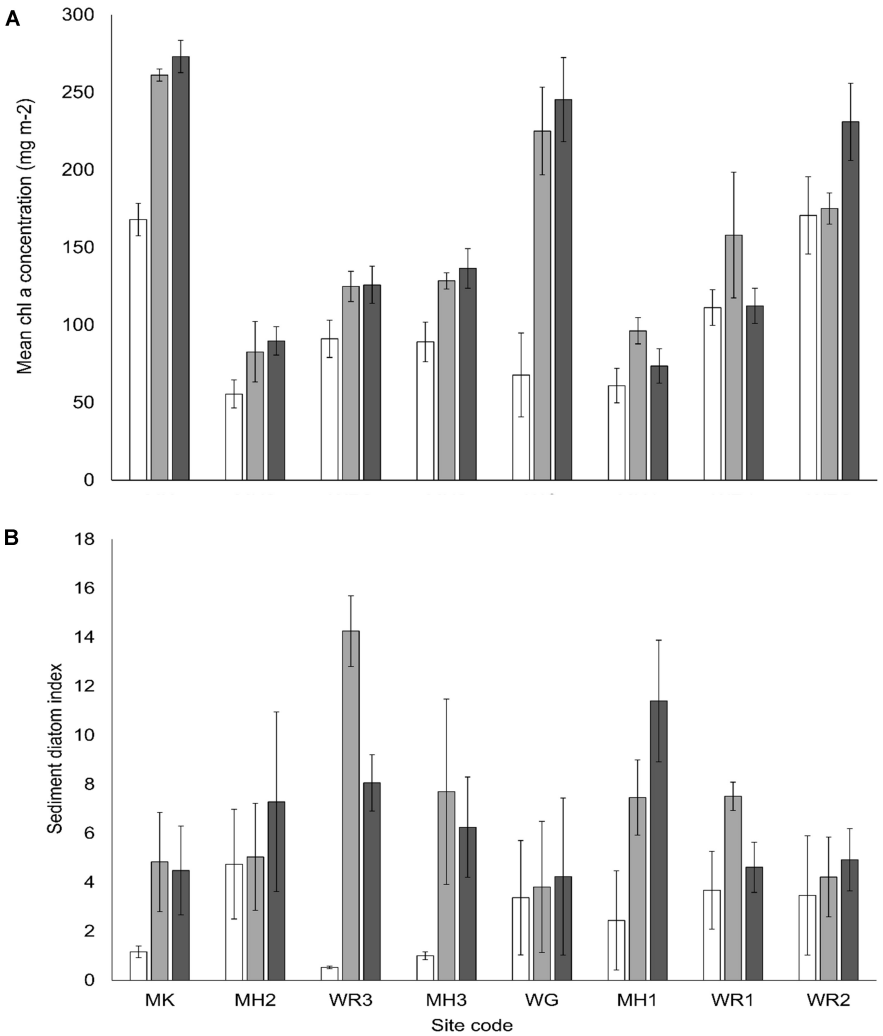

FIGURE 4 | (A) Mean chlorophyll a concentration and **(B)** mean diatom index of the sediment surface, across all sites and nutrient treatments (± SE, $n = 3$). Nutrient treatments; white bars – control plots (0 g N m^{-2} addition), light gray – medium plots (150 g N m^{-2} addition), dark gray – high plots (600 g N m^{-2} addition).

The diatom-associated FA biomarkers and overall lipid energy reserves of *M. liliana* were reduced by N enrichment suggesting that grazing on the MPB was diminished in our experimental plots. These changes are consistent with changes in dietary intake, as more diatom rich FAs were available in the sediment (Bell et al., 2003). This reduction in FA intake was not observed in *M. liliana* inhabiting Whangateau estuary. Here, *M. liliana* appeared to benefit and increase their uptake of nitrogen-stimulated MPB (diatom associated FAs). This is likely due to the relatively shallow, ebb-dominated nature of the estuary (Grace, 1972) and the associated advection of excess organic matter offshore (Middelburg and Herman, 2007). The tight recycling of nutrients in the bed allowed this low-turbidity system to remain productive and healthy. The depletion of lipid reserves can also result in a shift between different biomarkers, as specific FAs are differentially metabolized (Budge et al., 2001; Dridi et al., 2017). Despite the preservation of the DHA/EPA ratio, the ω3:ω6 PUFA ratios of bivalves were generally reduced in enriched plots. This suggests that bivalve nutritional quality was compromised (Jaschinski et al., 2008; Ruano et al., 2012). The higher proportion of bacterial FAs in *M. liliana* tissue suggests *M. liliana* ingested more bacteria or organic matter that had been processed via the microbial loop (Mayzaud et al., 1990; Gonçalves et al., 2017). The higher proportion of diatoms in the sediment and the shift in bivalve quality suggests the changes to the MPB community stimulated bacterial communities, which in turn lowered the quality of the bivalves. The shift in ω3:ω6 PUFA ratios is significant, as the transfer of ω3 PUFA, in particular EPA and DHA, is essential for the growth and reproduction in higher trophic levels and supports the provision of food and goods (fish, shellfish and Omega-3) from our coastal marine ecosystems (Kharlamenko et al., 2008; Twining et al., 2016).

Changes in the quality and quantity of food resources to secondary consumers has implications for trophic food webs, as intertidal bivalves are the major prey of many crustaceans, fish, and wading birds. As the condition of these bivalves

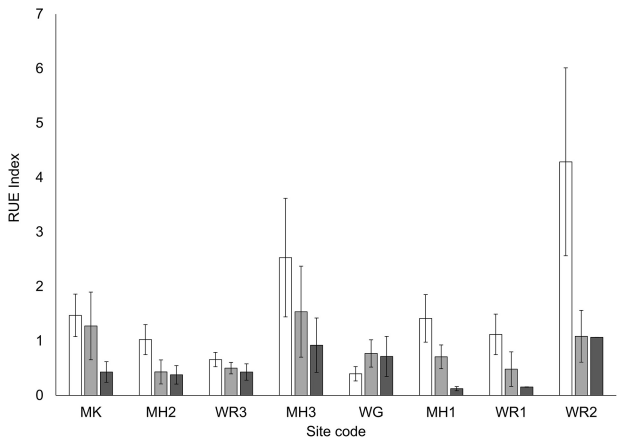

FIGURE 5 | Mean resource use efficiency (RUE), i.e., the ratio between chlorophyll a concentration and the sediment porewater concentration of the limiting nutrient [N in these systems (RUE calculations based on Eriksson et al., 2017)]. Nutrient treatments; white bars – control plots (0 g N m^{-2} addition), light gray – medium plots (150 g N m^{-2} addition), dark gray – high plots (600 g N m^{-2} addition).

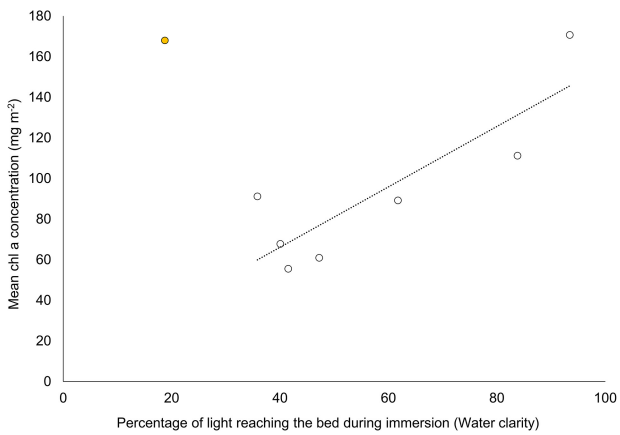

FIGURE 6 | Relationship between MPB biomass (chl a concentration, mg m^{-2}, ± SE, n = 3) and water clarity, see **Figure 2B** (r^2 = 0.73). Inclusion of site MK (shaded circle) reduced the explained variation (r^2) from 0.73 to 0.07.

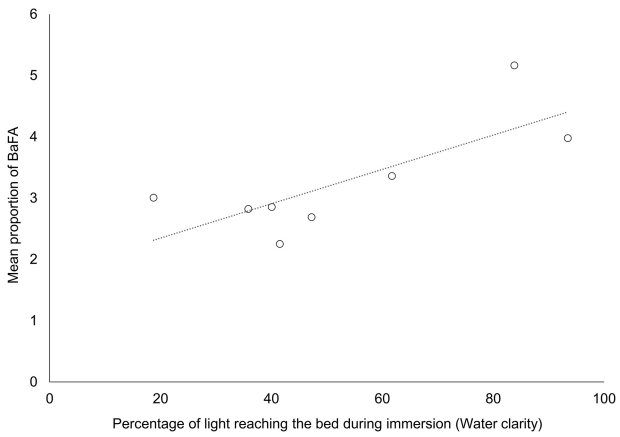

FIGURE 7 | Relationship between the water clarity and the mean proportion of bacteria-associated FAs (C15:0 + C17:0) in the sediment across ambient nitrogen conditions (control plots) in all sites. (r^2 = 0.67).

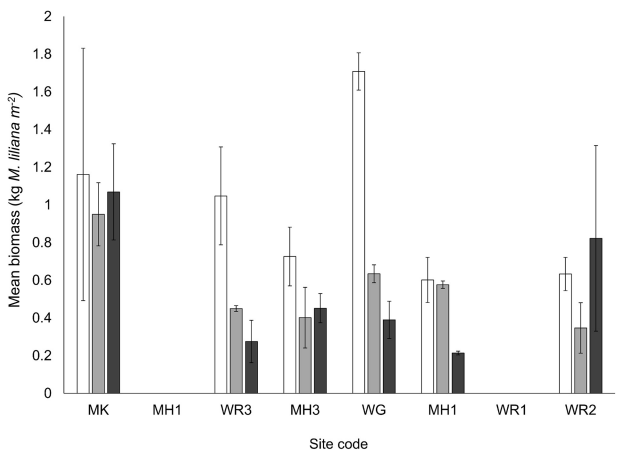

FIGURE 8 | Mean biomass (incl shell) of *M. liliana* specimens (20 – 30 mm length, kg dry weight bivalves m^2, ± SE, n = 3) as a function of site and nutrient enrichment treatment. Nutrient treatments; white bars – control plots (0 g N m^{-2} addition), light gray – medium plots (150 g N m^{-2} addition), dark gray – high plots (600 g N m^{-2} addition).

is altered their functional roles as prey for higher trophic levels and as grazers and stimulators of the MPB will also be altered (Thrush et al., 2006). While nutrient regeneration mediated by bioturbators such as *M. liliana* may become less influential on the MPB under higher external nitrogen loads, the utilization of nutrients by the MPB community would also likely decrease. This highlights the potential for top down processes to influence the MPB under N enrichment: Diatoms are proliferating under higher nitrogen concentrations not only due to the increase in nitrogen required for growth and reproduction but due to a decrease in grazing pressure. As FAs are essentially incorporated unaltered into the lipids of first order consumers, their FA profiles should reflect the FA profiles of the food they consume (Kharlamenko et al., 2001; Dalsgaard et al., 2003; Lebreton et al., 2011). Our data suggests the proportion of diatom-associated FAs in the bivalves decreased with nitrogen enrichment in the majority of sites alongside a concomitant increase in bacterial associated FAs. This could be due to the bivalves feeding less on the MPB due to N enrichment of the sites, or an increase in the metabolism of diatom-associated FAs. Direct chemical stress from other pollutants such as pesticides, pH, temperature and sedimentation have been observed to decrease feeding rates and nutrient uptake in several consumers (Patil, 2011; Wang et al., 2015; McCartain et al., 2017), which would in time reduce their biomass as fat stores are used. As bivalves tend to increase their metabolic activity to survive extended periods of stress from pollutants (Smolders et al., 2004; De Almeida et al., 2007; Patil, 2011) this

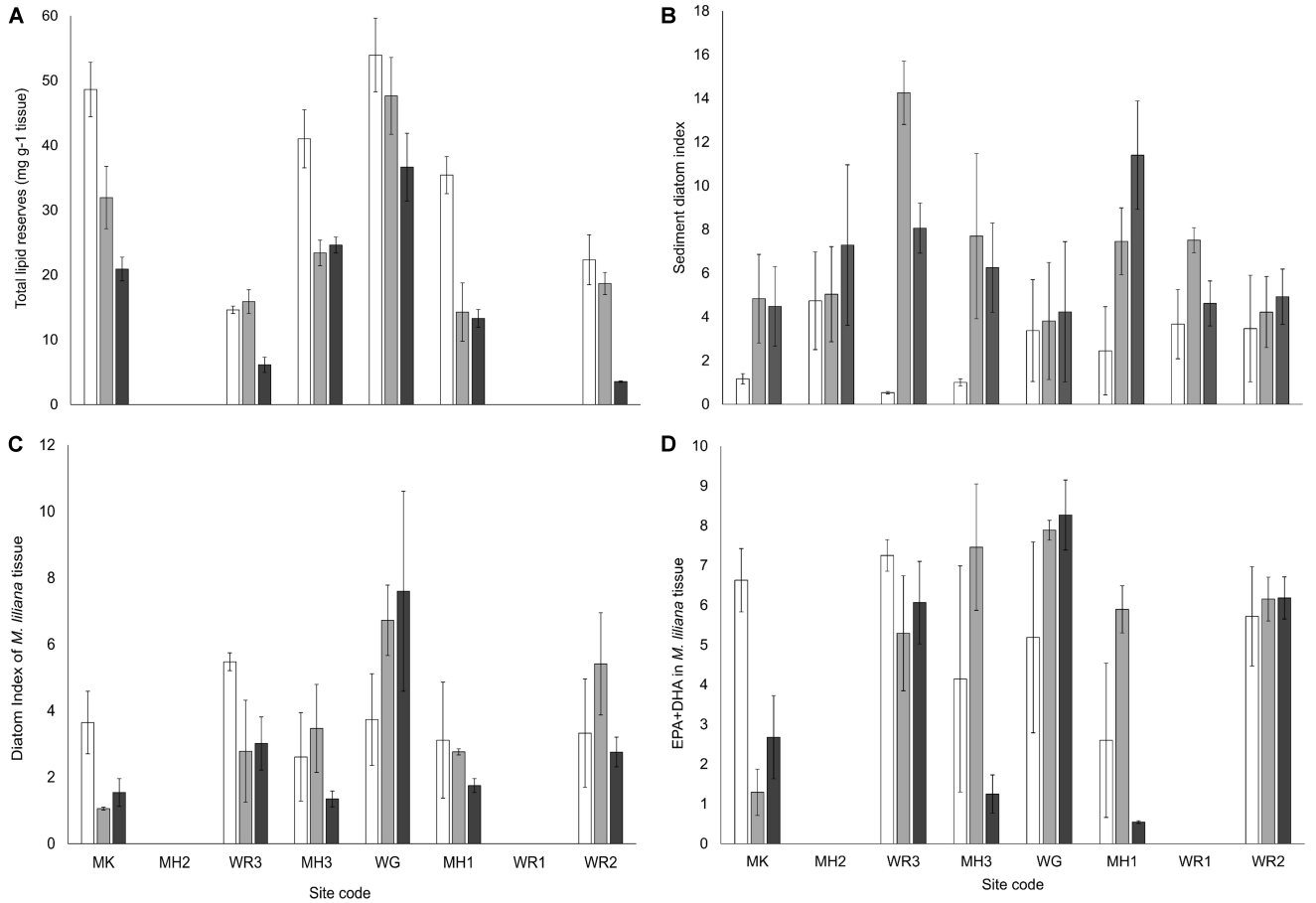

FIGURE 9 | (A) Mean total lipid reserves (mg g^{-1} DW tissue, ± SE, *n* = 3) from homogenized *M. liliana* specimens (3 individuals per sample, mean shell length 25 ± 4mm) across all sites and nutrient treatments. **(B)** Mean ratio of ω3:ω6 PUFAs from composite *M. liliana* tissue as a function of site and nutrient enrichment treatment. **(C)** Mean diatom index [16:1ω7 + 20:5ω3]/[18:1ω9 + 18:4ω3 + 22:6ω3] from composite *M. liliana* tissue. **(D)** Mean proportion of EPA [20:5ω3] + DHA [22:6ω3], extracted from composite *M. liliana* tissue (3 + individuals per 50 mg composite sample, ± SE, n = 3). Nutrient treatments; white bars – control plots (0 g N m^{-2} addition), light gray – medium plots (150 g N m^{-2} addition), dark gray – high plots (600 g N m^{-2} addition).

would further reduce biomass and lipid energy and FA reserves and potentially negatively impact their reproductive output.

Multivariate analysis of relationships between sediment FA biomarkers and environmental variables suggested that changes to the microbial community composition and quality was related to site-specific conditions such as the water clarity and subtle changes in the mud content of the sandy sediments. The effects of nutrient enrichment on FA biomarkers was modulated differently across the sites depending on the light availability. The functional role of intertidal microphytobenthos (MPB) in estuarine food webs have traditionally been characterized by their biomass, contribution to primary productivity and their influence on bacteria and nitrogen pathways at the sediment-water interface (MacIntyre et al., 1996; Serôdio and Catarino, 1999; O'Meara et al., 2017; Koedooder et al., 2019; Vaz et al., 2019). Our findings support previous studies where shifts in the MPB community were apparent with nutrient additions (Pinckney, 1995; Piehler et al., 2010). However, our experiment also reveals that the biosynthesis and transfer of essential FAs to consumers are rare but important components of the impacts of anthropogenic stressors on ecosystem function (see also Bachok et al., 2006; Bueno-pardo et al., 2018). Higher nitrogen inputs into low nutrient systems such as the ones we have studied herein can therefore alter the functional role of MPB as primary producers and as a basal food resource.

Across different sedimentary habitats resuspended MPB contribute substantially to water column productivity (Underwood and Kromkamp, 1999; Jones et al., 2017) and can even comprise up to 70% of the diet of harvested and farmed suspension feeders such as oysters, mussels and cockles (Sauriau and Kang, 2000; Dubois et al., 2007; Morioka et al., 2017). The MPB therefore support various coastal fisheries (Kritzer et al., 2016) and changes to the biosynthesis and transfer of essential FAs (EFAs) to key consumers may therefore have profound impacts on ecosystem functions through altering the functional role of the MPB and the biodiversity of fauna depending on their tolerance to high nutrient concentrations. Our investigation suggests that a key deep-dwelling tellinid bivalve that dominates

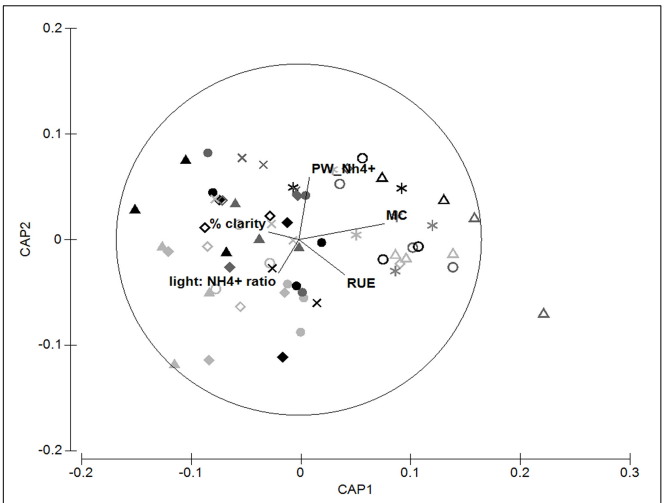

FIGURE 10 | Canonical analysis of principal components ordination of the quantity and quality indicators of the MPB and their relationship to environmental variables. Canonical axis 1 (δ^2 = 0.41) and canonical axis 2 (δ^2 = 0.15). PW NH4 + - porewater NH_4^+ concentration (0 – 2 cm depth). MC – mud content of the bed. RUE – resource use efficiency of the MPB (chl a:NH_4^+ ratio).Light:NH_4^+ ratio – The ratio between high-tide light and porewater NH_4^+ concentration.% clarity – The proportion of low tide light that reaches the PAR sensor during high tide, used as a proxy of turbidity. Symbols represent sites: Solid triangle – MH1; solid diamond – MH2; solid circle – MH3; open triangle – MK; open circle – WG; open diamond – WR1; star – WR2; cross – WR3. Colors represent nitrogen treatments: Light gray – control; dark gray – medium; black – high treated plots.

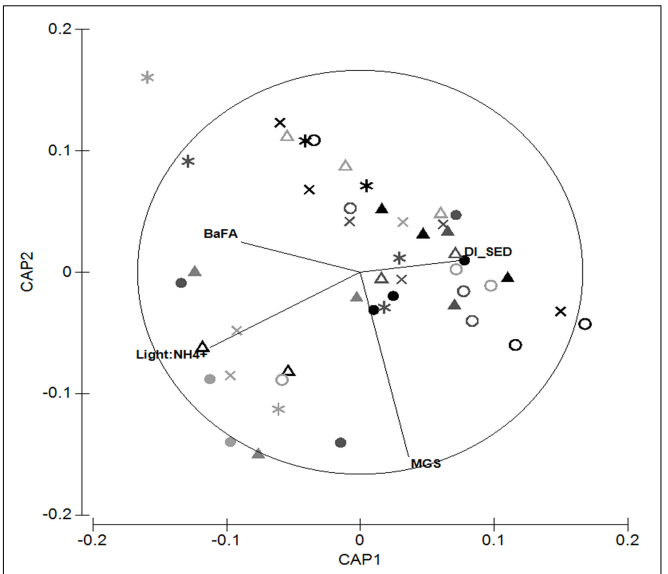

FIGURE 11 | Canonical analysis of principal components ordination of the quantity and quality indicators of *M. liliana* and the relationship with environmental and sedimentary variables. Canonical axis 1 (δ^2 = 0.30) and canonical axis 2 (δ^2 = 0.24). BaFA -C15:0 + C17:0 FAs associated with anaerobic and aerobic bacteria, DI_SED – Diatom index of the sediment surface. MGS – mean grain size. Light: NH_4^+ – ratio between high-tide light and porewater NH_4^+ concentration. Symbols represent sites: Solid triangle – MH1; solid circle – MH3; open triangle – MK; open circle – WG; star – WR2; cross – WR3. Colors represent nitrogen treatments: Light gray – control; dark gray – medium; black – high treated plots.

NZ estuaries, is negatively affected by nitrogen enrichment, and this could alter their role in soft sediment functions and their interactions with MPB and bacteria.

DATA AVAILABILITY STATEMENT

The datasets generated for this study are available on request to the corresponding author.

AUTHOR CONTRIBUTIONS

The New Zealand National Science Challenge Sustainable Seas, Dynamic Seas, Tipping Points project (CO1 × 1515) was responsible for the design and implementation of the larger field experiment, this involved many researchers in the implementation, maintenance and sampling of the experiment (see below). JAH conceived the manuscript and produced the first draft of the manuscript. JAH collected and processed fatty acid samples. JAH analyzed data with advice from JH. All authors contributed to the ideas presented in this manuscript, drafts of the manuscript and gave final approval for publication.

FUNDING

JAH was supported by the 'Oceans of Change Project'. ST, JH, CS, and CP were funded by the main project, The New Zealand National Science Challenge Sustainable Seas, Dynamic Seas, Tipping Points project (CO1 × 1515).

ACKNOWLEDGMENTS

The field campaign was conducted as part of a larger 'Tipping points' project funded through the National Science Challenge Sustainable Seas, which involved all authors and a nationwide group of collaborators to which we gratefully thank for the conception of the field experiment, the set-up and maintenance of the nitrogen enriched plots and deployed sensors throughout New Zealand. We would also like to thank the Seafloor Ecology Group at the University of Auckland for sample collection from the Auckland sites, Steph Mangan for the summary of PAR data and NIWA, Hamilton for processing porewater nutrient samples. We wish to thank Erica Zarate and Saras Green of the Mass Spectrometry Centre, Auckland Science Analytical Services. The University of Auckland, New Zealand for assistance with analysis of FAMEs by GC-MS, and to Raphael Bang for data processing.

SUPPLEMENTARY MATERIAL

The Supplementary Material for this article can be found online at: https://www.frontiersin.org/articles/10.3389/fmars.2020.00695/full#supplementary-material

REFERENCES

Anderson, M., Gorley, R. N., and Clarke, K. R. (2008). *PERMANOVA+ for PRIMER. Guide to Software and Statistical Methods*. Plymouth: PRIMER-E, Ltd.

Antonio, E. S., and Richoux, N. B. (2014). Trophodynamics of three decapod crustaceans in a temperate estuary using stable isotope and fatty acid analyses. *Mar. Ecol. Prog. Ser.* 504, 193–205. doi: 10.3354/meps10761

Bachok, Z., Mfilinge, P., and Tsuchiya, M. (2006). Food sources of coexisting suspension-feeding bivalves as indicated by fatty acid biomarkers, subjected to the bivalves abundance on a tidal flat. *J. Sustain. Sci. Manag.* 1, 92–111.

Balvanera, P., Pfisterer, A. B., Buchmann, N., He, J.-S., Nakashizuka, T., Raffaelli, D., et al. (2006). Quantifying the evidence for biodiversity effects on ecosystem functioning and services. *Ecol. Lett.* 9, 1146–1156. doi: 10.1111/j.1461-0248.2006.00963.x

Bell, J. G., McEvoy, L. A., Estevez, A., Shields, R. J., and Sargent, J. R. (2003). Optimising lipid nutrition in first-feeding flatfish larvae. *Aquaculture* 227, 211–220. doi: 10.1016/s0044-8486(03)00504-0

Berthold, M., Karsten, U., von Weber, M., Bachor, A., and Schumann, R. (2018). Phytoplankton can bypass nutrient reductions in eutrophic coastal water bodies. *Ambio* 47, 146–158. doi: 10.1007/s13280-017-0980-0

Bligh, E., and Dyer, W. (1959). A rapid method of total lipid extraction and purification. *Can. J. Biochem. Physiol.* 37, 911–917.

Brett, M. T., and Müller-Navarra, D. C. (1997). The role of highly unsaturated fatty acids in aquatic foodweb processes. *Freshw. Biol.* 38, 483–499. doi: 10.1046/j.1365-2427.1997.00220.x

Budge, S. M., Parrish, C. C., and Mckenzie, C. H. (2001). Fatty acid composition of phytoplankton, settling particulate matter and sediments at a sheltered bivalve aquaculture site. *Mar. Chem.* 76, 285–303. doi: 10.1016/s0304-4203(01)00068-8

Bueno-pardo, J., García-seoane, E., Sousa, A. I., Coelho, J. P., Morgado, M., Frankenbach, S., et al. (2018). Trophic web structure and ecosystem attributes of a temperate coastal lagoon (Ria de Aveiro, Portugal). *Ecol. Model.* 378, 13–25. doi: 10.1016/j.ecolmodel.2018.03.009

Burson, A., Stomp, M., Greenwell, E., Grosse, J., and Huisman, J. (2018). Competition for nutrients and light: testing advances in resource competition with a natural phytoplankton community. *Ecology* 99, 1108–1118. doi: 10.1002/ecy.2187

Byreddy, A. R., Gupta, A., Barrow, C. J., and Puri, M. (2016). A quick colorimetric method for total lipid quantification in microalgae. *J. Microbiol. Methods* 125, 28–32. doi: 10.1016/j.mimet.2016.04.002

Cahoon, L. B., and Safi, K. A. (2002). Distribution and biomass of benthic microalgae in Manukau Harbour, New Zealand. *New Zeal. J. Mar. Freshw. Res.* 36, 257–266. doi: 10.1080/00288330.2002.9517084

Camargo, J. A., and Alonso, Á (2006). Ecological and toxicological effects of inorganic nitrogen pollution in aquatic ecosystems: a global assessment. *Environ. Int.* 32, 831–849. doi: 10.1016/j.envint.2006.05.002

Cartaxana, P., Ribeiro, L., Goessling, J. W., Cruz, S., and Kühl, M. (2016). Light and O_2 microenvironments in two contrasting diatom-dominated coastal sediments. *Mar. Ecol. Prog. Ser.* 545, 35–47. doi: 10.3354/meps11630

Cnudde, C., Moens, T., Werbrouck, E., Lepoint, G., Van Gansbeke, D., and De Troch, M. (2015). Trophodynamics of estuarine intertidal harpacticoid copepods based on stable isotope composition and fatty acid profiles. *Mar. Ecol. Prog. Ser.* 524, 225–239. doi: 10.3354/meps11161

Consalvey, M., Jesus, B., Perkins, R. G., Brotas, V., Underwood, G. J. C., and Paterson, D. M. (2004). Monitoring migration and measuring biomass in benthic biofilms: the effects of dark/far-red adaptation and vertical migration on fluorescence measurements. *Photosynth. Res.* 81, 91–101. doi: 10.1023/b:pres.0000028397.86495.b5

Cook, P. L. M., Butler, E. C. V., and Eyre, B. D. (2004a). Carbon and nitrogen cycling on intertidal mudflats of a temperate australian estuary. I. Benthic metabolism. *Mar. Ecol. Prog. Ser.* 280, 25–38. doi: 10.3354/meps280025

Cook, P. L. M., Revill, A. T., Butler, E. C. V., and Eyre, B. D. (2004b). Carbon and nitrogen cycling on intertidal mudflats of a temperate Australian estuary. II. Nitrogen cycling. *Mar. Ecol. Prog. Ser.* 280, 39–54. doi: 10.3354/meps280039

Coutteau, P., Castell, J. D., Ackman, R. G., and Sorgeloos, P. (1996). The use of lipid emulsions as carriers for essential fatty acids in bivalves: a test case with juvenile *Placopecten magellanicus*. *J. Shellf. Res.* 15, 259–264.

Crain, C. M., Kroeker, K., and Halpern, B. S. (2008). Interactive and cumulative effects of multiple human stressors in marine systems. *Ecol. Lett.* 11, 1304–1315. doi: 10.1111/j.1461-0248.2008.01253.x

Cummings, V., Thrush, S., Hewitt, J., Norkko, A., and Pickmere, S. (2003). Terrestrial deposits on intertidal sandflats: Sediment characteristics as indicators of habitat suitability for *Recolonising macrofauna*. *Mar. Ecol. Prog. Ser.* 253, 39–54. doi: 10.3354/meps253039

Dalsgaard, J., St John, M., Kattner, G., Müller-Navarra, D., and Hagen, W. (2003). Fatty acid trophic markers in pelagic marine environment. *Adv. Mar. Biol.* 46, 227–340.

De Almeida, E. A., Bainy, A. C., De Melo Loureiro, A. P., Martinez, G. R., Miyamoto, S., Onuki, J., et al. (2007). Oxidative stress in *Perna perna* and other bivalves as indicators of environmental stress in the Brazilian marine environment: antioxidants, lipid peroxidation and DNA damage. *Compar. Biochem. Physiol.* 146, 588–600. doi: 10.1016/j.cbpa.2006.02.040

De Jonge, V. N., Elliott, M., and Orive, E. (2002). Causes, historical development, effects and future challenges of a common environmental problem: eutrophication. *Hydrobiologia* 475–476, 1–19. doi: 10.1007/978-94-017-2464-7_1

Douglas, E. J., Pilditch, C. A., Hines, L. V., Kraan, C., and Thrush, S. F. (2016). In situ soft sediment nutrient enrichment: a unified approach to eutrophication field experiments. *Mar. Pollut. Bull.* 111, 287–294. doi: 10.1016/j.marpolbul.2016.06.096

Dridi, S., Romdhane, M. S., and Cafsi, M. E. (2017). Nutritional quality in terms of lipid content and fatty acid composition of neutral and polar lipids in the adductor muscle of the oyster *Crassostrea gigas* (Thunberg, 1794) farmed in the Bizert lagoon (Tunisia) in relation with sexual cycle and environmen. *Egypt. J. Aquat. Res.* 43, 329–336. doi: 10.1016/j.ejar.2017.10.001

Drylie, T. P., Lohrer, A. M., Needham, H. R., Bulmer, R. H., and Pilditch, C. A. (2018). Benthic primary production in emerged intertidal habitats provides resilience to high water column turbidity. *J. Sea Res.* 142, 101–112. doi: 10.1016/j.seares.2018.09.015

Du, G., Yan, H., Liu, C., and Mao, Y. (2017). Behavioral and physiological photoresponses to light intensity by intertidal microphytobenthos. *Chin. J. Oceanol. Limnol.* 36, 293–304. doi: 10.1007/s00343-017-6099-0

Dubois, S., Orvain, F., Marin-léal, J. C., Ropert, M., and Lefebvre, S. (2007). Small-scale spatial variability of food partitioning between cultivated oysters and associated suspension-feeding species, as revealed by stable isotopes. *Mar. Ecol. Prog. Ser.* 336, 151–160. doi: 10.3354/meps336151

Emata, A. C., Ogata, H. Y., Garibay, E. S., and Furuita, H. (2004). Advanced broodstock diets for the mangrove red snapper and a potential importance of arachidonic acid in eggs and fry. *Fish Physiol. Biochem.* 28, 489–491. doi: 10.1023/b:fish.0000030637.26086.ab

Eriksson, B. K., Westra, J., Gerwen, I., Van Weerman, E., and Van Der, E. (2017). Facilitation by ecosystem engineers enhances nutrient effects in an intertidal system. *Ecosphere* 8:e02051. doi: 10.1002/ecs2.2051

Eyre, B. D., Ferguson, A. J. P., Webb, A., Maher, D., and Oakes, J. M. (2011). Metabolism of different benthic habitats and their contribution to the carbon budget of a shallow oligotrophic sub-tropical coastal system (southern Moreton Bay, Australia). *Biogeochemistry* 102, 87–110. doi: 10.1007/s10533-010-9424-7

Fearman, J., Bolch, C. J. S., and Moltschaniwskyj, N. A. (2009). Energy storage and reproduction in mussels, *Mytilus galloprovincialis*: the influence of diet quality. *J. Shellf. Res.* 28, 305–312. doi: 10.2983/035.028.0212

Ferguson, A. J. P., Eyre, B. D., and Gay, J. M. (2004). Benthic nutrient fluxes in euphotic sediments along shallow sub-tropical estuaries, northern New South Wales, Australia. *Aquat. Microb. Ecol.* 37, 219–235. doi: 10.3354/ame037219

Foley, J. A., DeFries, R., Asner, G. P., Barford, C., Bonan, G., Carpenter, S. R., et al. (2005). Global consequences of land use. *Science* 309, 570–574. doi: 10.1126/science.1111772

Fricke, A., Kihara, T. C., Kopprio, G. A., and Hoppenrath, M. (2017). Anthropogenically driven habitat formation by a tube dwelling diatom on the Northern Patagonian Atlantic coast. *Ecol. Indic.* 77, 8–13. doi: 10.1016/j.ecolind.2017.01.040

Galloway, A. W. E., Britton-Simmons, K. H., Duggins, D. O., Gabrielson, P. W., and Brett, M. T. (2012). Fatty acid signatures differentiate marine macrophytes at ordinal and family ranks. *J. Phycol.* 48, 956–965. doi: 10.1111/j.1529-8817.2012.01173.x

Galloway, A. W. E., and Winder, M. (2015). Partitioning the relative importance of phylogeny and environmental conditions on phytoplankton fatty acids. *PLoS One* 10:e0130053. doi: 10.1371/journal.pone.0130053

Gattuso, J.-P., Gentili, B., Duarte, C. M., Kleypas, J. A., Middelburg, J. J., and Antoine, D. (2006). Light availability in the coastal ocean: impact on the distribution of benthic photosynthetic organisms and contribution to primary production. *Biogeosci. Discuss.* 3, 895–959. doi: 10.5194/bgd-3-895-2006

Gonçalves, A., Marques, J., and Gonçalves, F. (2017). "Fatty acids' profiles of aquatic organisms: Revealing the impacts of environmental and anthropogenic stressors," in *Fatty Acids*, ed. A. Catala (London: IntechOpen), 89–118.

Grace, R. V. (1972). *The Benthic Ecology of the Entrance to Whangateau Harbour, Northland, New Zealand*. Auckland: University of Auckland.

Guo, F., Kainz, M. J., Valdez, D., Sheldon, F., and Bunn, S. E. (2016). The effect of light and nutrients on algal food quality and their consequent effect on grazer growth in subtropical streams. *Freshw. Sci.* 35, 1202–1212. doi: 10.1086/688092

Hickey, C. W., and Martin, M. L. (1999). Chronic toxicity of ammonia to the freshwater bivalve *Sphaerium novaezelandiae*. *Arch. Environ. Contam. Toxicol.* 36, 38–46. doi: 10.1007/s002449900440

Hicks, D. M., Shankar, U., Mckerchar, A. I., Basher, L., Lynn, I., Page, M., et al. (2011). Suspended sediment yields from New Zealand rivers. *J. Hydrol. New Zeal.* 50, 81–142.

Hill, W. R., Rinchard, J., and Czesny, S. (2011). Light, nutrients and the fatty acid composition of stream periphyton. *Freshw. Biol.* 56, 1825–1836. doi: 10.1111/j.1365-2427.2011.02622.x

Hodapp, D., Hillebrand, H., and Striebel, M. (2019). "Unifying" the concept of resource use efficiency in ecology. *Front. Ecol. Evol.* 6:233. doi: 10.3389/fevo.2018.00233

Hope, J. A., Paterson, D. M., and Thrush, S. F. (2019). The role of microphytobenthos in soft-sediment ecological networks and their contribution to the delivery of multiple ecosystem services. *J. Ecol.* 108:10.1111/1365-2745.13322.

Hopes, A., and Mock, T. (2015). Evolution of microalgae and their adaptations in different marine ecosystems. *eLS* 1–9. doi: 10.1002/9780470015902.a0023744

Howarth, R. W. (2008). Coastal nitrogen pollution: a review of sources and trends globally and regionally. *Harmful Algae* 8, 14–20. doi: 10.1016/j.hal.2008.08.015

Institute of Medicine [IOM] (2011). *Nutrition and Traumatic Brain Injury Improving Acute and Subacute*. Washington DC: The National Academies Press.

Jaschinski, S., Brepohl, D. C., and Sommer, U. (2008). Carbon sources and trophic structure in an eelgrass Zostera marina bed, based on stable isotope and fatty acid analyses. *Mar. Ecol. Prog. Ser.* 358, 103–114. doi: 10.3354/meps07327

Jesus, B., Brotas, V., Ribeiro, L., Mendes, C. R., Cartaxana, P., and Paterson, D. M. (2009). Adaptations of microphytobenthos assemblages to sediment type and tidal position. *Continent. Shelf Res.* 29, 1624–1634. doi: 10.1016/j.csr.2009.05.006

Jónasdóttir, S. H., Wilson, R. J., Gislason, A., and Heath, M. R. (2019). Lipid content in overwintering *Calanus finmarchicus* across the subpolar Eastern North Atlantic Ocean. *Limnol. Oceanogr.* 9999, 1–15.

Jones, H. F. E., Pilditch, C. A., Hamilton, D. P., and Bryan, K. R. (2017). Impacts of a bivalve mass mortality event on an estuarine food web and bivalve grazing pressure. *New Zeal. J. Mar. Freshw. Res.* 51, 370–392. doi: 10.1080/00288330.2016.1245200

Kharlamenko, V. I., Kiyashko, S. I., Imbs, A. B., and Vyshkvartzev, D. I. (2001). Identification of food sources of invertebrates from the seagrass Zostera marina community using carbon and sulfur stable isotope ratio and fatty acid analyses. *Mar. Ecol. Prog. Ser.* 220, 103–117. doi: 10.3354/meps220103

Kharlamenko, V. I., Kiyashko, S. I., Rodkina, S. A., and Imbs, A. B. (2008). Determination of food sources of marine invertebrates from a subtidal sand community using analyses of fatty acids and stable isotopes. *Russia. J. Mar. Biol.* 34, 101–109. doi: 10.1134/s106307400802003x

Knauer, J., and Southgate, P. C. (1999). A Review of the nutritional requirements of bivalves and the development of alternative and artificial diets for bivalve aquaculture. *Rev. Fish. Sci.* 7, 241–280. doi: 10.1080/10641269908951362

Koedooder, C., Stock, W., Willems, A., Mangelinckx, S., Marzinelli, E. M., and Campbell, A. H. (2019). Diatom-bacteria interactions modulate the composition and productivity of benthic diatom biofilms. *Front. Microbiol.* 10:1255. doi: 10.3389/fmicb.2019.01255

Kritzer, J. P., DeLucia, M. B., Greene, E., Shumway, C., Topolski, M. F., Thomas-Blate, J., et al. (2016). The importance of benthic habitats for coastal fisheries. *Bioscience* 66, 274–284. doi: 10.1093/biosci/biw014

Kromkamp, J., Peene, J., van Rijswijk, P., Sandee, A., and Goosen, N. (1995). Nutrients, light and primary production by phytoplankton and microphytobenthos in the eutrophic, turbid Westerschelde estuary (The Netherlands). *Hydrobiologia* 311, 9–19. doi: 10.1007/978-94-009-0117-9_2

Lebreton, B., Richard, P., Galois, R., Radenac, G., Pfléger, C., Guillou, G., et al. (2011). Trophic importance of diatoms in an intertidal *Zostera noltii* seagrass bed: evidence from stable isotope and fatty acid analyses. *Estuar. Coast. Shelf Sci.* 92, 140–153. doi: 10.1016/j.ecss.2010.12.027

Lepage, G., and Roy, C. C. (1986). Direct transesterification of all classes of lipids in a one step reaction. *J. Lipid Res.* 27, 114–120.

Lohrer, A. M., Halliday, N. J., Thrush, S. F., Hewitt, J. E., and Rodil, I. F. (2010). Ecosystem functioning in a disturbance-recovery context: contribution of macrofauna to primary production and nutrient release on intertidal sandflats. *J. Exper. Mar. Biol. Ecol.* 390, 6–13. doi: 10.1016/j.jembe.2010.04.035

Lohrer, A. M., Thrush, S. F., Lundquist, C. J., Vopel, K., Hewitt, J. E., and Nicholls, P. E. (2006). Deposition of terrigenous sediment on subtidal marine macrobenthos: response of two contrasting community types. *Mar. Ecol. Prog. Ser.* 307, 115–125. doi: 10.3354/meps307115

Lomstein, B. A., Blackburn, T. H., and Henriksen, K. (1989). Aspects of nitrogen and carbon cycling in the northern Bering Shelf sediment. I. The significance of urea turnover in the mineralization of NH4+.*Mar. Ecol. Prog. Ser.* 57, 237–247. doi: 10.3354/meps057237

Longphuirt, S. N., Lim, J. H., Leynaert, A., Claquin, P., Choy, E. J., Kang, C. K., et al. (2009). Dissolved inorganic nitrogen uptake by intertidal microphytobenthos: nutrient concentrations, light availability and migration. *Mar. Ecol. Prog. Ser.* 379, 33–44. doi: 10.3354/meps07852

Lorenzen, C. J. (1967). Determination of chlorophyll and pheo-pigments: *Spectrophotometric* equations. *Limnol. Oceanogr.* 12, 343–346. doi: 10.4319/lo.1967.12.2.0343

Lovelock, C. E., Feller, I. C., Ellis, J., Schwarz, A. M., Hancock, N., Nichols, P., et al. (2007). Mangrove growth in New Zealand estuaries: the role of nutrient enrichment at sites with contrasting rates of sedimentation. *Oecologia* 153, 633–641. doi: 10.1007/s00442-007-0750-y

MacIntyre, H. L., Geider, R. J., and Miller, D. C. (1996). Microphytobenthos: the ecological role of the 'secret garden' of unvegetated, shallow- water marine habitats. I. Distribution, abundance and primary production. *Estuar. Coasts* 19(2 part A), 186–201.

Marzetz, V., Koussoroplis, A., Martin-creuzburg, D., Striebel, M., and Wacker, A. (2017). Linking primary producer diversity and food quality effects on herbivores: a biochemical perspective. *Sci. Rep.* 7:11035.

Mayzaud, P., Claustre, H., and Augier, P. (1990). Dynamic of fatty acid changes during phytoplankton blooms produced in an enclosed experimental ecosystem. Influence of variable nutrient supply. *Mar. Ecol. Prog. Ser.* 60, 123–140. doi: 10.3354/meps060123

McCartain, L. D., Townsend, M., Thrush, S. F., Wethey, D. S., Woodin, S. A., Volkenborn, N., et al. (2017). The effects of thin mud deposits on the behaviour of a deposit-feeding tellinid bivalve: implications for ecosystem functioning. *Mar. Freshw. Behav. Physiol.* 50, 239–255. doi: 10.1080/10236244.2017.1364123

Middelburg, J. J., and Herman, P. M. J. (2007). Organic matter processing in tidal estuaries. *Mar. Chem.* 106, 127–147. doi: 10.1016/j.marchem.2006.02.007

Migné, A., Gévaert, F., Créach, A., Spilmont, N., Chevalier, E., and Davoult, D. (2007). Photosynthetic activity of intertidal microphytobenthic communities during emersion: in situ measurements of chlorophyll fluorescence (PAM) and CO 2 flux (IRGA) 1. *J. Phycol.* 43, 864–873. doi: 10.1111/j.1529-8817.2007.00379.x

Morioka, H., Kasai, A., Miyake, Y., Kitagawa, T., and Kimura, S. (2017). Food composition for blue mussels (*Mytilus edulis*) in the menai strait, UK, based on physical and biochemical analyses. *J. Shellf. Res.* 36, 659–668. doi: 10.2983/035.036.0315

Müller-Navarra, D. C., Brett, M. T., Liston, A. M., and Goldman, C. R. (2000). A highly unsaturated fatty acid predicts carbon transfer between primary producers and consumers. *Nature* 403, 74–77. doi: 10.1038/47469

Norkko, A., Hewitt, J. E., Thrush, S. F., and Funnell, G. A. (2006). Conditional outcomes of facilitation by a habitat-modifying subtidal bivalve. *Ecology* 87, 226–234. doi: 10.1890/05-0176

Norkko, J., Norkko, A., Thrush, S. F., Valanko, S., and Suurkuukka, H. (2010). Conditional responses to increasing scales of disturbance, and potential implications for threshold dynamics in soft-sediment communities. *Mar. Ecol. Prog. Ser.* 413, 253–266. doi: 10.3354/meps08745

O'Meara, T. A., Hillman, J. R., and Thrush, S. F. (2017). Rising tides, cumulative impacts and cascading changes to estuarine ecosystem functions. *Sci. Rep.* 7, 1–7.

Parker, J. G. (1983). A comparison of methods used for the measurement of organic matter in marine sediment. *Chem. Ecol.* 1, 201–209. doi: 10.1080/02757548308070802

Parrish, C. C., Abrajano, T. A., Budge, S. M., Helleur, R. J., and Hudson, E. D. (2000). Lipid and phenolic biomarkers in marine ecosystems: analysis and applications. *Handb. Environ. Chem.* 5, 193–223. doi: 10.1007/10683826_8

Patil, A. (2011). Protein changes in different tissues of freshwater bivalve parreysia cylindrical after exposure to indoxacarb. *Recent Res. Sci. Technol.* 3, 140–142.

Piehler, M. F., Currin, C. A., and Hall, N. S. (2010). Estuarine intertidal sandflat benthic microalgal responses to in situ and mesocosm nitrogen additions. *J. Exper. Mar. Biol. Ecol.* 390, 99–105. doi: 10.1016/j.jembe.2010.05.012

Pinckney, J. L. (1995). Impacts of seasonality and nutrients on microbial mat community structure and function mat community structure and function. *Mar. Ecol. Prog. Ser.* 123, 207–216. doi: 10.3354/meps123207

Pinturier-Geiss, L., Méjanelle, L., Dale, B., and Karlsen, D. A. (2002). Lipids as indicators of eutrophication in marine coastal sediments. *J. Microbiol. Methods* 48, 239–257. doi: 10.1016/s0167-7012(01)00326-8

Pratt, D. R., Pilditch, C. A., Lohrer, A. M., and Thrush, S. F. (2014). The effects of short-term increases in turbidity on sandflat microphytobenthic productivity and nutrient fluxes. *J. Sea Res.* 92, 170–177. doi: 10.1016/j.seares.2013.07.009

Pridmore, R. D., Thrush, S. F., Wilcock, R. J., Smith, T. J., Hewitt, J. E., and Cummings, V. J. (1991). Effect of the organochlorine pesticide technical chlordane on the population structure of suspension and deposit feeding bivalves. *Mar. Ecol. Prog. Ser.* 76, 261–271. doi: 10.3354/meps076261

Riekenberg, P., Oakes, J. M., and Eyre, B. (2017). Uptake of dissolved organic and inorganic nitrogen in microalgae-dominated sediment: comparing dark and light in situ and ex situ additions of 15N. *Mar. Ecol. Prog. Ser.* 571, 29–42. doi: 10.3354/meps12127

Risgaard-Petersen, N., Nicolaisen, M. H., Revsbech, N. P., and Lomstein, B. A. (2004). Competition between ammonia-oxidizing bacteria and benthic microalgae. *Appl. Environ. Microbiol.* 70, 5528–5537. doi: 10.1128/aem.70.9.5528-5537.2004

Ritchie, R. J. (2006). Consistent sets of spectrophotometric chlorophyll equations for acetone, methanol and ethanol solvents. *Photosynth. Res.* 89, 27–41. doi: 10.1007/s11120-006-9065-9

Rodil, I. F., Lohrer, A. M., Chiaroni, L. D., Hewitt, J. E., Thrush, F., Rodil, I. F., et al. (2011). Disturbance of sandflats by thin terrigenous sediment deposits: consequences for primary production and nutrient cycling. *Ecol. Appl.* 21, 416–426. doi: 10.1890/09-1845.1

Ruano, F., Ramos, P., Quaresma, M., Bandarra, N. M., and Pereira-da Fonseca, I. (2012). Evolution of fatty acid profile and condition index in mollusc bivalves submitted to different depuration periods. *Rev. Portuguesa Ciéncias Vet.* 111, 75–84.

Sauriau, P., and Kang, C. (2000). Stable isotope evidence of benthic microalgae-based growth and secondary production in the suspension feeder *Cerastoderma edule* Mollusca, Bivalvia) in the Marennes-Oleron Bay stable isotope evidence of benthic microalgae-based growth and secondary product. *Hydrobiologia* 440, 317–332.

Savage, C., Thrush, S. F., Lohrer, A. M., and Hewitt, J. E. (2012). Ecosystem services transcend boundaries: estuaries provide resource subsidies and influence functional diversity in coastal benthic communities. *PLoS ONE* 7:e42708. doi: 10.1371/journal.pone.0042708

Scheffer, M., and Van Nes, E. H. (2007). Shallow lakes theory revisited: various alternative regimes driven by climate, nutrients, depth and lake size. *Hydrobiologia* 584, 455–466. doi: 10.1007/978-1-4020-6399-2_41

Serôdio, J., and Catarino, F. (1999). Fortnightly light and temperature variability in estuarine intertidal sediments and implications for microphytobenthos primary productivity. *Aquat. Ecol.* 2, 235–241.

Serôdio, J., Ezequiel, J., Barnett, A., and Mouget, J. (2012). Efficiency of photoprotection in microphytobenthos: role of vertical migration and the xanthophyll cycle against photoinhibition. *Aquat. Microb. Ecol.* 67, 161–175. doi: 10.3354/ame01591

Simpson, S. L., Batley, G. E., and Chariton, A. A. (2013). Revision of the ANZECC/ARMCANZ sediment quality guidelines. *CSIRO Land Water Rep.* 08:132.

Singer, J. K., Anderson, J. B., Ledbetter, M. T., McCave, I. N., Jones, K. P. N., and Wright, R. (1988). An assessment of analytical techniques for the size analysis of fine- grained sediments. *J. Sediment. Petrol.* 58, 534–543.

Smolders, R., Bervoets, L., De Coen, W., and Blust, R. (2004). Cellular energy allocation in zebra mussels exposed along a pollution gradient: linking cellular effects to higher levels of biological organization. *Environ. Pollut.* 129, 99–112. doi: 10.1016/j.envpol.2003.09.027

Sprague, M., Dick, J. R., and Tocher, D. R. (2016). Impact of sustainable feeds on omega-3 long-chain fatty acid levels in farmed Atlantic salmon, 2006-2015. *Sci. Rep.* 6:21892.

Sterner, R. W., Elser, J. J., Fee, E. J., Guildford, S. J., and Chrzanowski, T. H. (1997). The light: nutrient ratio in lakes: the balance of energy and materials affects ecosystem structure and process. *Am. Nat.* 150, 663–684. doi: 10.1086/286088

Strandberg, U., Taipale, S. J., Hiltunen, M., Galloway, A. W. E., Brett, M. T., and Kankaala, P. (2015). Inferring phytoplankton community composition with a fatty acid mixing model. *Ecosphere* 6, 1–18.

Sundbäck, K., Alsterberg, C., and Larson, F. (2010). Effects of multiple stressors on marine shallow-water sediments: response of microalgae and meiofauna to nutrient-toxicant exposure. *J. Exper. Mar. Biol. Ecol.* 388, 39–50. doi: 10.1016/j.jembe.2010.03.007

Sundback, K., and Mcglathery, K. (2005). "Interactions between benthic macroalgal and microalgal mats," in *Interactions Between Macro-and Microorganisms in Marine Sediments*, eds E. Kristensen, R. R. Haese, and J. E. Kostka (Cham: Springer), 7–29. doi: 10.1029/ce060p0007

Sundbäck, K., Miles, A., and Linares, F. (2006). Nitrogen dynamics in nontidal littoral sediments: role of microphytobenthos and denitrification. *Estuar. Coasts* 29, 1196–1211. doi: 10.1007/bf02781820

Taipale, S. J., Vuorio, K., Strandberg, U., Kahilainen, K. K., Järvinen, M., Hiltunen, M., et al. (2016). Lake eutrophication and brownification downgrade availability and transfer of essential fatty acids for human consumption. *Environ. Intern.* 96, 156–166. doi: 10.1016/j.envint.2016.08.018

Tay, H. W., Bryan, K. R., and Pilditch, C. A. (2013). Dissolved inorganic nitrogen concentrations in an estuarine tidal flat. *J. Coast. Res.* 65, 135–140. doi: 10.2112/si65-024.1

Thrush, S. F., Hewitt, J. E., Cummings, V. J., Ellis, J. I., Hatton, C., Lohrer, A., et al. (2004). Muddy waters: elevating sediment input to coastal and estuarine habitats. *Front. Ecol. Environ.* 2, 299–306. doi: 10.2307/3868405

Thrush, S. F., Hewitt, J. E., Cummings, V. J., Green, M. O., Funnell, G. A., and Wilkinson, M. R. (2000). The generality of field experiments: interactions between local and broad-scale processes. *Ecology* 81, 399–415. doi: 10.1890/0012-9658(2000)081[0399:tgofei]2.0.co;2

Thrush, S. F., Hewitt, J. E., Gibbs, M., Lundquist, C., and Norkko, A. (2006). Functional role of large organisms in intertidal communities: community effects and ecosystem function. *Ecosystems* 9, 1029–1040. doi: 10.1007/s10021-005-0068-8

Thrush, S. F., Hewitt, J. E., Kraan, C., Lohrer, A. M., Pilditch, C. A., and Douglas, E. (2017). Changes in the location of biodiversity-ecosystem function hot spots across the seafloor landscape with increasing sediment nutrient loading. *Proc. R. Soc. B Biol. Sci.* 284:20162861. doi: 10.1098/rspb.2016.2861

Thrush, S. F., Hewitt, J. E., and Lohrer, A. M. (2012). Interaction networks in coastal soft-sediments highlight the potential for change in ecological resilience. *Ecol. Appl.* 22, 1213–1223. doi: 10.1890/11-1403.1

Tobias, C., Giblin, A., Mcclelland, J., Tucker, J., and Peterson, B. (2003). Sediment DIN fluxes and preferential recycling of benthic microalgal nitrogen in a shallow macrotidal estuary. *Mar. Ecol. Prog. Ser.* 257, 25–36. doi: 10.3354/meps257025

Tolhurst, T. J., Underwood, A. J., Perkins, R. G., and Chapman, M. G. (2005). Content versus concentration: effects of units on measuring the biogeochemical properties of soft sediments. *Estuar. Coast. Shelf Sci.* 63, 665–673. doi: 10.1016/j.ecss.2005.01.010

Townsend, M., Thrush, S. F., Hewitt, J. E., Lohrer, A. M., and Mccartain, L. (2014). Behavioural changes in the Tellinid bivalve *Macomona liliana* (Iredale, 1915) following exposure to a thin terrigenous sediment deposition event: evidence from time-lapse photography. *Cahiers Biol. Mar.* 55, 475–483.

Twining, C. W., Brenna, J. T., Hairston, N. G., and Flecker, A. S. (2016). Highly unsaturated fatty acids in nature: what we know and what we need to learn. *Oikos* 125, 749–760. doi: 10.1111/oik.02910

Underwood, G. J. C., and Kromkamp, J. C. (1999). Primary production by phytoplankton and microphytobenthos in estuaries. *Adv. Ecol. Res.* 29, 93–153. doi: 10.1016/s0065-2504(08)60192-0

Vargas, M. A., Rodríguez, H., Moreno, J., Olivares, H., Del Campo, J. A., Rivas, J., et al. (1998). Biochemical composition and fatty acid content of filamentous nitrogen-fixing cyanobacteria. *J. Phycol.* 34, 812–817. doi: 10.1046/j.1529-8817.1998.340812.x

Vaz, L., Frankenbach, S., Serôdio, J., and Dias, J. M. (2019). New insights about the primary production dependence on abiotic factors: Ria de Aveiro case study. *Ecol. Indic.* 106:105555. doi: 10.1016/j.ecolind.2019.105555

Veach, A. M., and Griffiths, N. A. (2018). Testing the light: nutrient hypothesis: insights into biofilm structure and function using metatranscriptomics. *Mol. Ecol.* 27, 2909–2912. doi: 10.1111/mec.14733

Volkenborn, N., Meile, C., Polerecky, L., Pilditch, C. A., Wethey, D. S., and Woodin, S. A. (2012). Intermittent bioirrigation and oxygen dynamics in permeable sediments: an experimental and modeling study of three tellinid bivalves. *J. Mar. Res.* 70:6.

Volkman, J. K., Barrett, S. M., Blackburn, S. I., Mansour, M. P., Sikes, E. L., and Gelin, F. (1998). Microalgal biomarkers: a review of recent research developments. *Organ. Geochem.* 29, 1163–1179. doi: 10.1016/s0146-6380(98)00062-x

Wang, Y., Li, L., Hu, M., and Lu, W. (2015). Physiological energetics of the thick shell mussel *Mytilus coruscus* exposed to seawater acidification and thermal stress. *Sci. Total Environ.* 514, 261–272. doi: 10.1016/j.scitotenv.2015.01.092

Wentworth, C. K. (1922). A scale of grade and class terms for clastic sediments. *J. Geol.* 30, 377–392. doi: 10.1086/622910

Woodin, S. A., Wethey, D. S., Hewitt, J. E., and Thrush, S. F. (2012). Small scale terrestrial clay deposits on intertidal sandflats: behavioral changes and productivity reduction. *J. Exper. Mar. Biol. Ecol.* 413, 184–191. doi: 10.1016/j.jembe.2011.12.010

Yang, D., Nam, S., Hwang, S. J., An, K. G., Park, Y. S., Shin, K. H., et al. (2016). Fatty acid biomarkers to verify cyanobacteria feeding abilities of herbivorous consumers. *J. Freshw. Ecol.* 31, 77–91. doi: 10.1080/02705060.2015.1025304

Zárate, E. V., Díaz De Vivar, M. E., Avaro, M. G., Epherra, L., and Sewell, M. A. (2016). Sex and reproductive cycle affect lipid and fatty acid profiles of gonads of *Arbacia dufresnii* (Echinodermata: Echinoidea). *Mar. Ecol. Prog. Ser.* 551, 185–199. doi: 10.3354/meps11711

Conflict of Interest: The authors declare that the research was conducted in the absence of any commercial or financial relationships that could be construed as a potential conflict of interest.

The reviewer DP declared a past co-authorship with one of the authors JH to the handling editor.

frontiers in Marine Science

ORIGINAL RESEARCH
published: 25 February 2020
doi: 10.3389/fmars.2020.00088

Stable Seasonal and Annual Alpha Diversity of Benthic Diatom Communities Despite Changing Community Composition

Leena Virta[1,2]*, *Janne Soininen*[1] and *Alf Norkko*[2,3]

[1] Department of Geosciences and Geography, University of Helsinki, Helsinki, Finland, [2] Tvärminne Zoological Station, University of Helsinki, Hanko, Finland, [3] Baltic Sea Centre, Stockholm University, Stockholm, Sweden

The global biodiversity loss has raised interest in the different facets of diversity, and the importance of diversity for ecosystem functions has been recognized. However, our knowledge on seasonal and inter-annual variation in the composition and diversity of communities is still poor. Here, we investigated the seasonal and inter-annual changes in taxonomic and functional community composition and diversity of benthic diatoms in a coastal habitat of the northern Baltic Sea, where seasonal and inter-annual variation of climate is pronounced. We found that the taxonomic and functional alpha diversity remained stable at seasonal and inter-annual level despite strong changes in community composition. However, alpha diversity decreased during an exceptionally warm winter possibly due to disturbances induced by the lack of ice. This may suggest that climate warming and consequently limited ice cover will affect the diversity of benthic communities.

Keywords: seasonal variation, annual variation, community composition, diversity, benthic diatoms, Baltic Sea, microphytobenthos

OPEN ACCESS

Edited by:
Vona Meleder,
Université de Nantes, France

Reviewed by:
Lourenço Soares Ribeiro,
Center for Marine and Environmental Sciences (MARE), Portugal
Du Guoying,
Ocean University of China, China

***Correspondence:**
Leena Virta
leena.virta@helsinki.fi

Specialty section:
This article was submitted to Marine Ecosystem Ecology, a section of the journal Frontiers in Marine Science

Received: *04 December 2019*
Accepted: *03 February 2020*
Published: *25 February 2020*

Citation:
Virta L, Soininen J and Norkko A (2020) Stable Seasonal and Annual Alpha Diversity of Benthic Diatom Communities Despite Changing Community Composition. Front. Mar. Sci. 7:88. doi: 10.3389/fmars.2020.00088

INTRODUCTION

The current global biodiversity crisis threatens all ecosystems and has increased interest in studying the diversity of different organisms on different scales. A great amount of research has resolved patterns of diversity and its effects on different aspects of ecosystem functioning and services, such as productivity (e.g., Smith, 2007; Cadotte et al., 2009) and nutrient cycling (e.g., Smetacek, 1999; Spilling et al., 2018). Some of these studies have presented snapshot results across spatial gradients (e.g., Virta et al., 2019) while others have included temporal variation (e.g., Morin et al., 2014), but most of them have neglected the strong seasonal and inter-annual variation that occurs across most parts of the globe (but see Hillebrand et al., 2010). Ignoring the seasonal and inter-annual changes in diversity undermines our ability to generalize biodiversity patterns, compromises inferences gained from monitoring programs and jeopardizes conservation efforts of valuable ecosystems.

The seasonal cycle of biotic communities is usually characterized by changes in taxonomic community composition induced by temporary species gain during favorable growing season and temporary species loss during more unfavorable conditions (Hobson and McQuoid, 1997). This results in seasonal changes in the functions of the community. However, this pattern can be altered by strong dispersal abilities and a large regional species pool that allow the replacement of temporarily transient species (Zobel, 1997), and thus, maintain steadily high local taxonomic diversity. Temporal changes in the taxonomy also affect the functional composition and diversity of the communities, which are often more effective than taxonomy in showing the relationship

between diversity and ecosystem functioning (Chapin et al., 2000). Furthermore, high taxonomic diversity supports functional redundancy (i.e., complementarity of species traits), which allows ecosystem stability throughout the year and also provides resilience against environmental change (Naeem et al., 2012). However, the temporal variation in functional diversity of communities in different ecosystems and habitats is still poorly known.

Diatoms are one of the most important groups of microorganisms in all aquatic ecosystems and account for as much as 20% of the total primary production on Earth (Nelson et al., 1995; Falkowski et al., 1998; Field et al., 1998). Different studies have agreed that the diversity of benthic diatom communities affects ecosystem productivity, although consensus on the direction of this effect has not been found. For example, Virta et al. (2019) showed that the diversity, especially functional alpha diversity, of benthic diatoms promotes ecosystem productivity, whereas Forster et al. (2006) found a negative relationship between diatom diversity and ecosystem productivity, which may be due to the dominance of a few highly productive species. However, considering the importance, high abundance and enormous diversity of benthic diatoms, it is surprising how little attention the temporal variation in their diversity has received.

To reduce these knowledge gaps, we present a study on the seasonal and inter-annual variation of the taxonomic and functional composition and diversity of benthic diatom communities. We conducted the study in the northern part of the Baltic Sea. The predominant climate zone in this area is a warm-summer humid continental climate with strong variations in air and water temperatures. Moreover, our sampling site was located in a generally shallow coastal archipelago area, which results in high seasonal and inter-annual variability in water temperature and annually occurring ice cover. Thus, biotic communities here experience strong temporal changes and are, thus, ideal for seasonal and inter-annual studies. Our specific research question and hypothesis was: *Does seasonal and inter-annual climatic variation affect the taxonomic and functional composition and alpha diversity of benthic diatom communities?* We hypothesized that the composition and diversity of communities would change significantly between seasons and climatically different years (Gilbert et al., 2010). We also predicted that we would find the lowest diversity during winter because of harsh conditions (Oberbeckmann et al., 2014).

MATERIALS AND METHODS

Study Area and Sampling

The temporal sampling site was located in a small, sheltered and shallow (<2 m) bay on the Finnish coast of the Baltic Sea, at the Hanko-peninsula (**Figure 1**). The bottom of the bay is muddy, with cobble-sized stones close to shores. Due to the sheltered

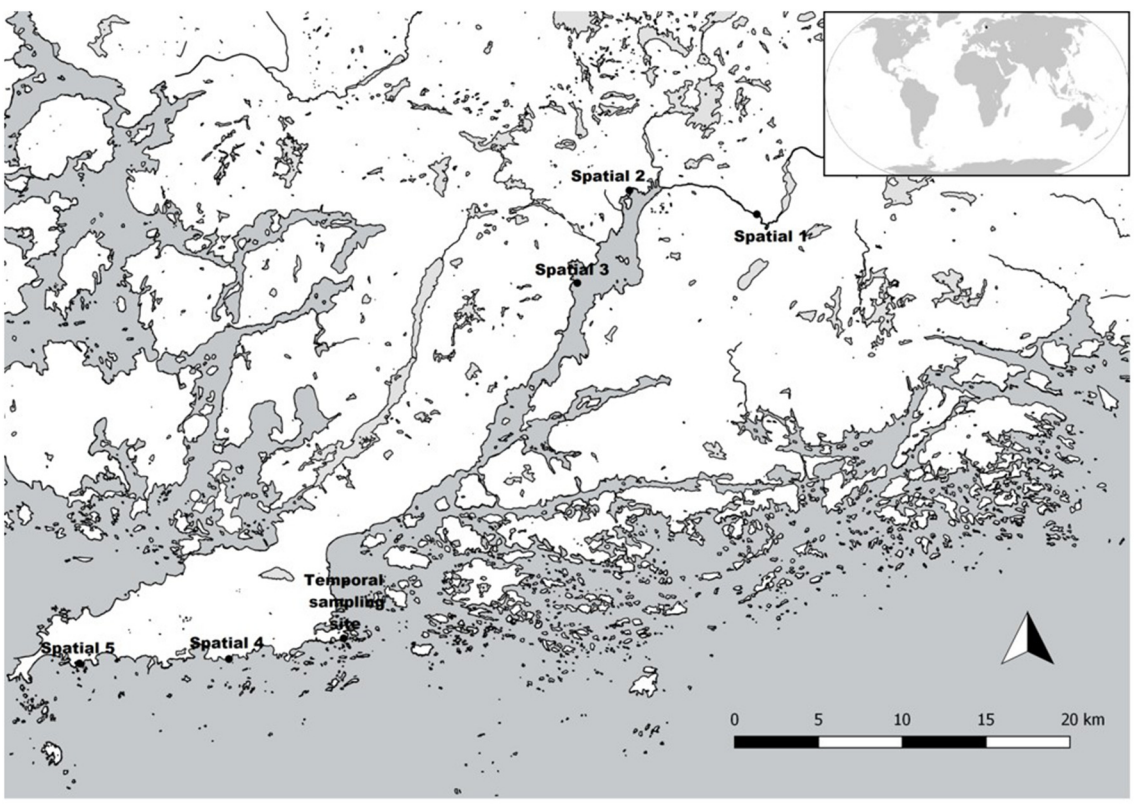

FIGURE 1 | Our temporal sampling site and five spatio-temporal sites along the Hanko Peninsula in southern Finland, Baltic Sea. Map layers derived from HELCOM (2019), European Environment Agency (2019), and SYKE (2019).

location, waves do not roll the stones, which form, thus, stable substrata for benthic diatoms. Climate in this area is a mixture of continental and oceanic climates, with strong seasonal and inter-annual variations. The average annual air temperature is ca. 6.8°C, and ice cover forms annually (Finnish Meteorological Institute, 2019). Water in the area is brackish with a salinity of 5–7. Thus, biotic communities are a mixture of brackish and freshwater species.

To provide more generality and context to the results from our intensively sampled site, we also collected spatio-temporal samples from five sites at three occasions (see below), hence 15 spatio-temporal samples altogether, and compared the temporal changes in diversity between these sites and our temporally intensive sampling site. These five sites were located at a distance of ca. 60 kilometers from the temporally intensive sampling site (**Figure 1**), and represent a gradient from a freshwater river Karjaanjoki, through its estuary Pojo Bay, to the brackish archipelago area at the coast of the Hanko-peninsula. Thus, biotic communities at these sites represent highly different environmental conditions in terms of salinity, nutrients, and exposure to wave action.

We conducted temporal sampling at two-week-intervals over a ca. two-year-period, 20 April 2017–29 May 2019, covering altogether a period of 111 weeks (**Supplementary Table 1**). We collected a total of 56 samples from natural stones following the recommendations of Kelly et al. (1998). We randomly selected 10 cobble-sized stones from depths of 20–50 cm, and avoided using the same stones again for at least eight following weeks, because of the required re-colonization time of benthic microalgae (Hillebrand and Sommer, 2000). We collected the biofilm by brushing the surfaces of stones with a toothbrush (25 cm^2/stone) and pooled the accumulated suspension into a composite sample. After sampling, we stored the samples in cold (+4°C) and dark conditions until further analyses. Our spatial samples for validation purposes were collected three times, June 2017, September 2017, and May 2019, following the same procedure.

Laboratory Analyses, Trait Analyses, and Temperature Calculations

We boiled the diatom samples in hydrogen peroxide (30% H_2O_2) to remove organic material, and mounted cleaned diatoms on slides using Naphrax (Brunel Microscopes Ltd., United Kingdom). We identified the diatoms (500 valves/sample) with a phase contrast light microscope with a 1,000× magnification to the lowest possible taxonomic level (typically species level). The identification followed Krammer and Lange-Bertalot (1986, 1988, 1991a,b), Snoeijs (1993), Snoeijs and Vilbaste (1994), Snoeijs and Potapova (1995), and Snoeijs and Kasperovicienè (1996). After identification, we transformed species counts into relative abundances.

To account for functional composition and diversity of diatom communities, we divided species to traits that are robust indicators of ecological behavior (Hodapp et al., 2016). We categorized species according to different classifications: size (biovolume classes: small < 1,000 μm/large > 1,000 μm), mobility (mobile/non-mobile), type of attachment [adnate/pedunculate (which was further divided to pad-attached/stalk-attached)/non-attached], colonization (colonial/non-colonial), guilds (low-profile/high-profile/motile/planktonic) (Rimet and Bouchez, 2012), and nitrogen-fixing abilities (nitrogen-fixer/non-nitrogen-fixer) (Passy, 2017). Each species was categorized according to all six classifications, which resulted in numerous possible combinations for classifying a certain species. For example, one of the common species, *Bacillaria paxillifera* (O.F. Müller) T.Marsson, was classified as large/mobile/non-attached/non-colonial/motile/non-nitrogen-fixer. As the measure of trait composition, we used the combination of traits of all the species present in the community. For the identification of traits, we used above mentioned species and trait literature, and Snoeijs et al. (2002) and Diatoms of North America (2019).

We derived average seasonal air temperatures of the study area from a weather station located in close proximity of our temporal sampling site, at Tvärminne Zoological Station (Finnish Meteorological Institute, 2019). Average seasonal water temperatures were derived from permanent loggers located close to the sampling site (Monicoast, 2019). These loggers by Finnish Meteorological Institute and later by Tvärminne Zoological Station have measured water temperature since the beginning of 1900.

Statistical Analyses

We divided our data into seasons according to thermal seasons (Finnish Meteorological Institute, 2019). Thermal seasons are characteristic to each location and each year. They are categorized as follows: thermal summer begins when daily average temperature rises permanently above +10°C, thermal fall when average daily temperature decreases below +10°C, thermal winter when average daily temperature decreases below 0°C, and thermal spring when average daily temperature rises permanently above 0°C.

To test if the diatom communities are significantly different between adjacent seasons and years, we ran analysis of similarities (ANOSIM), with Bray-Curtis distance (Clarke, 1993). ANOSIM is a distribution-free analog of one-way ANOVA, where values range between−1 and 1, 1 indicating total dissimilarity between groups and −1 greater dissimilarities within groups than between groups.

To illustrate season-specific patterns in taxonomic and functional community composition, we used Nonmetric Multidimensional Scaling (NMDS) with Bray-Curtis distance, and three dimensions for taxonomic composition and two dimensions for functional composition. We also calculated a centroid for the samples of each sampling season. We ran NMDS with the R packages vegan (Oksanen, 2019) and ggplot2 (Wickham, 2019).

To compare the taxonomic and functional alpha diversity in diatom communities between seasons, we used Shannon diversity index with logarithm base of b = 2 (Shannon and Weaver, 1962), which is a commonly used measure of diversity. Due to its sensitivity to rare species (Nagendra, 2002), it is a suitable index for studies concerning diatom communities, where

the majority of species is usually rare. Although species richness is the most commonly used measure of diversity, we decided not to include it as a parameter in this study. This decision was due to the large variation in species richness between samples and the fixed amount (500) of frustules identified per sample, which may have underestimated the number of species in speciose samples.

To test the significance of differences in taxonomic and functional diversity between seasons, we first computed one-way ANOVA test with season as a categorical factor. Then, we calculated pairwise significances between diversities of all seasons with Tukey Honest Significant Differences. We considered adjusted $p < 0.05$ to denote significant differences.

To validate the results of our temporal samples, we compared the degree of temporal beta diversity of our temporal sampling site with five other sites, which were sampled three times, using temporal beta diversity indices (TBI) (Winegardner et al., 2017). Our aim was to see whether the direction of change in diversity at our temporal site coincides with other five sites and, thus, to make our results more general. TBI is based on the Podani family of beta diversity and computes total temporal beta diversity as well as different components (species loss or species gain) of that beta diversity by forming pairs observed at time 1 (T1) and time 2 (T2). It computes species loss (bj) from T1 to T2 with the equation: bj = (y1j–y2j) if y1j > y2j, and species gain (cj) from T1 to T2 with the equation: cj = (y2j–y1j) if y2j > y1j. We ran the TBI for taxonomic temporal beta diversity with binary data using Bray-Curtis dissimilarities. The significances were computed using a parametric paired *t*-test with 9999 permutations. We ran the TBI with the R package adespatial (Dray et al., 2019).

All statistical analyses were conducted using R version 3.6.1 (R Development Core Team, 2019).

RESULTS

Total species richness in our temporal samples was 272, and species richness per sample varied between 31 and 70 (**Supplementary Table 1**). In general, all traits were present in all the samples, except planktonic guild, which was absent from nine samples and the nitrogen-fixing trait that was absent from 11 samples. Species abundances at sampling sites are presented in **Supplementary Table 2**, and trait classifications for all the species in **Supplementary Table 3**.

Thermal summer at our temporal site began on 19 May in 2017, 8 May in 2018 and 16 May in 2019, thermal fall on 6 October in 2017 and 24 September in 2018, thermal winter on 10 January in 2017–2018 (hereafter referred to as winter 2018) and 13 December in 2018–2019 (hereafter referred to as winter 2019), and thermal spring on 4 April in 2018 and 14 March in 2019 (Finnish Meteorological Institute, 2019). ANOSIM showed that the diatom communities were taxonomically and functionally different between most of the seasons (**Table 1**). Communities were also significantly different between the first and the second sampling year.

In the NMDS, compositions during most of the individual seasons formed clear clusters (**Figure 2**). These clusters showed cyclic annual variation in taxonomic and functional community composition. Taxonomic composition cycles showed clear differences between years, whereas functional composition cycles remained more similar between years.

TABLE 1 | Results of the ANOSIM to analyze the differences in taxonomic and functional community composition between **(A)** seasons and **(B)** years.

	Taxonomic		Functional	
	R	***p***	***R***	***p***
(A)				
Summer 2017–fall 2017	**0.857**	**0.002**	**0.926**	**0.001**
Fall 2017–winter 2018	0.183	0.073	0.024	0.361
Winter 2018–spring 2018	0.219	0.151	0.281	0.142
Spring 2018–summer 2018	**0.602**	**0.040**	0.377	0.122
Summer 2018–fall 2018	**0.337**	**0.013**	**0.312**	**0.039**
Fall 2018–winter 2019	**0.504**	**0.012**	**0.550**	**0.014**
Winter 2019–spring 2019	**0.466**	**0.025**	**0.611**	**0.007**
(B)				
2017/2018–2018/2019	**0.421**	**0.001**	**0.055**	**0.043**

Significant ($p < 0.05$) differences are bolded. Spring 2017 and summer 2019 were excluded from the analyses, because our sampling period only covered a part of them.

Despite considerable seasonal variation in air temperature (average seasonal temperature −4.0°C to 16.6°C) and water temperature (average seasonal temperature 0.6°C to 15.1°C), average seasonal diversity in our samples remained stable throughout the sampling period (**Table 2A**). Seasonal taxonomic diversity (Shannon diversity index) varied between 1.209 and 1.358, and seasonal functional diversity (Shannon diversity index) between 2.932 and 3.272. Season also appeared as a significant factor for both the taxonomic and functional diversity in the ANOVA (**Table 2B**). Taxonomic diversity was highest during winter 2018, which was a cold winter (average air temperature −4.0°C and solid ice cover at the sampling site for five consecutive sampling times), and lowest during winter 2019, which was a warm winter (average air temperature −1.5°C and solid ice cover at the sampling site for only two consecutive sampling times). Tukey multiple pairwise comparisons confirmed that the diversity of diatom communities was significantly different during the warm winter 2019 than during other seasons (**Table 2C**).

Our TBI analysis showed that temporal beta diversity was non-significant at the temporal sampling site and four of the spatio-temporal sites from June 2017 to September 2017, and from September 2017 to May 2019 (**Table 3**). The only significant temporal beta diversity occurred at the spatio-temporal sampling site 4, where the change was significant and negative from June 2017 to September 2017.

DISCUSSION

We studied the seasonal and inter-annual variation in the taxonomic and functional structure and diversity of littoral benthic diatom communities in the Baltic Sea, where seasons and years are climatically highly variable. Despite the importance

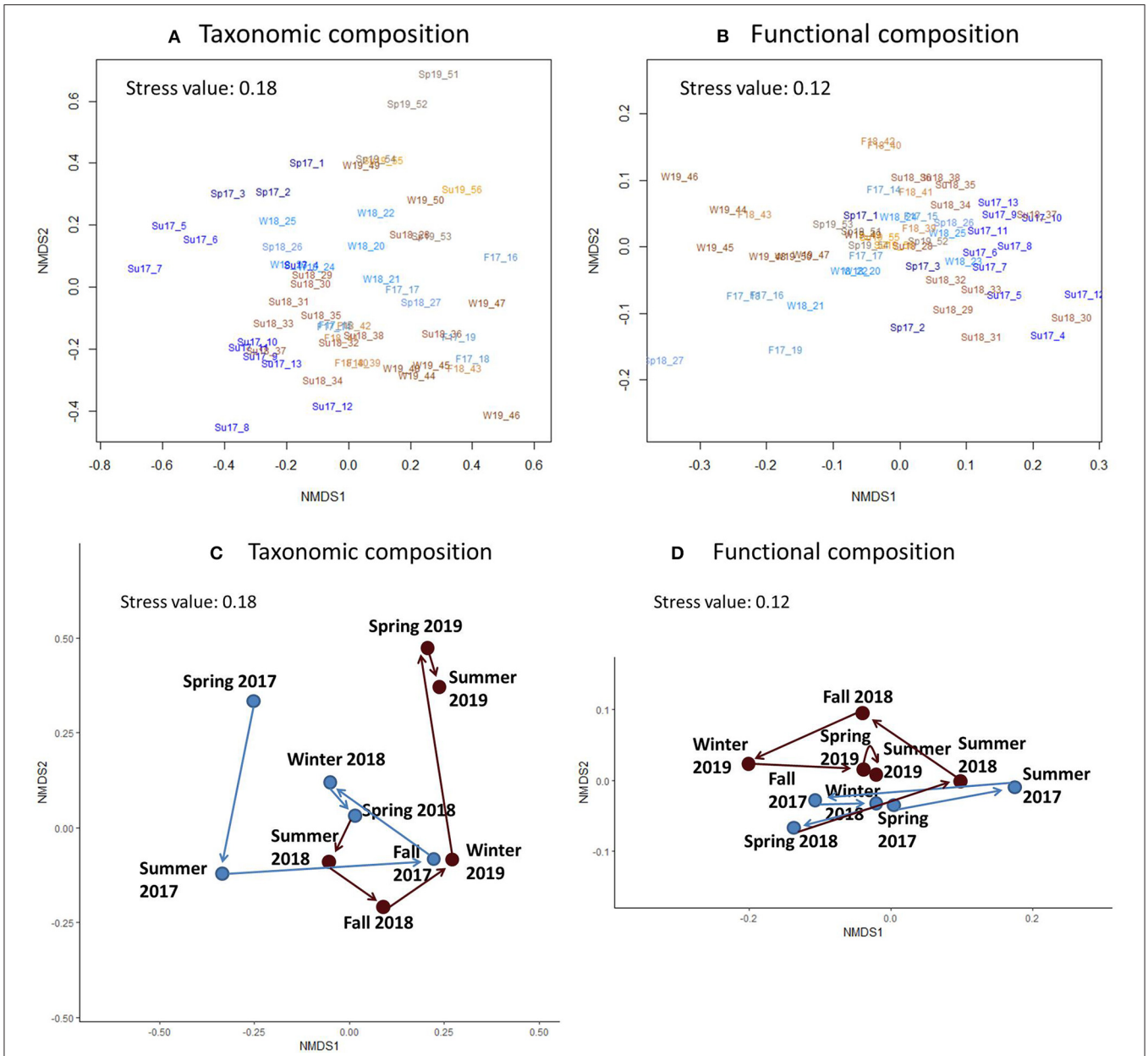

FIGURE 2 | Illustrations for Nonmetric Multidimensional Scaling (NMDS) for community composition. **(A,C)** Illustrate taxonomic composition, and **(B,D)** functional composition. **(A,B)** Illustrate all the sampling times. **(C,D)** Illustrate centroids calculated for the samples of each season, with arrows showing the directions of annual cycles in community composition. **(C,D)** Blue circles and arrows illustrate the cycle in community composition during the first sampling year, and the burgundy circles and arrows the cycle during the second sampling year. **(A,B)** Sp, spring; Su, summer; F, fall; W, winter; 17, year 2017; 18, year 2018; 19, year 2019. Numbers after the sampling year refer to the temporal order of samples.

of benthic communities for ecosystem functioning and services, seasonal and inter-annual changes are often overlooked, which compromises the effectiveness of monitoring and conservation efforts of these valuable ecosystems.

We collected samples at two-week-intervals for two consecutive years, from spring 2017 to summer 2019. There was considerable variation in air and water temperatures between seasons and years, year 2017–2018 featuring a cool summer and a cold winter, whereas 2018–2019 featuring the warmest ever recorded summer (Monicoast, 2019) and a mild winter. Due to the northern and continental/marine location of our sampling area, such strong seasonal and annual changes in climate are typical. Along with the climatic temperature changes, other factors that have previously been shown to affect diatom communities in the Baltic Sea and elsewhere, such as nutrient concentrations (Svensson et al., 2014), daytime length and light intensity (Yang and Flower, 2012), also vary seasonally in this area and may have had

TABLE 2 | (A) Mean and standard deviation for taxonomic and functional diversity (Shannon diversity index), water temperature and air temperature during seasons; **(B)** Results of the one-way ANOVA test to analyze the significance of the season for taxonomic and functional diversity; **(C)** Results of the Tukey Honest Significant Differences test to analyze pairwise differences between diversities of all seasons.

	Taxonomic diversity (Shannon diversity index)	Functional diversity (Shannon diversity index)	Water temperature (°C)	Air temperature (°C)	
(A)					
Season	Mean (SD)	Mean (SD)	Mean (SD)	Mean (SD)	
Summer 2017	1.289 (0.051)	3.195 (0.051)	13.6 (2.2)	14.0 (2.6)	
Fall 2017	1.243 (0.082)	3.089 (0.144)	6.8 (2.7)	4.1 (2.8)	
Winter 2018	1.358 (0.028)	3.217 (0.060)	0.6 (0.7)	−4.0 (4.3)	
Spring 2018	1.224 (0.173)	2.932 (0.356)	4.6 (1.6)	4.8 (2.2)	
Summer 2018	1.311 (0.031)	3.238 (0.071)	15.1 (4.7)	16.6 (3.6)	
Fall 2018	1.272 (0.041)	3.238 (0.107)	7.8 (2.2)	5.9 (4.0)	
Winter 2019	1.209 (0.056)	2.948 (0.132)	0.6 (0.7)	−1.5 (3.4)	
Spring 2019	1.315 (0.026)	3.272 (0.028)	4.0 (2.3)	4.8 (3.1)	
(B)					
	Df	**Sum of Squares**	**Mean Square**	**F value**	**Pr(>F)**
Season (taxonomic diversity)	9	0.056	0.006	2.176	0.041*
Season (functional diversity)	9	0.324	0.036	3.468	0.002**
(C)					
Taxonomic diversity	**Difference between means**	**Lower 95% confidence interval**	**Upper 95% confidence interval**	**Adjusted *p***	
Winter 2018 - winter 2019	−0.103	−0.202	−0.004	0.036*	
Functional diversity	**Difference between means**	**Lower 95% confidence interval**	**Upper 95% confidence interval**	**Adjusted *p***	
Summer 2017–winter 2019	−0.171	−0.338	−0.004	0.041*	
Summer 2018–winter 2019	−0.201	−0.365	−0.038	0.006**	
Fall 2018–winter 2019	−0.201	−0.399	−0.003	0.045*	
Winter 2019–spring 2019	0.225	0.013	0.437	0.030*	

*Only significant results are shown 0.001 ***, < 0.01 **, < 0.05 *. Spring 2017 and summer 2019 were excluded from the table, because our sampling period only covered a part of them.*

TABLE 3 | Temporal beta diversity according to temporal beta diversity indices (TBI) at our temporal sampling site and five spatial sites between **(A)** June 2017 and September 2017, and **(B)** September 2017 and May 2019.

	Temporal sampling site	Spatial sampling site 1	Spatial sampling site 2	Spatial sampling site 3	Spatial sampling site 4	Spatial sampling site 5
(A)						
TBI	0.504	0.487	0.443	0.392	**0.585**	0.293
p-value	0.1351	0.2336	0.5903	0.9212	**0.0015**	0.9999
Change	−	+	+	−	−	+
(B)						
TBI	0.525	0.544	0.517	0.491	0.545	0.386
p-value	0.3523	0.2108	0.4299	0.6488	0.2011	0.9966
Change	+	−	−	+	−	−

Significant values (p < 0.05) are bolded. TBI denotes total temporal beta diversity, + species gain, and – species loss.

an impact on the communities. In contrast, salinity, which often is the strongest driver of benthic diatom communities (Ulanova et al., 2009), remains highly similar throughout the year and was, thus, not likely to affect the communities in our study.

As we expected, this variation in environment led to highly variable taxonomic composition of communities between seasons and years, and also highly variable functional composition between seasons. Similar results of strong temporal variation have been found with different organisms in different ecosystems, such as soil microbes (Waldrop and Firestone, 2006), bacterioplankton (Van der Gucht et al., 2001), and fishes (Lazzari et al., 1999). However, our results disagree with several previous studies in the Baltic Sea, which have shown temporally stable community composition of benthic diatoms (Sabbe, 1993; Vilbaste et al., 2000). However, the duration of these studies has been remarkably shorter than ours, and they have been conducted on sedimentary soft bottoms, which may provide a more stable environment for the microphytobenthic organisms than stones.

However, the functional composition showed only low variation between years, and the alpha diversity of communities remained fairly stable between seasons and years. Such stable diversity patterns were discovered not only on our temporal sampling site but also on our five spatial sites, where we collected three samples during different seasons to validate our temporal results. This disagrees with studies conducted in other ecosystems, such as deep sea (Ramalho et al., 2014) and pelagic waters (Sabanci and Koray, 2011), but is in line with other benthic diatom studies in the Baltic Sea (Sabbe, 1993; Vilbaste et al., 2000). Reasons for the temporally stable diversity may include effective dispersal and large regional species pool, and consequent high functional redundancy of benthic microalgal communities. In other words, changing environmental conditions, such as water temperature, nutrients and light intensity, led to the disappearance of some species, but the seed bank, i.e., locally occurring resting stages of some species, the effective dispersal, and large regional species pool allowed them to be replaced by species that were favored by the new predominant conditions (Zobel, 1997). Hence, the communities were able to preserve high taxonomic diversity, which supported functional redundancy, i.e., complementarity of species traits that allows ecosystem stability throughout the year and also provides resilience against environmental change (Naeem et al., 2012).

Despite the similar result of temporally stable diversity in our study and other studies on benthic diatoms in the Baltic Sea, the diversity measured with Shannon's diversity index was remarkably lower in our study than in other studies in the same area. Our seasonal taxonomic mean diversity varied between 1.2 and 1.4, and seasonal functional mean diversity between 2.9 and 3.3, whereas, e.g., Vilbaste et al. (2000) found values of 2.8–5.2 for the taxonomic diversity of benthic diatom communities in the Gulf of Riga, Baltic Sea. Low diversity in our communities is astonishing, considering the fairly highly species richness, but we speculate that the low diversity is due to the dominance of a few species and, thus, low evenness of the communities.

Although the diversity of communities remained temporally fairly stable throughout our 2-year sampling period, we found the highest diversity of all seasons during the cold winter 2018 and the lowest diversity during the mild winter 2019. Taxonomic and functional diversity during the warm winter 2019 differed also significantly from several other seasons. Furthermore, the functional compositions of communities were different between winters, the cold winter 2018 featuring proportionally large amounts of large and high-growing species (traits: large-sized, pedunculate, pad-attached, colonial, and high-profile) and the warm winter 2019 small and mobile species (traits: small-sized, mobile, non-colonial, and motile). This finding of different response of small and large diatom species to environmental conditions is in agreement with Busse and Snoeijs (2002), who showed that small species were mostly affected by exposure to wave action and large species by salinity.

We speculate that the difference between winters in our study was due to differences in the duration of ice cover. Solid ice cover at the sampling site lasted for ca. 10 weeks during winter 2018 but only ca. 4 weeks during winter 2019. Microalgal studies in winter have concentrated on pelagic and sea-ice algae (e.g., Edgar et al., 2016; Enberg et al., 2018), which prevents comparing our results, but we speculate that low water temperature that always occurs during winter and wind-induced waves due to the lack of ice are cumulative stressors (Morin et al., 2015) that make species more vulnerable during ice-free winters. Thus, ice cover seems to be needed to protect high benthic diversity in winter. However, we only compared two consecutive years, and for broader conclusions on the effects of ice-cover or climate in general, studies covering longer time series are needed.

CONCLUSIONS

We showed that the diversity of benthic diatom communities is seasonally and inter-annually highly stable despite strong climatic variation and consequent changes in community composition. However, diversity seems to decrease during exceptionally warm winters possibly due to disturbances induced by the lack of ice. This may suggest that climate warming with smaller extent and shorter duration of ice cover will affect the diversity of benthic communities.

DATA AVAILABILITY STATEMENT

The raw data supporting the conclusions of this article will be made available by the authors, without undue reservation, to any qualified researcher.

AUTHOR CONTRIBUTIONS

LV, JS, and AN designed the study. LV conducted the field work, identified species, defined traits, conducted statistical analyses, and drafted the manuscript. All authors commented on the manuscript.

FUNDING

This work was supported by Walter and Andrée de Nottbeck Foundation (LV) and the Academy of Finland (Project ID 294853 to AN).

ACKNOWLEDGMENTS

We thank the staff at the Tvärminne Zoological Station: Tapio Rautalin and Jostein Solbakken for valuable help during winter sampling, and Noora Haavisto and Joanna Norkko for providing the climatic data.

SUPPLEMENTARY MATERIAL

The Supplementary Material for this article can be found online at: https://www.frontiersin.org/articles/10.3389/fmars.2020.00088/full#supplementary-material

Supplementary Table 1 | Sampling details.

Supplementary Table 2 | Species abundance table.

Supplementary Table 3 | Trait table.

REFERENCES

Busse, S., and Snoeijs, P. (2002). Gradient responses of diatom communities in the Bothnian Bay, Northern Baltic Sea. *Nova Hedwigia* 74, 501–525. doi: 10.1127/0029-5035/2002/0074-0501

Cadotte, M. W., Cavender-Bares, J., Tilman, D., and Oakley, T. H. (2009). Using phylogenetic, functional and trait diversity to understand patterns of plant community productivity. *PLoS ONE* 4:e5e5695. doi: 10.1371/journal.pone.0005695

Chapin, F. S., Zavaleta, E. S., Eviner, V. T., Naylor, R. L., Vitousek, P. M., Reynolds, H. L., et al. (2000). Consequences of changing biodiversity. *Nature* 405, 234–242. doi: 10.1038/35012241

Clarke, K. R. (1993). Non-parametric multivariate analyses of changes in community structure. *Aust. J. Ecol.* 18, 117–143. doi: 10.1111/j.1442-9993.1993.tb00438.x

Diatoms of North America (2019). Available online at: https://diatoms.org/ (accessed October 22, 2019).

Dray, S., Bauman, D., Blanchet, G., Borcard, D., Clappe, S., Guenard, G., et al. (2019). *Package "adespatial"*. Available online at: https://cran.r-project.org/web/packages/adespatial/adespatial.pdf (accessed October 15, 2019).

Edgar, R. E., Morris, P. F., Rozmarynowycz, M. J., D'souza, N. A., Moniruzzaman, M., Bourbonniere, R. A., et al. (2016). Adaptations to phytoautotrophy associated with seasonal ice cover in a large lake revealed by metatranscriptome analysis of a winter diatom bloom. *J. Great Lakes Res.* 42, 1007–1015. doi: 10.1016/j.jglr.2016.07.025

Enberg, S., Majaneva, M., Autio, R., Blomster, J., and Rintala, J. M. (2018). Phases of microalgal succession in sea ice and the water column in the Baltic Sea from autumn to spring. *Mar. Ecol. Prog. Ser.* 599, 19–34. doi: 10.3354/meps12645

European Environment Agency (2019). Available online at: https://www.eea.europa.eu/data-and-maps (accessed October 28, 2019).

Falkowski, P. G., Barber, R. T., and Smetacek, V. (1998). Biogeochemical controls and feedbacks on ocean primary production. *Science* 281, 200–206. doi: 10.1126/science.281.5374.200

Field, C. B., Behrenfeld, M. J., Randerson, J. T., and Falkowski, P. (1998). Primary production of the biosphere: integrating terrestrial and oceanic components. *Science* 281, 237–240. doi: 10.1126/science.281.5374.237

Finnish Meteorological Institute (2019). Available online at: https://en.ilmatieteenlaitos.fi/ (accessed October 22, 2019).

Forster, R. M., Creach, V., Sabbe, K., Vyverman, W., and Stal, L. J. (2006). Biodiversity-ecosystem function relationship in microphytobenthic diatoms of the Westerschelde estuary. *Mar. Ecol. Prog. Ser.* 311, 191–201. doi: 10.3354/meps311191

Gilbert, J. A., Field, D., Swift, P., Thomas, S., Cummings, D., Temperton, B., et al. (2010). The taxonomic and functional diversity of microbes at a temperate coastal site: a 'multi-omic' study of seasonal and diel temporal variation. *PLoS ONE* 5:e1e15545. doi: 10.1371/journal.pone.0015545

HELCOM (2019). Available onlione at: http://helcom.fi/baltic-sea-trends/data-maps (accessed October, 28 2019).

Hillebrand, H., Soininen, J., and Snoeijs, P. (2010). Warming leads to higher species turnover in a coastal ecosystem. *Glob. Change Biol.* 16, 1181–1193. doi: 10.1111/j.1365-2486.2009.02045.x

Hillebrand, H., and Sommer, U. (2000). Diversity of benthic microalgae in response to colonization time and eutrophication. *Aquat. Bot.* 67, 221–236. doi: 10.1016/S0304-3770(00)00088-7

Hobson, L. A., and McQuoid, M. R. (1997). Temporal variations among planktonic diatom assemblages in a turbulent environment of the southern Strait of Georgia, British Columbia, Canada. *Mar. Ecol. Prog. Ser.* 150, 263–274. doi: 10.3354/meps150263

Hodapp, D., Hillebrand, H., Blasius, B., and Ryabov, A. B. (2016). Environmental and trait variability constrain community structure and the biodiversity-productivity relationship. *Ecology* 97, 1463–1474. doi: 10.1890/15-0730.1

Kelly, M. G., Cazaubon, A., Coring, E., Dell'Uomo, A., Ector, L., Goldsmith, B., et al. (1998). Recommendations for the routine sampling of diatoms for water quality assessments in Europe. *J. Appl. Phycol.* 10, 215–224. doi: 10.1023/A:1008033201227

Krammer, K., and Lange-Bertalot, H. (1986). "Bacillariophyceae 1. Teil: naviculaceae," in *Süßwasserflora von Mitteleuropa,* eds H. Ettl, J. Gerloff, H. Heynig and D. Mollenhauer (Stuttgart: Gustav Fischer Verlag), 876.

Krammer, K., and Lange-Bertalot, H. (1988). "Bacillariophyceae 2. Teil: bacillariaceae, epithemiaceae, Surirellaceae," in *Süßwasserflora von Mitteleuropa,* eds H. Ettl, J. Gerloff, H. Heynig and D. Mollenhauer (Stuttgart: Gustav Fischer Verlag), 596.

Krammer, K., and Lange-Bertalot, H. (1991a). "Bacillariophyceae 3. Teil: centrales, fragilariaceae, eunotiaceae," in *Süßwasserflora von Mitteleuropa,* eds H. Ettl, J. Gerloff, H. Heynig and D. Mollenhauer (Stuttgart: Gustav Fischer Verlag), 576.

Krammer, K., and Lange-Bertalot, H. (1991b). "Bacillariophyceae 4. Teil: achnanthaceae, kritische ergänzungen zu navicula (Lineolatae) und Gomphonema," in *Süßwasserflora von Mitteleuropa,* eds H. Ettl, J. Gerloff, H. Heynig and D. Mollenhauer (Stuttgart: Gustav Fischer Verlag), 437.

Lazzari, M. A., Sherman, S., Brown, C. S., King, J., Joule, B. J., Chenoweth, S. B., et al. (1999). Seasonal and annual variations in abundance and species composition of two nearshore fish communities in Maine. *Estuaries* 22, 636–647. doi: 10.2307/1353051

Monicoast (2019). http://helsinki.fi/monicoast. (accessed October 25, 2019).

Morin, S., Bonet, B., Corcoll, N., Guasch, H., Bottin, M., and Coste, M. (2015). Cumulative stressors trigger incrased vulnerability of diatom communities to additional disturbances. *Microb. Ecol.* 70, 585–595. doi: 10.1007/s00248-015-0602-y

Morin, X., Fahse, L., de Mazancourt, C., Scherer-Lorenzen, M., and Bugmann, H. (2014). Temporal stability in forest productivity increases with tree diversity due to asynchrony in species dynamics. *Ecol. Lett.* 17, 1526–1535. doi: 10.1111/ele.12357

Naeem, S., Duffy, J. E., and Zavaleta, E. (2012). The functions of biological diversity in an age of extinction. *Science* 336, 1401–1406. doi: 10.1126/science.1215855

Nagendra, H. (2002). Opposite trends in response for the Shannon and Simpson indices of landscape diversity. *Appl. Geogr.* 22, 175–186. doi: 10.1016/S0143-6228(02)00002-4

Nelson, D. M., Treguer, P., Brzezinki, M. A., Leynaert, A., and Queguiner, B. (1995). Production and dissolution of biogenic silica in the ocean – Revised global estimates, comparison with regional data and relationship to biogenic sedimentation. *Global Biogeochem. Cy.* 9, 359–372. doi: 10.1029/95GB01070

Oberbeckmann, S., Loeder, M. G., Gerdts, G., and Osborn, A. M. (2014). Spatial and seasonal variation in diversity and structure of microbial biofilms on marine plastics in Northern European waters. *Fems Microbiol. Ecol.* 90, 478–492. doi: 10.1111/1574-6941.12409

Oksanen, J. (2019). *Package "vegan"*. Available onlone at: https://cran.r-project.org/web/packages/vegan/vegan.pdf (accessed October 22, 2019).

Passy, S. I. (2017). Framework for community functioning: synthesis of stress gradient and resource partitioning concepts. *PEERJ* 5:e3885. doi: 10.7717/peerj.3885

R Development Core Team (2019). *The R Project for Statistical Computing*. Retrieved from: http://www.R-project.org

Ramalho, S. P., Adao, H., Kiriakoulakis, K., Wolff, G. A., Vanreusel, A., and Ingels, J. (2014). Temporal and spatial variation in the Nazare Canyon (Western Iberian margin): Inter-annual and canyon heterogeneity effects on meiofauna biomass and diversity. *Deep-sea Res. Pt I* 83, 102–114. doi: 10.1016/j.dsr.2013.09.010

Rimet, F., and Bouchez, A. (2012). Life-forms, cell-sizes and ecological guilds of diatoms in European rivers. *Knowl. Manag. Aquat. Ec.* 406:01. doi: 10.1051/kmae/2012018

Sabanci, F. C., and Koray, T. (2011). Annual variation in the diversity, species richness and composition of the phytoplankton assemblages in the Izmir Bay (Eastern Aegean). *Turk. J. Fish Aquat. Sci.* 11, 303–314. doi: 10.4194/trjfas.2011.0215

Sabbe, K. (1993). Short-term fluctuations in benthic diatom numbers on an intertidal sandflat in the Westerschelde estuary (Zeeland, the Netherlands). *Hydrobiologia* 269, 275–284. doi: 10.1007/BF00028026

Shannon, C. E., and Weaver, W. (1962). *The Mathematical Theory of Communication*. Urbana, IL: University of Illinois Press.

Smetacek, V. (1999). Diatoms and the ocean carbon cycle. *Protist* 150, 25–32. doi: 10.1016/S1434-4610(99)70006-4

Smith, V. H. (2007). Microbial diversity-productivity relationships in aquatic ecosystems. *Fems. Microbiol. Ecol.* 62, 181–186. doi: 10.1111/j.1574-6941.2007.00381.x

Snoeijs, P. (1993). *Intercalibration and Distribution of Diatom Species in the Baltic Sea Volume 1*. Uppsala: Opulus Press.

Snoeijs, P., Busse, S., and Potapova, M. (2002). The importance of diatom cell size in community analysis. *J. Phycol.* 38, 265–272. doi: 10.1046/j.1529-8817.2002.01105.x

Snoeijs, P., and Kasperovicienė, J. (1996). *Intercalibration and Distribution of Diatom Species in the Baltic Sea Volume 4*. Uppsala: Opulus Press.

Snoeijs, P., and Potapova, M. (1995). *Intercalibration and Distribution of Diatom Species in the Baltic Sea Volume 3*. Uppsala: Opulus Press.

Snoeijs, P., and Vilbaste, S. (1994). *Intercalibration and Distribution of Diatom Species in the Baltic Sea Volume 2*. Uppsala: Opulus Press.

Spilling, K., Olli, K., Lehtoranta, J., Kremp, A., Tedesco, L., Tamelander, T., et al. (2018). Shifting diatom-dinoflagellate dominance during spring bloom in the Baltic Sea and its potential effects on biogeochemical cycling. *Front. Mar. Sci.* 5:327. doi: 10.3389/fmars.2018.00327

Svensson, F., Norberg, J., and Snoeijs, P. (2014). Diatom cell size, coloniality and motility: trade-offs between temperature, salinity and nutrient supply with climate change. *PLoS ONE* 9:e1e109993. doi: 10.1371/journal.pone.0109993

SYKE (2019). *Ladattavat Paikkatietoaineistot*. Available online at: https://www.syke.fi/fi-FI/Avoin_tieto/Paikkatietoaineistot (accessed October, 28 2019).

Ulanova, A., Busse, S., and Snoeijs, P. (2009). Coastal diatom-environment relationships in the brackish Baltic Sea. *J. Phycol.* 45, 54–68. doi: 10.1111/j.1529-8817.2008.00628.x

Van der Gucht, K., Sabbe, K., De Meester, L., Vloemans, N., Zward, G., Gillis, M., et al. (2001). Contrasting bacterioplankton community composition and seasonal dynamics in two neighbouring hypertrophic freshwater lakes. *Environ. Microbiol.* 3, 680–690. doi: 10.1046/j.1462-2920.2001.00242.x

Vilbaste, S., Sundback, K., Nilsson, C., and Truu, J. (2000). Distribution of benthic diatoms in the littoral zone of the Gulf of Riga, the Baltic Sea. *Eur. J. Phycol.* 35, 373–385. doi: 10.1080/09670260010001735981

Virta, L., Gammal, J., Järnström, M., Bernard, G., Norkko, J., and Norkko, A. (2019). The diversity of benthic diatoms affects ecosystem productivity in heterogeneous coastal environments. *Ecology* 100:e02765. doi: 10.1002/ecy.2765

Waldrop, M. P., and Firestone, M. K. (2006). Seasonal dynamics of microbial community composition and function in oak canopy and open grassland soils. *Microb. Ecol.* 52, 470–479. doi: 10.1007/s00248-006-9100-6

Wickham, H. (2019). *Package 'ggplot2'*. Available online at: https://cran.r-project.org/web/packages/ggplot2/ggplot2.pdf (accessed January 14, 2020).

Winegardner, A. K., Legendre, P., Beisner, B. E., and Gregory-Eaves, I. (2017). Diatom diversity patterns over the past c. 150 years across the conterminous United States of America: identifying mechanisms behind beta diversity. *Global Ecol. Biogeogr.* 26, 1303–1315. doi: 10.1111/geb.12640

Yang, H., and Flower, R. J. (2012). Effects of light and substrate on the benthic diatoms in an oligotrophic lakes: a comparison between natural and artificial substrates. *J. Phycol.* 48, 1166–1177. doi: 10.1111/j.1529-8817.2012.01201.x

Zobel, M. (1997). The relative role of species pools in determining plant species richness. An alternative explanation of species coexistence? *Trends Ecol. Evol.* 12, 266–269. doi: 10.1016/S0169-5347(97)01096-3

Conflict of Interest: The authors declare that the research was conducted in the absence of any commercial or financial relationships that could be construed as a potential conflict of interest.

frontiers in Marine Science

ORIGINAL RESEARCH
published: 25 February 2020
doi: 10.3389/fmars.2020.00036

Assessing Alternative Microscopy-Based Approaches to Species Abundance Description of Intertidal Diatom Communities

Lourenço Ribeiro[1,2], Vanda Brotas[2], Tania Hernández-Fariñas[3], Bruno Jesus[1] and Laurent Barillé[1]*

[1] EA 2160, Laboratoire Mer Molécules Santé, University of Nantes, Nantes, France, [2] Center for Marine and Environmental Sciences, Lisbon, Portugal, [3] IFREMER, LER/N, Avenue du Général de Gaulle, Port-en-Bessin-Huppain, France

OPEN ACCESS

Edited by:
David M. Paterson, University of St Andrews, United Kingdom

Reviewed by:
Graham J. C. Underwood, University of Essex, United Kingdom
Craig Plante, College of Charleston, United States

***Correspondence:**
Lourenço Ribeiro
llribeiro@fc.ul.pt

Specialty section:
This article was submitted to Marine Ecosystem Ecology, a section of the journal Frontiers in Marine Science

Received: *15 October 2019*
Accepted: *20 January 2020*
Published: *25 February 2020*

Citation:
Ribeiro L, Brotas V, Hernández-Fariñas T, Jesus B and Barillé L (2020) Assessing Alternative Microscopy-Based Approaches to Species Abundance Description of Intertidal Diatom Communities. Front. Mar. Sci. 7:36. doi: 10.3389/fmars.2020.00036

Diatoms usually dominate microphytobenthic biofilms in coastal and estuarine intertidal environments. Yet, functional studies on biofilms often skip species analysis because benthic diatoms are notoriously difficult to extract from sediments and challenging to identify at that taxonomic level. Valid, less time-consuming alternatives would surely be welcomed and increase the inclusion of community structure information in microphytobenthos (MPB) ecophysiological studies. Starting with an original 181-species abundances matrix (OSM), obtained during a 2-year spatial–temporal survey in a Tagus Estuary intertidal flat with contrasting sediment textures, the current study assessed the effectiveness of several approaches to species abundances analysis. The effect of excluding abundance data or rare species, the influence of taxonomic resolution, or the use of size-based metrics on biotic multivariate patterns was examined by an objective comparison that replicated these different approaches on three different levels: (1) inter-matrix correlations, (2) performance in several non-parametric multivariate analyses (ANOSIM, MDS), and (3) correlations with the environmental dataset. When compared with the OSM, all matrices had strong or very strong positive correlations. All discriminated successfully spatial patterns, separating well assemblages from sandy and muddy sediments, and all had significant correlations with the environmental dataset. Apart from the relative biovolume species matrix (BSM), only the species matrices were able to discriminate significantly temporal patterns. The exclusion of the rarest species (48% of total) had a negligible effect, with the common and original species abundances matrices having a $\rho > 0.99$ correlation. Of the alternative approaches to species abundances, species presence/absence and the genera abundances matrices yielded the best results overall. Genera presence/absence and the size-class matrices had intermediate performances, with the former performing comparatively poorly with regard to seasonal patterns. BSM had the lowest correlation with the environmental variable dataset ($\rho = 0.598$) and the worst overall performance in the other multivariate routines. This means that either a high-taxonomic resolution

qualitative analysis (i.e. species presence/absence) or, in alternatively, a genus-level analysis retaining abundance data may be sufficient to describe basic spatial differences in estuarine intertidal flats. However, if seasonal variations in mudflat diatom assemblage structure are to be detected, species-level abundance data are still necessary.

Keywords: diatoms, community structure, intertidal flats, microphytobenthos, multivariate analysis, taxonomic sufficiency

INTRODUCTION

Diatoms are usually the most ubiquitous and dominant microalgal component of the microphytobenthos (MPB) communities in intertidal estuarine and coastal areas (MacIntyre et al., 1996; Hamels et al., 1998; Méléder et al., 2007). They form dense biofilms on the sediment surface during low tides (Consalvey et al., 2004) and, through the production of extracellurar polymeric substances (EPS), play a pivotal role in intertidal sediment stabilization (Stal, 2010; Passarelli et al., 2014). Since Admiraal (1984) published his classic review on the ecology of estuarine sediment-inhabiting diatoms, research on MPB has greatly expanded in many different fields, such as nutrient cycling (Cabrita and Brotas, 2000), carbon transfers (Middleburg et al., 2000) or benthic–pelagic coupling (de Jonge and van Beusekom, 1995; Hernández Fariñas et al., 2017), biofilm vertical migration, and diatom photoprotective mechanisms (Van Colen et al., 2014; Marques da Silva et al., 2017). While the knowledge on the MPB functional aspects has improved decisively during that period, the structural aspects of these diatom-dominated communities (i.e. species taxonomy, distribution, and diversity) have been more scantily studied and only represent 20% of overall MPB publications of the last 30 years (Park et al., 2014).

This trend is a consequence of the inherent difficulty of sampling and identifying marine and coastal benthic diatoms, which is rooted in many causes: (1) benthic microalgae are notoriously difficult to extract from the sediment (Muylaert et al., 2002); (2) a paucity of comprehensive taxonomic monographs (Sullivan and Currin, 2002; Trobajo and Sullivan, 2010) makes species identification and intercomparison between studies problematic (Underwood and Barnett, 2006); (3) the number experienced diatomists (i.e. phycologists specialized in diatom taxonomy) that routinely work on MPB assemblages in the last decades is only a small fraction of the ones working in freshwater benthic systems or with coastal phytoplankton (Ribeiro, 2010). This means that research topics that rely on sound species-level identification and cell counts, such as distributional studies (Underwood et al., 1998) or the establishment of a diatom-based water quality index for estuaries, remain seriously underdeveloped (Trobajo and Sullivan, 2010).

Not surprisingly, current MPB functional studies tend to ignore species composition altogether and focus only on the MPB biofilm, in a "black-box" approach (Kociolek and Stoermer, 2001a; Underwood, 2005). Ideally, both structural and functional attributes of intertidal diatom assemblages should be investigated simultaneously (McIntire and Moore, 1977; Kociolek and Stoermer, 2001b) and there are recent examples where the ecophysiology of the biofilms was complemented with their species composition (Serôdio et al., 2012; Vieira et al., 2013; Cartaxana et al., 2015). However, there are often limitations that impede MPB ecologists from pursuing complementary detailed community descriptions to their main research aims, such as time, budget, and/or expert availability for collaborations. Therefore, alternatives to very labor-intensive species abundances datasets would surely be welcomed by MPB researchers eager to add a realistically achievable structural description of the diatom assemblages which could lead to a better understanding of the biofilm processes they are studying.

To our knowledge, this question has not been addressed within the context of MPB research (Ribeiro, 2010), although it has been consistently explored by community ecologists that rely on benthic invertebrate assemblages (Jones, 2008), phytoplankton (Carneiro et al., 2010), or freshwater diatoms from lentic and lotic systems (Kelly, 2013) as biological quality elements in environmental monitoring and bioassessment programs. Consequently, there has been a strong incentive to find more cost-effective alternatives to species-level analysis. Most of the discussion concerns taxonomic sufficiency, which is the minimum taxonomic resolution needed to meet the study objective (Ellis, 1985). According to this concept, only a small set of species (e.g. Clarke and Warwick, 1998) or easier-to-identify higher taxonomical levels (e.g. Olsgard et al., 1997; Lavoie et al., 2009; Menezes et al., 2010; Rimet and Bouchez, 2012a) may be required to adequately describe community patterns and their responses to natural or anthropogenic disturbances. Several other aspects concerning community description have also been pursued, such as: (1) the consequences of different transformations of abundances-by-sample data in multivariate analysis (e.g. Thorne et al., 1999; Heino, 2008); (2) the suitability of qualitative, presence/absence species datasets (Carballo and Naranjo, 2002); (3) the effect of rare species exclusion (e.g. Cao and Williams, 1999; Marchant, 1999); (4) the importance of cell size (Wunsam et al., 2002; Lavoie et al., 2006, 2010); and (5) the use of life-forms or ecological guilds as functional surrogates to taxonomic units (Simberloff and Dayan, 1991; Passy, 2007; Rimet and Bouchez, 2012b).

All these avenues warrant further investigations using intertidal diatom assemblage data. The works by Somerfield and Clarke (1995) and Olsgard et al. (1997, 1998) on marine macrofauna communities seem to provide a useful framework to do so. In this study, we tested the principle of taxonomic sufficiency on a dataset with a high taxonomic resolution collected by Ribeiro (2010). This dataset encompasses diatom communities in contrasting intertidal flats and provided an

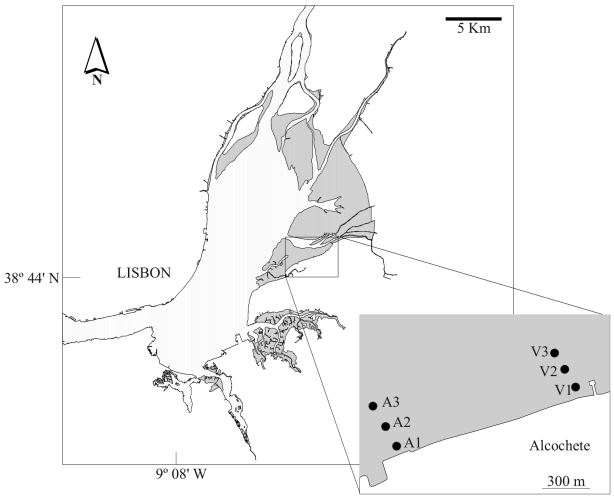

FIGURE 1 | Study area. Sampling stations identified by the letters in the box, gray areas represent intertidal areas.

opportunity to evaluate and test several alternative approaches to species-level community description in MPB research.

MATERIALS AND METHODS

Detailed descriptions of the study site, sampling procedures, environmental parameters, and diatom analysis (e.g. MPB extraction, slide preparation, and cell counts) are given elsewhere (Jesus et al., 2006, 2009; Ribeiro, 2010; Ribeiro et al., 2013). Sampling was conducted between 2003 and 2004 in a total of 12 bimonthly sampling campaigns. The sampling area consisted of two transects on the eastern shore of the Tagus estuary, each transect with three sampling stations running perpendicular to the shore (**Figure 1**). Sampling stations could be divided into three main groups, regarding their sediment texture: station A1 had fine and medium sands with almost no mud content; three stations were mainly composed by medium and coarse sands with an average mud fraction between 5 and 14% from the sandiest to the muddiest (i.e. A2 and A3 to V1, respectively); and two stations (V2 and V3) were muddy and had almost no sand content (Jesus et al., 2006; Ribeiro et al., 2013).

Matrices and Data Transformation

Ribeiro (2010) and Ribeiro et al. (2013) described in detail the spatial–temporal variation of this intertidal diatom community, its diversity patterns, and other features related to community physiognomy, such as life-form and size-class distributions. The original species abundance matrix (OSM) is composed by a total of 181 diatom taxa that were identified and counted in the 68 collected samples (Ribeiro, 2010; see **Supplementary Material** for original matrix). The abundances were standardized and are presented as relative percentages. All the derived matrices used in this study stem from the OSM, either by data transformation, species selection, and/or species abundance aggregation, with the objective of evaluating and comparing their performance using non-parametric multivariate tools, found in PRIMER® 6 software package (Clarke and Gorley, 2006). They are listed, together with their composition, type, transformation of data, and aims, in **Table 1**. They can be divided in two main groups that represent the two different facets of community structure analysis that are explored within the framework of the current study, namely metrics selection and taxonomic sufficiency.

Metrics Selection

These matrices retained their species-level resolution in order to test the effect of two main data transformations. Transformations downweigh the influence of dominant taxa to varying degrees (Field et al., 1982). OSM abundance data suffered the following transformations: (1) presence/absence. This transformation downweighs completely the species abundance data and shifts the emphasis to changes in taxonomic composition only (Clarke and Warwick, 2001). The aim of the presence/absence species matrix (0–1 SM) is to replicate an approach that only studies the assemblages qualitatively and, consequently, saves the time needed for cell counting; (2) biovolume. The biovolume species matrix (BSM) is based on the relative contribution of each taxon to the total biovolume of the assemblage (cf. Haubois et al., 2005) and can also be considered a severe data transformation. For each sample, the weighted relative biovolume of each taxon derived from its relative abundance and from its previously calculated median biovolume. This approach counters the over-estimation of the abundant small diatoms, which may actually contribute to a small fraction of the overall biomass (Hillebrand et al., 1999), while still retaining a high taxonomical resolution (Snoeijs et al., 2002). Cell biovolume calculation was based on equations proposed by Hillebrand et al. (1999) and derived from biometric measurements made by Ribeiro (2010).

Taxonomic Sufficiency

These matrices either aggregated species abundances to a higher taxonomic level or to a taxonomic surrogate or, in alternative, retained the species-level analysis to a restricted set of common species or to the species from a single genus. Three main approaches were followed:

(a) Taxa selection – two different lines were included in this approach: (1) Exclusion of rare taxa. A common species matrix (CSM), with no data transformation, included only species with more than two occurrences and/or that surpassed, at least in one sample, 1% of abundance and it was composed by 94 species. This allows a direct comparison with the OSM and, thus, to solely assess the effect of the exclusion of rare taxa. Ribeiro et al. (2013) used the same 94-species matrix but fourth-root transformed the abundance data. It is referred in the present study as Transformed Species Matrix (TSM) in order to allow a linkage between both works; (2) Focus on a single genus. *Navicula* was the most diverse and abundant genus in the OSM. The NAV matrix only retains the 29 species of *Navicula* and was root-transformed to counter the overwhelming preponderance of a handful of very abundant species.

TABLE 1 | Different matrices used in this study, with number of taxa, type and data transformation, as well as the details on the methodological approach of each dataset.

Approach		Matrix	Number of taxa/classes	Type and transformation of data	Methodological details of the approach
Metrics	Data transformation	Original species matrix (OSM)	181	Abundance; no transformation	Cell counts; high taxonomic resolution
		Species presence–absence (0–1 SM)	181	Qualitative; presence/absence	No cell counts; high taxonomic resolution
		Species biovolume (BSM)	181	Weighted relative biovolume	Cell counts; high taxonomic resolution; morphometric measurements
	Taxa selection	Common species matrix (CSM)	94	Abundance; no transformation	Cell counts; high taxonomic resolution; rare species exclusion
		Transformed species matrix (TSM)	94	Abundance; 4th root transformation	Cell counts; high taxonomic resolution; rare species exclusion
Taxonomic sufficiency		Navicula (NAV)	29	Abundance; root transformation	Cell counts; high taxonomic resolution but of just one genus
	Taxonomic resolution	Genera (GM)	57	Abundance; no transformation	Cell counts; low taxonomic resolution
		Genera presence–absence (0–1 GM)	57	Qualitative; presence/absence	No cell counts; low taxonomic resolution
	Taxonomic surrogacy	Size-classes (SCM)	4	Abundance; no transformation	Cell counts; morphometric measurements; no taxonomic identification

(b) Taxonomic resolution – the effect of reducing taxonomic resolution is tested in this approach. The species abundances found in OSM were aggregated to the genus level (57 genera) in a genus matrix (GM). Higher taxonomic levels were not pursued because suprageneric relationships in diatoms remain largely unknown (Cox, 2009) and a major restructuring of the current diatom classifications is still an ongoing process (Williams and Kociolek, 2007, 2010). A presence/absence GM (0–1 GM) was also created.

(c) Taxonomic surrogacy – One trait-based abundance matrix was assessed and compared with the taxonomy-based ones. The size-class matrix (SCM) were obtained from the OSM by simple aggregation of species abundance in the four size-classes described by Ribeiro (2010) and which comprised the very small ($<100\ \mu m^3$), small ($100–250\ \mu m^3$), medium-sized ($250–1000\ \mu m^3$), and large ($>1000\ \mu m^3$) diatoms. Given the low number of categories, the data were not transformed.

Matrix Comparison and Multivariate Analysis

Similarity matrices, also known as resemblance matrices, were constructed from the matrices listed in **Table 1** using the Bray–Curtis distance (Bray and Curtis, 1957). The multivariate patterns on these datasets were then compared to each other in three different ways:

(1) Inter-matrix correlations: Following the method described in Somerfield and Clarke (1995), the rank correlation coefficient (Spearman's ρ) between all the elements of any pair of similarity matrices with matching set of samples can be calculated. All inter-matrix rank correlations were determined, thus allowing a construction of a second similarity matrix, which was used as input matrix of a "second-stage" non-metric MDS (Somerfield and Clarke, 1995). This ordination permits simultaneous comparisons of all datasets and allows to perceive the relative effect of the different approaches and transformation of the data. Given that all matrices stem from the same OSM, they are not independently derived and a permutation test between resemblance matrices cannot be applied (Clarke, 1993).

(2) Effect on multivariate analyses (ANOSIM, MDS): Also following the approach proposed by Somerfield and Clarke (1995), the effect on subsequent non- parametric multivariate routines for each matrix listed in **Table 1** was examined. An analysis of similarities permutation test, with a two-way crossed (with no replicates) layout (ANOSIM, Clarke and Warwick, 1994), was done on each similarity matrix to examine the significance of differences between all stations and sampling dates. Multidimensional scaling (MDS) ordinations were performed to better visualize the multivariate patterns of different similarity matrices (Clarke, 1993; Clarke and Warwick, 2001).

(3) The relationships between patterns in multivariate structure and the environmental dataset collected simultaneously to the MPB sediment samples were examined using the BEST significance test procedure (Clarke et al., 2008). This analysis computes the Spearman's rank (ρ) correlation between the biotic and abiotic dissimilarity matrices and selects the subset of environmental variables that scores the highest ρ, thus choosing the combination of variables that maximizes the match between the biotic and abiotic datasets. In addition, the statistical significance of this match is given by a global match permutation test of the null hypothesis $\rho = 0$ (999 permutations of sample labels for a H_0 rejection at $p < 0.1\%$). The environmental dataset was

TABLE 2 | Pairwise Spearman's rank correlation between similarity matrices.

Matrices	OSM	0–1 SM	BSM	CSM	TSM	NAV	GM	0–1 GM
Original species matrix (OSM)								
Species presence–absence (0–1 SM)	0.8143							
Species biovolume (BSM)	0.7451	0.5057						
Common species matrix (CSM)	**0.9999**	0.8137	0.7445					
Transformed species matrix (TSM)	**0.9109**	**0.9709**	0.6154	**0.9108**				
Navicula (NAV)	0.8856	0.5812	0.7450	0.8854	0.7067			
Genera (GM)	0.8410	0.7623	0.5692	0.8410	0.8236	0.6094		
Genera presence–absence (0–1 GM)	0.7248	**0.9343**	0.4568	0.7246	0.8900	0.4978	0.6737	
Size-classes (SCM)	0.8655	0.7290	0.6099	0.8665	0.7978	0.7989	0.7033	0.6537

All correlations significantly different from zero by a permutation test at $p < 0.1\%$ (999 permutations) but as they all stem from the same original species matrix (OSM) this test is not independent. Correlations >0.9 are in bold.

the one used by Ribeiro et al. (2013) and included: tidal height; sediment temperature; light (i.e. Photosynthetic Photon Flux Density, PPFD); porewater salinity; NH_4^+, NO_2^-, NO_3^-, PO_4^{3-}, and SiO_2^- porewater concentrations; organic matter content (i.e. ash-free dry weight); and sediment grain size composition (following the Wentworth grade scale for grain size). Sediment water content had a very high Pearson's correlation with mud content (i.e. % grains < 63 μm), so only the latter was included in the analysis.

RESULTS

The interrelationships between the different approaches and the inter-matrix correlations (**Table 2**) can be visualized in the "second-stage" MDS (**Figure 2**), where a bigger proximity between two similarity matrices in the MDS ordination reflects a higher pairwise Spearman's rank correlation. The first striking result is the fact that original species matrix (OSM) and the CSM scored an almost perfect correlation ($\rho = 0.9999$), which can be perceived by the superposition of both points in **Figure 2**. The TSM scored slightly lower correlations with both OSM and CSM ($\rho = 0.911$), thus implying that the fourth-root transformation of the dataset had a greater effect than the reduction from initial 181 taxa (in the OSM) to 94 common taxa (both in CSM and TSM). This is further reinforced by the higher correlation of TSM to both species (0–1 SM, $\rho = 0.971$) and genera (0–1 SM, $\rho = 0.934$) presence/absence matrices, as both transformations reduce or nullify, in the case of the presence/absence, the weight and influence of the high abundances of the dominant species in the assemblages.

The 57-taxa genera abundance matrix (GM) scored a lower correlation to the OSM ($\rho = 0.841$) than the 29-taxa *Navicula* species abundance matrix (NAV, $\rho = 0.886$) or than the size-class abundance matrix (SCM, $\rho = 0.866$), which was composed of only four categories. The correlation between both genera matrices was also comparatively lower ($\rho = 0.674$) when compared to other inter-matrix correlations, namely between species-level ones. The exception was the species biovolume matrix (BSM) which, despite its high taxonomic resolution, scored the second lowest correlation with the OSM ($\rho = 0.745$). Moreover, its isolated

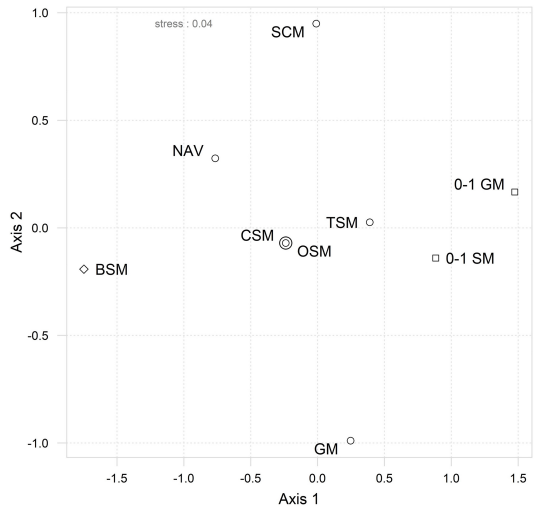

FIGURE 2 | Second-stage ordination by MDS of ranked inter-matrix pairwise Spearman rank correlations. Resemblance matrices included: Original (OSM), common (CSM), transformed (TSM) and *Navicula* species abundances matrices; species relative biovolume (BSM) and genera abundances (GM) datasets; species (0–1 SM) and genera (0–1 GM) presence–absence datasets; size-class abundances dataset (SCM). The symbols represent the type of metrics used in each matrix: abundance data (○), presence/absence (□), and weighted biovolume (◇).

position in MDS ordination (**Figure 2**) indicates comparatively low correlations with all other matrices. Nonetheless, all matrices scored a correlation above $\rho > 0.7$ with the OSM, which means that most of the matrices should give correlated to highly correlated patterns in their analyses (**Table 2**).

The MDS ordinations of the diatom assemblage data from the Tagus estuary (**Figure 3**) indicate that the overall patterns of community structure are mostly retained. Even as "raw data," available in the OSM, it clearly shows a distinction between diatom assemblages from sandy stations and assemblages from muddy stations (i.e. V2 and V3). The assemblages found in the low mud-content/fine sand station A1 are usually the furthest away from the mudflat ones, with the mixed sediment, muddy–sandy assemblages of stations A2, A3, and V1 between them.

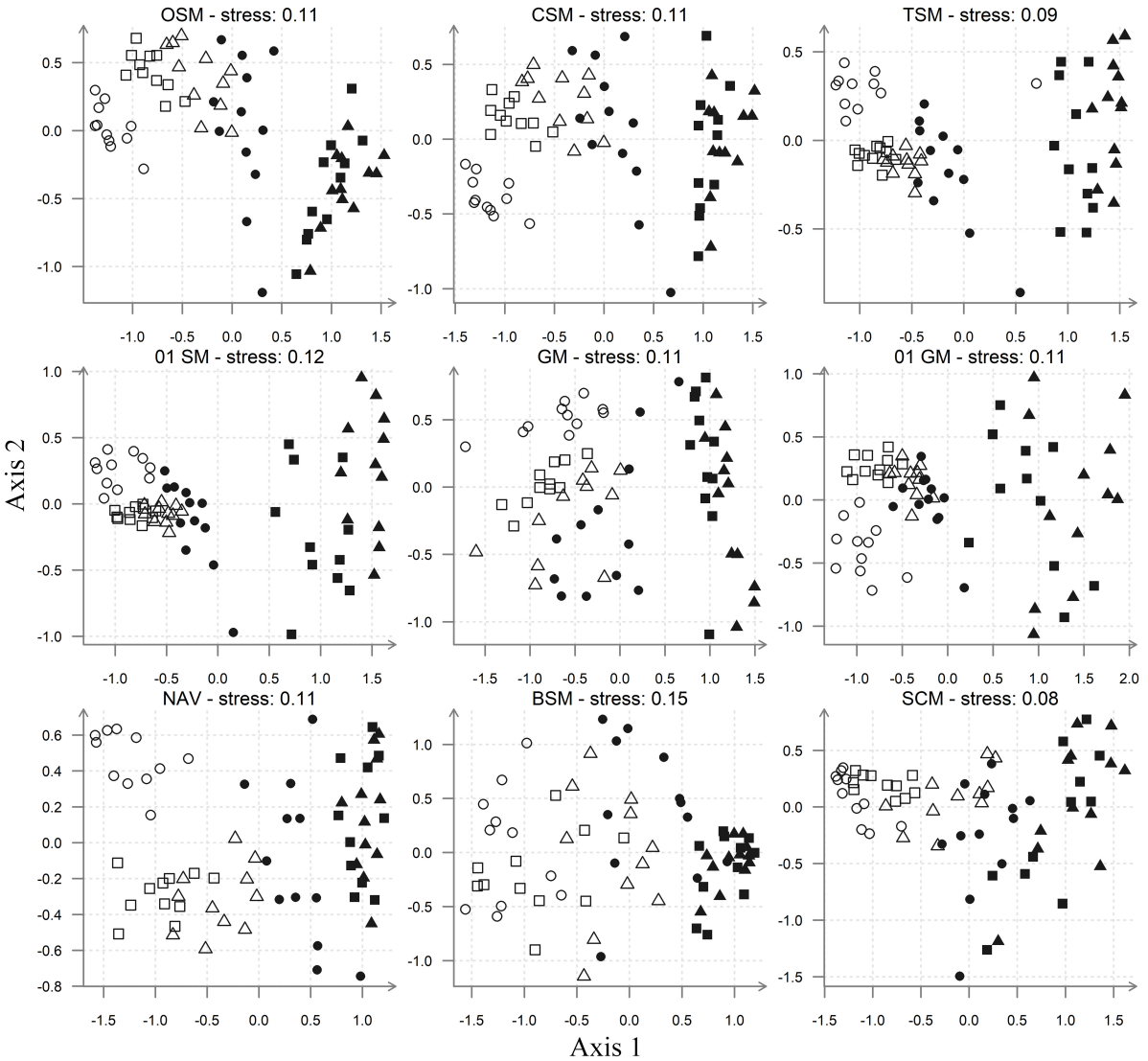

FIGURE 3 | MDS ordinations, based on Bray–Curtis similarity. Resemblance matrices included: Species (OSM, CSM, TSM, and *Navicula*) and genera (GM) abundances datasets; species relative biovolume dataset (BSM); species (0–1 SM) and genera presence–absence datasets (0–1 GM); size-class abundances datasets (SCM). Sampling stations: A1 (○), A2 (□), A3 (Δ), V1 (●), V2 (■), V3 (▲).

This pattern is repeated in all other ordinations, although in the case of the BSM it becomes much less obvious. Moreover, in the latter MDS, the mudflat samples cluster together, while the sandflat ones are much less aggregated, a pattern that is the inverse of the one observed in all other MDS ordinations. With all other species-level matrices (OSM, CSM, TSM, NAV, and 0–1 SM) it was also possible to separate clearly the assemblages of the station A1 from the other assemblages, collected in the mixed sediment, medium sandy stations (i.e. A2, A3, and V1). The separation between these two types of sandflat assemblages was less discernible with the genera and size-class matrices (**Figure 3**).

The results of the ANOSIM tests showed that all matrices were able to discriminate significantly the spatial differences, but only species-level matrices rejected both null hypotheses of the two-way ANOSIM test (**Table 3**). The genera presence/absence matrix (0–1 GM), with a significance probability of 16.3%, clearly failed to reject the null hypothesis that there were no temporal differences (test significance level $p < 0.01\%$), while the species biovolume (BSM), genera abundances (GM), and size-classes (SCM) matrices failed to reject the second null hypothesis at a much lower probability level. The global R for differences between sites ranged from 0.93 (TSM) to 0.67 (SCM). Apart from BSM, the species matrices had slightly higher R-values for both differences between sites and differences between sampling dates, when compared to the genera and size-classes matrices. The *Navicula* dataset had the highest global R for temporal differences

TABLE 3 | Comparison of different approaches used to study the multivariate structure of the diatom communities.

	Two-way ANOSIM global *R*	Non-rejected hypotheses in the two-way ANOSIM tests (*p*-values)	BEST (ρ)	Highest correlated environmental variable set
Original species matrix (OSM)	Sites: 0.855		0.83	Tidal height, coarse sand, medium sand, mud
	Date: 0.219			
Species presence–absence (0–1 SM)	Sites: 0.927		0.822	Mud
	Date: 0.190			
Species biovolume (BSM)	Sites: 0.629	H0 dates (0.2%)	0.598	Tidal height, coarse sand, mud
	Date: 0.172			
Common species matrix (CSM)	Sites: 0.857		0.829	Tidal height, coarse sand, medium sand, mud
	Date: 0.212			
Transformed species matrix (TSM)	Sites: 0.932		0.863	Mud
	Date: 0.308			
Navicula (NAV)	Sites: 0.884		0.749	Tidal height, coarse sand, mud
	Date: 0.337			
Genera (GM)	Sites: 0.735	H0 dates (0.2%)	0.772	Mud
	Date: 0.162			
Genera presence–absence (0–1 GM)	Sites: 0.840	H0 dates (16.3%)	0.857	Mud
	Date: 0.048			
Size-classes (SCM)	Sites: 0.673	H0 dates (0.4%)	0.71	Mud
	Date: 0.128			

The ANOSIM global test statistic (R), at a significance level $p < 0.01\%$, allows evaluating if the ability to discriminate sites and sampling dates is maintained. The BEST routine's test measures the link between the environmental dataset and the different matrices of the biotic data at $p < 0.1\%$ (999 permutations). Spearman's value (ρ) of the environmental variable subset that is highest correlated to the biotic datasets are also presented.

($R = 0.34$). Finally, the presence/absence matrices had a slightly higher global *R*-values for differences between sites than the corresponding species or genera abundance matrices, while a considerably lower global *R* for differences between sampling dates (**Table 3**).

The relationships between patterns in multivariate community structure and the environmental variables were examined using the BEST procedure. All biotic datasets had significant correlations ($p < 0.1\%$) with the selected environmental variable subsets, ranging from $\rho = 0.598$ (BSM) to $\rho = 0.863$ (TSM), which meant that the correlations between the biotic and abiotic datasets varied from moderate, in case of the biovolume and size-classes matrices, to strong in the case of the genera and species-level matrices (**Table 3**). These results were comparable to the other previous analyses. The species-level matrices had very similar correlation values, albeit not always selecting the same subset of environmental variables. The genera matrices both had "mud" as the highest correlated environmental variable, with the presence/absence dataset scoring a slightly higher correlation ($\rho = 0.86$).

DISCUSSION

Rare-Species Exclusion

The reduction of the diatom abundances matrix from the 181-taxa original matrix (OSM) to the 94-taxa CSM and TSM matrices had a negligible influence in the overall multivariate results. The Bray–Curtis similarity matrices derived from OSM and CSM had an almost perfect match, despite the exclusion of 48% of the initial taxa, and both had extremely high correlations with the TSM matrix, used in Ribeiro et al. (2013), which had the best results overall. The TSM matrix had the highest correlation between diatom community patterns and environmental variables (BEST test) and one of the top results in the ANOSIM test, where it performed slightly better in discriminating sampling dates than most of the other matrices. The current study seems to indicate that the comparatively slight gains in clarity were more a consequence of data transformation (i.e. fourth-root transformation of abundance data) than from the fact that the rare taxa were discarded. Nevertheless, it is likely that a combination of both steps was responsible for the clearer MDS ordination and cluster analysis results shown in that previous work.

Rare taxa exclusion can be somewhat arbitrary and may have a great impact in the overall results of several multivariate approaches (Cao et al., 1997, 2001; Cao and Williams, 1999) but it also eliminates accidental occurrences that cloud the final multivariate outcomes (Marchant, 1999). In a study that evaluated the effect of exclusion of diatom taxa on multivariate analysis in a large diatom dataset, Lavoie et al. (2009) concluded that the exclusion of taxa based on relative abundances could be confidently made until a ≥2% threshold, but that extra care must be taken when excluding taxa based on frequency of occurrence. In our study, a very conservative "cut-off" line was chosen (i.e. a ≥1% threshold and minimum of two occurrences in 68

samples) that allowed the elimination of allochthonous species (e.g. all phytoplanktonic taxa). However, as several authors argue, there is no biological justification for excluding rare species (Cao et al., 2001) and, contrary to PCA and DCA ordinations, the multivariate routines based on Bray–Curtis resemblance matrices do not require the exclusion of rare species (Clarke and Warwick, 2001). There are also no gains in time during diatom analysis, as the rarity of each species can only be established after the cell counts. Consequently, even though it is not a necessary step, the exclusion or rare species does not seem to hinder the multivariate analysis and may improve, even if slightly, the overall results.

Qualitative Analysis: Species Presence–Absence

Species composition studies only score the presence or the absence of taxa in each sample. High taxonomical resolution is maintained but there is no abundance data. This approach is much less time-consuming since scoring 300–600 individuals per sample is not necessary. Hence, its interest as a time-saving approach can be significant in large surveys. Our results showed that the species matrix based on binary data replicated well the several multivariate analyses outcomes and had a high correlation with the environmental variables dataset.

Taxonomical information alone seemed sufficient to spatially discriminate samples, but it had very weak temporal signal. This was anticipated, given that Ribeiro et al. (2013) concluded in that spatial differences were mainly brought about by changes in sediment texture, while temporal variations were mainly caused by seasonal shifts in abundance of a few dominant species from the mudflat assemblages and that the epipsammon-dominated assemblages had a stable structure throughout the 2-year study. The removal of abundance data eliminated the seasonal peaks of epipelic species and, thus, concealed the temporal patterns. The spatial patterns were retained because the taxonomic differences between the assemblages of each site were not affected. Therefore, it is to be expected that in large spatial surveys covering the salinity gradient of an estuary (e.g. Rovira et al., 2012) but also several sediment textures (e.g. Sabbe and Vyverman, 1991), qualitative data may prove to be sufficient to adequately describe the MPB communities. Likewise, it would also mean that if there are seasonal changes in silt content on a given tidal flat (e.g. Méléder et al., 2007), temporal variations are likely to be detected at the species level, even without abundance information. However, if a spatial study selects mudflats of similar sediment texture or grain size (Forster et al., 2006), or uses the lens-tissue method (Eaton and Moss, 1966) to selectively collect the epipelic fraction of the MPB (Thornton et al., 2002), spatial differences between diatom assemblages will mainly be caused by changes in the relative abundances of the most common species along the salinity and nutrient gradients (cf. Underwood et al., 1998). Therefore, the removal of abundance data would reduce much of those spatial differences in a similar fashion to what it did to the seasonal patterns of the mudflat assemblages of the Tagus estuary binary dataset.

Several authors advise against the use of binary data in monitoring studies. Lavoie et al. (2009) demonstrated that ordinations based on presence/absence data are only capable of gross separations between impacted and reference sites in large-scale monitoring studies, while Thorne et al. (1999) showed that clustering of Bray–Curtis similarities and ANOSIM analyses on binary matrices performed poorer than any other transformation of the same data (i.e. original, root, and fourth-root transformed data). Giving the same weight to all taxa may have major consequences when the community patterns are dependent on the abundance of a few dominant species. The current study shows that information taken from multivariate analysis based on binary, qualitative data may be enough to adequately display spatial patterns. But special caution is advised in larger spatial surveys, given the importance of abundance data in low-diversity, epipelon-dominated mudflat assemblages in estuarine areas.

Finally, a practical recommendation: in order to achieve a species-richness that falls in the expected asymptote of the species accumulation curve for the customary 300–600 valve count, at least 50 ocular fields should be screened when following presence–absence approach.

Taxonomic Sufficiency: Genus-Level Analyses

Genus-level abundance dataset had an intermediate correlation with the original species dataset (OSM) while the presence/absence matrix has one of the lowest. The overall multivariate spatial patterns were retained and the correlation with the environmental variables set was strong, but both matrices were incapable of significantly discriminating sampling dates. These results indicate, therefore, that information was lost by the reduction in taxonomical resolution but that change in intertidal diatom community structure can still be reflected at the genus-level.

The effect of taxonomic resolution in multivariate community patterns has been widely tested in freshwater and marine macroinvertebrate community studies (e.g. Dauvin et al., 2003; Anderson et al., 2005; Heino, 2008) and more rarely in freshwater diatom lotic communities (Rimet and Bouchez, 2012a). High correlations between species and genus richness (Hill et al., 2001; Passy and Legendre, 2006) and/or assemblage structure (Heino and Soininen, 2007) have been reported but Lavoie et al. (2009) found that genus-level multivariate analysis was only capable of detecting gross differences between impacted and reference sites in Canadian streams, mirroring the effects of presence/absence data transformation or of excessive exclusion of rare taxa.

The current study suggests the genus-level taxonomic resolution could be considered as sufficient to detect changes in community structure in coastal and estuarine intertidal areas, in particular when it is mainly caused by shifts in sediment texture. It should be noted, however, that seasonal patterns in the mudflat assemblages (i.e. in V2 and V3) were reduced to changes in the relative proportions of, essentially, three genera (i.e. *Navicula*, *Cylindrotheca*, and *Gyrosigma*). When the abundance data are discarded, the temporal signal disappears altogether at the genus-level but not at the species level (**Table 3**). As species-specific seasonal blooms (Ribeiro et al., 2013) are not recorded, temporal changes may become undetected with a reduction

of taxonomical resolution. Secondly in less diverse, epipelon-dominated assemblages, spatial differences brought by slight changes in sediment texture may not be detected at the genus-level. Finally, some information is bound to be lost when dealing with ubiquitous, abundant genera such as *Navicula*, which had high beta-diversity. The analysis of the 29-species *Navicula* set showed that it had a stronger correlation with the full species set than the genera datasets, thus underscoring the importance of this genus and of species-level community analysis. This impressive performance is an excellent example of the amount of variation and information that still exists within a single genus and, therefore, why the lack of sufficient taxonomic resolution in community ecology studies may be problematic (Kociolek and Stoermer, 2001a; Kociolek, 2005).

As in the case of the species-level binary data, more subtle spatial and temporal changes may pass undetected with the genus-level approach (Somerfield and Clarke, 1995; Hill et al., 2001; Lavoie et al., 2009). Some authors (e.g. Bowman and Bailey, 1997; Thorne et al., 1999) consider that preservation of abundance data is preferable to the maintenance of high taxonomic resolution in qualitative data. In our study the genus abundance matrix had lower discriminative power (ANOSIM) and lower correlation with the abiotic data (BEST) than the species presence/absence dataset. Interestingly, when binary data are coupled with lower taxonomical resolution the results were not considerably worse, except for the above mentioned temporal signal. The genus-level presence/absence had lower discriminative power (ANOSIM) but higher correlation with the abiotic data (BEST) than its species-level counterpart, as well as the genus abundance dataset. This result is in agreement with studies on marine and freshwater macrobenthic fauna (e.g. Olsgard et al., 1998; Heino, 2008), although the reasons for it are not entirely clear.

Diatom Cell Size and Biovolume

The effect of diatom cell size was assessed in two different ways: one discarded the taxonomic information and rearranged the abundance data in four size-classes, the other maintained the maximal taxonomic resolution but transformed the abundance data in a percentage of contribution to total biovolume. Both yielded poor results and the two lowest correlations to the OSM. They failed to detect temporal changes but still scored average to relatively high correlations with the environmental set and were able to discriminate the sites.

The use of size-classes does have the obvious advantage that almost no taxonomic expertise is needed, and that biometric data are easy to acquire and inter-calibrate. However, it should be noted that the four size-classes used in this study were originally established from this very dataset (i.e. OSM) and their distribution clearly reflected differences between the sampling stations (Ribeiro et al., 2013). Their applicability in other diatom distribution studies still needs to be tested. Nevertheless, the range of the four size-classes was not randomly chosen. A series of studies on the Baltic Sea epiphyton (Busse and Snoeijs, 2002, 2003; Snoeijs et al., 2002; Ulanova and Snoeijs, 2006), indicated that diatoms smaller than 1000 μm^3 and diatoms bigger than 1000 μm^3 responded differently to environmental gradients, namely to salinity and exposure to wave action, and recommended that both size-classes should be counted and analyzed separately. As for the smaller diatoms, the commonly attributed dominance of small diatoms in European mudflats (e.g. Admiraal et al., 1984; Haubois et al., 2005; Sahan et al., 2007) should, in fact, be attributed to a medium-sized group (i.e. 250–1000 μm^3) which is mainly composed of several *Navicula* species (Ribeiro et al., 2013). Finally, Ribeiro (2010) divided the <250 μm^3 group in two classes to stress the fact the very small diatoms (i.e. <100 μm^3) dominated the sandier sites (i.e. A1 and A2) but were not present in the mudflat ones, whereas the small diatoms (100–250 μm^3) size-class appeared both in sandflat and mudflat assemblages.

Studies by Haubois et al. (2005) and Lavoie et al. (2006) showed that both relative abundance and relative biovolume metrics obtained the same overall results but the explained percentage of species variance was higher with relative abundance data than with the relative biovolume metric. Haubois et al.'s (2005) study is particularly relevant because it was made on intertidal mudflat assemblages. It was able to show that, with this relative contribution to total biovolume, the epipelic assemblages were episodically dominated by large species. This temporal signal can also be perceived by a genus-level analysis (see above), as it is brought about by the species-specific blooms of large *Pleurosigma* and *Gyrosigma* species. Passy (2008) suggested that, in a lotic system, a small habit does confer resistance to disturbance of flow, grazing, and sinking and aids in dispersal, while a large habit is deemed advantageous in disturbance-free but nutrient-rich systems, where a tall stature provides a better access to nutrients and light, a greater surface for maximizing nutrient uptake rate, and a greater nutrient storage capacity. But she concluded that biovolume was more strongly related to density in the benthos than in the phytoplankton and that species distribution was a much more important descriptor of density at larger scales and a slightly better predictor than biovolume at local scales. In an intertidal system, dispersal seems less affected by cell size, as benthic diatoms of all types will be resuspended in estuaries and coastal areas (de Jonge and van Beusekom, 1992; Hernández Fariñas et al., 2017), but the size-class distribution will surely reflect sediment exposure, as smaller diatoms are spared from collision with sand grains, while larger ones are destroyed (Delgado et al., 1991). Sandflat assemblages are, therefore, invariably dominated by small diatoms (Asmus and Bauerfeind, 1994; Ribeiro et al., 2013), while in the mudflat assemblages the two size fractions of the motile epipelic group may well be a crude reflection of species-specific differences. They can also be playing, *per se*, a major role in biofilm cell micro-cycling and stratification, potentiating niche differentiation in epipelic biofilms, but the effect of size in MPB biofilm eco-physiology still needs to be explored. For example, in the particular case of the large species *Gyrosigma fasciola*, an inherent higher capacity of non-photochemical quenching (NPQ) seems to protect this species from high irradiances at lower temperatures, giving this species a competitive advantage in the winter

months (Serôdio et al., 2005), but these features cannot be attributed to size alone.

The current study indicates that cell size may be a crude way to separate assemblages from different sites, given that the overwhelming effect of hydrodynamic stress and sediment texture in soft-bottom intertidal areas (Paterson and Hagerthey, 2001) is also reflected in their size-class distribution. As for the usefulness of relative biovolume metrics, the extra time spent in biovolume calculations (Hillebrand et al., 1999) added to the already lengthy taxonomical identifications without bringing any extra clarity to overall results. Therefore, the applicability of species relative biovolume or size distribution does not seem particularly promising.

When to Keep the Species Abundances Approach

The current study proposes and compares several less labor-intensive options to the species abundances community analysis. It should be added, nonetheless, that some recent lines of MPB research do predicate on species abundances metrics or have much to gain when including them. This point is stressed by Underwood (2005), who highlighted how species composition influences biofilm function: not only there are significant differences in photosynthetic efficiency between epipelic diatom species (Oxborough et al., 2000), each taxon has its own migration pattern during a tidal exposure cycle, which in turn impacts the photophysiological response of individual cells but also of the biofilm as whole (e.g. Perkins et al., 2002; Paterson et al., 2003; Underwood et al., 2005). Moreover, Forster et al. (2006) and Vanelslander et al. (2009) depicted the effect of species richness and identity on epipelic biomass in both field and experimental conditions, while Barnett et al. (2015) showed clearly differences in the photophysiology of epipelic and epipsammic taxa. This latter example suggests that using growth-forms categories as surrogates to species-level analysis could be a valid alternative approach, but the allocation of diatom specimens to given a growth-form precludes a prior species-level identification in most cases and, thus, spending even more time and effort in assemblage description.

Microphytobenthos researchers should be aware that differences in biofilm function can be linked to both differences in species composition as well as to more conventional causes, such as nutrient concentration or photoacclimation (Underwood, 2005). For example, experimental settings that study the interactive effects of environmental variables on MPB biofilms (e.g. Cartaxana et al., 2015), or comparisons between light and O_2 microenvironments in natural intertidal sediments and their effect on biofilm photophysiology (e.g. Cartaxana et al., 2016) ideally require knowledge of species composition and their abundance (Underwood and Barnett, 2006). Furthermore, for research to be truly reproducible, peer-reviewed ecology journals should always include taxonomic information and how it was obtained (Vink et al., 2012). Unfortunately, it is not always possible to get this type of data and, hopefully, the current work provides a satisfactory way for MPB researchers to choose a valid alternative that is adequate to their studies objectives.

CONCLUSION

Many MPB ecologists lack satisfactory diatom identification skills or may have budget and/or time limitations that constrains them to complement their research with a sound description of taxonomic structure of the MPB biofilms they are studying. It is hoped that current work provides an objective way to evaluate and choose adequate surrogates to species-level diatom analysis in intertidal areas. All approaches tested in this study performed relatively well and replicated satisfactorily the multivariate patterns given by the species abundances dataset previously shown by Ribeiro et al. (2013), where very contrasting sediment textures were clearly reflected in differences in community structure, which were not only taxonomic but also in diatom size and functional group distribution. Even though all approaches were able to detect sharp environmental changes, there were enough differences between their multivariate routines' performances to establish a set of guidelines to be followed:

(1) Species presence/absence and genera abundances approaches were the most promising alternatives, with the latter performing slightly worse than the former. However, if a fast and crude spatial distinction of tidal flat assemblages from contrasting sediments is needed, probably the most adequate choice is a genus-level abundances matrix. This approach retains some of the abundance information and does not need great identification skills.
(2) Seasonal variations can only be confidently detected with species-level abundances. Species-specific blooms are responsible for the temporal shifts in the mudflat diatom assemblages and they disappear when using binary or genus-level datasets. Hence, neither the qualitative nor the genera approaches are advised in the case of temporal studies.
(3) The utility of size-classes as a surrogate classification seems limited, as it may not detect important environmental shifts, such as slight differences in sediment texture. However, their suitability in detecting nutrient gradients or light regimes should be further explored, as the size-classes presented here may well correspond to different niches in the epipelic assemblages usually found in mudflat environments.
(4) The weighted relative biovolume approach should be avoided. This method is very time-consuming and failed to detect important differences in the structure of assemblages collected from different sediments.

DATA AVAILABILITY STATEMENT

This article contains previously unpublished data. The name of the repository and accession number(s) are not available.

AUTHOR CONTRIBUTIONS

LR, BJ, and VB designed the fieldwork and outlined the sampling strategy. LR and BJ performed the sampling and laboratory analyses. LR, LB, and TH-F analyzed and interpreted the data. LR wrote the manuscript. All authors read, critically revised, and approved the final version of the manuscript.

FUNDING

This study was supported by a grant by the L'Agence Française pour la Biodiversité, AFB Grant number: 180906 – Convention Microphytobenthos Phase II, and also had the financial support of the Fundação para a Ciência e a Tecnologia (FCT) through UID/MAR/04292/2019. VB received a sabbatical grant from FCT SFRH/BSAB/142981/2018. VB also acknowledges funding from the European Union's Horizon 2020 Research and Innovation Programme grant agreement no. 810139: Project Portugal Twinning for Innovation and Excellence in Marine Science and Earth Observation – PORTWIMS.

ACKNOWLEDGMENTS

The authors are much obliged to P. Cartaxana and R. Mendes who assisted during sampling and laboratory work. The authors also thank the two reviewers for helpful comments that improved the manuscript.

SUPPLEMENTARY MATERIAL

The Supplementary Material for this article can be found online at: https://www.frontiersin.org/articles/10.3389/fmars.2020.00036/full#supplementary-material

REFERENCES

Admiraal, W. (1984). "The ecology of estuarine sediment-inhabiting diatoms," in *Progress in Phycological Research*, eds D. J. Chapman, and F. E. Round, (Bristol: Biopress), 269–322.

Admiraal, W., Peletier, H., and Brouwer, T. (1984). The seasonal succession patterns of diatom species on an intertidal mudflat: an experimental analysis. *Oikos* 42, 30–40.

Anderson, M. J., Connell, S. D., Gillanders, B. M., Diebel, C. E., Blom, W. M., Saunders, J. E., et al. (2005). Relationships between taxonomic resolution and spatial scales of multivariate variation. *J. Anim. Ecol.* 74, 636–646. doi: 10.1111/j.1365-2656.2005.00959.x

Asmus, R. M., and Bauerfeind, E. (1994). The microphytobenthos of Königshafen - spatial and seasonal distribution on a sandy tidal flat. *Helgol. Mar. Res.* 48, 257–276. doi: 10.1007/bf02367040

Barnett, A., Méléder, V., Blommaert, L., Lepetit, B., Gaudin, P., Vyverman, W., et al. (2015). Growth form defines physiological photoprotective capacity in intertidal benthic diatoms. *ISME J.* 9, 32–45. doi: 10.1038/ismej.2014.105

Bowman, M. F., and Bailey, R. C. (1997). Does taxonomic resolution affect the multivariate description of the structure of freshwater benthic macroinvertebrate communities? *Can. J. Fish. Aquat. Sci.* 54, 1802–1807. doi: 10.1139/f97-085

Bray, J. R., and Curtis, J. T. (1957). An ordination of the upland forest communities of southern wisconsin. *Ecol. Monogr.* 27, 326–349.

Busse, S., and Snoeijs, P. (2002). Gradient responses of diatom communities in the Bothnian Bay, northern Baltic Sea. *Nova Hedwig.* 74, 501–525. doi: 10.1127/0029-5035/2002/0074-0501

Busse, S., and Snoeijs, P. (2003). Gradient responses of diatom communities in the Bothnian Sea (northen Baltic Sea), with emphasis onresponses to water movement. *Phycologia* 42, 451–464. doi: 10.2216/i0031-8884-42-5-451.1

Cabrita, M. T., and Brotas, V. (2000). Seasonal variation in denitrification and dissolved nitrogen fluxes in intertidal sediments of the Tagus estuary, Portugal. *Mar. Ecol. Prog. Ser.* 202, 51–65. doi: 10.3354/meps202051

Cao, Y., Bark, A. W., and Williams, P. (1997). A comparison of clustering methods for river benthic community analysis. *Hydrobiologia* 347, 25–40.

Cao, Y., Larsen, D. P., and Thorne, R. S. J. (2001). Rare species in multivariate analysis for bioassessment: some considerations. *J. N. Am. Bethol. Soc.* 20, 144–153. doi: 10.2307/1468195

Cao, Y., and Williams, D. D. (1999). Rare species are important in bioassessment (Reply to the comment by Marchant). *Limnol. Oceanogr.* 44, 1841–1842.

Carballo, J. L., and Naranjo, S. (2002). Environmental assessment of a large industrial marine complex based on a community of benthic filter-feeders. *Mar. Pollut. Bull.* 44, 605–610. doi: 10.1016/s0025-326x(01)00295-8

Carneiro, F. M., Bini, L. M., and Rodrigues, L. C. (2010). Influence of taxonomic and numerical resolution on the analysis of temporal changes in phytoplankton communities. *Ecol. Indic.* 10, 249–255. doi: 10.1016/j.ecolind.2009.05.004

Cartaxana, P., Ribeiro, L., Goessling, J. W., Cruz, S., and Kühl, M. (2016). Light and O2 microenvironments in two contrasting diatom-dominated coastal sediments. *Mar. Ecol. Prog. Ser.* 545, 35–47. doi: 10.3354/meps11630

Cartaxana, P., Vieira, S., Ribeiro, L., Rocha, R. J., Cruz, S., Calado, R., et al. (2015). Effects of elevated temperature and CO2 on intertidal microphytobenthos. *BMC Ecol.* 15:10. doi: 10.1186/s12898-015-0043-y

Clarke, K. R. (1993). Non-parametric multivariate analyses of changes in community structure. *Austr. J. Ecol.* 18, 117–143. doi: 10.1111/j.1442-9993.1993.tb00438.x

Clarke, K. R., and Gorley, R. N. (2006). *PRIMER v6: User Manual/Tutorial*. Plymouth, UK: PRIMER-E.

Clarke, K. R., Somerfield, P. J., and Gorley, R. N. (2008). Testing of null hypotheses in exploratory community analyses: similarity profiles and biota-environment linkage. *J. Exp. Mar. Biol. Ecol.* 366, 56–69. doi: 10.1016/j.jembe.2008.07.009

Clarke, K. R., and Warwick, R. M. (1994). Similarity-based testing for community pattern: the 2-way layout with no replication. *Mar. Biol.* 118, 167–176. doi: 10.1007/bf00699231

Clarke, K. R., and Warwick, R. M. (1998). Quantifying structural redundancy in ecological communities. *Oecologia* 113, 278–289. doi: 10.1007/s004420050379

Clarke, K. R., and Warwick, R. M. (2001). *Change in Marine Communities: An Approach to Statistical Analysis and Interpretation*, 2nd Edn, Plymouth: PRIMER-E.

Consalvey, M., Jesus, B., Perkins, R. G., Brotas, V., and Paterson, D. M. (2004). Monitoring migration and measuring biomass in benthic biofilms: the effects of dark/far red adaptation and vertical migration on fluorescence measurements. *Photosynth. Res.* 81, 91–101. doi: 10.1023/b:pres.0000028397.86495.b5

Cox, E. J. (2009). What's in a name? – Diatom classification should reflect systematic relationships. *Acta Bot. Croat.* 68, 443–463.

Dauvin, J. C., Gomez Gesteira, J. L., and Salvande Fraga, M. (2003). Taxonomic sufficiency: an overview of its use in the monitoring of sublittoral benthic communities after oil spills. *Mar. Pollut. Bull.* 46, 552–555. doi: 10.1016/s0025-326x(03)00033-x

de Jonge, V. N., and van Beusekom, J. F. F. (1992). Contribution of resuspended microphytobenthos to total phytoplankton in the Ems estuary and its possible role for grazers Netherlands. *J. Sea Res.* 30, 91–105. doi: 10.1016/0077-7579(92)90049-k

de Jonge, V. N., and van Beusekom, J. F. F. (1995). Wind- and tide-induced resuspension of sediment and microphytobenthos from tidal flats in the Ems estuary. *Limnol. Oceanogr.* 40, 766–778.

Delgado, M., de Jonge, V. N., and Peletier, H. (1991). Sediment grain size effect on benthic microalgal biomass in shallow aquatic ecosystems. *Mar. Biol.* 108, 321–328.

Eaton, J. W., and Moss, B. (1966). The estimation of numbers and pigment content in epipelic algal populations. *Limnol. Oceanogr.* 11, 584–595. doi: 10.4319/lo.1966.11.4.0584

Ellis, D. (1985). Taxonomic sufficiency in pollution assessment. *Mar. Pollut. Bull.* 16:459. doi: 10.1016/0025-326X(85)90362-90365

Field, J. G., Clarke, K. R., and Warwick, R. M. (1982). A practical strategy for analysing multispecies distribution patterns. *Mar. Ecol. Prog. Ser.* 8, 37–52. doi: 10.3354/meps008037

Forster, R. M., Créach, V., Sabbe, K., Vyverman, W., and Stal, L. J. (2006). Biodiversity-ecosystem function relationship in microphytobenthic diatoms of the Westerschelde estuary. *Mar. Ecol. Prog. Ser.* 311, 191–201. doi: 10.3354/meps311191

Hamels, I., Sabbe, K., Muylaert, K., Barranguet, C., Lucas, C., Herman, P., et al. (1998). Organisation of microbenthic communities in intertidal estuarine flats, a case study from the Molenplaat (Westerschelde estuary, The Netherlands). *Eur. J. Protistol.* 34, 308–320. doi: 10.1016/s0932-4739(98)80058-8

Haubois, A.-G., Sylvestre, F., Guarini, J.-M., Richard, P., and Blanchard, G. F. (2005). Spatio-temporal structure of the epipelic diatom assemblage from an intertidal mudflat in Marennes-Oléron Bay, France. *Estuar. Coast. Shelf Sci.* 64, 385–394. doi: 10.1016/j.ecss.2005.03.004

Heino, J. (2008). Influence of taxonomic resolution and data transformation on biotic matrix concordance and assemblage-environment relationships in stream macroinvertebrates. *Boreal Environ. Res.* 13, 359–369.

Heino, J., and Soininen, J. (2007). Are higher taxa adequate surrogates for species-level assemblage patterns and species richness in stream organisms? *Biol. Conserv.* 137, 78–89. doi: 10.1016/j.biocon.2007.01.017

Hernández Fariñas, T., Ribeiro, L., Soudant, D., Belin, C., Bacher, C., Lampert, L., et al. (2017). Contribution of benthic microalgae to the temporal variation in phytoplankton assemblages in a macrotidal system. *J. Phycol.* 53, 1020–1034. doi: 10.1111/jpy.12564

Hill, B. H., Stevenson, R. J., Pan, Y., Herlihy, A. T., Kaufmann, P. R., and Johnson, C. B. (2001). Comparison of correlations between environmental characteristics and stream diatom assemblages characterized at genus and species levels. *J. N. Am. Benthol. Soc.* 20, 299–310. doi: 10.2307/1468324

Hillebrand, C., Dürselen, C. D., Kirschtel, D., Pollingher, U., and Zohary, T. (1999). Biovolume calculation for pelagic and benthic microalgae. *J. Phycol.* 35, 403–324.

Jesus, B., Brotas, V., Ribeiro, L., Mendes, C. R., Cartaxana, P., and Paterson, D. M. (2009). Adaptations of microphytobenthos assemblages to sediment type and tidal position. *Continent. Shelf Res.* 29, 1624–1634. doi: 10.1016/j.csr.2009.05.006

Jesus, B., Mendes, C. R., Brotas, V., and Paterson, D. M. (2006). Effect of sediment type on microphytobenthos vertical distribution: modeling the productive biomass and improving ground truth measurements. *J. Exp. Mar. Biol. Ecol.* 332, 60–74. doi: 10.1016/j.jembe.2005.11.005

Jones, F. C. (2008). Taxonomic sufficiency: the influence of taxonomic resolution on freshwater bioassessments using benthic macroinvertebrates. *Environ. Rev.* 16, 45–69. doi: 10.1139/a07-010

Kelly, M. (2013). Data rich, information poor? Phytobenthos assessment and the water framework directive. *Eur. J. Phycol.* 48, 437–450. doi: 10.1080/09670262.2013.852694

Kociolek, J. P. (2005). Taxonomy and ecology: further considerations. *Proc. Calif. Acad. Sci.* 56, 97–187.

Kociolek, J. P., and Stoermer, E. F. (2001a). Opinion: taxonomy and ecology: a marriage of necessity. *Diatom Res.* 16, 433–442. doi: 10.1080/0269249x.2001.9705529

Kociolek, J. P., and Stoermer, E. F. (2001b). Taxonomy and ecology: a marriage of necessity. *Diatom Res.* 16, 433–442. doi: 10.1080/0269249X.2001.9705529

Lavoie, I., Campeau, S., Fallu, M. A., and Dillon, P. J. (2006). Diatoms and biomonitoring: should cell size be accounted for? *Hydrobiologia* 573, 1–16. doi: 10.1007/s10750-006-0223-z

Lavoie, I., Dillon, P. J., and Campeau, S. (2009). The effect of excluding diatom taxa and reducing taxonomic resolution on multivariate analyses and stream bioassessment. *Ecol. Indic.* 9, 213–225. doi: 10.1016/j.ecolind.2008.04.003

Lavoie, I., Lento, J., and Morin, A. (2010). Inadequacy of size distributions of stream benthic diatoms for environmental monitoring. *J. N. Am. Benthol. Soc.* 29, 586–601. doi: 10.1899/09-062.1

MacIntyre, H. L., Geider, R. J., and Miller, D. C. (1996). Microphytobenthos: the ecological role of the "Secret Garden" of unvegetated, shallow-water marine habitats. I. Distribution, abundance and primary production. *Estuaries* 19, 186–201.

Marchant, R. (1999). How important are rare species in aquatic community ecology and bioassessment? A comment on the conclusions of Cao et al. *Limnol. Oceanogr.* 44, 1840–1841.

Marques da Silva, J., Cruz, S., and Cartaxana, P. (2017). Inorganic carbon availability in benthic diatom communities: photosynthesis and migration. *Philos. Trans. R. Soc. Lond. B Biol. Sci.* 372:20160398. doi: 10.1098/rstb.2016.0398

McIntire, C. D., and Moore, W.W. (1977). "Marine litoral diatoms: ecological considerations," in *The Biology of Diatoms*, ed. D. Werner, (Oxford: Blackwell Scientific Publications), 333–371.

Méléder, V., Rincé, Y., Barillé, L., Gaudin, P., and Rosa, P. (2007). Spatiotemporal changes in microphytobenthos assemblages in a macrotidal flat (Bourgneuf Bay, France). *J. Phycol.* 43, 1177–1190. doi: 10.1111/j.1529-8817.2007.00423.x

Menezes, S., Baird, D. J., and Soares, A. M. V. M. (2010). Beyond taxonomy: a review of macroinvertebrate trait-based community descriptors as tools for freshwater biomonitoring. *J. Appl. Ecol.* 47, 711–719. doi: 10.1111/j.1365-2664.2010.01819.x

Middleburg, J. J., Barranguet, C., Boschker, H. T. S., Herman, P. M. J., Moens, T., and Heip, C. H. R. (2000). The fate of intertidal microphytobenthos carbon: an *in situ* 13C-labeling study. *Limnol. Oceanogr.* 45, 1224–1234. doi: 10.4319/lo.2000.45.6.1224

Muylaert, K., Van Nieuwerburgh, L., Sabbe, K., and Vyverman, W. (2002). Microphytobenthos communities in the freshwater tidal to brackish reaches of the Schelde estuary (Belgium). *Belgian J. Bot.* 135, 15–26.

Olsgard, F., Somerfield, P. J., and Carr, M. R. (1997). Relationships between taxonomic resolution and data transformations in analyses of a macrobenthic community along an established pollution gradient. *Mar. Ecol. Prog. Ser.* 149, 173–181. doi: 10.3354/Meps149173

Olsgard, F., Somerfield, P. J., and Carr, M. R. (1998). Relationships between taxonomic resolution, macrobenthic community patterns and disturbance. *Mar. Ecol. Prog. Ser.* 172, 25–36. doi: 10.3354/meps172025

Oxborough, K., Hanlon, A. R. M., Underwood, G. J. C., and Baker, N. R. (2000). In vivo estimation of the photosystem II photochemical efficiency of individual microphytobenthic cells using high-resolution imaging of chlorophyll a fluorescence. *Limnol. Oceanogr.* 45, 1420–1425. doi: 10.4319/lo.2000.45.6.1420

Park, J., Kwon, B. O., Kim, M., Hong, S., Ryu, J., Song, S. J., et al. (2014). Microphytobenthos of Korean tidal flats: a review and analysis on floral distribution and tidal dynamics. *Ocean Coast. Manag.* 102, 471–482. doi: 10.1016/j.ocecoaman.2014.07.007

Passarelli, C., Olivier, F., Paterson, D. M., Meziane, T., and Hubas, C. (2014). Organisms as cooperative ecosystem engineers in intertidal flats. *J. Sea Res.* 92, 92–101. doi: 10.1016/j.seares.2013.07.010

Passy, S. I. (2007). Diatom ecological guilds display distinct and predictable behavior along nutrient and disturbance gradients in running waters. *Aquat. Bot.* 86, 171–178. doi: 10.1016/j.aquabot.2006.09.018

Passy, S. I. (2008). Species size and distribution jointly and differentially determine diatom densities in US streams. *Ecology* 89, 475–484. doi: 10.1890/07-0405.1

Passy, S. I., and Legendre, P. (2006). Power law relationships among hierarchical taxonomic categories in algae reveal a new paradox of the plankton. *Glob. Ecol. Biogeogr.* 15, 528–535. doi: 10.1111/j.1466-822X.2006.00246.x

Paterson, D. M., and Hagerthey, S. E. (2001). "Microphytobenthos in contrasting coastal ecosystems: biology and dynamics," in *Ecological Comparisons of Sedimentary Shores*, ed. K. Reise, (Berlin: Springer-Verlag), 105–125 doi: 10.1007/978-3-642-56557-1_6

Paterson, D. M., Perkins, R., Consalvey, M., and Underwood, G. J. C. (2003). "Ecosystem function, cell micro-cycling and the structure of transient biofilms," in *Fossil and Recent Biofilms: A Natural History of Life on Earth*, eds W. E. Krumbein, D. M. Paterson, and G. A. Zavarzin, (Dordrecht: Springer), 47–63. doi: 10.1007/978-94-017-0193-8_3

Perkins, R. G., Oxborough, K., Hanlon, A. R. M., Underwood, G. J. C., and Baker, N. R. (2002). Can chlorophyll fluorescence be used to estimate the rate of photosynthetic electron transport within microphytobenthic biofilms? *Mar. Ecol. Prog. Ser.* 228, 47–56. doi: 10.3354/meps228047

Ribeiro, L. (2010). *Intertidal Benthic Diatoms of the Tagus Estuary: Taxonomic Composition and Spatial-Temporal Variation (2 Volumes)*. Ph.D. Thesis, Universidade de Lisboa, Portugal.

Ribeiro, L., Brotas, V., Rincé, Y., and Jesus, B. (2013). Structure and diversity of intertidal benthic diatom assemblages in contrasting shores: a case study from the Tagus estuary. *J. Phycol.* 49, 258–270. doi: 10.1111/jpy.12031

Rimet, F., and Bouchez, A. (2012a). Biomonitoring river diatoms: implications of taxonomic resolution. *Ecol. Indic.* 15, 92–99. doi: 10.1016/j.ecolind.2011.09.014

Rimet, F., and Bouchez, A. (2012b). Life-forms, cell-sizes and ecological guilds of diatoms in European rivers. *Knowl. Manag. Aquat. Ecosyst.* 1:12. doi: 10.1051/kmae/2012018

Rovira, L., Trobajo, R., Leira, M., and Ibáñez, C. (2012). The effects of hydrological dynamics on benthic diatom community structure in a highly stratified estuary: the case of the Ebro Estuary (Catalonia, Spain). *Estuar. Coast. Shelf Sci.* 101, 1–14. doi: 10.1016/j.ecss.2011.12.033

Sabbe, K., and Vyverman, W. (1991). Distribution of benthic diatom assemblages in the Westerschelde (Zeeland, The Netherlands). *Belgian J. Bot.* 124, 91–101.

Sahan, E., Sabbe, K., Créach, V., Hernandez-Raquet, G., Vyverman, W., Stal, L. J., et al. (2007). Community structure and seasonal dynamics of diatom biofilms and associated grazers in intertidal mudflats. *Aquat. Microb. Ecol.* 47, 253–266. doi: 10.3354/ame047253

Serôdio, J., Cruz, S., Vieira, S., and Brotas, V. (2005). Non-photochemical quenching of chlorophyll fluorescence and operation of the xanthophyll cycle in estuarine microphytobenthos. *J. Exp. Mar. Biol. Ecol.* 326, 157–169. doi: 10.1016/j.jembe.2005.05.011

Serôdio, J., Ezequiel, J., Barnett, A., Mouget, J. L., Méléder, V., Laviale, M., et al. (2012). Efficiency of photoprotection in microphytobenthos: role of vertical migration and the xanthophyll cycle against photoinhibition. *Aquat. Microb. Ecol.* 67, 161–175. doi: 10.3354/ame01591

Simberloff, D., and Dayan, D. (1991). The guild concept and the structure of ecological communities. *Annu. Rev. Ecol. Syst.* 22, 115–143. doi: 10.1146/annurev.es.22.110191.000555

Snoeijs, P., Busse, S., and Potapova, M. (2002). The importance of diatom cell size in community analysis. *J. Phycol.* 38, 265–272. doi: 10.1111/j.1529-8817.2008.00628.x

Somerfield, P. J., and Clarke, K. R. (1995). Taxonomic levels, in marine community studies, revisited. *Mar. Ecol. Prog. Ser.* 127, 113–119. doi: 10.3354/meps127113

Stal, L. J. (2010). Microphytobenthos as a biogeomorphological force in intertidal sediment stabilization. *Ecol. Eng.* 36, 236–245. doi: 10.1016/j.ecoleng.2008.12.032

Sullivan, M., and Currin, C. (2002). "Community structure and functional dynamics of benthic microalgae in salt marshes," in *Concepts and Controversies in Tidal Marsh Ecology*, ed. M. P. Weinstein, (Cham: Springer), 81–106. doi: 10.1007/0-306-47534-0_6

Thorne, R. S. J., Williams, W. P., and Cao, Y. (1999). The influence of data transformations on biological monitoring studies using macroinvertebrates. *Water Res.* 33, 343–350. doi: 10.1016/s0043-1354(98)00247-4

Thornton, D. C. O., Dong, L. E., Underwood, G. J. C., and Nedwell, D. B. (2002). Factors affecting microphytobenthic biomass, species composition and production in the Colne Estuary (UK). *Aquat. Microb. Ecol.* 27, 285–300. doi: 10.3354/ame027285

Trobajo, R., and Sullivan, M. (2010). "Applied diatom studies in estuaries and shallow coastal environments," in *The Diatoms: Applications for the Environmental and Earth Sciences*, 2nd Edn, eds J. P. Smol, and E. F. Stoermer, (Cambridge: Cambridge University Press), 309–323. doi: 10.1017/cbo9780511763175.017

Ulanova, A., and Snoeijs, P. (2006). Gradient responses of epilithic diatom communities in the Baltic Sea proper. *Estuar. Coast. Shelf Sci.* 68, 661–674. doi: 10.1016/j.ecss.2006.03.014

Underwood, G. J. C. (2005). Microalgal (microphytobenthic) biofilms in shallow coastal waters: how important are species? *Proc. Calif. Acad. Sci.* 56, 162–169.

Underwood, G. J. C., and Barnett, M. (2006). "What determines species composition in microphytobenthic biofilms?," in *Functioning of Microphytobenthos In Estuaries*, eds J. Kromkamp, J. F. C. de Brouwer, G. F. Blanchard, R. M. Forster, and V. Créach, (Amsterdam: Royal Netherlands Academy of Arts and Sciences), 121–138.

Underwood, G. J. C., Perkins, R. G., Consalvey, M., Hanlon, A. R. M., Oxborough, K., Baker, N. R., et al. (2005). Patterns in microphytobenthic primary productivity: species-specific variation in migratory rhythms and photosynthesis in mixed-species biofilms. *Limnol. Oceanogr.* 50, 755–767. doi: 10.4319/lo.2005.50.3.0755

Underwood, G. J. C., Philiphs, J., and Saunders, K. (1998). Distribution of estuarine benthic diatom species along salinity and nutrient gradients. *Eur. J. Phycol.* 33, 173–183. doi: 10.1080/09670269810001736673

Van Colen, C., Underwood, G. J. C., Serôdio, J., and Paterson, D. M. (2014). Ecology of intertidal microbial biofilms: mechanisms, patterns and future research needs. *J. Sea Res.* 92, 2–5. doi: 10.1016/j.seares.2014.07.003

Vanelslander, B., De Wever, A., Van Oostende, N., Kaewnuratchadasorn, P., Vanormelingen, P., Hendrickx, F., et al. (2009). Complementarity effects drive positive diversity effects on biomass production in experimental benthic diatom biofilms. *J. Ecol.* 97, 1075–1082. doi: 10.1111/j.1365-2745.2009.01535.x

Vieira, S., Ribeiro, L., Marques, da Silva, J., and Cartaxana, P. (2013). Effects of short-term changes in sediment temperature on the photosynthesis of two intertidal microphytobenthos communities. *Estuar. Coast. Shelf Sci.* 119, 112–118. doi: 10.1016/j.ecss.2013.01.001

Vink, C. J., Paquin, P., and Cruickshank, R. H. (2012). Taxonomy and irreproducible biological science. *Bioscience* 62, 451–452. doi: 10.1525/bio.2012.62.5.3

Williams, D. M., and Kociolek, J. P. (2010). Classifications of convenience: the meaning of names. *Diatom Res.* 25, 213–216. doi: 10.1080/0269249x.2010.9705840

Williams, R. B., and Kociolek, J. P. (2007). Pursuit of a natural classification of diatoms: history, monophyly and the rejection of paraphyletic taxa. *Eur. J. Phycol.* 42, 313–319. doi: 10.1080/09670260701419921

Wunsam, S., Cattaneo, A., and Bourassa, N. (2002). Comparing diatom species, genera and in biomonitoring: a case study from streams in the Laurentians (Québec, Canada). *Freshw. Biol.* 47, 325–340. doi: 10.1046/j.1365-2427.2002.00809.x

Conflict of Interest: The authors declare that the research was conducted in the absence of any commercial or financial relationships that could be construed as a potential conflict of interest.

frontiers in Marine Science

ORIGINAL RESEARCH
published: 22 April 2020
doi: 10.3389/fmars.2020.00250

An Untargeted Metabolomic Approach for Microphytobenthic Biofilms in Intertidal Mudflats

Julie Gaubert-Boussarie[1], Soizic Prado[2] and Cédric Hubas[1]*

[1] Muséum National d'Histoire Naturelle, UMR BOREA, MNHN-CNRS-UCN-UPMC-IRD-UA, Station Marine de Concarneau, Concarneau, France, [2] UMR 7245, Unité Molécules de Communication et Adaptation des Micro-organismes, Muséum National d'Histoire Naturelle, Paris, France

Microphytobenthic (MPB) biofilms in intertidal muddy sediments play important ecological functions in coastal ecosystems. These biofilms are mainly composed of epipelic diatoms but also prokaryotes, with a dominance of bacteria, which excrete diverse extracellular polymeric substances (EPS) according to their environment. While numerous studies have investigated the main components of these EPS matrices via traditional colorimetric assays, their fine composition, notably in specialized metabolites, is still largely unknown. A better chemical characterization of these MPB biofilms is necessary, especially regarding the numerous functions their chemical components play for microorganisms (e.g., motility, cell protection, defense mechanisms, and chemical communication), but also for coastal systems (e.g., primary production, sediment stabilization, larval settlement of some invertebrates with high economical value). An alternative approach to traditional analyses is the use of untargeted metabolomic techniques, which have not yet been applied to such MPB biofilms. The objectives of the present study were to (a) propose a protocol for metabolic fingerprinting by LC-MS and GC-MS for metabolites analysis in polar and non-polar fractions in MPB biofilms extracted from mudflat sediment and to (b) apply this protocol to a case study: the effect of light exposure on the metabolomic fingerprint of the MPB biofilm community. We compared three extraction methods using different mixes of solvents and selected a methanol/chloroform mix (1:1), which gave better results for both techniques and fractions. We then applied the selected protocol to our case study using a short-term light exposure experiment in aquaria (7 days). The present study is the first using a detailed untargeted metabolomic approach on MPB biofilms from mudflat sediment and will provide a solid baseline for further work in this area.

Keywords: microphytobenthos, biofilms, mudflats, metabolomics, diatoms

OPEN ACCESS

Edited by:
João Serôdio, University of Aveiro, Portugal

Reviewed by:
Carina Rafaela Faria Da Costa Félix, Polytechnic Institute of Leiria, Portugal
Etelvina Figueira, University of Aveiro, Portugal

****Correspondence:***
Julie Gaubert-Boussarie
julieg1907@gmail.com

Specialty section:
This article was submitted to Marine Ecosystem Ecology, a section of the journal Frontiers in Marine Science

Received: *19 November 2019*
Accepted: *30 March 2020*
Published: *22 April 2020*

Citation:
Gaubert-Boussarie J, Prado S and Hubas C (2020) An Untargeted Metabolomic Approach for Microphytobenthic Biofilms in Intertidal Mudflats. Front. Mar. Sci. 7:250. doi: 10.3389/fmars.2020.00250

INTRODUCTION

Intertidal mudflats are key areas, forming the transition between terrestrial and aquatic environments, playing important ecological roles in estuarine ecosystems (Underwood and Kromkamp, 1999; Stal, 2003; Haro et al., 2019). These mudflats support extensive microphytobenthic (MPB) biofilm developing at the sediment/water interface in shallow water

environments (e.g., estuarine, intertidal areas, and sandy beach) (Pierre et al., 2014; Hubas et al., 2018). The species composition of MPB is diverse and often dominated by epipelic diatoms (Perkins et al., 2010), and composed of other eukaryotic (e.g., euglenids) and procaryotic (e.g., cyanobacteria and archaea) organisms. These biofilms contribute to the high productivity of intertidal mudflats and provide various ecosystem services such as nutrient recycling (carbon and nitrogen), sediment stabilization and larval settlement for invertebrates of high commercial value (Decho, 2000; Toupoint et al., 2012; Bohórquez et al., 2017). The microorganisms forming the MBP biofilm are entangled in a matrix of hydrated extracellular polymeric substances (EPS) exuded by the microphytobenthos, mainly by benthic diatoms (Pierre et al., 2014; Passarelli et al., 2015). These EPS constitute the cement holding cells in close proximity, allowing interaction, communication, metabolic cooperation or competition (Flemming and Wingender, 2010; Elias and Banin, 2012; Sutherland, 2017). EPS also play diverse fundamental roles in biofilms (e.g., motility of the pennate diatoms; Underwood and Paterson, 2003; Hanlon et al., 2006). Numerous studies have investigated the main components of these EPS matrices via traditional colorimetric assays, notably in their carbohydrate fraction (e.g., Underwood and Paterson, 2003; Hanlon et al., 2006; Pierre et al., 2010, 2014) but the chemical characterization of MPB biofilms, notably in small compounds (metabolites; typically $< 1{,}500$ Da) is still largely unknown. The biofilm matrix is able to absorb diverse small compounds and ions (Wotton, 2004; Hubas et al., 2018), increasing the chemical diversity of the 'dark matter of biofilms' (Flemming and Wingender, 2010; Flemming, 2016). Due to the complexity of microbial species assemblages in mudflat biofilms, the chemical analysis of synthesized compounds is challenging. A better chemical characterization of these MPB biofilms is therefore necessary, especially regarding the numerous functions their chemical compounds play for microorganisms and coastal areas. It is also crucial to better understand microbial interactions within natural MPB biofilms.

Metabolites are the end products of cellular regulatory processes (Fiehn, 2002). Traditionally, we distinguish primary metabolites, implied in metabolic pathways required for cell maintenance, survival, development and growth, from secondary or specialized metabolites, which are considered to be non-essential for the life of the producer organism but provide survival advantages in various ways (e.g., by improving nutrient availability, protecting against environmental stressors, and enhancing competitive interactions with other organisms or acting as a defense mechanism) (Kliebenstein, 2004; Kooke and Keurentjes, 2011). The production of specialized metabolites is strongly impacted by environmental signals, such as pH, light, carbon, and nitrogen sources or by organisms living in the same habitat. Accordingly, the metabolome (i.e., the set of metabolites) can provide a 'snapshot' of the physiological state of an organism at a given time (Fiehn, 2002; Kooke and Keurentjes, 2011).

The use of metabolomic techniques, notably through metabolomic fingerprinting approaches, allows the simultaneous analysis of a large set of metabolites and can thus be an alternative (or complementary) approach to traditional analyses for the study of MPB biofilms. In marine sciences, metabolomics is an emerging discipline that can bring useful information on the responses of marine organisms to environmental changes or stressors (Bundy et al., 2009), to assess health status (Dove et al., 2012) and to explore chemical communication between organisms (Gaillard and Potin, 2014).

Several studies explored the metabolomic response of marine microorganisms, such as diatoms or bacteria, to different factors. For example, a metabolomic approach has been used to study the metabolomic changes associated with the sexual reproduction in the marine diatom *Seminavis robusta* and to further isolate the sex pheromone implied (Gillard et al., 2013). Metabolite profiling was undertaken on 13 diatom cultures to assess their lipid diversity and to explore their metabolomic adaptation to nitrogen limitation (Bromke et al., 2015). Metabolomics has also been used to study chemically mediated interactions between bacteria and diatoms (Paul et al., 2013; Lépinay et al., 2018). However, studies of chemical profiles/metabolomic responses on complex assemblages such as natural biofilms are rare [Elias and Banin, 2012, an exception being the work of Chung et al. (2010) using GC-MS to study the chemical profile of subtidal biofilms according to substrata and age; and Bourke et al. (2017) using GC-MS and LC-MS to explore microalgae metabolism on permeable sediments]. Metabolomics could be a useful tool to better understand microbial interactions and communication in complex microphytobenthic communities of mudflat biofilms.

The objectives of the present study were to (a) propose a protocol for metabolomic fingerprinting by LC-MS and GC-MS for metabolites analysis in mid-polar and apolar fractions of MPB biofilms extracted from mudflat sediments and to (b) apply this protocol to a case study: the effect of light exposure on the metabolomic fingerprint of the MPB biofilm community, using a short-term aquaria experiment (7 days). Light dose and quality is an important environmental factor, notably for photosynthetic activity, microphytobenthic movement, and metabolites biosynthesis (Perkins et al., 2001; Li et al., 2014; Juneau et al., 2015). We thus explored the significant changes in metabolic production of MPB biofilms as a response to changes in light exposure. Identification of metabolites was also tentatively performed by using NIST 2017 database.

MATERIALS AND METHODS

Sampling

General Procedure and Site Description

Surface samples of mud sediment (depth of ∼1–2 cm) presenting dense microphytobenthic (MPB) biofilm (**Supplementary Figure S1**) were collected during low tide at the Marine Station of Concarneau (France; 47°52.5804′N; 3°55.026′W) in an empty breeding pond, supplied by the surrounding seawater from the Concarneau bay. Due to the particularity of this breeding pond, the biofilm growing at the sediment surface is never fully emerged during low tide (minimum 4–5 cm of seawater). A subsample of MPB biofilm was prepared for Scanning Electron Microscopy (SEM) observation. Briefly, the sample was cleaned in saturated potassium permanganate followed by concentrated HCl. After

acid cleaning, the sample was filtered on a polycarbonate membrane filter (Millipore GTTP, 0.2 μm), coated with gold and observed with a Sigma 300 (Zeiss) field-emission SEM equipped with a conventional Everhart–Thornley and in-lens detectors of secondary electrons at 1.5 kV.

Protocol Optimization for Metabolite Extraction

For the optimization of metabolite extraction, surface samples of mud sediment were collected in February 2019, placed in a tray and the MBP biofilm (top 2–5 mm depth) was collected with a spatula after sediment stabilization (15 samples). Samples were immediately frozen at −20°C until chemical extraction.

Short-Term Light Exposure Experiment

For the short-term light exposure experiment, surface samples of mud sediment were collected on the 13th March 2019 and directly randomly assigned to ten 1 L experimental tanks. The tanks were filled with seawater (around 4 cm of seawater layer on the sediment surface) and left overnight for sediment and biofilm stabilization. During the next morning, t0 samples of MBP biofilm (top 2–5 mm depth) were collected with a spatula and frozen at −20°C (10 samples). Five of the tanks were exposed to natural irradiance (NI; around 1 m from the window; mean irradiance of ca. 102 ± 19 μmol photon m^{-2} s^{-1}). The five remaining tanks were placed in an opaque box covered in the inside with foiled and exposed to higher artificial irradiance (AI). Light was provided by two LED sources (12 W, V-Lumtech®) supplying an irradiance of ca. 167 ± 23 μmol photon m^{-2} s^{-1} over a 11 h:13 h light:dark cycle, corresponding to the photoperiod at this time of the year. Experimental conditions (natural/higher artificial irradiance) were maintained during 7 days. At the end of the experiment (t7), MBP biofilm samples were collected and frozen at −20°C until chemical extraction (n = 5 per condition).

Sample Preparation

Extraction and Fractionation

MBP biofilm samples were freeze-dried prior to extraction. A mass of 200 mg was extracted three times with 3 mL of solvent in an ultrasonic bath during 30 min. Three mixtures of solvent were tested for metabolite extraction in terms of reproducibility and metabolites detection (n = 5 samples per test): M1 = MeOH (methanol)/$CHCl_3$ (chloroform) (1:1); M2 = H_20/MeOH/$CHCl_3$ (1:1:1); and M3 = H_20/MeOH/$CHCl_3$ (1.5:3.5:5) (see **Table 1**). Samples from the short-term light exposure experiment were treated with the mixture 1.

The organic phase was collected after centrifugation (1,800 g, 10 min). These steps were repeated three times and the organic phases were pooled and dried under N_2 at room temperature. The dried extracts were then resuspended in 1 mL of MeOH and fractioned by Solid Phase Extraction (Strata C18-E, 500 mg/6 mL, Phenomenex®) after cartridges cleaning (6 mL MeOH) and conditioning (6 mL H_2O), *via* three successive elutions: 6 mL of H_2O, 6 mL of MeOH and 6 mL of $CHCl_3$. The MeOH (mid-polar) and $CHCl_3$ (apolar) fractions were dried under N_2 before derivatization and were further analyzed separately to reduce the complexity of the extracts. Due to the high concentration in salts, which affects MS-based metabolomics analysis and can damage syringe and column, H_2O fractions were not analyzed. SPE also permitted to fractionate samples in two phases that could be analyzed separately: one expected to contain mostly polar to mid-polar metabolites (MeOH fraction) and the other to mostly consist of non-polar metabolites ($CHCl_3$ fraction).

TABLE 1 | Solvent mixtures used for metabolite extractions.

Mixture	H_20	MeOH	$CHCl_3$
1	0	50%	50%
2	33.3%	33.3%	33.3%
3	15%	35%	50%

Derivatization

Compounds were derivatized in order to be stable and volatile according to a standard protocol. First, 10 μL of ribitol (0.5 $mg.mL^{-1}$ in dH_2O) were added in MeOH fractions and 3 μL of tricosanoic acid (5 $mg.mL^{-1}$ in chloroform) were added in $CHCl_3$ fractions. Fractions were dried under N_2 prior to derivatization. Polar functional groups (e.g., -OH, -COOH, and -NH2; Liebeke and Puskás, 2019) are routinely transformed to TMS-derivatives via the well-establish two-step derivatization procedure involving methoxymation followed by trimethylsilylation (Roessner et al., 2000; Sogin et al., 2019). Recently, a modification of this standard procedure has been applied on different human, terrestrial and marine samples (e.g., urine, yeast, seagrass, corallines, and mangrove sediments) and has shown an increase of sensitivity (i.e., increase in metabolite signal intensity) (Liebeke and Puskás, 2019; Sogin et al., 2019). This method improvement includes a drying step between the methoxymation and trimethylsilylation and was thus employed on our MeOH fractions. First, 80 μL of methoxyamine hydrochloride dissolved in pyridine (20 $mg.mL^{-1}$) were added on the dried MeOH fractions. The mixture was ultrasonicated for 10 min and incubated for 90 min at 37°C in a thermal rotating incubator (120 rpm). The samples were then evaporated under N_2 to remove pyridine. Secondly, 100 μL of BSTFA + 1% TMCS were added and the samples were ultrasonicated for 10 min, briefly vortexed and incubated again for 30 min at 37°C in the thermal rotating incubator. The samples were evaporated again under N_2 to remove the BSTFA/TMCS and resuspended in MeOH for GC-MS analyses. Fatty acids are classically analyzed after transesterification to their corresponding fatty acid methyl esters (FAMEs) (e.g., Beale et al., 2018) the method presently used to derivatize compounds in our $CHCl_3$ fractions. One milliliter of BF_3-MeOH was added on the dried $CHCl_3$ fractions. The mixture was heated at 80°C for 10 min and cooled down at room temperature. Then, 1 mL of deionized water and 1 mL of $CHCl_3$ were added and vortexed before centrifugation at 1,800 g during 5 min. The lower phase was collected and used for GC-MS analyses.

Metabolomic Analyses

GC-MS

The MeOH and $CHCl_3$ fractions were analyzed on a gas chromatograph (7890B GC System- G1513A autosampler, Agilent Technologies®) coupled to a mass selective detector (5977B MSD, Agilent Technologies®) and a flame ionization detector (FID). Separation of metabolites was performed on an HP-5ms Ultra Inert column (30 m, 0.25 mm, and 0.25 μm, Agilent Technologies®) with helium as mobile phase. A volume of 1 μL of each sample was injected in splitless mode at 250°C. The injector temperature was set to 280°C and the FID detector to 300°C. Mass spectra were acquired in electron ionization mode at 70 eV between 35 and 600 m/z at a scan rate of 1.3 scan.s^{-1}. A constant flow rate was set to 1 mL.min^{-1}.

For the $CHCl_3$ fractions, the run started at 100°C for 1 min and increased by 15°C min^{-1} up to 215°C, by 5°C min^{-1} from 215 to 285°C and by 15°C min^{-1} from 285 to 325°C, followed by 3 min of post-run at 100°C. The total runtime was 28.33 min. For the MeOH fractions, the run started at 80°C for 1 min and increased by 10°C min^{-1} up to 325°C, holding 1 min at the final temperature. The run was followed by 3 min of post-run at 80°C for a total runtime of 26.5 min.

For both fractions, a solution with a mix of C8-C20 and C21-C40 alkanes (Fluka Analytical) was also injected for the determination of compound retention index. The identification of fatty acid methyl esters (FAMEs) was confirmed by comparison with a standard mixture (SupelCo 37 FAME mix). For each experiment and fraction, a quality control sample (QC) was prepared with 25 μL of each sample. It was used to monitor MS shift over time and to normalize data according to injection order. The run started with two blank injections, followed by 5 injections of the QC. Samples were then randomly injected, inserting one QC every five samples and two final blanks.

UHPLC-QToF

As LC-MS is more appropriate for polar, weakly polar and neutral compounds (Wang et al., 2015), only the MeOH fractions were analyzed with this technique. Metabolomic fingerprints of MeOH fractions were recorded on a Dionex Ultimate 3000 HPLC system coupled with a Maxis II^{TM} QTOF mass spectrometer (Bruker, MA, United States) fitted with an electrospray ionization (ESI) source. Metabolite separation was performed on a C18 Acclaim^{TM} RSLC Polar Advantage II (2.1 mm × 100 mm, 2.2 μm pore size) column (Thermo Scientific, MA, United States) at 40°C. The mobile phase consisted in a mix of H_2O + 0.1% formic acid (solvent A) and acetonitrile + 0.1% formic acid (solvent B). Injection volume was set to 2 μL and elution flow to 0.3 mL min^{-1}. The elution gradient profile was programmed as follows: 5% B during 2 min, increased up to 50% B from 2 to 9 min and to 90% B from 9 to 15 min, followed by an isocratic step of 90% B during 2 min. The initial conditions were gradually recovered from 17 to 19 min, and hold 3 min for column equilibration for a total runtime of 21 min. In the first half minute of each run, a sodium formate solution was injected directly as an internal reference for calibration. The acquisitions parameters of the ESI source were set as follows: electrospray voltage for the ESI source: 3,500 V, nebulizing gas (N_2) pressure: 35 psi, drying gas (N_2) flow: 8 mL min^{-1}, and drying temperature: 200°C. Mass spectra were recorded in positive ionization mode over the m/z range 100–1,300 at a frequency of 2 Hz. For MS/MS analysis, the cycle time was of 3 s. A quality control sample (QC) was prepared with 25 μL of each sample. It was used to check MS shift over time and to normalize data according to injection order. The run started with two blank injections, followed by 8 injections of the QC for mass spectrometer stabilization. Samples were then randomly injected, inserting one QC every five samples. A final blank was injected to check any memory effect of the compounds on the column.

Data Treatment and Statistical Analyses

GC-MS

Agilent data files acquired from GC-MS analyses were exported into mzXML files using MSconvert (Chambers et al., 2012). mzXML files were then processed using the eRah package (version 1.1.0; Domingo-almenara et al., 2016) under R performing preprocessing, peak deconvolution [min.peak.width = 2.5 (1.5 for MeOH fractions), min.peak.height = 2,500 (1,500 for MeOH fractions), noise. threshold = 500, avoid. processing.mz = c (73,149,207)], peak alignment [min.spectra.cor = 0.90, max. time.dist = 5 (3 for MeOH fractions), mz. range = 40:600] and missing compounds recovery (recMissComp function, minimum number of samples was set at 6). The matrix of compounds obtained was then filtered: peaks present in blanks (signal/noise ratio > 10) and those with higher coefficient of variation in pools (CV < 25%) were removed from the dataset. Finally, compounds annotation was performed by comparing mass spectra with NIST 2017 library completed with the calculation of Kovats' index (Van Den Dool and Kratz, 1963).

LC-MS

LC–MS raw data files were converted to mzXML files with MSconvert. mzXML files were then processed using the package XCMS for R software (R version 3.3.2, XCMS version 3.2.0). Optimized parameters for XCMS were used as follows: peak picking [method = "centwave", peakwidth = c(5,20), ppm = 10], retention time correction (method = "obiwarp", plottype = "deviation") with final grouping parameters (bw = 2, mzwid = 0.015) and filling in missing peaks.

Other parameters were set to default values. A matrix of compounds with peak intensity, m/z value and retention time was generated. The latter was filtered according to blanks and QC to remove technical variability using in-house R scripts [1-Filtering the matrix according to peaks present in blanks relative to pools (signal/noise ratio > 10), 2-filtering the matrix according to peaks coefficient of variation (CV) calculated on pool (CV < 20%) and 3-filtering the matrix according to autocorrelation between peaks]. Metabolites were annotated with constructor software (Bruker Compass DataAnalysis 4.4). Molecular network based on LC-MS/MS spectra were constructed with GNPS (M. Wang et al., 2016) using the following settings: precursor ion mass tolerance: 2 Da, fragment ion mass tolerance: 0.5 Da, min pairs cos: 0.7, minimum matched fragment ion: 6, node topK: 10 and minimum cluster size: 2. Resulting networks were

observed under Cytoscape 3.5.0 (Shannon et al., 2003). Metlin[1], MassBank, SIRIUS 4.0 (Böcker and Dührkop, 2016) and In-Silico MS/MS DataBase (ISDB) (Allard et al., 2016) were also used for putative annotation.

Data from LC-MS and GC-MS were normalized by log-transformation before statistical analyses. The relative standard deviations (%RSD = standard deviation/mean*100) were calculated for each metabolite (Parsons et al., 2009) to characterize measurement variability according to the solvent extraction mixtures. The percentage of total detected metabolites per sample was also calculated for each mixture used for metabolites extraction, for each dataset (i.e., MeOH fractions analyzed by GC-MS, MeOH fractions analyzed by LC-MS and $CHCl_3$ fractions analyzed by GC-MS) on the final matrix (after data analyses and filtering according to blanks and QC). The normality of the data distribution (%RSD and %compounds detected) was tested using the Shapiro–Wilk test but not confirmed. The non-parametric Kruskal–Wallis' test was thus used to identify differences between the percentages of RSD and metabolites detected according to the method, followed by *post hoc* Conover's test. To identify which significant factors were linked to the metabolites diversity, we used Permutational Multivariate Analysis of Variance using distance matrices (PERMANOVA, 9999 permutations, vegan package for R). Principal component analysis (PCA) was used to visualize the metabolome variation according to the irradiance condition and time (ade4 package for R). Powered Partial Least-Squares-Discriminant Analysis (PPLS-DA) were used to find the maximum covariance between our data set and their class membership. Permutational tests based on cross model validation (MVA.test and pairwise.MVA.test) were applied to test differences between groups (RVAideMemoire package) and correlation circles were drown to identify discriminating compounds (RVAideMemoire package). Wilcoxon signed-rank tests were used to identify differences in normalized intensities of discriminating compounds between sampling time (t0 vs. t7 samples) and Mann–Whitney–Wilcoxon tests to identify those between light treatments (NI vs. AI).

RESULTS

The MPB biofilm was dominated by diatoms, mainly by *Pleurosigma formosum* (**Figure 1A**), followed by *Gyrosigma balticum* (**Figure 1B**). Other abundant genera were characterized: *Entomoneis*, *Cocconeis*, *Falacia*, and *Campylodiscus*.

Protocol Selection for Metabolite Extraction

The resulting $CHCl_3$ and MeOH fractions obtained with M1, M2 or M3 were compared for extracting metabolites from MPB biofilms present in mudflat sediments.

In the $CHCl_3$ fractions analyzed by GC-MS, the RSDs were low and not significantly different according to the solvent mixtures used (median RSDs of 1.25, 1.15, and 1.47% for M1, M2, and M3, respectively; **Figure 2A**; KW = 1.13, $p = 0.57$). All three mixtures allowed to detect the same number of metabolites in these fractions (100% of total compounds detected, **Figure 2B**).

However, significant differences in reproducibility and number of detected metabolites were observed in the MeOH fractions analyzed by GC-MS and LC-MS (**Figures 2C,E**). In these fractions analyzed by GC-MS, a higher reproducibility was obtained with M1 and M2 (median RSDs of 8.47 and 13.28%, respectively, **Figure 2C**) while M3 gave significantly higher RSD (median RSD of 21.12%; *post hoc* $p < 0.05$). A higher number of metabolites were detected with M1 and M3 (96.96 ± 4.51 and 87.39 ± 18.08% of total detected metabolites, respectively; **Figure 2D**) but the variability in M3 appeared superior (standard deviation of 18.08%, four times higher compared to M1). A lower number of metabolites was detected in the same dataset with M2 (66.95 ± 11.23%; *post hoc* $p < 0.05$). In the same MeOH fractions analyzed by LC-MS (**Figure 2E**), low RSDs were obtained for all mixtures but M2 gave the lowest (median RSD 5.29%) compared to M1 and M3 which were not significantly different regarding the reproducibility (median RSDs of 6.42 and 6.45%, respectively; *post hoc* $p = 0.58$). A higher number of metabolites were detected with M3 (92.2 ± 7.8%), followed by M1 (85 ± 7.4%; **Figure 2F**). As for GC-MS analyses in these MeOH fractions, less metabolites were significantly detected in the same dataset with M2 (71.3 ± 6.3%). Combining results obtained with both techniques on the MeOH fractions (**Figures 2G,H**), we got a higher number of metabolites detected with M1 and M3 (91 ± 8.5 and 89.8 ± 13.4%, respectively) with a lower variability for M1, while not statistically supported [**Figure 2H**; KW = 14, $p < 0.05$, *post hoc* p(M1 vs. M3) = 0.98].

Collectively, we determined that solvent mixture 1 was more appropriate to reflect the chemical diversity of MPB biofilm and was used for the light exposure experiment.

Short-Term Light Exposure Experiment

$CHCl_3$ Fractions Analyzed by GC-MS

After GC-MS data analyses and the exclusion of artifactual and irreproducible peaks (coefficient of variation > 25%), a total of 56 features were highlighted in the $CHCl_3$ fraction (see **Supplementary Table S1** and **Supplementary Figure S2**). These features were tentatively annotated using NIST 2017 library and by comparison with a standard mixture for fatty acid methyl esters. Around 77% of the compounds could be annotated while 23% remain unknown. Among the annotated compounds (**Table 2** and **Figure 3**), a majority of fatty acids (FA) were displayed (53.5%), with a dominance of saturated FA (SFA; 30.2%) followed by monounsaturated FA (MUFA; 11.6%) and polyunsaturated FA (PUFA; 11.6%). Other families of molecules were highlighted such as alkenes (9.3%), alkanes (9.3%), fatty esters (7%), terpenes (7%), carboxylic acids (4.7%), phtalic acids (4.7%), a lactone (4,8,12-trimethyltridecan-4-olide; 2.3%), and an heterocyclic compound [3-(3,7-dimethyloct-6-enoxy)oxane; 2.3%]. Two compounds were assigned as plastic pollutants (ethyl 4-ethoxybenzoate and diethyl phtalate).

The effects of irradiance condition (natural: NI versus higher artificial: AI) and time on the metabolomic fingerprint of

[1]https://metlin.scripps.edu/

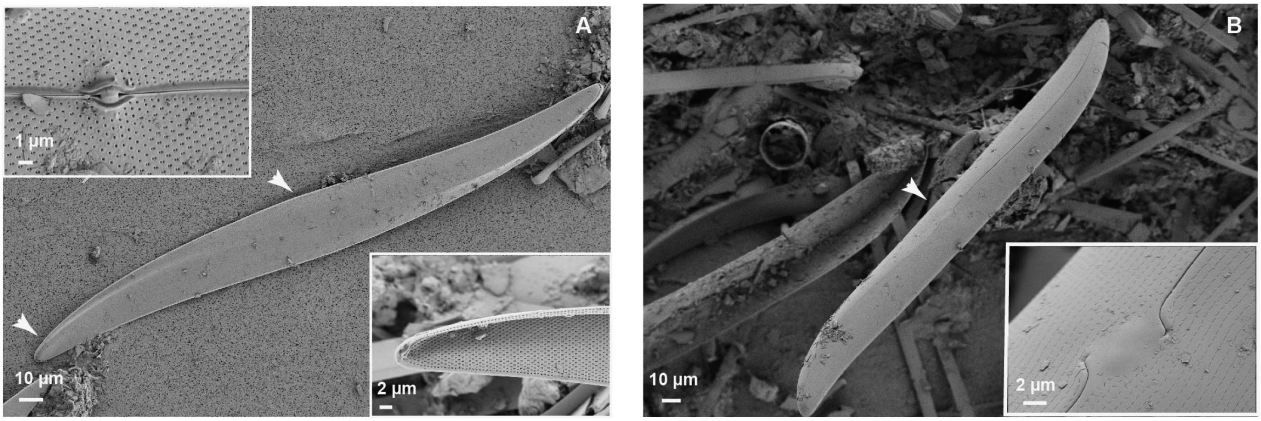

FIGURE 1 | Scanning electron microscopy (SEM) images of **(A)** *Pleurosigma formosum* with a focus on the central nodule structure (top left) and apical end structure (bottom right) and **(B)** *Gyrosigma balticum* with a focus on the central nodule structure (for all images: detector SE2, diaph 30.00).

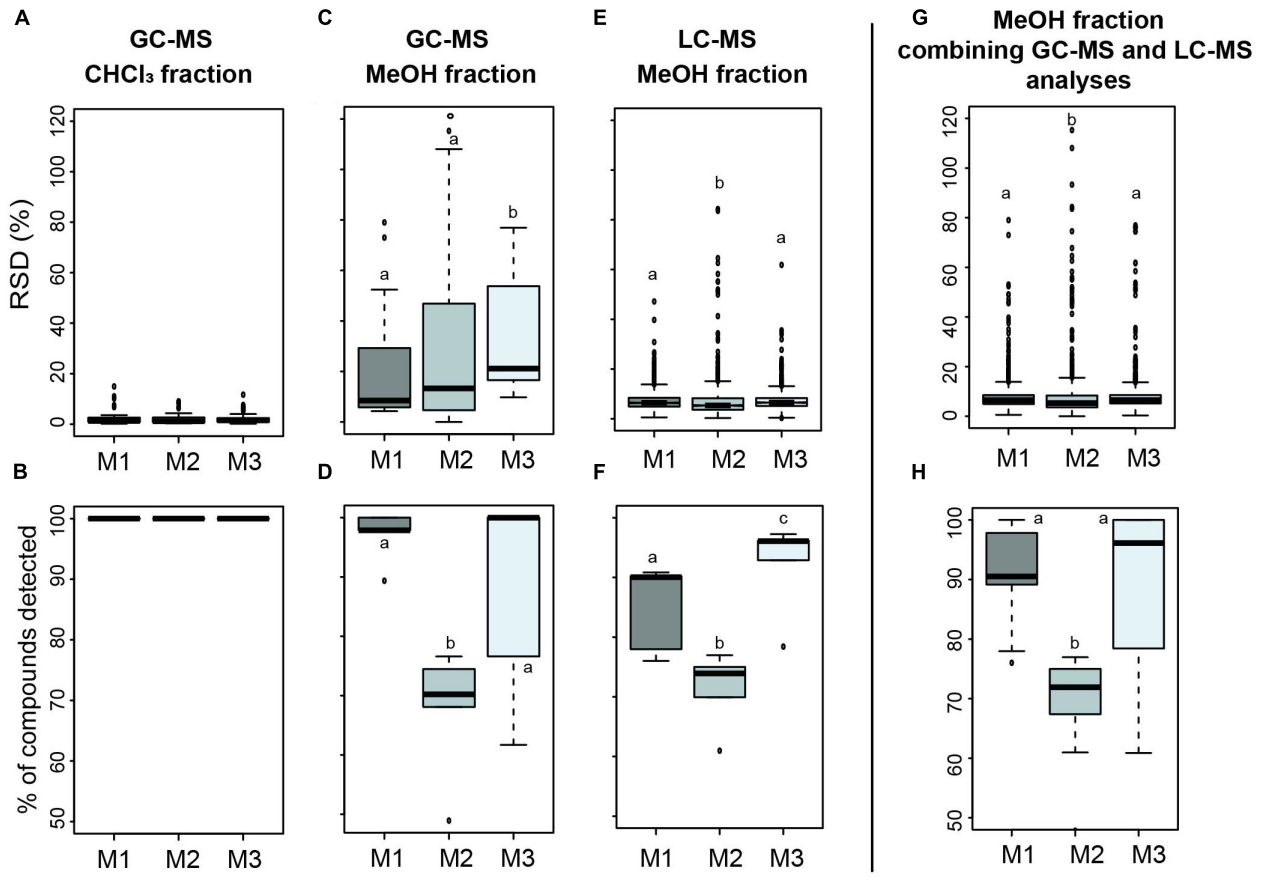

FIGURE 2 | Boxplots of the relative standard deviation (% RSD; **A,C,E,G**) and percentage of total detected metabolites **(B,D,F,H)** comparing the reproducibility associated with three solvent extraction mixtures according to the fraction ($CHCl_3$/MeOH) and the technique (GC-MS/LC-MS) used (M1 = MeOH/$CHCl_3$ (1:1), M2 = H_20/MeOH/$CHCl_3$ (1:1:1), and M3 = H_20/MeOH/$CHCl_3$ (1.5:3.5:5). Statistical analyses were performed using Kruskal–Wallis followed by *post hoc* Conover's test. Letters indicate distinct groupings based on *post hoc* pairwise comparisons among solvent mixtures ($p < 0.05$).

MPB biofilm were then investigated in this $CHCl_3$ fraction obtained by GC-MS. An unsupervised analysis (PCA) allowed to explain 53.47% of variance on the two first components (**Figure 4A**). The supervised analysis (PPLS-DA) highlighted the influence of time and light exposure on the metabolome of the MPB biofilm. Indeed, different metabolomic fingerprints

TABLE 2 | Annotated compounds in the $CHCl_3$ fraction of the MPB biofilm during the light exposure experiment (after data analyses and filtering).

Comp.	Molecular name	Chemical family	Raw formula	Match NIST	CAS number	Exp. RI	litt. RI
C13	1,4-benzenedicarboxylic acid	Phtalic acid	$C_8H_6O_4$	674*	120-61-6	1519	1515
C14	Dodecanoic acid	Fatty acid	$C_{12}H_{24}O_2$	564*	111-82-0	1526	1526
C17	Ethyl 4-ethoxybenzoate[§]	Carboxylic acid	$C_{11}H_{14}O_3$	819	23676-09-7	1540	1522
C21	Cetene	Alkene	$C_{16}H_{32}$	588*	629-73-2	1594	1592
C22	Hexadecane	Alkane	$C_{16}H_{34}$	510*	544-76-3	1601	1600
C23	Diethyl phtalate[§]	Phtalic acid	$C_{12}H_{14}O_4$	794		1612	1594
C24	Tridecanoic acid	Fatty acid	$C_{13}H_{26}O_2$	615*	1731-88-0	1627	1624
C27	12-methyltridecanoic acid	Fatty acid	$C_{14}H_{28}O_2$	688*	5129-58-8	1691	1686
C30	Heptadecane	Alkane	$C_{17}H_{36}$	720	629-78-7	1702	1700
C34	9-tetradecenoic acid	Fatty acid	$C_{14}H_{26}O_2$	856	56219-06-8	1710	1715
C36	Tetradecanoic acid (14:0)	Fatty acid	$C_{14}H_{28}O_2$	938	124-10-7	1727	1725
C37	Octadecane	Alkane	$C_{18}H_{38}$	705	593-45-3	1760	1800
C39	13-methyltetradecanoic acid	Fatty acid	$C_{15}H_{30}O_2$	828	1000424-50-7	1791	1779
C41	1-octadecene	Alkene	$C_{18}H_{36}$	890	112-88-9	1795	1793
C43	12-Methyltetradecanoic acid	Fatty acid	$C_{15}H_{30}O_2$	807	5129-66-8	1800	1788
C44	10-pentadecenoic acid	Fatty acid	$C_{15}H_{28}O_2$	912	1000426-92-2	1808	–
C45	Pentadecanoic acid (15:0)	Fatty acid	$C_{15}H_{30}O_2$	956	7132-64-1	1828	1820
C49	Neophytadiene	Terpene	$C_{20}H_{38}$	872	504-96-1	1843	1837
C50	Phytol	Diterpene	$C_{20}H_{40}O$	781	102608-53-7	1867	2116
C55	Neophytadiene	Terpene	$C_{20}H_{38}$	869	–	1887	1837
C57	Hexadeca-6,9,12-trienoic acid	Fatty acid	$C_{16}H_{26}O_2$	875	1000336-34-6	1904	1871
C62	9-hexadecenoic acid (16:1n-7)	Fatty acid	$C_{16}H_{30}O_2$	959	1120-25-8	1911	1898
C65	Hexadecanoic acid (16:0)	Fatty acid	$C_{16}H_{32}O_2$	953	112-39-0	1928	1926
C67	4,8,12-trimethyltridecan-4-olide	Lactone	$C_{16}H_{30}O_2$	744	220904-24-5	1952	–
C68	3-(3,5-Di-tert-butyl-4-hydroxyphenyl)propionic acid	Carboxylic acid	$C_{17}H_{26}O_3$	775	6386-38-5	1960	1943
C71	3-(3,7-dimethyloct-6-enoxy)oxane	Heterocyclic compound	$C_{15}H_{28}O_2$	737	–	1972	–
C76	1-eicosene	Alkene	$C_{20}H_{40}$	741	3452-07.1	1995	1995
C83	10-heptadecenoic acid	Fatty acid	$C_{17}H_{32}O_2$	929	–	2009	2016
C87	Heptadecanoic acid (17:0)	Fatty acid	$C_{17}H_{34}O_2$	831	1731-92-6	2028	2028
C89	Phytyl, 2-methylbutanoate	Phytyl fatty acid ester	$C_{25}H_{48}O_2$	832	–	2042	2441
C93	Phytyl, 2-methylbutanoate	Phytyl fatty acid ester	$C_{25}H_{48}O_2$	781		2071	2441
C95	6,9,12,15-Octadecatetraenoic acid (18:4n-3)	Fatty acid	$C_{18}H_{28}O_2$	863	73097-00-4	2097	2088
C98	9,12-Octadecadienoic acid (18:2n-6)	Fatty acid	$C_{18}H_{32}O_2$	887	2462-85-3	2103	2101
C99	9-octadecenoic acid	Fatty acid	$C_{18}H_{34}O_2$	913	112-62-9	2109	2110
C103	Stearic acid	Fatty acid	$C_{18}H_{36}O_2$	935	112-61-8	2129	2128
C114	Hexanoic acid, heptadecyl ester	Fatty ester	$C_{23}H_{46}O_2$	665*	–	2185	–
C119	1-docosene	Alkene	$C_{22}H_{44}$	907	1599-67-3	2195	2193
C123	5,8,11,14,17-eicosapentaenoic acid (20:5n-3)	Fatty acid	$C_{20}H_{30}O_2$	911	2734-47-6	2280	2282
C126	Eicosanoic acid	Fatty acid	$C_{20}H_{40}O_2$	684*	1120-28-1	2330	2329
C128	Tetracosane	Alkane	$C_{24}H_{50}$	687*	646-31-1	2400	2400
C133	4,7,10,13,16,19-docosahexaenoic acid (22:6n-3)	Fatty acid	$C_{22}H_{32}O_2$	830	2566-90-7	2467	2471
C137	Docosanoic acid	Fatty acid	$C_{22}H_{44}O_2$	627*	929-77-1	2532	2528
C147	Tetracosanoic acid	Fatty acid	$C_{24}H_{48}O_2$	650*	2442-49-1	2735	2728

Annotation was done with NIST 2017 and by comparison with a standard mixture for fatty acid methyl esters (comp, compound; RI, Van den Dool and Kratz Retention Index; exp, experimental; litt, litterature). [§] *Presumed anthropogenic contaminants from plastic origin. *Indicate a match with NIST 2017 library < 700.*

were observed between t0 and t7 samples independently of the irradiance condition (PPLS-DA, CER = 0.39, $p = 0.003$, *post hoc* $p < 0.05$ for each pair, **Figure 4B** and **Supplementary Table S2**), except for t0 NI versus t7 AI for which metabolomic changes were not statistically supported (*post hoc* $p = 0{,}108$, **Supplementary Table S2**). The irradiance condition was correlated with metabolomic changes after 7 days of treatment, between samples exposed to natural (t7 NI) and higher artificial irradiance [t7 AI; *post hoc* p(t7 AI vs. t7 NI) = 0.036; **Figure 4B**, **Supplementary Table S2**].

The metabolites significantly impacted by time or light exposure conditions were thus investigated (**Figure 5A**). Four of them majorly contributed to the metabolomic discrimination according to time (threshold 0.8; plastic pollutants were not considered): C39, C43, C56, and C93. All these compounds were significantly decreased at the end of the experiment

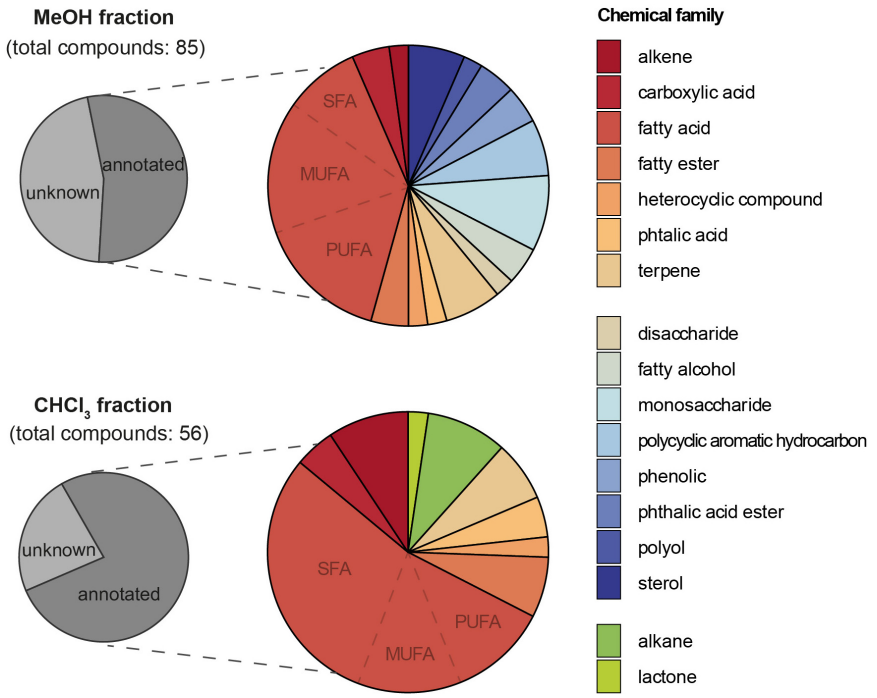

FIGURE 3 | Pie charts showing the proportions (from the total number of detected compounds) of annotated compounds and their chemical family in the MeOH and $CHCl_3$ fractions analyzed by GC-MS.

(**Figure 5B**). Two of them could be annotated as branched-chain fatty acids: 13- methyltetradecanoic acid (C39) and 12- methyltetradecanoic acid (43), one as a phytol derivative (C93, phytyl, 2-methylbutanoate) and C56 remained unknown. Other compounds significantly contributing to the metabolomic variation with time were found (with threshold = 0.7 on PPLS-DA loading plot, **Figure 5A**) and majorly tend toward a decrease by the end of the experiment (C14: dodecanoic acid, C19: unknown, C27: 12-methyltridecanoic acid, C36: tetradecanoic acid, C62: 9-hexadecenoic acid, C67: 4,8,12-trimethyltridecan-4-olide, C74: unknown, C75: unknown, C83: 10-heptadecenoic acid and C114: hexanoic acid, heptadecyl ester), excepted one metabolite which increased at t7 (C128: tetracosane) (see **Supplementary Figure S3**). Two metabolites correlated with the irradiance condition at t7 were also highlighted (threshold = 0.7, **Figure 5C**): C12 (unknown) and C30 (heptadecane), which are both decreased by the end of the experiment in samples exposed to higher artificial irradiance compared to those exposed to natural irradiance.

MeOH Fractions Analyzed by GC-MS and LC-MS

After GC-MS data treatment and filtering, 85 features were isolated in the MeOH fraction (see **Supplementary Table S3** and **Supplementary Figure S4**). As for the $CHCl_3$ fraction, the NIST 2017 library allowed us to annotated some compounds present in the MeOH fraction of MPB biofilm (around 54%) after data analyses and filtering (**Table 3** and **Figure 3**). A majority of fatty acids (39.1%) was also highlighted, dominated by PUFA and MUFA (15.2% each), followed by SFA (8.7%). Other compounds in smaller quantity were found and included mono- and disaccharides (8.7 and 2.2%), sterols (6.5%), terpenes (6.5%), fatty alcohols (4.3%), fatty esters (4.3%), carboxylic acids (4.3%), phenolics (4.3%), phtalic acid and phtalic acid esters (2.2 and 4.3%), a polyol (2.2%), an heterocyclic (2.2%) and an alkene (2.2%). Presumed anthropogenic contaminants from plastic origin were also identified among them, including some belonging to Polycyclic Aromatic Hydrocarbons (PAH, 6.5%).

The effects of light exposure and time on the metabolomic fingerprint of this MeOH fraction analyzed by GC-MS were then explored. The variance on the two first components of the PCA was explained by 73.4% (**Figure 4C**) and mainly due to a high intra-group variation in samples collected after 7 days of exposure to higher artificial irradiance (t7 AI). The irradiance condition was not statistically correlated with metabolomic changes in the MPB biofilm (PERMANOVA, $F = 0.49$, $p = 0.89$) neither to the time or their combination [PERMANOVA, F(time) = 2.14, p(time) = 0.06; F(time*irradiance) = 1.70, p(time*irradiance) = 0.13; PPLS-DA, CER = 0.619, $p = 0.146$, **Figure 4D**].

The effects of experimental conditions on the metabolomic fingerprint of MPB biofilms were finally explored in the same MeOH fraction analyzed by LC-MS. After data analyses and filtering, 2,547 features were considered in this fraction. The explained variance on axis 1–2 of the PCA was 62.65% (**Figure 4E**) and mainly due to a high intra-group variation in samples collected at t7 after exposure to higher artificial irradiance (t7 AI), as observed in the PCA for the same fraction analyzed by GC-MS. Only the time was correlated with metabolomic changes in this

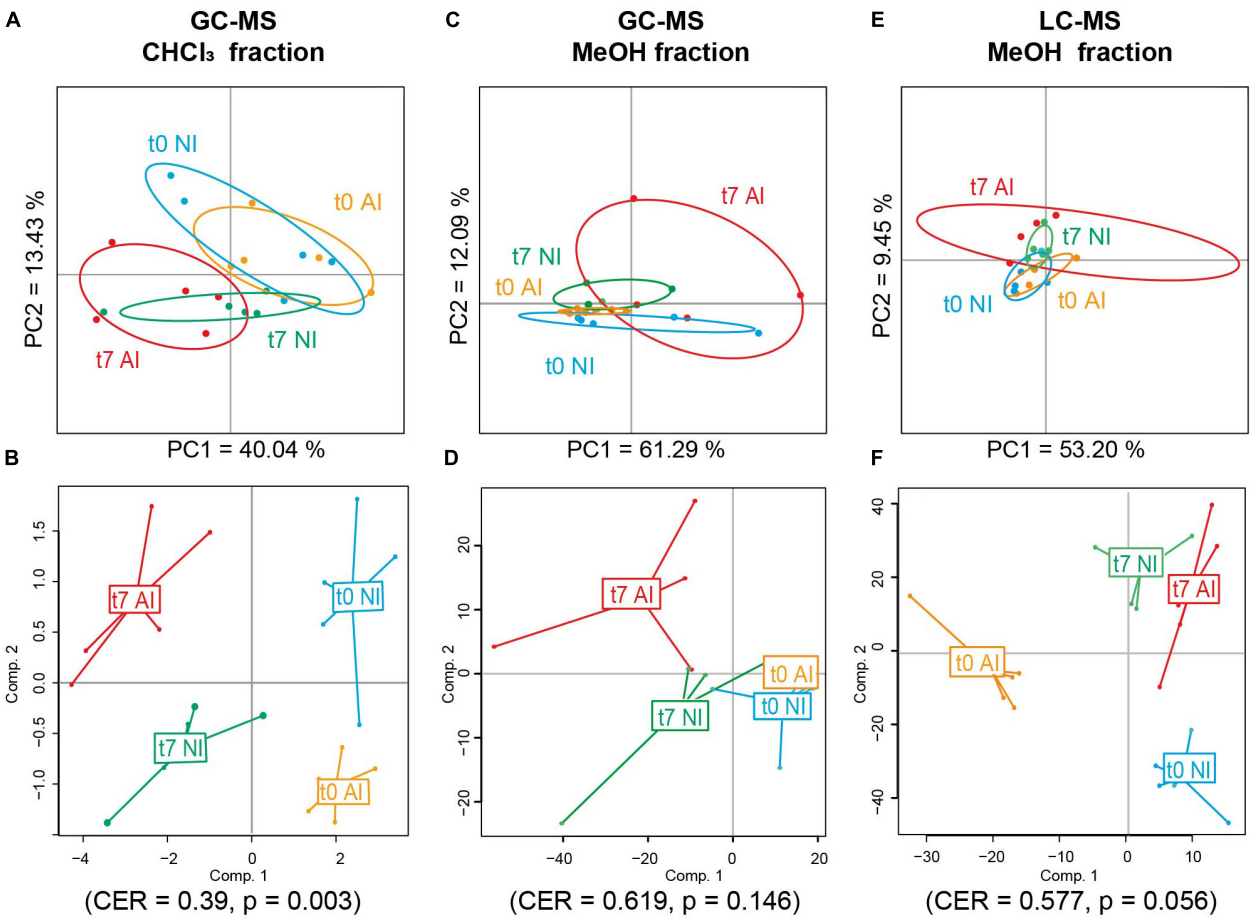

FIGURE 4 | Metabolomic fingerprint analyses of the MPB biofilm at the beginning (t0) and the end (t7) of the experiment depending of the light exposure conditions via unsupervised (Principal Component Analysis, PCA, **A,C,E**) and supervised discriminant (Powered Partial Least-Squares-Discriminant Analysis, PPLS-DA, **B,D,F**) analyses. The metabolome was analyzed by **(A,B)** GC-MS for $CHCl_3$ fractions, **(C,D)** GC-MS for MeOH fractions, and **(E,F)** LC-MS for MeOH fractions (NI: natural irradiance; AI: higher artificial irradiance). CER, classification error rate with *p*-value after double cross model validation.

fraction (PERMANOVA, F = 2.48, p = 0.019; PPLS-DA, CER = 0.105; p = 0.001), neither the effect of irradiance or the combination of factors was statistically supported [PERMANOVA, F(irradiance) = 0.96, p(irradiance) = 0.46; F(time*irradiance) = 0.8, p(time*irradiance) = 0.71; PPLS-DA, CER = 0.577, p = 0.056, **Figure 4F**]. Unfortunately, most probable raw formula of compounds correlated to time (**Supplementary Table S4**) did not match with any known compounds after the construction of a molecular network with GNPS and were not unambiguously identified by annotation against ISDB, MassBank and SIRIUS 4.0.

DISCUSSION

In this study, we detailed a protocol for untargeted metabolomic fingerprinting in MPB biofilms from mudflats. We selected a sonication-assisted extraction using organic solvents, a popular and easy to reproduce technique that has been widely applied on different types of marine samples (e.g., Fernandez-Varela et al., 2015; Bourke et al., 2017; Wilkinson et al., 2018; Gaubert et al., 2019). Three solvent extraction mixtures using different proportions of the commonly used methanol and chloroform (e.g., Kruger et al., 2008; Cajka and Fiehn, 2016; Kumar et al., 2016) have been tested. Using a biphasic mixture with a polar (MeOH + 0–33% H_2O) and a non-polar ($CHCl_3$) solvent, a wide range of compounds has been extracted, both hydrophilic and lipophilic, also increasing the molecular complexity of the MPB extracts. A good reproducibility (median RSDs < 1.5%) and the same high number of detected metabolites were equivalently obtained in the $CHCl_3$ fraction with all mixtures. Thus, we could not use this fraction to select the most appropriate solvent mixture for metabolite extraction. Based on the MeOH fraction analyzed by GC-MS and LC-MS, the mixture 1 (MeOH/$CHCl_3$ 1:1) has been retained as it gave a large number of detected metabolites with a good reproducibility. This is in accordance with the objective of the untargeted metabolomic fingerprinting approach. The mixture 3 showed similar results but the number of metabolites detected was more variable (13.4% for M3 vs. 8.5% for M1) while

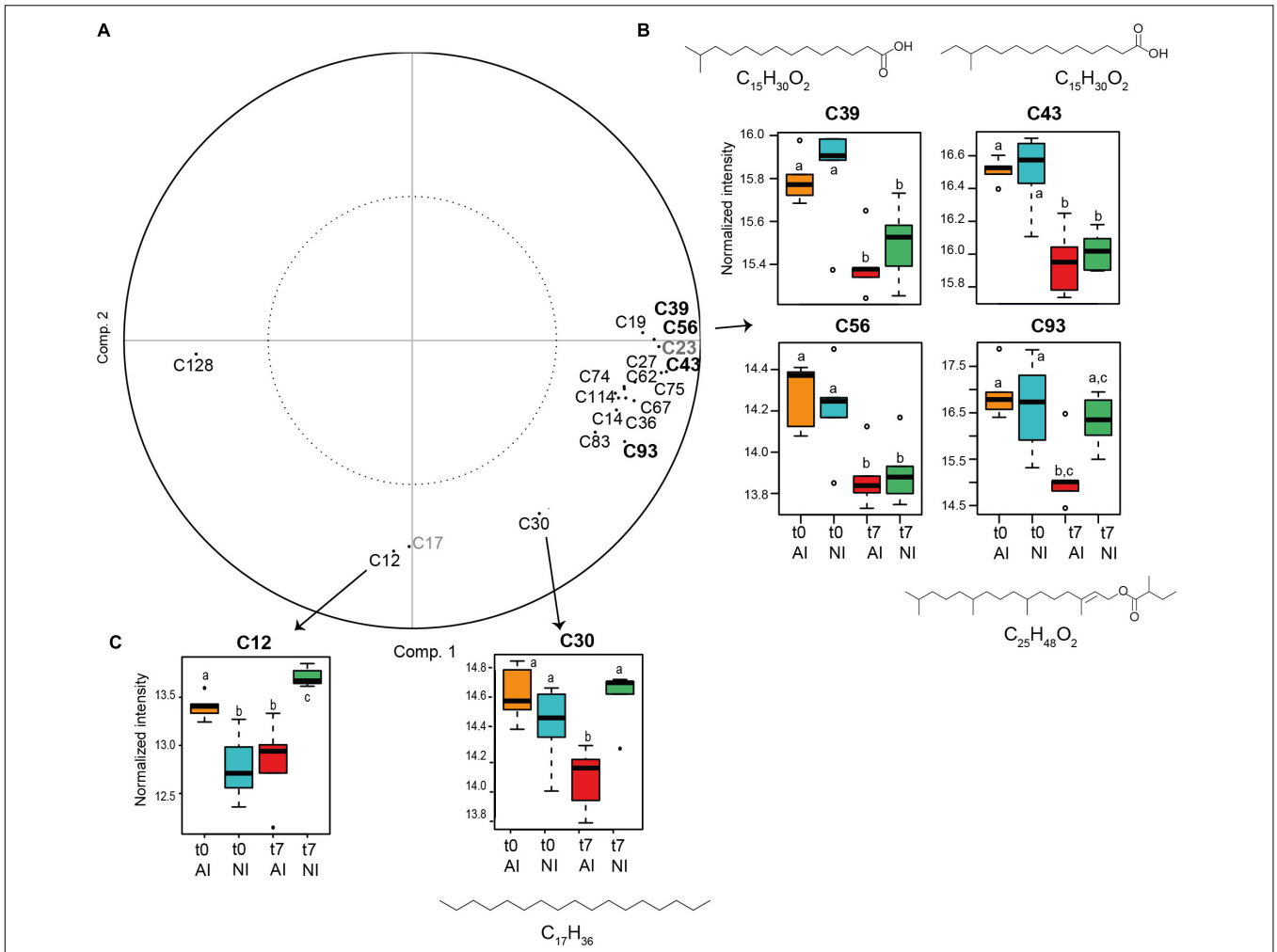

FIGURE 5 | (A) PPLS-DA loading in the $CHCl_3$ fraction (compounds in bold were selected with threshold = 0.8 and the others with threshold = 0.7. The two compounds in gray are plastic pollutants and were not considered). **(B)** Box plots of the compounds annotated in the $CHCl_3$ fraction responsible for metabolomic differences according to time (threshold = 0.8) and **(C)** to the light exposure condition at t7 (threshold = 0.7) (t0: beginning and t7: end of the experiment; NI: natural irradiance; AI: higher artificial irradiance). Ion intensities of metabolites are expressed as mean normalized intensities ± SD (log-transformed data, $n = 5$ per group). Statistical analyses were performed using Wilcoxon signed-rank tests to compare t0 vs. t7 samples and Mann–Whitney–Wilcoxon tests to compare light treatments. Letters indicate distinct groupings based on these tests for each compounds ($p < 0.05$). Chemical formulas are displayed for annotated compounds.

not statistically supported. The mixture 2 was dismissed as the number of metabolites detected was distinctly lower compared to other mixtures. The presently described experimental set up was then applied and validated on a case study: the effect of light exposure condition on the metabolome of MBP biofilms from mudflat sediments.

MPB biofilm samples collected at t0 and t7, under natural or higher artificial irradiance, were processed and the metabolite composition was analyzed by GC-MS. Among them, 46 and 43 features (in MeOH and $CHCl_3$ fractions, respectively) were putatively annotated based on a combinatorial matching of mass spectra and retention index. Both fractions displayed a majority of fatty acids (FA) with 12 to 24 carbon atoms among annotated compounds. This is not surprising as diatoms, one of the main components of MPB biofilm, are known for their richness in lipids (Nappo et al., 2009; Cointet et al., 2019). The presence and combination of some FA were characteristic of diatoms: 14:0, 16:0 and its metabolic derivatives 16:1n-7 and 16:4n-1 and the two PUFA 20:5n-3 (eicosapentaenoic acid, EPA) and 22:6n-3 (docosahexaenoic acid, DHA) (Dalsgaard et al., 2003; Kelly and Scheibling, 2012). The detection of 22:6n-3 and 18:4n-3 could reflect the presence of dinoflagellates (Budge and Parrish, 1998; Dalsgaard et al., 2003; Kelly and Scheibling, 2012). Fatty acids biomarkers of heterotrophic bacteria were also identified. They are composed of odd-numbered and iso- and anteiso-branched SFA and MUFA such as 15:0, 17:0, and 15:1 (e.g., 12-methyltetradecanoic acid; 13-methyltetradec-9-enoic acid; 13-methyltetradec-9-enoic acid), as well as cyclopropyl FA (Dalsgaard et al., 2003; Kelly and Scheibling, 2012).

Apart from FA, our study showed the high molecular diversity of the MPB biofilm, with numerous classes of compounds represented: alkenes, alkanes, fatty esters, terpenes, carboxylic

TABLE 3 | Annotated compounds in the MeOH fraction of the MPB biofilm during the light exposure experiment (after data analyses and filtering).

Comp.	Molecular name	Chemical family	Raw formula	Match NIST	CAS number	Exp. RI	Litt. RI
C10	Glycerol	Polyol	$C_3H_8O_3$	776	–	–	–
C42	Naphthalene, 1,2-dihydro- 1,1,6-trimethyl[§]	Polycyclic aromatic hydrocarbons	$C_{13}H_{16}$	645*	30364-38-6	1369	1354
C44	3-octen-2-ol	Fatty alcohol	$C_8H_{16}O$	620*	86297-58-7	1388	–
C51	Naphthalene, 1,7-dimethyl[§]	Polycyclic aromatic hydrocarbons	$C_{12}H_{12}$	769	573-37-1	1421	1404
C72	2,4-di-ter-butylphenol[§]	Phenolic	$C_{14}H_{22}O$	725	96-76-4	1515	1519
C108	Diethyl phtalate[§]	Phtalic acid	$C_{12}H_{14}O_4$	959	–	1605	1594
C137	Ribofuranose	Monosaccharide	$C_5H_{10}O_5$	825	–	1684	1624
C146	9-tetradecenoic acid	Fatty acid	$C_{14}H_{26}O_2$	919	56219-06-8	1708	1715
C155	Tetradecanoic acid (14:0)	Fatty acid	$C_{14}H_{28}O_2$	955	124-10-7	1728	1725
C179	10-pentadecenoic acid	Fatty acid	$C_{15}H_{28}O_2$	861	–	1806	–
C182	13-methyltetradec-9-enoic acid	Fatty acid	$C_{15}H_{28}O_2$	733	–	1812	–
C186	Pentadecanoic acid (15:0)	Fatty acid	$C_{15}H_{30}O_2$	947	7132-64-1	1828	1820
C191	Neophytadiene (isomer II)	Terpene	$C_{20}H_{38}$	928	504-96-1	1843	1837
C204	Neophytadiene (isomer I)	Terpene	$C_{20}H_{38}$	896	504-96-1	1867	1837
C207	Phytol	Diterpene	$C_{20}H_{40}O$	889	102608-53-7	1886	2116
C210	6,9,12,15-hexadecatetraenoic acid (16:4n-1)	Fatty acid	$C_{16}H_{24}O_2$	900	–	1892	1863
C216	9-hexadecenoic acid (16:1n-7)	Fatty acid	$C_{16}H_{30}O_2$	954	1120-25-8	1912	1898
C217	9,12-hexadecadienoic acid	Fatty acid	$C_{16}H_{28}O_2$	888	2462-80-8	1915	–
C223	Hexadecanoic acid (16:0)	Fatty acid	$C_{16}H_{32}O_2$	961	112-39-0	1931	1926
C226	Mannose	Monosaccharide	$C_6H_{12}O_6$	894	128705-67-9	1936	–
C229	Glucose	Monosaccharide	$C_6H_{12}O_6$	710	128705-73-7	1936	–
C238	Galactose	Monosaccharide	$C_6H_{12}O_6$	762	128705-64-6	1955	–
C239	3-(3,5-Di-tert-butyl-4-hydroxyphenyl)propionic acid	Carboxylic acid	$C_{17}H_{26}O_3$	722	6386-38-5	1956	1943
C241	1H-indene-4-acetic acid, 6-(1,1-dimethylethyl)-2,3-dihydro-1,1-dimethyl	Carboxylic acid	$C_{17}H_{24}O_2$	718	55591-05-4	1961	–
C248	3-(3,7-dimethyloct-6-enoxy)oxane	Heterocyclic comp.	$C_{15}H_{28}O_2$	725	–	1973	–
C254	Gamma-linolenic acid	Fatty acid	$C_{18}H_{30}O_2$	828	16326-32-2	1993	–
C259	9-heptadecenoic acid	Fatty acid	$C_{17}H_{32}O_2$	832	14101-91-8	2007	2003
C280	Phytyl, 2-methylbutanoate	Phytyl fatty acid ester	$C_{25}H_{48}O_2$	749	–	2070	2441
C286	6,9,12,15-octadecatetraenoic acid (18:4n-3)	Fatty acid	$C_{18}H_{28}O_2$	917	73097-00-4	2093	2088
C288	Pyrene	Polycyclic aromatic hydrocarbons	$C_{16}H_{10}$	632*	129-00-0	2099	2093
C293	9-octadecenoic acid	Fatty acid	$C_{18}H_{34}O_2$	883	13481-95-3	2109	2105
C297	Stearic acid	Fatty acid	$C_{18}H_{36}O_2$	911	112-61-8	2129	2128
C304	1-octadecanol	Fatty alcohol	$C_{18}H_{38}O$	820	18748-98-6	2157	2152
C316	1-docosene	Alkene	$C_{22}H_{44}$	721	1599-67-3	2195	2193
C332	3-chloropropionic acid, heptadecyl ester	Fatty ester	$C_{20}H_{39}ClO_2$	762	1000283-05-1	2296	–
C334	5,8,11,14,17-eicosapentaenoic acid (20:5n-3)	Fatty acid	$C_{20}H_{30}O_2$	801	1191-65-7	2298	–
C349	2- octyl-, cyclopropanedecanoic acid	Fatty acid	$C_{21}H_{40}O_2$	644*	10152-64-4	2411	–
C355	4,7,10,13,16,19-docosahexaenoic acid (22:6n-3)	Fatty acid	$C_{22}H_{32}O_2$	853	2566-90-7	2465	2471
C363	13-docosenoic acid	Fatty acid	$C_{22}H_{42}O_2$	914	1120-34-9	2509	2508
C373	2,4-bis (dimethylbenzyl) phenol[§]	Phenolic	$C_{24}H_{26}O$	708	2772-45-4	2539	2508
C376	Phthalic acid, di(2-propylpentyl) ester[§]	Phthalic acid ester	$C_{24}H_{38}O_4$	735	–	2560	2527
C393	Dioctyl terephthalate[§]	Phthalic acid ester	$C_{24}H_{38}O_4$	829	6422-86-2	2756	2766
C402	Lactose	Disaccharide	$C_{12}H_{22}O_{11}$	717	42390-78-3	2816	–
C431	Desmosterol	Sterol	$C_{27}H_{44}O$	813	18880-60-9	3081	3169
C439	Cholesterol	Sterol	$C_{27}H_{46}O$	877	1856-05-9	3101	3150
C444	Ergosta-7,22-dien-3-ol	Sterol	$C_{28}H_{46}O$	665*	55527-93-0	3145	3203

Annotation was done with NIST 2017 and by comparison with a standard mixture for fatty acid methyl esters (comp, compound; RI, Van den Dool and Kratz Retention Index; exp, experimental; litt, litterature). [§] *Presumed anthropogenic contaminants from plastic origin. *Indicate a match with NIST 2017 library < 700.*

acids, phtalic acids, heterocyclic compounds, lactones, mono- and disaccharides, sterols, fatty alcohols, phenolics and polyols. In the $CHCl_3$ fraction, hydrocarbons (alkenes and alkanes) were the second most represented groups among annotated features. Hydrocarbons are commonly found in diatoms, bacteria and cyanobacteria (e.g., Rontani and Volkman, 2005) and are products of the biodecarboxylation of fatty acids (Stonik and Stonik, 2015). The molecular diversity of the MeOH fraction was higher, with classes of compounds ranging from polar (e.g., monosacharides) to apolar compounds (e.g., alkenes). Interestingly, we annotated a short-chained oxylipin (3-octen-2-ol) closely similar to a self-stimulating oxylipin messenger (1-octen-3-ol) inducing defense in marine algae (Chen et al., 2019). Some marine diatoms are also known to possess volatile oxylipins belonging to unsaturated and polyunsaturated aldehydes (D'Ippolito et al., 2002; Ianora et al., 2004) but we did not find any in our study. A longer fatty alcohol with 18 carbons was also found in this fraction (1-octadecanol), indicator of an algal or bacterial contribution (Shiea et al., 1991; Rontani and Volkman, 2005). The presence of the terpene phytol in both fractions was not surprising as this compound is ubiquitous. Phytol has been found in cyanobacterial mats and photosynthetic bacterial mats (Shiea et al., 1991), diatoms (Stonik and Stonik, 2015), macroalgae (Santos et al., 2015), microalgae (Mendiola et al., 2008), and coccolithophorid (Riebesell et al., 2000). Phytol is generally considered to be the most abundant acyclic isoprenoid on earth as it represents the side chain of the chlorophyll, mainly chlorophyll *a* (Rontani et al., 1999; Rontani and Volkman, 2003; Kraub and Vetter, 2018). In our samples, phytol may arise from the hydrolysis of chlorophyll or bacteriochlorophyll. It may also originate from diatom chloroplasts where it can be biosynthesized by the methylerythritol (MEP) pathway (Masse et al., 2004; Stonik and Stonik, 2015). Another terpene, neophytadiene, was also found in both fractions. This terpene may be a phytol degradation product (Rontani and Volkman, 2003) and has been reported in some microalgae (López-Rosales et al., 2019) or macroalgae (Santos et al., 2015) and antimicrobial properties have been associated to this compound (e.g., Ahn et al., 2016).

Moreover, we found presumed anthropogenic contaminants from plastic origin in our samples, including some belonging to Polycyclic Aromatic Hydrocarbons (PAH). This is not surprising as these compounds, notably PAH, are ubiquitous and persistent environmental contaminants found in sediments and associated waters of urbanized estuaries and coastal areas (J. Wang et al., 2016; Baali and Yahyaoui, 2019). PAH can also come from natural sources through biodegradation by microorganisms (Baali and Yahyaoui, 2019).

Focusing on the chemical changes induced by the experimental conditions, we were able to highlight some compounds specifically correlated to the light exposure condition or time in the $CHCl_3$ fraction. Indeed, significant variations in the metabolomic fingerprinting were observed at the end of the experiment in samples exposed to natural vs. higher artificial irradiance. Only two metabolites driving these changes were highlighted, the hydrocarbon heptadecane and another unknown metabolite. The n-heptadecane is usually among the predominant hydrocarbons in cyanobacteria and cyanobacterial mats (Shiea et al., 1991; Grimalt et al., 1992; Dembitsky et al., 2001; Rontani and Volkman, 2005). It is also found in benthic diatoms, such as *Cocconeis scutellum* (Nappo et al., 2009). Some microalgae such as *Chlamydomonas variabilis* (Chlorophyceae) or *Nannochloropsis* sp. (Eustigmatophyceae) have the ability to synthesize heptadecanes and heptadecenes from the corresponding C18 FA by a light dependent way (Sorigué et al., 2016). As heptadecane was decreased by the end of the experiment in biofilms under AI, we may suppose that its conversion from C18 fatty acids was somehow down-regulated by our higher artificial irradiance treatment. While the function of these hydrocarbons is unknown, roles in regulating membrane properties or as cell signaling have been suggested (Sorigué et al., 2016).

Some metabolites were also correlated to metabolomic changes according to time and showed a decreased at t7. They mainly consisted of FA. Two of them were putatively annotated as branched-chain fatty acids with 15 carbons, which are, along with 15:0 and 17:0, typical of bacteria. Their decrease at t7 compared to t0 may be explained by a decrease of bacteria or their grazing by other organisms, such as bacterivorous nematodes (Hubas et al., 2010). The decrease of these compounds may also be explained by their degradation. One branched-chained SFA with 14 carbons was also identified, along with two SFA with 12 and 14 carbon atoms and two MUFA, including the 16:1n-7. An isoprenoid wax ester derived from phytol (phytyl fatty acid ester) was also decreased at t7 in higher artificial irradiance. In terrestrial plants, a large proportion of phytol and fatty acids is converted into fatty acid phytyl esters during stress or senescence in chloroplasts, to protect plant cell as free phytol shows membrane toxic properties (Lippold et al., 2014; Kraub and Vetter, 2018). In marine microorganisms, phytyl esters have been reported in dinoflagellates (Withers and Nevenzel, 1977), some microalgae species and bacteria (Rontani et al., 1999) and may serve as a potential energy storage (Rontani et al., 1999). We may therefore hypothesize that the decrease in this phytyl ester may reflect the consumption of some energy reserves. Another metabolite potentially derivated from phytol was putatively annotated as 4,8,12-trimethyltridecan-4-olide. This lactone may be a phytol degradation by-product metabolite, formed after lactonization of the isoprenoid metabolite 4-hydroxy-4,8,12-trimethyl-tridecanoic acid (Rontani et al., 1999). Only one metabolite correlated to the experimentation time increased at t7 (with the chosen threshold 0.7). This metabolite was annotated as tetracosane, a common long-chained saturated alkane found in marine microorganisms (Grimalt et al., 1992; Nappo et al., 2009; López-Rosales et al., 2019).

No significant effect of the light exposure condition was recorded in the metabolomic fingerprinting of the MeOH fraction with both GC-MS and LC-MS analyses. This result might be explained in part by our experimental conditions. Indeed, our higher artificial irradiance treatment (167 ± 23 µmol photon m^{-2} s^{-1}) was relatively low when compared to the natural conditions (102 ± 19 µmol photon m^{-2} s^{-1}) and compared with solar irradiance experienced in the natural habitat (up to 2,000 µmol photon m^{-2} s^{-1}). Moreover,

the photon flux of the natural light treatment was not constant compared to the AI condition as it depended on the natural environmental variations. This parameter might slightly influence the metabolomic variation of the biofilm and may be further taken into consideration. Only a metabolomic variation according to time was observed after LC-MS analyses in this fraction. This might be explained by the different nature of the compounds observed by LC-MS vs. GC-MS. As the experiment was short (7 days), some chemical changes may also take longer to take place in the mid-polar fraction of the MPB biofilm. It would be interesting to extent this preliminary experiment in order to get multiple time points and to test more irradiance conditions (with higher values).

CONCLUSION

This paper represents the first report about the metabolomic fingerprinting of MPB biofilms from mudflat sediments using an untargeted GC-MS and LC-MS metabolomic approach and will provide a baseline for further work in this area. Of the three extraction solvent mixtures tested, we concluded that using a MeOH:$CHCl_3$ (1:1) mixture provided the best compromise. The proposed protocol, detailing steps from sample collection to data analyses, was successfully applied to a case study: the impact of light exposure condition on the metabolome of MPB biofilm. While no metabolomic change was recorded in the MeOH fraction according to light exposure conditions, significant variations in the metabolomic fingerprinting of MPB biofilm were highlighted in the apolar fraction, according to the light exposure or time. Some metabolites correlated to these changes were identified and annotated. Our study demonstrated the interest of the metabolomic approach introduced here for rapid and simultaneous detection of metabolites from various groups and their respective chemical identification using available GC-MS databases. Both selected techniques are relevant to be used in combination for a broader analysis of metabolites. With its rich database, GC-MS allows a better identification of compounds and is particularly suitable for non-polar fractions. LC-MS, highly sensitive, is more appropriate for polar, weakly polar and neutral compounds (Wang et al., 2015). The metabolomic workflow introduced here on MPB biofilms has the potential to be adapted to further ecological studies on MPB biofilms in mudflat areas and would complete classical approaches on these biofilms. We focused on a global metabolomic study of the complex MPB biofilm (i.e., with no distinction between intra- and extracellular compounds, or between the endo- and exo-metabolome), but this workflow could be applied on the EPS fractions extracted through classical approach [Dowex resin (Jahn and Nielsen, 1995) or any other extraction methods (Takahashi et al., 2009)]. As numerous studies already investigated the EPS matrices composition (notably the carbohydrate fraction, highly polar) of the MPB biofilm, our study focused on mid-polar to apolar fractions. Metabolomics could help us to further understand the influence of various environmental factors on the MPB biofilm community and to explore the chemical communication between organisms. This approach would notably be pertinent to explore the diatom migration through the sediment. While this migration is known to take place in response to tidal and endogenous rhythms (Smith and Underwood, 1998), but also in response to environmental stress, this phenomenon still remained not fully understood. We cannot exclude that this diatom migration is, at least partially, coordinated through chemical communication, an hypothesis that could be further investigated via a metabolomic approach.

DATA AVAILABILITY STATEMENT

Metabolomics data have been deposited to the EMBL-EBI MetaboLights database (doi: 10.1093/nar/gks1004. PubMed) with the identifier MTBLS1378 (for LC-MS data) and MTBLS1379 (for GC-MS data). The complete LC-MS dataset can be accessed here https://www.ebi.ac.uk/metabolights/MTBLS1378 and https://www.ebi.ac.uk/metabolights/MTBLS1379 for the GC-MS dataset.

AUTHOR CONTRIBUTIONS

CH and JG-B designed the experiments and performed MPB biofilm sample collections. JG-B carried out extractions and fractionations, analyzed metabolomic fingerprints by GC-MS and LC-MS (with SP), performed data treatment and statistical analyses, and drafted the manuscript with input from CH and SP.

FUNDING

This study was supported by the BIO-Tide project, funded through the 2015–2016 BiodivERsA COFUND call for research proposals, with the national funders BelSPO, FWO, ANR, and SNSF. LC-MS fingerprints were acquired at the MNHN Bioorganic Mass Spectrometry Platform. The post-doctoral grant of JG-B was supported by the Regional Council of Brittany, SAD program and the META-Tide project. The Regional Council of Brittany, the General Council of Finistère, the urban community of Concarneau Cornouaille Agglomération and the European Regional Development Fund (ERDF) are acknowledged for the funding of the Sigma 300 FE-SEM of the Concarneau Marine Biology Station. MEB images were acquired thanks to the HULK project (FCT grant number 143255).

ACKNOWLEDGMENTS

We thank Elisabeth Nezan (Ifremer Concarneau) for the identification of *Gyrosigma balticum* and *Pleurosigma formosum*.

SUPPLEMENTARY MATERIAL

The Supplementary Material for this article can be found online at: https://www.frontiersin.org/articles/10.3389/fmars.2020.00250/full#supplementary-material

REFERENCES

Ahn, H. M., Kim, S., Hyun, S., Lim, S. R., Kim, H., Oh, J., et al. (2016). Effects of the timing of a culture temperature reduction on the comprehensive metabolite profiles of *Chlorella vulgaris*. *J. Appl. Phycol.* 28, 2641–2650. doi: 10.1007/s10811-016-0817-4

Allard, P., Péresse, T., Bisson, J., Gindro, K., Pham, V. C., Roussi, F., et al. (2016). Integration of molecular networking and In-Silico MS/MS fragmentation for natural products dereplication. *Anal. Chem.* 88, 3317–3323. doi: 10.1021/acs.analchem.5b04804

Baali, A., and Yahyaoui, A. (2019). *Polycyclic Aromatic Hydrocarbons (PAHs) and Their Influence to Some Aquatic Species*. London: IntechOpen, doi: 10.5772/intechopen.86213

Beale, D. J., Pinu, F. R., Kouremenos, K. A., Poojary, M. M., Narayana, V. K., Boughton, B. A., et al. (2018). Review of recent developments in GC – MS approaches to metabolomics-based research. *Metabolomics* 14:152. doi: 10.1007/s11306-018-1449-2

Böcker, S., and Dührkop, K. (2016). Fragmentation trees reloaded. *J. Cheminform.* 8:5. doi: 10.1186/s13321-016-0116-8

Bohórquez, J., McGenity, T. J., Papaspyrou, S., García-Robledo, E., Corzo, A., and Underwood, G. J. C. (2017). Different types of diatom-derived extracellular polymeric substances drive changes in heterotrophic bacterial communities from intertidal sediments. *Front. Microbiol.* 8:245. doi: 10.3389/fmicb.2017.00245

Bourke, M. F., Marriott, P. J., Glud, R. N., Hasler-Sheetal, H., Kamalanathan, M., Beardall, J., et al. (2017). Metabolism in anoxic permeable sediments is dominated by eukaryotic dark fermentation. *Nat. Geosci.* 10, 30–35. doi: 10.1038/ngeo2843

Bromke, M. A., Sabir, J. S., Alfassi, F. A., Hajarah, N. H., Kabli, S. A., Al-Malki, A. L., et al. (2015). Metabolomic profiling of 13 diatom cultures and their adaptation to nitrate-limited growth conditions. *PLoS One* 10:e0138965. doi: 10.1371/journal.pone.0138965

Budge, S. M., and Parrish, C. C. (1998). Lipid biogeochemistry of plankton, settling matter and sediments in Trinity Bay, Newfoundland. II. Fatty acids. *Org. Geochem.* 29, 1547–1559. doi: 10.1016/s0146-6380(98)00177-6

Bundy, J. G., Davey, M. P., Viant, M. R., Davey, ÆM. P., and Viant, M. R. (2009). Environmental metabolomics: a critical review and future perspectives. *Metabolomics* 5, 3–21. doi: 10.1007/s11306-008-0152-0

Cajka, T., and Fiehn, O. (2016). Toward merging untargeted and targeted methods in mass spectrometry-based metabolomics and lipidomics. *Anal. Chem.* 88, 524–545. doi: 10.1021/acs.analchem.5b04491

Chambers, M. C., Maclean, B., Burke, R., Amodei, D., Ruderman, D. L., Neumann, S., et al. (2012). A cross-platform toolkit for mass spectrometry and proteomics. *Nat. Biotechnol.* 30, 918–920. doi: 10.1038/nbt.2377

Chen, H., Yang, R., Chen, J., Luo, Q., Cui, X., Yan, X., et al. (2019). 1-Octen-3-ol, a self-stimulating oxylipin messenger, can prime and induce defense of marine alga. *BMC Plant Biol.* 19:37. doi: 10.1186/s12870-019-1642-0

Chung, H. C., Lee, O. O., Huang, Y., Mok, S. Y., and Kolter, R. (2010). Bacterial community succession and chemical profiles of subtidal biofilms in relation to larval settlement of the polychaete *Hydroides elegans*. *ISME J.* 4, 817–828. doi: 10.1038/ismej.2009.157

Cointet, E., Wielgosz-collin, G., Méléder, V., and Gonçalves, O. (2019). Lipids in benthic diatoms: a new suitable screening procedure. *Algal Res.* 39:101425. doi: 10.1016/j.algal.2019.101425

Dalsgaard, J., St John, M., Kattner, G., Müller-Navarra, D., and Hagen, W. (2003). Fatty acid trophic markers in the pelagic marine environment. *Adv. Mar. Biol.* 46, 225–340. doi: 10.1016/s0065-2881(03)46005-7

Decho, A. W. (2000). Microbial biofilms in intertidal systems: an overview. *Cont. Shelf Res.* 20, 1257–1273. doi: 10.1016/s0278-4343(00)00022-4

Dembitsky, V. M., Dor, I., Shkrob, I., and Aki, M. (2001). Branched alkanes and other apolar compounds produced by the Cyanobacterium *Microcoleus vaginatus* from the Negev Desert. *Russ. J. Bioorganic Chem.* 27, 110–119.

D'Ippolito, G., Iadicicco, O., Romano, G., and Fontana, A. (2002). Detection of short-chain aldehydes in marine organisms: the diatom *Thalassiosira rotula*. *Tetrahedron Lett.* 43, 6137–6140. doi: 10.1016/s0040-4039(02)01283-2

Domingo-almenara, X., Brezmes, J., Vinaixa, M., Samino, S., Ramirez, N., Ramon-, M., et al. (2016). eRah: a computational tool integrating spectral deconvolution and alignment with quantification and identification of metabolites in GC-MS-based metabolomics. *Anal. Bioanal. Chem.* 88, 9821–9829. doi: 10.1021/acs.analchem.6b02927

Dove, A. D. M., Leisen, J., Zhou, M., Byrne, J. J., Lim-hing, K., Webb, H. D., et al. (2012). Biomarkers of whale shark health: a metabolomic approach. *PLoS One* 7:e49379. doi: 10.1371/journal.pone.0049379

Elias, S., and Banin, E. (2012). Multi-species biofilms: living with friendly neighbors. *FEMS Microbiol. Rev.* 36, 990–1004. doi: 10.1111/j.1574-6976.2012.00325.x

Fernandez-Varela, R., Tomasi, G., and Christensen, J. (2015). An untargeted gas chromatography mass spectrometry metabolomics platform for marine polychaetes. *J. Chromatogr. A* 1384, 133–141. doi: 10.1016/j.chroma.2015.01.025

Fiehn, O. (2002). Metabolomics–the link between genotypes and phenotypes. *Plant Mol. Biol* 48, 155–171. doi: 10.1007/978-94-010-0448-0_11

Flemming, H. (2016). Biofilms: an emergent form of bacterial life. *Nat. Publ. Gr.* 14, 563–575. doi: 10.1038/nrmicro.2016.94

Flemming, H. C., and Wingender, J. (2010). The biofilm matrix. *Nat. Rev. Microbiol.* 8, 623–633. doi: 10.1038/nrmicro2415

Gaillard, F., and Potin, P. (2014). "Proteomics and metabolomics of marine organisms: current strategies and knowledge Fanny Gaillard and Philippe Potin abstract," in *Outstanding Marine Molecules: Chemistry, Biology, Analysis*, eds S. La Barre and J. M. Kornprobst (Weinheim: Wiley-VCH Verlag GmbH & Co. KGaA), 457–472. doi: 10.1002/9783527681501.ch21

Gaubert, J., Greff, S., Thomas, O. P., and Payri, C. E. (2019). Metabolomic variability of four macroalgal species of the genus *Lobophora* using diverse approaches. *Phytochemistry* 162, 165–172. doi: 10.1016/j.phytochem.2019.03.002

Gillard, J., Frenkel, J., Devos, V., Sabbe, K., Paul, C., Rempt, M., et al. (2013). Metabolomics enables the structure elucidation of a diatom sex pheromone. *Angew. Chemie Int. Ed.* 52, 854–857. doi: 10.1002/anie.201208175

Grimalt, J., Wit, R., Teixidor, P., and Albaiges, J. (1992). Lipid biogeochemistry of *Phormidium* and *Microcoleus* mats. *Adv. Org. Geochem.* 19, 509–530. doi: 10.1016/0146-6380(92)90015-p

Hanlon, A. R. M., Bellinger, B., Haynes, K., Xiao, G., and Hofmann, T. A. (2006). Dynamics of extracellular polymeric substance (EPS) production and loss in an estuarine, diatom-dominated, microalgal biofilm over a tidal emersion – immersion period. *Limnol. Oceanogr.* 51, 79–93. doi: 10.4319/lo.2006.51.1.0079

Haro, S., Brodersen, K. E., and Papaspyrou, S. (2019). Radiative energy budgets in a microbial mat under different irradiance and tidal conditions. *Microb. Ecol.* 77, 852–865. doi: 10.1007/s00248-019-01350-6

Hubas, C., Passarelli, C., and Paterson, D. M. (2018). "Microphytobenthic biofilms: composition and interactions," in *Mudflat Ecology. Aquatic Ecology Series*, Vol. 7, ed. P. G. Beninger (Cham: Springer), 63–90. doi: 10.1007/978-3-319-99194-8_4

Hubas, C., Sachidhanandam, C., Rybarczyk, H., Lubarsky, H. V., Rigaux, A., Moens, T., et al. (2010). Bacterivorous nematodes stimulate microbial growth and exopolymer production in marine sediment microcosms. *Mar. Ecol. Prog. Ser.* 419, 85–94. doi: 10.3354/meps08851

Ianora, A., Miralto, A., Poulet, S. A., Carotenute, Y., Buttino, T., Romano, G., et al. (2004). Aldehyde suppression of copepod recruitment in blooms of a ubiquitous planktonic diatom. *Nature* 429, 403–407. doi: 10.1038/nature02565.1

Jahn, A., and Nielsen, P. H. (1995). Extraction of extracellular polymeric substances (EPS) from biofilms using a cation exchange resin. *Pergamon* 32, 157–164. doi: 10.2166/wst.1995.0287

Juneau, P., Barnett, A., Méléder, V., Dupuy, C., and Lavaud, J. (2015). Combined effect of high light and high salinity on the regulation of photosynthesis in three diatom species belonging to the main growth forms of intertidal fl at inhabiting microphytobenthos. *J. Exp. Mar. Bio. Ecol.* 463, 95–104. doi: 10.1016/j.jembe.2014.11.003

Kelly, J. R., and Scheibling, R. E. (2012). Fatty acids as dietary tracers in benthic food webs. *Mar. Ecol. Prog. Ser.* 446, 1–22. doi: 10.3354/meps09559

Kliebenstein, D. J. (2004). Secondary metabolites and plant / environment interactions: a view through *Arabidopsis thaliana* tinged glasses. *Plant Cell Environ.* 27, 675–684. doi: 10.1111/j.1365-3040.2004.01180.x

Kooke, R., and Keurentjes, J. J. B. (2011). Multi-dimensional regulation of metabolic networks shaping plant development and performance. *J. Exp. Bot.* 63, 3353–3365. doi: 10.1093/jxb/err373

Kraub, S., and Vetter, W. (2018). Phytol and phytyl fatty acid esters: occurrence, concentrations and relevance. *Eur. J. Lipid Sci. Technol.* 120:1700387. doi: 10.1002/ejlt.201700387

Kruger, N. J., Troncoso-ponce, M. A., and Ratcliffe, R. G. (2008). 1H NMR metabolite fingerprinting and metabolomic analysis of perchloric acid extracts from plant tissues. *Nat. Protoc.* 3, 1001–1012. doi: 10.1038/nprot.2008.64

Kumar, M., Kuzhiumparambil, U., Pernice, M., Jiang, Z., and Ralph, P. J. (2016). Metabolomics: an emerging frontier of systems biology in marine macrophytes. *Algal Res.* 16, 76–92. doi: 10.1016/j.algal.2016.02.033

Lépinay, A., Turpin, V., Mondeguer, F., Grandet-Marchant, Q., Capiaux, H., Baron, R., et al. (2018). First insight on interactions between bacteria and the marine diatom *Haslea ostrearia*: algal growth and metabolomic fingerprinting. *Algal Res.* 31, 395–405. doi: 10.1016/j.algal.2018.02.023

Li, H., Lu, Y., Zheng, J., Yang, W., and Liu, J. (2014). Biochemical and genetic engineering of diatoms for polyunsaturated fatty acid biosynthesis. *Mar. Drugs* 12, 153–166. doi: 10.3390/md12010153

Liebeke, M., and Puskás, E. (2019). Drying enhances signal intensities for global GC – MS metabolomics. *Metabolites* 9:68. doi: 10.3390/metabo9040068

Lippold, F., Dorp, K., Abraham, M., Hölzl, G., Wewer, V., Yilmaz, L., et al. (2014). Fatty acid phytyl ester synthesis in chloroplasts of *Arabidopsis*. *Plant Cell* 24, 2001–2014. doi: 10.1105/tpc.112.095588

López-Rosales, A. R., Ancona-Canché, K., Chavarria-Hernandez, J. C., Barahona-Pérez, F., Toledano-Thompson, T., Garduño-Solórzano, G., et al. (2019). Fatty acids, hydrocarbons and terpenes of nannochloropsis and nannochloris isolates with potential for biofuel production. *Energies* 12:130. doi: 10.3390/en12010130

Masse, G., Belt, S. T., Rowland, S. J., and Rohmer, M. (2004). Isoprenoid biosynthesis in the diatoms *Rhizosolenia setigera* (Brightwell) and *Haslea ostrearia* (Simonsen). *Proc. Natl. Acad. Sci. U.S.A.* 101, 4413–4418. doi: 10.1073/pnas.0400902101

Mendiola, J. A., Santoyo, S., Cifuentes, A., Reglero, G., and Sen, F. J. (2008). Antimicrobial activity of sub- and supercritical CO 2 extracts of the green alga *Dunaliella salina*. *J. Food Prot.* 71, 2138–2143. doi: 10.4315/0362-028x-71.10.2138

Nappo, M., Berkov, S., Codina, C., Avila, C., Messina, P., Zupo, V., et al. (2009). Metabolite profiling of the benthic diatom *Cocconeis scutellum* by GC-MS. *J. Appl. Phycol.* 21, 295–306. doi: 10.1007/s10811-008-9367-8

Parsons, H. M., Ekman, D. R., Collette, W., and Viant, M. R. (2009). Spectral relative standard deviation: a practical benchmark in metabolomics. *Analyst* 134, 478–485. doi: 10.1039/b808986h

Passarelli, C., Meziane, T., Thiney, N., Boeuf, D., Jesus, B., Ruivo, M., et al. (2015). Seasonal variations of the composition of microbial biofilms in sandy tidal flats: focus of fatty acids, pigments and exopolymers. *Estuar. Coast. Shelf Sci.* 153, 29–37. doi: 10.1016/j.ecss.2014.11.013

Paul, C., Mausz, M. A., and Pohnert, G. (2013). A co-culturing/metabolomics approach to investigate chemically mediated interactions of planktonic organisms reveals influence of bacteria on diatom metabolism. *Metabolomics* 9, 349–359. doi: 10.1007/s11306-012-0453-1

Perkins, R. G., Lavaud, J., Serôdio, J., Mouget, J. L., Cartaxana, P., Rosa, P., et al. (2010). Vertical cell movement is a primary response of intertidal benthic biofilms to increasing light dose. *Mar. Ecol. Prog. Ser.* 416, 93–103. doi: 10.3354/meps08787

Perkins, R. G., Underwood, G. J. C., Brotas, V., Snow, G. C., Jesus, B., and Ribeiro, L. (2001). Responses of microphytobenthos to light: primary production and carbohydrate allocation over an emersion period. *Mar. Ecol. Prog. Ser.* 223, 101–112. doi: 10.3354/meps223101

Pierre, G., Graber, M., Orvain, F., Dupuy, C., and Maugard, T. (2010). Biochemical characterization of extracellular polymeric substances extracted from an intertidal mudflat using a cation exchange resin. *Biochem. Syst. Ecol.* 38, 917–923. doi: 10.1016/j.bse.2010.09.014

Pierre, G., Zhao, J. M., Orvain, F., Dupuy, C., Klein, G. L., Graber, M., et al. (2014). Seasonal dynamics of extracellular polymeric substances (EPS) in surface sediments of a diatom-dominated intertidal mudflat (Marennes-Oléron, France). *J. Sea Res.* 92, 26–35. doi: 10.1016/j.seares.2013.07.018

Riebesell, U., Revill, A. T., Holdsworth, D. G., and Volkman, J. K. (2000). The effects of varying CO 2 concentration on lipid composition and carbon isotope fractionation in *Emiliania huxleyi*. *Geochim. Cosmochim. Acta* 64, 4179–4192. doi: 10.1016/s0016-7037(00)00474-9

Roessner, U., Wagner, C., Kopka, J., Trethewey, R. N., and Willmitzer, L. (2000). Simultaneous analysis of metabolites in potato tuber by gas chromatography-mass spectrometry. *Plant J.* 23, 131–142. doi: 10.1046/j.1365-313x.2000.00774.x

Rontani, J., Bonin, P. C., and Volkman, J. K. (1999). Production of wax esters during aerobic growth of marine bacteria on isoprenoid compounds. *Appl. Environ. Microbiol.* 65, 221–230. doi: 10.1128/aem.65.1.221-230.1999

Rontani, J., and Volkman, J. K. (2003). Phytol degradation products as biogeochemical tracers in aquatic environments. *Org. Geochem.* 34, 1–35. doi: 10.1016/s0146-6380(02)00185-7

Rontani, J. F., and Volkman, J. K. (2005). Lipid characterization of coastal hypersaline cyanobacterial mats from the Camargue (France). *Org. Geochem.* 36, 251–272. doi: 10.1016/j.orggeochem.2004.07.017

Santos, S. A. O., Vilela, C., Freire, C. S. R., Abreu, M. H., Rocha, S. M., and Silvestre, A. J. D. (2015). Chlorophyta and Rhodophyta macroalgae: a source of health promoting phytochemicals. *Food Chem.* 183, 122–128. doi: 10.1016/j.foodchem.2015.03.006

Shannon, P., Markiel, A., Ozier, O., Baliga, N. S., Wang, J. T., Ramage, D., et al. (2003). Cytoscape: a software environment for integrated models of biomolecular interaction networks. *Genome Res.* 13, 2498–2504. doi: 10.1101/gr.1239303.metabolite

Shiea, J., Brassell, S., and Ward, D. (1991). Comparative analysis of extractable lipids in hot spring microbial mats and their component photosynthetic bacteria. *Org. Geochem.* 17, 309–319. doi: 10.1016/0146-6380(91)90094-z

Smith, D. J., and Underwood, G. J. C. (1998). Exopolymer production by intertidal epipelic diatoms. *Limnol. Oceanogr.* 43, 1578–1591. doi: 10.4319/lo.1998.43.7.1578

Sogin, E. M., Puskás, E., Dubilier, N., and Liebeke, M. (2019). Marine metabolomics: measurement of metabolites in seawater by gas chromatography mass spectrometry. *bioRxiv* [Preprint]. doi: 10.1101/528307

Sorigué, D., Légeret, B., Cuiné, S., Morales, P., Mirabella, B., Guédeney, G., et al. (2016). Microalgae synthesize hydrocarbons from long-chain fatty acids via a light-dependent pathway 1 [OPEN]. *Plant Physiol.* 171, 2393–2405. doi: 10.1104/pp.16.00462

Stal, L. J. (2003). Microphytobenthos, their extracellular polymeric substances, and the morphogenesis of intertidal sediments. *Geomicrobiol. J.* 20, 463–478. doi: 10.1080/713851126

Stonik, V., and Stonik, I. (2015). Low-molecular-weight metabolites from diatoms: structures. Biological roles and biosynthesis. *Mar. Drugs* 13, 3672–3709. doi: 10.3390/md13063672

Sutherland, I. W. (2017). "EPS – a complex mixture," in *The Perfect Slime: Microbial Extracellular Polymeric Substances (EPS)*, eds H. Flemming, T. Neu, and J. Wingender (London: IWA Publishing), 15–24.

Takahashi, E., Ledauphin, J., Goux, D., and Orvain, F. (2009). Optimising extraction of extracellular polymeric substances (EPS) from benthic diatoms: comparison of the efficiency of six EPS extraction methods. *Mar. Freshw. Res.* 60, 1201–1210. doi: 10.1071/MF08258

Toupoint, N., Mohit, V., Linossier, I., Bourgougnon, N., Olivier, F., Lovejoy, C., et al. (2012). Effect of biofilm age on settlement of *Mytilus edulis*. *Biofouling* 28, 985–1001. doi: 10.1080/08927014.2012.725202

Underwood, G. J. C., and Kromkamp, J. (1999). "Primary production by phytoplankton and microphytobenthos in Estuaries," in *Advances in Ecological Research Estuaries*, eds A. H. Fitter and D. G. Raffaelli (Cambridge, MA: Academic Press), 93–139.

Underwood, G. J. C., and Paterson, M. D. (2003). The importance of extracellular carbohydrate production by marine epipelic diatoms. *Adv. Bot. Res.* 40, 183–240. doi: 10.1016/s0065-2296(05)40005-1

Van Den Dool, H., and Kratz, P. D. (1963). A generalization of the retention index system including linear temperature programmed gas-liquid partition chromatography. *J. Chromatogr.* 11, 463–471. doi: 10.1016/s0021-9673(01)80947-x

Wang, J., Tan, Z., Peng, J., Qiu, Q., and Li, M. (2016). The behaviors of microplastics in the marine environment. *Mar. Environ. Res.* 113, 7–17. doi: 10.1016/j.marenvres.2015.10.014

Wang, M., Carver, J. J., Phelan, L. M., Sanchez, L. M., Garg, N., and Al, E. (2016). Sharing and community curation of mass spectrometry data with global

natural products social molecular networking. *Nat. Biotechnol.* 34, 828–837. doi: 10.1038/nbt.3597

Wang, Y., Liu, S., Hu, Y., Li, P., and Wan, J. B. (2015). Current state-of-the-art of mass spectrometry-based metabolomics studies – a review focusing on wide coverage, high throughput and easy identification. *R. Soc. Chem.* 5, 78728–78737. doi: 10.1039/C5RA14058G

Wilkinson, J. L., Hooda, P. S., Swinden, J., Barker, J., and Barton, S. (2018). Spatial (bio) accumulation of pharmaceuticals, illicit drugs, plasticisers, perfluorinated compounds and metabolites in river sediment, aquatic plants and benthic organisms. *Environ. Pollut.* 234, 864–875. doi: 10.1016/j.envpol.2017.11.090

Withers, N., and Nevenzel, J. (1977). Phytyl esters in a marine dinoflagellate. *Lipids* 12, 989–993. doi: 10.1007/bf02533324

Wotton, R. S. (2004). The ubiquity and many roles of exopolymers (EPS) in aquatic systems. *Sci. Mar.* 68, 13–21. doi: 10.3989/scimar.2004.68s113

Conflict of Interest: The authors declare that the research was conducted in the absence of any commercial or financial relationships that could be construed as a potential conflict of interest.

frontiers in Marine Science

PERSPECTIVE
published: 15 May 2020
doi: 10.3389/fmars.2020.00329

Artificial Light at Night: A New Challenge in Microphytobenthos Research

Elena Maggi[1] and João Serôdio[2]*

[1] Dipartimento di Biologia, CoNISMA – Consorzio Nazionale Interuniversitario per le Scienze del Mare, Università di Pisa, Pisa, Italy, [2] Department of Biology and CESAM – Centre for Environmental and Marine Studies, University of Aveiro, Aveiro, Portugal

Artificial light at night (ALAN) has been recently recognized as a globally widespread anthropogenic disturbance, characterized by different intensities and spectra, as well as spatial and temporal variability. Among marine organisms, those living on coastal areas are particularly exposed to artificial light. Some recent studies anticipated a potential for influences of ALAN on microphytobenthos (MPB) on rocky shores, either direct or indirectly mediated by trophic relationships. Here we emphasize the need for further investigations in different habitats, as well as on synergistic interferences with other stressors already impinging on coastal areas. The study of effects of ALAN poses new challenges in MPB research, including those related to the use of instruments for measuring both the light environment and the functioning of microbial photoautotrophs at night, and to the development of common monitoring approaches and manipulative experiments.

Keywords: light pollution, microphytobenthos, light intensity, light spectrum, temporal and spatial variability, trophic relationships, multiple stressors, challenges in sampling

OPEN ACCESS

Edited by:
Katherine Dafforn, Macquarie University, Australia

Reviewed by:
Damon Kai Bolton, University of New South Wales, Australia
Stuart Rees Jenkins, Bangor University, United Kingdom

****Correspondence:***
Elena Maggi
elena.maggi@unipi.it

Specialty section:
This article was submitted to Marine Ecosystem Ecology, a section of the journal Frontiers in Marine Science

Received: *30 November 2019*
Accepted: *21 April 2020*
Published: *15 May 2020*

Citation:
Maggi E and Serôdio J (2020) Artificial Light at Night: A New Challenge in Microphytobenthos Research. Front. Mar. Sci. 7:329. doi: 10.3389/fmars.2020.00329

INTRODUCTION

Artificial light at night (ALAN) is one of the most recently recognized sources of anthropogenic disturbance, globally widespread on both terrestrial and aquatic environments (Falchi et al., 2016; Davies and Smyth, 2017). ALAN is tightly related to the rate of urban development. For centuries, people have tended to concentrate on coastal areas and at the current rate of human population growth the spatial extent and magnitude of light pollution on these areas is expected to increase. The ALAN phenomenon is mostly due to the presence of outdoor night lights; these affect the surrounding abiotic environment both directly, through light sources of variable intensity (from a few to more than 100 lux) and indirectly, through the formation of a *skyglow*. The *skyglow* is a diffuse light field of low intensity (0.3–0.5 lux) visible as a glowing dome over built up areas and extending its influence on sub-urban and rural sites (Gaston, 2018). The most common direct sources of ALAN affecting coastal communities are represented by fixed lamps distributed along coastal streets, promenades, ports and marinas and potentially impacting estuarine mudflats, sandy beaches, rocky shores or artificial structures (**Figures 1A,B**). The intensity of light originating from a lamp rapidly declines within a few meters; therefore, the spatial arrangement of a given number of fixed lamps can create a scenario of alternating low and high light intensity areas, resulting in marked spatial variability in light pollution at the scale of a few to tens of meters (**Figure 1C**). It is worth noting that in coastal areas light pollution may also be related to the presence of intermitting and mobile sources, such as those associated with lighthouses or installed on commercial and tourist boats. The additional key feature of light sources, i.e., their emission spectrum,

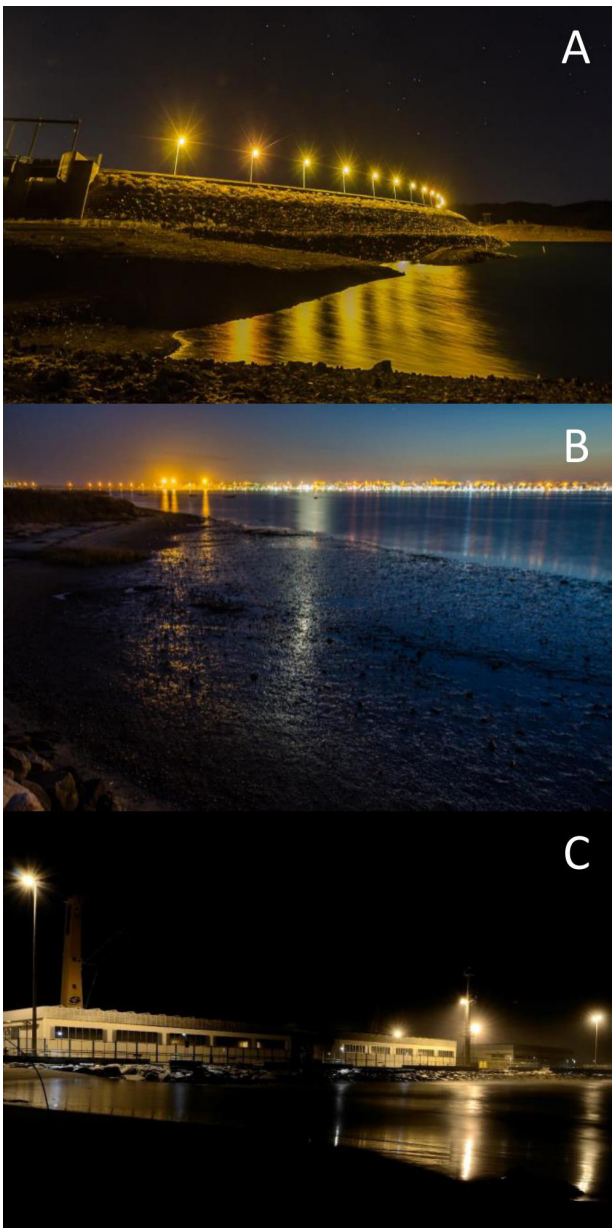

FIGURE 1 | Night light pollution caused by sources of artificial light located close (water damn, **A**) or relatively far away (intertidal estuarine mudflat, **B**), from water bodies and adjacent areas. **(C)** Example of alternating low and high intensity areas, along an artificial structure illuminated by streetlamps within a port. Photo credits: J. Serôdio **(A,B)** and M. Menconi **(C)**.

may also create vertical variability in the water column, due to specific attenuation patterns among different wavelengths (Tamir et al., 2017).

Knowledge on the effect of ALAN on coastal organisms and habitats is still fragmented, but published research has already highlighted a variety of impacts, including effects on settlement processes (both in invertebrates and bacteria; Davies et al., 2015; Maggi and Benedetti-Cecchi, 2018), changes in behavior (e.g., orientation of turtles, vertical migration of zooplankton and fish, anti-predator and locomotor activities, trophic pressure; e.g., Witherington and Bjorndal, 1991; Underwood et al., 2017; Ludvigsen et al., 2018; Duarte et al., 2019; Maggi et al., 2019) and composition of assemblages (Garratt et al., 2019; Maggi et al., 2020).

Among these studies, first evidences exist of impacts on intertidal microphytobenthos (MPB) (Maggi and Benedetti-Cecchi, 2018), but there is a need to further address the role of light pollution on key physiological and ecological aspects of MPB in different coastal habitats.

MICROPHYTOBENTHOS AND LIGHT ENVIRONMENT

The MPB plays a key functional role in a variety of coastal systems, representing one of the main groups of primary producers and a source of food for grazers in intertidal and shallow subtidal systems, either on soft bottoms or hard surfaces (Underwood and Kromkamp, 1999; Jenkins et al., 2001; Nagarkar et al., 2004; Al-Zaidan et al., 2006). MPB comprises a mix of autotrophic taxa that uses light as the primary energy source for photosynthesis. While it is known that light optima vary among (groups of) MPB species (Oxborough et al., 2000; Frankenbach et al., 2018), knowledge about low light requirements is almost null. It is known that some marine photolithotrophs can grow under natural conditions characterized by no more than 10 nmol photon m^{-2} s^{-1} (Raven et al., 2000). Although not aware of any experimental results, it is conceivable that motile diatoms might be capable of detecting and responding to low light levels, too; this hypothesis seems to be supported by the recent finding of phytochromes in pennate and centric diatoms (Fortunato et al., 2016). In fact, phytochromes can mediate the responses of plants to very low light intensities (e.g., "Very Low Fluence Responses" in seed germination; Sheerin and Hiltbrunner, 2017). Concerning motile diatoms, such responses would have a clear adaptive value in helping cells buried in ill-illuminated sediment layers (due to resuspension or bioturbation; Frankenbach et al., 2019) to reach the surface and regain photosynthetic activity and growth.

In addition to the role of light as a resource, seasonal changes in photoperiod play a fundamental role for MPB, the most obvious being related to the alternation between periods of high photosynthetic activity and net carbon fixation and those dominated by respiration. For cyanobacterial dominated MPB, the dark phase is also associated with the highest rates of nitrogen fixation (Sicora et al., 2019), while for MPB dominated by motile diatoms, common in fine sediment estuarine flats, these cycles are a main factor controlling diel vertical migrations (Round and Palmer, 1966; Consalvey et al., 2005; Coelho et al., 2011; Haro et al., 2019).

Given these premises, it is reasonable to expect that changes in night light conditions might affect MPB biology and ecology. Recent studies conducted in the Mediterranean showed, under lit conditions, a doubling in mean photosynthetic biomass and maximum photosynthetic efficiency of rocky shore MPB during early stages of the colonization process (Maggi and Benedetti-Cecchi, 2018), as well as an increase in temporal

variability of maximum photosynthetic efficiency, more evident on mature assemblages (Maggi et al., 2019). These results clearly point out that ALAN originating by direct sources of white LEDs, at relatively high intensity (30 lux), may influence the mechanisms related to photosynthetic activity, as well as the competitive interactions among different species composing MPB assemblages. In fact, the observed temporal variability suggests the occurrence of changes in composition and/or relative abundances of different taxa, possibly related to differences in species-specific sensitivities to light and in light optima (Maggi et al., 2019). If and how these effects are geographically consistent and pervasive among different habitats is currently unknown. It is undeniable, however, the potential key role of ALAN in disrupting vertical migratory cycles and ultimately primary productivity, as observed in silty mud MPB assemblages after 3 days under continuous light conditions (Haro et al., 2019).

In addition to high intensity light sources, MPB might be impacted by low light levels of a few lux, such as those experienced at some distance from a streetlamp or induced by brief flashes of light due to intermittent/variable sources (e.g., lighthouses, boats), as suggested by the previous discussion on low light requirements. Moreover, recent findings have confirmed an increase in photosynthetic biomass in the planktonic cyanobacteria *Microcystis aeruginosa* under very low irradiance at night (80 nmol m^{-2} s^{-1}, ∼6.6 lux) (Poulin et al., 2014).

As for different light spectra, the results of Grubisic et al. (2018) on freshwater periphyton assemblages suggest that the current transition from HPS lamps to white LEDs (Kyba, 2018) might increase the ecological impact of artificial light on aquatic primary producers.

Future investigations of ALAN effects on MPB should also consider the role of temporal variability. In fact, even constant artificial night lighting may have temporally variable effects. Hölker et al. (2015) revealed how natural seasonal changes in microbial community structure of freshwater habitats can be reduced under long-term lit conditions, with a shift from negative to positive net ecosystem production (NEP), driven by positive effects on the autotrophic component. Moreover, ALAN itself can be characterized by a marked temporal variability. For example, in some coastal localities, tourist activities are mainly concentrated during the warm season and light pollution originating from restaurants, beach resorts or boats might vary seasonally in intensity, spectrum and spatial variability.

Finally, the ecological effect of ALAN on MPB cannot be fully assessed without considering top-down and bottom-up effects related to their consumers (Leroux and Loreau, 2015; Lynam et al., 2017). Rates of grazing activity might be influenced by ALAN, with positive or negative effects cascading down to MPB, depending on the suppression or enhancement of consumers' metabolism, respectively (Maggi and Benedetti-Cecchi, 2018; Maggi et al., 2020). Potential changes in behavior of herbivores might even affect the spatial variability in the MPB biomass, as observed under increased water temperature (Como et al., 2014). Conversely, the effects on MPB might cascade up to their consumers, as an increase or decrease in availability of resources (Manfrin et al., 2018).

ALAN: AN ADDITIONAL STRESSOR IMPINGING ON COASTAL ASSEMBLAGES

Marine systems, including coastal ones, are currently impacted by a variety of global and local stressors, which can affect single organisms up to entire habitats in additive, synergistic or antagonistic ways (Halpern et al., 2008). ALAN is among the most recently recognized sources of anthropogenic disturbance in these areas and may interfere synergistically with various other stressors, such as the release of contaminants and waste (including plastic debris), eutrophication and warming. So far, very little is known about the possible interaction pathways of light pollution with other disturbances impinging on aquatic systems. To the best of our knowledge, the study by Pu et al. (2019) is the only one addressing this issue and highlighting the potential role of ALAN in alleviating the toxic effect of silver nanoparticles on litter decomposition in freshwater habitats. ALAN modified the dissolved concentration of AgNP by releasing the activity of decomposers' enzymes (inhibited by silver nanoparticles) and changing the microbial aquatic assemblage. Similarly, ALAN might modify the effect of other stressors usually covarying with light pollution in urban areas, such as eutrophication, changes in temperature due to the "heat island effect" or plastic debris (Grimm et al., 2008; Halfwerk and Slabbekoorn, 2015; Kirstein et al., 2019). Although not corroborated by any experimental data so far, the formulation of these hypotheses is supported by the knowledge that light is able to affect MPB growth in interaction with temperature and nutrients (e.g., Pivato et al., 2019; Rakotomalala et al., 2019). As for light and temperature, a recent study showed their key role for the development of biofilm on plastic debris, especially its photoautotrophic component (Misic and Covazzi Harriague, 2019). It is therefore possible that artificial light available at night might represent an additional factor shaping MPB colonizing these artificial substrates, and potentially interacting with resident MPB assemblages either in sandy, muddy or rocky coastal environments.

CHALLENGES IN SAMPLING ACTIVITIES

The study of potential ALAN effects on MPB poses several challenges regarding sampling activities. First, measurements of intensity and spectrum of ALAN in the field may be not as straightforward as in other situations. In fact, there is a limited availability of instruments specifically designed for measuring the light environment of microbial photoautotrophs in aquatic coastal habitats, where both water, sedimentation and presence of natural or artificial surfaces reflecting or absorbing light may create environmental heterogeneity at the scale of a few centimeters. Second, sampling and measurements of MPB under

night conditions require attention to avoid even short exposure to light, with the risk of triggering additional responses and confounding the effects of ALAN under study. A particularly relevant case regards the use of Pulse Amplitude Modulation (PAM) fluorometry (Schreiber et al., 1986), a technique extensively used to study MPB biofilms on tidal systems, both for measuring photo-physiological and productivity-associated parameters (Kromkamp et al., 1998; Consalvey et al., 2005), but also short-term variations in surface MPB biomass associated to migratory rhythms (Serôdio et al., 1997). This technique relies on the application of light pulses, of very low (measuring light) and very high intensity (saturation pulses) that, while considered non-invasive in most other experimental contexts, might confound the detection of effects and responses to ALAN. Considering the potential response of MPB species to even low light levels, we propose that the use of PAM fluorometry in the context of ALAN studies should be preceded by preliminary tests for possible artefactual effects and the eventual adaptation of currently applied experimental protocols. Preliminary tests should be carried out comparing different instrument settings, namely light intensity, frequency, and color (most portable instruments use only blue or red LEDs) used for both measuring light and saturating pulses, on the triggering of upward vertical migration or photo-physiological effects. It seems prudent to recommend that measurements of ALAN effects should be carried out on samples not previously exposed to instrument lights, and that all measurements required for optimization of instrument settings should be carried out on a separate set of samples.

To fill in the gaps of a still fragmented and local knowledge of the ALAN effect on MPB, we should aim at developing integrated common monitoring approaches to data collection. This might involve the optimization of available sensors, sensitive enough to measure ALAN-levels in heterogeneous environments such as coastal areas; as well as of instruments for non-destructive quantification of MPB biomass and functioning. Finally, research activities might include experimental manipulative studies, both in the field and under laboratory conditions, to unambiguously assess the potential effects of different light intensities, spectra, duration but also timing of night light application on MPB in different coastal habitats. In fact, variable effects might be related, among others, to the variability in natural night lighting caused by changing moon phases. It is known that information driven by moonlight is used as a cue by some organisms in aquatic habitats, such as corals and the Palolo worm for spawning (Caspers, 1984; Harrison et al., 1984), or zooplankton for ocean-scale mass vertical migration during Arctic winter (Last et al., 2016). For many other aquatic organisms characterized by relatively short life cycles (such as MPB), the potential role of chronobiology by moonlight has still not been elucidated and its study could reveal unexpected temporally variable effects of ALAN on different processes and mechanisms (Kronfeld-Schor et al., 2013).

DISCUSSION

Intensity, spectrum, spatial and temporal variability of ALAN are key features of a recently recognized source of anthropogenic disturbance, that is impinging on coastal organisms at a global scale. The role of light pollution on physiological and ecological aspects of MPB is still in its infancy, but some recent studies anticipate a potential for either direct or indirect influences on the spatial and temporal variability of biomass and diversity of MPB assemblages, mediated by trophic relationships (Maggi and Benedetti-Cecchi, 2018; Maggi et al., 2019, 2020), as well as for interactive effects with additional stressors (Pu et al., 2019). Here we emphasize the need for including ALAN among the new challenges in microphytobenthos research, through the development of common monitoring approaches and the unambiguous assessment of its potential effects on MPB by means of manipulative experiment.

AUTHOR CONTRIBUTIONS

EM and JS contributed to the conception of the study and approved the final submitted version. EM wrote the first draft of the manuscript.

ACKNOWLEDGMENTS

Thanks are due to FCT/MCTES for the financial support to CESAM (UIDP/50017/2020 + UIDB/50017/2020), through national funds.

REFERENCES

Al-Zaidan, A. S. Y., Kennedy, H., Jones, D. A., and Al-Mohanna, S. Y. (2006). Role of microbial mats in Sulaibikhat Bay (Kuwait) mudflat food webs: evidence from d13C analysis. *Mar. Ecol. Prog. Ser.* 308, 27–36. doi: 10.3354/meps308027

Caspers, H. (1984). Spawning periodicity and habitat of the Palolo worm eunice viridis (Polycheta, Eunicidae) in the Samoan islands. *Mar. Biol.* 79, 229–236. doi: 10.1007/BF00393254

Coelho, H., Vieira, S., and Serôdio, J. (2011). Endogenous versus environmental control of vertical migration by intertidal benthic microalgae. *Eur. J. Phycol.* 46, 271–281.

Como, S., Lefrancois, C., Maggi, E., Antognarelli, F., and Dupuy, C. (2014). Behavioral responses of juvenile golden gray mullet *Liza aurata* to changes in coastal temperatures and consequences for benthic food resources. *J. Sea Res.* 92, 66–73. doi: 10.1016/j.seares.2013.10.004

Consalvey, M., Perkins, R. G., Paterson, D. M., Underwood, G. J. C., Tomists, D. I. A., and Paterson, M. (2005). PAM fluorescence: a beginners guide for benthic diatomists. *Diatom Res.* 20, 1–22.

Davies, T. W., Coleman, M., Griffith, K. M., and Jenkins, S. R. (2015). Night-time lighting alters the composition of marine epifaunal communities. *Biol. Lett.* 11:20150080. doi: 10.1098/rsbl.2015.0080

Davies, T. W., and Smyth, T. (2017). Why artificial light at night should be a focus for global change research in the 21th century. *Glob. Chang. Biol.* 24, 872–882. doi: 10.1111/gcb.13927

Duarte, C., Quintanilla-Ahumada, D., Anguita, C., Manriquez, P. H., Widdicombe, S., Pulgar, J., et al. (2019). Artificial light pollution at night (ALAN) disrupts the

distribution and circadian rhythm of a sandy beach isopod. *Environ. Poll.* 48, 565–573. doi: 10.1016/j.envpol.2019.02.037

Falchi, F., Cinzano, P., Duriscoe, D., Kyba, C. C. M., Elvidge, D. G., Baugh, K., et al. (2016). The new world atlas of artificial night sky brightness. *Sci. Adv.* 2:377. doi: 10.1126/sciadv.1600377

Fortunato, A. E., Jaubert, M., Enomoto, G., Bouly, J. P., Raniello, R., Thaler, M., et al. (2016). Diatom phytochromes reveal the existence of far-red-light-based sensing in the ocean. *Plant Cell* 28, 616–628. doi: 10.1105/tpc.15.00928

Frankenbach, S., Azevedo, A. A., Reis, V., Dias, D., Vaz, L., Dias, J. M., et al. (2019). Functional resilience of PSII, vertical distribution and ecosystem-level estimates of subsurface microphytobenthos in estuarine tidal flats. *Cont. Shelf Res.* 182, 46–56. doi: 10.1016/j.csr.2019.05.018

Frankenbach, S., Schmidt, W., Frommlet, J., and Serôdio, J. (2018). Photoinactivation, repair and the motility-physiology trade-off in microphytobenthos. *Mar. Ecol. Prog. Ser.* 601, 41–57. doi: 10.3354/meps12670

Garratt, M. J., Jenkins, S. R., and Davies, T. W. (2019). Mapping the consequences of artificial light at night for intertidal ecosystems. *Sci. Total Environ.* 691, 760–768. doi: 10.1016/j.scitotenv.2019.07.156

Gaston, K. J. (2018). Lighting up the nighttime. *Science* 362:8226. doi: 10.1126/science.aau8226

Grimm, N. B., Golubiewski, N. E., Faeth, S. H., and Redman, C. L. (2008). Global change and the ecology of cities. *Science* 319, 756–760. doi: 10.1126/science.1150195

Grubisic, M., van Grunsven, R. H. A., Manfrin, A., Monaghan, M. T., and Holker, F. (2018). A transition to white LED increases ecological impacts of nocturnal illumination on aquatic primary producers in a lowland agricultural drainage ditch. *Environ. Poll.* 240, 630–638. doi: 10.1016/j.envpol.2018.04.146

Halfwerk, W., and Slabbekoorn, H. (2015). Pollution going multimodal: the complex impact of the human-altered sensory environment on animal perception and performance. *Biol. Lett.* 11:20141051. doi: 10.1098/rsbl.2014.1051

Halpern, B. S., Walbridge, S., Selkoe, K. A., Kappel, C. V., Micheli, F., D'Agrosa, C., et al. (2008). A global map of human impact on marine ecosystems. *Science* 319, 948–952. doi: 10.1126/science.1149345

Haro, S., Bohórquez, J., Lara, M., Garcia-Robledo, E., González, C. J., Crespo, J. M., et al. (2019). Diel patterns of microphytobenthic primary production in intertidal sediments: the role of photoperiod on the vertical migration circadian rhythm. *Sci. Tot. Env.* 9:13376. doi: 10.1038/s41598-019-49971-8

Harrison, P. L., Babcock, R. C., Bull, G. D., Oliver, J. K., Wallace, C. C., and Willis, B. L. (1984). Mass spawning in tropical reef corals. *Science* 223, 1186–1189. doi: 10.1126/science.223.4641.1186

Hölker, F., Wurzbacher, C., Weißenborn, C., Monaghan, M. T., Holzhauer, S. I. J., and Premke, K. (2015). Microbial diversity and community respiration in freshwater sediments influenced by artificial light at night. *Philso. Trans. R. Soc. B* 370:20140130. doi: 10.1098/rstb.2014.0130

Jenkins, S. R., Arenas, F., Arrontes, J., Bussel, J., Castro, J., Coleman, R. A., et al. (2001). European-scale analysis of seasonal variability in limpet grazing activity and microalgal abundance. *Mar. Ecol. Prog. Ser.* 211, 193–203. doi: 10.3354/meps211193

Kirstein, I. V., Wichels, A., Gullans, E., Krohne, G., and Gerdts, G. (2019). The Plastisphere – Uncovering tightly attached plastic "specific" microorganisms. *PLoS One* 14:e0215859. doi: 10.1371/JOURNAL.PONE.0215859

Kromkamp, J., Barranguet, C., and Peene, J. (1998). Determination of microphytobenthos PSII quantum yield efficiency and photosynthetic activity by means of variable chlorophyll fluorescence. *Mar. Ecol. Prog. Ser.* 162, 45–55.

Kronfeld-Schor, N., Dominoni, D., de la Iglesia, H., Levy, O., Herzog, E. D., Dayan, T., et al. (2013). Chronobiology by moonlight. *Proc. Biol. Sci.* 280:20123088. doi: 10.1098/rspb.2012.3088

Kyba, C. C. M. (2018). Is light pollution getting better or worse? *Nat. Astron.* 2, 267–269. doi: 10.1038/s41550-018-0402-407

Last, K. S., Hobbs, L., Berge, J., Brierley, A. S., and Cottier, F. (2016). Moonlight drives ocean-scale mass vertical migration of zooplankton during the Arctic winter. *Curr. Biol.* 26, 244–251. doi: 10.1016/j.cub.2015.11.038

Leroux, S. J., and Loreau, M. (2015). "Theoretical perspectives on bottom-up and top-down interactions across ecosystems," in *Trophic Ecology. Bottom-Up and Top-Down Interactions across Aquatic and Terrestrial Systems*, eds T. C. Hanley and K. J. La Pierre (Cambridge: Cambridge University Press), 3–28. doi: 10.1017/CBO9781139924856.002

Ludvigsen, M., Berge, J., Geoffroy, M., Cohen, J. H., De La Torre, P. R., Nornes, S. M., et al. (2018). Use of an autonomous surface vehicle reveals small-scale diel vertical migrations of zooplankton and susceptibility to light pollution under low solar irradiance. *Sci. Adv.* 4:9887. doi: 10.1126/sciadv.aap9887

Lynam, C. P., Llope, M., Möllmann, C., Helaouët, P., Bayliss-Brown, G. A., and Stenseth, N. C. (2017). Interaction between top-down and bottom-up control in marine food webs. *Proc. Nat. Acad. Sci. U.S.A.* 114:201621037. doi: 10.1073/pnas.1621037114

Maggi, E., and Benedetti-Cecchi, L. (2018). Trophic compensation stabilizes marine primary producers exposed to artificial light at night. *Mar. Ecol. Prog. Ser.* 606, 1–5. doi: 10.3354/meps12769

Maggi, E., Bertocci, I., and Benedetti-Cecchi, L. (2019). Light pollution enhances temporal variability of photosynthetic activity in mature and developing biofilm. *Hydrobiologia* 847, 1793–1802. doi: 10.1007/s10750-019-04102-2

Maggi, E., Bongiorni, L., Fontanini, D., Capocchi, A., Dal Bello, M., Giacomelli, A., et al. (2020). Artificial light at night erases positive interactions across trophic levels. *Funct. Ecol.* 34, 694–706. doi: 10.1111/1365-2435.13485

Manfrin, A., Lehmann, D., Grunsven, R. H. A., Larsen, S., Syväranta, J., Wharton, G., et al. (2018). Dietary changes in predators and scavengers in a nocturnally illuminated riparian ecosystem. *Oikos* 127, 960–969. doi: 10.1111/oik.04696

Misic, C., and Covazzi Harriague, A. (2019). Development of marine biofilm on plastic: ecological features in different seasons, temperatures, and light regimes. *Hydrobiologia* 835, 129–145. doi: 10.1007/s10750-019-3934-7

Nagarkar, S., Williams, G. S., Subramanian, G., and Saha, S. K. (2004). Cyanobacteria-dominated biofilms: a high-quality food resource for intertidal grazers. *Hydrobiologia* 519, 89–94.

Oxborough, K., Hanlon, A. R. M., Underwood, G. J. C., and Baker, N. R. (2000). In vivo estimation of the photosystem II photochemical efficiency of individual microphytobenthic cells using high-resolution imaging of chlorophyll a fluorescence. *Limnol. Oceanogr.* 45, 1420–1425. doi: 10.4319/lo.2000.45.6.1420

Pivato, M., Carniello, L., Moro, I., and D'Odorico, P. (2019). On the feedback between water turbidity and microphytobenthos growth in shallow tidal environments. *Earth Surf. Process. Landforms* 44, 1192–1206.

Poulin, C., Bruyant, F., Laprise, M.-H., Cockshutt, A. M., Vandenhecke, J. M.-R., and Huot, A. A. (2014). The impact of light pollution on diel changes in the photophysiology of *Microcystis aeruginosa*. *J. Plankton Res.* 36, 286–291. doi: 10.1093/plankt/fbt088

Pu, G., Zeng, D., Mo, L., He, W., Zhou, L., Huang, K., et al. (2019). Does artificial light at night change the impact of silver nanoparticles on microbial decomposers and leaf litter decomposition in streams? *Environ. Sci. Nano.* 2019, 1728–1739.

Rakotomalala, C., Guizien, K., Grangere, K., Lefebre, S., Dupuy, C., Orvain, M., et al. (2019). Modelling the functioning of a coupled microphytobenthic-EPS-bacterial system in intertidal mudflats. *Mar. Env. Res.* 150:104754. doi: 10.1016/j.marenvres.2019.104754

Raven, J. A., KÎbler, J. E., and Beardall, J. (2000). Put out the light, and then put out the light. *J. Biol. Ass. UK* 80, 1–25. doi: 10.1089/jwh.1998.7.297

Round, F. E., and Palmer, J. D. (1966). Persistent, vertical-migration rhythms in benthic microflora.: II. field and laboratory studies on diatoms from the banks of the river Avon. *J. Biol. Assoc.* 46, 191–214. doi: 10.1017/S0025315400017641

Schreiber, U., Schliwa, U., and Bilger, W. (1986). Continuous recording of photochemical and nonphotochemical chlorophyll fluorescence quenching with a new type of modulation fluorometer. *Photosynth. Res.* 10, 51–62. doi: 10.1007/BF00024185

Serôdio, J., Silva, J. M., and Catarino, F. (1997). Non-destructive tracing of migratory rhythms of intertidal benthic microalgae using in vivo chlorophyll a fluorescence. *J. Phycol.* 33, 542–553.

Sheerin, D. J., and Hiltbrunner, A. (2017). Molecular mechanisms and ecological function of far-red light signalling. *Plant Cell Environ.* 40, 2509–2529. doi: 10.1111/pce.12915

Sicora, C. I., Chiş, J., Chiş, C., and Sicora, O. (2019). Regulation of PSII function in *Cyanothece* sp. during a light–dark cycle. *Photos. Res.* 139, 461–473. doi: 10.1007/s11120-018-0598-5

Tamir, R., Lerner, A., Haspel, C., Dubinsky, Z., and Iluz, D. (2017). The spectral and spatial distribution of light pollution in the waters of the

northern Gulf of Aqaba (Eilat). *Sci. Rep.* 7:42329. doi: 10.1038/srep 42329

Underwood, C. N., Davies, T. W., and Queiros, A. M. (2017). Artificial light at night alters trophic interactions of intertidal invertebrates. *J. Anim. Ecol.* 86, 781–789. doi: 10.1111/1365-2656.12670

Underwood, G. C. J., and Kromkamp, J. (1999). Primary production by phytoplankton and microphytobenthos in estuaries. *Adv. Ecol. Res.* 29, 93–153. doi: 10.1016/S0065-2504(08)60192-0

Witherington, B. E., and Bjorndal, K. A. (1991). Influences of artificial lighting on the seaward orientation of hatchling loggerhead turtles *Caretta caretta*. *Biol. Conservat.* 55, 139–149.

Conflict of Interest: The authors declare that the research was conducted in the absence of any commercial or financial relationships that could be construed as a potential conflict of interest.

Advantages of publishing in Frontiers

OPEN ACCESS
Articles are free to read for greatest visibility and readership

FAST PUBLICATION
Around 90 days from submission to decision

HIGH QUALITY PEER-REVIEW
Rigorous, collaborative, and constructive peer-review

TRANSPARENT PEER-REVIEW
Editors and reviewers acknowledged by name on published articles

Frontiers
Avenue du Tribunal-Fédéral 34
1005 Lausanne | Switzerland

Visit us: www.frontiersin.org
Contact us: info@frontiersin.org | +41 21 510 17 00

REPRODUCIBILITY OF RESEARCH
Support open data and methods to enhance research reproducibility

DIGITAL PUBLISHING
Articles designed for optimal readership across devices

FOLLOW US
@frontiersin

IMPACT METRICS
Advanced article metrics track visibility across digital media

EXTENSIVE PROMOTION
Marketing and promotion of impactful research

LOOP RESEARCH NETWORK
Our network increases your article's readership